NUCLEAR PHYSICS

EDITORIAL BOARD

AUSTRALIA & NEW ZEALAND:	H. Messel (Sydney), M. L. Oliphant (Canberra)
AUSTRIA:	B. Karlik (Vienna), H. Thirring (Vienna)
BELGIUM:	M. de Hemptinne (Louvain), J. Verhaeghe (Ghent)
CANADA:	G. Volkoff (Vancouver)
DENMARK:	C. Møller (Copenhagen), S. Rozental (Copenhagen), G. E. Brown (Copenhagen)
FINLAND:	L. Simons (Helsinki)
FRANCE:	A. Berthelot (Saclay), S. Gorodetzky (Strasbourg)
GERMANY (DEM. REP.):	G. Hertz (Leipzig)
GERMANY (FED. REP.):	W. Gentner (Freiburg i. B.), J. H. D. Jensen (Heidelberg)
GREAT BRITAIN:	W. E. Burcham (Birmingham), T. H. R. Skyrme (Harwell)
HUNGARY:	L. Janossy (Budapest)
INDIA:	H. Bhabha (Bombay), R. Ramanna (Trombay)
IRISH REPUBLIC:	J. McConnell (Maynooth)
ISRAEL:	G. Racah (Jerusalem)
ITALY:	E. Amaldi (Rome)
JAPAN:	S. Kikuchi (Tokai), S. Tomonaga (Tokyo)
MEXICO:	M. Moshinsky (Mexico)
NETHERLANDS:	H. Brinkman (Groningen), S. R. de Groot (Leiden)
NORWAY:	E. Hylleraas (Oslo), A. Lundby (Oslo), H. Wergeland (Trondheim)
POLAND:	L. Infeld (Warsaw), J. Werle (Warsaw)
PORTUGAL:	J. M. Araújo (Porto), J. R. de Almeida Santos (Coimbra)
SOUTH AMERICA:	G. Beck (Saõ Paulo), J. Leite Lopes (Rio de Janeiro)
SPAIN:	J. M. Otero (Madrid), C. Sanchez del Rio (Madrid)
SWEDEN:	O. Klein (Stockholm), K. Siegbahn (Uppsala), I. Waller (Uppsala)
SWITZERLAND:	P. Huber (Basel), P. Scherrer (Zürich)
U.A.R. & ARAB COUNTRIES:	F. El Bedewi (Cairo), M. G. Nooh (Cairo)
U.S.A.:	H. H. Barschall (Madison, Wisconsin), S. Devons (New York), V. F. Weisskopf (Cambridge, Mass.)
U.S.S.R.:	M. A. Markov (Moscow), I. S. Shapiro (Moscow), D. V. Skobeltzyn (Moscow)
YUGOSLAVIA:	I. Supek (Zagreb)

NUCLEAR PHYSICS

JOURNAL DEVOTED TO THE EXPERIMENTAL AND THEORETICAL STUDY OF THE FUNDAMENTAL CONSTITUENTS OF MATTER AND THEIR INTERACTIONS

EDITOR: L. ROSENFELD - COPENHAGEN

VOLUME XXIV

APRIL 1961 — MAY 1961

NORTH-HOLLAND PUBLISHING COMPANY - AMSTERDAM

PRINTED IN THE NETHERLANDS

1.D.4 *Nuclear Physics* **24** (1961) 1—17; © *North-Holland Publishing Co., Amsterdam*

Not to be reproduced by photoprint or microfilm without written permission from the publisher

VIBRATIONS OF SPHERICAL NUCLEI

G. E. BROWN
NORDITA, *Copenhagen*
and
J. A. EVANS and D. J. THOULESS
Mathematical Physics Department,
University of Birmingham

Received 18 November 1960

Abstract: The particle-hole interaction is discussed as the mechanism for producing vibrational states in nuclei. The procedure is first illustrated by means of a schematic model, from which it is shown that the usual type of shell-model calculation must be extended to include correlations in the ground state of the nucleus before it can be applied to the calculation of vibrational states. Results of calculations in j—j coupling, but with zero-range forces, are given.

1. Introduction

Considerable experimental [1–5]) and theoretical [5, 6]) evidence suggests the existence of octupole vibrations in a large number of nuclei possessing spherical equilibrium shape. In this note we wish to indicate, that the particle-hole interaction produces a low-lying 3— state possessing an extremely large octupole moment and thus provides a natural mechanism for such a state. The techniques will be outlined in general form, however, so as to be applicable to other cases.

It has been suggested [7, 8, 9]) that the particle-hole interaction is the mechanism producing the dipole state (giant photonuclear resonance), and zero-range calculations showed it to be extremely effective both in transferring dipole strength to the dipole state and in raising the energy of the latter. In refs. [8, 9]) it was pointed out that the particle-hole interaction was generally repulsive in $T = 1$ states and attractive in $T = 0$ ones. If, therefore, a $T = 1$ state carrying most of the multipole moment goes up in energy, then one would expect a $T = 0$ one to come down. The simplest cases to consider are double closed-shell nuclei; it was pointed out in ref. [8]) that the valence particles played relatively little part in the state, except in determining its width. The simplest states to consider are those that arise from linear combinations of particles raised from one shell to the next, i.e., excitations of $\hbar\omega$ in the harmonic oscillator model. Now, whereas the dipole $T = 1$ state describes motion of neutrons against protons and, therefore, introduces no problems of spurious centre-of-mass motion, the dipole $T = 0$ state represents dipole motions of neutrons and

protons together and is, hence, almost completely spurious. In the Elliott and Flowers calculation [10]), for example, this state was removed and discarded before the secular matrix was diagonalized.

The next states one might look at are magnetic quadrupole or electric octupole states (these states have odd parity). We prefer now to look at the latter, since they are easily reached by inelastic particle scattering, and there is considerable evidence for their existence.

In this note we shall work mainly with a schematic model similar to that of refs. [7, 8]), quoting later results of shell-model calculations carried out in zero-range approximation. From the work with the schematic model it will become clear that the usual type of shell-model calculation will have to be modified considerably before being applied to the calculation of vibrational states because of the large energy shifts involved.

In section 2 we shall outline the treatment by the schematic model.

In section 3 we consider effects from correlations present in the ground-state of the nucleus, and in section 4 we will show the classical correspondence of our schematic model.

In the sections 5 and 6 we give results of shell-model calculations for O^{16} and Ca^{40} in zero-range approximation.

2. The Schematic Model

In ref. [8]) it was pointed out that we could represent the spin and isotopic spin character of a $T = 1$ particle-hole wave function as

$$\psi = \tfrac{1}{2}(P\uparrow + P\downarrow - N\uparrow - N\downarrow).$$

The particle-hole interaction consists of two types of terms as shown in fig. 1, direct terms D and exchange terms E. For a Wigner force the interaction in

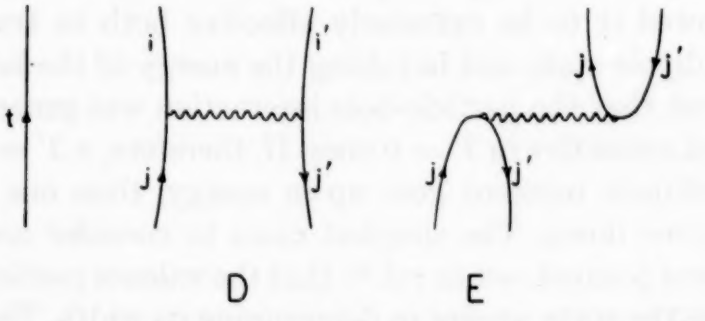

Fig. 1. Graphs corresponding to the direct terms D and the exchange terms E of the particle-hole interaction.

$T = 1$ states was D and in $T = 0$ states, $D-4E$. Although the interaction is more likely to be something like a Serber mixture plus a small spin-exchange, this will not look much different from the Wigner force in zero-range approxima-

tion which we can consider in formulating our schematic model and which seems to reproduce qualitative features.

We see that the interaction in $T = 0$ states is dominated by the exchange terms. With a zero-range Wigner force, D and E are equal, so that the interaction is $-3E$. Going to finite range decreases D compared with E, since the exchange term contains only one moment of the potential; i.e., in an expansion

$$V(\mathbf{r}_1-\mathbf{r}_2) = \sum_L V_L(r_1, r_2)P_L(\cos\theta_{12}) \tag{1}$$

only the term with $L = 3$ is involved in E for an octupole state. This is easy to see since the particle and hole coupled to angular momentum J can annihilate at a point as shown in fig. 1 only through the J^{th} term in the expansion (1). On the other hand, D depends on contributions from a large number of moments of the potential V_L, and going to finite range decreases the contribution † from large L. We shall consider mainly the exchange term, therefore.

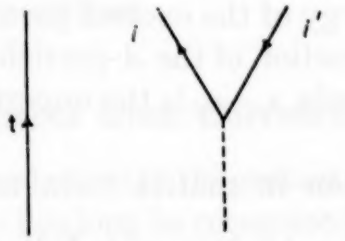

Fig. 2. Particle-hole creation by absorption of a γ-ray.

We note, now, that if the moment $V_L(r_1, r_2)$ were factorizable and proportional to $r_1{}^L r_2{}^L$, then the matrix element $V_{ii',jj'}$ between states ii' and jj', which we assume to be dominated by the exchange term, would be proportional to $D_{ii'} D_{jj'}$, where $D_{ii'}$ is the amplitude for absorption of an octupole γ-ray, leading to creation of a particle in state i and a hole in state i', as shown in fig. 2.

Now, in fact, $V_L(r_1, r_2)$ is nothing like $r_1{}^L r_2{}^L$ since V_L vanishes rapidly as the difference $|r_2-r_1|$ increases beyond 10^{-13} cm or so. However, we arrive at essentially the same representation of $V_{ii',jj'}$ if we keep all factors coming from angular integrals, but set all radial integrals entering into both $V_{ii',jj'}$ and $D_{ii'}$ equal (see ref. [7])). We shall, therefore, use

$$V_{ii',jj'} = \pm\mathscr{V} D_{ii'} D_{jj'}, \tag{2}$$

where $\mathscr{V}$ is a constant determining the strength of particle-hole interaction in the schematic model. The + sign refers to $T = 1$ states, the − sign to $T = 0$ ones, and $\mathscr{V}$ will in general have different magnitudes in the two cases. In the calculations we have carried out without approximating the radial integrals in this way, the calculated $V_{ii',jj'}$ have often differed quite a bit from those of the schematic model. However, it has generally been found that the $V_{ii',jj'}$ are large

† This point has been especially stressed by Ben Mottelson and Aage Bohr.

(and negative for $T = 0$ states) between states carrying large amplitudes $D_{ii'}$ and $D_{jj'}$ and that they are small between states having small transition amplitudes. This seems to be sufficient to guarantee that qualitative features will come out as in the schematic model.

Once one makes the above assumption about the $V_{ii',jj'}$ in the $T = 1$ dipole case, one obtains immediately the results of ref. [7]), finding in the degenerate case (all ε_i in the secular matrix of that reference equal) that the dipole state is

$$\Phi_{\mathrm{D}} = \sum D_{ii'}\varphi_{ii'}/\sqrt{\sum D_{ii'}^2}, \tag{3}$$

and that it is pushed up an amount $\sum_{ii'} \mathscr{V} D_{ii'}^2$ in energy. In dealing with the octupole case, we wish to obtain a solution for the case where all ε_i are not equal. Thinking of the situation using a simple-harmonic well, for example, one has octupole absorption to states of unperturbed energies $\hbar\omega$ and $3\hbar\omega$, and it may be important to include the latter.

We prefer now to change the notation of ref. [7]), so that ε_i is replaced by $\varepsilon_i - \varepsilon_{i'}$, where ε_i is the energy of the excited particle in the potential well representing the average interaction of the A-particles, and $\varepsilon_{i'}$ is the initial energy of the particle. In other words, $\varepsilon_i - \varepsilon_{i'}$ is the unperturbed energy of the particle-hole pair ii'.

The Schrödinger equation in matrix form now reads

$$(E - \varepsilon_i + \varepsilon_{i'})\psi_{ii'} = \pm \sum_{jj'} V_{ii',jj'}\psi_{jj'} \tag{4}$$

and using the approximation of the schematic model eq. (2) for $V_{ii',jj'}$, this is easily solved to give

$$\psi_{ii'} = \frac{ND_{ii'}}{E - \varepsilon_i + \varepsilon_{i'}}, \tag{4.1}$$

where N is a normalization constant,

$$N^2 = \left\{ \sum_{ii'} \frac{D_{ii'}^2}{(E - \varepsilon_i + \varepsilon_{i'})^2} \right\}^{-1}. \tag{4.2}$$

The energy of any given eigenstate may be found by taking the expectation value of the Hamiltonian. In the degenerate case (all $\varepsilon_i - \varepsilon_{i'}$ equal to a common value ε) the results are particularly simple, the amplitudes $\psi_{ii'}$ being

$$\psi_{ii'} = N' D_{ii'}, \tag{4.3}$$

with

$$(N')^2 = \{\sum_{ii'} D_{ii'}^2\}^{-1}, \tag{4.4}$$

and the energy of the vibrational state

$$E = \varepsilon - \mathscr{V} \sum_{ii'} D_{ii'}^2. \tag{4.5}$$

A slight generalization of the degenerate model is necessary to deal with the octupole case, since the absorbtion can proceed to states of unperturbed energies $\approx \hbar\omega$ and $\approx 3\hbar\omega$. Our schematic model would predict in this case

$$\psi = N\left\{\frac{\sum D^{(1)}_{ii'}\psi^{(1)}_{ii'}}{\hbar\omega - E} + \frac{\sum D^{(3)}_{ii'}\psi^{(3)}_{ii'}}{3\hbar\omega - E}\right\}, \tag{5}$$

where the upper suffices refer to states of energy $\hbar\omega$ and $3\hbar\omega$, respectively. Simple calculations then show that the second term has quite an important effect on increasing the octupole transition probability to the collective state. Another way of including the effect of higher transitions, as suggested by Ben Mottelson, would be to introduce an effective octupole charge. However, we believe that one should ultimately try to directly calculate the effect of the higher transitions. The experiments [12]) demand a higher transition probability than that obtained by Elliott and Flowers [10]), but we believe that this comes about from the effects of ground-state correlations, which we shall now discuss, as well as from the $3\hbar\omega$ transitions.

3. Effects from Correlations

The necessity of taking correlations in the ground state into account in plasma oscillations of an electron gas has long be recognized (See, for example, Sawada *et al.* [13]) or Ferrell and Quinn [14])). Their inclusion is necessary to reproduce the Bohm-Pines theory [15]) and to make correspondence with the classical theory.

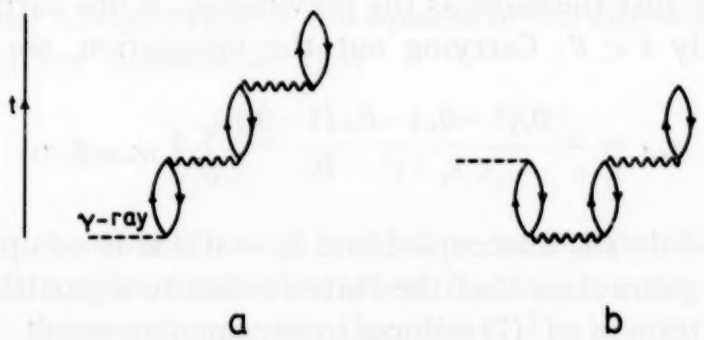

Fig. 3. a. Absorption of a γ-ray and subsequent processes. b. Interaction of two particles in the ground-state of the nucleus, forming two particle-hole pairs, and subsequent processes.

The necessity of including them in nuclear vibrational states has also been pointed out [16, 17]). We essentially rephrase the arguments of ref. [17]) in our schematic model. Since we deal now with vibrational states, we consider the exchange term of fig. 1, which is of main importance here. In fig. 3 we illustrate two processes which are topologically similar. Fig. 3a represents the process considered earlier, whereas fig. 3b represents two particles interacting in the ground state of the nucleus, forming two particle-hole pairs, one of which is

subsequently annihilated in absorbtion of the γ-ray. Clearly, the most convenient way of including processes of the type fig. 3b is to use Feynman techniques and allow for propagation in a chain either forwards or backwards in time. To this end we write down the Gell-Mann-Low wave function [18])

$$\psi(1, 2) = i \int\int \mathrm{d}\tau_5 \mathrm{d}\tau_6 S_{\mathrm{F}}(1, 5) S_{\mathrm{F}}(2, 6) \Gamma(5, 6) \psi(5, 6) \tag{6}$$

in their notation. Setting $t_1 = t_2 = t'$ and $t_5 = t_6 = t$, letting coordinate 5 refer to a particle and coordinate 6 to a hole for $t < t'$, and choosing

$$\Gamma(5, 6) = \delta(t_5 - t_6) V(5, 6), \tag{6.1}$$

we find in going over to an angular-momentum representation that

$$\psi_{ii'}(t') = i \int_{-\infty}^{\infty} \mathrm{d}t \, S_{\mathrm{F}i}(t' - t) S_{\mathrm{F}i'}(t' - t) V_{ii', jj'} \psi_{jj'}(t), \tag{6.2}$$

where

$$\begin{aligned} \psi_{ii'}(t) &\equiv \langle ii' | \psi(1, 2) \rangle = \chi_{ii'} \mathrm{e}^{-iEt'}, \\ S_{\mathrm{F}i}(t' - t) &= \begin{cases} i\theta_i \mathrm{e}^{-i\varepsilon_i(t'-t)}, & (t < t'), \\ -i(1-\theta_i) \mathrm{e}^{-i\varepsilon_i(t'-t)}, & (t > t'), \end{cases} \\ S_{\mathrm{F}i'}(t' - t) &= \begin{cases} -i(1-\theta_{i'}) \mathrm{e}^{i\varepsilon_{i'}(t'-t)}, & (t < t'), \\ i\theta_{i'} \mathrm{e}^{i\varepsilon_{i'}(t'-t)}, & (t > t'), \end{cases} \end{aligned} \tag{6.3}$$

and $\chi_{ii'}$ would be just the same as the previous $\psi_{ii'}$ if one carried out the integration over only $t < t'$. Carrying out the integration, we find

$$\chi_{ii'} = - \frac{\theta_i(1-\theta_{i'}) - \theta_{i'}(1-\theta_i)}{\varepsilon_i - \varepsilon_{i'} - E} \sum_{jj'} V_{ii', jj'} \chi_{jj'}, \tag{7}$$

where $\theta_i = 1$ if state i is unoccupied and $\theta_i = 0$ if it is occupied. That is, the factor $\theta_i(1-\theta_{i'})$ guarantees that the state i refers to a particle, the state i' to a hole. The first term in eq. (7) reduces to our previous result. The second term represents the effect of the excitation propagating backwards (these two parts are called $A_i^{(+)}$ and $A_i^{(-)}$ by Ferrell and Quinn [14])). Thus, although we started out with i labelling a particle and i' a hole (this designation referring to the bare vacuum, where one can unambigously talk about particles and holes because of the sharp discontinuity in occupation number at the Fermi energy), this convention has become reversed in the backwards part. However, particles can be created only in states of energy greater than the Fermi energy E_{F}, and holes in states of energy less than E_{F}. Thus, i' in the second case takes on precisely the same values as i in the first case. We can preserve the designation of particles by i and holes by i' if we interchange i and i' in the second term,

obtaining

$$\chi_{ii'} = -\frac{1}{\varepsilon_i - \varepsilon_{i'} - E} \sum_{jj'} \{V_{ii',jj'}\chi_{jj'} + V_{ii',j'j}\chi_{j'j}\},$$
$$\chi_{i'i} = +\frac{1}{\varepsilon_{i'} - \varepsilon_i - E} \sum_{jj'} \{V_{i'i,jj'}\chi_{jj'} + V_{i'i,j'j}\chi_{j'j}\}, \tag{8}$$

where $\chi_{ii'}$ refers to the forward-going part of the excitation, and $\chi_{i'i}$ refers to the backward-going part. The normalization is such [14, 21]) (see, also, eq. (14)) that

$$\sum_{ii'} |\chi_{ii'}|^2 - \sum_{ii'} |\chi_{i'i}|^2 = 1. \tag{8.1}$$

The quantities V will be discussed for the general case later. We note that if one includes only the exchange term of fig. 1, i.e., graphs of the type shown in fig. 3, then

$$V_{ii',jj'} = V_{ii',j'j} = V_{i'i,jj'} = V_{i'i,j'j}, \tag{8.2}$$

which is a great simplification. In this case we can add the two equations (8), obtaining

$$\chi_{ii'} + \chi_{i'i} = -\frac{2(\varepsilon_i - \varepsilon_{i'})}{(\varepsilon_i - \varepsilon_{i'})^2 - E^2} \sum_{jj'} V_{ii',jj'}(\chi_{jj'} + \chi_{j'j}), \tag{9}$$

showing that the secular equation describing only the forward going part can be modified rather trivially to give the squares of the eigenenergies E^2. In the schematic model one finds easily that

$$\chi_{ii'} = \frac{ND_{ii'}}{\varepsilon_i - \varepsilon_{i'} - E}, \quad \chi_{i'i} = \frac{ND_{ii'}}{\varepsilon_i - \varepsilon_{i'} + E}, \tag{9.1}$$

where N is again the normalization contant to be determined from eq. (8.1). We see that in the vibrational case when $E < \varepsilon_i - \varepsilon_{i'}$, the inclusion of the backwards-going terms enhances the absorption. The energy is given by the dispersion law †

$$1 = \sum \frac{2\mathscr{V} D_{ii'}^2 (\varepsilon_i - \varepsilon_{i'})}{(\varepsilon_i - \varepsilon_{i'})^2 - E^2}, \tag{9.2}$$

and it is seen that inclusion of the backwards terms lowers the energy still more. In fact, in the degenerate case (all $\varepsilon_i - \varepsilon_{i'}$ equal to ε)

$$E = \sqrt{\varepsilon^2 - 2\varepsilon \sum_{ii'} \mathscr{V} D_{ii'}^2}. \tag{9.3}$$

† This result has also been obtained by M. Baranger and Ben Mottelson.

The transition amplitude in the general case is given by

$$\mathscr{D} = \sum D_{ii'}(\chi_{ii'} + \chi_{i'i}), \tag{9.4}$$

if phase factors are chosen so that $D_{i'i} = D_{ii'}$, and, in the degenerate case, the transition probability is given by

$$|\mathscr{D}|^2 = \frac{\varepsilon}{E}\sum_{ii'} D_{ii'}^2, \tag{9.5}$$

that is, it is enhanced by the inclusion of backwards-going graphs by the factor ε/E. The transition probability to this one state then exhausts the energy-weighted sum rule, the inclusion of the backwards-going graphs being necessary for this [16, 17]).

4. Classical Correspondence

When the energy of the vibrational state becomes small compared with the single-particle excitations, the formulae shoud go over to those of the adiabatic case, and expanding in powers of $E/(\varepsilon_i - \varepsilon_{i'})$ we should regain the semiclassical description †. To make the correspondence more obvious, we go over to the notation $\omega_{ii'} = \varepsilon_i - \varepsilon_{i'}$, $\omega = E$. Then, with expansion in powers of $\omega/\omega_{ii'}$, eq. (9.2) becomes

$$\left(\frac{1}{2\mathscr{V}} - \sum \frac{D_{ii'}^2}{\omega_{ii'}}\right) - \omega^2 \sum \frac{D_{ii'}^2}{\omega_{ii'}^3} = 0. \tag{10}$$

This is to be compared with the adiabatic formula [19])

$$K\alpha + M\alpha'' = K\alpha - M\omega^2\alpha = 0, \tag{11}$$

where our formula (10) must be essentially $K - M\omega^2 = 0$ since no collective coordinate occurs. Here K represents the restoring force, and M, the inertial parameter. In fact, to within a constant, the coefficient of in eq. (10) is just the inertial parameter of the cranking model [20]). This is easy to see. The prescription of the cranking model is that one should add to the Hamiltonian

$$H = \sum_j H_0(j) = \sum_j (T_j + V_j) \tag{12}$$

describing the motion of particles in a spherical well V_j, the term

$$\delta H = \alpha \sum Y_L^0(\theta_j, \varphi_j) r_j^L \tag{12.1}$$

in describing L^{th} order vibrations; this additional term effectively distorts the shape of the well. Then

$$M = C \sum_{ii'} \frac{|\langle ii'| \dfrac{\partial}{\partial \alpha} |0\rangle|^2}{\omega_{ii'}} \tag{12.2}$$

† This was suggested by Aage Bohr.

where $|0\rangle$ is the uncorrelated ground state. But

$$\langle ii'|\frac{\partial}{\partial\alpha}|0\rangle = \frac{1}{\omega_{ii'}}\langle ii'|\left[H, \frac{\partial}{\partial\alpha}\right]|0\rangle$$
$$= -\frac{\langle ii'|\sum Y_L{}^0(\theta_j, \varphi_j) r_j{}^L|0\rangle}{\omega_{ii'}} = -\frac{\lambda D_{ii'}}{\omega_{ii'}}. \tag{12.3}$$

Substituting from eq. (12.3) back into (12.2) shows that the coefficient of ω^2 in eq. (10) is, to within trivial constants, equal to M. It is not surprising that our eq. (2) should lead us back to the cranking-model inertial parameter, for it would be exactly fulfilled if $V_L(r_1, r_2)$ were equal to $r_1{}^L r_2{}^L$ and we kept only the exchange terms. In this case keeping only the L^{th} term of the nucleon-nucleon force in the expansion (1) as a residual force between particles moving in a spherical well leads directly to the particles moving independently in a deformed well. The cranking model treats just this case. It is also not surprising that one must include ground-state correlations to make the classical correspondence, since this situation is known in the treatment of plasma oscillations in a metal [13, 14]).

As the number of terms in the sum of eq. (9.2) increase, or as the strength of the potential $\mathscr{V}$ increases, E moves down until it becomes zero, and any further increase in the aove factors would cause it to become imaginary. This is connected with the collapse of the nucleus into nonspherical equilibrium shape [21]).

5. Realistic Potentials

The calculations which are described in the next section were carried out by solving eq. (8), but it was not assumed that the potential has the simple form needed to give the schematic model of section 3. Eq. (8) is similar to a Schrödinger equation for a wave function with components $\chi_{ii'}$ and $\chi_{i'i}$, but there are some important differences. We give here a brief discussion of the general properties of eq. (8), since these properties must be understood to interpret the results of the calculations.

Eq. (8) can be written as a matrix equation

$$\begin{pmatrix} A & B \\ B & A \end{pmatrix}\begin{pmatrix} X \\ Y \end{pmatrix} = E\begin{pmatrix} X \\ -Y \end{pmatrix}, \tag{13}$$

where X is a column vector whose components are the numbers $\chi_{ii'}$, and Y is a column vector whose components are the numbers $\chi_{i'i}$. The equation takes this simple form, with A and B Hermitian matrices, if corresponding components of X and Y are $\chi_{ii'}$ and $\chi_{\bar{i}'\bar{i}}$, where a bar over an index denotes the time-reversed state. The matrix B has elements equal to $V_{ii',jj}$, and the matrix A has diagonal elements equal to $\varepsilon_i - \varepsilon_{i'} + V_{ii',ji'}$, and off-diagonal elements

$V_{ii',jj'}$. These matrices are Hermitian because of the time-reversal invariance of the shell-model energies and of the potential. Eq. (13) shows that the energy levels are given by the eigenvalues of the nonhermitian matrix

$$\begin{pmatrix} A & B \\ -B & -A \end{pmatrix},$$

and the peculiar properties of the solutions of this equation arise from the nonhermitian property.

The first thing to be noticed about eq. (13) is that for every positive eigenvalue E there is an equal negative eigenvalue $-E$, since eq. (13) implies

$$\begin{pmatrix} A & B \\ B & A \end{pmatrix} \begin{pmatrix} Y \\ X \end{pmatrix} = -E \begin{pmatrix} Y \\ -X \end{pmatrix}. \tag{13.1}$$

These negative solutions have no physical significance, but describe the same excited states as the positive solutions.

If we have two eigenvectors

$$\begin{pmatrix} X_m \\ Y_m \end{pmatrix} \quad \text{and} \quad \begin{pmatrix} X_n \\ Y_n \end{pmatrix}$$

with eigenvalues E_m and E_n, we get

$$\begin{aligned} E_n(X_m^\dagger Y_m^\dagger) \begin{pmatrix} X_n \\ -Y_n \end{pmatrix} &= (X_m^\dagger Y_m^\dagger) \begin{pmatrix} A & B \\ B & A \end{pmatrix} \begin{pmatrix} X_n \\ Y_n \end{pmatrix} \\ &= E_m^*(X_m^\dagger - Y_m^\dagger) \begin{pmatrix} X_n \\ Y_n \end{pmatrix}. \end{aligned} \tag{13.2}$$

Unless E_m^* and E_n are equal, we must have

$$X_m^\dagger X_n - Y_m^\dagger Y_n = 0, \tag{14}$$

and this replaces the usual orthogonality property of eigenvectors of a Hermitian matrix. This relation shows why the normalization of the eigenvectors given in eq. (8.1) is the natural one to choose in this problem.

A sufficient condition for the eigenvalues of eq. (13) to be real is that the eigenvalues of the Hermitian matrix

$$\begin{pmatrix} A & B \\ B & A \end{pmatrix}$$

should all be positive. This condition implies that

$$(X_n^\dagger Y_n^\dagger) \begin{pmatrix} A & B \\ B & A \end{pmatrix} \begin{pmatrix} X_n \\ Y_n \end{pmatrix} = E_n(X_n^\dagger X_n - Y_n^\dagger Y_n) \tag{15}$$

must be real and greater than zero, so E_n must be real. If the attractive part of the interaction is too strong, this condition breaks down, and imaginary eigen-

values, representing unstable modes of vibration, may appear. It can also be shown that, if this condition is satisfied, there is a complete set of eigenvectors of eq. (13). It follows that, for any X and Y,

$$(X^\dagger Y^\dagger)\begin{pmatrix} A & B \\ B & A \end{pmatrix}\begin{pmatrix} X \\ Y \end{pmatrix} \Big/ \left|(X^\dagger - Y^\dagger)\begin{pmatrix} X \\ Y \end{pmatrix}\right| \tag{15.1}$$

gives an upper bound for the magnitude of the lowest eigenvalue of eq. (13) [21]). This variational principle shows that we overestimate the excitation energy of the lowest excited state when, as in section 4, we consider only a restricted number of configurations.

Energy-weighted sum rules are particularly simple in this theory. We denote by Q the column vector whose components are matrix elements $Q_{ii'}$ of an operator, such as the octupole operator, between the occupied state i' and the unoccupied state i. The matrix element of this operator between the ground state of the system and the excited state of energy E_n in our theory is

$$\langle \Psi_n | Q | \Psi_0 \rangle = (X_n^\dagger Y_n^\dagger)\begin{pmatrix} Q \\ Q \end{pmatrix}. \tag{16}$$

The energy-weighted sum of the squares of these matrix elements is

$$\sum_n{}' \left| (X_n^\dagger Y_n^\dagger)\begin{pmatrix} Q \\ Q \end{pmatrix}\right|^2 E_n = \sum_n{}' (Q^\dagger Q^\dagger)\begin{pmatrix} A & B \\ B & A \end{pmatrix}\begin{pmatrix} X_n \\ -Y_n \end{pmatrix}(X_n^\dagger Y_n^\dagger)\begin{pmatrix} Q \\ Q \end{pmatrix}, \tag{16.1}$$

where the sum is taken over all positive energy eigenvectors. From the completeness of the set of eigenvectors, and from the symmetry between positive and negative energy eigenvectors, we can show that this equation gives

$$\sum_n{}' \left| (X_n^\dagger Y_n^\dagger)\begin{pmatrix} Q \\ Q \end{pmatrix}\right|^2 E_n = \tfrac{1}{2}(Q^\dagger - Q^\dagger)\begin{pmatrix} A & B \\ B & A \end{pmatrix}\begin{pmatrix} Q \\ Q \end{pmatrix} = Q^\dagger (A-B) Q. \tag{16.2}$$

If eq. (8.2) is satisfied, the interaction drops out of this expression, and the sum is the same as it would be in the unperturbed system. This is the case in either our schematic model or in our later calculations with zero-range forces. Consequently, neither of these is adequate to describe the enhancement of the energy-weighted sum rule through effects from exchange forces in the $T = 1$ case. However, it can be shown [21]) that this enhancement is contained in the formalism if one employs forces of finite range and demands self-consistency.

6. Calculations in *j*—*j* Coupling

The most important results of this work are calculations in which some ground state correlations have been included as described in the preceding sections. For completeness, however, we begin by reporting results of calculations in which such effects are not included. The procedure, in this case, is precisely the

same as that of the earlier paper on the dipole states [8]), and again the work is confined to the closed shell nuclei O^{16} and Ca^{40}. As before [8]), we indicate the effect of a realistic exchange mixture by calculating the matrices for both an ordinary force and a Soper Mixture.

If only 1 $\hbar\omega$ transitions are considered, the three configurations $p_{\frac{1}{2}}^{-1}d_{\frac{5}{2}}$, $p_{\frac{3}{2}}^{-1}d_{\frac{5}{2}}$ and $p_{\frac{3}{2}}^{-1}d_{\frac{3}{2}}$ give rise to an octupole state in O^{16}. The eigenvalues, together with the squares of the perturbed octupole moments (denoted by $\mathscr{D}$) are given in table 1a. As expected, most of the octupole strength is resident in

TABLE 1

Calculated energies and octupole strengths in O^{16}

	Ordinary force			Soper mixture		
	E (MeV)	$\mathscr{D}^2$ %	$E\mathscr{D}^2$ %	E (MeV)	$\mathscr{D}^2$ %	$E\mathscr{D}^2$ %
a. Without ground-state correlations	7.7	80		8.8	67	
	16.0	11		16.2	19	
	22.9	9		21.6	14	
		100%			100%	
b. With ground-state correlations	3.6	367	74	7.7	134	58
	18.8	13	12	16.0	24	22
	22.6	11	14	21.5	16	20
		391%	100%		174%	100%

$\mathscr{D}$ is proportional to the octupole transition amplitude $\langle \mathrm{ph}|Q_3|0\rangle$, where $Q_3 = r^3 Y_3^0(\theta, \varphi)$. The %'s are taken with respect to $\Sigma_{ii'} D_{ii'}^2$ and $\Sigma_{ii'} \varepsilon_{ii'} D_{ii'}^2$, where the sum is over unperturbed wave functions, and $\varepsilon_{ii'} = \varepsilon_i - \varepsilon_{i'}$, the unperturbed energy. All transitions considered are between adjacent shells, and the sums go only over such configurations.

the lowest level, the energy of which could be fitted to the experimental value simply by adjusting the interaction strength V_0. However, we thought it more useful to retain the value of V_0 which fitted the O^{16} dipole states [8]). The eigenvector obtained for this state agreed almost exactly with that of Elliott and Flowers, and consequently leads to their estimate of the lifetime. Using a reasonable value for the range parameter b of the wavefunctions, they obtained a lifetime three times too long. We shall show how this situation is improved by the introduction of ground state correlation effects.

For Ca^{40}, the results, in table 2a, are very similar. In this case, nine octupole

states can be formed from the configurations $d^{-1}f$, $d^{-1}2p$, and $2s^{-1}f$. Although the value of b^3 was increased in the ratio 40/16, V_0 was unaltered †.

Correlation effects were included for both nuclei by solving the matrix equation (13) numerically. In zero-range, the calculation of the matrix B is

TABLE 2

Calculated energies and octupole strengths in Ca^{40}

	Ordinary force			Soper mixture		
	E (MeV)	$\mathscr{D}^2$ %	$E\mathscr{D}^2$ %	E(MeV)	$\mathscr{D}^2$ %	$E\mathscr{D}^2$ %
a. Without ground-state correlations	6.0	62		6.3	43	
	8.7	13		9.2	7	
	9.8	15		10.2	36	
	11.1	0		11.3	0	
	12.6	2		12.6	2	
	14.2	2		14.8	4	
	16.5	3		16.1	7	
	16.6	1		16.5	0	
	17.9	2		17.2	1	
		100%			100%	
b. With ground-state correlations	1.9	512	72	5.4	109	45
	8.5	8	5	9.0	13	9
	9.5	16	11	9.9	39	29
	11.0	0	0	11.3	0	0
	12.6	2	2	12.6	2	2
	14.1	3	2	14.1	5	5
	16.5	4	5	16.1	8	9
	16.6	0	0	16.5	0	0
	17.9	2	3	17.2	1	1
		547%	100%		177%	100%

See table 1 for definition of the symbols.

rather simple. The phases of the unperturbed states can be chosen so that all the octupole moments $\mathscr{D}$ are positive and invariant under the interchange

$$i \to i', \quad i' \to i.$$

That is to say

$$D_{ii'} = D_{i'i}.$$

It follows then, that the part of the matrix element corresponding to zero total spin $S = 0$, is invariant under the interchange of particle and hole quantum numbers. A simple argument shows that under these circumstances the $S = 1$

† After these calculations were completed, it was pointed out to us by J. Blomquist that one should take the r.m.s. radius $(\overline{r^2})^{\frac{1}{2}}$ to be proportional to $A^{\frac{1}{3}}$ and not b. This would involve a substantial increase in V_0 for Ca^{40}, but would not change our results qualitatively.

part always changes sign. Now the $S = 1$ terms in the interaction can arise only as a result of spin-orbit forces, so that if the latter are negelected, the relations (8.2) must be satisfied (in zero-range approximation). In the present calculations, however, spin-orbit forces are included, and therefore B differs from the interaction part of A. Two important features of the results for O^{16} in table 1b, and for Ca^{40} in table 2b, are that for both types of force, the energies of the lowest states are lower than the corresponding ones in 1a and 2a, and that these lowest states have become very sensitive to the exchange mixture. It can be shown quite generally that the lowest eigenvalue must be lower than the lowest eigenvalue of the matrix A.

We now turn to a discussion of sum rules. Lane and Pendlebury [6]) have considered the fractions of certain sum rules exhausted by the lowest octupole states in various nuclei, including O^{16} and Ca^{40}. First they used the sum of squares of matrix elements

$$\sum_{ii'} D_{ii'}^2$$

and find, for the lowest 3^- state in O^{16} that

$$\mathscr{D}^2 \approx 0.64 \sum_{ii'} D_{ii'}^2. \tag{17}$$

Now, the total sum contains contributions from both $1\hbar\omega$ and $3\hbar\omega$ configurations, so that

$$\sum_{ii'} D_{ii'}^2 = \sum_{ii'} D_{ii'}^{(1)^2} + \sum D_{ii'}^{(3)^2},$$

where the upper suffices "1" and "3" refer to $1\hbar\omega$ and $3\hbar\omega$, respectively. It turns out for O^{16} that

$$\sum_{ii'} D_{ii'}^{(3)^2} = \tfrac{7}{3} \sum_{ii'} D_{ii'}^{(1)^2}.$$

Hence, from (17)

$$\mathscr{D}^2 = 0.64(1 + \tfrac{7}{3}) \sum_{ii'} D_{ii'}^{(1)^2} = 2.13 \sum_{ii'} D_{ii'}^{(1)^2} \tag{18}$$

Relation (18) is the more convenient form to use here because we have not explicitly included any $3\hbar\omega$ effects in our calculations. If the results of table 1b (for the Soper Mixture) are recalculated with a force strength V_0 which fits the lowest energy to the experimental value of 6.13 MeV †, then $\mathscr{D}^2$ rises from 134 % to 184 %. This latter figure is to be compared with the 213 % in (18).

If one does not simply renormalize, but tries to make an estimate, of what effect the $3\hbar\omega$ transitions would have on $\mathscr{D}^2$, one finds that they would give

† This "renormalization" may be thought of as taking some account of the $3\hbar\omega$ transitions, inclusion of which would push the level down. This is in the spirit of using an effective charge for γ-ray transitions.

rise to an enhancement of about 40 %, leading to

$$\mathscr{D}^2 = 1.34 \times 1.40 \times \sum_{ii'} D_{ii'}^{(1)2} = 1.88 \sum_{ii'} D_{ii'}^{(1)2},$$

in agreement with results from renormalizing the interaction.

It is interesting to consider the reason underlying our large $\mathscr{D}^2$. In the normal shell model, in which ground state correlations are not included, the orthonormality of the eigenvectors implies that,

$$\sum_p \mathscr{D}_p^2 = \sum_{ii'} D_{ii'}^{(1)2}, \tag{19}$$

where the index p goes over all perturbed states. From this it is clear that, for the lowest level,

$$\mathscr{D}^2 \leqq \sum_{ii'} D_{ii'}^{(1)2},$$

making the result (18) unobtainable. Of course, the situation would be improved by including $3\hbar\omega$ transitions, but it turns out that these do not mix in sufficiently strongly. It is, in any case, clear that there is no possibility within the framework of the shell model with $1\hbar\omega$ transitions of obtaining a correct value for the matrix element, and hence of the lifetime of the low 3^- resonance in O^{16}.

When ground state correlations are introduced, (19) is no longer satisfied, and indeed there is no theoretical limit on the left hand side; it will become infinite as the lowest eigenvalue drops to zero. In this case, provided only that zero range forces are used (and, in fact, for finite-range forces if self-consistency is enforced [21])),

$$\sum_p E_p \mathscr{D}_p^2 = \sum_{ii'} E_{ii'} D_{ii'}^{(1)2},$$

E_D and $E_{ii'}$ being the perturbed and unperturbed eigenvalues respectively. In the present case, we obtained with $E = 6.13$, the result

$$E\mathscr{D}^2 = 0.65 \sum_{ii'} E_{ii'} D_{ii'}^{(1)2}. \tag{20}$$

Now ideally, the total energy-weighted sum would be given by

$$\sum_{ii'} E_{ii'} D_{ii'}^2 = 8 \sum_{ii'} E_{ii'} D_{ii'}^{(1)2},$$

and (20) would become

$$E\mathscr{D}^2 = \frac{0.65}{8} \sum_{ii'} E_{ii'} D_{ii'}^2 = 0.08 \sum_{ii'} E_{ii'} D_{ii'}^2. \tag{21}$$

Increasing this by 40 % as before, we would obtain

$$E\mathscr{D}^2 \approx 0.11 \sum_{ii'} E_{ii'} D_{ii'}^2,$$

which, bearing in mind the uncertainties in this procedure, agrees quite well with the estimate of 0.18 of this sum rule given by Lane and Pendlebury [6]).

7. Summary

In this and a preceding paper [8]), the origin of vibrational states through the mixing of shell-model configurations by the particle-hole force has been discussed. The calculations carried out in these papers were only rough ones, and, in some cases, were inconsistent. For example, the enhancement of the energy-weighted sum rule obtained in [8]) resulted from the neglect of ground state correlations, as noted at the end of section 5. However, one can show [21]) that the introduction of finite range exchange forces works in the opposite direction, so that using our formalism, the energy-weighted sum rule comes out correct to first order in the amount of exchange force. Therefore, the effects of introducing forces of finite range and ground-state correlations seem to work against each other, and leaving both out probably gives better results than leaving either one out singly. This is, of course, no convincing excuse for not making better calculations, and ones with inclusion of both of these effects are now in progress. We note that the Elliott and Flowers calculation [10]) cannot be relied upon to give good results for the energy-weighted dipole sum rule, since it neglects ground-state correlations.

The $T = 1$ dipole and $T = 0$ octupole states are probably the vibrations of spherical nuclei easiest to see experimentally. However, our development points out the richness of possibility of other vibrational states, not yet observed. For example, a $T=1$ octupole state should exist somewhere below the $T = 1$ dipole state in energy. Here, again, the octupole strength will be split between two states because of the effect of spin. Calculations by E. Sanderson, carried out with zero-range forces as in [8]), predict energies of 18.5 and 25 MeV for these states in O^{16}. Another interesting possibility is the spin-flip $T = 1$ monopole state, suggested by Ben Mottelson and others. The simplest example of this would seem to be the 15 MeV state in Carbon, which consists of only one single-particle excitation. In heavier nuclei, a number of single-particle excitations will enter in. Another possibility is a giant $T = 1$, $M2$ resonance, which would be easily excited in inelastic particle scattering. It can be seen that a large number of possibilities exist, and with improved experimental techniques more states should be seen.

In conclusion, we should like to thank the many people with whom we have had pleasant discussions, including L. Castillejo, Ben Mottelson and T. H. R. Skyrme. We should also like to acknowledge receiving a preprint on work very closely related to the above by M. Barranger, who treats, in addition, quadrupole vibrations of partly-filled shells. Most of this work was carried out when

the first author (G. E. B.) was at the University of Birmingham, and we should like to thank Prof. R. E. Peierls for much encouragement and many interesting conversations.

References

1) B. L. Cohen, Phys. Rev. **105** (1957) 1549;
B. L. Cohen and A. G. Rubin, Phys. Rev. **111** (1958) 1568
2) M. Crut, D. R. Sweetman and N. S. Wall, Nuclear Physics **17** (1960) 655
3) R. H. Helm, Phys. Rev. **104** (1956) 1466
4) Fulbright, Lassen and Poulsen, Mat. Fys. Medd. Dan. Vid. Selsk. **31**, No. 10 (1959);
J. L. Yntema and B. Zeichman, Phys. Rev. **114** (1959) 815
5) McDaniels, Blair, Chen and Farwell, Nucler Physics **17** (1960) 614
6) A. M. Lane and E. D. Pendlebury, Nuclear Physics **15** (1960) 39
7) G. E. Brown and M. Bolsterli, Phys. Rev. Letters **3** (1959) 472
8) Brown, Castillejo and Evans, Nuclear Physics **22** (1960) 1
9) G. E. Brown and D. J. Thouless, Physica (to be published)
10) J. P. Elliott and B. H. Flowers, Proc. Roy. Soc. A **242** (1959) 57
11) Proc. Rehovoth Conf. on Nuclear Structure (North-Holland Publishing Co., Amsterdam 1958);
B. R. Mottelson, Varenna Lectures, 1960
12) Devons, Manning and Bunbury, Proc. Phys. Soc. A **68** (1955) 18
13) Sawada, Brueckner, Fukuda and Brout, Phys. Rev. **108** (1957) 507
14) R. A. Ferrell and J. J. Quinn, Phys. Rev. **108** (1957) 570
15) D. Bohm and D. Pines, Phys. Rev. **92** (1953) 609
16) R. A. Ferrell, Phys. Rev. **107** (1957) 1631
17) S. Fallieros, Thesis, University of Maryland, 1959
18) M. Gell-Mann and F. Low, Phys. Rev. **84** (1951) 350
19) A. Bohr and B. R. Mottelson, Mat. Fys. Medd. Dan. Vid. Selsk. **27**, No. 16 (1953)
20) D. R. Inglis, Phys. Rev. **97** (1955) 701
21) D. J. Thouless, Nuclear Physics **22** (1961) 78

1.D.2 *Nuclear Physics* **24** (1961) 18—27; © *North-Holland Publishing Co., Amsterdam*
Not to be reproduced by photoprint or microfilm without written permission from the publisher

A ROTATIONAL MODEL FOR Fe^{57}

R. D. LAWSON and M. H. MACFARLANE †
Argonne National Laboratory, Argonne, Illinois ††

Received 2 January 1961

Abstract: A model of Fe^{57} is examined, in which the odd neutron is considered to move in the field of an axially symmetric rotor. The effect of band mixing is included. For a prolate deformation with δ from 0.15 to 0.2, reasonable agreement with experiment is obtained for many of the properties of the states below 1 MeV in Fe^{57}. However, properties which depend on the intrinsic wave function of the $\frac{1}{2}^-$ ground state are in serious disagreement with experiment. The predictions of the model are insensitive to reasonable changes in the moment of inertia of the rotor and in the parameters (other than the deformation) characterizing the shape of the Nilsson potential.

1. Introduction

Although recent experimental studies have determined many of the properties of low-lying levels in Fe^{57} with considerable accuracy, interpretation of these data has been mainly qualitative. A conventional shell-model calculation would at the very least demand explicit consideration of three neutrons and two proton holes – a calculation which is prohibitively tedious. Similar difficulties, encountered in the (ds) shell, have been avoided by the use of rotational models [1–4]). The qualitative success of such calculations prompted us to examine an extreme single-particle rotational model of Fe^{57}.

The underlying physical picture is that of a single nucleon moving in the deformed field of an axially symmetric rotor. The parameters of this model are the moment of inertia of the rotor and the quantities characterizing the potential well. We have used a potential of the type discussed by Nilsson [5]) – a deformed harmonic oscillator with spin-orbit coupling. Our calculation differs from earlier studies of the rotational properties of light nuclei in that we do not allow ourselves the freedom to fix the positions of the unperturbed bands to give optimum agreement with experiment. Instead, we fix the parameters of the well and the rotor, and thereby determine the Hamiltonian of the model completely. All subsequent comparisons with experiment are made in terms of the eigenvalues and eigenfunctions of this Hamiltonian. The effects of band mixing introduced by the term $(\hbar^2/2\mathscr{I})\mathbf{I}\cdot\mathbf{j}$ in the Hamiltonian are, of course, very important since $\hbar^2/2\mathscr{I}$ is now more than ten times as great as in the

† Now at Department of Physics, University of Rochester, Rochester, New York.
†† Work performed under the auspices of the U. S. Atomic Energy Commission.

rare-earth region. We find in fact that the only significant parameter of our calculation is the deformation of the well; reasonable variations of the other parameters produce remarkably little change in the predictions of the model. Earlier calculations, wherein the positions of the bands were arbitrarily adjusted, suggest considerable sensitivity to the parameters of the model. This sensitivity is greatly reduced when the model is applied consistently.

Satisfactory agreement is obtained with the observed spectrum and with various of the static and dynamic properties of the levels of Fe^{57} below 1 MeV. However, quantities that depend on the intrinsic wave function of the $\frac{1}{2}^-$ ground state are in marked disagreement with experiment.

2. Calculation and Results

The Hamiltonian of our model is [6])

$$\begin{aligned} H &= \frac{\hbar^2}{2\mathscr{I}}\,[(\mathbf{I}-\mathbf{j})^2-(I_z-j_z)^2]+H_{\text{intrinsic}} \\ &= \frac{\hbar^2}{2\mathscr{I}}\,[I^2+j^2-2I_z{}^2]+\frac{\hbar^2}{2\mathscr{I}}\,(I_+j_-+I_-j_+)+H_{\text{intrinsic}}\,, \end{aligned} \tag{1}$$

where $\mathscr{I}$ is the moment of inertia of the rotor, $\mathbf{I}-\mathbf{j}$ the angular momentum of the core. The Nilsson Hamiltonian, $H_{\text{intrinsic}}$, has four adjustable parameters: the oscillator strength $\hbar\omega_0$, the deformation δ (or η) (ref. [6])), and the strengths of the added $\mathbf{l}\cdot\mathbf{s}$ and l^2 terms. The energy levels of this Hamiltonian for the (1f, 2p) shell and Nilsson's choice of parameters are shown in fig. 1.

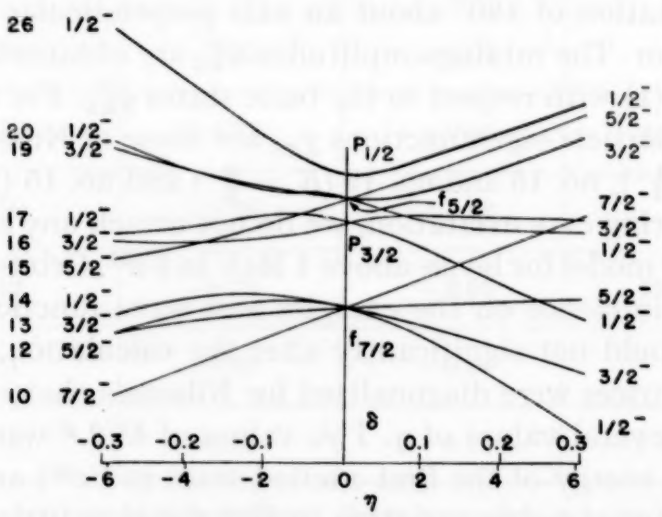

Fig. 1. Energy levels in the (1f, 2p) shell as a function of the deformation η. This diagram is part of fig. 5 in ref. [5]).

In a single-particle rotational model, all nucleons but the last are placed in pairs in the lowest available Nilsson orbits. The possibility of promoting such

pairs to unfilled levels is neglected, which is sensible only when there is a sizeable energy separation between the last core orbit and the first odd-particle orbit. In other words, it is not meaningful to apply a single-particle rotational model close to a crossing in the Nilsson level diagram. In the case of Fe^{57}, it will be seen from fig. 1 that for $-2 < \eta < 4$ no such crossings occur. Thus we may reasonably hope that our single-particle calculation will provide a good first approximation to a many-particle calculation with residual forces.

Difficulties with crossings in the Nilsson level diagram may already have been encountered in the (ds) shell. It is believed that beyond Si^{28} we are dealing with negative deformations [7]). In Si^{29} we then have a large energy separation between the last core orbit (Nilsson level no. 7) and the first single-particle orbits (no. 8 and no. 9). Accordingly one would expect, and indeed finds †, that the positive-parity levels in Si^{29} are well described by the model under consideration. On the other hand, in S^{33} the last core orbit can be either no. 8 or no. 9, which lie very close in energy and actually intersect for deformations in the region of interest. The expectations of the above "crossing" arguments are again borne out in practice [8]); the single-particle rotational model cannot give adequate agreement with experiment for S^{33}.

The wave function of the rth level of spin I in Fe^{57} is [9])

$$\Psi_M^{Ir} = \sum_{K,S} A_{KS}^{Ir} \phi_{MKS}^{Ir} = \sum_{K,S} A_{KS}^{Ir} \left\{ \sqrt{\frac{(2I+1)}{16\pi^2}} \, (1+R_1) D_{MK}^{I} \chi_{KS} \right\}, \tag{2}$$

where S distinguishes different intrinsic states of the same K and the operator R_1 produces a rotation of 180° about an axis perpendicular to the symmetry (z) axis of the rotor. The mixing amplitudes A_{KS}^{Ir} are obtained by diagonalizing the Hamiltonian (1) with respect to the basic states ϕ_{KS}^{Ir}. For positive deformations, the single-particle eigenfunctions χ_{KS} are those of Nilsson's orbits no. 20 and no. 26 ($K = \frac{1}{2}^-$), no. 16 and no. 19 ($K = \frac{3}{2}^-$) and no. 15 ($K = \frac{5}{2}^-$) (ref. [5])). Since we are ignoring core excitation, we do not attach any significance to the predictions of our model for levels above 1 MeV in Fe^{57}. Orbits no. 15 and no. 26 have only slight influence on the energies and wave functions below 1 MeV; their omission would not significantly alter the calculation.

The energy matrices were diagonalized for Nilsson's choice of single-particle parameters and several values of η. Two values of $\hbar^2/2\mathscr{I}$ were used: 0.14 MeV ($\frac{1}{6}$ the excitation energy of the first excited state in Fe^{56}) and 0.11 MeV. The fact that this rather sizeable variation in $\hbar^2/2\mathscr{I}$ makes little difference to the predictions of the model indicates that the precise value chosen for the moment of inertia is not of critical importance to the calculation. The resulting spectra are shown in fig. 2.

† See pp. 665–666 of ref. [17]).

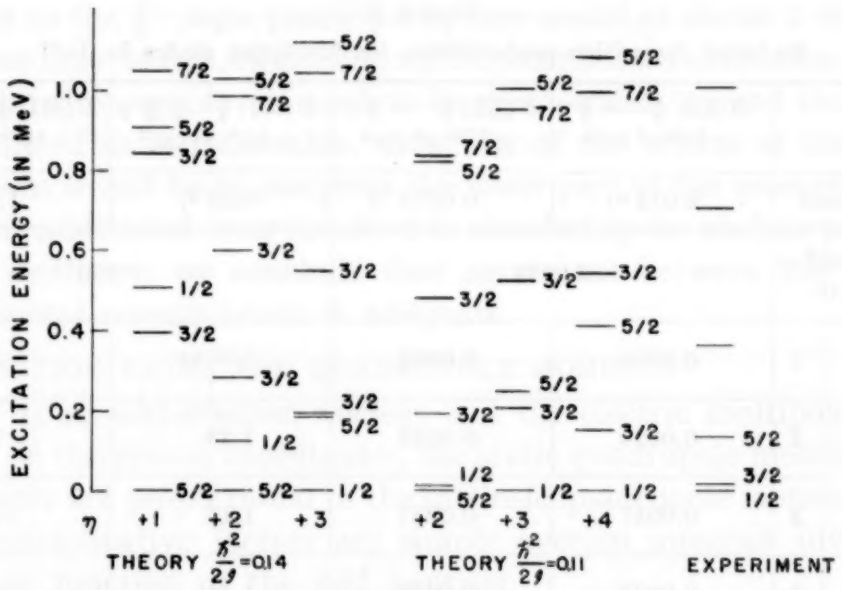

Fig. 2. Spectrum of Fe^{57}. The first three columns show the spectra obtained for positive deformation ($\eta = 1, 2$ and 3) and $\hbar^2/2\mathscr{I} = 0.14$ MeV. The next three columns are the resulting spectra when $\eta = 2, 3$ and 4 with $\hbar^2/2\mathscr{I} = 0.11$ MeV. Column 7 shows the experimental results.

TABLE 1

Static multipole moments and stripping widths of some of the low-lying states in Fe^{57} for various values of the deformation and moment of inertia of the rotor.

η		Magnetic moment of the ground state in n.m.	Magnetic moment of the first excited state in n.m.	Quadrupole moment of the first excited state in barns	$\frac{4\mathscr{S}_{\frac{3}{2}}^*}{2\mathscr{S}_{\frac{1}{2}}+4\mathscr{S}_{\frac{3}{2}}}$	$\mathscr{S}_{\frac{1}{2}}$
Experiment		+0.0903 [a])	−0.153 [b])	negative [13])	≈ 0.6 [11])	≈0.25 [18])
$\frac{\hbar^2}{2\mathscr{I}} = 0.14$ MeV	1	+0.39	−0.42	+0.04	0.51	0.012
	2	+0.58	+0.77	+0.05	450	0.002
	3	+0.70	+0.06	−0.02	3.32	0.002
$\frac{\hbar^2}{2\mathscr{I}} = 0.11$ MeV	2	+0.59	+0.75	+0.05	120	0.005
	3	+0.71	+0.02	−0.04	3.08	0
	4	+0.78	−0.53	−0.12	1.08	0.007

In calculating matrix elements of the magnetic dipole operators, a value of $Z/A = 0.464$ was taken for g_R. The quantity listed in column 5 is a measure of the relative strength of the proton groups to the third excited state $(\frac{3}{2}^-)^*$ and to the ground state doublet in Fe^{56}(d, p)Fe^{57}. $\mathscr{S}_{\frac{1}{2}}$ is the spectroscopic factor for the ground state.

[a]) G. W. Ludwig and H. H. Woodbury, Phys. Rev. **117** (1960) 1286

[b]) S. S. Hanna, J. Heberle, C. Littlejohn, G. J. Perlow, R. S. Preston and D. H. Vincent, Phys. Rev. Letters **4** (1960) 177

TABLE 2

Reduced transition-probabilities for low-lying states in Fe^{57}

η		$B(E2; \frac{5}{2}^- \to \frac{1}{2}^-)$ $\times 10^{48} e^2$ cm^4	$B(E2; \frac{5}{2}^- \to \frac{3}{2}^-)$ $\times 10^{48} e^2$ cm^4	$B(M1; \frac{5}{2}^- \to \frac{3}{2}^-)$ $\times 10^{30} e^2$ cm^2	$B(M1; \frac{3}{2}^- \to \frac{1}{2}^-)$ $\times 10^{30} e^2$ cm^2
Experiment		0.014 [a])	0.0074 [b])	0.23 [a])	1.4 [c])
Weisskopf estimate		0.0013		200	
$\frac{\hbar^2}{2\mathscr{I}} = 0.14$ MeV	1	0.0005	0.0003	0.0044	5.6
	2	0.0020	0.0028	1.23	7.3
	3	0.0047	0.0057	1.17	19.9
$\frac{\hbar^2}{2\mathscr{I}} = 0.11$ MeV	2	0.0023	0.0026	1.41	9.0
	3	0.0054	0.0052	1.22	24.1
	4	0.010	0.0074	0.83	47.8

[a]) A. T. G. Ferguson, M. A. Grace and J. O. Newton, Nuclear Physics **17** (1960) 9

[b]) G. R. Bishop, M. A. Grace, C. E. Johnson, A. C. Knipper, H. R. Lemmer, J. Perez y Jorba and R. G. Scurlock, Phil. Mag. **46** (1955) 951

[c]) H. R. Lemmer, O. J. A. Segaert and M. A. Grace, Proc. Phys. Soc. (London) A **68** (1955) 701

By use of standard techniques [9]), the energy eigenfunctions (2), were then used to calculate various moments and transition rates. The electromagnetic properties of the core enter the calculation through the gyromagnetic ratio g_R and the intrinsic quadrupole moment Q_0. The results are summarized in tables 1 and 2.

3. Comparison with Experiment

3.1. SPECTRUM

In Fe^{57} there are five known levels below 1 MeV (ref. [10])). The spins of the three lowest are well established, whereas that of the 365-keV state is fixed by stripping data [11]) as either $\frac{3}{2}^-$ or $\frac{1}{2}^-$. Nothing is known about the spin or parity of the state at 705 keV. From fig. 2 it is evident that the calculated and observed spectra are in moderate agreement for either value of the moment-of-inertia parameter and $\eta \approx 3$–4. A spin of $\frac{3}{2}^-$ rather than $\frac{1}{2}^-$ is predicted for the third excited state.

The 705-keV level is not observed in stripping † from Fe^{56} and is not prominent in pickup [12]) from Fe^{58}. These characteristics are consistent with its

† We wish to thank Dr. Parry for sending us his results prior to publication.

identification as the $\frac{7}{2}^-$ state predicted by our model at about 1 MeV. On the other hand, we may, in fact, be dealing with a complicated excitation of the core.

Our calculated energy levels tend to be more widely spread than is found experimentally. This is reasonable, since one of the effects of the neglected core excitations would be to compress the lower part of the predicted spectra. In view of the additional error involved in simulating the nuclear potential by a harmonic oscillator, we conclude that agreement between the theoretical and experimental energy levels is adequate.

3.2. E2 TRANSITION RATES AND QUADRUPOLE MOMENTS

Since Fe^{57} is an odd-neutron nucleus and the electric multipole operators depend only on the proton coordinates, the static quadrupole moments and E2 matrix elements are proportional to the intrinsic quadrupole moment Q_0 of the core. The multiplicative factors are simple overlap integrals involving the intrinsic wave function of the odd neutron.

The quadrupole moment of the first excited state is given by [9])

$$Q = Q_0 \sum_{KS} (A^{\frac{3}{2}1}_{KS})^2 \left\{ \frac{3K^2 - I(I+1)}{(I+1)(2I+3)} \right\}_{I=\frac{3}{2}}. \tag{3}$$

For $I = \frac{3}{2}$, the factor in brackets has a value of $+\frac{1}{5}$ when $K = \frac{3}{2}$ and $-\frac{1}{5}$ when $K = \frac{1}{2}$. Thus, although Q_0 is positive, a negative value can be obtained for Q provided that the internal wave function is predominately $K = \frac{1}{2}$. In this way we obtain agreement with the negative sign deduced by Bersohn [13]) for the quadrupole moment of the $\frac{3}{2}^-$ first excited state (See table 1).

For a uniformly charged spheroid, Q_0 is given [14]) † in terms of the deformation parameter δ by

$$Q_0 = \tfrac{4}{5}\, Ze\, R_0^2 \delta (1 + 0.17\delta + \ldots), \tag{4}$$

where R_0, the radius of the charge distribution, is taken in this calculation to be $1.2A^{\frac{1}{3}} \times 10^{-13}$ cm. Using this expression and the eigenfunctions (2), we obtain rather good agreement with the experimental values of $B(\mathrm{E2})$ for the transition from the $\frac{5}{2}^-$ level at 136 keV to the ground and first excited states (see table 2).

Since the matrix elements of the quadrupole operator depend directly on the distortion of the core, this satisfactory description of quadrupole moments and E2 transition rates suggests that a rotational model of Fe^{57} is not unreasonable.

3.3. M1 TRANSITION RATES AND MAGNETIC MOMENTS

The calculated magnetic moment of the first excited $\frac{3}{2}^-$ state is a sensitive function of the deformation. passing through the experimental value for η between 1 and 2 and again between 3 and 4. As we have seen, the larger value of deformation gives reasonable agreement with experiment both for the spectrum and for the electric quadrupole properties of Fe^{57}.

The matrix element of the M1 transition between the second $(\frac{5}{2}^-)$ and first

† See in particular eq. (V12) of ref. [14]) where in $\beta = (\frac{4}{3}\sqrt{\pi/5} \cdot \delta \approx 1.06\,\delta$.

($\frac{3}{2}^-$) excited states of Fe^{57} is overestimated by a factor of two (for $\eta \approx 4$). In rotational-model calculations in the (ds) shell, Paul has obtained about the same quality of agreement between theory and experiment for M1 transitions in F^{17} (see table 1 of ref. [1]), while Paul and Montague find larger discrepancies for M1 transitions in Na^{23} (see table 1 of ref. [4]). In analyzing M1 data in the rare-earth region, the standard procedure has been to treat the intrinsic matrix elements of the magnetic-dipole operator as empirical parameters. The values of these parameters required to fit the M1 transition rates frequently differ markedly from calculated values obtained from Nilsson's wave functions. It is, therefore, rather hard to compare our results with those obtained for M1 transitions in the rare-earth nuclei. Kerman, in his semiempirical analysis [9]) of band mixing in W^{183} (a nucleus similar to Fe^{57} in that it has an odd neutron, a ground-state spin of $\frac{1}{2}^-$, and an equilibrium deformation $\delta \approx 0.2$), obtains agreement to within 50 % for nine M1 matrix elements (see table 4 of ref. [9])), which is rather better than we have done. We conclude that the agreement between theory and experiment for the 122-keV M1 transition in Fe^{57} is marginal.

On the other hand, the calculated values of the ground-state magnetic moment and the M1 transition rate between the first excited state and ground state are quite clearly in disagreement with experiment. The discrepancy in the ground-state magnetic moment is very similar to that found in W^{183} and Os^{187} (see table 7b of ref. [15])). In each case we are dealing with a $\frac{1}{2}^-$ odd-neutron nucleus with a magnetic moment close to 0.1 nuclear magnetons. For such nuclei both the rotational model † and the shell model [16]) (even with configuration mixing) predict magnetic moments very close to the Schmidt value (0.638 nm). This disagreement indicates serious deficiencies in either the magnetic-moment operator or the ground-state nuclear wave function, or both. The fact that agreement with experiment for the 14-keV M1 matrix element is considerably worse than for the 122-keV matrix element suggests that the main trouble lies in the ground-state nuclear wave function.

3.4. STRIPPING AND PICKUP

The reaction $Fe^{56}(d, p)Fe^{57}$ has recently been studied [11]). Strong $l = 1$ transitions are observed to the unresolved ground-state doublet and to the third excited state at 365 keV; the excited state at 136 keV has $l = 3$.

In comparing these experimental data with the predictions of our model, the relevant quantities are the reduced widths θ^2. Since the spin of the target nucleus is zero, θ^2 for the rth level of spin I in Fe^{57} is given by [17]) ††

$$\theta^2(Ir) = \mathscr{S}(I, r)\theta_0{}^2(l),$$

$$\mathscr{S}(I, r) = \frac{2}{(2I+1)} \{\sum_{K,S} A^{Ir}_{KS} c^{I}_{KS}\}^2, \tag{5}$$

† See eq. (26) of ref. [5]).

†† See in particular eq. (III. 203) and p. 611 of ref. [17]).

where $\theta_0^2(l)$ is the appropriate single-particle reduced width and c^I_{KS} is the amplitude of angular momentum I in χ_{KS}.

We do not give quantitative estimates of the relative strength of $l = 1$ and $l = 3$ transitions because too little is known about the single-particle reduced widths. However, the large calculated spectroscopic factor $\mathcal{S}$ of the $\frac{5}{2}^-$ state (> 0.5 for all cases considered) is consistent with the fact that a strong $l = 3$ transition is observed.

In comparing the reduced widths of the two $l = 1$ transitions, only the spectroscopic factors $\mathcal{S}$ need be considered since the single-particle reduced width cancels. From table 1, we see that the calculated value of $[4\mathcal{S}_{\frac{3}{2}}^*/(2\mathcal{S}_{\frac{1}{2}}+4\mathcal{S}_{\frac{3}{2}})]$ for $\eta \approx 4$ is close to 1, in fair agreement with the observed value of 0.6.

The calculated contribution of the ground state to the combined $l = 1$ reduced width of the ground-state doublet is negligible, amounting to less than 1 % of the single-particle reduced width. This is in direct contradiction to the fact that an $l = 1$ transition to the Fe^{56} ground state is seen quite clearly [18]) in Fe^{57}(d, t)Fe^{56}. The strength of the transition in question indicates, very rougly, that the reduced width is about a quarter of the single-particle value. This discrepancy in the ground-state reduced width, involving a factor of between 20 and 30, is further clear indication that the ground-state wave function of our model is seriously defective.

4. Discussion

Within an oscillator shell, the Nilsson potential is characterized by three parameters. For the (1f, 2p) shell we may take these to be the deformation δ and the single-particle level separations in the limit of zero deformation, namely,

$$E(2p_{\frac{1}{2}})-E(2p_{\frac{3}{2}}) = \Delta(p)$$

and

$$E(1f_{\frac{5}{2}})-E(2p_{\frac{3}{2}}) = \Delta(fp).$$

So far we have followed Nilsson's original calculation, taking $\Delta(p) = 1.6$ MeV and $\Delta(fp) = 0.8$ MeV. To test the sensitivity of the model to changes in the parameters characterizing the single-particle potential, we repeated the calculation using $\Delta(p) = 1.5$ MeV, $\Delta(fp) = 0.5$ MeV and $\hbar^2/2\mathcal{I} = 0.14$. The spectra for $\eta = 2$ and $\eta = 3$ were not significantly altered from those shown in fig. 2. Furthermore, the overlap between corresponding eigenvalues (same value of η) from the two sets of single-particle parameters was in each case greater than 99 %. We conclude that the predictions of the model are insensitive to reasonable changes in the single-particle parameters, always remaining within the harmonic-oscillator approximation.

It does not seem possible to obtain agreement with experiment for a single-particle model with negative deformation. For $\eta = -2$, a $\frac{5}{2}$ ground state is

obtained, the next level lying at about 500 keV excitation. At $\eta = -4$ (see fig. 1) we encounter a crossing in the Nilsson diagram involving orbits no. 15 and no. 16 so that, as discussed earlier, an extreme single-particle model cannot be used. Finally, for $\eta = -6$, we obtain a $\frac{3}{2}$ ground state with the lowest $\frac{5}{2}$ state lying about 500 keV too high. Further, the second $\frac{3}{2}$ state is predicted to show no stripping from Fe^{56}, in disagreement with experiment.

Vervier and Bartholomew [19]) have discussed the levels of Fe^{57} in a qualitative fashion on the basis of a rotational model. Assigning $K = \frac{3}{2}$ to the first excited state, they are led by the negative sign of the observed quadrupole moment to select an oblate deformation, $\eta \approx -3$. As mentioned above, orbits no. 15 and no. 16 are then close to an intersection. Although Vervier and Bartholomew consider the promotion of pairs of particles among these levels (and level no. 17 which is close by), they neglect any residual pairing forces. In addition the effects of band mixing, which we have seen to be quite large, are not considered. Since the negative sign of the measured quadrupole moment can be obtained for positive deformation, the above argument for negative deformation is not conclusive.

In principle, the equilibrium deformation of a nucleus can be determined by minimizing the total energy as a function of deformation. Calculations in the (ds) shell [7]) predict a sharp change from prolate to oblate deformations around $A = 26$; such a change seems to be observed, but at $A = 28$–29. Thus we expect a change of sign in the deformation around the middle of the (fp) shell, probably somewhere between Fe and Ni. However, calculations of the type under consideration are not sufficiently reliable to locate it exactly.

The present model might also be expected to be applicable to Ni^{59}, which has the same (odd) number of neutrons as Fe^{57}. However, the ground-state spin of Ni^{59} is $\frac{3}{2}$, which we cannot obtain on the single-particle rotational model without proceeding to rather large negative deformations ($|\eta| \geqq 6$). Since a change of sign of η between Fe^{57} and Ni^{59} would not be unexpected, it is possible that a reasonable description of Ni^{59} could be obtained at $\eta \approx -4$ with a three-body rotational model including residual two-body interactions.

5. Summary and Conclusions

As a model of Fe^{57}, we consider a neutron in the deformed field of an axially symmetric rotor. Full account is taken of the mixing of rotational bands. For prolate shapes corresponding to δ between 0.15 and 0.2, a moderately accurate description is thereby obtained of many of the known properties of levels below 1 MeV in Fe^{57}. Serious discrepancies are, however, encountered for quantities which depend on the intrinsic wave function of the $\frac{1}{2}^-$ ground state.

The predictions of the model are remarkably insensitive to reasonable variations in the moment of inertia of the rotor and in the parameters (other than

the deformation) characterizing the deformed (harmonic-oscillator) potential. This significant fact is obscured if, instead of using the full rotational Hamiltonian, the relative positions of the pure bands are arbitrarily adjusted to fit the observed spectrum.

Since agreement with experiment for Fe^{57} is not fully satisfactory and, moreover, cannot be significantly improved by reasonable adjustments of the parameters of the model, the single-particle rotational picture must be refined. We might consider a many-particle rotational model, including residual two-body forces between the extra-core nucleons. Such a calculation would be similar in spirit and in degree of complication to conventional shell-model studies. Alternatively, we might carry the single-particle approach one step further, replacing the axially symmetric rotor by something better able to describe the Fe^{56} core. One such model is that of a neutron in the field of an asymmetric rotor.

References

1) E. B. Paul, Phil. Mag. **15** (1957) 311
2) G. Rakavy, Nuclear Physics **4** (1957) 375
3) A. E. Litherland, H. McManus, E. B. Paul, D. A. Bromley and H. E. Gove, Can. J. Phys. **36** (1958) 378
4) E. B. Paul and J. H. Montague, Nuclear Physics **8** (1958) 61
5) S. G. Nilsson, Mat. Fys. Medd. Dan. Vid. Selsk. **29**, No. 16 (1955)
6) A. K. Kerman, Mat. Fys. Medd. Dan. Vid. Selsk. **30**, No. 15 (1956)
7) Proc. Intern. Conf. on Nuclear Structure, Kingston, Sept. 1960 (North-Holland Publishing Co., Amsterdam, 1960) p. 441
8) R. Bhatt, to be published
9) A. K. Kerman, in Nuclear Reactions, ed. by P. M. Endt and M. Demeur (North-Holland Publishing Co., Amsterdam, 1959) vol. I, Ch. X)
10) Nuclear Data Sheets
11) A. W. Dalton, G. Parry, H. D. Scott and S. Swierszczewski, to be published
12) B. Zeidman, private communication
13) R. Bershon, Phys. Rev. Letters **4** (1960) 609
14) Alder, Bohr, Huus, Mottelson and Winther, Revs. Mod. Phys. **28**, (1956) 432
15) B. R. Mottelson and S. G. Nilsson, Mat. Fys. Skr. Dan. Vid. Selsk. **1**, No. 8 (1959)
16) H. Noya, A. Arima and H. Horie, Prog. Theor. Phys. (Japan) Supplement **8** (1958) **33**
17) M. H. Macfarlane and J. B. French, Revs. Mod. Phys. **32** (1960) 567
18) B. Zeidman, J. L. Yntema and B. J. Raz, Phys. Rev. **120** (1960) 1723
19) J. F. Vervier and G. A. Bartholomew, Proc. Intern. Conf. on Nuclear Structure, Kingston, Sept. 1960 (North-Holland Publishing Co., Amsterdam, 1960) p. 650

2.A.1:
2.J

Nuclear Physics **24** (1961) 28—35; © *North-Holland Publishing Co., Amsterdam*
Not to be reproduced by photoprint or microfilm without written permission from the publisher

THE $C^{12}(p, pn)C^{11}$ AND $Al^{27}(p, 3pn)Na^{24}$ CROSS-SECTIONS AT 591 MeV

K. GOEBEL, D. HARTING, J. C. KLUYVER †, A. KUSUMEGI ††† and H. SCHULTES
CERN, *Geneva*

Received 29 November 1960

Abstract: The absolute cross-sections of the reactions $C^{12}(p, pn)C^{11}$ and $Al^{27}(p, 3pn)Na^{24}$ were measured by exposing polythene and aluminium targets to the 591 MeV external proton beam of the CERN synchro-cyclotron. The proton flux was measured with a secondary emission chamber, calibrated by a counter telescope technique. The C^{11} and Na^{24} activity, induced in the targets, was determined by conventional counting methods, using calibrated Na^{22} and Na^{24} sources as primary standards. The measured cross-sections are 29.9 ± 1.5 mb and 11.0 ± 0.5 mb for the reactions $C^{12}(p, pn)C^{11}$ and $Al^{27}(p, 3pn)Na^{24}$ respectively.

1. Introduction

The C^{11} and Na^{24} activities, produced by bombarding carbon and aluminium respectively with high energy protons, have been used extensively for flux measurements in high energy beams, because of their convenient half-life, the high cross-section with which they are produced and the ease with which they can be distinguished from the activity of other reaction products. The cross-sections of the reactions $C^{12}(p, pn)C^{11}$ and $Al^{27}(p, p3n)Na^{24}$ have accordingly been measured in a number of laboratories [1, 2]) for energies ranging from threshold ud to 6 GeV for $C^{12}(p, pn)C^{11}$ and up to 3 GeV for $Al^{27}(p, 3pn)Na^{24}$.

The whole body of this work rests, however, on a comparatively small number of absolute cross-section measurements, as in many laboratories only the ratio of the cross-sections of the two reactions or the relative excitation function of one of them was measured. In the region between 500 MeV and 2 GeV incident proton energy in particular, only one series of measurements of the absolute cross-section of $C^{12}(p, pn)C^{11}$ has been reported [3]), whereas for the $Al^{27}(p, 3pn)Na^{24}$ cross-section, no absolute measurements have been made. This is especially unfortunate as the very low value of 25.5 ± 3.0 mb found by Burcham *et al.* [3]) for $C^{12}(p, pn)C^{11}$ at 650 MeV incident proton energy, which has been tentatively interpreted as a possible deviation from the otherwise energy independent behaviour of this cross-section at high energies, does not agree with the value of 31.0 ± 1.7 mb found at 660 MeV by Prokoshkin and Tiapkin [4]) via an indirect method. It seemed therefore worthwhile to determine the abso-

† Now at the University of Amsterdam, Amsterdam, Netherlands.
†† Now at the University of Kyoto, Kyoto, Japan.

lute value of both cross-sections at the energy of the external proton beam of the CERN sychro-cylotron (591 MeV) to provide one more reference point for the relative cross-section measurements in this energy region.

2. Experimental Method

Targets of either 0.3 g · cm^{-2} polythene plate or 10 mg · cm^{-2} aluminium foil were exposed to the external proton beam of the CERN synchro-cyclotron. The general lay-out is shown in fig. 1. After having been extracted by the regenerative method, the proton beam passes through a strong-focusing lens pair and is deflected by a bending magnet into a tube through the 560 cm thick heavy concrete shielding wall. By the combined focusing effect of the

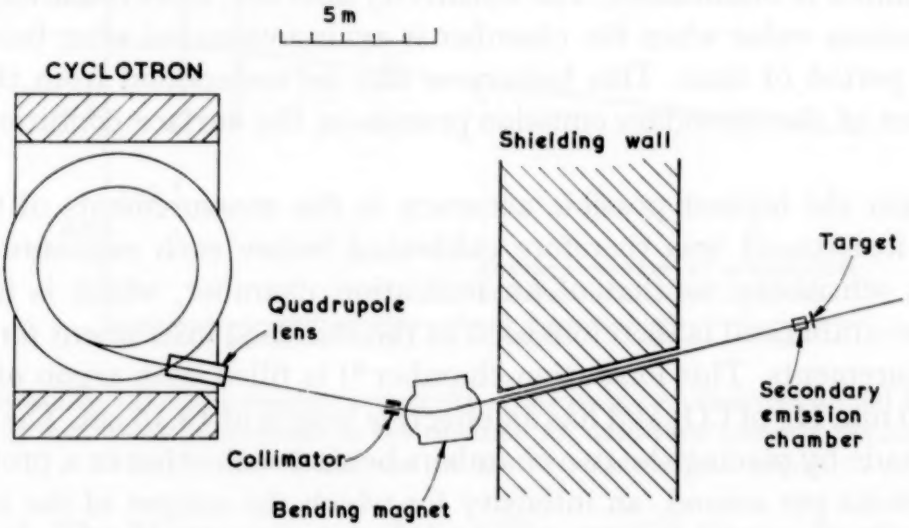

Fig. 1. Diagram of the proton beam layout.

lenses and the bending magnet, a beam spot of $4 \times 3\,cm^2$, containing 95 % of the total flux, is produced in the experimental room, 3 meters beyond the shielding wall. The beam travels through vacuum all the way to avoid contamination of the beam by neutrons or by protons of lower energy.

A secondary emission chamber [5]) was placed in the beam near this focus to measure the proton flux through the targets, which were mounted on the back of the chamber. The absolute number of C^{11} atoms produced during the exposure of the polythene targets was determined by counting the gamma-rays, produced by annihilation of the decay positons stopped in the target, with a 2.5 cm NaI scintillation gamma-ray spectrometer. The polythene plate was replaced at regular intervals by a calibrated Na^{22} source, which is also a positon emitter. From the ratio of the counting rates from the polythene and the Na^{22} source, the number of C^{11} atoms that was originally produced can be calculated.

The number of Na^{24} nuclei produced in the aluminium targets was determined by absolute β counting with Geiger-Müller counters. The absolute efficiency of these counters was measured with Na^{24} sources prepared from

standard solutions. The results were checked by measuring the activity of some suitable target samples directly with the β—γ coincidence technique.

3. Calibration of the Secondary Emission Chamber

To avoid background problems in the counting of the resultant activities, the exposures were made at a high proton beam flux, usually between 10^{10} and 10^{11} protons per second. The 20-plate secondary emission chamber [6]), that was used for measuring this flux, is a very convenient beam monitor, as it presents little material to the beam and has a strictly linear response even at high beam intensities. The sensitivity is constant within 2 % as long as the vacuum in the chamber is maintained. The sensitivity does not, however, always return to the previous value when the chamber is again evacuated after being out of use for a period of time. This behaviour can be understood from the strong dependence of the secondary emission process on the surface conditions of the foils.

To obtain the highest possible accuracy in the measurements of the beam flux, the instrument was therefore calibrated before each exposure by comparing its sensitivity to that of an ionization chamber, which is inherently much more stable and is therefore used as the standard instrument for all beam flux measurements. This ionization chamber [6]) is filled with argon of 638 mm Hg and 10 mm Hg of CO_2 and has an effective length of 13.15 cm. The comparison was made by placing the two chambers behind each other in a proton beam of 10^8 protons per second, an intensity for which the output of the ionization chamber was shown to be still linear with the beam flux. The ratio of the output currents of the two chambers, measured with two current integrators, is then also the ratio of their multiplication factors for 591 MeV protons. A typical value for this ratio is 2500.

The ionization chamber was calibrated once and for all by placing it in a beam of such low intensity, between 10^2 and 10^3 protons per second, that the number of protons in the beam could be counted with a counter telescope. Dead-time losses in the counting system could be corrected for by repeating the measurement at several beam intensities. These losses were not negligible even at these low beam intensities because of the unfavourable time structure of the proton beam, 55 bursts per second of 50 μs each. The output current of the ionization chamber was measured with the same current integrator that is also used at high beam intensities. This integrator [6]) was developed from a circuit of Lewis and Collinge [7]) and has an accuracy of better than 1 % over its whole range from 10^{-6} to 10^{-12} A. From these measurements, one series of which is shown in fig. 2, it was found that 10^{-9} coulomb of collected charge corresponds to $(4.86 \pm 0.10) \times 10^6$ protons of 591 MeV passing through the chamber. The multiplication factor of the ionization chamber is thus 1290 ± 25. The stability

of the ionization chamber was checked regularly by measuring its output when a Co^{60} source is placed in a standard position. It is better than 0.5 % over a period of more than a year.

The linearity of the secondary emission chamber was checked over a range of beam intensities from 10^9 to 10^{11} protons per second by polythene activation measurements. It is actually from these measurements that the $C^{12}(p, pn)C^{11}$ cross-section has been determined.

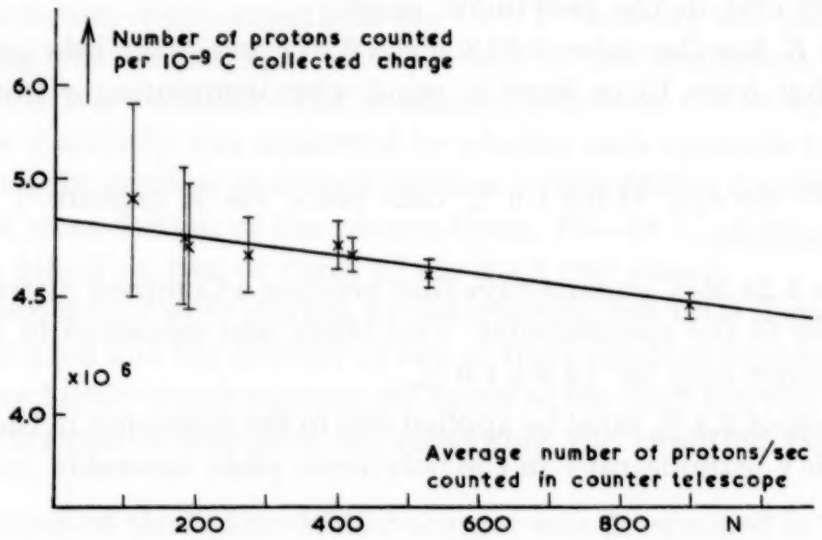

Fig. 2. A measurement of the absolute sensitivity of the ionization chamber for 591 MeV protons. The straight line, which corresponds to the equation for dead-time losses in the scaler counting the protons, is the best fit to the measurement points.

4. The Measurement of the $C^{12}(p, pn)C^{11}$ Cross-Section

The dimensions of the polythene targets were $18 \times 12 \times 0.3$ cm^3. Irradiation times varied, according to the proton beam flux, between 5 and 20 minutes for the six measurements that were made. After irradiation, the polythene plate was covered by a similar plate to stop all the decay positons, and the annihilation gamma-rays were counted with a 2.5 cm NaI crystal and photomultiplier placed 50 cm from the target assembly. The counter was followed by a conventional single-channel pulse-height analyser, adjusted such that the total-energy peak of the 0.51 MeV annihilation radiation was covered by the window. Every three minutes the polythene plate was replaced by an 80 μc Na^{22} source, calibrated to an accuracy of 2 % at the isotope division of AERE (Harwell) and these measurements were continued for three 20.5 min half-lives of the C^{11} activity. From the ratio of the counting rates due to the polythene and to the Na^{22} source, the cross-section σ of the reaction $C^{12}(p, pn)C^{11}$ can be calculated by means of the equation

$$\sigma = K \frac{N_c(t)}{N_{Na}} \frac{1}{NN_p} \frac{1}{e^{-\lambda t}(1-e^{-\lambda T})} A_{Na} \frac{\lambda\tau}{1-e^{-\lambda\tau}},$$

in which (the unit of time is 1 min) $N_c(t)$ is the number of counts due to the polythene activity, registered in a time interval τ, starting at the time t after the end of the exposure, N_{Na} the number of counts from the Na^{22} source in the same time interval τ, T the duration of the irradiation, λ the decay constant of C^{11}, 3.38×10^{-2} min^{-1}, A_{Na} the activity of the Na^{22} source at the time of the measurement in disintegrations per minute, N_p the beam flux in protons per minute, if necessary corrected for intensity fluctuations, and N the number of C^{12} atoms per cm^2 in the polythene plate.
The constant K has the value $0.89/0.854\times0.977$ and takes into account three corrections that have to be kept in mind when computing σ from the ratio $N_c(t)/N_{Na}$:

1) of the Na^{22} decays, 11.0 ± 1.0 % take place via K capture [8]) and do not produce positons.
2) Na^{22} emits 1.28 MeV gamma-rays that produce a Compton distribution over the window of the spectrometer. This effect was measured to increase the Na^{22} counting rate by 14.6 ± 1.0 %.
3) A correction of 2.3 % must be applied due to the difference in the absorption of 0.51 MeV gamma-rays in the polythene plate assembly and the Na^{22} container.

Inserting the results of the measurements into the equation for σ, the following values are obtained:

Sample No.	Calculated cross-section σ (mb)	Average proton beam intensity during irradiation ($\times10^{10}$p/sec)
1	29.1 ± 1.6	10
2	29.3 ± 1.6	6
3	30.1 ± 1.6	3
4	31.4 ± 1.6	3
5	29.6 ± 1.6	0.7
6	29.9 ± 1.6	0.2

The cross-section σ of the reaction C^{12}(p, pn)C^{11} for 591 MeV incident protons, found as the mean value of these figures, is

$$\sigma = (29.9\pm1.5)\times10^{-27}\ \text{cm}^2.$$

The error assigned to σ in each of the separate measurements is obtained by adding in quadrature the errors in the factors of the equation for σ. As this error is almost exclusively due to uncertainties in the calculation of σ from the measured numbers, rather than to statistics, the error assigned to the mean value of σ is almost the same as that of the separate measurements.

5. The Measurement of the $Al^{27}(p, 3pn)Na^{24}$ Cross-Section

As the Na^{24} activity, produced in aluminium by the incident protons, was measured by absolute β counting, thin targets of 10 mg cm^{-2} thickness and 15 cm diameter were used. As the half-life of Na^{24}(15h) is also much longer than that of C^{11}, irradiation times of several hours at a beam intensity of about 5×10^{10} protons per second were needed to obtain a sufficient counting rate.

After irradiation of the target foils the 1.9 h F^{18} activity was allowed to decay and counting was started 15 h after the end of the irradiation, i.e. after one half-life of the Na^{24} activity. The irradiated foils were cut in squares of 2×2 cm^2 and the β activity was measured by placing each square in turn at 50 mm distance from the window of an end-window Geiger-Müller counter. As a result of the small cross-section of the proton beam, 90—98 % of the total activity was always found on two or three of the 2×2 cm^2 pieces.

The measurements were started by determining the ratio between the total activity of the foil and the activity of two or three selected squares, after which only for these highly active squares the decay of the Na^{24} activity was followed for three consecutive half-lives by measuring the counting rate at regular intervals.

The efficiency of the Geiger-Müller counter was determined in two different ways [9]):

a) by direct calibration with Na^{24} standard sources, which were prepared from standard solutions † by depositing drops, that were accurately weighed, on sample supports of aluminium foil;

b) by measuring the absolute activity of some strongly activated target foil samples with the β—γ coincidence technique.

From these data the total activity $A(0)$ of the foil in disintegrations per minute at the end of the exposure can be calculated. The final accuracy for $A(0)$ of 2.9 % is mainly limited by the uncertainty in the calibration of the standard Na^{24} solutions.

The cross-section σ of the reaction Al^{27}(p, 3pn)Na^{24} follows from the equation

$$\sigma = \frac{A(0)}{N_p N(1-e^{-\lambda T})},$$

in which T is the duration of the irradiation in hours, λ the decay constant of Na^{24} ($\lambda = 4.60\times10^{-2}$ $hour^{-1}$), N the number of Al^{27} atoms per cm^2 of target foil, and N_p the beam flux in protons per minute, corrected for intensity variations of the beam during the exposure.

† Standard Na_2CO_3 solution from Teddington National Physics Laboratory. Standard NaCl solution from "Nuclear" Chicago. Absolute accuracy of both solutions was 3 %.

The results of the measurements are

Sample	Calculated cross-section σ (mb)
1	10.80 ± 0.5
2	11.20 ± 0.5
3	11.10 ± 0.5
4	11.20 ± 0.5
5	10.90 ± 0.5
6	10.75 ± 0.5
7	10.80 ± 0.5

from which a mean value for σ is found of

$$\sigma = (11.0 \pm 0.5) \times 10^{-27} \text{ cm}^2.$$

The main contributions to the error in σ are an uncertainty of 3 % in the absolute beam calibration (N_p) and the error of 2.9 % in $A(0)$ that was already mentioned.

6. Discussion

The value of 29.9 ± 1.5 mb for the cross-section of the reaction $C^{12}(p, pn)C^{11}$ at 591 MeV incident proton energy, found in the present measurements, agrees with the values of 30.4 ± 1.6 mb and 31.0 ± 1.7 mb obtained, at 560 MeV and 660 MeV incident proton energy respectively, by Prokoshkin and Tiapkin [4]). Their measurements are relative measurements, normalized to the absolute value of this cross-section obtained by Crandall *et al.* [10]) at 350 MeV incident proton energy. From these combined results it seems probable, that the low value of 25.5 ± 3.0 mb, obtained by Burcham *et al.* [3]) at 650 MeV incident proton energy in an absolute measurement, does not represent a real deviation from the energy independent behaviour of the $C^{12}(p, pn)C^{11}$ cross-section in this energy range.

For the $Al^{27}(p, 3pn)Na^{24}$ reaction, no previous measurements around 600 MeV proton energy are available. From the present measurements of this cross-section and that of the $C^{12}(p, pn)C^{11}$ reaction a ratio

$$\frac{\sigma_{C^{12}(p, pn)C^{11}}}{\sigma_{Al^{27}(p, 3pn)Na^{24}}} = 2.72 \pm 0.14$$

can be calculated, that should be compared with the value of 2.57 ± 0.13, which was obtained by Wolfgang and Friedlander [11]) in a direct measurement of this ratio at 600 MeV incident proton energy.

The authors wsih to thank Miss W. Riezler and Mr. W. Beck for technical help, and the operating staff of the synchro-cyclotron for their cooperation.

References

1) J. B. Cumming, G. Friedlander and C. E. Swartz, Phys. Rev. **111** (1958) 1386; the reader is referred to this article for earlier references
2) N. Horwitz and J. J. Murray, UCRL Report 8881 (1959)
3) W. E. Burcham, J. L. Symonds and J. D. Young, Proc. Phys. Soc. A **68** (1955) 1001; Proc. Phys. Soc., A **70** (1957) 824
4) Yu. D. Prokoshkin and A. A. Tiapkin, Sov. Phys. **5** (1957) 148
5) G. W. Tautfest and H. R. Fechter, Rev. Scient. Instr. **26** (1955) 229
6) D. Harting, J. C. Kluyver and A. Kusumegi, CERN Report 60—17 (1960)
7) I. A. D. Lewis and B. Collinge, Rev. Scient. Instr. **24** (1953) 1113
8) D. Strominger, J. M. Hollander and G. T. Seaborg, Rev. Mod. Phys. **30** (1958) 585
9) K. Goebel and H. Schultes, CERN Report 60—3 (1960)
10) W. E. Crandall, G. P. Milburn, R. V. Pyle and W. Birnbaum, Phys. Rev. **101** (1956) 329
11) R. L. Wolfgang and G. Friedlander, Phys. Rev. **96** (1954) 190; Phys. Rev. **98** (1955) 1871

2.F

Nuclear Physics **24** (1961) 36—42; © *North-Holland Publishing Co., Amsterdam*

Not to be reproduced by photoprint or microfilm without written permission from the publisher

SIMPLIFIED DISCUSSION OF BACKWARD PEAKING IN DIRECT INTERACTIONS

A. J. KROMMINGA and I. E. McCARTHY

Department of Mathematical Physics, University of Adelaide, Adelaide, South Australia

Received 6 December 1960

Abstract: A systematic semi-quantitative understanding of the shape and energy variation of the large backward peaks often observed in the angular distributions of products of direct interactions is given by the distorted wave Born approximation for a normal stripping-type process. The peaks are seen to result from the overlapping of the foci in the optical model wave functions for the positive energy particles as the scattering angle approaches 180°. The energy variation has the same period as would be given by $[j_L(kr_0)]^2$ but is displaced considerably in phase.

1. Introduction

When the angular distribution in reactions such as (α, p) [1,2,3]), (p, α) [4,5]) and (d, p) [6]) has been observed beyond 120° it has often been noticed that there is a sharp increase in the differential cross-section. This will be referred to as the backward peak or just the peak. It cannot be explained by the plane wave theory of such reactions. The size of the peak varies with energy, sometimes quite sharply, and with the state of the final nucleus.

In the experiments of the Japanese cyclotron group [1]) and of Priest, Tendam, and Bleuler [2]) the energy variation of the backward peaks in $C^{12}(\alpha, p)N^{15}$ has been studied in some detail. The peak height appears to oscillate with a period of about 10 MeV.

There have been several attempts to understand the mechanism responsible for the peaks. Within the framework of the Distorted Wave Born Approximation (DWBA) for a normal stripping-type process, Butler, Austern and Pearson [7]) suggested that they might be due to reflection from the far surface of the nucleus. On this model it is difficult to understand how the backward peaks could be much larger than the corresponding forward peaks as is often the case.

There have been suggestions that other mechanisms such as heavy particle stripping [8]) or compound nucleus contributions are responsible.

DWBA calculations by Tobocman [9]), Buck [10]) and Glendenning [11]) show evidence of such peaks and it seems possible that they can be explained within the framework of normal stripping theory.

The present work is an attempt to give a systematic semi-quantitative understanding of the shape and energy variation of the backward peaks based on the DWBA.

2. Properties of the Distorted Wave Functions

The matrix element in the DWBA may be written

$$M \propto (k^{(-)}/k^{(+)}) \int \mathrm{d}^3 r \varphi^{(+)}(\mathbf{r}) \varphi^{(-)*}(\mathbf{r}) \Psi(\mathbf{r}), \tag{1}$$

where $\varphi^{(+)}$ and $\varphi^{(-)*}$ are the wave functions of the incident and scattered particles whose momenta are $\hbar\mathbf{k}^{(+)}$ and $\hbar\mathbf{k}^{(-)}$ respectively. The function Ψ contains all the properties of the initial and final nuclei and the interaction; $\varphi^{(+)}$ and $\varphi^{(-)*}$ are optical model elastic scattering wave functions. If we write an optical model wave function in the form

$$\varphi(\mathbf{r}) = A(\mathbf{r}) \exp [iS(\mathbf{r})], \tag{2}$$

we can obtain a qualitative understanding of the effect of the distortion.

It has been shown by Eisberg, McCarthy and Spurrier [12]) that the wave function is easily understood in terms of the refraction and absorption of semi-classical particles. One expects $A(\mathbf{r})$ to be large on the surface of the nucleus near the incident particle, to decrease towards the far side because of the refraction and absorption, and to have a large sharp peak on the axis near the far side due to the focussing of the rays by the potential. Quantal calculations reproduce all these properties.

The focus has been discussed in more detail by McCarthy [13]). It can be quite well represented by a gaussian distribution in space whose half-width is about 1×10^{-13} cm. At low energies ($\approx$ 5 MeV) it is near the centre of the nucleus and subtends a large angle. At higher energies ($\approx$ 20 MeV) it is near the surface and subtends about 12° at the centre. The value of A at the focus is up to 10 times its value on the near surface for nucleons, and is comparable with the surface value for more strongly absorbed particles such as α-particles.

Examples of optical model wave functions [14]) have shown that $S(\mathbf{r})$ may be approximated by †

$$S(\mathbf{r}) \approx k(r) r \cos\theta + f(r). \tag{3}$$

The function $S(\mathbf{r})$ appears to be fairly linear in $\cos\theta$ over the whole range of $\cos\theta$. In some cases it deviates from its linear behaviour near $\cos\theta = \pm 1$ but the deviation is not at all great. This fact is of course the reason why the plane wave approximation is successful in predicting the positions of peaks in the angular distribution in cases where the focus is severely attenuated by absorption such as for (α, α') scattering.

In a discussion of an analytical approximation to the wave function which is highly successful for (α, α') scattering, McCarthy and Pursey [15, 16]) have shown that some averaging over k is necessary, but this is responsible only for rotating the angular distribution about the origin, and not for a substantial change in shape.

† For backward scattering we will neglect $f(r)$ in comparison with $K(r)r$.

McCarthy and Pursey [15]) suggested that the backward peaks in direct interaction angular distributions could be explained by the fact that, for backward scattering, the foci of both wave functions overlap. The term $A^{(+)}A^{(-)}$ in the integrand of the expression (1) increases within a few degrees as the scattering angle changes. It reaches a maximum at 180° where its value in the focal region is (for (α, p) reactions) about 10 times that on the other side of the nucleus. This model will be developed in the present article.

3. Qualitative Features of Backward Peaks

Some qualitative features of backward peaks in either experiments or exact distorted wave calculations can be understood in terms of the proposed idea that they are due to the overlap of the foci in the optical model wave functions.

a) In the 20 MeV region the backward peak always starts at about 150° [1–3]); this would be expected from the overlap of two foci of half-width about 12°. At lower energies (≈ 5 MeV) [4, 6]), the peaks start at smaller angles, since the foci subtend a larger angle.

b) Surface distorted wave calculations [10]) for the (d, p) peaks near 5 MeV are incapable of reproducing peaks, but volume calculations do reproduce them. This is because the focus at this energy is well inside the surface and is left out of a surface calculation.

c) Ground states do not give a (d, p) peak [10]) in the 5 MeV region but more excited states do. This may be because the radial part of $\Psi(\mathbf{r})$ is not large enough near the centre of the nucleus for ground states, but is larger for more excited states. It might, however, also be accounted for by the mechanism of section 4. Experiments at several different energies could distinguish between these two mechanisms.

d) The backward peaks in the distorted wave surface calculations of Glendenning [11]) for 15 MeV neutron inelastic scattering vary with the parameters of the calculation in the way expected from the model [13]). The peak is larger when the interaction radius is nearer the centres of the foci, it is smaller for larger imaginary potential when the foci are smaller (see fig. 9 of ref. [11])).

e) The backward peaks in the $F^{19}(p, \alpha)O^{16}$ data of Ogata [4]) get narrower as the proton energy increases from 8 MeV to 14 MeV corresponding to the proton focus moving further out and subtending a smaller angle.

Although the above evidence is highly suggestive that the focus overlap model is good for describing the backward peaks, it is not complete. We are now capable of saying why there are peaks, but we are left with the problem of why there are no peaks in some cases. This will be understood from the more quantitative discussion of section 4.

4. Energy Variation of the Backward Peaks

In order to get an idea of the energy variation of the backward peaks we shall make some simplifications to the distorted wave theory which are not expected to change the picture qualitatively.

We divide the integrand of the expression (1) into a "surface" and a "focus" term, and consider only the case where the scattering angle is 180° and the integrand is axially symmetric. The contribution from each term will be localized at one value of the radius. At energies less than 15 MeV, the equivalent radius for the focus term r_f is appreciably less than that for the surface term, r_s.

For the surface term we shall make the analytical approximation [15,16])

$$A^{(+)}(\mathbf{r}_s) = \exp(-\gamma \cos\theta^{(+)}), \quad A^{(-)}(\mathbf{r}_s) = \exp(\gamma \cos\theta^{(-)}), \tag{4}$$

where the $\theta^{(\pm)}$ are measured from the directions of the propagation vectors in free space $\mathbf{k}^{(\pm)}$, and γ is a constant which is roughly equal to 1 for most optical model wave functions in the relevant energy range.

The focus in $A^{(\pm)}$ is significant only for a very small range of $\cos\theta$, say from $\theta = 12°$ to 0° at 20 MeV, that is $0.98 \leqq \cos\theta \leqq 1$. It will be sufficient to represent $A^{(\pm)}$ in this region by square step functions of height $b^{(\pm)}$.

Setting

$$k^{(+)} + k^{(-)} = K, \quad \cos\theta = \chi, \tag{5}$$

the matrix element for 180° scattering becomes

$$M \propto (k^{(-)}/k^{(+)}) \left\{ \int_{-1}^{1} \mathrm{d}\chi \exp[i(K_s r_s + 2i\gamma)\chi] \int \mathrm{d}\varphi \Psi(r_s) \right.$$
$$\left. + b^{(+)} b^{(-)} \int_{0.98}^{1} \mathrm{d}\chi \exp[iK_f r_f \chi] \int \mathrm{d}\varphi \Psi(\mathbf{r}_f) \right\}. \tag{6}$$

In eq. (6) we have made the assumption discussed in section 2 that K_s is independent of χ. In the plane wave theory of angular distributions $K_s r_s$ is known to be energy dependent. Usually $\hbar K_s$ is taken to be the momentum transfer. Then the values of r_s which give the best agreement with angular distribution data vary with the incident energy. In an oversimplified picture this may be considered to arise from the fact that the values of K_s and K_f are more nearly equal to the difference in the propagation vectors measured from the bottom of the potential well at r_s and r_f respectively. We adopt the simplest parametrization, that is we assume that the appropriate value of r_s is given by fitting the plane wave approximation to the angular distribution data.

In most cases [11]) the dominant contribution to $\Psi(\mathbf{r})$ comes from one value of the angular momentum transfer L. We assume that this happens and put

$$\int \mathrm{d}\varphi \Psi(\mathbf{r}) = P_L(\cos\theta) R_L(r). \tag{7}$$

Let

$$a = b^{(+)} b^{(-)} R_L(r_t). \tag{8}$$

Neglecting the χ-dependence of $P_L(\chi)$ for $0.98 \leqq \chi \leqq 1$ we have

$$M \propto i^L j_L(K_s r_s + 2i\gamma) + a \left[\frac{1}{iK_t r_t} \exp(iK_t r_t \chi) \right]_{0.98}^{1}. \tag{9}$$

In the case of backward (α, p) reactions at about 20 MeV, we have

$$K_s r_s \approx K_t r_t \approx 10, \quad a \approx 10, \quad \gamma \approx 1.$$

Neglecting 2γ in comparison with $K_s r_s$ and using the asymptotic form of the spherical Bessel function for large argument, we have

$$M \propto (i^L/K_s r_s)\{\cos [K_s r_s - \tfrac{1}{2}(L+1)\pi] \cosh 2\gamma - i \sin[K_s r_s - \tfrac{1}{2}(L+1)\pi] \sinh 2\gamma\} + 0.02\, a \exp(iK_t r_t). \tag{10}$$

Putting $\cosh 2\gamma = \sinh 2\gamma = 3.5$ our final approximation for M is

$$M \propto (0.02\, a \cos K_t r_t \pm (3.5/Kr_s) \sin K_s r_s) + i(0.02\, a \sin K_t r_t \pm (3.5/Kr_s) \cos K_s r_s). \tag{11}$$

We have plus and minus signs for even and odd L respectively.

In the case we are considering, the coefficients of the sine and cosine terms in (11) are roughly equal, therefore the positions of the maxima and minima in the distribution of peak height against energy will be given by those of

$$\begin{aligned} |M|^2 &\propto (\cos K_t r_t \pm \sin K_s r_s)^2 + (\sin K_t r_t \pm \cos K_s r_s)^2 \\ &= 2(1 \pm \sin 2K_0 r_0), \end{aligned} \tag{12}$$

where

$$K_0 r_0 = \tfrac{1}{2}(K_s r_s + K_t r_t). \tag{13}$$

If we neglect the focus term we find maxima and minima in the energy distribution corresponding to those in the spherical Bessel function $j_L(K_s r_s)$. The fact that the argument of the Bessel function is complex in our case means that the minima are not zero, and there is a general rise in the differential cross-section towards the backward direction [15]). This, however, does not result in backward peaks. The addition of a focus term of comparable magnitude is necessary to produce the effect. The energy variation is then shifted considerably in phase from that for just the surface term. In the simple case considered above, the shift is $\frac{1}{4}\pi$.

In fig. 1 the heights of the experimental peaks at 170° (obtained by interpolation in the data of refs. [1, 2]) are plotted against the incident energy. The theory

may be compared with experiment by tabulating the values of r_0 necessary to fit maxima and minima at different energies and comparing them with values

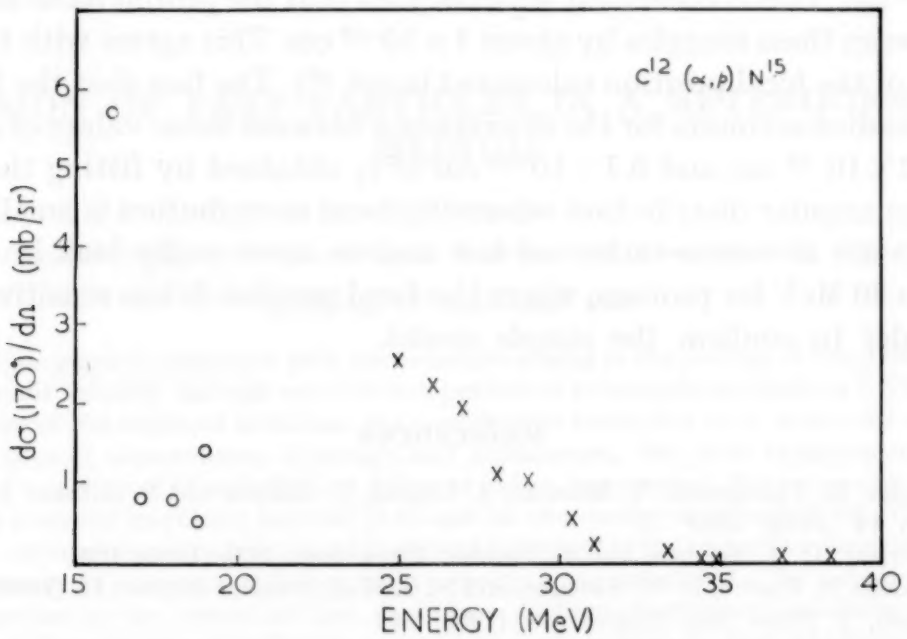

Fig. 1. Differential cross-sections at 170° in the C.M. system for $C^{12}(\alpha, p)N^{15}$ plotted against incident energy. The crosses represent interpolations in the data of ref. [1]), the circles represent interpolations in the data of ref. [2]).

r'_0 obtained near those energies from angular distributions. This is done in table 1.

TABLE 1

Values of r_0 obtained by fitting eq. (12) to the backward peaks in the experimental data of refs. [1, 2]) for $C^{12}(\alpha, p)N^{15}$. A maximum at about 15 MeV is assumed, and there is some indication of a maximum at 37 MeV. r'_0 is the value of r_0 obtained from plane wave stripping analysis of the angular distributions

E (MeV)	r_0 (10^{-13} cm)	r_0' (10^{-13} cm)
15 (max)	5.8	
17		5.9
18		5.5
19 (min)	5.8	
24 (max)	5.5	
33 (min)	5.1	
34.6		5.2
37 (max?)	5.2	

The maxima are much larger for lower incident energies as would be expected from eq. (11). Both $1/K_s r_s$ and (a) are larger for lower energies. The variation of a with energy must be noted. For $E \approx 40$ MeV the focus is near the outside of the nucleus and does not overlap the radial part of $\Psi(\mathbf{r})$ so much as at lower energies. Hence the backward peaks become very attenuated at these energies.

In the data of Ogata [4]) on $F^{19}(p, \alpha)O^{16}$, two minima are observed at about 9 MeV and 13.5 MeV. Corresponding values of r_0 are 4.7×10^{-13} cm and 5.2×10^{-13} cm. This is consistent with the idea that the proton focus moves outward between these energies by about 1×10^{-13} cm. This agrees with the energy variation of the focal position calculated in ref. [13]). The fact that the focus is at a smaller radius accounts for the discrepancy between these values of r_0 and the values 5.3×10^{-13} cm and 6.1×10^{-13} cm of r_s obtained by fitting the forward part of the angular distribution where the focal contribution is smaller. These arguments are of course rather ad hoc and we must really look in the range 15 MeV to 30 MeV for protons, where the focal position is less sensitive to energy, in order to confirm the simple model.

References

1) I. Nonaka, H. Yamaguchi, T. Mikumo, I. Umeda, T. Takata and S. Hitaka, J. Phys. Soc. (Japan) **14** (1959) 1260
2) J. R. Priest, D. J. Tendam and E. Bleuler, Phys. Rev. **119** (1960) 1301
3) P. R. Klein, H. Cindro, L. W. Swenson and N. S. Wall, Nuclear Physics **16** (1960) 374
4) H. Ogata, J. Phys. Soc. (Japan) **14** (1959) 707
5) I. Kumabe, C. L. Wang, M. Kawashima, M. Yada and H. Ogata, J. Phys. Soc. (Japan) **14** (1959) 713
6) D. A. Bromley, Proc. Intern. Conf. on Nuclear Structure (North-Holland Publishing Co., Amsterdam 1960), p. 272 (further references may be found in this article)
7) S. T. Butler, N. Austern and C. Pearson, Phys. Rev. **112** (1958) 1227
8) L. Madansky and G. F. Owen, Phys. Rev. **99** (1955) 1608
9) W. Tobocman, Proc. Intern. Conf. on Nuclear Structure, Kingston (1960) (North-Holland Publishing Co., Amsterdam 1960), p. 309
10) Buck, (reported by D. H. Wilkinson), Proc. Intern. Conf. on Nuclear Structure, Kingston (1960) (North-Holland Publishing Co., Amsterdam 1960), p. 37
11) N. K. Glendenning, Phys. Rev. **114** (1959) 1297
12) R. M. Eisberg, I. E. McCarthy and R. Spurrier, Nuclear Physics **10** (1959) 571
13) I. E. McCarthy, Nuclear Physics **11** (1959) 574
14) M. A. Melkanoff and J. Dyer, private communication
15) I. E. McCarthy and D. L. Pursey, to be published
16) I. E. McCarthy and D. L. Pursey, Proc. Intern. Conf. on Nuclear Structure, Kingston (1960) (North-Holland Publishing Co., Amsterdam 1960), p. 381

8.B:9.B *Nuclear Physics* **24** (1961) 43—61; © *North-Holland Publishing Co., Amsterdam*

Not to be reproduced by photoprint or microfilm without written permission from the publisher

EMISSION OF FAST PARTICLES IN A HETEROGENEOUS MEDIUM

M. L. TER-MIKAELYAN

Physical Institute of the Academy of Sciences of the Armenian SSR, USSR

Received 17 September 1960

Abstract: This paper is concerned with the radiation arising in the passage of relativistic particles of constant velocity through an arbitrary periodical heterogeneous medium †. The necessary condition of the origin of radiation, the condition of resonance (2.1), is derived on the basis of the laws of conservation of energy and momentum. The total radiation in a periodic medium is composed of radiations of different orders (harmonics). For each order of radiation there is a special frequency interval (2.6) and its own energy threshold (2.10). The radiation of each order is concentrated around the lower boundary of the respective spectrum intervals. The intensity of resonance radiation and its spectrum are calculated a) for a medium changing its properties by the cosinus law (sec. 4), b) for a medium of arbitrary periodicity with a weak change of density (sec. 4) and c) for a stratified medium (sec. 5), probably the most suitable for experimental purposes. Different effects influencing the accuracy of the formulas derived are analyzed in the last section. The properties of resonance radiation enumerated above can be applied in the physics of particles of ultra-high energy (secs. 5 and 6).

1. Introduction

The electromagnetic processes occurring in an arbitrary aggregate of fixed centres are known to possess a characteristic forward directionality at ultra-high energies. A direct corollary of this proposition is that large longitudinal distances, increasing with energy, can play an important role in these processes. Indeed, the momentum transferred to the medium along the direction of motion of the primary particle will equal

$$q_{\parallel} = p_0 - \sum_i \frac{(\mathbf{p}_i \mathbf{p}_0)}{p_0} . \tag{1.1}$$

Here $\mathbf{p}_0$ is the momentum of the incident particle and $\mathbf{p}_i$ are the momenta of the particles after the reaction.

Taking account of the energy conservation law

$$E_0 - \sum_i E_i = 0, \tag{1.2}$$

we can see that with relativistic energies and a well-pronounced direction, i.e., when $(\mathbf{p}_i \mathbf{p}_0)/p_0 \approx p_i \approx E_i$ the quantity $q_{\parallel}$, becomes small and decreases with increasing energy and directionality. From the uncertainty relation it follows

† Radiation in the random heterogeneous medium is discussed in ref. [3]) (see also the footnote on the next page).

that the effective longitudinal distances

$$l_{\text{eff}} \approx h/q_{\parallel} \tag{1.3}$$

can become rather large. It can readily be seen that at such large distances, different external effects can influence the interaction of two separate centres and lead to a sharp change of the usual cross sections. This reasoning was used by the author in investigating interference scattering and radiation in a crystal [1]) (see also the survey of ref. [2])), where the adjacent atoms in the lattice begin to act coherently owing to the growth of l_{eff} †.

The present work is concerned with the radiation produced by uniformly moving particles in a heterogeneous medium [3]). We shall see that the interference of the radiation arising in different heterogeneities will be essential because of the smallness of $q_{\parallel}$. Besides, the heterogeneities will lead to the radiation of quanta with lengths infinitesimally smalll compared with the dimensions of the heterogeneities. This will be another example confirming the importance of large longitudinal distances in radiation at ultra-high energies.

Since a uniformly moving particle produces only Cerenkov-Vavilov radiation in a homogeneous medium, below we shall consider the changes that this radiation undergoes in a heterogeneous medium. We shall see that in the case of a heterogeneous medium radiation will also exist in the range of frequencies exceeding the characteristic atomic frequencies wherein the dielectric constant is less than unity and no Cerenkov-Vavilov radiation possible.

The well-pronounced dependence of the radiation to be investigated below on the energy of the radiating particle can be used for detecting ultra-high energy particles. The cause of radiation in a heterogeneous medium can easily be detected if it is observed that the passage of photons through an opaque medium is always accompanied by scattering of light. Since the field of a charged particle is an aggregate of pseudophotons, the scattering of these pseudophotons on the heterogeneities of the medium is precisely the radiation of interest to us. The simplest example of radiation in a heterogeneous medium is the Ginsburg-Frank transition radiation [4]) arising as the charged particle crosses the border of two media. Frank [4]) considered the problem of summing the transitional radiation arising at many borders and showed that simple summation is possible if the distance between the borders exceeds l_{eff}.

Heterogeneities can be periodic or random functions of space. Periodic heterogeneities lead to the interference of radiation arising in different sections of a heterogeneous medium. As a result of interference phenomena a perceptible radiation in a periodic medium can appear only if the resonance condition, the derivation of which follows below, is fulfilled.

† In an article soon to be published by the "Uspekhi Fizicheskikh Nauk" the author attempts to present a survey of work on bremsstrahlung in crystals and to set down new results for these problems.

We shall assume that the medium changes its property periodically only along the z-axes and remains homogeneous in the x, y plane. Consider a particle the velocity of which forms an angle ψ with the direction of the z-axis and which emits a quantum of energy $\hbar\omega$ and momentum $\hbar\omega\sqrt{\varepsilon_0}/c$. The laws of conservation of longitudinal momentum and energy for this specific case will be rewritten as

$$q_{\parallel} = \frac{\mathbf{v}\delta\mathbf{p}}{v} - \frac{\hbar\omega}{c}\sqrt{\varepsilon_0}\cos\theta' = \frac{2\pi}{l}r\cos\psi, \tag{1.1}$$

$$\delta E = \hbar\omega = 0, \tag{1.2}$$

where θ' is the angle between the direction of the emitted quantum and the velocity $\mathbf{v}$; δE and $\delta\mathbf{p}$ are the changes of the energy and momentum of the particle, r is an arbitrary integer and l is the period of the medium. It will be emphasised that the radiation of the order of r in a periodic medium is impossible unless the momentum transferred to the lattice along the z-axis is equal to $2\pi\hbar r/l$.

2. The Condition of Resonance; Angular Distributions and Energy Threshold of Resonance Radiation

Since $\delta E = \mathbf{v}\delta\mathbf{p}$ for small changes of the energy of the particle, from the conservation laws (1.1) and (1.2) we immediately obtain the principal condition for radiation

$$\frac{\omega_{\text{eff}}}{v} = \frac{\omega}{v}\left(1 - \frac{v}{c}\sqrt{\varepsilon_0}\cos\theta'\right) = \frac{2\pi r}{l}\cos\psi. \tag{2.1}$$

The resonance condition (2.1) is equivalent in its physical content to the Bragg-Laue-Wulf condition in the diffraction of X-rays (see also refs. [1, 5]). From the condition (2.1) some noteworthy properties of the radiation under investigation follow. To begin with, the angle of the radiation of the quantum is given by the expression

$$\cos\theta' = \frac{c}{v\sqrt{\varepsilon_0}} - \frac{2\pi r c\cos\psi}{l\omega\sqrt{\varepsilon_0}}. \tag{2.2}$$

At $l \to \infty$ we arrive at the well-known relation for the angle of Vavilov-Cerenkov radiation. In contrast to the case $l \to \infty$, (2.2) can be fulfilled in a region. of frequencies considerably exceeding the characteristic atomic frequencies For such large frequencies the dielectric constant is of the form

$$\varepsilon = \varepsilon_0 + \Delta\varepsilon_1(z) = 1 - \frac{4\pi N e^2}{m_e\omega^2} - \frac{4\pi N' e^2}{m_e\omega^2}\varepsilon_1(z) \quad (\Delta\varepsilon_1(z) \ll \varepsilon_0). \tag{2.3}$$

Here N is the constant component of electric density and $N'\varepsilon_1(z)$ is the variable

one; obviously, the inequality $N'\varepsilon_1 \leqq N$ is always fulfilled. From the requirement $|\cos\theta'| \leqq 1$ we shall obtain

$$\frac{c}{v\sqrt{\varepsilon_0}}\left(1+\frac{v}{c}\sqrt{\varepsilon_0}\right) \geqq \frac{2\pi r\lambda}{l} \geqq \left(1-\frac{v}{c}\sqrt{\varepsilon_0}\right)\frac{c}{v\sqrt{\varepsilon_0}}, \tag{2.4}$$

where

$$\lambda = c/\omega\sqrt{\varepsilon_0}. \tag{2.5}$$

For the radiation of frequencies for which the dielectric constant is given by eq. (2.3) the right-hand part of the inequality (2.4) leads to two simultaneous conditions:

$$\frac{E}{h} \gg \omega_{\max}$$

$$= \frac{2b}{a}\left[1-\sqrt{1-4\left(1-\frac{v}{c}\right)\frac{b}{a^2}}\right]^{-1} \geqq \omega \geqq \frac{2b}{a}\left[1+\sqrt{1-4\left(1-\frac{v}{c}\right)\frac{b}{a^2}}\right]^{-1} = \omega_{\min}, \tag{2.6}$$

where the quantities a and b are equal to

$$a = \frac{2\pi cr}{l}, \qquad b = \frac{2\pi e^2}{m_e}N. \tag{2.7}$$

The inequalities (2.6) can be simplified for energies considerably exceeding the threshold energy (2.10)

$$\frac{E}{h} \gg \omega_{\max} \approx \frac{4\pi c}{l}\, r\left(\frac{E}{mc^2}\right)^2 \gtrsim \omega \gtrsim \frac{Ne^2 l}{m_e cr} \approx \omega_{\min}. \tag{2.6}$$

The left-hand part of the inequality (2.4) leads to the condition

$$\omega \geqq \pi cr/l. \tag{2.8}$$

The inequality (2.8) will automatically follow from (2.6) if we confine ourselves to the radiation the order of which satisfies the condition

$$r \ll r_{\max} = \frac{l}{2\pi}\left(\frac{4\pi Ne^2}{m_e c^2}\right)^{\frac{1}{2}}. \tag{2.9}$$

If (2.9) is fulfilled the interval of the frequencies radiated is given by the inequalities (2.6) from which follows the condition on the energy threshold when the radiation of the r-th order begins.

$$\frac{E}{mc^2} = \left(\frac{E}{mc^2}\right)_{\text{tr}} \geqq \frac{l}{rc}\sqrt{\frac{Ne^2}{\pi m_e}}. \tag{2.10}$$

From (2.9) it follows that the case under investigation can be realised only for

relativistic particles and therefore in all formulas beginning from (2.6) we put $v = c$ wherever possible.

The condition on the angle of radiation (2.2) in the case under consideration can be written as

$$\theta'^2 \approx \frac{4\pi r c \cos\psi}{l\omega} - \left(1 - \frac{v^2}{c^2}\right) - \frac{4\pi N e^2}{m_e \omega^2}. \tag{2.11}$$

It will be noted that $\cos\theta'$ becomes unity for radiation of the maximum and minimum frequencies (determined by (2.6)). For radiation of intermediate frequencies the radiation angle increases until it reaches the maximum

$$\theta' \approx \frac{r}{l}\left(\frac{m\pi c^2}{Ne^2}\right)^{\frac{1}{2}} \ll 1 \tag{2.12}$$

for frequencies merely twice as high as $\omega_{\min}$.

Let us now consider the radiation the order of which exceeds $r_{\max}$.

The interval of frequencies radiated into the front hemisphere is obtained from the condition (2.4)

$$\omega'_{\max} = \frac{2\pi v r}{l} \frac{1}{\left(1 - \frac{v}{c}\right)} \geqq \omega \geqq \frac{2\pi v}{l} r = \omega'_{\min}. \tag{2.13}$$

The radiation in this case will be directed at right angles to the trajectory at $\omega = \omega'_{\min}$ and along the trajectory at $\omega = \omega'_{\max}$. The radiation the order of which exceeds $r_{\max}$ decreases sharply with increasing r. Yet this case can be realized at arbitrary velocities. As we shall see below, the intensity of radiation of high order is small and the influence of small distortions of periodicity leading to the decrease of resonance radiation increases with the order of radiation. Summing up, it can be said that the radiation with the above properties (energy threshold, pronounced directionality, etc.) can be observed in the case $r_{\max} \gg 1$, i.e., if the period of the medium exceeds the quantity

$$l \gg l_1 = \left(\frac{m_e c^2 \pi}{Ne^2}\right)^{\frac{1}{2}}. \tag{2.14}$$

To avoid in experiment the influence of the photoeffect on the frequency region close to $\omega_{\min}$, where resonance radiation is concentrated, as we shall see, it is convenient in practise to choose solids for which $l \gtrsim 10^{-2}$ cm. Then (2.14) is always fulfilled with a considerable margin. The detailed analysis of the medium for which $l < l_1$ is omitted here for the sake of brevity.

3. Quasi-Classical Consideration

The Maxwell equations for a heterogeneous medium will preserve their conventional form and the only difference will consist in that the dielectrical

and magnetic permeabilities will be functions of the point x, y, z. We shall write the Maxwell equations for the Fourier field component selecting the time factor in the form $\exp(-i\omega t)$. The equations for the vector potential $\mathbf{A}$ can be written [6])

$$\Delta\mathbf{A}+\kappa^2\mathbf{A}-\operatorname{div}\mathbf{A}\cdot\operatorname{grad}(\lg\kappa^2)=-\frac{2\mu}{c}\int\mathbf{j}(t)e^{i\omega t}dt, \tag{3.1}$$

where

$$\kappa^2=\frac{\varepsilon\mu\omega^2}{c^2}, \qquad \varepsilon=\varepsilon_0+\Delta\varepsilon_1(z). \tag{3.2}$$

In the following we shall set $\mu=1$. We shall assume that the properties of the medium change only in one direction, along the z-axis. It will also be assumed that the current is directed along the z-axis

$$j_y=ev(z)\delta(x)\delta(y)\delta(z-z(t)). \tag{3.3}$$

An arbitrarily directed current can be considered by methods similar to those described below. It can be seen that for small angles of incidence and small angles of radiation the change reduces to replacing l by $l/\cos\psi$. In the case of incidence along the z-axis, eq. (3.1) turns into an equation for A_z. The components A_x and A_y can be assumed equal to zero. Thus, the polarization of the radiation under study is thereby determined, viz., the vector H of the resonance radiation is perpendicular to the plane containing the axis z and the wave vector $\mathbf{k}$.

The solution of eq. (3.1) will be sought in the form (the subscript z will be omitted in the following):

$$A(x,y,z)=\int A(k_x,k_y,z)\exp(ik_xx+ik_yy)dk_xdk_y. \tag{3.4}$$

The equation for

$$A(k_x,k_y,z)=A(q,z), \tag{3.5}$$

with

$$q=\sqrt{k_x^2+k_y^2}, \tag{3.6}$$

will be rewritten in the following manner

$$\varepsilon\frac{\partial}{\partial z}\left(\frac{1}{\varepsilon}\frac{\partial A(q,z)}{\partial z}\right)+\left(\frac{\omega^2}{c^2}\varepsilon-q^2\right)A(q,z)=-\frac{e}{2\pi^2c}\int v(z)\delta(z-z(t))e^{i\omega t}dt. \tag{3.7}$$

With an arbitrary dependence of ε_1 on z eq. (3.7) can be solved in general form in a quasi-classical approximation. The quasi-classical solutions of the corresponding homogeneous equation are of the well-known form (with accuracy to

the leading terms in quasi-classical expansion):

$$A_{1,2} = C_{1,2}\left(\frac{\varepsilon}{\kappa}\right)^{\frac{1}{2}} \exp\left\{\pm\int^{z}\kappa \mathrm{d}z\right\}, \tag{3.8}$$

where

$$\kappa = \sqrt{\frac{\omega^2}{c^2}\varepsilon - q^2}. \tag{3.9}$$

It will be noted that the possibility of reducing eq. (3.7) to a series of equations for a finite number of the functions in quasi-classical expansion calls for the fulfilment of the quasi-classical condition

$$\left|\frac{\varepsilon}{\kappa^2}\frac{\partial}{\partial z}\left(\frac{\kappa}{\varepsilon}\right)\right| \ll 1. \tag{3.10}$$

Actually we have to demand additionally that at distances of interest to us the change in the phase of the vector potential introduced by the subsequent terms of the expansion in the quasi-classical approximation would be small.

In the case of the medium considered below (sec. 4) this requirement can easily be fulfilled if we demand a more rigorous condition than eq. (3.10), viz.

$$\lambda \ll l. \tag{3.11}$$

After finding two linearly independent solutions (3.8) the Green's function of eq. (3.7) is constructed in the conventional manner [7]). The only point to be noted is that $G(z, z')$ should lead to waves diverging from the point $z = z'$ where the source is. Consequently (since the time factors have been chosen as $\exp(-i\omega t)$), $G(z, z')$ should be sought in the form

$$G(z, z') = \begin{cases} CA_1(q, z)A_2(q, z') & (z > z'), \\ CA_1(q, z')A_2(q, z) & (z < z'). \end{cases} \tag{3.12}$$

The Green's function is determined with an accuracy to a constant factor through this relation. If we additionally demand that the function $G(z, z')$ should satisfy eq. (3.7) in which the right-hand part is replaced by $-4\pi\varepsilon\delta(z-z')$, then the constant factor will be determined from the condition that the discontinuity of the derivative of the Green's function at the point $z = z'$ be equal to

$$G'(z'+0, z) - G'(z'-0, z') = -4\pi\varepsilon(z'). \tag{3.13}$$

Consequently, $C = 2\pi i$. The desired solution of eq. (3.7) can be written in the form

$$A(q, z) = \frac{ie}{4\pi^2 c}\left[\frac{\varepsilon(z)}{\kappa(z)}\right]^{\frac{1}{2}} \int \frac{v(t)\exp\left(i\omega t + i\left|\int_{z(t)}^{z}\kappa(z)\mathrm{d}z\right|\right)}{[\kappa(t)\varepsilon(t)]^{\frac{1}{2}}}\mathrm{d}t. \tag{3.14}$$

The absolute value signs in the exponent of the integrand of the expression denote that by the definition of the Green's function (3.12). we shall take only the positive values of the integral over z. We shall see in the following that actually we shall have to use (3.14) only for calculating the intensity of radiation into the front hemisphere $z \to \infty$ and since κ is by definition positive, the integral over z will always be positive.

Let us calculate the flux of energy passing through the x, y plane perpendicular to the trajectory of the particle (for the sake of simplicity we shall assume in the following that the particle moves uniformly and in a straight line). For this purpose it is necessary to calculate $[EH]_z = E_x H_y - H_x E_y$. The potential φ is determined from the conventional Lorenz condition and is equal to

$$\varphi = -\frac{ic}{\varepsilon\omega} \operatorname{div} \mathbf{A} = \frac{c}{\omega\varepsilon} \kappa A(q, z), \tag{3.15}$$

for, according to the quasi-classical condition (3.10), it is necessary to differentiate in (3.14) only the exponent of the integrand over the variable z.

The final expression for the flux of energy through the plane at a distance z from the origin of the coordinates and perpendicular to the trajectory for the entire time of motion is

$$S = \frac{8\pi^3 c^2 \mathrm{d}\omega}{\omega\varepsilon} \int_0^\infty q^3 \mathrm{d}q \kappa |A(q, z)|^2. \tag{3.16}$$

By virtue of the quasi-classical concept we can assume that the change of the properties of the medium scarcely affects the distribution of quanta, and therefore, we shall introduce the quantum radiation angle θ according to the relation

$$q = \frac{\omega}{c} \sqrt{\varepsilon_0} \sin\theta, \qquad \kappa_0 = \frac{\omega}{c} \sqrt{\varepsilon_0} \cos\theta = \sqrt{\frac{\omega^2}{c^2} \varepsilon_0 - q^2}.$$

The average deviation from the direction determined by the angle θ in a periodic medium is equal to zero (the mean squares at distances of the order of l_{eff} being infinitesimal).

4. Radiation in a Medium Changing Its Properties by the Cosinus Law

Let us calculate resonance radiation in a medium with a dielectric constant equal to

$$\varepsilon(\omega, z) = \varepsilon_0(\omega) + \Delta \cos\frac{2\pi z}{l}, \qquad \Delta \ll \varepsilon_0. \tag{4.1}$$

The calculation of the intensity is performed with the help of (3.14) and (3.16).

To simplify subsequent operation the quantity κ in (3.14) is expanded into the series

$$\kappa \approx \kappa_0 + \frac{1}{2}\frac{\omega^2}{c^2}\frac{\Delta\varepsilon_1}{\kappa_0}. \tag{4.2}$$

The expression for $A(q, z)$ at $z \to \infty$ and a constant velocity for the medium under cosideration is equal to

$$A(q, z) = \frac{iev}{8\pi^3 c}\left(\frac{\varepsilon}{\kappa}\right)^{\frac{1}{2}}\int \frac{\mathrm{d}t}{(\varepsilon\kappa)^{\frac{1}{2}}} \exp\left\{i\omega t + i\kappa_0(z - vt) + \frac{i\omega^2 \Delta l}{4\pi c^2 \kappa_0}\left(\sin\frac{2\pi z}{l} - \sin\frac{2\pi v t}{l}\right)\right\}. \tag{4.3}$$

If on the other hand (3.11) is fulfilled the dependence of the denominator of (4.3) on t can be neglected. Using a formula known from the theory of Bessel functions [8])

$$\exp\left(-iB\sin\frac{2\pi v t}{l}\right) = \sum_{r=-\infty}^{r=+\infty} J_r(B)\exp\left(-i\frac{2\pi v r t}{l}\right). \tag{4.4}$$

Eq. (4.3) can be represented as a sum of terms each of which contains a delta function of the form

$$\delta\left(\omega - \kappa_0 v - \frac{2\pi v}{l}r\right). \tag{4.5}$$

It can readily be seen that we have arrived at the condition of resonance (2.1) from which follows the expression for the cosinus of the radiation angle (2.2) and the interval of the frequencies radiated (2.4). Since we consider now the flux of energy through the plane $z \to \infty$, only positive radiation angles are possible and therefore the left-hand part of (2.4) has to be replaced for $c/v\sqrt{\varepsilon_0}$. After substituting the square of the modulus of eq. (4.3) into (3.16) and integrating over all angles we obtain the energy radiated in time T

$$\mathrm{d}I = \frac{e^2 v}{c^2}\omega \mathrm{d}\omega T \sum_r J_r^2(B)\left[1 - \left(\frac{c}{v\sqrt{\varepsilon_0}} - \frac{2\pi r c}{l\omega\sqrt{\varepsilon_0}}\right)^2\right]. \tag{4.6}$$

The expression in square brackets is $\sin^2\theta$ (see (2.2)). The quantity B in the argument of the Bessel function is equal to

$$B = \frac{l\Delta\omega}{4\pi c\sqrt{\varepsilon_0}\cos\theta}. \tag{4.7}$$

Before passing to the analysis of eq. (4.6) it will be recalled that the quasi-classical calculation we have used is not applicable close to the reversal points $\kappa = 0.$, i.e.

$$-\frac{2\pi r c}{l\omega\sqrt{\varepsilon_0}} + \frac{c}{v\sqrt{\varepsilon_0}} \gg \delta, \tag{4.8}$$

where δ is a small quantity determined by the least admissible quantities of

cos θ where the quasi-classical argument still applies. The restriction (4.8) should not affect the results (it is clear that (4.8) is automatically fulfilled for negative r if $c/v\sqrt{\varepsilon} \approx 1$).

(a) Let us proceed to the analysis of eqs. (4.6), (4.7), (2.4) and (2.2). Let us begin from the consideration of the frequencies which do not exceed the atomic ones. Let us consider certain terms of the series (4.6). If the condition

$$\frac{v}{c}\sqrt{\varepsilon_0} \geqq 1 \tag{4.9}$$

is fulfilled the term of the series (4.6) with $r = 0$ yields the intensity of Cerenkov radiation in a periodic medium and (4.8) and (2.4) are fulfilled automatically. Eq. (4.6) in this case differs from the Tamm-Frank formula only in that the unity in this formula is replaced by $J_0^2(B)$, decreasing the intensity of Cerenkov radiation. The quantity B (it will be recalled that $\lambda \ll l$, $\Delta \ll \varepsilon_0$) depends on the speed of the incident particle. Let us consider the term $r = -1$. The radiation angle is determined by the condition (2.2). The intensity is given by the term with $r = -1$ in eq. (4.6). To determine the interval of frequencies radiated, it is necessary to take into account, apart from the fulfilment of the condition (4.9), the right-hand part of the condition (2.4) which also imposes a condition on the allowable spectrum of the frequencies radiated. Let us consider the term with $r = +1$. The condition (4.8) will impose certain restrictions on the radiation frequency. At the same time (2.4) for $r = +1$ yields the interval of frequencies radiated. The comparison of the two conditions shows that only a small portion of the radiation spectrum about $\omega_{\min}$ cannot be described by eq. (4.6). This may prove inessential since for large values of B (i.e., when (4.8) is not fulfilled) the intensity will be small because of $J_n^2(B)$. The case $r = +1$ is interesting in that radiation can arise also when (4.9) is not fulfilled, i.e., below the Vavilov-Cerenkov radiation threshold. This reasoning can be extended for $r = \pm 2, \pm 3$; etc. It will be noted that radiation of positive order $r > 0$ can arise below the Cerenkov radiation threshold.

It should be emphasised once again that eqs. (4.6) fully describe the radiation with the restriction (4.8) for $\lambda \ll l$ and $\Delta \ll \varepsilon_0$. The radiation angle for each order is given by the condition (2.2) and the interval of frequencies radiated is determined by the condition (2.4) †.

Amatuni and Korkhmazyan [9]) obtained a formula for the radiation of order $r = 0, \pm 1$ for $\beta \ll 1$ and $\Delta \gg 1$ without the assumption $\lambda \ll l$. B. Bolotovsky kindly referred me to the work of Ginzburg and Eidman [10]) in which closely related results were obtained. In contrast to our assumption, the medium in this paper was assumed to be homogeneous and the charged particle replaced by an oscillator moving along the z-axis.

† The theory proposed in ref. [3]) can be applied in the case when the condition $\lambda \ll l$ is not fulfilled.

(b) Let us proceed now to the consideration of frequencies exceeding the characteristic atomic frequencies. Then we could use the limiting values ε and Δ in the form of (2.3) and the analysis of the formulas can be advanced considerably. It will be noted that only radiation of positive order $r > 0$ is possible at present.

In the case under consideration the right-hand part of the inequality (2.4) leads immediately to two inequalities (2.6) provided (2.9) is fulfilled. The energy threshold at which the radiation of a given order begins is determined by eq. (2.10) and the radiation angle is given by eq. (2.11).

If the radiation order exceeds $r_{\max}$ (2.9) the interval of frequencies radiated will be given by the inequality (2.13) instead of (2.6). This will lead to the argument of the Bessel function being considerably less than the index r for all values of ω. Therefore, since the indices $r \gtrsim r_{\max}$ are assumed large the numerical values of the Bessel functions will lead to insignificant intensity.

We return now to the case $r \ll r_{\max}$. As a result of the directionality of the radiation the expression in square brackets (4.6) can be simplified and the formula rewritten in the variables

$$y = \frac{b}{a\omega}, \tag{4.10}$$

$\mathrm{d}I$ having preliminarily been divided by $\hbar\omega$ and by vT. Then we have the equation

$$B = \alpha y, \qquad \alpha = \frac{N'}{N} r, \tag{4.11}$$

and for the number of the radiated quanta per unit path-length we have from (4.6)

$$m = \frac{4\pi}{137l} \sum_r r \int_{y_1}^{y_2} \frac{\mathrm{d}y}{y^2} J_r^2(\alpha y)\{y - y^2 - A\}, \tag{4.12}$$

where y_1 and y_2 correspond to the $\omega_{\min}$ and $\omega_{\max}$, while

$$A = \left(1 - \frac{v}{c}\right)\frac{b}{a^2}. \tag{4.13}$$

Note that $A \leqq \frac{1}{4}$, which determines the threshold energy. It will be mentioned that y_1 and y_2 are the roots of the expression in braces in (4.12).

Let us turn to the analysis of eq. (4.12). Using the asymptotic expression of Debay for the Bessel functions and the conventional expansion into an exponential series it can be shown that for $N' \ll N$ the principal contribution to (4.12) comes from the radiation of the first order. At $N' \approx N$ the radiation of high order also becomes essential for determining the total number of quanta.

To analyse the radiation spectrum let us return to eq. (4.6) or (4.12) without integrating over ω. It can readily be seen, proceeding from the properties of the

Bessel functions, that the overwhelming number of the quanta obtained will be concentrated close to $\omega_{\min}$.

The example considered above of a medium changing its properties by the cosinus law makes it possible to obtain the results for an medium of arbitrary periodicity for the case $N' \ll N$.

Just as before, we shall describe the properties of the medium through the dielectric constant (2.3). The variable part of ε will be expanded into the Fourier series

$$\varepsilon_1(z) = \sum_{r=1}^{\infty} a_r \cos\frac{2\pi z r}{l} + b_r \sin\frac{2\pi z r}{l}. \tag{4.15}$$

We shall omit the details of the calculation and adduce the final formula for the intensity of the radiation

$$\mathrm{d}I = \frac{e^2 v}{c^2}\omega \mathrm{d}\omega T \sum_r \frac{B_r^2 + B_{r'}^2}{4}\left[1 - \left(\frac{c}{v\sqrt{\varepsilon_0}} - \frac{2\pi r c}{l\omega\sqrt{\varepsilon_0}}\right)^2\right]. \tag{4.16}$$

The quantities B_r and $N_{r'}$ are equal to the quantity B (see (4.7)) multiplied by a_r/r and b_r/r respectively. The angular direction of radiation and the interval of the frequencies radiated are given by the formulas of sec. 2 for each order r

5. Stratified Medium

Since the stratified medium is the most convenient from the experimental point of view for using resonance radiation in the physics of high-energy particles, this section offers the derivation and investigation of the corresponding formulae in the general case for different thicknesses and arbitrary N', N. We shall use the formulae obtained above in quasi-classical approximation. The applicability of the quasi-classical approximation to the stratified medium calls for the smoothing out of the transition boundaries between the layers. This can always be done since large path-lengths of particles are essential for the production of radiation and therefore the result of interest to us does not depend on the sharpness of the boundaries. It will be noted furthermore that since the quasi-classical approximation leads to incorrect results for reflected waves, we should demand that the effects involving reflected waves be neglected. This will be achieved if the change of the dielectrical properties of the medium from the layer with the dielectrical constant ε_1 to the layer ε_2 will be small, i.e.,

$$\left|\frac{\varepsilon_1 - \varepsilon_2}{\varepsilon_1 + \varepsilon_2}\right| \ll 1 \tag{2.3}$$

In the region of frequencies exceeding the atomic ones which will interest us in the following, this condition is always fulfilled. Apart from (2.3) we shall

have to assume that $v \approx c$ and that the angles of radiation are small. The last condition will be fulfilled if (3.11) is fulfilled.

The energy radiated by a particle moving along the z-axis through a plane perpendicular to the trajectory of the particle and removed to a distance $z \to \infty$ from the origin of the coordinates is given by eq. (3.16) with $A(q, z)$ calculated by eq. (3.14).

We shall designate the integral in (3.14) through I

$$I = \int_{-\infty}^{+\infty} \frac{\exp\left((i\omega t + i\left|\int_{vt}^{z} \kappa \mathrm{d}z\right|\right)}{[\kappa(vt)\varepsilon(vt)]^{\frac{1}{2}}} \mathrm{d}t. \tag{5.1}$$

The calculation of S reduces to the calculation of the integral I for a stratified medium. We shall first consider the final number of the alternating layers of two different substances with dielectric constants ε_1 and ε_2,

$$\kappa_1 = \frac{\omega}{c}\sqrt{\varepsilon_1}\cos\theta, \qquad \kappa_2 = \frac{\omega}{c}\sqrt{\varepsilon_2}\cos\theta. \tag{5.2}$$

Let a layer out of the first substance ε_1 by $\Delta z_1 = v\Delta t_1$ thick and that out of the second substance ε_2 be $\Delta z_2 = v\Delta t_2$ thick. Let us designate the layers with the numbers from 1 to n, and let odd numbers describe the first medium and even numbers the second. For the sake of convenience let us choose n to be an even number, i.e., we shall have $\frac{1}{2}n$ layers of one medium and $\frac{1}{2}n$ of the other. In the following we shall let n tend to infinity (actually it will mean that the factor $|\sin \frac{1}{2}n\beta/\sin\beta|^2$ in I^2 — see (5.5) — can be replaced by

$$\tfrac{1}{2}n\pi \sum_{n=-\infty}^{n=+\infty} \delta(\beta - \pi r).$$

Let us designate as $t_1, t_2, \ldots t_n$ the times of entry of the particle into the first, second, etc. layers, and t_{n+1} the time of emission out of the last layer. Then the integral can be divided into a sum of integrals over t (from $-\infty$ to t_1; t_1 to t_2 etc. and from t_{n+1} to ∞). We shall discard the first integral from $-\infty$ to t_1 and the last from t_{n+1} to ∞ since they involve transition effects in the first and last boundary. Each integral can easily be calculated if the point z lies beyond the last layer. (In the following we should let z tend to infinity more rapidly than the number of the layers). The summation of the calculated integrals reduces to the summation of a geometrical progression. For I we obtain the final expression

$$I = \frac{1}{(\kappa_1\varepsilon_1)^{\frac{1}{2}}(\omega - \kappa_1 v)}\left\{\sum_{l=1}^{n-1} \mathrm{e}^{ir_l}(-1)^l + 1\right\} - \frac{1}{(\kappa_2\varepsilon_2)^{\frac{1}{2}}(\omega - \kappa_2 v)}\left\{\sum_{l=1}^{n-1} \mathrm{e}^{ir_l}(-1)^l + \mathrm{e}^{ir_n}\right\}, \tag{5.3}$$

where

$$\begin{aligned} r_1 &= (\omega-\kappa_1 v)\Delta t_1, \\ r_2 &= (\omega-\kappa_2 v)\Delta t_2+r_1, \\ r_3 &= (\omega-\kappa_1 v)\Delta t_3+r_2, \\ &\cdots\cdots\cdots\cdots\cdots \\ &\cdots\cdots\cdots\cdots\cdots \\ r_n &= (\omega-\kappa_2 v)\Delta t_n+r_{n-1}. \end{aligned} \tag{5.4}$$

For calculating (5.3) we assumed that the i-th plate is $\Delta z_i = v\Delta t_i$ thick. Eq. (5.3) will be used in the next section for calculating radiation with allowance for accidental deviations from the average thickness. For the time being we shall assume that all odd layers are Δz_1 and even Δz_2 thick. Then eq. (5.3) can be rewritten

$$I = 2\sin\tfrac{1}{2}(\omega-\kappa_2 v)\Delta t_2 \left| \frac{1}{(\varepsilon_1\kappa_1)^{\frac{1}{2}}(\omega-\kappa_1 v)} - \frac{1}{(\varepsilon_2\kappa_2)^{\frac{1}{2}}(\omega-\kappa_2 v)} \frac{\sin\frac{1}{2}n\beta}{\sin\beta} \right|, \tag{5.5}$$

where

$$2\alpha = (\omega-\kappa_1 v)\Delta t_1+(\omega-\kappa_2 v)\Delta t_2. \tag{5.6}$$

At sufficiently large n, I differs from zero where $\beta = \pi r$, i.e., the condition of resonance (2.1) is fulfilled in which $\psi = 0$ and $\sqrt{\varepsilon_0}$ is

$$\sqrt{\varepsilon_0} = \frac{\varepsilon_1^{\frac{1}{2}}\Delta z_1+\varepsilon_2^{\frac{1}{2}}\Delta z_2}{l} = 1-\frac{2\pi e^2}{m}N_{\text{eff}}, \tag{5.7}$$

$$N_{\text{eff}} = \frac{N_1+N_2\alpha}{1+\alpha}. \tag{5.8}$$

The sum of the thicknesses of two adjacent plates (the period of a stratified medium) is designated by l and their ratio by

$$\alpha = \frac{\Delta z_2}{\Delta z_1}. \tag{5.9}$$

The frequency interval for each order of radiation is given by eq. (2.6), with the condition (2.9). The angle of radiation of each order is determined by eqs. (2.11) and (2.12). The threshold energy for each harmonic is given by eq. (2.10). In all of the above formulae N_{eff} (5.8) should be understood by N. The case, mentioned by Frank [4]), of independent summation over different plates corresponds to resonance of a high order. If r is sufficiently large, then

$$\frac{\omega}{v}\left(1-\frac{v}{c}\sqrt{\varepsilon_0}\right) l \gg 1, \qquad (2.1')$$

i.e., the summation over r can be replaced by integration, or to put it more simply, $(\sin\frac{1}{2}n\beta/\sin\beta)^2$ in eq. (5.5) replaced by $\frac{1}{2}n$.

Substituting the $|I|^2$ thus found into eqs. (3.14) and (3.16) we shall obtain the angular distribution of radiation for the case when the inequality (2.1′) is fulfilled. The above condition is equivalent to one of the two inequalities: $\omega \gg \omega_{\max}$ or $\omega \ll \omega_{\min}$, where $\omega_{\max}$ and $\omega_{\min}$ are the maximum and minimum frequency of radiation for the first harmonic (see (2.6) at $r = 1$). As is clear from eq. (5.5) the quantity I will be small if

$$\omega \gg \sqrt{\frac{4\pi N_1 e^2}{m}} \frac{E}{mc^2} = \omega_0, \qquad N_1 > N_2,$$

i.e., the polarization of the medium will be essential provided $\omega \lesssim \omega_0$ (cf. ref.[1])). Thus for appreciable radiation in the frequency region $\omega \gg \omega_{\max}$ it is necessary to fulfil the inequality $\omega_{\max} \ll \omega_0$. From this inequality it directly follows that the energy of the particle should be considerably less than the threshold value for the first harmonic designated below by $(E/mc^2)_{1,\,\mathrm{tr}}$. Since in this case the radiation for harmonics with small r is forbidden and the radiation for high harmonics should, by virtue of the considerable overlapping of the respective frequency intervals, be summed, we arrive at the formula for the total number of quanta per unit path-length in the interval of frequencies $d\omega$. This formula is of the form (see the discussion in ref. [3])).

$$m = \frac{2}{137\pi l} \frac{d\omega}{\omega} \left[\ln \frac{2\pi N_1 e^2}{m\omega^2(1-v/c)} - 1 \right]. \tag{5.10′}$$

It should also be noted that energy losses up to the energies of the primary particle of the order of $(E/mc/)_{1,\,\mathrm{tr}}$ will grow linearly with the energy in accordance with eq. (5.10′). At higher energies the energy losses will be determined in practise by the first term of the series in eqs. (5.10) or (5.13) after multiplying by $\hbar\omega$. It can easily be seen that the losses emerge on to a plateau, i.e., cease to depend on the energy of the incident particle and come up to an insignificant quantity of the order 10^4 eV · cm²/gr in solid plates with an arbitrary period. Now let us turn to the general case.

Using the value of I found above, we can calculate by eq. (3.16) the flux of energy through the plane x, y at a larger distance from the layers. Let us integrate the result obtained over the angles of radiation. Then the final formula for the total number of quanta radiated by a relativistic particle of frequencies exceeding atomic frequencies per centimeter of stratified substance is

$$m = \frac{4p^2(1+\alpha)^2}{137l\pi} \sum_r \frac{1}{r} \int_{y_1}^{y_2} \frac{[y-A-y^2]}{(1-py)^2(1+p\alpha y)^2} \sin^2 \left[\frac{\alpha\pi r}{1+\alpha} - y\pi r \frac{\alpha p}{1+\alpha} \right] dy. \tag{5.10}$$

Here, we have

$$p = \frac{N_1 - N_2}{N_1 + N_2\alpha}. \tag{5.11}$$

The integration variable y is introduced according to eq. (4.10) and the integration limits over y are determined by the roots of the expression in the square brackets in the interval (5.10) and correspond to $\omega_{\min}$ and $\omega_{\max}$.

In building the radiation spectrum for each separate order it is more convenient to proceed from eq. (5.13) written in variables

$$\omega' = \frac{1}{yr} = \frac{\omega a}{rb}. \tag{5.12}$$

Note that the quantity rb/a (for energies considerably exceeding the threshold value (2.10)) is the lowest possible radiation frequency in the first harmonic

$$dm = \frac{4p^2(1+\alpha)^2}{137l\pi} \sum_r \frac{d\omega'}{r^3\omega'^3} \frac{\left[1-A\omega' r-\frac{1}{\omega' r}\right]}{\left(1-\frac{p}{\omega' r}\right)^2\left(1+\frac{p\alpha}{\omega' r}\right)^2} \sin^2\left[\frac{\alpha}{1+\alpha}\pi r-\frac{\pi\alpha p}{\omega'(1+\alpha)}\right]. \tag{5.13}$$

The spectrum for each harmonic will be described by a curve, the ordinate of which vanishes at $\omega' = \omega'_{\min} \approx 1/r$ and at $\omega' = \omega'_{\max} \approx a^2/br(1-v/c)$. The curve has a sharp maximum close to the left boundary of the spectrum. Let us adduce some numerical results for the total number of resonance quanta. Let $p \approx 1$ and α change from 1 to 10. The energies of the particles exceed the threshold value by a factor of $\sqrt{5}$ for the first order of radiation; or more strictly speaking, the parameter A (4.13) is selected equal to $A = 1/20r^2$. The quantity $m\Delta z_1 \times 10^3$ for different orders of r is listed in table 1. It will be noted that as the

TABLE 1

Numerical values of $m\Delta z_1 \times 10^3$

α \ r	1	2	3	4	5	10	20
1	1.94	2.34	1.89	1.57	1.35	0.86	0.54
2	2.51	1.96	1.62	1.26	1.09		
3	2.09	1.63	1.34	1.08	0.95		
4	2.24	1.47	1.15	0.95	0.81		
5	1.93	1.33	1.01	0.82	0.68		
6	1.63	1.19	0.88	0.74	0.61		
7	1.53	1.10	0.80	0.64	0.54		
8	1.44	1.02	0.74				
9	1.38	0.95	0.69				
10	1.33	0.91	0.66				

energy grows the total number of resonance quanta radiated at the first harmonic increases somewhat (≈ 40 %).

6. Concurrent Processes

6.1. "THERMAL" BACKGROUND

In this section we evaluate different effects modifying the conclusions given in the previous sections.

To begin with, let us consider the problem of the influence of accidental deviations from the ideal periodicity on the formulas of resonance radiation. This question is closely linked with a similar analysis of a thermal or diffuse background in the diffraction of X-rays. A similar study was also conducted in the investigation of interference radiation in a crystal [1]).

The analysis of accidental deviations will be exemplified for a heterogeneous medium considered in the previous section. We shall proceed from eq. (5.3). The quantities in (5.3) fluctuate about their average values owing to fluctuations in the thickness of the plates Δt_l. Since a heterogeneous medium indispensable for experiments must be created artificially, the question of the fluctuations reduces to that of the fluctuations in the thickness of different plates. In the case of a medium consisting of solid plates ($\frac{1}{2}n$ plates in all) located at a certain distance $\overline{\Delta z_2}$ from each other in gas, the fluctuations Δz_2 correspond to the inaccuracies in the spacing of plates and the fluctuations Δt_1 to the inaccuracies in the thickness of the plates themselves. Since we are dealing with the periodic medium in which all positions of identical plates are equivalent the fluctuations r_l should be equal for equivalent points. This can be written for example in the form

$$r_l = r_{l0} + (\omega - \kappa_l v)\xi_l, \tag{6.1}$$

or in the form

$$r_l = r_{l0} + (\omega - \kappa_1 v)\xi_{l1} + (\omega - \kappa_2 v)\xi_{l2}, \tag{6.2}$$

where the average square of accidental deviations is equal to $\overline{\xi_2^2}$ for even l and to $\overline{\xi_1^2}$ for odd l. The distribution of ξ_l is given by the Gaussian Law.

$$f_{1,2}(\xi_l)\mathrm{d}\xi_l = \frac{\mathrm{d}\xi_l}{\sqrt{\pi\overline{\xi_{1,2}^2}}} \exp\left(-\frac{\xi_l^2}{\overline{\xi_{1,2}^2}}\right). \tag{6.3}$$

By way of illustration let us consider a case when the deviation from the positions of equilibrium is determined by the condition (6.1). After averaging the modulus of the square of eq. (5.3) with the aid of eq. (6.3) we obtain in the conventional manner the following formula for the intensity of radiation in passing n boundaries:

$$S = \frac{e^2}{2\pi c}\theta^3 \mathrm{d}\theta \mathrm{d}\omega \left| \frac{1}{\varepsilon_1^{\frac{3}{4}}\left(1 - \frac{v}{c}\sqrt{\varepsilon_1}\cos\theta\right)} - \frac{1}{\varepsilon_2^{\frac{3}{4}}\left(1 - \frac{v}{c}\sqrt{\varepsilon_2}\cos\theta\right)} \right| (A_1 + A_2), \tag{6.4}$$

$$A_1 = n\left\{1-\tfrac{1}{2}\exp\left[-\frac{(\omega-\kappa_1 v)^2}{2}\overline{\xi_1^2}\right]-\tfrac{1}{2}\exp\left[-\frac{(\omega-\kappa_2 v)^2}{2}\overline{\xi_2^2}\right]\right\}, \quad (6.5)$$

$$A_2 = \frac{\sin^2\frac{1}{2}n\beta}{\sin^2\beta}\left[\exp\left[-\frac{(\omega-\kappa_2 v)^2}{2}\overline{\xi_2^2}\right]+\exp\left[-\frac{(\omega-\kappa_1 v)^2}{2}\overline{\xi_1^2}\right]\right.$$
$$\left.-2\cos(\omega-\kappa_1 v)\Delta t_1 \exp\left[-\frac{(\omega-\kappa_1 v)^2}{4}\overline{\xi_1^2}-\frac{(\omega-\kappa_2 v)^2}{4}\overline{\xi_2^2}\right]\right]. \quad (6.6)$$

The first term in (6.4) determines the "thermal background". The second term leads to resonance radiation formulas somewhat different from the formulae for the ideal heterogeneous medium. If

$$(\omega-\kappa_1 v)^2\overline{\xi_1^2} \ll 2, \qquad (\omega-\kappa_2 v)^2\overline{\xi_2^2} \ll 2, \quad (6.7)$$

the termal background goes to zero and the formulas do not differ from the case of radiation in the ideal medium. Otherwise the resonance term vanishes and the "amorphous" part only remains. It is not eworthy that the case (6.1) allows for the existence of resonance radiation even if one of the fluctuations is arbitrarily large, i.e., the conditions (6.7) are fulfilled only for one subscript.

6.2. INFLUENCE OF THE PLURAL SCATTERING PHOTOEFFECT AND OTHER EFFECTS

The formulae of sec. 3 are derived for particles whose velocity can change arbitrarily along the z-axis. This makes it possible to evaluate the error from the stopping of the particle and show that the stopping can be neglected provided the velocity of the particles change little over a length equal to the period of a medium.

The influence of the absorption of the quantum is considerably more essential. It can be readily seen that absorption must be negligible at distances of the order of the period of a medium, with the result that the resonance effects can be observed outside the optical region beginning from frequencies exceeding those of soft X-rays in the case of a hard plate. Since in this region of frequencies the absorption is caused chiefly by the photoeffect which depends strongly on the atomic number of the heterogeneous medium, the latter is better made of light substances, especially since the total number of resonance quanta produced per centimeter depends weakly on the density of the substances which enter eqs. (5.11), (5.10) and (5.13) through the quantity p.

Let us proceed to the consideration of the influence of multiple scattering on the resonance radiation. The angles typical of the radiation are given by eq. (2.11) and are of the order $\theta_1 \approx \sqrt{4\pi r\lambda/l}$. To neglect multiple scattering it is necessary that the angles of deviation of a particle at distances of the order

of the period should be considerably less than θ_1, i.e.,

$$\frac{E_s^2}{E^2}\frac{l}{L_{\text{eff}}} = \frac{E_s^2}{E^2}\left(\frac{\Delta z_1}{L_1} + \frac{\Delta z_2}{L_2}\right) \ll \frac{4\pi r\lambda}{l}. \tag{6.8}$$

Here $L_{1,2}$ is the electron radiation length in centimeters in the first and second media and

$$\frac{l}{L_{\text{eff}}} = \frac{\Delta z_1}{L_1} + \frac{\Delta z_2}{L_2}.$$

The condition (6.8) can be rewritten in the form

$$\omega \ll \left(\frac{E}{E_s}\right)^2 \frac{4\pi rc}{l^2} L_{\text{eff}} = \omega_s. \tag{6.9}$$

As has been repeatedly emphasised, the ratidation at each harmonic is strongly concentrated about the relevant $\omega_{\min}$ and therefore the scattering will have no essential effect on the results if $\omega_s \gg \omega_{\min}$. This leads to the condition on the energy of the particles

$$\frac{E}{mc^2} \gg \left(\frac{E}{mc^2}\right)_{\text{tr}} \sqrt{\frac{l}{L_{\text{eff}}}}\left(\frac{E_f}{mc^2}\right). \tag{6.10}$$

References

1) M. L. Ter-Mikaelyan, JETP **25** (1953) 296; Izv. Akad. Nauk SSSR, Ser. Fiz. **19** (1955) 657
2) E. L. Feinberg, Uspekhi Fiz. Nauk **58** (1956) 193
3) M. L. Ter-Mikaelyan, DAN SSSR **134** (1960) 318; JETP **39** (1960), 1693; Izv. Akad. Nauk of the Armenian SSR **14** (1961) (to be published)
4) V. L. Ginsburg and I. M. Frank (see Nobel lecture by I. M. Frank), Uspekhi Fiz. Nauk **18**, no. 3; **17**, no. 1
5) N. A. Khizhnyak and Ya. B. Feinberg, JETP **32** (1957) 4, 883
6) See for example, Grinberg, Selected questions of the mathematical theory of electric and magnetic fields (Gosudarstvennoye Tekhnitcheskoye Izdatelstvo, 1957)
7) V. I. Smirnov, Course of higher mathematics (Gostekhizdat, Moscow, 1957), Vol IV
8) G. N. Watson, Theory of Bessel functions (Izdatelstvo Inostrannoi Literaturi — Foreign Languages Publishing House — Moscow, 1949)
9) A. Ts. Amatuni and O. Korkhmazyan, Izv. Akad. Nauk of the Armenian SSR **13** (1960) 5
10) V. L. Ginsburg and V. Ya. Eidman, JETP **35** (1958) 1509

5

Nuclear Physics **24** (1961) 62—68; © *North-Holland Publishing Co., Amsterdam*

Not to be reproduced by photoprint or microfilm without written permission from the publisher

A SEARCH FOR PARITY-FORBIDDEN ALPHA-DECAY FROM THE 8.88 MeV (2^-) STATE IN O^{16}

W. KAUFMANN † and H. WÄFFLER

Nuclear Physics Division, Max-Planck-Institute for Chemistry (Otto-Hahn-Institut), Mainz, Germany

Received 2 January 1961

Abstract: The parity-forbidden alpha-decay of the O^{16} 8.88 MeV (2^-) state into $C^{12}+\alpha$ has been proved to be less frequent than the alpha-decay of the 9.58 (1^-) state by a factor $< 1.4\times10^{-6}$. From this experimental fact, an upper limit for the intensity F^2 of a possible opposite parity admixture to the 8.88 MeV state in O^{16} can be derived. It depends on the assumption made about Γ_α, the level width of a hypothetical 8.88 MeV (2^+) state in O^{16} and ranges between $F^2 \leqq 1.3\times10^{-12}$ to 1.3×10^{-11} according to $\Gamma_\alpha = 6$ keV to 0.6 keV.

1. Introduction

The self-interacting current hypothesis for weak interactions implies the occurrence of parity-forbidden transitions in nuclear processes [1]). As an example, in O^{16}, alpha-decay of the well-known "unnatural parity states" like 8.88 MeV (2^-), 10.94 MeV (0^-) and 11.07 MeV (3^+) should successfully compete with the E2, M1 and M2 gamma-cascades to the ground state (fig. 1) [2]). The frequency of those events nevertheless turns out to be extremely small: if F denotes the amplitude of the irregular (2^+) part of the O^{16} wave function describing the 8.88 MeV state, their probability is given by F^2 and takes, according to an order of magnitude estimate [1]), the value $F^2 \leqq 10^{-14}$.

Several attempts to observe parity-forbidden transitions, using different methods, have been reported [3–6]) ††. Upper limits only for F, ranging between 10^{-3} and about 10^{-5} ,could be given.

In the case of parity-forbidden alpha-decay, the allowed decay modes are radiative transitions which in general are slower than allowed alpha-decay by a factor of about 10^6. Such a strong inhibition for all modes of fast transitions from the state to be investigated is an indispensable condition for any experiment which aims to settle down the upper limit for F as far as possible. As far as the 8.88 MeV (2^-) state of O^{16} is concerned, the transition probability Γ_α could be evaluated from an experimentally observed alpha-decay rate. One then would obtain F^2 as the ratio

$$F^2 = \frac{\Gamma_{\alpha\,\mathrm{obs}}}{\Gamma_\alpha} = \frac{\Gamma_{\alpha\,\mathrm{obs}}}{\Gamma_{\mathrm{rad}}} \times \frac{\Gamma_{\mathrm{rad}}}{\Gamma_\alpha} \approx \frac{\Gamma_{\alpha\,\mathrm{obs}}}{\Gamma_{\mathrm{rad}}} \times 10^{-6}. \qquad (1)$$

† D 77, Mainz.

†† See ref. [5]) for further literature on this subject.

In this formula, $\Gamma_{\alpha\ \mathrm{obs}}$ denotes the level width, calculated from a really observed alpha-decay of the 8.88 MeV (2^-) state, whereas Γ_α belongs to the alpha-decay of a 8.88 MeV (2^+) state, corresponding to the irregular part of the wave function; Γ_α can be calculated from the single particle model, but the agreement with the experiment is rather poor. It seems preferable, therefore, to estimate it in a semi-empirical way. As it follows from eq. (1), the observation of an anomal alpha-decay rate of the 8.88 MeV state to one part in a million of other, normal alpha-decays of O^{16} would correspond to $F^2 = 10^{-12}$ by order of magnitude.

Unfortunately, since alpha-decaying levels are always broad, the tails of the normal alpha-groups may overlap the narrow parity-forbidden alpha-lines and

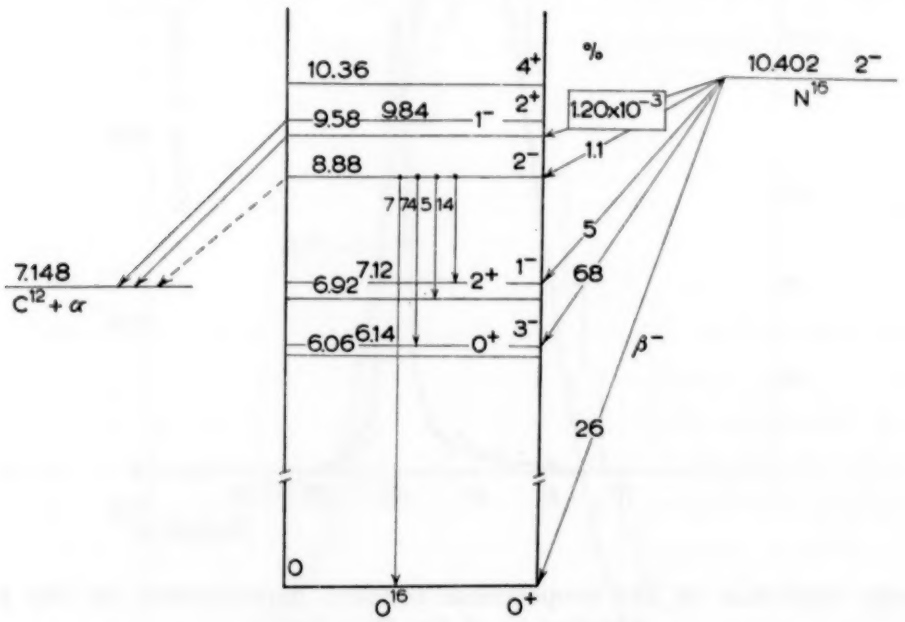

Fig. 1. Level scheme of O^{16} (taken from Ajzenberg and Lauritsen [2]). The framed number refers to the branching ratio measured in the present investigation.

thereby mask any effect. This is just the case for the 8.88 MeV state in O^{16}. The neighbouring 9.58 (1^-) state (fig. 1) decays by alpha-emission and is very broad, $\Gamma_\alpha = 650$ keV. On the other hand, if O^{16} is formed from the negaton-emitter N^{16} (half-life $T_{\frac{1}{2}} = 7.5$ s), the beta-decay branching to the 9.58 MeV state must be small, since it has not been observed up to now. If therefore N^{16} is produced by some kind of nuclear reaction, in radioactive equilibrium, the number of 9.58 MeV states formed per unit time is small compared to the corresponding number of 8.88 MeV states. This fact leaves a chance for an observation of the hypothetical, parity-forbidden alpha-decay.

2. Experimental Arrangement

The isotope N^{16} was produced by the reaction O^{16}(n, p)N^{16}. Commercially pure liquid CO_2 was irradiated with neutrons from 300 keV deuterons on tritium

(thick target). The continuously irradiated CO_2 expanded through a heated valve and a 6 m long, narrow copper tube into a proportional counter of 1 l counting volume. The gas flowed continuously through the counter, leaving it at atmospheric pressure.

The counter was made of brass with 8 cm inner diameter, 0.1 mm tungsten wire as anode and fitted with guard rings as described by Cockroft and Curran [7]). It worked at a voltage of 3200 V, corresponding to gas multiplication $M = 13$. Since with pure CO_2, the rise-time of the pulse generated in the counter shows appreciable variations (5 to 15 μs), a pulse integrating interstage RC coupling

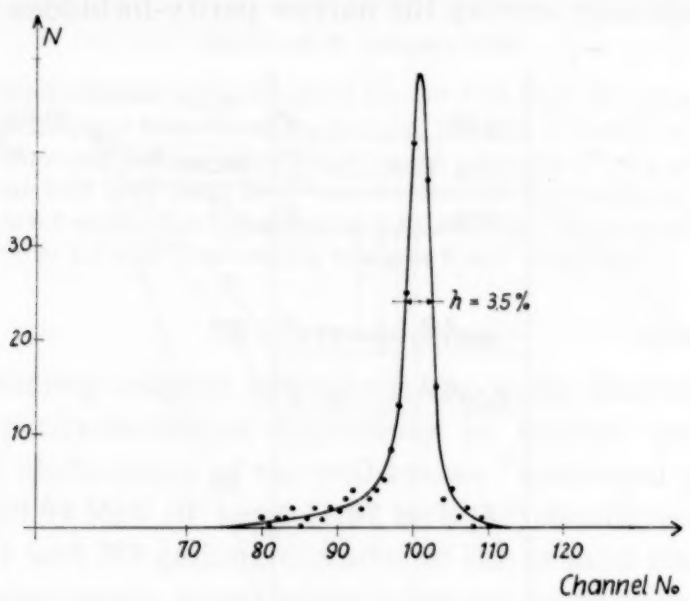

Fig. 2. Energy resolution of the proportional counter, demonstrated by the pulse-height distribution of the Po-α line.

of 17 μs time constant was introduced between cathode follower and first amplifier stage. The clipping time constant of the amplifier was kept correspondingly large (50 μs). A Sunvic 100-channel pulse-height analyzer was used in connection with the linear amplifier. Fig. 2 shows the pulse-height distribution from a thin layer of Po–α smeared on the inner surface of the counter wall.

Behind the proportional counter, the radioactive gas was allowed to stream around a thin-walled (0.1 mm Al) GM-tube. This tube counted the β^--particles from N^{16} and served as a monitor for the total decay rate. By comparing the number of alpha-particles (from the 9.58 MeV state) in the proportional counter with the beta-counts in the GM-tube, and after applying appropriate corrections, the branching-ratio of the beta-decay from N^{16} to the 9.58 MeV state in O^{16} could be calculated.

3. Results

The block-diagram in fig. 3 shows the pulse-height distribution of 50100

events, belonging to the decay of the O^{16}, 9.58 MeV state into $C^{12}+\alpha$ (background subtracted). It corresponds to 50 h of total measuring time. For a comparison of this spectrum with the Breit-Wigner one-level dispersion formula, several corrections have to be applied, namely, (i) wall-effects from the counter-tube, (ii) systematic coincidences between beta-particles and $(C^{12}+\alpha)$-decays,

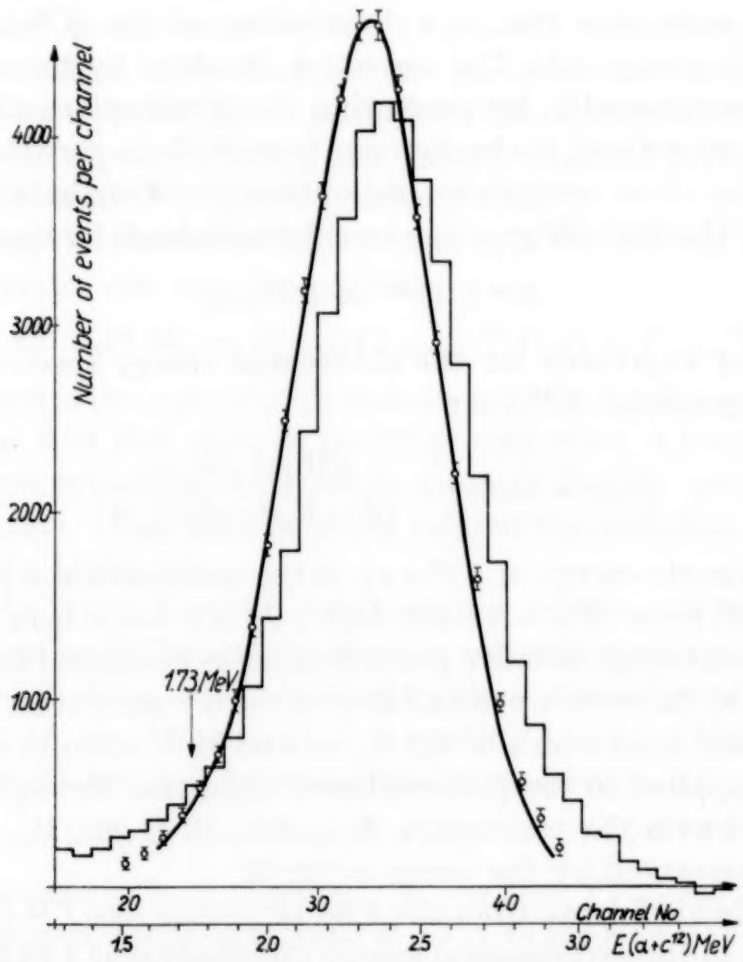

Fig. 3. Results of the experiment. Block-diagram: pulse-height distribution as measured from decay of N^{16}. Points: the same distribution, corrected as described in sec. 3. Full line: Breit-Wigner formula adapted to the two-step transition $N^{16} \rightarrow O^{16*}(9.58) \rightarrow C^{12}+\alpha$.

belonging to the same decay

$$N^{16} \xrightarrow{\beta^-} O^{16*} \rightarrow (C^{12}+\alpha)$$

and (iii) accidental coincidences between betas and $(C^{12}+\alpha)$:

(i) The total fraction of events undergoing energy diminution by wall effects and needing an appropriate correction is 12 %.

(ii) The maximum energy which a beta particle of minimum ionization can leave in the counter is 100 keV. This contribution involves a 50 keV shift in energy of the $(C^{12}+\alpha)$-spectrum.

(iii) The number of uncorrelated betas is 3×10^4/s. Since each of them generates a pulse of about 100 μs duration, the superposition of these pulses produces a small, nearly constant voltage at the coupling capacity to the amplifier input. The contribution of the ac-component of this voltage to the pulse-height spectrum can be neglected. The same is not true for the much less frequent accidental coincidences between one alpha and two, three or more betas. These events give rise to a broadening of the $(C^{12}+\alpha)$-distribution against the high-energy side. The correction involved by this effect has been determined experimentally, by comparing the distributions obtained for the Po–α line with and without the background from N^{16} beta-particles, respectively.

After applying these corrections, one obtains the distribution given by the points in fig. 3. The Breit-Wigner one-level formula leads for the two-step decay

$$N^{16} \overset{\beta^-}{\rightarrow} O^{16*} \rightarrow (C^{12}+\alpha)$$

to the following expression for the differential energy spectrum $N(\varepsilon)$ of the disintegration products $(C^{12}+\alpha)$:

$$N(\varepsilon) = \text{const} \times \frac{f(W_\beta)T_l(R,\varepsilon)}{(E-E_r)^2+(\frac{1}{2}\Gamma_{tot})^2}. \qquad (2)$$

Here, ε is the kinetic energy of $(C^{12}+\alpha)$, R the interparticle separation $C^{12}-\alpha$, E the 7.148 MeV$+\varepsilon$, $W_\beta = 10.402$ MeV$-E$ the total beta decay energy, $f(W_\beta)$ the beta-decay probability per unit time, as computed by Feenberg and Trigg [8]), $T_l(R,\varepsilon)$ the barrier penetrability of the C^{12} nucleus for alphas ($l = 1$), and Γ_{tot} the total level width of the $E_r = 9.58$ MeV state in O^{16}.
This formula, applied to the parity-allowed transition through the 9.58 MeV level and fitted with the parameters $R = 4.6\times10^{-13}$ cm, $\Gamma_{tot} = 0.65$ MeV is graphically represented by the curve in fig. 3.

A parity-forbidden decay from the 8.88 (2^-) state into $C^{12}+\alpha$ should mark itself as a peak in the experimental energy distribution at 1.73 MeV, as indicated by the arrow in fig. 3. As a more sensible test, a surplus over the theoretical curve, which is computed for a pure $9.58(1^-) \rightarrow (C^{12}+\alpha)$ decay, should be recognizable in this energy region. But as fig. 3 shows, the agreement between the experimental points and the curve is nearly perfect. Therefore, from this result, only an upper limit for a parity-violating process can be deduced.

The branching ratio for beta-decay to the 9.58 MeV level of O^{16} can be calculated from the effective counting volumes of the proportional counter ($V_P = 1010$ cm^3) and the GM-counter arrangement ($V_{GM} = 1.89$ cm^3). The volume of radioactive CO_2, entering the proportional counter at atmospheric pressure is $v = 0.15$ l/s.

In radioactive equilibrium, the counting ratio of GM-counter (betas) and proportional counter $(C^{12}+\alpha)$ is 156. The half-life of N^{16}, measured in our arrangement, came out as $T_{\frac{1}{2}} = 7.5\pm0.5$ s. With these figures one obtains for

the branchig ratio η and its mean error (n = number of decays per unit time) †

$$\eta = \frac{n_\beta(9.58)}{n_\beta(\text{total})} = (1.20 \pm 0.05) \times 10^{-5}.$$

4. Discussion

Our experiment, as illustrated by fig. 3, measures the ratio $n_\alpha(8.88)/n_\alpha(9.58)$ of the parity-forbidden alpha-decay to the parity-allowed one. No indication of a finite value for n_α (8.88) can be taken from the experiment, but nevertheless an upper limit for F^2, the intensity of a possible opposite parity admixture to the 8.88 MeV-state in O^{16}, may be deduced from it.

By introducing the number of beta-decays $n_\beta(8.88)$, leading from N^{16} to the O^{16} 8.88 MeV-state, one has the relation

$$n_\alpha(8.88)/n_\beta(8.88) = \Gamma_{\alpha\,\text{obs}}/(\Gamma_{\alpha\,\text{obs}} + \sum \Gamma_{\text{rad}}) \approx \Gamma_{\alpha\,\text{obs}}/\sum \Gamma_{\text{rad}}. \qquad (3)$$

Here, $\sum \Gamma_{\text{rad}}$ denotes the sum over all radiative widths for the gamma-cascades, leading from the 8.88 MeV state to the O^{16} ground state. A fraction amounting to 74 % of these transitions proceed to the 6.13 MeV 3^- state, by M1+E2 multipole radiation. The E2/M1 intensity ratio of this radiation has the experimental value 2 ± 1 (ref. [9])).

Most probable values for multipole radiation widths can be taken from a compilation given by Wilkinson [10]). Since in self-conjugate nuclei like O^{16}, the M1 transitions with $\Delta T = 0$ are inhibited by about two orders of magnitude [11]), one has to rely on the E2 transition. Assuming a most probable value of 2 Weisskopf units [12]) for this E2 transition, one obtains

$$\Gamma(\text{E2}) = 2 \times 1.2 \times 10^{-7} A^{\frac{4}{3}} E_\gamma^{\,5} = 1.5 \times 10^{-3}\ \text{eV}. \qquad (4)$$

Here, E_γ is measured in MeV. From eq. (4) one gets $\sum \Gamma_{\text{rad}} = 3 \times 10^{-3}$ eV. Now using the well-known [2]) beta-branching of 1.1 % to the 8.88 MeV state, together with the value $\eta = 1.20 \times 10^{-5}$ for the branching to the 9.58 MeV state, as given in section 3, one obtains from relation (3)

$$\Gamma_{\alpha\,\text{obs}}/\sum \Gamma_{\text{rad}} = n_\alpha(8.88)/n_\beta(9.58 \times \frac{1.20}{1.1} \times 10^{-3}$$

$$\approx n_\alpha(8.88)/n_\alpha(9.58) \times \frac{1.20}{1.1} \times 10^{-3}. \qquad (5)$$

An upper limit for this ratio can be deduced from fig. 3. Owing to the finite energy resolution of the counter equipment, by taking into account all broadening effects as discussed in section 3, the hypothetical narrow ($C^{12}+\alpha$)-line from the 8.88 MeV (2^-) state should appear in channels 23 and 24. From fig. 3,

† After completion of this work, we have been informed by Dr. Stevens (California Institute of Technology, Pasadena) that he has got quite the same value for this branching ratio. We are very indebted to Dr. Stevens for his communication.

one gets for the ratio $n_\alpha(8.88)/n_\alpha(9.58) = 0 \pm \delta/50100$ (δ is the mean standard deviation for channels 23 and 24).

From the 3930 events (effects plus background) registered in channels 23 and 24 one gets $\delta \approx 63$.

Since 1.1 % of the beta-decays from N^{16} proceed to the 8.88 MeV state, whereas 1.2×10^{-3} % only are going into the 9.58 MeV state, the parity-forbidden alpha-decay of the 8.88 MeV (2^-) state has a probalility smaller than the analogous decay of the 9.58 MeV (1^-) state by a factor $63/50100 \times (1.2/1.1) \times 10^{-3} = 1.37 \times 10^{-6}$. By taking 2δ as the error limit, one obtains from expression (5)

$$\Gamma_{\alpha\,\mathrm{obs}}/\sum\Gamma_{\mathrm{rad}} = \frac{126}{50100} \times \frac{1.2}{1.1} \times 10^{-3} = 2.74 \times 10^{-6}. \qquad (5a)$$

For calculating F^2 according to expression (1), one needs a numerical estimate for Γ_α, the decay probability of a hypothetical 8.88 MeV (2^+) state into ($C^{12}+\alpha$).

From the level systematics of light nuclei ($A \leqq 20$), one knows the reduced alpha-widths to range between about 0.01 and 1 single particle units [4]). There is one single exception, namely the 9.84 MeV (2^+) level in O^{16}, which has the extremely narrow reduced width of 0.0013 single-particle units, as follows from the measured value $\Gamma_\alpha(9.84) = 0.8$ keV. By making allowance for the fact, that the majority of the level widths observed in light nuclei is concentrated in the region of 0.1 single-particle units with a factor of about 3 either way, it seems reasonable to assume for Γ_α values corresponding to the range of 0.03 to 0.3 single-particle units. From these limiting values one easily calculates $0.6 \leqq \Gamma_\alpha \leqq 6$ keV. With these numbers, the following upper limit for F^2 is obtained:

$$F^2 \leqq 1.3 \times 10^{-11} \quad \text{to} \quad 1.3 \times 10^{-12}.$$

In concluding one must remark, that in the best case this experimental upper limit is higher by about an order of magnitude than the value to be expected according to Blin-Stoyle [1]).

References

1) R. J. Blin-Stoyle, Phys. Rev. **118** (1960) 1605
2) F. Ajzenberg-Selove and T. Lauritsen, Nuclear Physics **11** (1959) 1
3) N. Tanner, Phys. Rev. **107** (1957) 1203
4) D. H. Wilkinson, Phys. Rev. **109** (1958) 1603
5) F. Boehm and U. Hauser, Nuclear Physics **14** (1959) 615
6) Th. Mayer-Kuckuk and S. A. A. Zaidi, Zs. f. Phys. **159** (1960) 369
7) A. L. Cockroft and S. C. Curran, Rev. Sc. Instr. **22** (1951) 37
8) E. Feenberg and G. Trigg, Rev. Mod. Phys. **22** (1950) 400
9) J. A. Kuehner, A. E. Litherland, E. Almqvist, D. A. Bromley and H. E. Gove, Phys. Rev. **114** (1959) 775
10) D. H. Wilkinson, Phil. Mag. **1** (1956) 127
11) G. Morpurgo, Phys. Rev. **110** (1958) 721
12) V. F. Weisskopf, Phys. Rev. **83** (1951) 1073

1.D.4

Nuclear Physics **24** (1961) 69—83; © *North-Holland Publishing Co., Amsterdam*

Not to be reproduced by photoprint or microfilm without written permission from the publisher

RESIDUAL INTERACTION AND THE DEFORMATION OF NUCLEI

AKITO ARIMA †

Argonne National Laboratory, Argonne, Illinois ††

Received 4 November 1960

Abstract: The influence of short-range (delta-function) two-body interactions on the equilibrium deformation of nuclei at the beginning of the (2s—1d) shell has been studied. The moment of inertia, the equilibrium deformation, and the energy of β vibrations, have been calculated as a function of the strength of the interaction.

1. Introduction

Recently the collective model of the nucleus has succeeded in explaining many properties of nuclei, even in light nuclei for which the individual-particle model is a good approximation †††. In the p-shell nuclei, Kurath and Pičman have compared the wave functions derived by the intermediate-coupling shell model with the wave functions of the generator coordinate method [2]). They have found very good agreement. In the (2s—1d) shell, the spectrum of F^{19} can be understood by way of both the configuration mixing model [3]) and the collective model [4]). Many properties of the (2s—1d) shell nuclei have been successfully explained by the Nilsson model [5, 6]).

It we assume the single-particle model, in which every nucleon moves in a deformed well, the intrinsic energy given by the sum of the single-particle energies has a minimum at a finite deformation except in the case of the closed shell. Experimentally, nuclei near the magic numbers are spherical. Furthermore, the moment of inertia given by the cranking model is equal to that of a rigid body [7]), which is two to three times as large as the observed values [8]). These difficulties were removed by Bohr and Mottelson [9]) and Moszkowski [10]), who introduced the short-range residual interaction and found that this interaction reduced the equilibrium deformation from that given by the simple deformed-well model, and enough strong interaction makes nuclei spherical. The moment of inertia is also reduced considerably to be comparable with the observed value.

The eminent success of the theory of superconductivity [11]) has stimulated the application of the same ideas to nuclear structure [12]). On this line, Belyaev

† On leave of absence from the Institute for Nuclear Study, University of Tokyo. Permanent address after January, 1961: Department of Physics, University of Tokyo, Tokyo, Japan.

†† Work performed under the auspices of the U. S. Atomic Energy Commission.

††† The extensive literature about the collective model is cited in ref. [1]).

has discussed the effect of pairing correlations on the collective behavior of nuclei [13]). Kisslinger and Sorensen have calculated the many properties of spherical nuclei with a single closed shell by using a pairing force and a quadrupole-quadrupole interaction [14]). The energy gap can be obtained as the result of the pairing correlations and must play the important role in understanding the mechanism of nuclear structure. These theories are based on the new method used to explain superconductivity, and unfortunately the total number of nucleons is not conserved [13, 14]). The influence of the pairing force on the collective vibrations is studied by use of a perturbation expansion by Kerman [15]).

In this paper, the influence of the short-range interaction on the collective deformation is studied in the beginning of the (2s—1d) shell. However, the elegance of the above reterences is lost, because the large energy matrix should be numerically solved.

First, the single-particle approximation is adopted. Here every nucleon has the axially-symmetric deformed oscillator well, the volume of which is conserved. The short-range (δ-function) interaction is introduced only between the nucleons outside closed shells. The spin-orbit interaction is neglected. The secular equations are solved among the states which have the same shell model energies in the spherical case. This process yields the eigen-energies of the Hamiltonian which consists of the deformed-well shell-model Hamiltonian and the short-rang interactions. However, in order to know the intrinsic energy, half the sum of the deformed-shell-model potentials should be subtracted, because two-particle interactions which are replaced by the shell-model potentials should not be counted twice. The expectation values of this effective intrinsic Hamiltonian can be calculated and minimized as functions of the deformation. This equilibrium deformation is a function of the strength of the residual interaction. The greater the strength, the smaller the equilibrium deformation and enough strength suddenly gives spherical shape to nuclei. The moment of inertia is reduced by the residual interactions in two ways. The first is to increase the energy denominators of the Inglis formula [7]), and the second is to change the wave functions induced by the residual interaction.

The intensity of the short-range interaction can be estimated from the pairing energy of O^{18} by assuming that O^{17} and O^{18} are spherical and two neutrons in O^{18} are in the $1d_{\frac{5}{2}}$-shell. This intensity is not enough to make O^{19} and Ne^{20} be spherical, but O^{18} can be made spherical by an interaction only a little stronger than this. Therefore it can be said that O^{18} may be spherical, but O^{19} and Ne^{20} are already deformed. The moment of inertia is calculated in those nuclei, and the result for Ne^{20} is roughly in agreement with the experiment [16]). The properties of O^{18} can be understood by configuration mixing [3]), but the theoretical positions of the first 4^+ and the second 0^+ states are too low. The ratio of these excitation energies to the energy of the first excited state is about 2. Therefore,

it is interesting to calculate the vibrational energy as a function of the strength of the residual interaction. This vibrational energy has a minimum at the strength of interaction which changes nuclear shape from deformed to spherical. Around this minimum, the vibration energy of O^{18} is small and comparable to the first excitation energy. This calculation explains that the β vibrational energy is high in the vicinity of closed shells and becomes lower in the vibrational region and again goes up to higher values in the deformed region.

2. Intrinsic Hamiltonian

We assume that every nucleon moves in the deformed harmonic oscillator well, which is axially symmetric and has a fixed volume. The residual interaction is introduced among the nucleons outside the closed shell. The Hamiltonian of such a system is

$$H = H_0 + H', \tag{1}$$

$$H_0 = \sum_i \left[\frac{\hbar^2}{2m} \mathbf{p}_i^2 + \tfrac{1}{2} m\omega_0^2 \{ e^{2\alpha}(x_i^2 + y_i^2) + e^{-4\alpha} z_i^2 \} \right], \tag{2}$$

and

$$H' = \sum_{i>j}{}' V_{ij}, \tag{3}$$

where a prime restricts the summation to the outside particles, and the deformation parameter α is related to the usual parameter β by

$$\alpha = \tfrac{1}{4} \left(\frac{5}{\pi} \right)^{\frac{1}{2}} \beta = 0.316\beta. \tag{4}$$

The single-particle wave function is written as [17])

$$|n\lambda k\rangle = R_{n|\lambda|}(r) \frac{1}{\sqrt{2\pi}} \exp i\lambda\phi u_k(z), \tag{5}$$

$$R_{n|\lambda|}(r) = \frac{1}{|\lambda|!} \left(\frac{2\omega_1 m}{\hbar} \frac{(n+|\lambda|)!}{n!} \right)^{\frac{1}{2}} \sum_{i=0}^{n} (-1)^i \frac{|\lambda|!}{(i+|\lambda|)!} {}_nC_i \left(\frac{m\omega_1}{\hbar} r^2 \right)^{i+\frac{1}{2}|\lambda|} \tag{6}$$

and

$$u_k(z) = \left(\frac{m\omega_3}{\pi\hbar} \right)^{\frac{1}{4}} (2^k k!)^{-\frac{1}{2}} H_k \left(\sqrt{\frac{m\omega_3}{\hbar}}\, z \right) \exp\left(-\tfrac{1}{2} \frac{m\omega_3}{\hbar} z^2 \right), \tag{7}$$

where $\omega_1 = \omega_0 e^{\alpha}$, $\omega_3 = \omega_0 e^{-2\alpha}$, λ is the z component of the angular momentum, and (r, θ, z) are the cylindrical coordinates. The single-particle energy is

$$E_{n\lambda k} = (2n + |\lambda| + 1)\hbar\omega_1 + (k + \tfrac{1}{2})\hbar\omega_3. \tag{8}$$

The wave function of H_0 can be given as the Slater determinants. The eigen-

function of H is a linear combination of the eigenfunctions of H_0. The total sum (Λ) of λ, the total spin S, and the total isobaric spin T are good quantum numbers, provided that V_{ij} is a central force. Only the states with $S=0$, $T=1$ in O^{18} and with $S=T=0$ in Ne^{20} are considered. By the attractive interaction, the most symmetric states in the ordinary space are most depressed energetically, and this symmetry is conserved in H. We take the linear combinations of the Slater determinants to be the most symmetric in space, the spin singlet and the isobaric spin triplet in O^{18} and singlet in Ne^{20}. For example, the lowest state of H_0 for Ne^{20} is expressed by

$$\psi_0 = \frac{1}{\sqrt{4!}} \begin{vmatrix} |002\rangle_1\alpha_1\pi_1 & |002\rangle_1\beta_1\pi_1 & |002\rangle_1\alpha_1\nu_1 & |002\rangle_1\beta_1\nu_1 \\ |002\rangle_2\alpha_2\pi_2 & |002\rangle_2\beta_2\pi_2 & |002\rangle_2\alpha_2\nu_2 & |002\rangle_2\beta_2\nu_2 \\ |002\rangle_3\alpha_3\pi_3 & |002\rangle_3\beta_3\pi_3 & |002\rangle_3\alpha_3\nu_3 & |002\rangle_3\beta_3\nu_3 \\ |002\rangle_4\alpha_4\pi_4 & |002\rangle_4\beta_4\pi_4 & |002\rangle_4\alpha_4\nu_4 & |002\rangle_4\beta_4\nu_4 \end{vmatrix}$$

$$= |002\rangle_1|002\rangle_2|002\rangle_3|002\rangle_4 \frac{1}{\sqrt{4!}} \begin{vmatrix} \alpha_1\pi_1 & \beta_1\pi_1 & \alpha_1\nu_1 & \beta_1\nu_1 \\ \alpha_2\pi_2 & \beta_2\pi_2 & \alpha_2\nu_2 & \beta_2\nu_2 \\ \alpha_3\pi_3 & \beta_3\pi_3 & \alpha_3\nu_3 & \beta_3\nu_3 \\ \alpha_4\pi_4 & \beta_4\pi_4 & \alpha_4\nu_4 & \beta_4\nu_4 \end{vmatrix},$$

which is already the most symmetric and $S=0$, $T=0$. Generally the most symmetric wave functions having $S=0$ and $T=0$ are written as

$$\psi_n = \frac{1}{\sqrt{N}} \sum_{\mathrm{P}} \mathrm{P}|n_1\lambda_1 k_1\rangle_i|n_2\lambda_2 k_2\rangle_j|n_3\lambda_3 k_3\rangle_k|n_4\lambda_4 k_4\rangle_l \frac{1}{\sqrt{4!}} \begin{vmatrix} \alpha_1\pi_1 & \beta_1\pi_1 & \alpha_1\nu_1 & \beta_1\nu_1 \\ \alpha_2\pi_2 & \beta_2\pi_2 & \alpha_2\nu_2 & \beta_2\nu_2 \\ \alpha_3\pi_3 & \beta_3\pi_3 & \alpha_3\nu_3 & \beta_3\nu_3 \\ \alpha_4\pi_4 & \beta_4\pi_4 & \alpha_4\nu_4 & \beta_4\nu_4 \end{vmatrix}, \quad (9)$$

TABLE 1

Matrix element of the delta-function interaction. The matrix element $\frac{1}{2}\pi^{-1}\int R_{n_1|\lambda_1|}R_{n_2|\lambda_2|}R_{n_3|\lambda|_3}R_{n_4|\lambda_4|} \times \mathrm{d}r \int u_{k_1}u_{k_2}u_{k_3}u_{k_2}\mathrm{d}z$ is tabulated in the unit of $V_0 I$, where $I = \frac{1}{2}\pi^{-1}\int R_{00}^4 \mathrm{d}r \int u_0^4 \mathrm{d}z$. This matrix element is independent of the ordering of $(n_1\lambda_1 k_1)$. Therefore in the first column $(n_1\lambda_1 k_1)(n_2\lambda_2 k_2)(n'_1\lambda'_1 k'_1)(n'_2\lambda'_2 k'_2)$ is shown as the configuration.

Configuration	Matrix element	Configuration	Matrix element
$(100)^4$	$\frac{1}{2}$	$(100)\ (002)^3$	$\frac{1}{64}\sqrt{2}$
$(100)^3\ (002)$	$-\sqrt{\frac{1}{16}}$	$(020)^4$	$\frac{3}{8}$
$(100)^2\ (020)^2$	$\frac{1}{4}$	$(020)^2\ (011)^2$	$\frac{3}{16}$
$(100)^2\ (011)^2$	$\frac{1}{8}$	$(020)^2\ (002)^2$	$\frac{3}{32}$
$(100)^2\ (002)^2$	$\frac{3}{16}$	$(020)\ (011)^2\ (002)$	$\frac{1}{16}$
$(100)\ (020)^2\ (002)$	$\frac{1}{32}\sqrt{2}$	$(011)^4$	$\frac{3}{8}$
$(100)\ (011)^2\ (002)$	0	$(011)^2\ (002)^2$	$\frac{7}{32}$
$(100)\ (020)\ (011)^2$	$-\frac{1}{16}\sqrt{2}$	$(002)^4$	$\frac{41}{64}$

where P is the permutation operator and N is the number of permutations. Here, the wave function of the closed shell is abbreviated. In this paper, for simplicity, every single-particle state outside the closed shell is restricted by the relation

$$2n+|\lambda|+k = 2, \tag{10}$$

and we neglect the influence of the higher configuration mixing induced by H'. The delta function is assumed as for the residual interaction, and

$$V_{ij} = -V_0\delta(\mathbf{r}_i-\mathbf{r}_j). \tag{11}$$

The two-body matrix elements are given in table 1. The unit of these matrix elements is $V_0 I$, where

$$I = (m\omega_0/2\pi\hbar)^{\frac{3}{2}}.$$

The ratio $x = V_0 I/\hbar\omega_0$ is introduced to measure the strength of the residual interaction.

The eigenfunction u_n of H is a linear combination of ψ_i,

$$u_n = \sum_i c_{ni}\psi_i. \tag{12}$$

This u_n satisfies the equation

$$Hu_n = E_n(\alpha)u_n,$$

where $E_n(\alpha)$ is the eigenvalue. This $E_n(\alpha)$, however, is not the total intrinsic energy, because the two-body interactions which are approximated by the deformed average potential are counted twice. The effective Hamiltonian for the intrinsic motion is approximated by

$$\mathscr{H} = H-\tfrac{1}{2}\sum\tfrac{1}{2}m\omega_0{}^2\{e^{2\alpha}(x_i{}^2+y_i{}^2)+e^{-4\alpha}z_i{}^2\}. \tag{13}$$

The wave function u_n is no longer the eigenfunction of $\mathscr{H}$. However, we neglect the nondiagonal elements †, and therefore the intrinsic energy is given by the expectation value of $\mathscr{H}$,

$$\langle u_n|\mathscr{H}|u_n\rangle = \varepsilon_n(\alpha).$$

Here $\varepsilon_n(\alpha)$ includes the energy of the closed shells.

Without the residual interaction, $\varepsilon_0(\alpha)$ has minimum at a finite value of α. This minimum point moves towards smaller α as the interaction x increases. Two minima appear in a certain range of x. One of them is at $\alpha = 0$, and the other is at a finite α. The energies at these two minima are equal for some strength x_c. Beyond this strength x_c, the nucleus becomes suddenly spherical. This tendency can be seen in fig. 1.

† Recently it has been shown that the equilibrium deformation is unaltered in second and third order and that the fourth-order modification arising from the nondiagonal elements is very small. See ref. [18]).

The derivatives of $\varepsilon_0(\alpha)$ can be obtained by the equations

$$\frac{dE_0}{d\alpha} = \left\langle u_0 \left| \frac{\partial H}{\partial \alpha} \right| u_0 \right\rangle \tag{14}$$

and

$$\frac{d^2E_0}{d\alpha^2} = \left\langle u_0 \left| \frac{\partial^2 H}{\partial \alpha^2} \right| u_0 \right\rangle - 2\sum \frac{\left| \left\langle u_0 \left| \frac{\partial H}{\partial \alpha} \right| u_n \right\rangle \right|^2}{|E_0 - E_n|}. \tag{15}$$

These quantities can be calculated by using the eigenvectors $u_n(\alpha)$. In order

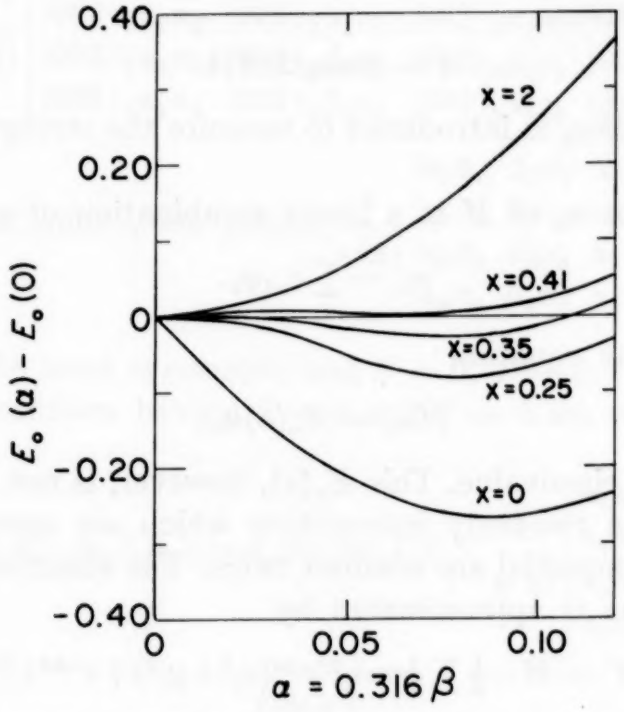

Fig. 1. Intrinsic energy curve $\varepsilon_0(\alpha)$. The expectation values of $\mathscr{H}$ in the lowest intrinsic state in O^{18} for several different values of x are shown as a function of the deformation parameter. Here $x = V_0 I/\hbar\omega_0$. Without the residual interaction, i.e., for $(x = 0)$, $\varepsilon_0(\alpha)$ has a minimum at a finite value of α. The stronger x, the smaller will be α_{eq}. For sufficiently strong x, $\varepsilon_0(\alpha)$ is lowest at $\alpha = 0$, and in this case the nucleus is spherical.

to know the derivatives of $\varepsilon_0(\alpha)$, the derivatives of

$$-\tfrac{1}{4}m\omega_0{}^2\langle u_0|\sum\{e^{2\alpha}(x_i{}^2+y_i{}^2)+e^{-4\alpha}z_i{}^2\}|u_0\rangle \tag{16}$$

should be calculated. For this purpose, this expectation value is calculated at the many values of α, and the derivatives are approximately estimated. Since the ground states are S-states for even-even nuclei at the origin of α, and since $\partial H/\partial\alpha$ is proportional to $\sum r_i{}^2 Y_{20}(\theta_i, \phi_i)$, the first derivative $dE(\alpha)/d\alpha$ should vanish at $\alpha = 0$. By the same kind of reasoning, the first derivative of the quantity (16) also vanishes at the origin of α. This means that the intrinsic

energy $\varepsilon_0(\alpha)$ of the ground state in the even-even nucleus has no linear dependence on α in the vicinity of $\alpha = 0$. This is not generally true in the case of the intrinsic excited states nor in the odd nuclei. The second derivative $d^2\varepsilon_0/d\alpha^2$ gives the restoring force of the β vibration. We define

$$C(\alpha) = \frac{d^2\varepsilon_0}{d\alpha^2}. \tag{17}$$

As long as C is negative at the origin of α, the nucleus cannot be spherical, because $\varepsilon_0(\alpha)$ has a maximum at $\alpha = 0$. If C is positive but small, there is another minimum at finite α which can be lower than the minimum at $\alpha = 0$. It is a very interesting problem to obtain the strength x_c for which the energy $\varepsilon_0(\alpha)$ is lowest at $\alpha = 0$ and the nucleus is to be spherical. Generally this is difficult, but it should be noticed that this x_c is close to that which makes $C = 0$. Therefore practically we can say that the condition for the existence of deformed nuclei is $C < 0$. The strength x_0 satisfying $C = 0$ rather easily found. In our cases,

$$x_0 = 0.36 \quad \text{and} \quad x_c = 0.42, \quad \text{for} \quad O^{18},$$

and

$$x_0 = 1.06 \quad \text{and} \quad x_c = 1.16 \quad \text{for} \quad Ne^{20}.$$

The strength x can be estimated from the pairing energy of O^{18}. We assume that O^{18} is spherical and two neutrons outside the closed shell are in the $1d_{\frac{5}{2}}$ shell. The pairing energy P, which can be obtained from the binding energies B of O^{16}, O^{17} and O^{18} is

$$P = B(O^{18}) + B(O^{16}) - 2B(O^{17}) = 3.93 \text{ MeV}. \tag{18}$$

This P is written in terms of a two-particle energy matrix for the residual interaction,

$$P = -\langle 1d_{\frac{5}{2}}^2 0 | V | 1d_{\frac{5}{2}}^2 0 \rangle = 0.789\, V_0 I. \tag{19}$$

Comparing this with (18), one obtains

$$V_0 I = 4.98 \text{ MeV}.$$

The harmonic oscillator spacing is roughly

$$\hbar\omega_0 = 41/A^{\frac{1}{3}} \text{ MeV}, \tag{20}$$

which gives 15.6 MeV for O^{18}. The ratio x comes out to be

$$x = 0.32. \tag{21}$$

The more detailed analysis of the paring energy indicates a little larger value of x[19], namely,

$$x \approx 0.5. \tag{22}$$

Even taking such ambiguity of x into consideration, we can conclude that Ne^{20} is deformed. Experimentally, the enhanced E2 transition probability of this nucleus suggests the deformation [16, 20]). The nucleus O^{18} is believed to be spherical; there is no evidence that this nucleus is deformed. The calculation shows that the strength $x = 0.5$ is enough to produce the spherical shape. The same sort of calculation is carried through in the nucleus O^{19}. The residual interaction depresses the state with $\Lambda = 0$ more than the one with $\Lambda = 1$ because the state with the $\Lambda = 0$ includes the S-states. The state with $\Lambda = 1$ is the lowest when strongly deformed but, by the above reason, the state with

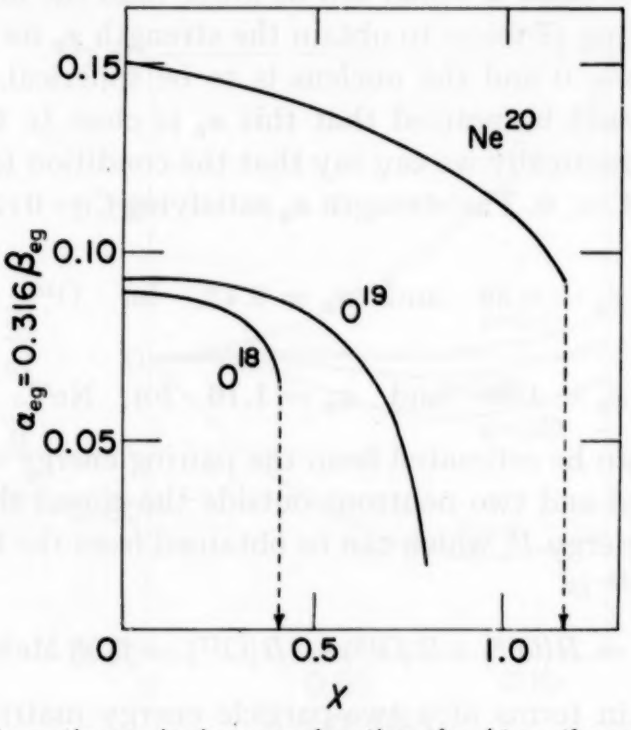

Fig. 2. Equilibrium deformation α_{eq} is given as a function of x. At x_c, the nucleus changes its shape from the deformed to spherical.

$\Lambda = 0$ becomes lower than that with $\Lambda = 1$ for an interaction strong enough to produce a spherical nucleus. Such a crossing occurs at $x \approx 0.8$. However, $x \approx 0.5$ should give this nucleus a stable deformation.

The equilibrium deformations are shown as functions of x in fig. 2.

3. Moment of Inertia and the Inertia Parameter of the β Vibration

The well known formula for the moment of inertia has been obtained by use of the method of Inglis [7]). By the cranking model, the moment of inertia I is written as

$$I = 2\hbar^2 \sum \frac{|\langle u_0|L_x|u_n\rangle|^2}{E_n - E_0} . \tag{23}$$

The moment of inertia by this formula results in the rigid-body value

$$I_{\text{rig}} = \sum m_i r_i^2. \tag{24}$$

The observed moment of inertia is about $\frac{1}{2}$ or $\frac{1}{3}$ of I_{rig}. Bohr and Mottelson [9]) and Moszkowski [10]) showed that the pair correlation reduced the moment of inertia. Griffin and Rich applied the formula derived by Belyaev to the rare earth nuclei and found good agreement [21]).

In this section, we evaluate I in (23) by using u_n obtained in the last section. We can separate this I into two parts: I_1 which has the large energy denominators in (23) and I_0 which has the small ones. Without the residual interaction,

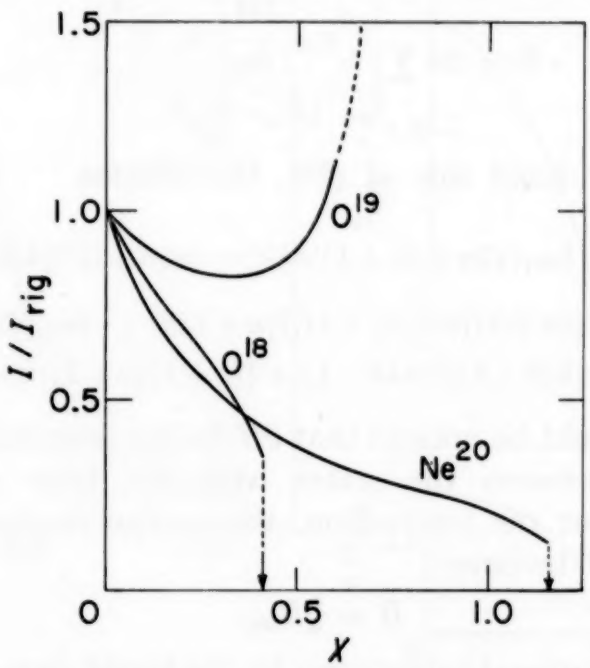

Fig. 3. Moment of inertia. The moment of inertia is reduced very much by the residual interaction in the even nuclei, while in odd nuclei this reduction is not so significant.

the large energy denominator is $\hbar\omega_0(e^{\alpha}+e^{-2\alpha})$, while the small one is $\hbar\omega_0$ $(e^{\alpha}-e^{-2\alpha})$. In I_1, the nucleons jump into the higher shells and in I_0 the nucleons jump into the orbits which are degenerate in the spherical shape. In magnitude I_1 is much smaller than I_0. This result enables us to neglect the small effect the interaction produces in I_1. The interaction has an important influence on I_0. First, the interaction modifies the energy denominators in (23). Secondly, this interaction significantly changes the wave functions. In the even-even nuclei, the lowest intrinsic state is depressed the most by the attractive potential, and then the energy denominators increase very much more than $\hbar\omega_0(e^{\alpha}-e^{-2\alpha})$. This effect, together with the change of the wave functions, reduces I very much. The ratio I/I_{rig} is shown as a function of x in fig. 3. However in O^{19} the energy denominators are decreased by the interaction, and this effect increases I, while the change of wave functions decreases I. Consequently,

I is almost the same as I_{rig} and it goes to infinity when the crossing occurs between the $\Lambda = 0$ state and the $\Lambda = 1$ state. Such a large moment of inertia can be seen [22]) in the groundstate band of Dy^{161}.

It is very interesting that I is greatly reduced by the residual interaction in even-even nuclei. The ratio I/I_{rig} ranges from 0.4 to 0.5 around $x = 0.4$.

As seen in the last section, O^{18} seems to be spherical. Here we calculate the β vibrational energy. Assuming axial symmetry, we cannot calculate the γ vibration. However, in the spherical nucleus, the two vibrational energies should be equal. In order to obtain the inertia parameter B, we can again use the Inglis formula [7]), which is

$$B = 2\hbar \sum \frac{\left| \left\langle u_0 \left| \frac{\partial H}{\partial \alpha} \right| u_n \right\rangle \right|^2}{(E_n - E_0)^3}. \tag{25}$$

To evaluate the right-hand side of (25), the relation

$$\begin{aligned} \frac{\partial H}{\partial \alpha} \Big| n\lambda k \Big\rangle = \hbar\omega_1 [& (2n+|\lambda|+1)|n\lambda k\rangle - \{n(n+|\lambda|)\}^{\frac{1}{2}}|n-1\lambda k\rangle \\ & - \{(n+1)(n+|\lambda|+1)\}^{\frac{1}{2}}|n+1\lambda k\rangle] - \hbar\omega_3[(2k+1)|n\lambda k\rangle \\ & + \{k(k+1)\}^{\frac{1}{2}}|n\lambda k-1\rangle + \{(k+1)(k+2)\}^{\frac{1}{2}}|n\lambda k+2\rangle] \end{aligned}$$

is useful. Here it should be noticed that $\partial H/\partial\alpha$ has diagonal elements or non-diagonal elements between the states with the large energy difference $\hbar\omega_0(e^{\alpha}+e^{-2\alpha})$. Without the interaction, the energy denominator in (25) is $\hbar\omega_0(e^{\alpha}+e^{-2\alpha})$, and B becomes

$$B \approx \tfrac{1}{4} B_{\text{irr}},$$

where B_{irr} is the irrotational value given by the liquid drop model [10]), namely

$$B_{\text{irr}} = 2m \sum_i r_i^2.$$

This B is small because of the large energy denominator in (25). By introducing the interactions, the intrinsic wave functions u_n are mixtures of ψ_i, and u_0 and u_n can have the same component ψ_i. Therefore $\partial H/\partial\alpha$ can have nonvanishing matrix elements between u_0 and u_n. The energy differences $(E_n - E_0)$ are much smaller than $2\hbar\omega_0$. Again we can separate B into B_0 and B_1 as done in the case of I, but this time the effect of the residual interaction in B_1 should be taken into consideration, because B_1 is not small compared with B_0. The quantity B_1 increases from $\frac{1}{4}B_{\text{irr}}$ as the interaction increases until $x = x_c$. Beyond x_c, the nucleus is spherical, and B_1 is independent of x and equal to $\frac{1}{4}B_{\text{irr}}$, while B_0 depends on x only through the energy denominators in (25). Therefore in the spherical region,

$$B = \tfrac{1}{4} B_{\text{irr}} + \frac{1}{x^3} B_{0s}. \tag{26}$$

Here B_0 takes the value B_{0s} for $x = 1$. As x increases, B decreases again to $\frac{1}{4}B_{\mathrm{irr}}$. The calculated B/B_{irr} is given in fig. 4a as a function of x.

The rigidity C is calculated by use of eq. (17) and the ratio C/C_{dis} is shown in fig. 4b, where

$$C_{\mathrm{dis}} = 2m\omega_0^2 \sum r_i^2.$$

The second derivative $\mathrm{d}^2E_0(\alpha)/\mathrm{d}\alpha^2$ is equal to C_{dis} when $x = 0$ or $x = \infty$, and therefore

$$C = \tfrac{3}{4}C_{\mathrm{dis}} \quad \text{for} \quad x = 0 \quad \text{or} \quad x = \infty.$$

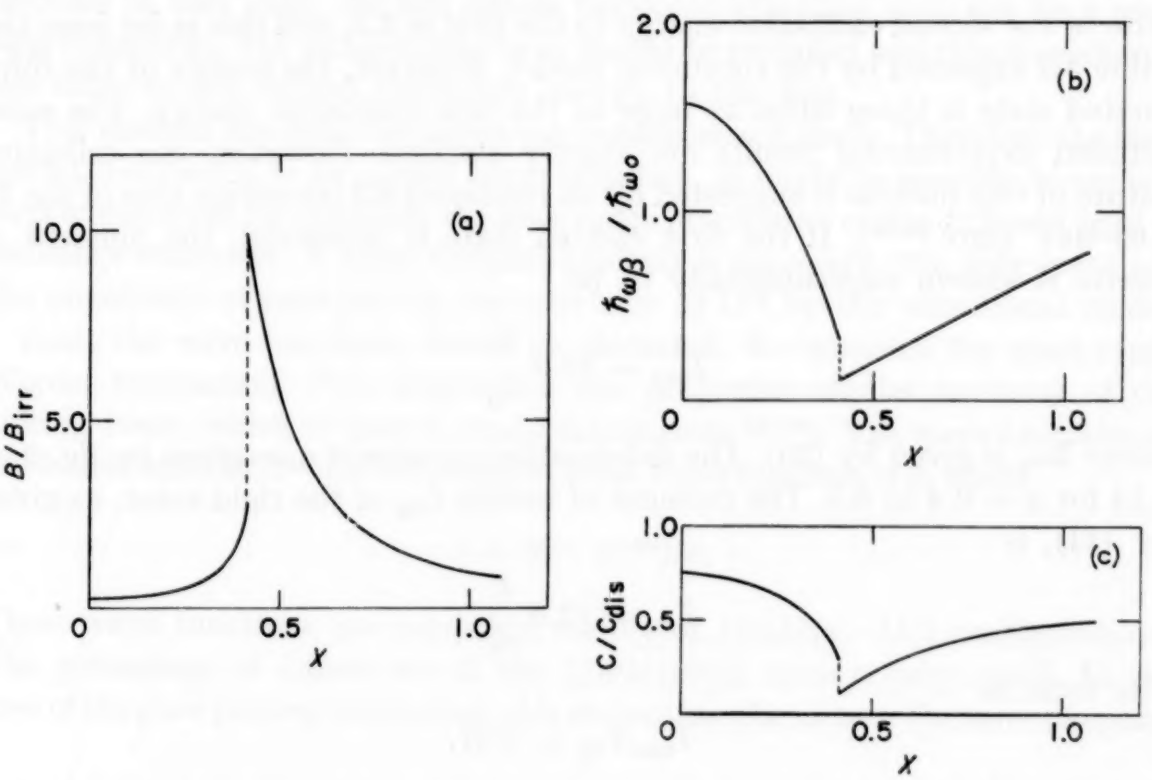

Fig. 4. (a) Inertia parameter. The ratio of the inertia parameter B to B_{irr} is plotted in O^{18} as a function of the strength of the residual interaction. (b) Rigidity. The ratio of the rigidity C to C_{irr} is plotted in O^{18} as a function of the strength of the residual interaction. (c) Beta vibrational energy $\hbar\omega_\beta$. The beta vibrational energy $\hbar\omega_\beta = \hbar\sqrt{C/B}$ is shown as a function of the strength of the residual interaction. This energy is very low around x_c.

Here the factor is due to the subtraction of half the shell-model potentials. The vibrational energy $\hbar\omega_\beta$ can be calculated by the equation

$$\hbar\omega_\beta = \hbar\sqrt{\frac{C}{B}}, \tag{27}$$

and this $\hbar\omega_\beta$ is shown in fig. 4c.

The dependence of $\hbar\omega_\beta$ on x is very interesting, because this suggests the dependence of the β vibrational energy on the number of nucleons outside the closed shells. The small values of x correspond to the strongly deformed nuclei far from the magic nuclei, where $\hbar\omega_\beta$ is high. Decreasing the number of nucleons

corresponds to increasing x, and $\hbar\omega_\beta$ decreass. We have spherical nuclei for fewer than a certain number of nucleons. In our case, $x > x_c$ gives spherical nuclei. As x increases beyond x_c, $\hbar\omega_\beta$ also increases. This situation reflects the fact that $\hbar\omega_\beta$ is greatest for nuclei near the magic number. These tendencies are observed experimentally [23]).

4. Discussions

As shown in sec. 2, the nuclei O^{19} and Ne^{20} seem to be deformed. In Ne^{20}, the ratio of the second excitation energy to the first is 2.5, and this is far from the value 3.3 expected by the rotational model. However, the energy of the third excited state is three times as large as the first excitation energy. The more detailed experimental results are eagerly awaited. However, the collective nature of this nucleus is suggested by an enhanced E2 transition rate of the 2^+ 1.63-MeV state [20, 24]). If the first excited state is rotational, the moment of inertia is known experimentally to be

$$I_{\text{exp}} = 27.8 \frac{\hbar}{\omega_0},$$

where $\hbar\omega_0$ is given by (20). The deformation parameter α, as given by fig. 2, is 0.14 for $x = 0.4$ to 0.5. The moment of inertia I_{rig} of the rigid rotor, as given by (24), is

$$I_{\text{rig}} = 41.5 \frac{\hbar}{\omega_0}.$$

The ratio is

$$I_{\text{exp}}/I_{\text{rig}} = 0.67.$$

The theoretical ratio is about 0.4, which agrees roughly with the observation.

In the odd nucleus O^{19}, the spin-orbit interaction should be taken into consideration because the single-particle energies are sensitive to the energy spectrum of the odd nucleus. Therefore, we cannot discuss this nucleus except for noting that this nucleus also is possibly deformed and the moment of inertia can be very large as discussed in the last section.

The nucleus O^{18} has been investigated by configuration mixing [3]). The spectrum and reduced width of the (d, p) reaction [25]) can be understood by this model. However, some question arises as to the position of the second and third excited states. The calculated energy of the second 0^+ state is too low, and the ratio of this excitation energy to the first excitation energy is about 1.4, while the experimental ratio [16]) is 2.0. The 4^+ state also has a low theoretical ratio 1.6, but the observed ratio 1.8 is rather large [16]). These high ratios suggested the possibility of vibrational excitations. By use of the cranking model, the vibrational energy was calculated in the last section. The strength $x = 0.45$ gives

the vibrational energy

$$\hbar\omega_\beta = 0.14\,\hbar\omega_0 \approx 2.2\ \text{MeV},$$

which is low enough to be comparable to the first excitation energy, 2.0 MeV. However, the fluctuation α is large, and

$$\Delta\alpha \approx (\hbar/2\sqrt{BC})^{\frac{1}{2}} = 0.07.$$

Because of this large $\Delta\alpha$, the simple harmonic vibration may not be a good approximation. The anharmonic term should be included and this may change the ratio of the second excitation energy to the first.

This nucleus has only two neutrons outside closed shells. Therefore the shell model is expected to be a good approximation. It might be possible to explain such a high ratio by assuming the long-range interaction or the different kind of exchange character. A more detailed analysis is necessary. We only point out the possibility of interpreting the spectrum of O^{18} by the vibrational model.

Last, the wave functions should be discussed. We assumed the short-range Wigner interaction. This interaction has properties similar to those of the pairing force, which is used in many calculations [13–15]). The wave functions of the lowest state in O^{18} are tabulated in table 2 as a function of δ, where

$$\delta = (e^{\alpha} - e^{-2\alpha})/x.$$

These wave functions are composed mainly of $\{(n\lambda k)(n-\lambda k)\}$ configurations. The percentage of admixture of the $\{(002)(100)\}$ state is very small. In the case of the pure pairing interaction, this state cannot be mixed. The same phenom-

TABLE 2

Ground-state wave function in O^{18}. The intrinsic wave function is expanded in terms of the eigenfunctions ψ_i of H_0: $\psi_0 = |002\rangle_1|002\rangle_2\,\chi(T=1,\ S=0)$, $\psi_1 = \frac{1}{2}\sqrt{2}\,\{|011\rangle_1|0-11\rangle_2 + |0-11\rangle_1|011\rangle_2\}\chi$, $\psi_2 = \frac{1}{2}\sqrt{2}\,\{|002\rangle_1|100\rangle_2 + |100\rangle_1|002\rangle_2\}\chi$, $\psi_3 = \frac{1}{2}\sqrt{2}\,\{|020\rangle_1|0-20\rangle_2 + |0-20\rangle_1|020\rangle_2\}$ and $\psi_4 = |100\rangle_1|100\rangle_2\chi$, where $\chi(T=1,\ S=0)$ is the isobaric and ordinary spin wave function.

δ \ n	0	1	2	3	4
0	0.1639	0.3386	0.0002	0.3386	0.1587
5	0.2587	0.3650	0.0003	0.2538	0.1223
10	0.3878	0.3515	0.0003	0.1729	0.0875
15	0.5319	0.3005	0.0004	0.1084	0.0588
20	0.6610	0.2350	0.0004	0.0652	0.0384
25	0.7586	0.1762	0.0004	0.0394	0.0253
30	0.8263	0.1314	0.0004	0.0246	0.0173
40	0.9030	0.0767	0.0003	0.0111	0.0090
50	0.9399	0.0487	0.0002	0.0059	0.0054

enon is seen in the other lower states in O^{18} and Ne^{20}. Therefore, as far as the lower states are considered, the important states ψ_i are those with every $(n\lambda k)$ and $(n-\lambda k)$ occupied, and the other states can be neglected. For δ larger than 30, only a few states ψ_i have probabilities larger than 5 % in u_0. This number is 2 in O^{18} and 4 in Ne^{20}, while the total number of the states is 5 in O^{18} and 18 in Ne^{20}. The probabilities of the lowest states u_0 of H_0 are almost 90 % for the large values of δ. Here, the energy difference $E_n - E_0$ is almost equal to the difference in the single-particle energies. In order to calculate the moment of inertia, the small admixture of the states which have configurations $\{(010)(0-10)\}$ and $\{(002)(100)\}$ in O^{18} and $\{(002)(002)\ (010)(0-10)\}$ and $\{(002)(002)(002)(100)\}$ in Ne^{20} are very important. Since these states have a nondiagonal matrix element L_x between the states $\{(002)(011)\}$ in O^{18} and $\{(002)(002)(002)(011)\}$ in Ne^{20}, which are the main ones in the states with $\Lambda = 1$, these configuration mixings change $\langle u_0|L_x|u_n\rangle$ by a rather large amount. By the first-order perturbation, these configuration mixings reduce the moments by the same amount as they were reduced by the change in the energy denominators in O^{18} and Ne^{20}. Generally both kinds of reductions are important in the even nuclei. Therefore if only the addition of the pairing energy to the energy denominators is taken into account, this energy should be assumed to be about twice those observed experimentally to obtain correct magnitudes of the moments in the rare earth region [21]). However, perturbation treatments of two-body interactions in large systems of Fermi particles have shown that the modification of the wave functions is such as to cancel exactly the effect of the energy shifts on the moment of inertia. This contradicts our result [26]). The reason of this contradiction may come partly from the periodic condition used by them.

The author would like to express his cordial thanks to Dr. D. R. Inglis for his kind discussions and encouragement throughout the work. He also thanks Drs. D. Kurath and A. Kerman for their kind interest and discussions. His best thanks are due to Dr. Hamermesh for his kind hospitality and also to Dr. F. Throw for his kind reading of the manuscript.

References

1) A. K. Kerman, Nuclear reactions (North-Holland Publishing Co., Amsterdam, 1959) Vol. 1, p. 427
2) D. Kurath and L. Pičman, Nuclear Physics **10** (1959) 313
3) J. P. Elliott and B. H. Flowers, Proc. Roy. Soc. Lond. A **229** (1955) 536; M. Redlich, Phys. Rev. **99** (1955) 1427
4) E. B. Paul, Phil. Mag. **2** (1957) 311
5) S. G. Nilsson, Mat. Fys. Medd. Dan. Vid. Selsk. **29**, No. 16 (1955) 16
6) A. E. Litherland, M. McManus, E. B. Paul, D. A. Bromley and H. Gove, Can. J. Phys. **36** (1958) 378
7) D. R. Inglis, Phys. Rev. **96** (1954) 1059; **97** (1955) 701

8) G. M. Temmer and N. P. Heydenburg, Phys. Rev. **99** (1955) 1609;
N. P. Heydenburg and G. M. Temmer, Phys. Rev. **100** (1955) 150;
Huus, Bjerregard and Elbeck, Mat. Fys. Medd. Dan. Vid. Selsk. **30**, No. 17 (1955)
9) A. Bohr and B. Mottelson, Mat. Fys. Medd. Dan. Vid. Selsk. **30**, No. 1 (1955)
10) S. A. Moszkowski, Phys. Rev. **103** (1956) 1328
11) J. Bardeen, L. N. Cooper and J. R. Schrieffer, Phys. Rev. **108** (1957) 1175;
N. N. Bogolyubov, JETP, USSR **34** (1958) 58; JETP, USSR **34** (1958) 73; Nuovo Cim. **7** (1958) 794
12) A. Bohr, B. R. Mottelson and D. Pines, Phys. Rev. **110** (1958) 936
13) S. T. Belyaev, Mat. Fys. Medd. Dan. Vid. Selsk. **31**, No. 11 (1959)
14) L. S. Kisslinger and R. A. Sorensen (to be published)
15) A. K. Kerman (to be published)
16) F. Ajzenberg-Selove and T. Lauritsen, Nuclear Physics **11** (1959) 1
17) T. Tamura, Phys. Rev. **111** (1958) 859
18) K. Lee and D. R. Inglis, Nuclear Physics (to be published)
19) H. Noya, A. Arima and H. Horie, Progr. Theoret. Phys. Suppl. **8** (1958) **33**
20) T. H. Kruse, R. D. Bent and L. J. Lidofsky, Phys. Rev. **119** (1960) 289
21) J. J. Griffin and M. Rich, Phys. Rev. **118** (1960) 850
22) D. Bés, Nuclear Physics **6** (1958) 645
23) R. K. Sheline, Revs. Mod. Phys. **32** (1960) 1
24) G. Rakavy, Nuclear Physics **4** (1957) 375
25) O. M. Bilaniuk and P. V. C. Hough, Phys. Rev. **108** (1957) 305
26) R. Amado and K. Brueckner, Phys. Rev. **115** (1959) 778

2.A.1:
2.E

Nuclear Physics **24** (1961) 84—88; *North-Holland Publishing Co., Amsterdam*
Not to be reproduced by photoprint or microfilm without written permission from the publisher

SECTIONS EFFICACES DES RÉACTIONS (p, n) ET (p, 2n) SUR Nd^{150}

J. OLKOWSKY, I. GRATOT et M. LE PAPE
C.E.N., *Saclay, France*

Reçu le 28 Octobre 1960

Abstract: Absolute cross sections have been measured for the reactions Nd^{150}(p, n)Pm^{150} and Nd^{150}(p, 2n)Pm^{149} ($E_p \leqq 11.1$ MeV). The sum of these cross sections is compared to that obtained by means of optical model. The agreement is satisfactory.

By using a simple model of evaporation, theoretical excitation functions are obtained, which renders a good account of experimental results.

1. Introduction

L'étude de l'interaction ^{150}Nd+p a été entreprise pour les raisons suivantes:

1) Nous avons montré [1]) que, dans le cas d'un noyau pratiquement sphérique comme ^{141}Pr, on pouvait, avec une bonne approximation, assimiler la section efficace de la réaction (p, n) à la section efficace totale pour une énergie de protons assez faible (inférieure à la barrière coulombienne). La section efficace de réaction était obtenue par le modèle optique qui suppose une symétrie sphérique au noyau cible. Il était intéressant ici de savoir si cette hypothèse est très restrictive ou non, ^{150}Nd étant un noyau très déformé.

2) ^{150}Nd est „entouré", dans la table des isotopes, de radioéléments de périodes et de propriétés bien caractéristiques. Comme nous opérons par des méthodes radiochimiques, il était possible d'étudier simultanément les différentes voies de l'interaction ^{150}Nd+p, tout au moins les plus importantes.

3) Pour l'émission compétitive d'un neutron ou de deux neutrons, Weisskopf et Ewing [2]) ont établi une formule donnant le rapport de probabilité de ces processus.

Pour que cette formule soit applicable il faut que:

a) l'énergie de liaison du proton soit supérieure à l'énergie de liaison du neutron, $B_p > B_n$;

b) l'énergie des particules incidentes x soit inférieure au seuil de la réaction (x, 3n).

En bombardant ^{150}Nd par des protons d'énergie $E_p \leqq 11.1$ MeV, nous satisfaisons à ces données.

Cette formule, vérifiée plusieurs fois [3]) dans le cas où les particules incidentes sont des α ne l'a pas encore été, à notre connaissance, pour des protons.

2. Méthode expérimentale

2.1. CIBLES

Le néodyme (sous forme d'oxyde) a la composition isotopique suivante (Oak-Ridge):

A	142	143	144	145	146	148	150
%	0.69	0.37	0.89	0.45	1.03	0.94	95.65

Les cibles sont constituées par un film de polystyrène à l'oxyde de néodyme déposé sur de l'aluminium de 10 μm. Les cibles ont des masses superficielles $\leqq 1$ mg/cm^2. On prépare un empilement de ces cibles, ce qui donne simultanément, pour chaque irradiation, les fonctions d'excitation de tous les produits formés.

2.2. IRRADIATIONS

Les conditions expérimentales sont les mêmes que dans notre autre travail [1]), c'est-à-dire utilisation du faisceau sorti de protons du cyclotron de Saclay ($E_{\mathrm{p\ max}} = 11.1$ MeV) et variation de l'énergie des protons incidents par absorption dans l'aluminium.

2.3. MONITORAGE

Nous avons mesuré le nombre de protons qui ont frappé l'empilement par deux méthodes différentes: 1) comme précédemment [1]) par la réaction ^{63}Cu(p,n)^{63}Zn, une feuille de cuivre pesée recouvrant tout l'empilement, et on mesure la quantité de ^{63}Zn formée; 2) en mesurant le courant de protons frappant la cible. Ces deux méthodes donnent des résultats comparables à 10 % près.

2.4. MESURES

On peut obtenir les fonctions d'excitation relatives de plusieurs façons: soit par les rayonnements γ ($E_\gamma = 320$ keV décroissant avec $T = 2$h7 pour ^{150}Pm, $E_\gamma = 285$ keV décroissant avec $T = 54$ h pour ^{149}Pm), soit par les rayonnements β.

Nous utilisons un spectromètre à cristal d'iodure de sodium et des compteurs Geiger du type cloche. Aucun traitement chimique n'est nécessaire, le seul produit gênant est ^{18}F produit sur l'oxygène de la cible. Pour les mesures de rayonnement γ, il ne gêne pas; pour les mesures de rayonnement β, nous l'éliminons par absorption, après les corrections nécessaires. Les compteurs Geiger sont étalonnés de façon absolue avec des étalons mesurés dans un compteur proportionnel 4π. Ceci permet de passer des sections efficaces relatives aux sections efficaces absolues. Ces mesures absolues tiennent compte des schémas. Nous avons utilisé ceux publiés dans la table des isotopes [4]).

Les seuls isotopes décelés comme produits de l'interaction ^{150}Nd+p sont:

^{150}Pm, ^{149}Pm en grande quantité, et ^{151}Pm en quantité très faible (provenant de la réaction ^{150}Nd (p, γ)). (Ces résultats seront publiés ultérieurement). La présence de ^{149}Nd qui aurait pu se former par les réactions (p, pn) ou (p, d) n'a pas été décelée dans les rayonnements γ et β, indiquant que, si ces réactions ont lieu, leurs sections efficaces sont très faibles.

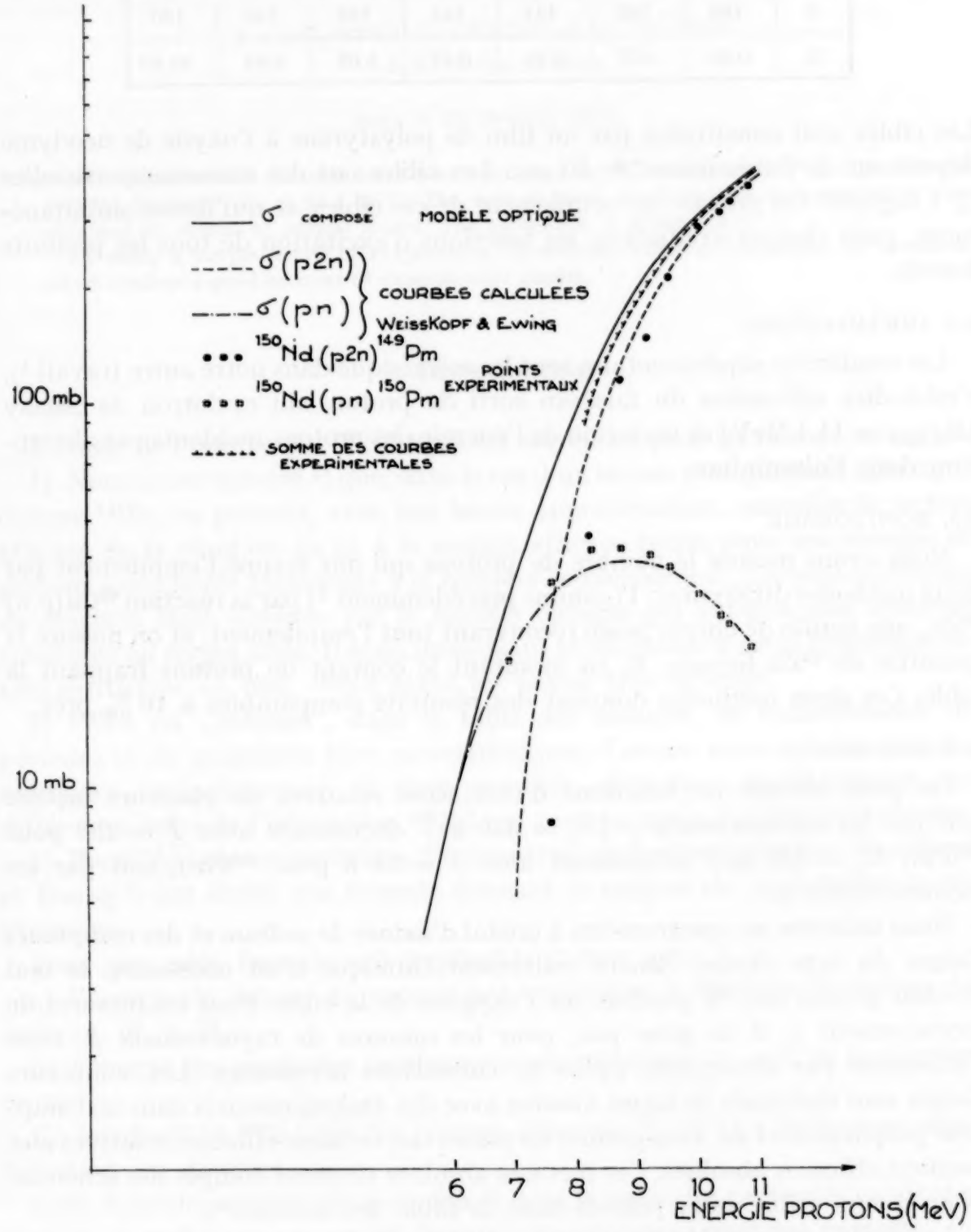

Fig. 1. Fonctions d'excitation de la réaction ^{150}Nd+p.

Les erreurs sur les sections efficaces absolues sont évaluées à $\pm 10\,\%$ vers $E_p = 11$ MeV et sont plus importantes quand l'énergie décroît car la définition en énergie devient plus médiocre et l'activité diminue.

3. Comparaison avec la théorie

La figure 1 représente la fonction d'excitation théorique de la réaction ^{150}Nd+p obtenue par le modèle optique de Bjorklund et Fernbach.

Les calculs ont été menés de la même façon que pour la réaction ^{141}Pr+p avec les mêmes paramètres [1]), soit $a = 0.65\,f$, $b = 1\,f$, $r_0 = 1.25\,f$ ($f = 10^{-13}$ cm). La courbe en pointillé représente la somme des fonctions d'excitation expérimentales (p, n) et (p, 2n). L'accord est satisfaisant. Il semble donc que: 1) les voies (p, n) et (p, 2n) représentent, à 10 % près environ, l'ensemble des voies ouvertes; 2) la déformation du noyau cible ne semble pas jouer un rôle important pour l'obtention de $\sigma_{\text{réaction}}$ par le modèle optique.

Weisskopf et Ewing ont établi la formule suivante [2])

$$\frac{\sigma(x,\,2n)}{\sigma(x,\,n)} = \frac{e^z}{1+z} - 1 \quad \text{avec} \quad z = \frac{\varepsilon_m - Q_{Bn}}{\theta},$$

ε_m étant l'énergie cinétique maximum du neutron émis, Q_{Bn} l'énergie de liaison du neutron dans ^{150}Pm et θ la température nucléaire.
Ceci, dans le cadre d'une théorie statistique des réactions, si les spectres des neutrons sont maxwelliens. Ceci a été montré expérimentalement pour des noyaux assez lourds et pour des énergies de particules incidentes pas trop élevées [5]).

Pour que cette formule s'applique, il faut que, pour le noyau cible, $B_p > B_n$. Pour ^{150}Nd, $B_p = 10.071$ MeV et $B_n = 6.996$ MeV. Ces énergies de liaison, ainsi que toutes celles nécessaires au calcul sont tirées de la table de Cameron [6]). Il faut encore que l'énergie des particules incidentes soit inférieure au seuil de la réaction (x, 3n). Dans notre cas, le seuil de la réaction ^{150}Nd(p, 3n) est 14.071 MeV [7]) et nous irradions avec des protons d'énergie maximum 11.1 MeV.

Pour le choix de la température nucléaire, nous avons utilisé la relation suivante reliant cette température à l'énergie des particules incidentes $E = a\theta^2$, où a est une constante dépendant de la masse du noyau. Nous avons pris [8]) $a = 10$.

Les sections efficaces s'obtiennent par les formules suivantes:

$$\sigma(\text{p, n}) = \sigma_{\text{réaction}}(1+z)e^{-z},$$
$$\sigma(\text{p, 2n}) = \sigma_{\text{réaction}}[1-(1+z)e^{-z})].$$

Sur la figure 1 sont représentées les fonctions d'excitation ainsi calculées. On constate que l'expérience les confirme bien, compte tenu des hypothèses simples qui sont à la base du calcul.

Nous remercions l'équipe de conduite du cyclotron pour les irradiations, ainsi que Monsieur Guillou pour les calculs de $\sigma_{\text{réaction}}$ faits à la machine Mercury-Ferranti de Saclay.

Bibliographie

1) J. Olkowsky, M. Le Pape et I. Gratot, Nuclear Physics **23** (1961) 164
2) V. F. Weisskopf et D. H. Ewing, Phys. Rev. **57** (1940) 472
3) H. L. Bradt et D. J. Tendan, Phys. Rev. **72** (1947) 1117;
E. L. Kelly et E. Segré, Phys. Rev. **75** (1949) 999;
G. M. Temmer, Phys. Rev. **76** (1949) 424
4) Table des isotopes, Rev. Mod. Phys. **30** (1958) 728
5) Albert, Anderson, Wong, Mc Shure et Walker, Wash. 1026 p. 59
6) A. G. W. Cameron, AECL-433 (1957)
7) A. H. Wapstra, Physica **21** (1955) 407
8) J. M. Blatt et V. F. Weisskopf, Theoretical nuclear physics, (Wiley, New York, 1952) p. **372**

2.F

Nuclear Physics **24** (1961) 89—101; © *North-Holland Publishing Co., Amsterdam*

Not to be reproduced by photoprint or microfilm without written permission from the publisher

γ RAYS FROM AN EXTRANUCLEAR DIRECT CAPTURE PROCESS

R. F. CHRISTY

Institute for Advanced Study, Princeton, New Jersey

and

IAN DUCK

Kellogg Radiation Laboratory, California Institute of Technology, Pasadena, California

Received 2 December 1960

Abstract: Direct electric dipole capture γ-ray transitions are calculated for a number of cases of charged particle capture in nuclei. It is found that when the γ-ray energy is sufficiently low – below about 2 MeV – the capture matrix element is determined by regions external to the usual "nuclear radius". A number of cases of this type are discussed and the calculations compared with experiment. The calculations are extended to the keV region in those cases when the process is of astrophysical interest.

1. Introduction

In many of the light nuclei, the cross section for the (p, γ) reaction shows a smooth variation with proton energy on which are superposed the resonances for the reaction in question. This smooth "background" cross section, the magnitude of which is characteristically $\approx 10^{-30}$ cm^2 at 1 MeV, is the subject of this note. In a number of cases, the angular distribution of the radiation follows the simple $\sin^2\theta$ law which is characteristic of a dipole oscillator oriented along the beam direction. This angular distribution results from an electric dipole p to s transition with no spin flip (i.e. the spin is uncoupled from the orbit). This simple angular distribution, combined with the smooth non-resonant excitation function, has led to the description of the process as direct capture [1]). The process apparently involves a transition from an initial state which does not involve any nuclear interaction to a final bound state. The absence of nuclear interaction in the initial state accounts for the absence of resonance and for the constancy of the spin which is not affected by the electric dipole radiation interaction but only by the nuclear force.

We have found that in a number of cases of this type of transition where the γ-ray energy is less than a few MeV, a straightforward calculation of the matrix element of the electric dipole moment, between an initial (undistorted) Coulomb wave function and a final bound state function of the residual nucleus, shows that the integrand rises to a maximum value at a radius which is in some cases many times the normal nuclear radius. Except at resonance, the irregular Coulomb function, since it strongly interacts with the nucleus, is comparable to the regular function at the nuclear radius. It is therefore negligibly small at

such large radii, which justifies its neglect in the calculation. These cases then, when the undisturbed regular Coulomb function dominates the matrix element, will have just those properties ascribed to the direct capture process.

These cases, when the dipole moment is determined entirely by those parts of the initial and final state wave functions which are exterior to what we normally think of as the nucleus, permit a more careful and detailed discussion of the value of the matrix element and of the (p, γ) cross section than is customary since the other nuclear particles and nuclear forces do not enter in such an explicit way.

In what follows we develop detailed expressions for this cross section. Our interest is twofold: On the one hand we have been interested in predicting the cross sections for a number of reactions at stellar energies, on the other hand, we are interested in the light thrown on the nucleus and its surface structure by measurement of these processes coupled with calculations.

2. Theoretical Basis

2.1. GENERAL EXPRESSIONS FOR THE CAPTURE CROSS SECTION

We consider the capture of a particle of mass M_1, and charge Z_1 by a target of mass M_2 and charge Z_2, to form a final state of the combined system. If the γ-ray energy is $E_\gamma = \hbar\omega$, the capture cross section for emission of electric dipole and electric quadrupole radiation of polarization m is, respectively,

$$\sigma_{1m} = \frac{16\pi}{9}\left(\frac{E_\gamma}{\hbar c}\right)^3 \frac{1}{\hbar v}|Q_{1m}|^2, \tag{1}$$

$$\sigma_{2m} = \frac{4\pi}{75}\left(\frac{E_\gamma}{\hbar c}\right)^5 \frac{1}{\hbar v}|Q_{2m}|^2. \tag{2}$$

The electric moments Q are given by

$$Q_{1m} = \frac{eM_1M_2}{M_1+M_2}\left(\frac{Z_1}{M_1} - \frac{Z_2}{M_2}\right)\int r Y^*_{1m}(\theta, \varphi)\Phi_f^*(r, \theta, \varphi)\Phi_1(r, \theta, \varphi)\mathrm{d}\tau, \tag{3}$$

$$Q_{2m} = e\left(\frac{M_1M_2}{M_1+M_2}\right)^2\left(\frac{Z_1}{M_1^2} + \frac{Z_2}{M_2^2}\right)\int r^2 Y^*_{2m}(\theta, \varphi)\Phi_f^*(r, \theta, \varphi)\Phi_1(r, \theta, \varphi)\mathrm{d}\tau, \tag{4}$$

where r, θ, φ are the relative coordinates of the (centres) of particles 1 and 2. We treat the nuclei involved as single particles since we attempt to evaluate the matrix elements only in the external region where they are separate.

For Φ_1 we use a wave function expressed in channel spin states Ψ_{Im_I} and in Coulomb functions $F_l(kr)$ and $G_l(kr)$ and including the nuclear phase shifts:

$$\begin{aligned}\Phi_1(r, \theta, \varphi) = \sum_{l_1=0}^{\infty} i^{l_1}\sqrt{4\pi(2l_1+1)}\,\frac{e^{i\eta_{l_1}}}{kr}\sum_{J_1 m_{J_1}}\langle Im_I l_1 0|J_1 m_{J_1}\rangle \\ \times[F_{l_1}(kr)+(G_{l_1}(kr)+iF_{l_1}(kr))e^{i\delta_{J_1}}\sin\delta_{J_1}]\sum_{m_{l_1}m'_I}\langle l_1 m_{l_1} Im'_I|J_1 m_{J_1}\rangle \\ \times Y_{l_1 m_{l_1}}(\theta, \varphi)\Psi_{Im'_I}.\end{aligned} \tag{5}$$

For Φ_f we also use a channel spin representation and a radial wave function $g_f(r)$ which we discuss in the next section:

$$\Phi_f(r,\theta,\varphi)=\sum_{I,m_{l_2},m_I''} a_I\langle l_2 m_{l_2} I m_I''|J_f m_{J_f}\rangle Y_{l_2 m_{l_2}}(\theta,\varphi)\Psi_{Im_I''}g_f(r). \tag{6}$$

In the above, l_1 is the initial orbit and l_2 the final; J_1 is the initial J and J_f the final one; we use the same symbol I for both the initial and final channel spin, anticipating that they will be the same. The a_I are coefficients related to the reduced width

We abbreviate

$$F_{l_1}(kr)+(G_{l_1}(kr)+iF_{l_1}(kr))e^{i\delta_{J_1}}\sin\delta_{J_1}=g_1(r).$$

2.2 ANGULAR INTEGRALS

The expression for Q_{1m} then reduces to

$$Q_{1m}=e\mu\left(\frac{Z_1}{M_1}-\frac{Z_2}{M_2}\right)\sum_{l_1 J_1 m_{J_1}} R_{1f1}a_I i^{l_1}e^{i\eta_{l_1}}\sqrt{3(2l_2+1)(2l_1+1)(2J_f+1)}(-1)^{1+l_2+I+J_1}$$
$$\times\begin{Bmatrix}1 & l_2 & l_1\\ I & J_1 & J_f\end{Bmatrix}\langle l_2 010|l_1 0\rangle\langle 1m J_f m_{J_f}|J_1 m_{J_1}\rangle\langle I m_I l_1 0|J_1 m_{J_1}\rangle, \tag{7}$$

where $R_{1f1}=\int r^2 dr g_f^*(r)g_1(r)/k$ and μ is the reduced mass.

If we want the angular distribution of the radiation, we cannot give a general simplification of the formula and must proceed from the above. We shall, instead, look now only at the total cross section which involves $\sum_m|Q_{1m}|^2$. This eliminates several interference terms and results in

$$\sum_{m,m_I,I}|Q_{1m}|^2$$
$$=e^2\mu^2\left(\frac{Z_1}{M_1}-\frac{Z_2}{M_2}\right)^2\sum_{l_1,J_1,I}a_I^2|R_{1f1}|^2 3(2J_f+1)(2J_1+1)\langle l_1,l_2\rangle\begin{Bmatrix}1 & l_2 & l_1\\ I & J_1 & J_f\end{Bmatrix}^2, \tag{8}$$

where $\langle l_1, l_2\rangle$ means the larger of l_1, l_2, and $\{\}$ is the 6-j symbol. Finally, we have

$$\sigma_1=\frac{16\pi}{9}\left(\frac{E_\gamma}{\hbar c}\right)^3\frac{1}{\hbar v}\frac{1}{(2J_2+1)(2S_1+1)}\sum_{m,m_I,I}|Q_{1m}|^2, \tag{9}$$

where J_2 is the J of the target nucleus and S_1 is the spin of the projectile.

In the case that δ_{J_1} is independent of J_1 we can sum over J_1 by writing

$$\Sigma_{J_1}(2J_1+1)\begin{Bmatrix}1 & l_2 & l_1\\ I & J_1 & J_f\end{Bmatrix}^2=\frac{1}{2l_2+1}.$$

In L–S coupling we can calculate a_I for the combination of a particle of spin S_1, internal $L_1=0$, with a target of J_2, L_2, S_2, and having relative orbital

angular momentum l_2, to form a final state J_f, L_f, S_f. We have then

$$a_I = \sum_{\substack{m_{l_2}, m_I, m_{l_f}, m_{S_f} \\ m_2, m_{S_1}, m_{L_2}, m_{S_2}}} \langle l_2 m_{l_2} I m_I | J_f m_{J_f} \rangle \langle J_2 m_2 S_1 m_{S_1} | I m_I \rangle$$

$$\times \langle L_2 m_{L_2} S_2 m_{S_2} | J_2 m_2 \rangle \langle l_2 m_{l_2} L_2 m_{L_2} | L_f m_{L_f} \rangle \langle S_2 m_{S_2} S_1 m_{S_1} | S_f m_{S_f} \rangle \langle L_f m_{L_f} S_f m_{S_f} | J_f m_{J_f} \rangle,$$

so that

$$a_I^2 = (2I+1)(2J_2+1)(2L_f+1)(2S_f+1) \begin{Bmatrix} I & L_2 & S_f \\ L_f & J_f & l_2 \end{Bmatrix}^2 \begin{Bmatrix} I & L_2 & S_f \\ S_2 & S_1 & J_2 \end{Bmatrix}^2. \quad (10)$$

This is so normalized that

$$\Sigma_{L_f S_f} a_I^2 = 1.$$

For quadrupole radiation we can similarly get

$$Q_{2m} = e\mu^2 \left(\frac{Z_1}{M_1^2} + \frac{Z_2}{M_2^2} \right) \Sigma_{l_1, J_1, m_{J_1}} R_{2fl} a_I i^{l_1} e^{i\eta_{l_1}} \sqrt{5(2l_2+1)(2l_1+1)(2J_f+1)} (-1)^{2+l_2+I+J_1}$$

$$\begin{Bmatrix} 2 & l_2 & l_1 \\ I & J_1 & J_f \end{Bmatrix} \langle l_2 020 | l_1 0 \rangle \langle I m_I l_1 0 | J_1 m_{J_1} \rangle \langle 2m J_f m_{J_f} | J_1 m_{J_1} \rangle, \quad (11)$$

where $R_{2fl} = 1/k \int r^3 \mathrm{d}r g_f^*(r) g_l(r)$, and

$$\sigma_2 = \frac{4\pi}{75} \left(\frac{E_\gamma}{\hbar c} \right)^5 \frac{1}{\hbar v} \Sigma_{m, m_I, I} |Q_{2m}|^2 \frac{1}{(2J_2+1)(2S_1+1)} \quad (12)$$

and

$$\Sigma_{m, m_I, I} |Q_{2m}|^2 = e^2 \mu^4 \left(\frac{Z_1}{M_1^2} + \frac{Z_2}{M_2^2} \right)^2 \Sigma_{l_1, J_1} a_I^2 |R_{2fl}|^2 5(2l_2+1)(2J_f+1)(2J_1+1)$$

$$\times \langle l_2 020 | l_1 0 \rangle^2 \begin{Bmatrix} 2 & l_2 & l_1 \\ I & J_1 & J_f \end{Bmatrix}^2. \quad (13)$$

2.3 RADIAL INTEGRALS

For the Coulomb wave functions, we use either the tables of Bloch *et al.* [2]) or, at low energy, where $\eta = Z_1 Z_2 e^2/\hbar v \gg \rho = kr$ at the important values of r and where $\eta\rho \gg 1$ we have used an expression of a WKB type †

$$F_l(\rho) \approx \frac{\sqrt{\rho}}{2(2\eta\rho)^{\frac{1}{4}}} \exp \left[-\pi\eta + 2\sqrt{2\eta\rho} - \frac{l^2}{\sqrt{2\eta\rho}} - \frac{\frac{1}{3}\rho^2}{\sqrt{2\eta\rho}} \right]. \quad (14)$$

Actually this expression is still acceptable at $2\eta = \rho$, $2\rho\eta = 1$. There is a corresponding approximation for G_l given by $F_l G_l \approx \frac{1}{2}\rho/(2\rho\eta)^{\frac{1}{2}}$.

† The WKB expressions used here are not the most accurate that we could devise but are approximated in order to permit analytical evaluation. They should not be used when the most careful calculation is attempted.

For the exterior bound state function $g_l(r)$, we use the Whittaker function which we write $W_{\alpha,l}(\kappa r)/r$ normalized at the nuclear radius r_n, to $u(r_n)/r$. Here $\alpha = Z_1 Z_2 e^2 \mu/\hbar^2 \kappa$ and $\kappa = (2\mu E_B/\hbar^2)^{\frac{1}{2}}$, where E_B is the binding energy. We define $W_{\alpha,l}(x)$ where $x = \kappa r$ by

$$W_{\alpha,l}(x) = \frac{(2x)^{-\alpha} e^{-x}}{(l+\alpha)!} \int_0^\infty t^{l+\alpha} e^{-t} \left(1+\frac{t}{2x}\right)^{l-\alpha} dt. \tag{15}$$

Unfortunately no general tabulation of this function appears to exist so that, except for certain special values of α, we must use various approximations depending on the values of α, x. For small x and $2\alpha x \ll 1$ we have the series expansion

$$\begin{aligned} W_{\alpha,l}(x) = {} & \frac{e^{-x}}{(2x)^l(\alpha-l-1)!\,(\alpha+l)!} \Bigg\{ \Sigma_{n=0}^{2l} \frac{(2l-n)!\,(\alpha-l+n-1)!}{n!} (-1)^n (2x)^n \\ & + (2x)^{2l+1}(-1)^{2l+1} \Sigma_{n=0}^{\infty} \frac{(\alpha+l+n)!}{n!\,(2l+1+n)!} (2x)^n \\ & \cdot [\psi(n)+\psi(n+2l+1)-\psi(\alpha+l+n)-\ln 2x] \Bigg\}, \end{aligned} \tag{16}$$

whereas asymptotically for large x $(2x > \alpha)$ we have

$$W_{\alpha,l}(x) \sim \frac{e^{-x}}{(2x)^\alpha} \left\{ 1 + \sum_{n=1} \frac{[(l+\frac{1}{2})^2-(\alpha+\frac{1}{2})^2] \ldots [(l+\frac{1}{2})^2-(\alpha+n-\frac{1}{2})^2]}{n!\,(2x)^n} \right\} \tag{17}$$

and for $2\alpha > x$, $2\alpha x > 1$, a WKB expression is appropriate:

$$W_{\alpha,l}(x) \approx \left(\frac{x}{2\alpha}\right)^{\frac{1}{4}} \exp\left[\alpha - \alpha \ln \alpha - 2\sqrt{2\alpha x} + \frac{l^2}{\sqrt{2\alpha x}} - \frac{\frac{1}{3}x^2}{\sqrt{2\alpha x}}\right]. \tag{18}$$

The quantity $\frac{1}{2}u^2(r_n)r_n$ we define as θ_{sp}^2 the single particle reduced width.

In calculating the radial matrix elements, we need the bound state Coulomb function W near the maximum of the integrand and at the nuclear radius. In addition, we need the regular Coulomb function F at the maximum of the integrand. We have found it convenient to calculate the matrix element in many cases by a saddle point type calculation where we approximate the integrand by a Gaussian. In this way we can obtain approximate analytic expressions for the cross section. Actually where high accuracy might be required, a numerical integration would be more appropriate. We distinguish a number of different cases according to the kind of approximation that is suitable for these functions.

For $\alpha \gg 1$ such as is the case (see below) for $Ne^{20}+p$, we find that the WKB approximation (18) can be used for W both at the maximum of the integrand and at the nuclear radius and in addition, provided $\eta \gg \rho$, the WKB approxi-

mation (14) can also be used for F. In fact, provided $\alpha > 1$ and $\eta > 1$ we can determine the maximum of the integrand from the WKB expressions for W and F. There results approximately for the dipole matrix element to which we confine our attention

$$(2\alpha x_m)^{\frac{1}{2}} = 12^{\frac{1}{3}}\alpha^{\frac{2}{3}}\left(\frac{E_B}{E_\gamma}\right)^{\frac{1}{3}}, \tag{19}$$

$$R_{1f1} \approx \frac{u(r_n)}{k\kappa^2 W_{\alpha, l_2}(x_n)}\frac{2}{3}\sqrt{2\pi}F_{l_1}(\rho_m)W_{\alpha, l_2}(x_m)x_m{}^2, \tag{20}$$

where $x_m = \kappa r_m$ is the location of the peak in the integrand.

If we substitute WKB expressions at ρ_m, x_m there results

$$R_{1f1} = \frac{u(r_n)3^{\frac{2}{3}}\sqrt{2\pi}(2\alpha)^{\frac{1}{3}}}{k^{\frac{1}{2}}\kappa^{\frac{5}{2}}W_{\alpha, l_2}(x_n)}\left(\frac{E_B}{E_\gamma}\right)^{\frac{5}{3}}\exp\left[-\pi\eta + \frac{(l_2{}^2 - l_1{}^2)}{12^{\frac{1}{3}}\alpha^{\frac{2}{3}}}\left(\frac{E_\gamma}{E_B}\right)^{\frac{1}{3}} - 1 + \alpha - \alpha\ln\alpha\right]. \tag{21}$$

If also $(2\alpha x_n)^{\frac{1}{2}} > 1$ then $W(x_n)$ can be replaced by a WKB expression giving

$$R_{1f1} = \frac{u(r_n)3^{\frac{2}{3}}\sqrt{2\pi}(2\alpha)^{7/12}}{k^{\frac{1}{2}}\kappa^{\frac{5}{2}}x_n{}^{\frac{1}{4}}}\left(\frac{E_B}{E_\gamma}\right)^{\frac{5}{3}}$$
$$\times\exp\left[-\pi\eta + \frac{(l_2{}^2 - l_1{}^2)}{12^{\frac{1}{3}}\alpha^{\frac{2}{3}}}\left(\frac{E_\gamma}{E_B}\right)^{\frac{1}{3}} - 1 + 2\sqrt{2\alpha x_n} - \frac{l_2{}^2}{\sqrt{2\alpha x_n}} + \frac{\frac{1}{3}x_n{}^2}{\sqrt{2\alpha x_n}}\right]. \tag{22}$$

For $\alpha < 1$ and $\eta > 1$ we can use the asymptotic expression (17) for W combined with the WKB expression for F. There results

$$(x_m)^{\frac{1}{2}} = (\tfrac{1}{2}\alpha)^{\frac{1}{2}} + (1.25 - \tfrac{1}{2}\alpha)^{\frac{1}{2}} \tag{23}$$

and

$$R_{1f1} = \frac{u(r_m)}{k\kappa^2 W_{\alpha, l_2}(x_n)}\left(\frac{2\pi}{(x_m)^{\frac{1}{2}}(1.25 - \frac{1}{2}\alpha)^{\frac{1}{2}}}\right)^{\frac{1}{2}} F_{l_1}(\rho_m)W_{\alpha, l_2}(x_m)x_m{}^2. \tag{24}$$

Here we can use the series for small x for $W(x_n)$.

For $\eta < 1$, the integral must be done numerically.

From these expressions we get the formulae (25)–(27) for σ_1, and $S = e^{2\pi\eta}E_{cm}\sigma_1$, where we have summed over J_1, and we write

$$\theta^2 = \frac{(2J_f + 1)\theta_{sp}^2}{(2J_2 + 1)(2S_1 + 1)(2l_2 + 1)}\sum_I a_I{}^2.$$

Then we have

$$\sigma_1 = \frac{32\pi}{3}\left(\frac{E_\gamma}{\hbar c}\right)^3\frac{e^2}{\hbar c}\frac{c}{v}\mu^2\left(\frac{Z_1}{M_1} - \frac{Z_2}{M_2}\right)^2\langle l_1, l_2\rangle\theta^2\frac{|R_{1f1}|^2}{u^2(r_n)r_n}, \tag{25}$$

or also

$$\sigma_1 = \frac{4\pi}{3}\left(\frac{E_\gamma}{E_B}\right)^3\left(\frac{E_B}{E_{cm}}\right)\frac{\hbar c}{e^2}m^2\left(\frac{Z_1}{M_1}-\frac{Z_2}{M_2}\right)^2\langle l_1, l_2\rangle\frac{\theta^2}{x_n}\left|\frac{R_{1fl}\,k^{\frac{1}{2}}\kappa^{\frac{5}{2}}}{u(r_n)}\right|^2\left(\frac{e^2}{mc^2}\right)^2 \quad (26)$$

and

$$S = \frac{4\pi}{3}\left(\frac{E_\gamma}{E_B}\right)^3\left(\frac{E_B}{mc^2}\right)\frac{\hbar c}{e^2}m^2\left(\frac{Z_1}{M_1}-\frac{Z_2}{M_2}\right)^2\langle l_1, l_2\rangle\theta^2\frac{e^{2\pi\eta}}{x_n}\left|\frac{R_{1fl}\,k^{\frac{1}{2}}\kappa^{\frac{5}{2}}}{u(r_n)}\right|^2 mc^2\left(\frac{e^2}{mc^2}\right)^2. \quad (27)$$

In the case that the low energy WKB expression (22) above is used for R_{1fl} we have

$$S = 8\pi^2\left(\frac{3E_B}{E_\gamma}\right)^{\frac{1}{3}}\left(\frac{E_B}{mc^2}\right)\frac{\hbar c}{e^2}\left[m\left(\frac{Z_1}{M_1}-\frac{Z_2}{M_2}\right)\right]^2\langle l_1, l_2\rangle\theta^2\frac{(2\alpha)^{7/6}}{x_n^{\frac{3}{2}}}$$

$$\times\exp\left[\frac{2(l_2^2-l_1^2)}{12^{\frac{1}{3}}\alpha^{\frac{2}{3}}}\left(\frac{E_\gamma}{E_B}\right)^{\frac{1}{3}}-2+4\sqrt{2\alpha x_n}-\frac{2l_2^2}{\sqrt{2\alpha x_n}}+\frac{\frac{2}{3}x_n^2}{\sqrt{2\alpha x_n}}\right]mc^2\left(\frac{e^2}{mc^2}\right)^2. \quad (28)$$

These approximate formulae, supplemented by some numerical integration, have been used to determine a number of cross sections in what follows. The treatment of the matrix element could certainly be improved, but it appears that the largest uncertainty by far is the value of the reduced width θ^2.

3. Specific Reactions

3.1. THE REACTION Be^7+p

The radiative capture of protons by Be^7 to form the ground state of B^8 is of interest in discussions of possible alternate [3]) chains in the generation of stellar energy. The binding energy is small (136 keV, $\alpha = 1.60$) so that a calculation that includes only the exterior contribution to the matrix element may be reasonably accurate for not too great proton energies.

We have calculated the cross section at very low energies using eq. (21) for the matrix element. For $W(x_n)$ we used the series expansion (16) for small x. We take $r_n = 4.1\times10^{-13}$ cm, $x_n = 0.31$. The capture is from an initial s state to a final p orbit. The angular distribution of the radiation should be spherical. For the reduced width evaluation for the final p state proton bound in B^8, we have assumed L–S coupling. Be^7 is described as $^2P_{\frac{3}{2}}$ and B^8 as $^3P_2$. The coefficient of fractional parentage is $\frac{1}{3}$. Taking $\theta^2_{sp} = 1\times\frac{1}{3}$ then $\theta^2 = \frac{25}{432}$.

Our result for S at very low energies is that S is constant below a few hundred keV and is $S_0 = 16\times10^{-3}$ keV · b. In this calculation the value of x_m at stellar energies is nearly 10 times the nuclear radius.

In order to compare with Kavanagh [4]) we have also calculated the cross section at 1 MeV by numerical integration. Here the peak contribution is at only twice r_n so that neglect of the interior contribution and of nuclear phase

shifts may not be entirely justified. However, the ratio of the S value at stellar energies to that at 1 MeV may still be more reliable than either individually since the uncertainty in θ^2 cancels. At 1 MeV we get $S = 11\times10^{-3}$ keV · b. This latter value agrees reasonably with Kavanagh's result of $S \approx 20\times10^{-3}$ keV · b and suggests that a suitable estimate of S_0, for purposes of stellar calculation, would be $S_0 \approx 30\times10^{-3}$ keV · b. These calculations differ slightly from estimates reported [3, 4]) already, primarily through the use of $\theta^2_{sp} = \frac{1}{3}$ rather than $\frac{1}{6}$, and slight changes in the approximations at low energy. These changes will not result in any significant change in the astrophysical calculation [5]).

3.2. THE REACTIONS He^3+He^4 AND H^3+He^4

The reaction $He^3+He^4 \rightarrow Be^7+\gamma$ is of some importance in the completion of the p–p chain of reactions in stars [3]). In order to complement the measurement [6]) of this reaction cross section at centre of mass energies above about 300 keV, and to enable a more accurate extrapolation to stellar energies, we have calculated the cross section for capture to the ground state and to the first excited state of Be^7. We have treated this as a two-body problem with the initial orbit of the two particles an s state and the final orbit a p state. This does not imply that Be^7 is well described as He^3 orbiting around He^4 in a p state, but rather that there is a significant amplitude to find Be^7 dissociated into a He^3 and a He^4 in a bound state. This is not unreasonable in the external region where we are interested in the matrix element although, as always, the calculated result is proportional to the reduced width.

In this case, there is some direct evidence on the reduced widths, available from the scattering experiments of Miller and Phillips [7]). These experiments indicate that the s wave interaction can be approximately represented by a hard sphere interaction whereas the p-wave phase shifts in the $\frac{3}{2}$ and $\frac{1}{2}$ states can be represented by resonance formulae associated with the ground and first excited states of Be^7. We have used these scattering data in the capture calculation in two ways. The s wave phase shift has been introduced into the initial state wave function where it makes only a small reduction in the matrix element at low energies since the main contribution is well outside the nucleus. The p wave phase shifts lead to values for the widths θ^2 of the two states in question to break up into He^3+He^4. There is considerable uncertainty in the combination of width and radius resulting from these experiments but we have chosen the values $r_n = 3.3\times10^{-13}$ cm, $\theta^2_{\frac{3}{2}} = 1.1$ and $\theta^2_{\frac{1}{2}} = 0.55$. The uncertainty in cross section resulting from these uncertainties is perhaps a factor of two.

For the ground state and excited state of Be^7, $\alpha = 0.66$ and 0.77 respectively. We have used eq. (23) for x_m leading to $x_m = 2.35$ and 2.40 in the two cases, $x_n = 1.20$ and 1.02 respectively. This leads to the use of eq. (20) for the matrix element where we have used the asymptotic expressions (17) for $W(x_m)$,

$W(x_n)$ and the WKB expression (14) for F at low energies. There results $S_{\frac{3}{2}}(E=0)=0.90$ keV · b, $S_{\frac{1}{2}}(E=0)=0.34$ keV · b, $S_{tot}(E=0)=1.24$ keV · b. At $\eta=1.585$, $E_\alpha=634$ keV, we have made numerical integrations of the matrix elements including the s state phase shifts. There results $S_{tot}(E_\alpha=$ $=635$ keV$)=0.54$ keV · b and the ratio of $S_{\frac{1}{2}}/S_{\frac{3}{2}}=0.37$, essentially the same as at $E=0$.

To compare these results with the measurements we note that our S is $\frac{3}{7}$ of that quoted [6]) since we use E_{cm}. The observed values in our notation are then $S_{obs}(635\text{ keV})=0.77$ keV · b. The calculated ratio of $S(E=0)/S(635\text{ keV})=$ $=2.3$ is larger than the experimental ratio 1.5. The calculated ratio is not too trustworthy in view of the different technique and approximations involved in the two cases. The experimental ratio is quite uncertain because of the inaccuracy of the low energy data. The low energy result is, however, sufficiently accurate to establish the role of this reaction in stars [5]).

The $H^3+He^4\rightarrow Li^7+\gamma$ reaction is the mirror of the He^3 reaction. In the absence of the corresponding scattering data, we have merely assumed the same radius and reduced widths as for the He^3 reaction. The binding energies here are greater so that $\alpha_{\frac{3}{2}}=0.264$ and $\alpha_{\frac{1}{2}}=0.294$. These lead to $x_m=2.02$ and 2.05; $x_n=1.50$, 1.35 respectively. Here the maximum lies so close to the nuclear radius that the neglect of the interior contribution can no longer be justified. The assumed hard sphere character of the s wave scattering leads to a node in the s wave function at the nuclear radius which is quite near where the maximum contribution would lie. This considerably reduces the exterior contribution so that only a numerical integration is trustworthy. Such a calculation gave $S_{\frac{3}{2}}$ (635 keV) $=0.05$ keV · b. This can be compared to the observed S_{tot} (635 keV) ≈ 0.034 keV · b.

3.3. THE REACTION $Ne^{20}+p$

The excited $\frac{1}{2}^+$ state of Na^{21} which is bound by only 26 keV should lead to a significant direct capture process if the reduced width is relatively large, and is of particular interest theoretically since the interaction takes place far from the nucleus. Here $\alpha=9.57$ and using WKB expressions for F and W leads to $x_m=5.58(E_B/E_\gamma)^{\frac{2}{3}}$ so that at low energies $r_m=30r_n$. These WKB formulae are relatively reliable up to about 1 MeV bombarding energy. The use of eq. (28) for the p to s transition leads to $S=236(E_B/E_\gamma)^{\frac{1}{3}}\theta^2\exp[-0.19(E_\gamma/E_B)^{\frac{1}{3}}]$ keV · b and $S(E=1\text{ MeV})=36.6\,\theta^2$ keV · b.

This reaction has been observed by Tanner [8]) † who measured $S(E\approx 1\text{ MeV})$ ≈ 11 keV · b. This would agree with the above calculation for $\theta^2\approx\frac{1}{3}$ which is quite large. The calculations quoted by Tanner differed slightly from that given here in the approximations used, and took $\theta^2=\frac{1}{4}$. The theoretical formula show a very considerable increase in S in going to stellar energies. The ratio

† See also the footnote on p. 1063 of ref. [7]).

$S(26\text{ keV})/S(1\text{ MeV}) = 4$ given by this formula would suggest $S(26\text{ keV}) \approx 44$ keV · b as given by Tanner.

3.4. THE REACTION $O^{16}+p$

The angular distribution ($\sin^2\theta$) of the radiation to the first excited ($S_{\frac{1}{2}}$) state of F^{17} makes it clear that both $p_{\frac{1}{2}}$ and $p_{\frac{3}{2}}$ initial states are contributing to the capture process in the same way and originally led Warren *et al.* [1]) to the suggestion that this reaction might be described as a direct capture process. We shall here treat this calculation by the same procedures as for the other reactions although more accurate and extensive calculations have been carried out by F. G. Nash [9]). We are indebted to G. M. Volkoff for sending us a copy of this thesis.

As for the $Ne^{20}+p$ reaction just discussed, the binding energy is here small enough (98 keV) so that $\alpha = 3.89$ is large. This permits use of the WKB formulae for F and W at x_m and x_n. We get $x_m = 4.12(E_B/E_\gamma)^{\frac{2}{3}}$, $x_n = 0.33$ so that the maximum in the matrix element is up to about 12 times the nuclear radius. There results $S = 45(E_B/E_\gamma)^{\frac{1}{3}}\theta^2 \exp[-0.35(E_\gamma/E_B)^{\frac{1}{3}}]$ keV · b which should be reliable up to 600 keV. This agrees with the observations reported by Tanner [8]) if θ^2 is taken to be $\frac{1}{3}$. This is not unreasonable since a rough calculation for a one particle 2s state gives $\theta^2 \approx \frac{1}{2}$. The calculations reported here do not have the same energy dependence as those quoted by Tanner although the absolute value is similar at ≈ 600 keV. It is not clear why this should be the case: those quoted by Tanner were preliminary numerical calculations before the approximate analytic methods above were developed.

The same procedure has also been used to estimate the capture to the $D_{\frac{3}{2}}$ state bound by 598 keV. The WKB approximations are not as reliable here. The result is $S = 0.26(E_B/E_\gamma)^{\frac{1}{3}}\theta^2 \exp[1.9(E_\gamma/E_B)^{\frac{1}{3}}]$ keV · b up to about 600 keV. This is only $\frac{1}{5}$ of the transition to the excited state at 600 keV and is less at lower energies. This ratio is in accord with experiment which indicates that this ratio is small.

3.5. INTERFERENCE OF DIRECT AND RESONANT CAPTURE

In the preceding, we have assumed that the dominant capture interaction was taking place so far from the nucleus that specific nuclear phase shifts could be neglected. This permitted us to use just F, the regular Coulomb function, in calculating the matrix element. Apart from potential phase shifts, which may become important, there is the case of resonance when the nuclear phase shift is certainly important since it necessarily becomes large. In this case, it is of interest to examine the nature of the interference between the resonant and direct reactions since this can be observed [10]).

In view of the usual energy dependence of the resonant phase shift, we can identify $G+iF$ as the relevant quantity, the square of the integral of which determines the resonance intensity whereas, if δ_0 is the potential phase shift,

the off resonance intensity is similarly given by $[\int (F \cos \delta_0 + G \sin \delta_0)]^2$ which equals $(\int F)^2$ in the case δ_0 is negligible. In any explicit example, of course, we would refer to the appropriate contributions from the two J values as indicated in sect. 2.

In some cases, as for example $C^{12}+p$, it has been of interest to compare the γ-ray width of the mirror nucleus $C^{13*} \rightarrow C^{13}+\gamma$ with that indicated by the resonance at 1.7 MeV in $C^{12}+p \rightarrow N^{13*} \rightarrow N^{13*}+\gamma$ observed by Woodbury [10]). Now only that part of the matrix element which is largely unaffected by Coulomb effects could legitimately be expected to be similar in the two cases. That is, the G^2 part of the matrix element is the part that may be equal in the two cases. This means that whenever F gives a large contribution, as it does in the examples being discussed, it will be necessary to extract just that part associated with G^2 for the purposes of mirror nucleus comparison. Such an analysis is in principle possible through the fact that $G+iF$ determines the phase of the resonant contribution compared to the non-resonant one when the potential phase shift is zero or is known from the scattering data. It can also be determined by comparing the resonance strength with the non-resonant strength at any particular angle. In this example, $N^{13*} \rightarrow N^{13*}+\gamma$, such an analysis indicates that only about half of the γ-ray width, i.e. about 30 ± 10 MeV out of about 50 ± 10 MeV, can be attributed to G^2 for purposes of comparison with the mirror.

In another example $O^{16}+p \rightarrow F^{17*} \rightarrow F^{17}+\gamma$, the non-resonant γ ray has been observed [11]) in the region of the p-wave resonance at 2.66 MeV. This means that not both the matrix elements of F and G vanish. As a consequence we can be sure that the resonance intensity F^2+G^2 cannot vanish. This prediction is in contradiction with the observation of ref. [11]) that this transition is not resonant.

4. Discussion

As a result of these calculations, we have found that the exterior contribution to the matrix element in a p–γ reaction will dominate for sufficiently small γ-ray energies and may already be important for γ-ray energies below two MeV. When this is the case, it is possible to calculate the capture cross section in terms of a single unknown parameter which we may call the reduced width of the final state. This unknown is, in fact, just the amplitude for the capture particle in the final state to be found far out in the barrier away from the target nucleus in its ground state.

In certain cases when, either from scattering or other experiments or from theory, we have some a priori knowledge of this reduced width, we can make an absolute calculation of the capture cross section. In other cases we may only be able to predict accurately the energy dependence of the cross section. The

results of such absolute calculations are seen, in the results given in sect. 3, to be quite reasonable.

In particular in the case of the capture by O^{16} to form the $S_{\frac{1}{2}}$ state of F^{17}, we would expect that a good calculation would be possible since this state is presumed to be well described by O^{16}+a 2s proton. For such a case, where we can set $\int u^2(r)\mathrm{d}r = 1$ as a normalization, we find that $\theta^2_{sp} \approx \frac{1}{2}$. Also, our approximate formulae should be improved when precise calculation is desired. A numerical integration at about 400 keV in this case shows that a correct result is about 1/1.6 times our approximate expression. Consequently the actual agreement with experiment is here very good. This agreement is, of course, somewhat sensitive to the radius r_n where the connection between the exterior function W and the interior function u is made. The calculated cross section is approximately proportional to the square of this radius in this case. We have intentionally chosen a radius significantly larger than the mean nuclear radius of electron scattering experiments in order to arrive more nearly at the radius where the nuclear forces have so decreased that the Coulomb forces become dominant. This radius is not only greater because of the range of the nuclear force but also because of the thickness of the nuclear surface. The value which we have chosen was taken to be $r_n = \frac{1}{2}(A_1^{\frac{1}{3}} + A_2^{\frac{1}{3}})e^2/mc^2 = 1.77\, r_e = 4.98 \times 10^{-13}$ cm $= 1.97(16)^{\frac{1}{3}} \times 10^{-13}$ cm. This is by a factor 1.8 greater than the mean nuclear radius.

At this point, it is convenient to reverse the argument. Once we are convinced that the matrix element is "extranuclear" we may use the cross section measurement at low energy as a direct measurement of the amplitude for finding a proton exterior to the nucleus in the final state. We find in these cases that the Coulomb barrier to the leaking out of such a proton is much smaller than would be obtained with a conventional nuclear radius and can be estimated correctly with a rather enlarged radius as we have done. These measurements can thus be used as a sensitive test of our understanding of the region of the nucleus where the nuclear attractive force changes into the Coulomb repulsion. The most direct way of approaching this problem through these results would be to compute directly from the cross section, the amplitude for finding the proton outside the nucleus. This can then be compared with any detailed theory or measurement of the nuclear surface.

One of us (R. F. C.) would like to thank Professor J. R. Oppenheimer for the hospitality of the Institute for Advanced Study, and to acknowledge the support of the National Science Foundation, which made it possible to write up this work. Support (of I. D.) by an Imperial Oil of Canada Fellowship is also acknowledged.

References

1) Warren, Laurie, James and Erdman, Can. J. Phys. **32** (1954) 563
2) Bloch, Hall, Broyles, Bouricius, Freeman and Breit, Rev. Mod. Phys. **23** (1951) 147
3) W. A. Fowler, Ap. J. **127** (1958) 551
4) Ralph W. Kavanagh, Nuclear Physics **15** (1960) 411
5) W. A. Fowler, Mémoires Soc. Roy. Sciences de Liège (1960)
6) H. D. Holmgren and R. L. Johnston, Phys. Rev. **113** (1959) 1556
7) P. D. Miller and G. C. Phillips, Phys. Rev. **112** (1958) 2048
8) Neil Tanner, Phys. Rev. **114** (1959) 1060
9) F. G. Nash, M. Sc. thesis, Univ. of British Columbia (1959)
10) H. H. Woodbury, A. V. Tollestrup and R. B. Day, Phys. Rev. **93** (1954) 1311
11) R. A. Laubenstein, M. J. W. Laubenstein, L. J. Koester and R. C. Mobley, Phys. Rev. **84** (1951) 12

2.G

Nuclear Physics **24** (1961) 102—106; ©*North-Holland Publishing Co., Amsterdam*

Not to be reproduced by photoprint or microfilm without written permission from the publisher

THE POLARIZATION OF PROTONS $Be^9(d, p)Be^{10}$ AND $Li^6(d, p)Li^7$ FOR 1.63 MeV DEUTERONS

A. M. K. VAN BEEK † and G. O. ANDRÉ

Fysisk Institutt, Norges Tekniske Høgskole, Trondheim, Norway

Received 27 October 1960

Abstract: The degree of polarization of the ground state protons of Be^{10} when Be^9 is bombarded with 1.63 MeV deuterons, has been found to be $P = +1\ \% \pm 7\ \%$ at an angle of 40°. Although the statistics in the lithium reaction are very poor we estimated the degree of polarization to be $-48\ \% \pm 16\ \%$ and $-63\ \% \pm 14\ \%$ for the ground state and first excited state protons respectively at 40°.

1. Introduction

The angular distributions of stripping reactions at deuteron energies well above the Coulomb barrier are successfully described by the Butler theory [1]). However, also at lower deuteron energies, even below the Coulomb barrier, stripping plays a dominant part in the reaction mechanism especially for light nuclei and it is often possible to decide upon the orbital angular momentum of the captured nucleon from the observed angular distributions [2, 3, 4]). Recent calculations by Tobocman [5]) who used a distorted-wave Born approximation give a still better fit to the angular distributions and even for heavier nuclei it seems possible to determine the angular momentum of the captured nucleon for relatively low incident deuteron energies. Though Butler's theory predicts zero polarization of the outgoing particles, Newns [6]) showed that the protons and neutrons from a stripping reaction are generally polarized. Experiments [7–10]) demonstrated, however, that the sign and magnitude of the polarization, were in contradiction with theory, although the general behaviour was understood [11]). The calculations by Tobocman seem to be successful in describing the polarization. The predicted values are strongly dependent on the choice of the optical model parameters involved, and more experimental information will be needed. In the present work some results obtained for the $Be^9(d, p)Be^{10}$ and $Li^6(d, p)Li^7$ reactions are discussed. These reactions were favourable since the Q-values are rather high, so that protons of sufficient energy are produced though the maximum deuteron energy obtainable with the Trondheim Van de Graaff-generator is rather low. Moreover we could compare the

† Present address: Natuurkundig Laboratorium der Rijksuniversiteit, Westersingel 34, Groningen (The Netherlands).

polarization values with measurements by one of us [3]) of the angular distributions for these reactions at the same deuteron energy. An interesting aspect of experiments at low deuteron energy could be the observation of an enhanced polarization due to Coulomb effects [12, 13]).

If we define a spin orientation in the $\mathbf{k}_d \times \mathbf{k}_p$ direction as positive, where $\mathbf{k}_d$ and $\mathbf{k}_p$ are the wave vectors of the incoming deuterons and the emitted protons respectively, then the polarization will be positive when $j_n = l_n + \frac{1}{2}$ and negative when $j_n = l_n - \frac{1}{2}$; j_n and l_n are the total spin and orbital angular momentum of the captured neutron. Therefore the sign of the polarization can give information about the spins of the levels involved in the reactions.

2. Experimental Procedure

A beam of about 5 μA of 1,63 MeV deuterons from the Van de Graaff-generator was focused on to a 90 μg/cm^2 Be^9 target and a 130 μg/cm^2 $Li^6{}_2O$-target †. Both targets were supported by a copper backing 0.12 mm thick. The total exposures were 60 μA hours and 50 μA hours respectively, measured with a

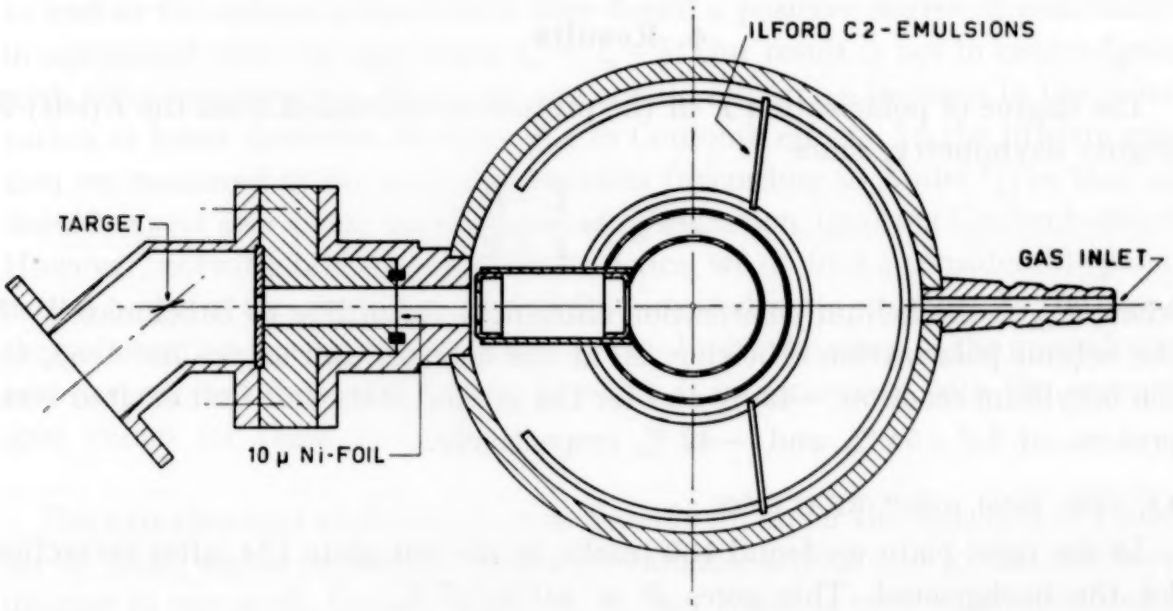

current integrator. The protons emitted at 40° (lab. angle) entered the scattering chamber through a 10 μm thick Ni foil. The chamber was filled with helium under a pressure of 2.5 or 1.5 atm respectively, helium being used as analyzer. Nuclear emulsions, Ilford C2, 200 μm thick, were positioned at 70° with respect to the proton beam, to the left and to the right, and facing the scattering volume at 15°. Slits, placed before the emulsions restricted the scattering angles of the protons. Before every exposure the helium chamber was evacuated and filled with 99.9 % pure heliumgas. Fig. 1 shows the apparatus.

† The targets were supplied by the Atomic Energy Establishment, Harwell, England.

Paraffin mixed with borax was placed between the s
the target so as to reduce the neutron background. A b
was performed by using the copper backing as a target.
must be zero in the direction perpendicular to the reactic
scattering chamber into such a position as a check of o
up-down experiment).

3. Track Analysis

An area of 14×17 mm of each plate was scanned wi
microscopes. Only tracks with dip angles between 9° a
angles of $\pm 20°$ were accepted, while we selected those p
started at the surface of the emulsion and had the relev
avoid personal errors the plates were scanned independ
The degree of polarization calculated from the scanned
the same in both cases †.

4. Results

The degree of polarization P of the protons is calcula
(right) asymmetry, since

$$PP_{\mathrm{He}} = \frac{L-R}{L+R},$$

where P_{He} is the helium polarization efficiency. Accordi
the helium polarization efficiency is, at the energies an
the beryllium reaction -43 % and for the ground state
protons of Li^7 -54 % and -42 % respectively.

4.1. THE $Be^9(d, p)Be^{10}$ REACTION

In the right plate we found 180 tracks, in the left plat
for the background. This gives $P = +0\ \% \pm 7\ \%$.

The errors are due to: (1) statistical errors, (2) misali
(3) misalignment of the angles under which the phot
positioned. The errors (2) and (3) were measured by

Because of the change of the differential cross sectio
emission of the protons from the target the asymmetry
experiment. Thus the final degree of polarization is 1 %
experiment showed no polarization.

† We thank Miss D. Ariëns Kappers and Mr. T. J. v. d. Linde for sca
and Mr A. C. C. Tenner, for valuable advice.

†† We should like to thank Dr K. W Brockman for putting the polar
(p, α)-scattering at our disposal.

Nuclear; Physics **24** (1961) 107—117 © *North-Holland Publishing Co., Amsterdam*
Not to be reproduced by photoprint or microfilm without written permission from the publisher

α) REACTIONS ON SOME LIGHT NUCLEI AT 13 MeV

N. CINDRO and M. CERINEO
Institute "Ruder Bošković", Zagreb, Yugoslavia
and
A. STRZAŁKOWSKI
The Centre of Nuclear Physics, Cracow, Poland

Received 26 October 1960

: Angular distributions of alpha particles from the reactions $B^{10}(d, \alpha)Be^{8}$, $B^{10}(d, \alpha)Be^{8*}$, $, \alpha)O^{17}$, $F^{19}(d, \alpha)O^{17*}$ have been studied with 13 MeV deuterons by means of thin llator technique. The results for B^{10} and F^{19} show a forward peaked distribution. An ıpted fit in terms of the Butler theory indicates the predominancy of direct processes in ıechanism of these reactions. The angular distribution for the reaction $Al^{27}(d, \alpha)Mg^{25}$ lso been measured. In this case it was not possible to separate the ground state from the ving excited states of Mg^{25}.
e absolute values of differential cross-sections have been measured in all cases.

1. Introduction

esults of the investigations of a large majority of medium energy reactions which proceed to a low lying level of the residual nucleus have predominancy of direct processes. This predominancy is manifested by ation from the isotropic or symmetric angular distribution, predicted ompound nucleus theory. The first processes of this kind to be discove- largely studied [1]) were the deuteron stripping and pick-up reactions, lowed by other reactions of the same type. Butler [2]) and others have tensive theoretical treatment of direct reactions, based on the analogy pping reactions. In the meantime, numerous examples of nonsymmetri- lar distributions in the range from 5—50 MeV with a large variety of ling particles have been found experimentally. The main interest, , was concentrated on the study of (n, p), (p, p′) and (α, p) reactions. kably good agreement with the theory has been found in several cases, the study of such relatively complex processes as (α, p) and (α, α′) s [3, 4]). It is natural therefore to consider [5]) reactions involving exchanges complex systems such as deuterons and α-particles, viz. (d, α) reactions, y in view of the relatively scarce experimental material existing. The (d, α) reactions at lower energies was conducted mostly with the aim of ng total cross sections or identifying states of residual nuclei [6]). How- ere have been relatively few measurements of angular distributions of

Paraffin mixed with borax was placed between the scattering chamber and the target so as to reduce the neutron background. A background experiment was performed by using the copper backing as a target. Since the polarization must be zero in the direction perpendicular to the reaction plane, we turned the scattering chamber into such a position as a check of our method (a so-called up-down experiment).

3. Track Analysis

An area of 14×17 mm of each plate was scanned with two Leitz binocular microscopes. Only tracks with dip angles between 9° and 23° and azimuthal angles of $\pm 20°$ were accepted, while we selected those proton tracks only that started at the surface of the emulsion and had the relevant range. In order to avoid personal errors the plates were scanned independently by two scanners. The degree of polarization calculated from the scanned number of tracks was the same in both cases †.

4. Results

The degree of polarization P of the protons is calculated from the L(left)-R (right) asymmetry, since

$$PP_{\mathrm{He}} = \frac{L-R}{L+R},$$

where P_{He} is the helium polarization efficiency. According to Brockman [14]) ††, the helium polarization efficiency is, at the energies and angles involved, for the beryllium reaction -43 % and for the ground state and first excited state protons of Li^7 -54 % and -42 % respectively.

4.1. THE Be^9(d, p)Be^{10} REACTION

In the right plate we found 180 tracks, in the left plate 174, after correction for the background. This gives $P = +0\ \% \pm 7\ \%$.

The errors are due to: (1) statistical errors, (2) misalignment of the target, (3) misalignment of the angles under which the photographic plates were positioned. The errors (2) and (3) were measured by an optical method.

Because of the change of the differential cross section [4]) over the angle of emission of the protons from the target the asymmetry is 1 % too low in our experiment. Thus the final degree of polarization is $1\ \% \pm 7\ \%$. The up-down experiment showed no polarization.

† We thank Miss D. Ariëns Kappers and Mr. T. J. v. d. Linde for scanning the plates accurately and Mr A. C. C. Tenner, for valuable advice.

†† We should like to thank Dr K. W Brockman for putting the polarization efficiency curves in (p, α)-scattering at our disposal.

4.2. THE $Li^6(d, p)Li^7$ REACTION

In this reaction it proved to be difficult to resolve the ground state protons and the first excited state protons from Li^7. By narrowing down the limits in which tracks could be accepted we achieved an approximate resolution of the peaks. However, the number of protons scattered to the right and to the left was very small. The sign of the polarization is negative both for the ground state protons and for the first excited state protons. After correction for the background tracks we found for the numbers of scattered ground state protons: left 27, right 16 and for the first excited state: left 50, right 29. The degree of polarization calculated from these numbers is $-48\,\% \pm 16\,\%$ for the ground state protons and $-63\,\% \pm 14\,\%$ for the first excited state protons.

5. Discussion

As we measured near the stripping peak [4]) in the beryllium reaction one may expect a small degree of polarization. Polarization measurements on this reaction have been reported by Hird *et al.* [8]) at a deuteron energy of 8.9 MeV. Close to and at the stripping maximum they found a positive degree of polarization in agreement with the spin value $j_n = l_n + \frac{1}{2}$. Our result is not in contradiction with these experiments. However, one should expect an increase in the polarization at lower deuteron energies due to Coulomb effects. In the lithium reaction we measured at the stripping maxima (according to André [3])) so that one should expect also a very small degree of polarization, ignoring Coulomb effects. However, notwithstanding our poor statistics, we do find a considerable polarization both for the ground state and first excited state protons. As the sign of the polarization is negative, $j_n = l_n - \frac{1}{2}$. This limits the spins of the ground state and first excited state of Li^7 to $\leqq \frac{3}{2}$, which is in agreement with the accepted spin values for these levels [2]).

The experimental work was done in Trondheim under the direction of Professor N. Hole, whom we want to thank for valuable advice and for his continued interest in our work. One of us (A. M. K. van Beek) is very much indebted to the Norwegian Scientific Research Council for a generous grant which enabled him to stay at the Physical Institute of the Technological University of Norway at Trondheim. The plates were scanned and the data worked out at the Physical Institute of Groningen University under the direction of Professor H. Brinkman, who suggested this work and to whom we are very much indebted for his guidance and for stimulating discussions.

References

1) S. T. Butler, Nuclear Stripping Reactions (Horowitz Publication, Sidney, 1957
2) F. Ajzenberg-Selove and T. Lauritsen, Nuclear Physics **11** (1959) 1

3) G. O. André, Nuclear Physics **15** (1960) 464
4) F. L. Canavan, Phys. Rev. **87** (1952) 136
5) W. Tobocman, Phys. Rev. **115** (1959) 98
6) H. C. Newns, Proc. Phys. Soc. A **66** (1953) 477
7) P. Hillman, Phys. Rev. **104** (1956) 176
8) B. Hird, J. A. Cookson and M. S. Bokhari, Proc. Phys. Soc. **72** (1958) 489
9) M. K. Juric and S. D. Cirilov, Phys. Rev. **112** (1958) 1224
10) R. G. Allas and F. B. Shull, Phys. Rev. **116** (1959) 996
11) H. C. Newns and M. Y. Refai, Proc. Phys. Soc. **71** (1958) 627
12) J. Yoccoz, Proc. Phys. Soc. A **67** (1959) 813
13) I. P. Grant, Proc. Phys. Soc. A **68** (1955) 244
14) K. W. Brockman, Phys. Rev. **110** (1958) 163

2.B:2.G *Nuclear; Physics* **24** (1961) 107—117 © *North-Holland Publishing Co., Amsterdam*
Not to be reproduced by photoprint or microfilm without written permission from the publisher

(d, α) REACTIONS ON SOME LIGHT NUCLEI AT 13 MeV

N. CINDRO and M. CERINEO
Institute "Ruđer Bošković", Zagreb, Yugoslavia
and
A. STRZAŁKOWSKI
The Centre of Nuclear Physics, Cracow, Poland

Received 26 October 1960

Abstract: Angular distributions of alpha particles from the reactions B^{10}(d, α)Be^{8}, B^{10}(d, α)Be^{8*}, F^{19}(d, α)O^{17}, F^{19}(d, α)O^{17*} have been studied with 13 MeV deuterons by means of thin scintillator technique. The results for B^{10} and F^{19} show a forward peaked distribution. An attempted fit in terms of the Butler theory indicates the predominancy of direct processes in the mechanism of these reactions. The angular distribution for the reaction Al^{27}(d, α)Mg^{25} has also been measured. In this case it was not possible to separate the ground state from the low-lying excited states of Mg^{25}.

The absolute values of differential cross-sections have been measured in all cases.

1. Introduction

The results of the investigations of a large majority of medium energy nuclear reactions which proceed to a low lying level of the residual nucleus have shown a predominancy of direct processes. This predominancy is manifested by the deviation from the isotropic or symmetric angular distribution, predicted by the compound nucleus theory. The first processes of this kind to be discovered and largely studied [1]) were the deuteron stripping and pick-up reactions, soon followed by other reactions of the same type. Butler [2]) and others have given extensive theoretical treatment of direct reactions, based on the analogy with stripping reactions. In the meantime, numerous examples of nonsymmetrical angular distributions in the range from 5—50 MeV with a large variety of bombarding particles have been found experimentally. The main interest, however, was concentrated on the study of (n, p), (p, p′) and (α, p) reactions. A remarkably good agreement with the theory has been found in several cases, even in the study of such relatively complex processes as (α, p) and (α, α′) reactions [3, 4]). It is natural therefore to consider [5]) reactions involving exchanges of more complex systems such as deuterons and α-particles, viz. (d, α) reactions, especially in view of the relatively scarce experimental material existing. The work on (d, α) reactions at lower energies was conducted mostly with the aim of measuring total cross sections or identifying states of residual nuclei [6]). However, there have been relatively few measurements of angular distributions of

(d, α) reactions above the energy of 10 MeV [5, 7]). Using a telescope counter technique Fisher and Fisher [5]) have made an extensive study of (d, α) reactions on nitrogen targets. Their results showed forward peaking in most cases, indicating a direct process for the mechanism of the reaction.

The following work has been undertaken with the aim of obtaining more experimental information about the (d, α) reactions which may help to throw some more light on the mechanism of these reactions. Moreover, the study of reactions involving complex particles may yield additional information on the problem of correlation of nucleons in nuclear matter, especially in light nuclei. With all this in mind we felt it was of interest to measure both the relative angular distributions and the absolute magnitude of the differential cross sections for several elements of different atomic masses.

2. Experimental Arrangement

The experiments were performed with the 13 MeV deuteron beam of the 120 cm cyclotron of the Centre of Nuclear Physics in Cracow (Poland). A 30 cm diameter scattering chamber was used. The chamber was provided with a vacuum-tight movable arm mounted on a phosphor-bronze strip. The

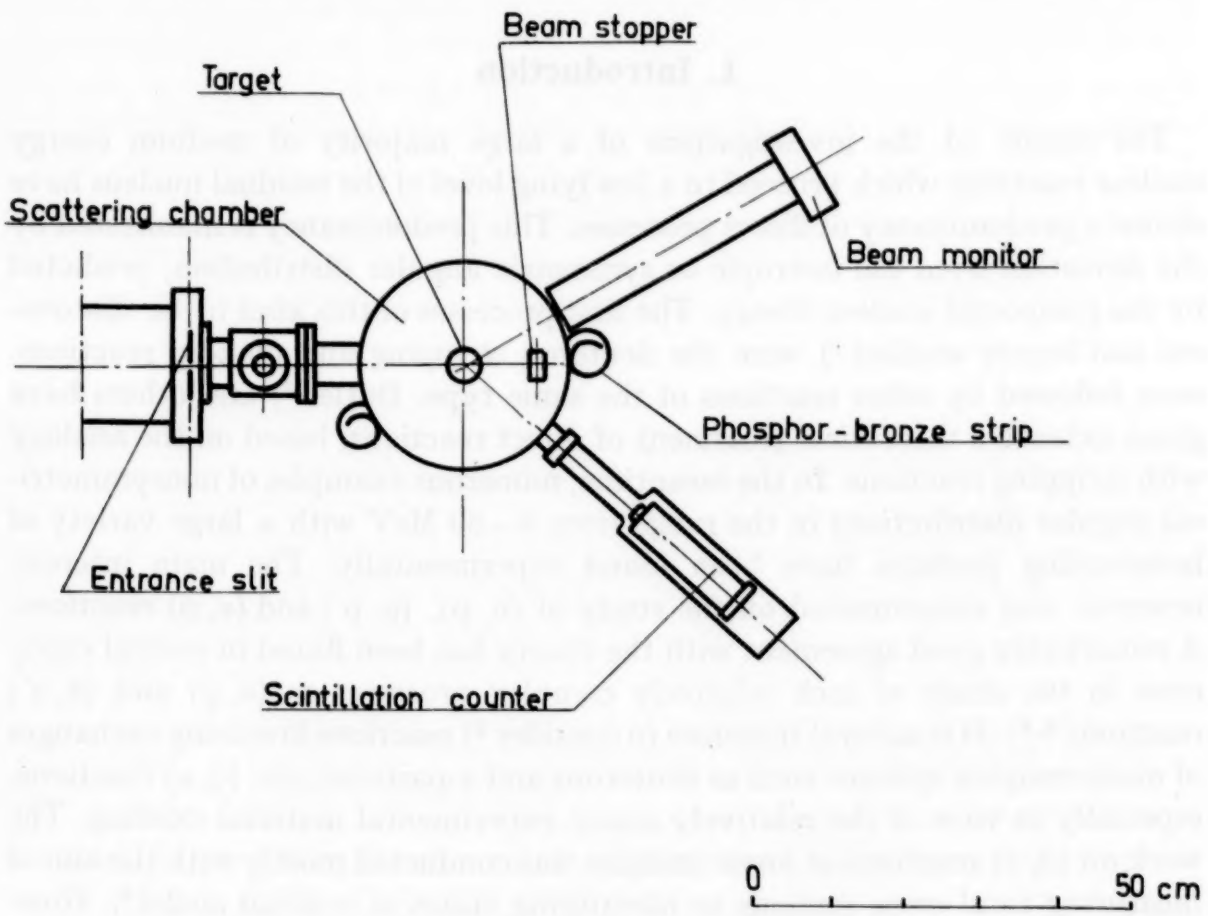

Fig. 1. General view of the experimental arrangement.

detector was placed inside the arm, at a distance of 30 cm from the target. Foils of teflon and of Al were used as targets for F^{19} and Al^{27}, while B^{10} targets were prepared by slurring natural boron powder in dissolved polystyrene. A solid target was obtained by evaporating the solvent. The reactions $B^{10}(d, \alpha)Be^{8}$ and $B^{11}(d, \alpha)Be^{9}$, both occurring for natural boron targets could easily be separated because of different Q-values. The thickness of the targets was 11 mg/cm² (boron+polystyrene), 7—10 mg/cm² (teflon) and 2 mg/cm²

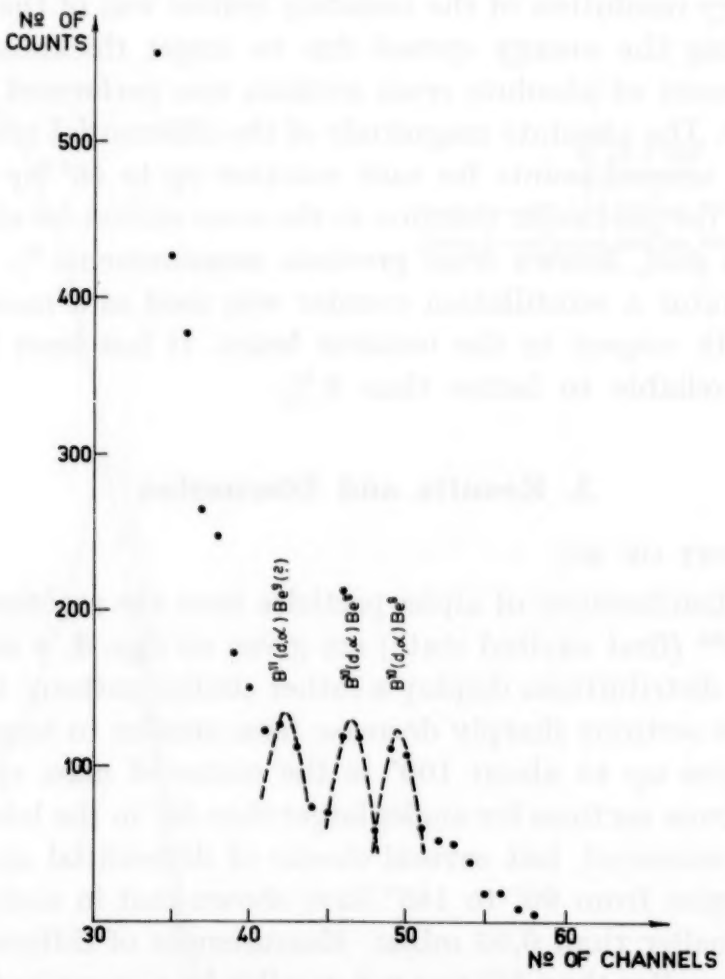

Fig. 2. Spectrum of pulses from particles emitted by the boron target bombarded with 13 MeV deuterons at $\theta_{lab} = 50°$.

(aluminium). The thickness of natural boron contained in polystyrene was 4 mg/cm². Care was taken that the beam spot, although about 0.7 cm in diameter and not always central, was not hitting the target frame. This was avoided by making targets 25 × 25 mm in dimensions. A general view of the experimental set-up is shown on fig. 1.

The detection of particles was performed by means of a thin scintillator, whose thickness was just enough to stop alpha particles of a given energy [8]). In this way particles with more energy or less specific ionization lose, in general, less energy in traversing the crystal, while particles with less energy are ruled

out by their smaller light output. By this method the use of a coincidence telescopic arrangement was avoided. Due to the dependence of the energy of the emitted alpha particles on the angle θ of emission, crystals of several different thicknesses had to be used for the same reaction.

The pulses from an EMI 6097B photomultiplier were fed through a standard equipment to a 100-channel amplitude analyzer. A typical spectrum of particles emitted by the boron target bombarded with 13 MeV deuterons is given in fig. 2. The energy resolution of the counting system was of the order of about 7—9 %, including the energy spread due to target thickness.

The measurement of absolute cross sections was performed by means of a beam integrator. The absolute magnitude of the differential cross sections was also checked at several points for each reaction up to 45° by comparing the cross section for the particular reaction to the cross section for elastic scattering of deuterons on gold, known from previous measurements [8]). In addition to the beam integrator a scintillation counter was used as a monitor at a fixed angle of 30° with respect to the incident beam. It has been found that the integrator was reliable to better than 5 %.

3. Results and Discussion

3.1. BOMBARDMENT OF B^{10}

The angular distributions of alpha particles from the reactions B^{10}(d, α)Be^8 and B^{10}(d, α)Be^{8*} (first excited state) are given on figs. 3, 4 and 5.

Both angular distributions display a rather similar pattern: in each case the differential cross sections sharply decrease from smaller to larger angles. Only the angular region up to about 100° in the centre of mass system has been measured. The cross sections for angles larger than 90° in the laboratory system have not been measured, but several checks of differential cross sections for angles in the region from 90° to 145° have shown that in each case the cross sections were smaller than 0.05 mb/sr. Measurement of differential cross sections for angles smaller than 25° was not possible by this method because of the steeply increasing number of elastically scattered deuterons and protons from (d, p) reactions on boron. The "tail" of these two peaks was large enough to smear out any structure in the region where peaks from alpha particles were expected. No definite conclusion about the behaviour of the cross sections in this region for the reactions studied could therefore be drawn.

A fit of the experimental data, using Butler's [2]) formula for the angular distribution of direct reactions has been attempted. Two processes which may contribute to the mechanism of these reactions have been considered: the "knock-out" and the "pick-up" process. Accordingly, modified Butler's formulae have been used [5]). All theoretical curves have been normalized to the experimental points at forward angles.

The curves on figs. 3, 4 and 5 represent the best fits obtained by calculating the cross sections for the pick-up and knock-out processes for reactions $B^{10}(d, \alpha)Be^8$ to the ground and first excited state. The l valus allowed by the

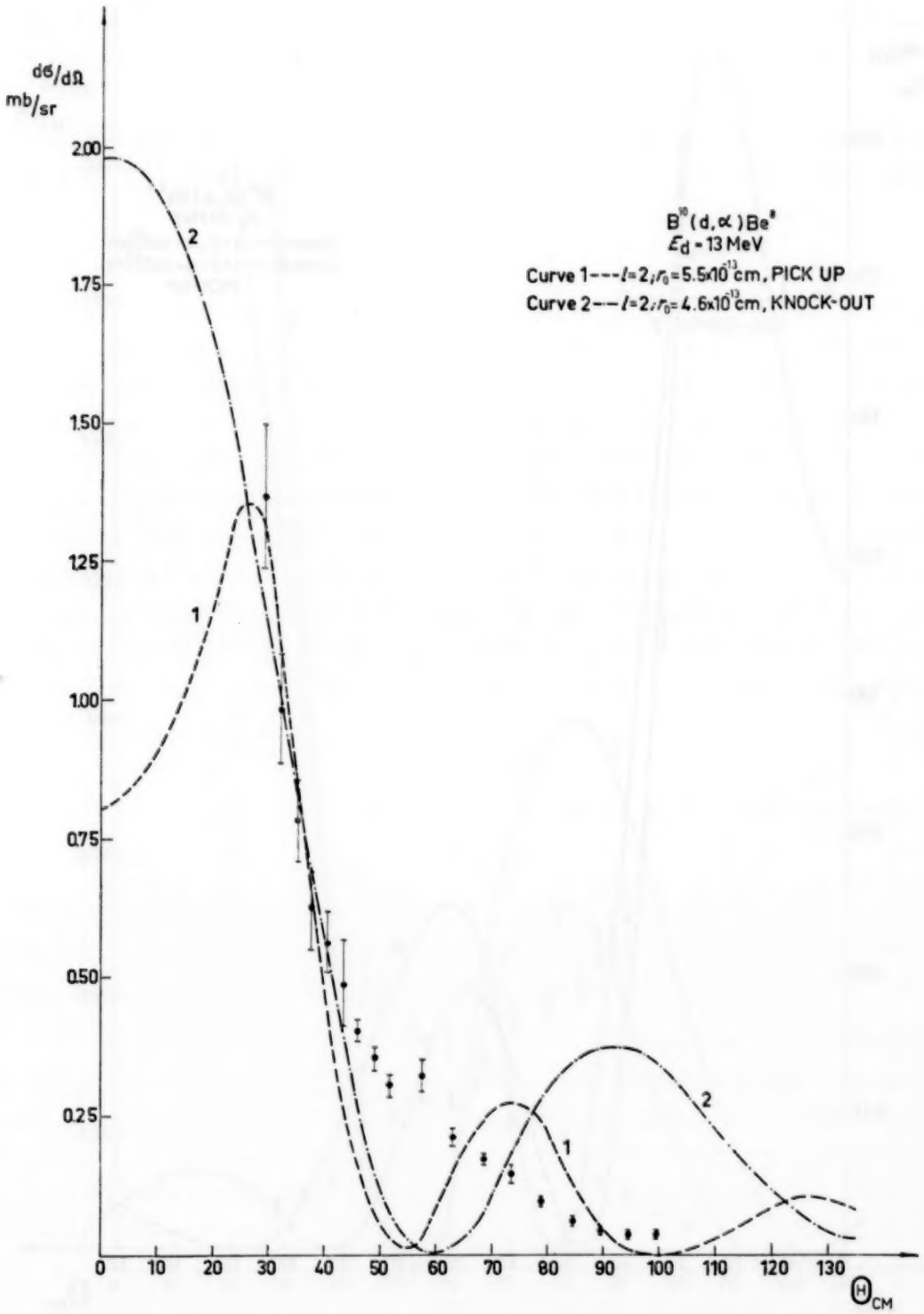

Fig. 3. Angular distribution of alpha particles from the reaction $B^{10}(d, \alpha)Be^8$ at 13 MeV deuteron energy. The curves represent theoretical fits with pick-up and knock-out calculations.

angular momentum selection rules are for the first reaction

$$l = 2, 4,$$

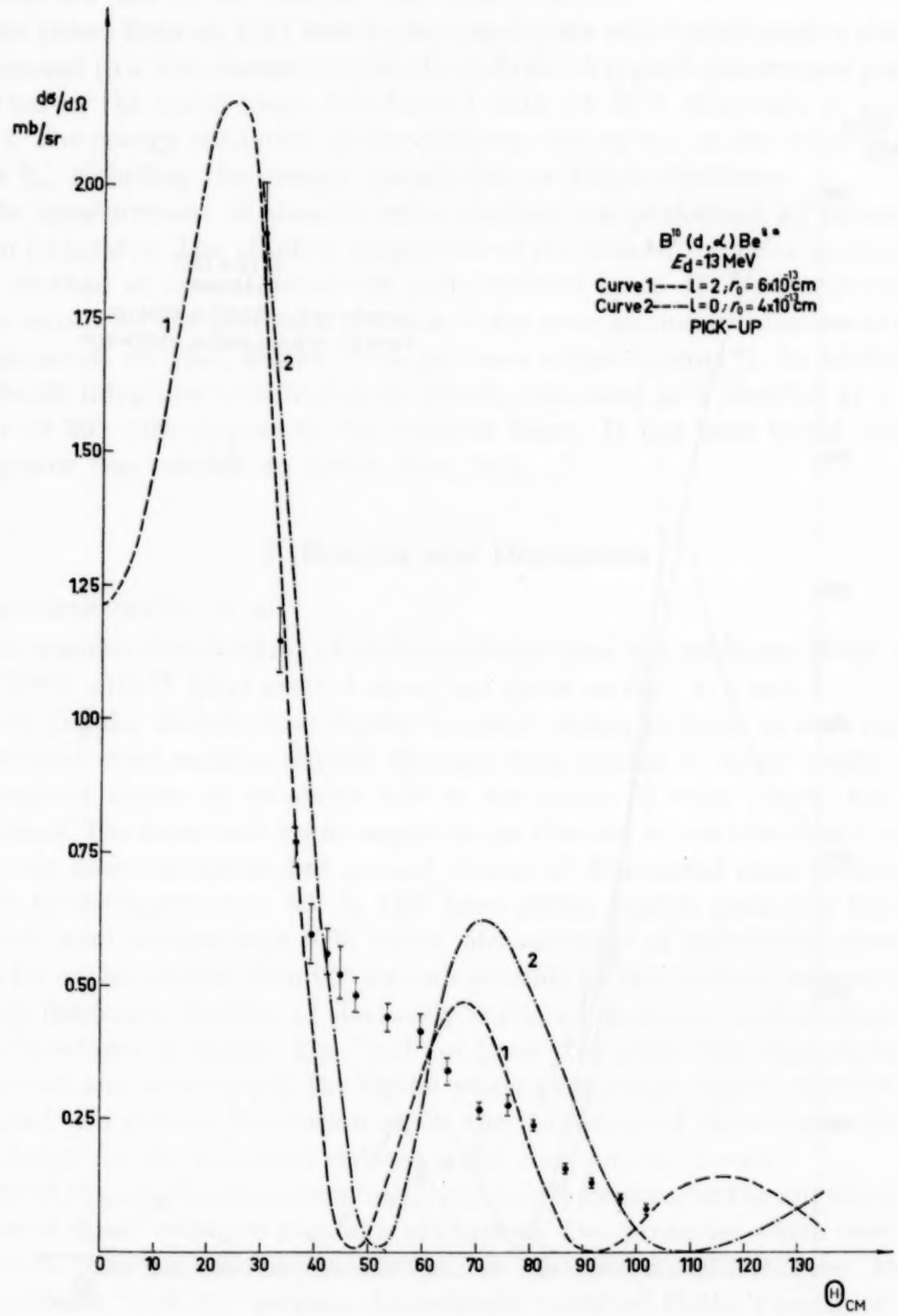

Fig. 4. Angular distribution of alpha particles from the reaction $B^{10}(d, \alpha)Be^{8*}$ at 13 MeV deuteron energy. The curves represent theoretical fits with pick-up calculations.

and for the second

$$l = 0, 2, 4, 6.$$

For the reaction $B^{10}(d, \alpha)Be^{8}$ g.s. the best fit was obtained with $l = 2$ curves.

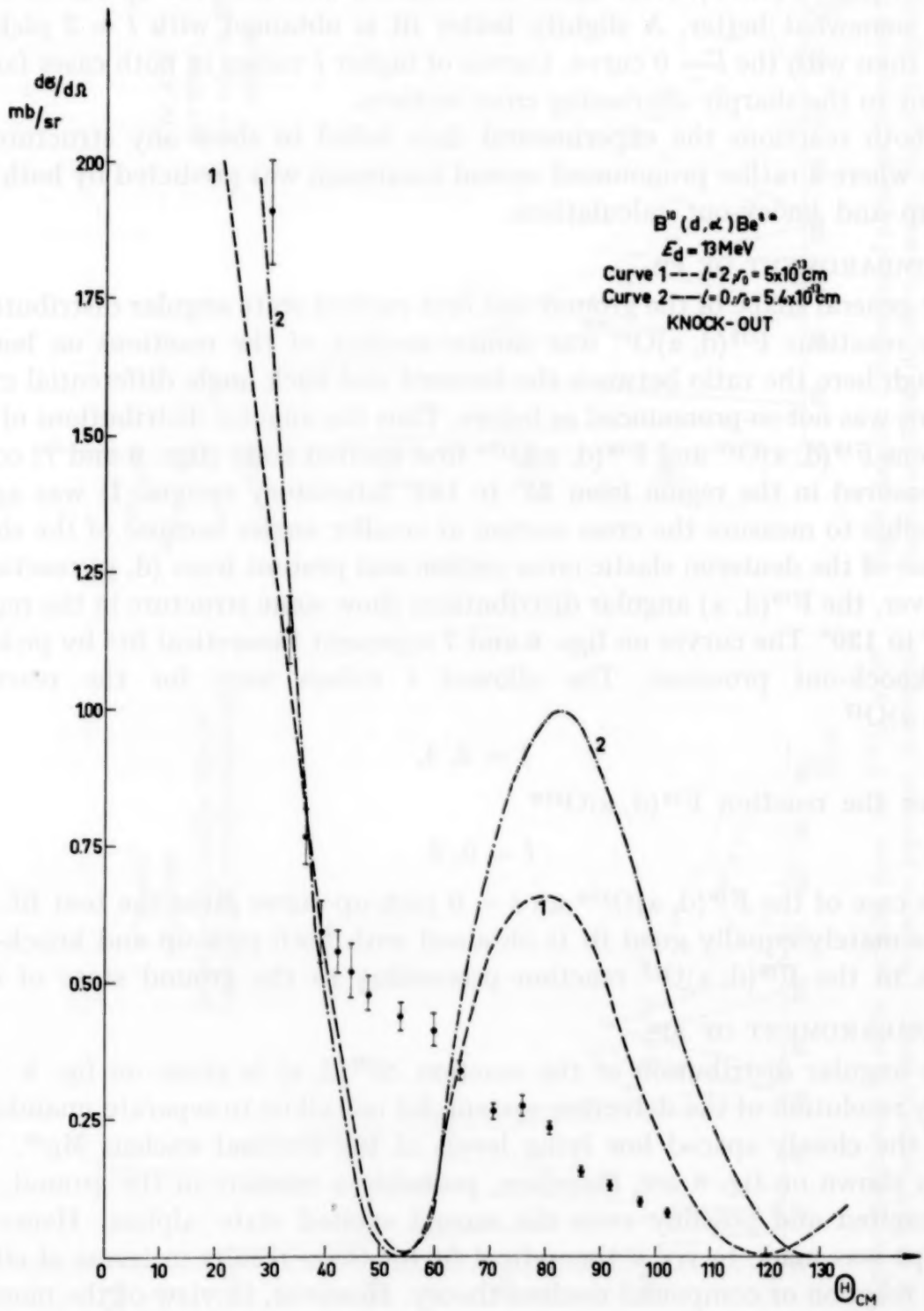

Fig. 5. Angular distribution of alpha particles from the reaction $B^{10}(d, \alpha)Be^{8*}$ at 13 MeV deuteron energy. The curves represent theoretical fits with knock-out calculations.

It appears that the pick-up process is a better approximation for the reaction mechanism than the knock-out process. The fact that it requires a larger radius is reasonable in view of the classical picture of the pick-up process. A similar situation is displayed by the angular distribution of $B^{10}(d, \alpha)Be^{8*}$ reaction (figs. 4 and 5). Here again fits obtained with the pick-up curves seem to be somewhat better. A slightly better fit is obtained with $l = 2$ pick-up curve than with the $l = 0$ curve. Curves of higher l values in both cases fail to account to the sharply decreasing cross sections.

In both reactions the experimental data failed to show any structure at angles where a rather pronounced second maximum was predicted by both the pick-up and knock-out calculations.

3.2. BOMBARDMENT OF F^{19}

The general shape of the ground and first excited state angular distributions of the reactions $F^{19}(d, \alpha)O^{17}$ was similar to that of the reactions on boron, although here the ratio between the forward and back angle differential cross sections was not so pronounced as before. Thus the angular distributions of the reactions $F^{19}(d, \alpha)O^{17}$ and $F^{19}(d, \alpha)O^{17*}$ first excited state (figs. 6 and 7) could be measured in the region from 25° to 145° laboratory system. It was again impossible to measure the cross section at smaller angles because of the sharp increase of the deuteron elastic cross section and protons from (d, p) reactions. However, the $F^{19}(d, \alpha)$ angular distributions show some structure in the region of 70° to 130°. The curves on figs. 6 and 7 represent theoretical fits by pick-up and knock-out processes. The allowed l values were for the reaction $F^{19}(d, \alpha)O^{17}$

$$l = 2, 4,$$

and for the reaction $F^{19}(d, \alpha)O^{17*}$

$$l = 0, 2.$$

In the case of the $F^{19}(d, \alpha)O^{17*}$ an $l = 0$ pick-up curve gives the best fit. An approximately equally good fit is obtained with both pick-up and knock-out curves in the $F^{19}(d, \alpha)O^{17}$ reaction proceeding to the ground state of O^{17}.

3.3. BOMBARDMENT OF Al^{27}

The angular distribution of the reaction $Al^{27}(d, \alpha)$ is given on fig. 8. The energy resolution of the detection system did not allow to separate unambiguously the closely spaced low lying levels of the residual nucleus Mg^{25}. The results shown on fig. 8 are, therefore, probably a mixture of the ground, the first excited and possibly even the second excited state alphas. Hence no attempt was made to try a theoretical fit for these results in terms of either direct reaction or compound nucleus theory. However, in view of the more or less symmetrical angular distribution, the predominancy of the direct processes seems to be improbable.

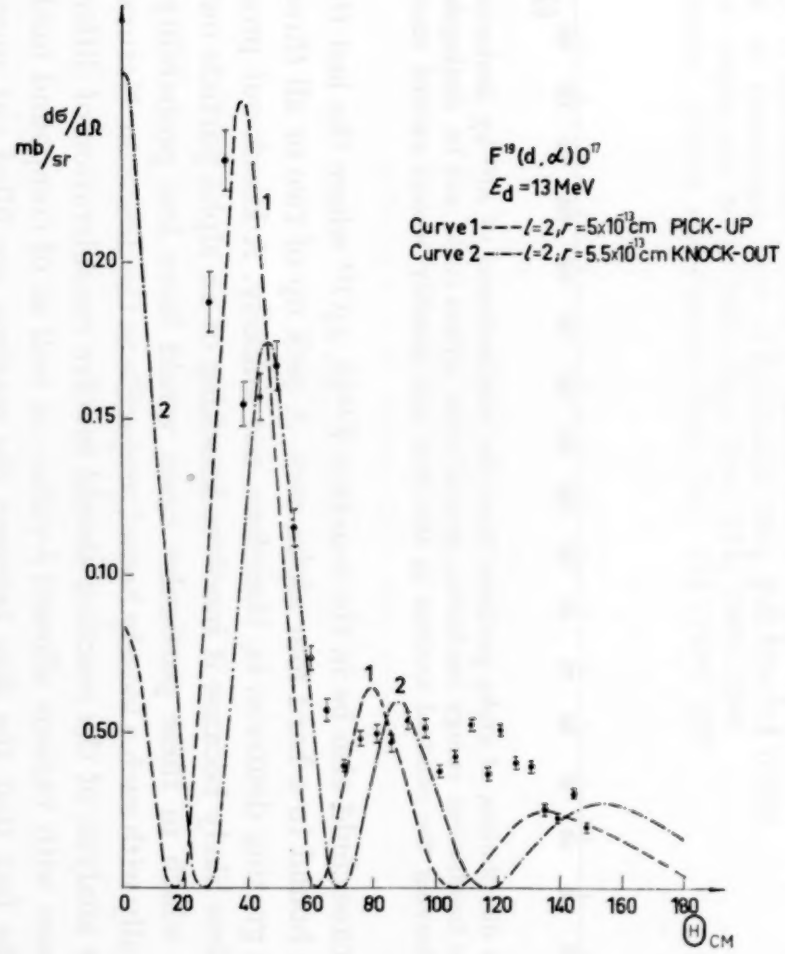

Fig. 6. Angular distribution of alpha particles from the $F^{19}(d, \alpha)O^{17}$ reaction at 13 MeV deuteron energy. The curves represent theoretical fits with pick-up and knock-out calculations.

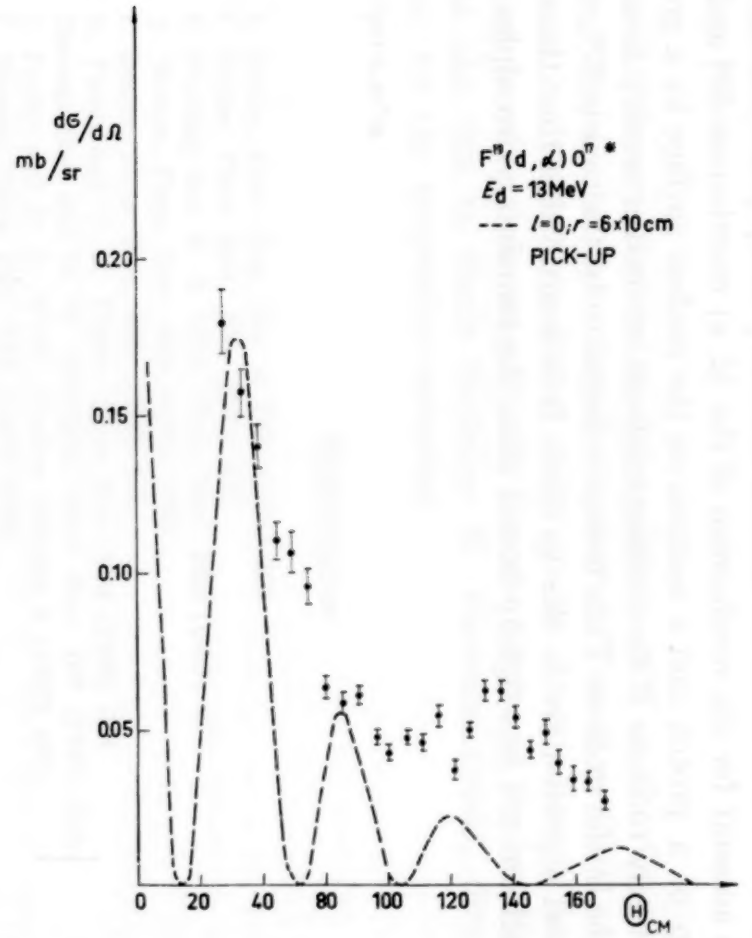

Fig. 7. Angular distribution of alpha particles from the $F^{19}(d, \alpha)O^{17*}$ reaction at 13 MeV deuteron energy. The curve represents a theoretical fit with pick-up calculation.

4. Conclusions

It appears from subsections 3.1 and 3.2 that the pick-up process is the most adequate to account for the mechanism of the (d, α) reaction on B^{10} and F^{19}. The pick up of a proton and a neutron on the nuclear surface by a grazing deuteron is likely to occur if the surface nucleons are rather weakly bound to the core of the initial nucleus. This, however, seems to be the case in B^{10}, where a neutron and a proton are in the 1p shell. It is conceivable that these two unpaired nucleons are less tightly bound than the remaining two alpha core.

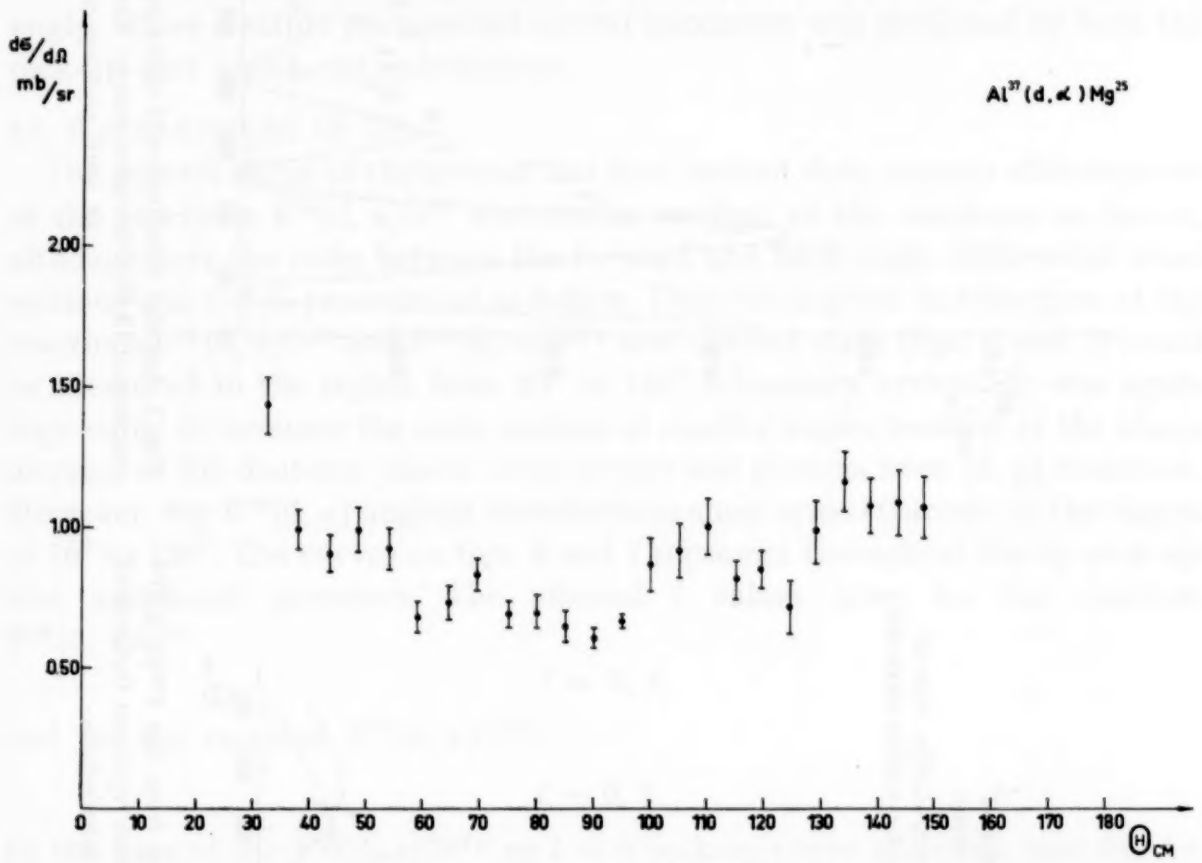

Fig. 8. Angular distribution of alpha particles from the bombardment of Al^{27} by deuterons of 13 MeV. Due to insufficient energy resolution, ground state alphas could not be distinguished from those leaving the residual nucleus in the first and possibly second excited state.

A similar case could also be in the reaction F^{19}(d, α)O^{17} where the last three nucleons are bound to a hard four alpha core. A pick up of two or all three of them by the grazing deuteron is, therefore, not unlikely. A knock-out process seems to be less likely because it involves knocking of an alpha particle out of the surface, which in these particular cases would have less probability to occur, especially with such a loosely bound projectile as the deuteron. Naturally, the complete analysis of the reaction should involve consideration of different direct processes with various allowed l-values as well as of compound nucleus processes. The fact that the dips between the maxima are filled out suggests

that the influence of nuclear absorption should also be taken into account [9]). In this analysis we have tried only to single out the prodominant mechanism of the reaction, which, in the cases of the reactions on B^{10} and F^{19} seems to be the pick-up process.

The authors are indebted to the cyclotron staff of the Cracow Centre of Nuclear Physics for operating the cyclotron. Two of us (N. C and M. C.) are also indebted to both the Polish and Yugoslav Atomic Energy Authorities for making possible their stay at the Cracow Centre of Nuclear Physics. They would also like to thank Professor H. Niewodniczanski, director of the Centre, for the hospitality extended.

References

1) S. T. Butler, Proc. Roy. Soc. A **208** (1951) 559
2) S. T. Butler, Phys. Rev. **106** (1957) 272
3) C. E. Hunting and N. S. Wall, Phys. Rev. **108** (1957) 901
4) H. J. Waters, Phys. Rev. **103** (1956) 1763;
S. T. Butler, Phys. Rev. **106** (1957) 272
5) G. E. Fisher and V. K. Fisher, Phys. Rev. **114** (1959) 553
6) E. Baumgartner and H. W. Fulbright, Phys. Rev. **107** (1957) 219;
F. J. Farley and R. E. White, Nuclear Physics **3** (1957) 561;
C. P. Browne, Phys. Rev. **104** (1956) 1598;
K. Lymhall and W. Weine, J. Inorg. and Nucl. Chem. **9** (1959) 193;
W. E. Moore, Univ. of Pittsburgh Tech. Rep. No. XI (1959);
C. P. Browne, Nuclear Physics **12** (1959) 662;
S. V. Starodubtzev and K. V. Makarunas, Dokladi A. N. USSR **129** (1959) 547
7) E. W. Hamburger, Univ. of Pittsburgh Tech. Rep. No. XI (1959)
8) N. Cindro and N. S. Wall, Phys. Rev. **119**(1960) 1340
9) Butler, Austern and Pearson, Phys. Rev. **112** (1958) 1227

1.E.1:
3.A

Nuclear Physics **24** (1961) 118—125; © *North-Holland Publishing Co., Amsterdam*
Not to be reproduced by photoprint or microfilm without written permission from the publisher

TRANSITIONS BETWEEN LOW-LYING EXCITED STATES OF Mn^{56} AND Ho^{166}

I. V. ESTULIN, A. S. MELIORANSKY and L. F. KALINKIN

Nuclear Physics Research Institute of the Moscow State University, Moscow, USSR

Received 14 September 1960

Abstract: The measurement of coincidences of cascade-quanta is used as a technique for investigating the low-lying levels of odd nuclei of Mn^{56} and Ho^{166} arising in the radiative capture of thermal neutrons. Reduced probabilities of M1 and E2 mixed radiative transitions with energies of 25 and 85 keV are found for Mn^{56}. The rotational band 0^-, 2^- (54.2 keV) and 4^- (174 keV) is detected in the strongly deformed nucleus Ho^{166}.

1. Introduction

A luminescent coincidence spectrometer [1]) was used for measuring soft cascade γ-quanta emitted from nuclei in the radiative capture of thermal neutrons. The sequence of measurements which was: evaluation of accidental coincidences, application of filters to allow for the "pedestal" resulting from hard γ-quanta, detection of the characteristic K-shell X-radiations etc., was described in our previous work [2]). The development of the techniques [3]) has made it possible to obtain quantitative data through the analysis of the coincidence spectrum: the absolute intensity of cascades, the coefficient of internal conversion of γ-quanta on atomic electrons and a sequence of radiative transitions.

In the general case the intensities of γ-quanta, n_{γ_1} and n_{γ_2}, in the cascade are not equal, as a result of additional transitions to the lower excited level or the internal conversion of γ-quanta. If N_c is the number of pulses from the γ-line detected in the coincidence spectrum and N_g is the number of pulses in the governing canal from the isolated γ-line, determined through the analysis of the spectrum into components, then the ratio N_c/N_g will be equal to

$$\frac{N_c}{N_g} = \frac{q}{n_g}\,\varepsilon\omega. \tag{1}$$

In this relation, q is the cascade intensity, which is of the same dimension as the intensity of γ-quanta n_g governing the coincidences, ε and ω are the effectiveness and the solid angle of the canal in which the coincidences are selected. The

value q/n_g will be different in governing the upper γ-quantum,

$$\frac{q}{n_g} = \frac{1}{(1+\alpha)_{\gamma_1}}, \tag{2a}$$

or the lower one,

$$\frac{q}{n_g} = \frac{n_{\gamma_2}}{n_{\gamma_1}(1+\alpha)_{\gamma_1}}, \tag{2b}$$

where α is the total coefficient of internal conversion of γ-quanta on atomic electrons, γ_1 denotes the lower γ-quantum and γ_2 the upper one. The respective expressions also hold for the detection of characteristic X-radiation.

Eqs. (1) and (2) were used in investigating the low-lying levels of Mn^{56} and Ho^{166}. The experimentally found ratio N_c/N_g determined $(q/n_g)_{exper}$, which was then compared with theoretical values for cases (2a) and (2b) for different radiation multipolarities. The results of this analysis are given below. The efficiency of the spectrometer ε and the solid angle ω were found from independent experiments. The technique is described in detail in ref. [3]).

Measurements of the coincidence spectrum were combined with those of a single spectrum with a view to determining absolute intensities in the number of γ-quanta per captured neutron [4]).

2. The Nucleus Mn^{56}

The spectrum of γ-quanta emitted in the radiative capture of thermal neutrons in Mn^{55} was investigated by a number of authors [5–8]). The present work is concerned with measurements of the energies and absolute intensities of the soft γ-quanta of the reaction $Mn^{55}(n, \gamma)Mn^{56}$ and coincidences among them. Apart from this, measurements were made of the coincidences between soft and hard γ-rays with energies close to the neutron binding energy in Mn^{56}. The results are represented in table 1.

TABLE 1

Results of the coincidence measurements

No.	Energy of γ-line (keV)	Intensity of γ-line in % per captured neutron	Coincides with γ-quanta (keV):
1	25±2	23 ±3	85, 108, >6200
2	85±2	18 ±2	25, 108, >6200
3	108±3	12 ±2	25, 85, >6200
4	190±4	2.5±0.5	[a]) >6200
5	217±4	11 ±2	>6200
6	280±5	8 ±3 [b])	>6200

[a]) The intensity of γ-quanta coinciding with the 25 keV γ-line was measured in the energy region up to 140 keV.

[b]) Intensity of 280 keV γ-line is determined from $\gamma-\gamma$-coincidences.

In the analysis of the results it was observed that the ratios of the areas of the photopeaks from 85 and 108 keV γ-quanta manifested in coincidences with the 25 keV γ-line are equal within errors to the ratios of the areas of the same γ-lines in the spectrum measured by a single-crystal spectrometer. In the coincidence spectrum with the sum of γ-lines 85 and 108 keV the areas of the photopeaks from these γ-quanta proved to be rather close. These facts indicate that the 108 keV γ-line is almost entirely due to the transition from the third excited level to the second (fig. 1). The upper limit of intensity of γ-quanta

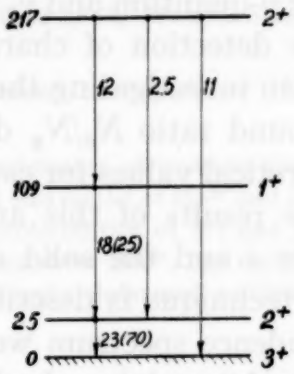

Fig. 1. Scheme of the low lying levels in Mn^{56}. The transition intensities are indicated.

involving a possible transition from the 109 keV level to the ground state, does not, according to this data, exceed 1.3 % per captured neutron. The technique of analysis of γ—γ-coincidences described in the previous section was used for determining the total conversion coefficients for the 25 and 85 keV γ-transitions. Table 2 represents experimental values and theoretical total conversion coefficients in the K, L and M shells[9]). Experimental data for the 85 keV radiative transition can be brought into agreement with theoretical values under the assumption either of the M2 transition or a mixture of multi-

TABLE 2

Total conversion coefficients

Transition energy (keV)		25				85			
Conversion coefficient $1+\alpha$	Theory	E1	M1	E2	M2	E1	M1	E2	M2
		3.36	2.37	79.7		1.05	1.05	1.83	1.55
	Experiment	3.0±0.2				1.4±0.2			
Multipolarity of transition		99 M1±1 E2				55 M1+45 E2			
Reduced probability	$B(M1)10^{-5}(e^2 \cdot b)$	0.83				0.3			
	$B(E2)(e^2 \cdot b)$	1.4				4			

poles M1+E2. The first possibility has to be rejected because the lifetime of the excited level is too long, which contradicts experiment [8]). Thus the 85 keV transition is a mixture of M1+E2 multipoles and consequently does not change the parity of the states. To the 109 keV level there is a direct transition of the E1 type from the initial state of Mn^{56} (2^- or 3^-, the first being more probable) realized in the capture of a thermal neutron [10]). Consequently the 109 and 25 keV states have positive parity.

The intense 25 keV γ-line in the spectrum can only result from a dipole transition. The measured value of the total internal conversion coefficient (table 2) is close to the theoretical one for the E1 transition. Yet the parities of the ground and first excited states are equal and there can be no such transition between them. The experimental value $(1+\alpha)$ for 25 keV exceeds the theoretical quantity for the M1 transition which warrants the conclusion that this transition is a mixture of multipoles M1+E2. A considerable difference between the conversion coefficients for the transitions of such multipolarities makes it possible to determine a low admixture of E2 radiation amounting to (0.8 ± 0.3) %.

The investigation of γ—γ-coincidences confirms the scheme of γ-transitions between the lower levels of Mn^{56} given in ref. [6]). The values of the multipolarities of 25 and 85 keV γ-transitions do not contradict the results of ref. [8]) in which the lifetimes of the first three excited levels of Mn^{56} were measured, nor those of ref.[11]) on the radiation of Cr^{56}. The results of ref. [8]) taken together with our data on conversion coefficients and multipolarity mixtures made it possible to calculate the experimental values of the reduced probabilities of the M1 and E2 transitions with energies 25 and 85 keV (table 2). The reduced probability of the 25 keV M1 transition was determined accurately to ±10 % and the rest accurately to ±50 %. The transitions of the M1 type are retarded as compared with those of the one-particle type by 10 to 40 times and the E2 transitions enhanced by two or three orders.

Similarly to the states of odd proton and neutron in the adjoining nuclei of Mn^{55} and Fe^{57}, the configuration $(f_{\frac{7}{2}})_{\frac{5}{2}}^3\, p_{\frac{3}{2}}$ corresponds to the ground state of Mn^{55}. The magnetic moment of the configuration of this kind is close to the experimental value [12]). The configuration $f_{\frac{7}{2}} f_{\frac{5}{2}}$ (ref. [11])) corresponds to the 109 keV level. From this level there is a M1+E2 transition to the 25 keV level (table 2) but no transition to the ground state. Therefore the configuration $f_{\frac{7}{2}} p_{\frac{3}{2}}$ can be ascribed to the 25 keV level, the 85 keV transition being assumed to be a neutron transition and the 25 keV transition the difference of energies of the states $(f_{\frac{7}{2}})_{\frac{5}{2}}^3$ and $f_{\frac{7}{2}}$. Probably the 217 keV level is described by a mixed configuration $(f_{\frac{7}{2}})_{\frac{5}{2}}^3+f_{\frac{7}{2}} f_{\frac{5}{2}}$ since from this level there are transitions, comparable in intensity, to all lower states. The above configurations of the ground state and the 217 keV level account for the largest probability of E1 transitions from the initial state of Mn^{56} (ref. [10])) in the case of a "direct" radiative capture of the neutron.

3. The Nucleus Ho^{166}

Soft γ-quanta arising in the reaction $Ho^{165}(n, \gamma)Ho^{166}$ with energies 120 and 145 were detected in refs. [13, 14]). The present work investigates the connection between these γ-quanta and the Ho^{166} levels populated in the β-decay of Dy^{166} (refs. [15, 16])). There was a hope of revealing a band of rotational levels since the odd nucleus of Ho^{166} is situated in the region of strongly deformed nuclei.

TABLE 3

Gamma-rays of the reaction $Ho^{165}(n, \gamma)Ho^{166}$

No.	Energy of γ-line (keV)	Intensity (in % per captured neutron)	Coincides with γ-line (keV):	Multipolarity of transition
	47 ± 2 [a])	$58\ \pm12$	47, 121, >1750	
1	56—66	$19\ \pm\ 5$ [b])	121	M1
2	82 ± 2	2.5	47, >1750	M1
3	121 ± 3	$16\ \pm\ 2$	47, >1750	E2
4	140 ± 3	$22\ \pm\ 3$		E1+M2

[a]) X-ray.
[b]) Strongly converted transition, total intensity is indicated.

Table 3 lists the energies and intensities of γ-quanta from the reaction $Ho^{165}(n, \gamma)Ho^{166}$. In the papers published before, γ-lines 1 and 2 are not indicated and the intensities of γ-lines 3 and 4 found in the present work differ somewhat from the results of ref. [13]) and especially from those of ref. [14]), where the data on the 121 keV γ-line seem to be erroneous. The 47 ± 2 keV peak is accounted for by the K-shell X-ray radiation of the Ho atom.

Four different series of measurements of coincidence spectra dealt with X-radiation, 121 and 140 keV γ-lines, and hard γ-quanta $E_\gamma > 1.75$ MeV. In these experiments no coincidences with 140 keV γ-quanta were found, which suggests, in agreement with ref. [17]) a large lifetime of the level from which the transition under consideration occurs. The 140 keV γ-transition can lead either to the ground state of Ho^{166} or to the first excited 54.2 keV state [16]) since it was impossible to detect the coincidences with these γ-quanta because of their considerable conversion on atomic electrons. In ref. [17]) the investigators determined the coefficient of internal conversion of the 140 keV γ-quanta in the K-shell ($\alpha_K \approx 0.4$) the value of which points to two possible multipolarity variants: E2 or E1 with a 5 % admixture of M2 [18]). An E2 transition so strongly retarded ($\tau = 2.14\times10^{-4}$ sec) [17]) is rather improbable but E1 transitions with a retardation factor of 10^{-6} to 10^{-9} are known. The intensity of the transition also is evidence for E1 multipolarity. Therefore it is more likely that the 140 keV γ-transition is a mixed one, which contradicts the assumption that it leads to the ground state. Consequently in the nucleus of Ho^{166} there is a 194 keV

level and a characteristic 3^+, as is shown in fig. 2. This accounts satisfactorily for the absence of transitions to the second excited level and the ground state.

In measuring coincidences with 121 keV γ-quanta there appears the 47 ± 2 keV peak corresponding within experimental error, to the K-radiation of Ho, but no other γ-lines are detected. Coincidences with 121 keV γ-quanta were also observed in the selection of X-radiation coincidences. Thus the 121 keV γ-quanta are located in a cascade with a strongly converted γ-line (designated through "y"), the conversion coefficient of this line on the electrons of the K-shell being $\alpha_K \geqq 10$. This evaluation of α_K excludes the possibility of

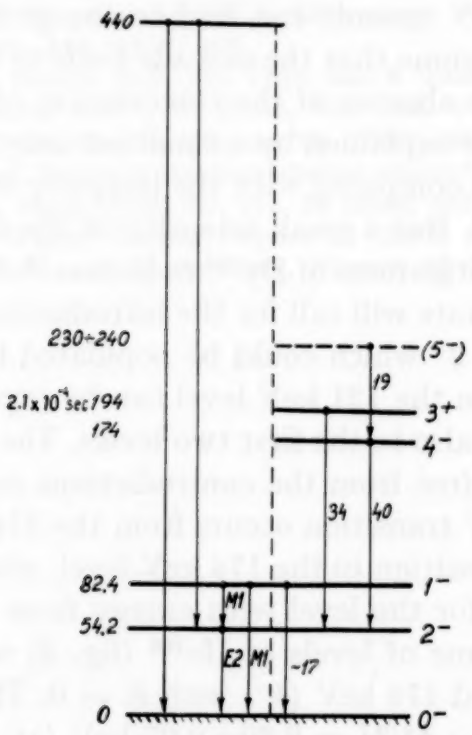

Fig. 2. Scheme of Ho^{166} levels. On the left side are shown the levels seen in the decay of Dy^{166} (ref. [16])). On the right side, those in the reaction (n, γ). The total transition intensities are indicated.

E1 and E2 transitions but allows the multipolarity of the M1 type with energies 55 to 65 keV or of the M2 type with energies 56 to 120 keV. If the energy of the transition under consideration $E_\gamma = 47\pm2$ keV coincides with the energy of K-radiation, the multipolarity of this transition can only be E1.

The intensity of the y-121 keV cascade is determined from eq. (1),

$$\left(\frac{q}{n_{120}}\right)_{\text{exper}} = 0.34\pm0.06. \tag{3}$$

This value was compared with the theoretical one under different assumptions about the multipolarity of the radiative transitions under consideration. If the 121 keV γ-transition is regarded as the upper one, the evaluation of the multi-

polarity of the converted transition, agrees with the value (3) and contradicts the estimates of multipolarity with respect to α_K. Therefore case 2a is rejected. A similar analysis for 47 keV γ-quanta leads to similar conclusions. Thus the lower transition has an 121 keV (case 2b). Using the experimental value of (3), we determine from an expression similar to (2b) the total intensity of the transition "y" : $n_y = 19$ % per captured neutron with the multipolarity of M1 or E2 121 keV γ-quanta. The multipolarity is found from the intensity of X-radiation measured in a single crystal spectrum (table 3) with allowance for the internal conversion of the detected γ-transitions in the K-shell, E2 being more preferable.

The intense y-121 keV cascade can lead to the ground state or the lowest excited levels. Let us assume that the cascade leads to the second excited level (fig. 2). In this case the absence of the coincidences of 121 keV with those of 82 keV would have to be explained by a small intensity of the direct transition (of the order of 5 %) as compared with the intensity of the cascade transition from the 82.4 keV level. But a small intensity of the direct transition contradicts the results of investigations of Dy^{166} radiation [17, 18]). The transition of the cascade to the ground state will call for the introduction of new levels of Ho^{166} with assignments 1^- or 2^- which could be populated in the β-decay of Dy^{166}. Besides, transitions from the 121 keV level can be expected to occur not only to the ground state but also to the first two levels. The scheme of γ-transitions represented in fig. 2 is free from the contradictions considered above. Under this scheme the 121 keV transition occurs from the 174 keV level. The assignment 5 ensuring the transition to the 174 keV level, when other transitions are suppressed, is selected for the level with energy from 230 to 240 keV.

In the proposed scheme of levels of Ho^{166} (fig. 2) one can see a rotational band $0(0^-)$, $54.2(2^-)$ and 174 keV (4^-) with $K = 0$. The moment of inertia of this rotational band $A = \hbar^2/2I = 9.20 \pm 0.07$ keV (at $B = 0.025 \pm 0.011$ keV) coincides with the calculations performed by L. K. Peker [19]) for odd nuclei with $K = 0$ and $J_0 = 0$. The 82.4 keV level through which 17 % of all transitions pass may be the beginning of a new rotational band with odd spins. In measuring coincidences with X-radiation and hard γ-quanta ($E_\gamma > 1.75$ MeV) 82.4 keV, γ-quanta and X-radiation not connected with the y-121 keV cascade are observed. Probably there is soft γ-radiation leading to the 82.4 keV energy level; yet we have discovered no corresponding γ-quanta. The Ho^{166} nucleus has a long-lived isomeric level with large spin (7^-) [20, 21]) and excitation energy ≈ 900 keV. This state can have $K = 7$ and the transition from this state to the levels detected will involve strong K-forbiddenness.

References

1) A. S. Melioransky, Instrum. and Meas. Engineering (in the press)
2) I. V. Estulin, A. S. Melioransky and L. F. Kalinkin, Nuclear Physics **16** (1960) 168;

A. S. Melioransky, I. V. Estulin, L. F. Kalinkin and B. S. Kudinov, JETP **38** (1960) 758
3) A. S. Melioransky, I. V. Estulin and L. F. Kalinkin, JETP (in the press)
4) I. V. Estulin, L. F. Kalinkin and A. S. Melioransky, Nuclear Physics **4** (1957)91
5) M. Reier and M. H. Shamos, Phys. Rev. **100** (1955) 1302
6) T. J. Kennet, L. M. Bollinger and R. T. Carpenter, Phys. Rev. Letters **1** (1958) 76
7) J. Urbanec, J. Kopecky and Kajfosz, Chezekoslovak Journal of Physics **9** (1959) 544
8) N. D'Angelo, Phys. Rev. **117** (1960) 510
9) M. E. Rose, Internal conversion coefficients (North-Holland Publishing Company, Amsterdam 1958)
10) L. V. Groshev, A. M. Demidov, V. N. Lutsenko and V. I. Pelekhov, Atlas of γ-ray spectra of the radiative capture of thermal neutrons (Moscow, 1958)
11) B. J. Dropesky, A. W. Schardt and T. T. Shull, Nuclear Physics **16** (1960) 357
12) R. W. Bauer and M. Deutsch, Phys. Rev. **117** (1960) 519
13) V. V. Sklyarevsky, E. P. Stepanov and B. A. Obinyakov, Atomnaya Energia **4** (1958) 22
14) J. E. Draper, Phys. Rev. **114** (1959) 268
15) R. G. Helmer and S. B. Burson, Bull. Am. Phys. Soc. **4** (1959) 427
16) J. S. Geiger, R. L. Graham and G. T. Ewan, Bull. Am. Phys. Soc. **5** (1960) 255
17) K. Alexander and V. Bredel, Nuclear Physics **16** (1960) 153
18) L. A. Sliv and N. M. Band, Tables of gamma-radiation internal conversion coefficients (1956)
19) L. K. Peker, Izv. Acad. Nauk SSSR, Ser. Fiz. **24** (1960) 365
20) P. Boskma and H. de Waard, Nuclear Physics **12** (1959) 533
21) H. Postma, A. R. Miedema and E. Smulders, Physica **25** (1959) 671

7.C

Nuclear Physics **24** (1961) 126—131; © *North-Holland Publishing Co., Amsterdam*

Not to be reproduced by photoprint or microfilm without written permission from the publisher

ON ISOBARIC EXCITATION OF NUCLEONS IN COLLISIONS WITH FAST PARTICLES

V. V. GLAGOLEV, V. PETRŽÍLKA and K. D. TOLSTOV

Joint Institute for Nuclear Research, High Energy Laboratory, Dubna, USSR

Received 15 September 1960

Abstract: An analysis is made of the possible contribution of isobaric states to collisions of nucleons with nucleons of momentum 10 GeV/c and π^--mesons of momentum 7 GeV/c. In both cases the excitation energy in the centre-of-mass system is identical.

The contribution of the isobaric states produced in the isotropic decay of an isobar with 1.24 GeV mass is shown to be small.

1. Introduction

The isobaric state of baryons corresponding to their own mass 1.24 GeV, spin $\frac{3}{2}$, and isobaric spin $\frac{3}{2}$ has been studied in several theoretical and experimental investigations. However, the short lifetime of the isobar has so far prevented observation of the nucleon in a state of isobaric excitation directly in experiment. Experimental data on the average multiplicity of particles, as well as a fraction of the cases of definite multiplicity, in inelastic collisions of nucleons with π^--mesons of momentum 7 GeV/c and protons of momentum 10 GeV/c are in agreement with calculation according to the Fermi statistical theory under the assumption that at the outset the excitation energy goes into the production of isobars and mesons. A study of angular and momentum characteristics of inelastic collisions yields information the analysis of which should, in principle, elucidate the question of the role of an isobaric state since the decay of the isobar has unique kinematics. Accordingly, we have analyzed the results of the experiments on the inelastic collisions of mesons with nucleons and protons with nucleons described in refs. [1, 2]).

2. Nucleon-Nucleon Collisions at 10 GeV/c

The question of the isobaric state in the collision with nucleons of protons with momentum 10 GeV/c was theoretically analyzed in refs. [3, 3a]). In ref. [4]) comparison was made with experiments and the contribution of the isobaric state was estimated to $\approx$ 20 %. In ref. [4a]) it was concluded that 50 % of pp-collisions at 6.2 GeV are described by an isobaric model. In ref. [4b]) the authors, analyzing the interactions of 4.5 GeV pions with photo-emulsion nuclei, explained

the results on the basis of an isobaric model. An approximate calculation with allowances for experimental data was previously mentioned in ref. [5]) (for a transverse momentum of nucleons ≈ 0.5 GeV/c). Let us now calculate the collision of a nucleon with a proton of momentum 10 GeV/c under the assumption that at first one or two isobars are produced, which disintegrate isotropically in their proper system into nucleon and pion. Let us consider the two variants when the isobars have a transverse momentum equal either to zero or to 0.5 GeV/c.

TABLE 1

Results of calculations for the collision of a proton and a nucleon

	$p_\perp$ (GeV/c)	Ψ^* angle of emission (c.m.s.)	Ψ angle of emission (lab. syst.)	β in lab. syst. (forward and backward)
2 isobars	0	0	0	0.992
	0	0	0	0.32
	0.5	15.5°	3°	0.99
	0.5	164.5°	41°10	0.52
isobar+nucleon	0	0	0	0.994
	0	0	0	0.28
	0.5	13°	2.5°	0.992
	0.5	167°	41°20	0.60

Table 1 represents the results of the calculation. The table shows that in the laboratory system it is practically inessential whether one or two isobars are formed and the calculation below will be performed for the two-isobar process.

In the proper system of the isobar the velocity of the meson during the decay of the system is equal to 0.86c, i.e., less than the velocity of the forward flying isobar in the laboratory system, and therefore the angular distribution in the laboratory system of the mesons arising from the decay of these isobars will be contained in a narrow front cone, making comparison with experiment difficult. Let us perform the calculation of the angular distribution of pions in the laboratory system for the decay of the isobars flying into the back hemisphere in the c.m.s. For the case $p_\perp = 0$ the calculation for the isotropy of the decay in the proper system reduces itself to finding the function $\mathrm{d}\cos\alpha^*/\mathrm{d}\cos\alpha$ by the conventional formula of angular transformation, where α^* and α are the angles of emission of the meson in the system of the isobar and the laboratory system, respectively. In the case $p_\perp \neq 0$ the isobar in the laboratory system moves at an angle Ψ, and the average angle of emission of the meson in the laboratory system $\bar{\alpha}$ depending on the angle α^* for $\bar{\alpha} \geqq \Psi$ is given by the

formula

$$\bar{\alpha}(\alpha^*) = \frac{1}{\pi}\int_{-\frac{1}{2}\pi}^{+\frac{1}{2}\pi} \arccos[\cos \Psi \cos \beta(\alpha^*) + \sin \Psi \sin \beta(\alpha^*) \sin \varphi]\mathrm{d}\varphi,$$

where $\beta(\alpha^*)$ is the angle of emission of the meson with respect to the motion of the isobar in the laboratory system and φ is the angle in a plane perpendicular to the motion of the isobar in the laboratory system. The calculation of $\bar{\alpha}(\alpha^*)$ was performed for the angle $\Psi = 41°$ corresponding to $p_\perp = 0.5$ GeV/c. The angular distribution in the laboratory system is expressed by the function d cos α^*/d cos $\bar{\alpha}$. Fig. 1 represents the pion angular distribution determined by

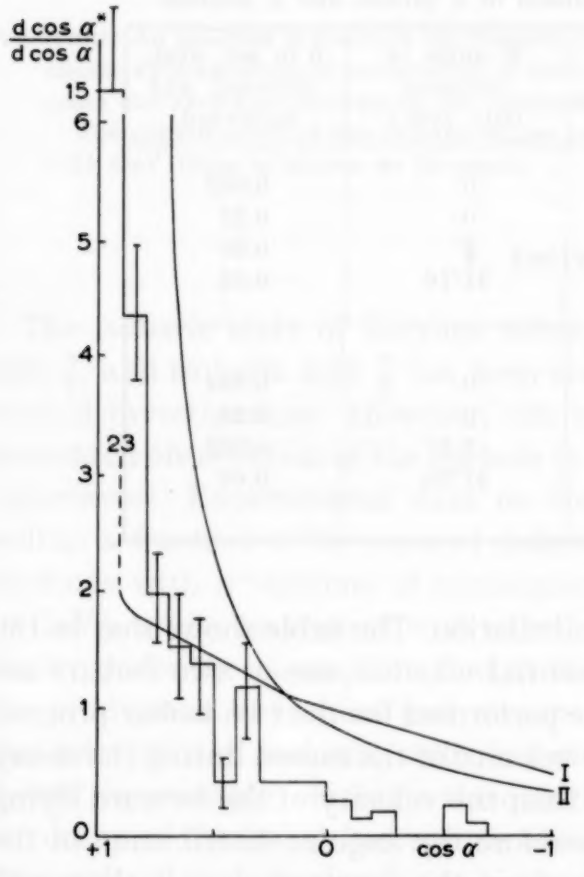

Fig. 1. π-meson spectrum for pp-collisions in the laboratory system. Curve I is the calculated spectrum for $p_\perp = 0$, curve II the calculated spectrum for $p_\perp = 0.5$ GeV/c.
The histogram shows the experimental spectrum.

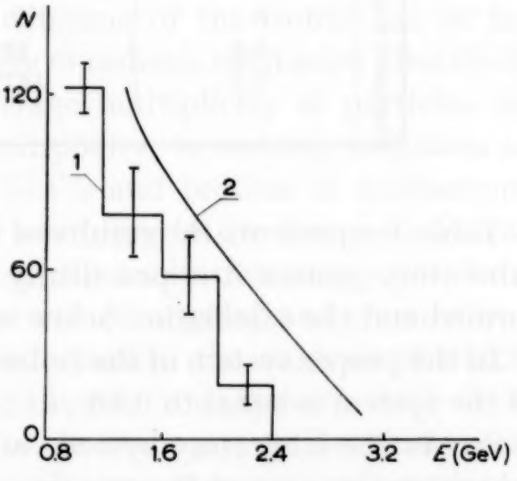

Fig. 2. Curve 1 is the experimental proton spectrum of (π^-, N)-collisions, curve 2 the restored average spectrum of isobars.

the function d cos α^*/d cos $\bar{\alpha}$ for all angles α of pions emitted in the decay of both isobars (curve I) and by the function d cos α^*/d cos $\bar{\alpha}$ for the decay of the isobar flying backward in the c.m.s. and for $\bar{\alpha} \geqq 41°$ (curve II). The histogram represented in fig. 1 gives the experimental angular distribution normalized to

the same area as curves I and II in pp-collisions, for stars with 2 and 4 prongs, and constructed in conformity with the data of ref. [6]). The proportion of mesons flying in the laboratory system into the back hemisphere is equal to 16 % for $p_\perp = 0$ and to 12 % for $p_\perp = 0.5$ GeV/c.

The experimental quantity $p_\perp$ amounts to 0.372 ± 0.025 GeV/c according to the data of ref. [2]), and consequently the meson angular distribution curve corresponding to this value must lie between curves I and II. The experimental value of the fraction of the mesons flying backward in the laboratory system is equal to 1.7 %. This small value, as well as the comparison of the histogram with the curves plotted for angles exceeding 90°, warrants the conclusion that the isobaric state plays no essential role in inelastic nucleon collisions. It will be noted that in the isobaric angular distribution of mesons in the centre-of-mass system 1 % of the colliding nucleon fly backward if their momentum is equal to 0.5 GeV/c in the laboratory system.

3. Pion-Nucleon Collisions at 7 GeV/c

Let us evaluate the contribution of the isobaric states produced in the collision of 7 GeV/c pions with nucleons. For this purpose an average spectrum of isobars was constructed on the basis of the experimental spectrum of protons † (fig. 2, curve 1). Use was made of the fact that in the two-particle decay of the isobar with a given energy the spectrum of protons in the laboratory system is constant from $E^{\mathrm{p}}_{\min} = \gamma_{\mathrm{is}}(E_0 - p_0\beta_{\mathrm{is}})$ to $E^{\mathrm{p}}_{\max} = \gamma_{\mathrm{is}}(E_0 + p_0\beta_{\mathrm{is}})$, where E_0 and p_0 are the energy and momentum of the proton in the system of the isobar. Hence the average value of the proton energy was determined for each isobar energy $E^{\mathrm{av}}_{\mathrm{p}} = \frac{1}{2}(E^{\mathrm{p}}_{\min} + E^{\mathrm{p}}_{\max})$ and the dependence $E_{\mathrm{is}}(E^{\mathrm{av}}_{\mathrm{p}})$ was plotted, the average spectrum of isobars being obtained on the basis of this dependence (fig. 2, curve 2). Thus we assume that the isobar is produced in all cases, even in those when a large momentum is transferred to the proton, which leads to overestimation.

Then it is assumed that the average angle of emission of isobars is the same as in the case of proton collinions,

$$\bar{\Theta}_{\mathrm{is}} = \arcsin\frac{\bar{p}_\perp}{\bar{p}} = \arcsin\frac{0.37}{1.01} = 21.5°.$$

At this value of $\bar{\Theta}_{\mathrm{is}}$ the angular pion distribution for the decay of isobars in the laboratory system of the coordinates is calculated (see fig. 3, curve 1), using the energy spectrum of isobars (fig. 2, curve 2) and assuming that the decay in the system of the isobar is isotropic. Plotted on the same graph is the experimental angular distribution of pions in the laboratory system for the case of collisions of 7 GeV pions with nucleons (fig. 3, curve 2). Both distributions are normalized to the same area. From comparing them it is obvious that the calculated frac-

† All experimental data used in this section is taken from ref. [1]).

tion of mesons flying backward is 15 % (or 16.5 %, for the case when at the beginning there is one meson and the isobar outgoing at 0°), while in the experiment this fraction is 2.1 %.

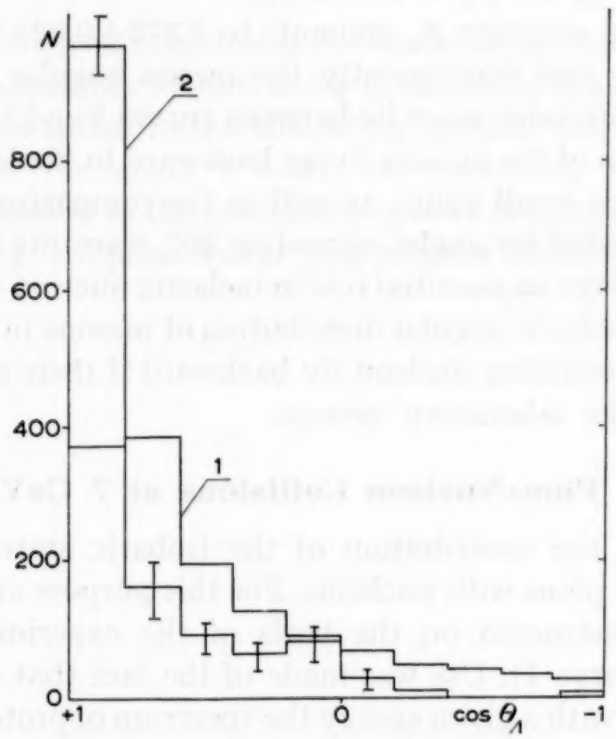

Fig. 3. Curve 1 is the calculated angular distribution of π-mesons from the decay of isobars, curve 2 is the experimental angular distribution of π-mesons in (π^-, N)-collisions.

It will be noted that for an isotropic angular distribution of pions with momentum 0.53 GeV/c in the c.m.s. of the pion and the nucleon we shall obtain 2 % pions flying backward in the laboratory system.

Then the probability of the isobaric state in (π^-, N)-interactions was considered on the basis of cases with an identified proton and one pion or several pions. For this purpose the energy $Q_{p,\pi}$ of the pair of proton and pion produced in the isobaric decay was calculated. The values $Q_{p,\pi}$ were determined for all possible proton-pion pairs. Altogether, 180 pairs in 88 (π^-, N)-collisions were calculated. The fraction of isobars was calculated through the ratio of the number of cases corresponding to the isobaric state to the number of all pairs multiplied by the average number $\bar{n}_\pi = 2.5$ of all charged pions in stars with an identified proton.

The limits of error for the quantity $Q_{p,\pi}$ can be determined to ± 15 % by the accuracy of measurements of the momenta $\mathbf{p}_p$ and $\mathbf{p}_\pi$. In accordance with this, $\Delta Q_{p,\pi} \leqq 25$ %, i.e., $Q^{(I^*)}_{p,\pi} = (160 \pm 40)$ MeV in the c.m.s. In this case the fraction of isobaric-state in (π^-, N)-interactions equals 13 %. If the error in determining $Q_{p,\pi}$ is assumed equal to 15 %, the fraction of the isobaric state processes decreases to 6 %.

The histogram in fig. 4 represents the distribution for all calculated proton-

pion pairs and the cross-hatched rectangular the fraction of isobars corresponding to $Q_{p,\pi}^{(I^*)} = (160 \pm 40)$ MeV. As is clear from the histogram, the isobaric fraction does not rise above the background of the extensive distribution in this portion of the spectrum.

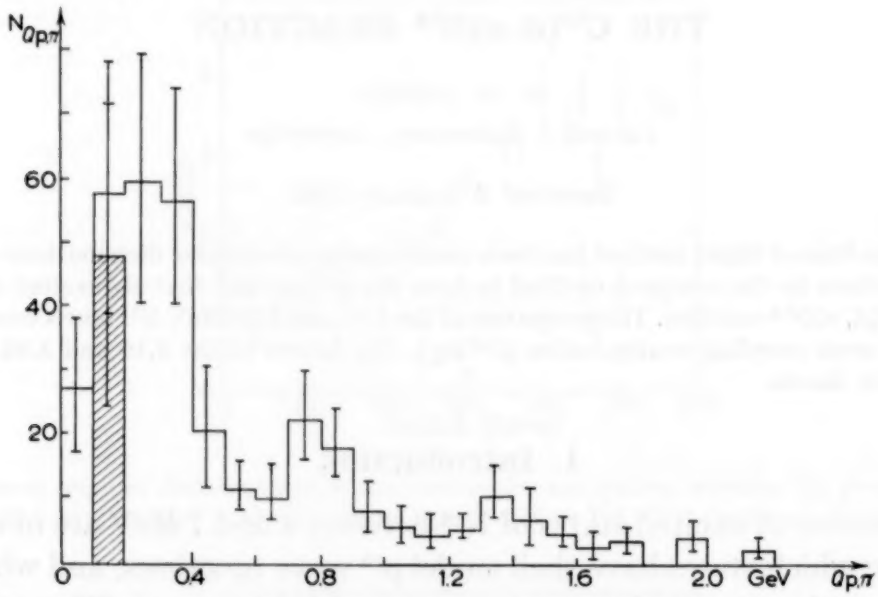

Fig. 4. Distribution of $Q_{p,\pi}$ for proton—π-meson pairs in (π^-, N)-collisions.

In accordance with the above-mentioned comparisons it can be concluded, similarly to the nucleon-nucleon case, that the production of isobaric states in (π^-, N)-interactions does not yield any essential contribution.

It will be noted that an isobar of mass 1.24 GeV has been used throughout these considerations. If we assume the participation of isobars with larger masses decaying into pion and nucleon, the calculated fraction of backward flying mesons is bound to increase.

In conclusion the authors express gratitude to M. M. Govorun for his help in the calculations, the authors of ref. [6]) for the introduction to their results and the authors of ref. [1]) for stimulating discussions.

References

1) V. A. Belyakov *et al.*, Preprint no. 530 of the Joint Institute of Nuclear Research; JETP **39** (1960) 937; Proc. 10th Conf. on High Energy Physics in Rochester (1960) p. 82
2) Wang Shou Feng *et al.*, Preprint no. 526 of the JINR
3) I. E. Tamm, Report 9th Conf. on High Energy Physics, Kiev (1959)
3a) I. M. Dremin and D. S. Chernavsky, JETP **38** (1960) 229
4) Wang Shou Feng *et al.*, Proc. 9th Conf. on High Energy Physics, Kiev (1959)
4a) H. Winzeler *et al.*, Nuovo Cim. **17** (1960) 8
4b) H. H. Aly and C. M. Fisher, Nuovo Cim. **17** (1960) 98
5) Proc. 6th Session of the Scientific Council of the Joint Institute for Nuclear Research, May (1959) (remarks of K. D. Tolstov)
6) T. Vishki *et al.*, Proc. 10th Conf. on High Energy Physics in Rochester (1960) p. 94

2.B:2.G

Nuclear Physics **24** (1961) 132—137; © *North-Holland Publishing Co., Amsterdam*

Not to be reproduced by photoprint or microfilm without written permission from the publisher

THE $C^{13}(d, n)N^{14}$ REACTION

A. N. JAMES

Cavendish Laboratory, Cambridge

Received 2 January 1961

Abstract: The time of flight method has been used to measure angular distributions and excitation functions for the neutrons emitted to form the ground and first six excited states of N^{14} in the $C^{13}(d, n)N^{14}$ reaction. The properties of the 4.91 and 5.69 MeV N^{14} levels were consistent with the weak coupling configuration ($C^{13}2s_{\frac{1}{2}}$). The nature of the 5.10 and 5.83 MeV levels remains in doubt.

1. Introduction

The properties of excited states of N^{14} between 4 and 7 MeV are of interest in determining which states have shell model p^{10} wave functions, and which states are formed predominantly by coupling a 2s or 1d proton to a C^{13} core [1]). In the first category only a 2^+ state is expected while four $T = 0$ states are expected in the second. Warburton *et al.* [1]) were able to make plausible the identification of these four states, 0^-, 2^-, 1^- and 3^-, with the 4.91, 5.10, 5.69 and 5.83 N^{14} states. Their arguments were based on an analysis of gamma-rays from $C^{13}+p$ ($Q = 7.55$ MeV) and on data from $C^{13}(d, n)N^{14}$. Benenson has observed $l = 0$ stripping for the 4.91 MeV level [2]) and Ranken *et al.* have measured relative gamma-ray yields [3]). Because of their unique parent character [4]) these states are expected to be formed in $C^{13}(d, n)N^{14}$ with large stripping reduced widths, by $l = 0$ for the 0^- and 1^- states, and $l = 2$ for the 2^- and 3^- states. Since the Q value for these levels is low (see table 1), angular distributions typical of stripping reactions should be observed even at low deuteron energy [5]).

2. Experimental

The time of flight apparatus of the Cavendish Laboratory's 1.4×10^6 V Cockcroft-Walton generator [6]) has been used to measure angular distributions and excitation functions for the neutrons emitted to form the ground and first six excited states of N^{14} in the $C^{13}(d, n)N^{14}$ reaction. Scintillation counters incorporating neutron discriminating Nuclear Enterprise N.E. 213 liquid scintillator [7]) were used with biases equivalent to neutron energies of 600 keV and 330 keV. For a bias of 600 keV and R.C.A. 7264 photomultiplier was used and gave a time resolution for the neutron groups in the time of flight spectrum of 6 ns. The lower noise current in an E.M.I. 6097 photomultiplier allowed a bias

of 330 keV with a neutron group time resolution [8]) of 8 ns. The flight paths were 3.5 and 1.5 m. The target was isotopically enriched carbon on 0.05 cm copper. It was less than 20 keV thick to 1.16 MeV protons. The time of flight spectrum

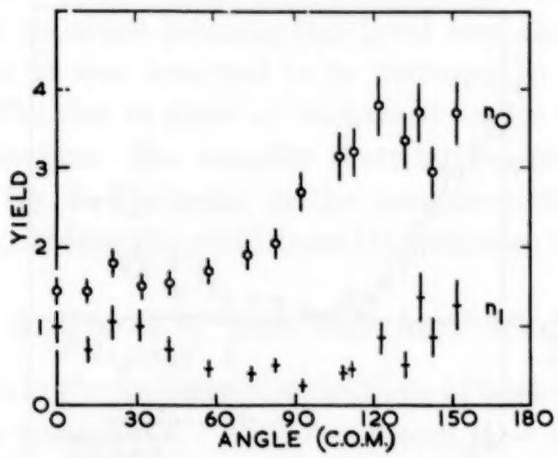

Fig. 1. Neutron angular distributions in the centre-of-mass system forming the ground state (n_0) and first excited 2.31 MeV state (n_1) of N^{14} at 1.2 MeV deuteron energy.

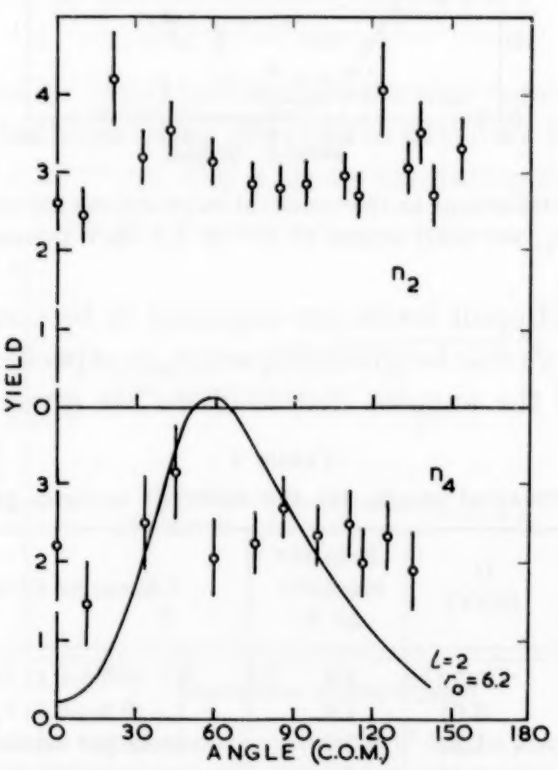

Fig. 2. Neutron angular distributions in the centre-of-mass system forming the 3.95 MeV (n_2) and 5.10 MeV (n_4) states of N^{14} at 1.2 MeV deuteron energy.

showed that the target contained significant amounts of C^{12} and deuterium. Allowance was made for the $C^{12}(d, n)N^{13}$ and $d(d, n)He^3$ reactions in extracting the neutron intensities of the $C^{13}(d, n)N^{14}$ reaction.

Figs. 1, 2 and 3 show the measured angular distributions at 1.2 MeV deuteron energy. Errors arising from corrections for counter efficiency [8]) are less than 10 % within any one of the distributions. The relative intensities of the neutron

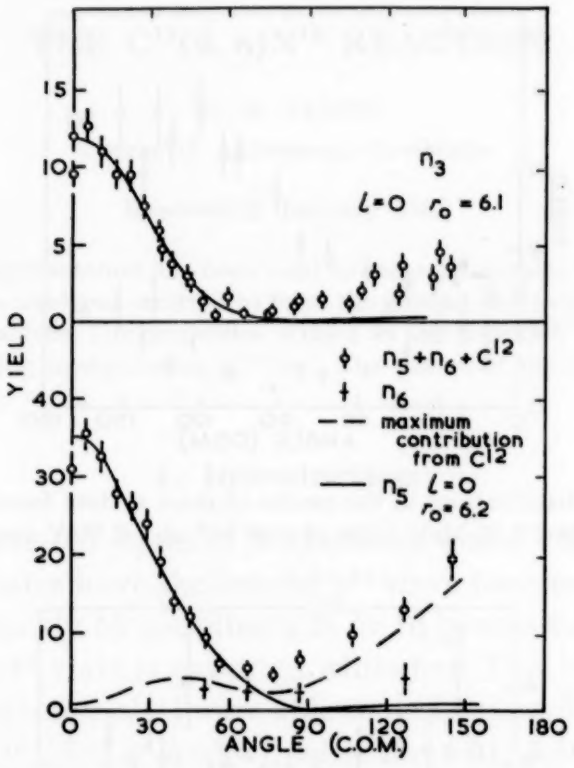

Fig. 3. Neutron angular distributions in the centre-of-mass system forming the 4.91 MeV (n_3) and 5.69 MeV (n_5, see text) states of N^{14} at 1.2 MeV deuteron energy.

groups forming the different levels are expected to be correct within 30 % (in particular the intensity ratio for groups n_3 and n_5 is expected to be within 10 %). The main features of the angular distributions are given in table 1.

TABLE 1

Experimental results for the different neutron groups

Group	E_x in N^{14} (MeV)	Q (MeV)	Relative intensity at 0°	Character of angular distribution
n_0	0	5.32	1.5	$1-(0.7\pm0.1)\cos\theta$
n_1	2.31	3.01	1.0	$1+(0.9\pm0.2)P_2(\cos\theta)$
n_2	3.95	1.37	3.0	Isotropic within 10 %
n_3	4.91	0.41	12.5	$l=0$ stripping, $r_0=6.1\times10^{-13}$ cm
n_4	5.10	0.22	2.5	Isotropic within 15 %
n_5	5.69	−0.37	33	$l=0$ stripping, $r_0=6.2\times10^{-13}$ cm
n_6	5.83	−0.51	3 ±1	Isotropic within 60 %

The experimental points for the 5.69 MeV level (n_5) shown in fig. 3 included the neutron groups C^{12}(d, n)N^{13} and n_6. At 0° the position of the peak in the

time of flight spectrum showed that the large intensity was due to the neutron group forming the 5.69 MeV level; less than 20 % of the intensity could have been from other groups. Four experimental points for the intensity of n_6 were determined between 50° and 130°. With the above limit on the intensity near 0°, the yield of neutrons forming this level was shown to have no strong variation with angle, it was assumed to be isotropic in obtaining the angular distribution of n_5. The rise in yield at backward angles could have come from the $C^{12}(d, n_0)N^{13}$ reaction. The angular distribution for this reaction at 1.2 MeV [8]) is shown in fig. 3. The error in the measurements of the intensity for n_5 at 0° caused by including the yield from this reaction was negligibly small.

3. The 4.91 and 5.69 MeV levels

The forward peaks in the angular distributions of both these levels were fitted by Butler stripping curves [9, 10]) † with $l = 0$ and $r_0 = 6.1 \times 10^{-13}$ cm (fig. 3). The ratio of the reduced widths with which the levels were formed was found to be

$$R = \frac{[(2J+1)\theta^2]_{5.69}}{[(2J+1)\theta^2]_{4.91}} = 2.8 \pm 0.5.$$

Angular distributions for these two levels were also measured in forward directions at 1 MeV. Again the peaks at 0° could be fitted by Butler stripping curves with $l = 0, r_0 = 6.1 \times 10^{-13}$ cm. Fig. 4 shows excitation functions at 0° for these

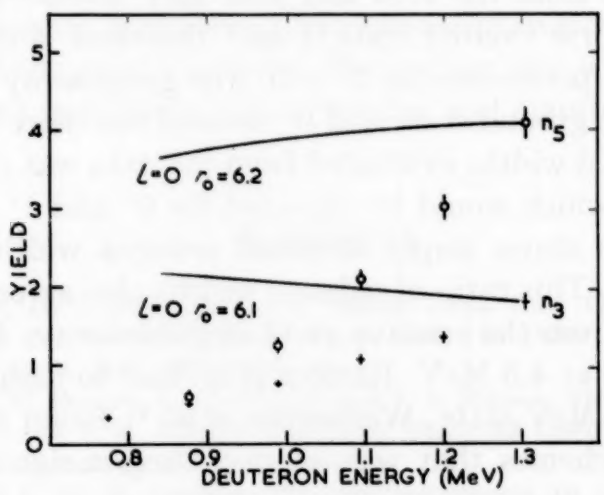

Fig. 4. Excitation functions (in the laboratory system) at 0° for the production of neutrons forming the 4.91 MeV (n_3) and 5.69 MeV (n_5) states in N^{14}. The curves are the predictions of Butler stripping theory (see text).

two groups; also shown are the theoretical excitation functions predicted by Butler stripping theory under the assumption that r_0 and θ^2 are independent of

† In ref. [9]), a correction which takes account of the Coulomb effect on the captured proton was used [4, 10]).

the deuteron energy. The ratios of reduced widths evaluated from the experimental excitation functions are given in table 2. The ratio is constant within the limits of experiment, indicating that the difference between theory and experiment shown in fig. 4 arises from neglecting the effects of barrier penetration by the deuteron.

TABLE 2

Ratios of reduced widths

E_d (MeV)	R
0.88	2.0±1.0
0.99	2.7±0.6
1.10	3.0±0.6
1.20	2.8±0.5
1.31	3.3±0.6

Stripping reactions in C^{13}(d, n)N^{14} with $l = 0$ restrict the spin and parity of the states produced in N^{14} to 0^- or 1^-. Warburton *et al.* [1]) considered the gamma-ray selection rules for transitions from 0^- and 1^- states to the 1^+, $T = 0$ ground state and the 0^+, $T = 1$ first excited state of N^{14}. They found that the decay of the 0^- level had to be to the ground state, and, if $T = 0$, the 1^- level would decay mainly to the first excited state, since the ground state transition would be forbidden by the isobaric spin selection rule for E1 radiation. The 5.69 MeV level was thought to be $J = 1$ from the strengths of the gamma-ray cascades from the 8.06 and 8.62 MeV levels [11]). It decayed predominantly to the first excited state [1]) and therefore would seem to be 1^- rather than 0^-, with preference for $T = 0$. The gamma-ray decay of the 4.91 MeV level was to the ground state and 0^- seemed the more likely assignment.

The ratio of reduced widths evaluated from the data was consistent with the theoretical value 3, which would be expected for 0^- and 1^- states of the type (C^{13}, $2s_{\frac{1}{2}}$), since such states imply identical reduced widths θ^2 equal to the single particle width. This ratio of reduced widths also agreed with that found by Ranken *et al.* [3]) from the relative yield of gamma-rays following deuteron bombardment of C^{13} at 4.5 MeV. Ranken *et al.* had to assume s wave proton capture for the 5.69 MeV state. Warburton *et al.* [1]) found no evidence in the gamma-ray decay schemes that was against these assignments.

4. The ground, 2.31 and 3.95 MeV levels

Excitation functions at 20° and 120° were measured for these three levels. They showed that the angular distributions of figs. 1 and 2 were in agreement with those of Green *et al.* [12]) at 860 keV. In particular the cos θ term for n_0 changed sign near 1.1 MeV where all the excitation functions indicated a weak broad resonance [13]). If the assumption is made that these three levels (all

belonging to the s^4p^{10} configuration) are populated by a compound nucleus process through the same resonance, then, from the forms of the angular distributions, that resonance must have $J = \frac{3}{2}^+$ and be formed by $l_d \geqq 1$.

5. The 5.10 and 5.83 MeV levels

On the assumption that these levels are of the type (C^{13}, $1d_{\frac{5}{2}}$) it is possible to predict, from the intensity of the groups n_3 and n_5, that the intensity at the maximum of the $l = 2$ stripping peak (fig. 2) would be four of the relative units used in table 1. [The ratio of the $2s_{\frac{1}{2}}$ to the $1d_{\frac{5}{2}}$ single particle reduced widths [4]) was taken as 2. No attempt was made to justify the assumption that distorting effects (see fig. 4) affected $l = 0$ and $l = 2$ stripping in the same way]. This intensity is very similar to that expected from compound nucleus formation (n_0, n_1 and n_2).

The shape of the experimental angular distributions, particularly for the 5.10 MeV level (n_4), favours compound nucleus formation rather than $l = 2$ stripping. If the 5.10 MeV level is formed by a compound nucleus process through the same resonance as the ground and first excited states, then the isotropic distribution observed indicates positive parity for this level; this interpretation must remain in doubt since levels of opposite parity are known to interfere in the compound nucleus ($\cos\theta$ term in the angular distribution of n_0).

The isotropic target was supplied by A.E.R.E. Harwell. This work was performed while the author held a Research Fellowship awarded by the Department of Scientific and Industrial Research. The author also wishes to acknowledge Mr. D. D. Stewart's invaluable aid in running and maintaining the Cockcroft-Walton generator.

References

1) E. K. Warburton, H. J. Rose and E. N. Hatch, Phys. Rev. **114** (1959) 214;
E. K. Warburton and W. T. Pinkston, Phys. Rev. **118** (1960) 733
2) R. E. Benenson, Phys. Rev. **90** (1953) 420
3) W. A. Ranken, T. W. Bonner, J. M. McCrary and T. A. Rabson, Phys. Rev. **109** (1958) 917
4) M. H. Macfarlane and J. B. French, Rev. Mod. Phys. **32** (1960) 567
5) D. H. Wilkinson, Phil. Mag. **3** (1958) 1185
6) A. N. James and C. M. P. Johnson, Nuclear Instruments **10** (1961) 68
7) F. D. Brooks, Nuclear Instruments **4** (1959) 151
R. B. Owen, Nucleonics **17**, no. 9 (1959) 92
8) A. N. James, Nuclear Physics **00** (1961) 000
9) C. R. Lubitz, Atomic Energy Commission Report AECU-3990 (1957) unpublished
10) S. T. Butler and O. M. Hittmair, Nuclear Stripping Reactions (Horowitz Publications, 1957)
11) D. H. Wilkinson and S. D. Bloom, Phil. Mag. **2** (1957) 63
12) L. L. Green, J. P. Scanlon and J. C. Willmott, Proc. Phys. Soc. A **68** (1955) 386
13) J. B. Marion and G. Weber, Phys. Rev. **102** (1956) 1355

8.A

Nuclear Physics **24** (1961) 138—142; © *North-Holland Publishing Co., Amsterdam*

Not to be reproduced by photoprint or microfilm without written permission from the publisher

DÉPENDANCE ANGULAIRE DE LA CORRÉLATION β—γ (POLARISÉ CIRCULAIRE) DANS Au^{198}

J. P. DEUTSCH † et P. LIPNIK †

Institut Interuniversitaire des Sciences Nucléaires, Centre de Physique Nucléaire de l'Université Catholique de Louvain, Belgique

Reçu le 18 novembre 1960

Abstract: Angular dependence of the beta-gamma circular polarization correlation in Au^{198} was measured. It can be described by a cosine function, which is the prediction of the so-called "ξ-approximation". A limit to a possible P_3-term in the distribution function is set by the ratio $A_3/A_1 = -0.13 \pm 0.25$.

1. Introduction

Il est utile de développer l'expression des divers observables d'une transition β, non-unique, une fois interdite, en série décroissante d'un paramètre $\xi = \frac{1}{2}\alpha Z/R$ (α, Z et R ont leur définition habituelle) [1, 2]. A part le cas où certains éléments de matrice nucléaires sont particulièrement petits (en raison d'une règle de sélection éventuelle) ou se compensent mutuellement, les termes successifs de cette série décroissent d'un facteur ξ. En ne retenant que le premier terme de la série, la forme du spectre d'une transition β une fois interdite non-unique se réduit à la forme statistique et l'anisotropie de la corrélation directionnelle β—γ s'annule.

Dans cette même approximation la dépendance angulaire de la corrélation β—γ (polarisé circulaire) se ramène à une loi en cosinus. Cette loi, nous avons voulu la vérifier dans le cas d'un noyau où les mesures de forme de spectre et de corrélation directionnelle ont montré la bonne applicabilité de cette approximation [3] ††.

2. Description de l'Expérience

La fraction 98.6 % des noyaux Au^{198} se désexcite vers l'état d'énergie de 411 keV du Hg^{198} [4]. Cette transition est du type une fois interdite, non-unique [3]. La valeur du paramètre ξ est [5] 16.2 ± 0.08. Les mesures [3] de la forme du spectre, de corrélation directionnelle β—γ, de corrélation β—γ (polarisé

† Chercheur agréé de l'I.I.S.N., Belgique.

†† La seule mesure de corrélation directionnelle β—γ (polarisé circulaire) d'une transition interdite publiée à ce jour [6] est celle de Sb^{124}; la loi en cosinus n'y est pas vérifiée. On sait d'ailleurs que l'approximation en ξ n'est pas applicable à ce noyau [7].

circulaire) et de corrélation β (polarisé)-γ indiquent que cette transition est bien décrite par l'approximation ξ. La petite déviation du spectre de la forme statistique [9]) n'est pas en désaccord avec cette affirmation. On s'attend donc à trouver dans la mesure de la corrélation directionnelle β—γ (polarisé circulaire) du Au^{198} une loi en cosinus.

Le dispositif expérimental se compose de deux canaux: un canal β pouvant tourner autour de la source et un canal γ précédé d'un polarimètre conique spécialement adapté à l'analyse des rayons γ de basse énergie (fig. 1). L'électro-

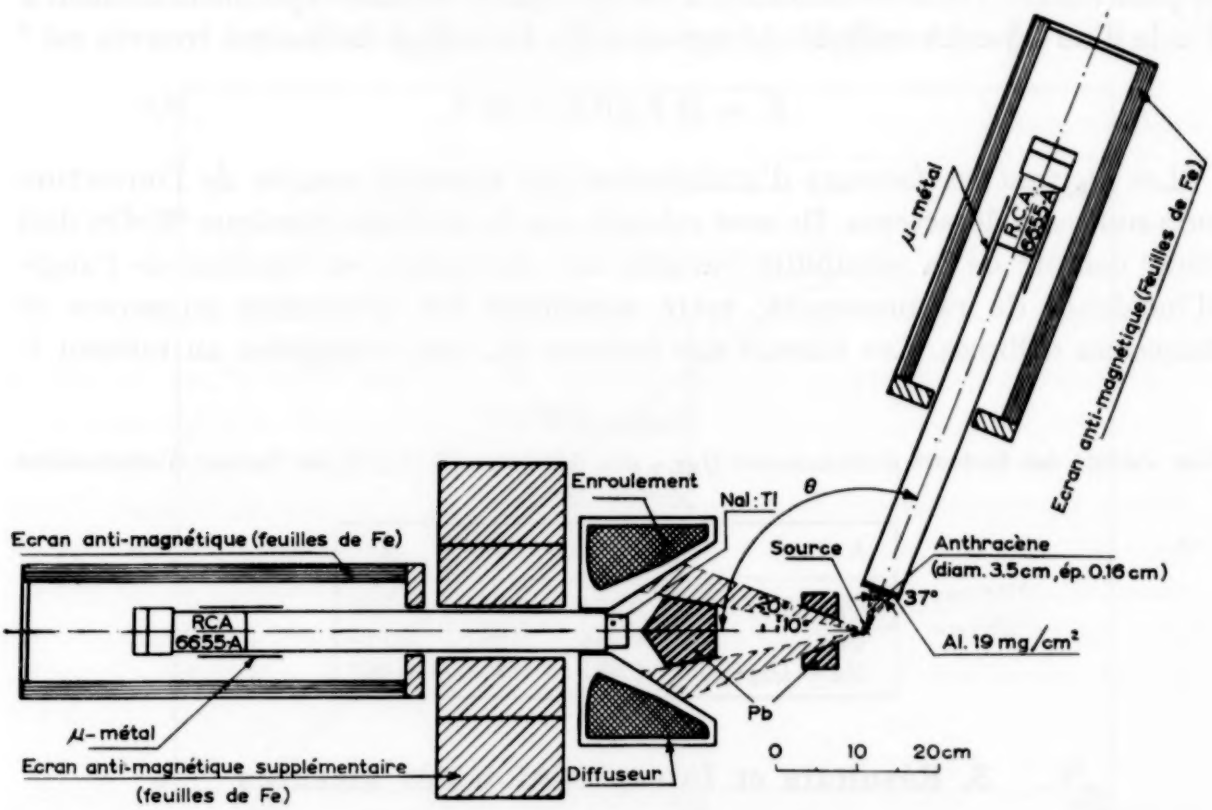

Fig. 1. Dispositif expérimental.

nique est du type classique "fast-slow". Cet ensemble et les techniques de mesure ont été décrits ailleurs [10, 11]).

La fonction de corrélation β—γ (polarisé circulaire) a la forme suivante:

$$W(\theta, \tau) = \sum_k (-\tau)^k A_k P_k(\cos\theta), \tag{1}$$

où $\tau = +1$ ou -1 pour des rayons γ polarisés circulaires droits ou gauches [15]). Si l'approximation ξ est valable, A_3/A_1 est de l'ordre de ξ^{-2}, c'est à dire 0.004 pour Au^{198}. Nous définissons un effet expérimental e par

$$e = 2\,\frac{N^+ - N^-}{N^+ + N^-}; \tag{2}$$

N^+ et N^- sont les nombres de coïncidences vraies obtenus pour les deux directions d'aimantation du polarimètre.

L'effet e est lié aux paramètres A_k de (1) par la relation

$$e(\cos\theta) = K\,\frac{A_1Q_1P_1(\cos\theta)+A_3Q_3P_3(\cos\theta)}{1+A_2Q_2P_2(\cos\theta)} = KA\,\frac{v}{c}\cos\theta; \qquad (3)$$

K caractérise le pouvoir analysant du polarimètre. Il a été calculé compte tenu de la contribution de (38 ± 5) % des rayons γ ayant subi deux diffusions dans le polarimètre. Cette contribution a été également vérifiée expérimentalement à l'aide d'un faisceau collimé de rayons γ [12]). La valeur de K ainsi trouvée est †

$$K = (3.2\pm0.3)\times10^{-2}.$$

Les Q_k sont les facteurs d'atténuation qui tiennent compte de l'ouverture non-nulle des détecteurs. Ils sont calculés par la méthode classique [14]). On doit tenir compte de la sensibilité variable des détecteurs en fonction de l'angle d'incidence du rayonnement; cette sensibilité été déterminée au moyen de faisceaux collimés. Les valeurs des facteurs Q_k sont consignées au tableau 1.

TABLEAU 1

Les valeurs des facteurs d'atténuation $Q_{k\beta,\gamma}$ des détecteurs β et γ et du facteur d'atténuation globale Q_k.

k	1	2	3
$Q_{k\beta}$	0.974	0.924	0.849
$Q_{k\gamma}$	0.966	0.887	0.774
$Q_k = Q_{k\beta}Q_{k\gamma}$	0.941	0.833	0.687

3. Résultats et Interprétation des Mesures

L'effet e mesuré en fonction de l'angle θ formé par l'axe des détecteurs β et γ est porté dans la fig. 2. Les points expérimentaux sont en bon accord avec la loi en cosinus prévue dans l'approximation en ξ pour la corrélation directionnelle $\beta-\gamma$ (polarisé circulaire).

L'effet obtenu à $\theta = 180°$ est

$$e(180°) = (1.28\pm0.07)\times10^{-2}.$$

Au moyen d'un polarimètre cylindrique classique Boehm et Wapstra [14]) obtiennent (0.75 ± 0.12) %, ce qui montre l'avantage des polarimètres coniques pour l'analyse des rayons γ dans ce domaine d'énergie.

Compte tenu de la valeur et de l'erreur de K rapportées plus haut, nous

† Suite à une remarque de R. M. Steffen nous avons inclu dans l'erreur l'influence d'une eventuelle non-saturation en surface du polarimètre sur une épaisseur de 0.5 mm.

obtenons à $\theta = 180°$ la valeur

$$A = 0.49 \pm 0.05.$$

Cette valeur est en accord avec celle obtenue par d'autres chercheurs [3, 14, 15, 16]).

En nous basant sur nos mesures de corrélation directionnelle $\beta-\gamma$ (polarisé circulaire), il devient possible de séparer dans le coefficient A les contributions des paramètres A_1 et A_3, coefficients de $P_1(\cos\theta)$ et $P_3(\cos\theta)$ dans la fonction de distribution:

$$W(\theta, \tau) = \sum_k (-\tau) A_k P_k(\cos\theta)$$
$$\approx 1 + A_2(\tfrac{3}{2}\cos^2\theta - \tfrac{1}{2}) + (-\tau)[A_1 + A_3(\tfrac{5}{2}\cos^2\theta - \tfrac{3}{2})]\cos\theta. \quad (4)$$

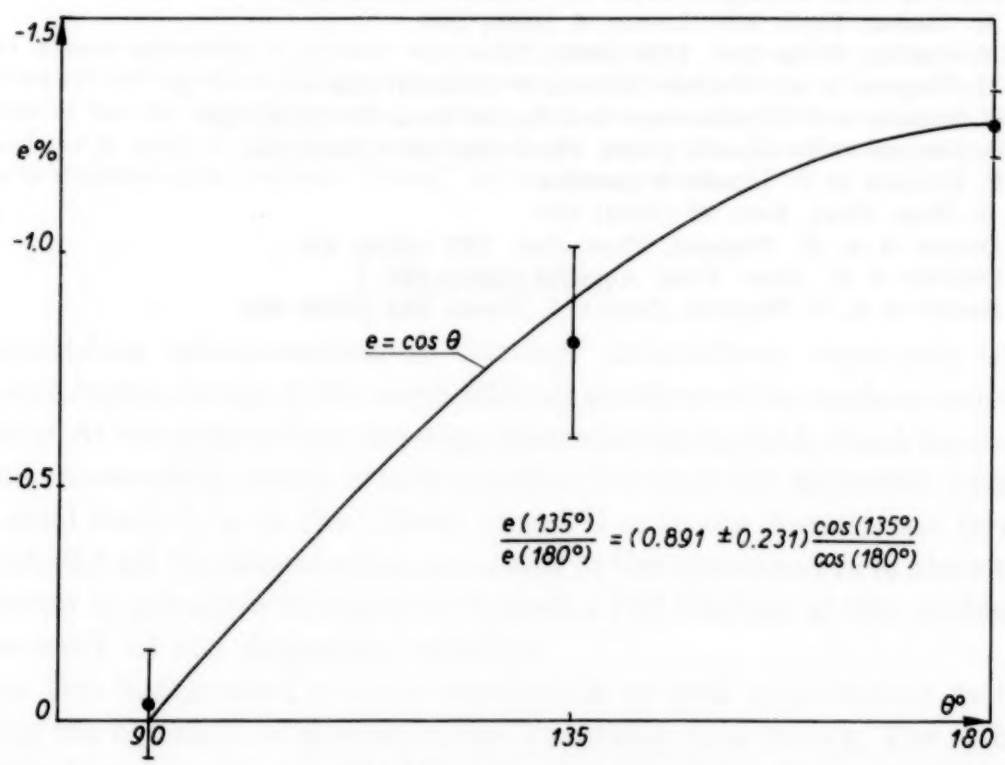

Fig. 2. Résultats expérimentaux.

Nous obtenons

$$A_1 = 0.46 \pm 0.10, \quad A_3 = -0.06 \pm 0.12.$$

Ces valeurs dépendent de K, c'est à dire du pouvoir analyseur calculé du polarimètre. Le rapport A_3/A_3 — par contre — peut être déterminé à partir de nos mesures, indépendamment de la valeur de K.

On trouve

$$A_3/A_1 = -0.13 \pm 0.25.$$

Nous avons dit plus haut que si l'approximation en ξ est applicable A_3/A_1 est de l'ordre de $(1/\xi)^2$ qui, dans le cas actuel, vaut 0.004. La valeur trouvée est en accord avec ces prévisions aux erreurs expérimentales près.

Nous avons eu des discussions intéressantes avec M. le Prof. R. M. Steffen; M. le Prof. M. de Hemptinne a bien voulu montrer l'intérêt qu'il portait à ce travail. Nous avons largement profité des conseils de Mr. le Prof. P. C. Macq. Nous tenons à leur exprimer nos plus vifs remerciements.

Références

1) E. J. Konopinski et E. G. Uhlenbeck, Phys. Rev. **60** (1941) 308
2) T. Kotani, Phys. Rev. **114** (1959) 795
3) R. M. Steffen, Phys. Rev. **118** (1960) 763, 768
4) Nuclear Date Sheets (National Research Council, Washington D.C.)
5) S. Fernbach, Rev. Mod. Phys. **30** (1958) 412
6) G. Hartwig et H. Schopper, Phys. Rev. Lett. **4** (1960) 293
7) R. M. Steffen, Phys. Rev. Letters **4** (1960) 290
8) R. M. Steffen, Phys. Rev. **118** (1960) 768
9) A. H. Wapstra *et al.*, Nuclear Physics **9** (1958/59) 538
10) J. P. Deutsch et P. Lipnik, Ann. Soc. Sc. de Brux. **73** (1959) 420
11) J. P. Deutsch et P. Lipnik, Journ. Phys. Rad. **21** (1960) 806
12) J. P. Deutsch et P. Lipnik, à paraître
13) M. E. Rose, Phys. Rev. **91** (1953) 610
14) F. Boehm et A. H. Wapstra, Phys. Rev. **109** (1956) 456
15) J. Berthier *et al.*, Helv. Phys. Acta **30** (1958) 483
16) F. Boehm et A. H. Wapstra, Zeitsch. f. Physik **152** (1958) 384

7.A

Nuclear Physics **24** (1961) 143—150; © *North-Holland Publishing Co., Amsterdam*

Not to be reproduced by photoprint or microfilm without written permission from the publisher

CONCERNING A "STRONG" COUPLING METHOD IN THE QUANTIZED FIELD THEORY

Ju. M. LOMSADZE

University of Uzhgorod, Ukraine, USSR †

Received 16 July 1960

Abstract: A new approximate method especially intended for "strong" coupling variants is proposed for solving the equation of motion in quantized field theory. This method revives the idea of the old "strong" coupling method, with the essential difference that in the new method use is made of the exact reduction of the interaction Hamiltonian of quantized fields to diagonal form, without "fixing" the nucleon current.

1. Introduction

The consistent interpretation of "strong" interactions, especially in the high-energy region, is one of the most difficult problem of the modern quantized field theory. At the present time the dispersion relation method, which has recently yielded encouraging results is very hopeful. Yet since the dispersion relations (in the usual form [2]), or in the Gilbert form [3, 4]) or in the Mandelstam form [5])) do not exhaust all the information contained in the quantized field theory, the latter cannot in principle be expected to yield a full solution of this problem in the framework of the dispersion relations.

Against this background it seems worthwhile to seek approximate methods for solving the equation of motion of the quantized field theory. The ultimate aim of this search is the construction of a consistent method, which can (in contrast to the perturbation method) be applied to "strong" interactions and at the same time be free from ineffectiveness (the functional integration method [6])), the restriction to low energies (Chew-Low method [7])), the impracticability of the renormalization programme (Tamm-Dankoff method [8])) and other defects of the approximate methods †† now in existence. A new approximate method, expressly intended for the "strong" interactions of quantized field theory variants is proposed below. The idea, just as the idea in the old "strong" coupling method [12]), consists in treating the interaction Hamilto-

† This work was reported on 14 May 1960 at the 2nd All-Union University Conference on Quantized Field and Fundamental Particles Theory in Uzhgorod (see ref. [1]).

†† As to "the modified method of perturbation" [9]), the problems of uniqueness (see ref. [11])) and of the convergence of the method still await final solution, although the principal difficulties of the method can be considered to have been overcome [10]).

nian $\hat{H}'$ as an "unperturbed Hamiltonian" and the free-field Hamiltonian $\hat{H}^0$ as a "small perturbation", in contrast to the perturbation method intended for "weak" coupling. Under the method proposed, the expansion will be performed in increasing powers of the Hamiltonian $\hat{H}^0$ and not of the Hamiltonian $\hat{H}'$. This obviously calls for such a representation of field operators in which the Hamiltonian $\hat{H}'$ (and not $\hat{H}^0$, as in perturbation method) would be diagonal.

In contrast to the conventional "strong" coupling method in which diagonalization was achieved at the expensive price of fixing the nucleon current, we shall put forth an exact method of bringing the Hamiltonian $\hat{H}'$ to diagonal form without any approximation.

2. The Choice of Representation of Schrödinger Field Operators

To be more specific, let us consider a case of interaction of proton (spinor) and π^0-meson (pseudoscalar hemitian) fields for which, in the canonical formalism chosen by us for the sake of convenience and clarity, we have ($\hbar = c = 1$):

$$\begin{aligned}
\hat{H}^0 &= \hat{H}_1^0 + \hat{H}_2^0, \\
\hat{H}_1^0 &= \int \mathrm{d}^3x \left(\tfrac{1}{2}\right)[\hat{\pi}^2(x) + (\nabla\hat{\varphi}(x))^2 + \mu^2\hat{\varphi}^2(x)], \\
\hat{H}_2^0 &= \int \mathrm{d}^3x(-i)[\hat{\Pi}(x)\gamma_4\boldsymbol{\gamma}\nabla\hat{\Psi}(x) + m\hat{\Pi}(x)\gamma_4\hat{\Psi}(x)], \\
\hat{H}' &= \int \mathrm{d}^3x(-g)\hat{\Pi}(x)\gamma_4\gamma_5\hat{\Psi}_p(x)\hat{\varphi}(x).
\end{aligned} \tag{1}$$

Here the Schrödinger operators, explicitly independent of time, of the π^0-meson field $\hat{\varphi}(x)$ and proton field $\hat{\Psi}_\alpha(x)$ and its canonical conjugate $\hat{\pi}(x)$ and $\hat{\Pi}_\alpha(x)$ obey the usual commutation relations

$$\begin{aligned}
[\hat{\varphi}(x), \hat{\pi}(x')]_- &= i\delta(x-x'), \\
[\hat{\Psi}_\alpha(x), \hat{\Pi}_\beta(x')]_+ &= i\delta_{\alpha\beta}\delta(x-x') \quad (\alpha, \beta = 1, \ldots 4).
\end{aligned} \tag{2}$$

The commutators (for the π^0-meson field) and anticommutators (for the proton field) not included are equal to zero.

Let us choose for the sake of simplicity the representation of γ-matrices, in which

$$\gamma_4\gamma_5 = -\rho_1\rho_3 = i\begin{pmatrix} 1 & & & \\ & 1 & & \\ & & -1 & \\ & & & -1 \end{pmatrix}, \tag{3}$$

and consider the following special representation for the field operators:

$$\hat{\varphi}(x) = \varphi(x), \quad \hat{\pi}(x) = -i\frac{\delta}{\delta\varphi(x)},$$

$$\hat{\Psi}_\alpha(x) = \begin{cases} \sqrt{\delta(0)}\,\sqrt{1-N}\,\hat{\lambda}(N)\hat{F}(N) & \text{for } \alpha = 1, 2, \\ \sqrt{\delta(0)}\,\hat{F}(N)\hat{\lambda}(N)\,\sqrt{1-N} & \text{for } \alpha = 3, 4, \end{cases} \tag{4}$$

$$\hat{\Pi}_\alpha(x) = i\hat{\Psi}_\alpha^+(x) = \begin{cases} i\sqrt{\delta(0)}\,\hat{F}(N)\hat{\lambda}(N)\sqrt{1-N} & \text{for } \alpha = 1, 2, \\ i\sqrt{\delta(0)}\,\sqrt{1-N}\,\hat{\lambda}(N)\hat{F}(N) & \text{for } \alpha = 3, 4, \end{cases}$$

$$N \equiv N_\alpha(x), \quad \delta(0) \equiv (2\pi)^{-3}V_\infty.$$

Here the operator $\hat{F}(N_\alpha(x))$ is defined by the following operation on some functional $\Phi[N_\beta(y)]$ of the four functions $N_\beta(y)$:

$$\hat{F}(N_\alpha(x))\Phi[N_\beta(y)] = \Phi[\delta_{xy}\delta_{\alpha\beta} - (2\delta_{xy}\delta_{\alpha\beta} - 1)N_\beta(y)], \tag{5}$$

(without summing over the indices). This means that the operator $\hat{F}(N_\alpha(x))$ affects only the value of the point x of the α-component of the $N_\beta(y)$-function, changing $N_\alpha(x)$ to $1-N_\alpha(x)$ (cf. a similar situation in usual formalism); other components and the value of the α-component at other points remaining unchanged. This operator can be expressed in explicit form

$$\hat{F}(N_\alpha(x)) = \sum_{n=0}^{\infty} \frac{(1-2N_\alpha(x)]^n}{n!} \frac{\partial^n}{\partial N_\alpha^n(x)}.$$

To determine the $\hat{\lambda}(N_\alpha(x))$-operator it is convenient to order (in any manner) all sets of the values of (y, β) so that it is possible to say which of each pair of values of (y', β') and (y'', β'') is larger. Then (as in the usual formalism):

$$\hat{\lambda}(N_\alpha(x)) = \prod_{(y,\beta)<(x,\alpha)} (1-2N_\beta(y)). \tag{6}$$

The volume V_∞ of three-dimensional space occurs in (4) because we have not introduced intermediate lattice points, but considered the space to be continous from the outset. Let us emphazise that V_∞ and $\delta(0)$ must be considered as mere "symbols", finite in the intermediate calculations, and tending to infinity only in the final result.

A direct check shows that the operators (4) actually obey the commutation relations (2). Let us now specify the physical meaning of the operator introduced. It is clear that $\varphi(x)$ must be considered as the value of the π^0-meson field at the point x of the space. In specifying the meaning of the function $N_\alpha(x)$ we must note that in the representation (4) the full charge operator and the Z-component of spin operator of the proton field are diagonal and have the form

$$\hat{e}_{\text{full}} = -ie\int \mathrm{d}^3x\hat{\Pi}(x)\hat{\Psi}(x) = e\int \mathrm{d}^3x\delta(0)[N_1(x)+N_2(x) - N_3(x)-N_4(x)]+2e\delta(0)V_\infty, \tag{7}$$

$$\hat{S}_z = -\tfrac{1}{2}i\int \mathrm{d}^3x\hat{\Pi}(x)\sigma_z\hat{\Psi}(x) = \tfrac{1}{2}\int \mathrm{d}^3x\delta(0)[N_1(x)-N_2(x)-N_3(x)+N_4(x)]. \quad (8)$$

Hence it follows that $N_\alpha(x)$ are the "coordinate" filling functions of the proton field, viz.: $N_1(x)$ and $N_2(x)$ are the numbers of protons at point x with the direction of spin along and against the Z axis, respectively; $N_3(x)$ and $N_4(x)$ are the numbers of anti-protons at the same point with the direction against and along the axis. The second term in (7) represents the infinite charge of the vacuum state, which can be normalized to zero as in the usual "momentum" representation (see below).

For the sake of clarity let us consider, for example, the state of our system of quantized fields, which is vacuum for the π^0-meson field and has one proton at some point x_0, with spin direction along the Z axis. The functional of this state in representation (4) has the form

$$\Phi_{0,1}[\varphi(y), N_\beta(y)] = C\delta[\varphi(y)]\delta[N_\beta(y)-\delta_{\beta 1}\delta_{yx_0}], \quad (9)$$

where the δ-functionals

$$\delta[\varphi(y)] = \prod_{(\infty)}\left(\frac{\mathrm{d}^3y}{2\pi}\right)\int \delta\lambda \exp\left[i\int \mathrm{d}^3y\lambda(y)\varphi(y)\right], \quad (10)$$

$$\delta[N_\beta(y)] = \left[\prod_{(\infty)}\left(\frac{\mathrm{d}^3y}{2\pi}\right)\right]^4\int \delta\lambda_1 \ldots \int \delta\lambda_4 \exp\left[i\sum_{\beta=1}^{4}\int \mathrm{d}^3y\lambda_\beta(y)N_\beta(y)\right], \quad (11)$$

and the constant C is determined from the normalization condition of the functional. According to the general principles of the quantum theory, $|\Phi[\varphi(y), N_\beta[y]]|^2$ is the probability density of finding the given distribution of the field φ and the numbers of filling N_β at every point of the space. As the functional $\Phi_{0,1}$ differs from zero only for the case $\varphi(y) \equiv 0$, $N_1(y) = \delta_{yx_0}$ and $N_{\beta\neq 1}(y) \equiv 0$, the functional (9) actually corresponds to the necessary one-proton state. This is also confirmed by the fact that the eigenvalues of the operators $\hat{e}_{\text{full}}$ and $\hat{S}_z$, belonging to the proper functional of these operators (9), are equal to $e+2e\delta(0)V_\infty$ and $\frac{1}{2}$ respectively. To obtain these results, it must be taken into account, that $\delta(0)\delta_{yx_0} = \delta(y-x_0)$.

Furthermore, on the basis of (5) we conclude that, to the accuracy of the constant factors, $\hat{\Psi}_{1,2}(x)$ and $\hat{\Pi}_{3,4}(x)$ are the absorption operators of proton and anti-proton at the point x and have the spin direction corresponding to the given subscript, and $\hat{\Pi}_{1,2}(x)$ and $\hat{\Psi}_{3,4}(x)$ are the production operators of proton and anti-proton with the same characteristics. Moreover, it is easy to find that the set of all functionals $\Phi[N_\beta(y)]$ different from zero only for functions $N_\beta(y)$ having only two values 0 or 1 is invariant with respect to the operators (4), that is, the Pauli principle is fulfilled automatically.

Now we are in a position to normalize to zero all the physical quantities of the vacuum state. As regards the proton field, it is sufficient to replace in all

operators corresponding to physical quantities, the usual product of spinor operators with their normal product (see, e.g., ref. [13])). This leads in particular, to the disappearance of the second term in eq. (7) for the total charge operator. For the π^0-meson field we probably can only use the direct way of subtracting from the operators corresponding to physical quantities the average values of them with respect to the vacuum state. It will be noted that the average value of the operator $\hat{H}'$ with respect to the π^0-meson vacuum is equal to zero and that only the first term in the operator $\hat{H}_1^0$ introduces a non-zero contribution into the average value of this operator with respect to the π^0-meson vacuum.

Finally it will be noted that in the representation (4) the Hamiltonian $\hat{H}'$ accurately reduces to the diagonal form

$$\hat{H}' = \int \mathrm{d}^3x(-g){:}\,\hat{\Pi}(x)\gamma_4\gamma_5\hat{\Psi}(x){:}\,\hat{\varphi}(x) = \int \mathrm{d}^3x\delta(0)\sum_{\beta=1}^{4} N_\beta(x)\varphi(x), \tag{12}$$

while the free Hamiltonians $\hat{H}_1^0$ and $\hat{H}_2^0$ are essentially operators containing, however, diagonal terms as well.

3. Transition to "Free Field Representation" and Approximate "Strong" Coupling Method

To solve the Schrödinger equation of the quantized fields system in the representation (4)

$$\left\{\hat{H}_1^0[\varphi(y), \hat{\pi}(y)]+\hat{H}_2^0[\hat{\Psi}(y), \hat{\Pi}(y)]+\hat{H}'-i\frac{\partial}{\partial t}\right\}\Phi[\varphi(y), N_\beta(y); t] = 0, \tag{13}$$

it is convenient to use the unitary transformation

$$\Phi[\varphi(y), N_\beta(y); t] = \mathrm{e}^{-iH't}\chi[\varphi(y), N_\beta(y); t], \tag{14}$$

leading to the Schrödinger equation in the "free-field represenation" (cf. the "interaction representation"):

$$\begin{aligned}&\left\{\hat{H}_1^0(t)+\hat{H}_2^0(t)-i\frac{\partial}{\partial t}\right\}\chi[\varphi(y), N_\beta(y); t] = 0,\\ &\hat{H}_1^0(t) \equiv \hat{H}_1^0[\varphi(y), \hat{\pi}(y, t)], \quad \hat{H}_2^0(t) \equiv \hat{H}_2^0[\hat{\Psi}(y, t), \hat{\Pi}(y, t)].\end{aligned} \tag{15}$$

The operators $\varphi(x)$, $\hat{\pi}(x, t)$, $\hat{\Psi}(x, t)$ and $\hat{\Pi}(x, t)$ referred to as the operators in "free-field representation" and now explicitly depending on time (with the exception of $\varphi(x)$) are determined by the following formulas, obtained in the usual way

$$\begin{aligned}&\hat{\pi}(x, t) = -g\delta(0)\sum_{\beta=1}^{4} N_\beta(x)t-i\frac{\delta}{\delta\varphi(x)},\\ &\hat{\Psi}_{1,2}(x, t) = \hat{\Psi}_{1,2}(x)\mathrm{e}^{-ig\varphi(x)t}, \quad \hat{\Psi}_{3,4}(x, t) = \hat{\Psi}_{3,4}(x)\mathrm{e}^{ig\varphi(x)t},\\ &\hat{\Pi}_{1,2}(x, t) = \hat{\Pi}_{1,2}(x)\mathrm{e}^{ig\varphi(x)t}, \quad \hat{\Pi}_{3,4}(x, t) = \hat{\Pi}_{3,4}(x)\mathrm{e}^{-ig\varphi(x)t}.\end{aligned} \tag{16}$$

The exact solution of eq. (15) can be represented in the form

$$\chi[\varphi(y), N_\beta(y); t] = \hat{S}(t, t_0)\chi[\varphi(y), N_\beta(y); t_0],$$
$$\hat{S}(t, t_0) \equiv \mathrm{T} \exp\left\{-i \int_{t_0}^{t} \mathrm{d}t[\hat{H}_1^0(t)+\hat{H}_2^0(t)]\right\}, \tag{17}$$

where T is the chronological Wick symbol. Of course, just as in the case of the analogous solution in the interaction representation, (17) is only an elegant form of recording, suitable for practical purposes only after it has been expanded into a McLauren series, in powers of the free Hamiltonians in the present case. For a particular case when $t_0 = -\infty$ and $t = +\infty$ we therefore have

$$\hat{S}(+\infty, -\infty) = \sum_{n=0}^{\infty} \frac{(-i)^n}{n!} \int \mathrm{d}t_1 \ldots \int \mathrm{d}t_n T[\hat{H}^0(t_1), \ldots, \hat{H}^0(t_n)], \tag{18}$$
$$\hat{H}^0(t) \equiv \hat{H}_1^0(t)+\hat{H}_2^0(t).$$

This expansion, along with that of the operator $\hat{S}(t, t_0)$ for finite t and t_0, can serve as the basis for specific practical calculations by the method of "strong" coupling. Using the orthonormality of the functionals $\chi[\varphi(y), N_\beta(y)]$ proper for the "operators" $\varphi(y)$ and $N_\beta(y)$ it is easy, in particular, to show that the matrix element M_{ij} of the transition from the ith state at the moment of time t_0 into the jth state at the moment of time t can be calculated by the formula

$$M_{ij} = \langle j|\hat{S}(t, t_0)|i\rangle \equiv \int \delta\varphi \int \delta N_1 \ldots \int \delta N_4 \chi_j^* \hat{S}(t, t_0)\chi_i. \tag{19}$$

Let us illustrate our method for the simplest example: "the proper energetic" process of the transition from the initial state ($t_0 = -\tau$) with one proton at the point x_0 and spin direction along the Z axis into the same final ($t = \tau$) state. In the first non-vanishing approximation in powers of the free Hamiltonians of the method of strong coupling only the contribution depending on the g part of the first term in the expression for the Hamiltonian $\hat{H}_1^0(t)$ (eq. (1)) will make a non-zero contribution

$$M_{01,01} = \langle 0, 1|-i \int \mathrm{d}^3x \int_{-\tau}^{\tau} \mathrm{d}t \tfrac{1}{2} g^2 \delta^2(0) \left[\sum_{\beta=1}^{4} N_\beta(x)\right]^2 t^2|0, 1\rangle$$
$$-\tfrac{1}{3} i g^2 \tau^3 \delta(0) \int \mathrm{d}^3x \delta(0)\delta_{xx_0} = -\tfrac{1}{3} i g^2 \tau^3 \delta(0), \tag{20}$$

where $\delta(0)$ corresponds in the usual formalism to the δ-function representing the law of the conservation of three-dimensional momentum. A similar, though more cumbersome, method can be used for calculating any other process, the initial and final states of which are described by a complete set of the dynamic variables $\varphi(y)$ and $N_\beta(y)$ — in an arbitrary approximation of the "strong" coupling method.

It will be noted that the transition to this unusual set of dynamic variables

was necessitated by the exact reduction of the Hamiltonian $\hat{H}'$ of field interaction to the diagonal form. Yet despite the novelty of the representation selected and certain difficulty arisin in comparison, based on this concept, of the strong coupling method with experiment, a detailed analysis of this representation can be of considerable interest aside from the idea of the method of strong coupling. The fact is that it is possible, in the framework of this concept, to gain a graphic idea of the complex motion of a quantum field system in the usual coordinates (and not momentum) space (the motion being, of course, quantum field motion and not a simple classical motion by a trajectory).

As to the possibility of comparing the results obtained under the proposed method with experiment there are two ways to do so. First, it is possible to change the experimental set-up and make $\varphi(y)$ and $N_\beta(y)$ directly observed quantities. Second, it is possible in principle to pass to the conventional momentum representation. Both possibilities, however, still need a detailed analysis.

In conclusion it will be emphasized that we have left out such problems calling for special investigation as the relativistically invariant (and not canonical) formulation of the proposed method of strong coupling, the realization of the renormalization programme and finally the possibility of constructing some calculational technique, along the lines of the Feynman-Dyson graph technique in the conventional perturbation method. Despite the clarity of the basic idea of the proposed method the problem of the actual magnitude of the dimensionless parameter of the expansion is not yet solved. This problem could be solved for example through the direct calculation of several first approximations of this method for some processes. Finally the problem of the possibility of applying this method to other more complex variants of quantized field is not yet clear either.

The author is indebted to V. Ya. Fainberg, Ye. S. Fradkin and D. V. Shirkov for valuable discussions of the present work.

Appendix

It will be noted that since the free Hamiltonian $\hat{H}_1^0$ of the π-meson field in our representation (4) contains the variational derivative $\delta/\delta\varphi(x)$, the use of the expansion of the operator $\hat{S}(t, t_0)$ in the series of the type of (18) may lead to some difficulties. One of these is due to the fact that any arbitrary finite power of $\delta/\delta\varphi(x)$ cannot change the character of the state functional which is of the form of the δ-functional $\delta[\varphi(x)-f(x)]$ but merely increases its singularity at $\varphi(x) = f(x)$. This difficulty, however, can be completely removed with the well-known Feynman technique of the "disentangling" of operators [14]). Namely it is possible to disentangle the operator $\hat{S}(t, t_0)$, given by (17), exactly with

respect to the operator $\hat{\pi}^2(x, t)$ and in any arbitrarily high approximation with respect to the other operators. A new series will arise as a result, with terms containing the operator $\delta/\delta\varphi(x)$ in the exponents. The meaning of this procedure is that the result of the action of these exponents on the state functional can be calculated in a closed form with the help of the expansion of this functional into a continuous Fourier integral and using the usual relation

$$F[\delta/\delta\varphi(x)] \exp\left\{i \int \mathrm{d}^3x\varphi(x)\lambda(x)\right\} = F[i\lambda(x)] \exp\left\{i \int \mathrm{d}^3x\varphi(x)\lambda(x)\right\}.$$

In this connection see ref. [15]).

References

1) Yu. M. Lomsadze, Programme and Theses of the Reports of the 2nd All-Union Inter-University Conference on Quantized Field and Fundamental Particles Theory in Uzhgorod (1960)
2) N. N. Bogolyubov, B. V. Medvedev and M. K. Polivanov, Problems of the Theory of the Dispersion Relations, GIFML (1958)
3) W. Gilbert, Phys. Rev. **108** (1957) 1078
4) L. A. Khalfin, DAN SSSR **130** (1960)
5) S. Mandelstam, Phys. Rev. **112** (1958) 1344
6) I. M. Gelfand and A. M. Yaglom, Usp. Mat. Nauk **11** (1956) 77
7) G. Chew and F. Low, Phys. Rev. **101** (1956) 1570
8) V. P. Silin and V. Ya. Fainberg, Usp. Fiz. Nauk **56** (1955) 569
9) Yu. M. Lomsadze, JETP **31** (1956) 887, Izvestia VUZ'ov (Fizika) No. **1** (1959) 88
10) Yu. M. Lomsadze, Problems of Modern Theory of Fundamental Particles (Uzhgorod 1959) No. 2, 182
11) D. A. Kirzsnitz, V. Ya. Fainberg and Ye. S. Fradkin, JETP **38** (1960) 239
12) G. Wentzel, Rev. Mod. Phys. **19** (1947) I
13) N. N. Bogolyubov and D. V. Shirkov, An Introduction to Quantum Field Theory (FIZMATGIZ 1957)
14) R. P. Feynman, Phys. Rev. **84** (1951) 108
15) Yu. M. Lomsadze, Reports of Uzhgorod University, No. **3** (1960) 25

1.E.1:
3.A

Nuclear Physics **24** (1961) 151—159; © *North-Holland Publishing Co., Amsterdam*
Not to be reproduced by photoprint or microfilm without written permission from the publisher

γ–γ ANGULARCORRELATION IN THE Ti^{48} (n, γ)Ti^{49} REACTION

B. KARDON, D. KISS, I. LOVAS and Z. ZÁMORI
Central Research Institute for Physics, Budapest

Received 16 December 1960

Abstract: The angular correlation of the γ-radiation resulting from the Ti^{48}(n, γ)Ti^{49} reaction has been measured for 0.34–1.38 MeV and 1.38–6.43 MeV cascades. The spin values of the 1.38 and 1.72 MeV levels of Ti^{49} as well as the multipolarity of the 0.34 MeV transition have been determined.

1. Introduction

The measurement of the (γ–γ) angular correlation is a very useful tool in nuclear spectroscopy. By means of this method the spin values of individual nuclear levels, multipolarity of the γ-radiation and in some cases the mixing parameter for mixed transitions can be determined. For isotopes of sufficiently long half life the use of γ–γ correlation technique for the study of the gamma cascades following radioactive decay is generally fairly convenient. For nuclear reactions induced by charged particles, background effects, however, are rather a nuisance. This difficulty due to the high neutron and gamma background is aggravated for (n, γ) reactions by the fact of the gamma spectrum being usually of composite nature so that the discrimination between the various components of the gamma cascade becomes highly problematical.

Despite these difficulties, it is of considerable interest to study the γ–γ angular correlation in (n, γ) reactions since in this way it is possible to investigate nuclear levels which cannot be excited by β-decay such as the levels above 2–2.5 MeV and those of nuclei having stable adjacent isobars.

In 1957 Trumpy [1]) was the first to succeed to measure the γ–γ angular correlation in the (n, γ) reaction. In 1959 such measurements were reported by Manning and Bartholomew [2]).

In the experiment reported in the following we have measured the γ–γ angular correlation in the Ti^{48}(n, γ)Ti^{49} reaction.

2. Experimental Apparatus

As thermal neutron source a horizontal channel of the Hungarian Research Reactor was used. The major part of the direct gamma radiation of the reactor was being absorbed by a bismuth plug, 20 cm long. The neutrons were passed to the 1.5 cm long, 1.2 cm diameter target through a boron carbide collimator,

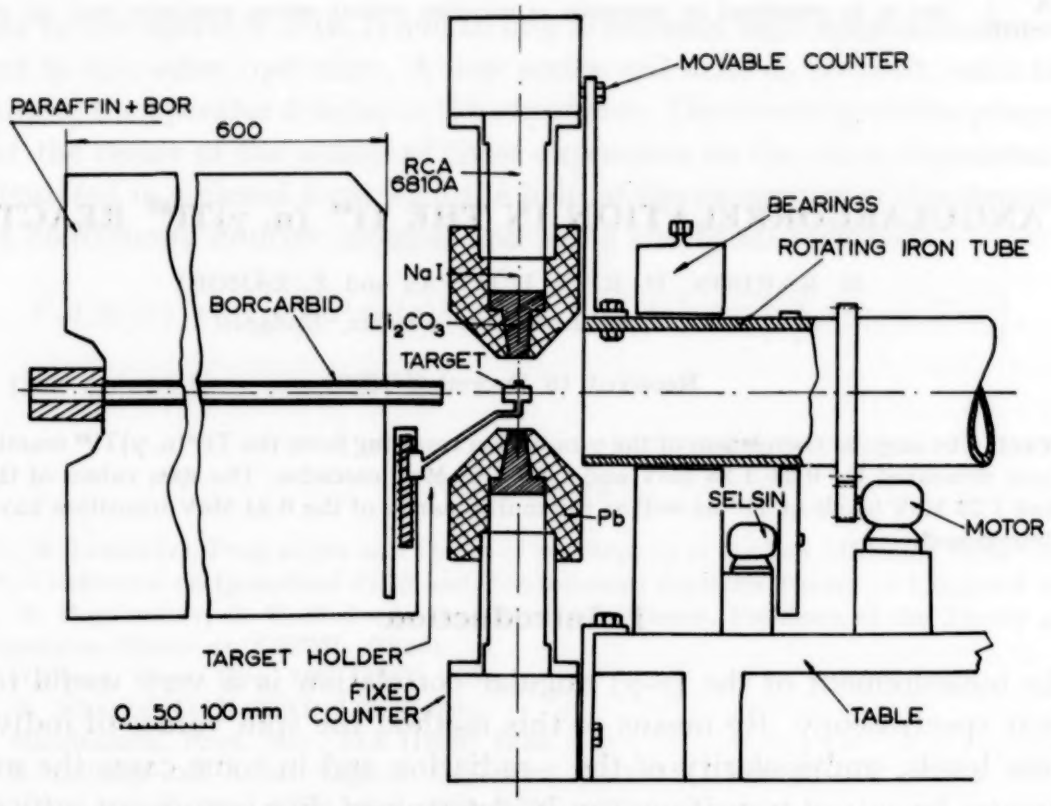

Fig. 1. The measuring arrangement.

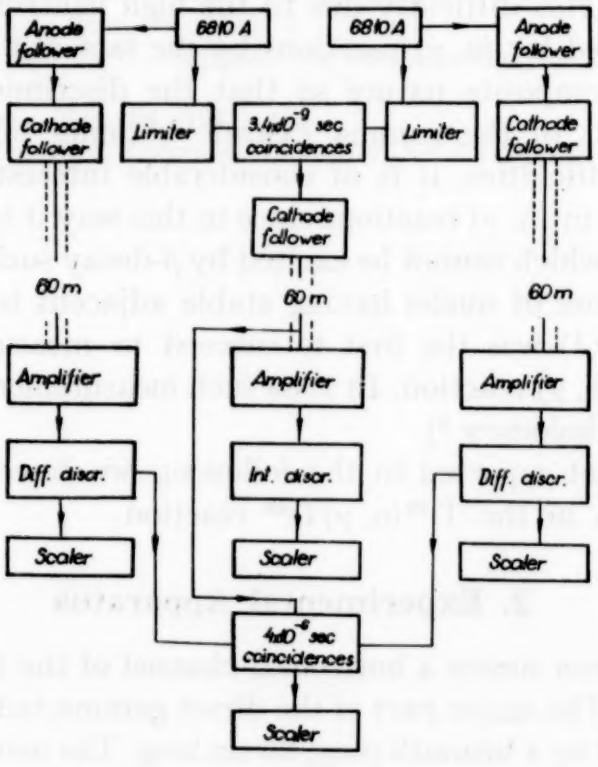

Fig. 2. The block diagram of the electronic apparatus.

60 cm long and 1.8 cm in diameter. The target consisted of compressed titanium powder on a thin plexiglass ring holder which could be centred by means of two fine adjusting screws.

Two scintillation counters served as detectors, each of them was a 5.1 cm × 3.8 cm diam. NaJ(Tl) crystal mounted on RCA 6810 A multiplier. One of them was kept in a fixed vertical position while the other was movable around the neutron beam as axis in a vertical plane from 90° to 270°. The measurements were performed both to the left and to the right of the 180° direction in three angular positions corresponding to $\cos^2\theta = 0$, 0.4 and 0.8. The motion of the counter was remote-controlled from the measuring laboratory with the use of a servo-mechanism turning and fixing the counter at the angle required. The outlay of the apparatus is shown in fig. 1.

The pulses coming from the multiplier were analysed by the usual fast-slow coincidence system. Its block diagram is shown in fig. 2. Each pulse coming from the multiplier plates was transmitted through a limiter stage to the fast coincidence unit. The two limiters consisted of two E 180F tubes connected in parallel. The fast coincidence unit was the well known Minton circuit using crystal diodes [3]) with a resolving time of 3.4×10^{-9} sec. With this circuit coincidences were obtainable for detector pulses of energies above 200 keV.

The pulses to be analysed were taken from the 12-th dynode of each multiplier. The energy resolution obtained for the Cs^{137} 661 keV line was 13 %.

3. Measurement

The thermal neutron intensity of the bombarding beam was 2×10^6 n/sec · cm^2. Since a considerable amount of neutrons which were scattered mainly by the target but also escaped through the shield was absorbed by the NaI crystal, the iodine became well activated and decayed through 2.02 MeV maximum energy ($T_{\frac{1}{2}} = 25$ min) β-emission. This β-radiation was detected with high efficiency by the crystal functioning as a 4π counter increasing thus considerably the background. This neutron background was reduced by the use of $LiCO_3$ absorber. Thus it has been achieved that the number of counts due to the activation of iodine was only 10 % of the total number of counts above the zero discrimination level set for the Ti(n, γ) reaction. The stray gamma background was screened off by lead collimators.

The rotational symmetry of the movable counter was determined partly by optics partly by direct measurement when the target was being adjusted until the movable counter yielded in each position the same counting rates. In order to eliminate the possibly remaining geometrical asymmetry, we used in the calculations the averages of the results obtained at the angles $180°+\theta$ and $180°-\theta$.

Errors due to some fluctuation in neutron intensity and to experimental

instabilities were minimized by frequently varying the angle of measurement. The measuring time at each angular position was 5 min.

The effective surfaces of the measuring crystals, situated at a distance of 8 cm from the target were about 7 cm^2 as determined by the lead collimators. Consequently, the counter solid angle was about 0.1 sr with respect to the centre of the target. Owing to finite target size and finite instrumental angular resolution some corrections were required. Since no corrections for finite radially extended targets have been reported in the literature, the value of the correction was determined directly as follows. For this purpose we utilized the electron pairs produced in the target by the high energy γ-radiation following neutron capture. The angular correlation in the annihilation radiation of the positons was measured with the apparatus set up for the actual experiment. The annihilation events and the (n, γ) reactions occur with about the same probability in each volume element of the target, consequently the measured angular correlation function $f(\delta)$ for annihilation radiation contains not only the effects due to the finite counter solid angle but those due to the finite target size too.

The function $f(\delta)$ thus obtained represents a Gaussian distribution with the half width 10°. The actual $(\gamma\text{–}\gamma)$ angular correlation function of the form

$$W(\theta) = \sum_k A_k P_k(\cos\theta)$$

has to be averaged over the $f(\delta)$ distribution. Making use of the addition theorem for Legendre polynomials, it can be proved that the correlation function averaged over the $f(\delta)$ distribution will be of the form [4])

$$\overline{W(\theta)} = \sum_k A_k Q_k P_k(\cos\theta).$$

Using now the experimental function $f(\delta)$ and applying the calculation method of Church *et al.* [5]), the following values were obtained:

$$Q_0 = 0.993, \quad Q_2 = 0.930.$$

As an experimental test the angular correlation of the Ni^{60} 1.33 and 1.17 MeV γ-lines was measured and the result was in fairly good agreement with the published data.

4. Results

The part which is now of interest in the decay scheme of Ti^{49} produced by slow neutron capture in the Ti^{48} isotope, is shown in fig. 3.

The purpose of our experiments was the study of the angular correlations in the A–E and D–E cascade transitions. Bretscher [6]) concluded from the angular distribution of the protons produced in the Ti^{48}(d, p)Ti^{49} reaction that the neutrons captured at the levels b and d have both the same orbital momentum, namely 1. Since the ground state of Ti^{48} has 0 spin and even parity, the parities of the two levels can be only negative and their spins must be $\frac{3}{2}$ or $\frac{1}{2}$.

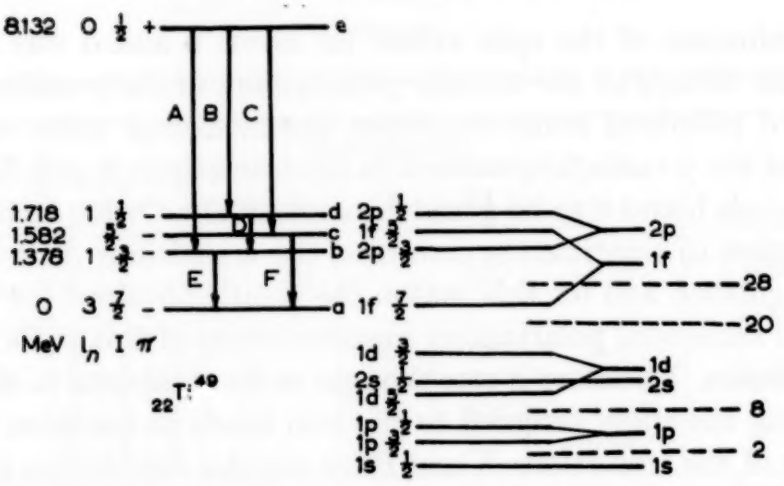

Fig. 3. Left: Decay scheme of Ti^{49}. Right: Shell model level system.

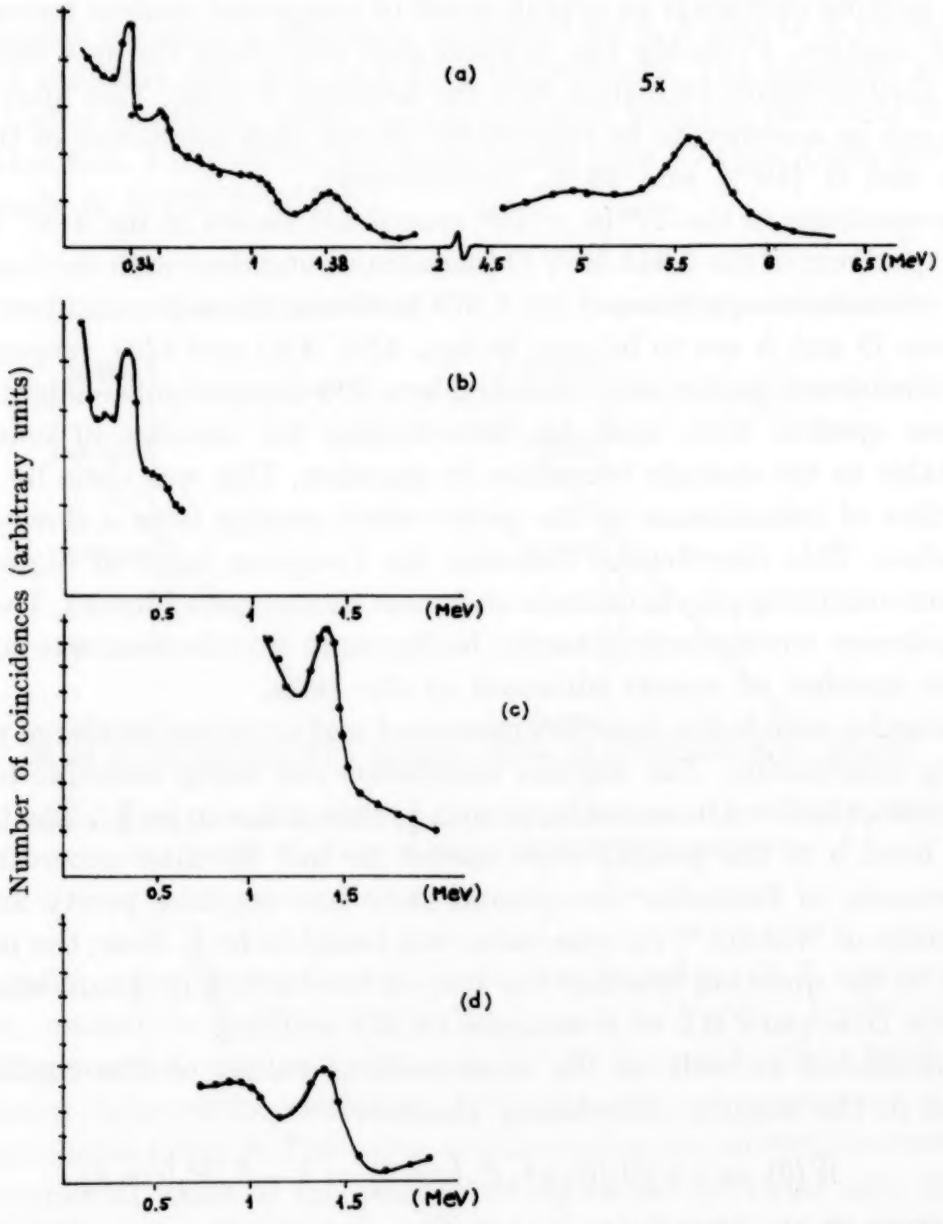

Fig. 4. The single and coincidence γ spectra in the $Ti^{48}(n, \gamma)Ti^{49}$ reaction, (a) single spectrum, (b) in coincidence with 1.38 MeV, (c) in coincidence with 0.34 MeV, and (d) in coincidence with 6.7 MeV.

The determination of the spin values for levels b and d was attempted by Trumpy [7]) who measured the circular polarization of the γ-radiation following the capture of polarized neutrons. From the measured value of the circular polarization of the γ-radiation emitted in the transitions A and B, he found the spins of the levels b and d to be $\frac{1}{2}$ and $\frac{3}{2}$, respectively. Owing to the rather poor energy resolution of scintillation counters, the transitions A and B cannot be clearly distinguished and for this reason the results obtained for Ti in the very ingenious and successful polarization measurements of this author still contain some uncertainties. Therefore it was thought to be of interest to check his result by determining the spins assigned to the two levels in question as well as the multipolarity of the transitions A and B by angular correlation measurements.

It seems highly probable from the calculations of Lane and Lynn [3]) that for Ti^{48} the neutron capture is an overall result of compound nucleus formation and of direct capture. Probably the neutron goes over from the free state in one step by electric dipole transition into the bounded P state. This form of direct capture can be assumed to be responsible for the high intensities of the transitions A and B (40 % and 29 %, respectively).

The γ-spectrum of the $Ti^{48}(n, \gamma)Ti^{49}$ reaction is shown in fig. 4(a). The coincidence spectrum of the 0.341 MeV D transition coincident with the transition E and the coincidence spectrum of the 1.378 MeV transition E coincident with the transitions D and A are to be seen in figs. 4(b), 4(c) and 4(d), respectively.

The coincidence spectra were recorded by a 100-channel pulse-height analyser and these spectra were used for determining the number of coincidences attributable to the cascade transition in question. This was done by counting the number of coincidences at the peaks which emerge from a slowly varying distribution. This distribution contains the Compton band of higher energy transitions occurring also in cascade and some chance coincidences. The number of coincidences corresponding to the background distribution was subtracted from the number of counts obtained at the peak.

The angular correlation function measured and corrected as above yields the following information. The angular correlation not being isotropic for any of the cascades, the level b cannot have spin $\frac{1}{2}$, thus it has to be $\frac{3}{2}^-$. The transition E from level b to the ground state cannot be but E2 since according to the measurements of Bretscher the ground state has negative parity and in the experiments of Walchli [9]) its spin value was found to be $\frac{7}{2}$. Now, the problem is reduced to the question whether the spin of level d is $\frac{3}{2}$ or $\frac{1}{2}$ and whether the transition D is pure M1 or a mixture of M1 and E2.

The predicted as well as the experimental values of the coefficient $\bar{A}_2$ involved in the angular correlation function

$$\overline{W}(\theta) = 1 + (Q_2/Q_0)A_2 P_2(\cos\theta) = 1 + \bar{A}_2 P_2(\cos\theta)$$

corrected for finite solid angle and finite target size are listed in table 1.

TABLE 1

Level spins and experimental and theoretical values of the coefficient $\bar{A}_2$

Cascade	I_a	I_b	I_d	I_e	Multipolarity A	Multipolarity D	Multipolarity E	$\bar{A}_2$ (th.)	$\bar{A}_2$ (exp.)
A–E 6.75–1.38	$\frac{7}{2}$	$\frac{3}{2}$		$\frac{1}{2}$	E1		E2	−0.067	-0.055 ± 0.01
D–E 0.34–1.38	$\frac{7}{2}$	$\frac{3}{2}$	$\frac{3}{2}$			E2	E2	0	-0.066 ± 0.01
	$\frac{7}{2}$	$\frac{3}{2}$	$\frac{3}{2}$			M1	E2	+0.054	
	$\frac{7}{2}$	$\frac{3}{2}$	$\frac{1}{2}$			E2	E2	+0.067	
	$\frac{7}{2}$	$\frac{3}{2}$	$\frac{1}{2}$			M1	E2	−0.067	

The angular correlation functions measured for A–E and D–E cascade transitions are shown in figs. 5(a) and 5(b), respectively. The magnetic transition being of higher multipole order, cannot compete with the electrical transition so that transition A is pure E1 and transition B pure E2 type. Consequently the A–E cascade is $\frac{1}{2}^+(E1)\frac{3}{2}^-(E2)\frac{7}{2}^-$.

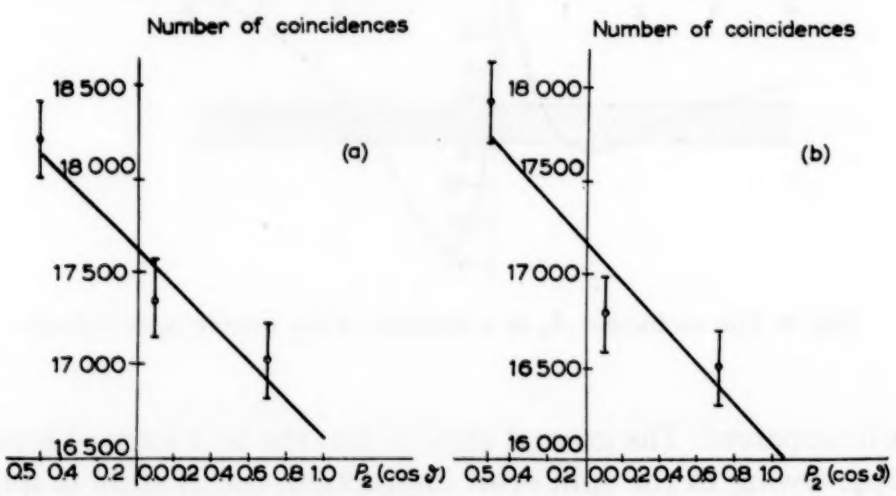

Fig. 5. The measured angular correlation functions (a) in the case of the 6.75–1.38 MeV transition and (b) in the case of the 0.34–1.38 MeV transition.

The angular correlation as measured for the transition D–E can be fitted in two ways, namely to $\frac{1}{2}^-(M1+E2)\frac{3}{2}^-(E2)\frac{7}{2}^-$ and to $\frac{3}{2}^-(M1+E2)\frac{3}{2}^-(E2)\frac{7}{2}^-$.

Assuming now the schemes $\frac{1}{2}^-(M1+E2)\frac{3}{2}^-(E2)\frac{7}{2}^-$ and $\frac{3}{2}^-(M1+E2)\frac{3}{2}^-(E2)\frac{7}{2}^-$, the predicted values of the coefficient $\bar{A}_2$ as a function of parameter $\delta \equiv \langle|E2|\rangle/\langle|M1|\rangle$ are shown in fig. 6. The value of this mixing parameter δ is restricted by the experimental value of the coefficient $\bar{A}_2$ to the intervals seen in fig. 6. Since $_{22}Ti^{49}$ lies immediately below the magic number 28, single particle tran-

sitions are predominant. For single particle transition, however, a strong competition of M1 and E2 radiations seems highly improbable and thus the assumption $\frac{3}{2}^-(M1+E2)\frac{3}{2}^-(E2)\frac{7}{2}^-$ cannot be true. The transition D is consequently to be considered pure M1. These results are consistent with the result of Trumpy's polarization measurement.

Considering that Ti^{49} contains an even number of protons and 27 neutrons, i.e. only one neutron less than the magic number 28 characteristic of the closed shell, the interpretation of the level structure from the shell model seems quite plausible. In fact, if we look at the term scheme determined by the shell model and illustrated in fig. 3(b), the analogy with the decay scheme of Ti^{49} will

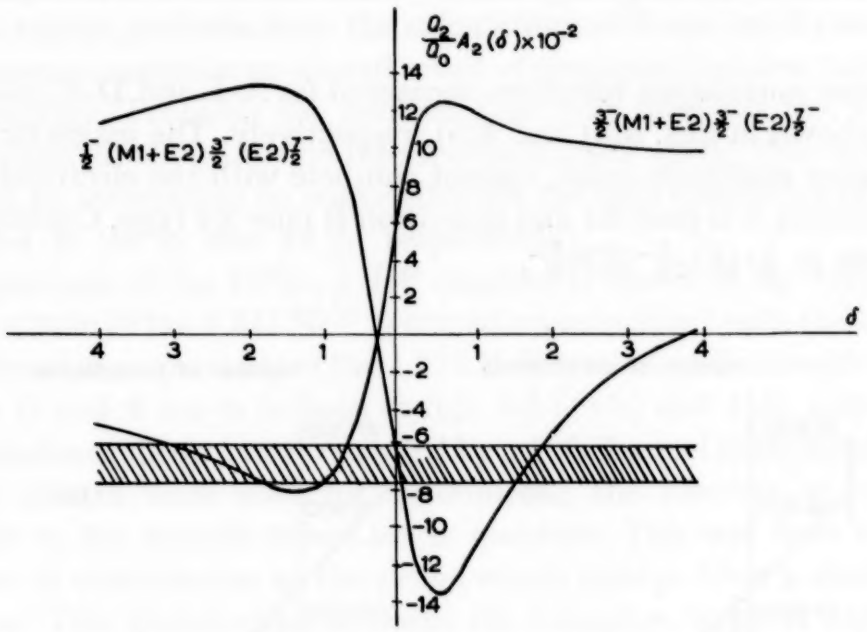

Fig. 6. The coefficient A_2 as a function of the mixing parameter δ.

become quite apparent. The ground state is $1f_{\frac{7}{2}}$, the first excited level $2p_{\frac{3}{2}}$ and the third $2p_{\frac{1}{2}}$. Owing to the spin orbit interaction, the 1f state is splitted into two sublevels. The lower has spin $\frac{7}{2}$, the higher spin $\frac{5}{2}$. This $1f_{\frac{5}{2}}$ state is probably identifiable with the level c of Ti^{49} at 1.582 MeV. The multipolarity of the transition C from level e to level c is in this case probably M2. The probability of transitions C is one order of magnitude less than that of transitions A or B. This fact seems to support the assumption that the transition C is M2 and the level c $\frac{5}{2}^-$. The full clarification of the problem, however, seems to require some further investigations.

Thanks are due to the Staff of the Hungarian Research Reactor for their help in carrying out the experiments and to our colleague Mr. J. Zimányi for very useful discussions.

References

1) G. Trumpy, Jener Publs. no. **13** (1957)
2) G. Manning and G. A. Bartholomew, Phys. Rev. **115** (1959) 401
3) G. H. Minton, Journ. of Res. of the NBS **57** (1956) 119
4) S. Frankel, Phys. Rev. **83** (1951) 673
5) E. L. Church and J. J. Kraushaar, Phys. Rev. **88** (1952) 419
6) M. M. Bretscher, J. O. Alderman, A. Elwyn and F. B. Shull, Phys. Rev. **96** (1954) 103
7) G. Trumpy, Nuclear Physics **2** (1956) 664
8) A. M. Lane and J. E. Lynn, Nuclear Physics **17** (1960) 563
9) H. E. Walchli, ORNL-1469, U. S. Atomic Energy Commission (1953)
10) L. V. Groshev, A. M. Demidov, V. M. Lutsenko and V. I. Pelekhov, Atlas of γ-ray spectra from radiative capture of thermal neutrons (Moscow, 1958)

7.C

Nuclear Physics **24** (1961) 160—162; © *North-Holland Publishing Co., Amsterdam*

Not to be reproduced by photoprint or microfilm without written permission from the publisher

RELATIVISTIC ONE-PION EXCHANGE NUCLEAR POTENTIAL

SURAJ N. GUPTA

Department of Physics, Wayne State University, Detroit, Michigan †

Received 6 December 1960

Abstract: The exact relativistic one-pion exchange nuclear potential is derived in the centre-of-mass system, and the relationship between the relativistic potential and the Schrödinger equation is discussed.

It was first observed by Taketani [1]) that, in spite of the large value of the pion-nucleon coupling constant, the perturbation theory can be applied to obtain the nuclear potential at all distances except in the immediate neighborhood of the nucleons. In particular, the one-pion exchange nuclear potential can be regarded as a fairly good approximation up to a minimum distance, somewhat larger than the pion Compton wavelength. Since the impact parameter can be expressed roughly in terms of the orbital angular momentum $\hbar\sqrt{l(l+1)}$ and the momentum $\mathbf{P}$ of the incident particle as

$$b \approx \frac{\hbar\sqrt{l(l+1)}}{|\mathbf{P}|}, \tag{1}$$

it follows that for low values of $|\mathbf{P}|$ and large values of l, the nucleon-nucleon scattering is essentially determined by the one-pion exchange interaction. Therefore, Moravcsik [2]) and Breit [3, 4]) have used the one-pion exchange nuclear potential to account for the higher angular momentum phase shifts in low-energy nucleon-nucleon scattering, which has led to an appreciable improvement of the earlier work on this problem.

Since the experimental data on nucleon-nucleon scattering extends over a considerable energy range, we shall derive the exact velocity-dependent one-pion exchange nuclear potential to see how far it differs from the usual static result. We shall also discuss the general relationship between the relativistic potential and the Schrödinger equation.

Let us consider the scattering of two nucleons, whose propagation four-vectors are p and q in the initial state and p' and q' in the final state. The one-pion exchange scattering matrix element for this process in the centre-of-mass

† Work supported in part by the U. S. National Science Foundation.

system is

$$S_2 = -i(2\pi)^4 \frac{g^2}{c\hbar}\,\delta(p+q-p'-q')\,\frac{1}{\mathbf{k}^2+\lambda^2} \cdot (\bar{\psi}^-(\mathbf{p}')\gamma_5\tau_i\psi^+(\mathbf{p}))(\bar{\psi}^-(\mathbf{q}')\gamma_5\tau_i\psi^+(\mathbf{q})), \quad (2)$$

where the various symbols have the same meaning as in an earlier paper [5]). Transforming the four-component Dirac spinors into the two-component Pauli spinors, we obtain without any approximation

$$\psi^{*-}(\mathbf{p}')\gamma_4\gamma_5\psi^+(\mathbf{p}) = \psi_L{}^{*-}(\mathbf{p}')\,\frac{\boldsymbol{\sigma}\cdot\mathbf{k}}{2p_0}\,\psi_L{}^+(\mathbf{p}), \quad (3)$$

where $\boldsymbol{\sigma}_i$ are the Pauli spin matrices, and $\psi_L{}^+(\mathbf{p})$ represents the so-called large components of $\psi^+(\mathbf{p})$ multiplied by an appropriate normalization factor to ensure that

$$\psi^{*-}(\mathbf{p})\psi^+(\mathbf{p}) = \psi_L{}^{*-}(\mathbf{p})\psi_L{}^+(\mathbf{p}). \quad (4)$$

Using (3), we can express (2) as

$$S_2 = (-i/c\hbar)(2\pi)^4\delta(p+q-p'-q')\psi_L{}^{*-}(\mathbf{p}')\psi_L{}^{*-}(\mathbf{q}')V_2(\mathbf{k})\psi_L{}^+(\mathbf{q})\psi_L{}^+(\mathbf{p}), \quad (5)$$

with

$$V_2(\mathbf{k}) = -\frac{g^2}{4p_0{}^2}\,(\boldsymbol{\tau}^{(1)}\cdot\boldsymbol{\tau}^{(2)})\,\frac{(\boldsymbol{\sigma}^{(1)}\cdot\mathbf{k})(\boldsymbol{\sigma}^{(2)}\cdot\mathbf{k})}{\mathbf{k}^2+\lambda^2}. \quad (6)$$

Thus, the nuclear potential is

$$V_2(\mathbf{r}) = (2\pi)^{-3}\int d\mathbf{k}\, e^{i\mathbf{k}\cdot\mathbf{r}}V_2(\mathbf{k}), \quad (7)$$

or, putting $\lambda\mathbf{r} = \mathbf{x}$,

$$V_2(\mathbf{x}) = \left(\frac{g^2}{4\pi c\hbar}\right)\left(\frac{Mc^2}{E}\right)^2\left(\frac{\mu c^2}{12}\right)\left(\frac{\mu}{M}\right)^2(\boldsymbol{\tau}^{(1)}\cdot\boldsymbol{\tau}^{(2)}) \times\left[\boldsymbol{\sigma}^{(1)}\cdot\boldsymbol{\sigma}^{(2)} + \left(1+\frac{3}{x}+\frac{3}{x^2}\right)S^{(1,2)}\right]\frac{e^{-x}}{x}, \quad (8)$$

where μ and M are the pion and nucleon masses respectively, and E is the energy of each nucleon in the initial or final state. The above potential can be used even after passing over from the interaction representation to the Schrödinger representation, provided that we can treat V_2 as small compared with E.

Since, according to our definition [5]) of a potential, V_2 represents the effective interaction energy, we can express the total energy of the system in the relativistic form as

$$W = 2(M^2c^4+c^2\mathbf{P}^2)^{\frac{1}{2}}+V_2, \quad (9)$$

or, neglecting the V_2^2 term,

$$\tfrac{1}{4}W^2-\tfrac{1}{2}V_2W-M^2c^4-c^2\mathbf{P}^2=0, \tag{10}$$

where $\mathbf{P}_1=\mathbf{P}$ and $\mathbf{P}_2=-\mathbf{P}$ are the momenta of the two nucleons. Hence, putting

$$W\Psi=2E\Psi$$

and

$$\mathbf{P}^2=-\hbar^2\nabla^2,$$

we obtain in the usual way the Schrödinger equation for the relative motion,

$$\left(\nabla^2+\frac{E^2-M^2c^4}{c^2\hbar^2}-\frac{V_2E}{c^2\hbar^2}\right)\Psi=0. \tag{11}$$

Substituting (8) in (11), we find that the above Schrödinger equation is in complete agreement with the recent result of Breit [3]).

References

1) M. Taketani, S. Nakamura and M. Sasaki, Progr. Theoret. Phys. **6** (1951) 581; Suppl. Progr. Theoret. Phys. no. **3** (1956)
2) P. Cziffra, M. H. MacGregor, M. J. Moravcsik and H. P. Stapp, Phys. Rev. **114** (1959) 880; M. H. MacGregor, M. J. Moravcsik and H. P. Stapp, Phys. Rev. **116** (1959) 1248; M. H. Macgregor and M. J. Moravcsik, Phys. Rev. Letters **4** (1960) 524
3) G. Breit and M. H. Hull, Nuclear Physics **15** (1960) 216
4) G. Breit, M. H. Hull, K. Lassila and K. D. Pyatt, Phys. Rev. Letters **4** (1960) 79; Phys. Rev., to be published
5) S. N. Gupta, Phys. Rev. **117** (1960) 1146

7.C

Nuclear Physics **24** (1961) 163—168; © *North-Holland Publishing Co., Amsterdam*

Not to be reproduced by photoprint or microfilm without written permission from the publisher

ELASTIC PHOTOPRODUCTION OF NEUTRAL PIONS FROM DEUTERIUM

ALLADI RAMAKRISHNAN, V. DEVANATHAN and G. RAMACHANDRAN †

University of Madras, Madras-25, India

Received 16 December 1960

Abstract: The elastic photoproduction of neutral pions from deuterium has been studied under the impulse approximation using the Chew-Low amplitude for the photoproduction of π^0 from nucleons. The differential cross-sections have been obtained at various photon energies (1.5, 2.0 and 2.5 in units of pion mass) and they are in good agreement with the available experimental values. Studies of the final spin state of the deuteron have also been made.

1. Introduction

The photoproduction of pions from deuterium has been studied earlier by many authors [1, 2]) using the impulse approximation. The elastic photoproduction of π^0 from deuterium is of particular importance for it presents no uncertainty regarding the final state of the system. A reliable calculation is possible in this case since the spatial wave function of the deuteron is known and the complete amplitude for the photoproduction of π^0 from nucleons is given by Chew *et al.* [3]). The differential cross-sections for the elastic photoproduction of π^0 from deuterium are obtained at various photon energies 1.5, 2.0 and 2.5 in units of the pion mass. A detailed comparison is made with the experimental results of Wolfe, Silverman and De Wire [4]), Davis and Corson [5]) and Rosengren and Baron [6]).

As Chew and Lewis [1]) have pointed out, it would be of interest to study the final spin state of the recoiling deuteron. The differential cross-sections for the various final spin states are also given separately for the incident photon of energy equal to twice the pion mass and it is found that they are nearly equal at large angles of pion emission, but at forward angles the $m_z = 0$ state predominates.

2. Calculation of the Cross-Section

Using the notation followed in ref. [2]), the matrix element for the photoproduction of π^0 from deuterons may be written as ††

† Junior Research Fellow, Council of Scientific and Industrial Research, India.

†† We use natural units in which $\hbar = c = 1$ and the pion mass is unity. Throughout this paper we use the notation followed in ref. [2]).

$$Q = \langle \mathrm{f}|T^{(1)} \exp(i\mathbf{D}\cdot\mathbf{r}_1)+T^{(2)} \exp(i\mathbf{D}\cdot\mathbf{r}_2)|\mathrm{i}\rangle, \tag{1}$$

where $|\mathrm{i}\rangle$ is the initial state represented by

$$|\mathrm{i}\rangle = 2^{-\frac{1}{2}}\{\mathrm{p}(1)\mathrm{n}(2)-\mathrm{p}(2)\mathrm{n}(1)\} \quad {}^3\chi_m u_\mathrm{d}(\varrho)(2\pi)^{-\frac{3}{2}} \tag{2}$$

and $|\mathrm{f}\rangle$ the final state which may either be charge-singlet or charge-triplet.

For the 'elastic' process $\gamma+\mathrm{D} \rightarrow \pi^0+\mathrm{D}$ the final state is

$$|\mathrm{f}\rangle = 2^{-\frac{1}{2}}\{\mathrm{p}(1)\mathrm{n}(2)-\mathrm{p}(2)\mathrm{n}(1)\} \quad {}^3\chi_m u_\mathrm{d}(\varrho) \exp\,(i\mathbf{D}\cdot\mathbf{R})(2\pi)^{-\frac{3}{2}}. \tag{3}$$

For the 'inelastic' process $\gamma+\mathrm{D} \rightarrow \pi^0+\mathrm{p}+\mathrm{n}$ we have the following final states:

(a) charge-singlet

$$|\mathrm{f_e}\rangle_\mathrm{S} = 2^{-\frac{1}{2}}\{\mathrm{p}(1)\mathrm{n}(2)-\mathrm{p}(2)\mathrm{n}(1)\} \quad {}^3\chi_m u_{t,\mathrm{e}}(\mathbf{k}\cdot\varrho) \exp\,(i\mathbf{D}\cdot\mathbf{R})(2\pi)^{-\frac{3}{2}}, \tag{4}$$

$$|\mathrm{f_o}\rangle_\mathrm{S} = 2^{-\frac{1}{2}}\{\mathrm{p}(1)\mathrm{n}(2)-\mathrm{p}(2)\mathrm{n}(1)\} \quad {}^1\chi_0 u_{t,\mathrm{o}}(\mathbf{k}\cdot\varrho) \exp\,(i\mathbf{D}\cdot\mathbf{R})(2\pi)^{-\frac{3}{2}}, \tag{5}$$

(b) charge-triplet

$$|\mathrm{f_e}\rangle_\mathrm{T} = 2^{-\frac{1}{2}}\{\mathrm{p}(1)\mathrm{n}(2)+\mathrm{p}(2)\mathrm{n}(1)\} \quad {}^1\chi_0 u_{t,\mathrm{e}}(\mathbf{k}\cdot\varrho) \exp\,(i\mathbf{D}\cdot\mathbf{R})(2\pi)^{-\frac{3}{2}}, \tag{6}$$

$$|\mathrm{f_o}\rangle_\mathrm{T} = 2^{-\frac{1}{2}}\{\mathrm{p}(1)\mathrm{n}(2)+\mathrm{p}(2)\mathrm{n}(1)\} \quad {}^3\chi_m u_{t,\mathrm{o}}(\mathbf{k}\cdot\varrho) \exp\,(i\mathbf{D}\cdot\mathbf{R})(2\pi)^{-\frac{3}{2}}. \tag{7}$$

The subscripts e and o refer to even and odd spatial parts of the wave function respectively. It can be shown that the contribution from the charge-triplet final state is almost negligible since the Chew-Low amplitudes for the photoproduction of π^0 from proton and neutron are nearly equal. The major contribution to the cross-section comes from the charge singlet final state (both elastic and inelastic). We shall, however, restrict ourselves to the "elastic process" wherein the final state is well-defined and presents no uncertainties.

The transition operator $T^{(j)}$ in (1) can be written as

$$T^{(j)} = \tfrac{1}{2}t_\mathrm{p}{}^{(j)}(1+\tau_3{}^{(j)})+\tfrac{1}{2}t_\mathrm{n}{}^{(j)}(1-\tau_3{}^{(j)}), \tag{8}$$

or as

$$T^{(j)} = \tfrac{1}{2}(t_\mathrm{p}{}^{(j)}+t_\mathrm{n}{}^{(j)})+\tfrac{1}{2}(t_\mathrm{p}{}^{(j)}-t_\mathrm{n}{}^{(j)})\tau_3{}^{(j)}, \tag{9}$$

where t_p and t_n are the amplitudes for the photoproduction of π^0 from proton and neutron and $\frac{1}{2}(1+\tau_3)$ and $\frac{1}{2}(1-\tau_3)$ the projection operators for the proton and neutron respectively. The τ_3 part in (9) does not connect the charge singlet states and the matrix element (1) ultimately reduces to

$$Q = \langle {}^3\chi_{m'}|\tfrac{1}{2}(t_\mathrm{p}{}^{(1)}+t_\mathrm{n}{}^{(1)})+\tfrac{1}{2}(t_\mathrm{p}{}^{(2)}+t_\mathrm{n}{}^{(2)})|{}^3\chi_m\rangle E, \tag{10}$$

where

$$\begin{aligned} E &= \int u_\mathrm{d}{}^*(\varrho) \exp\,(i\mathbf{k}_0\cdot\varrho)u_\mathrm{d}(\varrho)\mathrm{d}\varrho, \\ \mathbf{k}_0 &= \tfrac{1}{2}\mathbf{D} = \tfrac{1}{2}(\boldsymbol{\nu}-\boldsymbol{\mu}), \quad \varrho = \mathbf{r}_1-\mathbf{r}_2. \end{aligned} \tag{11}$$

Here, $\boldsymbol{\nu}$ is the momentum of the incident photon and $\boldsymbol{\mu}$ the momentum of the outgoing meson.

We shall use for t_p and t_n the complete amplitudes as given by Chew *et al.* [3])

$$t_p = \frac{2\pi}{\sqrt{\mu_0 \nu_0}} ef(F^+ + F^0), \tag{12}$$

$$t_n = \frac{2\pi}{\sqrt{\mu_0 \nu_0}} ef(F^+ - F^0). \tag{13}$$

In the above, F^0 is a small term which we shall neglect and, retaining only the dominant terms, F^+ can be written as

$$F^+ = i\boldsymbol{\sigma} \cdot \boldsymbol{\mu} \times (\boldsymbol{\nu} \times \boldsymbol{\varepsilon}) \frac{\mu_p - \mu_n}{4Mf^2} h^{+-} + \boldsymbol{\mu} \cdot \boldsymbol{\nu} \times \boldsymbol{\varepsilon} \frac{\mu_p - \mu_n}{4Mf^2} h^{++}, \tag{14}$$

where

$$h^{+-} = -\frac{2}{3\mu^3} e^{i\delta_{33}} \sin \delta_{33},$$

$$h^{++} = \frac{4}{3\mu^3} e^{i\delta_{33}} \sin \delta_{33},$$

μ_p, μ_n are the magnetic moments of the proton and the neutron respectively, ν_0 is the photon energy, ε its polarization, μ_0 the energy of the meson, $\boldsymbol{\sigma}$ is the spin operator for the nucleons and δ_{33} is the phase shift for the meson-nucleon scattering in the (3, 3) state. The other phase shifts are neglected.

We choose for our frame of reference the direction of the incident photon as z axis and the plane which contains the vectors $\boldsymbol{\nu}$ and $\boldsymbol{\mu}$ as $x-z$ plane. Let θ be the angle between $\boldsymbol{\nu}$ and $\boldsymbol{\mu}$.

Squaring, summing over final states and averaging over initial spin states and photon polarizations, we obtain

$$|Q|^2 = \frac{32}{27\mu^4} c^2 \lambda^2 \nu^2 \sin^2 \delta_{33} (1 + \tfrac{5}{2} \sin^2 \theta) |E|^2, \tag{15}$$

where $c = 2\pi ef/\sqrt{\mu_0 \nu_0}$, $\lambda = \mu_p - \mu_n / 4Mf^2$ and E is given by (11). Using the Hulthén wave function for the deuteron

$$u_d(\varrho) = \left[\frac{\alpha}{2\pi(1-\alpha\rho_1)}\right]^{\frac{1}{2}} \frac{e^{-\alpha\rho} - e^{-\beta\rho}}{\rho}, \tag{16}$$

one can evaluate

$$E = \frac{1}{1-\alpha\rho_1} \frac{2\alpha}{k_0} \left\{ \operatorname{arctg}\left(\frac{k_0}{2\alpha}\right) + \operatorname{arctg}\left(\frac{k_0}{2\beta}\right) - 2 \operatorname{arctg}\left(\frac{k_0}{\alpha+\beta}\right) \right\}. \tag{17}$$

The cross-section is given by

$$\frac{\mathrm{d}\sigma}{\mathrm{d}\boldsymbol{\mu}} = (2\pi)^{-2}|Q|^2\delta\left(\mu_0 + \frac{|\boldsymbol{\nu}-\boldsymbol{\mu}|^2}{4M} - \nu_0\right) \tag{18}$$

or

$$\frac{\mathrm{d}\sigma}{\mathrm{d}\mu_0\mathrm{d}\Omega} = (2\pi)^{-2}\mu\mu_0|Q|^2\delta\left(\mu_0 + \frac{|\boldsymbol{\nu}-\boldsymbol{\mu}|^2}{4M} - \nu_0\right). \tag{19}$$

The integration over $\mathrm{d}\mu_0$ can easily be performed if we make the justifiable assumption that the recoiling deuteron receives only momentum but no appreciable energy. Then

$$\frac{\mathrm{d}\sigma}{\mathrm{d}\Omega} = (2\pi)^{-2}\mu\mu_0|Q|^2, \tag{20}$$

where $\mu_0 = \nu_0$, $\mu = \sqrt{\mu_0^2-1}$ and $|Q|^2$ is given by (15).

3. Comparison with Experiments

Using (20) the differential cross-sections have been calculated at three photon energies 1.5, 2.0 and 2.5 in units of the pion mass and the results are represented in fig. 1. For completeness we also give the numerical results in table 1. Experi-

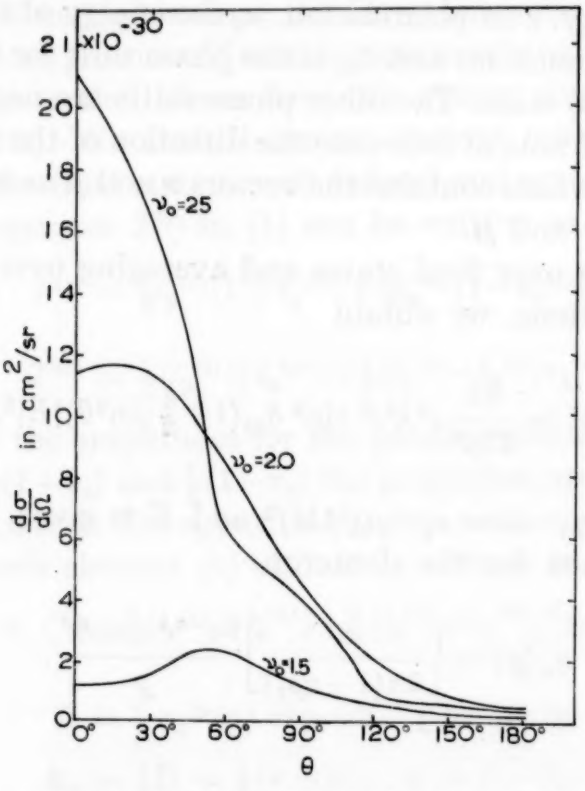

Fig. 1. Differential cross-section for the elastic photoproduction of π^0 from deuterium as a function of the angle of meson emission in the laboratory system for incident photon energies 1.5, 2.0 and 2.5 in units of pion mass.

mental results are available at photon energy of about 2 pion mass and they are plotted in fig. 2. The experimental values of Wolfe, Silverman and DeWire are for photons of 50 MeV spread centred at 280 MeV and those of Davis and Corson at 270 MeV. The results of Rosengren and Baron are the latest and they were obtained for photons of 30 MeV spread centred at about 280 MeV. The standard statistical errors are indicated in the figure. They apply only to relative cross-section at various angles and the absolute cross-section is subjected to a

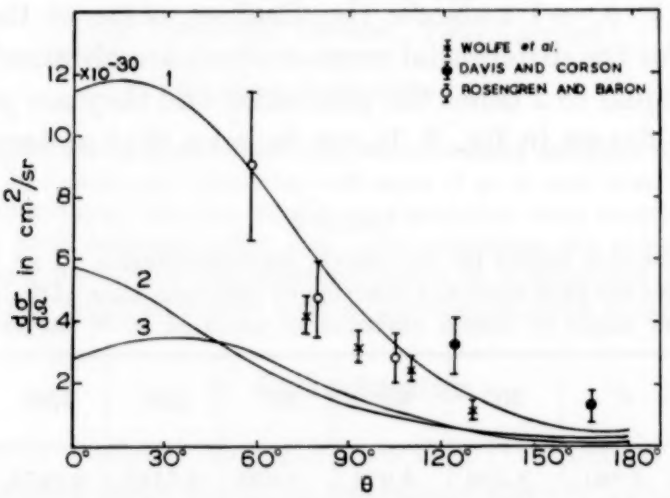

Fig. 2. Differential cross-section for the elastic photoproduction of π^0 from deuterium for an incident photon energy of 2 times the pion mass. Curve 1 is obtained from theory after summing over all final spin states. The experimental points are those of Wolfe *et al.* [4]), Davis and Corson [5]) and Rosengren and Baron [6]). Curves 2 and 3 are for particular final spin states $m_z = 0$ and $m_z = +1$ or -1.

TABLE 1

The differential cross-section $d\sigma/d\Omega$ for the elastic photoproduction of π^0 from deuterons as a function of photon energy and laboratory angle of meson emission in units of 10^{-30} cm²/sr.

ν_0 \ θ	0°	30°	60°	90°	120°	150°	180°
1.5	1.155	1.481	2.346	1.109	0.5961	0.2568	0.1439
2.0	11.44	11.50	8.549	4.642	2.065	0.8044	0.4360
2.5	21.18	16.66	6.198	4.085	1.028	0.5474	0.2912

further experimental error of 20 %. The general agreement of the theory with the experiments is good and especially the agreement with the results of Rosengren and Baron is remarkable.

4. Final Spin State of the Deuteron

Formula (15) was obtained after summing over the three final spin states ($m_z = +1, 0, -1$) of the recoiling deuteron. It would be of interest to study

the differential cross-section for π^0 production for each of the final spin states separately. The squares of the matrix elements are

$$|Q_{+1}|^2 = |Q_{-1}|^2 = \frac{8}{27\mu^4} c^2\lambda^2\nu^2 \sin^2\delta_{33}(1+4\sin^2\theta), \tag{21}$$

$$|Q_0|^2 = \frac{16}{27\mu^4} c^2\lambda^2\nu^2 \sin^2\delta_{33}(1+\sin^2\theta). \tag{22}$$

The subscripts $+1$, 0, -1 indicate the final m_z state of the deuteron. The numerical values for the differential cross-sections are obtained for the incident photon of energy equal to 2 times the pion mass and they are presented in table 2. Curves are also drawn in fig. 2. It can be seen that at large angles of pion

TABLE 2

The differential cross-section $d\sigma/d\Omega$ for the elastic photoproduction of π^0 from deuterons at a photon energy of 2 times the pion mass as a function of final spin state of the deuteron and laboratory angle of meson emission in units of 10^{-30} cm²/sr.

m_z \ θ	0°	30°	60°	90°	120°	150°	180°
+1	2.861	3.538	2.974	1.658	0.7183	0.2475	0.1090
0	5.722	4.423	2.602	1.326	0.6285	0.3094	0.2180
−1	2.861	3.538	2.974	1.658	0.7183	0.2475	0.1090

emission, the cross-sections for the different final spin states are nearly the same but at forward angles the $m_z = 0$ state predominates. Exact expressions for the cross-sections can also be derived if the initial target deuteron is polarized and the effect of circularly polarized photon beam on the polarized deuterons may also be investigated; although the experimental verification of these results will be rather difficult if not impossible.

One of us (G. R.) is grateful to the Council of Scientific and Industrial Research for the award of the Junior Research Fellowship.

References

1) G. F. Chew and H. W. Lewis, Phys. Rev. **84** (1951) 779;
M. Lax and H. Feshbach, Phys. Rev. **88** (1952) 509;
Y. Saito, Y. Watanabe and Y. Yamaguchi, Prog. Theor. Phys. **7** (1952) 103;
John Chappelear, Phys. Rev. **99** (1955) 254
2) V. Devanathan and G. Ramachandran, Nuclear Physics (in the press)
3) G. F. Chew *et al.*, Phys. Rev. **106** (1951) 1345
4) B. Wolfe, A. Silverman and J. W. DeWire, Phys. Rev. **99** (1955) 268
5) H. L. Davis and D. R. Corson, Phys. Rev. **99** (1955) 273
6) J. W. Rosengren and N. Baron, Phys. Rev. **101** (1956) 410

2.E

Nuclear Physics **24** (1961) 169—175; © *North-Holland Publishing Co., Amsterdam*

Not to be reproduced by photoprint or microfilm without written permission from the publisher

ON THE SPIN DEPENDENCE OF NEUTRON STRENGTH FUNCTIONS

KAMAL K. SETH

Duke University, Durham, North Carolina †

Received 1 December 1960

Abstract: The possibility of J dependence of s-wave neutron strength function S is examined empirically, (a) by comparing adjoining odd-mass ($I \neq 0$) and even ($I = 0$) nuclei, (b) by requiring that the strength function should vary smoothly with atomic weight for adjoining odd-mass nuclei with different spins, and (c) by comparing the average reduced widths for the various isotopes of uranium. It is concluded that S_J is proportional to $(2J+1)^{-1}$, and therefore that the optical potential should have a contribution which is dependent on target spin.

1. Introduction

A plot of s-wave neutron strength function †† S versus atomic weight A (fig. 1(a)), as derived from resolved resonance data [1]) exhibits a number of unexplained features, namely: (a) The data show an unusually large point scatter. (b) In spite of a lcak of data on even target nuclei †††, it is seen that for these nuclei S is invariably larger than for their odd-mass neighbours; the best illustration of this feature is found in Th^{232} and the transuranic elements in fig. 1(a). (c) In the region $A = 90$–130, the data points are much lower than the theoretical predictions [2, 3]) based on the optical model of the nucleus [4]). The effects (a) and (b) have gone by relatively unnoticed but the feature (c) has recently received great attention. Lane *et al.* [5]), and Sugie [6]) have invoked shell model arguments to explain this discrepancy qualitatively. As Sugie [6]) has pointed out Lane's argument based on the proximity to nucleon magic number N or $Z = 50$ cannot be primarily held responsible for effect (c), since no such marked discrepancy is found near $N = 82$, or at $Z = 82$ and $N = 126$. Sugie's own arguments are based on effect of parity conservation in the process leading to the neutron's absorption in order to form the compound nucleus. In the following we propose to show at least empirically, that the effect (c) is one manifestation of the J dependence of s-wave neutron strength function, the other manifestations being features (a) and (b).

† This work is supported in part by the U. S. Atomic Energy Commission.

†† We have limited ourselves in this paper to s-wave neutron strength functions only. The subscripts on S to be found elsewhere in this paper refer to J values for the -wave resonances and not to l as is sometimes done.

††† All statements made in this paper are in terms of target nuclei, as is customary in neutron physics. Henceforth we omit the word, "target", and consider it implied.

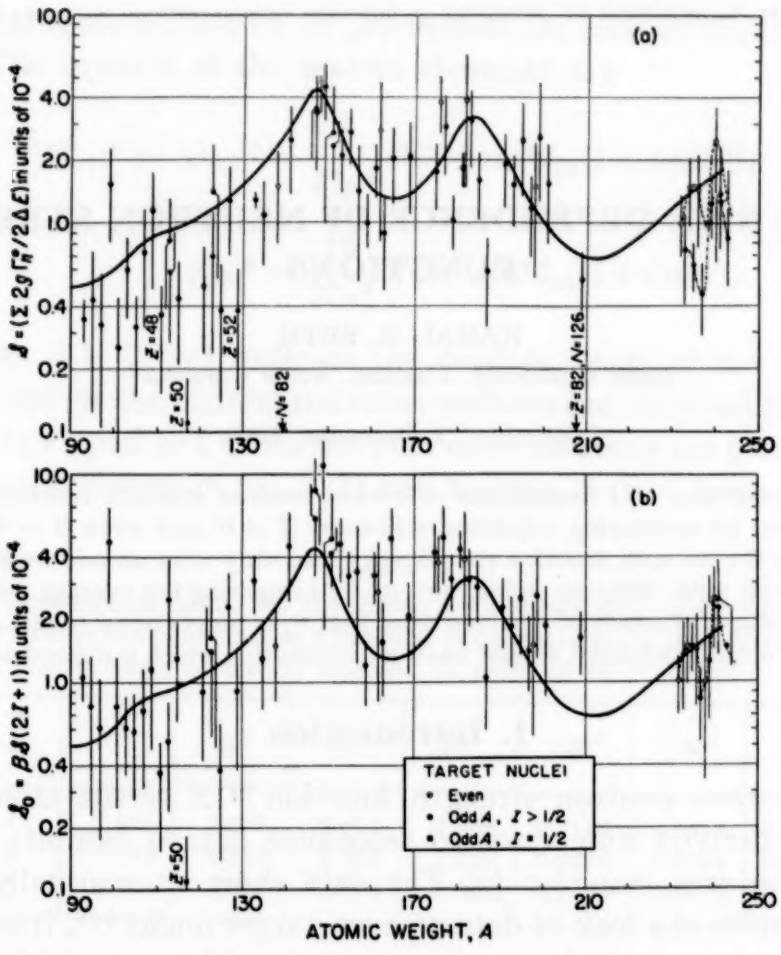

Fig. 1. (a) This figure shows $S = \Sigma(2g\Gamma_n^0/2\Delta E)$ versus atomic weight. The data are entirely from ref. [1]). The theoretical curve is due to Chase *et al.* [2]).

(b) This figure shows $S_0 = \beta S(2I+1)$ for the data in fig. 1(a), where $\beta = 1$ for even nuclei, $\beta = 0.3$ for all odd-mass nuclei with $I \neq \frac{1}{2}$ and $\beta = 0.5$ for odd-mass nuclei with $I = \frac{1}{2}$. Note the general improvement in point scatter, and improved agreement between odd-mass and even nuclei in the transuranic region, and the clear presentation of the theoretically predicted peak in the neighborhood of $A \approx 180$. The data in this figure suggest that the imaginary potential should be decreased from the value used by Chase *et al.* [2]) to yield higher peak values.

2. Analysis of data

The most direct method of demonstrating the J dependence would be to compare values of S for the two spin states of an odd-mass nucleus. Unfortunately, however, very little information is available on J values of resonances. For example there is not a single odd-mass nucleus for which 4 or more resonnances have been assigned to each spin state. The next best comparison, namely between strength functions of even-mass nuclei ($I = 0$) and the average (over the two spin states) strength function for adjoining odd-mass nuclei ($I \neq 0$) is similarly difficult. Due to inherently larger level spacings in even nuclei, very rarely have enough resonances been resolved by neutron fast-choppers to permit any statistically significant conclusion to be drawn. One exception to this is the transuranic region where both even and odd-mass

nuclei have been investigated carefully (see fig. 1(a)). Our present investigation was motivated by the obvious discrepancy in the strength function values of even and odd-mass nuclei in the transuranic region and the extreme point scatter in the region $170 \leqq A \leqq 200$ as seen in fig. 1(a).

In considering the available data we have imposed the following restrictions: (1) all resonance data that are not isotopically assigned were omitted from consideration; (2) whenever for a given isotope the number of resonances analyzed was $\leqq 3$, the data were rejected. Since in no case J assignments of $\geqq 4$ resonances were available for each spin state of an odd-mass nucleus, the data for $Ag^{107, 109}$, W^{183}, Pt^{195} and Hg^{199} were converted to the usual kind (i.e., Γ_n^0 converted to $2g\Gamma_n^0$) and then the strength function per spin state calculated in the usual manner. Subject to these restrictions *all* the data available in ref. [1]) are plotted in fig. 1.

Customarily, the "strength function per spin state", is obtained as

$$S \equiv \sum_{\Delta E} (\Gamma_n^0/\Delta E)$$

for even nuclei and in absence of positive identification of spin states of resonances as

$$S = \sum_{\Delta E} (''\Gamma_n^{0''}/2\Delta E)$$

for odd-mass nuclei. Since the compilation of widths [1]) lists Γ_n^0 for even nuclei and $2g\Gamma_n^0$ for odd-mass nuclei (these are the quantities determined by the conventional area analysis of neutron resonances), we may combine these two rules and state that the quantity S plotted in fig. 1(a) is obtained as

$$S \equiv \sum_{\Delta E} (2g\Gamma_n^0/2\Delta E)$$

for odd-mass as well as even-mass nuclei. We will now show that the interpretation of S as average strength function per spin state implies the definite assumption of J independence of $S_J \equiv (\bar{\Gamma}_n^0{}_J/D_J)$, or equivalently that $\bar{\Gamma}_{nJ}^0$ is proportional to $(2J+1)^{-1}$. We then show that the data suggest a different dependence of S_J on J and that for the "average strength function" per spin state for different odd-mass nuclei, the quantity to compare is not S but $S_0 = S(2I+1)$, where I is the target spin.

We have

$$S = \sum_{\Delta E} 2g\Gamma_n^0/2\Delta E = g_1 S_1 + g_2 S_2 = \{(2J_1+1)S_1 + (2J_2+1)S_2\}/\{2(2I+1)\},$$

where $S_1 = (\bar{\Gamma}_{n1}^0/D_{J_1})$ and $S_2 = (\bar{\Gamma}_{n2}^0/D_{J_2})$ and subscripts 1 and 2 refer to spin states $J_1 = I+\frac{1}{2}$ and $J_2 = I-\frac{1}{2}$.

Let us now consider a few simple possible dependences of S_J on J. In doing so we shall assume that $D_J \propto (2J+1)^{-1}$. This is a result which is based on statistical theories of level spacing and is strictly true only if J is not too

large [8]). Its essential truth has also been verified empirically [9]).

$$\text{(i)}\quad S_J = S'_0(2J+1)$$

This would correspond to the assumption that $\bar{\Gamma}_{nJ}{}^0$ is independent of J. We then obtain $S = 2S'_0\{(I+1)^2+I^2\}/(2I+1)$, from which it follows that a plot of S for neighbouring nuclei should show a larger value for the larger target spin. This is exactly opposite of what we find in fig. 1(a); the largest values of S actually correspond to even nuclei with $I = 0$.

$$\text{(ii)}\quad S_1 = S_2 = S_0'' = S.$$

In this case, $(\bar{\Gamma}_{nJ}/D_J)$ is independent of J. This is the usual assumption and is stated equivalently as $\bar{\Gamma}_{nJ} \propto (2J+1)^{-1}$. Under this assumption the different spin states in a given nucleus should have the same value of S if assignments of spin states are available, and a plot of S for different nuclei with different target spins should show smooth variation with atomic weight. In particular the neighbouring odd-mass and even-mass targets should show no sudden changes in S. As we see in fig. 1(a), none of these requirements are met by the actual data.

$$\text{(iii)}\quad S_J = S_0/(2J+1)$$

In this case, $\bar{\Gamma}_{nJ}{}^0 = \bar{\Gamma}_n{}^0(2J+1)^{-2}$. This yields $S = S_0/(2I+1)$. Thus a plot of $S_0 = S(2I+1)$ should show a smooth behaviour with atomic weight irrespective of the I value of the target nucleus, and whenever spin states of resonances are assigned, S_0 for the two spin states of an odd-mass nucleus should be the same. In order to take account of the empirical observation [9]) that $D_J \propto \beta D_0/(2J+1)$, where $\beta = 1$ for even target nuclei, $\beta \approx 0.3$ for odd-mass targets with $I > \frac{1}{2}$, and $\beta \approx 0.5$ for odd-mass target with $I = \frac{1}{2}$ †, we have plotted $S_0 = \beta S(2I+1)$ in fig. 1(b). We observe a significant improvement in point scatter especially in the region above $A = 170$, and a markedly improved agreement between the values for even and odd-mass nuclei in the region $A > 230$. It may be noted here that since the theoretical curves in figs. 1(a) and 1(b) were calculated with the optical model parameters chosen to yield the best fit to the data treated in the manner of fig. 1(a), we need not be too concerned about the deterioration of the quantitative fit to the data. It is important to notice however that the qualitative features of the theoretical curve are

† The value of β required to yield a smooth behaviour of D_0 with atomic weight is by no means constant – for example it must reflect variation of binding energy and pairing energy with the odd-even nature of the compound nucleus. However, in our choice of β above we have taken the average value 0.3, which yields the best agreement between even and odd-mass nuclei values in the transuranic region. It is found that this value yields good agreement in other regions of atomic weight where data for even nuclei exist for comparison. It is however found that $I = \frac{1}{2}$ nuclei show an erratic behaviour, both in the level spacing plot and the strength function plot. We have put $\beta = 0.5$ for these nuclei rather arbitrarily and achieved on an avarage a better agreement with the values for the neighbouring nuclei. We consider this change in β from 0.3 for odd-mass nuclei with $I \neq \frac{1}{2}$ to 0.5 for $I = \frac{1}{2}$ as entirely within the range of expected variation.

borne out much better by the data in fig. 1(b) than in fig. 1(a). The data in fig. 1(b) in general suggest a smaller value of the imaginary potential than was used in computing the theoretical curve shown. As far as the region $90 \leqq A \leqq 130$ is concerned we observe that while there is no significant improvement in point-scatter, almost an equal number of data points lie above and below the theoretical curve in fig. 1(b) while in fig. 1(a) almost all the experimental points are at least a factor 2 to 3 below the theoretical curve. The residual scatter in fig. 1(b) in the region $90 \leqq A \leqq 130$ follows closely the exceptionally large fluctuations (average $\approx$ 2 to 3 MeV) in neutron binding energies in this mass region. Such fluctuations are not taken into account here since we have kept β constant for all nuclei with $I > \frac{1}{2}$.

It is difficult to define a numerical criterion for demonstrating the improvement in point scatter in fig. 1(b) in absence of the best fit optical model curve for the data as presented in fig. 1(b). However, a crude measure of the point scatter can be obtained by computing the error $(1/n) \sum [(S/\bar{S})-1]^2$ and the corresponding quantity for S_0 over limited regions of atomic weight where neither S nor S_0 change rapidly. Such a calculation shows that there is no appreciable change in point scatter between figs. (1a) and 1(b) below $A = 170$, but that in the regions $A = 170$–185, 185–120 and 230–245 the errors in the S plot are 19 %, 21 % and 19 % respectively while those in the S_0 plot are correspondingly 3 %, 8 % and 12 % respectively. This kind of comparison does not take into account the possibility that some of the structure still included in these limited atomic weight regions (for example in the region $230 \leqq A \leqq 245$) may be real and does not do justice to fig. 1(b). For the region $230 \leqq A \leqq 245$, it is however possible to apply a more useful statistical test. If we make the hypothesis that the even and odd-mass nuclei with $A > 230$ come from populations with the same mean value of the attribute S or S_0, we can apply the usual "t-test" of statistics to test this hypothesis. Such a test gives the

TABLE 1

Averaged reduced width $\langle \bar{\Gamma}_n J^0 \rangle$ and $\bar{\Gamma}_n{}^0$ for various isotopes of uranium

Target nucleus	I	$\langle \bar{\Gamma}_n J^0 \rangle = \Sigma\, 2g\Gamma_n J^0/n$ in units of 10^{-4} eV [a]	$\bar{\Gamma}_n{}^0 = \begin{cases} \langle \bar{\Gamma}_n J^0 \rangle (2I+1)^2, & I \neq 0 \\ 4\bar{\Gamma}_n J^0, & I = 0 \end{cases}$ in units of 10^{-4} eV [a]
U^{233}	$\frac{5}{2}$	2.15 ± 0.65	77±23
U^{234}	0	19.2 ± 6.9	76±28
U^{235}	$\frac{7}{2}$	0.84± 0.23	54±14
U^{236}	0	21.6 ±10.0	86±40
U^{238}	0	22.8 ± 4.9	91±20

[a]) The errors on these numbers are calculated by putting the fractional error equal to $\sqrt{2/n}$, where n is the total number of resonances observed. While it is more common to calculate this error as being equal to $\sqrt{1/n}$ (as Porter and Thomas [10]) point out), for $\nu = 1$ distribution of reduced widths $\sqrt{2/n}$ is the correct estimate.

probability for this hypothesis being true for S as $\leqq 10\,\%$ while the corresponding probability for S_0 is $> 82\,\%$. This supports our claim that it is S_0 and not S which should be compared for different nuclei.

A further test of the correctness of our conclusion that $S_J \propto (2J+1)^{-1}$ is provided by table 1. The average reduced width as obtained by $\langle \bar{\Gamma}_{nJ}{}^0 \rangle \equiv \sum (2g\Gamma_{nJ}{}^0/n)$ for odd-mass nuclei and $\langle \bar{\Gamma}_{nJ}{}^0 \rangle = \Gamma_{nJ}{}^0/n$ for even nuclei (where n is the total number of resonances observed in either case), according to the assumption that $\bar{\Gamma}_{nJ}{}^0 = \bar{\Gamma}_n{}^0(2J+1)^{-2}$ actually gives $\langle \bar{\Gamma}_{nJ}{}^0 \rangle = \bar{\Gamma}_n{}^0/(2I+1)^2$ for odd-mass nuclei and $\langle \bar{\Gamma}_{nJ}{}^0 \rangle = \frac{1}{4}\bar{\Gamma}_n{}^0$ for even nuclei. Thus $\bar{\Gamma}_n{}^0 = \langle \bar{\Gamma}_{nJ}{}^0 \rangle (2I+1)^2$ (for odd-mass nuclei) and $\bar{\Gamma}_n{}^0 = 4\langle \bar{\Gamma}_{nJ}{}^0 \rangle$ for even-mass nuclei are the comparable quantities and not the $\langle \bar{\Gamma}_{nJ}{}^0 \rangle$ values as calculated directly. This is borne out vividly by table 1.

We thus find that all the collected empirical evidence is in favour of the assumption that $\langle \bar{\Gamma}_{nJ}{}^0 \rangle \propto (2J+1)^{-n}$, with $n = 2$, or $S_J = S_0/(2J+1)$. With a view to determining the limits of error on our value of $n = 2$, we have tried $n = 3$, and find that the point scatter in the corresponding plot of "strength function per spin state" becomes much worse than in fig. 1(b); this is specially true of the transuranic region. Also the agreement between the average "reduced widths" of table 1 is again lost. We therefore conclude that $n = 2$ to a fair degree of accuracy (error ± 0.5) and that closer limits on n cannot be set with the presently available data. The need for more spin state assignments and more resolved resonance data on even isotopes is obvious.

3. Theoretical Discussion

The theoretical justification for our empirical observation that s-wave neutron strength function for spin J, S_J is proportional to $(2J+1)^{-1}$ is not obvious. In the usual optical potential there is no term to take account of the spin of the target nucleus. There is some scattered experimental evidence [11]) that such a term may be required. Indeed, Feshbach [12]) has pointed out that since the real part of the optical potential "is for the most part just the shell model potential extrapolated to higher energy", it should contain some dependence on the character of the target nucleus, an additional potential say, of the form $\mathbf{I} \cdot \boldsymbol{\sigma} f(r)$ which would of course lead to a J dependent strength function for s-wave neutrons. Looking at neutron strength functions from the point of view of their intermediate coupling (or giant resonance) model, Lane, Thomas and Wigner [13]) also note that one should expect a difference in the behaviour of S_J for nuclei with $I = 0$ and those with $I \neq 0$, and also between S_1 and S_2 for the two spin states of a non-zero spin target nucleus. This follows since the corresponding single particle states which "weight" the levels of the "residual nucleus" are in general different in each case because of particle-particle interactions between the last two particles.

Whether or not the specific J dependence that we suggest is obtained from either of these approaches remains to be seen. Since the major improvement in the data by putting our J dependence occurs in the region where nuclei are appreciably deformed it is likely that this dependence arises, in part at least, from the coupling of the nuclear rotational motion to the compound nucleus excitation. Such a rotational-optical model [2]) has already met with considerable success in explaining the splitting of the s-wave strength function maximum in the neighbourhood of $A \approx 150$.

The author wishes to acknowledge the help of Miss Dorothy Brand in numerous computations. He is also thankful to Professor H. W. Newson for valuable advice and criticism.

References

1) D. J. Hughes, B. A. Magurno and M. K. Brussel, Neutron cross sections (U. S. Government Printing Office, Washington 1960), BNL-325, 2nd ed., suppl. no. 1
2) Chase, Wilets and Edmonds, Phys. Rev. **110** (1958) 1080
3) K. McVoy, Phys. Rev. **118** (1960) 1323
4) Feshbach, Porter and Weisskopf, Phys. Rev. **96** (1954) 448
5) Lane, Lynn, Melkonian and Rae, Phys. Rev. Lett. **2** (1959) 424
6) A. Sugie, Phys. Rev. Lett. **4** (1960) 286
7) Carter, Harvey, Hughes and Pilcher, Phys. Rev. **96** (1954) 113
8) J. M. B. Lang and K. J. LeCouteur, Proc. Phys. Soc. **67A** (1954) 586
9) H. W. Newson, private communication
10) C. E. Porter and R. G. Thomas, Phys. Rev. **104** (1956) 483
11) R. A. Vanetsian, A. P. Klutcharev and E. D. Fedtchenko, C. R. Cong. Intern. de Physique Nucléaire (Paris, 1959), p. 607
12) H. Feshbach, Nuclear Spectroscopy, Part B, ed. by F. Azenberg-Selove (Academic Press, New York, 1960) p. 1046
13) A. M. Lane, R. G. Thomas and E. P. Wigner, Phys. Rev. **98** (1955) 693

10.D *Nuclear Physics* **24** (1961) 176; ©*North-Holland Publishing Co., Amsterdam*

BOOK REVIEW

W. D. ALLEN, *Neutron Detection* (Newnes, London 1960. 144 p. 15s.)

The scope of this book is very wide, and the variety of readers for whom it is intended is very great, in the sense that it includes both some interesting remarks for people who even do not know that a nuclear cross section is an area, and chapters for persons with a more extensive knowledge of the subject; however, readers at an intermediate stage might miss finer details. About half the text deals with the subject indicated by the title, i.e. methods for neutron detection, while the other half gives a great variety of applications of the detectors without in any way being exhaustive.

The first chapter after the introduction treats of the reactions used in neutron detection, one section of it a little confusingly entitled "The (n, p) and similar reactions", which is to be interpreted as the scattering of neutrons on hydrogen and similar processes. The next chapter, which is devoted to instruments for neutron detection, starts with ionization chambers — the behaviour of electrons and ions in gases and a little about the difficulties encountered in manufacturing — and as special examples it takes up boron-lined and fission chambers. Then follow proportional counters — especially the BF counter — and scintillation counters. At the end of the chapter the reader is told a little about nuclear emulsions and cloud chambers.

The following chapters present special features of the applications of the detectors, such as measurement of fast flux, neutron spectrometry including time-of-flight spectrometry, measurement of slow neutron flux, health monitoring, and source calibration. These chapters give the author occasion to touch on a great many special features of neutron detection.

All the figures which are of common interest are very appropriately gathered in appendices after the text, and a great number of references are assembled in a very clear way at the end of the book.

Although, as stated in the preface, the book covers only materials available up to the end of 1957, it can be recommended to those who wish to get a first orientation about the subject and a very good introduction to the literature.

J. Schiellerup Petersen

3.B

Nuclear Physics **24** (1961) 177—195; © *North-Holland Publishing Co., Amsterdam*

Not to be reproduced by photoprint or microfilm without written permission from the publisher

PENETRATION MATRIX ELEMENTS AND NUCLEAR STRUCTURE EFFECTS IN Tl^{203}

T. R. GERHOLM, B.-G. PETTERSSON, B. VAN NOOIJEN †
and Z. GRABOWSKI ††
Institute of Physics, University of Uppsala, Uppsala, Sweden

Received 16 January 1961

Abstract: Gamma-gamma, electron-gamma and gamma-electron directional correlation experiments on the $d_{\frac{3}{2}}$(400 keV) $d_{\frac{3}{2}}$(279 keV)$s_{\frac{1}{2}}$ cascade in Tl^{203} are reported. The following results were obtained:

$$A_2(\gamma\gamma) = -0.130 \pm 0.006, \quad A_2(e\gamma) = -0.011 \pm 0.004, \quad A_2(\gamma e) = -0.030 \pm 0.003.$$

In addition the K-conversion coefficient of the 400 keV transition was determined from the coincidence experiments. The value obtained is

$$\beta_1^K(400\ \text{keV}) = 0.145 \pm 0.007.$$

The experiments were performed in order to search for nuclear structure effects in the M1 internal conversion process. These effects are expected to be negligible in the *l*-allowed (400 keV) transition. This is confirmed by the experiments which are in perfect agreement with the theory assuming no nuclear structure effects. Large nuclear structure effects are to be expected for the strongly retarded *l*-forbidden (279 keV) transition. This is also confirmed by the angular correlation experiments. It is shown that all experimental data are consistent with a λ-value of $+76 \pm 1$, where λ is defined as the ratio of the penetration matrix element and the normal gamma ray matrix element. The value for the weighting factor $C(Z, k)$ was taken to be 0.0260. The errors for λ given here do not include the uncertainty in the weighting factor which is supposed to be known to within ± 10 %. The agreement between the theory and the experimental results is further improved if the particle parameters are corrected for the finite size of the nucleus in the E2 conversion process.

1. Introduction

During the past ten years the process of internal conversion has been subject to a great deal of theoretical interest. In 1949 Rose and co-workers [1, 2]) published extensive calculations of internal conversion coefficients based on the so called "point nucleus" approxiination. Later Sliv [3–5]) pointed out that the finite size of the nucleus may cause considerable deviations from the results obtained in this approximation. Particularly large effects were to be expected for M1 K-shell conversion coefficients for heavier elements. These predictions were experimentally confirmed [6, 7]). New calculations of the internal conversion coefficients for the K and L subshells, taking into account screening and finite

† On leave from: Technische Hogeschool, Delft, Holland.
†† On leave from: Instytut Badań Jadrowych, Krakow, Poland.

size effects, were published by Sliv and Band [8, 9]) and also by Rose [10]). Rose also gives unscreened M subshell coefficients and tabulates the radial matrix elements used for the calculation of the K-shell coefficients in the point nucleus, unscreened, approximation. The calculations of Sliv and Band and those of Rose are based on somewhat different models, but the results are expected to be in close agreement. Although this holds for most of the tabulated values there exist some discrepancies not yet explained.

The taking into account of finite size effects has considerably improved the agreement between theoretical and experimental values. However, some experimentally determined conversion coefficients differ markedly from both Sliv and Band's and from Rose's values. Substantial deviations were found [11]) for some slow E1 transitions among the heaviest elements. The 85 keV transition in Pa^{231}, for instance, seems to exhibit L_I and L_{II} conversion coefficients which are 10–20 times higher than the theoretical values, while the L_{III} coefficient seems to be normal. Much smaller, but still significant deviations have been found for some M1 (ref. [12])) and E2 (refs. [13, 14])) coefficients.

A possible explanation for these anomalies was offered when Church and Weneser [15]) showed that, contrary to what has been generally accepted previously, internal conversion coefficients may depend on the details of the nuclear structure. The nuclear structure effects are generally small but under certain circumstances they may cause considerable deviations from the theoretical values calculated by Sliv and Band and by Rose. This comes about in the following way.

The interaction between the conversion electron and the nucleus takes place through the intermediary of the radiation field. The strength of the radiation field is proportional to the gamma ray matrix element, which comprises the nuclear structure dependent factors. At the first sight one might expect that the internal conversion coefficients should be independent of the details of the nuclear structure, since the internal conversion coefficient is defined as the ratio of conversion electron intensity to gamma ray intensity. The gamma ray matrix element therefore should be expected to be divided out.

This is true, however, only as long as the interaction is assumed to take place *outside* the nucleus. But, since the conversion electron penetrates into the nuclear matter there will be an interaction between the electron and the transition charges and currents in the interior of the nucleus. The form of this interaction is different and gives rise to "penetration matrix elements" which are not necessarily proportional to the gamma-ray matrix elements. Nuclear structure dependent factors, therefore, generally remain in the expression for the internal conversion coefficient.

Intuitively one might expect that these "dynamic" effects can give rise only to minute deviations, since the region of overlap between the nuclear and electron wave functions is a very small fraction of the total area under the

electron wave function. This is indeed generally the case and is reflected in the theory by a small weighting factor, of the order of a few percent or less for the nuclear structure dependent factors in the expression for the conversion coefficient.

The small weighting of the nuclear structure dependent factors may, however, be counterbalanced if there is a strong reduction of the gamma-ray matrix element, while the penetration matrix element still has its dimensional value. In other words: anomalous nuclear structure dependent conversion coefficients are to be expected for transitions for which specific nuclear selection rules forbid electromagnetic emission without imposing similar restrictions on the conversion matrix elements. The most striking example is the E0-transitions which are to be found not only in $0+ \rightarrow 0+$ transitions but quite generally in competition with M1 and E2 in all nuclear transitions between levels of the same spin and parity. The prediction has already been experimentally confirmed [16]).

Among the M1 transitions those classified as l-forbidden appear to be the most promising as far as the observability of the penetration matrix element is concerned. For M1 transitions of the type $\Delta I = 1$, no, and $\Delta l = 2$, the gamma-ray matrix element is equal to zero (for pure shell model states) but in the penetration matrix element there is an additional spin dependent term $\hat{r}(\boldsymbol{\sigma} \cdot \hat{r})$, which combines the $\Delta l = 2$ states [15]). It has been known for some time [17, 18]) that the l-forbidden M1 transitions are strongly retarded when compared to the (allowed) single particle M1 transition rates. This demonstrates the validity of the l-selection rule and indicates that shell-model wave functions should give a reasonably good zero-order approximation.

In this way it has become possible to use the conversion electron as a probe particle to measure the distribution of charges and currents in the nucleus in much the same way as in the high energy electron scattering experiments at Stanford by Hofstadter and co-workers.

The theory has been worked out by Church and Weneser [15]) and more recently by Green and Rose [19]). Applications of the theory to specific nuclear problems have been published by Nilsson and Rasmussen [20]) (E1 transitions), Reiner [21, 22]) (M1 transitions in the deformed region) Kisslinger [23]) (l-forbidden M1 in Tl^{203}) and recently by Church and Weneser [24]) (E1 transitions). The picture that emerges from these studies has recently been reviewed by Church and Weneser [25]).

The existence of penetration matrix elements will result not only in an anomalous internal conversion coefficient but it will also appear as a deviation from the normal electron-gamma angular correlation pattern. The particle parameters used for the angular correlation coefficients are closely related to the internal conversion coefficient. The values for the particle parameters can be predicted from a knowledge of the anomalous conversion coefficient [26]).

Therefore a comparison between the experimentally determined conversion coefficient and the angular correlation may serve as a check of the theory.

The odd thallium isotopes present rather unique possibilities in this respect since for these isotopes there is an *l*-allowed M1 transition immediately followed by a cascading *l*-forbidden M1 transition of nearly the same energy. It is therefor possible to compare the conversion matrix elements for these two different types of transitions in the same nucleus. Of course, according to the theory, only the forbidden transition should exhibit anomalous conversion properties.

Deutch and Goldberg [27]) have recently published an experimental study of this kind for Tl^{203}. The interpretation of their results, however, is very confusing. For this reason it was decided to remeasure the electron-gamma and gamma-gamma angular correlations in Tl^{203} with improved statistical accuracy and to extend the investigation to the neighbouring and very similar nucleus Tl^{201}, which has recently been subject to some experimental studies at this institute [28]). The results of our work are reported in the present paper, devoted to Tl^{203}, and the following one [48]) †, which deals with Tl^{201}.

2. Experiments

The gamma-gamma correlation experiments were performed with an automatic directional correlation apparatus described elsewhere by Lindqvist [29]). For the conversion electron-gamma correlation experiments an instrument was used which consists of a "medium thick" lens spectrometer with the source located outside the region of the magnetic field and a 6.4 cm diam. by 5.1 cm NaI(Tl) scintillation detector, which can be rotated around the source (5.f. fig. 1). A description of this instrument has been published by Gerholm and Pettersson [30]).

The magnetic spectrometer was adjusted to a resolution of 5 %, which for this instrument corresponds to a transmission of about 2%. A typical electron spectrum is shown in fig. 2.

The sources were first centered with respect to the magnetic spectrometer, thereupon, the centre of rotation of the gamma channel was carefully adjusted to coincide with the centre of the source. An example of the scintillation spectra obtained in the gamma-channel is shown in fig. 3. For the centering of the gamma-channel the discriminator level was set at the position indicated by S. The gamma-electron coincidences, however, were taken with the discriminator level raised to C. The position of S with respect to the 279 keV photopeak, corresponds to the position of C relative to the 400 keV peak. When the gamma-channel had been centered the single counting rates at the 90°, 180°, and 270° positions were found to be equal to within 0.5 %. The remaining differences in gamma-counting rates were corrected for by dividing the number

† In the text this paper will be referred to as (II).

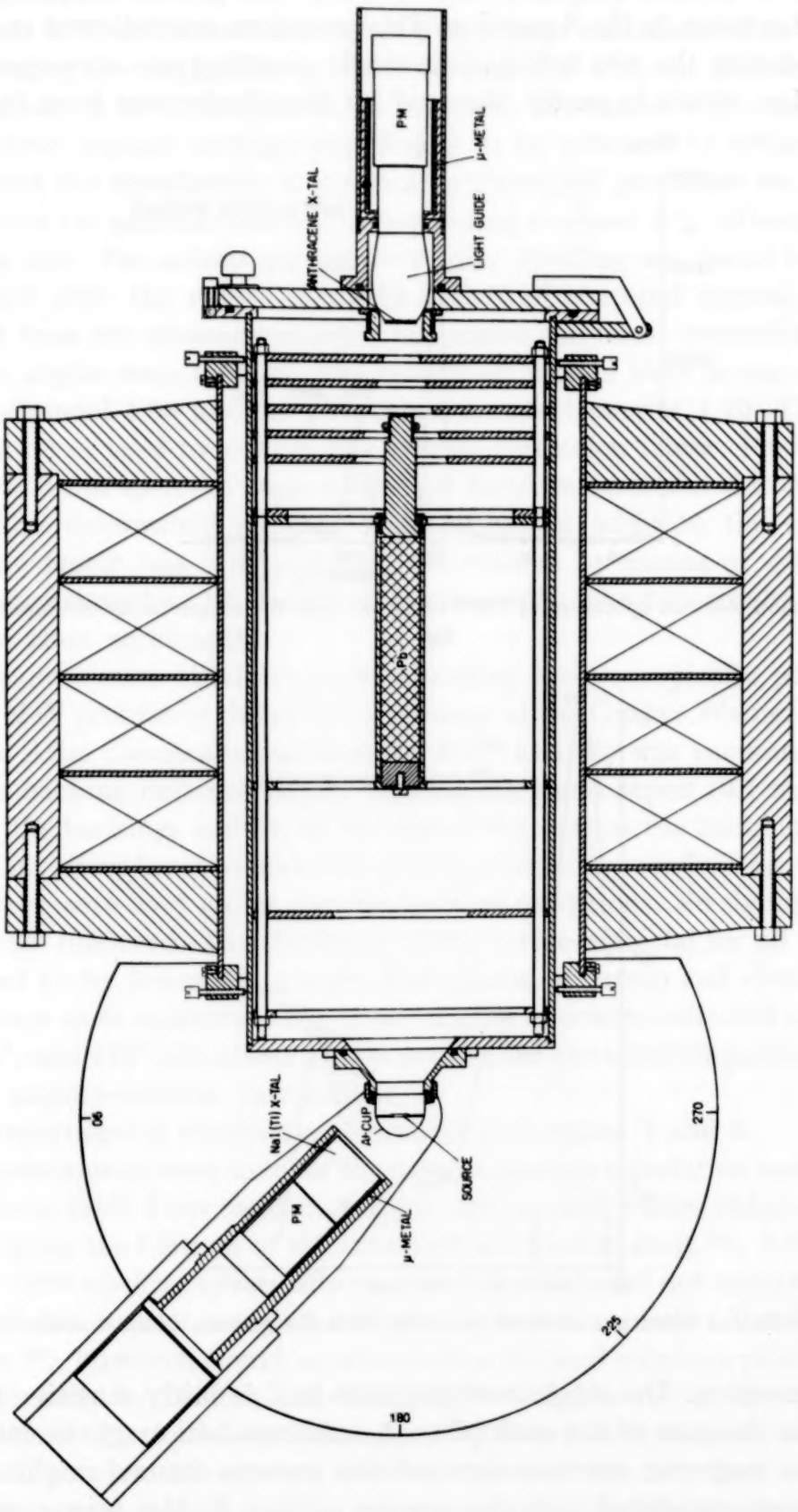

Fig. 1. Electron-gamma angular correlation spectrometer used for the experiments reported in the present and in the following paper (II).

of coincidences, recorded with the discriminator level at C by the gamma single counting rates taken in the S position. This procedure was followed in order to avoid introducing the 400 keV gamma single counting rate corresponding to the C position, which is partly obscured by the interference from the strong

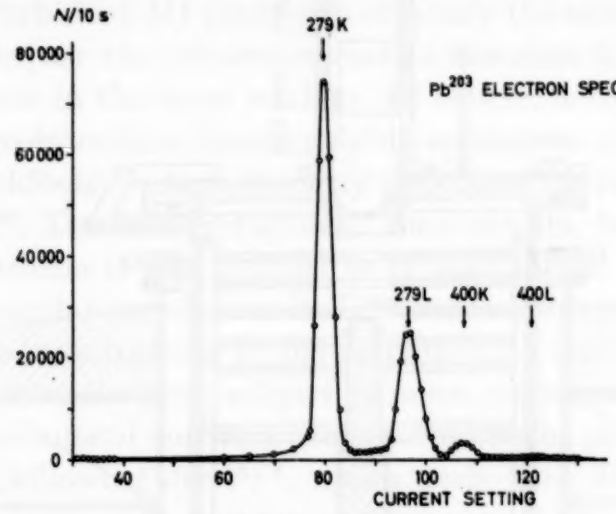

Fig. 2. Conversion electron spectrum of Pb^{203} recorded with the magnetic spectrometer shown in fig. 1.

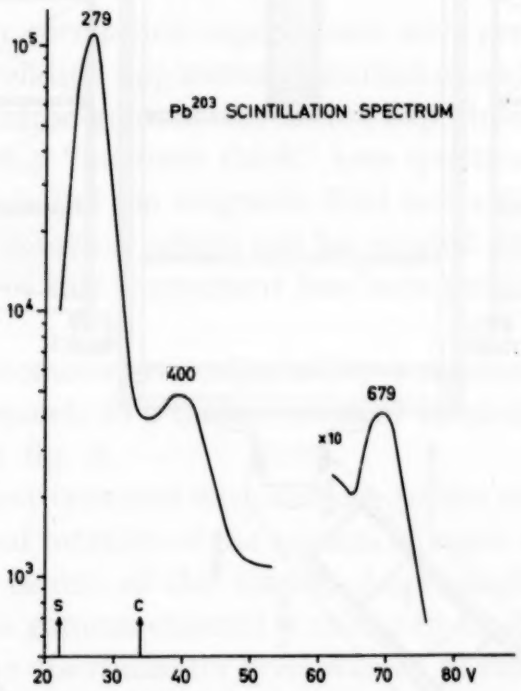

Fig. 3. Scintillation spectrum of Pb^{203} recorded with the gamma channel shown in fig. 1.

279 keV transition. The single counting rate at C is fairly sensitive to minor variations in the gain of the multiplier. A small residual magnetic interaction between the magnetic spectrometer and the gamma-channel might result in gain variations correlated with the angular setting. In this way a systematic error may be introduced.

The gamma-counting rate at S, however, is proportional to the 400 keV single rate at C, and insensitive to fairly large gain variations. This was verified by measuring the single rates at 90°, 180°, and 270° with the discriminator level varied about ± 10 % around the S position. The ratios of the counting rates at the three angular settings were found to be constant to within 0.2 %.

To check the significance of the gamma correction procedure we deliberately de-centered the gamma-channel corresponding to about 4 % difference in single counting rate. The anisotropy obtained after dividing was found to be in good agreement with the values obtained with well centered sources.

Apart from the above-mentioned correction the usual corrections for finite aperture angles were applied. The correction factors were in our case for the gamma-channel 1.06 and for the magnetic spectrometer 1.10. The standard procedure was used to obtain the gamma correction factor. For the spectrometer the finite aperture angle correction factor was calculated from the photographically determined electron trajectories. In addition the spectrometer correction factor was independently determined by means of a special "P_2-baffle" experiment to be described elsewhere [31]). The two results were found to be in close agreement.

The sources were obtained by bombarding spectroscopically pure thallium with 40 MeV protons in the syncro-cyclotron at the Gustav Werner Institute in Uppsala. After chemical separation the Pb^{203} activity was vacuum-evaporated onto the backing material. Mylar (0.9 mg/cm^2) and zapon (0.1 mg/cm^2) were used for the backings and for all but one of the sources the backing was coated with a thin silver layer to make the source electrically conducting. Four different sources were used under varying backing conditions. No significant differences were observed. The thickness of the active material for all sources was estimated to be below 50 μg/cm^2. Both gamma-electron and electron-gamma correlations were measured. The total number of counts collected at the angles 90°, 180°, and 270° was about 50 000 per run for the electron-gamma as well as for the gamma-electron correlations.

The experimental results are summarized in tables 1 and 2.

The same sources were used for the gamma-gamma correlation measurements. As shown in table 2 our measured $A_2(\gamma\gamma)$ agrees with values obtained by other groups. Since the lifetime of the intermediate level is short [32]), 2.9×10^{-10} sec, and the Tl^{203} nucleus spherically symmetric one should not expect any attenuation of the angular correlation due to extra nuclear fields. Van Nooijen and Wapstra [33]), however, found an attenuation for lead sulphate powder sources. A careful study by Deutch and Goldberg [27]) failed to reveal any evidence for perturbations. Lindqvist and Marklund [34]) found no difference between solid and liquid sources. In view of these results and the fact that our observed anisotropy agrees with the earlier results we are led to the conclusion that our gamma-gamma results represent the true unperturbed correlation.

TABLE 1

Experimental results obtained in the present work for electron-gamma and gamma-electron correlations

	Source	Backing cond.	true/acc.	Result
gamma-electron correlation	1	0.9 mg/cm² mylar+silver	15	$-(0.035 \pm 0.008)$
	2a	0.9 mg/cm² mylar	5	$-(0.030 \pm 0.006)$
	2b	0.9 mg/cm² mylar	10	$-(0.0325 \pm 0.011)$
	3a	zapon+silver	6	$-(0.029 \pm 0.008)$
	3b	zapon+silver	7	$-(0.027 \pm 0.009)$
	4a	zapon+silver	5	$-(0.024 \pm 0.008)$
	4b	zapon+silver	8	$-(0.034 \pm 0.008)$
			average value	$-(0.030 \pm 0.003)$
electron-gamma correlation	1	0.9 mg/cm² mylar+silver	75	$-(0.007 \pm 0.008)$
	2	0.9 mg/cm² mylar	24	$-(0.001 \pm 0.007)$
	3a	zapon+silver	20	$-(0.019 \pm 0.008)$
	3b	zapon+silver	24	$-(0.014 \pm 0.0075)$
	4	zapon+silver	21	$-(0.015 \pm 0.0065)$
			average value	$-(0.011 \pm 0.004)$

TABLE 2

Summary of experimental results obtained from direction correlation experiments on Tl^{203}

$A_2(\gamma e)$	$A_2(\gamma\gamma)$	$A_2(e\gamma)$	Ref.
-0.052 ± 0.015	-0.151 ± 0.010	-0.036 ± 0.010	[27]
	-0.107 ± 0.007		[47]
	-0.128 ± 0.003		[34]
	-0.128 ± 0.007		[33]
-0.030 ± 0.003	-0.130 ± 0.006	-0.011 ± 0.005	[a]
$\delta_2^2 = \frac{M1}{E2} = 0.45 \pm 0.05$			[42]

[a]) present work.

Consequently, since the same sources were used in the electron-gamma experiments, also these correlations should be unaffected by static, extranuclear fields.

In principle, however, the electron-gamma correlations may be subject to attenuation effects other than those discussed above. A scattering of the conversion electrons in the source and in the backing gives rise to a smearing out of the angular correlation. An estimate of this attenuation based on the theory of Frankel [35]) shows that under the source conditions used in our experi-

ment the scattering attenuation is negligible for the 400 keV conversion-electrons and less than two percent for the 279 keV electrons.

Finally, a few words should be said about the so called "K-hole effect". It has been suggested [36]) that a strong, time dependent, perturbation may appear due to the interaction between the nuclear magnetic dipole moment and the magnetic field produced by the unpaired electron left in the K-shell after K-conversion (or K-capture). Some experimentalists [37, 38]) claim to have found evidence for this effect. If present, the K-hole attenuation would make it almost impossible to draw conclusions from conversion electron correlations and perhaps also from gamma-gamma correlations following K-capture.

A special electron-gamma correlation experiment on Hg^{197m} was undertaken in order to investigate a possible existence of a K-hole effect. The details of this experiment are reported in a following paper [39]). The conclusion reached, however, is that there is no evidence for an attenuation due to the vacancy in the K-shell in the case of Hg^{197m} provided the source is deposited onto an electrically conducting layer.

3. Interpretation of the Experimental Values

The experimentally determined A_2 coefficients may be written as products

$$A_2(\gamma\gamma) = F_2(400\gamma)F_2(279\gamma), \tag{1}$$

$$A_2(\mathrm{e}\gamma) = F_2(400\,\mathrm{e})F_2(279\gamma), \tag{2}$$

$$A_2(\gamma\mathrm{e}) = F_2(400\gamma)F_2(279\mathrm{e}), \tag{3}$$

where the F_2 coefficients are given by †

$$F_2(400\gamma) = \frac{1}{1+\delta_1^2}\{\delta_1^2 F_2^{\mathrm{m}} + 2\delta_1 F_2 + F_2^{\mathrm{e}}\}_{400}, \tag{4}$$

$$F_2(400\mathrm{e}) = \frac{1}{1+p_1^2}\{p_1^2 b_2^{\mathrm{m}} F_2^{\mathrm{m}} + 2p_1 b_2 F_2 + b_2^{\mathrm{e}} F_2^{\mathrm{e}}\}_{400}, \tag{5}$$

$$F_2(279\gamma) = \frac{1}{1+\delta_2^2}\{\delta_2^2 F_2^{\mathrm{m}} + 2\delta_2 F_2 + F_2^{\mathrm{e}}\}_{279}, \tag{6}$$

$$F_2(279\mathrm{e}) = \frac{1}{1+p_2^2}\{p_2^2 b_2^{\mathrm{m}} F_2^{\mathrm{m}} + 2p_2 b_2 F_2 + b_2^{\mathrm{e}} F_2^{\mathrm{e}}\}_{279}. \tag{7}$$

The F-functions were taken from the tables published by Ferentz and Rosenzweig [40]), and the b_2^{e} particle parameters from a recent paper by A. K. Ustinova [41]). The nuclear structure dependence of the angular correlation is

† Note that the mixing ratios are defined as $\delta^2 = \mathrm{M1/E2}$. This convention is in accordance with Church and Weneser [15]) but is the inverse of the most commonly used. The sign convention for δ is the same as in ref. [40]).

reflected by the variation with λ of the parameters p, b_2^{m} and b_2. λ is defined as

$$\lambda = \frac{M_e}{M_\gamma}, \tag{8}$$

where M_e is the penetration matrix-element and M_γ the gamma-ray matrix element.

The b_2^{m} and b_2 particle parameters given in table 3 were computed at the electronic computer FACIT in Stockholm, using the method given in ref. [26]).

TABLE 3

The particle parameters $b_2^{\mathrm{m}}(\lambda)$ and $b_2(\lambda)$ for $Z = 81$, $E = 279$ keV

λ	b_2	b_2^{m}
−10	−0.1162	+0.0480
− 5	−0.1199	+0.0529
0	−0.1246	+0.0587
5	−0.1305	+0.0660
10	−0.1385	+0.0752
15	−0.1495	+0.0871
20	−0.1661	+0.1027
25	−0.1932	+0.1221
30	−0.2447	+0.1351
50	−0.0644	−0.2949
55	−0.0198	−0.1949
60	+0.0044	−0.1440
65	+0.0194	−0.1136
70	+0.0297	−0.0936
75	+0.0371	−0.0796
80	+0.0427	−0.0691
85	+0.0471	−0.0611
90	+0.0507	−0.0547

The value $C(Z, k) = 0.0260$ has been used in the calculations.

The values for the radial matrix elements were obtained by linear interpolation in Rose's tables [10]). The mixing parameter b_2 was also corrected for the finite nuclear size effects in the E2 conversion process. For this correction the method described in the Appendix was used. The E2-finite size correction to b_2 was found to be quite small. The results, given in table 3, are in good agreement with the values published by Deutch and Goldberg [27]), who obtained values for b_2^{m} and b_2 for $\lambda = -19$, -3, $+1$, $+5$, and $+21$ by interpolation between values calculated for $Z = 78$ and $Z = 83$.

Finally, the parameters p_1 and p_2 are defined as

$$p_1 = \delta_1 \sqrt{\frac{\beta_1^{\mathrm{K}}(\lambda = 1)}{\alpha_2^{\mathrm{K}}}} \tag{9}$$

and

$$p_2 = \delta_2 \sqrt{\frac{\beta_1{}^{K}(\lambda = 1)}{\alpha_2{}^{K}}} \{1-(\lambda-1)C(Z, k)\}^2, \tag{10}$$

where $\beta_1{}^{K}(\lambda = 1)$ and $\alpha_2{}^{K}$ are the M1 and E2 conversion coefficients calculated by Sliv and Band and $C(Z, k)$ is the weighting factor tabulated by Church and Weneser [15]) †. The sign of p is equal to the sign of δ.

3.1. GAMMA-GAMMA CORRELATION

The mixing ratio δ_2 has been accurately determined by McGowan and Stelson [42]) by means of a polarization direction correlation following Coulomb excitation. They found

$$\delta_2 = +0.67 \pm 0.04.$$

This result is in good agreement with the value obtained from the K/L and the L-subshell ratios (cf. table 4), but less significance should be given to the

TABLE 4

δ_2, determined from the conversion ratios [28]) and from the polarization-direction measurement by McGowan and Stelson [42])

Conversion ratios	Exp.	$1/\delta_2{}^2$	
		Rose	Sliv
K/L_I+L_{II}	3.9 ± 0.1	2.6 ± 0.5	2.0 ± 0.4
L_I+L_{II}/L_{III}	4.8 ± 0.1	2.3 ± 0.2	2.5 ± 0.3
McGowan and Stelson		2.25 ± 0.25	

latter figures because of the uncertainties in the L-subshell coefficients and the possible existence of nuclear structure effects in the M1 conversion coefficients.

Using (6) and McGowan and Stelson's value for δ_2 one obtains

$$F_2(279\gamma) = -0.99 \pm 0.01. \tag{11}$$

The $F_2(279\gamma)$ is very insensitive to δ_2 and for this reason $F_2(400\gamma)$ and $F_2(400\mathrm{e})$ can be accurately determined from the experimental values for $A_2(\gamma\gamma)$ and $A_2(\mathrm{e}\gamma)$.

Our results give

$$F_2(400\gamma) = +0.130 \pm 0.006, \tag{12}$$

$$F_2(400\mathrm{e}) = +0.011 \pm 0.004. \tag{13}$$

† The values for $C(Z, k)$ given in ref. [15]) should be corrected for a factor of $\sqrt{\frac{3}{2}}$ omitted in the calculations (cf. ref. [26])).

As pointed out by Deutch and Goldberg the mere fact that $F_2(400\gamma)$ and $F_2(400\mathrm{e})$ are both positive rules out the less probable spin assignment of $\frac{3}{2} \rightarrow \frac{3}{2} \rightarrow \frac{1}{2}$ not excluded from gamma-gamma correlations and determines the sign of δ_1 to be positive. From (4) and (12) one obtains

$$\delta_1 = +40^{+10}_{-7},$$

corresponding to an admixture of $0.06^{+0.03}_{-0.02}$ percent E2.

3.2. ELECTRON-GAMMA CORRELATION

No nuclear structure effects are to be expected for the l-allowed transition. Hence the experimentally measured $F_2(400\mathrm{e})$ should be in agreement with the value obtained from (5) and (9), using the value given above for δ_1 and the normal, nuclear structure independent, particle parameters. The experimental value is

$$F_2(400\mathrm{e})(\mathrm{exp}) = +0.011 \pm 0.004, \tag{14}$$

which is to be compared with the theoretical value. From Biedenharn and Rose [46]) one gets

$$b_2^{\mathrm{m}}(\text{point nucleus}) = +0.110, \quad b_2(\text{point nucleus}) = -0.268,$$

corresponding to a theoretical value

$$F_2(400\mathrm{e})(\text{point nucleus}) = +0.0074 \pm 0.0006. \tag{15}$$

A still better agreement is obtained if the particle parameters are corrected for the finite nuclear size †. The corrected values are

$$b_2^{\mathrm{m}}(\text{finite size}) = +0.126, \quad b_2(\text{finite size}) = -0.267,$$

and

$$F_2(400\mathrm{e})\ (\text{finite size}) = +0.0090 \pm 0.0007. \tag{16}$$

3.3. THE 400 keV K-CONVERSION COEFFICIENT

The $F_2(400\mathrm{e})$ is very insensitive to the parameter λ. A minor disagreement between theoretical and experimental values therefore requires very large λ-values, in disagreement with what one should expect from the theory.

Due to the insensitivity of $F_2(400\mathrm{e})$ to nuclear structure effects our angular correlation experiments do not exclude the possibility of a large λ-value. This would be seen, however, from a comparison between the experimentally determined conversion coefficient and the theoretical value for $\lambda = 1$, obtained from Sliv and Band's tables.

The conversion coefficient of the 400 keV transition has been measured by Nijgh *et al.* [43]) who got

$$\alpha_{\mathrm{K}}{}^{(400)}\ (\mathrm{Nijgh}) = 0.118 \pm 0.011.$$

† The method used for this correction is explained in the Appendix of (II).

Deutch and Goldberg [27]) confirmed this value using the relation

$$\alpha_K^{(400)}(\text{exp}) = \alpha_K^{(279)}\ (\text{exp})\ \frac{N_\gamma^{(279)} N_e^{(400)}}{N_\gamma^{(400)} N_e^{(279)}}$$

and got †

$$\alpha_K^{(400)}\ (\text{Deutch and Goldberg}) = 0.123 \pm 0.015.$$

However, these two experiments are not independent since Deutch and Goldberg use Nijgh's *et al.* value for the $N_\gamma^{(279)}/N_\gamma^{(400)}$ ratio.

The conversion coefficient of the 400 keV transition can be independently determined, with a considerable degree of accuracy, from our electron-gamma and gamma-electron coincidence experiments. It is easily seen that, provided the source to detector distance is kept constant and the beta-transmission of the magnetic spectrometer (equal to the effective solid angle times the detection efficiency) is the same in the two experiments the following relation will hold exactly:

$$\alpha_K^{(400)} = \alpha_K^{(279)}\ \frac{\bar{C}(400\text{e}{-}279\gamma)\varepsilon^{(400)} q^{(400)}}{\bar{C}(400\gamma{-}279\text{e})\varepsilon^{(279)} q^{(279)}}; \tag{16}$$

$\alpha_K^{(279)}$ is the K-conversion coefficient of the 279 keV transition. This has been very accurately measured by several independent groups [6, 7]). The coefficients $\bar{C}(400\text{e}{-}279\gamma)$ and $\bar{C}(400\gamma{-}279\text{e})$ are the measured counting rates averaged over the angles and with minor corrections applied for the background of random coincidences and for the decay of the source during the course of the experiment; ε is the total crystal efficiency for the gamma-ray in question and q is the probability that the pulse produced will be accepted by the discriminator. Since only the ratio $\varepsilon_\gamma^{(400)} q^{(400)}/\varepsilon_\gamma^{(279)} q^{(279)}$ appears, the value found for $\alpha_K^{(400)}$ should be fairly insensitive to the errors in the absolute values for ε and q.

A separate experiment was made in order to determine this ratio. In a fixed geometry we compared the coincidence and single counting rates for Au^{198} and Tl^{203} sources. One has

$$\frac{\varepsilon^{(412)}\, q^{(412)}}{\varepsilon^{(279)}\, q^{(279)}} = \frac{\bar{C}(\beta{-}412\gamma)N(400\text{e})(1{-}\kappa_{\text{tot}}^{(279)})}{\bar{C}(400\text{e}{-}279\gamma)N(\beta)(1{-}\kappa_{\text{tot}}^{(412)})}$$

The value for $\varepsilon^{(412)} q^{(412)}/\varepsilon^{(279)} q^{(279)}$ thus determined becomes 0.765 ± 0.03 in good agreement with the value obtained from the tables of theoretically calculated crystal efficiencies published by Heath *et al.* [44]), namely 0.745. Moreover, we could also use our experimental data to calculate the absolute crystal effi-

† In fact the figure given by Deutch and Goldberg is 0.117 ± 0.015. This value, however, is based on a ratio $N_\gamma^{(279)}/N_\gamma^{(400)} = 18.5 \pm 2$ erroneously quoted from Nijgh *et al.*, who obtained a slightly higher value, namely 19.5 ± 1.5. We have introduced this minor correction to Deutch and Goldberg's experimental value.

ciency for these gamma-rays energies. Our values agree with those calculated by Heath *et al.* to within 5 %.

The values for $\alpha_K^{(400)}$ obtained from (16) using our experimentally determined ratio of the crystal efficiencies are summarized in table 5. The weighted mean value becomes

$$\alpha_K^{(400)}(\text{exp., present work}) = 0.145 \pm 0.007,$$

which is in perfect agreement with the theoretical value obtained by log-log interpolation in Sliv and Band's tables,

$$\beta_1^K(\lambda = 1, \text{ Sliv}) = 0.148.$$

TABLE 5

$\alpha_K(400)$ from coincidence experiments

Run	$\alpha_K(400)$ [a])
1	0.145 ± 0.008
2	0.143 ± 0.011
3	0.148 ± 0.008
4	0.147 ± 0.008
Average	0.145 ± 0.007

[a]) Calculated from eq. (16) with $\varepsilon_\gamma^{(400)} q^{(400)} / \varepsilon_\gamma^{(279)} q^{(279)} = 0.745 \pm 0.020$ and $\alpha_K(279) = 0.163 \pm 0.003$.

The disagreement between our experimental value for the 400 keV K-conversion coefficient in Tl^{203} and the values given by Nijgh *et al.* and by Deutch and Goldberg seems to be due primarily to the value for $N_\gamma^{(279)}/N_\gamma^{(400)}$ given by Nijgh *et al.* who got $N_\gamma^{(279)}/N_\gamma^{(400)} = 19.5 \pm 1.5$, while our data correspond to a somewhat higher value, namely 23 ± 1. However, the value given for $N_\gamma^{(279)}/N_\gamma^{(400)}$ by Nijgh *et al.* depends on the value used for $\alpha_K^{(412)}$(Hg 198) which was quoted from Wapstra *et al.* [45]). We have recently been able to show that Wapstra's *et al.* value is somewhat too low. In this way the discrepancy between the experimental values for $\alpha_K^{(400)}$ (Tl-203) is removed.

Therefore, we can finally conclude that our experimental results for the electron-gamma angular correlation and for the internal conversion coefficient of the 400 keV transition are in accordance with the theoretical prediction that for the allowed M1 transition the penetration matrix element is negligible. The nuclear structure effects, therefore, do not affect the internal conversion process to any detectable amount and the conversion coefficient is correctly given by the "surface current" model used by Sliv and Band.

3.4. GAMMA-ELECTRON CORRELATION

The analysis of the experimental results for this correlation is similar to the electron-gamma analysis discussed above. However, in this case we have to

consider the λ-dependence of p, b_2^{m} and b_2. From (2) and (3) we get

$$\frac{A_2(\gamma\mathrm{e})}{A_2(\gamma\gamma)} = \frac{F_2(279\mathrm{e})}{F_2(279\gamma)} = +0.235\pm0.035. \tag{17}$$

Using, as before, $F_2(279\gamma) = -0.99\pm0.01$ we get from the experiment †

$$F_2(\mathrm{e}) = -0.23\pm0.04, \tag{18}$$

to be compared with the theoretical expression

$$F_2(\mathrm{e}\lambda) = \frac{\delta^2 \frac{\beta_1(\lambda)}{\alpha_2} b_2^{\mathrm{m}}(\lambda) F_2^{\mathrm{m}} + 2\delta \sqrt{\frac{\beta_1(\lambda)}{\alpha_2}}\, b_2(\lambda) F_2 + b_2^{\mathrm{e}} F_2^{\mathrm{e}}}{1+\delta^2 \frac{\beta_1(\lambda)}{\alpha_2}}. \tag{19}$$

From this comparison it is possible to determine λ. In general one will have two possible λ-values which both give agreement between the theoretical expression (19) and the experimentally determined $F_2(\mathrm{e})$.

However, as already pointed out λ can also be independently determined from the K-shell internal conversion coefficient. From $\alpha_{\mathrm{K}}(\mathrm{exp})$ and δ one gets

$$\beta_1(\mathrm{exp}) = \frac{(1+\delta^2)\alpha_{\mathrm{K}}(\mathrm{exp}) - \alpha_2(\mathrm{Sliv})}{\delta^2}. \tag{20}$$

Using the experimental values [6, 42]) for δ and $\alpha_{\mathrm{K}}(\mathrm{exp})$ one has

$$\beta_1(\mathrm{exp}) = 0.360\pm0.03, \tag{21}$$

which is to be compared with the theoretical expression

$$\beta_1(\lambda) = \beta_1(\mathrm{Sliv})\{1-(\lambda-1)C(Z,k)\}^2. \tag{22}$$

Again the comparison between the theoretical expression and the experimental result gives two possible solutions.

If the internal conversion theory including the nuclear structure (i.e. λ) dependent factors is correct one of the two λ-values defined from $F_2(\mathrm{e}\lambda)$ should agree with one of the two λ values obtained from $\beta_1(\lambda)$. To get a unique value for λ it is therefore necessary to determine both $F_2(\mathrm{e})$ and β_1.

This comparison is illustrated in fig. 4. The experimental value for β_1 gives as one solution $\lambda = 2.3\pm0.3$ corresponding to an almost negligible contribution of the penetration matrix element to the internal conversion process. The second solution becomes $\lambda = +76\pm0.6$ which in fact means that the penetration matrix element plays a dominant role.

In the lower part of fig. 4 a similar comparison is made for the angular correlation experiment. The first solution becomes $\lambda = +15.5\pm2.5$ in obvious disagreement with the values found above. The second solution, however, is

† From now on we delete the indices. All factors refer to the 279 keV transition.

$\lambda = +80 \pm 5$. Since this is in good agreement with the large λ-value found from the internal conversion coefficient we conclude that the proper λ-value is (for $\delta = +0.65$) $\lambda = 76 \pm 1$.

In fig. 4, δ is taken to be $+0.65$. However, as seen in (19) and (22) the theoretical curves both depend on δ. In fig. 5 we have chosen a different representation in order to illustrate that it is impossible to get agreement between the internal conversion coefficient and the angular correlations for any reason-

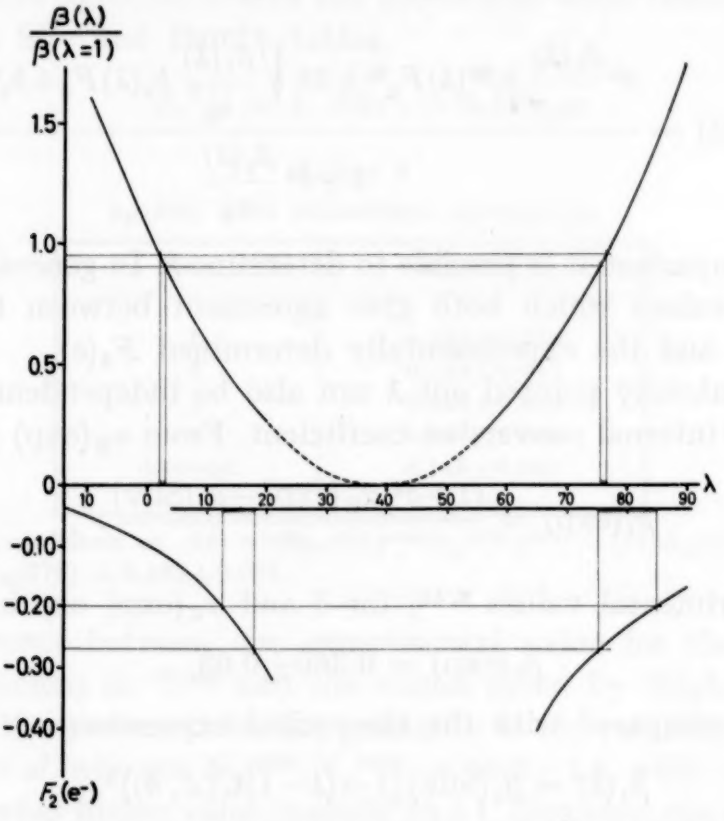

Fig. 4. To illustrate the existence of large nuclear structure dependent effects in the K-conversion process of the 279 keV transition in Pb^{203}. Upper half of the figure: the theoretical K-shell M1 conversion coefficient $\beta_1(\lambda)$ divided by the finite size corrected value β_1(Sliv) as a function of λ. Lower half of the figure: the theoretical angular correlation function $F_2(e\lambda)$ as a function of λ. Horizontal lines correspond to the experimental values (with errors). Consistent results are obtained for $\lambda = +76 \pm 1$. The theoretical curves correspond to $\delta = +0.65$.

able value of δ if λ is assumed to be small. In the $1-(\lambda-1)\,C(Z, k)$ versus δ plane the regions determined by the experimental value for the ratio $F_2(e)/F_2(\gamma)$ (eqs. (6) and (19)) and α_K(eqs. (20) and (22)) should overlap. In this way one can determine simultaneously both λ and δ.

As seen in the figure the region of overlap is in accordance with the δ-value given by Stelson and McGowan and the value obtained from the K/L and L subshell ratios (cf. Table 4). It is also evident that the small values for λ corresponding to $1-(\lambda-1)C(Z, k) \approx +1$ have to be excluded.

We would like to point out that our experimentally measured gamma-

electron anisotropy is *larger* than the theoretical value predicted for $\lambda = 1$ (c.f. fig. 4). For our interpretation we use the ratio $F_2(e)/F_2(\gamma)$ i.e. the ratio of the experimentally measured $A_2(\gamma e)/A_2(\gamma\gamma)$. The same sources were used in both experiments. An attenuation present in the gamma-gamma correlation must also appear in the gamma-electron correlation. If our gamma-electron correlation has been subject to an additional attenuation due to scattering of the conversion electrons the correct value for $A_2(\gamma e)$ would be larger than assum-

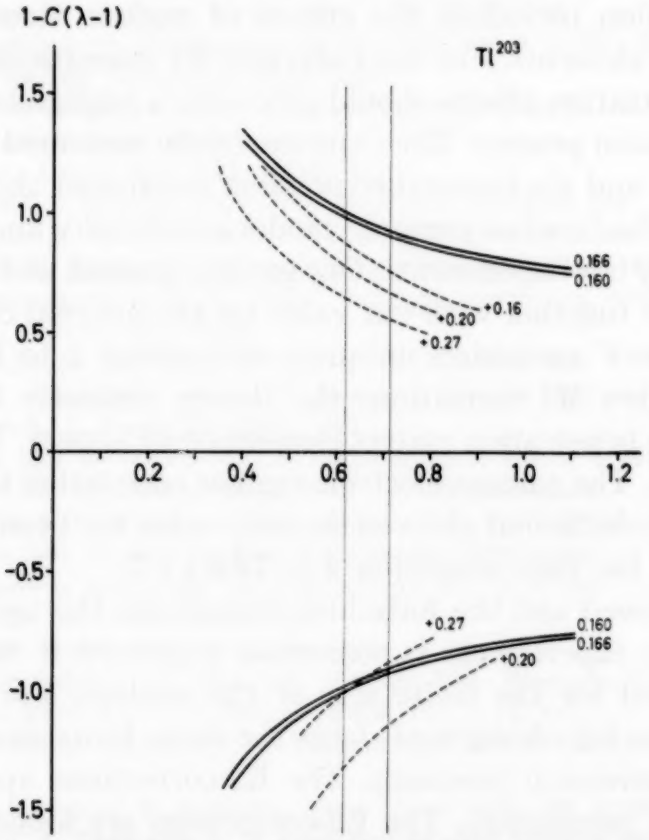

Fig. 5. To illustrate the δ dependence of the results obtained from experimental determinations of the K-conversion coefficient and the angular correlations. In the $1-(\lambda-1)C(Z, k)$ versus δ plane are given the theoretical curves corresponding to the experimental values for the conversion coefficient (solid curves) and for the ratio $F_2(e)/F_2(\gamma)$ (dashed curves). The vertical lines for $\delta = +0.67 \pm 0.04$ correspond to the values for the M1/E2 mixing ratio given in ref. [42]). The vertical lines intersect the overlap area at $1-(\lambda-1)C(Z, k) \approx -1$ which for $C(Z, k) = 0.0260$ gives $\lambda = +76 \pm 1$.

ed in our interpretation. This, of course, would imply that the disagreement between the experimental result and the theoretical predictions for $\lambda = 1$ is even larger than assumed above.

The value for λ obtained above depends on the value taken for the weighting factor $C(Z, k)$. In our limits of error we have not included the uncertainty in this function, which was obtained by interpolation in the tables given by Church and Weneser [15, 26]) as $C = 0.0260$. The uncertainty in the present calculations of $C(Z, k)$ is about ± 10 %, and this consequently gives the main contribution

to final errors for λ. It should be observed, however, that the present uncertainty concerning $C(Z, k)$ does not affect our interpretation above. The decisive factor is $(\lambda-1)C(Z, k)$. A change in $C(Z, k)$ simply implies a change in the corresponding λ-value.

4. Conclusions

Our experimental results are in complete agreement with the present theory of internal conversion including the effects of nuclear structure dependent penetration matrix elements. For the *l*-allowed M1 transitions the theory predicts that the penetration effects should give only a negligible contribution to the internal conversion process. The experimentally measured electron-gamma angular correlation and the internal conversion coefficient should therefore be in agreement with the "surface current" model used by Sliv and his co-workers. This is confirmed by our experiments. Our gamma-gamma and electron-gamma angular correlations together with our value for the internal conversion coefficient for the 400 keV transition uniquely determines λ to be $\lambda = 1.4 \pm 1.0$.

For the *l*-forbidden M1 transitions the theory indicates that fairly large contributions of the penetration matrix elements may appear. This is confirmed by the experiments. The gamma-electron angular correlation together with the internal conversion coefficient gives as the only value for λ compatible with the experimental data for this transition $\lambda = 76.0 \pm 0.7$.

For both the allowed and the forbidden transitions the agreement between the theory and the experiments is somewhat improved if the particle parameters are corrected for the finite size of the nucleus. For the *l*-forbidden transition, where the E2 admixture is large the static finite size affects both the M1 and the E2 conversion processes. The E2-corrections appear in both b_2^e and b_2 (the mixing parameter). The E2-corrections are found to be small but tend to improve the agreement between theory and experiments.

References

1) M. E. Rose, G. M. Goertzer, B. I. Spinrad, J. Harr and P. Strong, Phys. Rev. **83** (1951) 79
2) M. E. Rose, in Beta- and Gamma Ray Spectroscopy, ed. by K. Siegbahn (North-Holland Publishing Co., Amsterdam, 1955) Ch. XIV
3) L. A. Sliv, JETP **21** (1951) 770
4) L. A. Sliv and M. A. Listengarten, JETP **22** (1952) 29
5) L. A. Sliv, Journ. de Phys. et du Radium **16** (1955) 523
6) A. H. Wapstra and G. J. Nijgh, Nuclear Physics **1** (1956) 245
7) C. Nordling, K. Siegbahn, E. Sokolowski and A. H. Wapstra, Nuclear Physics **1** (1956) 326
8) L. A. Sliv and I. M. Band, Coefficients of Internal Conversion of Gamma Radiation, Part I, K shell (Physico-Technical Institute, Academy of Science, Leningrad 1956) (issued in USA as Report 57 ICC K1, Physics Department, University of Illinois, Urbana, Illinois)
9) L. A. Sliv and I. M. Band, Tables of Gamma Ray Conversion Coefficients, Part II, L-shell (Physico-Technical Institute, Academy of Science, Leningrad 1958) (issued in USA as Report 58 ICC L1, Physics Department University of Illinois, Urbana, Illinois)

10) M. E. Rose, Internal Conversion Coefficients (North-Holland Publishing Co., Amsterdam, 1958)
11) F. Asaro, F. S. Stephens, J. M. Hollander and I. Perlman, Phys. Rev. **117** (1960) 492
12) E. S. Snyder and S. Frankel, Phys. Rev. **106** (1957) 755
13) K. O. Nielsen, O. B. Nielsen and M. A. Waggoner, Nuclear Physics **2** (1957) 476
14) F. K. McGowan and P. H. Stelson, Phys. Rev. **107** (1957) 1674
15) E. L. Church and J. Weneser, Phys. Rev. **104** (1956) 1382
16) T. R. Gerholm and B. G. Pettersson, Phys. Rev. **110** (1958) 1119
17) L. Spruch and A. Rotenberg, Phys. Rev. **103** (1956) 365
18) H. de Waard and T. R. Gerholm, Nuclear Physics **1** (1956) 281
19) T. A. Green and M. E. Rose, Phys. Rev. **110** (1958) 105
20) S. G. Nilsson and J. O. Rasmussen, Nuclear Physics **5** (1958) 617
21) A. S. Reiner, Nuclear Physics **5** (1948) 544
22) A. S. Reiner, Structure Effects in the Interaction between Nuclei and Atomic Electrons, Thesis, University of Amsterdam, 1958
23) L. S. Kisslinger, Phys. Rev. **114** (1959) 292
24) E. L. Church and J. Weneser, Bull. Am. Phys. Soc. **5** (1960) 231
25) E. L. Church and J. Weneser, Ann. Rev. Nucl. Science **10** (1960) 193
26) E. L. Church, M. E. Rose and J. Weneser, Phys. Rev. **109** (1958) 1299; electron radial matrix elements are tabulated in M. E. Rose, Internal Conversion coefficients (North-Holland Publishing Co., Amsterdam, 1958)
27) B. I. Deutch and N. Goldberg, Phys. Rev. **117** (1960) 818
28) J. Lindskog, E. Bashandy and T. R. Gerholm, Nuclear Physics **16** (1960) 175
29) T. Lindqvist, Ark. f. Fysik **12** (1957) 495
30) T. R. Gerholm and B. G. Pettersson, Nuclear Instruments **4** (1959) 107
31) T. R. Gerholm, R. Othaz and M. El-Nesr (to be published)
32) E. Bashandy, T. R. Gerholm and J. Lindskog, Ark. f. Fysik **17** (1960) 421
33) B. van Nooijen and A. H. Wapstra, Physica **23** (1957) 404
34) T. Lindqvist and I. Marklund, Nuclear Physics **3** (1957) 367
35) S. Frankel, Phys. Rev. **83** (1951) 673
36) H. Frauenfelder, Phys. Rev. **82** (1951) 549;
see also H. Frauenfelder, in Beta and Gamma Ray Spectroscopy, ed. by Kai Siegbahn (North-Holland Publ. Co., Amsterdam, 1955) Ch. XIX (1)
37) H. Aeppli, M. Albers-Schönberg, H. Frauenfelder and P. Scherrer, Helv. Phys. Acta **25** (1952) 339
38) F. Gimmi, E. Heer and P. Scherrer, Helv. Phys. Acta **29** (1956) 147
39) B. G. Pettersson, J. Thun and T. R. Gerholm, Nuclear Physics **24** (1961) 223
40) M. Ferentz and N. Rosenzweig, Table of F-coefficients, ANL report 5324
41) A. K. Ustinova, JETP **37** (1960) 216
42) F. K. McGowan and P. H. Stelson, Phys. Rev. **109** (1958) 901
43) G. J. Nijgh, A. H. Wapstra, L. T. M. Ornstein, N. Salomons-Grobben, J. R. Huizenga and O. Almén, Nuclear Physics **9** (1958/59) 528
44) R. L. Heath, AEC Research and Development report IDO-16408, Phillips Petroleum Co., Atomic Energy Div. Idaho Falls, Idaho;
S. H. Vegors, Jr., L. L. Marsden and R. L. Heath, AEC Research and Development report IDO-16370, Phillips Petroleum Co., Atomic Energy Division, Idaho Falls, Idaho
45) A. H. Wapstra, G. J. Nijgh, N. Salomons-Grobben and L. T. M. Ornstein, Nuclear Physics **9** (1958/59) 538
46) L. C. Biedenharn and M. E. Rose, Revs. Mod. Phys. **25** (1953) 729
47) J. Varma, Phys. Rev. **94** (1954) 1688
48) B. G. Pettersson, T. R. Gerholm, Z. Grabowski and B. van Nooijen, Nuclear Physics **24** (1961) 196

1.E.1:
3.B

Nuclear Physics **24** (1961) 196—222; © *North-Holland Publishing Co., Amsterdam*
Not to be reproduced by photoprint or microfilm without written permission from the publisher

PENETRATION MATRIX ELEMENTS AND NUCLEAR STRUCTURE EFFECTS IN Tl^{201}

B.-G. PETTERSSON, T. R. GERHOLM, Z. GRABOWSKI † and B. VAN NOOIJEN ††

Institute of Physics, University of Uppsala, Uppsala, Sweden

Received 16 January 1961

Abstract: The study of nuclear structure effects in internal conversion discussed in part (I) (preceding paper) has been extended to the neighbouring nucleus Tl^{201}. Gamma-gamma, electron-gamma and gamma-electron correlations have been measured. The following results have been obtained:

$$\begin{aligned}
A_2(946+907\gamma\text{–}330\gamma) &= +0.72 \pm 0.04,\\
A_2(946+907\gamma\text{–}330\mathrm{e}) &= +0.210\pm 0.007,\\
A_2(361\gamma\text{–}330\gamma) &= -0.20 \pm 0.08,\\
A_2(361\gamma\text{–}330\mathrm{e}) &= -0.09 \pm 0.01,\\
A_2(361\mathrm{e}\text{–}330\gamma) &= +0.001\pm 0.004,\\
A_2(585\gamma\text{–}330\mathrm{e}) &= +0.022\pm 0.015,\\
A_2(585\gamma\text{–}361\mathrm{e}) &= -0.013\pm 0.008.
\end{aligned}$$

From coincidence and single counting rates the following conversion coefficients were determined:

$$\alpha_K^{(330)} = 0.113\pm 0.008, \qquad \alpha_K^{(361)} = 0.21\pm 0.025, \qquad \alpha_K^{(585)} = 0.06\pm 0.01.$$

A decay scheme including 17 transitions and 9 excited states has been established. The angular correlations and conversion coefficients were used to determine the spins and parities for the first, second and fifth excited states as well as the multipolarities, characters and mixing ratios of the most intense transitions.

The results have been analyzed in terms of nuclear structure effects in the conversion process. Our conclusions reached in part (I) have been confirmed, i.e. for the $d_{\frac{3}{2}} \rightarrow d_{\frac{3}{2}}$ M1 transition there is no evidence for nuclear structure effects in agreement with what is to be expected from the theory.

For the strongly retarded *l*-forbidden $d_{\frac{3}{2}} \rightarrow s_{\frac{1}{2}}$ M1 transition the experimental data are in complete agreement with the theory for $\lambda = +74\pm 3$, where λ is defined as the ratio of the penetration matrix element and the corresponding gamma ray matrix element. The value for the weighting factor $C(Z, k)$ was taken to be 0.0274. The errors for λ given here do not include the uncertainty in the weighting factor which is supposed to be known to within ± 10 %. Thus the evidence for large nuclear structure effects in the internal conversion process found for the 279 keV transition in Tl^{203} (cf. ref. [15])) has been confirmed for the analogous 330 keV transition in Tl^{201}. The λ-values for these two transitions are in close agreement.

Corrections for static finite size effects in the E2 conversion process have been applied and as in the case of Tl^{203} these corrections were found to be small.

It is concluded that the present formulation of the theory of internal conversion, including nuclear structure dependent factors, is fully consistent with the experimental data. Experimentally determined penetration matrix elements provide new pieces of information about the nuclear structure. It is shown that in order to get a unique determination of the λ-parameter it is necessary to determine both the internal conversion coefficient and the electron-gamma angular correlation.

† On leave from: Instytut Badań Jadrowych, Krakow, Poland.
†† On leave from: Technische Hogeschool Delft, Holland.

1. Introduction

In the preceding paper [15]) † we have discussed an experimental study of the conversion matrix elements for the $d_{\frac{5}{2}}$ (400 keV)$d_{\frac{3}{2}}$ (279 keV)$s_{\frac{1}{2}}$ cascade in Tl^{203}. It was decided to extend the experiment to the neighbouring nucleus Tl^{201}. The main features of the two decay-schemes are very similar. It will be shown below that in analogy to Tl^{203} there is in Tl^{201} a stop over transition from the second excited state. This cascade can be described as $d_{\frac{5}{2}}$ (361 keV)$d_{\frac{3}{2}}$ (330 keV) $s_{\frac{1}{2}}$. The lifetime of the intermediate level has recently been measured to be $(7\pm2)\times10^{-11}$ sec [1]), corresponding to an M1 retardation factor of 380 ± 110 to be compared with the retardation of 1000 ± 110 for the corresponding transition in Tl^{203}. The competing E2 transitions are in both cases somewhat enhanced, enhancement factors being 17.4 ± 6.3 for Tl^{201} and 9.2 ± 1.5 for Tl^{203}, respectively. For constant gamma ray matrix elements the M1/E2 mixing ratio †† varies as the inverse of the transition energy. The reduced retardation of M1 and the increased enhancement of E2 compensate for this effect. This explains that the M1/E2 mixing ratios are almost exactly equal in Tl^{201} and Tl^{203}.

However, the energy released in the decay of Pb^{201} is considerably higher than in the case of Pb^{203}. Therefore several higher levels are found to be excited in the decay of Pb^{201}. This gives rise to a fairly complicated decay scheme and introduces several complications in the angular correlation experiments in particular since the decay scheme has not yet been firmly established. For the cascade of interest in this connection, however, it is possible to arrange the experiment in such a way that the difficulties caused by the uncertainties in the decay scheme can be circumvented.

2. Remarks Concerning the Decay of Pb^{201} and the Angular Correlation Experiments in Tl^{201}

Bergkvist *et al.* [2]) have studied the decay of Pb^{201} with a high resolution double focusing beta-ray spectrometer. In table 1 we have summarized the energies and relative intensities of the K-conversion lines assigned to Tl^{201}.

It has been shown by means of electron-electron coincidences that the 361 keV and 330 keV transitions are strongly in coincidence. Delayed coincidence experiments by Lindskog *et al.* [1]) show that the 361 keV transition preceeds the 330 keV transition and since the latter has the by far strongest intensity it should go from the first excited state to the ground state. The first excited level is then placed at 330 keV. The second excited state is situated at 692 keV since the 361 keV transition is one of the strongest in the decay. The 692 keV line then corresponds to a cross-over transition to the ground state.

† This paper will be referred to as (I).

†† As in (I) we adopt the convention δ^2 = M1/E2 (cf. footnote on page 185).

Further information concerning the decay scheme can be obtained from electron-gamma coincidences. The magnetic spectrometer used for the angular correlation studies was operated in coincidence with a NaI(Tl) scintillation spectrometer. The results of these coincidence studies are summarized in table 2.

TABLE 1

Summary of Tl^{201} transitions given by Bergkvist *et al.* [2])

Transition energy in keV	K conversion intensity
129.1	
284.4?	0.7
310.0	0.5
330.3	100
361.2	25
394.3	0.6
405.6	2.7
585	1.9
692	0.6
708?	0.3
766	1.0
825?	0.4
907	1.3
946	1.6
1099	0.2

TABLE 2

Electron-gamma coincidence studies of some transitions in Tl^{201}

Transition	Coincidence with 330 e	Coincidence with 361 e
330		yes
361	yes	
405	yes	?
585	yes	yes
692	no	no
766	yes	no
907	?	no
946	yes	no
1099	no	no
1300	yes	yes
1400	no	no

As seen in table 2 the 692 keV transition is not in coincidence with the 361 keV and 330 keV lines.

From the coincidence data given in table 2 it is possible to place a level at 1277 keV de-excited by the 946 keV transition to the first excited state and by the 585 keV transition to the second excited state. The 1097 keV, 766 keV and

405 keV lines correspond, according to the energy relations and the coincidence data, to the de-excitation of a level at 1097 keV. Furthermore the coincidence information places a level at about 2012 keV † de-excited by the 1300 keV transition to the second excited state. The 907 keV line found to be in non-coincidence with the 361 keV line and possibly, in coincidence with the 330 keV line could be placed to correspond to a level either at 1237 keV or at 907 keV but the coincidence relations favour the 907 keV alternative. Tentatively one may place a level at 1406 to be de-excited by the 129 keV, 310 keV and 1406 keV transitions respectively. The 2012 keV level may be de-excited by the 284 keV

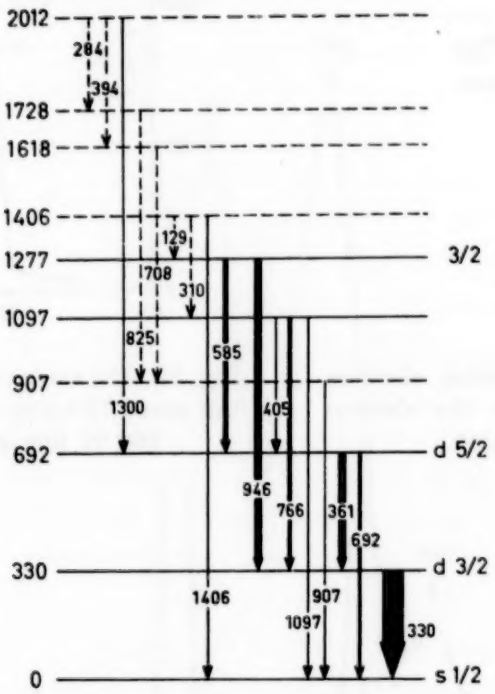

Fig. 1. Tentative decay scheme of Tl^{201} based on energy relations and coincidence studies.

and 394 keV transitions feeding two levels at 1728 keV and 1618 keV de-excited by the 825 keV–907 keV cascade and the 708 keV–907 keV cascade to the ground state, respectively.

A tentative decay scheme based on these considerations is given in fig. 1. The levels and transitions given in solid lines are those supported by coincidence experiments. In addition we have also given five less certain levels and seven transitions in broken lines, of which all but the 907 keV transition have intensities less than 1 % of the 330 keV transition. In this way we have placed all the transitions assigned to Tl^{201} by Bergkvist *et al.*

By means of atomic beam resonance the ground state spin of Tl^{201} has recently [3]) been measured and found to be $\frac{1}{2}$ in accordance with the shell model level assignment $s_{\frac{1}{2}}$. Since the 330 keV transition is a M1/E2 mixture and since

† The energy of this level is less accurately known since the 1300 keV transition has only been seen in our scintillation spectrum.

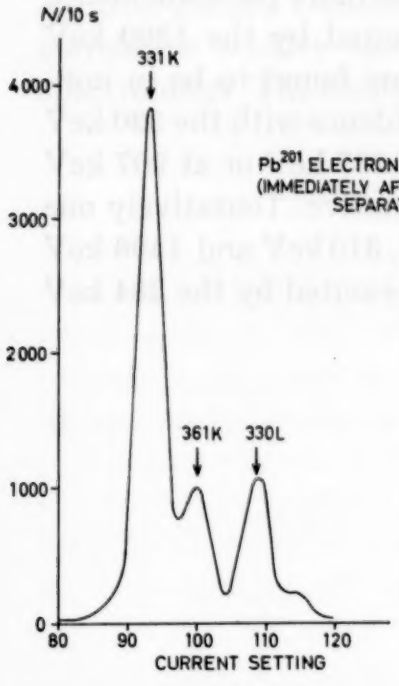

Fig. 2a. Part of the Tl^{201} conversion electron spectrum taken immediately after the electromagnetic isotope separation.

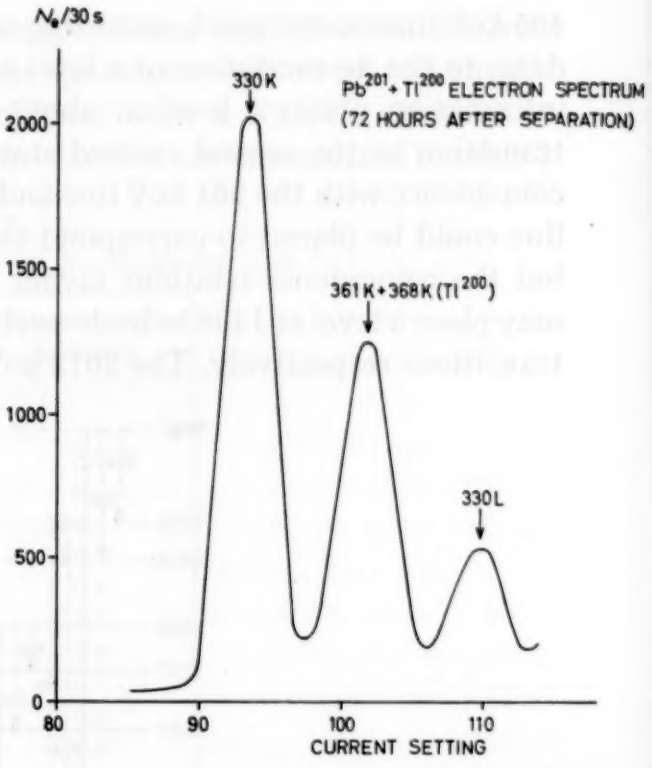

Fig. 2b. The same part of the spectrum as shown in fig. 2 but taken 72 hours after the separation. Note the Tl^{200} 368 K line growing in during the decay.

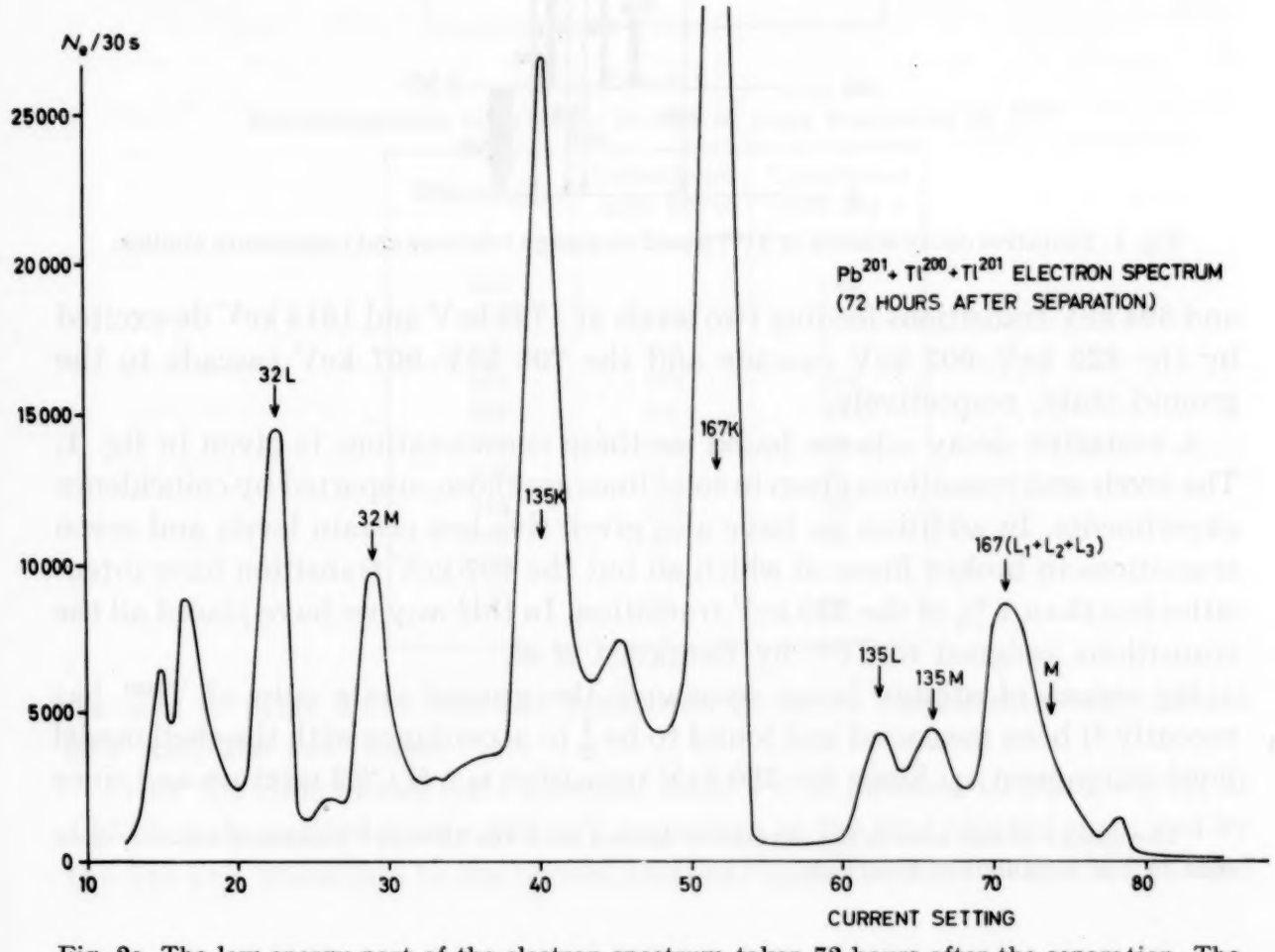

Fig. 2c. The low energy part of the electron spectrum taken 72 hours after the separation. The conversion lines shown in the figure are Hg^{201} lines growing in as the Pb^{201} source decays to Tl^{201}.

the M1 component has been found to be strongly retarded, the first excited state definitely corresponds to the shell model level at $d_{\frac{3}{2}}$. As will be seen below the 361 keV transition is of almost pure M1 character and hence the possible spin values for the second excited level become $\frac{1}{2}+$, $\frac{3}{2}+$ or $\frac{5}{2}+$, but of these all but the last alternative can be ruled out by means of the angular correlation results. Thus we may give the second excited level the shell model assignment $d_{\frac{5}{2}}$.

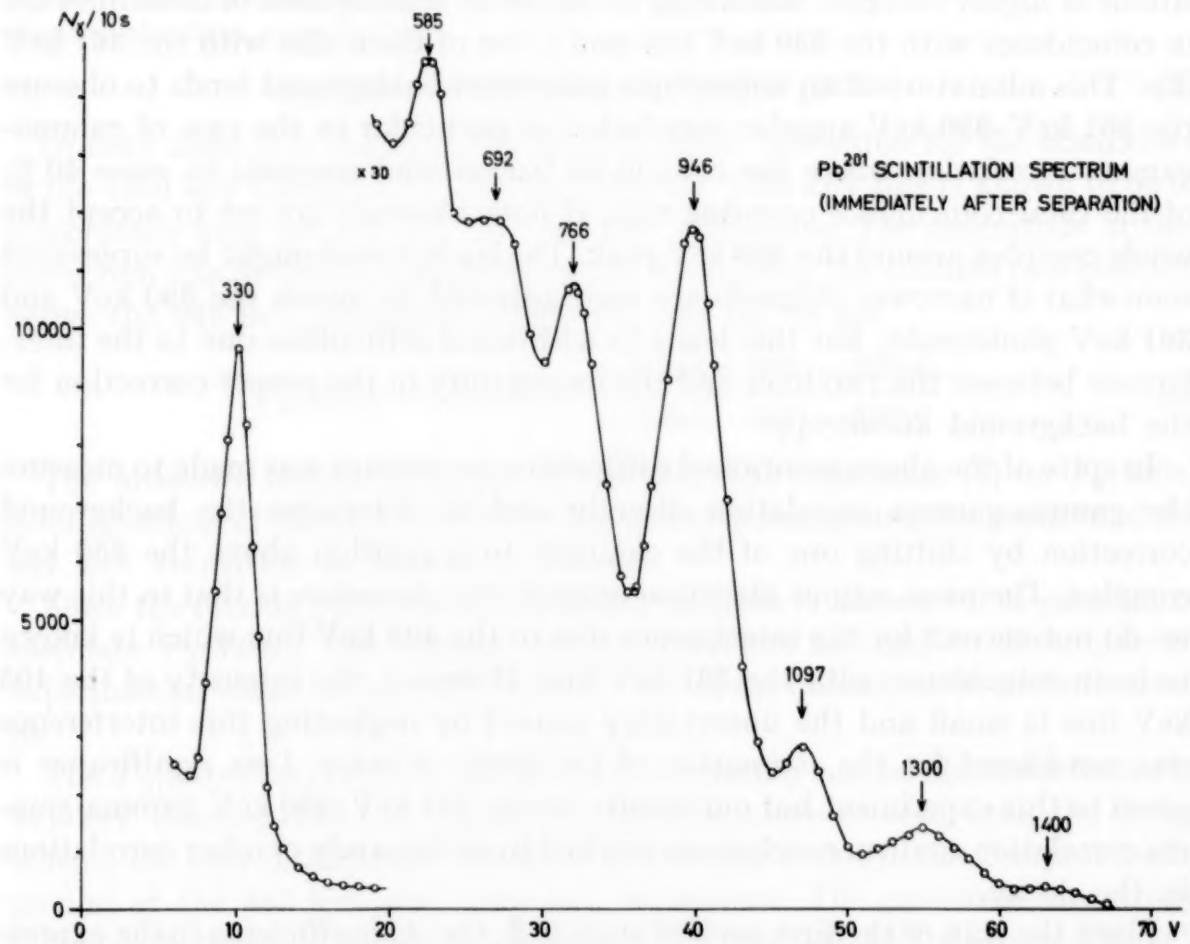

Fig. 3. Scintillation spectrum of Pb^{201} recorded in the gamma channel immediately after the separation.

Finally according to our angular correlations the level at 1277 could be either $\frac{3}{2}$ or $\frac{1}{2}$, but the $\frac{3}{2}$ assignment seems more probable because of the fairly intense feeding directly to this level from the $\frac{5}{2}$-ground state in the mother isotope Pb^{201}.

In this way we have established the positions, spin and parity and shell model assignments of the two first excited levels in Tl^{201}. We have not attempted a further investigation of the decay scheme, since for our present purpose we are only interested in the conversion matrix elements for the $d_{\frac{5}{2}}$ (361 keV) $d_{\frac{3}{2}}$(330 keV)$s_{\frac{1}{2}}$ cascade.

Our experiment is based on a comparison between gamma-gamma and electron-gamma angular correlations. Because of the good resolution of the

magnetic spectrometer the conversion lines of interest for our experiment can easily be distinguished and do not interfere with neighbouring lines present in the spectrum (cf. fig. 2). Unfortunately this is not the case in the gamma channel. As seen in fig. 3 the broad peak at about 350 keV is composed of a complex of photopeaks due to the 310 keV, 330 keV, 361 keV, 394 keV and 405 keV transitions, all superimposed on a weak Compton background due to the transitions of higher energies. According to the decay scheme most of these lines are in coincidence with the 330 keV line and a few of them also with the 361 keV line. This admixture of an anisotropic coincident background tends to obscure the 361 keV–330 keV angular correlation in particular in the case of gamma-gamma correlation where the coincident background amounts to some 40 % of the total coincidence counting rate, if both channels are set to accept the whole complex around the 350 keV peak. The background might be suppressed somewhat if narrower channels are used adjusted to match the 330 keV and 361 keV photopeaks, but this leads to additional difficulties due to the interference between the two lines and the uncertainty in the proper correction for the background anisotropy.

In spite of the above mentioned difficulties an attempt was made to measure the gamma-gamma correlation directly and to determine the background correction by shifting one of the channels to a position above the 350 keV complex. The most serious objection against this procedure is that in this way we do not correct for the interference due to the 405 keV line which is known to be in coincidence with the 361 keV line. However, the intensity of the 405 keV line is small and the uncertainty caused by neglecting this interference was considered for the estimation of the limits of error. Less significance is given to this experiment but our results for the 361 keV–330 keV gamma-gamma correlation confirm conclusions reached from the study of other correlations in the decay.

Since the spin of the first excited state is $\frac{3}{2}$, the A_4 coefficients in the expression for the correlation functions involving the 330 keV cascade are equal to zero. This was, in fact, confirmed in the gamma-gamma correlations where the experimentally determined A_4 coefficients were found to be zero within the limits of experimental errors. The general expression for the angular correlation becomes

$$W(\theta) = 1 + A_2 P_2(\cos\theta), \tag{1}$$

where the A_2 coefficient is a product of two F_2-functions one of which refers to the initial and the other to the following transition in the cascade.

As seen from the decay-scheme and table 2, of all the transitions in the 350 keV complex, only the 330 keV line is in coincidence with the 946 keV transition and, perhaps, also with the 907 keV transition. It is possible to take advantage of this fact in order to derive the information of interest for our present purpose.

If one of the two gamma channels is set to accept the complex peak around 946 keV and the other channel is set at the 330 keV photo-peak, we get for the A_2 coefficient the following expression:

$$A_2\{(946+907)\gamma\text{–}330\gamma\} = F_2^*(\gamma)F_2(330\gamma), \tag{2}$$

where the $F_2^*(\gamma)$ is an "effective" F_2 corresponding to some weighted average of the $F_2(946\gamma)$ and (maybe) the $F_2(907\gamma)$. In the same way we obtain for the gamma-electron correlation

$$A_2\{(946+907)\gamma\text{–}330\text{e}\} = F_2^*(\gamma)F_2(330\text{e}). \tag{3}$$

In both cases it is necessary to apply a minor correction for the admixture of the 1280 keV Compton background since the 1280 keV line is known to be in coincidence with the 361 keV and 330 keV transitions. The magnitude of this correction was determined experimentally by shifting the channel to a position above the 946 keV photopeak. From (2) and (3) we get

$$F_2(330\text{e}) = F_2(330\gamma)\frac{A_2\{(946+907)\gamma\text{–}330\text{e}\}}{A_2\{(946+907)\gamma\text{–}330\gamma\}}. \tag{4}$$

The unknown factor $F_2^*(\gamma)$ is divided out. The expression (4) for $F_2(330\text{e})$ is independent of the above mentioned ambiguity concerning the position of the 907 keV transition in the decay scheme.

Since the mixing ratio of the 330 keV transition is known † it is possible to calculate $F_2(330\gamma)$. The relation (4) can therefore be used to determine an experimental value for $F_2(330\text{e})$, which is one of the quantities we are interested in.

The $F_2(361\text{e})$ function for the 361 keV transition can be obtained from the 361 keV electron–330 keV gamma correlation, since as seen from the decay scheme the only disturbing admixture in this case is due to the Compton background of the 585 keV and 1280 keV transitions. The measured anisotropy therefore becomes a weighted average of the true 361 keV electron–330 keV gamma anisotropy and the 361 keV electron–(585+1280) keV Compton background anisotropy. The true A_2-coefficient is obtained from the experimental value $A_2(\text{exp})$ by means of the relation

$$A_2(\text{true}) = \frac{(1+s)A_2(\text{exp})}{1+s\,F_2(\text{Compton})/F_2(330\gamma)}, \tag{5}$$

where the weighting factor s is given by

$$s = \frac{\bar{C}(\text{Compton})}{\bar{C}(330\gamma)}. \tag{6}$$

$\bar{C}(\text{Compton})$ and $C(330\gamma)$ are the coincidence counting rates averaged over all angles. These relations were used in order to derive the $A_2(\text{true})$ from the

† Cf. discussion below.

measured anisotropy. Finally one has

$$F_2(361\text{e}) = \frac{A_2(\text{true})}{F_2(330\gamma)}, \tag{7}$$

from which we get the $F_2(361\text{e})$ since the $F_2(330\gamma)$ is known.

From the 361 keV gamma–330 keV electron cascade we obtain in exactly the same way the true A_2 coefficient for this cascade and by making use of the already determined $F_2(330\text{e})$ we get

$$F_2(361\gamma) = \frac{A_2(361\gamma\text{–}330\text{e})}{F_2(330\text{e})}. \tag{8}$$

However, $F_2(361\gamma)$ will be less accurately determined since the coincidence background admixture is considerably larger in this case. It is, however, possible to check the value for $F_2(361\gamma)$ obtained from (7) by means of a comparison between the $A_2(361\gamma\text{–}330\gamma)$ experimentally determined (cf. above) and the value obtained by multiplying the $F_2(361\gamma)$ with the known value for $F_2(330\gamma)$ since

$$A_2(361\gamma\text{–}330\gamma) = F_2(361\gamma)F_2(330\gamma). \tag{9}$$

Finally, we also measured the following two gamma-electron correlations:

$$A_2(585\gamma\text{–}361\text{e}) = F_2(585\gamma)F'_2(361\text{e}), \tag{10}$$

$$A_2(585\gamma\text{–}330\text{e}) = F_2(585\gamma)\,F_2(330\text{e})\,\frac{W(\frac{5}{2}\,\frac{5}{2}\,\frac{3}{2}\,\frac{3}{2};\,21)}{W(\frac{5}{2}\,\frac{5}{2}\,\frac{3}{2}\,\frac{3}{2};\,01)}. \tag{11}$$

Bothe these A_2 coefficients were found to be very small. For the 585γ–361e correlation this is to be expected since the $F_2'(361\text{e})$ is small for this almost pure M1 transition. The Racah coefficients coupling the 585 keV and 330 keV transitions leaving the intermediary 361 keV transition unobserved reduces the $A_2(585\gamma\text{–}330\text{e})$ by about 30 %. The fact that the $A_2(585\gamma\text{–}330\text{e})$ is found to be small is then primarily due to a small value for $F_2(585\gamma)$. From the experimental $F_2(585\gamma)$ it is possible to determine $\delta(585)$.

The $A_2(585\gamma\text{–}361\text{e})$ can be used to determine the upper limits for systematic errors, due for instance to a minute residual magnetic interaction between the spectrometer and the gamma channel.

In this way we have obtained the four F_2-functions of interest for the analysis of the conversion matrix elements. In addition we need the conversion coefficients for the 361 keV and 330 keV transitions, none of which has been measured hitherto. It is, however, possible to determine these quantities with a considerable degree of accuracy from our electron-gamma coincidence data. For the 330 keV transition we obtain

$$\kappa_{\text{K}}^{(330)} = \frac{\bar{C}\{(946+907)\gamma\text{–}330\text{e}\}}{\omega f N\{(946+907)\gamma\}}, \tag{12}$$

where $\bar{C}$ is the coincidence counting rate averaged over all angles, ω the transmission of the magnetic spectrometer (equal to the effective solid angle times the detection efficiency) and κ_K is the conversion probability closely related to the internal conversion coefficient

$$\alpha_K = \frac{\kappa_K}{1-\kappa_K\{1+(L+M+\ldots)/K\}}. \tag{13}$$

The K/(L+M+ . . .) ratio is known from the magnetic spectrometer measurements. The transmission of the spectrometer has been measured in three different ways: (1) by means of a calibrated Cs^{137} source, (2) by an experimental calibration using the formula (12) and the 400 keV–279 keV cascade in Tl^{203} where the 279 keV K conversion coefficient has been very accurately determined by several independent groups [4]) and (3) from the 165 keV(M4)–134 keV (E2) cascade in Hg^{197m} making use of the fact that the 165 keV transition is known to be converted to at least 99.7 %. As shown in table 3 the values for ω obtained in these three different ways are in good agreement.

TABLE 3

Summary of spectrometer transmission calibrations

Method used	Spectrometer transmission ω
Calibr. Cs^{137} source	1.12×10^{-2}
Coinc. exp. with Tl^{203} (see text)	1.13×10^{-2}
Coinc. exp. with Hg^{197m}	1.14×10^{-2}
Accepted value	$(1.13\pm0.03)\times10^{-2}$

The main uncertainty in our value for α_K, therefore, stems from the remaining factor f in (12). The factor f is the fraction of $N\{(946+907)\gamma\}$ that is in coincidence with the 330 keV transition. Since we are not sure about the position of the 907 keV transition in the decay scheme we can only assume as extreme cases either 100 % or 0 % coincidence coupling between the 907 keV and the 330 keV transitions. Together with the relative gamma intensities of the 947 keV and the 907 keV transitions this gives the extreme values for f.

In exactly the same way we can also determine the 330 keV conversion coefficient from the 330e–361γ coincidence runs.

Finally, using a slightly modified procedure, we can determine the same conversion coefficients also from the 361e–330γ coincidences together with the relative K line intensities of the 330 keV and 361 keV lines and the gamma single counting rate due to the 330 keV transition. The appropriate relation becomes

$$\kappa_K^{(330)} = \frac{\bar{C}\,(361e\text{–}330\gamma)}{\omega N(330\gamma)}\,\frac{N(330e)}{N(361e)}, \tag{14}$$

which holds exactly. The coefficient $\bar{C}$ is averaged over all angles and corrected for random coincidences. The value obtained from (14) is not subject to the uncertainties caused by the coincidence fraction f in (11) and gives therefore the most precise figure for $\alpha_K^{(330)}$.

Once $\alpha_K^{(330)}$ is determined the $\alpha_K^{(361)}$ can be easily found by means of the relation

$$\alpha_K^{(361)} = \alpha_K^{(330)} \frac{\bar{C}\,(361\text{e}{-}330\gamma)\,\varepsilon^{(361)}\,q^{(361)}}{\bar{C}\,(330\text{e}{-}361\gamma)\,\varepsilon^{(330)}\,q^{(330)}}, \tag{15}$$

which is also exact provided only that the transmission is kept constant. The coincidence counting rates are averaged over all angles and corrected for random coincidences; ε is the efficiency of the scintillation crystal and q is the probability that the pulse produced will be accepted within the discriminator channel. Since (14) contains only the ratios of $\varepsilon^{(361)}/\varepsilon^{(330)}$ and $q^{(330)}/q^{(361)}$ the uncertainties in the absolute values for ε and q give only a minor contribution to the errors in $\alpha_K^{(361)}$, which therefore will be determined with essentially the same degree of accuracy as $\alpha_K^{(330)}$.

3. Experiment

The instruments used for the gamma-gamma and for the electron-gamma correlations were the same as used for the Tl^{203} study [15]).

Sources were produced by (p, 3n) and (p, 5n) reactions with pure thallium in the synchrocyclotron at the Werner Institute in Uppsala. The bombarding energy was 60 MeV. In order to obtain pure Pb^{201} sources the lead activity produced was electromagnetically isotope separated directly on to the 1 mg/cm^2 Al backing used in all our angular correlation experiments.

The correlation runs were stopped after about two halflives. This precaution was taken mainly to avoid perturbations that otherwise might appear due to a minor admixture of Pb^{200} in the separated sources. Both Pb^{201} and Pb^{200} ultimately decay to Hg^{201} and Hg^{200} respectively. Fortunately the levels in Hg^{201} are all below 167 keV [2]) and the decay of Tl^{201}, therefore, does not cause any difficulties in the angular correlation experiments. However, in Hg^{200} levels of considerably higher energies are populated and the cascading transitions to the ground state may possibly affect our correlations. With the precautions taken the total admixture of Tl^{200} during the measuring period was certainly less than 1 %. An estimate of the amount of Tl^{200} admixture was obtained from a measurement of the electron spectrum 72 hours after the electromagnetic separation. The second strongest line in the Tl^{200} decay is to be found at 1205 keV, i.e. in the valley between the 1099 and the 1280 keV photopeaks.

In a similar way the initial Pb^{202} activity was measured to be less than 3 %.

The sources were first carefully centred with respect to the magnetic spectro-

meter and thereupon the centre of rotation of the gamma channel was adjusted to coincide with the centre of the source. After centering the gamma single counting rate was equal for all angles to within 1 % and the residual variations

TABLE 4

Summary of electron-gamma, gamma-electron and gamma-gamma angular correlations studied in Tl^{201}

Source no.	Coincidence combination	Background/true	Measured A_2
1	330e–360γ	0.4 $\pm$0.05	-0.031 ± 0.010
2			-0.044 ± 0.004
3			-0.025 ± 0.015
4			-0.048 ± 0.005
2	330e-background		$+0.081\pm0.005$
			$+0.076\pm0.007$
	330e–360γ	$A_2^{true} = -0.09\pm0.011$	
5	360e–330γ	0.14$\pm$0.02	$+0.001\pm0.003$
5	360e–background		0.000 ± 0.005
	360e–330γ	$A_2^{true} = +0.001\pm0.004$	
6	330e–946γ	0.07$\pm$0.02	$+0.191\pm0.008$
7			$+0.195\pm0.004$
8			$+0.180\pm0.015$
5	330e-background		$+0.02\ \pm0.02$
7			
	330e–946γ	$A_2^{true} = 0.210\pm0.007$	
6	330e–585γ	$A_2^{true} = +0.022\pm0.015$	
8	360e–585γ	$A_2^{true} = -0.013\pm0.008$	
2	330γ-360γ	0.6 $\pm$0.05	-0.025 ± 0.005
3			-0.037 ± 0.008
5			-0.012 ± 0.006
3	330γ background		$+0.277\pm0.01$
	360γ background		$+0.255\pm0.01$
	330γ–360γ	$A_2^{true} = -0.20\pm0.08$	
9	330γ–946γ	0.35$\pm$0.03	$+0.54\ \pm0.008$
10			$+0.54\ \pm0.010$
11			$+0.565\pm0.010$
10	330γ-background		$+0.07\ \pm0.03$
10	946γ-background		$+0.05\ \pm0.03$
	330γ–946γ	$A_2^{true} = 0.72\pm0.04$	

were corrected for in the usual way by dividing the coincidence counting rate with the gamma single counting rate. A slightly different procedure was used in one case, namely for the 361γ–330e correlation, where the centering and the normalization was made by means of the total complex around 350 keV in

order to avoid introducing a possible systematic error caused by the interference of the unresolved strong 330 keV photopeak on the gamma single counting rate at 361 keV. Minor gain variations in the electron multiplier due to a residual magnetic interaction between the two channels could otherwise have given rise to a false angular dependence in the single counting rate.

The angular setting was changed every 300 seconds and coincidences were taken for the angles 90°, 135°, 180° and 225° in the gamma-gamma runs and for the angles 90°, 180° and 270° in the electron-gamma runs. 11 sources were used to obtain the 24 runs, summarized in table 4. As seen in the table corresponding runs generally taken with different sources are in good agreement. The A_2 (measured) given in the table have been corrected in the usual way for the finite aperture angles in the two channels. The aperture angle corrections were the same as in the Tl^{203} experiment, i.e. 1.06 for the gamma channel and 1.10 for the electron channel.

Since no attenuation effects due to extra nuclear field effects were found for the Tl^{203} correlations we assume that there is no observable attenuations in the Tl^{201} case either, in particular since the lifetime of the intermediate state is even shorter in this case. For the sources used in the electron-gamma correlations no attenuation due to electron scattering in the source and in the backing support is to be expected. Our average A_2 (true) given in table 4 should therefore correspond to the real unperturbed angular correlations for the corresponding cascades.

3.1a. CONVERSION COEFFICIENT OF THE 330 keV TRANSITION

The conversion coefficient of the 330 keV transition was determined from the coincidence counting rates averaged over all angles and from the corresponding single counting rates by means of the relations (12), (13) and (14).

TABLE 5

Summary of experimental values for $\kappa_K^{(330)}$

Method used	$\kappa_K^{(330)} \times 10^2$
$\frac{\bar{C}(330e^- - 361\gamma)}{N(361\,\gamma)}$	10.0 ± 0.7
$\frac{\bar{C}(361e^- - 330\gamma)}{N(330\,\gamma)}$	9.1 ± 0.7
$\frac{C(330e^- - 946\gamma)}{N(946\,\gamma)}$	$\geqq 7.4$
N_0 determined in the $C(361\ e^- - 330\,\gamma)$ run	10.1 ± 0.6
Adopted average	9.8 ± 0.6

The results obtained are summarized in table 5. The value for the effective transmission of the spectrometer was taken from table 3.

3.1b. CONVERSION COEFFICIENT OF THE 361 keV TRANSITION

This conversion coefficient was obtained from the already determined $\alpha_K^{(330)}$ and from the 361e–330γ and 361γ–330e coincidence runs using the relation (15). For the ratio $\varepsilon^{(361)}/\varepsilon^{(330)}$ a value of 0.95 was used obtained from the tables published by Heath [5]). The uncertainty in $q^{(361)}/q^{(330)}$ was taken into account for the estimation of the errors. The experimental result was

$$\alpha_K^{(361)} = 0.21 \pm 0.025.$$

This value shows that the 361 keV transitions is of predominantly M1 character.

3.2a. (946+907) keV–330 keV CORRELATIONS

As shown in table 4 we have found the following values for the gamma-electron and gamma-gamma correlations:

$$A_2\{(946+907)\gamma\text{–}330\text{e}\} = F_2^*(\gamma)F_2(330\text{e}) = +0.210 \pm 0.007, \quad (2)$$

$$A_2\{(946+907)\gamma\text{–}330\gamma\} = F_2^*(\gamma)F_2(330\gamma) = +0.72 \pm 0.04, \quad (3)$$

where $F_2^*(\gamma)$ is the "effective" F_2 function defined above.

The factor $F_2(330\gamma)$ is a function of the M1/E2 mixing ratio $\delta(330)$ of the 330 keV transition. A value for $\delta(330)$ can be obtained from the conversion ratios recently measured by Lindskog *et al.* [1]). Due to the possible existence of anomalous conversion matrix elements in the case of this retarded M1 transition a determination of the mixing ratio from the conversion ratios might be in question. However, it seems possible to draw conclusions on the basis of an analogy between the two very similar transitions in Tl^{203} and Tl^{201}. As shown in table 6 the sub-shell ratios for these two transitions are remarkably similar indicating that the mixing ratios of the 279 keV transition in Tl^{203} and the 330 keV transition in Tl^{201} are almost exactly equal. The mixing ratio of the 279

TABLE 6

Comparion between mixing ratios in Tl^{203} and Tl^{201} (quoted from Lindskog *et al.* [1]))

	Tl^{203} 279 keV transition			Tl^{201} 330 keV transition		
Shell	Ratio	Mixing ratio (E2/M1)		Ratio	Mixing ratio (E2/M1)	
		Rose	Sliv		Rose	Sliv
K/L_I+L_{II}	3.9 ± 0.1	2.6 ± 0.5	2.0 ± 0.4	4.2 ± 0.2	2.9 ± 0.6	2.1 ± 0.6
L_I+L_{II}/L_{III}	4.8 ± 0.1	2.3 ± 0.2	2.5 ± 0.3	6.5 ± 0.5	2.2 ± 0.3	2.3 ± 0.4
McGowan and Stelson [6])		2.25 ± 0.25				

keV transition has been accurately determined by means of a polarization-direction experiment due to McGowan and Stelson [6]). Their value is independent of the conversion matrix elements. The fact that the value obtained from the conversion ratios is in agreement within the limits of error, with McGowan and Stelson's value shows that the dynamic effects do not show up to any observable amount in the conversion ratios of the 279 keV transition in Tl^{203}. We assume that this holds also for the analogous 330 keV transition in Tl^{201} and obtain in this way

$$\delta(330) = \sqrt{\frac{M1}{E2}} = +0.68 \pm 0.07.$$

As in the case of Tl^{203} the sign of δ must be positive. This can be seen as follows. Regardless of the sign of $\delta(330)$, $F_2(330e)$ is always negative. Since (2) and (3) have the same sign, $F_2(330\gamma)$ must also be negative, which is only possible for a positive $\delta(330)$.

The value for $\delta(330)$ determined in this way is not very precise and may be slightly affected by dynamic factors in spite of the fact that no such effects were seen in the case of Tl^{203}. Most fortunately, however, the $F_2(330\gamma)$ function has a broad maximum around our value for $\delta(330)$ (cf. fig. 4). The value for

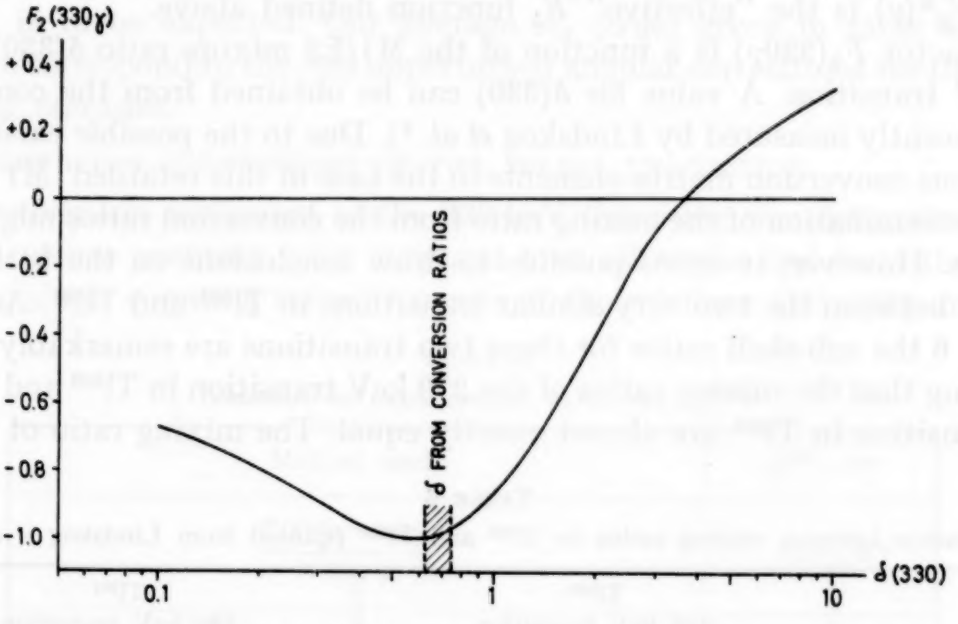

Fig. 4. Determination of $F_2(330\gamma)$ value from the $\delta(330)$ value given in table 6.

$F_2(330\gamma)$ is, therefore, very accurately determined in spite of the above-mentioned uncertainties in $\delta(330)$. For $\delta(330) = 0.68 \pm 0.07$ we get

$$F_2(330\gamma) = -0.99 \pm 0.01.$$

Using this value for $F_2(330\gamma)$ we get from (2), (3) and (4)

$$F_2(330e) = -0.29 \pm 0.025.$$

3.2b. 361 keV ELECTRON–330 keV GAMMA CORRELATION

Using the value of $F_2(330\gamma)$ obtained above and our experimental A_2 given in table 4 we get

$$A_2(361\text{e}-330\gamma) = F_2(361\text{e})F_2(330\gamma) = +0.001\pm0.004,$$
$$F_2(361\text{e}) = -0.001\pm0.004. \tag{16}$$

3.2c. 361 keV GAMMA–330 keV ELECTRON CORRELATION

From the experimental A_2 value found for this correlation (table 4) and the $F_2(330\text{e})$ obtained in the preceding section we get

$$A_2(361\gamma—330\text{e}) = F_2(361\gamma)F_2(330\text{e}) = -0.09\pm0.01,$$
$$F_2(361\gamma) = +0.31\pm0.06. \tag{17}$$

It has already been shown that the internal conversion coefficient for the 361 keV transition indicates an almost pure M1 character. Consequently the

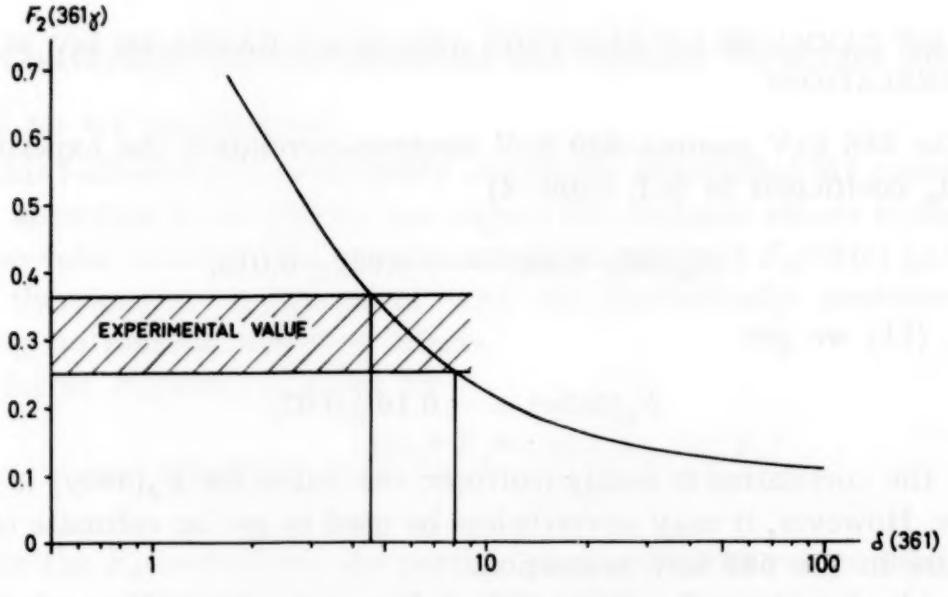

Fig. 5. Determination of $\delta(361)$ from the experimental $F_2(361\gamma)$ value derived from the gamma-electron correlation.

possible spin assignments for the second excited level are $\frac{1}{2}$, $\frac{3}{2}$ and $\frac{5}{2}$. From $F_2(361\text{e})$ and $F_2(361\gamma)$ it can be shown that there is only one possible alternative, namely $\frac{5}{2}$, corresponding to the shell model level at $d_{\frac{5}{2}}$. From $F_2(361\gamma)$ and the spin sequence $\frac{5}{2} \rightarrow \frac{3}{2}$ the mixing ratio of the 361 keV transition is determined. We obtain (cf. fig. 5)

$$+4.55 \leqq \delta(361) \leqq +8.0.$$

In agreement with the conversion coefficient the angular correlation shows that the 361 keV transition is almost pure M1 with an E2 admixture of some 3 %. This may be compared with the analogous 400 keV transition in Tl^{203} where the E2 admixture was found to be 0.06 % [$\delta(400, Tl^{203}) = +41 \pm 7$, cf. preceding paper].

3.2d. 361 keV GAMMA–330 keV GAMMA CORRELATION

From $F_2(361\gamma)$ and $F_2(330\gamma)$ we can predict a value for $A_2(361\gamma\text{–}330\gamma)$

$$A_2^{\text{predicted}}(361\gamma\text{–}330\gamma) = -0.31 \pm 0.06.$$

This value is to be compared with the experimental result given in table 4. As already mentioned this gamma-gamma correlation is difficult to determine because of the large contribution of anisotropic background. Nevertheless we get a reasonable agreement between the predicted and the experimental A_2 coefficients.

3.2e. 585 keV GAMMA–330 keV ELECTRON AND 585 keV GAMMA–361 keV ELECTRON CORRELATIONS

For the 585 keV gamma–330 keV electron-correlation the experimentally found A_2 coefficient is (c.f. table 4)

$$A_2(585\gamma\text{–}330\text{e}) = +0.022 \pm 0.015.$$

From (11) we get

$$F_2(585\gamma) = -0.10 \pm 0.07.$$

Since the correlation is nearly isotropic the value for $F_2(585\gamma)$ is very inaccurate. However, it may nevertheless be used to get an estimate of the E2 admixture in the 585 keV transition.

It may be seen from the (946+907) keV gamma-330 keV angular correlations that the spin of the 1279 keV level must be $\frac{1}{2}$ or $\frac{3}{2}$. The conversion coefficient of the 585 keV transition can be estimated from

$$\kappa_K^{(585)} = \kappa_K^{(330)} \frac{N(330\text{e})}{\bar{C}(585\gamma\text{–}330\text{e})} (1 - \kappa_{tot}^{585}) \Omega \varepsilon(585) R^{(361)}, \qquad (18)$$

where Ω is the solid angle of the gamma counter and $R^{(361)}$ is the fraction of all transitions from the 691 keV level that goes through the 361 keV transition. Though the value for the conversion coefficient of the 585 keV transition, obtained from (18) is not very accurate it is sufficient to be used as a guide for

the multipolarity and character assignment. We get

$$\alpha_K^{(585)} = 0.06 \pm 0.01,$$

in accordance with the theoretical value from Sliv and Band for an M1 transition ($\beta_1 = 0.056$, $\alpha_2 = 0.0125$, $\beta_2 = 0.12$). A pure E2 can be excluded and the spin of the 1272 keV level becomes $\frac{3}{2}$.

For the spin sequence $\frac{3}{2} \rightarrow \frac{5}{2}$ and a predominantly M1 transition the correlation experiments give

$$+3.7 \leqq \delta(585\gamma) \leqq +4.5,$$

corresponding to an E2 admixture of about 6 % in accordance with the experimental $\alpha_K^{(585)}$.

The 585 keV gamma-361 keV electron correlation was found to be nearly isotropic as one should expect since the F'_2(361e) is small (= +0.024). This may be considered as experimental check for systematic errors present in our experiment. It is seen from table 6 that these errors should be well within the limits of statistical errors given in the table.

4. Conversion Matrix Elements and Nuclear Structure Effects

4.1. THE 361 keV TRANSITION

For this l-allowed and presumably essentially unretarded M1 transition one should, according to the theory, not expect the dynamic effects to show up to any observable amount. The experimentally determined F_2(361e) and α_K(361) should therefore be in agreement with the theoretically predicted values, assuming no nuclear structure effects.

The factor F_2(361e) is given by

$$F_2(361\mathrm{e}) = \frac{p^2 b_2^{\mathrm{m}} F_2^{\mathrm{m}} + 2p b_2 F_2 + b_2^{\mathrm{e}} F_2^{\mathrm{e}}}{1+p^2}. \tag{19}$$

Using for the F_2-coefficients and particle parameters the values obtained from Biedenharn and Rose's tables and for the mixing parameter †

$$p = \delta \sqrt{\frac{\beta_1(\lambda = 1)}{\alpha_2}} \tag{20}$$

the value $+9.8 \leqq p \leqq +17.0$, corresponding to the δ(361) values given above and the $\beta_1(\lambda = 1)$ and α_2 obtained from Sliv and Band's tables, the theoretical value for F_2(361e) becomes

$$F_2(361\mathrm{e}, \text{theor.}) = -0.0055 \pm 0.0025.$$

† The parameter λ is defined in part (I). The value $\lambda = 1$ corresponds to the "surface current" model used by Sliv and Band.

TABLE 7

The particle parameters $b_2^m(\lambda)$ and $b_2(\lambda)$ for $Z = 81$, $E = 330$ keV

λ	b_2	b_2^m
−10	−0.1762	0.0771
−5	−0.1809	0.0852
0	−0.1868	0.0951
5	−0.1950	0.1077
10	−0.2055	0.1239
15	−0.2205	0.1452
20	−0.2435	0.1734
25	−0.2822	0.2074
30	−0.3569	0.2080
55	0.0254	−0.2482
60	0.0490	−0.1911
65	0.0644	−0.1548
70	0.0751	−0.1299
75	0.0831	−0.1119
80	0.0892	−0.0981
85	0.0940	−0.0874
90	0.0979	−0.0787

The value $C(Z, k) = 0.0274$ has been used in the calculations.

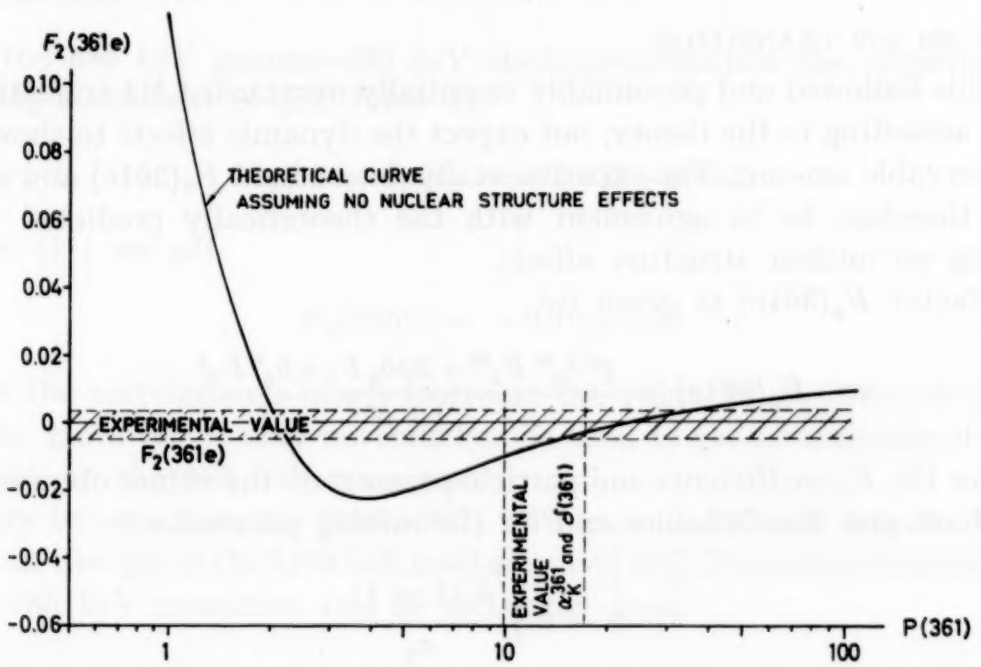

Fig. 6. Comparison between theory and experimental results for the 361 keV transition.

The particle parameters given in Biedenharn and Rose are calculated in the point nucleus approximation. Taking (static) finite size effects into account we get slightly modified values for b_2^m and b_2(cf. table 7), which result in

$$F_2(361\text{e, theor.}, \lambda = 1) = -0.006 \pm 0.0031,$$

in good agreement with the experimental value obtained above (cf. fig. 6).

However, due to cancellation the $F_2(361e)$ is very insensitive to λ, i.e. to nuclear structure effects, and large λ values cannot be excluded from the angular correlation results. For a predominant M1 transition, however, the conversion coefficient becomes a fairly sensitive measure of λ, since

$$\beta_1(\lambda) = \beta_1(\lambda = 1)\{1-(\lambda-1)C(Z, k)\}^2, \tag{21}$$

where $C(Z, k)$ is tabulated by Church and Weneser [7] †

The experimental β_1 is obtained from the conversion coefficient $\alpha_K(361)$ and the mixing ratio $\delta(361)$,

$$\beta_1(\text{exp}) = \frac{(1+\delta^2)\alpha_{\text{exp}}-\alpha_2}{\delta^2}. \tag{22}$$

From α_{exp}, $\delta(361)$ and eq. (22) we get, using the theoretical value for α_2 obtained from Sliv and Band,

$$\beta_1(\text{exp}) = 0.22\pm0.025$$

in perfect agreement with the theoretical value for $\lambda = 1$ obtained from Sliv and Band

$$\beta_1(\lambda = 1) = 0.20.$$

The λ values compatible with our experimental results are according to (21) and (19)

$$-3 \leqq \lambda \leqq +1.5.$$

4.2. THE 330 keV TRANSITION

For this strongly retarded M1 transition nuclear structure effects are expected to show up in $F_2(e)$ and α_K. The $F_2(330e)$ function is given by

$$F_2(e) = \frac{p^2(\lambda)b_2^{m}(\lambda)F_2^{m}+2p(\lambda)b_2(\lambda)F_2+b_2^{e}F_2^{e}}{1+p^2(\lambda)}. \tag{23}$$

The particle parameters b_2^{m} and b_2 were calculated using the methods outlined in the Appendix. The values for the radial matrix elements were obtained by linear interpolation in tables of Rose [8]. The calculations were performed with the electronic computer FACIT in Stockholm. The results are given in table 7.

For our interpretation we use the representation discussed in (I). Fig.7

† The values for $C(Z, k)$ given in ref. [7]) should be corrected for a factor $\sqrt{\frac{3}{5}}$ omitted in the calculations [12]).

(upper part) shows $\beta_1(\lambda)$ and (lower part) $F_2(e, \lambda)$ versus λ for $\delta = +0.65$. Our experimental results are consistent with the following values:

$$\beta_1 \rightarrow \lambda = 1 \pm 3 \quad \text{or} \quad \lambda = 74 \pm 2, \qquad F_2(e) \rightarrow \lambda = 22.5 \pm 1.5 \quad \text{or} \quad \lambda = 76 \pm 3.$$

Obviously the small λ-values have to be excluded, while the value $\lambda \approx 75$ gives good agreement between the theory and our conversion coefficient and angular correlation measurements.

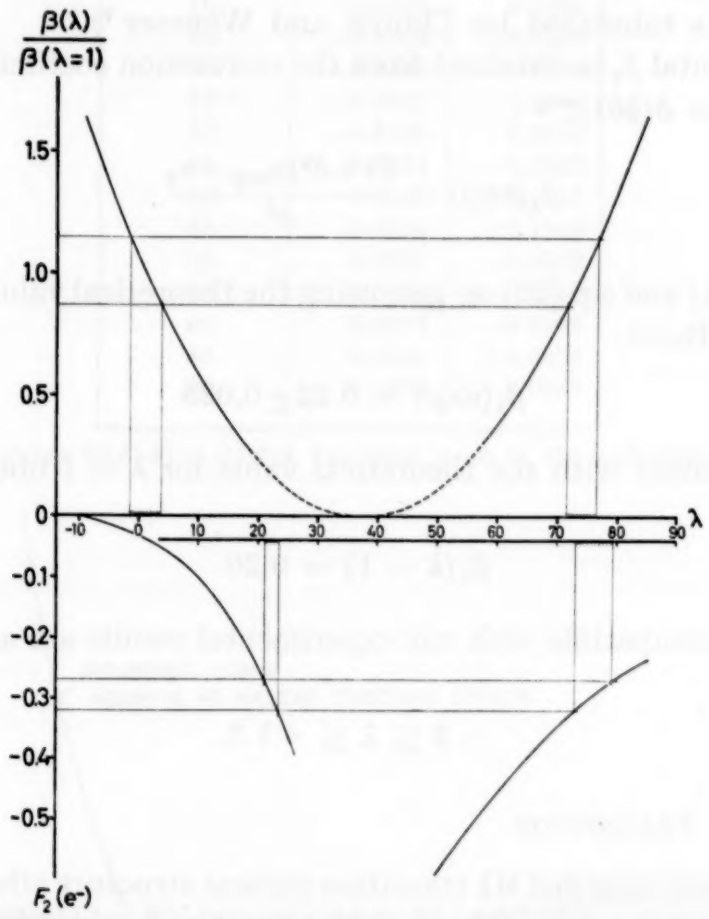

Fig. 7. To illustrate the existence of large nuclear structure dependent effects in the K-conversion process of the 330 keV transition in Tl^{201}. Upper half of the figure: The theoretical K-shell M1 conversion coefficient $\beta_1(\lambda)$ divided by the finite size corrected value $\beta_1(\text{Sliv})$ as a function of λ. Lower half of the figure: The theoretical angular correlation function $F_2(e\lambda)$ as a function of λ. Horizontal lines correspond to the experimental values (with errors). Consistent results are obtained for $\lambda = +74 \pm 2$ .The theoretical curves correspond to $\delta = +0.65$.

The interpretation of our experimental results, however, depends on the value chosen for the mixing ratio $\delta(330)$. As mentioned above the value $\delta = +0.68 \pm 0.07$ was determined from the K/L and L-subshell ratios. The large λ-value obtained above shows that the M1 internal conversion process is strongly affected by the penetration effects. Nevertheless the $K/(L_I + L_{II})$ should be fairly insensitive to λ. This is confirmed in the case of Tl^{203}(cf. table 6).

To illustrate how a change in δ will effect our results we have also reproduced

our results in the $1-(\lambda-1)C(Z,k)$ versus δ representation (cf. (I)). There is clearly no region of agreement for any value of δ around $1-(\lambda-1)C(Z,k) \approx 1$, i.e. for small λ-values. But there is an overlap area around $1-(\lambda-1)C(Z,k) \approx -1$ corresponding to $\lambda \approx +70$ and $\delta \approx +0.7$ in agreement with the value obtained from the conversion ratios.

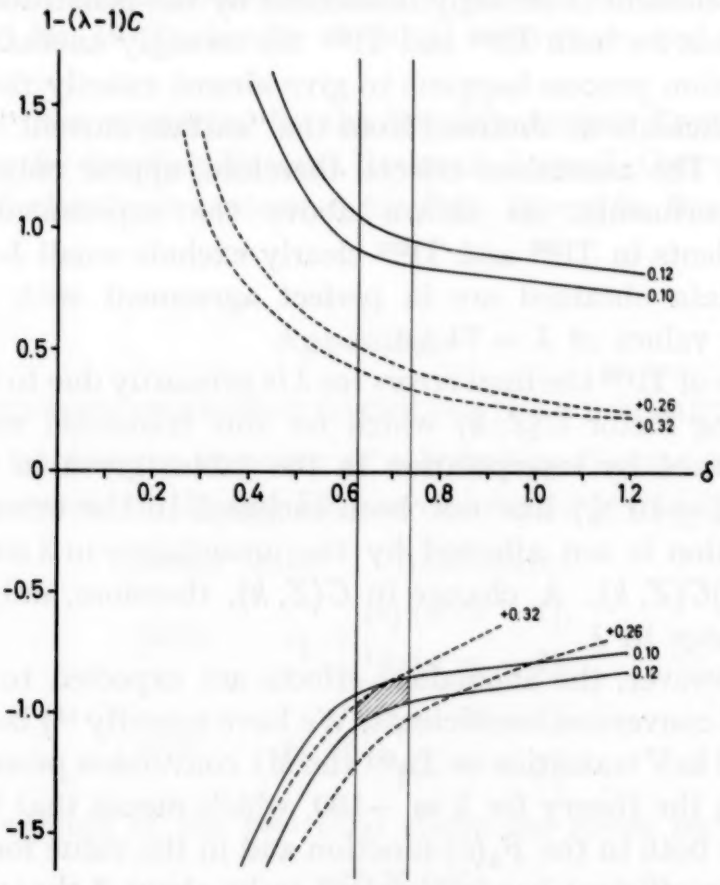

Fig. 8. To illustrate the δ dependence of the results obtained from experimental determinations of the K-conversion coefficient and the angular correlations. In the $1-(\lambda-1)C(Z,k)$ versus δ plane are given the theoretical curves corresponding to the experimental values for the conversion coefficient (solid curves) and for the ratio $F_2(e)/F_2(\gamma)$ (dashed curves). The vertical lines for $\delta = +0.68 \pm 0.07$ correspond to the values for the M1/E2 mixing ratio obtained from the K/L_I+L_{II} and L_I+L_{II}/L_{III} ratios (cf. table 6 and ref. [1])). The vertical lines intersect the overlap area at $1-(\lambda-1)C(Z,k) \approx -1$, which for $C(Z,k) = 0.0274$ gives $\lambda \approx 75$.

As in the case of Tl^{203}(cf. (I)) we observe a value for the ratio $A_2(\gamma e)/A_2(\gamma\gamma)$ which is *larger* than the theoretical prediction for $\lambda = 1$. The disagreement is even more pronounced in the case of Tl^{201}. Scattering of the conversion electrons would tend to reduce this ratio and consequently imply an increased discrepancy for $\lambda = 1$ as compared to the value used in our interpretation above.

5. Conclusions

The conclusions reached in (I) have been confirmed. For the allowed M1 transition the theory and the experimental results show no disagreement and,

as the theory predicts, the nuclear structure dependent conversion matrix element can in this case be neglected in comparison with the normal conversion matrix element, which for this allowed transition is expected to have its dimensional value.

For the *l*-forbidden and strongly retarded M1-transition the internal conversion matrix element is strongly influenced by the penetration effects. It is a curious fact that for both Tl^{203} and Tl^{201} the strongly anomalous M1 K-shell internal conversion process happens to give almost exactly the same internal conversion coefficients as obtained from the "surface current" model used by Sliv and Band. The anomalous effects, therefore, appear only in the angular correlation experiments. As shown above the experimentally measured $A_2(\gamma, \mathrm{e})$ coefficients in Tl^{203} and Tl^{201} clearly exclude small λ-values, but the experimental data obtained are in perfect agreement with the theoretical predictions for values of $\lambda = 74 \pm 3$.

As in the case of Tl^{203} the final errors for λ is primarily due to the uncertainty in the weighting factor $C(Z, k)$ which for this transition was taken to be 0.0274 as obtained by interpolation in the tables given in refs. [7, 12]). This uncertainty ($\leqq \pm 10\,\%$) has not been included in the errors given above. Our interpretation is not affected by the uncertainty in λ since the decisive factor is $(\lambda - 1)C(Z, k)$. A change in $C(Z, k)$, therefore, only means a corresponding change in λ.

Generally, however, the anomalous effects are expected to appear also in the M1 internal conversion coefficients. We have recently [14]) been able to show that for the 482 keV transition in Ta^{181} the M1 conversion process gives a good agreement with the theory for $\lambda \approx -100$, which means that the penetration effects show up both in the $F_2(\mathrm{e})$-function and in the value for β_1. In fact the M1 conversion coefficient has been found to be about 8 times as large as the value tabulated by Sliv and Band.

The existence of large nuclear structure dependent contributions to the internal conversion matrix elements for retarded M1 transitions has opened up the possibility of using the penetration matrix elements to determine the distribution of transition charges and currents in the nucleus. Thus, for these M1 transitions, the internal conversion process provides additional information about the nuclear structure. As shown above both measurements of internal conversion coefficients and electron-gamma angular correlations are necessary for a unique determination of the relative weight of the penetration matrix elements. From a measurement of the lifetime of the nuclear level the absolute value of the penetration matrix element can be obtained.

The authors wish to express their sincere gratitude to Professor Kai Siegbahn for having provided excellent research facilities. We are also much indebted to Drs. E. L. Church and J. Weneser for their valuable comments on the theoreti-

cal aspects of this work in particular concerning the calculations of the particle parameters. The numerical computations of these parameters were performed at the electronic computor FACIT in Stockholm. We wish to thank Mr. L. von Sydow for his valuable aid in coding the programme for the computor. We also thank the cyclotron and isotope separator crews of the Werner Institute for several irradiations and separations. Finally, we wish to thank fil. mag. Inga-Britt Häller and Mr. W. Parker for chemical separations and vacuum evaporations.

The work has been supported by the Swedish Atomic Energy Commission and, in part, by the Swedish Natural Research Council. One of us (B. v. N.) thanks the Netherland's Organisation for Pure Scientific Research (Z.W.O.) for a grant.

Appendix

A.1. STATIC FINITE SIZE CORRECTION TO THE PARTICLE PARAMETERS b_2^{m}, b_2 and b_2^{e}

K-conversion implies the emission of a bound $s_{\frac{1}{2}}$ electron into one of two final continuum states. In M1 and E2 conversions these transitions are

bound state: final state:

$$\text{(M1)} \qquad s_{\frac{1}{2}} \rightarrow \begin{cases} s_{\frac{1}{2}}\,(\kappa = -1), \\ d_{\frac{3}{2}}\,(\kappa = +2), \end{cases}$$

$$\text{(E2)} \qquad s_{\frac{1}{2}} \rightarrow \begin{cases} d_{\frac{3}{2}}\,(\kappa = +2), \\ d_{\frac{5}{2}}\,(\kappa = -3). \end{cases}$$

The relative weights of the two final states are given by [9])

$$T_{\mathrm{m}} = \frac{e^{i\delta_2} R_2(\mathrm{m})}{e^{i\delta_{-1}} R_{-1}(\mathrm{m})}$$

and

$$T_{\mathrm{e}} = 2\,\frac{e^{i\delta_2}}{e^{i\delta_{-3}}}\,\frac{R_2(\mathrm{e})}{R_{-3}(\mathrm{e})},$$

where δ_κ are the appropriate Coulomb phases and $R_\kappa(\mathrm{m/e})$ the electron radial matrix elements.

The particle parameters are given by

$$b_2^{\mathrm{m}}(\mathrm{M1}) = 1 - 2\,\frac{|1-T_{\mathrm{m}}|^2}{2+|T_{\mathrm{m}}|^2},$$

$$b_2(\mathrm{M1+E2}) = \frac{\mathrm{Re}\; e^{i(\theta_{\mathrm{e}}-\theta_{\mathrm{m}})}\left(1+\dfrac{2}{T_{\mathrm{m}}{}^*}\right)\left(1-\dfrac{2}{T_{\mathrm{e}}}\right)}{\sqrt{5}\sqrt{\left(1+\dfrac{2}{|T_{\mathrm{m}}|^2}\right)\left(1+\dfrac{6}{|T_{\mathrm{e}}|^2}\right)}}$$

and

$$b_2^{e}(\mathrm{E2}) = 1+\tfrac{2}{5}\frac{|3+T_e|^2}{6+|T_e|^2}.$$

The conversion coefficients become the sum of the two partial conversion coefficients

$$\alpha_K(\mathrm{M1}) = \frac{2\pi\alpha k}{3}\{2|R_{-1}|^2+|R_2|^2\},$$

$$\alpha_K(\mathrm{E2}) = \frac{\pi\alpha k}{15}\{3|R_{-3}|^2+2|R_2|^2\}.$$

Rose [8]) has tabulated the radial matrix elements in the unscreened, point nucleus, approximation. From these matrix elements the particle parameters [9]) and the internal conversion coefficients [10]) have been calculated. Later the effects of the finite size of the nucleus was taken into account for the calculation of conversion coefficients [8]). The particle parameters, however, are at present only available in the point nucleus approximation.

For the analysis of the electron-gamma angular correlation experiments it was necessary to take finite nuclear size effects into consideration. These will affect the Coulomb phases and the radial matrix elements. It has been shown [11]) recently, however, that the phase differences are almost uneffected. For this reason we have neglected the change in the phase factors. A comparison with the finite size corrected phases tabulated by Sliv and Volchok showed that this was well justified in our case.

A.2. THE M1 CONVERSION PROCESS

The predominant transition is the $s_{\frac{1}{2}} \rightarrow s_{\frac{1}{2}}$ which for heavier elements and low energy transitions is known to be strongly affected by the nuclear finite size. This effect can be taken into account in an approximate way [12]) by adding a pure imaginary increment $i\varepsilon$ to the radial matrix element R_{-1} tabulated by Rose. This imaginary increment is determined by the equation

$$\beta_1^{K}(\mathrm{Sliv}) = \frac{2\pi\alpha k}{3}\{2|R_{-1}-i\varepsilon|^2+|R_2|^2\}.$$

Having determined $i\varepsilon$ we replace R_{-1} in the expression above with a modified radial matrix element $R'_{-1} = R_{-1}-i\varepsilon$. In this way the *static* effects are taken into account.

To correct for the dynamic i.e. λ-dependent effects, we add an additional imaginary increment to R'_{-1} and obtain a λ-dependent radial matrix element

defined as

$$R''_{-1} = R^{\text{Rose}}_{-1} - i\left\{\varepsilon + (\lambda-1)C(Z,k)\frac{\beta_1{}^{\text{K}}(\text{Sliv})\sqrt{\dfrac{3}{4\pi\alpha k}}}{\sqrt{\beta_1{}^{\text{K}}(\text{Sliv})-\beta_1{}^{\text{K}}(\kappa=+2)}}\right\}.$$

The particle parameters $b_2{}^{\text{m}}$ and b_2 are calculated using R''_{-1} and $R_2{}^{\text{Rose}}$ †.

A.3. THE E2 CONVERSION PROCESS

Due to cancellation in the radial matrix elements for the $s_{\frac{1}{2}} \rightarrow d_{\frac{3}{2}}$ transition, the dominant transition in this case is the one to the state of higher j. This is expected to be practically unaffected by the finite size effects and explains why the E2 conversion coefficients are only slightly different in the point nucleus and finite size approximations. This, however, does not necessarily imply that the finite size effects can be safely neglected in the calculations of $b_2{}^{\text{e}}$ and b_2, since the angular correlation parameters depend on the ratio of the amplitudes of the two possible final states, while the conversion coefficient is proportional to the sum of the square of the amplitudes. Recently, Ustinova [13]) has calculated the parameter $b_2{}^{\text{e}}$ in the finite size approximation (surface current model). The deviations from the point nucleus values, tabulated by Biedenharn and Rose, were found to be fairly small ($\leqq 5$ % for the transitions of interest in our case). We have estimated the E2 finite size effects on the mixing parameter, making use of Ustinova's results. The method is similar to the M1 correction discussed above. To the point nucleus value for $R_2(\text{e})$ a pure imaginary increment $i\varphi$ was added. The value for $i\varphi$ was determined by the requirement

$$b_2{}^{\text{e}}(\text{Ustinova}) = 1+\tfrac{2}{5}\frac{|3+T'_{\text{e}}|^2}{6+|T'_{\text{e}}|^2},$$

where T'_{e} is defined as

$$T'_{\text{e}} = 2\frac{e^{i\delta_2}}{e^{i\delta_{-3}}}\frac{R'_2(\text{e})}{R_{-3}(\text{e})}.$$

To check the method the E2 conversion coefficient was calculated using $R'_2(\text{e})$ instead of the point nucleus $R_2(\text{e})$. The conversion coefficient thus obtained should be approximately corrected for the nuclear finite size effects and consequently be in reasonable agreement with the values given by Sliv and Band. This was found to be the case. Our calculated conversion coefficients agree to within a few tenth of a percent with the finite size values, but differ by some percent from the point nucleus E2 conversion coefficients.

The b_2 parameters thus corrected for static nuclear finite size effects are nearly equal to the point nucleus values.

† These calculations were performed at the electronic computer FACIT in Stockholm. We would like to point out that the programme for $b_2{}^{\text{m}}(\lambda)$ and $b_2(\lambda)$ is available to those who may be interested.

Note added in proof: Through the courtesy of Professor L. A. Sliv of the Physico-Technical Institute of Leningrad we obtained his finite size and screening corrected radial matrix elements for $Z = 81$, 84, 88 and 92. This allows us to check the approximate method outlined in the Appendix to the present paper. A comparison shows, on the whole, a very good agreement and we may now conclude that our particle parameters corrected for the finite size of the nucleus should be correct to within a few per cent.

We would like to express our sincere gratitude to Professor Sliv and his co-workers for having provided us with these radial matrix elements prior to publication.

References

1) J. Lindskog, E. Bashandy and T. R. Gerholm, Nuclear Physics **16** (1960) 175
2) K. Bergkvist, I. Bergström, C. Herrlander, S. Hultberg, H. Slätis, E. Sokolowski, A. Wapstra and T. Wiedling, Phil. Mag. **46** (1955) 65
3) I. Lindgren, C. M. Johansson and S. Axensten, Phys. Rev. Letters **1** (1958) 473
4) A. H. Wapstra and G. J. Nijgh, Nuclear Physics **1** (1956) 245
5) R. L. Heath, AEC Research and Development Report IDO-16408, Phillips Petroleum Co., Atomic Energy Div., Idaho Falls Idaho (1957);
S. M. Vegors, Jr., L. L. Marsden and R. L. Heath, AEC Research and Development Report IDO-16370, Phillips Petroleum Co., Atomic Energy Division, Idaho Falls, Idaho (1958)
6) F. K. McGowan and P. H. Stelson, Phys. Rev. **109** (1958) 901
7) E. L. Church and J. Weneser, Phys. **104** (1956) 1382
8) M. E. Rose, Internal Conversion Coefficients (North-Holland Publishing Co., Amsterdam, 1958)
9) L. C. Biedenharn and M. E. Rose, Revs. Mod. Phys. **25** (1953) 729
10) M. E. Rose, G. H. Goertzel, G. I. Spinrad, J. Harr and P. Strong, Phys. Rev. **83** (1951) 79
11) L. A. Sliv and B. A. Volchok, Tables of Coulomb phases and amplitudes, AEC-report 2875 (1957)
12) E. L. Church, M. E. Rose and J. Weneser, Phys. Rev. **109** (1958) 1299
13) A. K. Ustinova, JETP **37** (1960) 216
14) Z. Grabowski, B.–G. Pettersson, T. R. Gerholm and J. E. Thun, Nuclear Physics **24** (1961) 251
15) T. R. Gerholm, B.–G. Pettersson, B. van Nooijen and Z. Grabowski, Nuclear Physics **24** (1961) 177

3.C

Nuclear Physics **24** (1961) 223—242; © *North-Holland Publishing Co., Amsterdam*

Not to be reproduced by photoprint or microfilm without written permission from the publisher

MAGNETIC AND QUADRUPOLE INTERACTIONS IN Hg^{197m}. ANGULAR CORRELATIONS

B.-G. PETTERSSON, J. E. THUN and T. R. GERHOLM

Institute of Physics, University of Uppsala, Uppsala, Sweden

Received 16 January 1961

Abstract: A series of electron-gamma angular correlation studies of the 165 keV–134 keV cascade in Hg^{197m} and the 130 keV–279 keV cascade in the decay-product Au^{197m} are reported. The experiments have been undertaken primarily to settle the much discussed problem of the possible existence of a time dependent coupling between the nucleus and the electron core excited by virtue of a preceding conversion or electron-capture process.

For the Au^{197m} cascade no observable attenuations of the angular correlation pattern were found due to the short lifetime (2.3×10^{-11} s) of the intermediate level. In Hg^{197m}, where the corresponding lifetime is 1×10^{-8} s, the correlation was found to be attenuated by a static quadrupole interaction for carrier-free sources deposited onto different metal and insulator backings. No measurable attenuation due to an interaction with the electron core was seen for metallic source backings. However, an additional attenuation attributed to the after-effects of the conversion-process was found for sources embedded in insulating environments. The interplay between the two different types of interaction gives a complicated attenuation mechanism, which, however, can be disentangled by means of time-differential angular correlations. A direct proof of the existence of an attenuation-effect due to the excitation of the electron core is furnished by a magnetic decoupling experiment, confirming the results obtained in the correlation experiments.

1. Introduction

The angular correlation between successive nuclear transitions is frequently used to determine nuclear characteristics, such as the multipolarities, characters and mixing ratios of the transitions as well as the spins and parities of the levels involved. Provided the experimentally obtained angular correlation represents the true unperturbed relative directional distribution pattern one can infer the relevant nuclear parameters in a straight-forward way from the theory of angular correlations [1]).

It is well known that extranuclear fields can cause strong perturbations of the angular correlation. The nuclear magnetic dipole moment couples to external magnetic fields and the nuclear quadrupole moment will cause a similar coupling to electric field gradients. In both cases the coupling results in a precession around the external field (gradient) axis. If the coupling is sufficiently strong the nuclei change their initial orientation resulting in a wipe out of the angular correlation. It is evident that knowledge of the magnitude of these effects is of importance for the interpretation of the experimental results.

In most crystals strongly inhomogeneous fields are known to be present. Therefore one should quite generally expect a quadrupole coupling to take place in solid sources. To what extent this will result in an attenuation of the angular correlation depends not only on the lifetime of the intermediate level and the strength of the coupling but also on the resolving time and the time delay used in the coincidence arrangement.

For an isotropic source, i.e. a random distribution of nuclear spin orientations, a static (time independent) interaction can never give rise to a complete attenuation of the angular correlation. Under the condition that the signals from the second detector are not delayed with respect to the first and that the resolving time of the coincidence circuit is much longer than the lifetime of the intermediate level, the attenuation will approach a certain maximum value with increasing strength of coupling. This limit of maximum attenuation is called the "hard core" value. Under these conditions an attenuation below the hard core limit unambiguously shows that the static interactions alone cannot explain the perturbation mechanism. With delayed angular correlations it is, however, quite possible to get values below the hard core limit. In fact one might even get anisotropies with the reversed sign.

The theory of the perturbation of the angular correlation caused by extranuclear fields has been worked out in some detail by Abragam and Pound [2]). Steffen [3]) has written a review article on the subject dealing with both theoretical and experimental results.

While the origin and nature of the quadrupole interaction mechanism seems to be well understood this is not the case for another kind of coupling which is of a time-dependent character. It has been suggested [4]) that as a consequence of the after-effects of a formation of a hole in the electron core caused by internal conversion or electron capture there might be a magnetic coupling between the nucleus and the magnetic field produced by the excited and ionized atomic core. However, the hole will be very rapidly filled up – theoretical estimates indicate a recovery time by means of radiative transitions and Auger-effect of the order of 10^{-14}–10^{-15} s. During this time the hole diffuses to the outermost electron shell. Because of the Auger transitions several new holes will be created leaving the atom in a highly ionized state. The final recovery depends on the availability of free electrons to fill up the holes in the outer shell and neutralize the ion. In a conducting material such as a metal, free electrons from the conduction band are readily available. If the radioactive nuclei are embedded in a metallic environment one should therefore expect the total recovery time to be much too short compared to the precession period to allow for any attenuation. But if the radioactive atoms are placed in an insulator the atom might remain ionized for a considerable time perhaps giving rise to an attenuation of the angular correlation pattern. The coupling to the atomic shell has been discussed by Goertzel [5]), Brady and Deutsch [6]), Sunyar *et al.* [7]) and by Frauenfelder [4, 8]).

If present, the effect might influence gamma-gamma correlations following electron capture but it has its most important bearing on angular correlations involving conversion electrons.

2. Survey of Earlier Work

In spite of serious efforts from several different groups the problem of the hole-effect is not at all clear. Evidence for the existence of a hole effect has been reported for Cd^{111}, Hf^{181} and Hg^{197m} while a search for the effect in Te^{121} and Te^{123} revealed no indications for its existence. Aeppli *et al.* [9]) found in an early gamma-gamma correlation experiment on Cd^{111} attenuations below the hard core value for ionic crystal sources, which were taken as evidence for the hole-effect, the hole being formed by the preceding K-capture. This interpretation appeared to be confirmed when Kraushaar and Pound [10]) measured the Cd^{111m} correlation which goes through the same intermediate level and found attenuations to the hard core value *but never below*. The large attenuations observed by Kraushaar and Pound showed, however, that the correlation was strongly perturbed by the static quadrupole coupling. The Swiss group [11]) found this to be true also for the Cd^{111} correlation and concluded "that the attenuations observed could be largely and perhaps entirely explained by the quadrupole interaction hypothesis". In 1953 Steffen [12]) reported several Cd^{111} measurements with non-metallic sources below the hard core value. Those results were interpreted in terms of the hole effect. In 1956, however, Steffen [13]) published the results of a series of very careful experiments on Cd^{111}. It was then found that only two out of some 20 different sources gave values below the hard core value. Steffen has later found that these two exceptions probably can be explained by source impurities [14]). Thus there seems to be no remaining evidence for the presence of the hole effect in Cd^{111}. Gimmi *et al.* [15]) in 1956 reported electron-gamma correlations measured in Hf^{181}. Comparing gamma-gamma and electron-gamma correlations for the same cascade, they concluded that the latter was subject to an additional attenuation attributed to the after-effects of the hole formation. The attenuation factor was found to be 0.5. The same correlations were later studied by Snyder and Frankel [16]). Their result for the electron-gamma correlation is in disagreement with that of Gimmi *et al.* and revealed no evidence for any hole attenuation within the limits of experimental errors.

Goldberg and Frankel [17]) studied Te^{121} and Te^{123} and measured K-electron-gamma and K-electron-K-electron correlations. From the analysis of their results they were led to the conclusion that their correlations were not subject to any detectable amounts of attenuation. Thus the Te^{121} and Te^{123} cascades show no evidence for the hole effect.

An experimental study of Hg^{197m} especially aimed at an investigation of the

after-effects of hole-formation has been reported by the Pennsylvania group. The experimental results obtained were at first interpreted as evidence for the existence of the effect [18]) but upon further experimental studies [19]) it was concluded that the attenuation observed was due solely to quadrupole coupling.

The same correlation has been investigated by Gimmi *et al.* [15]) and also by Breitenberger [20]), who claim to have found evidence for the existence of the hole-attenuation effect. The Swiss group measured K-electron-gamma correlations and found that their results could be explained by assuming an attenuation due to the after-effects of the hole formation to about 50 % of the full anisotropy, i.e. an attenuation coefficient of the same magnitude as they found for the Hf^{181} correlation.

Breitenberger got a nearly unperturbed correlation for sources embedded in aluminium metal, while a source encapsuled in a non-conducting aluminium oxide environment, showed an *isotropic* distribution, which can be explained in terms of a strong hole-effect in non-conducting media.

3. Introductory Remarks

For our present experiment we have chosen Hg^{197m} for the following reasons:

1) Earlier experiments, discussed above, have given contradictory results. Some seem to indicate the presence of the hole effect.

2) The lifetime of the intermediate level is long enough to allow for time differential experiments and yet sufficiently short to let a fast but strong "on-off" hole effect compete with a weaker but always present quadrupole coupling.

3) The isotope can easily be obtained in carrier-free form on any kind of backing material.

4) Finally, there is in the decay product Au^{197m} a suitable cascade, which goes through an intermediate level of much shorter lifetime so that the Au^{197m}

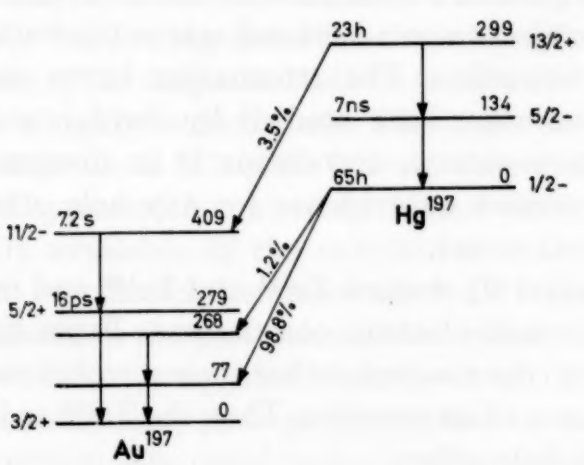

Fig. 1. Decay scheme of Hg^{197m}.

correlation can be used to simulate a switch off of the quadrupole and, probably, also the magnetic coupling. In this way one can under identical source conditions study the effect of the charging up of the source during the decay.

The decay scheme of Hg^{197m} given in fig. 1 has been established by R. Joly *et al.* [21]). The 23 h isomer decays partly through the $i_{\frac{13}{2}}(M4(+E5))f_{\frac{5}{2}}(E2)\ p_{\frac{1}{2}}$ cascade to the Hg^{197} ground state and partly by an electron capture branch to the $h_{\frac{11}{2}}$ isomer in Au^{197}. From the latter state there is a $h_{\frac{11}{2}}(E3)\ d_{\frac{3}{2}}(M1+E2)d_{\frac{5}{2}}$ cascade to the ground state in Au^{197}. The lifetimes of the intermediate levels in these two cascades have both been measured. From delayed coincidences a value of $t_{\frac{1}{2}} = (7.0 \pm 0.2) \times 10^{-9}$ s has been found [22]) in Hg^{197} and from the $B(E2)$ determined by means of Coulomb excitation, one obtains $t_{\frac{1}{2}} = 1.6 \times 10^{-11}$ s for the $d_{\frac{5}{2}}$ level in Au^{197}.

The particle parameters used for the interpretation of the measured $e_K^- - \gamma$ correlation have been taken from Biedenharn and Rose [1]). The particle parameters are calculated for a point nucleus. The influence on the particle parameters of the nuclear finite size can, however, in this case be safely neglected. A calculation by A. K. Ustinova [25]) shows that the M4 particle parameter is changed by less than 1 % if finite size effects are taken into account.

For intensity reasons the 130 keV electron-279 keV gamma correlation was measured with the 130 keV L-peak focused in the magnetic spectrometer. Unfortunately no comparison can be made with the theory for this correlation since the particle parameters for L-conversion have not yet been calculated. As already stated this correlation was measured in order to study the effect of source charge on the angular correlation.

Depending on the source conditions the angular correlation can be more or less attenuated due to a static quadrupole interaction and/or a time-dependent coupling caused by the after-effects of the hole formation. The attenuation can be expressed by an attenuation factor G. Thus

$$A_2(\text{exp}) = G_2 A_2(\text{unperturbed}). \tag{1}$$

The quadrupole interaction may be expressed in terms of a precession angular velocity ω_0, which for the Hg^{197m} is given by

$$\omega_0 = \frac{3}{20\hbar} eQ \frac{\partial^2 V}{\partial z^2}, \tag{2}$$

where eQ is the nuclear quadrupole moment and $(\partial^2 V)/(\partial z^2)$ represents the field gradient. The quantity $\Delta\nu_Q$ frequently used to describe quadrupole interactions is closely related to ω_0. In our case one has

$$\Delta\nu_Q = \frac{10\omega_0}{3\pi}. \tag{3}$$

The precession around the field gradient gives rise to an attenuation of the

angular correlation. The actual attenuation observed, however, depends sensitively on the instrumental parameters τ_0 and t_d, i.e. the resolving time of the coincidence circuit and the time delay used to record delayed coincidences. For the spin $\frac{5}{2}$ of the intermediate level, Abragam and Pound have given the following expression for the attenuation factor:

$$G_2(t) = \tfrac{1}{5}\{1+\tfrac{13}{7}\cos\omega_0 t+\tfrac{10}{7}\cos 2\omega_0 t+\tfrac{5}{7}\cos 3\omega_0 t\}. \quad (4)$$

The $G_2(t)$ given in eq. (4) represents the attenuation factor as measured in a time-differential experiment, i.e. a measurement where the resolving time of the coincidence circuit τ_0 is very short compared to the precession period. Furthermore the lifetime of the intermediate level should be of the same order of magnitude as the precession period if the experiment should be feasible. These requirements are generally not fulfilled. The actually observed $\bar{G}_2(t)$ then becomes a weighted average obtained from eq. (4) by integration.

We have evaluated the different $\bar{G}_2$ from eq. (4) for the three different time delay settings used in our experiment. For simplicity we denote these "fast", "normal" and "delayed". In all three settings τ_0 is the same, but in the fast position t_d is negative, but $t_d+\tau_0$ still positive, so that only the first prompt fraction of the gamma rays will be accepted. The fact that our coincidence resolving curve is not rectangular in shape gives rise to some complications which are discussed below.

The normal position corresponds to the maximum of the delayed coincidence counting rate. Our resolving time is sufficiently long ($\tau_0 > 2\tau_n$), such that we can replace the limits of integration by 0 and ∞. The expression for $\bar{G}_2$ (normal) then becomes

$$\bar{G}_2\,(\text{normal}) = \tfrac{1}{5}\left(1+\tfrac{13}{7}\frac{1}{1+(\omega_0\tau_n)^2}+\tfrac{10}{7}\frac{1}{1+(2\omega_0\tau_n)^2}+\tfrac{5}{7}\frac{1}{1+(3\omega_0\tau_n)^2}\right). \quad (5)$$

For the fast position the slope of the coincidence resolving curve has to be taken into account in the integration. For the resolving time used in our experiment the fast slope was to a good approximation described by an exponential slope with a drop-off rate corresponding to a virtual half-life of about 3.5 ns, which is of the same order of magnitude as the half-life in question, 7.0 ns.

The net effect of this exponentially decaying window-curve is to reduce the weight of the delayed and more strongly attenuated coincidences. To take this into account we may simply replace the decay-constant λ_n by an effective decay-constant given by

$$\lambda_{\text{eff}} = \lambda_n+\lambda_s, \quad (6)$$

where λ_s is the slope of the prompt coincidence curve corresponding to a drop off rate, τ_s at the steep end of the resolving curve. In other words, we get

$\bar{G}_2$(fast) from expression (5) simply by replacing τ_n by τ_{eff} given by

$$\tau_{eff} = \tau_n \frac{\tau_s}{\tau_s + \tau_n}. \tag{7}$$

Finally, the delayed position corresponds to a positive time-delay which, expressed in units of the nuclear lifetime, is obtained from the coincidence counting rate,

$$\frac{C(\text{delayed})}{C(\text{normal})} = \int_0^{t_d} e^{-\lambda_s(t_d-t)} \lambda_n e^{-\lambda_n t} dt + \int_{t_d}^{\infty} \lambda_n e^{-\lambda_n t} dt. \tag{8}$$

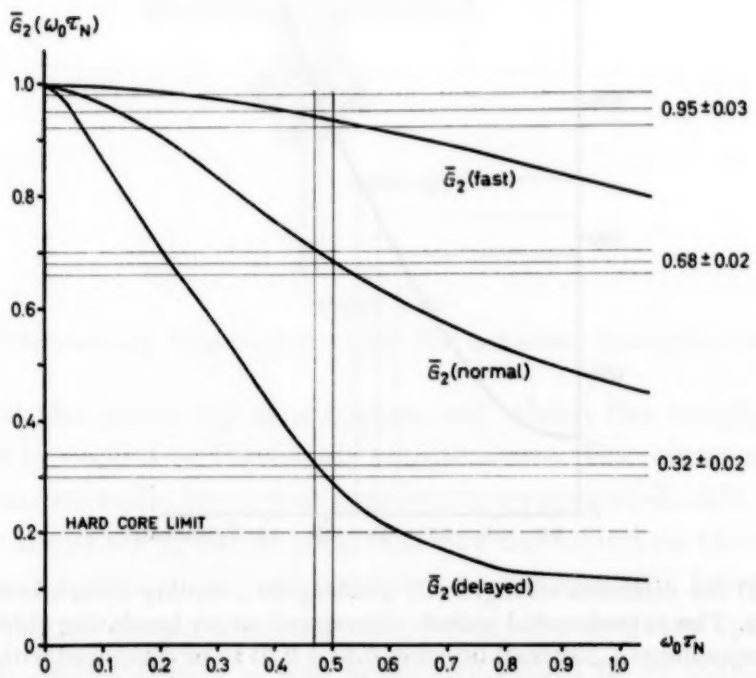

Fig. 2. The attenuation factors $\bar{G}_2$(fast), $\bar{G}_2$(normal) and $\bar{G}_2$(delayed) given as functions of the strength of the quadrupole coupling. Experimental values corresponding to sources on Au backings are shown.

The coincidence counting rate C should be normalized to the same single counting rate in the electron (or gamma) channel. The slope of the resolving curve is then taken into account in the first integral.

The expression for $\bar{G}_2$(delayed) becomes for $\lambda_s = 2\lambda_n$ to a good approximation

$$\bar{G}_2(\text{delayed}) = \tfrac{1}{5}\left(1 + \tfrac{13}{7}\frac{\cos\omega_0 t_d}{1+(\omega_0\tau_n)^2} + \tfrac{10}{7}\frac{\cos 2\omega_0 t_d}{1+(2\omega_0\tau_n)^2} + \tfrac{5}{7}\frac{\cos 3\omega_0 t_d}{1+(3\omega_0\tau_n)^2}\right), \tag{9}$$

where t_d is obtained from eq. (8).

Fig. 2. gives the attenuation factors as functions of the strength of the quadrupole coupling.

Note that in the limit of strong coupling ($\omega_0\tau_n \gg 1$) the three different $\bar{G}_2$

approach the limiting hard core value

$$\bar{G}_2(\text{hard core}) = 0.2.$$

If an attenuation not caused by a static electric quadrupole interaction is present, the interplay between the couplings will obviously result in a complicated perturbation mechanism.

In order to see whether only a static quadrupole interaction can explain the

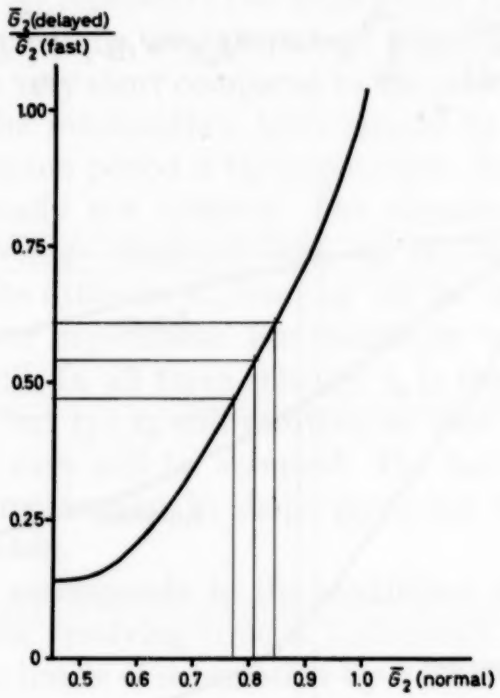

Fig. 3. $\bar{G}_2$ (normal) for different strengths of quadrupole coupling determined by the ratio $\bar{G}_2$ (delayed)/$\bar{G}_2$ (fast). The experimental values correspond to an insulating rubber hydrochloride backing. The corresponding $\bar{G}_2$ (normal) becomes 0.81 ± 0.04 to be compared with the experimental values for A_2 (normal) given in table 2.

observed attenuations, we can, however, utilize the correlations measured at our three different delay positions.

Fig. 3 gives the ratio $\bar{G}_2(\text{delayed})/\bar{G}_2(\text{fast})$ as a function of $\bar{G}_2(\text{normal})$. We can thus use this graph to determine the value for $\bar{G}_2(\text{normal})$ from the experimentally determined ratio $A_2(\text{delayed})/A_2(\text{fast})$. If only a static quadrupole interaction is able to account for the attenuations found, the value $A_2^* = A_2(\text{normal})/\bar{G}_2(\text{normal})$ should correspond to the true undisturbed correlation.

4. Present Experiment

4.1. SOURCE AND APPARATUS

The Hg^{197m} activity was obtained by bombarding natural gold by 18 MeV protons in the synchro-cyclotron at the Werner-Institute, Uppsala. The

target material was in the form of a 0.1 mm thick gold foil. This was removed from the target-holder and placed in the mercury evaporation vessel shown in fig. 4. The irradiated gold foil was placed at the bottom of the quartz tube. After evacuating the vessel to about 0.1 mm pressure, the quartz tube was sealed off. It was then heated from outside to 600 °C. The source backing is

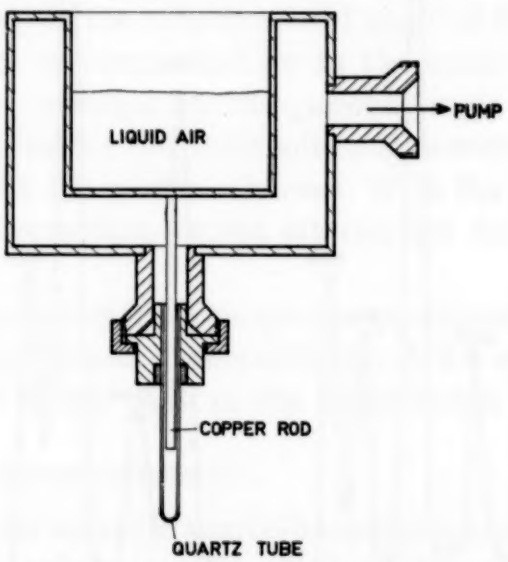

Fig. 4. The mercury evaporation vessel. For a further description see ref. [26]).

pressed against the lower tip of a copper rod which fits snugly in the quartz tube. This rod is cooled to liquid air temperature. For some of the sources a thin and circular metallic layer was previously evaporated onto the backing. In the latter case about 50 % of the total activity deposited on the source backing. The activity was found to be well confined to the metallic layer. For insulator sources, i.e. without evaporated metallic layer, the activity spread out over a larger area but about 10–20 % was generally found to be concentrated to the spot, where the diameter is 4 mm which corresponds to the lower tip of the rod. This part was punched out and mounted on a separate zapon backing.

Since the bombarding energy is below the threshold for (p, 2n) reactions the only mercury isotope produced is Hg^{197m}. Some active gold will be produced by (p, p) and (p, pn) reactions but these do not evaporate at the fairly low temperature used for outgassing the mercury from the gold target. Thus our sources are deposited onto the backing in a carrier-free and pure form.

Certain precautions had to be taken in order to avoid a minute quantity of gold evaporating together with the mercury activity. It will be seen later that the anisotropies for gold and silver backings are quite different. From a series of measurements evaporating the activity onto a silver-backing, we found that an evaporation temperature of 600 °C was sufficiently low to avoid any influence from evaporated gold. If the temperature is increased above 900 °C, however, enough gold, even if scarcely visible, is evaporated to give the typical "gold-attenuation" independent of the backing material used.

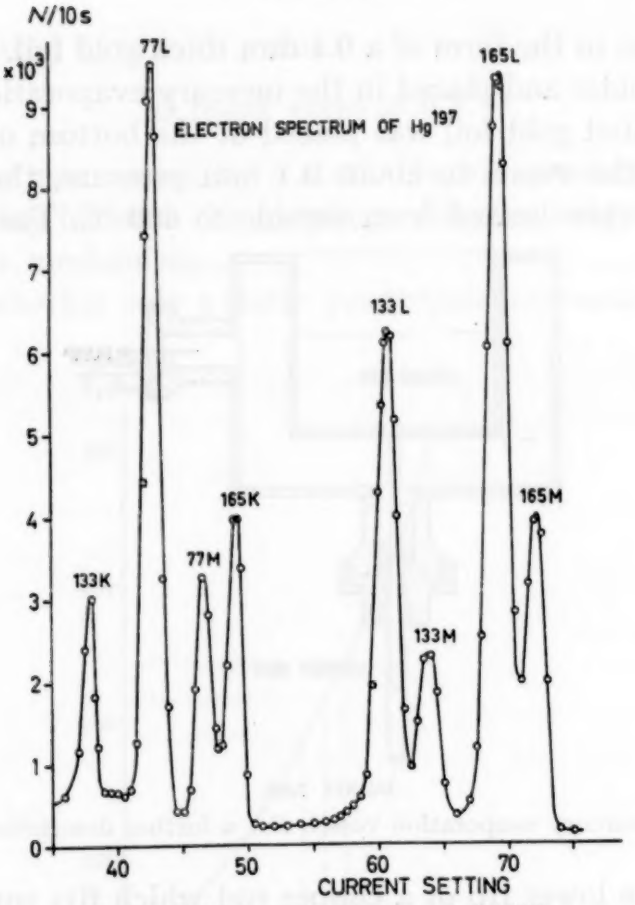

Fig. 5. Electron spectrum of Hg^{197m}.

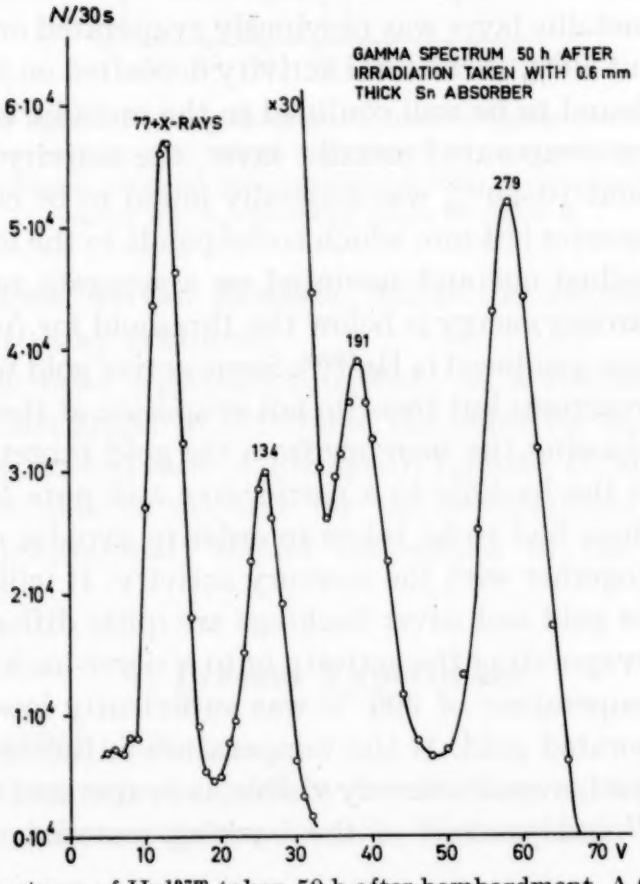

Fig. 6. Scintillation spectrum of Hg^{197m} taken 50 h after bombardment. A 0.6 mm thick Sn-absorber is used to reduce the 77 keV+X-ray peak.

An electron-gamma angular correlation spectrometer with magnetic momentum selection was used for the angular correlation experiments. This instrument has been described elsewhere [23]). The sources were centered with respect to the axis of the magnetic spectrometer and thereupon the axis of rotation of the gamma-detector was adjusted to coincide with the centre of the source. The minute residual variation in the effective solid angle of the gamma-detector at various angular settings was corrected for in the usual way by dividing the number of coincidences recorded by the gamma single counting rate.

Correction factors applied for the finite solid angles were 1.10 for the magnetic spectrometer and 1.07 for the gamma channel. With the source thickness used in our experiments no correction for the attenuation due to source scattering has to be applied.

Representative spectra taken in the magnetic spectrometer and in the gamma-channel are shown in figs. 5 and 6, respectively. A 0.6 mm thick tin absorber was used to reduce the X-ray peak in the scintillation spectrum.

4.2. METALLIC SOURCE ENVIRONMENTS

The results obtained for metallic source-backings are summarized in table 1. As seen, the obtained A_2 values are different for different metals. Moreover the anisotropies measured in the "normal" and "delayed" positions are considerably lower, except for silver, than those measured in the "fast" position. This, of course, clearly indicates the presence of an attenuation mechanism.

The last column gives A_2* which should represent the true A_2 value if the attenuations found are due to a static quadrupole interaction only. As is seen the A_2*-values for different metal backings show good mutual agreement.

To ascertain that the A_2*-values found correspond to the true correlation, a comparison with the theoretically predicted A_2-values should be made.

For intensity reasons the measurements presented in table 1 all refer to L-electrons for which no particle-parameters have been calculated.

It should also be mentioned that all A_2-terms given in table 1 have been calculated from the formula $A_2=2A/(3+A)$, where A is the anisotropy. Thus an eventual A_4-term has not been taken into consideration. This is certainly justified, as the A_4-term is small, in fact, less than 10% of the A_2-term. Further, the A_2-values given in table 1 are used only to determine the relative attenuation factors.

For a direct comparison with the theoretically predicted value the 165K–134γ correlation was measured. Silver was chosen as backing-material for this measurement since the quadrupole attenuation was found to be particularly small for this backing material. The A_2 term predicted for the 165K–134γ correlation, of course, depends on the multipolarities and mixing ratios for the 165 keV and 134 keV transitions and the spin-sequence, which, however, is known to be $\frac{13}{2}$(M4+E5)$\frac{5}{2}$(E2)$\frac{1}{2}$. We discard a possible admixture of M3 in competition with the E2 transition.

TABLE 1

Summary of experimental results for metal source backings

Source backing	Source no.	165L–134γ correlation			
		A_2 (fast)	A_2 (normal)	A_2 (delayed)	A_2*
Ag	1	0.204±0.006	0.195±0.005	0.188±0.007	
	2	0.204±0.006	0.198±0.006		
	3		0.182±0.006		
	4		0.198±0.005		
	5		0.198±0.012		
	6		0.198±0.006		
	7		0.184±0.007		
	Average	0.204±0.005	0.194±0.004	0.188±0.007	0.199±0.004
Au	8	0.185±0.007	0.136±0.005	0.060±0.007	
	9		0.137±0.007	0.065±0.007	
	10		0.124±0.007		
	11		0.135±0.007		
	12		0.140±0.007		
	13		0.130±0.007		
	14		0.127±0.005		
	15		0.141±0.007		
	Average	0.185±0.007	0.133±0.004	0.063±0.005	0.193±0.007
Al	16	0.200±0.018	0.141±0.008	0.080±0.019	
	17		0.147±0.009		
	Average	0.200±0.018	0.144±0.006	0.080±0.019	0.197±0.015
Ga	18		0.167±0.010		
Ga (heated)	19		0.149±0.010		
		130L–279γ-correlation			
Ag	2		0.308±0.008		
Au	9		0.314±0.007		

For the very similar isotope Hg^{199m} about 0.8 % E5 gamma admixture in the corresponding M4 transition has been reported by Pound and Wertheim [24]). If the same reduced matrix-elements in the two isotopes are assumed, the change in energy from Hg^{199m} (368 keV) to Hg^{197m} (165 keV) will reduce the E5 admixture in Hg^{197m} by a factor of five. Further the K-conversion probability is about 15 times higher for M4 than for E5 in the 165 keV transition. The contribution to the K-conversion peak of E5 radiation could thus be calculated to be $\lesssim 0.01$ %. When the uncertainty in the E5/M4 mixing ratio is taken into account the theoretically predicted values become $A_2 = 0.236 \pm 0.003$ and $A_4 = -0.026$.

Since the A_4 term is small compared to A_2 only the anisotropy A was measured and A_2 calculated from the formula

$$G_2 f_2 A_2 = \frac{2A}{3+A} + \frac{G_4 f_4 A_4 (3A-5)}{4(3+A)}. \tag{10}$$

The theoretical A_4 term is used in the small correction term in eq. (10) and f_2 and f_4 are the correction factors for the finite solid angles.

The value found after correction for $\bar{G}_2$ (normal) $= 0.975 \pm 0.015$ was $A_2 = 0.232 \pm 0.006$. This is in perfect agreement with the theoretical value for a pure M4 and E2 cascade.

4.3. INSULATOR SOURCE ENVIRONMENT

As seen in table 2, the values for A_2* (insulator) are considerably lower than the values for A_2*(metal) summarized in table 1. This clearly shows the presence of an attenuation different from the static quadrupole interaction.

TABLE 2

Summary of experimental results for insulator source backings

Source backing	Source no.	165L–134γ correlation			
		A_2 (fast)	A_2 (normal)	A_2(delayed)	A_2*
Rubber hydrochloride	20		0.142±0.011		
	21	0.131±0.007	0.120±0.007	0.071±0.008	
	22		0.129±0.006		
	Average	0.131±0.007	0.127±0.007	0.071±0.008	0.157±0.010
Mylar	23	0.115±0.012	0.101±0.006	0.060±0.012	0.127±0.013
Al_2O_3	24		0.098±0.017	0.051±0.016	
MgO	25	0.124±0.014	0.119±0.010	0.068±0.014	0.147±0.017
		130L–279γ correlation			
Mylar	23		0.320±0.023		

Before we proceed to interpret this attenuation in terms of a time-dependent coupling due to the after-effects of the hole-formation, we must rule out the possibility that the attenuation of A_2*(insulator) is due to deflections of the electrons by the electric charge built up on the insulated source during the emission of conversion electrons. In order to study this problem the 130 keV-L electron-279 keV gamma correlation in the decay of Hg^{197m} to Au^{197m} was

measured on both metallic and insulator source backings. The lifetime of the 279 keV level, 2.3×10^{-11} s, is short enough to make attenuations from electric or magnetic interactions unlikely. No difference between metallic and insulator sources was found in this case.

4.4. CONCLUDING REMARKS

Our delayed angular correlation studies of the 165 keV M4+E5 electron – 134 keV E2 gamma cascade are consistent with the following picture of the attenuation mechanism. Immediately after the conversion process the hole formed in the K-shell moves out to the outermost orbit creating several new holes during its way out through Auger transitions thus leaving the atom in a highly ionized and probably excited state. This first phase of the recovery process is estimated to take only some 10^{-14} to 10^{-15} s which is too short to affect the orientation of the nucleus.

During the second phase of the recovery process the ion picks up electrons from its surroundings and finally ends up in its neutralized ground state. The time required for this recovery depends on the availability of free electrons, i.e. on the nature of the environment, which in our case is the backing material into which the active Hg^{197m} atoms have been deposited in carrier-free form. In the metal backings this time is very short and should not result in any observable attenuation of the angular correlation pattern. Thus the attenuations observed are expected to be of a pure quadrupole character. When corrected for the quadrupole attenuation the angular correlation is expected to give the true unperturbed correlation which is obtained from the known $\frac{1}{2}^{3}$(M4+E5)$\frac{5}{2}$(E2)$\frac{1}{2}$ spin and multipolarity sequence, using the particle parameters given by Biedenharn and Rose. The small E5 admixture gives only a minor contribution to the uncertainty in the electron-gamma angular correlation because of the much higher K-conversion probability for M4 with respect to E5.

As shown above, these expectations have been confirmed in our experiments. The attenuation mechanism in metallic environment is of a pure quadrupole character. When corrected for the quadrupole attenuation, the A_2 coefficient is in perfect agreement with the theoretical unperturbed A_2 coefficient. Thus we may write $A_2(t_d, \text{metals}) = \tilde{G}_2(Q, t_d)A_2(\text{unperturbed})$, where $A_2(t_d, \text{metals})$ is the experimentally measured A_2-coefficient at the delay position t_d and $\tilde{G}_2(Q, t_d)$ is the corresponding quadrupole attenuation factor.

In insulators, however, the atom will remain in its ionized and excited state for a longer period of time. During this period the electronic core will have paramagnetic properties. As a consequence of the presence of incomplete electronic shells, the nucleus is exposed to a strong magnetic field, which may be of the order 10^5–10^6 G. The nuclear spin **I** will start precessing around the atomic spin **J**, i.e. a hyperfine structure interaction. Under normal circumstances **J** is randomly orientated and will be subject to rapid fluctuations in time due to

the filling up of the electronic shells, radiative transitions and relaxation phenomena. The net result, however, might be an additional attenuation of the angular correlation pattern, provided the hfs interaction lasts sufficiently long to cause a deorientation of the nuclear spin system.

If this time is comparable to the lifetime of the nucleus the attenuation mechanism becomes a very complicated mixture of time-dependent hfs interaction (presumably of magnetic character) and the static quadrupole coupling. If this occurs it should, in the general case, not be possible to fit our observed relative attenuations to the theoretical curve obtained from the theory by Abragam and Pound.

If, however, the hfs interaction is shorter than the nuclear lifetime, but still long enough to result in an attenuation of the angular correlation, the hfs-interaction may be described as a fast "on-off" kind of coupling present immediately after the K-conversion. As a consequence of this short but strong hfs interaction, the unperturbed A_2-coefficient drops to a somewhat smaller value $A_2(0)$ given by $A_2(0) = G_2(0)\, A_2$ (unperturbed), where $G_2(0)$ is the attenuation factor corresponding to the "on-off" hfs interaction. Thereupon the weaker but static quadrupole coupling takes over further reducing the anisotropy. Since the latter attenuation mechanism is due solely to quadrupole coupling, it should follow the theoretical $\tilde{G}_2(Q, t_d)$ obtained from Abragam and Pound's theory, with A_2 (unperturbed) replaced by $A_2(0)$. In other words the A_2-coefficient measured at a time-delay position t_d should be given by A_2 (t_d, insulators) $= G_2(0)\tilde{G}_2(Q, t_d)A_2$(unperturbed).

Our delayed angular correlations are consistent with the latter alternative. Thus we conclude that in addition to the quadrupole interaction there is an additional fast "on-off" kind of coupling present immediately after the K-conversion. When the observed anisotropies are corrected for the quadrupole attenuation, $G_2(0)$ is determined to be 0.74 ± 0.04, i.e. an attenuation of about 25 %.

As already stated $G_2(0)$ is presumably due to a (magnetic) hfs interaction, i.e. a coupling between the nuclear spin **I** and the spin of the atomic shell **J**. This hypothesis might be unambiguously confirmed if we could find the means to decouple **I** and **J**. If our hfs-hypothesis is correct, the decoupled system should give pure quadrupole interaction in both metallic and insulating source environment. When a correction is made for this quadrupole interaction, the insulator sources should give the true, unperturbed correlation, just as the metallic sources have been found to do.

5. Decoupling Experiment

Such a decoupling of **I** and **J** should be possible to obtain with the aid of an external magnetic field applied in the direction of the emission of the conversion electrons (longitudinal decoupling). If the interaction energy between the

external magnetic field **B** and the magnetic moment $\boldsymbol{\mu}_e$ of the electron core is larger than the hfs interaction, a decoupling will take place, i.e.

$$\boldsymbol{\mu}_e \cdot \mathbf{B} > \boldsymbol{\mu}_n \cdot \mathbf{B}_J,$$

where $\boldsymbol{\mu}_n$ is the nuclear magnetic moment and $\mathbf{B}_J$ is the magnetic field at the nucleus caused by the unpaired electron orbits. The required strength of the external field, then becomes $B > \boldsymbol{\mu}_n \cdot \mathbf{B}_J/\mu_e$. A field of a few thousand G should be quite sufficient to achieve complete decoupling. When decoupling

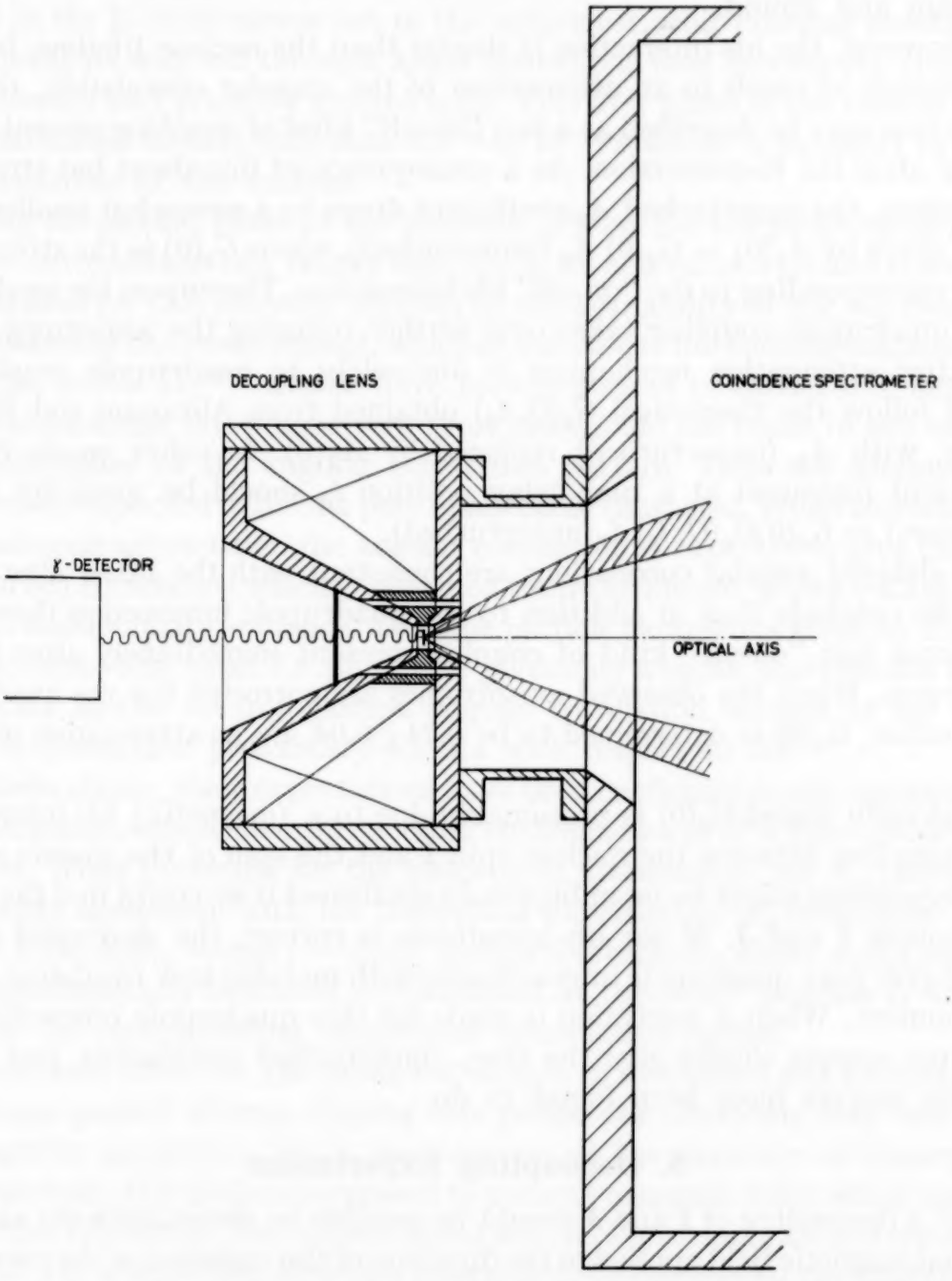

Fig. 7. Experimental set-up in the magnetic decoupling experiment.

has been obtained **I** and **J** both precess around the axis of the external field which is chosen to coincide with the quantization axis in the angular correlation experiment. The precession of **I** around this axis will, of course, not give rise to any attenuations of the angular correlation pattern since the population of the nuclear m-substates remains unaffected. Transitions between atomic m-substates and changes in the atomic spin configuration during the neutralization process will not change the nuclear spin orientation. An unperturbed angular correlation should then be observed.

The quadrupole interaction, however, gives the usual quadrupole attenuation. This can be neglected for the short time during which the paramagnetic properties remain but is expected to give the usual attenuation $(G_2(Q, t_d))$ when the final recovery has occurred.

There is a slight complication due to the fact that the electron trajectories are somewhat modified by the presence of the external field. The decoupling magnet was designed such that this effect was minimized.

A necessary requirement for the magnet producing the external field is that its influence on the electron trajectories in the magnetic spectrometer should be small. A magnet of the electron-lens type, easily giving a sufficiently strong and also well confined field, was considered the best choice. Preliminary experiments showed that the field from such a magnetic lens did not influence the spectrometer resolution, but gave a considerable increase in transmission due to a deflection of electrons with emission angles larger than those normally accepted into the spectrometer aperture cone.

The experimental arrangement is shown in fig. 7. As seen in fig. 7, coincidences were only recorded in a fixed position, corresponding to an average angle of 180° between the detected electrons and gamma rays.

Keeping this angle constant to a great extent simplifies the problem of avoiding systematic errors in the measurements.

5.1. EXPERIMENT

Careful checks showed that the magnetic field produced in the decoupling lens did not influence the gamma-counter. However, the spectrometer transmission increased by about 50 %, due to the focussing action of this field. Only normalizing the coincidence counting rate to the electron single counting rate is not sufficient in such a case, as the larger solid angle accepted also means a change in the geometrical correction factor f for the spectrometer. This correction factor can, in principle, be calculated from the observed increase in transmission of the spectrometer. Using a metallic backing, however, this factor can also be directly measured in a straightforward way. The decoupling experiment was thus performed with three different source backings, namely silver, gold and mylar. The runs with the metallic source backings were measured in order to get the correction factor f_B.

Coincidences were counted for periods of 1000 s with the field in the decoupling lens on and off. The decoupling field was determined to be approximately 3000 G. The single electron counting rate was recorded simultaneously with the coincidences. The ratio N_c/N_β showed only statistical fluctuations for both field on and off during the measuring periods.

For the 180° position used in our experiments the appropriate expressions become

$$W_0(\text{metal}) = 1+f_0 G_2(Q, t_d, \text{metal})A_2, \tag{11}$$

$$W_B(\text{metal}) = 1+f_B G_2(Q, t_d, \text{metal})A_2, \tag{12}$$

$$W_0(\text{insul.}) = 1+f_0 G_2(0)G_2(Q, t_d, \text{insul.})A_2, \tag{13}$$

$$W_B(\text{insul.}) = 1+f_B G_2(Q, t_d, \text{insul.})A_2. \tag{14}$$

The index 0 corresponds to measurement without and the index B to measurement with the external magnetic field. From the eqs. (11)–(14) the two unknown parameters f_B and $G_2(0)$ can be determined.

As seen from eqs. (11–14) the expression δ, defined as

$$\delta = \frac{W_B - W_0}{W_0} = \frac{\left(\frac{N_c}{N_e}\right)_B - \left(\frac{N_c}{N_e}\right)_0}{\left(\frac{N_c}{N_e}\right)_0}, \tag{15}$$

is expected to be negative for metallic backings since $f_B < f_0$ but positive for insulator sources where $f_B < f_0$ but $f_B > f_0 G_2(0)$. As seen in table 3 this was experimentally confirmed. From the observed δ values, the values for f_B and $G_2(0)$ were calculated.

TABLE 3

Results of the decoupling experiments

Source backing	A_2 (exp) [a]	$\delta = \frac{\left(\frac{N_c}{N_e}\right)_B - \left(\frac{N_c}{N_e}\right)_0}{\left(\frac{N_c}{N_e}\right)_0}$	f_B/f_0	$G_2(0)$
Ag	0.160±0.003	−0.026 ±0.004	0.806±0.030	
Au	0.110±0.003	−0.023 ±0.005	0.761±0.050	
Mylar	0.083±0.005	+0.0092±0.004	0.795±0.030 [b]	0.71±0.04

[a] Not corrected for attenuation and finite aperture angles and measured without the decoupling magnet.

[b] Average adopted.

Using directly the experimentally measured A_2 (exp) coefficients we get from the relations above

$$\frac{f_B}{f_0} = 1+\delta_{\text{metal}}\{1+A_2^{-1}(\text{exp. metal})\} \tag{16}$$

and

$$G_2(0) = \frac{1+\delta_{\text{metal}} \cdot \{1+A_2^{-1}(\text{exp metal})\}}{1+\delta_{\text{insul.}} \cdot \{1+A_2^{-1}\ (\text{exp insul.})\}}. \tag{17}$$

The results are summarized in table 3. For the insulator backing (mylar) we get $G_2(0) = 0.71 \pm 0.04$. This is in good agreement with the value obtained from the delayed angular correlation experiments discussed above.

6. Conclusions

The attenuations found for the different *metallic* source environments are fully consistent with a pure quadrupole interaction mechanism. Strictly speaking, our experimental results do not completely rule out the possibility of an additional rapidly vanishing attenuation mechanism present immediately after the K-conversion process. However, if at all present, such an on-off coupling could not give larger attenuations than 5 %. This can be seen from the fact that our experimental A_2-coefficient for the 165 keV electron-134 keV gamma cascade, when corrected for the quadrupole attenuation only, becomes $A_2 = 0.232 \pm 0.006$, which agrees to within 5 % with the theoretical value for a pure M4+E2 cascade, $A_2 = 0.236$.

For *insulator* source environments, however, the situation is different. Here the experiments show that there exists in addition to the quadrupole interaction mechanism a rapidly vanishing coupling. This fast ón-off coupling attenuates the angular correlation to some 75 % of the unperturbed value. The decoupling experiment shows that this attenuation mechanism is due to an **I–J** coupling. It must, therefore, be understood in terms of after-effects of hole formation.

As in the metallic sources there is, of course, also in the insulator environment case a quadrupole coupling giving rise to a further attenuation of the angular correlation pattern.

We conclude that for lifetimes of the intermediary level in the nanosecond region (and possibly even shorter) the attenuations caused by the after-effects of hole formation can by no means be neglected, whenever the radioactive atoms are embedded in an insulating medium.

After-effects of hole formation are to be expected not only for conversion electron-gamma angular correlations but also for gamma-gamma correlations immediately following K-capture and probably also beta-decay. In the latter case the holes are formed by the "shake off" of electrons when the electron-core readjusts itself to the new atomic number.

We express our sincere gratitude to Professor Kai Siegbahn for his encouraging support and for the excellent research facilities provided. Thanks are also due to the cyclotron crew at the Werner Institute for a considerable number of gold-irradiations.

References

1) L. C. Biedenharn and M. E. Rose, Revs. Mod. Phys. **25** (1953) 729
2) A. Abragam and R. V. Pound, Phys. Rev. **92** (1953) 943
3) R. M. Steffen, Phil. Mag. Suppl. **4** (1955) 294
4) H. Frauenfelder, Phys. Rev. **82** (1951) 549
5) G. Goertzel, Phys. Rev. **70** (1946) 897
6) E. L. Brady and M. Deutsch, Phys. Rev. **78** (1950) 558
7) A. Sunyar, D. Alburger, G. Friedlander, M. Goldhaber and G. Scharff-Goldhaber, Phys. Rev. **79** (1950) 181
8) H. Frauenfelder, in Beta and Gamma Ray Spectroscopy, edited by K. Siegbahn (North-Holland Publ. Com., Amsterdam, 1955)
9) H. Aeppli, A. S. Bishop, H. Frauenfelder, M. Walter and W. Zünti, Phys. Rev. **82** (1951) 550
10) J. J. Kraushaar and R. V. Pound, Phys. Rev. **92** (1955) 522
11) M. Albers-Schönberg, E. Heer, T. B. Novey and R. Rüetschi, Phys. Rev. **91** (1953) 199
12) R. M. Steffen, Phys. Rev. **90** (1953) 1119
13) R. M. Steffen, Phys. Rev. **103** (1956) 116
14) Private communication to E. S. Snyder and S. Frankel (see ref. [16]))
15) F. Gimmi, E. Heer and P. Scherrer, Helv. Phys. Acta **29** (1956) 147
16) E. S. Snyder and S. Frankel, Phys. Rev. **106** (1957) 755
17) N. Goldberg and S. Frankel, Phys. Rev. **100** (1955) 1350
18) J. V. Kane and S. Frankel, Bull. Am. Phys. Soc. **1** (1956) 171
19) H. H. Coburn, J. V. Kane and S. Frankel, Phys. Rev. **105** (1957) 1293
20) E. Breitenberger, Proc. Phys. Soc. **69** (1956) 566
21) R. Joly, J. Brunner, J. Halter and O. Huber, Helv. Phys. Act. **28** (1955) 403
22) T. Suter, P. Reyes-Suter and T. R. Gerholm, (in press)
23) T. R. Gerholm and B.–G. Pettersson, Nuclear Instruments **4** (1959) 107
24) R. V. Pound and G. K. Wertheim, Phys. Rev. **102** (1956) 396
25) A. K. Ustinova, JETP **37** (1960) (10) 216
26) W. C. Parker, Nuclear Instruments **8** (1960) 354

3.B

Nuclear Physics **24** (1961) 243—250; © *North-Holland Publishing Co., Amsterdam*

Not to be reproduced by photoprint or microfilm without written permission from the publisher

EXPERIMENTAL DETERMINATION OF THE CONVERSION COEFFICIENT OF THE 412 keV E2 TRANSITION IN Hg^{198}

B.-G. PETTERSSON, J. E. THUN and T. R. GERHOLM

Institute of Physics, University of Uppsala, Uppsala, Sweden

Received 16 January 1961

Abstract: The K-conversion coefficient of the 412 keV transition in Hg^{198} has been measured using a coincidence method. The result obtained $\alpha_K = 0.0305 \pm 0.0010$ is in agreement with the theoretical value for a pure E2 transition as calculated by Rose and by Sliv and Band. We disagree with recent results obtained by the internal-external conversion method.

1. Introduction

The theoretical tabulations of internal conversion coefficients by Rose [1]) and by Sliv and Band [2]) are under normal circumstances supposed to be accurate to within a few percent. Appreciable deviations are to be expected only for certain strongly retarded transitions, primarily of E1 or M1 character, for which nuclear structure dependent penetration matrix elements [3]) may affect the internal conversion coefficients. For E2 transitions the theory indicates that nuclear structure effects should be negligibly small. For this reason conversion coefficients of pure E2 transitions are frequently used as references in relative measurements of conversion coefficients and transition intensities.

Recently, however, some doubt has been shed on the validity of the theoretical E2 conversion coefficients. McGowan and Stelson [4]) report experimental K-conversion coefficients which are *larger* than the theoretical values. They found for Er^{166}, Yb^{170} and Hf^{176} deviations of +13, +23 and +20 % respectively. On the other hand there have been several measurements on other isotopes which have given values which are *lower* than the theoretical figures. Deviations as large as −20 % have been reported.

None of these deviations can be understood theoretically, but it would be particularly embarrassing if such large deviations *in both directions* really exist.

Several experimental determinations of the 412 keV E2 transition in Au^{198} have been reported. As seen in table 1 there is no significant difference between Rose's value and that of Sliv and Band, but all experimental figures hitherto reported are below these theoretical values with the single exception of Simon's early result. The discrepancy is particularly large for the values given by de Vries and by Hultberg and co-workers. It should be observed, however, that the experimental results are not entirely independent since Hultberg *et al.* at

Vanderbilt University and at Berkeley, as well as de Vries, use the same method, i.e. a comparison in a magnetic spectrometer between the intensities of external and internal conversion lines. Moreover, the efficiencies of the photoelectric converters used were all calculated from Hultberg's [5]) theory using the electronic computor in Stockholm. An error in the converter efficiency used in these calculations, therefore, affects all these experimental values in the same way. However, de Vries also measured the conversion coefficient by comparing the K-peak with the intensity of the continuous beta spectrum and got consistent results, though lower than that of Wapstra who also used the beta-continuum method.

TABLE 1

Experimental and theoretical values of the conversion coefficient of the 412 keV E2 transition in Hg^{198}

α_K	Method	Ref.
0.030 $\pm$0.001	e/β	P. Hubert [12])
0.0275$\pm$0.0030	e–γ coinc.	O. Huber *et al.* [13])
0.0307$\pm$0.0004	e/β	L. Simons [14])
0.0281$\pm$0.0005	e/β	A. H. Wapstra [15])
0.0241$\pm$0.0012	e/β	C. de Vries [16])
0.0252$\pm$0.0013	ext/int.	C. de Vries [16])
0.0241$\pm$0.0010	ext/int.	S. Hultberg *et al.* [17])
0.0244$\pm$0.0008	ext/int.	J. H. Hamilton *et al.* [18])
0.0298		L. A. Sliv and I. M. Band [1])
0.0302		M. E. Rose [2])

We have recently finished an electron-gamma angular correlation study [6]) of the 400 keV–279 keV cascade in Tl^{203}. During the course of these measurement we determined the K-conversion coefficient of the 400 keV M1 transition. Our result is

$$\alpha_K = 0.145 \pm 0.007,$$

in perfect agreement with the theoretical value obtained from Sliv and Band [2]) which by log-log interpolation becomes

$$\alpha_K(\text{Sliv and Band}) = 0.148.$$

Our result, however, is in disagreement with an experimental value reported by Nijgh *et al.* [7]), who got

$$\alpha_K = 0.118 \pm 0.011,$$

i.e. a deviation of -20 % from the theoretical value given above. However, it appears that the value given by Nijgh *et al.* is related to the above mentioned

K-conversion coefficient of the 412 keV transition in Au^{198}. Nijgh *et al.* obtained their value from a combination of four different experiments:

(1) a comparison of the X-ray peak (N_X, Hg^{198}) and the 412 keV gamma ray peak ($N_{412\gamma}$, Hg^{198}) in the scintillation spectrum of Au^{198},

(2) a comparison of the X-ray peak (N_X, Tl^{203}) and the 279 keV gamma-ray peak ($N_{279\gamma}Tl^{203}$) in the scintillation spectrum of Hg^{203},

(3) a comparison of the 279 keV gamma ray peak ($N_{279\gamma}$, Tl^{203}) and the 400 keV gamma ray peak ($N_{400\gamma}$, Tl^{203}) in the scintillation spectrum of Pb^{203},

(4) a comparison between the K-conversion line intensities of the 279 keV and the 400 keV transitions in Pb^{203} studied in a magnetic beta-ray spectrometer, i.e. N_{279K}, Tl^{203} and N_{400K}, Tl^{203}, respectively. Combining these results one obtains

$$\alpha_K^{400}(Tl^{203}) = \alpha_K^{412}(Hg^{198}) \left[\frac{N_{400K}}{N_{279K}}\right]_{Pb^{203}} \cdot \left[\frac{N_{400\gamma}}{N_{279\gamma}}\right]_{Pb^{203}} \left[\frac{N_X}{N_{279\gamma}}\right]_{Hg^{203}} \left[\frac{N_{412\gamma}}{N_X}\right]_{Au^{198}}. \quad (1)$$

This rather complicated procedure has the advantage that one avoids introducing any correction for the variation of the efficiency of the scintillation crystal with the energy. On the other hand the value finally obtained for $\alpha_K^{400}(Tl^{203})$ depends on the value of $\alpha_K^{412}(Hg^{198})$. The fact that the value for $\alpha_K^{400}(Tl^{203})$ is lower than the theoretical and our experimental value indicates that the reason might be due to an erroneous value for the $\alpha_K^{412}(Au^{198})$. In fact our value for the 400 keV-K-conversion coefficient in Tl^{203} corresponds to

$$\alpha_K^{412}(Hg^{198}) = 0.033 \pm 0.004,$$

if we use the values given by Nijgh *et al.* The result, thus obtained, is in agreement with the theory within the experimental errors. The main uncertainty in our value stems from the errors in the proportionality factor between the two conversion coefficients.

Thus our results indicate that both conversion coefficients are in fact in agreement with the theoretical values. In order to verify this conclusion we have also made a separate determination of the Hg^{198} 412 keV K-conversion coefficient using, again, the electron-gamma coincidence method.

2. Experiments

The source was produced by irradiating pure gold in the R1 reactor in Stockholm in a flux of about 10^{12} n/cm^2 · sec for about 5 days. The goldactivity thus produced was evaporated in vacuum onto a 1 mg/cm^2 thick Al-backing. The thickness of the active goldlayer was approximately 30 μg/cm^2.

To determine the transmission of the spectrometer we used Hg^{197m} produced by bombarding gold with 19 MeV protons in the syncro-cyclotron at the Gustav

Werner's Institute in Uppsala. The mercury activity was evaporated in vacuum onto a 20 μg/cm^2 gold spot previously evaporated onto a 0.9 mg/cm^2 mylar foil by means of a special mercury evaporation technique described elsewhere [8]).

For our experiments we used the electron-gamma angular correlation spectrometer designed by Gerholm and Pettersson [9]). In the Au^{198} runs a part of the beta-continuum was focussed in the spectrometer and the 412 keV gamma-ray was recorded in coincidence. In the Hg^{197m} calibration runs the L-conversion line of the 165 keV M4 transition was focussed in the spectrometer and the cascading 134 keV gamma-ray was recorded in coincidence. In both cases the source to gamma detector distance was chosen as short as possible. In order to eliminate angular correlation effects the gamma-detector was placed at an angle of 126° with respect to the direction of emission of the electrons for which angle the P_2-polynomial in the angular-correlation expression becomes zero. Earlier experiments have shown that the A_4 coefficient is negligibly small.

The appropriate expressions become for the Hg^{197} experiment

$$\varepsilon_C \omega p_L^{(165)} = \frac{C(134\gamma, 165L)}{N(134\gamma)}, \tag{2}$$

and for the Au^{198} experiment

$$\varepsilon_C \omega p_K^{(412)} = \frac{C(412\gamma, \beta) N(412K)}{N(\beta) N(412\gamma)}. \tag{3}$$

In (2) and (3) $\omega p_L^{(165)}$ and $\omega p_K^{(412)}$ are the detection-probabilities per 165 keV and 412 keV transition repectively. The quantity ω is defined as the effective transmission of the magnetic spectrometer and $p_L^{(165)}$ and $p_K^{(412)}$ are related to the corresponding conversion probabilities $\kappa_L^{(165)}$ and $\kappa_K^{(412)}$ as will be discussed below. The factor ε_C is the efficiency of the coincidence circuit which is assumed to be the same in both experiments (cf. below). The quantities $C(134\gamma, 165L)$ and $C(412\gamma, \beta)$ are the coincidence counting rates corrected for random coincidences. $N(134\gamma)$ and $N(412\gamma)$ are the counting rates in the gamma channel corrected for the general background and for minor contributions from the Compton background of transitions of higher energy, and $N(\beta)$ in (3) is the counting rate in the magnetic spectrometer, which is set at an energy of 500 keV, i.e. above the 282 keV endpoint of the beta-branch to the second excited state. An eventual small admixture of Au^{199} produced by the reaction $Au^{198}(n, \gamma)Au^{199}$ will not influence the measurements as the maximum energies in the last isotope are $E_\beta = 460$ keV and $E_\gamma = 208$ keV respectively. Finally, $N(412K)$ is the counting rate due to the 412 keV K-conversion line only, when the instrument is set at the maximum of the K-peak. In order to subtract the contribution from the beta-continuum the spectrum was taken and

a Kurie plot of the beta-continuum made. From this the relative contributions of conversion electrons and beta-rays were determined. The uncertainties in these corrections were taken into account in the evaluation of the limits of errors and give only a minor contribution to the final errors.

Our experiment is based on the assumption that the transmission ω of the instrument is the same in the Hg^{197} calibration runs and the Au^{198} measurements. There are three objections against this basic assumption. First one might expect that the effective transmission of the instrument depends slightly on the finite dimensions of the source and the centering of the source on the optical axis of the spectrometer. To investigate this several independent calibrations with different Hg^{198} sources were made. From these experiments it was found that the spectrometer transmission varies slightly with the geometry of the source. The uncertainty in ω thus introduced gives, however, only a minor contribution to the final errors in ω. As shown below the uncertainty in $\kappa_L^{(165)}$ is the main limiting factor.

Secondly, the energy difference between the 165 keV L line and the 412 keV K-line may change the effective transmission if the detector is somewhat energy dependent. To investigate this the pulse height spectrum in the anthracene scintillation detector was recorded. It was found that even with the 165 keV K-line focussed in the instrument the conversion electrons produced a peak which was well separated from the dark current background. In the actual experiment the higher energy L conversion line was used.

Finally, one might object that the transmission of the beta-ray spectrometer could possibly vary somewhat with the energy of the focussed electrons. If, due to remanence or saturation effects in the iron yoke, the shape of the magnetic field is somewhat different at different field settings, the electron trajectories are not exactly conformal. Consequently the effective transmission becomes energy dependent. If this happens, however, it would also appear as a deviation from the linear relation between spectrometer coil current and momentum ($B\rho$) of the focussed electrons. Furthermore, the line-profiles would become distorted and one would observe a deviation from the linear Kurie-plot of allowed spectra. Since none of these effects are present within the energy range of interest in this connection we conclude that the transmission is constant.

The coincidence counting rate is of course proportional to the efficiency (ε_C) of the coincidence circuit. It is of importance that this is the same in both experiments. For sufficiently long resolving times one approaches a constant value generally interpreted as 100 % coincidence counting efficiency. To make sure that our coincidence circuit was insensitive to variations in the resolving time we deliberately used a fairly long resolving time setting ($2\tau_0 = 10^{-7}$ sec) and confirmed the insensitivity by reducing $2\tau_0$ by a factor of two without any observable change in the true coincidence counting rate.

The coincidence resolving curve (coincidence counting rate versus time delay

inserted in the two channels) was recorded and for the resolving times used in our experiment it was found to exhibit a long flat plateau also generally regarded as an indication that the coincidence efficiency is 100 %. During our experiment the coincidences were taken at the middle of the plateau. Our coincidence counting rate should therefore be independent of minor variations in the instrumental time delays. The time delay between the emission of the conversion-electron and the appearance of the corresponding pulse at the output of the scintillation detector depends on the energy of the conversion electron. This energy dependent time delay increases with decreasing energy due to longer time of flight through the spectrometer and a longer response time of the scintillation detector. The variation of the instrumental time delay becomes larger the lower the energy is.

To make sure that our coincidence efficiency was insensitive to energy variations we measured the coincidence counting rate for both K and L electrons and determined the ratios $C(134\gamma, 165\mathrm{K})/N(165\mathrm{K})$ and $C(134\gamma, 165\mathrm{L})/N(165\mathrm{L})$. These were found to be equal within the limits of statistical errors of one percent. With these precautions we feel safe to conclude that the efficiency of the coincidence circuit was the same (though not necessarily 100 %) in both experiments and independent of reasonable variations in resolving time and conversion electron energy.

For obvious reasons $p_{\mathrm{K}}^{(412)}$ is equal to the 412 keV K-conversion probability ($\kappa_{\mathrm{K}}^{(412)}$) provided of course, that the spectrometer is set to focus the peak of the 412 keV K-conversion line. If $\kappa_{\mathrm{tot}}^{(412)}$ is the total conversion probability of the 412 keV transition, the 412 keV K-conversion coefficient becomes

$$\alpha_{\mathrm{K}}^{(412)} = \frac{\kappa_{\mathrm{K}}^{(412)}}{1-\kappa_{\mathrm{tot}}^{(412)}}. \tag{4}$$

For the same reasons $p_{\mathrm{K}}^{(165)}$ may be obtained from the K : L : M ratios and the total conversion coefficient of the 165 keV transition. It is, however, preferable to use the 165 keV L-line for the calibrations, partly because the L-conversion probability is nearly 3 times as large as the K-conversion probability resulting in an improved statistical accuracy in the final result. More important, however, is that the systematical errors are much reduced if the L-line is used, since, the maximum relative error for a given $\kappa_{\mathrm{X}}^{165}$ is

$$\frac{\Delta\kappa_{\mathrm{X}}}{\kappa_{\mathrm{X}}} = 2\,\frac{\Delta \mathrm{X}}{\mathrm{X}}\left(1-\frac{\mathrm{X}}{\mathrm{K}+\mathrm{L}+\mathrm{M}}\right), \tag{5}$$

where X denotes one of the K, L or M intensities.

There is, however, a minor difficulty associated with the use of the L-electrons. Since the L-peak is not single but composed of the closely spaced triplet of $\mathrm{L_I}$, $\mathrm{L_{II}}$ and $\mathrm{L_{III}}$, the peak counting rate is not quite a true measure of the

total L-intensity. In our experiment the L-lines are not resolved but the separation of the L-components gives rise to a broadening of the line. By folding the L lines, using the K-line profile and the $L_I : L_{II} : L_{III}$ ratios we have obtained a relation between the peak counting rate and the total L-intensity. This becomes

$$N_L(\text{total}) = (1.04 \pm 0.01) N_L(\text{peak}).$$

The errors in the proportionality factor comes from the uncertainties in the line profile and the L_I, L_{II} and L_{III} ratios. Using this relation we have determined the K : L : M ratios † from the peak counting rates:

$$K : L : M = 100 : 272 : 110,$$

while a direct comparison between areas under the line profiles gave

$$K : L : M = 100 : 271 : 111.$$

The close agreement between these two results is probably accidental but justifies our folding procedure. The results thus obtained are in good agreement with the conversion-spectrum published by Coburn, Kane and Frankel [10]) and also, with the theoretical K : L : M ratios for this pure M4 transition. Our value, however, deviates somewhat from the results obtained by Huber *et al.* [11]), who got

$$K : L : M = 100 : 226 : 87.$$

The 165 keV M4 transition in Hg^{197m} is more than 99.7 % converted [10]) and $\kappa_L^{(165)}$ therefore becomes

$$\kappa_L^{(165)} = \frac{1}{1 + K/L + M/L + \ldots} = 0.564.$$

Using our relation between the L peak counting rate and the total L intensity we get

$$p_L^{(165)} = \frac{\kappa_L^{(165)}}{1.04 \pm 0.01}.$$

Using the value for ω determined from (2) we obtain from (3) $\kappa_K^{(412)} = 0.0292 \pm 0.0009$,
and with $\kappa_{tot} = \kappa_K(1 + L/K + M/K)$ this gives

$$\alpha_K^{(412)} = \frac{\kappa_K^{(412)}}{1 - \kappa_{tot}^{(412)}} = 0.0305 \pm 0.0010,$$

in good agreement with our less accurate value obtained from the Tl^{203} experiment.

† The M-lines are so closely spaced that there is no appreciable broadening of the M-complex. M-electrons, therefore, may be considered as mono-energetic.

3. Conclusion

Our result $\alpha_K = 0.0305 \pm 0.0010$ is in agreement with the theoretical values given by Rose $\alpha_K = 0.0302$ and by Sliv and Band $\alpha_K = 0.0298$. We disagree, however, with some recent results obtained from comparison with the beta-continuum and in particular with those obtained by the photoelectric method. On the basis of our two independent results for the E2 conversion coefficient of the 412 keV transition we feel that the calculated converter efficiencies are somewhat too low at least in the lower energy region.

We should also like to point out that the electron-gamma coincidence method, where it can be applied, is probably the most straightforward and accurate method for the determination of internal conversion coefficients.

References

1) M. E. Rose, Internal Conversion Coefficients (North-Holland Publishing Co., Amsterdam, 1958)
2) L. A. Sliv and I. M. Band, Tables of Gamma Ray Conversion Coefficients (Physico-Technical Institute, Academy of Science, Leningrad, 1958), issued in USA as Report 57 ICE KI, Physics Department, University of Illinois
3) E. L. Church and J. Weneser, Phys. Rev. **104** (1956) 1382
4) F. K. McGowan and P. H. Stelson, Phys. Rev. **107** (1957) 1674
5) S. Hultberg and R. Stockendal, Ark. f. Fysik **14** (1959) 565
6) T. R. Gerholm, B.–G. Pettersson, B. van Nooijen and Z. Grabrowski, Nuclear Physics **24** (1961) 177
7) G. J. Nijgh, A. H. Wapstra, L. Th. M. Ornstein, N. Salomons-Grobben, K. R. Huizenga and O. Almén, Nuclear Physics **9** (1958/59) 528
8) W. C. Parker, Nuclear Instruments **8** (1960) 354
9) T. R. Gerholm and B.–G. Pettersson, Nuclear Instruments **4** (1959) 107
10) H. H. Coburn, J. V. Kane and S. Frankel, Phys. Rev. **105** (1957) 1293
11) O. Huber, F. Humbel, H. Schneider, A. de-Shalit and W. Zünti, Helv. Phys. Acta **24** (1951) 127
12) P. Hubert, Compt. Rend. **232** (1951) 2201
13) O. Huber *et al.*, Helv. Phys. Acta **25** (1952) 3
14) L. Simons, Phys. Rev. **86** (1952) 570
15) A. H. Wapstra, Nuclear Physics **9** (1958/59) 538
16) C. de Vries, Thesis, Amsterdam 1960
17) S. Hultberg *et al.*, private communication
18) J. H. Hamilton, W. F. Frey and S. Hultberg, Bull. Am. Phys. Soc. **5** (1960) 449

3.B: 3.C

Nuclear Physics **24** (1961) 251—268; © *North-Holland Publishing Co., Amsterdam*

Not to be reproduced by photoprint or microfilm without written permission from the publisher

PENETRATION MATRIX ELEMENTS AND NUCLEAR STRUCTURE EFFECTS IN Ta^{181}

Z. GRABOWSKI, B.-G. PETTERSSON, T. R. GERHOLM and J. E. THUN

Institute of Physics, University of Uppsala, Uppsala, Sweden

Received 16 January 1961

Abstract: Gamma-gamma and electron-gamma angular correlations in Ta^{181} have been measured. The following results were obtained:

$$\begin{aligned}
G_2A_2(133\gamma+137\gamma-482\gamma) &= -0.065\pm0.003,\\
G_2A_2(137\gamma-482\gamma) &= -0.04\ \pm0.015,\\
G_2A_2(133\mathrm{K}-482\gamma) &= -0.118\pm0.005,\\
G_2A_2(137\mathrm{K}-482\gamma) &= +0.030\pm0.013,\\
G_2A_2(133\gamma+137\gamma-482\mathrm{K}) &= -0.005\pm0.003,\\
A_2(346\gamma-136\mathrm{K}) &= +0.02\ \pm0.01.
\end{aligned}$$

The quadrupole attenuation factor G_2 was determined by delayed angular correlations and found to be the same in the gamma-gamma and electron-gamma correlations. The value obtained is $G_2 = 0.22\pm0.015$. An independent determination of G_2 based on a comparison between our $G_2A_2(133\gamma+137\gamma-482\gamma)$ and the value for $A_2(133\gamma+137\gamma-482\gamma)$ obtained by other groups using low viscosity liquid sources gave $G_2 = 0.23\pm0.015$.

In addition the following two conversion coefficients were determined from electron-gamma coincidence data:

$$\alpha_K(133) = 0.54\pm0.08, \quad \alpha_K(482) = 0.026\pm0.002.$$

The results have been used to analyze the 482 keV conversion process in terms of nuclear structure dependent conversion matrix elements. The 482 keV transition is of mixed E2/M1 character. The mixing ratio becomes $\delta(482) = 6.4\pm0.8$. The M1 conversion process is strongly affected by the penetration terms. The M1 conversion coefficient is about 10 times larger than the normal finite size corrected value. From the conversion coefficient and the angular correlations the parameter λ, defined as the ratio of the penetration matrix element and the normal gamma-ray matrix element, becomes $-70 \geqq \lambda \geqq -125$. The large λ-value is a consequence of the large retardation of the 482 keV M1 transition. For the strongly retarded 133 keV E2 transition, however, the conversion process is found to be normal.

It is concluded that the spin of the 619 keV level is $+\frac{5}{2}$ in disagreement with earlier tentative assignments.

1. Introduction

It has been observed recently [1]) that for certain strongly retarded magnetic dipole transitions large anomalies appear in the internal conversion process. The cause of these anomalies is the presence of so called penetration matrix elements in the internal conversion process. The penetration matrix element has only a small weight when compared to the normal gamma-ray matrix element. The small weighting, however, may be counterbalanced if the gamma-ray matrix element is considerably smaller than its dimensional value, i.e. if the

electromagnetic transition is much retarded. A necessary requirement is, of course, that the penetration matrix element for the same nuclear transition should be essentially unaffected and thus have its dimensional value.

These requirements are fulfilled for the l-forbidden ($\Delta l = 2$) M1 transitions between pure shell model states. In the deformed region l is no longer a good quantum number and the l-selection rule is expected to break down. However, for strongly deformed nuclei the asymptotic quantum numbers introduced by Nilsson forbid M1 and also E2 single particle transitions between certain single particle configurations [2]). Moreover, collective M1 and E2 transitions between different rotational bands are, of course, forbidden in the lowest order.

In Ta^{181} there is a mixed M1–E2 transition from the $\frac{5}{2}+$ excited state at 482 keV to the $\frac{7}{2}+$ ground state. In the Nilsson model the two states are classified as $|I, K, \pi\rangle = |\frac{5}{2}, \frac{5}{2}+\rangle \rightarrow |\frac{7}{2}, \frac{7}{2}+\rangle$, in other words as a transition between two different rotational bands. Both M1 and E2 transitions are forbidden by the selection rules of the appropriate asymptotic quantum numbers.

The $|\frac{5}{2}, \frac{5}{2}+\rangle$ and the $|\frac{7}{2}, \frac{7}{2}+\rangle$ states originate from the shell model states at $d_{\frac{5}{2}}$ and $g_{\frac{7}{2}}$, respectively. Consequently the 482 keV M1 (but not the E2) transition is expected to be forbidden also in the shell model picture. De Waard [3]) has measured the halflife for the 482 keV level. The result, 1.06×10^{-8} sec, together with the known (cf. below) E2/M1 mixing ratio indicates that both the M1 and the E2 transitions are much slower than predicted by the Weisskopf formula. The retardation factors are $R(\mathrm{M1}) = 2\,500\,000$ and $R(\mathrm{E2}) = 35$.

Large anomalies are expected to show up in the M1 internal conversion process. In a recent review article Church and Weneser have analyzed the 482 keV transition [4]). From published values for the conversion coefficient and angular correlations they conclude that existing experimental data indicate that the penetration matrix element might in fact be important. The λ-value, defined as the ratio of the penetration matrix element to the gamma ray matrix element, was found to be $-7 \leqq \lambda \leqq -150$. The uncertainties in the experimental values given for the conversion coefficient and for the E2/M1 mixing ratio do not allow for a more precise value for λ. In fact, $\lambda = +1$, which means complete absence of penetration effects in the conversion process, is barely excluded. The anomaly found for the M1 conversion coefficient could, as pointed out by the authors, be removed by increasing the theoretical E2 conversion coefficient by some 7 to 8 %.

The penetration effects should also be seen in the electron-gamma angular correlations, but published results [5, 6]) are too inaccurate to allow for any conclusions concerning the value for λ, though large positive values are excluded.

An experimental study of the 482 keV transition in Ta^{181} especially aiming at a search for penetration effects in the internal conversion process is apparently called for.

2. Remarks Concerning Angular Correlations and Internal Conversion Coefficient Measurements in Ta^{181}

For the analysis of the internal conversion process of the 482 keV transition in Ta^{181} we are interested in the following three parameters: the K-conversion coefficient, the E2/M1 mixing ratio and the ratio of the angular correlation functions $F_2(482\ \mathrm{K})/F_2(482\gamma)$.

The decay scheme of $Hf^{181} \rightarrow Ta^{181}$ has been studied by several experimenters [7, 8]). The relevant part of the decay scheme is given in fig. 1. As seen from

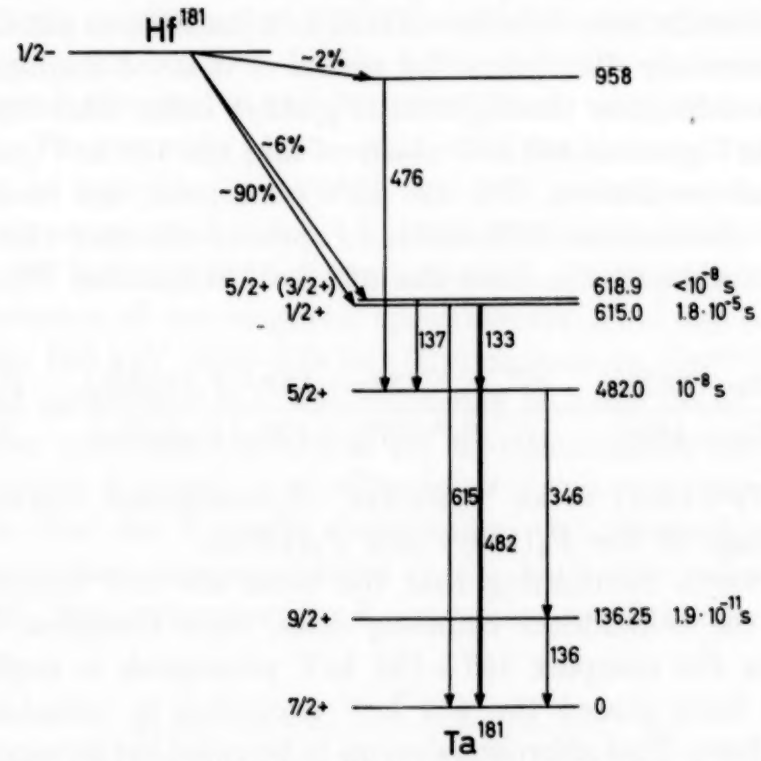

Fig. 1. Decay scheme of $Hf^{181} \rightarrow Ta^{181}$ based on A. V. Borovikov *et al.* [8]).

the decay scheme there are several transitions of nearly the same energy. Since these cannot be resolved in the scintillation spectrum certain complications arise in the gamma-gamma and electron-gamma angular correlation experiments. The difficulties, however, can be overcome for the correlations of interest in this connection. This will be discussed below.

There is an additional complication caused by the long half-life of the 482 keV level and by the large quadrupole moment of the strongly deformed Ta^{181} nucleus. Angular correlations for transitions cascading through the 482 keV level are expected to be strongly attenuated. There are two ways of overcoming this difficulty.

For gamma-gamma correlations the attenuations can be removed in the usual way by making use of low viscosity liquid sources. In this way the true, unperturbed, angular correlation may be obtained.

For gamma-electron correlations, however, one has to use solid sources and hence the correlation will be strongly attenuated. However, from the gamma-electrons and gamma-gamma correlations measured with the same source one can determine the ratio of the A_2-coefficients

$$\frac{A_2(\gamma e)}{A_2(\gamma\gamma)} = \frac{G'_2 F_2(\gamma_1) F_2(e_2)}{G''_2 F_2(\gamma_1) F_2(\gamma_2)}. \tag{1}$$

Consequently the ratio $F_2(e_2)/F_2(\gamma_2)$ can be determined, independently of attenuations, provided only $G'_2 = G''_2$. This ratio can be used for the analysis of the angular correlations. Whether it is in fact justified to put G'_2 equal to G''_2 can be experimentally determined by means of delayed angular correlations.

We want to determine the $F_2(482e)/F_2(482\gamma)$ ratio. This can be obtained from the 133 keV gamma-482 keV electron and the 133 keV gamma-482 keV gamma angular correlations. The 137 keV photopeak, not resolved from the 133 keV peak, presents no difficulties in spite of the fact that the 137 keV transition is in coincidence with the 482 keV transition. The ratio simply becomes

$$\frac{A_2(137\gamma+133\gamma-482\mathrm{K})}{A_2(137\gamma+133\gamma-482\gamma)} = \frac{G'_2 F_2^*(137\gamma+133\gamma) F_2(482\mathrm{K})}{G''_2 F_2^*(137\gamma+133\gamma) F_2(482\gamma)} = \frac{F_2(482\mathrm{K})}{F_2(482\gamma)}, \tag{2}$$

where $F_2^*(137\gamma+133\gamma)$ is an "effective" F_2-coefficient corresponding to a weighted average of the $F_2(133\gamma)$ and $F_2(137\gamma)$.

It may be worth mentioning that the weak 476 keV transition does not contribute to the coincidence counting rates, since Compton background of this line under the complex 137+133 keV photopeak is negligible. Earlier experimenters have placed the 476 keV transition in coincidence with the 137+133 keV lines. This alternative seems to be ruled out by recent coincidence experiments reported in ref. [8]). However, even if the 476 keV line would be in coincidence with the 137+133 keV complex our results would remain essentially unaffected.

TABLE 1

K conversion coefficients

Transition energy (keV)	α_K	Ref.
133	0.48 ±0.02	[9])
	0.49	[7])
	0.50 ±0.06	[6])
	0.54 ±0.08	present work
482	0.032±0.04	[9])
	0.027	[7])
	0.023±0.02	[6])
	0.026±0.02	present work

The second factor of importance for our analysis is the K conversion coefficient of the 482 keV transition. This has been experimentally determined by several independent groups [6, 7, 9]). The results are given in table 1. However, it can also be experimentally determined by means of 133 keV electrons-482 keV gamma coincidences. The conversion probability $\mathscr{H}_K(482)$ is obtained from

$$\mathscr{H}_K(482) = \frac{N(482\mathrm{K})C(133\mathrm{K}-482\gamma)}{N(133\mathrm{K})N(482\gamma)q(133-482)\omega}, \tag{3}$$

where $N(482\mathrm{K})$ and $N(133\mathrm{K})$ are the peak counting rates on the K conversion lines in a magnetic spectrometer. $C(133\mathrm{K}-482\gamma)$ is the coincidence counting rate obtained with the 133 keV K line focussed in the spectrometer and the 482 keV photopeak accepted in the gamma-channel, where the single counting rate is $N(482\gamma)$. The quantity $q(133-482)$ is the fraction of all 133 keV transitions which are in coincidence with the 482 keV transition; the fraction q is obtained with an accuracy of about 3 % from the known relative intensities of the competing 482 keV and 346 keV transitions [7]). The remaining factor in (3) is the transmission ω of our magnetic spectrometer. This has been calibrated by means of the 165 keV (M4)–134 keV(E2) cascade in Hg^{197m}. The method applied for this calibration has been discussed in some detail in ref. [10]). To eliminate angular correlation effects in (3) the coincidences were taken in the 126° position (where $P_2(\cos\theta) = 0$). The detector was at a close distance from the source such that the $P_4(\cos\theta)$ contribution was smeared out. Moreover, the angular correlation was attenuated to the hard core value.

From $\mathscr{H}_K(482)$ thus determined the K conversion coefficient is obtained from the relation

$$\alpha_K = \frac{\mathscr{H}_K}{1-\mathscr{H}_K\left(1+\dfrac{L+M+N}{K}\right)}, \tag{4}$$

where the $(L+M+N)/K$ ratio was taken from the measured electron spectrum.

The last parameter of importance for the analysis of the conversion matrix element of the 482 keV transition is the mixing ratio $\delta(482)$, which here is defined as

$$\delta^2 = \frac{\mathrm{E2}}{\mathrm{M1}}. \tag{5}$$

The sign of δ is chosen in accordance with the notation used by Biedenharn and Rose [11]).

In principle $\delta(482)$ can be derived from the $F_2(482\gamma)$ which appears in the expression for the A_2 coefficient of the 133 keV gamma–482 keV gamma correlation,

$$A_2(133\gamma-482\gamma) = F_2(133\gamma)F_2(482\gamma). \tag{6}$$

However, this A_2 coefficient cannot be obtained directly from our corresponding gamma-gamma correlation. There are two corrections to be taken into account, one for the large attenuation to be expected in our experiments with solid sources and another for the admixture of the unresolved 137 keV–482 keV correlation.

The appropriate attenuation factor is obtained by comparing our measured A_2-coefficient for the (133+137) keV gamma–482 keV gamma cascade with the true A_2 coefficient for the corresponding unperturbed correlation.

Studies of the (133+137) keV gamma–482 keV gamma correlation has been published by McGowan [12]), Snyder and Frankel [6]), Lindqvist and Karlsson [13]), and by Debrunner *et al.* [14]). The results given in table 2 are in good agreement. McGowan also measured delayed angular correlations and obtained the same results, which is a sensitive criterion for absence of perturbations. Debrunner *et al.* [14]) arrived to the same conclusion by comparing the possible attenuations of their measured A_2 and A_4 terms.

The second problem concerns the admixture of the 137 keV–482 keV coincidences. To overcome this difficulty a triple coincidence experiment was performed. Owing to the long half-life of the 615 keV level (18.1 ± 0.3 μs) [15]) the 133 keV transition will not give coincidences with the beta-particles feeding this level. The lifetime of the 619 keV level is much shorter ($< 10^{-8}$ s). Fast coincidences between beta-particles and the 482 keV gamma-ray can thus be used to select the decays via the 137 keV transition. A (β–γ–γ) triple coincidence experiment will therefore give the pure 137 keV–482 keV gamma-gamma correlation.

Since the attenuation factor can be measured and the relative gamma-ray intensities of the 137 keV and 133 keV transitions are known [7]), the true unperturbed $A_2(133\gamma-482\gamma)$ is easily derived from the measured $A_2(137\gamma+133\gamma-482\gamma)$ and $A_2(137\gamma-482\gamma)$.

The ground state spin of the Ta^{181} nucleus has been measured [16]) to be $\frac{7}{2}$. From the 482 keV level there is a 346 keV–136 keV cascade to the ground state. The 136 keV level is the first excited state, reached in Coulomb-excitation, and has been interpreted as the first rotational state above the $\frac{7}{2}$ ground state. It must have a spin of $\frac{9}{2}$. From the 346 keV gamma–136 keV gamma correlation [14]) and from a measurement of the angular distribution of the 136 keV gamma-rays after Coulomb-excitation of the 136 keV level [17]) it can be shown that the spin of the 482 keV level must be $\frac{5}{2}$. Debrunner *et al.* have shown that there are three alternative spin sequences compatible with the measured $A_2(133\gamma-482\gamma)$, but the $\frac{5}{2}$ spin assignment to the 482 keV level rules out two of these leaving as the only possible alternative $\frac{1}{2} \rightarrow \frac{5}{2} \rightarrow \frac{7}{2}$ as first suggested by de Waard.

Thus the 133 keV transition becomes a mixture of E2+M3. In order to determine the value for the $F_2(133\gamma)$ we have to know the M3 admixture.

Under normal circumstances the M3 transition probability is vanishingly small in competition with E2. However, the long half-life of the 615 keV level shows that the E2 transition must be strongly retarded. Therefore a contribution of M3 cannot be excluded off hand. The retardation of E2 can be understood from the selection rules of the asymptotic quantum numbers assigned to the $\frac{1}{2}$ and $\frac{5}{2}$ levels in the Nilsson model.

The penetration matrix elements are expected to be very small for the E2 K conversion process since this leads primarily to the $d_{\frac{1}{2}}$ continuum state which is known to be very insensitive to nuclear finite size effects. An experimental confirmation of this prediction can be obtained by means of the 133 keV electron–482 keV gamma cascade. From the measured $A_2(133\mathrm{K}-482\gamma)$ and $A_2(133\gamma-482\gamma)$ coefficients we obtain the ratio

$$\frac{A_2(133\mathrm{K}-482\gamma)}{A_2(133\gamma-482\gamma)} = \frac{F_2(133\mathrm{K})}{F_2(133\gamma)}, \tag{7}$$

which is independent of the attenuations. As shown below this ratio is in good agreement with the theoretical prediction for a nuclear structure independent pure E2 transition. It should be observed that the angular correlation is expected to be very sensitive to small M3 admixtures since the theoretical M3 K-conversion coefficient is 80 times larger than the E2 coefficient. This, effectively, increases the M3 admixture by two orders of magnitude. Unfortunately it is not possible to make any quantitative analysis since the particle parameter for an E2+M3 mixing has not been calculated.

Further information concerning the maximum amount of M3 admixture can be derived from the conversion coefficient of the 133 keV transition. This conversion coefficient is easily obtained from our electron-gamma and gamma-electron coincidence measurements. One has

$$\mathscr{H}_{\mathrm{K}}(133) = \frac{C(133\mathrm{K}-482\gamma)}{N(482\gamma)\omega q(482-133)}, \tag{8}$$

where $q(482-133)$ is the fraction of all 482 keV transitions which are in coincidence with the 133 keV transition. From $\mathscr{H}_{\mathrm{K}}$ we get the internal conversion coefficient α_{K} using (4). From the value for α_{K} we can determine or place an upper limit for the M3 admixture. This means that we now know the $F_2(133\gamma)$ and are able to use the experimental $A_2(133\gamma-482\gamma)$ to determine $F_2(482\gamma)$ from (6). Finally, from F_2 (482γ) we get $\delta(482)$.

3. Experiments

The Hf^{181} activity was produced by neutron irradiation at DIDO in Harwell at a neutron flux of 10^{14} n/cm^2 · sec. Spectroscopically pure HfO_2 enriched to

93.3 % in Hf^{180} was irradiated for three weeks. The active HfO_2 was dissolved in HNO_3 and vacuum evaporated from a wolfram strip onto a 0.6 mg/cm² aluminium foil. The evaporation temperature was kept sufficiently low to avoid simultaneous wolfram evaporation. The sources were estimated to have a thickness of less than 10 μg/cm².

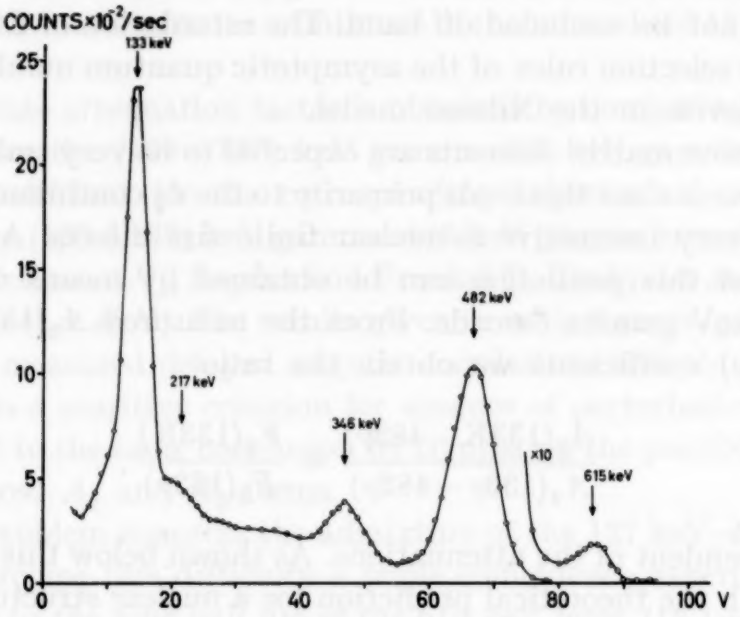

Fig. 2. Scintillation spectrum of Hf^{181} taken with a 0.6 mm Sn absorber.

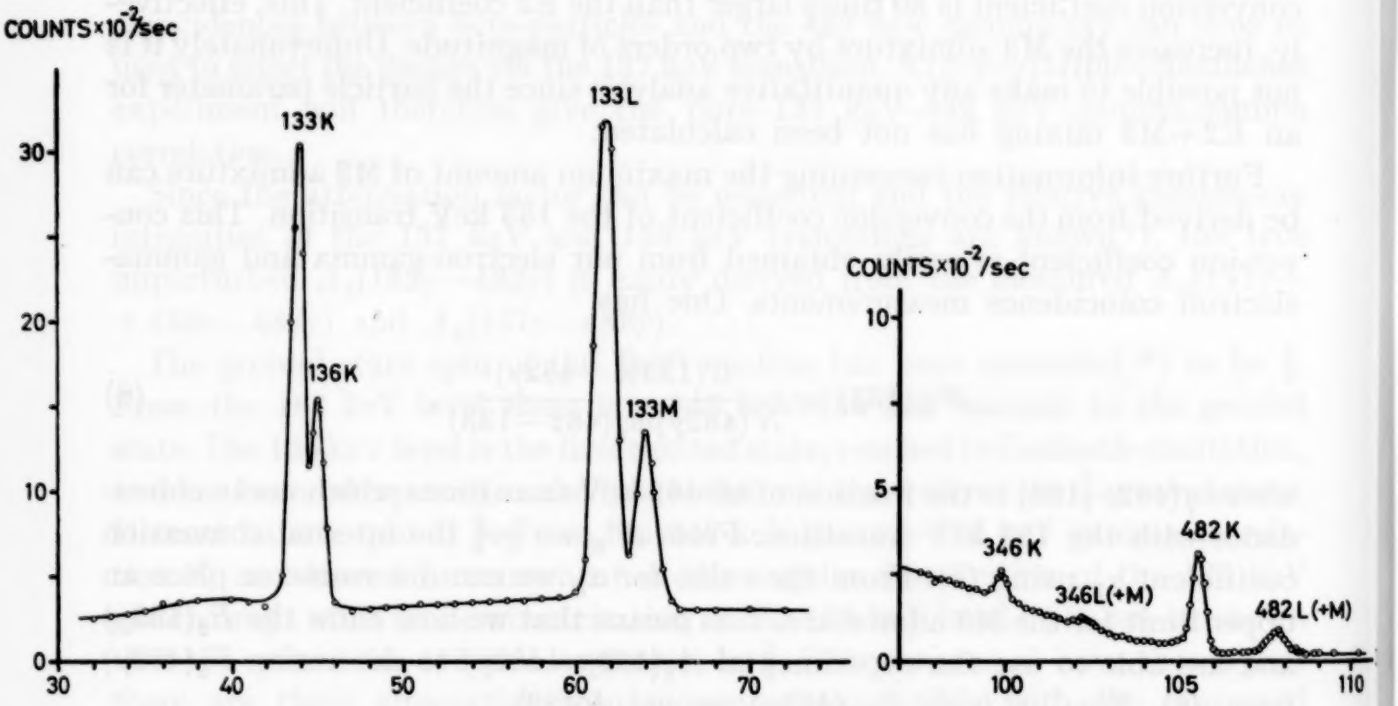

Fig. 3. Electron spectrum of Hf^{181}.

The only contamination is due to the Hf^{175} activity. Judging from our electron spectra this contamination was less than 1 % and did not interfere with our Hf^{181} experiments.

The gamma-gamma correlations were measured with an automatic instrument described by Lindqvist [19]). For the triple coincidence experiment, discussed above, the gamma-gamma correlation instrument was gated with pulses taken from a third scintillation detector placed near the source. In this detector a 1 mm thick anthracene crystal was used to record the beta-particles in coincidence with the 137 keV–482 keV cascade. The electron-gamma correlations were studied in an electron-gamma angular correlation spectrometer constructed by Gerholm and Pettersson [20]). The sources were first centred with respect to the optical axis of the magnetic spectrometer and thereupon the centre of rotation of the gamma-channel was adjusted to coincide with the centre of the source. Residual minute variations, less than 0.2 %, in the gamma-counting rate at different angles were corrected for in the usual way by dividing the coincidence counting rate with the gamma single counting rate. The magnetic spectrometer was adjusted to a resolution of 1.5 % for the 133 keV electron-482 keV gamma correlations and to a resolution of 3 % for the 133+137 keV gamma–482 keV electron correlations. The 136 keV electron–482 keV gamma correlation was measured with a resolution of 1.5 %.

In figs. 2 and 3, a scintillation spectrum and an electron spectrum of Hf^{181} are shown.

3.1. STUDIES OF THE ATTENUATION OF THE ANGULAR CORRELATIONS

Our angular correlation experiments have been made with solid sources. Owing to the long lifetime of the 482 keV level and the large quadrupole moment of the Ta^{181} nucleus large attenuations of the angular correlations are to be expected. As pointed out above these attenuations will not affect our interpretations, provided only that the basic assumption $G'_2 = G''_2$ is correct. In other words we assume that the gamma-gamma and the gamma-electron correlations measured with the same source are equally attenuated.

The theory of the quadrupole interaction mechanism has been worked out by Abragam and Pound [21]). It follows from their theory that the attenuation factors are functions of the parameters ω_0, t_0 and τ_0, i.e. the quadrupole precession frequency, the time-delay and the resolving time of the coincidence arrangement respectively. Provided these parameters are the same

$$G'_2(\omega_0, t_0, \tau_0) \equiv G''_2(\omega_0, t_0, \tau_0).$$

However, the attenuation factors might be very sensitive functions of the three parameters. Minor differences in t_0 and τ_0 and a slight variation of ω_0 with time due to ageing effects in the source could therefore possibly effect our results if not proper precautions are taken. To make sure that our results

were unaffected by t_0 and τ_0 the same coincidence circuit was used in both the gamma-gamma and the gamma-electron correlations and the resolving time was taken to be long ($2\tau_0 = 7\times10^{-8}$ s) compared to the nuclear half-life.

As shown in ref. [22]) the precession period can be determined by means of delayed angular correlations. The value for ω_0 was determined in this way for both the gamma-gamma and the gamma electron correlations. The precession period was found to be equal. Thus aging effects, possibly present in the sources, could not significantly alter our results, in particular since our gamma-gamma and gamma-electron experiments were "sandwiched" in time.

From the product of the precession frequency and the lifetime of the excited state τ_N, determined as $4 \leqq \omega_0\tau_N \leqq 12$ in our delayed angular correlation studies, the appropriate attenuation factor for the "time-integral", i.e. with $\tau_0 \gg \tau_N$, experiments was calculated. The result is $G_2 = 0.22\pm0.015$, which is slightly higher than the "hard-core" limit of $G_2 = 0.20$. Since in the hard-core limit G_2 approaches a constant value, independent of ω_0, t_0 and τ_0, the fact that our experimental value are very close to this limit serves as an additional precaution. Minor variations in ω_0, t_0 and τ_0 should not affect our "time integral" correlations used for the interpretation below.

Finally, by comparing our "time integral" gamma-gamma correlations obtained with solid sources with the corresponding results obtained with low viscosity liquid sources, we can get an independent experimental determination of the attenuation factor. As seen in table 2 the result is $G_2 = 0.23\pm0.015$ in good agreement with the value obtained from our delayed angular correlations and the theory of Abragam and Pound. This agreement may be taken as an additional support for the conclusion that the angular correlation measured with low viscosity sources in fact represents the true unperturbed correlation.

3.2. THE (133+137) keV GAMMA – 482 keV K ELECTRON AND THE (133+137) keV GAMMA – 482 keV GAMMA CORRELATIONS

The same source was used to measure these two correlations. 3 gamma-electrons and 5 gamma-gamma runs were taken. As an additional precaution these were "sandwiched" in time. The results, summarized in table 2 are

$$G_2A_2(133\gamma+137\gamma-482\mathrm{K}) = -0.005\pm0.003,$$
$$G_2A_2(133\gamma+137\gamma-482\gamma) = -0.065\pm0.003.$$

Thus we get

$$\frac{F_2(482\mathrm{K})}{F_2(482\gamma)} = +0.08\pm0.05.$$

3.3. THE K CONVERSION COEFFICIENT OF THE 482 keV TRANSITION AND THE 133 keV TRANSITION

The K conversion coefficients of these two transitions is obtained from the 133 K-482γ coincidence counting rate and the corresponding single counting

rates $N(133\text{K})$, $N(482\gamma)$ and $N(482\text{K})$ using the formulae (3), (4), and (8). It is necessary to know the coincidence coupling constants $q(133-482)$ and $q(482-133)$.

TABLE 2

Directional correlations measured in Ta^{181}

Correlation measured	G_2A_2	A_2	Ref.
$(133+137)\gamma$–$482\,\gamma$		-0.291 ± 0.006	[6]
		-0.280 ± 0.004	[12]
		-0.230 ± 0.012	[13]
		-0.281 ± 0.010	[14]
	-0.065 ± 0.003	-0.295 ± 0.030	present work
$(133+137)\gamma$–482 K	-0.033 ± 0.014	-0.165	[6]
	-0.005 ± 0.003	-0.022 ± 0.015	present work
$137\gamma-482\gamma$	-0.04 ± 0.015	$-0.17\ \pm0.09$	present work
133 K$-482\,\gamma$	$-0.13\ \pm0.02$	-0.65	[6]
	-0.118 ± 0.005	$-0.52\ \pm0.06$	present work
137 K$-482\,\gamma$	$+0.030\pm0.013$	$+0.13\ \pm0.06$	present work
136 K$-346\,\gamma$		$+0.02\ \pm0.01$	present work

The probability that a 133 keV transition is followed by a 482 keV transition, i.e. $q(133\text{–}482)$, depends on the branching ratio of the 482 keV and the 346 keV transitions. This branching ratio has been determined by Boehm and Marmier with a crystal diffraction spectrometer and a high resolution solenoidal beta-ray spectrometer. A minor correction has also been applied to the 482 keV single counting rates due to the admixture of the 476 keV transition, not resolved in our experiment. Using the relative intensities given by Boehm and Marmier we get $q(133-482) = 0.85\pm0.025$.

In the same way the probability that a 482 keV transition is preceeded by a 133 keV transition, i.e. $q(482-133)$, depends on the branching ratio of the 133 keV transition and the sum of the transition intensities of the 137 keV and the 476 keV lines. The relative transition intensities were taken from Boehm and Marmier and from our relative K-line intensities of the 133 keV and 137 keV transitions. The value thus obtained becomes $q(482-133) = 0.93\pm0.02$.

The conversion probabilities obtained from the coincidence experiments become

$$\mathscr{H}_K(482) = 0.0258\pm0.0015, \quad \mathscr{H}_K(133) = 0.229\pm0.012.$$

To determine the conversion coefficients we have measured the K/L+M+N ratios. Our results are

$$(\text{K}/(\text{L}+\text{M}+\text{N}))_{482} = 3.8\pm0.3, \quad (\text{K}/(\text{L}+\text{M}+\text{N}))_{133} = 0.68\pm0.03,$$

and from (4) we get (cf. table 1)

$$\alpha_K(482) = 0.026 \pm 0.002, \quad \alpha_K(133) = 0.54 \pm 0.08.$$

3.4. THE (133+137) keV GAMMA – 482 keV GAMMA AND THE 137 keV GAMMA – 482 keV GAMMA CORRELATIONS

As mentioned above we want to determine the 133 keV gamma-482 keV gamma correlation. Because of the presence of the 137 keV transition the measured correlation becomes a mixture of the 137 keV and 133 keV gamma-482 keV gamma correlations. To correct for the admixture of the 137 keV-gamma-482 keV gamma correlation one has to know the relative gamma intensities and the $A_2(137\gamma-482\gamma)$. Boehm and Marmier have determined the relative intensities with a crystal diffraction spectrometer of high resolution, such that the two gamma-lines were well separated. The beta-gamma-gamma triple coincidence experiment discussed above selects the 137 keV gamma-482 keV gamma cascade and gives for the A_2-coefficient

$$G_2A_2(137\gamma-482\gamma) = -0.04 \pm 0.015.$$

The (137+133) keV gamma-482 keV gamma results summarized in table 2 give

$$G_2A_2(137\gamma+133\gamma-482\gamma) = -0.065 \pm 0.003.$$

From our $A_2(137\gamma-482\gamma)$ and the relative gamma intensities given by Boehm and Marmier we get

$$G_2A_2(133\gamma-482\gamma) = -0.066 \pm 0.004.$$

Finally, if we apply the same correction to the unperturbed $A_2(137\gamma+133\gamma-482\gamma)$ measured with low viscosity sources we get, for the unperturbed correlation

$$A_2(133\gamma-482\gamma) = -0.284 \pm 0.013.$$

3.5. THE 133 keV K ELECTRON – 482 keV GAMMA AND THE 137 keV K ELECTRON – 482 keV GAMMA CORRELATIONS

In these cases there is no interference with the 137 keV transition since the two K-lines are clearly separated. The results are summarized in table 2 and give

$$G_2A_2(133\mathrm{K}-482\gamma) = -0.118 \pm 0.005,$$
$$G_2A_2(137\mathrm{K}-482\gamma) = +0.030 \pm 0.013.$$

4. Interpretations

Of the three factors of importance for our analysis of the penetration matrix elements in the 482 keV transition two have been obtained above namely the ratio $F_2(482\mathrm{K})/F_2(482\gamma)$ and $\alpha_K(482)$. It remains to settle the problem of the

E2/M1-mixing ratio of the 482 keV transition. To determine this we first analyze the 133 keV transition. As shown above this is a $\frac{1}{2}(E2+M3)\frac{5}{2}$ transition. An observable M3 admixture cannot be excluded since the E2 transition is known to be very much retarded.

From the L subshell ratios [7]) $L_I : L_{II} : L_{III} = 0.26 : 1.26 : 1$ it is seen that the transition is of predominantly E2 character. The theoretical subshell ratios are 0.20 : 1.23 : 1 for E2 and 1.2 : 0.20 : 1 for M3.

A small M3 admixture should appear in the gamma-gamma angular correlation. However, the 133 keV electron-482 keV gamma correlation becomes a much more sensitive measure of a small M3 admixture since the 133 keV theoretical M3 K conversion coefficient is about 80 times larger than the E2 coefficient. Therefore already the ratio

$$\frac{G_2A_2(133\text{K}-482\gamma)}{G_2A_2(133\gamma-482\gamma)} = \frac{F_2(133\text{K})}{F_2(133\gamma)} = 1.8\pm0.2$$

can be used to investigate the M3 admixture in the 133 keV transition. Unfortunately the E2+M3 mixing parameter has not yet been calculated and no quantitative analysis is possible. However, our value for the ratio $F_2(133\text{K})/F_2(133\gamma)$ given above agrees, within the limits of error, with the theoretical value for a pure E2 transition

$$\frac{F_2(133\text{K, E2})}{F_2(133\gamma\text{, E2})} = 1.84.$$

We therefore conclude that the M3 admixture is negligibly small.

The large retardation of the E2 transition may, however, give rise to anomalous conversion matrix elements. If this were the case our conclusion above might be wrong. This problem can be settled by comparing the experimental and the theoretical K-conversion coefficients. Log-log interpolation in Sliv and Band's tables give for a pure E2 transition

$$\alpha_2 = 0.49$$

in agreement with our experimental value

$$\alpha_K(133) = 0.54\pm0.08.$$

Thus we may conclude that even for this very strongly retarded E2 transition (the retardation factor is 400) the penetration matrix elements have a negligible weight when compared to the normal conversion matrix elements.

Once the pure E2 nature of the 133 keV transition has been established we may use the value for $A_2(133\gamma-482\gamma)$ obtained above to determine $F_2(482\gamma)$, since

$$F_2(482\gamma) = \frac{A_2(133\gamma-482\gamma)}{F_2(133\gamma)} = 0.53\pm0.025,$$

where the value for $F_2(133\gamma) = -0.535$ is taken from Ferentz and Rosenzweig's tables [23]). In fig. 4, $F_2(482\gamma)$ is given as a function of $\delta(482)$. The experimental value for $F_2(482\gamma)$ given above corresponds to

$$\delta(482) = 6.4 \pm 0.8.$$

As discussed above the 137 keV gamma-482 keV gamma correlation was measured in the triple coincidence experiment primarily to obtain the corrections to be applied to the mixed (133+137) gamma correlations. The result

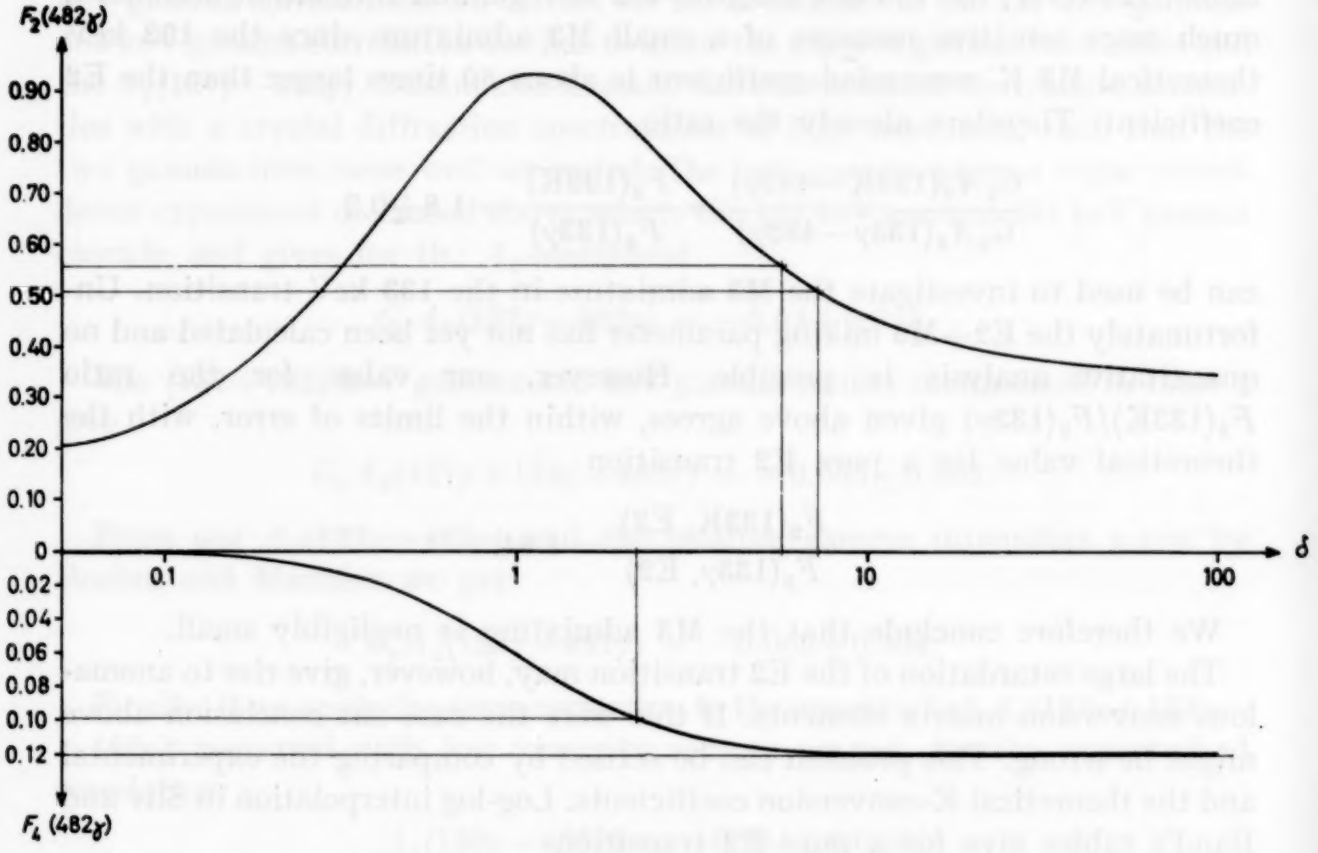

Fig. 4. The functions $F_2(482\gamma)$ and $F_4(482\gamma)$ versus $\delta(482\gamma)$. The experimental results (horizontal lines) determines the mixing ratio to be δ (482) = $+6.4 \pm 0.8$.

obtained may be used, however, to determine the spin of the 619 keV level and the mixing ratio of the 137 keV transition. From the values given above for $A_2(137\gamma-482\gamma)$, $A_2(137\mathrm{K}-482\gamma)$ and $F_2(482\gamma)$, we get

$$F_2(137\gamma) = -0.32 \pm 0.20, \quad F_2(137\mathrm{K}) = +0.25 \pm 0.13.$$

These two values are only compatible with a $+\frac{5}{2}$ assignment, corresponding to a unique first forbidden beta transition to this level. The empirical log *ft* value 8.5 ± 0.5 for such a transition is in agreement with the experimental value 8.4. For the mixing ratio E2/M1 we get

$$\delta(137) = +2.3 \pm 0.9.$$

Our $+\frac{5}{2}$ assignment is in disagreement with the value $+\frac{3}{2}$ suggested by Mottelson and Nilsson [2]), who considered the 619 keV level as the first member of a rotational band starting with the 615 keV spin $\frac{1}{2}$ state.

5. The Penetration Matrix Elements of the 482 keV Transition

It may be seen already from the M1 internal conversion coefficient that the conversion process is strongly anomalous. From our experimental values for $\delta(482)$ and $\alpha_K(482)$ we get for the partial M1 conversion coefficient

$$\beta_1(\text{exp}) = 0.40 \pm 0.15,$$

to be compared with the value obtained from Sliv and Band's tables

$$\beta_1(\text{Sliv}) = 0.0482.$$

The partial E2 conversion coefficient was assumed to be unaffected by penetration effects. This assumption seems to be well justified on the basis of our results obtained for the pure E2 133 keV transition discussed above. We have also recently confirmed [1, 10]) that for Tl^{203}, Tl^{201} and Hg^{198} the experimental E2 conversion coefficients agree with the values tabulated by Sliv and Band and by Rose.

The large discrepancy found for the M1 conversion coefficient is a consequence of the appearance of a penetration matrix element in the internal conversion process. The magnitude of this matrix element is determined by the parameter λ, defined as

$$\lambda = \frac{M_e}{M_\gamma}, \tag{9}$$

where M_e is the penetration matrix element and M_γ is the normal gamma-ray matrix element. According to Church and Weneser the expression for $\beta_1(\lambda)$ becomes

$$\beta_1(\lambda) = \beta_1(\text{Sliv})\{1-(\lambda-1)C(Z,k)\}^2, \tag{10}$$

where $C(Z,k)$ is a weighting function tabulated by Church and Weneser [24]). Thus λ cannot be uniquely determined from the conversion coefficient alone. To each experimental value for $\beta_1(\lambda)$ correspond two possible λ-values.

However, λ can also be obtained from the electron-gamma angular correlation experiments since $F_2(482\text{K})$ is a function of λ

$$F_2(482\text{K}) = \frac{b_2^{\,m} F_2^{\,m} + 2p b_2 F_2 + p^2 b_2^{\,e} F_2^{\,e}}{1+p^2}, \tag{11}$$

where p is defined as

$$p = \delta \sqrt{\frac{\alpha_2}{\beta_1(\text{Sliv})[1-(\lambda-1)C(Z,k)]^2}}. \tag{12}$$

In (11) the values for F_2^m, F_2 and F_2^e are taken from Ferentz and Rosenzweig [23]). The particle parameters may be taken from Biedenharn and Rose,

TABLE 3

The particle parameters $b_2^m(\lambda)$ and $b_2(\lambda)$ for different values of λ.

λ	b_2	b_2^m
−100	−0.3627	0.0847
−75	−0.3660	0.1035
−50	−0.3732	0.1293
−40	−0.3777	0.1429
−30	−0.3834	0.1596
−20	−0.3906	0.1807
−10	−0.4000	0.2080
0	−0.4129	0.2446
10	−0.4314	0.2956
20	−0.4603	0.3697
30	−0.5095	0.4740

The value $C(Z, k) = 0.020$ was used in the calculations

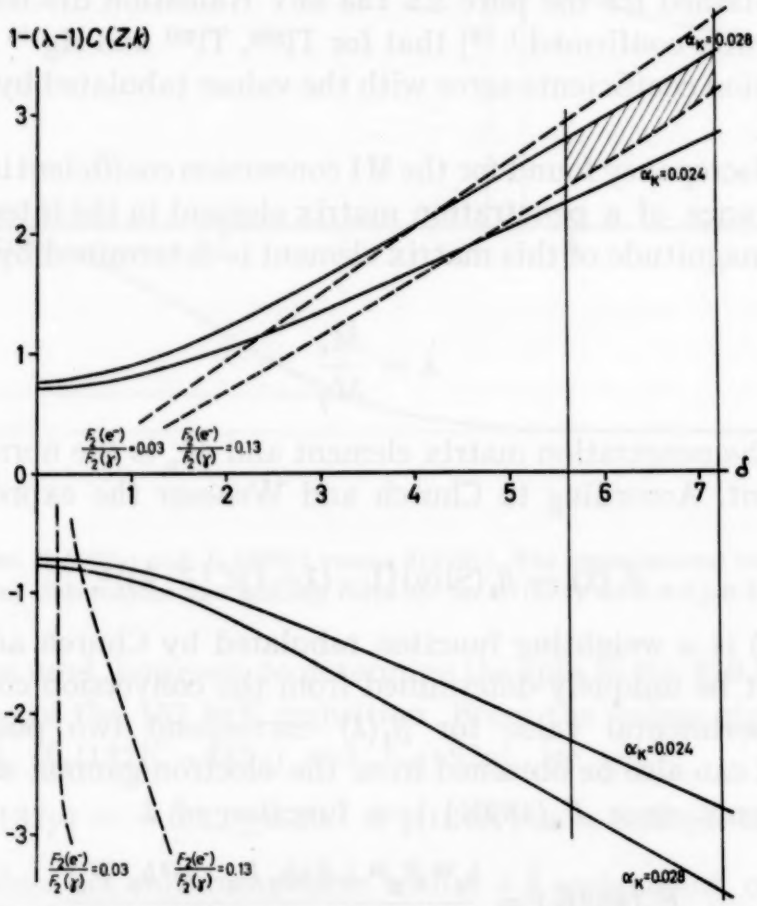

Fig. 5. The function $1-(\lambda-1)C(Z, k)$ versus $\delta(482)$. Solid curves are determined by the internal conversion coefficient and the dashed curves by the ratio $F_2(482\,e)/F_2(482\gamma)$ The vertical lines represents the limits for the mixing ratio as determined in fig. 4. The shaded area corresponds to values for $1-(\lambda-1)C(Z, k)$ in agreement with the experimental data. For $C(Z, k) = +0.020$ one obtains $-75 \geqq \lambda \geqq -125$. The M1 conversion coefficient is therefore about 10 times larger than the value given by Sliv and Band.

but since these calculations have been performed in the point nucleus approximation the values given in the tables have to be corrected in two ways: "Static" finite size effects have to be taken into account in both the E2 and the M1 conversion processes. In addition a correction for the "dynamic" or penetration effects, has to be applied to the particle parameters involved in the M1 conversion process. Thus the "static" correction affects all three particle parameters, while the "dynamic" correction applies only to b_2^{m} and b_2. These two become functions of λ. The procedure for these corrections has been described in a preceding paper [1]). For the calculation of $b_2^{\mathrm{m}}(\lambda)$ and $b_2(\lambda)$ the electronic computor FACIT in Stockholm was used. The calculated values are shown in table 3.

In fig. 5 we give in a $1-(\lambda-1)C(Z, k)$ versus δ plane the curves defined by the experimental values for $F_2(482\mathrm{K})/F_2(482\gamma)$ and $\alpha_{\mathrm{K}}(482)$. As shown in the figure there is a region of overlap for positive values of $1-(\lambda-1)C(Z, k)$. It is also seen in the figure that our experimental values for $\delta(482)$ agrees with the overlap area. The shaded area corresponds to values for λ and δ in agreement with the experimental results. If $C(Z, k)$ is taken to be $+0.020$ one has

$$-70 \geqq \lambda \geqq -125.$$

6. Conclusions

The results obtained above show that this strongly retarded M1 transition is largely affected by the presence of a penetration matrix element. We have recently found similar effects for the l-forbidden M1 transitions in Tl^{203} and Tl^{201}. In the latter case, however, the anomaly is only seen in the gamma-electron angular correlation experiment. Due to an accidental coincidence, the internal conversion coefficient for these l-forbidden transitions in Tl^{203} and Tl^{201} are almost exactly equal to the values tabulated by Sliv and Band, while the angular correlation experiments showed that the value for λ must be about $+76$. In the general case, however, the penetration effects are expected to show up both in the angular correlations and in the internal conversion coefficient. This is illustrated by the 482 keV transition in Ta^{181} where the experimental value for β_1 is *one order of magnitude larger* than the value obtained from Sliv and Band's tables. To get a unique determination of λ it is necessary to measure angular correlations as well as to determine the internal conversion coefficient.

The values for λ obtained for the 482 keV transition and for the l-forbidden transitions in Tl^{203} and Tl^{201} are of the same order of magnitude but of opposite signs.

The penetration matrix element determined here provides new information concerning the structure of the Ta^{181} nucleus not available in any other ways. The experimental λ value may be compared to theoretical values obtained from various nuclear models. The Nilsson model, used to describe the Ta^{181} nucleus, for example, predicts [4]) $|\lambda| \approx 600$.

We are indebted to the Director of this Institute, Professor Kai Siegbahn, for the excellent research facilities provided. Thanks are further due to Mr. W. C. Parker for his help in preparing the sources. The work has been sponsored by the U. S. Air Research and Development Command. One of us (Z. G.) expresses his gratitude to the Swedish Institute for Cultural Exchange for a fellowship.

References

1) T. R. Gerholm, B.–G. Pettersson, B. van Nooijen and Z. Grabowski, Nuclear Physics **24** (1961) 177;
B.–G. Pettersson, T. R. Gerholm, Z. Grabowski and B. van Nooijen, Nuclear Physics **24** (1961) 196
2) B. R. Mottelson and S. G. Nilsson, Mat. Fys. Skr. Dan. Vid. Selsk. **1**, No. 8 (1959)
3) H. de Waard, Physica **18** (1952) 1151
4) E. L. Church and J. Weneser, Ann. Rev. Nucl. Science **10** (1960) 193
5) F. Gimmi, E. Heer and P. Scherrer, Helv. Phys. Acta **29** (1956) 147
6) E. S. Snyder and S. Frankel, Phys. Rev. **106** (1957) 755
7) F. Boehm and P. Marmier, Phys. Rev. **103** (1956) 342
8) A. V. Borovikov, V. S. Gvozdev, I. A. Kondurov and Y. L. Khazdov, Izvest. Akad. Nauk, SSSR, Ser. Fiz. **23** (1959) 1448
9) F. K. McGowan, Phys. Rev. **93** (1954) 163
10) B.–G. Pettersson, J. E. Thun and T. R. Gerholm, Nuclear Physics **24** (1961) 243
11) L. C. Biedenharn and M. E. Rose, Revs. Mod. Phys. **25** (1953) 729
12) F. K. McGowan, Phys. Rev. **93** (1954) 471
13) T. Lindqvist and E. Karlsson, Ark. f. Fysik **12** (1957) 519
14) P. Debrunner, E. Heer, W. Kundig and R. Ruetschi, Helv. Phys. Acta **29** (1956) 463
15) J. E. Draper and R. L. Hickok, Phys. Rev. **108** (1957) 1280
16) J. H. Gisolf and P. Zeeman, Nature **132** (1933) 566
17) F. K. McGowan and P. H. Stelson, Phys. Rev. **109** (1958) 901
18) H. de Waard, Thesis, University of Groningen (1954)
19) T. Lindqvist, Ark. Fysik **12** (1957) 495
20) T. R. Gerholm and B.–G. Pettersson, Nuclear Instruments **4** (1959) 107
21) A. Abragam and R. V. Pound, Phys. Rev. **92** (1953) 943
22) B.–G. Pettersson, J. E. Thun and T. R. Gerholm, Nuclear Physics **24** (1961) 223
23) M. Ferentz and N. Rosenzweig, Table of *F*-coefficients, ANL report 5324
24) E. L. Church, M. E. Rose and J. Weneser, Phys. Rev. **109** (1958) 1299

2.E

Nuclear Physics **24** (1961) 269—273; © *North-Holland Publishing Co., Amsterdam*

Not to be reproduced by photoprint or microfilm without written permission from the publisher

SUR LA DÉTERMINATION DU POTENTIEL IMAGINAIRE DANS LE MODÈLE OPTIQUE

J. OLKOWSKY et J. RAYNAL

C.E.N. Saclay, Gif-sur-Yvette, S. et O., France

Reçu le 9 décembre 1960

Abstract: The Bjorklund-Fernbach optical model is applied to the determination of the imaginary potential W fitting the $^{141}_{59}Pr_{82}$+p reaction cross-section at energy less than 11.1 MeV. One finds that $\sigma_{reaction}$ is more sensitive to the shape of the imaginary potential than to its depth.

1. Introduction

Le modèle optique, tel qu'il est décrit dans le travail de Feshbach, Porter et Weisskopf [1]) permet de calculer la section efficace de réaction. La partie imaginaire du potentiel complexe décrit l'absorption correspondant à la formation du noyau composé.

En ce qui concerne la diffusion élastique, le modèle optique ne fournit pas un seul ensemble de paramètres pour interpréter l'expérience mais plusieurs. En particulier, le potentiel imaginaire W est mal déterminé.

On admet [2, 3]) que c'est la section efficace de réaction qui doit être la plus sensible à W. Mais la mesure de $\sigma_{réaction}$ est difficile. A haute énergie, on peut déterminer $\sigma_{réaction}$ par une méthode de transmission [4]). Pour des protons d'énergie inférieure à 15 MeV environ, on ne peut utiliser cette méthode sans risque d'erreurs importantes.

Nous avons essayé de voir si $\sigma_{réaction}$ pouvait être assimilé à σ(p, n) tout au moins dans un cas favorable. L'expérience [5]) a porté sur la réaction $^{141}_{59}Pr_{82}$+p, l'énergie des protons étant $\leqq$ 11.1 MeV.

Pour écrire que $\sigma_{réaction} \approx \sigma$(p, n) dans ce cas, il faut s'assurer que:

1) la réaction (p, n) procède par l'intermédiaire d'un noyau composé,

2) les autres réactions énergétiquement possibles sont négligeables.

Les arguments utilisés sont développés dans un autre article [5]).

Remarquons que l'on ne possède actuellement aucune donnée sur l'importance de la diffusion élastique „composée". Il semble toutefois logique que la compétition des réactions (p, n) et diffusion élastique composée dépende étroitement du seuil de la réaction (p, n). Au-dessous de ce seuil la diffusion élastique composée existe seule. Au-dessus, la réaction (p, n) devient de plus en plus compétitive si l'énergie croît. Pour $^{141}_{59}Pr_{82}$ le seuil de la réaction (p, n) est bas [6]): 2.53 MeV.

2. Calculs de $\sigma_{\text{réaction}}$ dans le cas de $^{141}_{59}Pr_{82}+p$

Les calculs de $\sigma_{\text{réaction}}$ ont été faits en prenant le modèle optique de Bjorklund et Fernbach [7,8]) avec les paramètres

$$a = 0.65 \text{ fm}, \quad b = 1 \text{ fm}, \quad r_0 = 1.25 \text{ fm}.$$

Rappelons [5]) que le noyau ^{141}Pr est pratiquement sphérique. Il possède une couche fermée de neutrons $N = 82$ et son moment quadrupolaire est voisin de $0 (Q = 0.05)$.

Les détails de la programmation du modèle optique à la machine Mercury-Ferranti de Saclay sont donnés dans l'article de Beurtey *et al.* [9]).

Nous avons fait varier les paramètres V et W pour étudier leur influence sur $\sigma_{\text{réaction}}$. Nous avons limité les calculs à deux énergies incidentes: 6 et 10 MeV. Les figs. 1 et 2 représentent les résultats obtenus: les points indiquent les valeurs effectivement calculées et les flèches σ(p, n) expérimental avec les barres d'erreur.

On constate que, pour $V = 45 \pm 1$ MeV, de larges variations de W changent peu $\sigma_{\text{réaction}}$. Cette valeur de $V = 45 \pm 1$ MeV (avec $r_0 = 1.25$ fm) est donnée par Bjorklund [10]) comme la meilleure pour interpréter les résultats concernant la polarisation et la diffusion élastique pour des énergies de particules incidentes comprises entre 7 et 14 MeV. Cette valeur de V ne dépend pas du nombre de masse A de la cible (au-dessus de l'aluminium).

La variation de $\sigma_{\text{réaction}}$ en fonction de W n'est pas monotone. Elle présente, pour certaines valeurs de V, des résonances géantes. Sur la fig. 3, les déphasages indiquent une résonance $\frac{3}{2}^-$ dans la région de 55 à 60 MeV et des résonances $\frac{3}{2}+$ et $\frac{5}{2}+$ entre 40 et 45 MeV. Dans les régions de résonances la section efficace de réaction ne donne aucune indication sur W.

L'effet de ces résonances pourrait être éliminé en divisant $\sigma_{\text{réaction}}$ par un paramètre qui représente l'intensité du faisceau dans la région où le potentiel imaginaire existe: la section efficace de diffusion élastique d'origine nucléaire σ_N. Les calculs ont montré que le rapport $\sigma_{\text{réaction}}/\sigma_N$ varie uniformément en fonction de W quel que soit V dans le cas de la fig. 1. Malheureusement, pour des noyaux aussi lourds et le domaine d'énergie envisagé, on ne peut atteindre σ_N. En effet rappelons [11]) que la section efficace de diffusion élastique $\sigma(\theta)$ peut s'écrire sous la forme

$$\sigma(\theta) = \sigma_{\text{Ruth}} + \sigma_N + \sigma_I,$$

σ_I provenant de termes d'interférence entre σ_{Ruth} et σ_N; on ne peut connaître σ_N que par l'intermédiaire des paramètres du modèle optique.

Meyer et Hintz [12]) ont remarqué que la valeur calculée pour la section efficace de réaction avec les paramètres utilisés pour la diffusion élastique était plutôt faible par rapport aux valeurs mesurées et ont suggéré d'augmenter la part du potentiel imaginaire en dehors du noyau. Dans le modèle optique utilisé

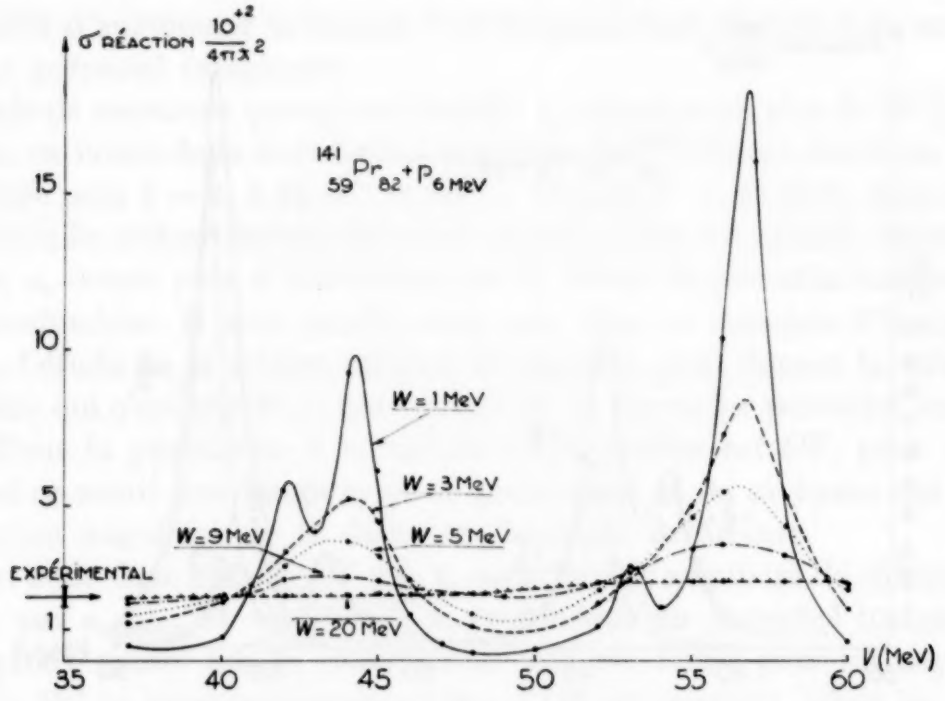

Fig. 1. La section efficace $\sigma_{\text{réaction}}$ pour une énergie incidente de 6 MeV.

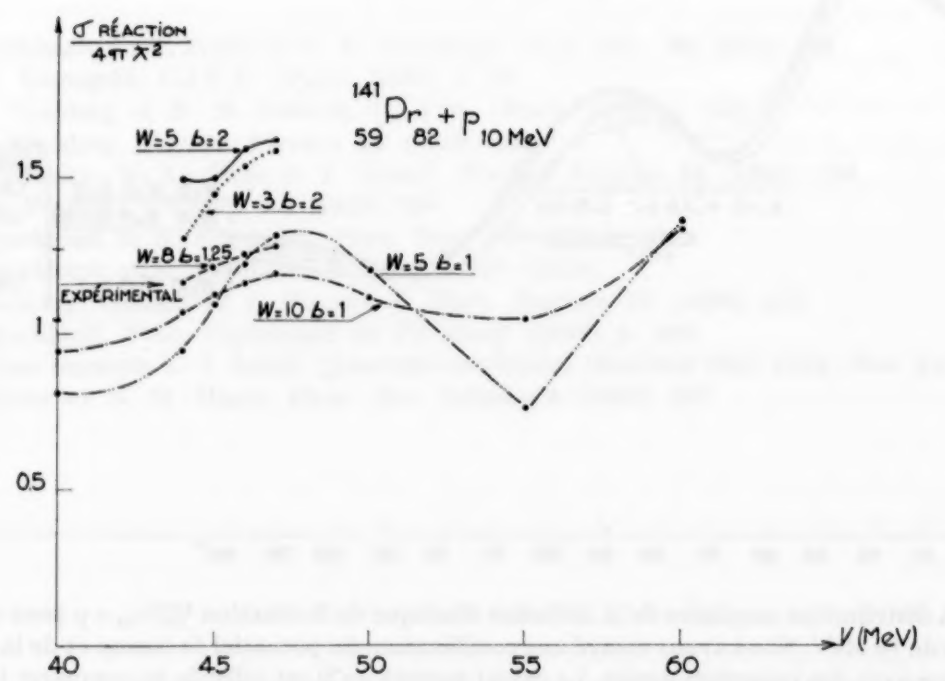

Fig. 2. La section efficace $\sigma_{\text{réaction}}$ pour une énergie incidente de 10 MeV.

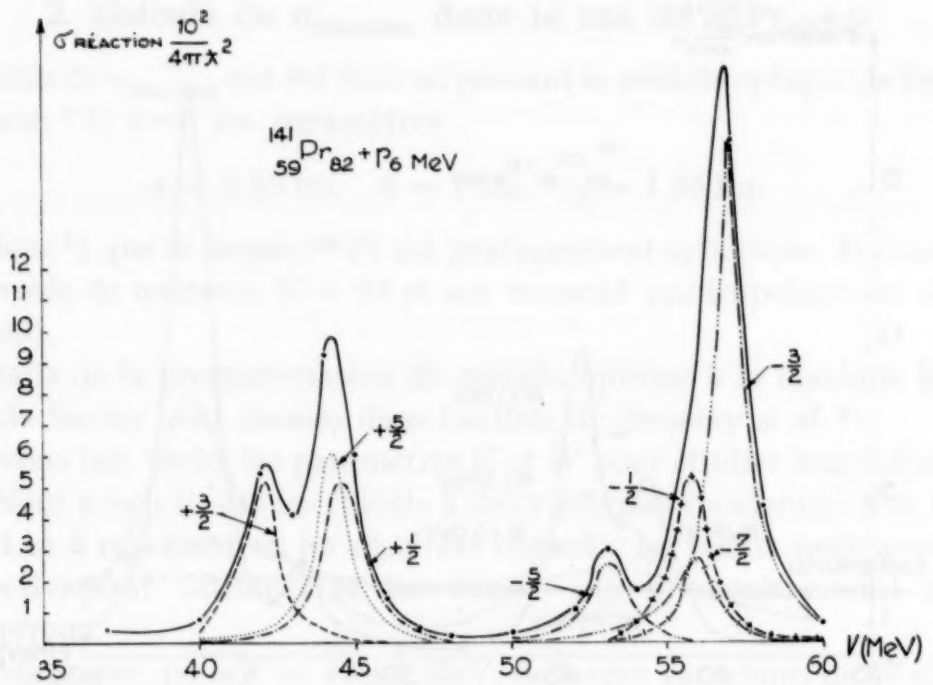

Fig. 3. La section efficace $\sigma_{\text{réaction}}$ pour une énergie incidente de 6 MeV et pour $W = 1$.

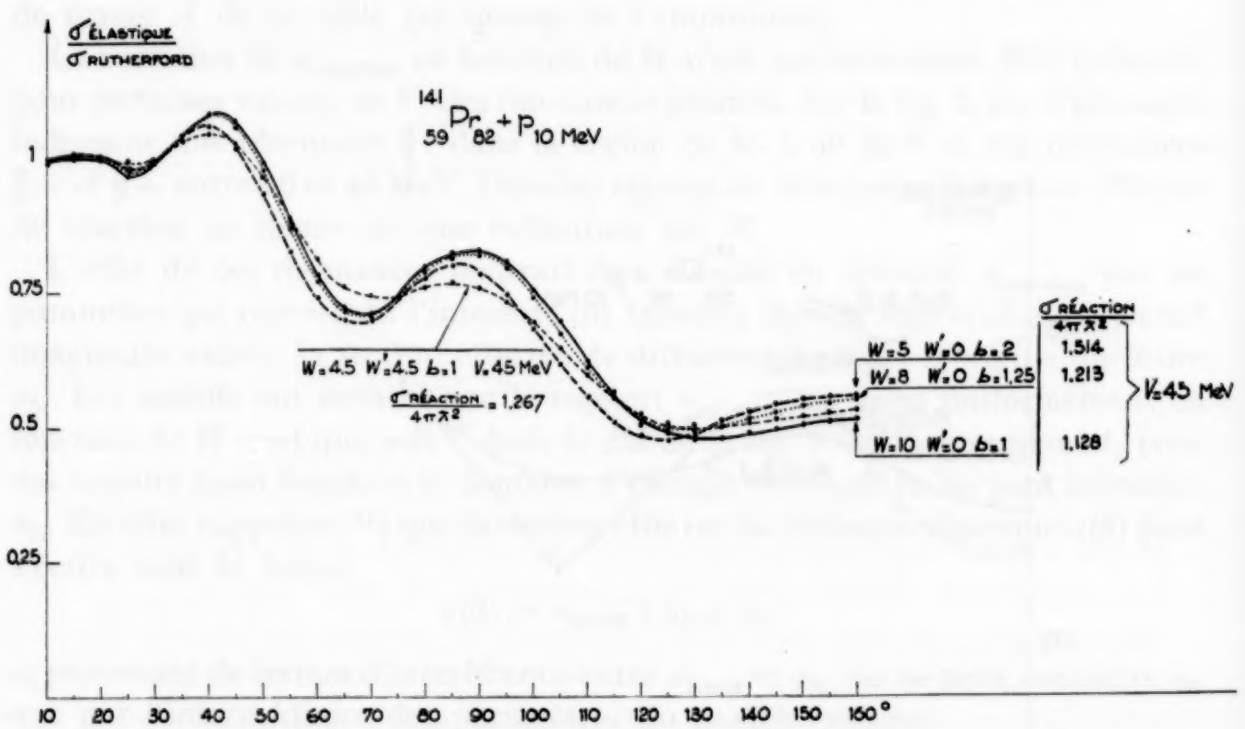

Fig. 4. La distribution angulaire de la diffusion élastique de la réaction $^{141}_{59}Pr_{82}$ + p pour une énergie incidente de 10 MeV. Nous avons essayé une combinaison du potentiel de Saxon et de la gaussienne à la surface avec des intensités égales. Le calcul montre qu'il est difficile de comparer les résultats de potentiels aussi différents qu'une gaussienne décroissant en exp $(-r^2)$ et un potentiel de Saxon qui décroît en exp $(-r)$.

ici, il suffit d'augmenter la largeur b de la gaussienne centrée à la surface qui décrit le potentiel imaginaire.

Les calculs montrent que si b est doublé, σ_r augmente de plus de 30 % (fig. 2). La faible variation de la distribution angulaire de la diffusion élastique (fig. 4) a été vérifiée pour $b = 1$, 1.25 et 2 et $bW = 10$ pour $V = 45$ MeV. Sans remettre en question les valeurs habituellement adoptées pour ces calculs, on peut affirmer que σ_r donne plus d'indications sur la forme du potential imaginaire que sur sa profondeur. Il nous semble donc que, dans ce domaine d'énergie et de noyaux, l'étude de la section efficace de réaction peut donner la valeur d'un paramètre qui n'est pas W et qui dépend de la forme du potentiel imaginaire choisi. Pour la gaussienne à la surface ce paramètre est bW, pour un autre potentiel ce serait une fonction de sa profondeur et de sa forme qui laisse la distribution angulaire de la diffusion élastique invariante.

Ici, on peut donc obtenir bW par la distribution angulaire de diffusion élastique, b par $\sigma_{\text{réaction}}$ et en déduire la profondeur du potentiel imaginaire W. Remarquons encore que la polarisation (qui est faible pour un noyau aussi lourd que Pr) ne varie pratiquement pas si bW est constant (dans les trois cas calculés de la fig. 4).

Nous remercions Monsieur Guillou qui a fait les calculs à la machine Mercury-Ferranti de Saclay, Madame Pillard pour une partie des calculs numériques, Messieurs C. Bloch et R. Beurtey pour des discussions utiles.

Bibliographie

1) H. Feshbach, C. E. Porter et V. F. Weisskopf, Phys. Rev. **96** (1954) 448
2) A. E. Glassgold, C.I.P.N. (Paris, 1958) p. 30
3) T. J. Gooding et R. M. Eisberg, C.I.P.N. (Paris, 1958) p. 420
4) T. J. Gooding, Nuclear Physics **12** (1959) 241
5) J. Olkowsky, M. Le Pape et I. Gratot, Nuclear Physics **23** (1961) 164
6) A. H. Wapstra, Physica **21** (1955) 385
7) F. Bjorklund et S. Fernbach, Phys. Rev. **109** (1958) 1295
8) F. Bjorklund et S. Fernbach, U.C.R.L.-5028 (1958)
9) R. Beurtey, Guillou et J. Raynal, J. Phys. Radium **21** (1960) 402
10) F. Bjorklund, Proc. Conférence de Pittsburg (1957) p. 206
11) Voir par exemple L. I. Schiff, Quantum mechanics (McGraw Hill, 1949, New York) p. 120
12) V. Meyer et N. M. Hintz, Phys. Rev. Letters **5** (1960) 207

2.D. *Nuclear Physics* **24** (1961) 274—299; © *North-Holland Publishing Co., Amsterdam*
Not to be reproduced by photoprint or microfilm without written permission from the publisher

AN EXPERIMENTAL TEST OF THE STATISTICAL THEORY OF NUCLEAR REACTIONS

D. L. ALLAN

Atomic Energy Research Establishment, Harwell, England

Received 19 December 1960

Abstract: The 14 MeV differential (n, p) cross sections of about 40 nuclei have been measured at 120° to the incident neutrons using a photographic plate method. The results are compared with the cross sections calculated according to the statistical theory of nuclear reactions and it is shown that good agreement exists between theory and experiment provided a level density function of the form $\exp 2(aU)^{\frac{1}{2}}$ with $a \approx {}^{1}/_{10}A$ is used and the pairing energy δ is taken into account. Experimental values of δ and the nuclear temperatures are given. The (n, np) cross sections of 13 of the nuclei have been measured and the results are discussed in terms of a reaction mechanism based on the statistical model.

1. Introduction

The fundamental assumption of the statistical theory of nuclear reactions [1]) is that nuclear reactions proceed via an intermediate compound nucleus which subsequently decays in a variety of ways which are independent of the way the compound nucleus was formed. The theory predicts that the energy spectra of the emitted particles should be peaked at energies well below the incident energy (for incident energies > 10 MeV) and that the angular distributions of the emitted particles should be approximately isotropic. The theory also predicts absolute cross sections.

It is well known that for incident energies > 10 MeV there have been many experiments which have shown these predictions to be wrong (e.g. refs. [2–7])). Angular distributions have been measured which are far from isotropic, being peaked strongly in the forward direction, and the energy spectra exhibit strong groups of particles emitted with energies only a little below the incident energy.

These discrepancies are now attributed to direct interaction processes in which the incident particles interact with only a few nucleons within the nucleus. Such processes are in complete contrast with compound nucleus processes in which the incident particle shares its energy and angular momentum with all the particles in the nucleus. Direct interaction processes occur during the early stages of any sufficiently high energy nuclear reaction. They represent a preliminary phase of the reaction during which particles may be ejected from the nucleus before the conditions implicit in the compound nucleus definition have had time to establish themselves.

Discrepancies between the statistical theory predictions and the experimental results are most pronounced when (i) the Coulomb barrier strongly inhibits compound nucleus processes and (ii) the observations are made in such a way that direct interaction processes are exaggerated. E.g., this is the case when particle detectors are set up at low angles and are biased to register high energy particles only or when detectors are adjusted to detect deuterons only (pick-up processes).

Many of the phenomena attributed to direct interactions have been discovered relatively recently and there has been a natural tendency to make observations in the energy region 10–30 MeV in such a way that the direct effects are most pronounced. As a result, an unconscious bias towards exaggerating the overall importance of direct interaction effects in this energy region can be detected in the literature.

The work reported here is an attempt to reverse this bias – to conduct an experiment in which it is the compound nucleus processes which are exaggerated. This bias has been introduced in the following ways:

(i) By studying (n, p) reactions at 14 MeV. With uncharged incident particles there is no Coulomb barrier to impede compound nucleus formation and, although compound nucleus processes are favoured even more strongly in (n, n′) reactions where no Coulomb barrier is involved at all, (n, p) reactions permit a more thorough test of the statistical theory because the cross sections depend more sensitively upon the effects of competition from other reactions. In addition, the effect of other variables such as the Q value of the reaction can be tested.

(ii) By choosing neutron deficient target nuclei. When such nuclei undergo (n, p) reactions they are transformed into nuclei lying closer to the nuclear stability line and, because of favourable Q values, compound nucleus decay by proton emission is favoured. Most of the target nuclei studied had atomic numbers between 11 and 30. In this region, the Coulomb barrier does not seriously impede proton emission and the incidence of the closed shells at $N, Z = 20, 28, 40$ has the effect of giving some of the nuclei anomalously high (positive) (n, p) Q values.

(iii) By detecting the protons at 120° to the incident protons. At this angle the direct interaction contribution to (n, p) reactions is known to be small [3–5, 36, 41, 42]).

(iv) By using photographic plate detectors. Experimenters employing scintillation counters have to take special precautions if they wish to measure protons in the energy range 2–4 MeV because of the large background caused by neutrons and γ-rays, but there are no special difficulties in observing the higher energy protons. On the other hand, photographic plates record clear unambiguous tracks in the 2–4 MeV region whereas the very long (and usually rare) high energy tracks are very tedious to meas-

ure. Thus, for experimenters working with photographic plate detectors, there is a strong incentive to select the more neutron deficient target nuclei for study because they give high yields of low energy protons resulting from compound nucleus decay.

We have measured the 14 MeV differential (n, p) cross sections at 120° for about 40 targets using a photographic plate method in which tracks caused by protons from up to six different targets were recorded simultaneously in a single plate under completely equivalent conditions. One of the targets was always a standard Fe^{54} target and the results were converted to absolute values using the previously measured Fe^{54}(n, p) and Fe^{54}(n, np) cross sections [4]). The results have been corrected for the contributions from (n, np) reactions and, for convenience of comparison with other results, the cross sections are presented in the integrated form:

$$4\pi \left[\frac{\partial\sigma}{\partial\theta}\right]_{120°},$$

where $[\partial\sigma/\partial\theta]_{120°}$ is the differential cross section actually measured.

2. Apparatus and Method

The apparatus is illustrated in fig. 1. A 2.5 cm × 2.5 cm 300 μm Ilford C2 photographic plate (P) was cemented in the centre of an 8 cm diameter aluminium disc (D) and it was surrounded by a 2.54 cm wide annular band (B) made of 0.05 cm gold sheet. This band was provided with six 20 × 12 mm rectangular windows (W) through which charged particles from up to six 2 × 1 cm targets (T) could pass to the plate, the target material being deposited on strips of 0.01 cm gold foil cemented to the outside of the band. The target-photographic plate assembly was placed inside a slightly larger cylindrical drum (C) also lined with 0.05 cm gold so that, apart from the target materials, the only material visible from a point on the surface of the photographic emulsion was gold with a thickness of at least 0.06 cm. This thickness is considerably greater than the range of a 14 MeV proton in gold.

The assembly described above was placed inside an aluminium alloy vacuum chamber and placed in such a position with respect to the 14 MeV neutron source S that the angle (S$\hat{T}$P) between the neutrons incident upon the targets and the protons reaching the photographic plate was 120° for all targets. Attached to the outer case of the vacuum chamber, and mounted axially, was a 15 cm length of 13 mm diameter copper rod (A) which effectively screened the photographic plate from direct neutrons.

With this arrangement, the photographic plate detected charged particles emitted by up to six different targets simultaneously, together with a small background caused mainly by proton recoils due to direct and room scattered

neutrons. To maintain circular symmetry, scanning was confined to a central circular area of the plate 7 mm in diameter. The position co-ordinates, range and angular orientation (α) in the emulsion plane of tracks caused by protons which could have come from the band of targets were recorded, and histograms giving the number of tracks $N(\alpha)d\alpha$ in each 2° interval throughout the angular

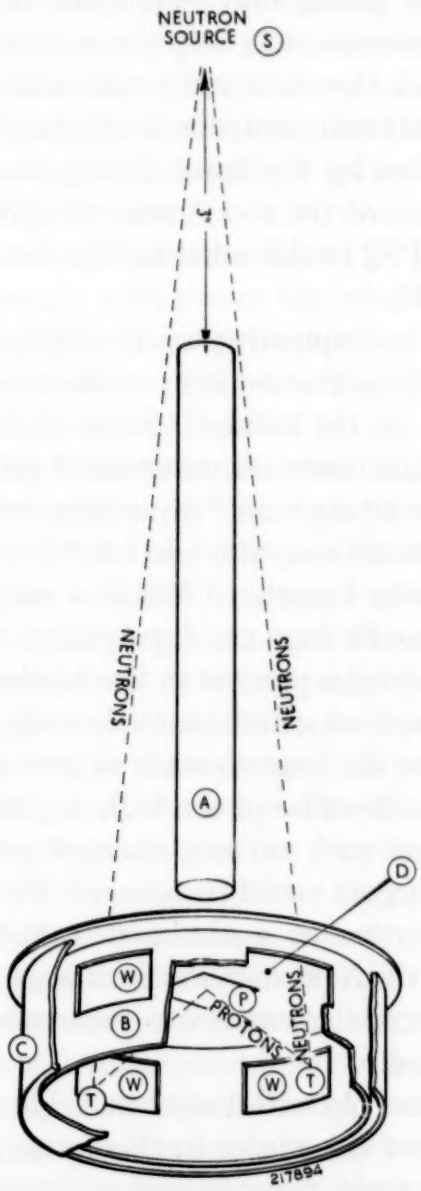

Fig. 1. The experimental set-up.

range $\alpha = 0°–360°$ were prepared. The histograms exhibited six well resolved peaks superimposed upon a small uniform background. The number of tracks in each peak determined the relative proton yield from each target and the intensity of tracks in the valleys between the peaks provided the background measurement. One of the targets was always a standard Fe^{54} target and, since the absolute cross sections of the reactions $Fe^{54}(n, p)\,Mn^{54}$ and $Fe^{54}(n, np)Mn^{53}$

are known [4, 5]), it was possible to convert the proton yields to absolute differential cross sections at 120°.

To ensure that the background was isotropic and uniform with respect to track length the drum containing the targets and photographic plate was continuously rotated during the neutron exposures by a small electric clock motor with a geared drive giving one revolution in two minutes. With this arrangement one could be certain that only the targets (which rotated with the plate) could have produced the observed peaks and all errors caused by the anisotropy of the room scattered neutrons, and neutron energy variations due to the finite angle subtended by the band of targets at the source, were completely eliminated. The axis of the rod A was at right angles to the deuteron beam and the half angle (PŜT) subtended by the band B and the plate at the neutron source S was 8.5°.

Most of the targets were isotropically pure (> 90 %) and they were deposited upon the 0.01 cm gold strips as the element, oxide or carbonate (halogen targets were prepared from silver or tin halides). Some of the deposits were electroplated and others were laid down as compacted powders to form layers of thickness varying from 6 to 40 mg · cm^{-2} according to the results of preliminary yield determinations. It was necessary to add 0.2 to 0.5 mg · cm^{-2} of polystyrene binder to some of the powder targets to obtain a mechanically stable deposit. Exposures made with 5 to 10 mg · cm^{-2} polythene targets showed that the background due to the hydrogen present in the binder was completely negligible. A Pb_3O_4 target was exposed simultaneously with the oxide and carbonate targets in order to measure the contribution of protons from the O^{16}(n, p)N^{16} reaction ($Q = -9.6$ MeV). Because of the high negative Q values of the (n, p), (n, np) and (n, d) reactions with carbon, charged particle emission from the carbon in the carbonate targets could be ignored. For some of the lower yield targets, background measurements made in the rather limited angular regions occupied by the valleys in the $N(\alpha)$ distributions were not sufficiently accurate. For these targets, therefore, the exposures were made with one of the six target windows unoccupied.

This work is concerned mainly with target nuclei in the atomic number range $Z = 11$–30 because most of the nuclei in this range gave large proton yields. Each set of targets in this range was exposed separately to three photographic plates and all three plates were scanned. The three plates were orientated at various angles (in the plane of D) with respect to the targets to provide a means of detecting the possible existence of an angle bias amongst the scanners. The agreement between the scanners was good and no angle bias was found.

A few nuclei in the range $Z = 33$–53 were studied but the proton yield from targets in this group were mostly comparable to or less than the background. As a rule only one plate was exposed to each set of targets in this group and all the targets were prepared from materials having the natural isotropic composition.

In general, both (n, p) and (n, np) reactions contributed to the observed proton yields and, to begin with, the two contributions were separated using the procedure described in an earlier paper [4]). The quantity $\ln(N(\varepsilon)/\sigma_p(\varepsilon)\varepsilon)$ was plotted against ε, where $N(\varepsilon)$ is the observed number of protons emitted into a 0.5 MeV energy interval with average energy ε and $\sigma_p(\varepsilon)$ is the inverse cross section for reforming the compound nucleus by bombarding the (excited) residual nucleus by protons of energy ε. For most of the nuclei studied the points on such a plot could be fitted by two straight lines, one lying in the higher proton energy region ($\varepsilon > 5$ MeV), where the (n, np) reaction is normally energetically forbidden and the other, which had roughly 3 times the slope, lying in the low energy region ($2 < \varepsilon < 5$ MeV) where both (n, p) and (n, np) reactions contributed to the yield. It was assumed that for the (n, p) protons alone the quantity $\ln(N(\varepsilon)/\sigma_p(\varepsilon)\varepsilon)$ varied linearly with ε over the whole range of proton energies from 2–12 MeV. Consequently a linear extrapolation of the (n, p) line into the 2–5 MeV region provided a means of determining the (n, p) yield alone.

Since most of the targets studied gave some (n, np) yield, and there was a low energy proton yield from the oxide and carbonate targets due to the O^{16}(n, p)N^{16} reaction, it was later found convenient to restrict the $N(\alpha)$ histograms to protons having ranges between 80 μm and 240 μm. The 80 μm cut-off (corresponding to protons with energies $\approx$ 3 MeV) removed most of the (n, np) contribution, completely eliminated the oxygen contribution and greatly reduced the background. The upper range limit was imposed for convenience, there being very few tracks with ranges exceeding 240 μm. Roughly 60 % of the (n, p) cross section was included within these range limits and this part of the cross section was determined with good accuracy. The remaining 40 % of the (n, p) cross section was regarded as a correction, the magnitude of which depended on some theoretical estimate of the shape of the (n, p) spectrum in the steeply falling region below the 3 MeV low energy cut off.

It was found that the magnitude of this correction was not very sensitive to the value of the nuclear temperature (i.e. to the slope of the line $\ln(N(\varepsilon)/\sigma_p\varepsilon)$), to the Coulomb barrier cut off which enters into the quantity σ_p or to departures of $\ln(N(\varepsilon)/\sigma_p\varepsilon)$ from linearity. The ratio of the cross section between the range limits to the whole (n, p) cross section was also very constant from one nucleus to another so that many of the results given in the next section apply equally well to the uncorrected portion of the (n, p) yield. All the cross section results (targets: $Z = 11$–30) have been corrected for the isotopic composition of the targets.

3. Results and Discussion

3.1. (n, p) CROSS SECTIONS FOR NUCLEI $Z = 11$–30

The results of the measurements expressed in the form $\sigma_{exp} = 4\pi[\partial\sigma/\partial\theta]_{120°}$ mb, where $[\partial\sigma/\partial\theta]_{120°}$ mb is the differential cross section at 120° normalised to

TABLE 1

14 MeV (n, p) cross sections for target nuclei with $Z = 11$–30

Target nucleus	σ_{exp}(n, p) I (mb)	Error (mb)	Q_p (ref. [8]))	σ_{theor}(n, p) Theory A (mb)	σ_{theor} (n, p) Theory B (mb)	σ_{exp}(n, p) II (mb)	σ_{exp}(n, p) at 14 MeV obtained by other authors (mb)
Na^{23}	57	20	−3.60	62	33	50	34±15 [13])
Mg^{24}	118	16	−4.73	141	148	110	191±35 [13])
							200±10 [25])
							109±10 [46]) [a])
Mg^{25}	67	10	−3.01	63	41	63	45±18 [13])
							60±10 [27]) [b])
Mg^{26}	27	7				27	50± 5 [27]) [b])
Al^{27}	87	11	−1.81	91	72	76	52± 9 [13]), 79±6 [28])
							115±10 [29]), 87±7 [30]);
							55±10 [31]) [a]), 53±5 [32])
Si^{28}	243	22	−3.87	262	186	246	220±51 [13])
							250±10 [25])
							375±20 [26])
P^{31}	184	14	−0.70	133	109	114	64± 8 [13])
							91± 9 [28])
							86± 7 [35])
S^{32}	365	25	−0.93	427	430	289	254±10 [12])
							369±44 [13])
							285±20 [46]) [a])
Cl^{35}	125	38	+0.61	206	200	107	
Ca^{40}	451	38	−0.54	428	444	298	
Ti^{46}	203	21	−1.58	243	209	196	520 [32]) [b])

Ti^{47}	112	15	+0.18	115	100	111	230±40 [32] b)
Ti^{48}	29	8	−3.21	58	51	29	93±32 [13]), 58±8 [32] b)
V^{51}	20	7	−1.68	22	20	23	27± 4 [13])
Cr^{50}	265	21	−0.26	296	324	277	
Cr^{52}	74	10	−3.21	47	38	67	78±11 [13])
							119±10 [26])
Cr^{53}	44	7	−1.70	28	26	48	
Mn^{55}	43	7	−2.04	18	12	45	
Fe^{54}	382	13	+0.09	424	383	382	306 [5]) a), 375 [4]) a)
Fe^{56}	82	7	−2.92	51	33	86	97±12 [13])
							124±12 [28])
							144±19 [30])
							72± 7 [37]), 75 [5]) a)
Co^{59}	81	10	−0.78	35	25	61	82± 8 [43]) b)
Ni^{58}	440	27	+0.36	444	358	430	560±110 [33])
							237±20 [43]) b)
							560± [5]) a), 440 [4]) a)
							270 [42]) a, b)
Ni^{60}	124	9	−2.03	83	60	134	87 [5]) a), 200 [4]) a)
Cu^{63}	118	9	+0.72	89	68	105	98 [4]) a)
Zn^{64}	179	18	+0.21	238	258	171	386±58 [13]), 216 [39])
							284±20 [43]) b)
							≈200 [40]) a)
Zn^{66}	34	4	−1.85	45	43	35	100±17 [13])
							77± 8 [43]) b)
Zn^{67}	41	7	+0.21	53	38	33	

a) Proton yield measurements (corrected for (n, np) yield and direct interaction component).
b) 14.8 MeV measurements.

the value [4]) for Fe^{54}, are given in column 2 of table 1. The experimental errors given in column 3 were obtained by combining the statistical error associated with the track counting with the error of the extrapolation procedure described in sect. 2. A plot of σ_{exp}(n, p) against the atomic number Z of the even target nuclei is given in fig. 2. The solid circles give the cross sections for the lightest even isotope and the open circles for the next lightest isotope †. Fig. 3 gives the same data for the odd-neutron and odd-proton target nuclei. These two figures show that for targets with $Z = 11$–30, the cross section σ(n, p) is greatest at or near closed shells ($Z = 20$, 28) and falls to a minimum value between closed shells. It is natural to associate this fluctuation with the fluctuation of the (n, p) Q-value as one passes through a closed shell region.

The Q-values [8]) of the (n, p) reactions studied in this work are given in column 4 of table 1. When Q is plotted against Z for the even (lightest and next to lightest) nuclei and for the odd-neutron and odd-proton nuclei separately, curves similar to figs. 2 and 3 with peaks near $Z = 20$ and 28 are obtained.

In figs. 4 and 5, σ_{exp}(n, p) is plotted against Q value separately for the even and odd-mass nuclei. The points lie on three curves according to whether $Z \leqq 20$, $20 < Z \leqq 28$ (29) or 28 (29) $< Z$, this regular behaviour following directly from the form of the dependence of Q on Z. The numbers appearing alongside the experimental points are the atomic numbers Z of the target nuclei. Let us look first at the points lying near the uppermost curves of figs. 4 and 5: the cross-section σ_{exp}(n, p) rises steadily as Q becomes less negative, reaching a maximum value near the closed shell at $Z = 20$ and meanwhile Z changes from 12(11) to 20(15). With a further increase in Z, Q returns to a large negative value but the cross section points now lie on a lower curve because, while Z has been increasing, the Coulomb barrier height of the nuclei has been increasing also. Again, as Q becomes less negative, there is a smooth rise in σ_{exp}(n, p) up to a second maximum corresponding to the positive Q values near $Z = 28$. With an increase of Z to 30, the Q values become negative again and the increased Coulomb barrier depresses the cross sections so that the experimental points for 28(29) $< Z$ lie on the bottom curves of figs. 4 and 5. However, a closer inspection of these figures will show that there can be no simple empirical relation giving σ(n, p) in terms of the parameters Q and Z alone. The cross sections for $Z = 30$ are depressed below the values for $Z = 28$, 29 by amounts which are much too large in comparison with the variation of σ_{exp} (n, p) with Z (for a fixed Q value) in other parts of these graphs. So far, however, we have ignored the effect of level density fluctuations near closed shells.

According to the statistical theory of nuclear reactions, the cross section of a reaction depends sensitively upon the level density of the product nucleus and of

† In figs. 2–7, the open circles at the ends of the stippled arrows are the revised cross sections for the three light isotopes discussed in section 3.9.

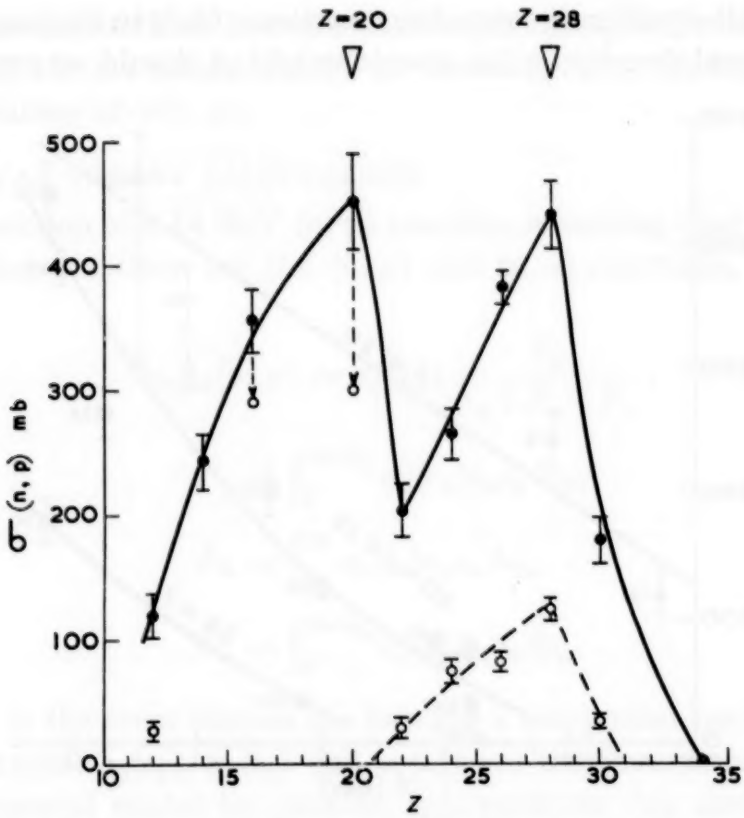

Fig. 2. A plot of σ_{exp}(n, p) against Z for the even target nuclei (see text).

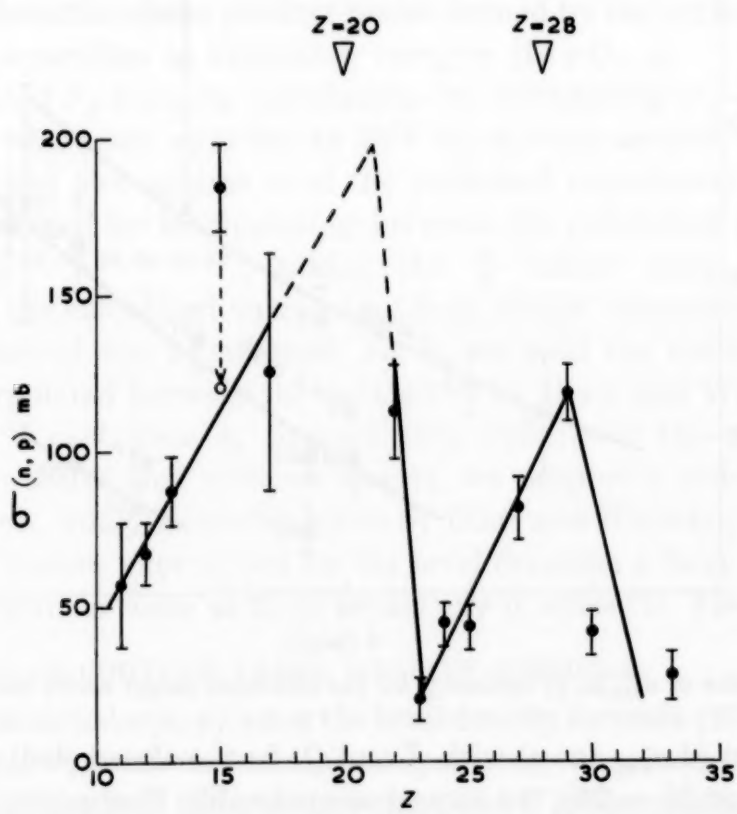

Fig. 3. A plot of σ_{exp}(n, p) against Z for the odd-proton and odd-neutron target nuclei (see text).

the products of all significant competing reactions. Only in the case of a smooth dependence of level density on the atomic weight A should we expect to find a

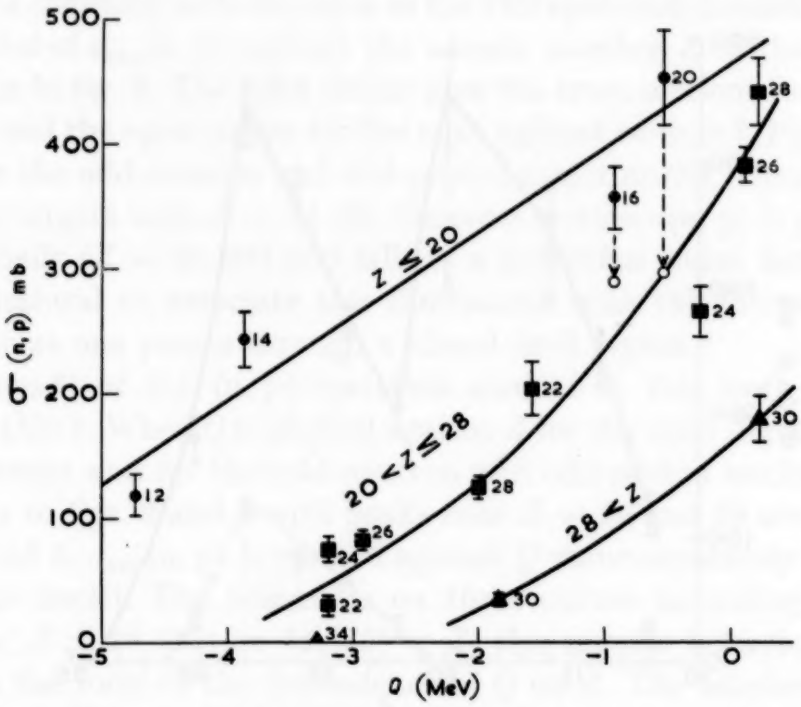

Fig. 4. A plot of σ_{exp}(n, p) against Q for the even target nuclei (see text).

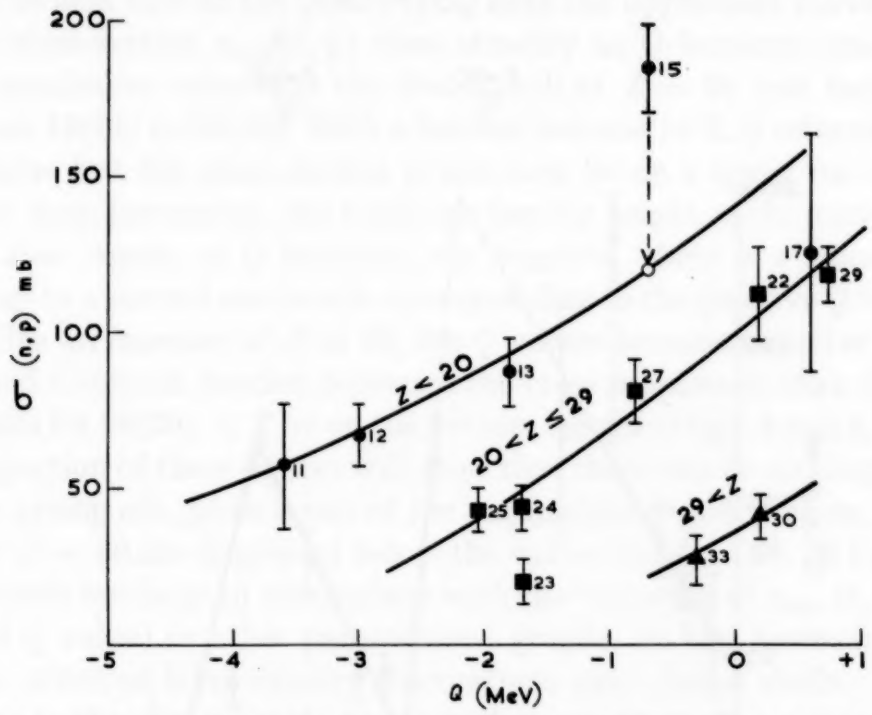

Fig. 5. A plot of σ_{exp}(n, p) against Q for the odd-mass target nuclei (see text).

smooth variation of σ_{exp} (n, p) with Z and Q. In the closed shell region we are considering (Z or $N = 28$), we expect considerable fluctuations in the level density and these will cause sudden changes in σ_{exp} (n, p) which are independent

of the Q value fluctuations. In order to examine this question more thoroughly we have used the statistical theory of Weisskopf and Ewing [1]) to calculate theoretical values of σ(n, p).

3.2. STATISTICAL THEORY CALCULATIONS

The cross section of a 14 MeV (n, p) reaction, assuming that the only significant competing reactions are the (n, n) and (n, α) reactions, is given by the equations

$$\sigma_{\text{theor}}(\text{n, p}) = \sigma_{\text{c}}(14)\,\frac{F_{\text{p}}}{F_{\text{p}}+F_{\text{n}}+F_{\alpha}}\,, \tag{1a}$$

$$F_{\text{p}} = \int_0^{14+Q_{\text{p}}} \sigma_{\text{p}}(\varepsilon_{\text{p}})\varepsilon_{\text{p}}\rho_{\text{p}}\,\text{d}\varepsilon_{\text{p}}, \tag{1b}$$

$$F_{\text{n}} = \int_0^{14} \sigma_{\text{n}}(\varepsilon_{\text{n}})\varepsilon_{\text{n}}\rho_{\text{n}}\,\text{d}\varepsilon_{\text{n}}, \tag{1c}$$

$$F_{\alpha} = \int_0^{14+Q_{\alpha}} \sigma_{\alpha}(\varepsilon_{\alpha})\varepsilon_{\alpha}\rho_{\alpha}\,\text{d}\varepsilon_{\alpha}, \tag{1d}$$

where $\sigma_{\text{c}}(14)$ is the cross section for forming a compound nucleus by 14 MeV incident neutrons; $\sigma_{\text{p}}(\varepsilon_{\text{p}})$, $\sigma_{\text{n}}(\varepsilon_{\text{n}})$ and $\sigma_{\alpha}(\varepsilon_{\alpha})$ are the inverse cross sections for forming compound nuclei by protons (p), neutrons (n) and α-particles (α) having energies ε_{p}, ε_{n} and ε_{α}. The quantity Q_{p} is the Q value of the (n, p) reaction and Q_{α} is the Q value of the reaction (n, α). The quantities ρ_{n}, ρ_{p} and ρ_{α} are the level densities of the product nuclei formed by the emission of neutrons, protons and α-particles at excitation energies $(14+Q-\varepsilon)$.

We eliminated F_{α} from our calculations by substituting $\sigma'_{\text{c}} = \sigma_{\text{c}} - \sigma(\text{n}, \alpha)$ for σ_{c} in eq. (1a), where σ(n, α) is the 14 MeV (n, α) cross section. σ_{c} was obtained from a smoothed plot against A of the published experimental values [9]) and (n, α) was obtained by interpolating between the published (n, α) activation cross sections [10–13, 28, 30, 35, 43]), taking the Q values into account. Since $\sigma(\text{n}, \alpha) \ll \sigma_{\text{c}}$, the calculated values σ_{theor}(n,p) do not depend at all sensitively upon the values of σ(n, α) assumed. For σ_{p} we used the values calculated by Shapiro, interpolated between the data given by Blatt and Weisskopf [14]) with $r_0 = 1.5\times10^{-13}$ cm. Since σ_{n} changes very little over the neutron energies represented in the 14 MeV neutron spectra, we adopted a constant value of σ_{n} for each nucleus, using the curves given by Blatt and Weisskopf [14]) (p. 348) for $\varepsilon_{\text{n}} = 2$ MeV. Various expressions for the level densities ρ have been suggested, and we will examine some of these separately in subsects. 3.3–3.8.

3.3. LANG AND LE COUTEUR LEVEL DENSITY FORMULA

First, we calculated σ(n, p) using the level density formula (27) given by Lang and Le Couteur [15]), with the nuclear temperature t obtained from the formula $U = \frac{1}{8}At^2 - t$, where A is the atomic weight and U is the excitation energy. The results of these calculations are given in fig. 6 in the form of the ratio

$\sigma_{exp}(n, p)/\sigma_{theor}(n, p)$ plotted against Z, the upper plot giving the results for the odd-mass target nuclei and the lower plot for the even targets. The indicated errors are those arising from the errors in σ_{exp} only; they do not include errors associated with the parameters used in the calculations.

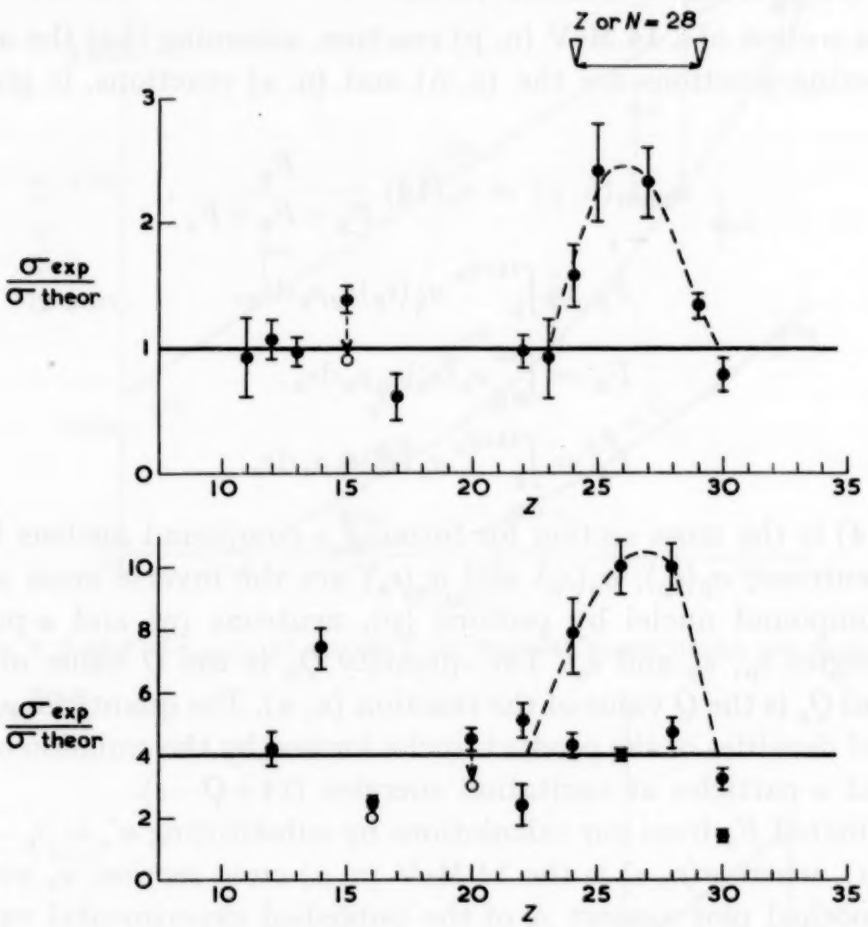

Fig. 6. A plot of the ratio $\sigma_{exp}(n, p)/\sigma_{theor}(n, p)$ against Z for the odd-mass nuclei (upper part) and for the even nuclei (lower part).

Apart from two points in the closed shell region the ratios for the odd nuclei are close to unity, indicating good agreement between theory and experiment. This is very gratifying as the calculated (n, p) cross sections have not been normalised in any way. The lower plot shows that for the even nuclei the experimental cross sections are roughly 4 times the calculated values with an excursion of up to 10 times in the closed shell region. The factor of 4 discrepancy is a well known effect which can be explained in terms of a shift in the position of the effective ground state of a nucleus [16]) caused by nucleon pairing. This shift has the value δ MeV for even nuclei, roughly $\frac{1}{2}\delta$ MeV for odd-proton and odd-neutron nuclei and zero for odd nuclei, where δ is the so-called pairing energy. In an (n, p) reaction with an even target nucleus the product nucleus is odd whereas the product formed by the principle competing reaction (the (n, n′) reaction) is even. Thus, in the statistical theory calculations, the pairing energy

δ appears as a fictitious negative Q value [17]) associated with the (n, n') reaction and it therefore enhances the emission of protons by reducing the competing neutron emission. When the target nucleus is odd the pairing energies of the products formed by the competing reactions are each roughly equal to $\frac{1}{2}\delta$ and this parameter may be ignored. This explains why good agreement between the experimental and theoretical cross sections was obtained for the odd-mass nuclei (fig. 6, upper plot) without introducing the pairing energy into the calculations.

3.4. EXPERIMENTAL DETERMINATION OF δ-VALUES

We have calculated the values of δ required to give agreement between theory and experiment for the even target nuclei (i.e. δ was adjusted to make $\sigma_{exp}/\sigma_{theor} = 1$). The results of this calculation are presented in fig. 7 together with

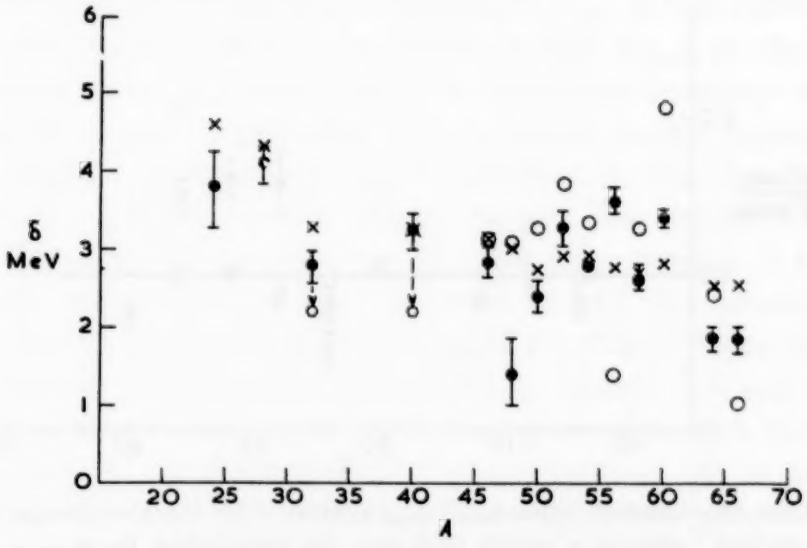

Fig. 7. A plot of the pairing energy δ against A for the even nuclei.
Value of δ required to give agreement with experiment.
× Cameron's values of δ (semi-empirical mass formula).
○ Dostrovsky *et al.* (semi-empirical mass formula with shell corrections).

the values derived by Cameron [17]) from his semi-empirical mass formula and the values given by Dostrovsky *et al.* [18]), which take shell effects into account. These "experimental" values of δ have not been normalised and the agreement both in absolute magnitude and with the general trend of the Cameron values is very good. Thus, a measurement of the compound nucleus component of the (n, p) cross section of an even nucleus, where we have direct competition between reactions leading to even and odd product nuclei, provides a sensitive method of measuring the pairing energy δ. The effect of the pairing energy can be seen rather directly by comparing the experimental (n, p) cross sections (column 2, table 1) of the three zinc isotopes with the corresponding (n, p) Q values. To within the experimental errors, σ_{exp}(n, p) for the even nucleus Zn^{66}

is equal to σ_{exp}(n, p) for the odd-neutron nucleus Zn^{67} in spite of the fact that the Q value is 2.06 MeV more negative. This equality of the cross sections follows naturally if we take $\delta = 2.06$ MeV for Zn^{66}. The effect of pairing energy is again apparent in the Zn^{64}(n, p) reaction, for the Zn^{64}(n, p) cross section is roughly 4 times the Zn^{67}(n, p) cross sections although the Q-values are identical (Compare also Fe^{56}/Co^{59} giving $\delta = 2.14$ MeV). Similarly if the data of figs. 4 and 5 are plotted on the same graph, the curves representing the (n, p) cross sections of nuclei belonging to the same Z-group are displaced by δ MeV with respect to each other.

3.5. LANG AND LE COUTEUR LEVEL DENSITY FORMULA WITH CAMERON'S δ-VALUES (THEORY A)

Fig. 8 presents the recalculated ratios $\sigma_{exp}/\sigma_{theor}$ for the even target nuclei obtained by inserting Cameron's values of δ into the calculation for σ_{theor}.

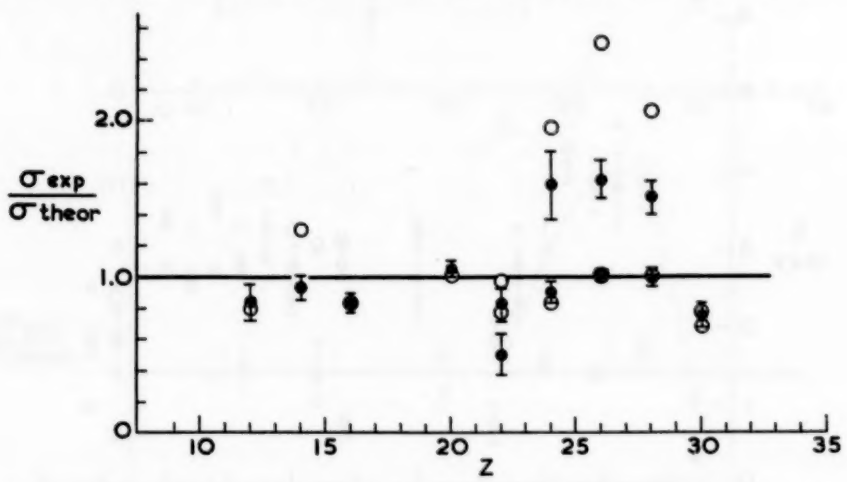

Fig. 8. A plot of the recalculated ratios $\sigma_{exp}/\sigma_{theor}$ against Z for the even nuclei, obtained by inserting Cameron's values of δ into the calculation for σ_{theor}.

● Lang and Le Couteur level density formula.

○ $\rho = \exp 2(aU)^{\frac{1}{2}}$ with $a = {}^{1}/_{10}A$.

As one would expect from the good agreement evident from fig. 7, most of the points now lie close to the line $\sigma_{exp}/\sigma_{theor} = 1$. The four points which lie off this line correspond to target nuclei in the closed shell region (Z or $N = 28$). Thus, when the pairing energy is taken into account the experimental and theoretical cross sections of both odd-mass and even-mass nuclei are in very good agreement, with the exception of a few nuclei in the region N or $Z = 28$. We will attribute these deviations to level density fluctuations in the vicinity of closed shells. The actual values of the calculated cross sections (theory A) are given in column 5 of table 1.

3.6. SIMPLE FERMI GAS MODEL LEVEL DENSITY FORMULA $\rho = C \exp[2(aU)^{\frac{1}{2}}]$ (THEORY B)

The Lang and LeCouteur formula is based upon the Fermi gas model of the nucleus but it includes refinements which allow for the incomplete rigidity of

the nucleus and the effect of surface oscillations. In order to see the extent to which these refinements contributed to the good agreement between theory and experiment described above, the (n, p) cross sections were recalculated using the simple formula first given by Weisskopf [19]) in 1937 and which has frequently been used for statistical theory calculations:

$$\rho = C \exp\left[2(aU)^{\frac{1}{2}}\right]. \tag{2}$$

Here, a is a constant which is connected with the nuclear temperature T_{np} by the relation $U = aT_{\mathrm{np}}^2$. The constant C does not enter into our calculations because we are concerned only with level density ratios †.

We first of all derived the values of the parameter a from the experimental proton spectra. As mentioned in section 2, the slope of the line $\ln(N(\varepsilon_{\mathrm{p}})/\sigma_{\mathrm{p}}(\varepsilon_{\mathrm{p}})\varepsilon_{\mathrm{p}})$ as a function of ε_{p} gives the nuclear temperature T_{np}. It was assumed that this temperature corresponded to the excitation energy U_{peak} at the peak of the proton spectrum, since it is there that the statistical accuracy of the proton yields $N(\varepsilon_{\mathrm{p}})$ is best and consequently it is the points in this region which have the greatest weight in determining T_{np}. In addition to this, the (n, np) component is generally negligible in this energy region. The parameter a was then found from the relation $a_{\mathrm{exp}} = U_{\mathrm{peak}}/T_{\mathrm{np}}^2$ (see also subsect. 3.10). A rough proportionality was found to exist between a and the atomic weight A, the average value of A/a for 15 nuclei being 11.5 ± 3 MeV^{-1} (we excluded from this average the three light nuclei mentioned in subsect. 3.9 and nuclei which gave very low proton yields). This value of a agrees well with the mean value given by Thomson [45]). Dostrovsky *et al.* [18]) have used eq. (2) to calculate excitation functions for a number of nuclear evaporation processes. In their calculations they used values of a equal to $\frac{1}{10}A$, $\frac{1}{20}A$ and $\frac{1}{40}A$. We calculated σ_{theor}(n, p) using $a = a_{\mathrm{exp}}$, $\frac{1}{10}A$ and $\frac{1}{20}A$ and, in agreement with Dostrovsky *et al.*, found that σ_{theor} did not depend very sensitively upon the value of a. The results of the calculations with $a = \frac{1}{10}A$ (theory B) are given in column 6 of table 1. The agreement between the two sets of theoretical cross sections (theory A and theory B) is good and most of the discrepancies can be accounted for by the use of different Q values ††. The new results do not affect the essential features of figs. 2–7. For example, the values of $\sigma_{\mathrm{exp}}/\sigma_{\mathrm{theor}}$ calculated according to both theory A and theory B for the even nuclei are plotted together in fig. 8.

† That is, we assume that C is identical for isobaric nuclei and that level density fluctuations caused by the odd-neutron character of the nucleus and by closed shells are accounted for by δ and a.

†† For "theory A" the Q values were obtained from the tables of Wapstra [20]); for "theory B" and figs. 4 and 5 we used the more recent values given in table 1 which were obtained from tables compiled by Ashby and Catron [8]). Some of these values differed a little from the values used in theory A. E.g. Na^{23} (−3.4 MeV), Cl^{35} (+0.4 MeV), V^{51} (−1.4 MeV), Cr^{50} (−0.6 MeV), Fe^{54} (+0.3 MeV), and Ni^{58} (+0.6 MeV).

3.7. THE CONSTANT TEMPERATURE FORMULA $\rho = C \exp(-\varepsilon/T)$

It is sometimes suggested [14]) that level densities can be represented sufficiently accurately for the purpose of statistical theory calculations by the expression $\rho = C \exp -\varepsilon/T$, where ε is the emitted particle energy, T is the nuclear temperature and C is a constant. This formula implies that the nuclear temperature is independent of excitation energy and that the quantity $\ln \rho(\varepsilon) = \ln(N(\varepsilon)/\sigma(\varepsilon)\varepsilon)$ is a linear function of ε. Ericson [21]) has suggested that T is virtually independent of excitation energy if the excitation energy is not too high. On the other hand, the level density formulae based on the Fermi gas model (e.g. the Lang and Le Couteur formula and the relation $\rho = C \exp [2(aU)^{\frac{1}{2}}]$) require that $U = aT^2$ (or an equivalent relation) and the relation between $\ln \rho$ and ε (or U) exhibits a slight downward concavity at small values of ε (or large values of U). In principle, the experimental values of $\ln \rho$ plotted as a function of ε should enable us to decide between these two level density relations. The statistical accuracy of the experimental values of $\ln \rho$ was good enough for this purpose in the case of the targets giving the highest (n, p) yields but, unfortunately, these targets gave a very high (n, np) proton yield in the very energy region where we might expect to observe the downward concavity. Targets which gave no (n, np) yield invariably gave a low (n, p) yield and the statistical accuracy is poor. In fact, in every case the two types of level density formulae fitted the experimental $\ln \rho$ curves over the region which was free from (n, np) contamination equally well.

However, it is possible to compare the two types of level density formulae by comparing the values of σ_{theor}(n, p) which they yield. We have already seen in subsect. 3.5 and 3.6 that the Fermi gas type of level density formula (theories A and B) lead to values of σ_{theor} which agree rather well with the experimental values σ_{exp}. When σ_{theor} was calculated using the constant temperature level density formula the values turned out to be consistently 2.5–3 times smaller than σ_{exp}; that is, our calculations definitely favour the Fermi gas type of dependence.

Since the magnitude of an (n, p) cross section is determined by competition between the (n, n′) and (n, p) reactions it must be determined very largely by the ratio of the level densities $\rho_{\text{p}}/\rho_{\text{n}}$ of the residual nuclei produced by these reactions averaged over regions of excitation energy a few MeV wide. The average energy of the emitted neutrons ($\approx$ 2 MeV) is several MeV less than that of the protons ($\approx$ 5 MeV), with the result that neutron emission tends to leave the residual nucleus with several MeV more excitation energy than proton emission (it should be remembered that Q and δ also effect the average effective excitation energies). Thus, the experimental (n, p) cross section values provide a rough means of comparing the level densities of isobaric nuclei at excitation energies several MeV apart.

It is instructive therefore to plot curves representing the two level density

relations $\rho = \exp(-\varepsilon/T)$ and $\rho = \exp[2(aU)^{\frac{1}{2}}]$ on the same graph, normalising them at the excitation energy corresponding to 5 MeV proton emission. If we read off the value of level density corresponding to 2 MeV neutron emission we find that the first formula gives a value 2.5–3 times the second, thus explaining why the calculations based on the constant temperature formula overestimated the (n, n') reaction at the expense of the (n, p) reaction by this factor. We conclude, therefore, that the Fermi gas type of level density formula, which has a downward concavity in the excitation energy region corresponding to neutron emission, is more in accord with the values σ_{exp}(n, p) obtained in these experiments.

3.8. NEWTON'S LEVEL DENSITY FORMULA

Another formula based on the Fermi gas model of the nucleus has been given by Newton [44]) and σ_{theor}(n, p) was calculated for a few of the nuclei studied in this work using this author's level density formula. The calculated values were much too high, however, and the nuclear temperatures were roughly 50 % greater than the experimentally determined temperatures.

3.9. CORRECTION OF EXPERIMENTAL (n, p) CROSS SECTIONS USING THE RELATION $\rho = C \exp[2(aU)^{\frac{1}{2}}]$

The procedure for separating the contributions from the (n, p) and (n, np) reactions described in sect. 2 involved a linear extrapolation of the quantity $\ln(N(\varepsilon)/\sigma_{\text{p}}(\varepsilon)\varepsilon)$ into the low energy region where the (n, np) protons were observed. This procedure is not consistent with the conclusion reached in subsect. 3.7 that the relation $\rho = C \exp[2(aU)^{\frac{1}{2}}]$ gives a better description of the level density than the relation $\rho = C \exp(-\varepsilon/T)$. We have accordingly recalculated σ_{exp}(n, p) using the preferred relation $\rho = C \exp[2(aU)^{\frac{1}{2}}]$ with $a = \frac{1}{10}A$. The new values are given in the column 7 of table 1. It will be seen that with the exception of three light nuclei the new values, designated σ_{exp} (n, p) II, differ very little from the old (σ_{exp}(n, p)I, column 2). The three exceptions (P^{31}, S^{32} and Ca^{40}) all have very low proton binding energies, a circumstance which causes the (n, np) spectrum to dominate the whole proton spectrum and leads to $\ln(N(\varepsilon)/\sigma(\varepsilon)\varepsilon)$ plots to which only a single straight line having a slope corresponding to a temperature $T_{\text{np}} = 1.2$ MeV can be fitted. This temperature is intermediate between the values of T_{np}(1.5 MeV) and T_{nnp}(0.5 MeV) obtained for other nuclei having comparable mass numbers (see table 2).

These three values of σ_{exp}(n, p) are represented in figs. 2–7 by the open circles located at the end of stippled arrows. The only significant changes these values introduce is to reduce the slope of the $Z \leqq 20$ line in fig. 4 and to reduce the heights of the peaks at $Z = 20$ in figs. 2 and 3.

3.10. NUCLEAR TEMPERATURE ($Z = 11$–30)

As mentioned in sect. 2, the temperature T_{np} of the residual nuclei formed in (n, p) reactions can be determined from the slope of the graphical relation between the quantity $\ln(N(\varepsilon)/\sigma_p(\varepsilon)\varepsilon)$ versus ε. Because it is necessary to measure a large number of tracks to define the proton spectrum $N(\varepsilon)d\varepsilon$ at all accurately, we have been able to derive values of T_{np} for only 17 out of the 27 nuclei studied in the $Z = 11$–30 range. These results are given in table 2, where it will

TABLE 2

Nuclear temperatures $T_{np}(Z = 11$–$30)$

Nuclei	T_{np} (MeV)
Mg^{24}, Al^{27}, Si^{28}	1.5 ± 0.2
P^{31}, S^{32}, Ca^{40}	1.2 ± 0.1 [a]
Ti^{46},	1.25 ± 0.1
Cr^{50}, Cr^{52}, Fe^{54}, Fe^{56}, Ni^{58}, Ni^{60}, Cu^{63}, Zn^{64} Zn^{66}, Zn^{67}	1.1 ± 0.1

[a]) This value corresponds to a mixture of (n, p) and (n, np) reactions (see subsect. 3.9).

be seen that the T_{np} values have been divided into four groups. The individual values fluctuate slightly within each group but these variations are not statistically significant. These results are on the whole consistent with the temperatures obtained from the formula $U = aT^2$ with $a = \frac{1}{10}A$ and with U taken as the excitation energy corresponding to the peak of the proton spectrum ($\varepsilon_p \approx 5$ MeV). At the same time it is important to note that the above relations lead to values of T_{nn} which are over twice the temperatures observed in 14 MeV inelastic scattering experiments. E.g., in the case of Fe^{56}, we have $a = 5.6$ MeV^{-1} and $U = 14 - \varepsilon_n - \delta = 9$ MeV ($\varepsilon_n = 2$ MeV, $\delta \approx 3$ MeV) which leads to $T_{nn} \approx 1.3$ MeV. The observed 14 MeV value of T_{nn} is 0.6 MeV [22, 23]).

The values obtained for T_{nnp}, the temperature of the residual nucleus formed in an (n, np) reaction, varied between 0.3 and 0.4 MeV for all the nuclei listed in table 4.

3.11. (n, p) CROSS SECTIONS FOR NUCLEI WITH $Z > 30$

The targets in this group were prepared from materials having the natural isotopic composition and only one plate was exposed to each set of six targets. The results are given in table 3 and, in addition, the results for arsenic ($Z = 33$) and selenium ($Z = 34$) have been included in figs. 2–5. Apart from arsenic, the only elements giving proton yields significantly different from zero were zirconium ($Z = 40$), molybdenum ($Z = 42$) and antimony ($Z = 51$). Thus, we have a result which is similar to that found for the $Z = 11$–30 group: the maximum 14 MeV (n, p) cross sections occur for target nuclei lying close to the closed proton shells at $Z = 40$ and 50.

TABLE 3
14 MeV(n, p) cross sections for target nuclei $Z = 33$–53 (natural isotopic mixture)

Target element	Z	σ_{exp}(n, p) mb (this work)	σ_{exp}(n, p) obtained by other authors (mb)
As	33	27± 5	
Se	34	<14	
Br	35	<14	
Sr	38	22±17	(Sr^{88}) 17±2 [25])
Zr	40	62±12	87±22 [36]) [a])
Mo	42	120±20	
Ag	47	<14	3.5±0.7
Cd	48	<14	3.8±0.4
In	49	<14	1.6±0.3
Sn	50	<15	(Sn$^{116, 120}$) < 1 } 0°±15° [38]) [a])
Sb	51	11± 6	40 ±2
Te	52	<5	<1
I	53	<5	

[a]) Proton yield measurements.

3.12 (n, np) CROSS SECTIONS FOR NUCLEI WITH $Z = 11$–30

The experimental values of σ(n, np) are given in table 4. Since these (n, np) cross sections were obtained by subtracting the (n, p) cross sections from the total proton emission cross sections, the absolute errors associated with σ(n, np) are roughly equal to the absolute errors of the corresponding (n, p) cross sections. The sodium, magnesium, titanium, calcium and chromium targets were prepared from the oxides and carbonates of these elements and consequently there was a large yield of low energy protons from the O^{16}(n, p)N^{16} reaction. The correction for these protons (deduced from the Pb_3O_4 target yield) was so large that it was decided to exclude the results for these elements from table 4, apart from those for Ca^{40} and Cr^{50} which gave particularly large (n, np) yields.

Let us now examine these values of σ(n, np) on the basis of the (n, np) reaction mechanism outlined in earlier papers [4]). A similar analysis has been given by Colli *et al.* [24]). According to this mechanism an (n, np) reaction takes place in two independent stages. In the first stage a neutron is evaporated ((n, n′) reaction) and in the second a proton is evaporated from the still highly excited nucleus. Evaporation of a neutron having energy ε_n leaves the nucleus with excitation energy $U_n = 14 - \varepsilon_n$. The energy spectrum of these neutrons $N(\varepsilon_n)d\varepsilon_n \propto F_n d\varepsilon_n$ (see eq. (1c)) may be regarded also as an excitation energy spectrum $N(U_n)dU_n$ giving the probability that the nucleus is left with excitation energy U_n after evaporating a neutron. In general, the nucleus can reduce this energy U_n by proton, neutron or γ-emission and the probabilities for the occurrence of these processes can be expressed in terms of the partial widths Γ_p, Γ_n and Γ_α, respectively. Second neutron emission ((n, 2n) reaction) is possible only if $U_n > B_n$, and proton emission ((n, np) reaction) if $U_n > B_p$,

TABLE 4

14 MeV (n, np) cross sections for target nuclei $Z = 11$–30

	Target nucleus	σ_{exp}(n, np) (mb)	σ_{exp}(n, p) (mb)	$\frac{\sigma_{nnp}}{\sigma_{np}}$	R	$\frac{F_n}{F_p}$	α		σ_{theor}(n, np) (mb)	σ_{exp}(n, np) obtained by other authors (mb)
even	Si^{28}	27±22	246	0.11	0	4.91	(∞)	$\bar{\alpha} = 0.51$	0	
	S^{32}	105±25	289	0.36	0.52	1.40	0.49		158	
	Ca^{40}	205±38	298	0.69	0.69	1.63	0.62		252	
	Cr^{50}	153±21	277	0.55	0.44	2.92	0.43		210	
	Fe^{54}	218±13	382	0.57	0.66	2.41	0.36		308	220 [4])*
										224 [5])*
	Fe^{56}	35± 7	86	0.41	0	3.97	(∞)		0	
	Ni^{58}	343±27	430	0.80	0.61	2.85	0.46		314	160±40 [33])
										220 [4])*
	Ni^{60}	51± 9	134	0.38	0.12	22.00	(0.14)		80	60 [4]) *
										68 [5])*
	Zn^{64}	281±18	171	1.64	0.54	4.56	0.67		321	≈370 [41])*
	Zn^{66}	50± 4	35	1.43	0.13	32.30	(0.34)		91	
odd-proton	Al^{27}	53±11	76	0.70	0.52	11.75	0.11	$\bar{\alpha} = 0.17$	79	70 [4])*
										85 [31])*
	P^{31}	163±14	114	1.43	0.65	7.90	0.28		100	
	Cu^{63}	152± 9	105	1.45	0.45	19.60	0.13		158	130 [4])*

where B_n and B_p are the binding energies of neutrons and protons in the target nucleus. For most of the nuclei studied $B_p < B_n$ and consequently there is a region of excitation energy $B_p < U_n < B_n$ where proton or γ-emission are the only processes possible (i.e. $\Gamma_n = 0$). When the amount by which U_n exceeds B_p is small, the Coulomb barrier impedes proton emission and $\Gamma_p \ll \Gamma_\gamma$. The experimental spectra show that the yield of protons with energies below 2 MeV is negligible and so, for the purposes of our calculation, we shall assume that protons must have an energy of at least 2.5 MeV to compete effectively against γ-emission. It is possible for competition from neutron emission to begin when $U_n > B_n$ and, because the (n, np) protons have energies well below the Coulomb barrier, we expect this competition to be rather severe. However, the neutrons themselves must penetrate an angular momentum barrier and for this reason we shall assume that competition from the (n, 2n) reaction becomes dominant only when the neutrons have an energy of (B_n+1) MeV. We note that for most of the nuclei in table 4, $B_n - B_p \approx 3$ MeV, so that 1 MeV neutrons compete on the average with 4 MeV protons. Although it is obvious that some protons will be emitted in the region where $U_n > (B_n+1)$ (i.e. a sharp cut-off does not really exist), we shall simplify the problem by supposing that proton emission ((n, np) reaction) is possible only when first neutron emission leaves the nucleus with an excitation energy within the sharply defined limits $(B_p+2.5) < U_n < (B_n+1)$MeV. Let us denote the ratio of the area under the excitation energy spectrum $N(U_n)\mathrm{d}U_n = N(14-\varepsilon_n)\mathrm{d}\varepsilon_n$ between these limits to the area of the whole spectrum by R. Then we have

$$\sigma(\mathrm{n}, \mathrm{np}) = \sigma(\mathrm{n}, \mathrm{n}') \times R \times \alpha, \tag{3}$$

where $\sigma(\mathrm{n}, \mathrm{n}')$ is the cross section of all processes in which a neutron is evaporated in the first stage of compound nucleus decay and $\alpha = \Gamma_p/(\Gamma_p+\Gamma_\gamma)$. Since

$$\sigma(\mathrm{n}, \mathrm{n}') = \sigma(\mathrm{n}, \mathrm{p}) F_n/F_p,$$

we have

$$\sigma(\mathrm{n}, \mathrm{np}) = \sigma(\mathrm{n}, \mathrm{p}) \times \frac{F_n}{F_p} \times R \times \alpha, \tag{4a}$$

or

$$\alpha = \frac{\sigma(\mathrm{n}, \mathrm{np})}{\sigma(\mathrm{n}, \mathrm{p})} \times \frac{1}{R} \times \frac{F_p}{F_n}. \tag{4b}$$

Thus we can determine α by using the experimental values of $\sigma(\mathrm{n}, \mathrm{np})$ and $\sigma(\mathrm{n}, \mathrm{p})$, the values of R obtained from the theoretical (n, n') spectra, and the values of F_p and F_n which were used when calculating the theoretical values $\sigma_{\mathrm{theor}}(\mathrm{n}, \mathrm{p})$. The values of α obtained are given in column 7 of table 4. If we exclude the values enclosed in brackets, which correspond to cases where R is either zero or very small (for these cases the area under the curve $N(\varepsilon_n)\mathrm{d}\varepsilon_n$

between the limits is too small to yield an accurate determination of α), we see that the α values may be divided into two groups according to whether the target nucleus is even or odd-proton. The averaged values of α for these two groups are $\bar{\alpha} = 0.51$ and 0.17, respectively. This distinction between even-mass and odd-mass nuclei provides yet another instance of the effect of nucleon pairing on level density. The products of (n, np) reactions with even target nuclei are odd-proton whereas with odd-proton target nuclei the products are even. As mentioned in subsect. 3.3, the effective ground state of an even nucleus is raised by $\frac{1}{2}\delta$ MeV with respect to that of an odd-proton nucleus. Consequently Γ_p, and therefore $\bar{\alpha}$ also, will be rather smaller on the average for odd-proton target nuclei. The constant $\bar{\alpha}$ should not be taken too seriously, however. In particular, because of our neglect of neutron competition in the region $B_n < U < (B_n+1)$, we should not regard $\bar{\alpha}$ as a reliable measure of Γ_p/Γ_γ. In the region where neutron competition is possible Γ_n will sometimes be significant and $\bar{\alpha}$ will then contain a component which depends on Γ_n as well as on Γ_p and $\Gamma_\gamma(\alpha' = \Gamma_p/(\Gamma_n+\Gamma_p+\Gamma_\gamma).)$ This will be the case when neutron emission is favoured by pairing effects. For example, (n, 2n) reactions with odd-proton target nuclei are favoured (Γ_n large) by the fact that the product nuclei are odd; this will reduce α' independently of the value of Γ_p.

In the last column but one of table 4 we present the values of σ(n, np) calculated according to eq. (4a) using the theoretical values of σ(n, p) and F_n/F_p (theory B) and the values of $\bar{\alpha}$ given in table 4. The calculated values follow the fluctuations of the experimental cross sections sufficiently well to justify the proposed reaction mechanism. It should be mentioned that the average excitation energy of the residual nucleus formed in a 14 MeV (n, np) reaction is only $\approx$ 2 MeV and we must therefore expect considerable fluctuation in the level densities. Moreover, the assumption of fixed values of $\bar{\alpha}$ for the two groups of nuclei implies that the ratios of the level densities of the nuclei formed by proton and γ-emission are constant within each group. This also is clearly unrealistic.

3.13. COMPARISON WITH 14 MeV (n, p) CROSS SECTIONS OF OTHER AUTHORS

Most of the 14 MeV (n, p) cross section data reported in the literature were derived from activation measurements in which the yields of the radioactive products formed specifically in (n, pγ) reactions were measured. These cross sections are integrated (n, p) cross sections and consequently contain contributions from both compound nucleus and direct (n, pγ) processes. It is important to note, however, that they contain no contribution from the (n, pn) reaction (in which a neutron is emitted after proton emission) because this reaction leads to a different final nucleus. On the other hand, cross section measurements based on proton yield measurements include the (n, pn) component but, as stated in the Introduction, the method used in the work reported here was specifically

designed to exclude the direct interaction component. There are no reliable methods of assessing the magnitidus of either the direct components of (n, pγ) cross sections or the compound nucleus components of (n, pn) cross sections. We therefore have the rather unsatisfactory situation whereby we may expect the activation cross sections to be either smaller or larger than (or accidentally equal to) the cross sections obtained from proton yield measurements according to whether $\sigma(\mathrm{n, p}\gamma)_{\mathrm{direct}} \geqq$ or $< \sigma(\mathrm{n, pn})_{\mathrm{compound\ nucleus}}$.

The published 14 MeV (n, p) cross sections are given in the last column of tables 1 and 3. Those marked [a]) are based on proton yield measurements; consequently they include the (n, pn) component but have been corrected for the direct interaction component. Although there are one or two cases where the cross sections for a particular isotope do not agree amongst themselves, it is possible to make some general observations about these data. (i) There are no cases where σ_{exp}(n, p) II (or the other proton yield results) significantly exceed the activation cross sections. (ii) Some of the activation cross sections exceed the proton yield cross sections by $\approx$ 100 mb or more (e.g. Mg^{24}, $Ti^{46, 47}$, Zn^{64}?). (iii) More generally the activation cross sections exceed the proton yield values by 0–40 mb.

We can conclude therefore that, in general, $\sigma(\mathrm{n, p})_{\mathrm{direct}} = (0\text{–}40\ \mathrm{mb}) + \sigma(\mathrm{n, pn})$. The magnitude of σ(n, pn) is determined partly by the (n, p) Q value (Q_{np}) and partly by the competition between γ-emission and neutron emission from the (n, p) product nucleus. The binding energy of a neutron in the nucleus formed by an (n, pγ) reaction is generally $\approx$ 7 MeV so that if $Q_{\mathrm{np}} \approx 0$ MeV, emission of a 1 MeV second neutron is energetically possible provided that the (first) proton was emitted with an energy $\varepsilon_{\mathrm{p}} \lesssim 6$ MeV. If we assume that a neutron is always emitted when more than 1 MeV is available to it, then σ(n, pn) could be as much as $\frac{1}{2}\sigma$(n, p) although it would fall off rapidly with increasingly negative values of Q_{np}. But as we saw in subsect. 3.12 for the similar case of the (n, np) reaction, competing emission processes are strongly influenced by odd-even effects and it turns out that (n, pγ) reactions with both even and odd-proton targets are favoured by pairing effects. Of the nuclei studied in this work, only in the case of the odd-neutron target nuclei Ti^{47} and Zn^{67} do we have a situation where the (n, pn) reaction is favoured by both the value of Q_{np} ($\approx$ 0 MeV) and by pairing effects. Thus, for most of the nuclei studied σ(n, pn) is probably rather small, perhaps not more than $\frac{1}{6}\sigma$(n, p). This means that $\sigma(\mathrm{n, p})_{\mathrm{direct}}$ is usually between 20–60 mb and sometimes exceeds 100 mb. These values are in accord with the published estimates of $\sigma(\mathrm{n, p})_{\mathrm{direct}}$ [4, 5, 42]), and agree also with the values calculated by Brown and Muirhead [34]), although not with the individual values given by these authors.

The values of σ_{exp}(n, p) given in column 3 of table 3 for Sr^{88} (82.7 % abundant) and Zr are in good agreement with the published values [25, 36]) (apart from Sr^{88}, all the cross sections in table 3 are based on proton yield measurements).

The cross section survey was extended to $Z = 53$ mainly for the purpose of investigating the results of a similar survey carried out at forward angles ($0 \pm 15°$) by Eubank, Peck and Zatzick [38]). These authors found that the (n, p) cross section for Sb($Z = 51$) was at least 40 times that for Sn($Z = 50$). In agreement with their work, we found that the proton yield from most of these targets was too small to be resolved from the background. The yield from Sb was just significant, although the cross section turned out to be much smaller than that found by Eubank *et al.* [38]). The same group have also measured the angular distribution of the protons from Sb and identified a forward peaked and an "isotropic" component [39]). They pointed out that if this second component were truly isotropic it would represent an integrated cross section of 74 ± 6 mb. Their measurements were confined to angles less than 60°, however, and our 120° measurements show that the proton yield is actually very small at backward angles. It follows therefore that most of the proton yield measured by Peck *et al.* [39]) (22 mb forward of 60°) must have been due to direct interactions.

4. Conclusions

The conclusion of this work may be summarised as follows:

(i) The compound nucleus components of 14 MeV (n, p) cross sections for targets with $Z = 11$–30 vary from ≈ 20 mb to ≈ 450 mb and show a strong dependence on whether the target nucleus contains an even or odd number of neutrons and protons. The magnitude of the cross section is also strongly influenced by the incidence of closed shells at $Z, N = 20$ and 28. These cross section fluctuations can be well accounted for by the statistical model of the nucleus in terms of Q value and level density fluctuations near closed shells, and by pairing effects. In the region $Z = 30$–53 the (n, p) cross sections are considerably smaller but exhibit similar fluctuations near the closed shells at $Z, N = 40$ and 50.

(ii) Comparison of the proton yield (n, p) cross section measurements with 14 MeV (n, p) activation cross sections show that the (n, p) direct interaction component probably varies between ≈ 20 mb and ≈ 100 mb. However, this method of estimating the direct component is not very reliable because of the unknown magnitude of the (n, pn) cross section.

(iii) In the region $Z = 11$–30 (n, np) cross sections vary between 0 and ≈ 300 mb. The cross sections can be well accounted for by the statistical model in terms of fluctuations of the binding energies of neutrons and protons in the target nucleus and by pairing effects.

The author thanks Mrs. M. J. Bathe, Miss E. I. Harrison, Mrs. A. S. Lane and Miss P. Stopana for scanning the plates and Mr. G. V. Ansell for operating

the 14 MeV neutron generator. He also thanks the Electromagnetic Separator Group, A. E.R.E., Harwell for providing the separated isotopes and preparing the targets.

References

1) V. E. Weisskopf and D. H. Ewing, Phys. Rev. **57** (1940) 472
2) B. L. Cohen, Phys. Rev. **105** (1957) 1549
3) L. Rosen and L. Stewart, Phys. Rev. **99** (1955) 1052
4) D. L. Allan, Proc. Phys. Soc. A **70** (1957) 195; Nuclear Physics **6** (1958) 464, **10** (1959) 348
5) P. V. March and W. T. Morton, Phil. Mag. **3** (1958) 143, **3** (1958) 577
6) L. Colli, F. Cuelbar, S. Micheletti and M. Pignanelli, Nuovo Cim. **14** (1959) 81
7) L. Colli, U. Faccini and S. Micheletti, Nuovo Cim. **5** (1957) 502
8) V. J. Ashby and H. C. Catron, UCRL 5419 (1959)
9) D. J. Hughes and R. B. Schwartz, Brookhaven National Laboratory Report, BNL **325**
10) H. G. Blosser, C. D. Goodman and T. H. Handley, Phys. Rev. **110** (1958) 531
11) R. S. Scalan and R. W. Fink, Nuclear Physics **8** (1958/59) 139
12) L. Allen, Jr., W. A. Biggers, R. J. Prestwood and R. K. Smith, Phys. Rev. **107** (1957) 1363
13) E. B. Paul and R. L. Clarke, Canad. J. Phys. **31** (1953) 267
14) J. M. Blatt and V. F. Weisskopf, Theoretical Nuclear Physics (Wiley, New York, 1952)
15) J. M. B. Lang and K. J. LeCouteur, Proc. Phys. Soc. A **67** (1954) 586
16) H. Hurwitz and H. A. Bethe, Phys. Rev. **81** (1951) 898
17) A. G. W. Cameron, Canad. J. Phys. **36** (1958) 1040
18) I. Dostrovsky, Z. Fraenkel and G. Friedlander, Phys. Rev. **116** (1959) 683
19) V. F. Weisskopf, Phys. Rev. **52** (1937) 295
20) A. H. Wapstra, Physica **21** (1955) 367
21) T. Ericson, Nuclear Physics **11** (1959) 481
22) P. H. Stelson and C. Goodman, Phys. Rev. **82** (1951) 69
23) E. R. Graves and L. Rosen, Phys. Rev. **89** (1953) 343
24) L. Colli, U. Facchini, I. Iori, M. G. Marcazzan and A. M. Sona, Nuovo Cim. **13** (1959) 730
25) A. V. Cohen and P. H. White, Nuclear Physics **1** (1956) 73
26) B. D. Kern, W. E. Thompson and J. M. Ferguson, Nuclear Physics **10** (1959) 226
27) M. J. Nurmia and R. W. Fink, Nuclear Physics **8** (1958) 139
28) S. G. Forbes, Phys. Rev. **88** (1952) 1309
29) C. S. Khurana and H. S. Hans, Nuclear Physics **13** (1959) 88
30) S. Yasumi, J. Phys. Soc. Japan, **12** (1957) 443
31) G. Brown, G. C. Morrison, H. Muirhead and W. T. Morton, Phil. Mag. **2** (1957) 785
32) A. Poularis and R. W. Fink, Phys. Rev. **115** (1959) 989
33) K. M. Purser and E. W. Titterton, Austral. J. Phys. **12** (1959) 103
34) G. Brown and H. Muirhead, Phil. Mag. **2** (1957) 473
35) J. A. Grundle, R. L. Henkel and B. L. Perkins, Phys. Rev. **109** (1958) 425
36) Se Hee Ahn, J. R. Hearst, J. H. Roberts and E. N. Strait (to be published)
37) G. W. McClure and D. W. Kent, Journal of the Franklin Institute **260** (1959) 238
38) H. P. Eubank, R. A. Peck, Jr., and M. R. Zatzick, Nuclear Physics **10** (1959) 418
39) R. A. Peck, Jr., H. P. Eubank and R. M. Howard, Nuovo Cim. **14** (1959) 397
40) Wash-191 (1956) AEC
41) A. H. Armstrong and L. Rosen, Nuclear Physics **19** (1960) 40
42) I. Kumabe and R. W. Fink, Nuclear Physics **15** (1960) 316
43) I. L. Preiss and R. W. Fink, Nuclear Physics **15** (1960) 326
44) T. D. Newton, Canad. J. Phys. **34** (1956) 804
45) D. B. Thomson, Thesis, Los Alamos Scientific Laboratory (1960)
46) L. Colli, I. Iori, G. Marcazzan, F. Margari, A. M. Sona and P. G. Sona, Nuovo Cim. **17** (1960) 634

8.A

Nuclear Physics **24** (1961) 300—312; © *North-Holland Publishing Co., Amsterdam*

Not to be reproduced by photoprint or microfilm without written permission from the publisher

INELASTIC π^--NUCLEON INTERACTIONS AT 7.5 GeV

L. C. GROTE, U. KRECKER, U. KUNDT, K. LANIUS, G. MANSKE and H. W. MEIER

Kernphysikalisches Institut der Deutschen Akademie der Wissenschaften zu Berlin, Zeuthen/Berlin

Received 11 November 1960

Abstract: In a stack of NIKFI-R-emulsions, which was irradiated at Dubna with negative pions, we identified 111 inelastic π^--nucleon collisions. The angular distribution of the emitted particles, their momenta and transverse momenta were investigated and compared with the results of Beljakov *et al.* [1]). Discussion of the results shows that the interactions can be partly ascribed to pion-pion collisions. For those collisions, the radius of the interaction volume could be estimated to be $\Delta r_{\pi\pi} \gtrapprox 1.0 \times 10^{-13}$ cm. For the remainder of the pion-nucleon-collisions we obtained $\Delta r_{\pi N} \gtrapprox 0.4 \times 10^{-13}$ cm.

1. Introduction

The extraction of a negative pion beam of about 7 GeV from the Dubna Synchrophasotron made it possible to study the pion-nucleon interactions in this energy range also. During the last Rochester conference an emulsion group from Dubna (Beljakov *et al.* [1])) presented experimental results on inelastic pion-nucleon interaction at 7 GeV. In the following we report some preliminary results on the same subject, because our results differ partly from those of the Dubna group.

2. Experimental Procedure

From the Joint Institute of Nuclear Research (Dubna) we got a stack consisting of one hundred emulsion sheets of the type NIKFI-R with 400 μm thickness and dimensions 10×20 cm^2. The stack had been exposed to the π^--beam of (7.5 ± 0.6) GeV energy and 4×10^3 particles per cm^2 intensity. The μ^--meson contamination was (5 ± 2) %. The stack was processed in our laboratory.

The plates were scanned by following along the tracks of the primary pions with $450\times$ magnification. About 60 cm track length could be followed by one scanner per hour. Every track was investigated by at least two scanners. Examining a total of 309.9 m we found 759 interactions †. Single scatterings with a scattering angle $< 5°$ were not counted as an interaction. In 652 out of the 759 cases the event occurred at a distance $\geqq 20$ μm from glass and emulsion surface of the processed emulsion respectively. Measurements have been made only for this group of events. Making use of exactly the same criteria for the

† Taking into account the results and corrections described in this paper the mean free path for inelastic interactions of negative pions of 7.5 GeV energy in emulsion proved to be (38.6 ± 1.4) cm.

identification of π-nucleon interactions as the Dubna group †, we selected out of the 652 interactions 112 events, denoted in the following as pion-nucleon interactions. Therefore, the relative frequency of the π-nucleon interactions is (17.2 ± 1.5) %. In ref. [1]) at a pion energy of 7 GeV out of 5300 events 535 have been selected which fulfilled the criteria for π-nucleon interactions, i.e. the relative frequency is (10.1 ± 0.4) %.

The difference between the frequency found in Dubna and in our laboratory is beyond statistical errors. We suppose that the reason for this discrepancy is predominately a scanning-effect. The Dubna group investigated every track only once††.

TABLE 1

Scanning efficiency in %

	a	b	c	a+b, b+c, c+a
All events	97.2 ± 0.8	97.8 ± 0.7	95.9 ± 0.9	100
π–N-collisions	91 ±3	92 ±3	88 ±4	99
π–p-collisions with two secondaries	77 ±7	79 ±7	83 ±7	96
π–p-collisions with two secondaries after elimination of the π–e-collisions	79 ±8	76 ±7	89 ±7	97

In table 1 are tabulated the scanning efficiencies of the three laborants, who made the scanning along the tracks. The scanning efficiency for detecting π-nucleon interactions is remarkably smaller than that for all interactions. The percentage of π-nucleon interactions, which have not been found by single scanning, is (51 ± 8) %. In order to study the tendency of this selective overlooking we determined the efficiency for finding the π–p-events with two secondary tracks. The results are tabulated in the third row. One can see that the efficiency for finding such events is smaller. In 75 % of all cases the reason for the selective overlooking of the two prong π–p-interactions was that the scanner missed the origin of the event and followed one of the secondary tracks. From our results it seems to be possible, that in ref. [1]) a remarkable proportion of all π-nucleon interactions has not been found. Especially events with a small number of prongs, in which one of the secondary tracks is nearly parallel to the primary track (see also fig. 4), have been overlooked. In addition to the 112 inelastic π-nucleon interactions we found 29 single scattering events with a solid scattering angle θ between 1° and 5° in the laboratory system. In order to separate the elastic scattering events from the inelastic ones, we made scattering

† Private communication by I. M. Gramenitsky.

†† Private communication by Prof. K. D. Tolstov and Prof. W. Petržilka.

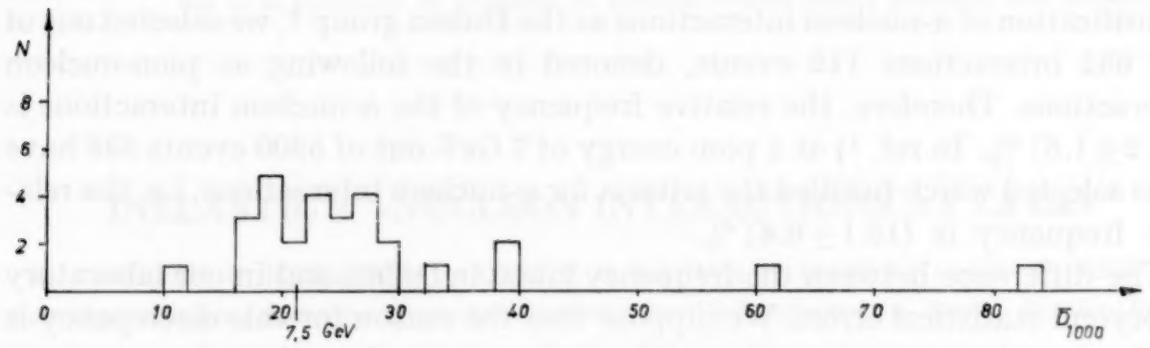

Fig. 1. Mean values of the second differences of the secondaries from one prong stars with scattering angles between 1° and 5°. $\bar{D}_{1000}$ is given in units of 0.01 μm.

TABLE 2

Spurious scattering values

Cell length (μm)	Spurious scattering (μm)
500	0.083 ± 0.016
1000	0.120 ± 0.045
2000	0.18 ± 0.12

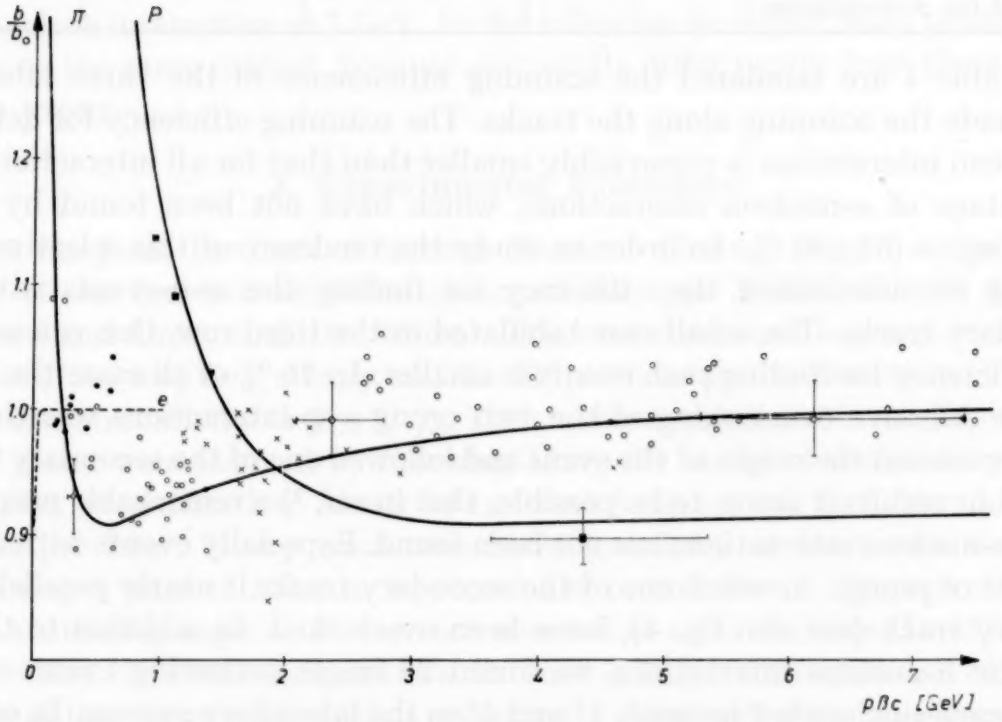

Fig. 2. Ionisation versus pβc for all measured tracks.
○ — identified pions, ■ — identified protons,
× — not identified tracks (supposed pions),
● — identified electrons.

measurements at all 29 secondary tracks †. At each track we measured at least 30 cells of 1000 μm. In fig. 1 we plotted the distribution of the mean values of the second differences related to a cell length of 1000 μm. From this distribution we identified 5 of the scattering events as inelastic. Furthermore we could identify 2 scattering events with $\theta < 1°$ as inelastic π-nucleon interactions.

All secondary tracks of the inelastic π-nucleon interactions having a dip angle $\leqq 5°$ in the unprocessed emulsion were identified by ionisation and scattering measurements. Corrections had been made for "spurious scattering" in our plates. The values of spurious scattering for different cell lengths are given in table 2. About 40 cells have been measured on every track. The cell length was chosen in such a way that the condition $D_{\text{signal}}/D_{\text{noise}} \geqq 2$ was fulfilled; the mean error of the relative blob density was not larger than 3 %. The measured values are plotted in fig. 2. The curves were taken from the paper by Barkas and Young [2]). The dashed curve is valid for electrons.

The fact that there are many measured points in the region where the pion curve and the electron curve are crossing makes it reasonable to suppose that several secondary tracks are not pions but electrons. We studied therefore all two prong events which were selected as pion-proton interactions using the Dubna criteria with one secondary track making an angle $\theta < 1°$ relative to the primary direction. Indeed, we could show that only two out of 10 events of this type were really pion-nucleon interactions. The remaining 8 events proved to be pion-electron collisions. In the fourth row of table 1 we tabulated the efficiency for detecting the two prong π–p-interactions after the elimination of the π–e-collisions.

From the measured secondary tracks we could identify 70 as $\pi^{\pm}$-mesons and 6 as protons. The energy distribution of these pions in the laboratory system leads us to the assumption that all 27 tracks, which could not be identified, are caused by pions. This corresponds with the results of ref. [1]). All the following distributions of angles, momenta etc. underlie the measured secondary tracks. For the tracks with dip angles $> 5°$ we made geometrical corrections.

3. Results

Table 3 shows the observed frequencies of the secondary particles for inelastic π–p- and π–n-interactions respectively. In the second row are tabulated the frequencies normalized to 100. We made a correction for the loss of two prong π–p-interactions (cf. table 1). In the third row we tabulated the corresponding frequencies given in ref. [1]), also normalized to a total of 100 events. Within the large limits of statistical errors the two distributions approximately correspond with one another. In the fourth row are given the frequencies calculated by Barashenkov [3]) on the basis of statistical theory of multiple

† All scattering measurements were done with the Kernspurmeßmikroskop (KSM) of VEB C. Zeiß, Jena.

TABLE 3

Observed frequencies of the secondary particles

	π^-–p					π^-–n			
Number of prongs	0	2	4	6	8	1	3	5	7
Berlin	3 5±3	30 54±10	15 26±7	6 11±4	2 4±3	16 29±7	28 51±10	11 20±6	0 0
Dubna [1])	4±1	48± 4	42±4	5±1	1±0.5	23±3	59± 5	15±2	3±1
Statistical theory[3])		46.0	44.0	6.0	0.1	17.0	57.5	18.5	2.0

TABLE 4

Mean numbers of prongs

	$\bar{n}_{\pi-p}$	$\bar{n}_{\pi-n}$	$\bar{n}$	$\bar{n}_{\pi\pm}$	$\bar{n}_p$
Berlin	3.1±0.2	2.8±0.2	2.9±0.15	2.7	0.2
Dubna	3.0	3.0	3.0±0.1	2.5	0.5

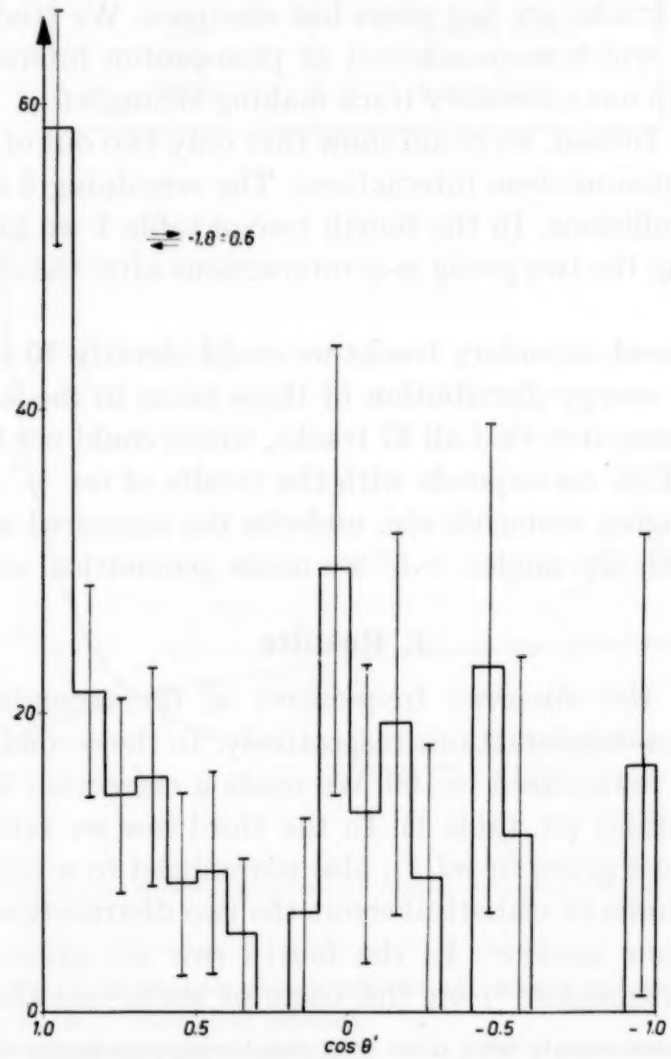

Fig. 3. Angular distribution of the pions from all interactions (π–N-system).

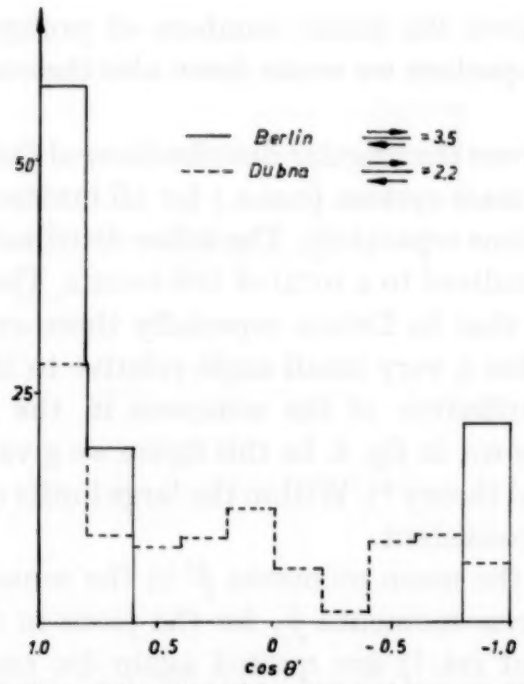

Fig. 4. Angular distribution of the pions from one and two prong events (π–N-system).

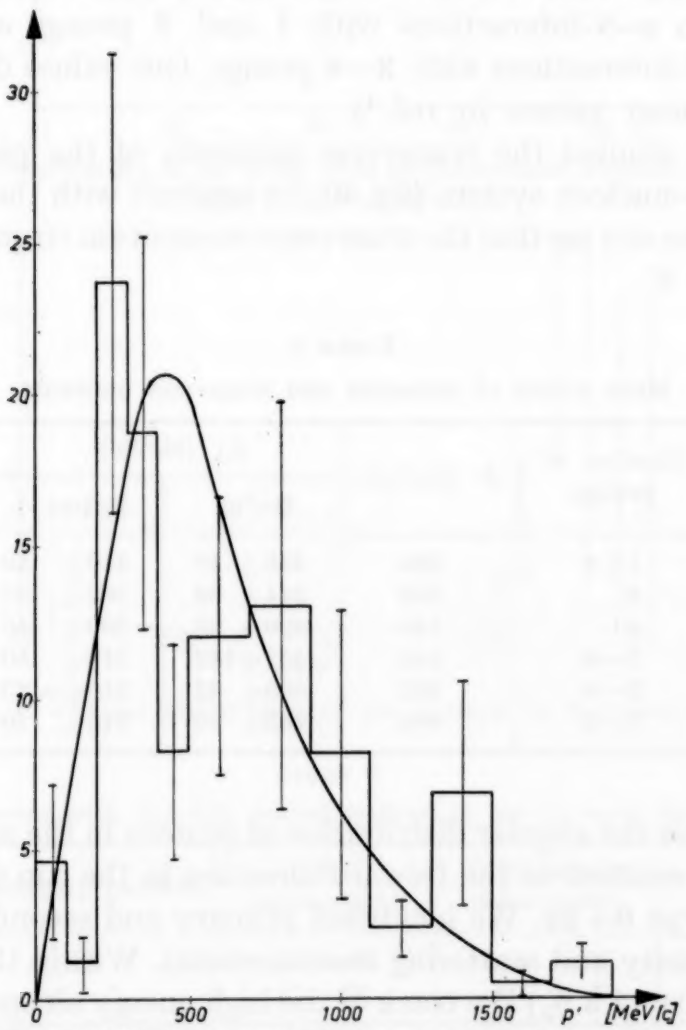

Fig. 5. Momentum distribution of the pions from all interactions (π–N-system).

production. Table 4 gives the mean numbers of prongs resulting from our measurements. For comparison we wrote down also the corresponding values of ref. [1]).

In figs. 3 and 4 are given the angular distributions of the emitted pions in the pion-nucleon centre of mass system (c.m.s.) for all interactions and for the one and two prong interactions separately. The latter distribution is compared with that of ref. [1]), also normalized to a total of 100 events. The comparison of these distributions indicates that in Dubna especially those events are overlooked, in which one track makes a very small angle relative to the primary direction.

The momentum distribution of the π-mesons in the pion-nucleon system normalized to 100 is shown in fig. 5. In this figure we give also the distribution resulting from statistical theory [3]). Within the large limits of experimental errors the distributions are consistent.

In table 5 are given the mean momenta $\bar{p}'$ in the π-nucleon system and the mean values of transverse momenta $\bar{p}_\perp$ for the pions in different groups. The corresponding values of ref. [1]) are quoted again for comparison.

It is remarkable, that there are deviations between our mean values for $\bar{p}_\perp$, corresponding to π–N-interactions with 1 and 2 prongs and those corresponding to π–N-interactions with 3—8 prongs. Our values deviate from the corresponding mean values in ref. [1]).

We have also studied the transverse momenta of the pions versus their angles θ' in the π-nucleon system (fig. 6). In contrast with the observations at high energy jets we can see that the transverse momentum strongly changes with increasing angle θ'.

TABLE 5

Mean values of momenta and transverse momenta

Number of prongs	$\bar{p}'$ (MeV/c)	$\bar{p}_\perp$ (MeV/c)	
		Berlin	Dubna [1])
1+2	595	233± 19	310± 40
3	563	344± 83	260± 30
4	740	500± 93	360± 40
5—8	546	458±142	310± 50
3—8	607	425± 42	310±≈25
1—8	604	385± 49	310± 20

In fig. 7 is given the angular distribution of protons in the π-nucleon system. The sole proton emitted in the forward direction in the c.m.s. comes from an interaction of type $0+2\pi$. We identified primary and secondary particles by relative blob density and scattering measurements. Within the limits of error of the blob density (2.3 %) the track of the high energy secondary particle can be assigned to a proton (or antiproton). The possibility of a K-meson, however,

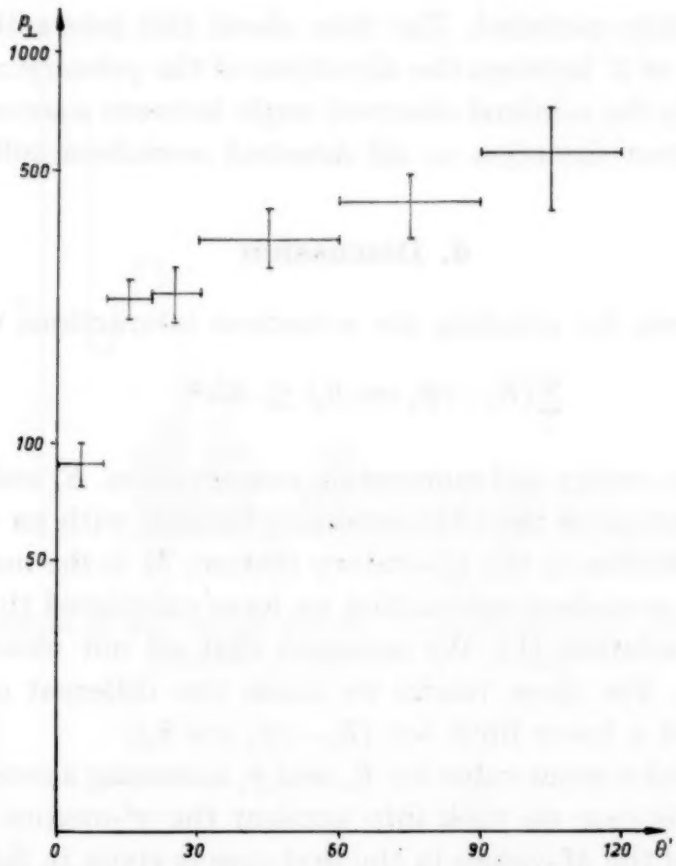

Fig. 6. Transverse momentum $p_\perp$ of the pions from all interactions plotted as a function of the angle θ' (π–N-system).

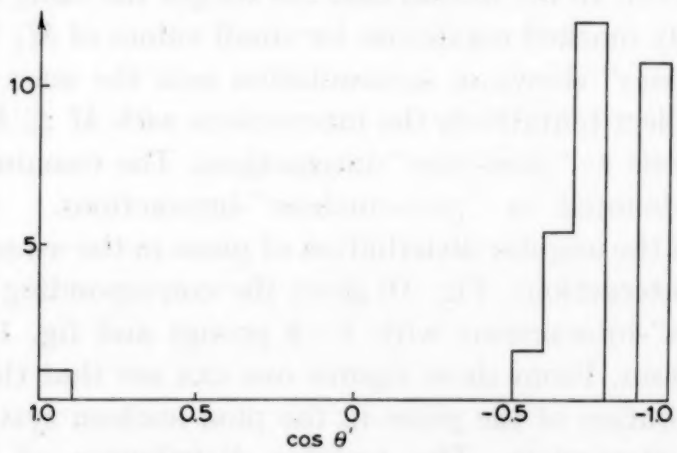

Fig. 7. Angular distribution of the protons (π–N-system).

TABLE 6

Data about the event with the sole proton emitted in the forward direction (c.m.s.)

Primary particle	Secondary particle	θ (lab-system)	Total energy (lab-system)	$p_\perp$
π	p [a])	0° 5′	4545 MeV	40 MeV/c
	π	2° 48′	407 MeV	21 MeV/c

[a]) Traversing a range of 2.34 cm the proton causes a star 0+4 p.

cannot be completely excluded. The data about this interaction are given in table 6. The angle of 5′ between the directions of the primary π-meson and the secondary proton is the minimal observed angle between a secondary track and the primary π-meson direction at all detected π-nucleon collisions.

4. Discussion

One of the criteria for selecting the π-nucleon interactions was the relation

$$\sum_i (E_i - cp_i \cos\theta_i) \leqq Mc^2, \tag{1}$$

which follows from energy and momentum conservation. E_i and p_i are the total energy and momentum of the i-th secondary particle with an angle θ_i relative to the primary direction in the laboratory system, M is the mass of the target particle. For each π-nucleon interaction we have calculated the "target mass" with the help of relation (1). We assumed that all not identified minimum tracks were pions. For these tracks we made two different estimations:

1) we calculated a lower limit for $(E_i - cp_i \cos\theta_i)$;

2) we determined a mean value for E_i and p_i assuming a constant transverse momentum; in this case we took into account the π^0-mesons too.

The distribution of the M-values in the first case is given in fig. 8. The "target masses" of the π-nucleon interactions with $\geqq 3$ prongs are cross hatched within the same distribution. In the second case too we got the same type of distribution with a strongly marked maximum for small values of M. The distribution of the "target masses" shows an accumulation near the mass of the π-meson.

Therefore we collect tentatively the interactions with $M \leqq M_\pi$ in one group, denoting such events as "pion-pion"-interactions. The remaining events form a second group denoted as "pion-nucleon"-interactions.

In fig. 9 is given the angular distribution of pions in the π-nucleon system for the "pion-pion"-interactions. Fig. 10 gives the corresponding distribution for the "pion-nucleon"-interactions with 1—3 prongs and fig. 11 for all "pion-nucleon"-interactions. From these figures one can see that the asymmetry of the angular distribution of the pions in the pion-nucleon system is caused by the "pion-pion"-interactions. The angular distribution of "pion-nucleon"-interaction seems to be nearly isotropically.

TABLE 7

Mean values of the transverse momenta

	$\bar{p}_\perp$ (MeV/c)
pion-nucleon collisions with 1—3 prongs	408±94
pion-nucleon collisions with 1—8 prongs	453±65
pion-pion collisions	192±18

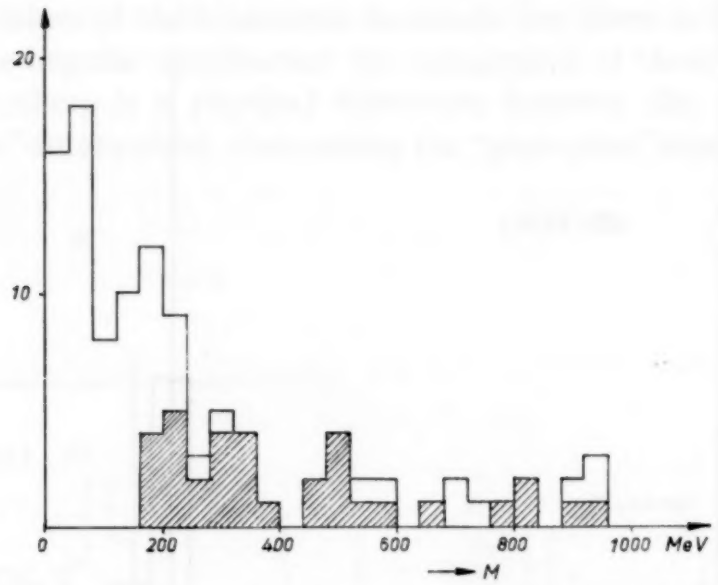

Fig. 8. Minimum values of the "target masses" of all interactions. The cross hatched areas represent events with $\geqq 3$ prongs.

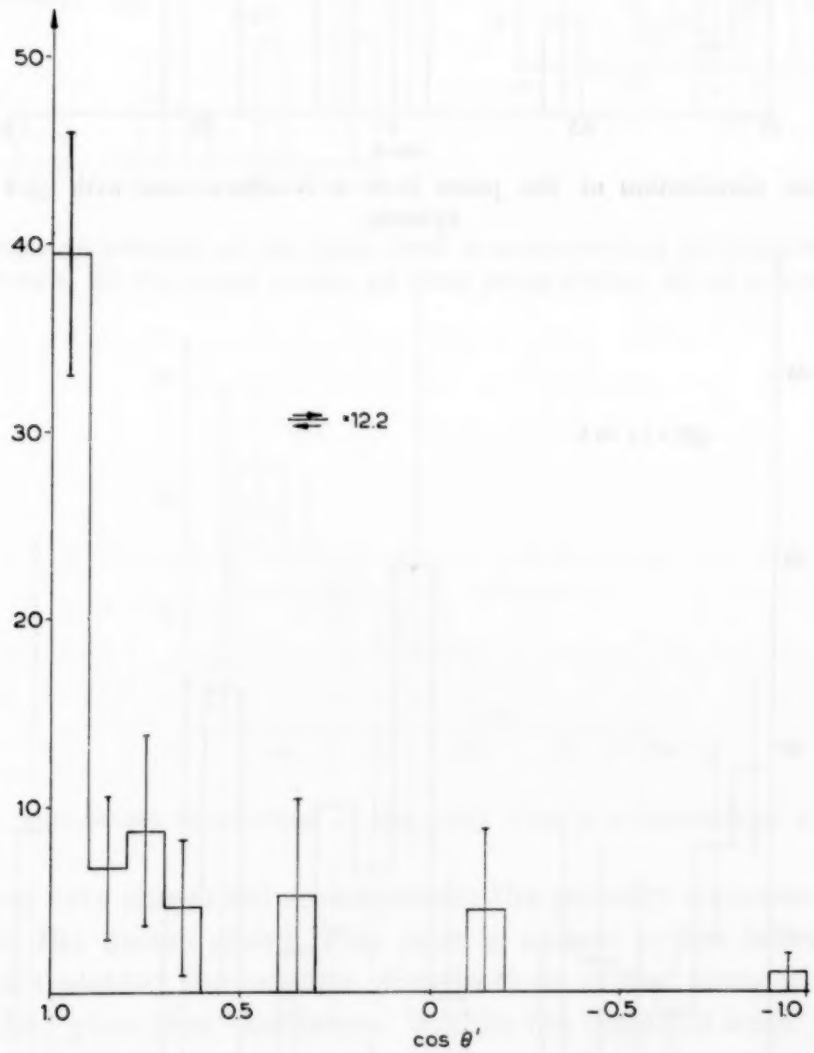

Fig. 9. Angular distribution of the pions from π–π-interactions (π–N-system).

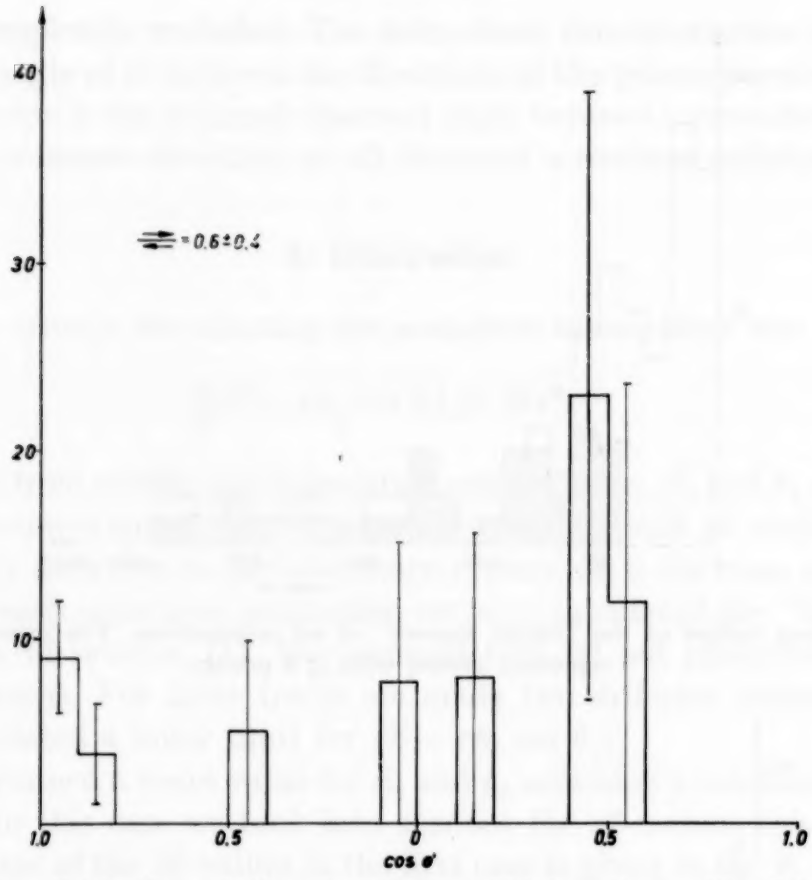

Fig. 10. Angular distribution of the pions from π–N-interactions with $\leqq 3$ prongs (π–N-system).

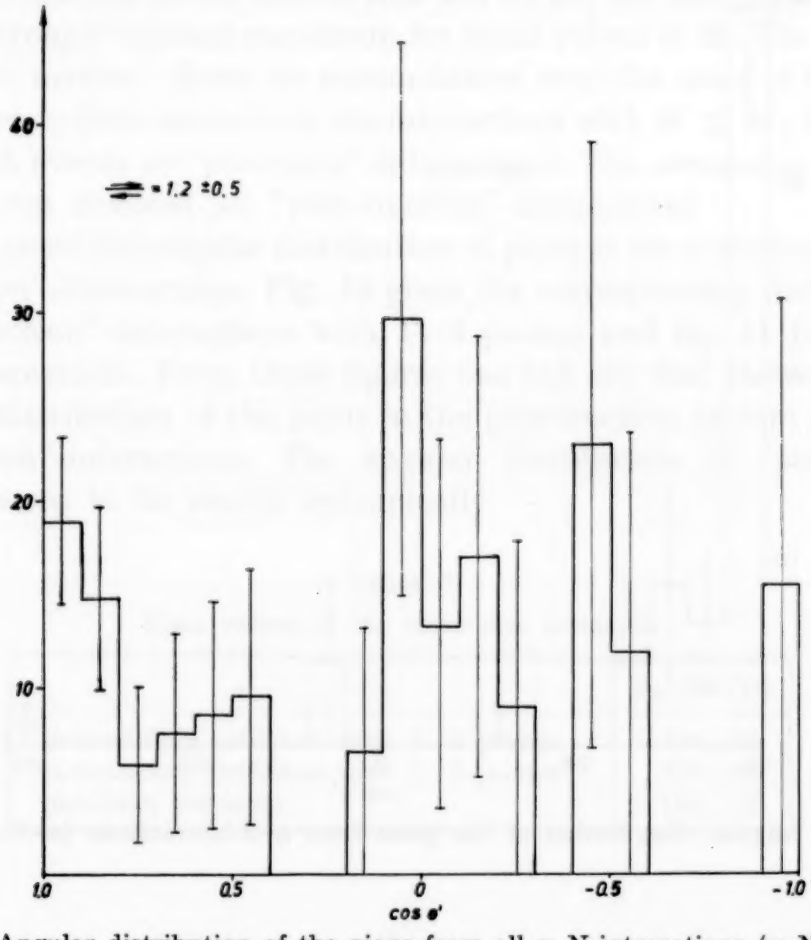

Fig. 11. Angular distribution of the pions from all π–N-interactions (π–N-system).

The mean values of the transverse momenta are given in table 7. Just as in the case of the angular distribution the comparison of these mean values also suggests that there is a physical difference between the "pion-pion"- and "pion-nucleon"-interactions. Concerning the "pion-pion"-interactions we made

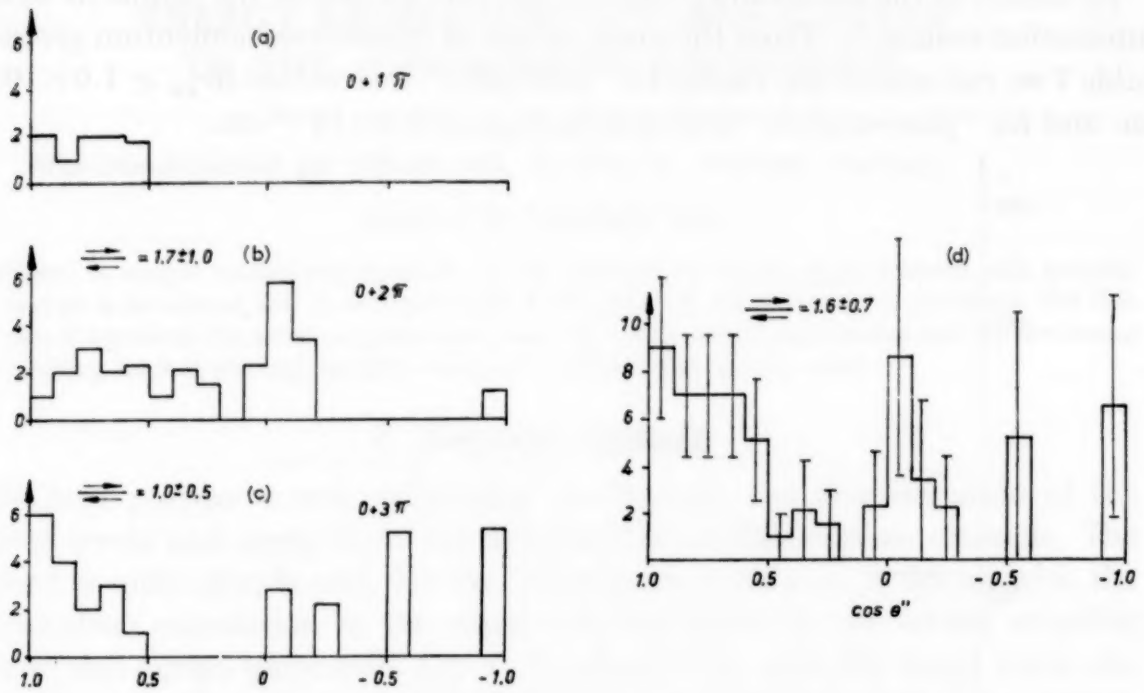

Fig. 12. Angular distribution of the pions from π–π-interactions (π–π-system); (a) one prong events, (b) two prong events, (c) three prong events, (d) all π–π-events.

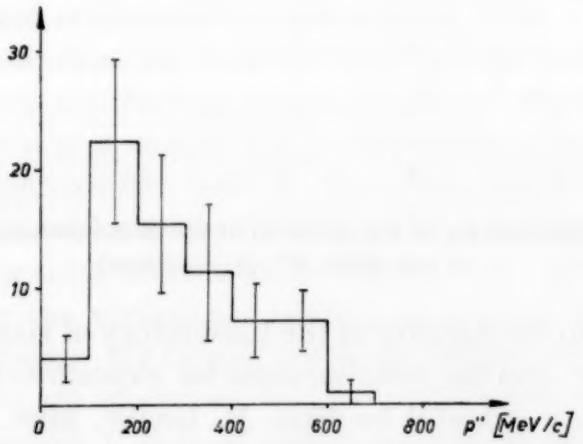

Fig. 13. Momentum distribution of the pions from π–π-interactions (π–π-system).

the following very simplified assumptions: the primary π-meson interacts with a pion from the meson cloud. This pion is at rest in the laboratory system. In fig. 12 are plotted the angular distributions of the pions in the pion-pion c.m.s. for the "pion-pion" collisions. Within the limits of error these distributions are isotropic.

In fig. 13 is shown the momentum distribution of π-mesons in the pion-pion c.m.s.

The transverse momentum of the pions versus the angle of emission θ'' in the pion-pion c.m.s. is plotted in fig. 14.

By means of the uncertainty relation one gets an idea of the radius Δr of the interaction volume [1]). From the mean values of transverse momentum given in table 7 we calculated this radius for "pion-pion"-interaction $\Delta r_{\pi\pi} \gtrsim 1.0 \times 10^{-13}$ cm and for "pion-nucleon"-interaction $\Delta r_{\pi N} \gtrsim 0.4 \times 10^{-13}$ cm.

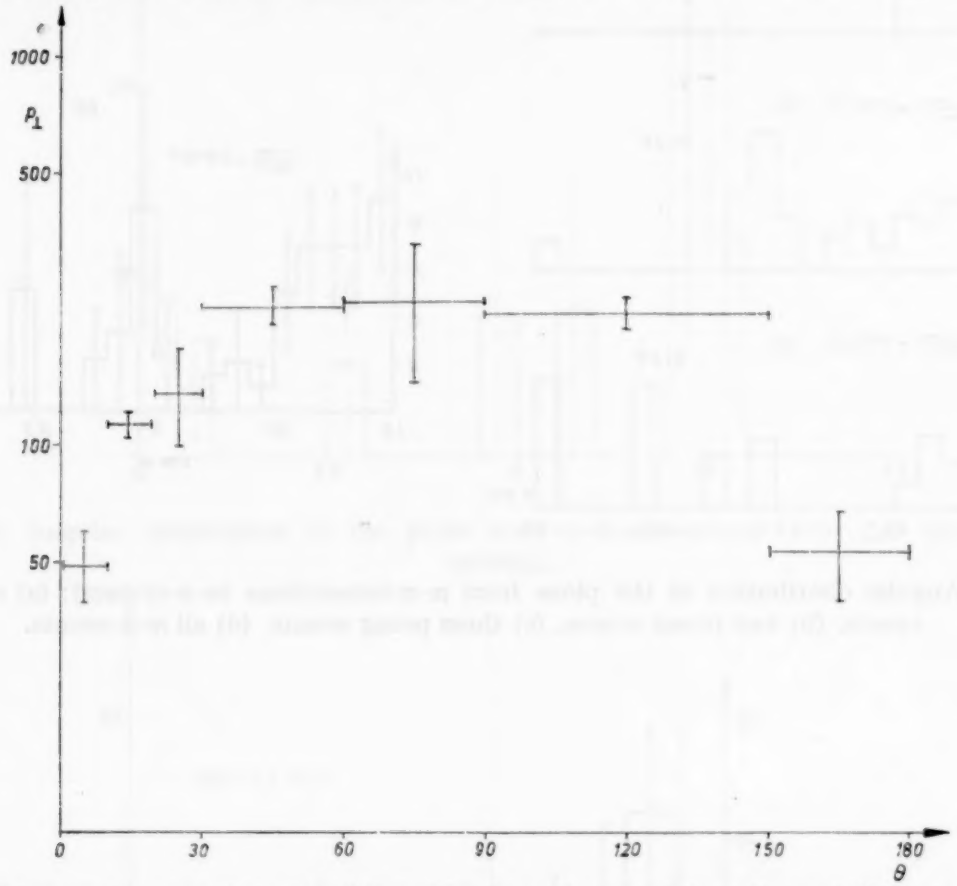

Fig. 14. Transverse momentum $p_\perp$ of the pions from the π–π-interactions plotted as a function of the angle θ'' (π–π-system).

We are indebted to the director of the Laboratory of High Energies in Dubna, Prof. W. I. Weksler, and his collaborators for exposure of the emulsion stack. The authors are very grateful to Miss. R. Bielke, Miss. I. Kussatz, Mrs. L. Schubert, Mrs. S. Stösser, Miss C. Student, Mr. W. Bernard and Mr. P. Landrock for the aid in scanning and measuring.

References

1) W. A. Beljakov, Wan Chu-Fen, W. W. Glagolev, N. Dalchashav, R. M. Lebedev, N.N. Melnikowa, W. A. Nikitin, W. Petržilka, W. A. Swiridov, M. Suk and K. D. Tolstov, Dubna, preprint R 530 (1960)
2) W. H. Barkas and D. M. Young, UCRL 2579 (1954)
3) W. S. Barashenkov, Dubna, preprint R 540 (1960)

6.B

Nuclear Physics **24** (1961) 313—317; © *North-Holland Publishing Co., Amsterdam*

Not to be reproduced by photoprint or microfilm without written permission from the publisher

A NEW VARIATIONAL METHOD FOR CALCULATING EXCITED ENERGY LEVELS AND ITS APPLICATION TO THE ANHARMONIC OSCILLATOR

KAZUO YAMAZAKI

Max-Planck-Institut für Physik und Astrophysik, München, Germany

Received 21 November 1960

Abstract: A simple variational method for the calculation of the excited levels of a quantal system is developed and as an illustration it is applied to the anharmonic oscillator. For this case it agrees in the weak coupling limit with the perturbation calculation and for the strong coupling limit it also agrees with the exact values within a 1 % error.

1. General Method

We here propose a new variational method for the determination of the excited levels and apply it to the anharmonic oscillator as an example. The method is quite simple and, for the anharmonic oscillator, it agrees with the perturbation calculation in the weak coupling limit; in the strong coupling limit it also agrees quite well, say up to about 1 %, with the exact value obtained by numerically solving the Schrödinger equation with a computer. For the n-th excited level it is in principle possible to use the usual variational method, if we know the exact 0-th, . . ., $(n-1)$-th state vectors; among the state vectors which are orthogonal to these exact 0-th, . . . $(n-1)$-th state vectors, we choose a suitable trial function and find the best one by the variational method; then we can find an upper bound for the n-th excited level. But in the real problems it is almost always impossible to know the exact state vectors. If we use approximate 0-th to $(n-1)$-th state vectors, we are in trouble, especially since we know that rather good eigenvalues can be obtained with rather poor associated state vectors. This is the difficulty usually encountered in applying the variational method to excited levels.

Our idea is the following. We choose a suitable simple trial function and the variational parameters are so chosen that the expression $\langle n|H^2|n\rangle - \langle n|H|n\rangle^2$ becomes as small as possible †; it is, of course, zero for the exact n-th state. This requirement has another nice feature, namely it gives us a possibility to estimate the error in E_n by computing ††

$$\frac{\langle n|H^2|n\rangle - \langle n|H|n\rangle^2}{2\langle n|H|n\rangle^2}.$$

† A similar variational method was used in another context by H. Preuss [4]). I am indebted to Dr. Preuss for this information.

†† The factor $\frac{1}{2}$ is due to the squaring.

However, this is generally an overestimate of the error in E_n, because the above expression is the ratio of the sum of the non-diagonal elements and the diagonal element, thus it refers rather to the error of the state vector $|n\rangle$. (Compare with table 1 at the end of this paper). It is regrettable that even though we use here the variational method we cannot say that the values so obtained give an upper bound of the true value (see table 1). This is so, because we give up the requirement of the orthogonality of the state vectors, as remarked above. Because of its simplicity, the possibility of the estimate of errors and the rather surprising agreement with the exact values, we can hope that our method may have some application in the problems of field theory, as for example in that of mass determination in the Heisenberg theory of elementary particles [1]), or in the domain of solid state physics.

2. Anharmonic Oscillator

The Hamiltonian of the anharmonic oscillator is given by (we use the notation of Heisenberg [2]))

$$H = \tfrac{1}{2}(p^2+x^2)+\tfrac{1}{4}\lambda x^4 \quad \text{with} \quad [p, x] = -i. \tag{1}$$

Let us now put

$$p = \frac{-i}{\sqrt{2\alpha}}(a-a^*), \quad x = \sqrt{\tfrac{1}{2}\alpha}(a+a^*), \tag{2}$$

where a^* and a are creation and annihilation operators satisfying the usual commutation relations

$$[a, a^*] = 1, \quad [a, a] = [a^*, a^*] = 0. \tag{3}$$

The point is here that we introduce a variational parameter α which is adjusted differently for each level. If we want to calculate the n-th excited level E_n, the corresponding α_n is determined from the condition

$$\delta(\langle n|H^2|n\rangle-\langle n|H|n\rangle^2) = 0, \tag{4}$$

where

$$|n\rangle = \frac{a^{*n}}{\sqrt{n!}}|0\rangle, \quad a|0\rangle = 0. \tag{5}$$

The state $|n\rangle$ seems to be just the usual free harmonic oscillators's n-th excited state but through (2) this $|n\rangle$ is implicitly a function of the parameter α_n. The various $|n\rangle$ are not orthogonal to each other, as we can see from the fact that the x-represensative $\langle x|n\rangle$ is the Hermite polynomial with the argument $x/\sqrt{\alpha_n}$.

A method in spirit similar to the above was proposed by Kaiser [3]) in the framework of the new Tamm-Dancoff approximation. In some cases it may

have advantages because of the possible ease with which it is extended to field theory. The superiority of our method is its simplicity, the possibility of the estimate of errors and, for the anharmonic oscillator, a better agreement with the exact values, as already emphasized above.

To carry out the actual calculation we proceed as follows. First we put (2) into (1) and express H and H^2 in terms of a, a^* and the parameter α, and then perform the ordering of all the operators in H and H^2 in the normal product form of Wick (the a stand to the right and the a^* stand to the left). The following formula is useful for the ordering of the operators x^8, p^4 . . .:

$$(a\pm a^*)^{2n} = \sum_{j=0}^{n} \frac{([a, a^*])^n}{j!\ 2^j} \sum_{i=0}^{2n-2j} \frac{(\pm 1)^{n+i}(2n)!}{(2n-2j-i)!\ i!} (a^*)^{2n-2j-i} a^i. \tag{6}$$

By taking the expectation values of the well-ordered H and H^2 in the state $|n\rangle$ given by (5), the non-diagonal parts with respect to the number operator a^*a drop out. It is quite easy to re-express these well-ordered operators in terms of the number operator a^*a. Thereupon we use (5) with $\langle n|a^*a|n\rangle = n$. After all this we find, for arbitrary n,

$$\begin{aligned}
&\langle n|H|n\rangle = \tfrac{1}{4}\left(\alpha+\frac{1}{\alpha}\right)(2n+1)+\frac{3\lambda\alpha^2}{16}(2n^2+2n+1),\\
&\langle n|H^2|n\rangle-\langle n|H|n\rangle^2\\
&\quad=\tfrac{1}{8}\left(\alpha-\frac{1}{\alpha}\right)^2(n^2+n+1)+\frac{\lambda\alpha^2}{8}\left(\alpha-\frac{1}{\alpha}\right)(2n^3+3n^2+7n+3)\\
&\quad+\frac{\lambda^2\alpha^4}{256}(34n^4+68n^3+278n^2+244n+96).
\end{aligned} \tag{7}$$

From (4) and (7) α_n is seen to satisfy the equation

$$\begin{aligned}
&2(\alpha_n{}^4-1)(n^2+n+1)+(\lambda\alpha_n{}^3)(3\alpha_n{}^2-1)(2n^3+3n^2+7n+3)\\
&\quad+\tfrac{1}{4}(\lambda\alpha_n{}^3)^2(17n^4+34n^3+139n^2+122n+48)=0.
\end{aligned} \tag{8}$$

This equation fixes the value of α_n as function of λ (the redundant solution can be simply rejected ty the requirements that α_n be real and positive and $\alpha_n \to 1$, for $\lambda \to 0$). Inserting this value of α_n into the expression $\langle n|H|n\rangle$ in (7) we get out energy level E_n in the form

$$E_n = \tfrac{1}{4}\left(\alpha_n+\frac{1}{\alpha_n}\right)(2n+1)+\frac{3\lambda\alpha_n{}^2}{16}(2n^2+2n+1). \tag{9}$$

For the case $\lambda \ll 1$ the solution of (8) is clearly $\alpha_n = 1+O(\lambda)+\ldots$; thus our energy levels are given by

$$E_n = (n+\tfrac{1}{2})+\frac{3\lambda}{16}(2n^2+2n+1)+O(\lambda^2)+\ldots, \quad \lambda \ll 1, \tag{10}$$

which agrees with the usual perturbation calculation. In the strong coupling limit, $\lambda \gg 1$, the first four α become

$$\alpha_0^{-1} = 1.219\lambda^{\frac{1}{3}}, \quad \alpha_1^{-1} = 1.413\lambda^{\frac{1}{3}}, \quad \alpha_2^{-1} = 1.537\lambda^{\frac{1}{3}}, \quad \alpha_3^{-1} = 1.648\lambda^{\frac{1}{3}}. \quad (11)$$

The corresponding E_n, their error by comparison with the exact values, and the rough estimate of error $\langle n|H^2|n\rangle - \langle n|H|n\rangle^2/2\langle n|H|n\rangle^2$ are tabulated in table 1. We see the agreement is excellent. For further comparison we have also quoted the values of Heisenberg [2]) and of Kaiser [3]), which are obtained with the new Tamm-Dancoff method and its modification, respectively. In the last column of table 1 we have also quoted the values obtained by the simple variation method which will be discussed below.

TABLE 1

Comparison of the calculated energy values with the exact ones

	E_n^e Exact value [2])	E_n eq. (9)	error	$\frac{\langle n\|H^2\|n\rangle - \langle n\|H\|n\rangle^2}{2\langle n\|H\|n\rangle^2}$	Heisenberg [2])	Kaiser [1])	E_n^V S.V.M.
$E_0\lambda^{-\frac{1}{3}}$	0.4208	0.4309	+2.2%	0.129	0.421 [a])	0.421 [a])	0.4292
$E_1\lambda^{-\frac{1}{3}}$	1.5079	1.5293	+1.4%	0.027	1.574	1.566	1.5269
$E_2\lambda^{-\frac{1}{3}}$	2.9587	2.9531	−0.2%	0.020	2.889	3.008	2.9513
$E_3\lambda^{-\frac{1}{3}}$	4.6210	4.6100	−0.2%	0.015	5.311	4.659	4.5933

[a]) The E_0 value cannot be calculated, in principle, by the new Tamm-Dancoff method. Here we take the exact value as reference level for the excited states.

3. Comparison with Simple Variational Method

Lastly we want to compare our method with the simple variational method (quoted in the following as S.V.M.), namely, that in which the same trial function (5) is used but the variational parameters α are determined simply from $\delta\langle n|H|n\rangle = 0$, instead of (4). Let us denote the n-th energy level obtained by S.V.M., that given by our eq. (9), and the exact one, by E_n^V, E_n and E_n^e, respectively.

Then it is clear that $E_n^V \leqq E_n$ (for arbitraly n), because E_n^V is the minimum among all possible E_n (α). Now, for the ground state, clearly $E_0^e \leqq E_0^V$. The 1st excited state is an odd function owing to the special symmetry of our Hamiltonian (1), $H(x) = H(-x)$, the exact ground state function is an even function. As our trial function $\langle x|1\rangle$ is an odd function, it is orthogonal to the exact ground state function. Thus it is clear that $E_1^e \leqq E_1^V$. From this argument we know without any explicit calculation that

$$E_0^e \leqq E_0^V \leqq E_0, \quad E_1^e \leqq E_1^V \leqq E_1.$$

This means that for the ground and 1st excited state, S.V.M. gives better results than our eq. (9). But for the higher excited state there is no inequality, $E_n^{\mathrm{e}} \leqq E_n^{\mathrm{v}}$. In these cases our method should give better results than S.V.M. The numerical results summarized in table 1 show that this is actually the case, although numerically the difference is small. The above comparison with the S.V.M. shows clearly the validity of our method. For the ground state it is always poor, while for the excited state it is in general excellent. In general our method and S.V.M. are complementary in the sense that if we know some general symmetry properties of the systems we can use them for the orthogonality of the trial function and exact state vector; then S.V.M. is better; otherwise, for the general excited state, our method is better.

The author wishes to thank Professor W. Heisenberg for the interest and encouragement in this work, and also Dr. R. M. Ahrens for the kind reading of the manuscript.

References

1) H. P. Dürr, W. Heisenberg, H. Mitter, S. Schlieder and K. Yamazaki, Zeits. f. Naturf. **14** (1959) 441
2) W. Heisenberg, Nachr. d. Gött. Akad. d. Wiss. (1953) p. 111
3) H. J. Kaiser, Thesis, Dresden 1959; Ann. d. Phys. **6** (1960) 131
4) H. Preuss, Zeits. f. Naturf. **13** (1958) 439

1.E.1:
3.A

Nuclear Physics **24** (1961) 318—321 ©*North-Holland Publishing Co., Amsterdam*

Not to be reproduced by photoprint or microfilm without written permission from the publisher

INVESTIGATIONS ON THE DECAY SCHEME OF I^{131} IN THE LOW ENERGY REGION OF GAMMA-RAYS

Gy. MÁTHÉ, T. SCHARBERT and D. BERÉNYI

Institute of Nuclear Research of the Hungarian Academy of Sciences, Debrecen 1, *Pf.* 51, *Hungary*

Received 17 October 1960

Abstract: The region below 364 keV energy of gamma radiation deriving from the decay of I^{131} was examined by scintillation techniques with ordinary as well as with sum-coincidence methods. A new cascade of 156—210 keV (of an intensity of ≈1 % in relation to the cross-over transition) from a level of 364 keV into the ground state was found. Furthermore the existence of the 177 keV line was confirmed by our studies.

1. Introduction

I^{131} is one of the best known artificial radioactive isotopes. The procedure of clarification of its decay scheme is dealt with by Siegbahn's handbook of nuclear spectroscopy in the chapter of illustrative examples [1]). At the same time, the Nuclear Data Sheets [2]) summarizing all the data on the individual isotopes contains also a gamma-ray line with a question mark at 280 keV, and it does

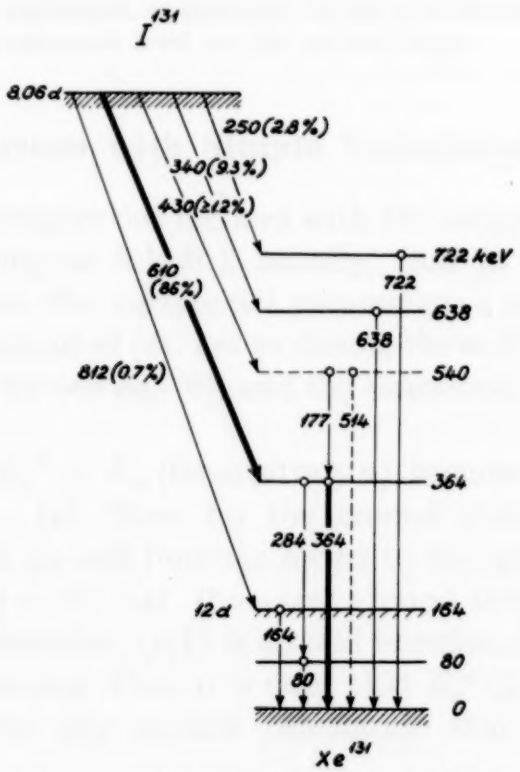

Fig. 1. Decay scheme of I^{131} from the book of Dželepov and Peker.

not represent the 540 keV level of Xe^{131} from which the 177 keV gamma-ray line found also by two authors [3–4]) is supposed to begin. Seaborg and collaborators also omit this level in their recent Table of Isotopes [5]), while the same level is plotted by Dželepov and Peker with dotted line in their book of the decay-scheme of radioactive nuclei [6]). (The decay-scheme reported by them can be seen in fig. 1.)

The ordinary and sum-coincidence [7]) spectra of the gamma-radiations deriving from the decay of I^{131} in the energy region below 364 keV were examined by the authors using scintillation techniques. The applied NaI(Tl) crystals were 3.8 cm by 3.8 cm in size and the multipliers were of RCA 6342 type. The resolution of the analyzing crystal was $\approx$ 7.5 % at the 661 keV γ-ray line of Cs^{137}. The resolving time of the coincidence circuit τ was $\approx 8 \times 10^{-8}$ sec.

2. Results and Discussions

Setting the sum-channel at the 364 keV peak, the sum-coincidence spectrum visible in fig. 2 was obtained. As it is well known, when this sum-coincidence

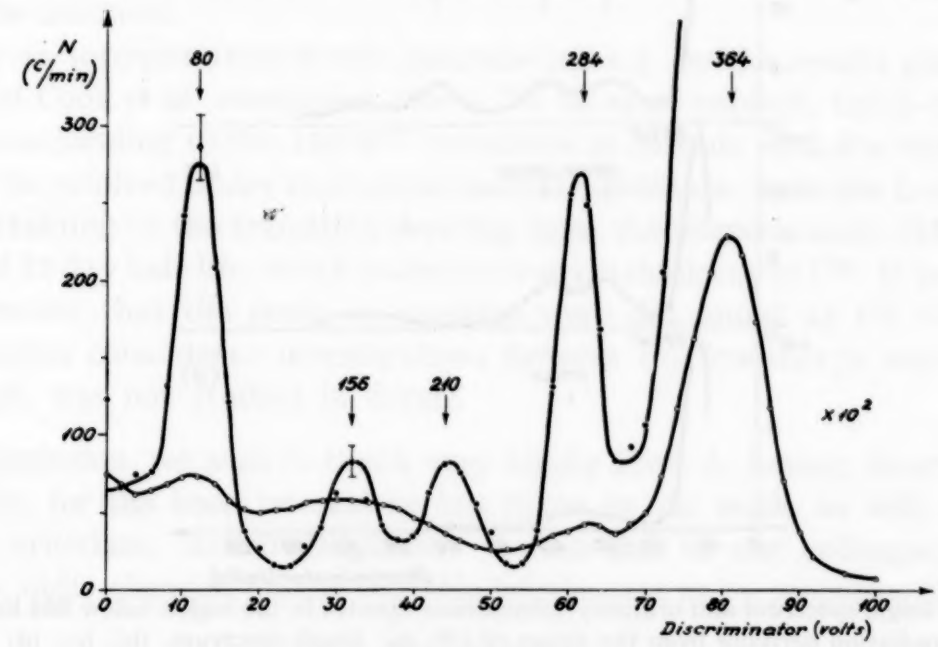

Fig. 2. Sum-coincidence spectrum (black dots) in the region below 364 keV energy of gamma radiation deriving from the decay of I^{131}. Sum-channel at the 364 keV peak. The single spectrum is also shown (open circles)

method [7]) is used, only the peak pairs pertaining to gamma lines in cascade appear in the spectrum, and at these peaks, the areas below the peaks are equal within the limit of error. As can be seen in fig. 2, in addition to the 80 and 284 keV lines, there is another cascade of 156—210 keV with an intensity about five times less than that of the former lines. These new peaks cannot come from the Compton-effect, both because an anti-Compton shield had been placed between the crystals and because such peaks can only appear in the case of

higher-energy lines actually in cascade. These problems in the case of the sum-coincidence method were studied by us in more detail [8]). Thus, the appearence of the peaks in question cannot be caused by an instrumental effect.

The same spectrum, as can be seen in fig. 2, was also obtained in the case of a source prepared from a shipment of I^{131} arriving at a later date, while in the case of identical sources, the ratios of the peaks were also unchanged as a function of the time. Thus, contamination is out of question. It is otherwise sufficiently well excluded also by the sum-coincidence method itself.

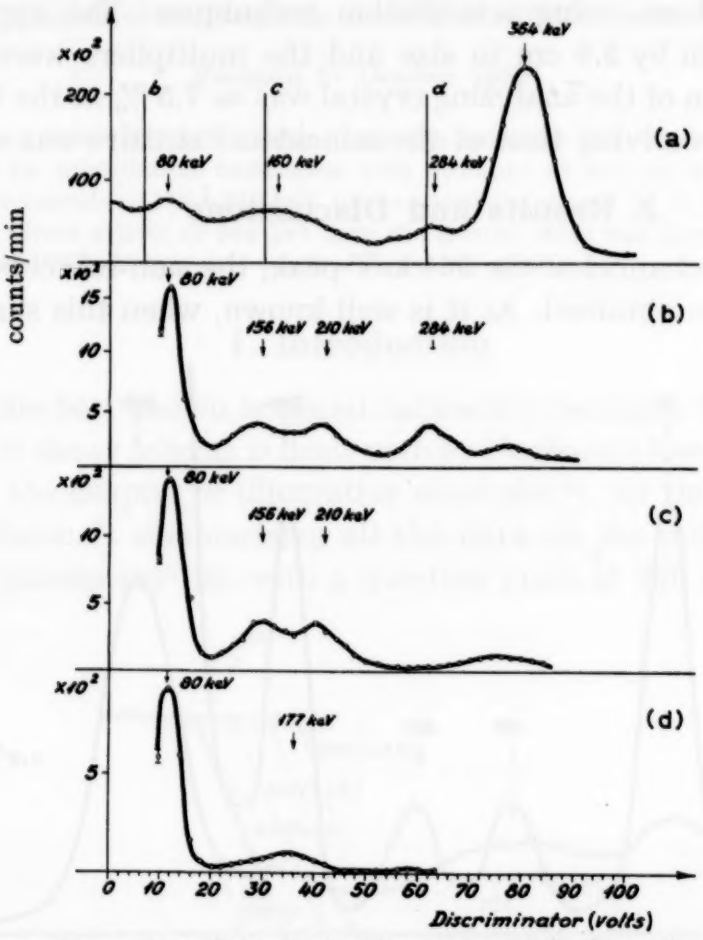

Fig. 3. The single spectrum and ordinary coincidence spectra in the region below 364 keV energy of gamma radiation deriving from the decay of I^{131}. (a) Single spectrum. (b), (c), (d) Ordinary coincidence spectra. The selecting discriminator is integrally set accordingly at points marked b, c, d in fig. 3(a).

The existence of the 156—210 keV gamma-lines in cascade is also proved by the results of ordinary coincidence measurements, which were made in the former energy region of the gamma-radiations of Xe^{131}. These results are shown in figs. 3(b), 3(c) and 3(d). In the first case, the selecting discriminator was integrally set in such a way that the analyzing spectrometer should detect all gamma lines in coincidence (cf. fig. 3(a)). It is seen that in this case, too, the two peaks in the sum-coincidence spectrum are present. The same is true in the case when the selecting channel selects only gamma radiation above 150 keV (fig. 3(c)). If, how-

ever, in the selecting channel, gamma lines above 280 keV are detected, the two peaks in the coincidence spectrum will disappear (fig. (3d)) denoting that the two lines in question only coincide with each other, but are not in cascade with a gamma-radiation of higher energy. In this latter case, however, at 176 keV an additional peak appears, which may be indentified with the 177 keV line reported in refs. [3, 4]). Thus, its presence of the decay of I^{131} is confirmed by our measurements.

The peak appearing in our experiment at 210 keV must be made to correspond to the γ-line found at 208 keV by Cook and collaborators [9]) and designated by a question mark in the Nuclear Data Sheets [2]). Up to now, this line could not be inserted into the decay-scheme. On the basis of our measurements the following may be pointed out. The 364 keV level of Xe^{131} deexcites to the ground state with greatest probability through a direct transition. In parallel with this, a 284—80 keV cascade of greater probability and a 156—210 keV cascade of lesser probability (with an intensity of $\approx 1\,\%$ in relation to the direct transition) also occur. Thus, at 156 or 210 keV, an additional level must be assumed.

Such an interpretation is not contradicted e.g. by the results given in the paper of Cook *et al.* mentioned above. To be more explicit, the L-conversion line corresponding to the 156 keV transition in cascade with the 208 keV line cannot be resolved under their experimental conditions, from the L-conversion line pertaining to the transition deriving from the isomeric state (164 keV) of Xe^{131} of 12 day half-life, which is also involved in the decay of I^{131}. It is probable, furthermore, that the peaks in question were not found up till now in the scintillation coincidence investigations because the low-energy region of the spectrum was not studied in detail.

In conclusion, we wish to thank very kindly Prof. A. Szalay, director of our Institute, for the keen interest he has taken in our work, as well as for his helpful criticizm. Acknowledgement is also due to our colleague, Dr. Cs. Ujhelyi, radio-chemist, for the valuable help he gave us by preparing the source.

References

1) K. Siegbahn, Beta- and Gamma-Ray Spectroscopy (North-Holland Publishing Co., Amsterdam, 1955) p. 696
2) Nuclear Data Sheets, National Academy of Sciences (National Research Council, Washington) NRC 58-6-42 and 58-6-37
3) J. M. Cork, W. C. Rutledge, A. E. Stoddard, C. E. Branyan and W. J. Childe, Phys. Rev. **81** (1951) 482
4) W. G. Smith and J. M. Hollander, Phys. Rev. **101** (1956) 746
5) D. Strominger, J. M. Hollander and G. T. Seaborg, Revs. Mod. Phys. **30** (1958) 707
6) B. S. Dželepov and L. K. Peker, Decay schemes of radioactive nuclei (Academy of Sciences of the USSR, Moscow-Leningrad, 1958)
7) A. M. Hoogenboom, Nuclear Instruments **3** (1958) 57
8) Gy. Máthé, T. Scharbert and D. Berényi, Acta Phys. Hung., to be published
9) D. Moe, G. E. Owen and C. Sharp Cook, Phys. Rev. **75** (1959) 1270

1.E.6

Nuclear Physics **24** (1961) 322—325; © *North-Holland Publishing Co., Amsterdam*

Not to be reproduced by photoprint or microfilm without written permission from the publisher

CONCERNING THE CALCULATION OF THE NUCLEAR MOMENT OF INERTIA

S. T. BELIAEV

I. V. Kurchatov Atomic Energy Institute, USSR Academy of Sciences, Moscow, USSR

Received 27 September 1960

Abstract: Using the generalized method of canonical transformation an expression for the nuclear moment of inertia is found with allowances for nucleon pairing. The result in the main coincides with that obtained earlier by A. Migdal by the Green's function method.

The moment of inertia of deformed nuclei taking account of superfluidity (i.e., Cooper nucleon pairing) was calculated in ref. [1]) in the framework of the adiabatic perturbation theory (cranking model). As was shown by A. B. Migdal with the help of the Green's functions [2]), the cranking-model procedure is insufficient, since the rotation changes the Cooper pairs themselves, which leads to an additional term in the moment of inertia. In the present note it will be shown that the consistent application of the canonical transformation method leads to the same results.

Nucleons in a deformed self-consistent field are described by the Hamiltonian

$$H = \sum_{\nu_1} (\varepsilon_{\nu_1} - \lambda) a_{\nu_1}{}^{\dagger} a_{\nu_1} - \tfrac{1}{2} \sum \langle 12|C|2'1' \rangle a_1{}^{\dagger} a_2{}^{\dagger} a_{2'} a_{1'}, \qquad (1)$$

where $a_{\nu_1}{}^{\dagger}(a_{\nu_1})$ are the creation (annihilation) operator of a nucleon in the state $\nu_1 \equiv 1$; $\varepsilon_{\nu_1} \equiv \varepsilon_1$ is the energy of this single-particle state and λ is the chemical potential of the system.

Nucleon pairing can be treated by means of the canonical transformation to the quasi-particles

$$a_\nu = u_\nu \alpha_\nu + v_\nu \alpha_{\tilde{\nu}}{}^{\dagger}, \quad \text{that is} \quad \alpha_\nu = u_\nu a_\nu - v_\nu a_{\tilde{\nu}}{}^{\dagger}, \qquad (2)$$

where $\tilde{\nu}$ denotes the state corresponding to the time reversal of state ν (and having the same energy †) and the transformation coefficients satisfy the conditions

$$u_{\tilde{\nu}} = u_\nu, \quad v_{\tilde{\nu}} = -v_\nu, \quad u_\nu{}^2 + v_\nu{}^2 = 1, \qquad (3)$$

and are selected under the requirement that the terms with $\alpha\alpha$ and $\alpha^{\dagger}\alpha^{\dagger}$ in the Hamiltonian should vanish after transformation. This requirement is known

† If $|\nu\rangle = |nljm\rangle$, then $|\tilde{\nu}\rangle = (-1)^{j+m}|nlj-m\rangle$.

to be equivalent to the minimization of the quasi-particle vacuum state (determined as $\alpha\Psi_0 = 0$)

$$\Psi_0 = \prod_{|\nu|} (u_\nu + v_\nu \overbrace{a_\nu^\dagger a_{\tilde{\nu}}^\dagger}) |0\rangle. \tag{4}$$

The calculation of average values with the function (4) is equivalent to the independent averaging of pairs of operators such as †

$$\langle a_1^\dagger a_2^\dagger a_{2'} a_{1'}\rangle = \langle a_1^\dagger a_{1'}\rangle_0 \langle a_2^\dagger a_{2'}\rangle_0 - \langle a_1^\dagger a_{2'}\rangle_0 \langle a_2^\dagger a_{1'}\rangle_0 + \langle a_1^\dagger a_2^\dagger\rangle_0 \langle a_{2'} a_{1'}\rangle_0. \tag{5}$$

Only the "diagonal" expressions differ from zero,

$$\langle a_1^\dagger a_1\rangle_0 = v_1^2, \quad \langle a_1^\dagger a_{\tilde{1}}^\dagger\rangle_0 = \langle a_{\tilde{1}} a_1\rangle_0 = u_1 v_1. \tag{(6)}$$

To obtain the moment of inertia, we shall search for the lowest state of the system with a fixed average value of the angular momentum about the axis of rotation X. For this purpose we shall add the following term to the Hamiltonian

$$H_\omega = -\omega \hat{J}_x = -\omega \sum_{1,2} \langle 1|j_x|2\rangle a_1^\dagger a_2 \tag{7}$$

and determine the Lagrangian factor ω from the condition $\hat{J}_x = J_x$.

When the term H_ω is added to the Hamiltonian the prohibition for the production of quasi particle pairs $\alpha^\dagger\alpha^\dagger$ is violated and cannot be restored by simple change of coefficients of u_ν and v_ν in eq. (2). In order to eliminate the terms $\alpha\alpha$ and $\alpha^\dagger\alpha^\dagger$ in the total Hamiltonian $H' = H + H_\omega$ we shall perform an additional canonical transformation of a more general type [3])

$$\alpha_\nu \to \alpha_\nu(\omega) + \sum_{\nu'} f_{\nu\nu'} \alpha_{\tilde{\nu}}^\dagger(\omega). \tag{8}$$

The coefficients $f_{\nu\nu'}$ involve the rotational term H_ω ($f_{\nu\nu'} \approx \omega$). These coefficients can be assumed to be small and considered only in the first non-vanishing order. From the conditions of the canonical nature of transformation (8) and from the symmetry in the sign of ω it follows that

$$f_{\nu\nu'} + f_{\tilde{\nu}'\tilde{\nu}} = 0, \quad f_{\nu\nu} = 0. \tag{9}$$

For new quasi-particles $\alpha_\nu(\omega)$ (corrected for rotation) the vacuum state differs from (4) and, as follows from (8) is of the form

$$\begin{aligned} \Psi_\omega &= \exp\{\tfrac{1}{2} \sum_{\nu\nu'} f_{\nu\nu'} \alpha_\nu^\dagger \alpha_{\tilde{\nu}'}^\dagger\} \Psi_0 \\ &= \exp\{\tfrac{1}{2} \sum_{\nu\nu'} f_{\nu\nu'} (u_\nu a_\nu^\dagger - v_\nu a_{\tilde{\nu}}) (u_{\nu'} a_{\tilde{\nu}'}^\dagger + v_{\nu'} a_{\nu'})\} \Psi_0. \end{aligned} \tag{10}$$

It will be noted that the function (10) is not normalized,

$$(\Psi_\omega, \Psi_\omega) = \exp\,(\tfrac{1}{2} \sum_{\nu\nu'} |f_{\nu\nu'}|^2).$$

† Eq. (5) shows that the canonical transformation method is equivalent to the generalized Hartree-Fock method [3]).

To determine the coefficients $f_{\nu\nu'}$, let us demand the minimum of the average value of the total Hamiltonian H' in the state (10). For averages calculated with the function (10) the relation (5) still holds, but apart from the diagonal quantities

$$\begin{aligned}\langle a_1^\dagger a_1\rangle &= v_1^2+(u_1^2-v_1^2)\sum_2|f_{12}|^2,\\ \langle a_1^\dagger a_{\tilde 1}^\dagger\rangle &= \langle a_{\tilde 1}a_1\rangle = u_1v_1-2u_1v_1\sum_2|f_{12}|^2,\end{aligned}\tag{11}$$

the non-diagonal expressions also differ from zero,

$$\begin{aligned}\langle a_1^\dagger a_2\rangle &= (u_1v_2-v_1u_2)f_{12}^*,\\ \langle a_1 a_{\tilde 2}^\dagger\rangle &= \langle a_{\tilde 2}a_1\rangle^* = (u_1u_2+v_1v_2)f_{12}^*.\end{aligned}\tag{12}$$

In (11) and (12) we took account of the relation

$$f_{12}^*+f_{21}=0,\tag{13}$$

which can be confirmed by direct calculation.

Calculating the average values of H and H_ω with the help of (11) and (12) we shall obtain

$$\begin{aligned}\langle H\rangle &= W_0+\tfrac12\sum_{12}(E_1+E_2)|f_{12}|^2\\ &-\tfrac12\sum\langle 1\tilde 2|G|\tilde 2'1'\rangle(u_1u_2+v_1v_2)(u_{1'}u_{2'}+v_{1'}v_{2'})f_{12}^*f_{1'2'}\\ &+\tfrac12\sum(\langle 1\tilde 1'|G|\tilde 2'2\rangle-\langle 1\tilde 1'|G|2\tilde 2'\rangle)(u_1v_2-v_1u_2)(u_{1'}v_{2'}-v_{1'}u_{2'})f_{12}^*f_{1'2'},\end{aligned}\tag{14}$$

$$\langle H_\omega\rangle = -\omega\langle\hat J_x\rangle = -\omega\sum\langle 1|j_x|2\rangle(u_1v_2-v_1u_2)f_{12}^*,\tag{15}$$

where W_0 is the term which does not contain $f_{\nu\nu'}$ and E is the energy of quasi-particles

$$\begin{aligned}E_1 &= \sqrt{(\tilde\varepsilon_1-\lambda)^2+\Delta_1^2},\\ \tilde\varepsilon_1 &= \varepsilon_1-\sum_2(\langle 12|G|21\rangle-\langle 12|G|12\rangle)v_2^2,\quad \Delta_1=\sum_2\langle 1\tilde 1|G|\tilde 22\rangle u_2v_2.\end{aligned}\tag{16}$$

The quantity Δ (a gap in a quasi-particle spectrum) describes particle pairing. The parameters u and v can be expressed through Δ:

$$u_1^2=\tfrac12\left(1+\frac{\tilde\varepsilon_1-\lambda}{E_1}\right),\quad v_1^2=\tfrac12\left(1-\frac{\tilde\varepsilon_1-\lambda}{E_1}\right).$$

Varying $\langle H\rangle+\langle H_\omega\rangle$ with respect to f_{12}^* (with allowances for (9) and (13)) we shall obtain the integral equation for determining f_{12}

$$\begin{aligned}&(E_1+E_2)f_{12}-\sum_{1'2'}\langle 1\tilde 2|G|\tilde 2'1'\rangle(u_1u_2+v_1v_2)(u_{1'}u_{2'}+v_{1'}v_{2'})f_{1'2'}\\ &\quad+\sum_{1'2'}(\langle 1\tilde 1'|G|\tilde 2'2\rangle-\langle 1\tilde 1'|G|2\tilde 2'\rangle)(u_1v_2-v_1u_2)(u_{1'}v_{2'}-v_{1'}u_{2'})f_{1'2'}\\ &\quad=\omega(u_1v_2-v_1u_2)\langle 1|j_x|2\rangle.\end{aligned}\tag{17}$$

Using (17), eq. (14) can be written as

$$\langle H\rangle = W_0+\tfrac{1}{2}\omega^2 \sum (u_1v_2-v_1u_2)\langle 1|j_x|2\rangle f^*_{12}/\omega, \tag{18}$$

or, after eliminating ω with the help of (15), we obtain

$$\langle H\rangle = W_0+J_x^2/2\mathscr{I},$$

where the moment of inertia $\mathscr{I}$ is determined by the expression

$$\mathscr{I} = \sum_{12} \langle 2|j_x|1\rangle (u_1v_2-v_1u_2) f_{12}/\omega. \tag{19}$$

It is convenient to represent $\mathscr{I}$ as a sum of separate terms. From (17) and (19) we find

$$\mathscr{I}=\mathscr{I}^{(1)}+\mathscr{I}^{(2)}+\mathscr{I}^{(3)}, \quad \mathscr{I}^{(1)} = \sum_{12} \frac{|\langle 1|j_x|2\rangle|^2}{E_1+E_2}\,(u_1v_2-v_1u_2)^2, \tag{20}$$

$$\mathscr{I}^{(2)} = \sum_{121'2'} \frac{\langle 2|j_x|1\rangle}{E_1+E_2}\,\langle 1\tilde{2}|G|\tilde{2}'1'\rangle (u_1v_2-v_1u_2)(u_1u_2+v_1v_2)(u_{1'}u_{2'}+v_{1'}v_{2'})f_{1'2'}/\omega, \tag{21}$$

$$\mathscr{I}^{(3)} = -\sum_{121'2'} \frac{\langle 2|j_x|1\rangle}{E_1+E_2}\,(\langle 1\tilde{1}'|G|\tilde{2}'2\rangle-\langle 1\tilde{1}'|G|2\tilde{2}'\rangle) \times (u_1v_2-v_1u_2)^2(u_{1'}v_{2'}-v_{1'}u_{2'})f_{1'2'}/\omega, \tag{22}$$

where the quantity $f_{\nu\nu'}$ is defined as the solution of eq. (17).

The Cranking model gives only the first term $\mathscr{I}^{(1)}$ †. This method is equivalent to taking account of only the diagonal corrections to average values (11), which naturally can be done without transcending the framework of the transformation (2). The non-diagonal average values (12) give rise to additional terms. The term $\mathscr{I}^{(2)}$ (coinciding with that found in ref. [2])) takes account of the effect of rotation on pairing. The additional term $\mathscr{I}^{(3)}$ describes the change of a self-consistent nucleon field in rotation. If there is no pairing ($\Delta = 0$), the term $\mathscr{I}^{(1)}$ is equal to the rigid-body value of the moment of inertia, decreases with the increasing Δ and vanishes as $\Delta \to \infty$ ††. The term $\mathscr{I}^{(2)}$ vanishes at $\Delta = 0$ and approaches the hydrodynamical value for irrotational flow at $\Delta \to \infty$ [2]). The term $\mathscr{I}^{(3)}$ introduces a correction to $\mathscr{I}^{(1)}$ of the order of $A^{-\frac{1}{3}}$, but it may become more important for the nuclei with small deformation.

† See ref. [1]). The difference in the factor 2 is due to the independent summation over the states ν and $\tilde{\nu}$ in eq. (20).

†† The limit $\Delta \to \infty$ means, in fact, the condition $\hbar\omega \ll \Delta \ll \varepsilon_F$ where $\hbar\omega$ is the distance between different shells and ε_F the Fermi energy.

References

1) S. T. Beliaev, Mat. Fys. Medd. Dan. Vid. Selsk. **31**, No. 11 (1959)
2) A. B. Migdal, JETP **37** (1959) 249; Nuclear Physics **13** (1959) 655
3) N. N. Bogolyubov, Uspekhi Fiz. Mat. Nauk **67** (1959) 549

1.D.1

Nuclear Physics **24** (1961) 326—333; © *North-Holland Publishing Co., Amsterdam*

Not to be reproduced by photoprint or microfilm without written permission from the publisher

NUCLEAR INTERACTIONS IN THE SHELL MODEL

S. P. PANDYA and S. K. SHAH

Physical Research Laboratory, Ahmedabad 9, India †

Received 24 November 1960

Abstract: A central two-body interaction that fits the energy levels of the $(d_{\frac{3}{2}})(d_{\frac{3}{2}})$ and $(d_{\frac{3}{2}})(d_{\frac{3}{2}})^{-1}$ configurations observed in K^{38} and Cl^{36} is deduced. It is shown that this does not explain the very small splittings of the $s_{\frac{1}{2}}$-particle doublets in P^{30}, P^{32} etc.

1. Introduction

During the last decade the nuclear shell model has enjoyed many remarkable successes. In recent years the work of Brueckner and others has also provided it with a strong qualitative justification for many of its basic assumptions. However, even the phenomenology of the shell model can hardly be regarded as being in a satisfactory state yet. For example, the independent particle wavefunctions are in all calculations approximated by the harmonic oscillator wavefunctions for obvious reasons of simplicity, and we have no rigorous estimate of how far the quantitative results would change if some other type of independent particle wavefunctions were to be used for the calculations. Again our knowledge of the effective perturbation interaction introduced to split up the degeneracy of many states of the same configuration is hardly satisfactory. Different authors have chosen different interactions for calculations for various groups of nuclei. The interactions chosen are almost always velocity-independent, central, and smooth (no hard-cores or singularities) two-body forces, with several arbitrary parameters. The only justification for a given choice of parameters is generally that it fits the problem in hand adequately.

For p-shell nuclei, Rosenfeld or Inglis interaction appears to give quite good results. Bilaniuk and French [1]) have shown however that these interactions cannot explain the observed very small s-particle doublet splittings in light nuclei. Moreover an analysis of the experimental data on deuteron stripping reactions on Calcium isotopes led French and Raz [2]) to pronounce the Rosenfeld interaction as inadequate for explaining these data. On the other hand recently Komoda [3]) has found the Rosenfeld interaction to be quite satisfactory for explaining the pairing energies and the magnetic moments of Ca isotopes.

Thieberger [4]) has determined the parameters of the central two-body

† Work supported by the Department of Atomic Energy, India and M. S. University of Baroda, Baroda.

interaction H_{12} from study of the ground state binding energies of a large number of nuclei, $A = 12$–60. While the justification for the use of pure spherical jj coupling wavefunctions for all such nuclei is itself in some doubt, it is also clear that the procedure adopted gives an average interaction, wiping out the configuration-dependence of H_{12} if any exists, and the results perhaps show only the insensitivity of the binding energy calculations to the choice of the wavefunctions and H_{12}. Arima [5]) has made similar calculations for the $2s_{\frac{1}{2}}$ and $1d_{\frac{3}{2}}$ shells, also with satisfactory results, and has derived the parameters of the two-body interaction consisting of central, tensor and spin-orbit forces. While Thieberger obtains a Serber-type two-body interaction, Arima does not.

Although very little is known of the three-body or many-body effective interactions in nuclei, it seems that they may conveniently be ignored for the purpose of the shell model calculations [6]). However, regarding the importance of the role of velocity-dependence of the interactions or of non-central spin-dependent forces, our knowledge is far from satisfactory. It is not unreasonable to expect that such residual effective nuclear interactions in the shell model may be configuration dependent. Of this aspect too there exists no systematic investigation.

In this paper we make an attempt to derive somewhat differently information on the nature of the effective two-body nuclear interaction (assumed central and velocity-independent) operative in the region of nuclei with $A = 30$–40. Our emphasis is on relative separations of the whole group of energy levels of the given configurations, since the interaction is primarily introduced to explain these. The energy levels of the odd nuclei in the $d_{\frac{3}{2}}$ shell are first analysed in section 2 with the help of some of the hole-particle theorems established earlier by one of the authors [7]). This provides us with a simple central interaction which correctly accounts for the splitting of the energy levels of the $(d_{\frac{3}{2}})^2$ configuration. It is well known that the states of a neutron-proton configuration $(s_{\frac{1}{2}})(l_j)$ form a close doublet, such as observed in nuclei Al^{28}, P^{30}, P^{32}, etc. Since the splitting of these doublet states depends only upon the strength of the spin-dependent part of the neutron-proton interaction, an analysis of such splittings would provide us with information on the spin-dependence of the effective nuclear forces. This is next done in section 3, and in section 4 the results thus obtained are compared with the results obtained in section 2.

2. Odd Nuclei in the $d_{\frac{3}{2}}$ Shell

In this section we shall analyse the low-lying energy levels of the odd nuclei Cl^{34}, Cl^{36} and K^{38}, which may be described in the jj coupling scheme in terms of the configurations $(d_{\frac{3}{2}})$ $(d_{\frac{3}{2}})$, $(d_{\frac{3}{2}})(d_{\frac{3}{2}})^{-1}$ and $(d_{\frac{3}{2}})^{-1}$ $(d_{\frac{3}{2}})^{-1}$ respectively. We shall assume also harmonic oscillator type radial dependence of the particle wavefunctions. A brief remark was made regarding the level schemes of Cl^{34}

and Cl^{36} by one of the authors earlier [7]). Now we shall discuss these nuclei in somewhat more detail in view of the additional available experimental data.

The known levels of Cl^{34} are $J = 0^+$ (ground state), 3^+ (0.145 MeV), and levels of unknown spin-parity at 1.1 MeV, 1.9 MeV, 2.7 MeV and above [8]). The earlier analysis [7]) predicted the identification of the 1.1 and 1.9 MeV levels with the 1^+ and 2^+ levels of the $(d_{\frac{3}{2}})(d_{\frac{3}{2}})$ configuration, unless there remains an undiscovered level in Cl^{34} below 2.5 MeV. If the jj coupling scheme were exactly valid in these nuclei, we would expect the level schemes of Cl^{34} and K^{38} to be identical. However, the energy levels known in K^{38} are 3^+ (ground state), 0^+ (0.123 MeV) and a level of unknown spin-parity (but very probably $T = 0$) at 0.44 MeV [9]). It is generally agreed that the jj coupling scheme has a better validity near the end of the subshell than at the beginning, the excellent validity of the jj coupling has been demonstrated for the low levels of Cl^{38} and K^{40}, and whereas the level spectrum of S^{33} (or Cl^{33}) shows many low levels (three levels below 2.5 MeV), no level below 2.5 MeV is seen in K^{39}. These considerations suggest that the energy levels of the $(d_{\frac{3}{2}})(d_{\frac{3}{2}})$ configuration are seen to a better approximation in K^{38} rather than in Cl^{34}. Although $J = 2^+$ level is not seen here, the $0^+ - 2^+$ separation can be taken as 2.15 MeV in view of the observed 2^+ state in A^{38} at this excitation energy. Finally, the observed $T = 0$ level at 0.44 MeV in K^{38} may be identified as remaining $J = 1^+$ level of the $(d_{\frac{3}{2}})(d_{\frac{3}{2}})$ configuration.

We now apply eq. (1) of ref. [7]) to evaluate the energy levels of the configuration $(d_{\frac{3}{2}})(d_{\frac{3}{2}})^{-1}$ expected to be seen in Cl^{36}. The result gives $J = 2^+$ (ground state), 3^+ (0.93 MeV), 1^+ (1.47 MeV) and 0^+ (4.23 MeV). The experimental data on Cl^{36} have been discussed by Segel [10]) and Endt and Braams [8]). Allowing for the configuration mixing effects (i.e. departure from exact jj coupling) which may displace the pure configuration states by ≈ 0.1 MeV, it is easy to identify the calculated states $J = 2^+$, 3^+ and 1^+ with the observed ground state, 0.79 MeV, and 1.60 MeV states. The remaining $J = 0$ state is quite high and is difficult to identify. The results of the earlier analysis and the assignments of Endt and Braams are in agreement with these results. Further explicit measurements of spins and parities in these nuclei will enable us to refine the analysis and also estimate the amount of departure from strict jj coupling scheme.

The result of the above arguments is that we have been able to interpret the experimental data to obtain the relative energy splittings of the levels of the neutron-proton configurations $(d_{\frac{3}{2}})(d_{\frac{3}{2}})$ and $(d_{\frac{3}{2}})(d_{\frac{3}{2}})^{-1}$ with errors of at most $\approx 10\ \%$.

We write the two-body neutron-proton interaction as

$$H_{12} = [A_0 + A_1 M + A_2 B + A_3 MB] J(r_{12}), \tag{1}$$

where M, B are the space- and spin-exchange operators, and A_k are the constants. The function $J(r_{12})$ is for convenience chosen to be of the Gaussian type,

$$J(r_{12}) = \exp[-(|\mathbf{r}_1 - \mathbf{r}_2|/r_0)^2]. \tag{2}$$

For the configuration of equivalent nucleons $(d_{\frac{3}{2}})(d_{\frac{3}{2}})$ we have in the states $J = 0, 2, MB = -1$ and in the states $J = 1, 3, MB = +1$. This enables us to write the interactions for these states in a simpler form:

$$H_{12} = (a_{\pm} + b_{\pm}\boldsymbol{\sigma}_1 \cdot \boldsymbol{\sigma}_2)J(r_{12}) \quad \text{for} \quad MB = \mp 1, \tag{3}$$

$$a_{\pm} = A_0 \mp A_3 + \tfrac{1}{2}(A_2 \mp A_1), \qquad b_{\pm} = \tfrac{1}{2}(A_2 \mp A_1). \tag{4}$$

Matrix elements of H_{12} can be easily evaluated for various states, and we write the energy of a state with spin J as

$$E_J = a_{\pm} E_J^{(a)} + b_{\pm} E_J^{(b)}. \tag{5}$$

Table 1 lists the numerical values of $E_J^{(a)}$ and $E_J^{(b)}$ for $\lambda = r_0/r_d = 0.8$, and 1.0 where r_d is the parameter in the radial wavefunction $\exp[-(r/r_d)^2]$.

TABLE 1

The coefficients $E_J^{(a)}$ and $E_J^{(b)}$ for various values of J and λ

	J	0	1	2	3
$\lambda = 0.8$	$E_J^{(a)}$	0.1248	0.0946	0.0645	0.0946
	$E_J^{(b)}$	−0.1372	−0.0477	−0.0274	0.0597
$\lambda = 1.0$	$E_J^{(a)}$	0.1877	0.1542	0.1207	0.1542
	$E_J^{(b)}$	−0.1653	−0.0846	−0.0330	0.0834

It is well known [7, 11]) that there exists a simple relationship between the matrix elements of the Wigner and $\boldsymbol{\sigma}_1 \cdot \boldsymbol{\sigma}_2$ interactions for the states of neutron-proton configurations $(j_1)(j_2)$ and $(j_1)^{-1}(j_2)$, viz.,

$$\begin{aligned} E_J^{(a)}[(j_1)(j_2)] &= -E_J^{(a)}[(j_1)^{-1}(j_2)], \\ E_J^{(b)}[(j_1)(j_2)] &= E_J^{(b)}[(j_1)^{-1}(j_2)]. \end{aligned} \tag{6}$$

Therefore, by comparing the relative separations of the states $J = 0$, 2 and $J = 1$, 3 of the configurations $(d_{\frac{3}{2}})(d_{\frac{3}{2}})$ and $(d_{\frac{3}{2}})(d_{\frac{3}{2}})^{-1}$ deduced earlier, we can at once obtain the values of $a_{\pm}$ and $b_{\pm}$. For example, we obtain from table 1 and eq. (6) for the separations $E_2 - E_0$ in K^{38} and Cl^{36}, and $\lambda = 1.0$,

$$-0.0670 a_+ + 0.1323 b_+ = 2.15 \text{ MeV},$$

and

$$0.0670\, a_+ + 0.1323\, b_+ = -4.23 \text{ MeV}.$$

This gives

$$\begin{aligned} a_+ &= -44.3 \text{ MeV}, \\ b_+ &= -\ 7.9 \text{ MeV}. \end{aligned} \tag{7}$$

Similarly we obtain

$$b_- = -2.6 \text{ MeV}. \tag{8}$$

Unfortunately, one cannot obtain a_- in this fashion, but one can obtain it by evaluating the separation of say $J = 2,3$ and using the above values of a_+ and $b_\pm$. We find

$$a_- = -44.9 \text{ MeV}. \tag{9}$$

Table 2 lists the values of A_0, A_1, A_2 and A_3 thus obtained for $\lambda = 0.8$ and 1.0. The results do not appear to be very sensitive to the range parameter λ.

TABLE 2

The parameters of the two-body central interaction (1) determined from analysis of the $d_{\frac{3}{2}}$-shell are listed in the first two columns, and those determined from analysis of the $(s_{\frac{1}{2}})(l_j)$ doublets are listed in the third and fourth columns for $\lambda = 0.8$ and 1.0

	$\lambda = 0.8$	$\lambda = 1.0$	$\lambda = 0.8$	$\lambda = 1.0$
A_0	−46.9	−39.3		
A_1	+5.4	+5.3		
A_2	−13.6	−10.5	−2.3	−1.5
A_3	−3.6	−3.1	−10.8	−6.8

We have shown that by assuming only the validity of the jj coupling scheme and absence of many-body forces, we can assign with a reasonable certainty spins and parities to many low lying levels of K^{38} (and Cl^{34}) and Cl^{36}, and with the help of the level schemes thus constructed we have decuced a simple two-body interaction which accounts for these. Conversely, one may now say that with the assumption of the interaction (1) with the parameters listed in table 1, and the validity (even approximate) of the jj coupling scheme, one is able to predict the low lying levels of the odd nuclei in the $d_{\frac{3}{2}}$ shell, belonging to the configurations $(d_{\frac{3}{2}})(d_{\frac{3}{2}})$ or $(d_{\frac{3}{2}})(d_{\frac{3}{2}})^{-1}$.

3. The $s_{\frac{1}{2}}$-Particle Doublets

To study the nuclear interactions which produce the observed very small splittings of the $s_{\frac{1}{2}}$-particle doublets in nuclei near $A = 30$, we again assume jj coupling scheme and harmonic oscillator radial wavefunctions. We shall also assume $r_s = r_d$ for the extension parameters of the radial wavefunctions. The wavefunction of a state of spin J obtained from coupling of an $s_{\frac{1}{2}}$ proton to an l_j neutron shall be written in the obvious notation $\langle s\frac{1}{2} \times lj : JM|$, where the $\times$ denotes the vector coupling. The technique of evaluating the matrix elements of a two-body interaction operator (1) for such states is well known, but we shall briefly sketch a derivation here, as it will be of use in our subsequent calculations involving non-central spin-dependent forces. The above wavefunction can

be transformed to the L–S coupling form as

$$\langle s\tfrac{1}{2}\times lj : JM| = \sum_{S=0,1} [(2j+1)(2S+1)]^{\frac{1}{2}} W(\tfrac{1}{2}jSl; J\tfrac{1}{2})\langle (0l)l\times(\tfrac{1}{2}\tfrac{1}{2})S : JM|, \quad (10)$$

where $W(abcd; ef)$ is the Racah coefficient.

The two-body interaction (1) is now written as

$$H_{12} = [a+bM+\alpha\boldsymbol{\sigma}_1\cdot\boldsymbol{\sigma}_2+\beta\boldsymbol{\sigma}_1\cdot\boldsymbol{\sigma}_2 M]J(r_{12}), \quad (11)$$

with

$$\begin{aligned} a &= A_0+\tfrac{1}{2}A_2, \qquad \alpha = \tfrac{1}{2}A_2, \\ b &= A_1+\tfrac{1}{2}A_3, \qquad \beta = \tfrac{1}{2}A_3. \end{aligned} \quad (12)$$

As is well known the matrix elements of the first two terms of (11) give J-independent (but l-dependent) contributions to the energy of the state, viz.,

$$E_J^{(0)} = aF^{(0)}(0l0l)+bF^{(l)}(0ll0)/(2l+1), \quad (13)$$

where $F^{(0)}$ and $F^{(l)}$ are the radial direct and exchange integrals. The matrix elements of the spin-dependent terms can also be written down at once as

$$E_J^{(1)} = [\alpha F^{(0)}(0l0l)+\beta F^{(l)}(0ll0)/(2l+1)]\tfrac{3}{2}(-1)^{l+J+1}(2j+1) \times W(\tfrac{1}{2}j\tfrac{1}{2}j; l1)W(\tfrac{1}{2}j\tfrac{1}{2}j; J1). \quad (14)$$

Hence the knowledge of the splitting of the doublet immediately gives us the value of $[\alpha F^{(0)}+\beta F^{(l)}/(2l+1)]$.

We shall now apply these results to the doublets $(s_{\frac{1}{2}})(s_{\frac{1}{2}})$, $(s_{\frac{1}{2}})(d_{\frac{5}{2}})$ (see footnote †) and $(s_{\frac{1}{2}})(d_{\frac{3}{2}})$ which one may expect to see as ground states in P^{30}, Al^{28} and P^{32} respectively, and also as excited states in some of these or other nuclei. A result that follows directly from eq. (14) is

$$\Delta(s_{\frac{1}{2}}\times d_{\frac{5}{2}}) = \tfrac{3}{2}\Delta(s_{\frac{1}{2}}\times d_{\frac{3}{2}}), \quad (15)$$

where Δ denotes the doublet splittings E_2-E_3 and E_2-E_1 for the two cases. The experimental results show however, $\Delta(s_{\frac{1}{2}}\times d_{\frac{5}{2}}) = 0.031$ MeV and $\Delta(s_{\frac{1}{2}}\times d_{\frac{3}{2}}) = 0.077$ MeV from Al^{28} and P^{32} ground state doublets. Our conclusions should therefore be tempered by the knowledge that the jj coupling assumption may not be valid even for the ground states of these nuclei. We shall later remark generally on these other discrepancies we shall observe ††.

In P^{30} the ground and the first excited state at 0.685 MeV are easily interpreted as the $J = 1, 0$ states of the $(s_{\frac{1}{2}})(s_{\frac{1}{2}})$ doublet. These data, combined with

† Note that for jj coupling $\Delta(d_{\frac{5}{2}}\times s_{\frac{1}{2}}) \equiv \Delta(d_{\frac{5}{2}}{}^{-1}\times s_{\frac{1}{2}})$.

†† Recently excited states in Si^{28} have been observed [12]) corresponding to the ground state doublet of Al^{28}. In this case the observed splitting is $\Delta = 0.065$ MeV which would improve the agreement substantially. One may easily argue that the spherical jj coupling shell model has a better validity in Si^{28} rather than in Al^{28}.

the doublet splitting in P^{32} and eq. (14), give

$$\left.\begin{aligned} 0.165(\alpha+\beta) &= -0.685 \\ 0.060\alpha+0.009\beta &= -0.077 \end{aligned}\right\} \lambda = 1.0,$$
$$\left.\begin{aligned} 0.105(\alpha+\beta) &= -0.685 \\ 0.035\alpha+0.007\beta &= -0.077 \end{aligned}\right\} \lambda = 0.8. \qquad (16)$$

The values of A_2 and A_3 derived from these equations are given in table 2.

Unfortunately not enough is known of the spins and parities of the excited states of P^{30} and P^{32} to enable us to identify more such $s_{\frac{1}{2}}$-particle doublets. When additional information of several doublets in the same nucleus is available, it would be possible to evaluate more precisely not only the spin-dependent but also the spin-independent part of the two-body interaction.

4. Discussion

It is clear that there exists a very real discrepancy between the parameters of the spin-dependent part of the central two-body interaction determined from the $(s_{\frac{1}{2}})(l_j)$ doublet splittings and from the splitting of the levels of the $(d_{\frac{3}{2}})(d_{\frac{3}{2}})$ and $(d_{\frac{3}{2}})(d_{\frac{3}{2}})^{-1}$ configurations. That the discrepancy is outside the limits of errors can be seen from the fact that if the spin-dependent interaction obtained from the d-shell analysis is used to evaluate the s-doublet splittings, we obtain $\Delta(s_{\frac{1}{2}}\times s_{\frac{1}{2}}) = 0.93$ and 1.13 MeV, and $\Delta(s_{\frac{1}{2}}\times d_{\frac{3}{2}}) = 0.25$ and 0.32 MeV for $\lambda = 0.8$ and 1.0 respectively. The discrepancy for the $(s_{\frac{1}{2}}\times s_{\frac{1}{2}})$ doublet is not so serious as that for the $(s_{\frac{1}{2}}\times d_{\frac{3}{2}})$ doublet. This perhaps suggests the presence of non-central spin-dependent terms in the two-body interaction. If such terms would displace the energy levels by 0.1–0.2 MeV in the right direction, the discrepancy would be resolved. One may also note that while such small contritions to the energy of the levels by the non-central interactions would be important for $(s_{\frac{1}{2}})(l_j)$ doublets, they would be relatively insignificant for other configurations, and hence their neglect in the $d_{\frac{3}{2}}$-shell may be justified.

Of course, the above discrepancies (including that between the observed and expected splitting of the ground state doublet in Al^{28}) may also be attributed to failure of jj coupling or of the spherical shell model etc. However, our attempt has been to see how far one may succeed in understanding the observed level schemes in a large group of nuclei in terms of simple assumptions for angular momentum coupling and two-body interactions.

In conclusion, we feel that the results presented here show that it is not possible to define a simple unique central two-body interaction which will with the assumption of jj coupling scheme explain the low lying energy levels ascribable to different configurations. Such a simple interaction must either be regarded as configuration-dependent or may have to be modified by introducing additional non-central or velocity-dependent terms.

References

1) O. M. Bilaniuk and J. B. French, Nuclear Physics **17** (1960) 435
2) J. B. French and B. J. Raz, Phys. Rev. **104** (1956) 1411
3) T. Komoda, Prog. Theor. Phys. **24** (1960) 201
4) R. Thieberger, Phys. Rev. **116** (1959) 713
5) A. Arima, Prog. Theor. Phys. **19** (1958) 421
6) S. P. Pandya and J. B. French, Ann. Phys. **2** (1957) 166
7) S. P. Pandya, Phys. Rev. **103** (1956) 956; **108** (1957) 1311
8) P. M. Endt and C. M. Braams, Revs. Mod. Phys. **29** (1957) 683
9) Y. Hashimoto and W. R. Alford, Phys. Rev. **116** (1959) 981
10) R. E. Segel, Phys. Rev. **113** (1959) 844
11) C. Schwartz, Phys. Rev. **94** (1954) 95
12) P. M. Endt and A. Heyligers, Physica **26** (1960) 230;
S. Hinds and R. Middleton, Proc. Phys. Soc. **76** (1960) 545

2.E: 2.L

Nuclear Physics **24** (1961) 334—339; © *North-Holland Publishing Co., Amsterdam*

Not to be reproduced by photoprint or microfim without written permission from the publisher

THE ELASTIC SCATTERING OF 29 MeV He^3 BY Al, V AND Cu

G. W. GREENLEES, J. S. LILLEY, P. C. ROWE

Department of Physics, University of Birmingham

and

P. E. HODGSON

Clarendon Laboratory, Oxford

Received 9 December 1960

Abstract: Absolute differential cross sections are presented for the elastic scattering of 29 MeV He^3 by Al, V and Cu in the angular range 15°–80° (c.m.). The results are fitted by an optical model potential with a Saxon-Woods form factor and no spin orbit term.

1. Introduction

The elastic scattering of medium energy protons and neutrons has been studied extensively in recent years and considerable success has been achieved in the analysis of the data in terms of the optical model [1]). Theoretical justification for the use of such a model in the case of proton and neutron elastic scattering has been given by several authors [2]). More recently, attempts have been made to fit similar results for heavier particles in terms of the optical model. Although the theoretical justification for such a procedure is uncertain, satisfactory fits to the data have been obtained. In particular the elastic scattering of deuterons [3]) alpha particles [4, 5, 6]) and nitrogen ions [7]) have all been analysed in this way. In all cases strong surface absorption of the particles is indicated by the relative insensitivity of the fit to the depth of the central potential provided the surface form is retained. This feature verifies the essential correctness of the semi-classical sharp cut-off model of Blair [8]) which has been used in the analysis of alpha particle elastic scattering results [9]).

A recent paper [10]) presented results on the variation of the elastic scattering of He^3 with both energy and angle which were analysed in terms of the Blair model. A later paper [11]) analysed these results in terms of the optical model. The present paper provides more detailed results for the He^3 elastic differential cross-sections at 29 MeV using Al, V and Cu targets, together with an analysis in terms of the optical model. Similar data for C, Ne and A has recently been obtained by Aguilar *et al.* [12]) and for C, Al, Ti, Ni and Nb by Wegner and Hall [13]).

2. Method and Apparatus

The 29.4 MeV extracted He^3 beam from the Nuffield 152 cm cyclotron passed

through a screening wall and entered a 30.5 cm scattering chamber [14]). This chamber is fitted with a scintillation counter which can be set at any angle between 15° and 165° to the incident beam. The overall angular definition of the scattering was $\pm 1°$ and the counter setting was accurate to 0.2°. The scintillation counter consisted of a 3 mm NaI(Tl) crystal and Dumont 6292 photomultiplier and the pulse height spectra were recorded on a 100-channel pulse-height analyser; the energy resolution was 2–3 %. The targets were in the form of foils and the beam traversing the target was collected in a Faraday cup and integrated.

3. Results

Absolute differential cross-sections for elastic scattering were calculated directly from the observed spectra. Typical spectra at three angles are shown in fig. 1. No particle discrimination was available in the detect orso that all charged

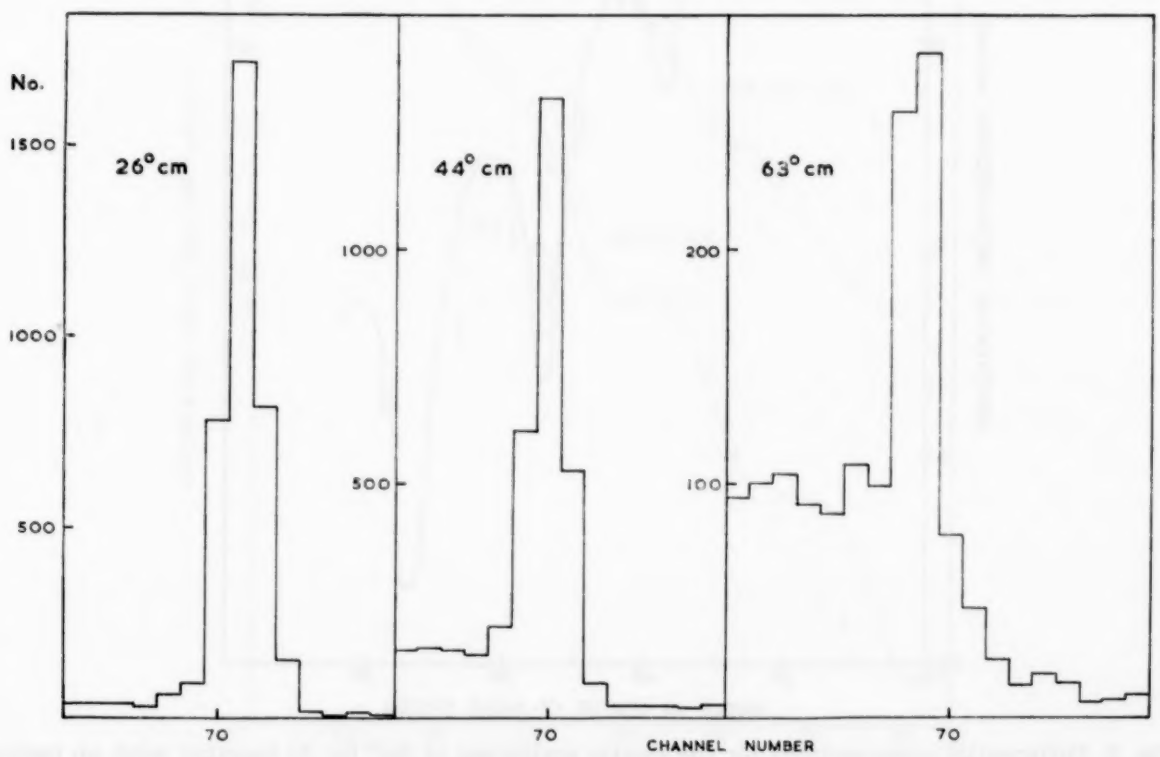

Fig. 1. Typical pulse height spectra obtained using a Cu target and an incident beam of 29.4 MeV He^3 particles.

particles were recorded with equal efficiency. This was immaterial at forward angles ($< 40°$) where the elastic cross-section was the dominant one. At larger angles the He^3 elastic peak was superimposed on a significant background of other charged particles and this together with a contribution from unresolved inelastic groups entailed a correction. The extent of this correction can be seen in the 63° curve of fig. 1. The relative accuracy of the results is estimated at 3 %

in general and the absolute accuracy at 7 %. The differential cross sections obtained with Al, V and Cu are given in figs. 2 and 3.

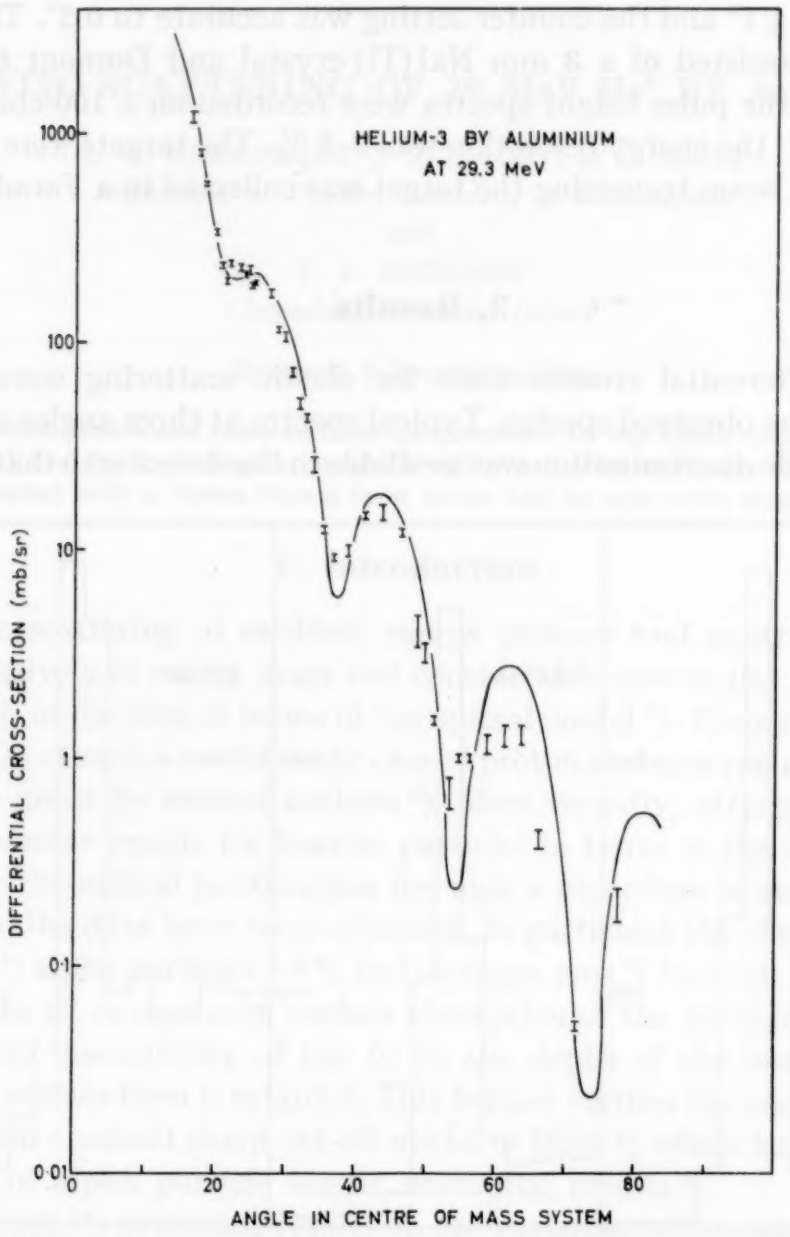

Fig. 2. Differential cross-sections for the elastic scattering of He^3 by Al together with an optica model fit (full line). The mean energy of scattering was 29.3 MeV. The parameters of the optica model curves are given in table 1.

4. Analysis and Discussion

These results were analysed by assuming that the interaction between the He^3 and the target nucleus can be represented by a two body potential of the form

$$V(r) = V_C(r) + (U + iW)f(r),$$

where $V_C(r)$ is the Coulomb potential taken to be that due to a uniformly charged sphere of radius $R_C = 1.3\,A^{\frac{1}{3}}$, the quantities U and W are the refracting and absorbing nuclear potentials and $f(r) = \{1+\exp[(r-R)/a]\}^{-1}$ is the Saxon-Woods radial form factor with nuclear radius $R = r_0 A^{\frac{1}{3}}$ and surface diffuseness a. Spin-orbit forces are not included as their strength is unknown

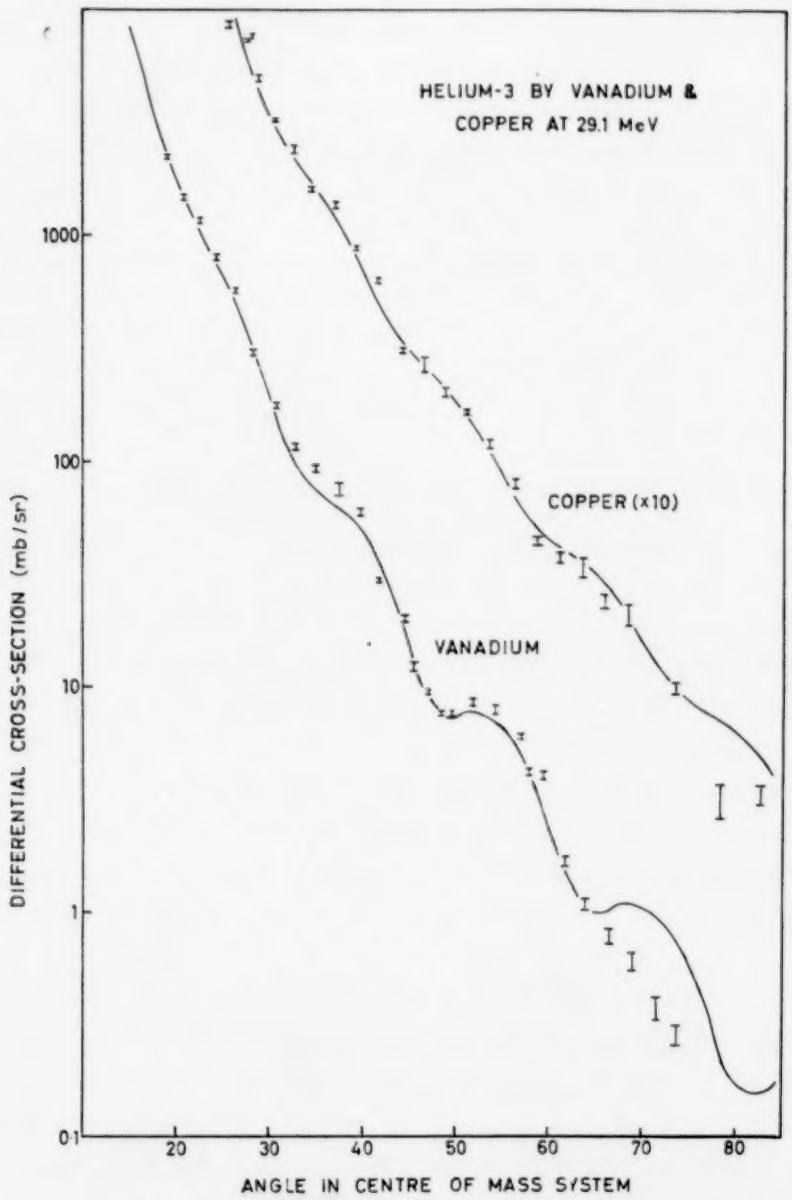

Fig. 3. Differential cross-sections for the elastic scattering of He^3 by V and Cu together with optical model fits (full lines). The mean energy of scattering was 29.1 MeV. The parameters of the optical model curves are given in table 1.

and their effect on the differential cross section is likely to be small. If suitable numerical values are chosen for the potential parameters the corresponding Schrödinger wave equation for the interaction may be solved to give the observable quantities by the methods described elsewhere [15]). All the calculations were carried out on the Oxford University Mercury Computer.

The four parameters U, W, r_0 and a were systematically varied to minimise

$$\Delta_N = \sum_N \left(\frac{(\mathrm{d}\sigma/\mathrm{d}\Omega)_{\mathrm{exp}} - (\mathrm{d}\sigma/\mathrm{d}\Omega)_{\mathrm{theor}}}{\delta(\mathrm{d}\sigma/\mathrm{d}\Omega)_{\mathrm{exp}}} \right)^2 ,$$

where the summation extends over all the N experimental points. As the relative values of the cross-sections are more accurately known than the absolute ones each experimental distribution was normalised to the calculated one by multiplying it by the factor A that minimises Δ. The parameters giving the best fit to the data are given in table 1, and the corresponding differential

TABLE 1

Parameters of the best fit potentials, the calculated reaction cross-sections and the values of Δ_N for the N measured points. The quantity A is the normalisation constant by which the experimental distribution must be multiplied to agree with the theoretical one.

Nucleus	$-U$ (MeV)	$-W$ (MeV)	r_0 (fm)	a (fm)	σ_R (mb)	N	Δ_N	A
Al	45	30	1.57	0.63	1258	40	2623	1.05
V	27	30	1.52	0.72	1521	30	567	0.97
Cu	20	30	1.60	0.73	1739	32	1119	0.91

cross-sections are compared with experiment in figs. 2 and 3. The factors A are consistent with 1.00 ± 0.07, as they should be. For the reasons discussed elsewhere [16]), it is impossible to put firm limits on the best values of the potential parameters while the reaction cross-sections are unknown and the effects of the spin-orbit forces have not been taken into account. It is found, however, that the cross-sections are more sensitive to r_0 and a than to U and W. This is what would be expected as the elastic scattering process is essentially a surface interaction [11]).

We wish to express our thanks to Professors W. E. Burcham, F. R. S. and D. H. Wilkinson, F. R. S. for their continuing interest, to the Cyclotron Scattering Group for help in recording the results, to the Director of the Oxford University Computing Laboratory for the use of the Mercury computer, to Dr. B. Buck and Mr. R. N. Maddison for their work on the computer programme, and to Miss N. Reynolds, Miss S. Tilley and the staff of the Computing Laboratory for their assistance. Two of us (J. S. L. and P. C. R.) acknowledge financial support from the Department of Scientific and Industrial Research.

References

1) Proc. Intern. Conf. on the Nuclear Optical Model, Florida (1959)
2) G. E. Brown, Rev. Mod. Phys. **31** (1959) 893

3) M. Melkanoff, Proc. Intern. Conf. on the Nuclear Optical Model, Florida (1959)
4) G. Igo, Phys. Rev. Letters, **1** (1958) 72
5) G. Igo, and R. M. Thaler, Phys. Rev. **106** (1957) 126
6) W. B. Cheston and A. E. Glassgold, Phys. Rev. **106** (1957) 1215
7) C. E. Porter, Phys. Rev. **112** (1957) 1722
8) J. S. Blair, Phys. Rev. **95** (1954) 1218
9) D. D. Kerlee, J. S. Blair and G. W. Farwell, Phys. Rev. **107** (1957) 1343
10) G. W. Greenlees and P. C. Rowe, Nuclear Physics **15** (1960) 687
11) P. E. Hodgson, Nuclear Physics **21** (1960) 28
12) J. Aguilar, W. E. Burcham, J. B. A. England, A. Garcia, P. E. Hodgson, P. V. March, J. S. C. McKee, E. M. Mosinger and W. T. Toner, Proc. Roy. Soc. A **257** (1960) 13
13) H. E. Wegner and W. S. Hall, Bull. Am. Phys. Soc. **3** (1958) 338
14) G. W. Greenlees, B. C. Haywood, L. G. Kuo and M. Petravic, Proc. Phys. Soc. A **70** (1957) 331
15) B. Buck, R. N. Maddison and P. E. Hodgson, Phil. Mag. **5** (1960) 1181
16) P. E. Hodgson, J. Aguilar, J. B. A. England and A. Garcia, Nuclear Physics **22** (1960) 138

2.A.1

Nuclear Physics **24** (1961) 340—345; © *North-Holland Publishing Co., Amsterdam*

Not to be reproduced by photoprint or microfilm without written permission from the publisher

ACTIVATION CROSS SECTIONS FOR (n, p) REACTIONS IN SOME MEDIUM-WEIGHT NUCLEI WITH D+D NEUTRONS

J. J. VAN LOEF †

Instituto de Física y Matemáticas, Universidad de Chile, Santiago

Received 17 November 1960

Abstract: Activation cross sections for (n, p) reactions with D+D neutrons are reported on $_{26}Fe^{54}$, $_{28}Ni^{61}$ and $_{30}Zn^{67}$ and compared with previously published (n, p) cross sections in $_{26}Fe^{56}$, $_{28}Ni^{58}$ and $_{30}Zn^{64}$. The (n, p) cross sections of the even target nuclei are much greater than those of the odd neutron nuclei; among even nuclei they are highest for 28 closed shell Fe^{54} and Ni^{58}.

1. Introduction

The (n, p) cross section of many nuclei has been measured by different authors with neutrons originating from the H^3(d, n)He^4 reaction [1–4]), whereas cross section data are rather scarce at neutron energies below 12 MeV. At lower neutron energies the (n, p) reaction in most nuclei is suppressed due to either an unfavourable Q value or a too high Coulomb penetration barrier. Furthermore on applying the well-known activation technique to measure the cross section, a reasonable activity can be obtained only in nuclei with a suitable half-life.

The investigation of the (n, p) cross sections at low neutron energies is of some advantage since competing reactions are in general of less importance. As reactions of low order [5]) are not known to occur, the interpretation of these cross sections usually is based on the statistical theory of nuclear reactions [6]). On applying this theory in the analysis of experimental (n, p) and (n, α) cross sections, Bullock and Moore [7]) determined the odd-even dependence of nuclear level density parameters. However, additional experimental data particularly for odd neutron target nuclei are useful in order to complete such an analysis. Furthermore it would be of interest to investigate whether shell effects, observed at 14 MeV [8]), also appear at low neutron energy. Finally, it seems worthwhile to verify whether the (n, p) cross sections decrease with increasing neutron number at constant Z, as observed by Levkovskii [9]) at 14 MeV.

From a practical point of view, the knowledge of (n, p) cross sections with D+D neutrons is important, since according to Wille and Fink [10]), the T+D neutron source can be contaminated appreciably by neutrons originating from

† Private address: De Boschwal, Maarsbergen, Holland

the $H^2(d, n)He^3$ reaction. Thus the determination of activation cross sections at 14 MeV in a number of cases may be complicated by the presence of low energy neutrons. In this paper we report on activation cross sections for (n, p) reactions with D+D neutrons in Fe^{54}, Ni^{61}, and Zn^{67}, and we will compare them with earlier published (n, p) cross sections of Ni^{58} and Zn^{64} [11, 12]).

2. Experimental Procedure and Results

The (n, p) activation cross sections were determined through observation of induced radioactivities according to the method developed by Segré [13]). The activities induced in the samples were detected with a NaI(Tl) scintillation spectrometer. Gamma rays accompanying beta-decay or K capture in the product nucleus were observed.

TABLE 1

Information concerning the reactions studied

Reaction	Abundance (%)	Q value (MeV)	Half-life	Gamma ray (keV)	Branching (%)
$Fe^{54}(n, p)Mn^{54}$	5.8	+0.40	290 days	840	100
$Ni^{58}(n, p)Co^{58}$	67.8	+0.39	71 days	810	99
$Ni^{61}(n, p)Co^{61}$	1.25	−0.51	1.65 hours	71	100
$Zn^{64}(n, p)Cu^{64}$	48.9	+0.20	12.8 hours	annihilation	19
$Zn^{67}(n, p)Cu^{67}$	4.1	+0.20	61 hours	184	43

The nuclei which have been studied in this paper are listed in the first column of table 1. These nuclei were chosen because of suitable Q values of the (n, p) reaction, convenient half-lives of the induced activities, the large fraction of decays which yielded γ-rays, and the availability of samples of high purity. As relatively large amounts of material were required, only naturally-occurring isotopic mixtures were used. The isotopic abundances are given in the second column. The Q values of (n, p) reactions in the different nuclei are based on Nuclear Data Sheets [14]), whereas the half-lives of the induced activities, the principal gamma rays and their branching ratio are given as quoted in the review article by Strominger *et al* [15]). It is interesting to note that the gamma-ray decay schemes of these nuclei are very simple.

The irradiations with D+D neutrons were performed with the 800-keV University of Chile cascade generator, the characteristics of which are described in a previous paper [11]). The energy spread of the neutron beam which the sample intercepted was 200 keV or less and was mainly determined by the target thickness and the finite angle subtended by the sample. During the irradiations the neutron flux was monitored by a conventional BF_3 long counter.

The desired activity was identified both by γ-ray energy and by half-life, and in general no decay other than the expected one was found. In iron however,

a gamma ray of 0.845 MeV with a decay time of 2.6 hours was attributed to Mn^{56} from neutron capture by manganese, which in a small quantity was present. Thus the measurement of the Mn^{54} activity was started two days after the end of the irradiation so that Mn^{56} had decayed completely.

As the activities of the low-abundant isotopes were expected to be low, the gamma rays were measured with a Harshaw NaI(Tl) well-type scintillation counter (crystal size: 4.7 cm in diameter and 5 cm high with a hole of 1.6 cm in diameter and 3.7 cm deep) and a 20-channel pulse-height analyzer (Eldorado Electronics Pa-400). The crystal was shielded with 5 cm of lead in order to obtain the best signal-to-background ratio. The spectrometer was calibrated with Ce^{144}, Fe^{59}, Cs^{137} and Na^{22} standard gamma-ray sources.

The (n, p) cross sections of Fe^{54}, Ni^{61} and Zn^{67} were based on previously measured activation cross sections of the Ni^{58}(n, p)Co^{58} and Zn^{64}(n, p)Cu^{64} reactions, respectively [11, 12]). As the 840 keV gamma ray of Mn^{54} has about the same energy as the principal gamma ray in Co^{58} decay, a comparison was made between the induced radioactivities in iron and nickel. Samples of iron and nickel, 1.5 cm in diameter and 1 cm in height, were irradiated in succession at 600 keV deuteron energy during 24 hours each. From the intensity ratio of the photopeaks of the Mn^{54} and Co^{58} gamma rays of about 1 to 50, the ratio of integrated neutron flux, the difference in number of target nuclei and growth factor, the cross sections of (n, p) reactions in Fe^{54} and Ni^{58} resulted to be the same within 10 %.

The 71 keV gamma ray of Co^{61}, obtained through the (n, p) reaction in Ni^{61}, was measured in irradiated nickel, and compared with the Co^{58} activity which was present in the same sample. By taking into account the isotopic abundance, the growth factor, the counting efficiency, the gamma-ray self absorption and a correction for the X-ray escape peak, the ratio of (n, p) cross sections of Ni^{58} and Ni^{61} was found to be about 60 to 1. The major source of error in the Co^{61} activity came from the determination of the gamma-ray self absorption factor in nickel.

The principal gamma ray of 184 keV belonging to the 61 hour decay of Cu^{67} was masked by the very pronounced backscattering peak at 175 keV due to the annihilation radiation of Cu^{64} with a 12.8 hour half-life. Therefore a search was also made for the partially converted 92 keV gamma ray of the first excited state of Zn^{67}, which appears in the decay of Cu^{67}. Both from the decay constant of the broad maximum at 175 keV and the shape of the pulse-height distribution measured at different time intervals after the end of the irradiation, an estimate was made of the Cu^{67} activity. From this result, an upper limit of 10 % was assigned to the ratio of cross sections of (n, p) reactions in Zn^{67} and Zn^{64}, respectively.

Cross sections of (n, p) reactions in Fe^{54}, Ni^{58} and Zn^{64} at 2.6, 3.3 and 3.6 MeV neutron energy respectively were obtained by simultaneously irradiating samp-

les placed at various positions around the D+D neutron source, whereas (n, p) cross sections of Ni^{61} and Zn^{67} were determined at 3.3 MeV only. In table 2 the measured activation cross sections are given together with their

TABLE 2

Activation cross sections for (n, p) reactions

Target nucleus	Type	σ(n, p) (mb) [a]	Neutron energy (MeV) [b]	Ref.
$_{28}Ni^{61}$	odd neutron	3 ± 1.5	3.3±0.2	
$_{30}Zn^{67}$	odd neutron	<5	3.3±0.2	
$_{26}Fe^{54}$	even	210 ±20	3.6±0.1	
		190 ±20	3.3±0.1	
		150 ±15	2.6±0.2	
$_{28}Ni^{58}$	even	195 ±15	3.6±0.1	[12]
		170 ±20	3.3±0.1	
		175 ±15	2.6±0.2	[12]
$_{30}Zn^{64}$	even	56.5± 4.0	3.6±0.1	[11]
		51.5± 5.0	3.3±0.1	
		26.5± 2.0	2.6±0.2	[11]

[a]) Standard deviations are relative.

[b]) The neutron energy spread at the sample due to target thickness and angular spread.

relative standard deviations. The absolute cross sections are based on the activation cross sections of the Ni^{58}(n, p)Co^{58} and Zn^{64}(n, p)Cu^{64} reactions, which are 195±30 mb and 56.5±9.0 mb respectively at 3.55 MeV neutron energy [11, 12]).

3. Discussion

Two types of target nuclei have been studied in this paper namely $_{even}X^{odd}$ and $_{even}X^{even}$, which through the (n, p) reaction lead to $_{odd}X^{odd}$ and $_{odd}X^{even}$, respectively. The nuclei Ni^{61} and Zn^{67} belong to the first group, and Fe^{54}, Ni^{58} and Zn^{64} to the second. A striking result is that the experimental (n, p) cross sections of the even target nuclei are much greater than those of the odd neutron nuclei for neutrons with energies between 2.6 and 3.6 MeV. Likewise the average (n, p) cross section of S^{32} is by a factor of two to three higher than the corresponding reaction cross section of P^{31} [16]), in spite of strong competition of the (n, α) reaction in S^{32}.

By comparing (n, p) cross sections of even-even nuclei at equivalent neutron energies, reaction cross sections of both Fe^{54} and Ni^{58} are by an order of magnitude greater than those of Zn^{64} and Fe^{56}, the latter reported by Terrell and Holm [17]). This may be due to the influence of shell structure, as Fe^{54} has a 28 closed neutron shell, and Ni^{58} has a 28 closed proton shell. Recently Allan [18]) has shown that (n, p) cross sections at 14 MeV reach maximum values at $Z=20$ and 28 and a minimum value occurs at an intermediate value of Z.

Although the (n, p) reaction is strongly energy dependent, cross sections of different nuclei are comparative as long as the Q value is about the same [18]). As neutron scattering competes with the (n, p) reaction in the first place, the cross section of the latter depends on the relative probability that a proton or a neutron is emitted from the compound nucleus. According to the statistical theory of nuclear reactions [6]), these probabilities depend among other things on the level density of the residual nucleus. On analyzing existing (n, p) and (n, α) cross section data, Bullock and Moore [7]) determined the odd-even dependence of nuclear level density parameters. The results of their study confirm that the effective level densities are highest for an odd nucleus and lowest for an even one. As a consequence, the cross section for (n, p) reactions in even target nuclei should be higher than that in odd neutron nuclei, which is consistent with our findings. However at the relatively low energies of the incoming neutrons, the statistical treatment of the residual nucleus may not be appropriate. In the Ni^{58}(n, p)Co^{58} reaction the excitation of the Co^{58} ground state seems to predominate for neutron energies between 2 and 4 MeV [19]). Likewise primarily ground state protons were measured in the K^{39} (n, p) A^{39} reaction below 3.5 MeV neutron energy [20]).

Levkovskii [9]) observed that (n, p) cross sections at 14 MeV neutron energy depend on the neutron excess in the target nucleus. Similarly in the nuclei we have studied in this paper, (n, p) cross sections are systematically higher for the neutron deficient isotope. According to Lane [21]), the potential for neutrons tends to be deeper in nuclei where the neutron excess is smaller. This might slow down the reemission of neutrons and therefore favour the (n, p) reaction in some cases.

References

1) Colli, Facchini, Iori, Marcazzan and Sona, Nuovo Cim. **13** (1959) 730 (for earlier references, see this paper)
2) K. H. Purser and E. W. Titterton, Australian J. Phys. **12** (1959) 103
3) Kern, Thompson and Ferguson, Nuclear Physics **10** (1959) 226
4) I. L. Preiss and R. W. Fink, Nuclear Physics **15** (1960) 326
5) V. F. Weisskopf, Suppl. Progr. Theor. Phys. **11** (1959) 52
6) J. M. Blatt and V. F. Weisskopf, Theoretical Nuclear Physics (John Wiley and Sons, New York, 1952)
7) R. E. Bullock and R. G. Moore, Jr., Phys. Rev. **119** (1960) 721
8) Eubank, Peck, Jr., and Zatzick, Nuclear Physics **10** (1959) 418 ($Z = 50$); M. R. Zatzick and H. P. Eubank, Bull. Am. Phys. Soc. **4** (1958) 141 ($Z = 20$)
9) V. N. Levkovskii, JETP **4** (1957) 291; **6** (1958) 1174
10) R. G. Wille and R. W. Fink, Phys. Rev. **118** (1959) 242
11) J. Rapaport and J. J. van Loef, Phys. Rev. **114** (1959) 565
12) González, Rapaport and Van Loef, Phys. Rev. **120** (1960) 1319
13) Segré, Greisen, Linenberger and Miskel, Atomic Energy Commission Report MDDC-228, 1946 (unpublished)
14) Nuclear Data Sheets, National Academy of Sciences, National Research Council, Washington, D.C.

15) Strominger, Hollander and Seaborg, Revs. Mod. Phys. **30** (1958) 585
16) D. J. Hughes and R. B. Schwartz, Brookhaven National Laboratory, Report BNL-325, 2nd edition (1959)
17) J. Terrell and D. M. Holm, Phys. Rev. **109** (1958) 2031
18) D. L. Allan, Proc. of the Kingston Conf. (North-Holland Publishing Co., Amsterdam, 1960) p. 838
19) P. A. Moldauer, private communication
20) Haenni, Bass and Bonner, Bull. Am. Phys. Soc. **5** (1960) 248
21) A. M. Lane, as quoted by Schiffer, Lee and Zeidman, Phys. Rev. **115** (1959) 427

8.B

Nuclear Physics **24** (1961) 346—352; © *North-Holland Publishing Co., Amsterdam*

Not to be reproduced by photoprint or microfilm without written permission from the publisher

A REMARK ON THE ISOBARIC SPIN SPACE

Th. A. J. MARIS

Instituto de Física, Universidade do Rio Grande do Sul, Pôrto Alegre, Brasil

Received 26 August 1960

Abstract: Usually a physical meaning is given only to half of the solutions of the Klein-Gordon equation for a 4-component spinor. It is shown that the isobaric spin degrees of freedom of a free fermion-isofermion field can be simply interpreted by considering all the solutions of the Klein-Gordon equation to be meaningful. Explicit expressions for the isobaric spin operators in spinor and configuration space quantities are given. The conserved current of one of the isobaric spin components is the axial vector current.

It is the purpose of this note to show that a completely γ^5-invariant Dirac theory contains degrees of freedom which can be interpreted as corresponding to the isobaric spin of a fermion-isofermion field.

At present we restrict ourselves to the kinematics of the problem and treat therefore only the free field equation. It will however become clear that the following interpretation is possible in any really γ^5-invariant theory in which the Dirac-equation with non-zero mass appears.

We first consider the unquantized Dirac field. The transition from the Klein-Gordon equation to the Dirac equation consists of the following well known linearization procedure. The equation

$$(\Box^2 - m^2)\psi = 0 \tag{1}$$

may be written

$$\left(\gamma^\mu \frac{\partial}{\partial x^\mu} + m\right)\left(\gamma^\nu \frac{\partial}{\partial x^\nu} - m\right)\psi = 0.$$

The solutions of the two Dirac equations

$$\left(\gamma^\mu \frac{\partial}{\partial x^\mu} + m\right)\psi_1 = 0 \tag{2a}$$

and

$$\left(\gamma^\mu \frac{\partial}{\partial x^\mu} - m\right)\psi_2 = 0 \tag{2b}$$

form together a complete set from which the solutions of (1) can be found by superposition. Usually, one then arbitrarily chooses one of the two eq. (2), arguing that the theories resulting from each of the two equations are physically identical.

This choice destroys the γ^5-invariance which eq. (1) possesses and we suspect that it conceals also the isobaric spin degrees of freedom of the fermion-isofermion fields. In fact, considering for definiteness ψ as the nucleon field, we will show that the two fields ψ_1 and ψ_2 in eqs. (2) can in a natural way be interpreted as the proton and the neutron fields. It would seem, that, similarly as the "positive and negative energy solutions" of the Dirac equations correspond to particles with opposite charges, the "positive and negative mass states" correspond to particles with opposite isobaric spins.

The only assumption we make is that eq. (1) represents the free nucleon field. Thus the equation pair (2) generates a basic set of solutions. It may be written

$$\left(\gamma^\mu \frac{\partial}{\partial x^\mu} I + m\tau_3\right) \Psi = 0, \tag{3}$$

in which

$$\Psi = \begin{pmatrix} \psi_1 \\ \psi_2 \end{pmatrix}.$$

τ_i stands here, and in the following, for a Pauli spin matrix and I denotes the unit matrix. We uniquely characterize a complete set of solutions of eq. (1) by the index 1 or 2 of eqs. (2) and by the eigenvalues of the helicity and four momentum operators:

$$-i\sigma_j \frac{\partial}{\partial x^j} \psi_{i\lambda k_\mu} = \lambda |\mathbf{k}| \psi_{i\lambda k_\mu} \quad (\lambda = \pm 1), \tag{4}$$

$$-i \frac{\partial}{\partial x^\mu} \psi_{i\lambda k_\mu} = k_\mu \psi_{i\lambda k_\mu} \quad (-k^\mu k_\mu = m^2). \tag{5}$$

$\gamma^5 \psi_{1\lambda k_\mu}$ solves eqs. (2b), (4) and (5). Therefore

$$\gamma^5 \psi_{1\lambda k_\mu} = \text{constant } \psi_{2\lambda k_\mu}$$

and thus

$$\psi_{1\lambda k_\mu} = \text{constant } \gamma^5 \psi_{2\lambda k_\mu}.$$

Normalizing $\psi_{2\lambda k_\mu}$ so that the constant equals 1, one gets

$$\gamma^5 \Psi_{\lambda k_\mu} = \tau_1 \Psi_{\lambda k_\mu}, \quad \text{with} \quad \Psi_{\lambda k_\mu} = \begin{pmatrix} \psi_{1\lambda k_\mu} \\ \psi_{2\lambda k_\mu} \end{pmatrix}.$$

From this equation and eq. (3) it follows that, acting on $\Psi_{\lambda k_\mu}$, one can replace τ_1 by $\gamma^5 I$, τ_2 by $(i/m)\gamma^5 \gamma^\mu \, \partial/\partial x^\mu I$ and τ_3 by $-(1/m)\gamma^\mu \, \partial/\partial x^\mu I$.

Forgetting now about the 8-component symbol Ψ and returning to the 4-component of eq. (1), we define the components of the isobaric spin vector t_i by

$$(t_1, t_2, t_3) = \tfrac{1}{2}\left(\gamma^5, \frac{i}{m} \gamma^5 \gamma^\mu \frac{\partial}{\partial x^\mu}, -\frac{1}{m} \gamma^\mu \frac{\partial}{\partial x^\mu}\right) \tag{6}$$

and rotations in isobaric spin space by the transformation

$$\psi \to \exp[i\varepsilon_j t_j]\psi,$$

or explicitly

$$\psi \to \exp\left[\tfrac{1}{2}\left(i\varepsilon_1\gamma^5 - \varepsilon_2 \frac{1}{m}\gamma^5\gamma^\mu \frac{\partial}{\partial x^\mu} - \varepsilon_3 \frac{i}{m}\gamma^\mu \frac{\partial}{\partial x^\mu}\right)\right]\psi.$$

These transformations clearly leave eq. (1) invariant. Eq. (2) are eigenvalue equations for t_3 and each one is consequently only invariant under rotations around the 3-axis. Eq. (2a) corresponds to the proton ($t_3 = +\frac{1}{2}$) and (2b) to the neutron ($t_3 = -\frac{1}{2}$). If one disregards one of these equations, one can describe only one of the particle types and loses the possibility of rotating the fields around the 1- and 2-isospin axes.

The next step to be taken is the quantization of the ψ-field. As will become clear later, the commonly used equal time commutation rules for Dirac spinors are essentially still true for our 4-component nucleon field. However, the usual formulation of these rules is clearly not invariant under the defined rotations in isospace and the relations are incomplete, because of the additional degrees of freedom present. Expressing this last fact somewhat differently, one may say that the commutator function obeys in our case a second order equation and is therefore not determined only by its values on a hypersurface.

To find the desired commutation rules, we first define the proton- and neutron annihilation and creation operators by expanding the field operator in the solutions of eqs. (2a) and (2b) with the help of the corresponding projection operators:

$$\psi_\alpha(x) = \psi_{1\alpha}(x) + \psi_{2\alpha}(x),$$

with (7)

$$\psi_1(x) = \tfrac{1}{2}\left(1 - \frac{1}{m}\gamma^\mu \frac{\partial}{\partial x^\mu}\right)\psi(x) \quad \text{and} \quad \psi_2(x) = \tfrac{1}{2}\left(1 + \frac{1}{m}\gamma^\mu \frac{\partial}{\partial x^\mu}\right)\psi(x).$$

We further expand ψ_1 and ψ_2, employing the usual notation for the spinor eigenfunctions,

$$\begin{aligned}
\psi_{1\alpha}(x) &= \sum_{r=1,2} \int \mathrm{d}^3k \{a_{1r} u_{r\alpha} \mathrm{e}^{i(\mathbf{k}\cdot\mathbf{x} - k_0 x_0)} + b_{1r}^\dagger v_{r\alpha} \mathrm{e}^{-i(\mathbf{k}\cdot\mathbf{x} - k_0 x_0)}\}, \\
\psi_{2\alpha}(x) &= \sum_{r=1,2} \int \mathrm{d}^3k \{a_{2r} v_{-r\alpha} \mathrm{e}^{i(\mathbf{k}\cdot\mathbf{x} - k_0 x_0)} + b_{2r}^\dagger u_{-r\alpha} \mathrm{e}^{-i(\mathbf{k}\cdot\mathbf{x} - k_0 x_0)}\}.
\end{aligned} \tag{8}$$

It is clarifying to study the isobaric spin transformations of the a's and b's. As an example we consider the transformation

$$\psi'(x) = \mathrm{e}^{2i\alpha T_1}\psi(x)\mathrm{e}^{-2i\alpha T_1} = \mathrm{e}^{i\alpha\gamma^5}\psi(x),$$

where T_1 is the first component of the isobaric spin, which we will later express in terms of the field operators. Expanding ψ' in the operators a' and b' as in (8) and using the relations

$$\gamma^5 u_{-r\alpha} = v_{r\alpha}, \qquad \gamma^5 v_{-r\alpha} = u_{r\alpha},$$

one finds

$$\begin{aligned} e^{2i\alpha T_1} a_{1r} e^{-2i\alpha T_1} &= a'_{1r} = a_{1r} \cos\alpha - i a_{2r} \sin\alpha, \\ e^{2i\alpha T_1} a_{2r} e^{-2i\alpha T_1} &= a'_{2r} = a_{2r} \cos\alpha - i a_{1r} \sin\alpha. \end{aligned} \tag{9}$$

The following equation is generally valid:

$$\begin{pmatrix} a'^{\dagger}_{1r} \\ a'^{\dagger}_{2r} \end{pmatrix} = e^{-i\alpha\tau_i} \begin{pmatrix} a^{\dagger}_{1r} \\ a^{\dagger}_{2r} \end{pmatrix}. \tag{10}$$

For the antiparticles follows in the same way

$$\begin{pmatrix} -ib'^{\dagger}_{2r} \\ +ib'^{\dagger}_{1r} \end{pmatrix} = e^{-i\alpha\tau_i} \begin{pmatrix} -ib^{\dagger}_{2r} \\ +ib^{\dagger}_{1r} \end{pmatrix}. \tag{11}$$

The T-transformations accomplish just what one desires, namely they mix neutrons with protons and anti-neutrons with anti-protons without affecting the spin coordinates. The difference in the indices of the creation operators of (10) and (11) expresses the fact that the (diagonal) third component of the isobaric spin of an anti-particle is opposite to that of the corresponding particle.

The situation with respect to the other rotations in isospace is exactly analogous to the one just considered.

We now postulate the usual quantization rules for the proton and neutron creation and annihilation operators; in particular we take the operators corresponding to opposite orientations of the isobaric spin to be anti-commuting. From eqs. (10) and (11) and the analogous relations for the other rotations one may see that these quantization rules are invariant under isobaric spin transformations.

From expansion (8) follow now, in the usual way, the commonly used equal time commutation rules for the neutron and proton field operators ψ_1 and ψ_2. From

$$\psi = \psi_1 + \psi_2$$

one finds then for $x_0 = x'_0$

$$\{\psi_\alpha^{\dagger}(x), \psi_\beta(x')\}_+ = 2\delta_{\alpha\beta}\delta(x-x'), \tag{12}$$

all other anti-commutators vanishing.

These are, except for the factor 2, the usual rules. As remarked earlier they are, although correct, incomplete and not manifestly invariant under isobaric spin transformations.

One may find the invariant and complete set of free field commutation rules by using (8), starting from the postulated rules between the a's and b's. It is, however, simpler to verify the following invariant relations directly by inspection:

$$\{\bar{\psi}_\alpha(x'), \psi_\beta(x)\}_+ = 2i\gamma^\mu_{\alpha\beta} \frac{\partial}{\partial x^\mu} \Delta(x-x'), \tag{13}$$

all other anti-commutators vanishing.

Both sides of relation (13) obey the Klein-Gordon equation and by application of the projection operators (7) one obtains the well-known commutation rules for the solutions of the Dirac eqs. (2a) and (2b). Of course, (13) reduces to (12) for $x_0 = x'_0$.

We now go over to the construction of the isobaric spin operators T_i, taking as an example T_1. We want a hermitian, space-time independent, operator T_1 with

$$[T_1, \psi] = t_1 \psi. \tag{14a}$$

From definition (6) and eqs. (7) it follows that

$$[T_1, \psi_1] = \tfrac{1}{2}\gamma^5 \psi_2, \quad [T_1, \psi_2] = \tfrac{1}{2}\gamma^5 \psi_1. \tag{14b}$$

Adding the condition of a zero vacuum expectation value, one finds uniquely from (14)

$$T_1 = -\tfrac{1}{4}\int \psi_2^\dagger \gamma^5 \psi_1 + \psi_1^\dagger \gamma^5 \psi_2 \, \mathrm{d}^3x - \text{the transposed.} \tag{15}$$

Expressing ψ_1 and ψ_2 in ψ by relations (7), one may write

$$T_1 = -\frac{i}{4m^2}\int \bar{\psi} \overleftrightarrow{\frac{\partial}{\partial x^0}} \gamma^5 \gamma^\mu \frac{\partial \psi}{\partial x^\mu} \, \mathrm{d}^3x \, - \text{transp.}$$

The symbol $\overleftrightarrow{\partial}/\partial x$ has the meaning

$$A \overleftrightarrow{\frac{\partial}{\partial x}} B = \tfrac{1}{2}\left(A \frac{\partial B}{\partial x} - \frac{\partial A}{\partial x} B\right).$$

On quite the same way one finds in general

$$T_i = \frac{i}{2m^2}\int \bar{\psi} \overleftrightarrow{\frac{\partial}{\partial x^0}} t_i \gamma^\mu \frac{\partial \psi}{\partial x^\mu} \, \mathrm{d}^3x \, - \text{transp.}, \tag{16}$$

with the t_i's defined in (6), and for the baryon number

$$B = \int \psi_1^\dagger \psi_1 + \psi_2^\dagger \psi_2 \, \mathrm{d}x^3 \qquad - \text{transp.}$$

$$= \frac{i}{2m^2}\int \bar{\psi} \overleftrightarrow{\frac{\partial}{\partial x^0}} \gamma^\mu \frac{\partial \psi}{\partial x^\mu} \, \mathrm{d}^3x \, - \text{transp.}$$

The operator

$$Q = T_3 + \tfrac{1}{2}B = \int \psi_1^\dagger \psi_1 \, \mathrm{d}^3x \, - \text{transp.}$$

is the proton number operator and measures therefore the electric charge.

From (14a) and the analogous relations for the other isobaric spin components and the baryon number, it follows that

$$[T_i, T_j] = iT_k \quad \text{etc., and} \quad [B, T_i] = 0.$$

These relations can also be demonstrated directly with the help of eq. (13).

The T_i's are the fourth components of the divergenceless isobaric spin currents

$$\mathcal{T}_i{}^\mu = \frac{i}{2m^2}\,\bar{\psi}\,\frac{\overleftrightarrow{\partial}}{\partial x_\mu}\,t_i\,\gamma^\nu\,\frac{\partial\psi}{\partial x^\nu} - \text{transp.}$$

and are consequently independent of the integration surface taken. Furthermore they are invariant under continuous Lorentz transformations and hermitian. Therefore, one may indeed say that the T_i's have the properties commonly attributed to the isobaric spin operators.

The T_i-operators are not invariant under the discrete transformations. For example, the parity transformation is accompanied by an inversion through the 3-axis, and the charge conjugation through the 1-axis in isospace.

The parity situation is interesting †. We take this transformation to be

$$\psi'(\mathbf{x}, t) = \eta\gamma^4\psi(-\mathbf{x}, t).$$

From eqs. (7) it follows that

$$\psi'_1(x) = \eta\gamma^4\psi_1(-x), \qquad \psi'_2(x) = \eta\gamma^4\psi_2(-x), \tag{17}$$

and from eq. (8) that the proton and neutron have different parities. Because experimentally the π^+ and π^- have a different parity from the (np)-pair, their parity is positive in our formulation. From eqs. (6), (16) and expression (18) below it follows then that the π^0 has a negative parity. One may observe from eqs. (15) and (17) that the T^+-current is identical to the axial vector current, which is now conserved because of the different signs of m in eqs. (2).

What has been shown in this paper is that the usual 8-component theory of a free fermion-isofermion field can rather easily be written in a 4-component form which is invariant under certain transformations. These transformations have all the properties of rotations in isobaric spin space.

Thus far nothing new has been introduced in the physics of the problem. But if we assume that the proposed transformations still represent the isobaric spin rotations of a fermion-isofermion field in the case of interactions, then strong restrictions on an admissible theory result. In the case of interactions other fields will contribute to the conserved isobaric spin currents $\mathcal{T}_i{}^\mu$. For example, the isospin currents of the π-meson field are given by the well-known expression:

$$\phi_2\,\frac{\partial\phi_3}{\partial x^\mu} - \phi_3\,\frac{\partial\phi_2}{\partial x^\mu}, \quad \text{etc.} \tag{18}$$

† The author thanks Dr. J. Tiomno for a helpful remark on this point.

Apologies are due for the lack of references. The present note has an about equally strong connection with many papers on the isobaric spin space and the author neither wanted to disturb this symmetry nor to burden this short note with a long list of references. He is thankful to Drs. M. A. Melvin, D. Dillenburg and Gerhard Jacob for many stimulating discussions. The stay of the author in Brasil has been made possible by the support of Comissão Supervisora do Plano dos Institutos (COSUPI) Conselho Nacional de Pesquisas and the Division of Scientific Development of the Organization of the American States.

2.C: 2.F

Nuclear Physics **24** (1961) 353—371; © *North-Holland Publishing Co., Amsterdam*

Not to be reproduced by photoprint or microfilm without written permission from the publisher

THE $C^{13}(p, n)N^{13}$ REACTION CROSS SECTION FROM THRESHOLD TO 13 MeV

P. DAGLEY †, W. HAEBERLI and J. X. SALADIN

University of Wisconsin, Madison, Wisconsin ††

Received 2 January 1961

Abstract: The cross section for the $C^{13}(p, n)N^{13}$ reaction has been measured at 0° from threshold to 13.1 MeV and at 90° from threshold to 5.3 MeV. Resonances have been observed, some of which can be attributed to known states in N^{14}. No indication was found of a neutron group leading to the first excited state in N^{13} but above 8 MeV there is evidence for neutrons leading to the second or third excited state. In the energy range between threshold and 13 MeV fifty angular distributions of the neutrons leading to the ground state of N^{13} have been determined. The angular distributions are similar in shape over energy intervals of two or three MeV. At the end of an interval the angular distributions change character quite suddenly. Over much of the energy range there is pronounced backward peaking with a secondary maximum near 50° and no forward peak. Above 11.4 MeV the angular distributions are in qualitative agreement with a simple direct interaction calculation. The differential cross sections were integrated to give the total cross section for the reaction.

1. Introduction

Below 5.3 MeV the $C^{13}(p, n)N^{13}$ reaction has been studied with good resolution by several authors [1–5]) but at higher energies measurements have been made only by the stacked foil technique [6, 7]). The newly installed tandem Van de Graaff accelerator at the University of Wisconsin provided the opportunity to extend the studies to higher energies with high resolution. The 90° beam analysing magnet provides an energy resolution which has been estimated [8]) to be about 5×10^{-4}.

During the last few years much effort has been made to explain the angular distribution of particles emitted in nuclear reactions. Particularly familiar is the stripping theory, which as a whole has been very successful for (d, p) and (d, n) reactions and their inverse. A direct interaction model valid for other types of reactions as well has more recently been proposed by Butler [9]). This model considers a mechanism in which the impinging particle interacts only with one or a few nucleons at the nuclear surface, rather than giving rise to the formation of a compound nucleus. The shape of the angular distribution should be very similar to those characteristic of stripping reactions. According to

† Now at Chadwick Laboratory, University of Liverpool, England.

†† Work supported by the U. S. Atomic Energy Commission and by the Graduate School from funds supplied by the Wisconsin Alumni Research Foundation.

Butler [9]) such a process should be particularly important when only a small energy exchange is involved in the reaction and when the final nucleus is left in a low-lying state. The $C^{13}(p, n)N^{13}$ reaction to the ground state should be a good example. C^{13} and N^{13} are mirror nuclei having an odd nucleon outside a tightly bound C^{12} core. This suggests the possibility that the reaction is dominated by a direct interaction between the incoming proton and the odd neutron. It was one of the aims of the present experiment to investigate to what extent this is the case.

The relative positions of the energy levels involved in the $C^{13}(p, n)$ reaction are summarized in ref. [10]). The threshold of the reaction occurs for a proton energy of (3.2372 ± 0.0016) MeV (ref. [11])). Excitation energies in the compound nucleus N^{14} greater than 10.55 MeV are being reached by the reaction. As the bombarding energy is increased above 5.78 it becomes energetically possible for the reaction to proceed to the first excited state in N^{13} with the emission of a second group of neutrons of lower energy. Similarly a third and fourth group of neutrons might appear above 7.02 and 7.07 MeV, respectively. At 5.325 MeV the $C^{13}(p, pn)C^{12}$ reaction also becomes energetically possible.

2. Apparatus

2.1. THE TARGET CHAMBER

The target chamber is shown in fig. 1. The material is principally stainless steel, the body A of the chamber being made from two domestic mixing bowls having a wall thickness of about 0.04 cm. This avoided the need for heavy flanges close to the target and simplified the construction.

The beam pipe B is fixed to the upper half and a glass-windowed part C was set in above it so that the front of the target could be viewed by the camera of the closed-circuit television system. The camera provided quite a large mass relatively close to the chamber but an experimental check showed that scattering of neutrons by the camera did not measurably affect the results.

A beam stop D was supported from a bracket soldered to a copper tube which passed through the wall of the chamber. The stop was cooled by blowing air through the tube.

The lower half of the chamber carried a shaft and a wheel E from which 10 targets F could be supported. The shaft passed through a double teflon seal and was driven by a selsyn motor. The double seal was provided with an intermediate pumping tube so that a differential pumping system could be used, but it was not necessary to do this.

Except for the teflon seals on the shaft the O-rings used were made of Viton † which has a very low rate of outgassing. These rings were used without grease

† Viton-A compound 514 D, supplied by the Minnesota Rubber Company, 3630 Woodale Avenue, Minneapolis 16, Minnesota.

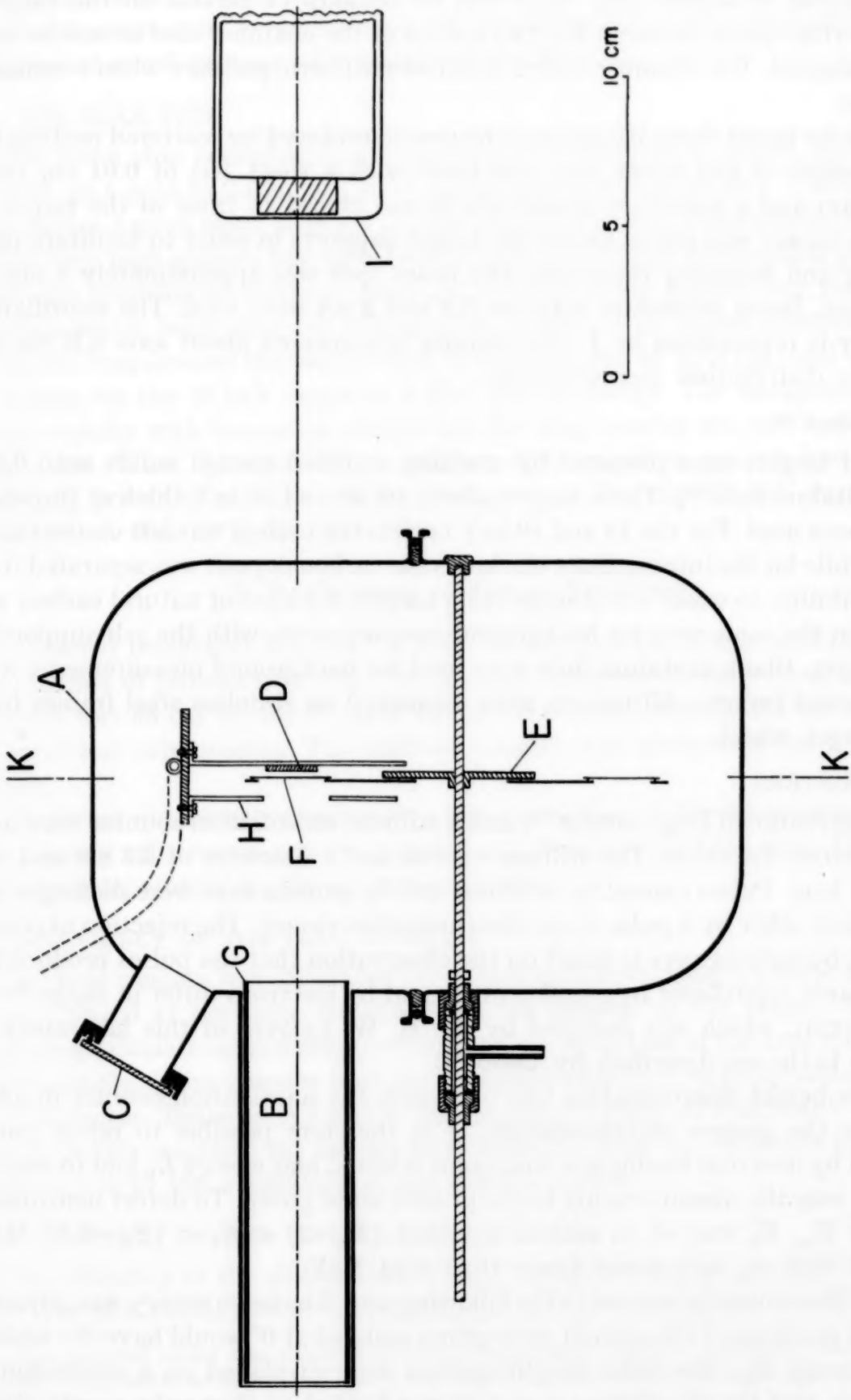

Fig. 1. Experimental apparatus. A – Target chamber. B – Beam tube. C – Observation window. D – Beam stop. E – Wheel supporting targets. F – Target. G – Tantalum liner. H – Tantalum diaphragm. I – Detector.

and helped to ensure that there was no buildup of carbon on the targets. The O-ring spacer between the two halves of the chamber also served to keep them aligned. The chamber sealed under atmospheric pressure when evacuated for use.

In order to cut down background neutrons produced by scattered protons the last section of the beam pipe was lined with a sheet (G) of 0.01 cm thick tantalum and a tantalum diaphragm H was placed in front of the target. A quartz viewer was put in one of the target supports in order to facilitate positioning and focussing the beam. The beam spot was approximately 1 mm in diameter. Beam intensities between 0.3 and 2 μA were used. The scintillation counter is represented by I. The counter was rotated about axis KK for the angular distribution measurements.

2.2. TARGETS

Solid targets were prepared by cracking enriched methyl iodide onto 0.001 cm tantalum foils [12]). Three targets about 10, 20 and 50 keV thick at threshold have been used. For the 10 and 50 keV targets the carbon was left on the tantalum, while for the intermediate thickness the carbon deposit was separated from the tantalum to make a self-supporting target. A target of natural carbon was made in the same way for background measurements with the self-supporting C^{13} target. Blank tantalum foils were used for background measurements with the backed targets. All targets were supported on stainless steel frames from the target wheel.

2.3. COUNTERS

A conventional long counter [13]) and a stilbene scintillation counter were used for neutron detection. The stilbene crystal had a diameter of 2.5 cm and was 1.2 cm long. Pulses caused by neutrons and by gamma rays were distingiushed from each other by a pulse shape discrimination circuit. The rejection of counts caused by gamma rays is based on the observation that the pulses produced in an organic scintillator by recoil protons and by electrons differ in shape [14, 15]). The circuit, which was designed by Mr. H. W. Lefevre of this laboratory, is similar to the one described by Owen [16]).

Pulse height discrimination was used with the scintillation counter in addition to the gamma discrimination. It is therefore possible to reject pulses caused by neutrons having less than some selected bias energy E_b and to restrict in this way the measurements to the ground state group. To detect neutrons of energy E_n, E_b was set in such a way that $(E_n-2) < E_b < (E_n-0.5)$ MeV, except that E_b was never lower than 0.74 MeV.

The discriminator was set in the following way. The beam energy was adjusted so that neutrons of the ground state group emitted at 0° would have the desired bias energy E_b. The pulse height spectra were displayed on a multichannel analyser and the discriminator was then adjusted so that only counts above

the midpoint of the high energy cut-off of the spectrum were recorded. During the subsequent runs at higher energies the recorded counts represented the number of recoil protons whose energy exceeded E_b.

2.4. THE BEAM STOP

The beam stop consisted of a 1.2 cm diameter deposit of nickel, enriched † in Ni^{58}, on a gold backing. Ni^{58} has a (p, n) threshold of 9.48 MeV [8]) and therefore makes a good beam stop for use with a long counter. Unfortunately nickel has a very high gamma ray yield which caused a serious overloading problem with the scintillation counter. Gold has a much lower gamma ray yield and made a better beam stop for this counter in spite of its higher neutron yield. With the long counter the background from nickel was 30 % of the total number of counts for the 20 keV target at 9 MeV proton energy. The background was rising rapidly with increasing energy and the long counter was not used above this point. With the scintillation counter, discrimination against low energy neutrons provided a much smaller background. For the 50 keV target the background was 25 % at 13 MeV.

3. Evaluation of Cross Sections

A current integrator was used in order to measure the charge and therefore the number of protons collected. The distance between the target and the long counter was 55 cm for the 0° yield measurements and 105 cm for the angular distribution experiments. The stilbene counter was always 29 cm from the target.

The other quantities entering into the evaluation of the cross sections are the counter efficiencies and the number of C^{13} atoms per unit area. They are discussed separately in the following sections.

3.1. EFFICIENCY OF THE LONG COUNTER

The long counter was calibrated on several occasions using a Pu–Be neutron source placed at the same distance from the counter as the target. Allen [13]) describes calculations and measurements of the deviation of the true efficiency of the standard long counter from the efficiency obtained by calibration with a Pu–Be source. Between 0.2 and 6 MeV neutron energy (3.4–9.2 MeV proton energy in this reaction) the maximum deviation is 6 %. No allowance has been made for it in the evaluation of the cross sections.

3.2. EFFICIENCY OF THE SCINTILLATION COUNTER

The efficiency of the stilbene scintillation counter is the product of two factors. The first factor relates the number of neutrons entering the crystal to the

† The enriched nickel was obtained from the Oak Ridge National Laboratory and had an isotopic composition of 99.6 % Ni^{58}, 0.3 % Ni^{60} and 0.1 % Ni^{62}. The chemical purity was given as 99.8 %, the main impurity being 0.2 % copper.

number n_r of recoil protons produced in the crystal. It was calculated † from the dimensions of the scintillator and the total neutron cross sections of hydrogen and carbon. The second factor relates the number n of counts observed to the number n_r of recoil protons. It was assumed that $n = n_r(E_n - E_b)/E_n$, where E_n is the neutron energy and E_b is the neutron energy corresponding to the discriminator setting.

This method does not require any knowledge of the non-linear relationship between energy and pulse height for recoil protons in stilbene. However, it is assumed that the energy distribution of the recoil protons produced by mono-energetic neutrons has a rectangular shape. This is true if the n-p scattering is isotropic in the centre-of-mass system and if multiple scattering and edge effects are negligible. These effects distort the spectrum but are to some extent compensatory and have not been taken into account in the evaluation of the data. The magnitude of the errors caused by these effects is discussed in subsection 5.1.

No account was taken of the reported directional asymmetry of crystalline scintillators [17]).

3.3. THICKNESS OF THE TARGETS

The target thicknesses at threshold were measured for the two thinner targets by the rise method [18]). The thicknesses were equivalent to 10.6 and 19.8 keV. The relative thickness of these two targets was also determined by comparing the yields at several energies. The thickness of the third target was found only by comparison of its yield to that from the 19.8 keV target. It was found to be 2.6 times as thick as this target, or about 50 keV at threshold.

The abundance of C^{13} in the targets was measured by comparing the rate of rise of the yield curve near threshold for the enriched targets with that of natural carbon for which the abundance of C^{13} is known [19]). The relative abundance of C^{13} was found to be 51 ± 3 %. The value given by the supplier †† was 40 to 60 %.

The number of C^{13} atoms in the target was derived from the abundance and equivalent thickness using the stopping cross section given by Whaling [20]). The 19.8 keV target was found to have 5.1×10^{18} atoms/cm^2 with an accuracy of about 8 %. As an additional check the number of C^{13} atoms in this target was also determined by comparing the neutron yield which it produced with the yield obtained for an "infinitely" thick target of natural carbon. If the stopping power and the abundance of C^{13} in natural carbon are known, the number of C^{13} atoms in the enriched target follows from the comparison of the integral over the enriched target yield curve from threshold to E_p and the

† See ref. [17]) for a discussion of stilbene as a neutron detector.

†† Isomet Corporation, Palisades Park, New Jersey.

yield at E_p of a thick target of natural carbon. This method which does not depend on the measurement of the target thickness by the rise method gave a value of 4.9×10^{18} atoms/cm^2. A mean value of $(5.0\pm0.4)\times10^{18}$ atoms/cm^2 was used for the evaluation of the cross sections.

4. Energy Calibration

The momentum of the protons passing through the analysing magnet was assumed to be proportional to the frequency given by the proton resonance flux meter. Under this assumption the relation between proton kinetic energy E in eV and the frequency f of the nuclear resonance fluxmeter [8]) is

$$E\left(1+\frac{E}{2\varepsilon}\right)=kf^2g^2/M,$$

where g is the charge of the ion in units of the electronic charge, E/ε is the ratio of the kinetic energy to the rest mass energy and M is the proton mass in atomic mass units. During the experiment k was determined several times by means of the accurately known threshold of the $C^{13}(p, n)$ reaction [11]). The result was $k=(2.008\pm0.002)10^{-8}$. An additional measurement was made for the $Al^{27}(p, n)$ reaction threshold at [8]) 5.800 MeV leading to the result $k=(2.011\pm0.002)\times10^{-8}$.

The analysing magnet of the Chalk River tandem accelerator is identical in design and construction to that used in the present experiment. The Chalk River group [8, 21]) performed calibration measurements for magnetic fields equivalent to proton energies up to 14.5 MeV and found no measurable variation of k between proton energies of 3 and 14.5 MeV. The assumption that the two magnets are identical is supported by the close agreement of k measured at Chalk River [$k=(2.011\pm0.002)\times10^{-8}$] with our values. The proton energies were computed using the value $k=2.008\times10^{-8}$.

5. Results and Errors

5.1. YIELD AT 0° AND 90°

The forward yield was measured up to 9 MeV with the long counter and from 4.3 to 13.1 MeV with the stilbene counter biased so that only neutrons leading to the ground state of N^{13} were recorded. In order to detect narrow resonances points were taken in energy increments of 5 to 10 keV below 9 MeV and 25 keV at higher energies. The 90° yield was measured with the long counter only. The results are shown in figs. 2 and 3. The cross sections are in the laboratory system. For the sake of clarity some points have been omitted from the curves, particularly where scintillation counter data are coincident with long counter data. Between 4.3 and 5.4 MeV the long counter curve is 10 to 30 % lower than the stilbene counter curve. There is good agreement between the two in the energy

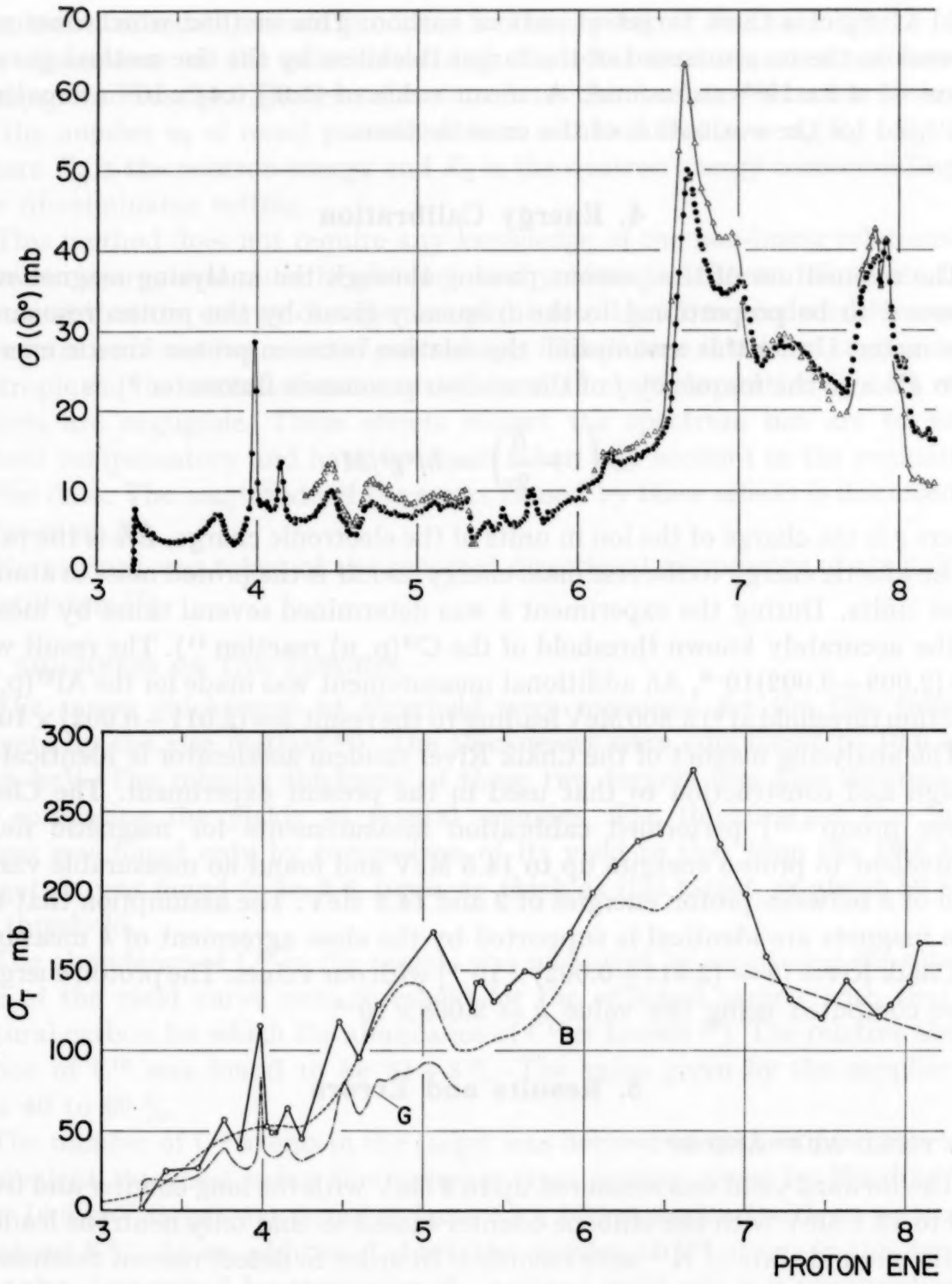

Fig. 2. Upper part: The $C^{13}(p, n)N^{13}$ reaction cross section (per unit solid angle) at 0°. Abscissa and ordinates are given in the laboratory system. The open triangles represent the cross section to the ground state of N^{13} only, the dots the cross section for all neutrons. Lower part: Total

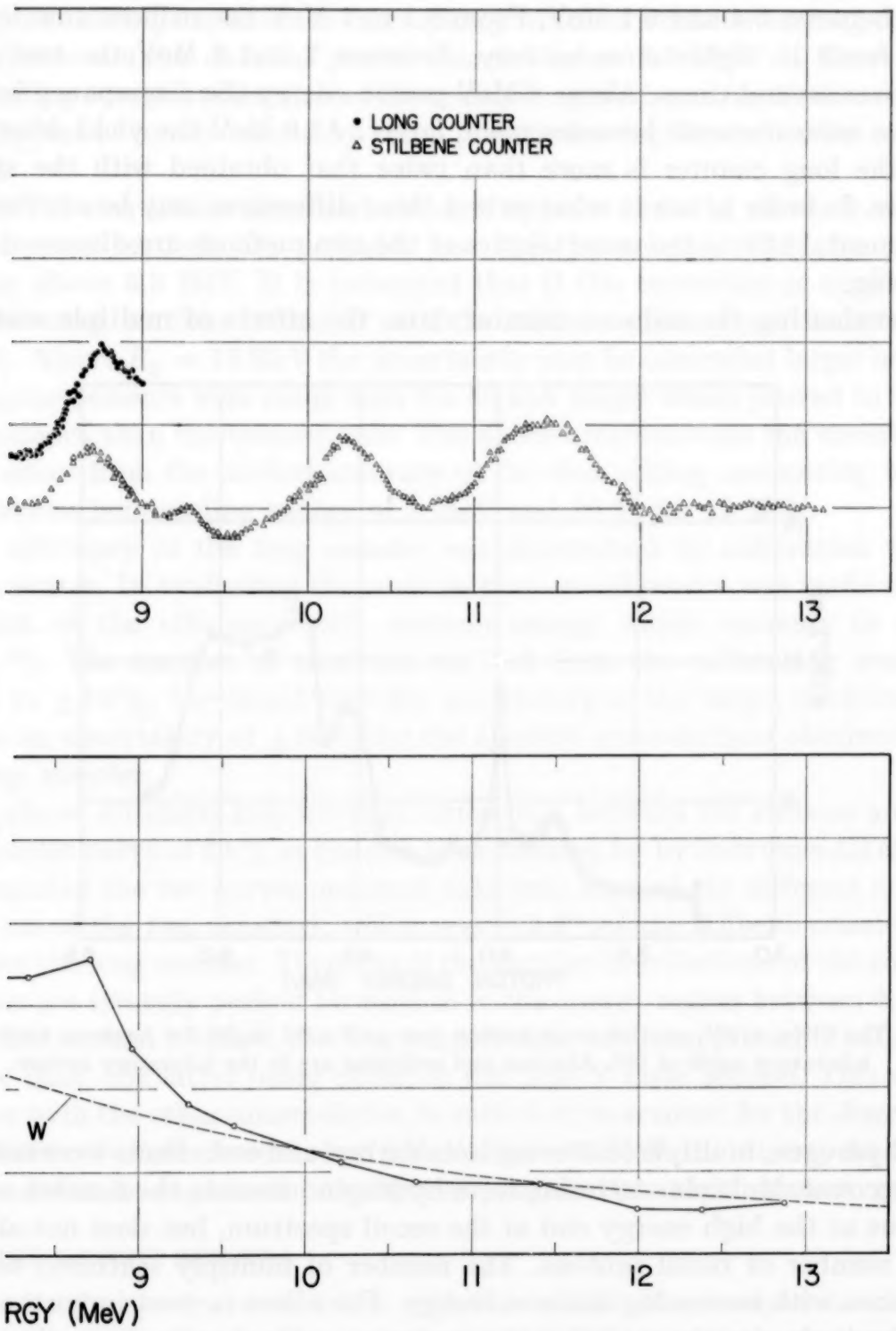

cross section of the $C^{13}(p, n)N^{13}$ reaction to the ground state of N^{13} as a function of the proton laboratory energy. The open circles represent the present data. The results of Gibbons and Macklin [5] (G), Blaser *et al.* [6] (B), and Whitehead and Foster [7] (W) are also shown for comparison.

range between 5.4 and 6.1 MeV. From 6.1 to 7 MeV the stilbene counter data again result in higher cross sections. Between 7 and 8 MeV the two curves cross over several times. Above 8 MeV proton energy the discrepancy between the two measurements becomes much larger. At 9 MeV the yield determined with the long counter is more than twice that obtained with the stilbene counter. In order to see to what extent these differences may be attributed to instrumental effects the uncertainties of the two methods are discussed in the following.

In evaluating the stilbene counter data, the effects of multiple scattering

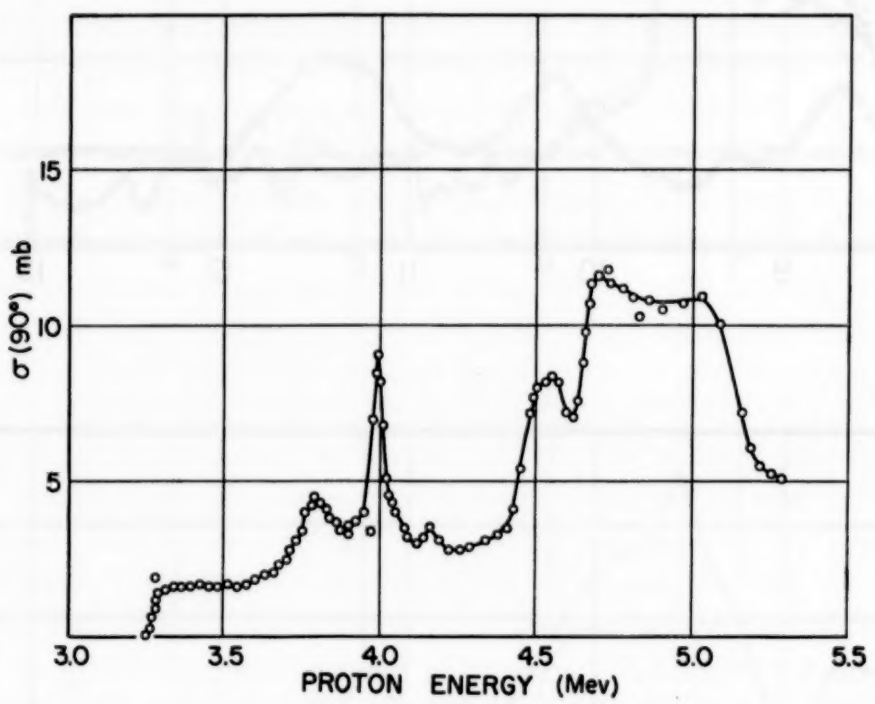

Fig. 3. The $C^{13}(p, n)N^{13}$ reaction cross section (per unit solid angle) for neutrons emitted at a laboratory angle of 90°. Abscissa and ordinates are in the laboratory system.

from hydrogen, multiple scattering from carbon and end effects were not taken into account. Multiple scattering from hydrogen increases the number of recoil protons at the high energy end of the recoil spectrum, but does not alter the total number of recoil protons. The number of multiply scattered neutrons decreases with increasing neutron energy. The effect is most important when the bias is close to the cut-off of the spectrum and leads to cross sections which are too high. Estimates based on graphical integration of calculated recoil spectra [17]) indicate that the magnitude of this effect is 30 % for a proton energy of 4.3 MeV, drops to a minimum of about 5 % at 5.3 MeV and then rises to 12 % for 13 MeV proton energy. Multiple scattering from carbon also leads to too high a cross section by an amount which decreases monotonically from 15 % to 3 % as the bombarding energy increases from 4.3 to 13 MeV. Thus

multiple scattering explains the discrepancy which exists between long counter and stilbene counter data for proton energies below 5.3 MeV. At the highest bombarding energies about half of the multiple scattering correction is compensated by loss of counts caused by recoil protons leaving the end of the stilbene crystal.

From the corrections discussed above it appears that the absolute stilbene counter cross sections are probably too high by roughly 10 % for proton energies above 5.3 MeV. It is estimated that if this correction is applied the absolute cross sections obtained with the stilbene counter are uncertain to ± 20 %. Above $E_p = 10$ MeV the uncertainty may be somewhat larger because these measurements were made with the 50 keV target which proved to be less homogeneous than the thinner ones. The above error includes the uncertainty which arises from the limited accuracy of the bias setting amounting to 4 % for a proton bombarding energy of 5 MeV and 10 % for 13 MeV.

The efficiency of the long counter was determined by calibration with a Pu–Be source. In evaluating the cross sections no allowance was made for the variation of the efficiency with neutron energy which amounts to about ± 6 % [13]). The number of neutrons emitted from the calibrating source is known to ± 10 %. Combined with the uncertainty of the target thickness one obtains an uncertainty of ± 20 % for the absolute cross sections obtained with the long counter.

The above estimates indicate that differences between the stilbene and the long counter curve of 20 % or less can be accounted for by instrumental effects. In comparing the two curves one must take into account the different angular resolution of the two counters, which was $\pm 2.2°$ for the stilbene counter and $\pm 15°$ for the long counter. Therefore if the angular distributions of the emitted neutrons are strongly peaked forward as in the energy region between 6.5 and 7 MeV and around 7.8 MeV, the long counter data will be appreciably below the stilbene data, the latter being closer to the true 0° cross section. This effect, together with the other uncertainties, is sufficient to account for the discrepancies between the two curves below 8 MeV. Above 8 MeV the discrepancies are large and can be explained only by the presence of other neutron groups.

5.2. PULSE HEIGHT SPECTRA

Pulse height spectra were taken with the scintillation counter to identify neutron groups leading to the excited states of N^{13}. A typical spectrum with background subtracted is shown in fig. 4 for $E_p = 10.21$ MeV, $\theta = 0°$. The step labelled A corresponds to ground state neutrons ($E_n = 7.19$ MeV). Neutron groups leading to the first and to the second or third excited state ($E_n = 4.76$, 3.51, 3.56 MeV) are expected to produce steps at the points labeled B and C. There is no evidence for a group at B. The curve rises again near C indicating the presence of one or both of the other groups. Marion *et al.* [22]) looked for the

neutron group to the first excited state at threshold but were unable to find any evidence for it.

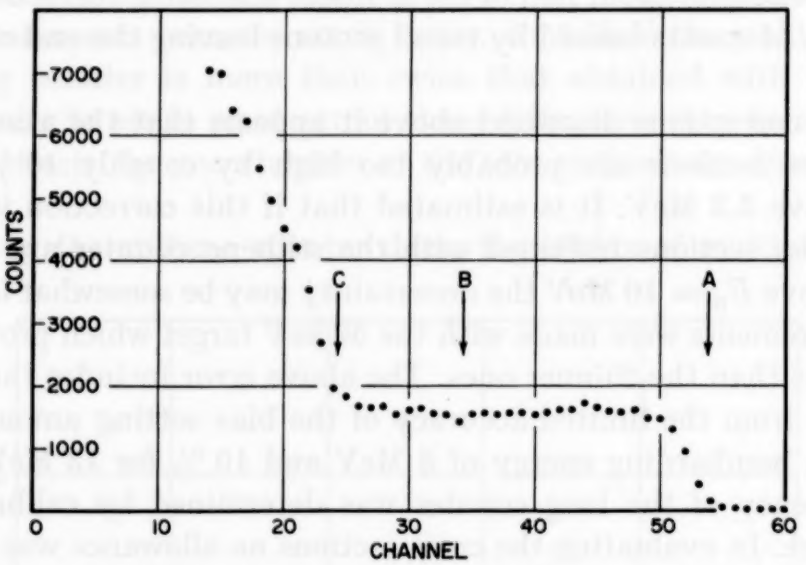

Fig. 4. A typical pulse height spectrum produced by neutrons from the C^{13}(p, n) reaction in a stilbene counter. The measurement is for $E_p = 10.21$ MeV, $\theta = 0°$. The positions where steps are expected from neutron groups leading to the ground state, the first excited state and the second or third excited states are marked by A, B and C, respectively.

At $E_p = 7.9$ MeV some measurements with a recoil-counter telescope were made. No neutron group leading to the first excited state could be detected. An upper limit of 5 % can be set on the intensity of neutrons to the first excited state relative to the intensity of ground state neutrons.

5.3. ANGULAR DISTRIBUTIONS

Fifty angular distributions were measured between threshold and 13 MeV. Measurements were made every 15° from 0° to 165° with the scintillation counter and to 135° with an additional measurement at 140° with the long counter. The bias conditions for the stilbene detector were such that only ground state neutrons were detected. The long counter was used up to 5.3 MeV and the scintillation counter from 4.47 MeV upwards. In the region of overlap the results obtained with the two counters were consistent. The cross sections were transformed into the centre-of-mass system using the tables of Marion *et al.* [23]) and are displayed in fig. 5. The different curves are displaced with respect to each other in order to avoid confusion.

Bair *et al.* [4]) have measured angular distributions up to 4.6 MeV. The shapes of their angular distributions are in very good agreement with the present data. Angular distribution measurements up to 5.3 MeV were reported recently by Albert *et al.* [24]). Above 3.4 MeV there is good agreement in the angular dependence of the cross section. Below 3.4 MeV their measurements show pronounced forward peaking which has not been observed in the present work.

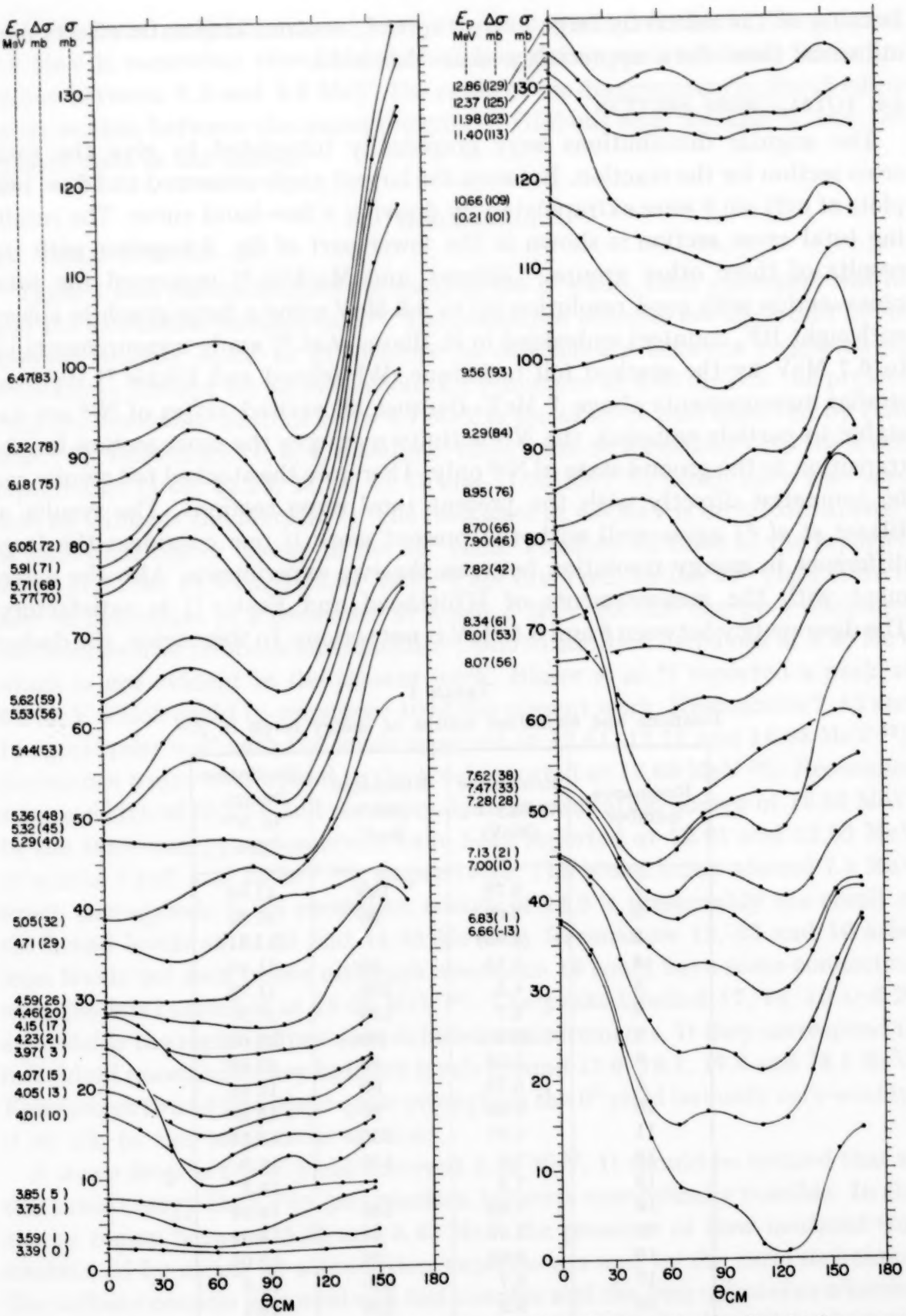

Fig. 5. Angular distributions of the neutrons from the $C^{13}(p, n)N^{13}$ reaction leading to the ground state of N^{13}. The cross sections (per unit solid angle) and the scattering angles are given in the centre-of-mass system. The bombarding energy refers to the laboratory system. The curves are displaced vertically by an amount indicated for each curve by $\Delta\sigma$. To obtain the cross section subtract $\Delta\sigma$ from the value given by the ordinate.

Because of the relatively large energy spread, neutron kinematic effects may influence their data appreciably near threshold.

5.4. TOTAL CROSS SECTION

The angular distributions were graphically integrated to give the total cross section for the reaction. Between the largest angle measured and $\theta = 180°$ plots of $\sigma(\theta) \sin \theta$ were extrapolated by drawing a free-hand curve. The resulting total cross section is shown in the lower part of fig. 2 together with the results of three other groups. Gibbons and Macklin [5]) measured the total cross section with good resolution up to 5.3 MeV using a large graphite sphere with eight BF_3 counters embedded in it. Blaser *et al.* [6]) made measurements up to 6.7 MeV by the stacked foil technique. Whitehead and Foster [7]) reported similar measurements above 7 MeV. Because all excited states of N^{13} are unstable to particle emission, the N^{13} activity measures the cross section for the transition to the ground state of N^{13} only. Therefore the stacked foil results can be compared directly with the present total cross sections. The results of Blaser *et al.* [6]) agree well with the present work if one considers the large difference in energy resolution between the two experiments. Also the agreement with the measurements of Whitehead and Foster [7]) is satisfactory. The discrepancy between 8 and 9.5 MeV is not serious. In this region, the dashed

TABLE 1

Positions and estimated widths of energy levels in N^{14}

Resonance number	Resonance energy E_p (MeV)	Etsimated width (keV)	Excitation energy in N^{14} (MeV)
1	3.76	100	11.04
2	3.98	30	11.24
3	(4.05)		(11.31)
4	4.15	40	11.40
5	4.5	100	11.73
6	4.7	150	11.91
7	(5.44)	(60)	(12.60)
8	5.53	50	12.68
9	5.72	60	12.86
10	6.20	70	13.30
11	6.67	250	13.74
12	7.0	150	14.0
13	7.3		14.3
14	7.85	150	14.83
15	7.93	50	14.91
16	8.03	50	15.00
17	8.7	350	15.6
18	9.3	150	16.1
19	10.2	400	17.0
20	11.4	600	18.1

curve is based only on measured points at 8.2, 8.8 and 9.9 MeV. The point at 8.8 MeV is somewhat above the dashed line giving some evidence for an increase between 8.2 and 8.8 MeV. The cause of the disagreement in the absolute cross section between the measurements of Gibbons and Macklin [5]) and the present data is not known.

6. Discussion

6.1. YIELD CURVES

Table 1 lists the resonances observed in the 0° yield, their estimated widths and the excitation energies in N^{14}. The resonance energies are uncertain by an amount roughly equal to $\frac{1}{2}\Gamma$ because of interference between neighbouring resonances. Except for an indication of a resonance at 4.05 MeV in the present data the resonance pattern up to 4.7 MeV is the same as that observed by Bair *et al.* [3, 4]). Resonances 1, 2, 4, 5 and 6 in table I can be identified with the levels reported at 11.07, 11.23, 11.38, 11.73 and 11.95 MeV [10]) which have also been seen by Gibbons and Macklin [5]). The resonance at 4.5 MeV is broad and appears at somewhat higher energy in the 90° yield. Possibly all three of the reported levels at 11.60, 11.73 and 11.91 MeV [10]) are involved. In the 90° yield there is also an indication of a resonance at about 5 MeV. At this energy a resonance has been seen by Gibbons and Macklin [5]) who in addition listed one at 4.85 MeV which is not evident in the present work. Blaser *et al.* [6]) reported a peak at 6.2 MeV which could be resonance 10 of the present work. Resonances 7, 11 and 14 agree quite well with the levels reported at 12.61, 13.71 and 14.84 MeV [10]). Resonance 8 may correspond to the level reported at 12.68 MeV [10]). Resonance 9 has a width of 60 keV and corresponds to an excitation energy of 12.86 MeV. In the same energy region levels have been reported at 12.81 and 12.93 MeV of widths 7 keV and 22 keV [10]), respectively. The broad hump around 7.3 MeV which corresponds to an excitation energy of 14.3 is presumably the result of the broad levels at 14.22 and 14.43 MeV [10]). Resonances 12, 15 and 16 arise from levels not seen before although resonance 16 could have some connection with the level reported at 15.09 MeV [10]). The peaks labelled 17, 18, 19 and 20 are outside the region of previous detailed measurements. If they correspond to individual resonances they indicate levels around 15.6, 16.1, 17.0 and 18.1 MeV. Resonances 19 and 20 appear quite strongly in the 0° yield but only very weakly, if at all, in the total cross section.

A sharp drop in the 0° yield occurs at 5.32 MeV. It should be noticed that at this same energy the $C^{13}(p, pn)$ reaction becomes energetically possible. In the energy region between 5.32 and 5.42 MeV the presence of slow neutrons was established by means of attenuation experiments and by the ratio technique. The stilbene counter was used as a fast counter and the long counter or a boron-loaded scintillator as a slow neutron detector. Very likely these slow neutrons must be attributed to the $C^{13}(p, pn)C^{12}$ reaction.

Fig. 6. Three-dimensional plot of the angular distributions of $C^{13}(p, n)$ neutrons leading to the ground state of N^{13} as a function of the bombarding energy. The angles and cross sections are in the centre-of-mass system. The proton energy is in the laboratory system. The plot is split up in an arbitrary way.

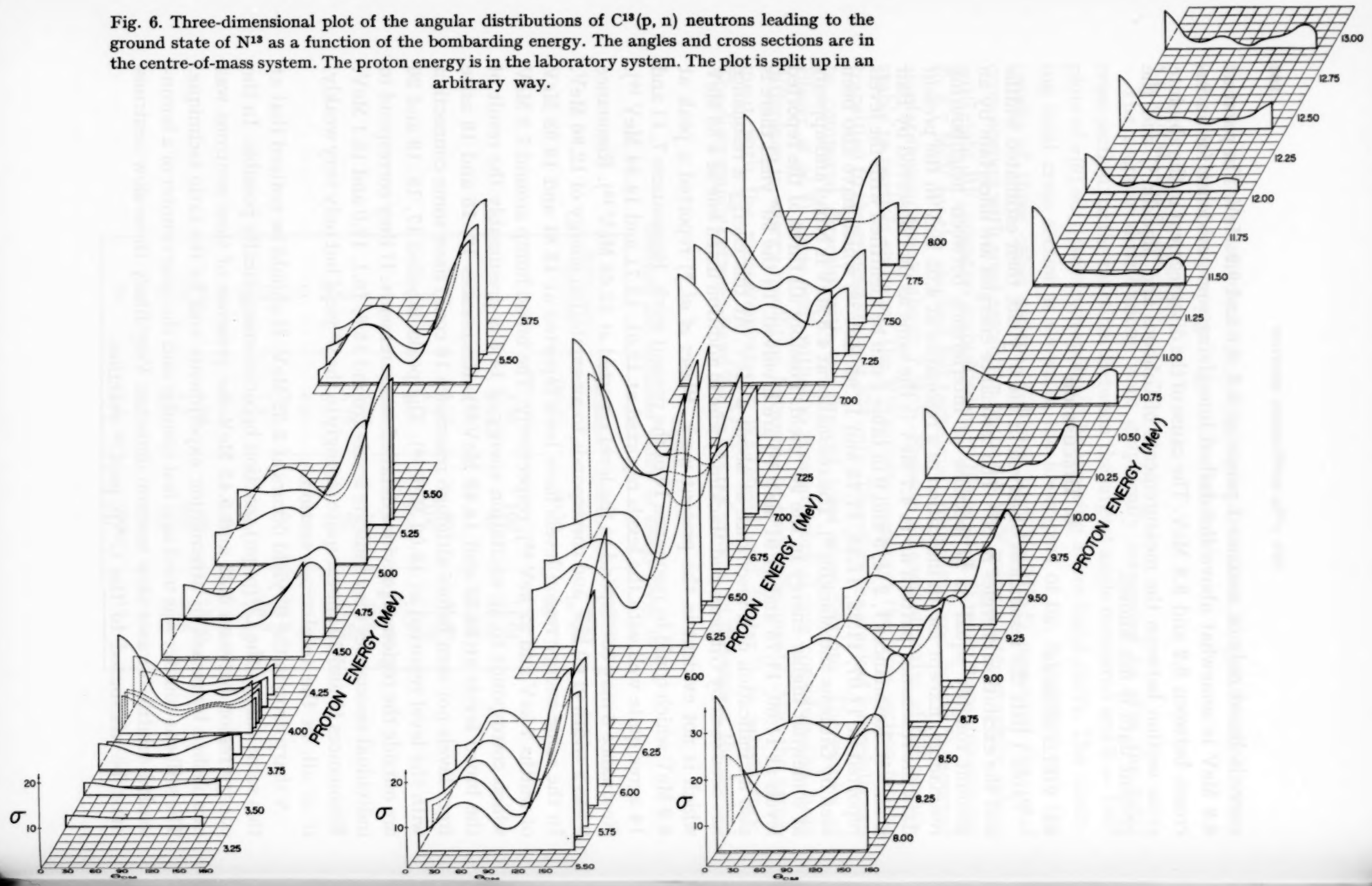

The lower part of fig. 2 shows the total $C^{13}(p, n)N^{13}$ cross section. The measured points are connected by straight lines. The average value of the total cross section rises gradually with increasing energy, reaches the geometric cross section at 6.7 MeV and then decreases with increasing energy.

6.2. ANGULAR DISTRIBUTIONS AND REACTION MECHANISM

Figure 6 presents the cross sections of fig. 5 in a way which is more suitable for a qualitative discussion. The outstanding feature of these angular distributions is that their shape remains qualitatively the same over energy intervals of roughly 2 MeV, and that the transition from one such interval to another is sudden. The shape of the distributions remains very constant, for instance between 5.0 and 6.5 MeV, where the cross section is small at 0°, rises to a broad maximum at 50°, followed by a minimum near 115° and a large rise at back angles. Essentially the same pattern occurs again between 8 and 9.6 MeV, except that in these distributions the cross section drops again beyond 150°. For energies between 6.5 and 8 MeV and 10 to 13 MeV the cross sections have a forward peak and a rise toward back angles, with one or sometimes two secondary maxima in between. Somewhat similar angular distributions also occur near 4 MeV.

The fluctuations which occur in the differential and total cross section as a function of bombarding energy (fig. 2) already indicated that the reaction is strongly influenced by resonances. One can therefore not expect the shape of the angular distributions to be entirely in agreement with a direct interaction picture. However, it has been observed in deuteron stripping reactions that the main features of the angular distribution can remain the same even though the reaction goes through a resonance [25]). This is seen to happen in the $C^{13}(p, n)$ reaction as well. A good example is again the region between 5 and 6.5 MeV where the 0° cross section has several resonances causing the cross section to fluctuate by more than factor of two without drastic effects on the shape of the angular distributions, i.e. angular distributions taken on and off a sharp resonance are the same. To some extent the same comment applies to the interval between 6.5 and 8 MeV. However, what appears unusual here is the occurrence of angular distributions which vary slowly with energy, but which change from one mode to another quite suddenly.

The direct interaction between the incoming proton and a neutron on the surface of the nucleus which was proposed by Butler [9]) leads to forward peaked angular distributions. A calculation as described in section III of ref. [9]) was performed for $E_p = 10$ MeV. The observed shape of the angular distribution for proton energies above 11.4 MeV and angles less than 100° is in fair agreement with this calculation. However, this may well be accidental since the behaviour at lower energies makes it appear quite possible that the shape of the angular distribution will change again as the bombarding energy is increased further.

The only feature common to all angular distributions is the rise of the cross section towards large angles. For instance at $\theta = 135°$ without exception the angular distributions are rising. It is in the *backward* hemisphere where the angular distributions remain qualitatively the same. Actually if the angular distributions were fore-aft reversed ($\theta \to \pi - \theta$) they would show a maximum between 0° and 30° followed by a minimum between 60° and 90°, i.e. they would appear much like the results of the direct interaction model mentioned above. Possibly the consistent backward rise in the C^{13}(p, n)N^{13} cross sections arises in part from "heavy particle stripping". This mechanism, which was proposed by Madansky and Owen [26–28]) to explain backward peaking in the B^{11}(d, n)C^{12} reaction, would in our case require a large probability for collision between the incoming proton and the C^{12} core of C^{13}.

We should like to thank Mrs. B. Rosen for preparing the carbon targets and Mr. H. W. Lefevre for the use of the pulse shape discriminating circuit. We are also indebted to Mr. R. R. Borchers for his help during the experiment and for preparing the programs for the calculation of neutron energies. In the latter connection we wish to thank Dr. K. R. Symon of the Midwestern Universities Research Association for granting us the facilities of the IBM-704 computer. We also thank Mr. S. J. Moss for performing the direct interaction calculation at 10 MeV.

Note added in proof: In the meantime measurements have been made of the neutron spectra at 0° for $E_p = 7.96$, 8.92 and 9.99 MeV, using the pulsed-beam time-of-flight technique †. At 7.96 MeV the neutron group to the first excited state of N^{13} was found to have an intensity of less than 4 % of the ground state group, in agreement with subsect. 5.2. The relative intensities of the neutron groups to the ground state, the first excited state and the second or third excited state are 1 : 0.4 : 1.3 for $E_p = 8.92$ MeV and 1 : 0.1 : 2.2 for $E_p = 9.99$ MeV.

† We thank Mr. H. W. Lefevre for performing these measurements.

References

1) H. T. Richards, R. V. Smith and C. P. Browne, Phys. Rev. **80** (1950) 524
2) R. E. Adamson, W. W. Buechner, W. M. Preston, C. Goodman and D. M. Van Patter, Phys. Rev. **80** (1950) 985
3) J. K. Bair, J. D. Kington and H. B. Willard, Phys. Rev. **90** (1953) 575
4) J. K. Bair, H. O. Cohn and H. B. Willard, Phys. Rev. **119** (1960) 2026
5) J. H. Gibbons and R. L. Macklin, Phys. Rev. **114** (1959) 571
6) J. P. Blaser, F. Boehm, P. Marmier and P. Scherrer, Helv. Phys. Acta **24** (1951) 465
7) A. B. Whitehead and J. S. Foster, Can. J. Phys. **36** (1958) 1276
8) D. A. Bromley, A. J. Ferguson, H. E. Gove, J. A. Kuehner, A. E. Litherland, E. Almqvist and R. Batchelor, Can. J. Phys. **37** (1959) 1514
9) S. T. Butler, Phys. Rev. **106** (1957) 272

10) F. Ajzenberg-Selove and T. Lauritsen, Nuclear Physics **11** (1959) 1
11) R. O. Bondelid and C. A. Kennedy, Phys. Rev. **115** (1959) 1601
12) J. D. Seagrave, Phys. Rev. **85** (1952) 197
13) W. D. Allen, in Fast Neutron Physics, ed. by Marion and Fowler (Interscience, New York, 1960) part I, p. 361
14) G. T. Wright, Proc. Phys. Soc. **B 69** (1956) 358
15) F. D. Brooks, Progr. Nucl. Phys. **5** (1956) 252
16) R. B. Owen, Nucleonics **17**, no. 9 (1959) 92
17) C. D. Swartz and G. E. Owen, in Fast Neutron Physics, ed. by Marion and Fowler (Interscience, New York, 1960) part I, p. 211
18) R. F. Taschek and A. Hemmendinger, Phys. Rev. **74** (1948) 373
19) A. O. Nier, Phys. Rev. **77** (1950) 789
20) W. Whaling, Handbuch der Physik, edited by S. Flügge (Springer-Verlag, Berlin, 1958) Vol. 34, p. 193
21) H. E. Gove, J. A. Kuehner, A. E. Litherland, E. Almqvist, D. A. Bromley, A. J. Ferguson and P. H. Rose, R. P. Bastide, N. Brooks and R. J. Connor, Phys. Rev. Letters **1** (1958) 251
22) J. B. Marion, T. W. Bonner and C. F. Cook, Phys. Rev. **100** (1955) 91
23) J. B. Marion, T. I. Arnette and H. C. Owens, ORNL-2574 (TID 4500)
24) R. D. Albert, S. D. Bloom and N. K. Glendenning, Phys. Rev., submitted
25) M. T. McEllistrem, K. W. Jones, Ren Chiba, R. A. Douglas, D. F. Herring and E. A. Silverstein, Phys. Rev. **104** (1956) 1008
26) L. Madansky and G. E. Owen, Phys. Rev. **99** (1955) 1608
27) G. E. Owen and L. Madansky, Phys. Rev. **105** (1957) 1766
28) T. Fulton and G. E. Owen, Phys. Rev. **108** (1957) 789

2.F

Nuclear Physics **24** (1961) 372—387; © *North-Holland Publishing Co., Amsterdam*

Not to be reproduced by photoprint or microfilm without written permission from the publisher

(d, α) REACTIONS ON C^{12}, O^{16} AND Mg^{24}

F. PELLEGRINI †

University of Pittsburgh, Pittsburgh, Pennsylvania ††

Received 2 January 1961

Abstract: The energy spectra of alpha particles from bombardment of C^{12}, O^{16} and Mg^{24} with 15 MeV deuterons have been measured at many angles between 10° and 90° (laboratory system) by means of an ionization chamber with a resolution in energy of about 1.2 %. The alpha groups leading to the 1.74 MeV, $T = 1$, 0^+ level of B^{10} and to the 2.31 MeV, $T = 1, 0^+$ level of N^{14} were not observed. The 2.22 MeV level of Na^{22} was slightly excited for angles of observation less than 40° (laboratory system) but for higher angles it appeared with an intensity comparable with the intensity of other $T = 0$ levels of Na^{22}. Angular distributions and absolute cross sections corresponding to the ground, 0.72, 2.15 and 3.58 MeV states of B^{10} to the ground state of N^{14} and to the ground 0.58, 0.89, 1.53 and 2.58 MeV states of Na^{22} are reported. The general shape of these angular distributions indicates that the (d, α) reactions, leading to the low lying states of the residual nuclei, proceed by a direct surface interaction.

Attempts to fit the data with plane and distorted wave calculation have been done.

1. Introduction

It has been observed by some authors [1]) that the angular distributions of α particles from reactions initiated by deuterons with an energy up to 21 MeV on light nuclei are frequently peaked in the forward direction and may exhibit an oscillatory behaviour. In several cases attempts have been made to fit the experimental data with the simple direct interaction theories [2]) treating the deuteron and the alpha particle as single particles and representing them by simple plane wave also during the interaction. At the present time the agreement found, even if not so good, was limited to only few of the angular distributions obtained. It is of interest, therefore, to see how in a larger number of experimental results, the theories can reproduce the shape of the angular distributions and how much improvement can be achieved by introducing distorted wave calculations [3]).

For this purpose we made an extensive study of (d, α) reactions and as targets we chose C^{12}, O^{16} and Mg^{24} which a priori seemed to be most interesting for understanding the mechanism of the reaction.

† On leave of absence from C.I.S.E.'s laboratories Milano and now at the University of Milano Physics Department.

†† Work done at Sarah Mellon Scaife Radiation Laboratory and supported by the joint program of the Office of Naval Research and U. S. Atomic Energy Commission.

In addition the nuclear properties of the residual nuclei B^{10}, N^{14} and Na^{22}, belonging to the series of nuclei with $A = 4n+2$ and $N = Z$, are of particular interest since they contain low lying $T = 1$ states.

2. Experimental Apparatus

These experiments were performed with the 15 MeV deuteron beam of the University of Pittsburgh 119 cm cyclotron. The beam was energy-analysed by

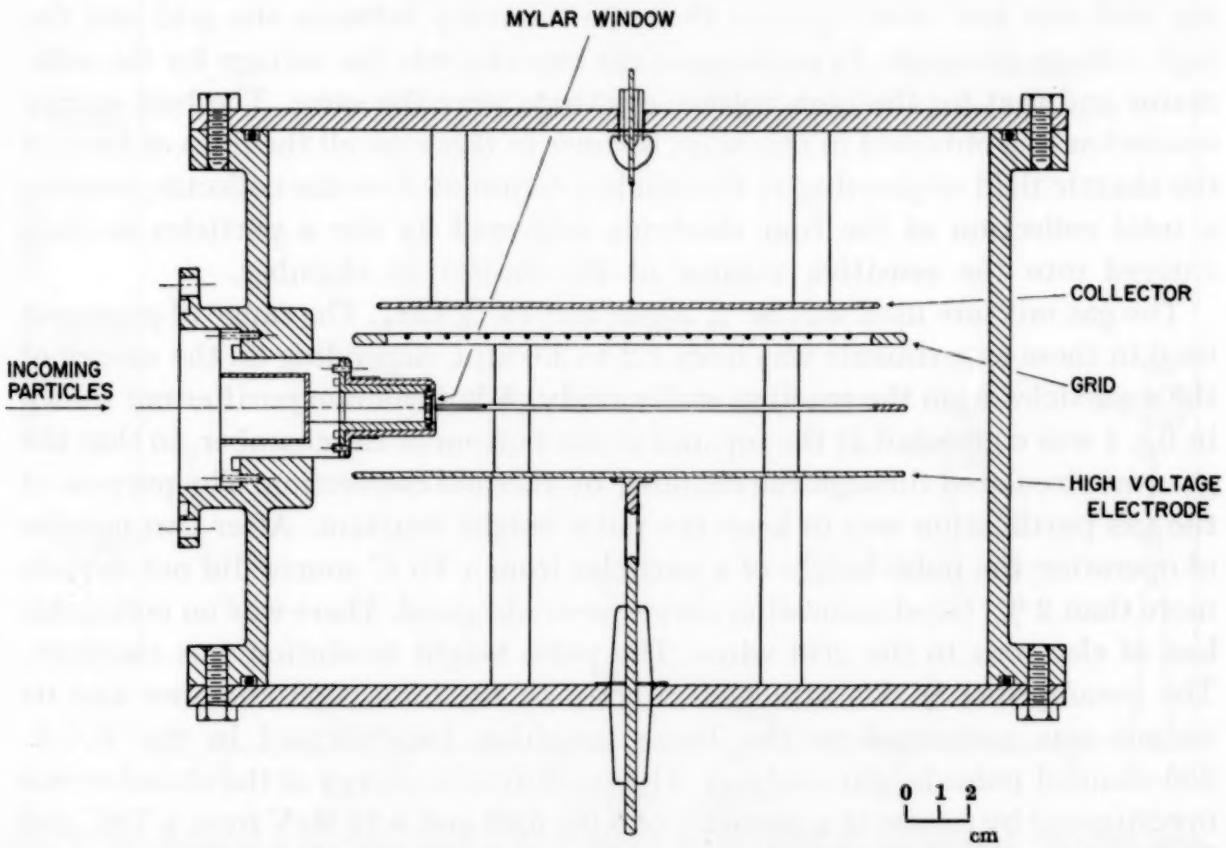

Fig. 1. Gridded ionization chamber used as α particles detector.

two magnets, focused on thin targets of the elements being studied and collected in a Faraday cup.

The α particles were detected by means of a fast ionization chamber of the electron collection type, having the geometry shown in fig. 1. The α particles passed through a 6 μm mylar window coated on its inner surface with a thin evaporated film of aluminium. The collector was a strip of brass about 1 cm wide and was supported by two insulators of teflon. The grid was made of 0.15 mm tungsten wire with a centre to centre spacing of 2 mm. The grid, guard ring and high voltage electrode were all of trapezoidal shape and were supported by four teflon insulators. The window was held in a removable collimator, which was made of a brass conductor and a plexiglass insulator. The mylar window was supported by a polished brass surface containing 37 holes of 1 mm

located in a regular pattern within a 0.9 cm diameter circle. The seals of the brass collimator to insulator and of the insulator to the grounded chamber wall were made by O-ring gaskets. The purpose of the guard ring was to connect electrically the final brass part of the collimator to the desired voltage. A resistance voltage divider distributed the voltage to the several electrodes. The high voltage electrode was maintained at about 2500 V and the grid at about 1660 V.

Under these conditions the electric field intensity between the collector and the grid was four times greater than the intensity between the grid and the high voltage electrode. In performing the experiments the voltage for the collimator and that for the high voltage electrode were the same. The best energy resolution was obtained in this way, because in this case all the lines of force of the electric field originating at the window terminated on the collector, causing a total collection of the first electrons delivered by the α particles as they entered into the sensitive volume of the ionization chamber.

The gas mixture used was 90 % argon and 10 % CH_4. The range of pressures used in these experiments was from 1.2 to 3.0 atm, depending on the energy of the α particles from the reaction under study. A hot calcium purifier not shown in fig. 1 was connected at the top and at the bottom of the chamber, so that the gas was circulated through the chamber by thermal convection. The purpose of the gas purification was to keep the pulse height constant. After two months of operation the pulse height of α particles from a Th C′ source did not deviate more than 2 %. Good saturation curves were obtained. There was no noticeable loss of electrons to the grid wires. The pulse height resolution was excellent. The preamplifier [4]) was attached directly to the ionization chamber and its output was connected to the linear amplifier incorportead in the R.C.L. 256-channel pulse-height analyser. The resolution in energy of the chamber was investigated by means of α particles of 6.05, 6.09 and 8.78 MeV from a ThC and ThC′ source. The full width at half maximum of the 8.78 MeV α particles was 114 keV and for α particles of 16 MeV was about 190 keV. This width was mainly due to the electronics and the thickness of the targets. The noise due to the ionization chamber was negligible. In our case the chamber noise involved only the straggling, the induction of positive ions and the loss of electrons to the grid wires.

Particular care was taken in the choice of the collector in order to reduce the capacitance and after several trials the strip of brass previously mentioned was adopted.

Before doing our experiments, we took particular care to study the background in order to minimize it. The detector was put in the target room near the scattering chamber. We studied the spectrum of α particles from a ThC–ThC′ source in the presence of such background. Fig. 2 shows how the background was decreased by a large amount by using a smaller sensitive volume.

This background was mainly due to the neutrons and gamma rays crossing the sensitive volume of the chamber. In all experiments a continuous low-lying spectrum of pulses from fast deuterons entering through the window was observed. The highest pulses of this sort were due to deuterons having energy to traverse the total length of the sensitive volume of the chamber. Generally, the corresponding energy limit was between 5 and 8 MeV, depending on the pressure of the gas.

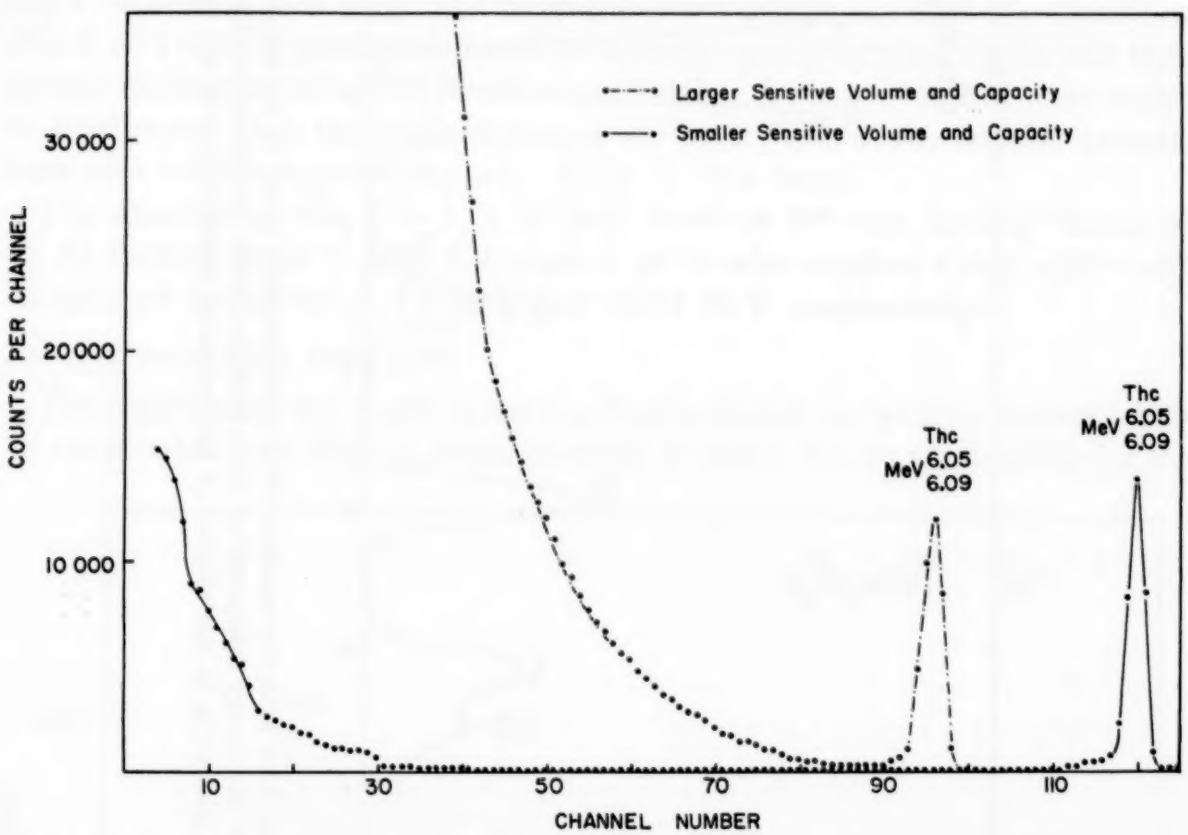

Fig. 2. Spectrum of α particles from a Th C source in presence of background obtained with a current deuteron beam of about 0.2 μA. It is evident how the use of a smaller sensitive volume and capacity shifts the background towards low energy while the pulses of the α particles are shifted towards higher channel numbers.

3. Results

3.1. THE REACTION $C^{12}(d, \alpha)B^{10}$

The target of C^{12} was prepared by cracking methyl iodide (CH_3I) on a thin tantalum strip. Fig. 3 shows the spectrum of α particles obtained at 24° (laboratory system). The energy groups correspond to the known level structure of B^{10} as reported by F. Ajzenberg-Selove and T. Lauritsen [5]). Above the 5.16 MeV level of B^{10} the level spacing is so small that our energy resolution is insufficient to separate individual peaks and permit their assignment to known levels. The rise of the spectrum shown below 4.5 MeV energy represents the onset of the deuteron background. The energy groups indicated by an arrow at

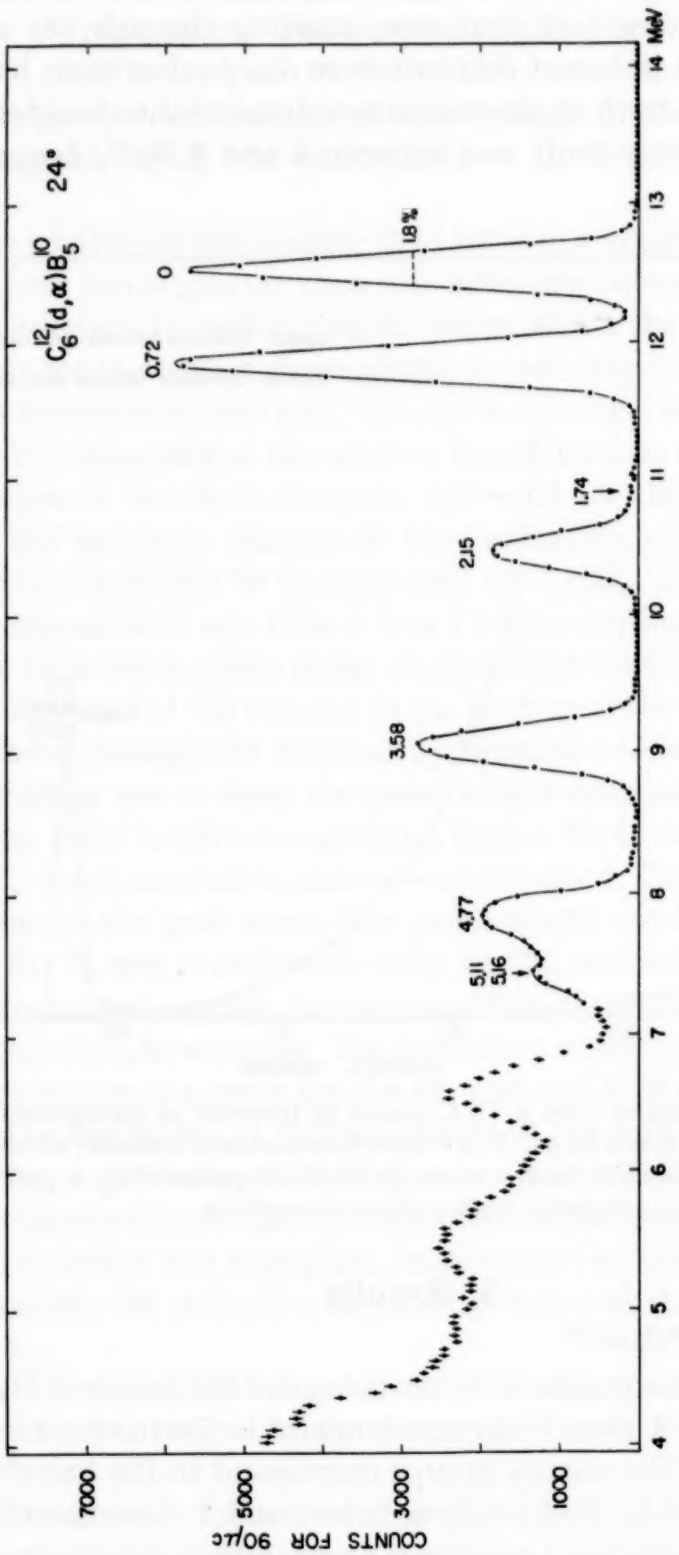

Fig. 3. Spectrum of α particles from the reaction $C^{12}(d, \alpha)B^{10}$ obtained at 24° in the laboratory system. The abscissa are the energy dissipated by the α particles inside the ionization chamber without corrections for absorption in the window of the ionization chamber and in the target

an excitation energy of 1.74 and 5.11–5.16 MeV correspond to the $T = 1$ levels of B^{10} which should not be excited in this reaction. As the 5.16 MeV level is so close to the 5.11 MeV level we cannot recognize which one of these levels contributes to the spectrum. Therefore we cannot decide whether or not the isobaric spin selection rule is obeyed. The $T = 1$, 1.74 MeV level is well separated from the $T = 0$, 2.15 MeV level and it was observed for all the angles of observation with an intensity lower than 4 % of the intensity of the neighbouring $T = 0$, 2.15 MeV level. But in this case we cannot say that the absence of this $T = 1$ state is good evidence of the isobaric spin selection rule. In fact the α groups leading to this level involve a transition from a 0^+ initial state into a 0^+ final state. Thus the conservation of the parity and of the angular momentum also inhibit appreciably any decay to this level.

The absence of the $T = 1$, 1.74 MeV level of B^{10} was already found by A. El Bedewi *et al.* [6]) and J. Català *et al.* [7]) who studied $C^{12}(d, \alpha)B^{10}$ with energies of deuterons of 8.9 MeV and 19.17 MeV, respectively.

3.2. THE REACTION $O^{16}(d, \alpha)N^{14}$

The target used was 6 μm mylar $C_{10}(H_2O)_4$ coated on both its surfaces with an evaporated gold film to avoid possible wrinkles due to the heating by the

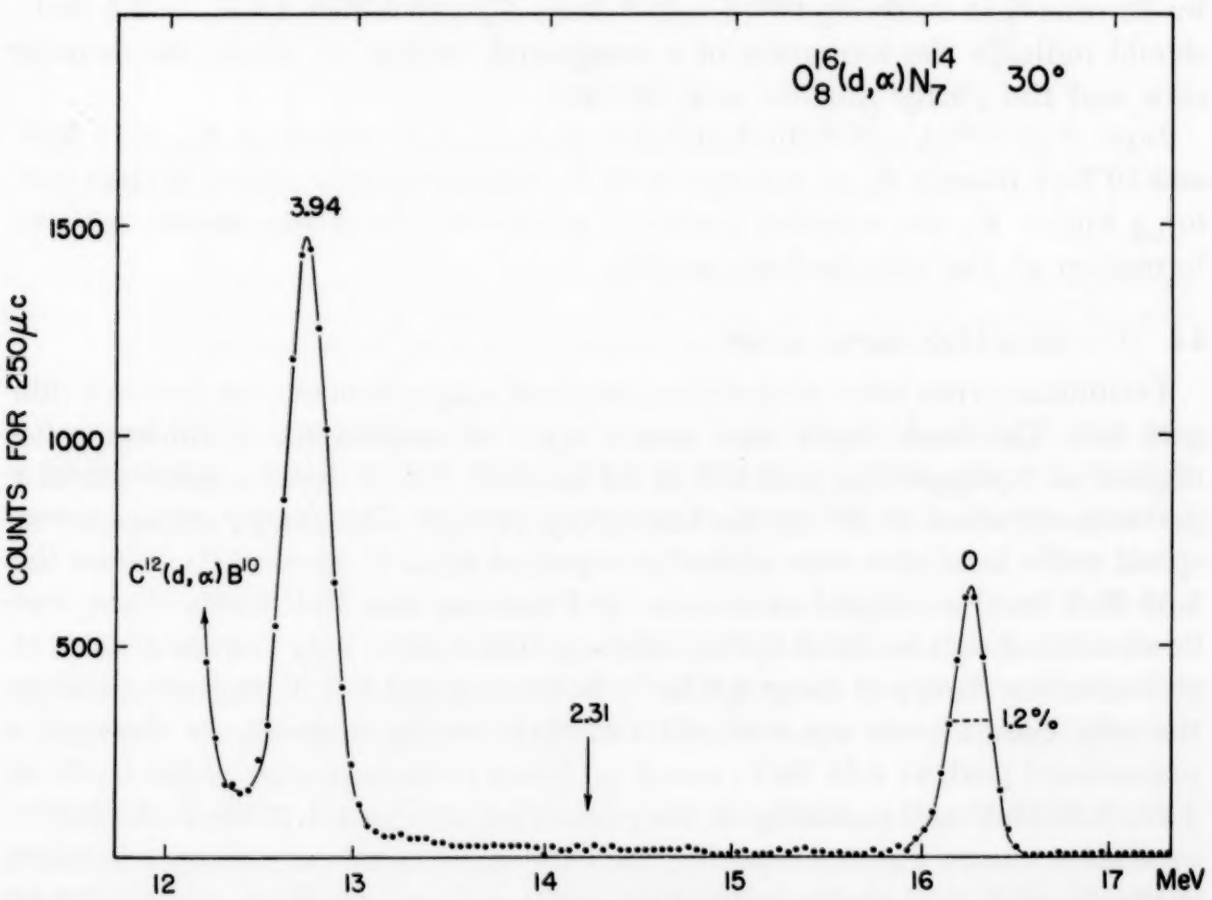

Fig. 4. Spectrum of α particles from the reaction $O^{16}(d, \alpha)N^{14}$ obtained at 30° in the laboratory system. The scale energy gives the energy dissipated inside the ionization chamber.

beam. In order to determine the stability of the target under exposure to the beam, runs were taken on the same day with different targets. No sensible variation was observed in the relative cross section and the variation of the absolute cross section was within ± 25 %. Fig. 4 shows a spectrum of α particles obtained at 30 degrees in the laboratory system. The energy groups correspond to the known levels of N^{14}. The absence of the $T = 1$, 2.31 MeV level is consistent with the isobaric spin selection rule and with the conservation of parity and angular momentum, since the transition is $0^+ \rightarrow 0^+$ as in the previous case of the 1.74 MeV level of B^{10} from $C^{12}(d, \alpha)B^{10}$. The abundance of the $T = 1$, 2.31 MeV group was less than 3 % of the abundance of the $T = 0$ ground state at all the angles of observation.

It is interesting to observe that in $O^{16}(d, \alpha)N^{14}$ the ratio of the intensities of the forbidden $T = 1$, 2.31 MeV level and the ground state of N^{14} changes with the incident energy of the deuterons (E_d). C. Brown [8]) with E_d ranging from 5.5 MeV to 7.5 MeV observed this ratio to be on the average 0.05; Freementle *et al.* [9]) observed at $E_d = 19$ MeV this ratio to be 0.036.

The appearance of the forbidden group at different bombarding energies must not be interpreted as a violation of both conservation rules; in fact the resonance yield curve of α particles leading to the first excited state of N^{14} found by Browne [8]) in studying $O^{16}(d, \alpha)N^{14}$ from $E_d = 5.5$ MeV to $E_d = 7.5$ MeV, should indicate the formation of a compound nucleus in which the isobaric spin and the parity are not well defined.

Now, if in $O^{16}(d, \alpha)N^{14}$ the forbidden group is less excited at $E_d = 15$ MeV and 19 MeV than at $E_d = 5.5$ and 7.5 MeV, this is probably due to the fact that for a higher E_d the reaction proceeds mostly by direct interaction without formation of the intermediate system.

3.3. THE REACTION $Mg^{24}(d, \alpha)Na^{22}$

Preliminary runs were made with a target of magnesium evaporated on a thin gold foil. The final target used was a layer of magnesium of thickness 0.3 mg/cm^2 on a supporting gold foil of 0.2 mg/cm^2. Fig. 5 shows a spectrum of α particles obtained at 25° in the laboratory system. The energy groups correspond to the level structure of Na^{22} as reported by C. P. Browne [10]). Above the 3.53 MeV level we should expect the 3.71 and the 3.94 MeV levels. These two levels are not well resolved by the detector, which gives only one component at an excitation energy of about 3.9 MeV. Between 4 and 5 MeV excitation energy the only known levels are 4.32 and 4.47 MeV. As fig. 5 shows, we observed a pronounced peak at 4.53 MeV, which probably is the resultant of the levels at 4.32, 4.47 MeV and partially of the close level at about 4.77 MeV. At higher excitation energy the level spacing becomes smaller and our energy resolution is insufficient to separate individual peaks and permit their assignment to known levels. Furthermore, looking at the peaks at the excitation energy be-

tween 6 and 8 MeV, they appear significantly wider than the resolution of our equipment, indicating that only a small fraction of the higher excited states show up as single peaks. The energy group labelled N^{14} is due to the reaction $O^{16}(d, \alpha)N^{14}$ ground state from an impurity of O^{16} in the target. The $T = 1$, 2.31 MeV level of N^{14}, previously investigated, does not appear. The 3.94 MeV level of N^{14} should occur close to the 2.97 and 3.07 MeV levels of Na^{22}. The 4.91, 5.10, 5.69 MeV and higher levels of N^{14} should appear in the region above 4 MeV excitation energy of Na^{22}, partially altering the spectrum obtained.

In studying the angular distribution we directed our attention only to the first few excited levels of Na^{22} up to the 2.58 MeV level, where the only extra-

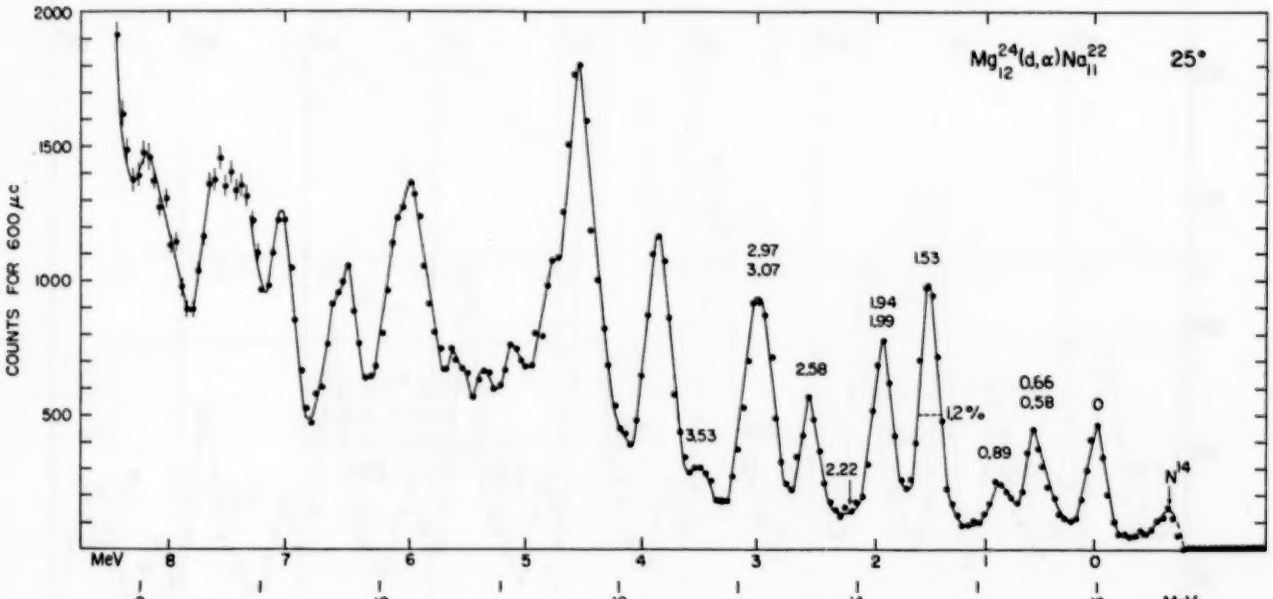

Fig. 5. Spectrum of α particle from the reaction $Mg^{24}(d, \alpha)Na^{22}$ obtained at 25° in the laboratory system. The scale above the axis gives the excitation energy of the residual nucleus. The scale below the axis gives the energy dissipated inside the ionization chamber.

neous α particles group was due to the ground state of N^{14}. Possible groups of α particles arising from the bombardment of deuterons in the Mg^{25} and Mg^{26} isotopes of the natural targets have not been observed. In fact the Q-values of the $Mg^{25}(d, \alpha)Na^{23}$ and $Mg^{26}(d, \alpha)Na^{24}$ reactions are 7.04 and 2.88 MeV, respectively. Their difference from the Q-value of the $Mg^{24}(d, \alpha)Na^{22}$, which is 1.954 MeV, should have led easily, by studying the observed spectra at several angles, to the identification of levels not belonging to the Na^{22} nucleus. The background due to the supporting gold foil of the target was almost negligible in all the spectra observed.

The Na^{22} nucleus has been one of the most recently investigated in order to establish the energies of the first and second $T = 1$ states. Temmer and Heydenburg [11]), from investigation of the $Ne^{20}(He^3, p\gamma)Na^{22}$ and $F^{19}(\alpha, n\gamma)Na^{22}$ reactions, have proposed the 0.66 MeV, $J = 0^+$ level as the first $T = 1$ state.

Krone and Singh [12]), by studying the $Ne^{21}(p, \gamma)Na^{22}$ reaction, conclude that the second $T = 1$ state is the 2.2 MeV $J = 2^+$ level. Judging by the excitation in energy of the first level in the neighbouring isobar Ne^{22}, they indicate the 0.92 MeV, $J = 0^+$ level as the possible first $T = 1$ state. However, C. P. Browne [10]), by investigating the $Mg^{24}(d, \alpha)Na^{22}$ and $Mg^{25}(p, \alpha)Na^{22}$ reactions, concludes that the first $T = 1$ state is the 0.66 MeV level, by exciting this level with the second reaction and not with the first one.

In our experiment the $T = 1$, 0^+, 0.66 MeV level is so close to the 0.58 MeV level that our energy resolution is insufficient to give any information about its intensity. For the 2.22 MeV level indicated by an arrow in fig. 5, even if its

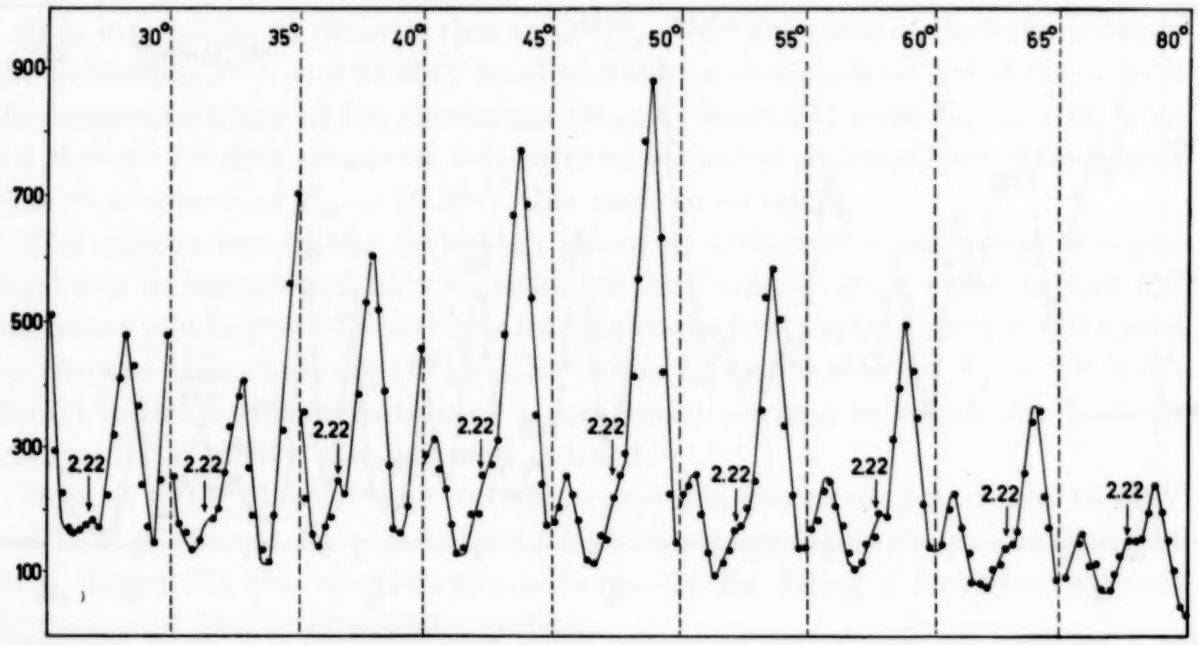

Fig. 6. Spectrum of the α groups leading to the 2.22 MeV state of Na^{22} as appeared at the different angles of observation. Even if the 2.22 MeV level is not well separated from the neighbouring levels 1.99–1.94 MeV, it is evidently a component of this group.

existence at 25° is very questionable, it appeared for angles higher than 40° (lab. system) with an intensity which was comparable with the intensity of the 0.58, 0.89, 2.58 and 3.53 MeV levels of Na^{22}. Fig. 6 shows how the 2.22 MeV level appeared at the several angles of observation. This result, coupled with the fact that if the 0.66 MeV level is the first $T = 1$ state, the second $T = 1$ state should be expected at an excitation energy lower than 2.22 MeV, leads to the conclusion that the 2.22 MeV level is not a $T = 1$ but a $T = 0$ level.

On the other hand this second $T = 1$ state should be found in the region about 2 MeV where the only known levels are 1.99 and 1.94 MeV. Nothing can be said about the intensity of each of these two levels, which are too close to be separated with our energy resolution. However, C. P. Browne [10]) observed both components in $Mg^{24}(d, \alpha)Na^{22}$.

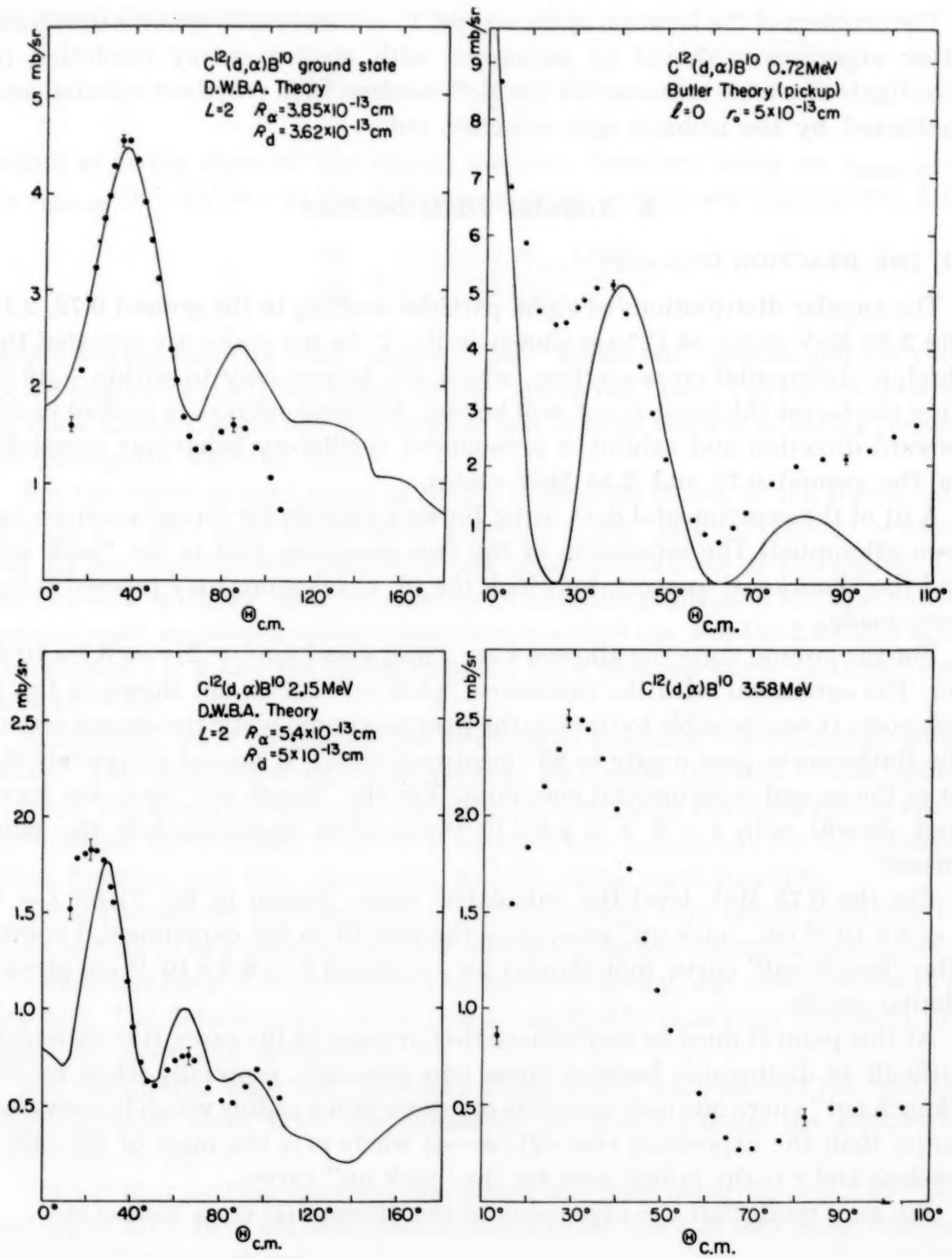

Fig. 7. Angular distributions of the α particles leading to the ground, 0.72, 2.15 and 3.58 MeV states of B^{10} from C^{12}(d, α)B^{10} reaction. The solid curves for the ground state and the 2.15 MeV state were calculated with distorted waves using $l = 2$, $R_\alpha = 3.85 \times 10^{-13}$ cm, $R_d = 3.62 \times 10^{-13}$ cm and $l = 2$, $R_\alpha = 5.4 \times 10^{-13}$ cm, $R_d = 5 \times 10^{-13}$ cm, respectively. The solid curve for the 0.72 MeV state was calculated on Butler's theory for "pick up" process with $l = 0$, $r = 5 \times 10^{-13}$ cm[13].

The problem of the location of the second $T = 1$ state still remains unsolved. Other experiments should be performed with greater energy resolution to investigate the level structure of the Na^{22} nucleus with reactions affected and unaffected by the isobaric spin selection rule.

4. Angular Distributions

4.1. THE REACTION $C^{12}(d, \alpha)B^{10}$

The angular distributions of alpha particles leading to the ground 0.72, 2.15 and 3.58 MeV states of B^{10} are shown in fig. 7. In the scales are reported the absolute differential cross sections, which are known only to within ± 40 % since the target thickness is not well known. All these curves are peaked in the forward direction and exhibit a pronounced oscillatory behaviour especially for the ground 0.72 and 2.15 MeV states.

A fit of the experimental data using Butler's formula for direct reactions has been attempted. The separation of the two processes, that is the "pick up" and the "knockout" process, by which the (d, α) reactions may proceed [1]) has been made.

For the ground state the allowed l are 2 and 4 and for $l = 2$, $r = 3.6 \times 10^{-13}$ cm. The agreement with the calculated "pick up" curve, not shown in fig. 7, was poor. It was possible to fit only the first maximum while the second zero of the Butler curve goes nearly to 85° (centre-of-mass). It missed completely the fit of the second experimental maximum. For the "knock out" case, the curve (not shown) with $l = 2$, $r = 4.5 \times 10^{-13}$ cm gives approximately the same answer.

For the 0.72 MeV level the calculated curve (shown in fig. 7) for $l = 0$, $r = 5 \times 10^{-13}$ cm, "pick up" case, gives the best fit to the experimental points. The "knock out" curve (not shown) for $l = 0$ and $r = 6.5 \times 10^{-13}$ cm gives a similar result.

At this point it must be emphasized that, in most of the cases, it is extremely difficult to distinguish between these two processes, especially when for the "knock out" curve one uses as radius of interaction a radius which is somewhat larger than the expression $r(m-2)/(m-4)$ where m is the mass of the initial nucleus and r is the radius used for the "pick up" curve.

We may recall that the expression of the differential cross section is

$$\frac{d\sigma}{d\Omega} \propto \left[\frac{G_l(y) j_l(x) + x j_{l-1}(x)}{x^2 + y^2}\right]^2,$$

where $x = q(\Theta)r$ and $y = Kr$ are related to the momentum transfer and to the binding energy while $G_l(y)$ is a constant factor depending on l and y. The momentum transfers in a "pick up" and in a "knock out" process are related

by the following expression:

$$q(\Theta)_{\text{knock out}} = \frac{m-4}{m-2}\, q(\Theta)_{\text{pick up}},$$

where m is the mass of the initial nucleus; therefore using as $r_{\text{knock out}} = r_{\text{pick up}}\ (m-2)/(m-4)$ the differential cross section will assume the form

$$\frac{\mathrm{d}\sigma}{\mathrm{d}\Omega} \propto \left[\frac{cj_l(x)+xj_{l-1}(x)}{x^2+c^2}\right]^2,$$

where x is the same for both "pick up" and "knock out" process and the value of the constant c is slightly bigger for the "knock out" case. The curves obtained in these circumstances are very similar and in most cases it is hardly possible to distinguish between them.

For the higher excited states of B^{10} the theoretical curves do not fit the data. For the 2.15 MeV state the allowed l are 0 and 2; the "pick up" curve $l = 0$ does not fit the experimental points for any reasonable choice of the radius. The curve $l = 2$ "pick up" case, in order to fit only the position of the first experimental peak, requires a radius larger than 9×10^{-13} cm. For the 3.58 MeV state the allowed l is 2 and the radius required for a pick up curve is larger than 10×10^{-13} cm.

A distorted wave calculation has been made assuming a pure surface interaction. This interaction was approximated by a delta function on the nuclear surface. The distorted wave was obtained by employing the black sphere model as modified by McIntyre *et al.* [13]); it requires two parameters for the deuteron wave function and two parameters for the alpha wave function.

These parameters were guessed at and the results were sealed assuming the cross section to be a function of $KR\Theta$, where R refers to the radius parameter of the wave functions. The normalization, being arbitrary, was also adjusted to fit the data. The details of the calculation as applied to (α, α') are discussed in a paper by Rost and Austern [3]).

For the ground state and 2.15 MeV state of B^{10}, we obtained the best fits with distorted wave Born approximation (D.W.B.A.) using the parameters indicated on fig. 7.

For the first excited state the agreement was poor using $R_\alpha = 5\times 10^{-13}$ cm and $R_d = 4.7\times 10^{-13}$ cm. The calculated curve for the 3.58 MeV state does not fit the experimental points.

4.2. THE REACTION $O^{16}(d, \alpha)N^{14}$

In fig. 8 is shown the angular distribution corresponding to the ground state of N^{14}. The absolute differential cross section indicated on the scales is known only to within $\pm 25\ \%$ as previously mentioned.

The Butler curve for $l = 0$ and $r = 4.2 \times 10^{-13}$ cm "knock out" case shown in fig. 8 yields the best fit obtainable. To fit with a "pick up" curve we had to use too small a radius.

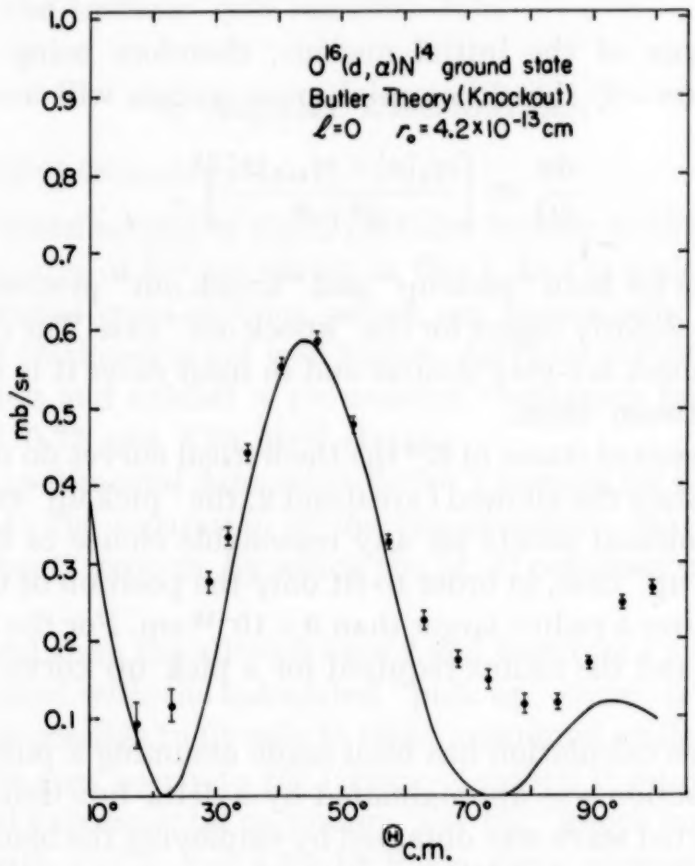

Fig. 8. Angular distribution of the ground state of N^{14} from $O^{16}(d, \alpha)N^{14}$. The solid curve was calculated for the "knock out" process of Butler's theory with $r = 4.2 \times 10^{-13}$ cm and $l = 0$.

The distorted wave calculation does not fit the data.

4.3. THE REACTION $Mg^{24}(d, \alpha)Na^{22}$

In figs. 9 and 10 are shown the angular distributions of alpha particles leading to the ground, 0.58, 0.89, 1.53 and 2.58 MeV states of Na^{22} †). The absolute differential cross sections are given within ± 30 % for the non-uniformity of the target. The general shape of these curves is similar to those obtained on C^{12} and O^{16} indicating a pure direct surface interaction.

The best fits obtained with D.W.B.A. theory are shown in fig. 9 for the ground state and for the 0.89 MeV state, while the agreement for the other states was poor.

The Butler calculations give poor agreement for the ground state and the 0.58 MeV state. They do not fit the 0.89 MeV state and give reasonable fits for

† The error indicated in all the curves obtained includes the uncertainties due to the statistics and to the background.

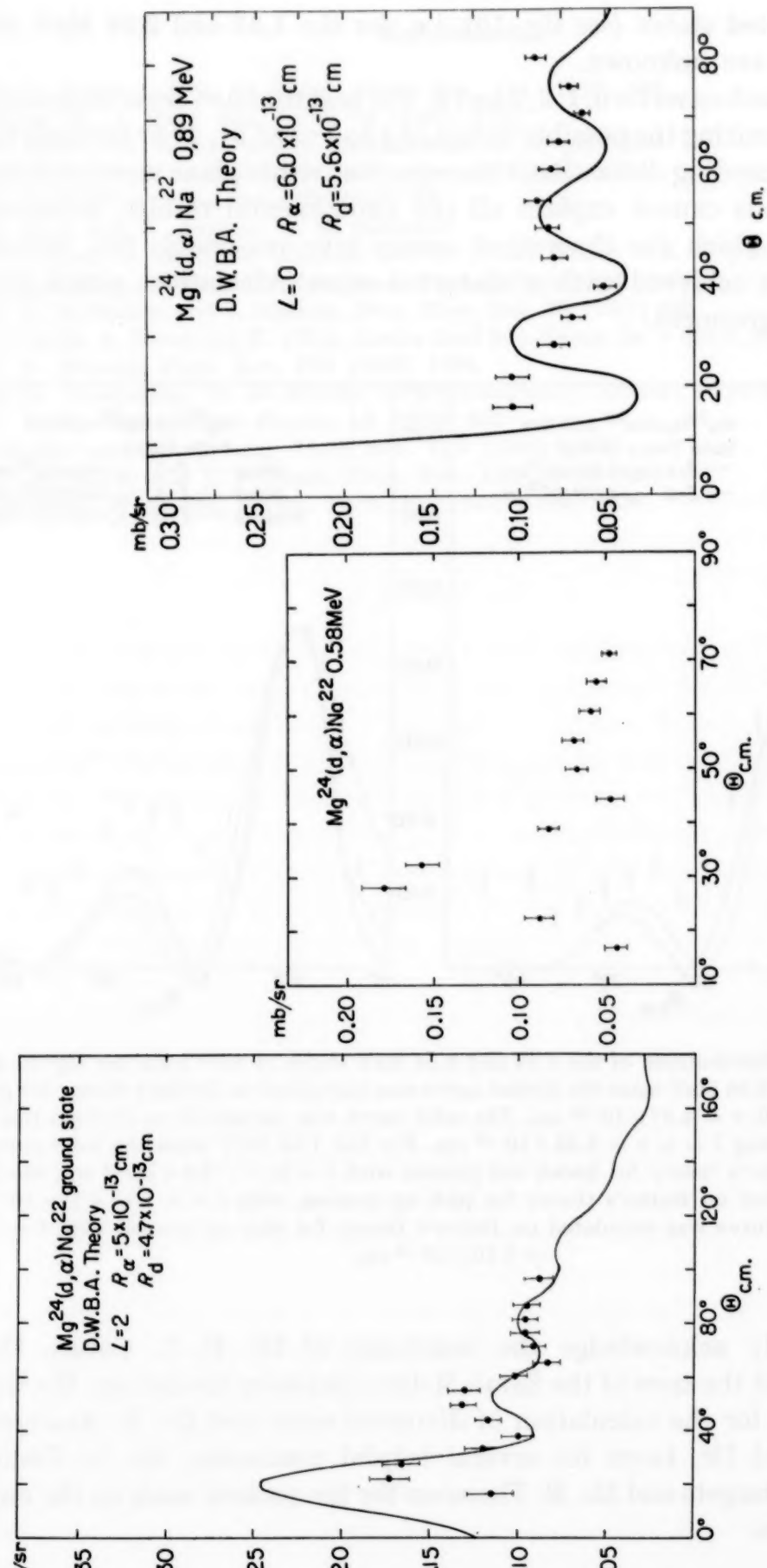

Fig. 9. Angular distributions of the ground, 0.58 and 0.89 MeV states of Na^{22} from the Mg^{24}(d, α) Na^{22} reaction. The solid curves were calculated with distorted wave Born approximation (D.W.B.A.) using for the ground state $R_\alpha = 5 \times 10^{-13}$ cm, $R_d = 4.7 \times 10^{-13}$ cm, $l = 2$ and for the 0.89 MeV state $R_\alpha = 6 \times 10^{-13}$ cm, R_d 5.6×10^{-13} cm, $l = 0$.

the higher excited states (see fig. 10), i.e. for the 1.53 and 2.58 MeV states, whose parities are unknown.

We tried for both cases $l=0, 1, 2, 3$ and 4. The best fits have been obtained with $l=0$ and $l=4$, limiting the possible values of J to 1^+ and 3^+, 4^+ 5^+ for both levels.

From the preceeding discussion it emerges that either plane wave or distorted wave calculations cannot explain all the experimental results. However, in those cases in which the theoretical curves give reasonable fits, noticeable improvement is achieved with a distorted wave calculation, which gives a much better agreement.

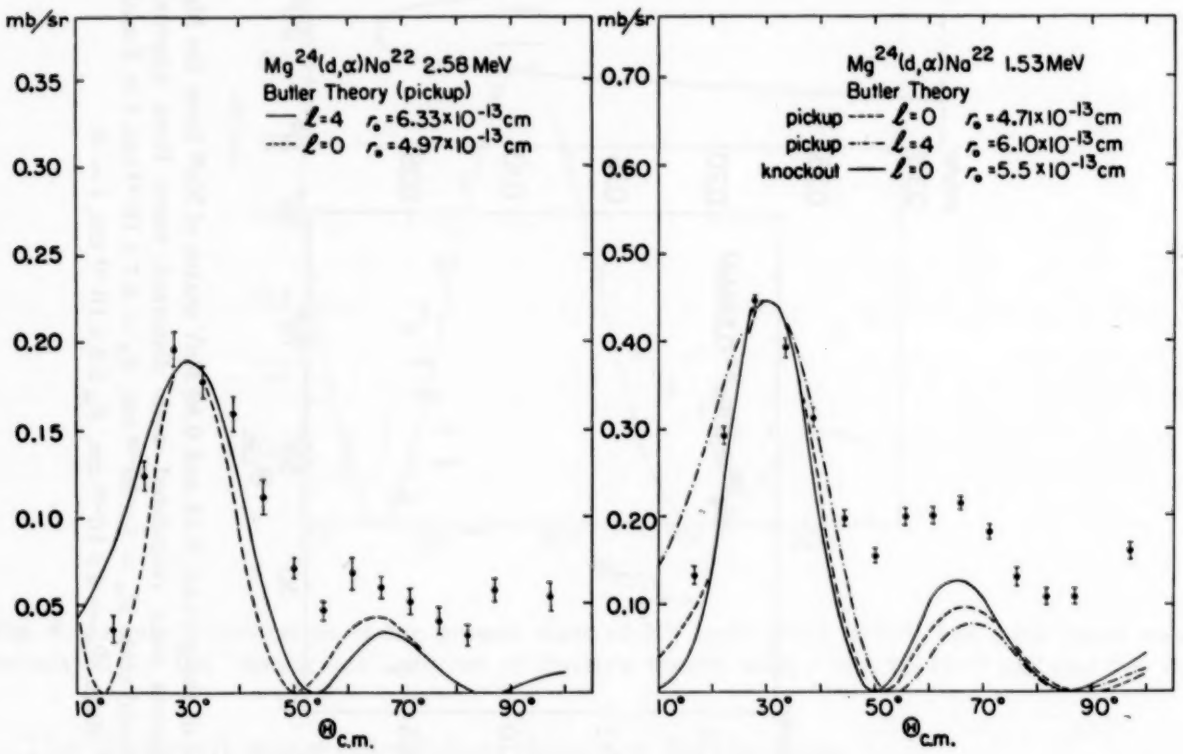

Fig. 10. Angular distributions of the 1.53 and 2.58 MeV states of Na^{22} from the $Mg^{24}(d, \alpha)Na^{22}$ reactions. For the 2.58 MeV state the dotted curve was calculated on Butler's theory for pick up process using $l = 0$, $r = 4.97 \times 10^{-13}$ cm. The solid curve was calculated on Butler's theory for pick-up process using $l = 4$, $r = 6.33 \times 10^{-13}$ cm. For the 1.53 MeV state the solid curve was calculated on Butler's theory for knock out process with $l = 0$, $r = 5.5 \times 10^{-13}$ cm; the dotted curve was calculated on Butler's theory for pick up process, with $l = 0$, $r = 4.71 \times 10^{-13}$ cm; the point dotted curve was calculated on Butler's theory for pick up process with $l = 4$, $r = 6.10 \times 10^{-13}$ cm.

We gratefully acknowledge the assistance of Dr. B. L. Cohen, Dr. K. Quisinberry and the crew of the Sarah Mellon cyclotron laboratory. We wish to thank E. Rost for the calculation of distorted wave and Dr. N. Austern, Dr. S. Yoshida and Dr. Isoya for several helpful comments, Mr. G. Fodor for furnishing the targets and Mr. B. Thomson for his patient work on the numerical calculations.

References

1) G. E. Fisher and V. K. Fisher, Phys. Rev. **114** (1959) 533;
Chuin Hu, J. Phys. Soc. Japan **15** (1960) 1741;
N. Cindro, M. Cerineo and A. Strzalkowski, to be published
2) Austern, Butler and McManus, Phys. Rev. **97** (1955) 132;
El.-Nadi, Proc. Phys. Soc. **70** (1957) 62
3) E. Rost and N. Austern, to be published
4) C. Cottini, E. Gatti, G. Giannelli and G. Rozzi, Nuovo Cim. **2** (1955) 988
5) F. Ajzenberg-Selove and T. Lauritsen, Nuclear Physics **11** (1960) 1
6) F. A. El Bedewi and I. Hussein, Proc. Phys. Soc. **70** (1957) 233
7) J. Catala, A. Bonet and E. Villar, Anales Real Soc. Espan. fis. y quim. Madrid **54** (1958) 241
8) C. P. Browne, Phys. Rev. **104** (1956) 1598
9) R. G. Freemantle, W. M. Gibson, O. J. Prowse and J. Rotblat, Phys. Rev. **92** (1953) 1268
10) C. P. Browne, Nuclear Physics **12** (1959) 662
11) Temmer and Heydenburg, Phys. Rev. **111** (1958) 1663
12) R. W. Krone and J. J. Singh, Phys. Rev. **117** (1960) 1562
13) McIntyre, Wang and Becker, Phys. Rev. **117** (1960) 1337

8.C

Nuclear Physics **24** (1961) 388—399; © *North-Holland Publishing Co., Amsterdam*

Not to be reproduced by photoprint or microfilm without written permission from the publisher

ON THE NATURE OF THE ELECTROMAGNETIC FIELD

TETSUO GOTŌ

Department of Physics, College of Science and Engineering, Nihon University, Tokyo

Received 5 December 1960

Abstract: Attempting to identify the electromagnetic field as an affine connexion for spinors, we investigate the nature of the electromagnetic interaction and the electric charge. All spinors interact with the electromagnetic field. Possibility of charge independence is studied. In our opinion, the violation of the charge independence by the electromagnetic field is caused by the violation of the flatness of space-time.

1. Introduction

Models of elementary particles have been proposed by many authors from various points of view. Especially, one of the most important aims of the theories and models already proposed is to derive the isobaric multiplets on the basis of simple or intuitive assumptions, for phenomenologically the isobaric multiplets of strongly interacting particles are the most characteristic.

Though the isobaric multiplet structure is an important character of the strongly interacting particles, it is worth remembering that the isobaric spin seems to be closely connected with the electric charge. Why are there special relations between the electric charge and the third component of the isospin? And why is the symmetry of the charge independence violated by the electromagnetic interaction? Also other internal quantum numbers, the strangeness and the nucleon number, seem to have close connection with the electric charge. Thus, it may be considered that the internal structure of elementary particles is essentially related to the electric charge. Although the theories and models proposed by many authors have symmetries convenient for explaining the phenomenological symmetry of the charge independence and can derive the degeneracies of the mass eigenvalues, they cannot explain clearly the reason why the quantum numbers are related to the electric charge and the reason why the symmetry of the charge independence is violated and the mass levels are split by the existence of the electromagnetic interaction. For example, in the model of the rigid body or the model of the relativistic rotator [1]) there exist internal rotational degrees of freedom which seem to correspond to the isospin. We cannot, however, understand the reason why the internal rotation of the rigid body is related to the electric charge. In Heisenberg's non-linear theory [2]), the problem of the electric charge and the electromagnetic field will

not be clear until the dynamical problem is solved. Thus, on the basis of this theory, we cannot say anything about the relation between the electric charge and the isospin at the present stage. In the composite model and the related theories [3]), it seems that the electromagnetic field has a special situation among many other fields. Of course, it is easy to say that the electromagnetic field is also a composite one. If it is so, however, we cannot say anything about the relation between the electric charge and the isospin until the dynamical problem is solved.

It seems to us that the symmetry of the charge independence and the violation of the charge independence by the presence of the electromagnetic interaction are the most important features of the internal structure of the strongly interacting particles. In our opinion, this fact has an intimate relation to the nature of the electromagnetic field and the electric charge. So we hope that the relation between the electric charge and the isospin and the reason for the violation of the symmetry in the presence of the electromagnetic interaction will be understood by the study of the nature of the electromagnetic field and the electric charge.

After Einstein's gravitation theory, there have been many attempts to unify the electromagnetic field and the gravitational field. At that time, however, physicists did not know the variety of elementary particles or fields and then the unified theory was only an academic one and had no connection with the problem of the structure of elementary particles. Recently, Hara [4]) attempted to amalgamate the so-called isospace and the usual four dimensional space-time by interpreting geometrically the electromagnetic field and the electric charge on the basis of Kaluza's five-dimensional unified theory [5]). In Kaluza's theory, the metric tensor of the five-dimensional space is composed of the electromagnetic field and the gravitational field. Thus the electromagnetic field is essentially related to the space-time structure. The charge is proportional to the momentum canonically conjugated to the fifth coordinate. Hara showed that Klein's coordinate transformation contained the rotation group in the three-dimensional Lorentz space (not Euclidean space!). Anyhow, in his theory, the electromagnetic field occupies a special place among many other fields, as does the gravitational field. And this fact played an essential role in the amalgamation of the isospace and the ordinary space-time.

In contrast with Hara's opinion, we attempt to interpret the electromagnetic field geometrically in the framework of the ordinary four-dimensional space-time and to study the nature of the electric charge.

In general, the structure of a space is prescribed by a metric tensor g_{ik} and an affine connexion Γ^i_{jk}. However, when we need to treat spinor quantities, an affine connexion Γ_k for spinor quantities, which is 4×4 matrix, must be also given. Thus, the structure of a space is perfectly determined by three quantities g_{ik}, Γ^i_{jk} and Γ_k. When we assume that Γ^i_{jk} is symmetric, i.e. $\Gamma^i_{jk} = \Gamma^i_{kj}$, it is

expressed by the metric tensor g_{ik} and its derivatives. However, even in this case, Γ_k is not determined uniquely. The equations for determining Γ_k are invariant under the transformation $\Gamma_k \to \Gamma_k + iA_k$, where $A_k(x)$ is an arbitrary vector field. Thus, if we treat spinor quantities, it is necessary to prescribe a vector field $A_k(x)$. We identify this vector field with the electromagnetic field. From this viewpoint, the electromagnetic field is closely related to the structure of space-time.

A similar idea to the above concerning the electromagnetic field was already proposed by H. Weyl [7]). In his unified theory, Weyl attempted to introduce the electromagnetic field in an affine connexion Γ^i_{jk} for tensorial quantities. At that time, the importance of spinor quantities was not recognized. After the discovery of the Dirac equation, the generalization of the equation in the presence of the gravitational field was made and then the theory of spinors in curved space was developed [8]). Infeld and van der Waerden [8]) pointed out the arbitrariness of Γ_k and suggested that we made use of this arbitrariness for introducing the electromagnetic field. In this note, we intend to develop this idea about the electromagnetic field.

From the viewpoint stated above, the electromagnetic field and the gravitational field are the fields which prescribe the structure of space-time and occupy a special position among many other fields. In contrast with the gravitational field, the electromagnetic field has a special relation to spinor quantities. In our opinion, the effect of the presence of the electromagnetic field appears only when there exist dynamical quantities described essentially by spinors. In section 2, we summarize some mathematical results and discuss the parallel displacement for spinor and tensorial quantities. We show in section 3 that the electric charge must be considered as a dynamical quantity described essentially by a spinor. As the electric charge and the electromagnetic field are intimately connected and from our viewpoint the electromagnetic field prescribes the character of space-time for spinor quantities, it is natural that the electric charge and spinors should be closely related to each other. After considering the dynamical nature of the electric charge, we discuss the possibility of introducing the isospin and the strangeness in sections 4 and 5. In section 6, we consider the gauge transformation and some miscellaneous problems.

In this note, we do not intend to construct a realastic model for unified description of elementary particles, but to clarify the nature of the electromagnetic field and the electric charge and to discuss the possibility of introducing some internal variables (viz. the isospin, the strangeness and the nucleon number).

2. Spinors in Curved Space

In this section, let us survey some geometrical characters of spinors in a generally curved space. Throughout this note we consider four component

spinors. The precise formulation of spinor theory in curved space was given by Infeld and van der Waerden; we follow here, for the sake of simplicity, a paper by Schrödinger and Bargmann [8]).

There are three fundamental quantities in a given space: a metric tensor g_{ik}, generalized Dirac matrices $\gamma^{\alpha}_{\beta,k}$ and an affine connexion $\Gamma^{\alpha}_{\beta,k}$ for spinors. (For the suffices of world tensors we use Latin letters and for those of spinors Greek letters). An affine connexion Γ^{i}_{jk} is expressed in terms of g_{ik} and its derivatives on assumption of symmetric affinity, i.e. $\Gamma^{i}_{jk} = \Gamma^{i}_{kj}$. The following relations hold between these fundamental quantities:

$$\gamma_i\gamma_k+\gamma_k\gamma_i = 2g_{ik}, \tag{2.1}$$

$$\frac{\partial\gamma_i}{\partial x_l} - \Gamma^{j}_{il}\gamma_j+\Gamma_l\gamma_i-\gamma_i\Gamma_l = 0, \tag{2.2}$$

$$\Phi_{kl}\gamma_i-\gamma_i\Phi_{kl} = R^{j}_{kli}\gamma_j, \tag{2.3}$$

where

$$\Phi_{kl} = \frac{\partial\Gamma_l}{\partial x_k} - \frac{\partial\Gamma_k}{\partial x_l} +\Gamma_l\Gamma_k-\Gamma_k\Gamma_l \tag{2.4}$$

and R^{j}_{kli} is a Riemann's curvature tensor, i.e.

$$R^{i}_{klm} = -\frac{\partial\Gamma^{i}_{kl}}{\partial x_m} + \frac{\partial\Gamma^{i}_{km}}{\partial x_l} + \Gamma^{i}_{jl}\Gamma^{j}_{km}-\Gamma^{i}_{jm}\Gamma^{j}_{kl}. \tag{2.5}$$

From eq. (2.1), generalized matrices γ_k's are determined by a given metric tensor g_{ik}. And using eqs. (2.2)–(2.5), we obtain

$$\Phi^{kl} = -\tfrac{1}{4}R_{klij}S^{ij} +\tfrac{1}{2}ief_{kl}1, \tag{2.6}$$

where

$$S^{ij} = \tfrac{1}{2}[\gamma^i\gamma^j-\gamma^j\gamma^i], \quad \gamma^i = g^{ik}\gamma_k, \tag{2.7}$$

1 denotes the 4×4 unit matrix and f_{kl} is an arbitrary antisymmetric tensor. Then, if we assume that there is no gravitational field, or that the space-time is flat, Γ_k is almost determined and the result is as follows:

$$\Gamma^{\alpha}_{\beta,k} = \tfrac{1}{2}ieA_k(x)\delta_{\beta}{}^{\alpha}, \tag{2.8}$$

where $A_k(x)$ is an arbitrary real vector field and e is a constant. (The reason why Γ_k must be pure imaginary in (2.8) is not clear only from eqs. (2.1)–(2.7). A precise discussion is given by Infeld and van der Waerden.) The tensor f_{ik} is expressed by $A_k(x)$ as follows:

$$f_{ik} = \frac{\partial A_k}{\partial x_i} - \frac{\partial A_i}{\partial x_k}. \tag{2.9}$$

The covariant derivative of a spinor field $\psi^\alpha(x)$ is defined by

$$\psi^\alpha_{|k}(x) = \partial_k \psi^\alpha(x) - \Gamma^\alpha_{\beta,k}\psi^\beta(x), \tag{2.10}$$

and in the case of no gravitational field becomes

$$\psi^\alpha_{|k}(x) = \partial_k \psi^\alpha(x) - \tfrac{1}{2}ieA_k(x)\psi^\alpha(x) = (\partial_k - \tfrac{1}{2}ieA_k(x))\psi^\alpha(x). \tag{2.11}$$

Now, we consider the parallel displacement of tensorial and spinor quantities. For example, we consider the parallel displacement of a vector p^i (not a vector

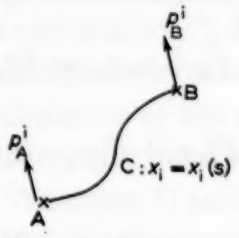

Fig. 1.

field) given at a point A from a point A to a point B along a given curve $C(C : x_i = x_i(s))$; see fig. 1. In this case, we must treat the following equation as an initial value problem:

$$\frac{dp^i}{ds} + \Gamma^i_{jk}p^j\frac{dx^k}{ds} = 0. \tag{2.12}$$

Similarly, if we consider the parallel displacement of a spinor (not a spinor field but a spinor given at a point A), the following equation must be studied:

$$\frac{d\xi^\alpha}{ds} + \Gamma^\alpha_{\beta,k}\frac{dx^k}{ds}\xi^\beta = 0. \tag{2.13}$$

If there is no gravitational field, the equations (2.12) and (2.13) become †

$$\frac{dp^i}{ds} = 0, \tag{2.12'}$$

$$\frac{d\xi}{ds} + \tfrac{1}{2}ieA_k(x)\frac{dx^k}{ds}\xi = 0. \tag{2.13'}$$

Then, as far as we treat tensorial quantities in the case of no gravitational field, we can consider that the space-time is flat. However, if we must treat spinors, we cannot consider the space-time to be flat even if there is no gravitational field. In order to consider the space-time to be completely flat, the electromagnetic field $A_k(x)$ must also be zero.

† With regard to eq. (2.13′) we remark, that, as will be shown by eq. (2.14), we of course can obtain the equation of parallel displacement for ξ as $d\xi/ds = 0$ by a suitable choice of the coordinate system in spin space. However, the choice of the coordinate system in spin space should depend on the curve or integral path C.

From now, since we confine ourselves to the usual Minkowski space, it is sufficient to take Γ_k as given by the eq. (2.8). And then for the parallel displacement we need to consider eqs. (2.12′) and (2.13′). Integrating (2.13′) we obtain that

$$\xi^\alpha = \xi_0{}^\alpha \exp\left[-\tfrac{1}{2}ie\int_C \mathrm{d}x_k A^k(x)\right], \tag{2.14}$$

where $\xi_0{}^\alpha$ is an initial value given at a point A.

If $A_k(x) = \partial_k \Lambda(x)$, i.e. $f_{ik} = 0$, the phase factor in (2.14) is independent of the path C and expressed by $-\frac{1}{2}ie[\Lambda(x_B)-\Lambda(x_A)]$. If $A_k(x)$ is time independent and the curve C is closed in the three-dimensional sense, i.e. there is only a static magnetic field, the phase factor becomes $\frac{1}{2}ie\int_C \mathbf{A}\mathrm{d}\mathbf{x} = \frac{1}{2}ie\int_S$ not $\mathbf{A}\mathrm{d}\mathbf{S}$ and this is just the magnetic flux in the closed circuit C. It may be worth-while to remark that this fact is similar to that of Bohm's Gedanken-Experiment [9]) which illustrates a peculiar function of the electromagnetic potential $A_k(x)$ in quantum mechanics. From (2.13′), we can see easily that

$$\frac{\mathrm{d}}{\mathrm{d}s}(\bar{\xi}\xi) = 0, \quad \frac{\mathrm{d}}{\mathrm{d}s}(\bar{\xi}\gamma_k\xi) = 0, \quad \text{etc.} \tag{2.15}$$

These facts can be easily understood by remembering that $(\bar{\xi}\xi)$, $(\bar{\xi}\gamma_k\xi)$ etc. are ordinary tensorial quantities and there is no effect of the electromagnetic field on ordinary tensorial quantities. (See eq. (2.12′)).

3. The Electric Charge as a Dynamical Variable

It is well known that the electric charge of a strongly interacting particle and the third component of its isospin are linearly dependent on each other. Then, if the isospin results from quantization of an internal dynamical quantity, the electric charge must also be considered as a dynamical quantity. Therefore, in pre-quantum theory or classical mechanics, the electric charge is susceptible to any arbitrary magnitude. The discrete character of the charge of the existing elementary particles can be interpreted as the result of the quantum condition for an internal dynamical variable.

Since we suppose the electromagnetic field to be an affine connexion for spinors, it is natural to consider that a dynamical variable related to the electric charge is described essentially by a spinor quantity.

Now, let us study the motion of a particle in a completely flat space (e.g. $A_k(x) = 0$). And let us suppose that the particle has an internal dynamical variable described by a spinor ξ. If the quantity described by ξ is not affected by any force, i.e. ξ does not change with time, the equations of motion for such a particle are given by

$$\frac{\mathrm{d}^2x^i}{\mathrm{d}s^2} = 0, \quad \frac{\mathrm{d}\xi}{\mathrm{d}s} = 0, \tag{3.1}$$

and the Lagrange function is then given as

$$\mathscr{L} = \tfrac{1}{2}m \frac{dx^k}{ds}\frac{dx_k}{ds} + \tfrac{1}{2}i\left[\bar{\xi}\frac{d\xi}{ds} - \frac{d\bar{\xi}}{ds}\xi\right]. \tag{3.2}$$

However, in the case of $\Gamma_k = \frac{1}{2}i\,A_k(x)$ (e.g. the presence of the electromagnetic field), the fact that ξ is not affected by any force or ξ does not change with time is not expressed by $d\xi/ds = 0$, but by

$$\frac{d\xi}{ds} + \tfrac{1}{2}ieA_k(x)\frac{dx^k}{ds}\xi = 0. \tag{3.3}$$

This means, that we must change d/ds to $d/ds + \frac{1}{2}ie\,A_k dx^k/ds$ for spinors. For tensorial quantities, we need no change for any operation.

Then, the Lagrange function (3.2) becomes

$$\mathscr{L} = \frac{m}{2}\frac{dx^k}{ds}\frac{dx_k}{ds} + i\bar{\xi}\frac{d\xi}{ds} - \tfrac{1}{2}eA_k\frac{dx^k}{ds}\bar{\xi}\xi \tag{3.2'}$$

and Euler's equations derived from (3.2') are

$$\frac{d^2x_k}{ds^2} = \frac{e}{2m}\bar{\xi}\xi f_{ki}\frac{dx^i}{ds}, \quad i\frac{d\xi}{ds} = \tfrac{1}{2}eA_k\frac{dx^k}{ds}\xi, \tag{3.3}$$

where

$$f_{ki} = \frac{\partial A_i}{\partial x_k} - \frac{\partial A_k}{\partial x_i}$$

represents the field tensor. As is easily shown by (3.3), the following conservation law is valid:

$$\frac{d}{ds}(\bar{\xi}\xi) = 0. \tag{3.4}$$

Because of the first equation of (3.3), $\frac{1}{2}\bar{\xi}\xi$ expresses the total charge of the particle and the charge conservation law is expressed by an equation like (3.4). The magnitude of the total charge $\frac{1}{2}\bar{\xi}\xi$ may have any value, chosen as initial value.

Eq. (3.3) is similar to the ordinary equations for a charged particle. There is only the one difference that in our case the total charge must be considered not as a parameter but as a dynamical variable. The interpretation of the electromagnetic field as an affine connexion for spinor quantities is consistent with the interaction between the electromagnetic field and a charged particle. If $A_k(x) = \partial_k \Lambda(x)$, the field strength $f_{ik} = 0$, the path of the particle is straight and $\xi = e^{\frac{1}{2}ie\Lambda(x)}\xi_0$; therefore, if we transform ξ to $e^{\frac{1}{2}ie\Lambda(x)}\xi$, the equation (3.3) becomes identical with (3.1). Thus, in the case $f_{ik} = 0$, the space-time can be considered to be perfectly flat.

Now, it is clear that the internal variables described by spinors have an intimate connection with the electric charge and the dynamical quantities described by tensorial quantities have no relation to the electric charge. Thus it is hoped that the internal quantum numbers related to the electric charge are expressed by dynamical variables of spinor quantities.

4. On Charge Independence

The dynamical vaiables discussed in the previous section do not contribute to the energy of the particle, they stick to the particle. However, if the internal variable ξ varies, it contributes to the energy of the particle. For example, let us consider the following Lagrangian (in the absence of the electromagnetic field):

$$\mathscr{L} = \tfrac{1}{2} m_0 \frac{\mathrm{d}x^k}{\mathrm{d}s} \frac{\mathrm{d}x_k}{\mathrm{d}s} + i\bar{\xi} \frac{\mathrm{d}\xi}{\mathrm{d}s} - M^2(\bar{\xi}, \xi), \tag{4.1}$$

where M is a function of $\bar{\xi}$ and ξ only. From this Lagrangian, we obtain the Hamiltonian

$$H = \frac{1}{2m_0} p^k p_k + M^2(\bar{\xi}, \xi) \tag{4.2}$$

and then $M(\bar{\xi}, \xi)$ gives the rest energy of the particle. Now, since M is dependent on ξ and $\bar{\xi}$, the mass of the particle is also a dynamical variable. And as ξ is a Lorentz spinor, the motion of ξ contributes to the angular momentum of the particle. Even if the particle is at rest, i.e. its momentum is zero, it has in general an angular momentum which is caused by a motion of the internal variable ξ. Thus, it is clear that the three quantities, e.g. the spin, the mass and the electric charge of the particle are correlated with each other through the dynamical variable ξ.

In quantum theory, $M(\bar{\xi}, \xi)$ plays a role of a mass operator. Hence, if $M(\bar{\xi}, \xi)$ has a symmetry property or is invariant under a transformation, the mass eigenvalue of the particle, in general, degenerates. Thus, if the transformation is represented by a rotation group in a three-dimensional Euclidean space, we can consider that the particle forms the so-called iso-multiplet and the transformation can be identified with a rotation in iso-space.

Actually, there exists such a transformation. It is well-known that the linear transformation given by Pauli and Gürsey [10]) is isomorphic to the rotation group in the three-dimensional Euclidean space,

$$\xi \to \xi' = a\xi + b\gamma_5 C^{-1}\bar{\xi}, \quad \bar{\xi} \to \bar{\xi}' = a^*\bar{\xi} + b^*\xi C\gamma_5, \tag{4.3}$$

where

$$|a|^2 + |b|^2 = 1.$$

This transformation is independent of the Lorentz transformation for ξ. The infinitesimal generators of this transformation are given by

$$T_1 = \tfrac{1}{2}[\bar{\xi}\gamma_5 C^{-1}\bar{\xi} - \xi C\gamma_5 \xi], \quad T_2 = \tfrac{1}{2}i[\bar{\xi}\gamma_5 C^{-1}\xi + \xi C\gamma_5 \xi], \quad T_3 = \tfrac{1}{2}\bar{\xi}\xi. \tag{4.4}$$

It is a remarkable fact that $T_3 = \frac{1}{2}\bar{\xi}\xi$ is identical with the total charge discussed in the previous section. Thus, if $M(\bar{\xi}, \xi)$ is invariant under the P-G transformation (4.3), we can introduce a dynamical variable corresponding to the isospin. From our viewpoint, it is easy to understand that the charge independence is violated by the presence of the electromagnetic interaction: the electric charge is not invariant but transforms as T_3 and hence the electromagnetic interaction is not invariant under the transformation (4.3). In our opinion, the presence of the electromagnetic field means that the flatness of space-time is violated for spinor quantities. Then, it is considered that the violation of the charge independence reflects that of the flatness of space-time.

As already pointed out, ξ has an angular momentum. Thus, the magnitude of the isospin is restricted by the magnitude of an ordinary spin. The infinitesimal generators of the Lorentz transformation for ξ is given by

$$L_{kl} = \tfrac{1}{2}i\bar{\xi}[\gamma_k, \gamma_l]\xi. \tag{4.5}$$

By comparing T_3 with the third component of the angular momentum L_{12}, it is easy to see that the states possessing integral spin have an integral isospin and the states possessing half-integral spin have half-integral isospin †.

5. Strangeness and Fermion Number

Now, let us consider the strangeness and the nucleon number. The strangeness is also the quantum number which is related to the electric charge. Then, as in the case of the isospin, we introduce another dynamical variable η which is described essentially by a spinor. Such a dynamical quantity defines an electric charge $\frac{1}{2}\bar{\eta}\eta$. The angular momentum of η is also similar to that of ξ. Then, the possible total angular momenta of the particle which has two internal variables ξ and η are given by the following table:

ξ spin	η spin	total spin
integer	integer	integer
integer	half integer	half integer
half integer	integer	half integer
half integer	half integer	integer

The ξ spin is the same as the isospin (Cf. section 4).

As shown in the previous section, the integral and the half integral character of ξ angular momentum is the same as that of the isospin. Then, identifying $\bar{\eta}\eta$

† This discussion is made on the assumption of the quantization rule $\{\bar{\xi}, \xi\}_+ = 1$.

with strangess is, we hope, sufficient to explain the existing experimental facts by means of two internal dynamical variables ξ and η.

Finally, in the case of half-integral total angular momentum, the wave functions resulting from the quantization procedure have to be described by spinor fields. Then, electromagnetic interaction with the spinor fields is necessarily introduced by virtue of the space-time structure: the derivative ∂_k for spinor fields must be replaced by the covariant derivative $\partial_k - \Gamma_k = \partial_k - \frac{1}{2}ieA_k(x)$ for the sake of covariance. Hence, the total charge of spinor fields is given by $\frac{1}{2}(\bar{\xi}\xi + \bar{\eta}\eta + 1)$. The last term, 1, can be called the fermion number, because it must be added in the case of fermions. The fermion number just corresponds to the nucleon number introduced phenomenologically.

6. Concluding Remarks

6.1. ON GAUGE TRANSFORMATIONS

From our viewpoint, the theory is invariant under the transformation

$$\xi \to \xi' = e^{\frac{1}{2}ie\Lambda}\xi, \quad \eta \to \eta' = e^{\frac{1}{2}ie\Lambda}\eta,$$

$$\begin{aligned}
&\psi(x) \to \psi'(x) = e^{\frac{1}{2}ie\Lambda}\psi(x) && \text{for spinor fields,} \\
&\phi(x) \to \phi'(x) = \phi(x) && \text{for tensor fields,} \\
&p_k \to p'_k = \begin{cases} p_k + \frac{1}{2}e(\bar{\xi}\xi + \bar{\eta}\eta + 1)\partial_k\Lambda & \text{for spinor fields,} \\ p_k + \frac{1}{2}e(\bar{\xi}\xi + \bar{\eta}\eta)\partial_k\Lambda & \text{for tensor fields,} \end{cases} && (6.1) \\
&A_k(x) \to A'_k(x) = A_k(x) - \partial_k\Lambda(x).
\end{aligned}$$

This corresponds to the usual gauge transformation for strongly interacting particles. If $A_k(x) = \partial_k\Lambda(x)$, it is, of course, possible to eliminate the affine connexion $A_k(x)$ for spinors by the so-called gauge transformation. Hence there is no physical effect of $A_k(x)$. A similar state of affairs exists for the gravitational field. If the affine connexion for tensorial quantities satisfies the integrability condition (i.e. if the parallel displacement does not depend on the path), we can make Γ^i_{jk} zero by a suitable coordinate transformation. In such a case, Riemann's curvature tensor is zero, i.e. $R_{ijkl} = 0$, and we call the space flat. Similarly, we may call the space flat for spinors if the field tensor f_{ik} vanishes. The gauge transformation by which we can make $A_k = 0$ just corresponds to the suitable coordinate transformation by which we can make $\Gamma^i_{jk} = 0$.

6.2. PRESENCE OF GRAVITATIONAL FIELD

If the gravitational field is present, the dynamical properties of the electric charge become important. In such a case, the motion of a particle is influenced

by the interaction between the charge variable and the gravitational field. For example, we show the generalization of the equations of motion (3.1) in the case of a general curved space:

$$\frac{\mathrm{d}^2x^i}{\mathrm{d}s^2}+\Gamma^i_{jk}\frac{\mathrm{d}x^j}{\mathrm{d}s}\frac{\mathrm{d}x^k}{\mathrm{d}s}=\frac{i}{m}\bar{\xi}\Gamma_k\xi\frac{\mathrm{d}x^k}{\mathrm{d}s},\quad \frac{\mathrm{d}\xi^\alpha}{\mathrm{d}s}=\Gamma^\alpha_{\beta,k}\frac{\mathrm{d}x^k}{\mathrm{d}s}\xi^\beta, \tag{6.2}$$

where Γ_k's are in general 4×4 matrices. Even if the electromagnetic potential $A_k=0$, the Γ_k do not vanish and are determined by the gravitational field $g_{ik}(x)$. Thus, we can distinguish in principle between motions of charged or uncharged particles by the use of the gravitational field even if there is no electromagnetic field.

6.3. SUMMARY

In this note, we discuss the possibility of identifying the electromagnetic field with an affine connexion for spinors in ordinary four dimensional space time. In this way the electric charge has intimate relations to the dynamical quantities described essentially by spinors. In our opinion, the isospin and the strangeness correspond to internal variables represented by spinors ξ and η. We have not examined the physical meaning of these variables. The variables ξ and η may correspond to degrees of internal rotation of two rigid bodies † or to internal variables of a composite system of two particles having Zitterbewegung. The discussion given in this note is not influenced essentially by any assumption about the nature of ξ and η .It is essential in our discussion that these quantities must be described by spinors. From our viewpoint, the effect of the electromagnetic field appears only when there exist spinors as dynamical variables. All spinors, no matter whether they are fields or not, necessarily have an electric charge and thus interact with the electromagnetic field. The violation of the charge independence by the electromagnetic field is the result of a curvature of space-time. The conservations of the third component of the isospin of the strangeness are naturally interpreted as the conservation of $\bar{\xi}\xi$ and $\bar{\eta}\eta$, even if the electromagnetic interaction exists.

The author wishes to thank Professors T. Toyoda, T. Okabayashi and H. Suura for their stimulating discussions.

† A composite system of two rotators is discussed by H. Fukutome [11]).

References

1) T. Nakano, Prog. Theor. Phys. **15** (1956) **333**;
T. Takabayashi, Prog. Theor. Phys. **23** (1960) 915 (see also the refs. of this paper)
2) H. P. Dürr, W. Heisenberg, H. Mitter, S. Schlieder and K. Yamazaki, Zs. f. Naturf. **14a** (1959) **441**

3) Y. Katayama and M. Taketani, (preprint);
Z. Maki, M. Nakagawa, Y. Ohnuki and S. Sakata, Prog. Theor. Phys. **23** (1960) 1174
4) O. Hara, Prog. Theor. Phys. **21** (1959) 919;
see also O. Klein, Nuclear Physics **4** (1957) 667
5) P. G. Bergmann, Introduction to the Theory of Relativity (Prentice-Hall, New York, 1955)
6) E. Schrödinger, Space-Time Structure (Cambridge University Press, 1954)
7) H. Weyl, Space, Time and Matter (translated into English by H. L. Brose) (Dover Publ., New York, 1950)
8) E. Schrödinger, S. B. Preutz Akad. Wiss. (1943) 105;
V. Bargmann, S. B. Preutz Akad. Wiss. (1932) 346;
L. Infeld and B. L. van der Weerden, S. B. Preutz Akad. Wiss. (1939) 380
9) Y. Aharonov and D. Bohme, Phys. Rev. **115** (1959) 485
10) W. Pauli, N. C. **6** (1957) 204
F. Gürsey, N. C. **7** (1958) 411
11) H. Fukutome, Soryushiron-kenkyu (mimeographed circular in Japanese) **20** (1959) 311

1.B:3.A

Nuclear Physics **24** (1961) 400—411; © *North-Holland Publishing Co., Amsterdam*

Not to be reproduced by photoprint or microfilm without written permission from the publisher

MEASUREMENT OF THE ENERGY OF THE GAMMA RADIATION FROM NEUTRON CAPTURE BY HYDROGEN

J. E. MONAHAN, S. RABOY and C. C. TRAIL

Argonne National Laboratory, Argonne, Illinois †

Received 16 January 1961

Abstract: A scintillation spectrometer with an anticoincidence annulus of NaI is used to measure the energy of the gamma ray that follows the capture of a neutron by hydrogen. The measurement is made simultaneously with the calibration of the spectrometer system in terms of six reference gamma rays. The results indicate a value of 2219 ± 2 keV for the binding energy of the deuteron. A discussion of this result relative to other measurements of this and related quantities is presented.

1. Introduction

The application of computational techniques [1]) to the analysis of the spectra of gamma rays obtained with a scintillation spectrometer with an anticoincidence annulus of sodium iodide [2]) has led to convenient and precise determinations of the energies of gamma rays [3]). It was decided to apply this technique to the measurement of the energy of the gamma ray resulting from the capture of neutrons by hydrogen. In a review article by Wapstra [4]), the weighted average of measured values of the binding energy of the deuteron is calculated to be 2226.4 ± 1.8 keV. Subsequently this has become the value commonly accepted in the literature. It was the objective of this experiment to measure with comparable accuracy a related quantity, namely the energy of the gamma ray following neutron capture by hydrogen. Our results indicate a value of 2219 ± 2 keV for the deuteron binding energy.

The discrepancy between these values is obviously greater than that conventionally accepted as statistical. It is necessary, therefore, to devote a considerable part of this discussion to an analysis of possible systematic errors in our own as well as in other measurements of this quantity.

2. Experimental Procedure

The technique of measurement is similar to that described in ref. [3]). In order to minimize drifts due to changes in amplifier gain as well as pulse-height shifts due to different counting rates, the spectrum of the capture gamma ray is obtained simultaneously with the spectra of various reference gamma rays.

† This work was performed under the auspices of the U. S. Atomic Energy Commission.

The sources and the energies of the "standards" used in this experiment are Na^{24} (2753.3±1.0 keV and 1368.6±0.3 keV) [5], Y^{88} (1836.2±1.7 keV and 898.7±0.8 keV) [3] and Bi^{207} (1063.9±0.4 keV [6]) and 570.8±0.5 keV [3])).

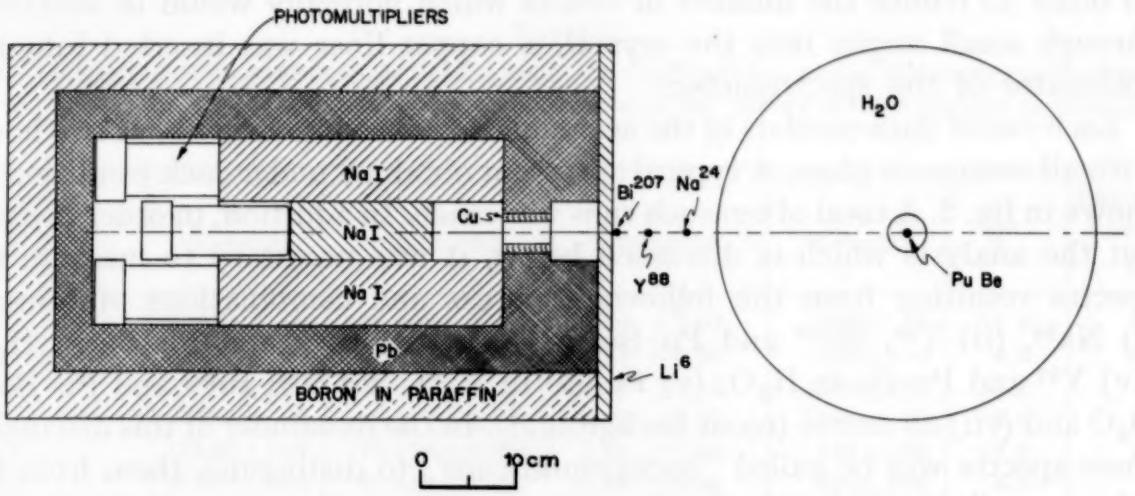

Fig. 1. Experimental arrangement of sources for the measurement of the energy of the gamma ray resulting from capture of neutrons by hydrogen.

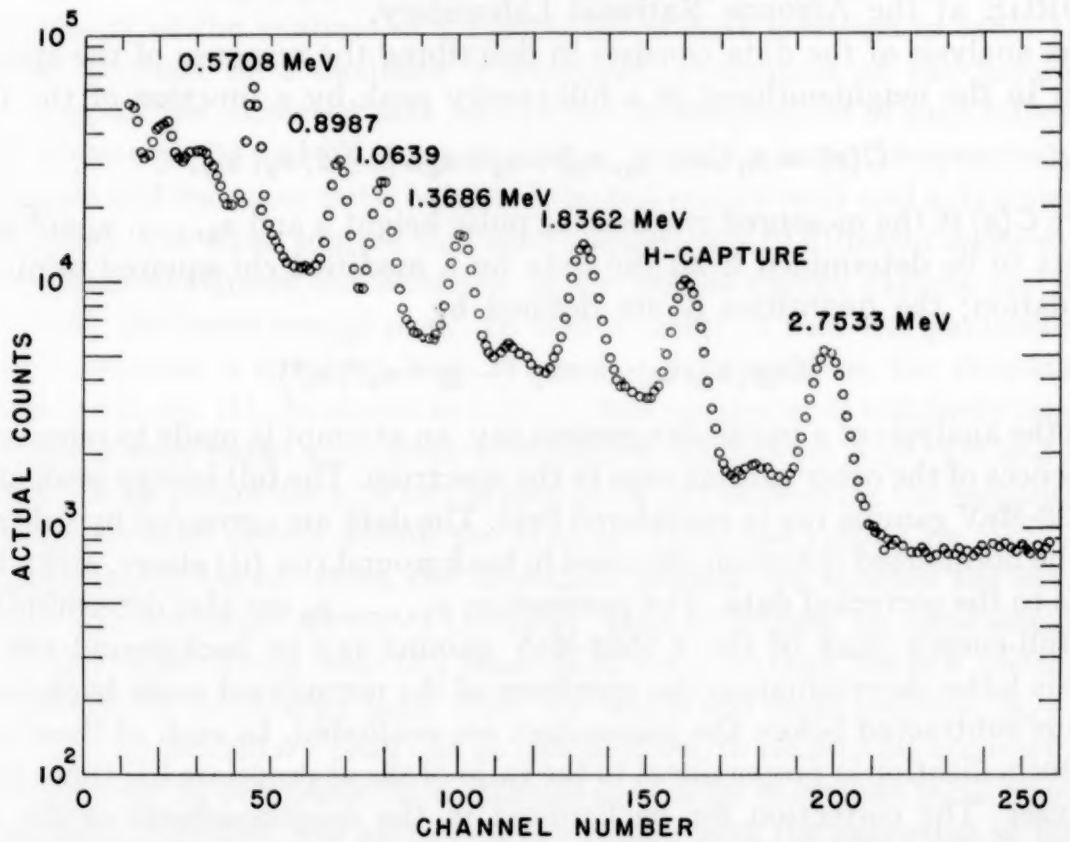

Fig. 2. Spectrum of gamma rays obtained by simultaneous exposure of the scintillation spectrometer to radioactive sources (Na^{24}, Y^{88} and Bi^{207}) and Pu–Be source in a barrel of water.

The experimental arrangement is shown in fig. 1. A Pu–Be neutron source immersed in a barrel of water (40 cm high and 40 cm in diameter) served as the source of capture gamma rays. The radioactive sources (Na^{24}, Y^{88} and Bi^{207})

were placed between the barrel of water and the spectrometer. The latter is protected from background by 2.5 cm of boron-loaded paraffin and 5 cm of lead. A 0.64 cm shield of Li^6 is placed between the spectrometer and the sources. In order to reduce the number of events which normally would be scattered through small angles into the crystal, a copper liner was inserted into the collimator of the spectrometer.

Each run of data consists of the accumulation of counts over about two hours with all sources in place. A typical spectrum obtained under such conditions is shown in fig. 2. A total of ten such runs was made. In addition, in order to carry out the analysis which is discussed below, it was necessary to measure the spectra resulting from the following sources and combinations of sources: (i) Na^{24}, (ii) Y^{88}, Bi^{207} and Pu–Be in H_2O, (iii) Bi^{207} and Pu–Be in H_2O, (iv) Y^{88} and Pu–Be in H_2O, (v) Pu–Be in H_2O, (vi) Y^{88}, Bi^{207} and Pu–Be in D_2O and (vii) no source (room background). In the remainder of this discussion these spectra will be called "background runs" to distinguish them from the "data runs" obtained with all sources in place. The data are recorded on punched paper tape in a form suitable for direct use on the digital computer GEORGE at the Argonne National Laboratory.

The analysis of the data consists in describing the response of the spectrometer in the neighbourhood of a full-energy peak by a function of the form

$$C(x) = \alpha_1 G(x; \alpha_2, \alpha_3) + \alpha_4 + \alpha_5 G(x+d; \alpha_2, \alpha_3), \tag{1}$$

where $C(x)$ is the measured response at pulse height x and $\alpha_1, \ldots, \alpha_5$ are parameters to be determined from the data by a modified chi-squared minimum calculation; the quantities G are defined by

$$G(y; \alpha_2, \alpha_3) = \exp\left[-(y-\alpha_2)^2/\alpha_3^2\right]. \tag{2}$$

In the analysis of a particular gamma ray, an attempt is made to remove the influences of the other gamma rays in the spectrum. The full-energy peak of the 2.7533-MeV gamma ray is considered first. The data are corrected by subtracting the normalized spectrum obtained in background run (ii) above, and a fit is made to the corrected data. The parameters $\alpha_1, \ldots, \alpha_5$ are also determined for the full-energy peak of the 2.7533-MeV gamma ray in background run (i). In this latter determination the spectrum of the normalized room background (vii) is subtracted before the parameters are evaluated. In each of these cases the normalization is proportional to the ratio of the appropriate life times of the analyzer. The correction for background in the neighbourhood of the full-energy peak of the capture gamma ray is considered next. The effect of the neutron background, as determined in background run (vi), is subtracted from this peak in the data runs after normalization of the background run to the life time of the analyzer as before. The influence of the Na^{24} source is removed by subtracting the spectrum of this isolated source, background run (i), with a

normalization determined by the ratio of the areas of the full-energy peaks of the 2.7533-MeV gamma ray of the data run and background run (i). This procedure is repeated for each of the full-energy peaks in the data runs.

TABLE 1

Values of parameters from least-squares fit of $\alpha_1 \exp[-(x-\alpha_2)^2/\alpha_3^2]+\alpha_4$ to the full-energy peak of gamma rays in a typical set (run 123) of data in the measurement of the energy of the hydrogen capture gamma ray.

Energy (MeV)	α_1 (Counts)	α_2 (Channels)	α_3 (Channels)	α_4 (Counts)	χ^2	Expected value of χ^2
2.7533	11650± 40	198.020±0.013	5.74 ±0.02	387± 18	11.6	19
2.2 (unknown)	6360± 90	159.951±0.028	5.13 ±0.09	350±100	8.5	11
1.8362	7760±160	133.077±0.031	4.45 ±0.12	300±180	11.2	9
1.3686	27150± 80	100.407±0.007	3.66 ±0.01	1200± 40	6.3	12
1.0639	15150±140	79.016±0.022	3.28 ±0.04	140± 70	17.6	11
0.8987	17070±170	67.612±0.017	2.82 ±0.04	690±160	4.3	4
0.5708	37040±220	44.730±0.010	2.253±0.018	190±120	5.2	4

The result of the analysis of a typical set of data is shown in table 1. The analysis consists of a modified χ^2-minimum evaluation of the parameters $\alpha_1, \ldots, \alpha_5$ for the corrected data runs in the neighbourhood of each full-energy peak. From eqs. (1) and (2) it is seen that α_1 and α_2 represent, respectively, the amplitude and the mean pulse height of the full-energy peak and α_3 is a measure of its width. For those sources that emit gamma rays of different energies, it is not possible to remove the influence of the higher energy gamma ray in the vicinity of the lower energy peak. To take account of this the parameter α_4, which represents a constant level of counts superposed on the Gaussian, is introduced in eq. (1). As shown in table 1, this parameter is relatively large for the lower energy peaks associated with each of the sources Na^{24}, Y^{88} and Bi^{207}. Finally a fifth parameter α_5 is introduced in eq. (1) to describe the response due to back-scattered events within the crystal. These are caused by large-angle Compton scattering in which the degraded gamma ray escapes the detector through the entrance aperture, therefore, fails to trigger an anticoincidence pulse. This type of event leads to a small peak not more than 250 keV lower than the mean of the full-energy peak. Since the width and mean position, (α_2-d) in eq. (1), of this secondary peak can be calculated with reasonable accuracy, it is necessary only to determine its amplitude α_5 in order to include these events in the response function. For all full-energy peaks, with the exception of that at 2.7533 MeV, the contribution to the full-energy peak by α_5 is essentially zero. Even in the case of the 2.7533-MeV peak, the correlation between α_2 and α_5 is sufficiently small that any reasonable value of α_5 produces a negligible shift in α_2.

The calculated value of χ^2 provides a measure of the "goodness of fit" of the response function eq. (1) to the observed spectrum. The calculated and expec-

TABLE 2

Mean positions of full-energy peaks of all gamma rays, and parameters obtained from fit of each set of data to the relation $E = a+bx+cx^2$, which relates the energy of a gamma ray to its pulse height

Energy of gamma ray (MeV)		Mean position of peak									
		Run 116	Run 117	Run 122	Run 123	Run 125	Run 126	Run 147	Run 148	Run 149	Run 150
Energy of gamma ray (MeV)	2.7533	195.32 ±0.04	197.76 ±0.04	199.583 ±0.016	198.020 ±0.013	195.674 ±0.018	199.72 ±0.04	190.201 ±0.033	186.27 ±0.04	183.92 ±0.04	181.026 ±0.026
	1.8362	131.103 ±0.013	133.148 ±0.016	134.251 ±0.021	133.077 ±0.031	131.571 ±0.030	134.262 ±0.018	128.109 ±0.028	125.494 ±0.023	123.858 ±0.027	121.778 ±0.027
	1.3686	98.489 ±0.017	100.354 ±0.017	101.381 ±0.009	100.407 ±0.007	99.272 ±0.007	101.440 ±0.013	96.643 ±0.022	94.659 ±0.017	93.530 ±0.015	91.846 ±0.024
	1.0639	77.465 ±0.016	79.180 ±0.020	79.895 ±0.016	79.016 ±0.022	78.138 ±0.017	79.853 ±0.024	76.142 ±0.020	74.621 ±0.024	73.723 ±0.026	72.334 ±0.011
	0.8987	66.151 ±0.015	67.800 ±0.006	68.387 ±0.017	67.612 ±0.017	66.890 ±0.016	68.357 ±0.018	65.233 ±0.016	63.968 ±0.019	63.241 ±0.026	61.950 ±0.021
	0.5708	43.491 ±0.007	44.955 ±0.022	45.416 ±0.008	44.730 ±0.010	44.292 ±0.008	(not in this run)	43.292 ±0.013	42.472 ±0.012	41.988 ±0.010	41.062 ±0.008
Parameters	a	−65.9 ±1.4	−80.6 ±1.7	−81.5 ±1.2	−74.7 ±1.4	−76.4 ±1.7	−74.9 ±5.5	−81.5 ±1.8	−83.6 ±1.6	−84.0 ±1.9	−80.0 ±1.5
	b	14.69 ±0.03	14.53 ±0.03	14.412 ±0.023	14.48 ±0.03	14.66 ±0.03	14.31 ±0.09	15.12 ±0.04	15.46 ±0.03	15.64 ±0.04	15.91 ±0.03
	$100c$	−0.130 ±0.013	−0.101 ±0.014	−0.105 ±0.010	−0.098 ±0.012	−0.103 ±0.015	−0.075 ±0.034	−0.114 ±0.017	−0.124 ±0.016	−0.118 ±0.018	−0.143 ±0.016
	χ^2	3.7	2.2	3.0	4.3	5.9	6.4	4.6	3.4	4.9	3.7

tation value for this quantity are listed for each full-energy peak in the last two columns of table 1.

The mean positions α_2 of the full-energy peaks of all the gamma rays for all the runs are presented in table 2. For each run, the energy E of the gamma ray is related to the mean position by the quadratic function

$$E = a+b\alpha_2+c\alpha_2^2. \quad (3)$$

The six reference energies thus provide an over-determined set of equations of the form of eq. (3) for the calibration of an energy scale. The considerations which led to a preference of the quadratic relation (3) over a linear relation are discussed in refs. [1, 3]). The resulting determinations of the energy of the hydrogen capture gamma ray are listed in table 3. The weighted average of this set of data is 2217.2 ± 1.5 keV for the hydrogen capture gamma ray. This gives the value 2218.5 ± 1.5 keV for the binding energy of the deuteron.

TABLE 3

Results of 10 determinations of the neutron-capture gamma ray in hydrogen, with assumption of a quadratic relationship between energy and mean position

Run	Position of mean of capture gamma ray (channel)	Energy (keV)
116	157.840 ± 0.031	2220.1 ± 1.5
117	160.059 ± 0.033	2219.2 ± 1.5
122	161.247 ± 0.039	2215.3 ± 1.2
123	159.951 ± 0.028	2215.6 ± 1.3
125	158.089 ± 0.033	2215.8 ± 1.5
126	161.371 ± 0.027	2215.0 ± 2.4
147	153.839 ± 0.032	2217.6 ± 1.6
148	150.734 ± 0.031	2218.6 ± 1.5
149	148.762 ± 0.027	2217.1 ± 1.5
150	146.356 ± 0.032	2217.8 ± 1.5

Weighted average 2217.2 ± 1.5 keV (error increased to allow for systematic deviation from quadratic fit). Binding energy of the deuteron: 2219 ± 2 keV. (This result contains an adjustment for systematic errors, see text.)

In order to determine the effect, if any, that small-angle scattering of the gamma rays in H_2O would have on these measurements, the following experiment was performed. A source of Ce^{144} which decays through Pr^{144} to Nd^{144} was placed in the centre of a barrel of water. The technique used for the measurement of the hydrogen capture gamma ray was used to measure the energy of the 2.18-MeV gamma ray emitted by Nd^{144}. We obtained the value 2184.1 ± 1.9 keV for this measurement, which is to be compared with the value 2186.0 ± 2.2 keV, the result of our previous direct measurement of this transition for a

source out of water [3]). The errors associated with these measurements include a measure of the systematic error in the method. To obtain a value for the effect of the water we consider the random errors which are 0.7 keV and 0.4 keV for the source out of water and in the water respectively. The effect of the water is to give an apparently lower result by 1.9 ± 0.8 keV. We add this number to our measured value of the energy of the hydrogen-capture gamma ray.

A measure of the systematic error in the method is reported [3]) in the measurement of the gamma rays from Ce^{144}. Gamma rays with energies of 0.696 MeV and 1.487 MeV are in cascade and the sum of the determination of their energies is compared with the measurement of the 2.186-MeV crossover mentioned above. This sum is measured to be 2183.7 keV with a 0.5 keV random error. The difference between these measurements is 2.3 ± 0.8 keV. Since the χ^2 test of the fit to the energy calibration curves indicate a systematic error in both measurements, we conclude that the measurement of the energy of the crossover gamma ray is too high by 1.2 keV with a systematic uncertainty of 1.1 keV.

When we combine the corrections for the effect of the water and the systematic differences of the method, and when we combine the statistical error of 1.0 keV with the systematic error of 1.1 keV, we obtain for our best value for the binding energy of the deuteron 2219 ± 2 keV.

3. Discussion of Results

As mentioned previously, the result of this measurement is lower than the value usually quoted in the literature. In fact the discrepancy is sufficient to indicate that one, or possibly both, of these values includes some unsuspected systematic error. For this reason this section will include a discussion not only of the present experiment but also of some independent measurements of the binding energy of the deuteron and of related quantities.

3.1. THE PRESENT MEASUREMENT

The technique discussed above is, of course, not an absolute measurement but depends on a calibration of the pulse-height scale in terms of the independently measured energies of a set of gamma transitions. In addition, the accuracy of this method depends on the validity of using eq. (3) to represent the calibration over the energy interval of this set of gamma ray energies.

It is possible that some of the energies of the standards used in this experiment are in error, and, although there is some theoretical justification [1]) for our choice of eq. (3), it is also possible that this representation is not entirely adequate for the energy calibration. However, since the use of six standard gamma-ray energies provides an over-determined set for our assumed calibration function, it is possible to obtain "best" (in the sense of least-squares) values for the parameters a, b, and c in eq. (3) and also to test the adequacy of eq. (3) by an approximate calculation of χ^2. In the ten data runs the latter calculation re-

sulted in values of χ^2 which are from 1.1 to 3.2 times the expected value. Thus eq. (3) seems to give no statistically significant deviation from the "correct" calibration function.

Moreover, any random deviation introduced by the use of eq. (3) can be included, at least approximately, in our final results by renormalizing our error estimates so that χ^2 takes on its expectation value. This has been done for each data run; and in combining the ten runs the errors have been treated as entirely systematic and averaged in the same manner as the mean energy. The error estimates, therefore, are considered to be relatively conservative.

There exists one possible flaw in the above argument. Because of the disproportionate weight with which the 2.7533 MeV standard enters into the calculations, particularly in the determination of the value of the parameter c in eq. (3), an error of magntiude ε in this standard energy will be reflected as an error of about $\frac{1}{2}\varepsilon$ in the measured value of the binding energy of the deuteron. Thus the difference between the present result and that quoted by Wapstra [4]) would require that ε be about 15 keV if this difference were to be attributed entirely to this standard. This corresponds to slightly more than a full channel in our pulse-height response. It is difficult to believe that any combination of errors in the determination of the energy of this standard and in our measurement of the corresponding value of α_2 could account for this difference.

If subsequent measurements should indicate that an incorrect value of any standard energy was used in this experiment, the results presented in tables 2 and 3, are complete enough to enable any interested party to recalculate the value of the binding energy of the deuteron.

3.2. OTHER MEASUREMENTS

Measurements of the $H^3(p, n)He^3$ threshold are among the experiments from which precise evaluations of the binding energy of the deuteron have been made. The Q value of this reaction, when combined with the end point of the beta decay of tritium, gives the difference in mass between the neutron and the hydrogen atom. This difference, when combined with the mass difference between H_2 and D, gives the binding energy of the deuteron.

The threshold for neutron production by the reaction $H^3(p, n)He^3$ was measured to be 1019 ± 1.0 keV by Taschek *et al.* [7]). This threshold energy was determined by calibrating the electrostatic analyzer against the $Al^{27}(p, \gamma)Si^{28}$ resonance at 993. 3 keV as measured by Herb *et al.* [8]). The calibration of the energy scale was checked against the 873.5-keV resonance in $F^{19}(p, \alpha\gamma)O^{16}$ and the $Li^7(p, n)Be^7$ threshold [8]).

Bonner and Butler [9]) have reported a value of 1020.3 ± 1.5 keV for the $H^3(p, n)He^3$ threshold. These authors calibrated their magnetic analyzer against the 873.5-keV resonance in $F^{19}(p, \alpha\gamma)O^{16}$ and the 993.3-keV resonance[8]) in $Al^{27}(p, \gamma)Si^{28}$.

A group at the Naval Research Laboratory [10]) has measured the $H^3(p, n)He^3$ threshold to be 1019.7 ± 0.5 keV. This group made an "absolute" measurement, using an electrostatic analyzer to determine the proton energy.

If the Q values reported in these threshold measurements are combined with the weighted average of 18.1 ± 0.2 keV for the end-point energy of the beta-decay of tritium as reported by King [11]) and with a value 1441.3 ± 0.6 keV for the H_2-D doublet difference, which is the average of two recent determinations [12, 13]), the respective values obtained for the binding energy of the deuteron are 2222.3 ± 1.3 keV, 2223.3 ± 1.8 keV, and 2222.7 ± 0.8 keV. These results would be increased by 0.5 keV if the value of the beta-decay energy of tritium (18.6 ± 0.1 keV) obtained by Porter [14]) is used.

This agreement is somewhat illusory. The Rice [9]) and Los Alamos [7]) groups used the $Al^{27}(p, \gamma)Si^{28}$ resonance at 993.3 keV to calibrate their accelerators. In addition to the value of 993.3 keV for the energy of this resonance as measured by Herb *et al.* [8]), the following values are to be found in the literature: 990.8 ± 0.2 keV by Bumiller *et al.* [15]), 992.4 ± 0.5 keV by Bondelid and Kennedy [16]) and 994.0 ± 1.0 keV by S. E. Hunt *et al.* [17]). An earlier bit of work in Copenhagen [18]) reports on a series of $Al(p, \gamma)$ resonances. Resonances at 986 ± 2 keV and 994 ± 2 keV are reported. The 986-keV level of Broström *et al.* is indentified as the resonance at 991 keV by the authors of a survey article [19]), but these same reviewers report the 994 keV without adjustment of the energy scale.

In our work on the $F^{19}(p, \alpha\gamma)O^{16}$ resonances [20]) in which we used the scintillation spectrometer with an anticoincidence annulus, we found that the relative intensities of the gamma rays of energy 6.1 MeV, 6.9 MeV and 7.1 MeV change as the proton energy is varied over the resonance. Also, at any particular proton energy, the angular distribution differs measurably from one of these gamma rays to another. Upon shifting to a plain NaI crystal and a pulse-height discriminator, it was possible to shift the position of the resonance at 1.385 MeV by large amounts by varying the bias condition on the discriminator. It is suggested, therefore, that each of the measurements mentioned in the previous paragraph may have been concerned with different quantities and that the spread in the results represent a spread in the experimental conditions. In fact, it is possible that the various experimental groups may have been looking at different resonances. This calibration energy is, of course, quite critical in the measurement of the $H^3(p, n)He^3$ threshold, and consequently in these determinations of the binding energy of the deuteron. For example, the value 990.8 keV, if used for the $Al^{27}(p, \gamma)$ resonance, would lead to a value of about 2220 keV for the deuteron binding energy.

The report of the experiment at the Naval Research Laboratory [10]) indicates that their absolute measurement of the threshold of $H^3(p, n)He^3$ would be in disagreement with the earlier measurements [7, 9]) if their own value of the

$Al^{27}(p, \gamma)$ resonance [16]) had been used. Their claim of agreement with the earlier measurements, therefore, cannot be maintained.

Each of these measurements of the $H^3(p, n)$ threshold used some system of BF_3 counters combined with a paraffin moderator as a neutron detector. In order to determine the threshold energy it is necessary to extrapolate from values of the measured neutron yield above threshold. Such an extrapolation presupposes knowledge about the shape of the yield curve which depends not only on the reaction itself but also on the response of the detector system (as a function of energy). It is difficult to make a proper assessment of the uncertainty in the results introduced by this procedure.

A direct measurement of the energy of the gamma rays emitted after capture of neutrons by hydrogen was made by Bell and Elliott [21]). Their method involves the use of a beta-ray spectrometer to analyze the photoelectrons ejected from a uranium radiator by the capture gamma ray. A 13 cm thickness of paraffin irradiated in the thermal column of a reactor was the source of the capture rays. The value of the deuteron binding energy obtained by these authors is 2230 ± 7 keV. In the two runs used for this determination, the signal-to-noise ratio is about 1.08 and 1.06, respectively. An accurate determination of the background is necessary for a precise measurement of the position of the peak since this background is changing rapidly with energy in the region of the peak. The background measurement is obtained by the substitution of lucite for the uranium radiator. The contribution to the background by the continuum of gamma rays producing photoelectrons from the uranium radiator will not be detected by the lucite measurement. Similarly, the calibration standard, the 2.615-MeV gamma ray in ThC'', is measured with the reactor off. Its peak position is superposed upon a qualitatively different spectrum. Our own work indicates that serious systematic errors may be introduced by poor signal-to-background ratios and by inadequate methods for determining the background.

Direct measurements of the photodisintegration energy of the deuteron have been made in at least two laboratories [22, 23]). Both these measurements are threshold measurements and use a bremsstrahlung beam produced by monoenergetic electrons. The neutron yield is determined as the energy of the electrons is varied and an extrapolation procedure is devised to determine the threshold of the disintegration process. The values of the deuteron binding energy obtained by this method are 2226 ± 3 keV (Mobley and Laubenstein [22])) and 2227 ± 3 keV (Noyes *et al.* [23])).

The extrapolation procedure of Mobley and Laubenstein depends on the assumption that the yield of photoneutrons is directly proportional to a power of the energy excess above threshold. This was justified by a plausibility argument which is of questionable validity for the range of energies measured. The combination of the behaviour of the photodisintegration cross section [24]) and the intensity distribution of the bremsstrahlung beam gives an energy depend-

ence for the photoneutron yield which differs quite markedly from a direct power law for energies only a few keV above threshold. The energy of the electron beam is determined by reference to the $Li^7(p, n)\ Be^7$ threshold with the proton beam of the electrostatic accelerator.

As was noted by Marion [25]), the threshold measurement for $Li^7(p, n)Be^7$ can serve as an energy calibration point for charged particle accelerators but may be somewhat unreliable as a measurement of the Q values of the reaction. It must be emphasized, however, that the same reasoning demands that the experimental conditions of the absolute measurement must be reproduced in order to use these measurements for energy standards. The limitations associated with the neutron counter, i.e. long counter [26]), and with threshold measurements may cause systematic errors. Mobley and Laubenstein do not describe the counter, its shape, or position used in the calibration process.

The experiment by Noyes *et al.* consists of a similar measurement of the photodisintegration of the deuteron by a bremsstrahlung beam. The energy of the electron beam, however, is measured absolutely with an electrostatic analyzer. The extrapolation technique is based on a different power law from that of Mobley and Laubenstein, and again no quantitative estimate is made of the error introduced by approximating the photoneutron yield by a pure power law. There is a serious question about the detection of neutrons in this experiment. A BF_3 counter, at about 120° to 140° to the beam and a D_2O target is embedded in about 30 kg of paraffin. The quantity of paraffin is sufficiently large to compete with the BF_3 counter, particularly for neutrons near threshold. This competition probably introduces a prejudice against the data points near the actual threshold.

All the results which have been discussed in this section seem to indicate a rather close grouping of the values of the deuteron binding energy for those measurements which are essentially similar. This would suggest the possibility of systematic differences due to the method of measurement. In such a case it is rather unrealistic to average all these measurements in the same manner as with quantities exhibiting random differences.

A group at Livermore [27]) has reported a direct measurement of the energy of the capture gamma ray with a bent crystal spectrometer. Their mean value of the binding energy of the deuteron is given as 2225 keV as computed from the following set of measurements: 2224 ± 6 keV, 2224 ± 16 keV, 2228 ± 3 keV and 2222 ± 2 keV. The data thus exhibit a large spread with the "best" values at the extremes of the range. It is difficult to define a reasonable statistical estimate of the error to be assigned to the average of such a set. The Bragg angle for this energy is very small, so that the reflected beam is very close to the main beam direction. The background is known to be appreciable and is changing very rapidly. The report does not indicate how this background is measured or what corrections have been made for the background.

We gratefully acknowledge the help received in setting up this experiment from J. Peregrin of the Argonne National Laboratory. We are indebted to R. Julke of the Applied Mathematics Division of Argonne for the actual program on the digital computer. The patience and cooperation of L. Nelson and J. Nelson and their staffs at the computer are appreciated. Finally we must express our appreciation for the illuminating and encouraging discussions with G. R. Ringo.

References

1) J. E. Monahan, S. Raboy and C. C. Trail, to be published
2) C. C. Trail and Sol Raboy, Rev. Sci. Instr. **30** (1959) 425
3) J. E. Monahan, S. Raboy and C. C. Trail, to be published
4) A. H. Wapstra, Physica **21** (1955) 367;
Encyclopedia of Physics (Springer-Verlag, Berlin, 1958), vol. 18, Part 1, p. 1
5) A. Hedgran and D. Lind, Ark. Fys. **5** (1952) 177 and private communication
6) D. E. Alburger, Phys. Rev. **92** (1953) 1257
7) R. F. Taschek, H. V. Argo, A. Hemmindinger and G. A. Jarvis, Phys. Rev. **76** (1949) 325
8) R. G. Herb, S. C. Snowden and O. Sala, Phys. Rev. **75** (1949) 246
9) T. W. Bonner and J. W. Butler, Phys. Rev. **83** (1951) 1091
10) R. O. Bondelid, J. W. Butler, C. A. Kennedy and A. del Callar, Phys. Rev. **120** (1960) 887
11) R. W. King, Revs. Mod. Phys. **26** (1954) 327
12) J. Mattauch and R. Bieri, Z. Naturforsch. **9A** (1954) 303;
J. Mattauch and H. Hintenberger, Report on the activity of the Swiss study commission for atomic energy from 1946 to 1958, Experimental Supplement VIII p. 50 (1960)
13) R. A. Dermirkhanov, T. I. Gutkin, V. V. Dosokhov and A. D. Rudenko, J. Nuclear Energy **3** (1956) 251
14) F. T. Porter, Phys. Rev. **115** (1959) 450
15) F. Bumiller, H. H. Staub and H. E. Weaver, Helv. Phys. Acta **29** (1956) 83
16) R. O. Bondelid and C. A. Kennedy, Phys. Rev. **115** (1959) 1601
17) S. E. Hunt, R. A. Pope, D. V. Freck and W. W. Evans, Phys. Rev. **120** (1960) 1740
18) K. J. Broström, T. Huus and R. Tangen, Phys. Rev. **71** (1947) 661
19) P. M. Endt and C. M. Braams, Revs. Mod. Phys. **29** (1957) 683
20) J. E. Monahan, S. Raboy and C. C. Trail, to be published
21) R. E. Bell and L. G. Elliott, Phys. Rev. **74** (1948) 1552: Phys. Rev. **79** (1950) 283
22) R. C. Mobley and R. A. Laubenstein, Phys. Rev. **80** (1950) 309
23) J. C. Noyes, J. E. Van Hoomissen, W. C. Miller and B. Waldman, Phys. Rev. **95** (1954) 396
24) H. A. Bethe, Elementary Nuclear Theory (Wiley, New York, 1947) p. 58
25) J. B. Marion, University of Maryland, Physics Department, Technical Report 184 (July 1960) (unpublished)
26) A. O. Hanson and J. L. McKibben, Phys. Rev. **72** (1947) 673
27) E. L. Chupp, R. W. Jewell, Jr., and W. John, Phys. Rev. **121** (1961) 234

9.B

Nuclear Physics **24** (1961) 412—421; © *North-Holland Publishing Co., Amsterdam*

Not to be reproduced by photoprint or microfilm without written permission from the publisher

MEASUREMENT OF THE COLLISION MEAN FREE PATH OF PENETRATING SHOWER PRODUCING COSMIC RAY NEUTRONS IN LEAD

G. BOZÓKI, E. FENYVES and L. JÁNOSSY

Central Research Institute of Physics, Laboratory for Cosmic Rays, Budapest

Received 28 June 1960

Abstract: The collision mean free path of penetrating shower producing cosmic ray neutrons was measured with an anticoincidence counter arrangement in lead. The detector selected neutrons having a mean energy of about 30 GeV. The collision mean free path and the corresponding collision cross section were found to be $\lambda_c^{Pb} = (208 \pm 12)$g/cm^2 and $\sigma_1^{Pb} = (1652 \pm 95)$mb, respectively. From this the inelastic nucleon-nucleon cross section was estimated to be $\bar{\sigma}_1 = (24 \pm 5)$mb. Comparison of these results with those obtained at accelerator energies shows, that the inelastic or collision cross section of neutrons as well as the inelastic nucleon nucleon cross section in lead very probably remain constant from 1 GeV to about 30 GeV.

1. Introduction

Several authors have measured the collision mean free path and the corresponding collision cross section † of penetrating shower producing cosmic ray particles in different materials. Since the mean energy of these particles is in the 10 GeV—100 GeV region, comparison of the results of these measurements with those obtained at accelerator energies (1 GeV—10 GeV) indicate the general trend of the collision cross section with energy [1, 2]). Furthermore it is possible, using the nuclear density distributions known from electron scattering experiments [3, 4]), to estimate from the measured collision cross sections the inelastic nucleon-nucleon cross section [5, 6, 7, 8, 9]) at cosmic ray energies and compare it with those obtained at accelerator energies.

It had been observed earlier [2]) that the collision cross section in different materials as well as the corresponding nucleon-nucleon cross section were significantly higher at cosmic ray energies than those measured with accelerators at several GeV. Recently, however, Brenner and Williams [8]) have found a collision cross section in iron near 50 GeV which is not greatly different from the cross sections measured at the cosmotron with ≈ 1 GeV neutrons and protons. Similar results were found also by Kocharian *et al.* [9, 10]) for lead at lower energies (0.9—34 GeV).

† The collision cross section, also called inelastic or reaction cross section by different authors, is given by an experimental definition, and corresponds at high energies to the particle-production cross section [8]).

In the present experiment we have measured the collision cross section of cosmic ray neutrons having a mean energy of about 30 GeV in lead. The method of measurement was worked out originally by Rossi and Regener [11]) and by Jánossy and Rochester [12]) and used later by several authors [13, 14, 1]). It is based on the attenuation measurement of neutrons producing penetrating showers in a detector and not interacting in the absorber placed above the detector †. The collision cross scction obtained does not deviate significantly from those measured in accelerators with 1—5 GeV neutrons. The inelastic nucleon-nucleon cross section derived is also equal within the limits of error to the values found for (p—p) interactions at accelerator energies.

2. Experimental Arrangement

The experimental arrangement consisted of a penetrating shower detector, an anti-coincidence counter shield and a lead absorber of variable thickness

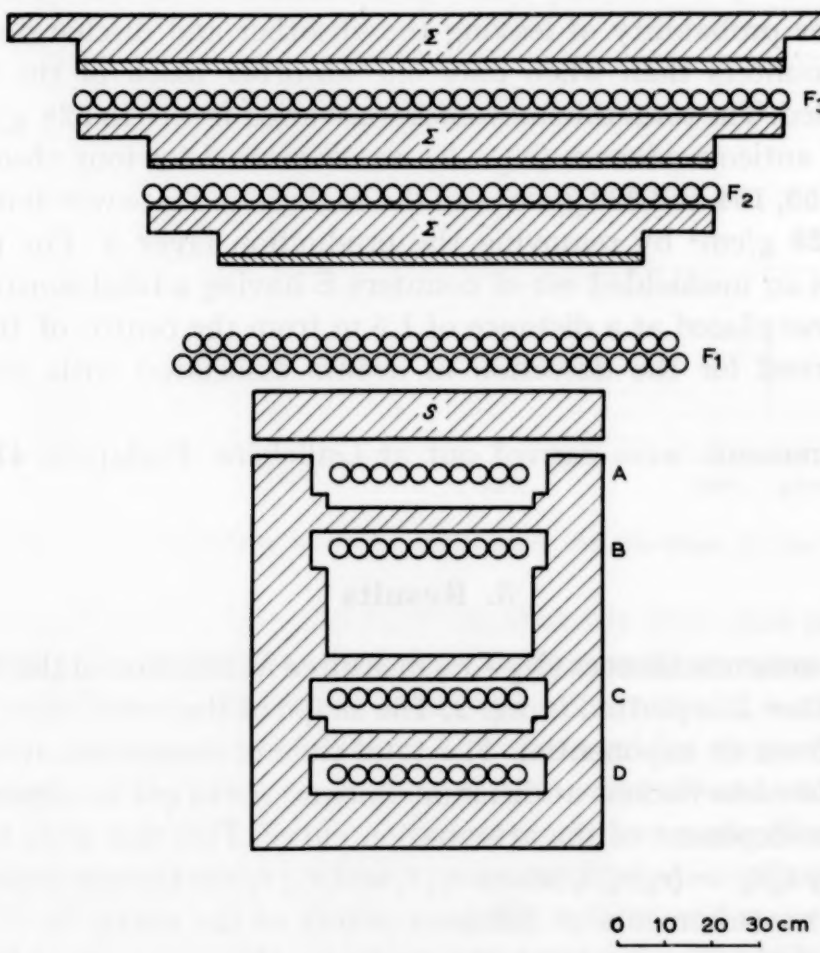

Fig. 1. The experimental arrangement.

† A detailed description of this method as well as the discussion of possible spurious effects was given by the authors in ref. [1]).

(fig. 1). The penetrating shower detector was the same apparatus that was used previously for the measurement of the absorption length of penetrating shower producing particles [15]). It consisted of four counter sets A, B, C and D embedded in a lead block. Events (N_2) by which at least two counters of each of the four sets were discharged, were selected by discriminators. As it was shown in ref. [15]) these events correspond to penetrating showers having a mean energy of about 30 GeV. The penetrating shower detector was covered with a 10 cm lead layer S in which the showers were produced.

The anticoincidence counter shield consisting of three counter sets connected in parallel ($F_1+F_2+F_3 = F$) served for the discrimination of penetrating showers produced by neutrons not interacting in the lead absorber Σ from those produced by charged primaries or interacting neutrons. To exclude events produced by interacting neutrons more effectively [1]), the absorber Σ was subdivided into three layers and these were placed between and above the anticoincidence counters so that the maximum thickness of each layer was not more than 10 cm [16]). In this way ionizing secondaries of the interacting neutrons have a greater probability of leaving the absorber and discharging the anticoincidence counters than when only one absorber block of the same total thickness is used. The total thickness of Σ was varied from 0 to 328 g/cm² lead †.

The rate of anticoincidences (N_2—F) was measured for four absorber thicknesses $\Sigma = 0$, 55, 164 and 328 g/cm² and the background rate was determined for $\Sigma = 0$ and 328 g/cm² by removing the production layer S. For part of the measurements an unshielded set of counters E having a total sensitive surface of 3200 cm² was placed at a distance of 1.5 m from the centre of the arrangement and served for the detection of events associated with extensive air showers.

The measurements were carried out at Csillebérc, Budapest, 410 m above sea level.

3. Results

The rate of anticoincidences (N_2—F) measured as function of the thickness of the lead absorber Σ is plotted in fig. 2. The shape of the curve does not deviate significantly from an exponential. The total time of measurement was divided up between the observations at different thicknesses to get maximum information about the exponent of the attenuation curve. This was done by choosing approximately $t_i/t_k = (r_k/r_i)^{\frac{1}{2}}$, where r_i, t_i and r_k, t_k are the corresponding rates and times of measurements at different points of the curve [17]).

Correction of the measured data for background counts caused by μ-mesons was not necessary. Such a correction is, as shown in ref. [15]), only of the order of

† The lead absorber layers were held by iron slabs of thickness 2.0, 1.0 and 2.0 cm, which were left permanently above the anticoincidence counter sets F_1, F_2 and F_3.

several percent for a penetrating shower detector without an anticoincidence counter shield; thus using the present anticoincidence arrangement consisting of counters having efficiencies higher than 99.9 % [18]) the background due to μ-mesons can be neglected. This was proved also experimentally by measuring the rate of anticoincidences at $\Sigma = 0$ and 328 g/cm² when the shower producing layer was removed (fig. 2, dotted curve).

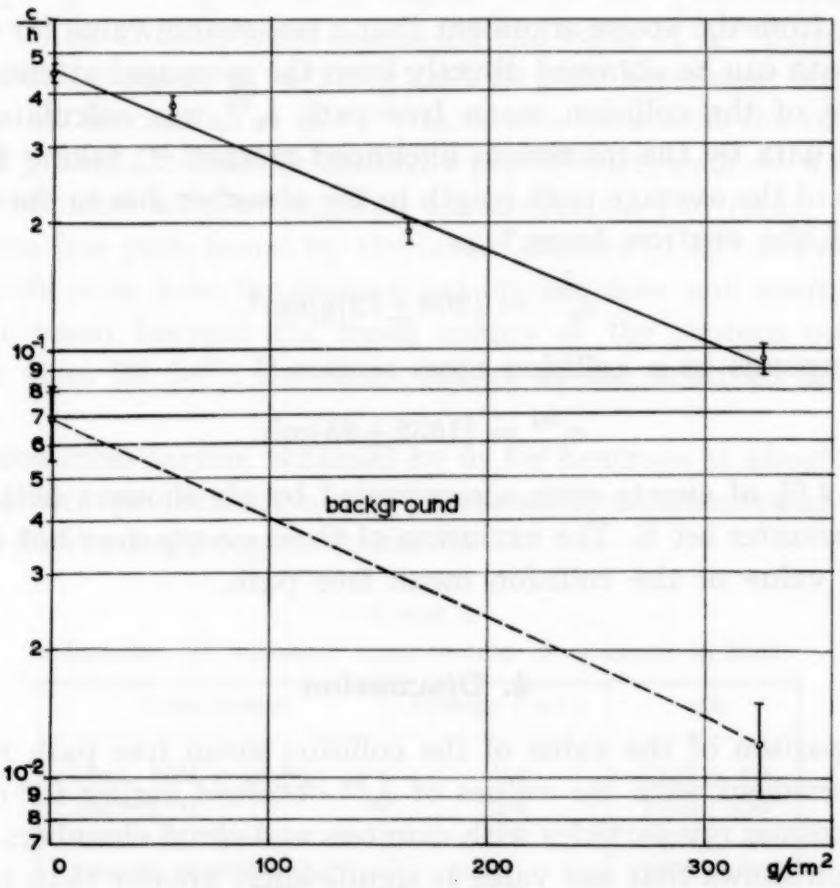

Fig. 2. The rate c/h of anticoincidences (N_2—F) versus the thickness of the lead absorber.

The slope of this curve does not differ significantly from that measured with the producing layer, indicating that this "background" is caused also mainly by neutrons producing penetrating showers in the frame or in the lead block itself, and therefore no correction need be introduced for their contribution to the attenuation curve. There are, however, two other effects which might influence the value measured for the collision mean free path. These are a) the effect of electrons accompanying high energy neutrons and reducing the rate of anticoincidences at $\Sigma = 0$ by discharging the anticoincidence counters, and b) the decrease with increasing absorber thickness of the probability of ionizing secondaries produced in nuclear interactions to escape from the absorber and discharge the anticoincidence counters. The slight significance of the first effect can be shown by measuring the rate of anticoincidences (N_2—F) with 55 g/cm²

lead placed above the top anticoincidence counters F_3. It can be seen clearly from fig. 2 that the point measured at 55 g/cm² fits, within the limits of error, quite well the value expected for a strictly exponential attenuation curve calculated from the measured values. The same argument can be used to show that the second effect does not seriously change the slope of the attenuation curve by measuring the rate of anticoincidences at the medium absorber thickness $\Sigma = 164$ g/cm².

It is clear from the above argument that a reasonable value for the collision mean free path can be obtained directly from the measured attenuation curve.

The value of the collision mean free path λ_c^{Pb} was calculated from the uncorrected data by the maximum likelihood method [19]) taking into account the increase of the average path length in the absorber due to the non-parallel character of the neutron beam † as

$$\lambda_c^{Pb} = (208 \pm 12) \text{g/cm}^2, \tag{1}$$

which corresponds to a collision cross section ††

$$\sigma_1^{Pb} = (1652 \pm 95) \text{mb}. \tag{2}$$

Roughly 2 % of events were accompanied by air showers detected by the unshielded counter set E. The exclusion of these events does not significantly change the value of the collision mean free path.

4. Discussion

The comparison of the value of the collision mean free path found in the present experiment with the values of λ_c^{Pb} obtained earlier for charged and uncharged cosmic ray particles with counters and cloud chambers in the same energy region shows that our value is significantly greater than the weighted mean of the earlier results [2, 22]), which is close to the "geometrical" collision mean free path ($\lambda_{geom}^{Pb} \approx 160$ g/cm²). We cannot give any reasonable explanation for this discrepancy. It must be emphasized, however, that some of the earlier counter measurements giving smaller values of λ_c^{Pb} were selected from a greater experimental material according to the penetrating power or multiplicity of secondaries; this was done so as to exclude more effectively neutrons interacting in the top absorber. The selection of the experimental material may cause however, some bias in the results obtained, which cannot be estimated easily.

Furthermore, in some of these measurements an appreciable correction for the background was needed. This treatment may also cause, apart from in-

† For the estimation of the average path length of neutrons in the absorber it was assumed, that their differential angular distribution around the vertical is proportional to $\cos^7 \vartheta$ [20]).

†† A preliminary value of λ_c^{Pb} and σ_1^{Pb} was given at the Moscow Cosmic Ray Conference, July 1959 [21]).

creasing significantly the statistical error, some systematic shift of the results. For that very reason the experimental conditions of our measurements were chosen so that no correction was needed for the background.

More recently Brenner and Williams [8]) have measured the collision mean free path and the corresponding collision cross section of cosmic ray protons and neutrons for iron near 50 GeV with a similar method and found a value of $\lambda_c^{Fe} = 152 \pm 7$ g/cm², significantly higher than the geometrical one, $\lambda_{geom}^{Fe} \approx 100$ g/cm². The authors have calculated the value of λ_c^{Pb} corresponding to their experimental result as ≈ 210 g/cm², in good agreement with the value obtained by us. Kocharian *et al.* [9, 10]) have also measured the collision mean free path of protons in lead for different proton energies from 0.9 GeV up to 34 GeV determined with a magnetic spectrograph. The mean value of the collision mean free path found by the latter authors [9]), $\lambda_c^{Pb} = 198 \pm 10$ g/cm², deviates significantly from the geometrical one; it does not confirm however, directly our result because the mean energy of the protons measured was much lower than 30 GeV, the mean energy of the neutrons in the present experiment.

The collision cross section obtained by us for neutrons at about 30 GeV can be compared with the inelastic neutron cross sections measured at accelerators in the 1—5 GeV energy region (table 1).

TABLE 1

Inelastic (or collision) cross section of neutrons in lead

Experiment	Energy (GeV)	mb
Coor, Hill *et al.* [23])	1.4	1727 ± 45
Barrett [24])	3.6	1930 ± 300
Atkinson, Hess *et al.* [25])	4.5	1660 ± 90
present experiment	≈30	1652 ± 95

These data suggest that the value of the inelastic (or collision) cross section of neutrons in lead remains constant from about 1 GeV up to about 30 GeV. This result is in good agreement with the results of Brenner and Williams [8]) who found the same constancy of the inelastic cross section in iron up to about 50 GeV. From the constancy of the nucleon-nucleus inelastic cross section one can expect that the effective elementary nucleon-nucleon cross section $\bar{\sigma}_1$ — the average of σ_1^{np} and σ_1^{nn} — is not very different at 30 GeV from the cross section measured directly for nucleon-nucleon collisions at accelerator energies.

The effective elementary cross setion $\bar{\sigma}_1$ contributing to the collision cross section as measured with the present experimental method corresponds at these energies essentially to the inelastic (meson-producing) cross section [8]) and must therefore be compared with the inelastic nucleon-nucleon cross section measured at accelerators.

The value of $\bar{\sigma}_1$ was derived from the collision cross section measured in lead by a transparency calculation worked out originally by Heitler and Jánossy [5]) and Fernbach, Serber and Taylor [6]) for uniform and generalized later by Williams [7]) for tapered nuclear density distribution.

According to this the collision cross section of a high energy neutron scattered by a nucleus represented by the nuclear density distribution $\rho(r)$ has the form [7])

$$\sigma_1 = \int_0^\infty [1-e^{-F(b)}]2\pi b db, \tag{3}$$

where b is the impact parameter of the collision and

$$F(b) = \int_{-\infty}^{\infty} K((b^2+s^2)^{\frac{1}{2}})ds, \tag{4}$$

the integral of the absorption coefficient $K(r) = \rho(r)\bar{\sigma}_1$ of the bombarding neutron along its path s (fig. 3).

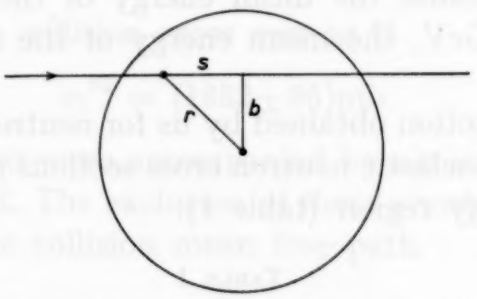

Fig. 3. The path s of a neutron through the nucleus; b is the impact parameter.

It was assumed that the nuclear density distribution has the same form as the charge density distribution determined by electron scattering experiments, i.e. that the spatial distribution of neutrons is the same as that of protons; this was also experimentally proved [26]). Hofstadter *et al.* [3, 4]) have found that the charge distribution for medium and heavy nuclei can be represented by a homogeneous smoothed density distribution of the type

$$\rho(r) = \frac{\rho_0}{1+\exp[(r-c)/z]}, \tag{5}$$

where c corresponds to the "half density" radius, z is the surface thickness parameter and ρ_0 the density parameter ($\rho_0 \approx$ central density). For lead the values $c \approx 6.5\times10^{-13}$ cm and $z \approx 0.5\times10^{-13}$ cm were found experimentally [4]).

The effect of the finite range of nucleon-nucleon interaction was taken into account according to Williams [7]) in a phenomenological manner by folding the density $\rho(r)$ with a function $F(|r-r'|)$ so as to obtain an effective nuclear density,

$$\rho'(r') = \int (\rho(r)F(|r-r'|)d^3r. \tag{6}$$

The effective density has been computed for a square well interaction

$$F(|r-r'|) = \begin{cases} \dfrac{1}{\frac{4}{3}\pi\lambda\!\!\!^{-}_{\pi}{}^{3}} & \text{for} \quad r < \lambda\!\!\!^{-}_{\pi}, \\ 0 & \text{for} \quad r > \lambda\!\!\!^{-}_{\pi}. \end{cases} \tag{7}$$

The value of $\bar{\sigma}_1$ obtained by the transparency calculation is very sensitive to the choice of the "half density" radius c, a small change in c corresponding to a very large change in $\bar{\sigma}_1$. Thus the contribution to the error of $\bar{\sigma}_1$ resulting from the inaccuracy of the determination of c for lead by electron scattering experiments is much greater than that resulting from the statistical error of σ_1^{Pb} obtained in our measurements. This difficulty can be overcome in the following way [8]).

Both σ_1^{Pb} and $\bar{\sigma}_1$ were measured very accurately at accelerator energies (see tables 1 and 2). Assuming that σ_1^{Pb} and $\bar{\sigma}_1$ are constant in the energy region between 1 GeV and 6 GeV their weighted mean values can be estimated as $\sigma_1^{\mathrm{Pb}} = 1717 \pm 40$ mb and $\bar{\sigma}_1 = 26 \pm 2$ mb.

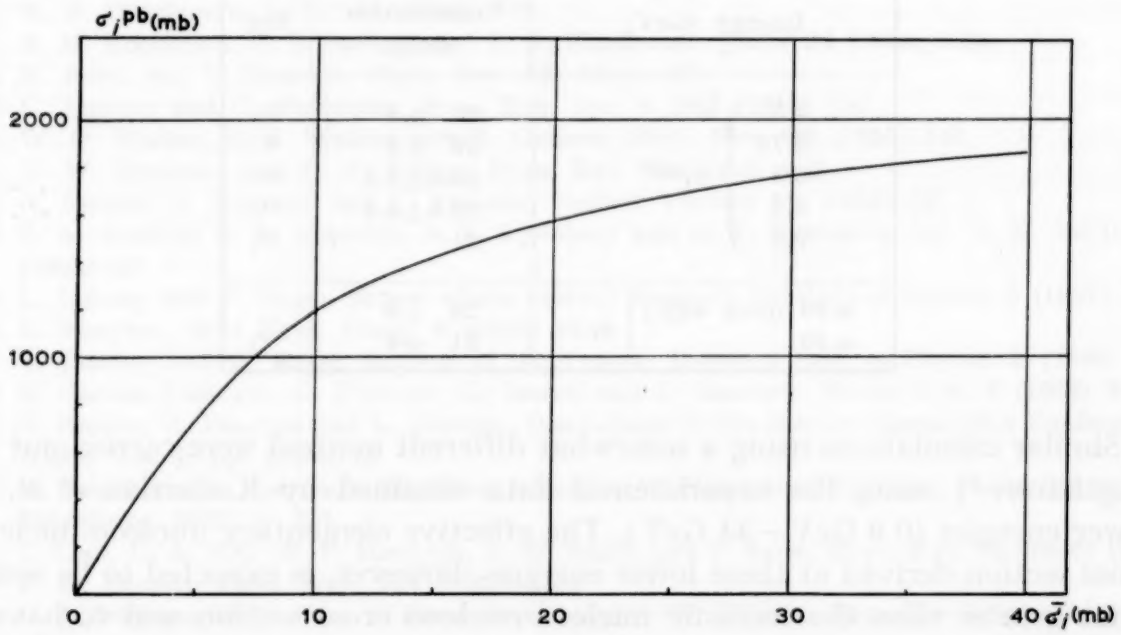

Fig. 4. The transparency curve for lead.

Substituting these values in eq. (3) and (4), using a fixed value of $z = 0.54 \times 10^{-13}$ cm taken from electron scattering experiments [27]) and varying the value of c, the "effective" half density radius best fitting the experimental cross sections can be estimated with a high accuracy as 6.67×10^{-13} cm. Due to the fact that in our case the values of σ_1^{Pb} are, within the limits of error, equal at accelerator and cosmic ray energies, the same will hold for the values of $\bar{\sigma}_1$. This means that in our case small inaccuracies in the original assumptions of the transparency calculation do not influence significantly the results and the

whole treatment was used rather for the evaluation of the statistical error of $\bar{\sigma}_1$ from the transparency curve than for that of its absolute value.

The transparency curve for lead is plotted in fig. 4. It can be seen from the transparency curve that our experimental result for the collision cross section in lead, $\sigma_1^{Pb} = 1652 \pm 95$ mb, corresponds — taking into account also the error in the estimate of c — to an inelastic nucleon-nucleon cross section at about 30 GeV

$$\bar{\sigma}_1 = 24 \pm 5 \text{ mb}. \tag{8}$$

This value is in a good agreement with the inelastic nucleon-nucleon cross section estimated in a similar way from the collision cross section measured for iron at 50 GeV [8]) and both values are not significantly different from the inelastic (p—p) cross sections measured at accelerators in the 1 GeV—10 GeV energy region (table 2).

TABLE 2

Inelastic nucleon-nucleon cross sections

Energy (GeV)		Cross section (mb)	Ref.
1.5	σ_1^{pp}	27 ±3	[28])
2.75		26 ±3	[28])
5.3		26.8±5.5	[28])
6.2		22.6±5.3	[28])
9.0		21	[28])
≈30 (pres. exp.)	$\bar{\sigma}_1$	24 ±5	
≈50		21 ±4	[8])

Similar calculations using a somewhat different method were carried out by Begzhanov [9]) using the experimental data obtained by Kocharian *et al.* at lower energies (0.9 GeV—34 GeV). The effective elementary nucleon-nucleon cross section derived at these lower energies, however, is expected to be somewhat greater than the inelastic nucleon-nucleon cross section and to have a value between the inelastic and total cross section. Indeed, the value found for the elementary cross section (32 ± 3 mb) agrees well with the above expectations.

5. Conclusion

Our results show that the inelastic (or collision) cross section of neutrons in lead remains, within the limits of error, constant from about 1 GeV up to about 30 GeV, and further they confirm the conclusion of ref. [8, 9]) about the constancy of the inelastic nucleon-nucleon cross section in the energy region 1 GeV—50 GeV.

We are indebted to Prof. K. Sitte for valuable discussions. We wish to thank also Mr. K. Ziegelmann for his assistance in running the equipment and Mr. G. Domokos and Miss M. Horváth for helping in the numerical calculations.

Note added in proof: The collision mean free path of 30 GeV neutrons in lead measured in the present experiment ($\lambda_c^{Pb} = 208 \pm 12$ g/cm^2) is in good agreement with the value of 200 g/cm^2 published just now of the mean free path of 24 GeV protons accelerated by the CERN proton synchrotron [29]).

References

1) G. Bozóki, E. Fenyves and L. Jánossy, Nuclear Physics **1** (1956) 501
2) R. W. Williams, Phys. Rev. **98** (1955) 1393
3) R. Hofstadter, Rev. Mod. Phys. **28** (1956) 214
4) R. Hofstadter, Ann. Rev. Nucl. Sci. **7** (1957) 231
5) W. Heitler and L. Jánossy, Proc. Phys. Soc. A **62** (1949) 374
6) S. Fernbach, R. Serber and T. B. Taylor, Phys. Rev. **75** (1949) 1352
7) R. W. Williams, Phys. Rev. **98** (1955) 1387
8) A. E. Brenner and R. W. Williams, Phys. Rev. **106** (1957) 1020
9) R. B. Begzhanov, JETP **34** (1958) 775
10) N. M. Kocharian, G. S. Saakian and Z. A. Kirakosian, JETP **35** (1958) 1335
11) B. Rossi and V. Regener, Phys. Rev. **58** (1940) 837
12) L. Jánossy and G. Rochester, Proc. Roy. Soc. A **182** (1943) 180
13) W. D. Walker, S. P. Walker and K. Greisen, Phys. Rev. **80** (1950) 545
14) H. W. Boehmer and H. S. Bridge, Phys. Rev. **85** (1952) 863
15) G. Bozóki, E. Fenyves and L. Jánossy, Nuclear Physics **11** (1959) 531
16) S. A. Azimov, N. A. Dobrotin, A. L. Ljubimov and K. P. Ryshkova, Izv. A. M. SSSR **17** (1953) 80
17) L. Jánossy and E. Rupp, Report of the Central Research Institute of Physics **5** (1957) 188
18) E. Fenyves, Acta Phys. Hung. **4** (1955) 363
19) L. Jánossy and E. Rupp, Reports of the Central Research Inst. of Physics **8** (1960) 71
20) M. Cervasi Fidecaro, G. Fidecaro, G. Marini and L. Mezzetti, Nuovo Cim. **9** (1958) 38
21) G. Bozóki, E. Fenyves and L. Jánossy, Proceedings of the Moscow Cosmic Ray Conference (1959) Vol. I, pp. 170–173
22) M. Deutschmann, Kosmische Strahlung, edited by W. Heisenberg (Springer, Berlin-Göttingen Heidelberg, 1953) p. 101
23) T. Coor, D. A. Hill, W. F. Hornyak, L. W. Smith and T. Snow, Phys. Rev. **98** (1955) 1369
24) P. H. Barrett, Phys. Rev. **114** (1959) 1374
25) H. J. Arkinson, W. N. Hess, V. Perez-Mendez and R. W. Wallace, Phys. Rev. Letters **2** (1959) 168
26) A. Abashian, R. Cool and J. W. Cronin, Phys. Rev. **104** (1956) 885
27) L. R. B. Elton, Nuclear Physics **5** (1958) 173, **8** (1958) 396
28) V. I. Veksler, Report on the 9-th International Conference on High Energy Physics, Kiev (1959)
29) A. Ashmore, G. Cocconi, A. N. Diddens and A. M. Wetherell, Phys. Rev. Lett. **5** (1960) 576

1.E.1:
3.A

Nuclear Physics **24** (1961) 422—430; © *North-Holland Publishing Col, Amsterdam*

Not to be reproduced by photoprint or microfilm without written permission from the publisher

THE 5.3 SEC ISOMER OF W^{183}

C. J. GALLAGHER, Jr., and H. L. NIELSEN

Institute for Theoretical Physics, University of Copenhagen, Denmark

Received 17 January 1961

Abstract: A 5.3 sec isomer of W^{183} has been chemically separated from its parent 5.2 d Ta^{183}. The radiations from the isomer have been observed with a xenon proportional counter and a NaI scintillation crystal and have energies of 46, 52, ≈ 105 and ≈ 160 keV. Gamma-gamma coincidence measurements involving the photons have been made. On the basis of these results and previously reported high resolution measurements of the decays of Ta^{183} and Re^{183}, the energy of the isomeric level is assigned as 309.49 keV, and its spin and parity as $\frac{9}{2}+$.

1. Introduction

The energy levels of beta stable W^{183} have been investigated through studies of the beta decay of Ta^{183} (ref. [1])), the electron capture decay of Re^{183} (ref. [2])), fast and slow neutron reactions on wolfram [3–5]) and Coulomb excitation of the W^{183} levels directly [6–8]). The very careful work of Murray *et al.* [1]), using both high resolution gamma-ray and beta-ray spectroscopy, established the decay scheme of Ta^{183} shown in fig. 1. In their analysis of the experimental data, Murray *et al.*

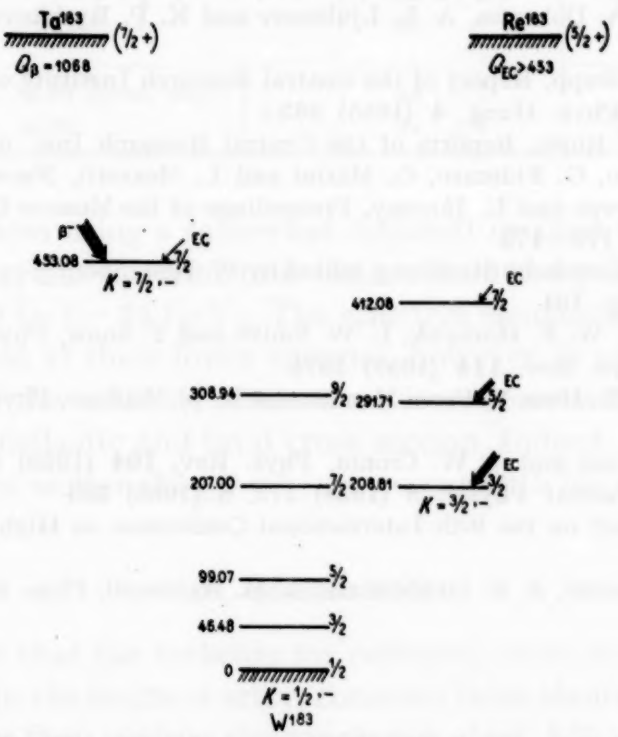

Fig. 1. Level scheme of W^{183} and levels populated by the decays of Re^{183} and Ta^{183}. The level scheme is as originally proposed by Murray *et al.* The analysis of the level scheme into intrinsic and rotational states was first proposed by Kerman.

were able to fit all but two of the observed transitions into the decay scheme shown. One of these transitions unassigned in the decay scheme, at 102.49 keV, they assigned as an M2 transition on the basis of the K and L_I conversion coefficients (35 and 6, respectively) and the observed conversion in only the L_I shell. Kerman [9]) analyzed the level spectrum and showed that it could be described in terms of intrinsic and rotational states as shown in fig. 1, assuming, however, that some of the states were highly K-admixed by the Coriolis interaction. Thulin *et al.*, investigating the decay of Re^{183} by the use of photographic-recording permanent-magnet spectrographs, found that all of the transitions they observed fit into the level scheme proposed by Murray *et al.* with no evidence for the conversion lines of the 102.49 keV transition [2]). Gallagher *et al.*, using longer exposures than Thulin *et al.* on the same equipment, were also unable to find any evidence for the 102.49 keV transition [10]). Der Mateosian and Goldhaber produced a 5.5 s isomer in wolfram by slow neutron reactions on wolfram, and reported that there were $\approx$ 80 keV electrons in the sample [3]). From the halflife and the electron energy they calculated that the isomeric transition was probably E3 or M3. Campbell and Goodrich reported gamma rays of 0.12 and 0.17 MeV for this isomer [4]). Poë has produced this isomer by fast neutrons on wolfram and has reported that the gamma-ray spectrum of the isomer included K X-rays (60 keV) and two gamma rays at 105 and 155 keV with an approximate ratio of intensities of 10 : 2.5 : 1, respectively. In Coulomb excitation experiments, the 99.07 and 46.48 keV levels have definitely been excited [6, 7]). Transitions of 162 and 292 keV have also been observed and assigned as arising from the excitation of the 208.81 keV $\frac{3}{2}$-level and the 292 keV $\frac{5}{2}$-level [8]).

We have investigated the beta decay of Ta^{183} again in an attempt to establish the position of the level in W^{183}, which de-excites by the M2 transition reported by Murray *et al.* In so doing we have isolated and studied the decay of a 5.3 s isomer in W^{183} which is populated by Ta^{183} decay.

2. Experimental

The 5.2 d Ta^{183} was produced by a 2 d irradiation of natural tantalum in a thermal neutron flux of 10^{14} n/cm^2 · s. The tantalum activity was adsorbed from a weak HF-solution on top of a small column (3mm $\times$ 1 mm diameter) containing Dowex 1 $\times$ 10 anion-exchange resin of a grain size corresponding to a settling rate in water of 2–4 mm/min. Elution of wolfram activity was performed with a 0.3 *M* HF–1*M* HCl mixture [11]). An activity with a 5.3 s halflife was found in the eluate.

Determination of the halflife was carried out using a well-type scintillation crystal in connection with a single-channel analyzer set to accept the W K X-rays and a scaler. A few drops of the eluate were transferred to the detector

immediately upon elution and photographs of the scaler were taken approximately every second for some minutes. A scaler counting the line current frequency of 50 Hz was photographed in the same picture. In this way, simultaneous values of accumulated counts and time were obtained. Analysis of the data

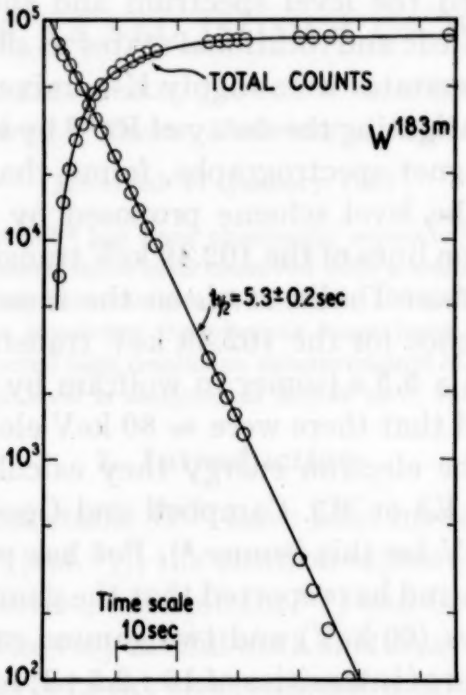

Fig. 2. Decay curve for the 5.3 s W^{183m} eluted from a Dowex 1 × 10 cm ion exchange resin column loaded with radioactive Ta^{183}. The decay curve was measured directly by photographing the register of the scaler in the counting circuit at 1 or 2 s intervals.

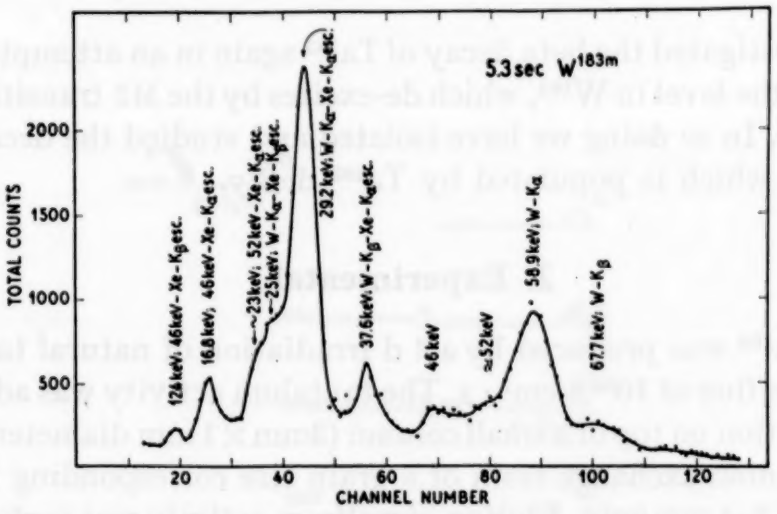
5.3sec W183m
TOTAL COUNTS
CHANNEL NUMBER
12keV; 46keV - Xe - Kβ esc.
16.8keV; 46keV - Xe - Kα esc.
~23keV; 52keV - Xe - Kα esc.
~25keV; W - Kα - Xe - Kβ esc.
292keV; W - Kα - Xe - Kα esc.
37.6keV; W - Kβ - Xe - Kα esc.
46keV
≈52keV
58.9keV; W - Kα
67.7keV; W - Kβ

Fig. 3. An Xe proportional-counter spectrum of the low energy radiations from 5.3 s W^{183m} obtained by repeated rapid extractions of W^{183m} from the parent Ta^{183}. Room and source background were subtracted after each extraction.

yields a halflife for the activity of 5.3±0.2 s (fig. 2).

Applying the same chemical technique, we measured the gamma-ray spec-

trum of the activity, using a 7.6 cm × 7.6 cm diameter NaI(Tl) crystal as well as a xenon-filled proportional counter (gas pressure: 2 atm) and gamma-gamma coincidences. A 256-channel pulse-height analyzer was used in all of these measurements †. Statistically significant numbers of counts were obtained in all three measurements by repeated rapid extractions, subsequently counting the decays of the isomer for 30 intervals. In order to account properly for the source background and analyzer dead time, which varied from extraction to extraction, we used the complement and lifetime operating modes of the analyzer to subtract the background after each extraction.

The proportional counter spectrum (fig. 3) was energy calibrated, using sources of Cs^{137} and Tl^{204} (emitting Ba and Hg X-rays, respectively). Besides the strong W K_α and W K_β lines, and their corresponding Xe-escape peaks, photopeaks and escape peaks of transition of 46 keV and 52 keV are present. The intensity ratio of the 46 keV line to the W K_α is $\approx \frac{1}{10}$.

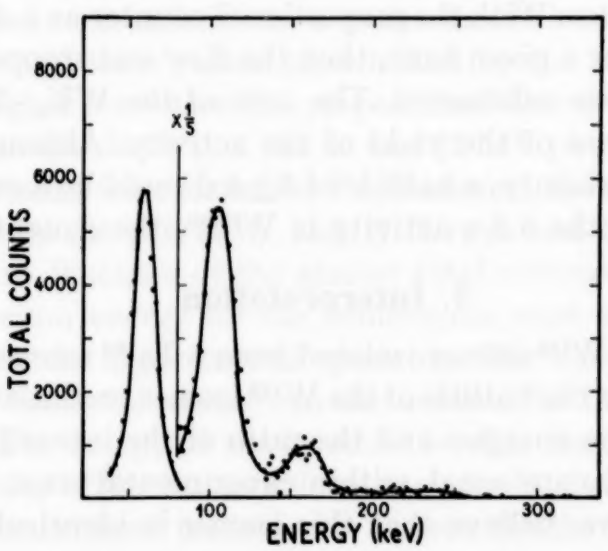

Fig. 4. A NaI scintillation crystal pulse-height spectrum of the radiations from 5.3 s W^{183m}. The spectrum was obtained in a manner identical to that described in the caption of fig. 3.

The NaI spectrum is shown in fig. 4. The energy spectrum was calibrated with a W^{178}–Ta^{178} equilibrium mixture, Na^{22} and Cd^{109}. From fig. 4 it can be seen immediately that the spectrum contains peaks at 55, 105 and 160 keV. The experimental ratio of the peak intensities is 100 : 19 : 3.5, respectively. Pronounced coincidence sum peaks were observed at ≈ 105 and ≈ 160 keV when the solid angle was increased. In order to obtain an estimate of the energy of the isomeric level using sum coincidences, we measured the spectrum of the isomer with a source placed against the crystal. The sum background showed a definite cutoff at ≈ 260 keV.

† Manufactured by Radiation Counter Laboratories, Skokie, Ill., USA.

Gamma-gamma coincidence measurements using a conventional fast-slow coincidence circuit were made, gating on all three photon peaks, but because of the necessity for large initial counting rates and large geometries, we probably also observed coincidences with sum peaks. Quite unambiguously, however, the $\approx$ 55 keV photon is coincident with 55, 105 and 160 keV photons. The 160 keV transition was only strongly coincident with K X-rays, and some 160–105 keV coincidences were observed. The ratio of 55 to 105 keV photons was 2.5 times less than the same ratio in the single spectrum, however.

The mass assignment of the activity was made by determining the elution yield of the activity as a function of time. The experimental technique was a modified version of Campbell and Nelson's [12]). A Dowex 1×10 column, as described above, but in which the Ta activity was evenly distributed on the resin, was continuously eluted with a 0.3 *M* HF–1*M* HCl mixture, which was recirculated in a steady flow to the top of the column. The system was shielded so that only a suitable length of the tubing immediately below the column was exposed to the detector. With the proportional counter as a detector, the spectrum was recorded for a given time, then the flow was stopped, and the "background" spectrum was subtracted. The area of the WK_α–Xe K_α escape line was used as a measure of the yield of the activity. Although the method is subject to some uncertainty, a halflife of 6 ± 4 d could be ascribed to the yield, thus indicating that the 5.3 s activity is W^{183m}, the daughter of 5.2 d Ta^{183}.

3. Interpretation

The halflife of the W^{183} isomer isolated from a Ta^{183} source is, within experimental error, equal to the halflife of the W^{183} isomer produced by neutron reactions on wolfram. The energies and the ratio of the intensities of the gamma transitions we observe are equal, within experimental error, to those reported by Poë. We, therefore, believe that this isomer is identical to that reported earlier.

Our experimental data alone would not be enough to permit us to assign the energy, spin, or parity of the isomeric level, but taken together with the careful work of Murray *et al.* and Thulin *et al.* we believe we can assign all three.

The energy of the isomer can be deduced in the following way. We have established that it is populated relatively strongly in the decay of Ta^{183}, hence probably has been observed in the work of Murray *et al.* Furthermore, because Murray *et al.* report only two unassigned transitions (the difference between which, or the sum of which, does not correspond to any energy sum or difference in the W^{183} level scheme) it is probable that (1) one of the unassigned transitions is the isomeric transition; (2) this transition populates one of the levels reported by Murray *et al.* The first argument is reasonable because the 102.49 keV transition has been assigned an M2 multipolarity. Secondly, on the basis that the intensity of the other unassigned transition has an intensity only about $\frac{1}{4}$

the strength of the 102.49 transition (and is an M1+E2), we do not believe it can reasonably be assigned as a transition alone depopulating a level populated by the isomeric transition. Also because the isomer decays by at least two transitions, we conclude that the isomeric decay populates at least one of the levels reported by Murray *et al.*

An examination of the W^{183} level scheme shows that only one of all the levels previously assigned in W^{183} satisfies the requirements imposed by the fact that the highest energy transition in the spectrum of the isomer is 160 keV. That is the 207.00 keV level previously assigned as the $\frac{7}{2}$-rotational state of the $K = \frac{1}{2}$ rotational band. Using the relative gamma intensities and conversion coefficients reported by Murray *et al.* for the transitions depopulating this level and the subsequently populated levels, and for the 102.49 keV isomeric transition, we conclude that, if this is the level populated by the isomer, the NaI spectrum of the isomer should (1) have peaks at $\approx$ 55 keV (K X-rays, 46.48 and 52.59 keV photons), $\approx$ 105 keV (99.07, 102.49, and 107.93 keV photons) and $\approx$ 160 keV (160.53 keV photons); and (2) these peaks should have the intensity ratio 100 : 19.8 : 3.5. Both of these points are checked by the experimental results. In addition, the higher resolution Xe proportional-counter study of the low-energy photon spectrum shows just the 46 and 52 keV photon and W K X-ray peaks expected with this interpretation. Furthermore, the principal sum peaks should be 2 K X-rays (at 110 keV), and K X-rays and 107.93 keV photons (at $\approx$ 160 keV) with (because of the almost total conversion of the isomeric transition) a maximum energy for the coincidence sum peak at $\approx$ 260 keV, again as observed in the experimental spectrum. The strong coincidence-sum peaks predicted by this level scheme can also account for the apparent 160–105 keV coincidences. The energy of the isomeric level is thus 309.49 keV.

The spin and parity of the isomeric level can also be deduced, assuming the M2 assignment of the isomeric transition is correct. (In the following discussion we assume that there are no transitions with energies $\lesssim$ 30 keV). The K conversion coefficient reported by Murray *et al.* is 35, which is considerably larger than the theoretical value of Sliv and Band [13]) of 27.6. However, Murray *et al.* normalized their experimental conversion coefficient to the theoretical value for an M1 which had not been corrected for finite nuclear size effects, which results in an error of 20 % in this case †. When this correction is applied, the experimental conversion coefficient is 28, in excellent agreement with theory. However, the L-subshell ratio reported by Murray *et al.*, $\alpha_{LI} : \alpha_{LII} : \alpha_{LIII} = 4.8 : - : -$, differs from the theoretical ratio for an M2, $\alpha_{LI} : \alpha_{LII} : \alpha_{LIII} = 6.94 : 0.83 : 1.58$ [13]). We have not experimentally checked this apparent discrepancy between theory and experiment. The assignment of the transition as M2 is therefore at present only partially consistent with theory.

† The conversion coefficients used in obtaining the ratio of transition intensities (i.e. $I_{\gamma 55}$:$I_{\gamma 110}$:$I_{\gamma 160}$) reported in the paragraph above were also reduced by 20 %.

We shall, however, accept Murray *et al.*'s assignment of the transition as M2 on the basis of the K-conversion coefficient, and assign it to populate the 207.00 keV level to which Murray *et al.* assigned negative parity. The parity of the isomer is therefore positive. Because the isomer is populated by a beta branch with log $ft = 8.5$ (calculated from Moszkowski's nomograph [14]), using a beta-decay energy calculated from the beta-endpoint energy of 615 keV for the transition to the 453.08 keV level, the decay fraction carried by the 102.49 keV transition reported by Murray *et al.* and the energy we have assigned to the isomeric level) from the Ta^{183} ground state, which is probably $\frac{7}{2}+$ (although $\frac{9}{2}-$ is possible), the level is expected to have a spin in the range $\frac{5}{2}$ to $\frac{9}{2}$. Because the level is not populated by the decay of Re^{183}, which has been postulated to have a $\frac{5}{2}+$ ground state [2]), the assignment of $\frac{5}{2}+$ or $\frac{7}{2}+$ seems unlikely, leaving $\frac{9}{2}+$ as the best possibility. Such an assignment is consistent with the systematics of energy levels in this region, as a $\frac{9}{2}+$ state is generally assigned [15]) as the ground state of nuclei with $N = 107$, and hence should be a low lying excited state in a nucleus with $N = 109$. If Ta^{183} has a $\frac{9}{2}$-ground state, an additional possibility is $\frac{11}{2}+$, but we consider this latter assignment less probable.

If the isomeric level is $\frac{9}{2}+$, the 210.4 keV cross-over M2 to the $\frac{5}{2}-$ state at 99.07 keV is possible. We can set an upper limit on the intensity of this cross-over transition as $\leqq \frac{1}{5}$ the intensity of the 160 keV transition. This is ≈ 80 times less than energy considerations alone would predict. However, the very large hindrance of the 102.49 keV transition (see below) indicates that it probably occurs only through small admixtures in the wave functions; hence, the weakness of the branch to the 99.07 keV level may not be especially significant.

The decay scheme we propose involving the isomer is shown in fig. 5.

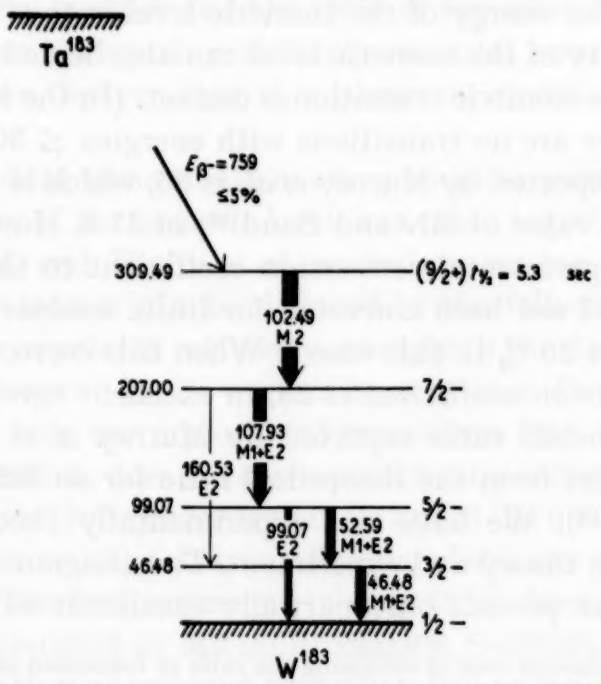

Fig. 5. The Ta^{183} decay scheme involving the 5.3 s W^{183} isomer.

4. Discussion

The log $ft = 8.5$ observed for the beta decay to the isomeric level is large for an allowed transition. Furthermore, although in the asymptotic-limit classification of the Nilsson states † the levels would be 404 ($\frac{7}{2}+$) and 624 ($\frac{9}{2}+$) and the transition would be hindered, the log ft for the same transition observed in Lu^{177} decay is 6.3. Such variations in the log ft for a given transition have been observed before [15]) but as yet have not been satisfactorily explained in a quantitative way.

The argument we have used to assign a spin and parity to the isomer is largely dependent on the M2 assignment of the 102.49 keV transition, which we assign as the isomeric transition. In addition to the discrepancy in the L-subshell conversion of the transition, the isomer is extremely retarded for an M2. The hindrance factor for the radiative transition relative to single-particle rates [16])

$$F_{M2} = \frac{t_{\frac{1}{2}}(\text{exp})}{t_{\frac{1}{2}}(\text{theor})} = 1.6 \times 10^7$$

is, we believe, a larger hindrance than has hitherto been observed for an M2 transition. Such a large hindrance might, of course, be associated with the $\nu = 2 (\nu = \Delta K - L)$ K forbiddenness of the transition [17]).

In view of the long halflife of the isomer it is surprising that an E3 transition does not compete. The hindrance for a 102.5 keV E3 would be $\approx 10^2$. However, the L-subshell ratio reported by Murray *et al.* effectively rules this out, as theoretically $\alpha_{LI} : \alpha_{LII} : \alpha_{LIII} = 0.84 : 32 : 25$ for an E3 transition.

Most surprising to us, however, is that the E1 transition which might be expected to occur between $\frac{9}{2}+$ and $\frac{7}{2}-$ states is very weak, if present at all, at least on the basis of the conversion coefficient. Even if we assume that the isomeric transition is pure E1 (ignoring the question of the large conversion coefficient), the hindrance factor for the radiative transition is $F_{E1} = 1.95 \times 10^{15}$, which certainly classifies it as the most highly retarded K-forbidden E1 (considering $\nu = 3$) yet observed.

We thank Professor Niels Bohr for the excellent working conditions in his laboratory. The participation of one of us (C. J. G.) in this research was made possible by a U. S. National Science Foundation Postdoctoral Fellowship.

† See ref. [15]) for a discussion about the use of the asymptotic limit selection rules.

References

1) Murray, Boehm, Marmier and Du Mond, Phys. Rev. **97** (1955) 1007
2) Thulin, Rasmussen, Gallagher, Smith and Hollander, Phys. Rev. **104** (1956) 471

3) E. Der Mateosian and M. Goldhaber, Phys. Rev. **76** (1949) 187
4) E. C. Campbell and M. Goodrich, private communication quoted in Strominger, Hollander and Seaborg, Revs. Mod. Phys. **30** (1958) 585
5) A. J. Poë, Phil. Mag. **46** (1955) 611
6) Huus, Bjerregård and Elbek, Mat. Fys. Medd. Dan. Vid. Selsk. **30**, No. 17 (1956)
7) Chupp, Clark, Du Mond, Gordon and Mark, Phys. Rev. **107** (1957) 745
8) P. H. Stelson and F. K. McGowan, Phys. Rev. **99** (1955) 112;
F. K. McGowan and P. H. Stelson, Phys. Rev. **109** (1958) 901
9) A. K. Kerman, Mat. Fys. Medd. Dan. Vid. Selsk. **30**, No. 15 (1956)
10) Gallagher, Strominger and Unik, Phys. Rev. **110** (1958) 725
11) Gallagher, Nielsen and Nielsen, Phys. Rev. to be published
12) E. C. Campbell and F. Nelson, J. Inorg. Nuclear Chem. **3** (1956) 233
13) L. A. Sliv and I. M. Band, Publication of the Leningrad Physico-Technical Institute (reproduced in USA as Reports 57 ICC K **1** and 58 ICC-L **1** by the Physics Department, University of Ill., Urbana, Illinois, USA)
14) S. A. Moszkowski, Phys. Rev. **82** (1951) 35
15) B. R. Mottelson and S. G. Nilsson, Mat. Fys. Skr. Dan. Vid. Selsk. **1**, No. 8 (1959)
16) S. A. Moszkowski, in Beta- and Gamma-Ray Spectroscopy, edited by K. Siegbahn (North Holland Publishing Company, Amsterdam, 1955) Ch. XIII p. 391
17) Alaga, Alder, Bohr and Mottelson, Mat. Fys. Medd. Dan. Vid. Selsk. **29**, No. 9 (1955)

2.D: 2.F

Nuclear Physics **24** (1961) 431—442; © *North-Holland Publishing Co., Amsterdam*

Not to be reproduced by photoprint or microfilm without written permission from the publisher

PROTONS AND DEUTERONS FROM Ni^{58} BOMBARDED BY 14.8 MeV NEUTRONS

R. N. GLOVER and K. H. PURSER

Department of Nuclear Physics, Australian National University, Canberra

Received 20 December 1960

Abstract: Using a counter telescope, energy spectra and angular distributions are measured for protons emitted from Ni^{58} at 14.8 MeV incident neutron energy. The angular distributions indicate for the direct interaction contribution $l = 0$ and $l = 2$ transitions to unresolved levels near the ground state of the residual Co^{58} nucleus. Transitions with $l = 1$ to states of higher excitation demonstrate the presence of odd parity levels. Below 6 MeV proton energy, the distributions are isotropic. Nuclear temperatures of 1.35 ± 0.03 MeV and 0.50 ± 0.03 MeV are found for the reactions (n, pγ) + (n, pn) and (n, np) respectively. The total cross section for proton emission is 830 ± 70 mb. Partial cross sections are: (n, pγ) + (n, pn) 430 mb compound nucleus, 60 mb direct interaction; (n, np) 340 mb.

Deuteron emission is established, the total cross section for the (n, d) reaction being 25 ± 6 mb. The angular distribution of the most prominent deuteron group suggests unresolved transitions to the $\frac{7}{2}^-$ Co^{57} ground state and a new state at approximately 0.5 MeV. The presence of an $l = 1$ transition implies approximately 13 % p-wave admixture in the Ni^{58} ground state configuration.

1. Introduction

Many studies of proton emission from elements bombarded with approximately 14 MeV neutrons have been reported. It is possible to derive information on

1) the direct interaction process, with particular interest in observing transitions to individual levels of the residual nucleus;
2) the compound nucleus contribution;
3) cross sections;

and simultaneously, if protons and deuterons can be distinguished, on

4) the (n, d) pick-up reaction.

Therefore to carry out any detailed study an experiment should measure angular distributions and separate deuterons from protons. The major effort in the past has been devoted to measurement of energy spectra at a given angle, usually in the forward direction, and has provided little quantitative data. The particle detection techniques generally used have been nuclear emulsions and counter telescopes. The former suffers from difficulties in distinguishing protons from deuterons in the energy range of interest, namely 1–10 MeV [1]) and in attaining adequate statistical accuracy. On the other hand, because of the complexity of counter telescope techniques, angular distributions have seldom

been measured, and then only at large angular intervals and without separation of deuterons from protons. The present counter telescope and associated equipment were designed for experiments at 14.8 ± 0.3 MeV neutron energy to provide as much of the information noted above as possible.

The energy spectrum of protons emitted from Ni^{58} or natural nickel at a given forward angle has been measured previously [1–4]). Verbinskii *et al.* [5]) employing simple counting techniques obtained a crude angular distribution for all protons of energy > 6 MeV from natural nickel. The results suggested little anisotropy. Excessive background prevented measurements below 6 MeV. Colli *et al.* [6]) observed the spectrum from natural nickel at 18°, 45°, 90° and 135° and noted, at all energies in the range 3.5–15 MeV, minima at 90° and a small excess of counts at 18°. The design of their counter telescope [7]) suggests that the former effect is related to appreciable neutron scattering at 90°. With one exception [3]) these experiments were carried out at 14.1 MeV neutron energy. At 14.8 MeV, angular distributions have been reported by Kumabe and Fink [8]) using nuclear emulsions but the statistical accuracy is low and the energy intervals wide. Some forward peaking was observed but almost entirely at proton energies below 7 MeV so that identification with the direct interaction mechanism is dubious. At energies below 4 MeV a minimum at 90° was claimed.

In short proton angular distributions have not been measured adequately and neither the presence of direct interaction effects nor deuteron emission has been established.

2. Experimental Method

The telescope and associated circuitry and techniques have been described elsewhere [9]). For clarity a block diagram (fig. 1) illustrates the operation of the equipment. The counter telescope was capable of measuring angular distributions in the range 0–150° with angular resolution varying from ±7° at 30° to ±4° at backward angles, and negligible scattering (2 %) of incident neutrons. The target to be studied was located in a 'clean' neutron cone defined by means of a fast coincidence between the counter detecting recoil α-particles from the t(d, n)α reaction and the telescope scintillation counter. Particle identification was dependent on the fact that, when the ionisation loss dE/dx and energy E pulses are applied to the X and Y plates of a cathode ray tube, particles of different mass produce separate hyperbolae.

To establish that angular distributions were measured accurately, the angular distribution of recoil protons from a thin polythene radiator was measured from 0° to 65° on each side of the 0° position and shown to give the expected ($\cos\theta$) dependence.

The details of the Ni^{58} target were: diameter 2.7 cm, thickness 10 mg/cm^2, total weight 61.9 mg, composition 95.6 % Ni^{58} and 4.4 % Ni^{60}, platinum target backing 0.12 mm thick.

This target was set at a distance of 13 cm from the tritium target, at which point the diameter of the defined neutron cone was slightly greater than 2.9 cm. The cone normally contained 3×10^6 neutrons/sec, corresponding to 8×10^8 neutrons/sec into 4π. It was possible to use high flux mainly because of the powerful discrimination of the particle identification system against random

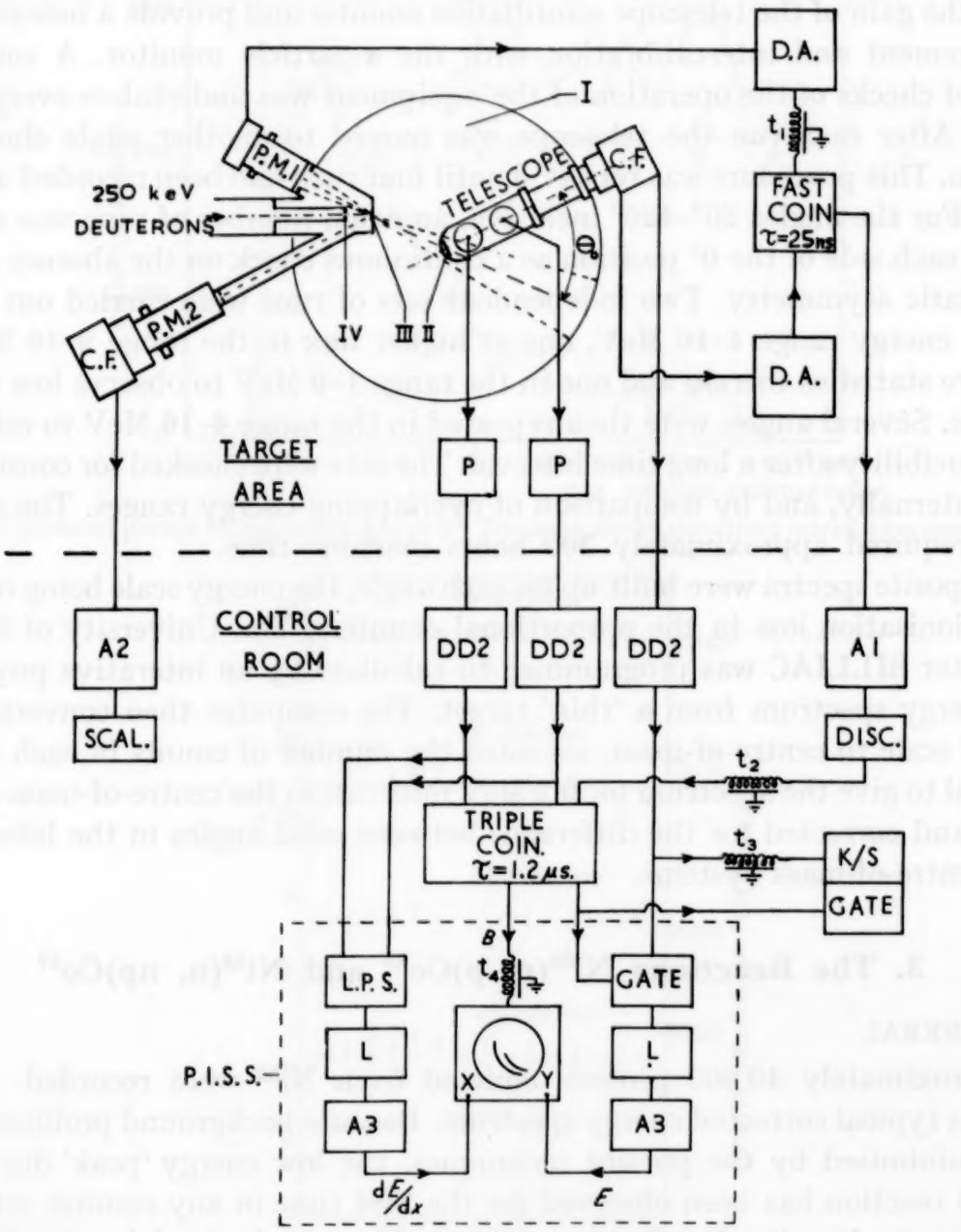

Fig. 1. I: Angular distribution table. II: Target under study. III: Tritium target. IV: Stop, diam. 2 mm, at 2.5 cm from tritium target to prevent movement of defined neutron cone. PM1: Recoil α-particle detector; plastic scintillator 0.05 mm thick on RCA 6655A photomultiplier. PM2: α-particle flux monitor; CsI crystal 0.05 mm thick on Dumont 6292 photomultiplier. CF: Cathode follower. P: Preamplifier. DA: Distributed amplifiers Hewlett Packard Types 460A+B. DD2: Fairstein double delay line amplifier. A1, A2: Conventional high gain amplifiers. P.I.S.S.: Particle identification and selection system. LPS: Least pulse selector. L: Pulse lengthener. A3: Long tailed pair amplifier. B: Brightening pulse to cathode ray tube grid.

events. Ten angles were studied, a run at each angle consisting of exposure of the Ni^{58} target and then the platinum blank. The cathode ray tube display was filmed, each frame corresponding to a fixed number of recoil α-monitor counts i.e. the same integrated flux. The method of film analysis has been described elsewhere [9]). Between each run the thin polythene radiator was exposed at 0° to check the gain of the telescope scintillation counter and provide a neutron flux measurement and intercalibration with the α-particle monitor. A complete series of checks of the operation of the equipment was undertaken every eight hours. After each run the telescope was moved to another angle chosen at random. This procedure was repeated until four runs had been recorded at each angle. For the angles 20°–120° inclusive, an equal number of runs was carried out on each side of the 0° position as a continuous check on the absence of any systematic asymmetry. Two independent sets of runs were carried out in the proton energy range 4–16 MeV, one at higher flux in the range 9–16 MeV to improve statistics therein and one in the range 1–9 MeV to observe low energy protons. Several angles were then repeated in the range 4–16 MeV to establish reproducibility after a long time interval. The sets were checked for consistency both internally, and by comparison of overlapping energy ranges. The experiment required approximately 300 hours machine time.

Composite spectra were built up for each angle, the energy scale being corrected for ionisation loss in the proportional counters. The University of Sydney computer SILLIAC was programmed to calculate by an interative procedure the energy spectrum from a 'thin' target. The computer then converted the energy scale to centre-of-mass, adjusted the number of counts in each energy interval to give the spectrum for 0.2 MeV intervals in the centre-of-mass energy scale, and corrected for the difference between solid angles in the laboratory and centre-of-mass systems.

3. The Reactions Ni^{58}(n, p)Co^{58} and Ni^{58}(n, np)Co^{57}

3.1. GENERAL

Approximately 40 000 protons emitted from Ni^{58} were recorded. Fig. 2 shows a typical corrected energy spectrum. Because background problems have been minimised by the present techniques, the low energy 'peak' due to the (n, np) reaction has been observed for the first time in any counter telescope experiment. Angular distributions (figs. 3–5) were obtained by dividing the spectra into 1 MeV intervals. In contrast to previous results [6, 8]) the angular distributions were isotropic below 6 MeV (fig. 3) showing neither forward peaking at low energies nor minima at 90°.

Precautions were taken during fabrication of the target at A.E.R.E., Harwell, during transit and after receipt to avoid water or other hydrogenous contamination. Its absence could not be checked directly by looking for recoil protons

near 0° since, from the Q-value of the (n, p) reaction, ($+0.36$ MeV [10]), protons leaving Co^{58} in the ground state or low-lying levels would have similar energies. However, such contamination distributed uniformly throughout the nickel

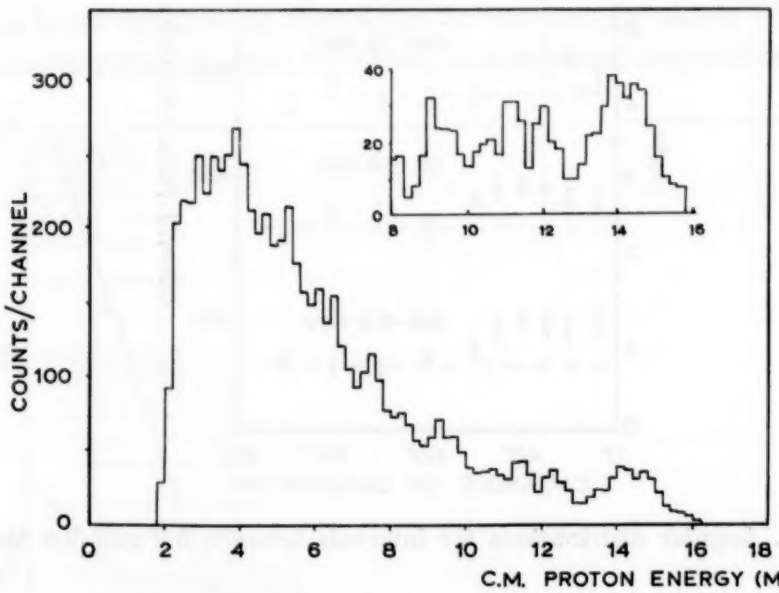

Fig. 2. Corrected proton energy spectrum at 0°. The inset shows the direct interaction contribution.

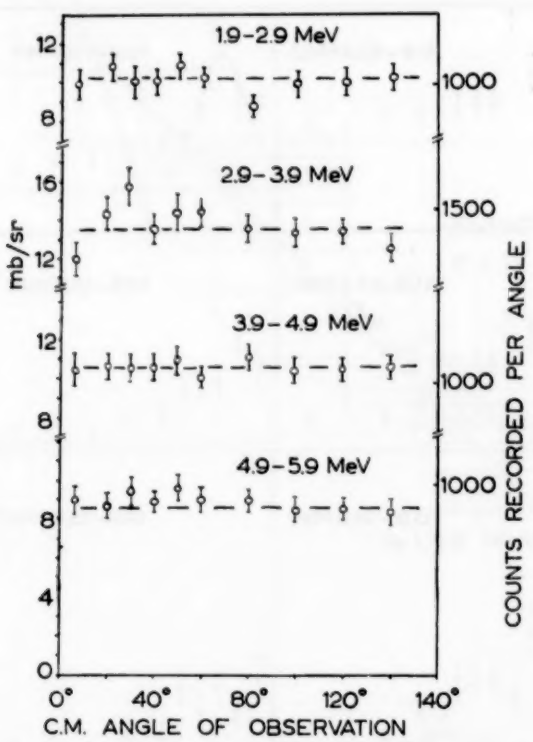

Fig. 3. Angular distributions 1.9–5.9 MeV; broken lines represent the compound nucleus contribution calculated from the ordinates of the points lying on the lines defining the temperatures (fig. 6).

layer could only account for protons in the range 14–15 MeV. It was concluded therefore that the excess of high energy protons (fig. 2, inset) was not due to contamination.

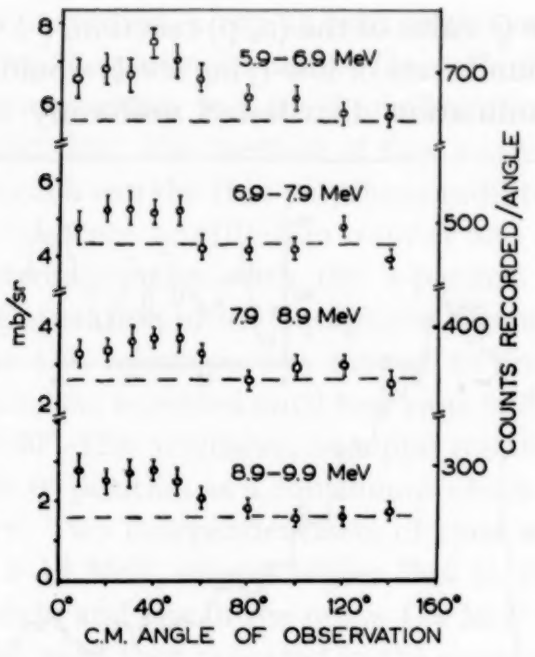

Fig. 4. Angular distributions for intervals between 5.9 and 9.9 MeV.

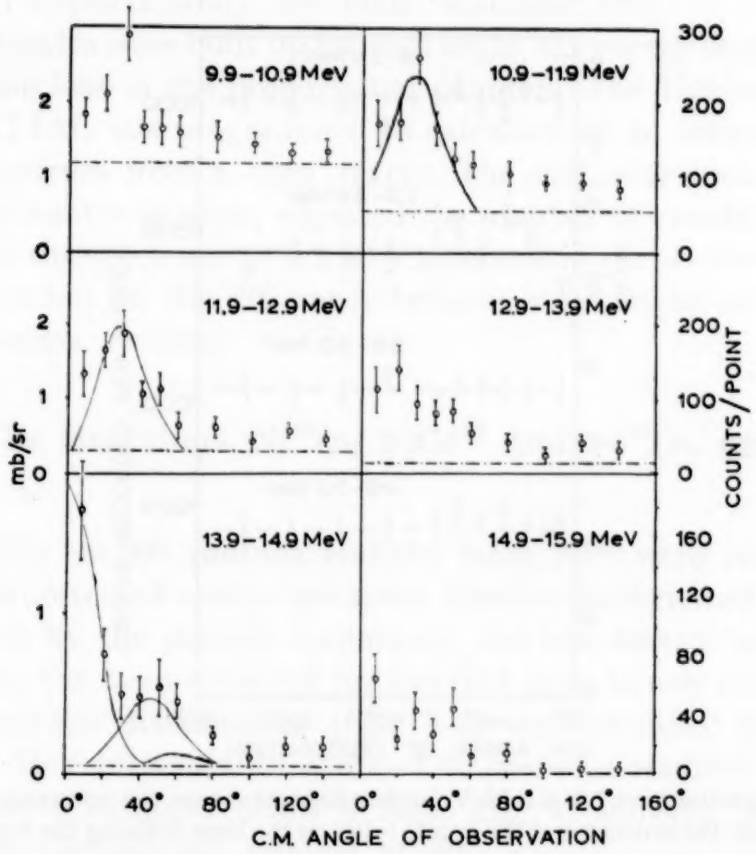

Fig. 5. Angular distributions for intervals between 9.9 and 15.9 MeV. Fits for $l = 1$ are shown for the intervals 10.9–11.9 MeV and 11.9–12.9 MeV, and $l = 0$ and $l = 2$ fits for the interval 13.9–14.9 MeV. Since these intervals are arbitrary, that for 12.9–13.9 MeV may contain contributions from the intervals above and below.

3.2. COMPOUND NUCLEUS CONTRIBUTION

The nuclear temperatures derived from a conventional statistical theory plot (fig. 6) were 1.35 ± 0.03 MeV and 0.50 ± 0.03 MeV for the reactions (n, pγ)+(n, pn) and (n, np) respectively. In the former case the temperature was obtained from a least squares fit restricted to the energy range 7.0–9.0 MeV since at high proton energies the plot deviated in a manner suggestive of a significant

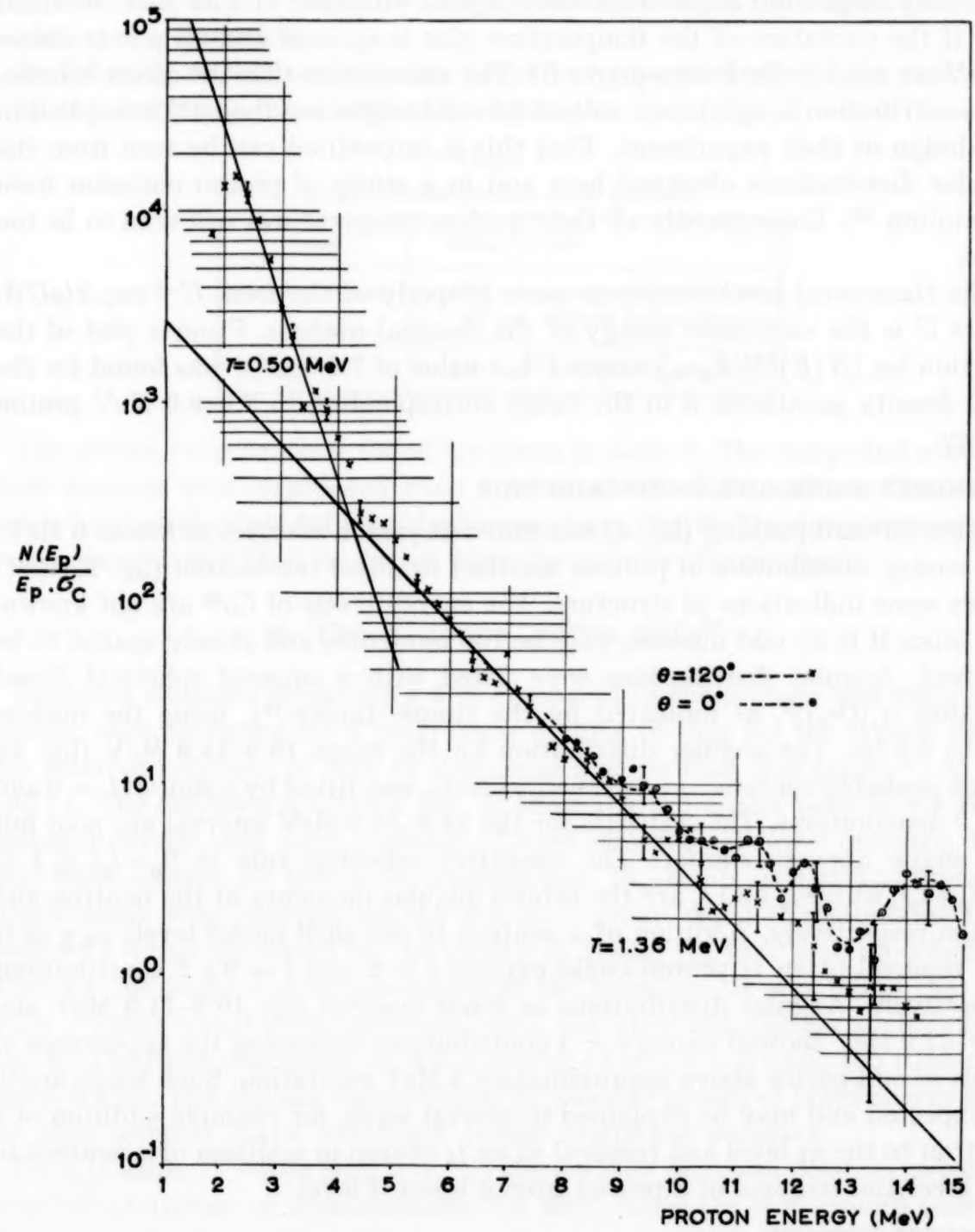

Fig. 6. Conventional statistical theory plot at 120° using the cross sections for compound nucleus formation derived by Shapiro [11]).

direct interaction contribution. The (n, np) temperature agrees with that of Kumabe and Fink [8]). However, their (n, pγ)+(n, pn) temperature of 1.0 MeV appears to be influenced by protons from the (n, np) reaction. If only points above 7 MeV are considered it increases to 1.25 MeV. Storey *et al.* [12]) have reported an (n, pγ)+(n, pn) temperature of (1.58$\pm$0.05) MeV from observation of the proton spectrum above 4 MeV with a scintillation counter subtending an extremely large solid angle. This value agrees with that of 1.52 MeV obtained here if the curvature of the temperature plot is ignored and all points above 7 MeV are used in the least squares fit. The assumption that the direct interaction contribution is significant only at forward angles less than 45° is implicit in the design of their experiment. That this is unjustified can be seen from the angular distributions observed here and in a study of proton emission from aluminium [13]). Consequently all their nuclear temperatures will tend to be too large.

The theoretical level density is more properly of the form $U^{-2}\exp 2(aU)^{\frac{1}{2}}$, where U is the excitation energy of the residual nucleus. From a plot of the function $\log [N(E)U^2/E_p\sigma_c]$ versus $U^{\frac{1}{2}}$, a value of 7.8 MeV^{-1} was found for the level density parameter a in the range corresponding to 7.0–9.0 MeV proton energy.

3.3. DIRECT INTERACTION CONTRIBUTION

Some forward peaking (fig. 4) was noted at proton energies as low as 6 MeV. The energy distribution of protons ascribed to direct interaction (fig. 2, inset) shows some indications of structure. The energy levels of Co^{58} are not known, but, since it is an odd nucleus, may be too numerous and closely spaced to be resolved. Angular distributions were fitted with a squared spherical Bessel function $[j_l(Qr_0)]^2$, as indicated by the simple theory [14]), using the nuclear radius 5.6 fm. The angular distribution for the range 13.9–14.9 MeV (fig. 5), which probably contains several energy levels, was fitted by a sum of $l = 0$ and $l = 2$ distributions. The statistics for the 14.9–15.9 MeV interval are poor but the shape appears similar. The operative selection rule is $|l_n - l_p| \leqq 1 \leqq |l_n + l_p|$, where l_n and l_p are the orbital angular momenta of the neutron and proton respectively. Addition of a neutron to the shell model levels $p_{\frac{1}{2},\frac{3}{2}}$ or $f_{\frac{5}{2}}$ and removal of an $f_{\frac{7}{2}}$ proton could explain $l = 2$ and $l = 0+2$ contributions respectively. Angular distributions at lower energies e.g. 10.9–11.9 MeV and 11.9–12.9 MeV showed strong $l = 1$ contributions indicating the appearance of levels of odd parity above approximately 3 MeV excitation. Such levels are to be expected and may be explained in several ways, for example addition of a neutron to the $g_{\frac{9}{2}}$ level and removal of an $f_{\frac{7}{2}}$ proton or addition of a neutron to a p level and removal of a proton from a lower d level.

3.4. CROSS SECTIONS

Although the fast neutron flux was measured absolutely to an accuracy of

3 % (by simultaneous comparison of two independent methods, namely recoil α-particle detection [15]) and detection of recoil protons with the counter telescope [16])), absolute cross sections do not depend on knowledge of the fast neutron flux. Since the Ni^{58} target and polythene radiator were exposed to the neutron beam in identical geometry within the telescope the Ni^{58} total cross section depends only on

1) the ratio of Ni^{58} counts to recoil proton counts for the same number of detected α-particles;
2) the ratio of Ni^{58} nuclei in the target to hydrogen nuclei in the radiator;
3) the scattering cross-section for hydrogen.

TABLE 1

Experimental proton cross sections

total	830±70 mb
(n, pγ+n, pn)	430 mb (compound nucleus) 60 mb (direct interaction)
(n, np)	340 mb (compound nucleus)

The proton cross sections found are given in table 1. The compound nucleus cross sections were calculated from spectra obtained from the ordinates of points lying on the lines defining the temperatures (fig. 6). The direct interaction cross section could then be found from the angular distributions.

4. The Reaction Ni^{58}(n, d)Co^{57}

Deuteron emission of intensity 3 % compared to the protons was observed. Spectra were corrected by a programme similar to that for the proton data. The relative response of NaI to deuterons and protons was taken [17]) to be 0.96 : 1. The deuteron spectrum (fig. 7) showed a prominent peak at 8.4 MeV deuteron energy, and some evidence of level structure at lower energies. The total cross section for the (n, d) reaction was 25±6 mb. Theoretical angular distributions were derived for the 8.4 MeV group using the tabulations of Lubitz [18]) which are based on the theory of Butler [19]), and were modified to allow for the finite angular resolution of the telescope. It was found that no single l value would give agreement with the observed angular distribution (fig. 8). The most reasonable fit was a mixture $l = 1$, $l = 3$ using the (Gamow) radius 6.4 fm. The angular distributions for possible groups of lower energy had the same general shape but much poorer statistical accuracy.

For a Q-value of −5.69 MeV (ref. [10])) the 8.4 MeV deuteron peak corresponds to a Co^{57} excitation of approximately 0.5 MeV. Since the Ni^{58} ground state is 0^+, only one l value is allowed for a transition to each final state. Therefore the angular distribution must correspond to two levels which, from the resolution

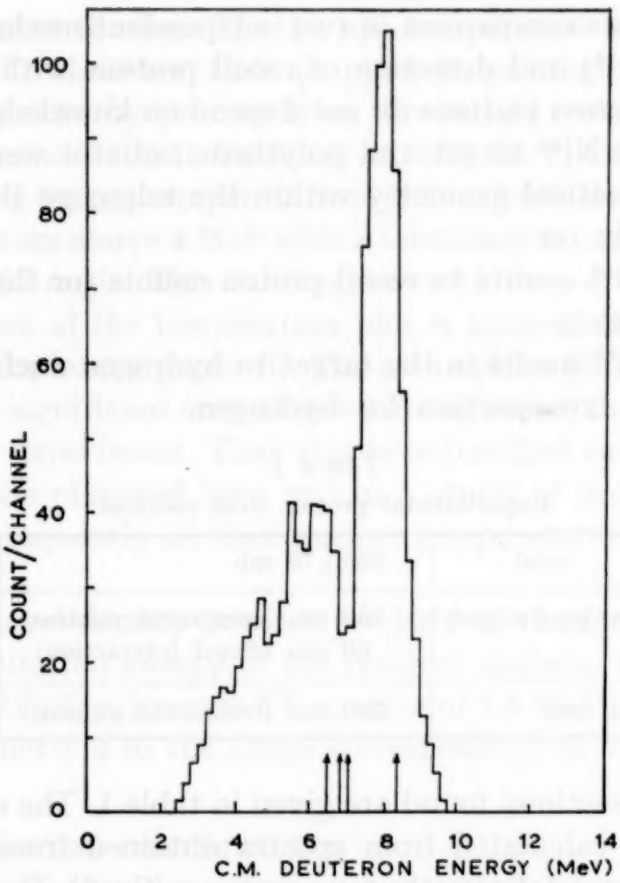

Fig. 7. Deuteron energy spectrum summed over the angles 0°–80°.

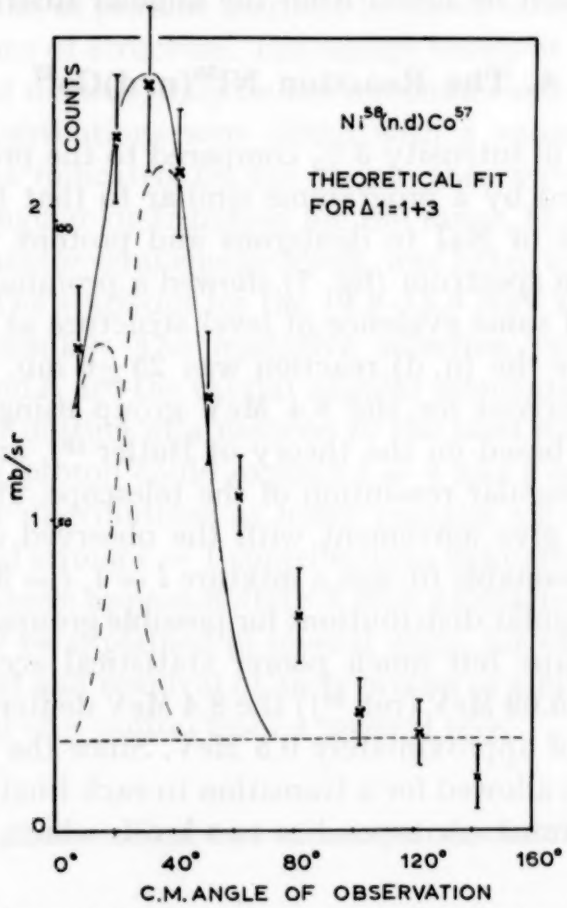

Fig. 8. Angular distribution of 8.4 MeV deuteron group, showing $l = 1+3$ fit. The broken lines represent the $l = 1$ and $l = 3$ contributions and the 'isotropic' component.

observed for 8.15 MeV deuterons from the (n, d) reaction on aluminium [13]), may be estimated to be 0.5 MeV apart. However, Co^{57} levels reported from the decay of Ni^{57} [20, 21]) are 0($\frac{7}{2}^-$), 1.36($\frac{3}{2}^-$), 1.49 ($\frac{1}{2}^-$) and 1.89 MeV ($\frac{5}{2}^-$). It seems reasonable to identify the $l = 3$ component as the ground state transition due to pick up of an $f_{\frac{7}{2}}$ proton from the closed shell and postulate an error of approximately 0.3 MeV in the Q value or in the experimental energy scale. The former possibility may be supported by a bump in the Ni^{58} proton spectrum of Jack and Ward [4]) which, if due to deuterons, can also be shown to correspond to a Co^{57} excitation of approximately 0.5 MeV assuming the Q-value used here and a relative response of CsI to deuterons and protons of 1.04 : 1 (ref. [22])). To explain the $l = 1$ transition, a new level at approximately 0.5 MeV with spin $\frac{1}{2}^-$ or $\frac{3}{2}^-$ is required. This may be in conflict with the Ni^{57} decay data of Konijn *et al.* [21]) who carried out a coincidence search for γ-rays of energy approximately 0.5 MeV and deduced an upper intensity limit of 1 % of the total γ-ray emission.

The presence of $l = 1$ transition(s) implies that the Ni^{58} ground state configuration contains p-wave admixture. The reduced widths, extracted as described by Macfarlane and French [23]), for the $l = 1$ and $l = 3$ transitions were 0.005 and 0.038 respectively indicating 13 % admixture. Assuming jj-coupling the spectroscopic factor S would have a value of 8, suggesting a value of 0.005 for the single particle reduced width θ_0^2(1f). This seems not inconsistent with θ_0^2(1f) = 0.012 in the range A = 17–45 (ref. [23])), if θ_0^2 decreases by a factor of 2–3 at the end of the shell as has been observed for the 1d shell [23]).

The authors are indebted to Messrs. E. Weigold and G. Hogg for assistance in recording the data and to Professor E. W. Titterton for many discussions.

References

1) D. L. Allan, Proc. Phys. Soc. A **70** (1957) 195
2) L. Colli and U. Facchini, Nuovo Cim. **5** (1957) 309
3) L. Colli, M. Pignanelli, A. Rytz and Z. Zurmühle, Nuovo Cim. **9** (1958) 280
4) W. Jack and A. Ward, Proc. Phys. Soc. **75** (1960) 833
5) V. V. Verbinskii, T. Hurliman, W. E. Stephens and E. J. Winhold, Phys. Rev. **108** (1957) 779
6) L. Colli, U. Facchini, I. Iori, M. G. Marcazzan and A. Sona, Nuovo Cim. **13** (1959) 730
7) M. G. Marcazzan, A. M. Sona and M. Pignanelli, Nuovo Cim. **10** (1958) 155
8) I. Kumabe and R. W. Fink, Nuclear Physics **15** (1960) 316
9) R. N. Glover, K. H. Purser and E Weigold, Nuclear Instruments, to be published
10) V. J. Ashby and H. C. Catron, UCRL 5419 (1959)
11) M. M. Shapiro, Phys. Rev. **90** (1953) 171
12) R. S. Storey, W. Jack and A. Ward, Proc. Phys. Soc. **75** (1960) 526
13) R. N. Glover and E. Weigold, Nuclear Physics, to be published
14) N. Austern, S. T. Butler and H. McManus, Phys. Rev. **92** (1953) 350
15) J. Benveniste, A. C. Mitchell, C. D. Schrader and J. H. Zenger, UCRL 5619 (1959); Nuclear Instruments **7** (1960) 306
16) S. J. Bame, E. Haddad, J. E. Perry and R. K. Smith, Rev. Sci. Inst. **28** (1957) 997

17) J. D. Seagrave, Phys. Rev. **97** (1955) 757
18) C. R. Lubitz, AECU **3990** (1957)
19) S. T. Butler, Nuclear Stripping Reactions (Wiley, New York, 1957)
20) J. Konijn, B. van Nooijen, P. Mostert and P. M. Endt, Physica **22** (1956) 887
21) J. Konijn, H. L. Hagedoorn and B. van Nooijen, Physica **24** (1958) 129
22) R. A. Peck, H. P. Eubank and J. Lowe, Rev. Sci. Inst. **30** (1959) 703
23) M. H. Macfarlane and J. B. French, NYO 2846 (1959); Rev. Mod. Phys. **32** (1960) 567

1.E.1

Nuclear Physics **24** (1961) 443—455; © *North-Holland Publishing Co., Amsterdam*

Not to be reproduced by photoprint or microfilm without written permission from the publisher

LEVELS IN Ho^{162} AND Dy^{162}

M. JØRGENSEN, O. B. NIELSEN and O. SKILBREID

Institute for Theoretical Physics, University of Copenhagen, Denmark

Received 19 December 1960

Abstract: An activity with half-life 11.8 min, representing the ground state of Ho^{162}, has been isolated by a recoil method from the 68 min Ho^{162} activity which belongs to an isomeric level about 90 keV above the ground state. A decay scheme for the Ho^{162} levels is proposed, indicating the following levels in Ho^{162}: ground state, $(K, I^{\pi}) = (1, 1^+)$; 38.5 keV $(1, 2^+)$; 86.5 keV (1.3^+); $\approx$ 90 keV $(6, 6^-)$. In Dy^{162} the following levels are proposed: 81 keV $(0, 2^+)$; 266 keV $(0, 4^+)$; 549 keV $(0, 6^+)$; 1485 keV $(5, 5^-)$. Single-particle assignments in the Nilsson-Mottelson scheme can be proposed for the unpaired particles of the ground state and the 90 keV states of Ho^{162} as well as of the 1485 keV level of Dy^{162}, based on the above spins and the fact that the K-capture transitions from Ho^{162} are allowed unhindered.

1. Introduction

The single-particle states characterizing the ground states and low energy excited states of odd-mass nuclei are now so well established throughout the regions of deformed nuclei [1]) that an identification of the intrinsic excitations in odd and even deformed nuclei seems within scope. The lowest levels of an odd nucleus probably correspond to configuration with the odd proton and the odd neutron left in the single-particle states identified as low lying levels in neighbouring odd-mass nuclei. Each configuration contains two levels corresponding to parallel or antiparallel coupling of the angular momenta of the proton and the neutron [2]).

Due to a pairing correlation, the ground states of even nuclei are depressed in energy and thereby separated from the single-particle excitations by a gap of 1–2 MeV, in which energy gap only collective excitations of the ground-state structure are found [3, 4]). The intrinsic excitations are expected to correspond to configurations of two unpaired protons or neutrons. An identification of such configurations thus also provides information on the size of the energy gap.

Since, in general, more than one low lying proton or neutron state in an odd-mass nuclei is known, the number of possible intrinsic states in even and odd nuclei is often considerable, making an unambiguous interpretation impossible. However, the situation is somewhat simpler if β-transitions with log ft values $\leqq 5$ occur. Such allowed unhindered transitions can take place only if the proton and neutron involved in the decay have the same asymptotic quantum numbers [1]).

In all the odd-mass Ho-isotopes, the odd proton is assigned [1]) the orbital $\frac{7}{2}^-[5, 2, 3]$. Allowed unhindered β-transitions are observed in six cases between this proton and the neutron state $\frac{5}{2}^-[5, 2, 3]$. For Ho^{162}, Mihelich *et al.* [5]) have reported a half-life of 67 min. This relatively short period might suggest that the same proton and neutron states are involved in the decay to Dy^{162}.

In addition, Mihelich *et al.* observed strong E2 transitions of 283, 185 and 81 keV, which could be identified as the $6^+ \rightarrow 4^+ \rightarrow 2^+ \rightarrow 0^+$ cascade in the ground state rotational band of Dy^{162}. The more detailed investigation of the decay scheme described here shows that two different levels of Ho^{162} decay with K-capture transitions with log $ft \approx 4.7$. Accordingly, it is possible to identify the single-particle configurations for both levels as well as for a 1485 keV excited level in Dy^{162}.

2. Experimental Methods

The Ho^{162} activity was produced in the $Tb^{159}(\alpha, n)$ reaction. Targets for the cyclotron bombardments and sources for the β- and γ-ray spectrometers were prepared according to techniques described elsewhere [6–9]). Although the α-particle energy was only 20 MeV, the $(\alpha, 2n)$ reaction was also rather intense, and Ho^{161} and Ho^{162} were formed in about equal amounts. The low energy radiation of Ho^{162} could thus only be studied on sources prepared in an isotope separator [6]). A few milligrams of the rare earth oxide bombarded in the cyclotron were immediately transferred to the ion source, and a chlorine containing vapour, in this case $C Cl_4$, was introduced. Volatile chlorides of the rare earths are then formed and ionized in the ion sources with high efficiency. By this method, separations could be carried out in one hour with an efficiency of about 10 %. Also the sources used for the isolation of the 11.8 min ground state of Ho^{162} by a recoil method were produced in the isotope separator.

Since Ho^{161} emits no high energy radiation, the positon spectrum and the high energy conversion line spectrum of Ho^{162} could be studied on sources prepared by chemical methods.

Due to the short life of Ho^{162}, the technique described in refs. [7, 8]) had to be speeded up by a factor of two. Thus, the dissolution of the target material, the application of the rare earth chloride solution on the macro-cation exchange column, and the separation of Tb from the earlier eluted by-products Ga and Er with α-hydroxy-isobutyrate, were performed in the course of 75 min. The subsequent operations, viz., the application of the acidified Tb-fraction on the micro-cation exchange column and the elution with ammonium lactate succeeded by ignition of the aluminium foil on which the activity was deposited, were also performed in 75 min. In most cases, the β-ray sources were ready for use about 2.5 h after termination of the cyclotron bombardment.

Single γ-ray spectra and γ–γ-coincidence spectra were measured in conven-

tional scintillation spectrometers equipped with 7.5 cm × 7.5 cm NaI-crystals and multi-channel analyzers. Conversion lines, the positon spectrum, and e–γ coincidence spectra were measured in a six-gap β-ray spectrometer equipped with automatic point-to-point recording. The detailed technique applied for the e–γ coincidence measurements has been described in ref. [10]).

3. Experimental Results

3.1. GAMMA RAY MEASUREMENTS

The γ-ray spectrum of an isotopically pure source is shown in fig. 1. In addition to the K X-ray and the 81, 185, and 283 keV γ-rays of the ground

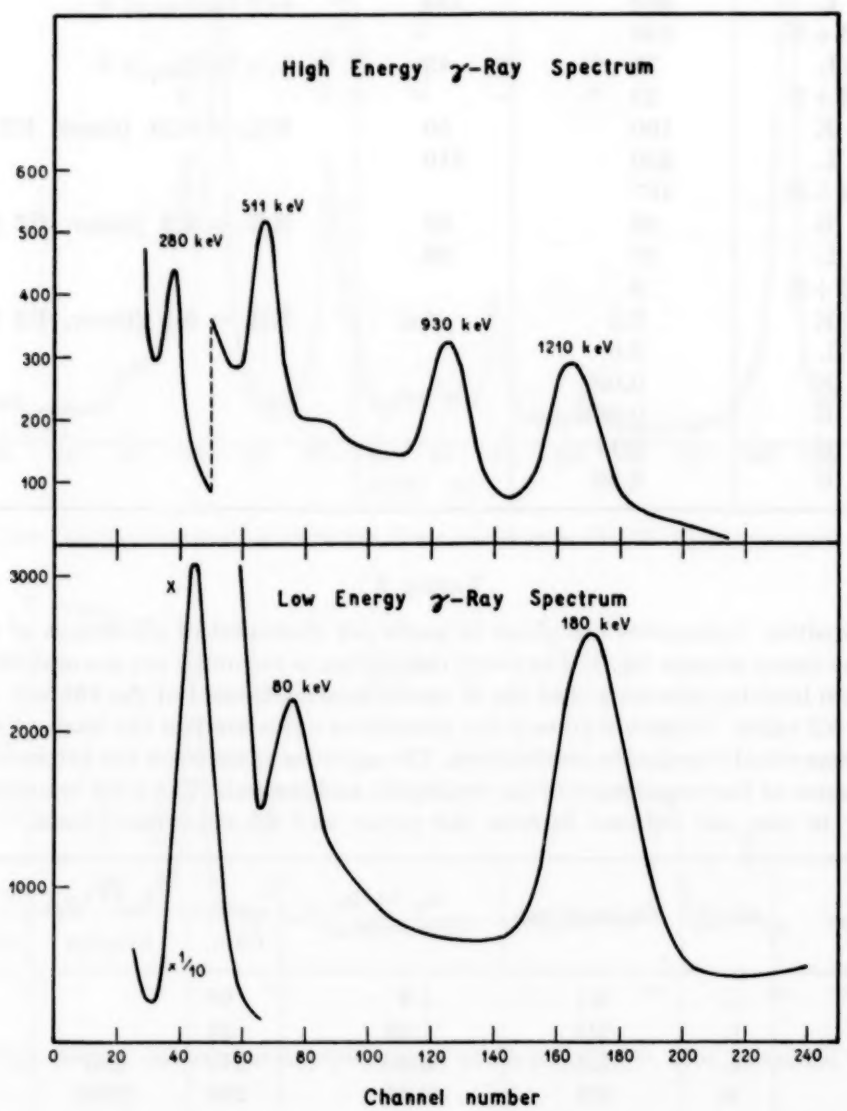

Fig. 1. Single γ-ray spectrum of 68 min Ho^{162} measured with a 7.5 cm × 7.5 cm NaI-crystal.

state rotational band, two intense high energy peaks of ≈ 935 and ≈ 1210 keV are present. The peak at 510 keV is strongly self-coincident in 180° geometry,

but not at 90°, and is thus due to annihilation radiation. The intensities are given in tables 2 and 3, which summarize the quantitative results of the experiments.

TABLE 1

Internal conversion lines. Energies are based on the accurate data of Mihelich *et al.* The 38.5 and 58.0 keV transitions are assumed to take place in Ho^{162} and not in Dy^{162}. The two sets of intensities are normalized on the line $K_{184.8}$.

E (keV)	Shell	Intensity of line		
		Present investigation	Mihelich *et al.*	
38.5	L	395	135	$L_I+L_{II}/L_{III} \geqq 5$
	M+N	140		
58.0	L	75	43	$L_I+L_{II}/L_{III} \geqq 5$
	M+N	25		
80.8	K	190	50	K/L = 0.54 (theor. E2 0.55)
	L	350	310	
	M+N	107		
184.8	K	59	59	K/L = 2.2 (theor. E2 2.4)
	L	27	29	
	M+N	9		
282.8	K	7.5	8.5	K/L = 3.4 (theor. E2 3.7)
	L	2.0		
884	K	0.025		
915	K	0.025		
935	K	0.17		
1215	K	0.20		

TABLE 2

Transition intensities. Intensities are given in parts per thousand of all decays of 68 min Ho^{162} according to the decay scheme fig. 7. The γ-ray intensities in column 7 are normalized with respect to the conversion lines by assuming that the K conversion coefficient of the 185 keV transition has the theoretical E2 value. Column 6 gives γ-ray intensities calculated on the basis of the conversion lines and the theoretical conversion coefficients. The agreement between the intensities of columns 6 and 7 is a measure of the consistency of the multipole assignments. The total transition intensities in the last column include the γ-ray and all conversion lines.

E (keV)	I_{Line}	Shell	Assignment	α_K or α_L (theoretical)	I_γ			$I_{trans.}$
					Calc.	Singles	Coinc.	
38	395	L	M1	4.4	90			625
58	75	L	M1	1.40	53			660
81	350	L	E2	3.20	110	105		760
185	59	K	E2	0.21	280	(280)		375
283	7.5	K	E2	0.060	125	145		135
884	0.025	K				190		
915	0.025	K						
935	0.17	K	E1	0.00120	140		127	140
1215	0.20	K	E1	0.00075	265	295	245	265

3.2. CONVERSION LINE MEASUREMENTS

The conversion line intensities are given in table 1 and used in table 2 for the assignment of multipole orders and for the calculation of the transition intensities. In addition to the lines representing the transitions known from the γ-ray

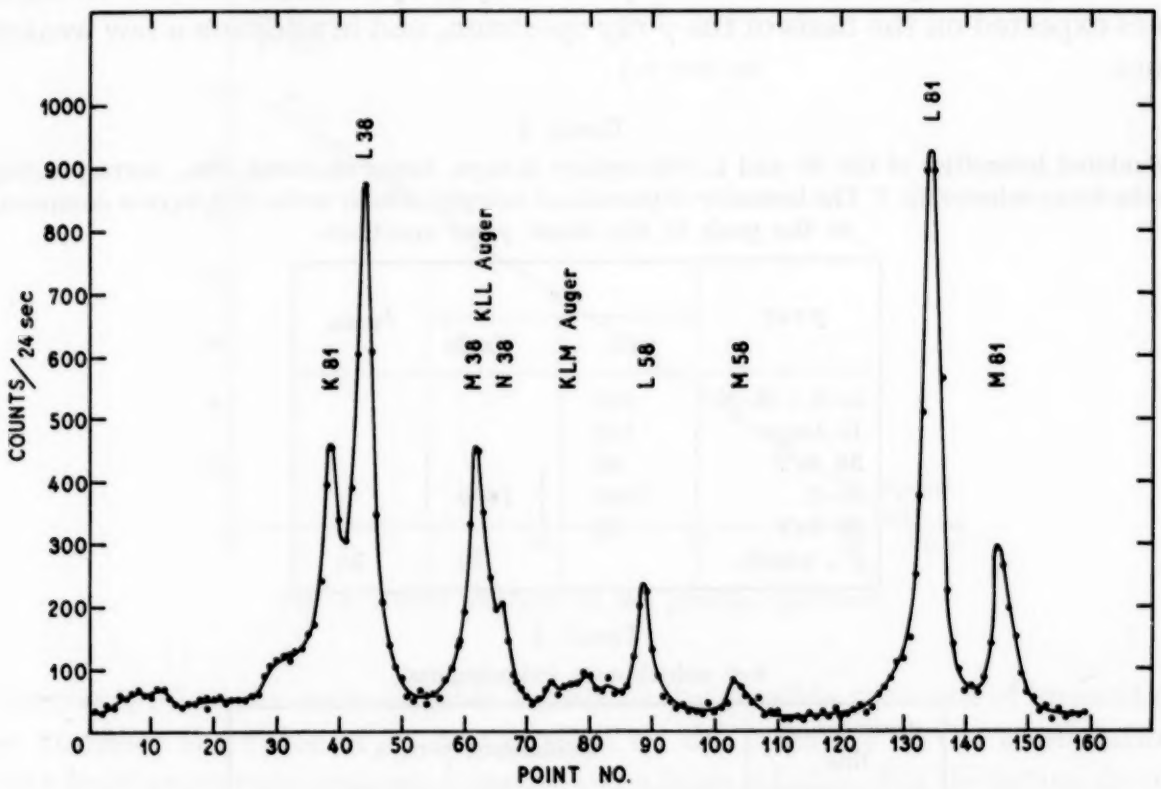

Fig. 2. Low energy internal conversion lines of 68 min Ho^{162}. Not corrected for decay.

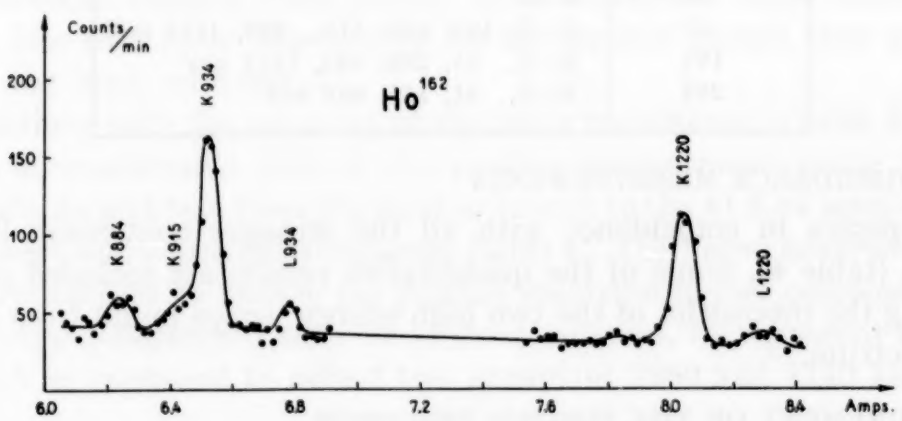

Fig. 3. High energy internal conversion lines of 68 min Ho^{162}. Not corrected for decay.

spectrum, L and M conversion lines of two intense transitions of 38.5 and 58.0 keV are present (fig. 2). These lines have earlier been observed by Mihelich *et al.* and assigned predominant M1 multipole order from $L_I : L_{II} : L_{III}$ ratios. The M1 nature is confirmed by the present $L_I + L_{II} : L_{III}$ ratios. As 58 keV is higher

than the K binding energy in Ho and Dy, an unobserved K conversion line of a few keV must be assumed and, since the theoretical K/L ratio for low energy M1 transitions is 6.8, it must be rather intense and represent the larger number of the 58 keV transitions.

The high energy conversion line spectrum (fig. 3) contains the two stronger lines expected on the basis of the γ-ray spectrum, and in addition a few weaker lines.

TABLE 3

Calculated intensities of the K- and L+M-capture X-rays, Auger electrons, etc., corresponding to the decay scheme fig. 7. The intensity of photons of energies similar to the KX-rays is compared to the peak in the single γ-ray spectrum

γ-ray	I_γ		$I_{trans.}$
	calc.	single	
L–X+M–X	160		
K-Auger	105		
38 keV	90		
K–X	1440	1800	
58 keV	53		
β^+, annih.		70	35

TABLE 4

e–γ coincidence experiments

Conversion line	Coincident γ-rays
38	K–X
58	none
81	K–X, 185, 283, 510, 935, 1215 keV
185	K–X, 81, 283, 935, 1215 keV
283	K–X, 81, 185, 935 keV

3.3. e–γ COINCIDENCE MEASUREMENTS

γ-ray spectra in coincidence with all the stronger conversion lines were measured (table 4). Some of the quantitative results are included in table 2, confirming the intensities of the two high energy γ-rays found from the single γ-ray spectrum.

3.4. MEASUREMENT OF THE POSITON SPECTRUM

The annihilation peak (fig. 1) indicates the presence of a positon group sufficiently intense for a measurement in the β-ray spectrometer. The annihilation radiation from the unseparated source used for this measurement was somewhat more intense than that of the isotopically pure sources, indicating the presence of some positon emitting impurities which were not easily removed completely by the fast chemical technique employed. A measurement of the half-life of the

positon spectrum revealed, however, that the main component decayed with a 68 min period as do the other radiations from Ho^{162}.

Fig. 4 shows a Fermi analysis of the positon spectrum. A measurement of the intensity relative to the conversion lines indicates that the positon spectrum

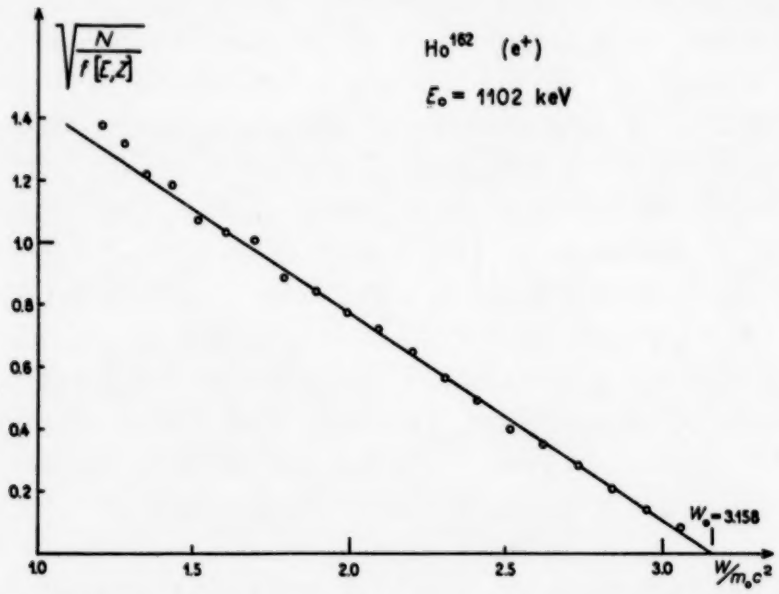

Fig. 4. Fermi analysis of the positon spectrum.

represents 50 of the units of table 2. Due to the possible presence of impurities we consider the value of 35 units, based on the intensity of the annihilation peak from an isotope separated source, to be more reliable. For the actual decay energy and Z-value, the ratio between K-capture and β^+ emission is 16 (ref. [11])), and the electron capture from higher shells represents three times the β^+-intensity. The transitions represented by the positon groups thus amount to $\approx$ 700 of the units of table 2.

A comparison with the intensity of the other transitions in table 2 makes it clear that a considerable part of the positon decays must excite the Dy^{162} ground state. In addition there is a positon branch to the 81 KeV level established by the e–γ coincidence measurements (table 4). The Fermi analysis (fig. 4) is not accurate enough to resolve the positon spectrum in two components with 80 keV energy difference. Under these circumstances, the apparent end point of 1100 keV is supposed to reflect two groups of 1060 and 1140 keV.

4. The Decay Scheme

γ–γ and e–γ coincidence measurements (table 4) show that the two high energy transitions are coincident with the 81 and 185 keV transitions, and the 935 keV ray further with 283 keV. They thus originate in one level at about 1485 keV (fig. 7), of spin 5^-, since it decays with E1 transitions to levels of 6^+

and 4^+. The half-life of Ho^{162} indicates a low *ft*-value, and the spin of the level decaying to the 5^- state is thus, 4, 5 or 6.

A positon transition to the 81 keV level is established by annihilation radiation coincident with the line L_{81}, but not with K_{185} and K_{283}. It has already been mentioned that the total strength of the positon spectrum can only be explained by assuming a strong branch to the ground state of Dy^{162}, which is further confirmed by the fact that the annihilation peak in the γ-ray spectrum coincident with the 81 keV lines is considerably weaker than in the single γ-ray spectrum. These β^+-transitions to levels with spin 0^+ and 2^+ can scarcely originate in a level which also decays to the 5^- state, and they thus point to the existence of a second state in Ho^{162} with low spin.

Since the positon spectrum exhibits the same decay period of 68 min as the other radiations, a possible second state of shorter half-life must be fed from the 68 min state by an isomeric transition, if the possibility of incidental coincidence of the periods is neglected. The 38 and 58 keV transitions, which from their intensities and coincidence relations are difficult to place in the Dy^{162} level scheme, can at least tentatively be considered involved in such a scheme.

5. The Isolation of an 11.8 min Activity of Ho^{162}

Recently, Asaro *et al.* [12]) have isolated 16 h Am^{242} from 150 y Am^{242} by a method utilizing the nuclear recoil caused by the internal conversion electrons

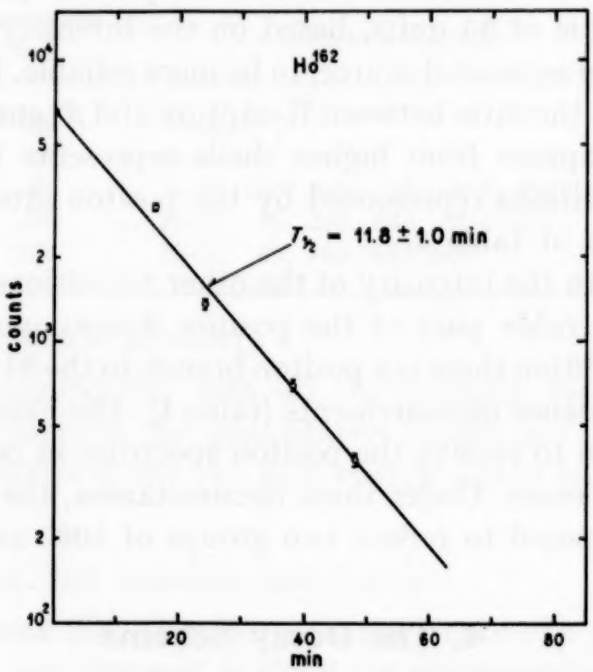

Fig. 5. Decay curve for the short lived Ho^{162}.

from a 48 keV isomeric transition. A similar procedure was adopted here, since the cases seem analogous.

The recoils were collected on platinum foils placed a few mm in front of an isotope separated source of 68 min Ho^{162}. Since it evidently is of decisive importance that the radioactive atoms are placed on the surface of the source backing, the ion beam in the isotope separator was slowed down before reaching the target foil. Normally, the ions are accelerated to an energy of about 50 keV,

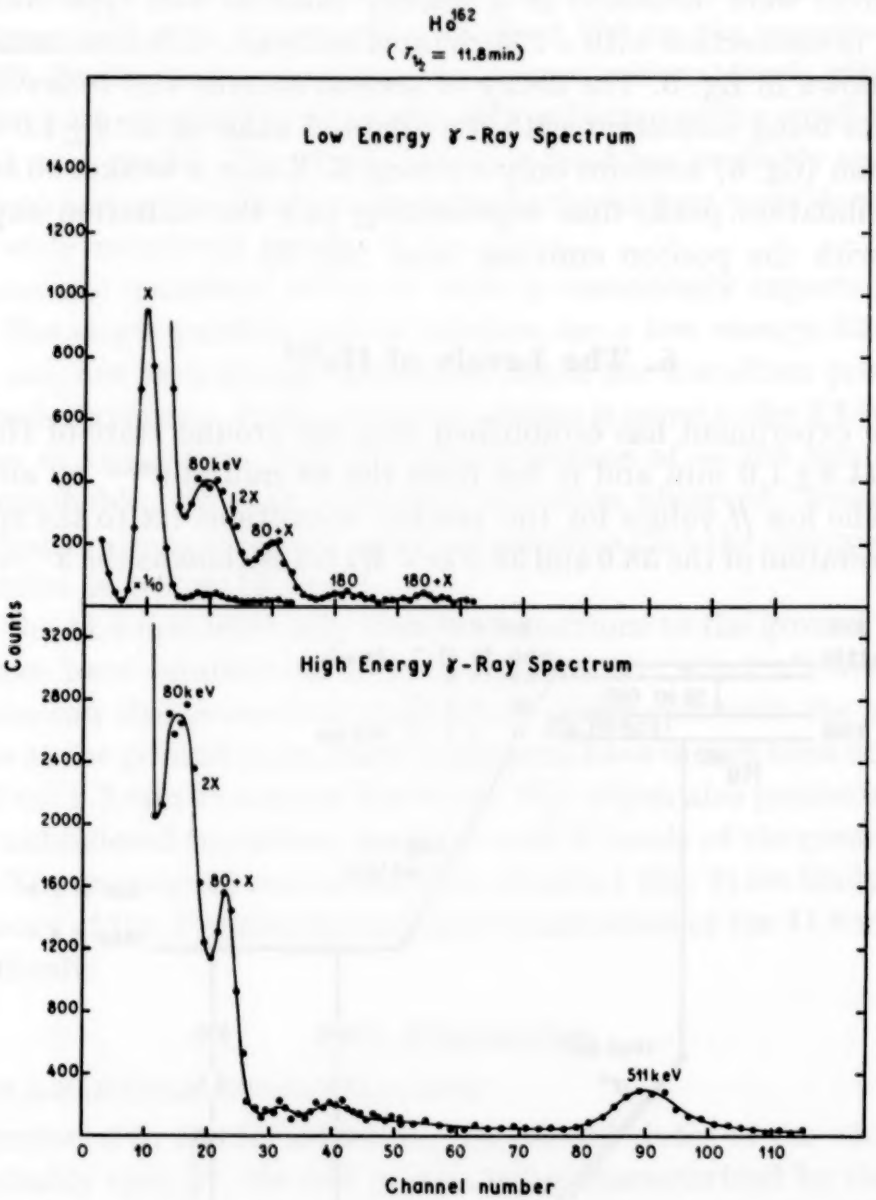

Fig. 6. Single γ-ray spectrum of 11.8 min Ho^{162} measured with a 5.0 cm × 5.0 cm well-type NaI-crystal.

corresponding to a range of ≈ 5 $\mu g/cm^2$ in the target, but, in the present case, the energy was reduced to ≈ 100 eV. The same technique has earlier been described in connection with the preparation of targets for Van der Graaff accelerators [13]).

The collection turned out to be three times more efficient in vacuum than in

the atmosphere, whereas the application of an electric field between the source and the collector caused a further improvement by a factor of two, indicating that the recoils, at least partly, leave the source as positive ions. In the most favourable cases the net efficiency amounted to $\approx 0.5 \times 10^{-3}$, yielding samples of 50 000 counts integrated.

These sources were measured in a heavily shielded well type NaI-crystal, 5 cm × 5 cm, in connection with a 256-channel analyzer. A determination of the half-life is shown in fig. 5. The decay of several sources was followed, all the measurements being consistent with the adopted value of 11.8 ± 1.0 min. The γ-ray spectrum (fig. 6) contains only a strong K X-ray, a weaker 80 keV γ-ray, and the annihilation peak, thus representing just the radiation expected in connection with the positon emitting level (fig. 7).

6. The Levels of Ho^{162}

The above experiment has established that the ground state of Ho^{162} has a half-life of 11.8 ± 1.0 min and is fed from the 68 min Ho^{162m} by an isomeric transition. The low *ft* values for the positon transitions fix to the spin to 1^+.

An interpretation of the 58.0 and 38.5 keV M1 transitions as the $3^+ \rightarrow 2^+ \rightarrow 1^+$

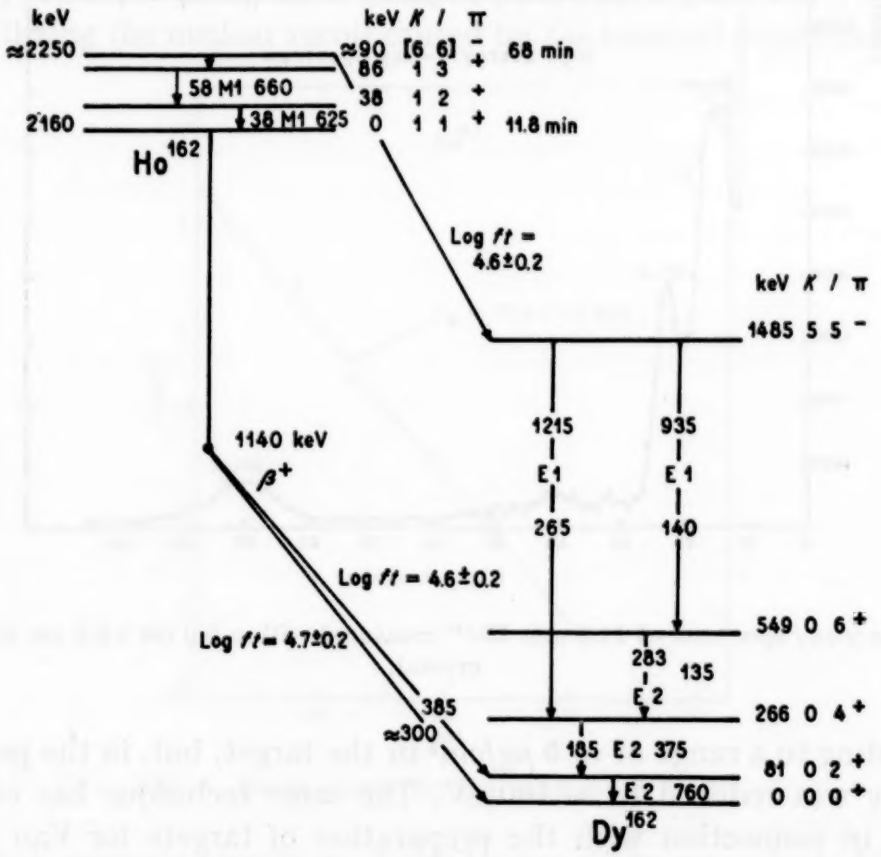

Fig. 7. The proposed decay scheme for Ho^{162m}. The transitions are labelled with the energy in keV, the multipole order, and the intensity in parts per 1000 of all decays.

cascade in the rotational band of this 1^+ ground state is suggested by their energy ratio which is extremely close to the theoretical value 3 : 2. Recalling that the 38.5 keV transition almost exclusively proceeds through L and M conversion, and the 58.0 keV transition mainly by K conversion, their coincidence relations (table 1) tend to confirm that they form a cascade, and it is seen from table 2 and fig. 7 that the calculated intensities, 625 and 660, respectively, agree well with the intensity of about 700 for the transitions from 11.8 min Ho^{162}. Furthermore, transitions between rotational levels with $I = 1$ in an odd nucleus are expected to proceed by M1 radiation with a small E2 admixture as in odd mass nuclei. The 68 min isomeric level has probably spin 6^- (see the Discussion) and is thus likely to deexcite to the highest possible member of the ground state rotational band.

The isomeric transition to the 3^+ level is accordingly expected to be of E3 nature. The single-particle unit of lifetime for a low energy E3 transition is about 1 sec, not very energy dependent, since the transition proceeds mainly by internal conversion. If the proposed scheme is correct, the E3 transition is K forbidden of two orders, and the actual lifetime of ≈ 100 min $= 6\times 10^3$ sec seems reasonable. No such transition has been observed, however, and the above considerations are based on the assumption that the energy of the isomeric transition is below 10 keV †.

From the 11.8 min level only the two transitions to the ground state band of Dy^{162} have been established. It is likely, however, that allowed unhindered transitions can also proceed to other states of low spin with the same intrinsic structure as the ground state. Such transitions have in fact been observed in the decay of the 9.3 min 1^+ state of Ta^{178} (ref. [14])), which also proceeds mainly with allowed unhindered transitions to the 2^+ and 0^+ levels of the ground state band of Hf^{178}. The unassigned conversion lines of table 1 (fig. 3) are likely to be related to the decay of the 1^+ state, but a closer examination of the 11.8 min activity is very difficult.

7. Discussion

7.1. SINGLE-PARTICLE CONFIGURATIONS

As mentioned in the Introduction, the ground states of the odd Ho isotopes have probably spin $\frac{7}{2}^-$, the odd proton being characterized by the asymptotic quantum numbers [5, 2, 3]. In the Dy^{161} ground state, the odd neutron is assigned the orbital $\frac{5}{2}^+$[6, 4, 2], and other low lying neutron states are probably $\frac{5}{2}^-$[5, 2, 3] and $\frac{3}{2}^-$[5, 2, 1]. The three K-capture transitions from the levels of Ho^{162} (fig. 7) are clearly classified as allowed unhindered, log ft being < 5, and must involve the transformation of a $\frac{7}{2}^-$[5, 2, 3] proton into a $\frac{5}{2}^-$[5, 2, 3] neutron.

† *Note added in proof:* A line at $\approx$ 8.5 keV with an intensity $\approx$ 300 of the above units has now been observed. It is interpreted as the M line of a $\approx$ 10 keV transition.

In the 1^+ ground state of Ho^{162}, the $\frac{7}{2}^-[5, 2, 3]$ proton is probably coupled to the $\frac{5}{2}^-[5, 2, 3]$ neutron. This configuration transforms into one with two neutrons of $\frac{5}{2}^-[5, 2, 3]$, corresponding to the paired ground state configuration of the even Dy^{162}. In the same scheme, the configuration of the isomeric Ho^{162} state is a $\frac{7}{2}^-[5, 2, 3]$ proton and a $\frac{5}{2}^+[6, 4, 2]$ neutron, which by the decay to the 1485 keV level in Dy^{162} is changed into a configuration of two unpaired neutrons $\frac{5}{2}^-[5, 2, 3]$ and $\frac{5}{2}^+[6, 4, 2]$.

The spin of 1^+ for the ground state of Ho^{162} agrees with the rules of the most favourable coupling of the odd particles as proposed by Gallagher and Moszkowski [15]). The same rules predict for Ho^{162m} 6^- rather than 1^-.

In odd mass nuclei, the moment of inertia is somewhat higher than in neighbouring even nuclei due to a contribution from the odd particle [1]). For odd nuclei, as for states of unpaired particles in even nuclei, contributions from two particles are expected. The moment of inertia for the assumed $\frac{5}{2}^-[5, 2, 3]$ neutron state in Dy^{161} is 20 % higher than for the ground state of Dy^{162}, and for a $\frac{7}{2}^-[5, 2, 3]$ proton state in Ho^{163} it is 27 % higher [1]). It is thus consistent with the above coupling scheme that the moment of inertia for the Ho^{162} ground state, as indicated by the energy spacing in the rotational band, is 41 % higher.

An analysis of even-odd mass differences and the β-decay systematics in the rare earth region indicates an energy gap of the order of 1600 keV for neutrons and 1800 keV for protons [16]). It is thus plausible that the lowest intrinsic excitation encountered in Dy^{162} involves the breaking of a neutron, and not of a proton pair. According to the first approximation of the theory of Bardeen *et al.* [17]), a very high density of quasi-particle states is expected just above the energy gap, and one or more of these states are then easily shifted down by additional interactions. Thus it is to be expected that the energy of the lowest excitation is somewhat smaller than the formal gap.

7.2. BRANCHING RATIOS

The theoretical branching ratio for β-transitions from the $(K, I^\pi) = (1,1^+)$ state of Ho^{162} to the 0^+ and 2^+ levels of the ground state rotational band of Dy^{162} is 2 : 1 [18]). Fig. 7 indicates an experimental value closer to 1. The two intensities are found, however, as differences and must not be considered very accurate.

If the isomeric level in Ho^{162}, as assumed in the above discussion, is 6^-, it can also decay to the 6^- and 7^- levels of the rotational band of the 1485 keV state in Dy^{162}. No transitions originating in these levels have been seen. The theoretical branching ratio, corrected for the energy dependence, for the transitions to 5^-, 6^- and 7^-, is 1 : 0.12 : 0.006. If the 6^- and 7^- levels were excited according to this estimate, the transitions from the 7^- would not have been observed, whereas the transitions deexciting the 6^- level would be about our limit of detection.

The authors are indebted to Professor Niels Bohr for the excellent working conditions in his Institute. The work was strongly stimulated through illuminating discussions with Professors A. Bohr and B. R. Mottelson, and Drs. S. G. Nilsson and C. J. Gallagher.

References

1) B. R. Mottelson and S. G. Nilsson, Mat. Fys. Skr. Dan. Vid. Selsk. **1**, No. 8 (1959)
2) A. Bohr and B. R. Mottelson, Mat. Fys. Medd. Dan. Vid. Selsk. **27**, No. 16 (1953)
3) A. Bohr, B. R. Mottelson and D. Pines, Phys. Rev. **110** (1958) 936
4) S. T. Belyaev, Mat. Fys. Medd. Dan. Vid. Selsk. **31**, No. 11 (1959)
5) J. W. Mihelich, B. Harmatz and T. H. Handley, Phys. Rev. **108** (1957) 989
6) K. O. Nielsen and O. Skilbreid, Nuclear Instruments **2** (1958) 15
7) S. Bjørnholm, O. B. Nielsen and R. K. Sheline, Nature **178** (1956) 1110
8) P. Gregers Hansen and R. K. Sheline, Nuclear Instruments **2** (1958) 39
9) S. Bjørnholm, P. Dam, H. Nordby and N. O. Roy Poulsen, Nuclear Instruments **5** (1959) 196
10) P. Gregers Hansen, O. B. Nielsen and R. K. Sheline, Nuclear Physics **12** (1959) 88
11) P. F. Zweifel, Phys. Rev. **107** (1957) 329
12) F. Asaro, I. Perlman, J. O. Rasmussen and S. G. Thompson, UCRL-9047, May 1960
13) B. Elbek, M. C. Olesen and O. Skilbreid, Nuclear Physics **10** (1959) 294
14) C. J. Gallagher, H. L. Nielsen and O. B. Nielsen, Phys. Rev. (in print)
15) C. J. Gallagher and S. A. Moszkowski, Phys. Rev. **111** (1958) 1282
16) S. G. Nilsson, private communication
17) J. Bardeen, L. N. Cooper and J. R. Schrieffer, Phys. Rev. **108** (1957) 1175
18) G. Alaga, K. Alder, A. Bohr and B. R. Mottelson, Mat. Fys. Medd. Dan. Vid. Selsk. **29**, No. 9 (1955)

2.A.1 *Nuclear Physics* **24** (1961) 456—464; © *North-Holland Publishing Co., Amsterdam*
Not to be reproduced by photoprint or microfilm without written permission from the publisher

ABSOLUTE CROSS SECTION OF THE $K^{39}(n, p)A^{39}$ REACTION FOR 2.5-MeV NEUTRONS

W. R. DIXON and J. H. AITKEN
Division of Applied Physics, National Research Council, Ottawa, Canada

Received 16 December 1960

Abstract: The cross section for the $K^{39}(n, p)A^{39}$ reaction, at a neutron energy of 2.46 MeV, has been measured to be 96 ± 6 mb. The experimental method consists of taking coincidences between the events in a KI(Tl) scintillation crystal and the He^3 particles which are produced simultaneously with neutrons in the d–d reaction.

1. Introduction

The reactions $K^{39}(n, p)A^{39}$ and $K^{39}(n, \alpha)Cl^{36}$ at neutron energies of a few MeV were first observed in KI(Tl) scintillation crystals by Scott and Segel [1]). By combining the target and detector, the difficulty of getting low-energy charged particles out of a target was circumvented, and high yields were obtained. In table 1 the reactions expected for a neutron energy $E_n = 2.46$ MeV are listed, together with the maximum and minimum energies which the emitted particle can assume. The reactions listed for K^{41} are not expected to be prominent in the spectrum of emitted particles, since the isotopic abundance of K^{41} is only 6.8 %.

TABLE 1

Maximum and minimum energy of emitted particle in laboratory system for $E_n = 2.46$ MeV

Reaction	Q (MeV	E_{min} (MeV)	E_{max} (MeV)
$K^{39}(n, p)A^{39}$	0.20	2.41	2.66
$K^{39}(n, p)A^{39*}$	−1.04	1.24	1.42
$K^{41}(n, p)A^{41}$	−1.80	0.53	0.65
$K^{39}(n, \alpha)Cl^{36}$	1.36	3.10	3.67
$K^{39}(n, \alpha)Cl^{36*}$	0.58	2.43	2.94
$K^{41}(n, \alpha)Cl^{38}$	−0.09	1.88	2.31

Subsequently to the work of Scott and Segel, Kienle and Segel [2]) have studied the application of the $K^{39}(n, p)A^{39}$ reaction to neutron spectrometry, and Lindström and Neuert [3]) have shown that absolute cross sections can be simply obtained for some of the reactions listed in table 1. When the source of neutrons is the d–d reaction, the detection of the associated He^3 particles has the effect of "tagging" a beam of neutrons going in a direction approximately opposite

to the direction of the He^3 particles. To obtain the absolute cross section, one counts both the total number of He^3 particles detected, and the number of coincidences between the He^3 detector and identifiable events in the KI(Tl) crystal. If the KI(Tl) crystal is wide enough to encompass completely the tagged neutron beam, one has the following simple relation:

Number of coincidences
= (number of He^3 particles detected) × (number of atoms/cm^2) × cross section.
Using this method, Lindström and Neuert have obtained the following results:

$$\sigma(n, \alpha) = 36 \text{ mb} \pm 10\ \%,$$
$$\sigma(n, p) = 45 \text{ mb} \pm 10\ \%,$$

for the ground-state K^{39} reactions at $E_n = 2.59$ MeV.

We have done a similar experiment, and have obtained quite different results, namely

$$\sigma(n, p) = 96 \pm 6 \text{ mb}$$

at $E_n = 2.46$ MeV, while $\sigma(n, \alpha)$ is only about 6 mb. (In both experiments the neutron energy spread is of the order of 0.1 MeV). Details of our measurements are reported below. Preliminary reports of studies of these reactions have also been made by Haenni, Bass and Bonner [4]).

2. Experimental Arrangement

Fig. 1 shows the general arrangement of the experimental apparatus. Deuterons are accelerated to 100 keV in a Texas Nuclear Corporation neutron generator, and allowed to strike a thin brass target. After a few minutes time, deuterium builds up on the surface of the brass, and neutrons are produced in the d–d

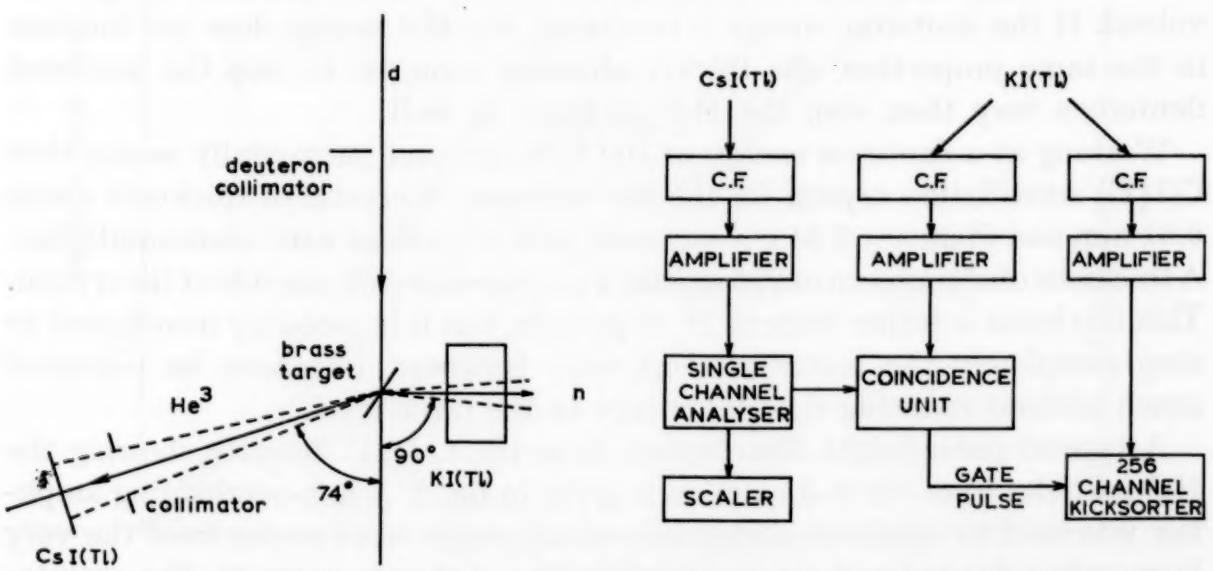

Fig. 1. The experimental arrangement (approximately to scale) and block diagram of the electronics.

reaction. The neutrons at 90° are detected in a KI(Tl) crystal, while the associated He^3 particles, at 74°, are detected in a thin CsI(Tl) crysal. A block diagram of the electronic circuits is also shown in fig. 1.

It should be noted that small variations in the position of the deuteron beam do not affect the measured cross section, provided that the KI(Tl) crystal always encompasses the tagged neutron beam. A collimator was used on the deuteron beam to avoid the consequences of large excursions.

2.1. THE He^3 DETECTOR

In order to make absolute cross-section measurements, the He^3 detector must be able to discriminate against protons and tritons from the d(d, p)t reaction, against deuterons scattered elastically from the target, and against light emitted from the target. Since the He^3 energy is rather low (e.g. 792 keV at 90° for a deuteron energy of 100 keV), the main difficulty arises from scattered deuterons and light. Lindström and Neuert [3]) have used a proportional counter with a mica window, with the gas pressure chosen so that the He^3 particles gave the biggest pulses. Okhuysen *et al.* [5]) have used an organic scintillator with a thin aluminium absorber as a He^3 detector, in spite of the small pulse size from heavily ionizing particles. Shapiro and Higgs [6]) have used a magnetic field to deflect the He^3 particles into a windowless detector so situated that light from the target could not enter it. Working at a somewhat higher deuteron energy (900 keV), Franzen, Huber and Schellenberg [7]) have avoided scattered deuterons by using a gas target, but their He^3 detector did not discriminate against protons and tritons.

It should be noted that the ability to discriminate with absorbers between elastically scattered deuterons and associated He^3 particles is best at low deuteron energies, simply from the point of view of the particle energies involved. If the deuteron energy is increased, the He^3 energy does not increase in the same proportion; the thicker absorber required to stop the scattered deuterons may then stop the He^3 particles as well.

Working at a deuteron energy of 100 keV, we have successfully used a thin CsI(Tl) scintillation crystal for the He^3 detector. A crystal of thickness about 0.51 mm and diameter 2.54 cm was used with a DuMont 6467 photomultiplier. A thickness of aluminium of 225 $\mu g/cm^2$ was evaporated on one side of the crystal. This thickness is rather critical. It stops light, but it is probably insufficient to stop completely the scattered deuterons. However, it cannot be increased much without reducing the He^3 energy to the noise level.

A typical pulse-height distribution from the CsI(Tl) detector showing the He^3 particles from the d–d reaction is given in fig. 2. A non-overloading amplifier was used to eliminate distortions which might have arisen from the very large pulses due to the d–d tritons and protons (off scale in fig. 2). The peak-to-valley ratio in fig. 2 did not stay constant from day to day. This effect has also

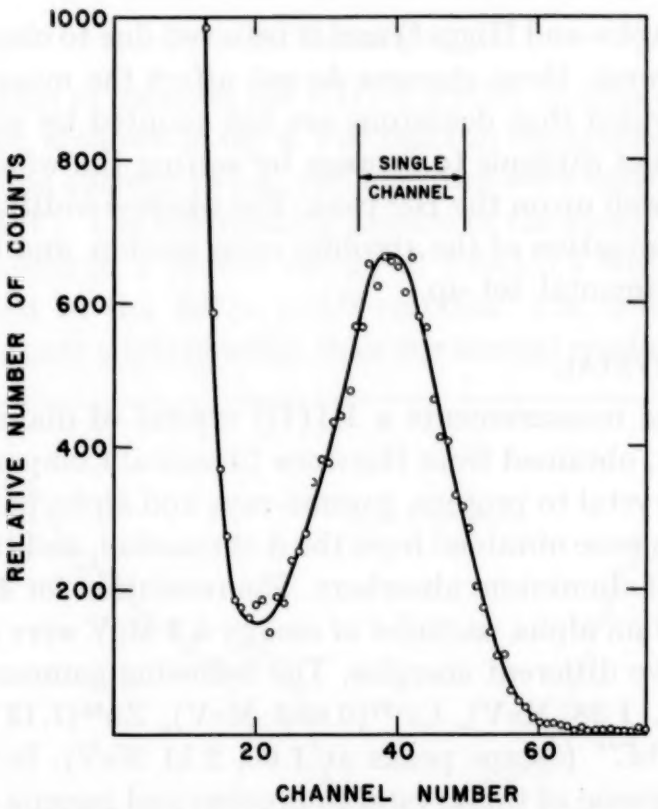

Fig. 2. The pulse-height distribution due to He^3 particles in the CsI(Tl) detector. Pulses due to d–d tritons and protons are off-scale to the right.

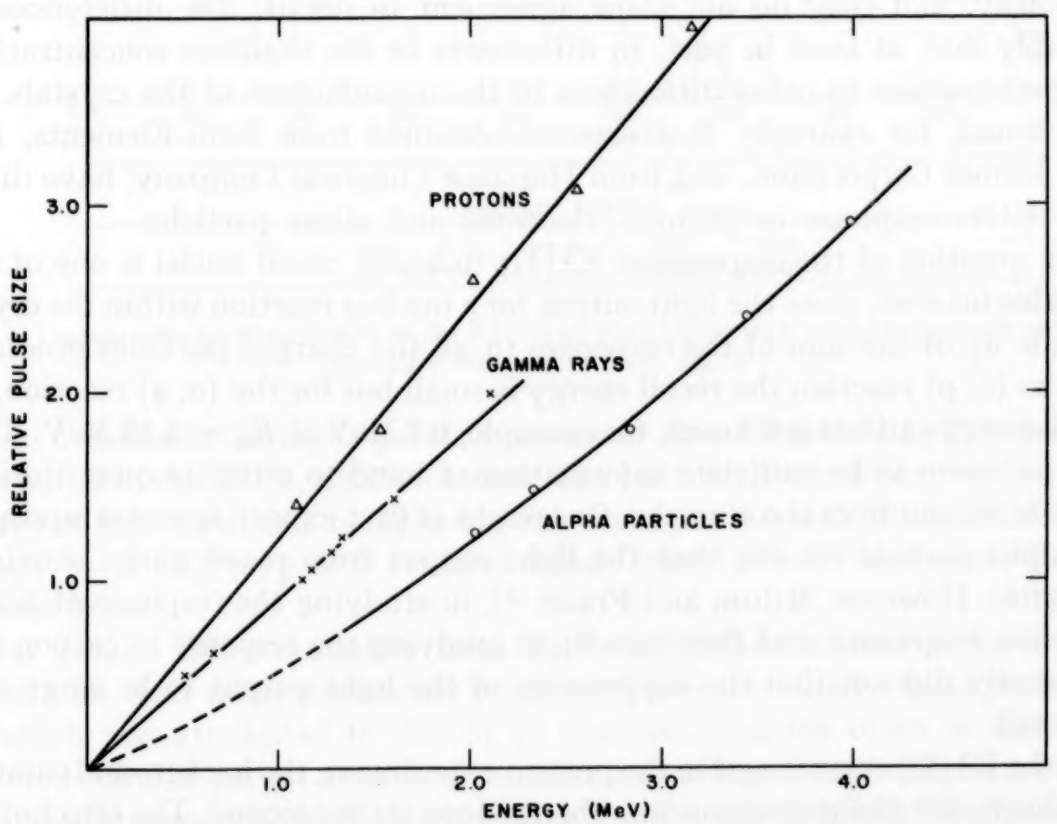

Fig. 3. Response of the KI(Tl) crystal to protons, gamma rays and alpha particles.

been noted by Shapiro and Higgs [6]) and is believed due to changes in the deuterium target. However, these changes do not affect the measured value of the cross section provided that deuterons are not counted by mistake in the He^3 detector. This is not difficult to arrange by setting the window of the single-channel analyzer well up on the He^3 peak. The window width is of course irrelevant in the determination of the absolute cross section, and this fact was used to test the experimental set-up.

2.2. THE KI(Tl) CRYSTAL

For most of the measurements a KI(Tl) crystal of diameter 1.91 cm and thickness 1.27 cm, obtained from Harshaw Chemical Company, was used. The response of this crystal to protons, gamma-rays and alpha particles is shown in fig. 3. The protons were obtained from the d–d reaction, and their energy varied by the insertion of aluminium absorbers. The resolution for 3.2 MeV protons is about 9 %. Polonium alpha particles of energy 5.3 MeV were used, with the air path varied to give different energies. The following gamma-ray sources were used: Na^{22}(0.511, 1.28 MeV), Cs^{137}(0.662 MeV), Zn^{65}(1.12 MeV), Co^{60}(1.17, 1.33 MeV) and ThC″ (escape peaks at 1.60, 2.11 MeV). It can be seen from fig. 3 that the response of this crystal to protons and gamma rays is essentially linear, while the response to alpha particles is non-linear.

A number of studies [3, 8–12]) of the response of KI(Tl) crystals have been made previously, and they do not show agreement in detail. The differences are probably due, at least in part, to differences in the thallium concentrations, and perhaps also to other differences in the manufacture of the crystals. We have found, for example, that crystals obtained from Semi-Elements, Inc., from Isomet Corporation, and from Harshaw Chemical Company, have different relative response to protons, electrons and alpha particles.

The question of the response of KI(Tl) to heavy recoil nuclei is one of considerable interest, since the light output for a nuclear reaction within the crystal is made up of the sum of the responses to all the charged particles produced. For the (n, p) reaction the recoil energy is small but for the (n, α) reaction, the recoil energy can be significant, for example, 0.7 MeV at $E_n = 2.46$ MeV. There does not seem to be sufficient information at hand to estimate quantitatively the light output from recoil nuclei. One might at first expect, from extrapolating the alpha-particle results, that the light output from recoil nuclei should be negligible. However, Milton and Fraser [13]), in studying the response of KI(Tl) to fission fragments, and Burcham [10]), in studying the response to carbon ions, apparently did not find the suppression of the light output to be as great as expected.

In the KI(Tl) crystal used in the present experiment, the background counting rate due to K^{40} disintegrations was about 80 counts per second. The effect of this background was to contribute chance coincidences at energies up to 1.5 MeV.

3. Results

A typical spectrum of pulses in the KI(Tl) crystal, in coincidence with pulses in the He^3 detector, is shown in fig. 4. For this run the accelerating voltage was 100 kV, the deuteron current 18 μA, and neutrons were detected at an angle of 90° ($E_n = 2.46$ MeV). The outstanding feature of the spectrum in fig. 4 is the peak (a) which comes at a proton energy of 2.65 ± 0.1 MeV. From table 1 it must be attributed to the $K^{39}(n, p)A^{39}$ reaction. The width of peak (a) is 11–12 %, which is only slightly wider than the normal resolution. The peak (b)

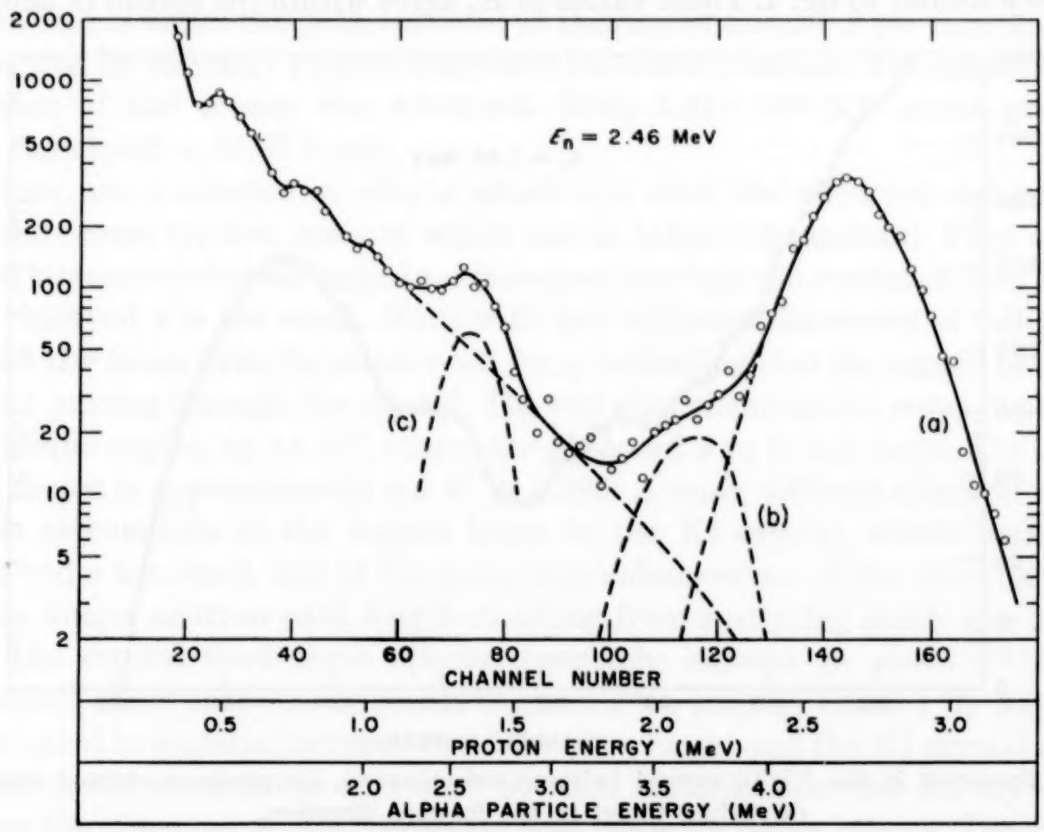

Fig. 4. Typical coincident spectrum in the KI(Tl) crystal. The energy scales for protons and alpha particles were taken from fig. 3.

in fig. 4 comes at an alpha-particle energy of about 3.6 MeV and is therefore attributed to the $K^{39}(n, \alpha)Cl^{36}$ reaction. The peak (c) in fig. 4 comes at a proton energy of 1.35 MeV, and an alpha-particle energy of 2.6 MeV; it is probably due mostly to the $K^{39}(n, p)A^{39*}$ reaction which leaves the A^{39} nucleus in its first excited state.

Our results differ markedly from those of Lindström and Neuert [3]), who found that their main peak could be divided into two nearly equal peaks, one of which was attributed to the (n, p) reaction, and the other to the (n, α) reaction. Over a period of several months, and using several different experimental arrangements, we have at no time found a splitting comparable to that found by Lindström and Neuert. In the hope that there might be a significant

splitting at some other temperature, a KI(Tl) crystal was cooled with liquid air, and the peak examined as the crystal warmed up again to room temperature, but no significant splitting was found at any intermediate temperature.

We have also examined the spectrum at some other neutron energies, by changing the angle at which the neutrons were observed. In particular a value $E_n = 2.55$ MeV was chosen in order to approach more closely the value used by Lindström and Neuert, $E_n = 2.59$ MeV. (It was not possible to determine the absolute cross section at this angle of observation.) The spectrum observed was very similar to fig. 4. These values of E_n agree within the spread in neutron

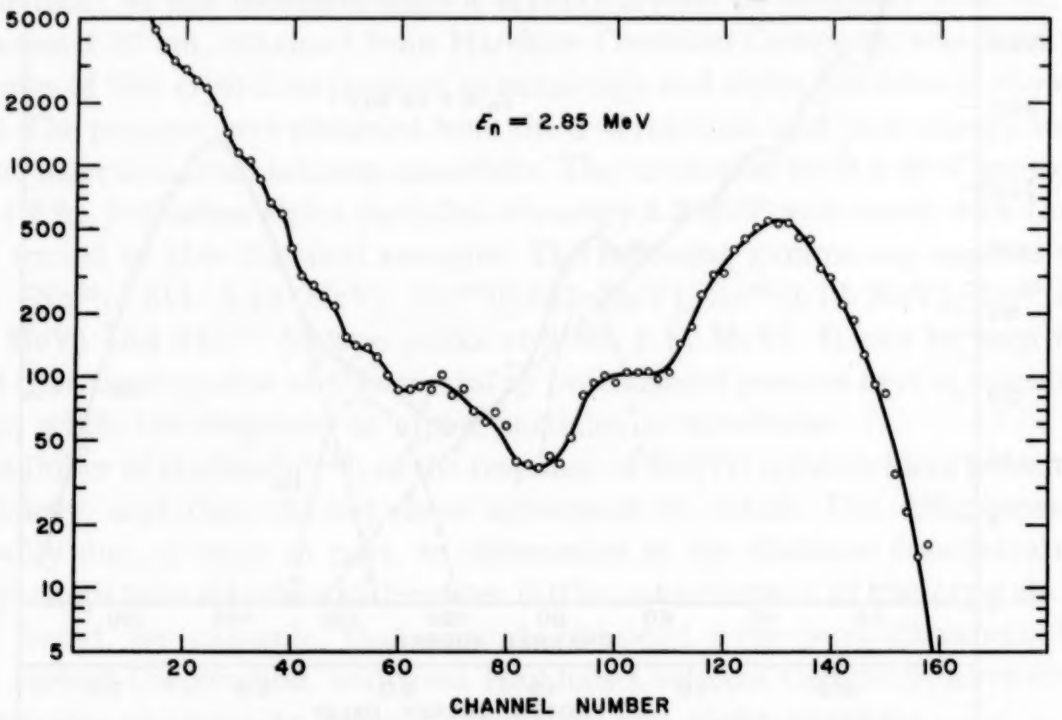

Fig. 5. Spectrum in the KI(Tl) crystal (without coincidences), for neutrons emitted from the deuterium target in the forward direction.

energy in both experiments, which is of the order of 0.1 MeV †. Thus resonance structure in the (n, p) and (n, α) excitation curves cannot be the explanation of the discrepancy between our results and those of Lindström and Neuert.

The spectrum for the neutrons emitted in the forward direction ($E_n = 2.85$ MeV) is shown in fig. 5. This run was made with a much smaller KI(Tl) crystal weighing 0.44 g, without coincidences. In this case the (n, α) peak is relatively more prominent than for $E_n = 2.46$ MeV. As a rough estimate, we have, at $E_n = 2.46$ MeV,

$$\frac{\sigma(n, \alpha)}{\sigma(n, p)} \approx 0.06,$$

† This spread arises mostly from the spread in angle for neutrons in the tagged beam. Another factor, of less importance, is the spread in deuteron energy arising from the slowing down of deuterons in the thick target.

and at $E_n = 2.85$ MeV,

$$\frac{\sigma(n,\alpha)}{\sigma(n, p)} \approx 0.14.$$

These ratios are clearly subject to rather large errors because of the uncertainty in separating out the low intensity alpha-particle peak.

The absolute cross section for the reaction $K^{39}(n, p)A^{39}$, without corrections, is calculated to be 97 ± 6 mb at $E_n = 2.46$ MeV. This figure is based on a total of 5826 true coincidences under the peak in a time of 549 min. Accidental coincidences under the peak occurred at the rate of about 0.8 per min, and were measured by inserting a 5 μsec delay into one of the channels. The corresponding number of He^3 counts was 4 562 093. With 1.31×10^{22} K^{39} atoms per cm^2, the calculated σ is 97.5 mb.

There are a number of effects which can alter the observed value of the absolute cross section, some of which can be taken into account. First of all it must be ensured that all tagged neutrons pass through the crystal; if they do not, the observed σ is too small. Runs with two different diameters of collimators on the He^3 beam gave the same result for σ, indicating that the tagged beam was in fact passing through the crystal. The fact that the neutrons enter the crystal at oblique angles, up to 10°, causes the observed σ to be too large. The correction factor is approximately $\cos 5° = 0.995$. A more difficult effect to correct for is attenuation of the tagged beam in the KI crystal, which makes the observed σ too small, and at the same time enhancement of the observed σ due to the longer neutron path length resulting from scattering inside the crystal. For the crystal used these effects separately amount to about 10 %; the combined effect has been estimated to give a σ too large by about 1 %. Neutrons attenuated in material between the deuterium target and the KI crystal reduce the observed σ; neutrons scattered by such material into the KI crystal increase the observed σ. No correction was made for these effects. The factors listed so far have mainly to do with absorption and scattering of the tagged neutron beam. Absorption of the He^3 particles as they emerge from the brass target does not affect the calculated value of σ. If, however, scattered deuterons are counted as He^3 particles by mistake, the observed σ will be too low. As already noted, care was taken to be well up on the He^3 peak with the single channel analyzer (see fig. 2) in order to avoid this possibility. There is also the question of resolving-time losses in the He^3 scaler; these should be negligible at the counting rates used. Finally there is an uncertainty of a few percent in estimating the area under the $K^{39}(n, p)$ peak.

If we make a correction of 1.5 % for the oblique paths for unscattered neutrons, for the enhancement of path length due to scattering and for the attenuation of the neutron beam, we obtain finally a value

$$\sigma(n, p) = 96 \pm 6 \text{ mb}.$$

The statistical error is only ± 1.3 %; the much larger error quoted is to allow for the uncertainties discussed above.

4. Conclusions

The cross section for the $K^{39}(n, p)A^{39}$ reaction at a neutron energy of 2.46 MeV has been measured to be 96 ± 6 mb, while the $K^{39}(n, \alpha)Cl^{36}$ cross section at the same neutron energy is found to be about 6 mb.

Note added in proof: According to T. W. Bonner (private communication) there are rapid variations in the cross section in the region of 2.5 MeV, so that the measured cross section will depend to a considerable extent on the spread in neutron energy. Our estimate of the total spread in neutron energy in the present experiment, namely 100 keV, should perhaps be increased somewhat to allow for the elastic scattering of the He^3 particles in the target. However this is not a large effect because the effective thickness of the target is very small, being determined by the range of 100 keV deuterons.

References

1) M. J. Scott and R. E. Segel, Phys. Rev. **102** (1956) 1557
2) P. Kienle and R. E. Segel, Brookhaven National Laboratory Progress Reports, BNL 502 and BNL 515 (1958)
3) G. Lindström and H. Neuert, Zeits. f. Naturf. **13a** (1958) 826
4) Haenni, Bass, Bonner, Davis, Gabbard and Retz-Schmidt, Bull. Am. Phys. Soc. **4** (1959) 97; Haenni, Bass and Bonner, Bull. Am. Phys. Soc. **5** (1960) 248
5) Okhuysen, Bennett, Ashe and Millett, Rev. Sci. Inst. **29** (1958) 982
6) P. Shapiro and R. W. Higgs, Phys. Rev. **108** (1957) 760
7) Franzen, Huber and Schellenberg, Zeits. f. Naturf. **10a** (1955) 820
8) J. F. Raffle and E. J. Robbins, Proc. Phys. Soc. **65** B (1952) 320
9) W. T. Link and D. Walker, Proc. Phys. Soc. **66** A (1953) 767
10) W. E. Burcham, Proc. Phys. Soc. **70** A (1957) 309
11) Franzen, Peelle and Sherr, Phys. Rev. **79** (1960) 742
12) P. Kienle and R. E. Segel, Phys. Rev. **113** (1959) 909
13) J. C. D. Milton and J. S. Fraser, Phys. Rev. **96** (1954) 1508

2.L: 7.A

Nuclear Physics **24** (1961) 465—473; © *North-Holland Publishing Co., Amsterdam*

Not to be reproduced by photoprint or microfilm without written permission from the publisher

A CONVERGENT SET OF INTEGRAL EQUATIONS FOR SINGLET PROTON-PROTON SCATTERING

S. CIULLI † and J. FISCHER ††

Joint Institute for Nuclear Research, Laboratory of Theoretical Physics, Dubna, USSR

Received 10 October 1960

Abstract: Elastic nucleon-nucleon scattering is studied by using the two-dimensional spectral representation of Mandelstam. In this first paper, the convergence problem arising from the combination of the forward dispersion relation with the unitarity condition on the physical cut is solved via a conformal transformation.

1. Introduction

A set of integral equations for the elastic scattering of protons on protons in the singlet state was obtained by using the two-dimensional spectral representation of Mandelstam. The method is based on a new approach recently introduced in Dubna [1]). We shall briefly recall its fundamental idea. The dispersion relations are written only for such angles (forward and backward scattering) for which they are simple enough and at which there are no spectral functions in the unphysical region. Then the dispersion relations are differentiated with respect to $\cos\theta$ at these points. In the entire region $-1 \leqq \cos\theta \leqq +1$ the amplitude $M(q^2, \cos\theta)$ is represented by a Taylor expansion around these points and these series are substituted into the unitarity condition. The partial waves can also be determined in terms of these Taylor coefficients.

However, this approach (as will be shown) leads, on the physical cut, to a problem of convergence [5]), since the cosine singularities of M located in the non-physical region $\cos\theta > 1$ restrict the convergence of the Taylor expansion also in the physical region. Indeed, the cosine of the nearest singularity is $1+\mu^2/2q^2$ and approaches the forward scattering point asymptotically as q^2 increases ††† (see fig. 1). In the *physical region*, the expansion around $\cos\theta = 1$ converges only for $\cos\theta > 1-\mu^2/2q^2$ and, consequently, a certain $q^2_{\max}$ exists so

† On leave of absence from the Institute of Atomic Physics, Bucharest, Roumania.

†† On leave of absence from the Physical Institute of the Czechoslovak Academy of Sciences, Prague.

††† We use the following notation: q is the length of the centre-of-mass momentum in the reaction $N+N \to N+N$, θ the c.m. scattering angle, and M the "causal amplitude" defined, for instance, in ref. [2]) or ref. [3]).

that

$$1-\frac{\mu^2}{2q_{\max}^2}=-1, \quad \text{or} \quad q_{\max}^2=\tfrac{1}{4}\mu^2.$$

At $q>q_{\max}$ the convergence circle of the Taylor expansion around $\cos\theta=1$ does not cover the entire physical region $-1\leqq\cos\theta\leqq 1$ and therefore this series cannot be used in the unitarity condition.

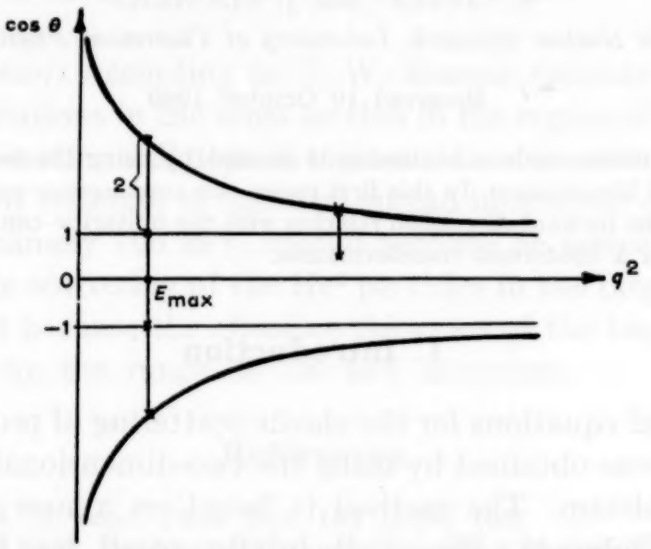

Fig. 1. The boundary of the cosine sungularities.

In the N+N → N+N process, the corresponding $E_{\max}=2\sqrt{(m^2+q_{\max}^2)}$ is extremely small, not larger than 10 MeV in the laboratory system. (If symmetry is taken into account and an expansion in $(\cos^2\theta-1)$ is used, $E_{\max}$ can be shifted up to 49.4 MeV). Yet it is desirable to ensure the convergence of the Taylor series at least up to the threshold of the first inelastic process NN → NNπ (290 MeV), for which the simple unitarity condition still holds.

2. A Convergent Cosine Expansion

For this purpose we make a conformal transformation of the complex cosine plane

$$w=\frac{1-z^2}{\alpha^2-z^2}, \quad z=\cos\theta, \quad \alpha^2=1+2\,\frac{\mu^2}{q^2}+\frac{\mu^4}{2q^4} \tag{1}$$

(see fig. 2) and we show that the series

$$\sum \left.\frac{\partial^n M}{\partial w^n}\right|_{\substack{z^2=1\\(w=0)}} \frac{w^n}{n!}$$

converges in the whole interval $-1\leqq z\leqq 1$ for any observable energy. Below

49.4 MeV where the power series in $\cos^2\theta$ also converges, the series in w yields a better approximation if the same number of terms is taken. A rapidly convergent set of integral equations is thus obtained.

The properties of this conformal transformation as well as the reasons for the choice of its form are given in Appendix 1, and some quantitative estimations in Appendix 2.

3. The Unitarity Condition

Let us now turn to the unitarity condition. On the physical cut, it has the following form (in the c.m. system):

$$\operatorname{Im} M(q^2, z) = \tfrac{1}{2}\frac{m^2}{(4\pi)^2}\frac{q}{\sqrt{q^2+m^2}}\int M^\dagger(q^2, z_1)M(q^2, z_2)\mathrm{d}z_1\,\mathrm{d}\varphi, \tag{2}$$

where

$$z_2 = zz_1 - \sqrt{1-z^2}\sqrt{1-z_1^2}\cos\varphi.$$

At this stage, an expansion of M into partial waves is frequently performed to obtain the unitarity condition for the partial waves. In the forward-scattering method, however, only the properties of M near $\cos\theta = 1$ are used and the partial wave amplitudes can therefore be determined only by integrating the Taylor series. Since each power of w contains an infinite number of partial waves, the simultaneous use of the w power series and the partial wave expansion leads to a re-ordering problem. Each coefficient of one expansion is written as a combination of an infinite sum of the coefficients of another expansion. In practical calculations, however, one has to restrict oneself to a finite number of terms and thus the transition from one expansion to another leads to additional errors. For this reason we avoided the partial wave expansion and used only the power series in w. All integrals in (2) can be performed by direct calculation.

Writing now the singlet amplitude $M_{ss}(q^2, z)$ as

$$\mathcal{M}_{ss}(q^2, z)\,\frac{1-\boldsymbol{\sigma}_1\cdot\boldsymbol{\sigma}_2}{4},$$

we expand $\mathcal{M}_{ss}(q^2, z)$ in w^n and take only three terms:

$$\mathcal{M}_{ss}(q^2, z) \approx a_0(q^2)+a_1(q^2)w+a_2(q^2)w^2. \tag{3}$$

Then, we obtain from (2) and its derivatives with respect to z

$$\operatorname{Im}\mathcal{M}_{ss}(q^2, 1) \approx \tfrac{1}{2}\frac{m^2}{(4\pi)^2}\frac{q}{\sqrt{q^2+m^2}}\sum_{i,j=0}^{2} a_i^* a_j K_{ij}^{(0)},$$

$$\left.\frac{\partial \operatorname{Im}\mathcal{M}_{ss}}{\partial z}\right|_{z=1} \approx \tfrac{1}{2}\frac{m^2}{(4\pi)^2}\frac{q}{\sqrt{q^2+m^2}}\sum_{i,j=0}^{2} a_i^* a_j K_{ij}^{(1)},$$

$$\left.\frac{\partial^2 \operatorname{Im}\mathcal{M}_{ss}}{\partial z^2}\right|_{z=1} \approx \tfrac{1}{2}\frac{m^2}{(4\pi)^2}\frac{q}{\sqrt{q^2+m^2}}\sum_{i,j=0}^{2} a_i^* a_j K_{ij}^{(2)},$$

where

$$K_{ij}^{(n)} = \frac{\partial^n}{\partial z^n}\int_0^{2\pi}\int_{-1}^{1} w_1{}^i w_2{}^j \, dz_1 \, d\varphi|_{z=1}.$$

The quantities $K_{ij}^{(n)}$ depend only on the energy (via α^2, see eq. (1)) and are easily obtained. Their explicit form is

$$K_{00} = 4\pi,$$

$$K_{10} = 4\pi - 2\pi\,\frac{\alpha^2-1}{\alpha}\ln\frac{\alpha+1}{\alpha-1},$$

$$K_{11} = K_{20} = 2\pi\,\frac{3\alpha^2-1}{\alpha^2} - \pi\,\frac{(3\alpha^2+1)(\alpha^2-1)}{\alpha^3}\ln\frac{\alpha+1}{\alpha-1},$$

$$K_{21} = \frac{\pi}{2\alpha^4}(15\alpha^4-4\alpha^2-1) - \frac{3\pi}{4\alpha^5}(5\alpha^4+2\alpha^2+1)(\alpha^2-1)\ln\frac{\alpha+1}{\alpha-1},$$

$$K'_{00} = K'_{10} = K'_{20} = 0,$$

$$K'_{11} = \frac{\pi}{6\alpha^4}(3\alpha^4-2\alpha^2+3) - \frac{\pi}{4\alpha^5}(\alpha^2+1)(\alpha^2-1)^2\ln\frac{\alpha+1}{\alpha-1},$$

$$K'_{21} = \frac{\pi}{24\alpha^6}(15\alpha^6-7\alpha^4-7\alpha^2+15) - \frac{\pi}{16\alpha^7}(5\alpha^4+6\alpha^2+5)(\alpha^2-1)^2\ln\frac{\alpha+1}{\alpha-1},$$

$$K''_{00} = K''_{10} = K''_{20} = 0,$$

$$K''_{11} = -\frac{\pi}{120\alpha^6(\alpha^2-1)}(45\alpha^8-90\alpha^6-64\alpha^4+90\alpha^2-45) + \frac{\pi}{16\alpha^7}(3\alpha^4+2\alpha^2+3)(\alpha^2-1)^2\ln\frac{\alpha+1}{\alpha-1},$$

$$K''_{12} = -\frac{\pi}{480\alpha^8(\alpha^2-1)}(225\alpha^{10}-375\alpha^8+90\alpha^6-398\alpha^4+645\alpha^2-315) + \frac{\pi}{64\alpha^9}(15\alpha^6+15\alpha^4+13\alpha^2+21)(\alpha^2-1)^2\ln\frac{\alpha+1}{\alpha-1},$$

$K_{ij}^{(n)} \equiv K_{ji}^{(n)}$, $K_{22}^{(n)}$ is neglected.

In the integral equations the two-pion contribution to the unphysical cut yields an inhomogeneous term which will be denoted by χ. We have not studied in detail this term, or any other contributions to the unphysical cut. They can be taken from refs. [3, 4]) offering thorough analysis of them. Nevertheless, we hope the method of using only forward scattering will enable us to obtain a simpler form of χ.

4. Integral Equations for Singlet Scattering

Since we write the integral equations only for the singlet scattering, we can take advantage of the fact that in the expansion of M into the "physical"

amplitudes

$$M = \alpha+\beta(\boldsymbol{\sigma}_1\cdot\mathbf{n})(\boldsymbol{\sigma}_2\cdot\mathbf{n})+\gamma(\boldsymbol{\sigma}_1\cdot\mathbf{n}+\boldsymbol{\sigma}_2\cdot\mathbf{n})$$
$$+\delta(\boldsymbol{\sigma}_1\cdot\mathbf{m})(\boldsymbol{\sigma}_2\cdot\mathbf{m})+\varepsilon(\boldsymbol{\sigma}_1\cdot\mathbf{l})(\boldsymbol{\sigma}_2\cdot\mathbf{l})$$

the dispersion relations for α, β, δ and ε have a simple form in the nonrelativistic approximation (see ref. [2])). The singlet amplitude $\mathscr{M}_{ss}$ in these terms,

$$\mathscr{M}_{ss} = +\alpha-\beta-\delta-\varepsilon,$$

does not contain the γ-term.

The integral equations have the following form:

$$a_0 = \frac{f^2}{\mu^2}\frac{-4q^2}{4q^2+\mu^2}+\chi_{ss}|_{t=0}+\frac{1}{2\pi}\left(\frac{m}{4\pi}\right)^2\int_0^\infty \frac{q'}{\sqrt{q'^2+m^2}}\frac{\sum_{i,j=0}^{2}K_{ij}a_i^*a_j}{q'^2-q^2}\,dq'^2,$$

$$a_1 = (\alpha^2-1)q^2f^2\left(\frac{1}{(4q^2+\mu^2)^2}-\frac{1}{\mu^4}\right)-(\alpha^2-1)q^2\left.\frac{d\chi_{ss}}{dt}\right|_{t=0}$$
$$-\frac{1}{2\pi}\left(\frac{m}{4\pi}\right)^2(\alpha^2-1)q^2\int_0^\infty\frac{1}{2q'\sqrt{q'^2+m^2}}\frac{\sum_{i,j=1}^{2}K'_{ij}a_i^*a_j}{q'^2-q^2}\,dq'^2, \quad (3)$$

$$2a_2 = \frac{\alpha^2+3}{2}a_1+(\alpha^2-1)^2q^42f^2\left(\frac{1}{(4q^2+\mu^2)^3}-\frac{1}{\mu^6}\right)+(\alpha^2-1)^2q^4\left.\frac{d^2\chi_{ss}}{dt^2}\right|_{t=0}$$
$$+\frac{1}{2\pi}\left(\frac{m}{4\pi}\right)^2(\alpha^2-1)^2q^4\int_0^\infty\frac{1}{4q'^3\sqrt{q'^2+m^2}}\frac{\sum_{i,j=1}^{2}K''_{ij}a_i^*a_j}{q'^2-q^2}\,dq'^2.$$

In these equations, we used $f^2 = (\mu^2/4m^2)g^2$.

As usual in the forward scattering case, one subtraction must be performed. However, this subtraction is to be applied only to the first equation, because the second and the third one have a correct behaviour at infinity. This was achieved by using constant momentum transfer dispersion relations instead of the constant angle ones.

5. Conclusions

The integral equations are written for the first three coefficients of (2) and not for the partial waves. As has been said above, we used this unusual expansion (2) to avoid additional errors arising from the simultaneous use of two expansions. But there is also another circumstance favouring this approach.

The NN → NN scattering amplitude is known to contain many waves so that the partial wave expansion converges very slowly. To obtain a true picture without using too many approximation terms, we must expand $M(q^2, z)$ into a

more convenient set of functions. Owing to the method used we can confine ourselves only to the power expansions around $\cos\theta = 1$.

Strictly speaking, the "most rapidly convergent" expansion of $M(q^2, z)$ is that in the powers of M itself in which it reaches itself to the trivial identity $M \equiv M$. But M is not known unless the equations are solved: the a priori information known about M concerns only the location of the poles and cuts. Within the scope of this information, the most rapidly convergent expansion will be one in powers of a function with the same location of singularities as M. A function of this type is given in Appendix 1, but it is too complex for practical calculations. Our w-function, which is much simpler, is a somewhat worse approximation to this ideal case, but, as the numerical estimations show (see Appendix 2), three coefficients in (2) are quite sufficient.

It is a pleasure for us to acknowledge frequent stimulating discussions we had with Professor H. Y. Tzu and Dr. D. V. Shirkov. We also wish to thank Dr. V. S. Vladimirov and E. V. Maikov for their helpful discussions concerning the mathematical aspects of this work.

Appendix 1

A.1.1. CONFORMAL TRANSFORMATION

To secure the convergence of the power expansion around $\cos^2\theta = 1$ in the entire physical region $0 \leqq \cos^2\theta \leqq 1$ we transformed the left half-plane limited by the straight line C′ into the inside of the unit circle C′ of the complex plane $w = (1 - \cos^2\theta)/(\alpha^2 - \cos^2\theta)$ (see fig. 2). The point $\cos^2\theta = 1$ obviously becomes $w = 0$.

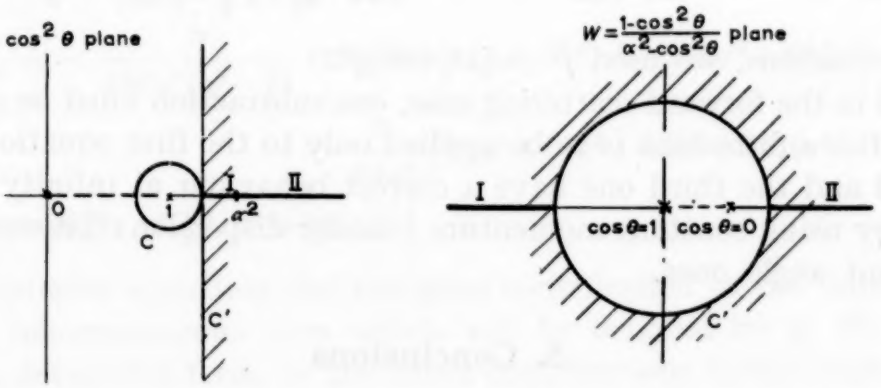

Fig. 2. The $\cos^2\theta$ plane and the w plane. The circle C is the convergence limit of the $\cos^2\theta$ expansion, whereas the straight line C′ and the circle of the w-plane give the convergence limit of the w-expansion.

The power expansion around $w = 0$ is convergent in each point inside the unit circle, for the amplitude has no singularities in this region. All physical points are contained in this circle and therefore the w-power expansion can be used in the integrals of the unitarity condition without any additional precautions.

A1.2. CONVERGENCE RATES

There is a great variety of conformal transformations ensuring the convergence of the corresponding Taylor expansions in the whole physical region. It is well known that the Taylor expansion behaves for $n \to \infty$ as the geometrical series $(r/R)^n$, where R is the convergence radius and $r = |w|$. Naturally, the most convenient would be a transformation for which r/R would have a minimum value in all physical points. Such an optimal transformation $w_M(z)$ actually exists and we shall show that it transforms the cut complex plane D_{Max} (see fig. 3) into the unit circle. This is equivalent to the statement that for any other conformal transformation $w_1(z)$ converting an arbitrary domain

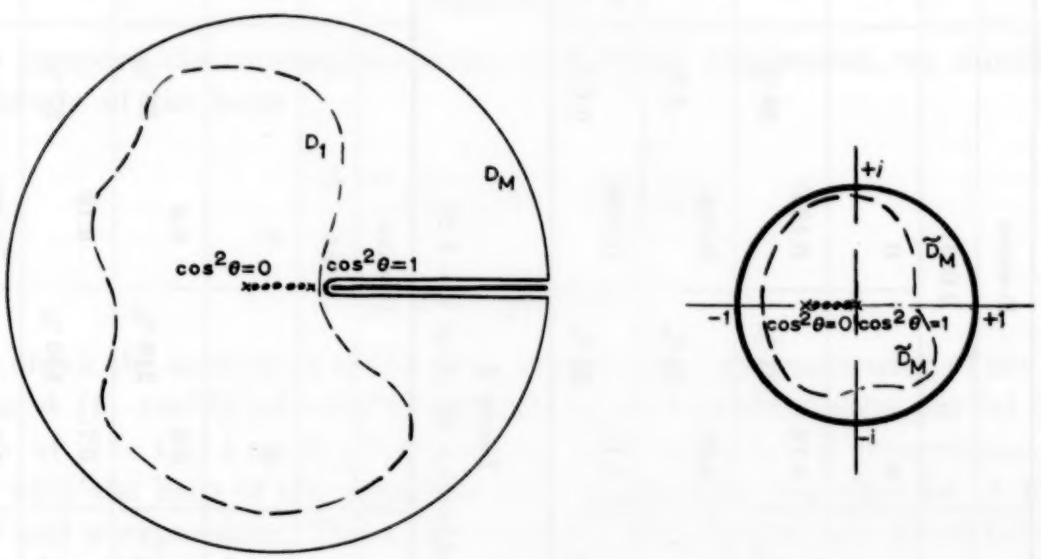

Fig. 3. The optimal transformation of the $\cos^2\theta$ plane into the w plane.

$D_1 \subset D_M$ (not containing points of the z-cut!) into the unit circle, the inequality

$$r_1 \equiv |w_1(P)| \geqq r_M \equiv |w_M(P)| \quad (R_1 = R_M = 1)$$

holds for each point $P \in D_1$.

To prove this, we observe that $w_M(z^2)$ transforms D_1 into a domain $\tilde{D}_1$ contained in the unit circle $\tilde{D}_M$. The function $w_M = f(w_1)$ which transforms the w_1-unit circle into $\tilde{D}_1$ is analytical and has the following properties:

$|f(P)| \leqq 1$ for each P contained in the w_1-unit circle, $f(0) = 0$ because both $w_1(z)$ and $w_M(z)$ transform the point $\cos^2\theta = 1$ into the origin.

Now, the well known Schwartz lemma † requires

$$|w_M| \leqq |w_1|$$

for all points w_1 contained in the unit circle.

† If $f(z)$ is analytical for all $|z| < R$ and if $|f(z)| \leqq M$ and $f(0) = 0$, it follows $|f(z)| \leqq M|z|/R$.

TABLE 1

Approximations for A at $\tau = \frac{4}{3}$

	S-wave		D-wave		G-wave	
Exact value	1.386		0.0831		0.0071	
One term approx.	1.9 35 %	1.9 35 %	0	0	0	0
Two term approx.	1.17 −15 %	1.30 −6 %	0.14 63 %	0.105 26 %	0	0.005 −30 %
Three term approx.	1.49 7 %	1.403 1 %	0.05 −39 %	0.078 −5 %	0.015 113 %	0.0082 17 %
Four term approx.	1.33 −4 %	1.383 −0.2 %	0.10 22 %	0.0836 0.6 %	0.001 −83 %	0.0064 −9 %

TABLE 2

Approximations for A at $\tau = 1.28$

	S-wave		D-wave		G-wave	
Exact value	2.10		0.265		0.047	
One term approx.	4 91 %	4 91 %	0	0	0	0
Two term approx.	−0.2 −108 %	1.4 −33 %	0.8 216 %	0.4 58 %	0	0.045 −4 %
Three term approx.	5 142 %	2.4 12 %	−0.7 −350 %	0.19 −27 %	0.2 361 %	0.056 16 %
Four term approx.	−2 −195 %	1.99 −5 %	1.7 528 %	0.298 12 %	−0.4 −1034 %	0.040 −14 %

A1.3. THE OPTIMAL TRANSFORMATION

The optimal transformation w_M can readily be constructed with the help of the Joukowsky transformation. By means of the transformation $u = (2\tau^2 - z^2 - 1)/(z^2 - 1)$ the cut of the z^2 plane goes into a cut between $u = -1$ and $u = +1$, and $u_{(z^2=1)} = \infty$. This cut can then be transformed into the unit circle (and $u = \infty$ into the origin) by means of the transformation $\frac{1}{2}(w_M + (1/w_M)) = u$. Thus

$$w_M = -1 + 2\,\frac{\tau^2 - 1 - (\tau^2-1)^{\frac{1}{2}}(\tau^2 - z^2)^{\frac{1}{2}}}{z^2 - 1}.$$

Appendix 2

To compare the convergence rates of different expansions, we consider an amplitude of the form

$$A = \frac{1}{\tau + \cos\theta} + \frac{1}{\tau - \cos\theta},$$

where

$$\tau^2 = \tfrac{1}{2}(1 + \alpha^2).$$

To check the accuracies of the first, second, etc., approximation of the $\cos^2\theta$ and $w = (1 - \cos^2\theta)/(\alpha^2 - \cos^2\theta)$ expansions, we calculate some partial coefficients of $A = 1/(\tau + \cos\theta) + 1/(\tau - \cos\theta)$, first exactly, by integrations, and then with the help of the approximative expressions provided for A by the $\cos^2\theta$ and w expansions. These approximative expressions are listed below, in the first and second columns respectively, the errors being expressed in %. Table 1 is calculated for $\tau = \frac{5}{3}$, for which both expansions are convergent. Table 2 is calculated for $\tau = 1.28$ for which the expansion in $\cos^2\theta$ is divergent, the w-expansion remaining, naturally, convergent. This τ corresponds to the laboratory nucleon energy of 72 MeV, but if the one-pion pole is subtracted and τ represents the location of the beginning of the two-pion singularity, this value corresponds to the inelastic threshold 290 MeV.

References

1) Efremov, Meshcheryakov, Shirkov and Tzu, preprint JINR E-539;
Ho Tso-hsin, Hsien Ding-chang and W. Zoellner, preprint JINR D-547, also in JETP **39** (1960) 1660
2) M. L. Goldberger, Y. Nambu and R. Oehme, Annals of Physics **2** (1957) 226
3) D. Amati, E. Leader and B. Vitale, Nuovo Cim. **17** (1960) 68
4) M. L. Goldberger and R. Oehme, Annals of Physics **10** (1960) 153
5) S. Ciulli and J. Fischer, preprint of the Joint Institute for Nuclear Research E-675; JETP (in the press)

1.B

Nuclear Physics **24** (1961) 474—479; © *North-Holland Publishing Co., Amsterdam*

Not to be reproduced by photoprint or microfilm without written permission from the publisher

THE $^1S_0$ NUCLEON INTERACTION IN THE BOUNDARY CONDITION MODEL

E. L. LOMON †

Department of Physics, Massachusetts Institute of Technology Cambridge, Massachusetts

and

M. NAUENBERG ††

Cornell University, Ithaca, New York †††

Received 19 December 1960

Abstract: The nucleon-nucleon interaction model consisting of an energy independent boundary condition with an exponential potential tail is solved analytically for S states. The range of the potential is chosen to be approximately half of a meson Compton wavelength. The three remaining model parameters are fitted to the $^1S_0$ scattering length, effective range, and 210 MeV phase shift. The strength of potential required is in agreement with the expectations of a meson theory. The phase shifts predicted at other energies between 0 and 310 MeV are satisfactory.

1. Introduction

It has been proposed that the short range strong interactions may be represented by boundary conditions which, due to the large effective virtual energies, are slowly varying with the total energy of the system [1, 2]).

Recent work has indicated that a precise fit to all the nucleon-nucleon interaction data may be obtained in terms of energy independent boundary conditions at a fixed boundary radius r_0 and a potential tail, outside r_0, consistent with the predictions of meson theory [3, 4]). The limited analytic investigation developed earlier [5]) and presented in detail below has for many purposes been superseded by the extensive numerical calculations already completed or presently underway. However a description of the analytic results is useful in exhibiting the sensitivity of the predictions to the input parameters, and the general structure of the result. We show that the model is capable of fitting the low as well as the high energy data.

In sect. 2 the well-known analytic solution for the wave function in an exponential potential is extended to the case at hand. In this case the inner region of the potential is replaced by requiring the logarithmic derivative of

† On leave from McGill University, Montreal, Canada.

†† Present address: Institute for Advanced Study, Princeton, New Jersey.

††† This work is supported in part through AEC Contract AT(30-1)-2098, by funds provided by the U. S. Atomic Energy Commission, the Office of Naval Research and the Air Force Office of Scientific Research.

the wave function at a radius r_0 to be constant. The resulting exact solution is expressed in terms of untabulated functions, Bessel functions of arbitrary imaginary order. However an expansion in momentum gives an exact expression for the scattering length in terms of Bessel functions of integral order. Furthermore an expansion in the effective strength of the potential tail gives a rapidly convergent algebraic expression for the phase shift at all energies.

In sect. 3 the parameters of the model are fitted to the unique set of $^1S_0$ phase shifts given by experiment. To reduce the number of parameters meson theoretical arguments are produced to indicate that the range of the exponential tail should be approximately one half of a meson Compton wavelength. The sensitivity of the fit to this assumption is easily estimated and the effect on other parameters of altering the range is shown. It turns out that the potential depth parameter agrees well with the estimates of a meson theory. It is noteworthy that the model fitted at low and high energies interpolates well at 40 MeV, where other models have had some difficulty.

2. The Solution of the Model

The interaction in the $^1S_0$ state is represented by an exponential potential tail $V = -B\exp(-r/d)\,(r > r_0)$ and the boundary condition

$$r_0\left(\frac{\psi'_s}{\psi_s}\right)_{r_0} = f_0, \tag{1}$$

where ψ_s is the wave function in the scattering potential. The wave function in the potential region has the well-known solutions [6]) normalized to plane waves asymptotically

$$U\ (r) = r\psi(r) = \Gamma(1+2kdi)e^{-(2kd\ \ln\ bd)i}J_{2kdi}(2bde^{-r/2d}),$$
$$U^*(r) = r\psi^*(r),$$

where $b^2 = MB/\hbar^2$ (for an attractive potential, $B > 0$ and b^2 is real) and $\hbar k$ is the relative momentum. The wave function for scattering with a phase shift δ_0 is then $\psi_s = \psi - e^{2i\delta_0}\psi^*$. Putting ψ_s in (1) we obtain

$$\tan\delta_0 = -i\frac{(f_0+1)[U-U^*]_{r_0} - r_0\left[\dfrac{dU}{dr} - \dfrac{dU^*}{dr}\right]_{r_0}}{(f_0+1)[U+U^*]_{r_0} - r_0\left[\dfrac{dU}{dr} + \dfrac{dU^*}{dr}\right]_{r_0}} \tag{2}$$

$$= \frac{(f_0+1)[\mathrm{Im}\,\Lambda - \tan kr_0\,\mathrm{Re}\,\Lambda] + kr_0[\mathrm{Re}\,\Lambda + \tan kr_0\,\mathrm{Im}\,\Lambda] + Z\dfrac{r_0}{2d}\left[\mathrm{Im}\dfrac{\partial\Lambda}{\partial Z} - \tan kr_0\,\mathrm{Re}\dfrac{\partial\Lambda}{\partial Z}\right]}{(f_0+1)[\mathrm{Re}\,\Lambda + \tan kr_0\,\mathrm{Im}\,\Lambda] - kr_0[\mathrm{Im}\,\Lambda - \tan kr_0\,\mathrm{Re}\,\Lambda] + Z\dfrac{r_0}{2d}\left[\mathrm{Re}\dfrac{\partial\Lambda}{\partial Z} + \tan kr_0\,\mathrm{Im}\dfrac{\partial\Lambda}{\partial Z}\right]},$$

where $\Lambda = \Lambda_{ip}(2Z)$ (ref. [7])) with $Z = bd\exp(-r_0/2d)$ and $p = 2kd$.

Expanding the above in kd one can obtain the scattering length (as defined by $k \cot \delta_0 = -1/a_0 + \frac{1}{2}\rho_0 k^2 + \ldots$)

$$a_0 = -2d \frac{(f_0+1)[\frac{1}{2}\pi N_0(2Z) - (c+\ln bd)J_0(2Z)] - \frac{r_0}{d} Z[\frac{1}{2}\pi N_1(2Z) - (c+\ln bd)J_1(2Z)]}{(f_0+1)J_0(2Z) - \frac{r_0}{d} ZJ_1(2Z)}, \quad (3)$$

where $C = 0.5772$ is Euler's constant [7]).

One can also obtain the effective range by expanding further in kd. However it proves useful to expand first in Z. Because of the rapid convergence of the Bessel functions we get an adequate representation for the required range of parameters.

For all kd we obtain to fourth order in the expansion of the Λ functions

$$\begin{aligned}
\operatorname{Re} \Lambda &= 1-(1+p^2)^{-1}Z^2+(2-p^2)(1+p^2)^{-1}(4+p^2)^{-1}\tfrac{1}{2}Z^4, \\
\operatorname{Im} \Lambda &= (1+p^2)^{-1}pZ^2[1-\tfrac{3}{2}(4+p^2)^{-1}Z^2], \\
\operatorname{Re} \frac{\partial \Lambda}{\partial Z} &= -2Z(1+p^2)^{-1}[1-(2-p^2)(4+p^2)^{-1}Z^2], \\
\operatorname{Im} \frac{\partial \Lambda}{\partial Z} &= 2Zp(1+p^2)^{-1}[1-3(4+p^2)^{-1}Z^2].
\end{aligned} \quad (4)$$

Eqs. (4) can be substituted into eq. (2) and used to obtain δ_0 for all k. We also expand in $kr_0 \equiv r_0 p/2d$ to give

$$kr_0 \cot \delta_0 = \frac{\alpha+\beta(kr_0)^2+\ldots}{\gamma+\delta(kr_0)^2+\ldots},$$

where

$$\alpha = (f_0+1) - Z^2\left[f_0+1+2\left(\frac{r_0}{2d}\right)\right] + \tfrac{1}{4}Z^4\left[f_0+1+4\left(\frac{r_0}{2d}\right)\right] + \left(-\tfrac{1}{36}Z^6\left[f_0+1+6\left(\frac{r_0}{2d}\right)\right]\right),$$

$$\beta = (f_0+1)\left(\frac{2d}{r_0}\right)^2 + 1 + Z^2\left[f_0\left(\frac{2d}{r_0}\right)+1\right] - \tfrac{1}{16}Z^4\left(\frac{2d}{r_0}\right)^2\left[3(f_0+1)+18\left(\frac{r_0}{2d}\right)+20\left(\frac{r_0}{2d}\right)^2\right],$$

$$\gamma = -f_0 + Z^2\left[(f_0+1)\left(\frac{2d}{r_0}\right)+(f_0+2)+2\left(\frac{r_0}{2d}\right)\right] - \tfrac{1}{8}Z^4\left[3(f_0+1)\left(\frac{2d}{r_0}\right)+2(f_0+6)+8\left(\frac{r_0}{2d}\right)\right]$$
$$+\left\{\frac{Z^6}{216}\left[11\left(\frac{2d}{r_0}\right)(f_0+1)+66+6f_0+36\left(\frac{r_0}{2d}\right)\right]\right\},$$

$$\delta = -f_0\left(\frac{2d}{r_0}\right)^2 - \tfrac{1}{3}(f_0+1) + Z^2\left[\left(\frac{2d}{r_0}\right)+\tfrac{1}{3}(f_0+1)+\tfrac{2}{3}\left(\frac{r_0}{2d}\right)\right]$$
$$+Z^4\left(\frac{2d}{r_0}\right)^3\left[\tfrac{3}{32}(f_0+1)+\tfrac{3}{16}(3-f_0)\left(\frac{r_0}{2d}\right)+\tfrac{3}{8}\left(\frac{r_0}{2d}\right)^2-\left(\frac{f_0+1}{12}\right)\left(\frac{r_0}{2d}\right)^3-\tfrac{1}{3}\left(\frac{r_0}{2d}\right)^4\right],$$

giving

$$\frac{a_0}{r_0} = -\frac{\gamma}{\alpha} \tag{5}$$

and

$$\tfrac{1}{2}\frac{\rho_0}{r_0} = \frac{1}{\gamma}\left[\beta - \frac{\alpha\delta}{\gamma}\right] = \frac{1}{\gamma}\left[\beta + \frac{\delta r_0}{a_0}\right] \approx \frac{\beta}{\gamma}. \tag{6}$$

The last approximation in eq. (6) is possible because of the physically large value of a_0/r_0.

Eq. (5) can also be obtained directly from eq. (3) by expanding the latter in Z^2. We have done so to order Z^6, the added results for α and γ being shown in brackets above. Because of the near vanishing of α it is numerically disastrous to expand a_0 into a power series in Z^2. It is anyway convenient to leave $\tan\delta_0$, a_0 and ρ_0 in the above form as rational functions in Z^2.

The accuracy of the above expansion can be checked by comparing eqs. (3) and (5) or by noting the relative size of successive terms in the experimental region of the parameters. For the parameters derived below, the exact a_0 is 1.03 of the Z^6 approximation and 0.8 of the Z^4 approximation. The large error in the Z^4 approximation is however due to the small value of α, and the sixth order term is actually only 1 % of the leading term. It can be assumed then that the error in ρ_0 is about 1 %. For $\tan\delta_0$ the accuracy is considerably better, as the large value of p improves the convergence of the Λ function. At 210 MeV the fourth order terms in Λ and $\partial\Lambda/\partial z$ are about 10 % of the second order terms and 1 % of the first order terms. The Z^6 corrections are likely to be negligible.

3. Fitting the Data

We shall fit to the scattering length, the effective range and the 210 MeV phase shift in the $^1S_0$ state. We have, however, four independent parameters in the model, f_0, r_0, B and d, and must pick one of them on a theoretical basis. The range of the potential is determined primarily by the pion Compton wavelength. We choose $d \approx \frac{1}{2}\hbar/m_\pi c$ rather than $\hbar/m_\pi c$ for two reasons. (i) The fourth order contribution [8]) is strong compared to the second order potential in the region of 1 fm, thus effectively shortening the range. (ii) We are using an exponential rather than the shorter tailed Yukawa potential and can roughly compensate at low energies by decreasing the range parameter. In any case r_0 and f_0 are insensitive to changes in d, and $d\sqrt{B}$ is approximately a constant giving us the variation in B for different choices of d.

It can be seen from (4) that at $kr_0 = \frac{1}{2}\pi$ and $p^2 \to \infty$

$$\tan\delta_0 = \frac{-(f_0+1)+\dfrac{r_0}{2d}Z^2}{\frac{1}{2}\pi}.$$

This is small and negative when the criterion for large a_0 is satisfied. Thus $r_0 \approx \pi/2k'$, where k' is a momentum at which $\delta_0 \approx 0$. A trial value of r_0 was chosen by the above criterion, then (5) was used to get a rough trial relation between (f_0+1) and Z^2, and (6) to give a second relation. Small adjustments were then made to fit (3), (6) and (2) at 210 MeV simultaneously.

For $f_0 = -0.25$, $r_0 = 0.77$ fm, $d = 0.7$ fm and $Z^2 = 0.46$ (which is equivalent to $B = 117$ MeV) we obtain

$$a_0 = -25 \text{ fm}, \quad \rho_0 = 2.72 \text{ fm} \quad \text{and} \quad \delta_0(210 \text{ MeV}) = 2.3°.$$

The quantities ρ_0 and δ_0 are in sufficient agreement with the data [9]) considering the experimental error and the Z^2 approximation. The resonating denominator in eq. (3) makes a_0 so sensitive to Z^2 or (f_0+1) that shifting a_0 to -21 fm corresponds to a 1 % shift in either of these parameters. The phase shift at 40 MeV was calculated from the above parameters and is 41.2°; at 310 MeV the phase shift is predicted to be $-11.7°$, and at 142 MeV $+12.2°$ in reasonable agreement with experiment.

4. Conclusions

The model, after being fitted to the scattering length, the effective range and the 210 MeV phase shift yields the correct 40 MeV, 140 MeV and 310 MeV phase shifts. The interpolation at 40 MeV is a non trivial consequence as a hard core model tends to result in a smaller 40 MeV phase shift after fitting the other data [10]). It is also satisfactory that the depth of the potential is in reasonable agreement with that predicted by fourth order meson theory, in calculations such as that by Gartenhaus [8]).

We have demonstrated the feasibility of using a meson theoretical tail and replacing the inner region by an energy independent boundary condition for all the $^1S_0$ data from 0 to 310 MeV. We also have simple analytic relations for the dependence of the data on the model parameters; showing that r_0 is given approximately by the energy at which the phase shift changes sign, and that the large scattering length implies a certain simple relation between the strength of the boundary interaction f_0 and the strength of the potential b.

Other calculations [3, 4]) have already shown that a rough fit over the energy range is possible for all the phase shifts. A complete fit is now underway [11]).

References

1) H. Feshbach and E. Lomon, Phys. Rev. **102** (1956) 891
2) V. F. Weisskopf, Phys. Rev. **116** (1959) 1615
3) A. Tubis, in Nuclear Forces and the Few Nucleon Problem, ed. by T. C. Griffiths and E. A. Powers (Pergamon Press, New York, 1960) p. 83
4) D. P. Saylor, F. A. Bryan and R. E. Marshak, Phys. Rev. Let. **5** (1960) 266

5) E. Lomon and M. Nauenberg, Bull. Am. Phys. Sec. **3** (1958) 183
6) P. Morse and H. Feshbach, Methods of Theoretical Physics (McGraw-Hill, New York, 1953) pp. 1670ff
7) E. Jahnke and F. Emde, Tables of Functions (Dover, New York, 1945)
8) S. Gartenhaus, Phys. Rev. **100** (1955) 900
9) M. H. MacGregor and M. J. Moravcsik, Phys. Rev. Let. **4** (1960) 524;
K. Gotow and E. Heer, Phys. Rev. Let. **5** (1960) 111;
E. Lomon and R. C. Stabler, Nuovo Cim. **15** (1960) 150;
G. Breit *et al.*, Phys. Rev. **120** (1960) 2227
10) J. L. Gammel and R. M. Thaler, Phys. Rev. **107** (1957) 291;
MacGregor, Moravcsik and Noyes, UCRL-5582-T (1959)
11) A. Tubis, private communication

8.A

Nuclear Physics **24** (1961) 480—487; © *North-Holland Publishing Co., Amsterdam*

Not to be reproduced by photoprint or microfilm without written permission from the publisher

ASYMMETRY OF THE ANGULAR DISTRIBUTION OF ELECTRONS FROM $\mu \to$ e—DECAY

I. I. GUREVICH, B. A. NIKOLSKY and S. A. ALI-ZADE

I. V. Kurchatov Atomic Energy Institute of the Academy of Sciences of the USSR, Moscow, USSR

Received 29 September 1960

Abstract: The asymmetry of the angular distribution of electrons from $\mu \to$ e decay was studied in magnetic fields by detecting the $\pi \to \mu \to$ e decays in photoemulsion. As a result it is found that longitudinal magnetic fields from 20 000 to 30 000 G do not cancel totally the depolarising effect of the medium (photoemulsion) on the μ-meson.

1. Introduction

The angular distribution of $\pi \to \mu \to$ e decay electrons is described by the relation

$$\frac{\mathrm{d}N}{\mathrm{d}\Omega} = \frac{1}{4\pi} \quad (1 - a \cos \vartheta). \tag{1}$$

The theoretical value of the asymmetry parameter a for V–A interaction and two-component neutrino is equal to $a = \frac{1}{3}$. The difficulty of an experimental check of this prediction lies in the fact that the μ-meson when stopped in a condensed medium depolarizes and thus, in investigating the angular distribution of electrons from $\mu \to$ e decay the quantity $a^* = Pa$ is determined, where P is the degree of the residual polarization of the μ-meson stopped in the given medium. The quantity P differs for different substances and does not lend itself to direct determination. Orear *et al.* [1]) considered the mechanism of depolarization of a stopped μ-meson as a consequence of the production of muonium. The degree of polarization of this kind essentially depends on the strength of the external magnetic field whose direction coincides with that of the spin of the μ-meson:

$$a^* = a \left(1 - \frac{0.5}{1+x^2}\right). \tag{2}$$

Here, $x = \mu H / \Delta E$, where μ is the magnetic moment of the μ-meson, H the magnetic field and ΔE the energy of the hyperfine splitting of muonium (1.84×10^{-5} eV). A more detailed analysis of the depolarization mechanism in the production of muonium, taking account of multiple electron exchange, was

performed by Ferrell *et al.* [2]). The dependence they obtained is of the form

$$a^* = a\left(1 - \frac{0.5}{1+x^2+\tau^{-2}}\right)^n. \tag{3}$$

Here, n is the number of electron exchanges, and τ the average lifetime of the muonium atom in units $\hbar/\Delta E = 3.58\times 10^{-11}$ sec. With an adequate choice of the parameters n and τ, eq. (3) describes the dependence $a^*(H)$ sufficiently well for fields up to $\approx$ 10 000 G. At the same time it follows from eq. (3) that a longitudinal magnetic field of sufficiently high strength leads to a practically total elimination of the depolarization of the μ-meson in the production of muonium. The present work is concerned with investigating the asymmetry of the angular distribution of $\pi \to \mu \to$ e decay electrons in magnetic fields up to 35 000 G and thus elucidating the dependence $a^*(H)$ in a wide interval of variation of the magnetic field strength H. The possibility of checking eq. (3) on the strength of these data enables us to specify the mechanism of depolarization of the μ-meson in a substance, which is essential in the experimental determination of the magnitude of the coefficient a (see eq. (1)).

2. Experimental Set-Up

The emulsion chambers placed in magnetic fields were irradiated by slow π^+-mesons, which stopped in the chamber. In scanning, those events of $\pi \to \mu \to$ e decay were selected in which the direction of emission of the μ-meson formed an angle $\beta_\mu = 0°$ to 30° or $\beta_\mu = 180°$ to 150° with the direction of the field. To determine the latter use was made of X-ray lines which were traced on the emulsion before the cassette was examined.

In scanning the emulsion special care was taken to eliminate the systematic errors stemming from different efficieny in the detection of different cases of $\pi \to \mu \to$ e decay. Such cases of the $\pi \to \mu$ decay were only considered when the end of the μ-meson was not closer than at a distance of $\Delta_\mu = 15$ μm off the surface of the developed emulsion layer. Out of the the 177 850 cases of $\pi \to \mu$ decay satisfying the selection rule with respect to β_μ, only 66 cases were found in which no $\mu \to$ e decay electron was observable. When scanning, no measurement was made of the angle formed by the emission of the electron with the direction of the magnetic field H; the only projection of the angle α on the surface of the emulsion was measured, the magnitude of the coefficient a^* in eq. (1) being determined as

$$a^*_{\text{exp}} = 2\,\frac{N(\alpha > 90°) - N(\alpha < 90°)}{N(\alpha > 90°) + N(\alpha < 90°)}, \tag{4}$$

where the angle of the emission of the electron α was counted from the direction of the projection of the μ-meson onto the direction of the field H. The value of

the coefficient a^*_{exp} determined from eq. (4) is somewhat underestimated owing to the precession of the μ-meson spin around the direction of the magnetic field H. The value a^* corrected for this effect is obtained as follows:

$$a^* = \frac{a^*_{exp}}{\langle \cos \beta_\mu \rangle}. \tag{5}$$

Here, $\langle \cos \beta_\mu \rangle$ is the average cosinus of the angle between the direction of the field and the spin (or the momentum) of the μ-meson. The values $\langle \cos \beta_\mu \rangle$ for the selected cases of $\pi \to \mu$ decay were determined experimentally.

3. Results and Discussions

Altogether there have been selected 177 850 events of $\pi \to \mu \to$ e decay satisfying the selection rules with respect to β_μ and Δ_μ described in sect. 2. The number of the $\pi \to \mu \to$ e decay events in fields of different strength are given in table 1.

TABLE 1

Numbers of $\pi \to \mu \to$ e decay events for fields of different strength H

Magnetic field (G)	Number of cases
405	9 705
805	13 430
1 610	11 617
2 370	10 005
10 000	30 331
20 000	8 851
27 000	17 557
35 000	17 715
Emulsions with higher content of gelatine 27 000	58 639

Out of the 177 850 events of $\pi \to \mu \to$ e detected and scanned no case of $\mu \to 3$e decay or any other anomalous kind of μ-meson decay was detected. There was one case of decay of the μ-meson into electron, neutrino, anti-neutrino and (virtual) γ-quantum with the conversion of the latter into a negaton-positon pair [8]) (Dalitz effect),

$$\mu \to \mathrm{e} + \nu + \tilde{\nu} + \mathrm{e} + \mathrm{e}.$$

The value of the coefficient a^* obtained by eq. (4) and corrected in accordance with eq. (5) for emulsions with normal gelatinous content is represented in table 2. The table also lists the values a^* for μ-mesons flying along and against the direction of the magnetic field H.

The data represented in table 2 are plotted in figs. 1 and 2 alongside experi-

mental results obtained by other authors [1, 3–7]). Here we have $P = 3a^*$ and $X = H/1580$. Figs. 1 and 2 also represent the value P_{exp} for emulsions with higher gelatinous content for the value $X = 17.1$ (see table 3).

Table 3 lists the values a^* for "diluted" emulsions, i.e., emulsions with higher gelatinous content in a field $H = 27\,000$ G. The degree of dilution of the emul-

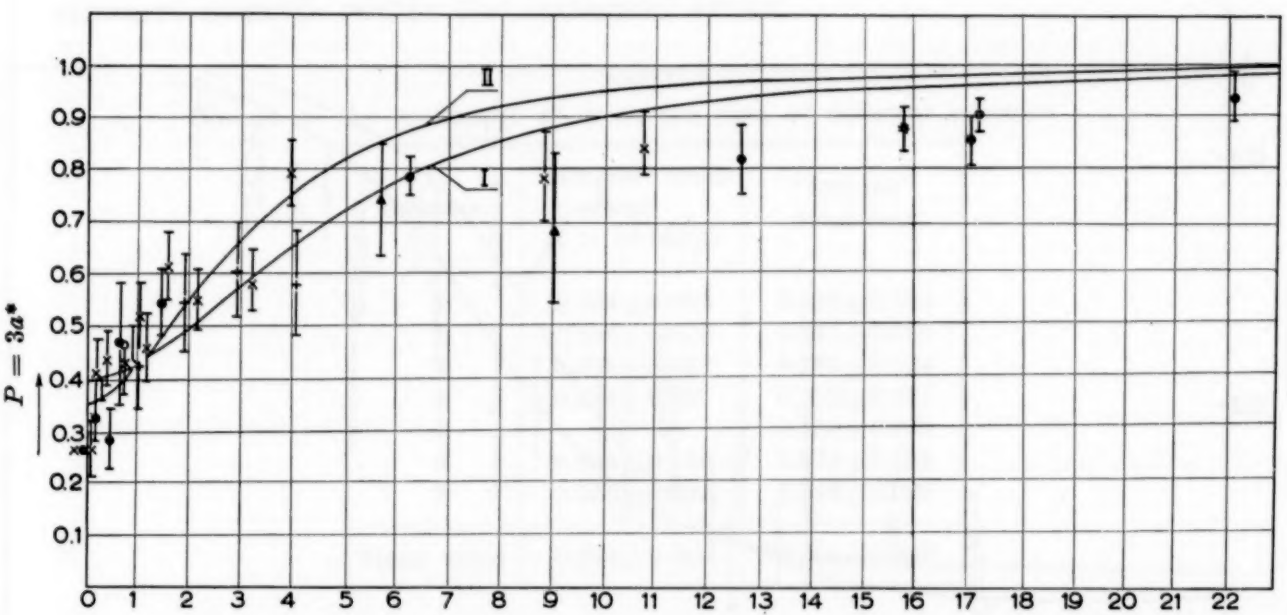

Fig. 1. Experimental data on the dependence $P = f(X)$, where $P = 3a^*$ and $X = H/1580$. The smooth curve I corresponds to the theoretical dependence $P = f(X)$ of eq. (3) for the values $n = 22$, $\tau = 0.30$. This curve corresponds in the best way to the experimental data in the interval of X from 0 to 22.15. Curve II corresponds to the theoretical dependence (3) for the values $n = 12$ and $\tau = 0.44$ and corresponds in the best way to the experimental data in the interval of X from 0 to 4.09.

○ Gurevich *et al.* [6]). + Sens *et al.* [3, 7]). × Waissenberg [5]). △ Orear *et al.* [1]). ▲ Barkas *et al.* [4]). ✱ Lynch *et al.* [7]). • Present work. ⊙ "Deluted" emulsions (present work).

TABLE 2

Values of the coefficients $a^* = Pa$ obtained for different strengths of the longitudinal magnetic field H. The quantities $a^*(\uparrow)$ refer to μ-mesons moving along the field ($\beta_\mu < 30°$) and $a^*(\downarrow)$ to those moving against the field ($\beta_\mu > 150°$); the δa^* are the standard errors ($\delta a^* = 2/\sqrt{N}$).

H (G)	405	805	1 610	2 370	10 000	20 000	27 000	35 000	10 000 35 000
$a^*(\uparrow)$	0.115	0.115	0.170	0.165	0.262	0.277	0.296	0.317	0.284
$\delta a^*(\uparrow)$	0.030	0.027	0.023	0.030	0.017	0.032	0.023	0.023	0.011
$a^*(\downarrow)$	0.114	0.077	0.185	0.202	0.264	0.266	0.273	0.309	0.277
$\delta a^*(\downarrow)$	0.03	0.027	0.028	0.030	0.017	0.032	0.023	0.023	0.011
a^*	0.114	0.096	0.178	0.184	0.263	0.272	0.284	0.313	0.281
δa^*	0.021	0.020	0.020	0.020	0.012	0.023	0.016	0.016	0.008

sion is described by the ratio of the volume of gelatine to the total volume of the emulsion, $V_{gel}/V_{gel}+V_{tgBr}$. For the normal emulsion this ratio amounts to 0.51. For comparison table 3 also lists the value $a^*(H = 27\,000$ G) for the emulsion with normal gelatinous content.

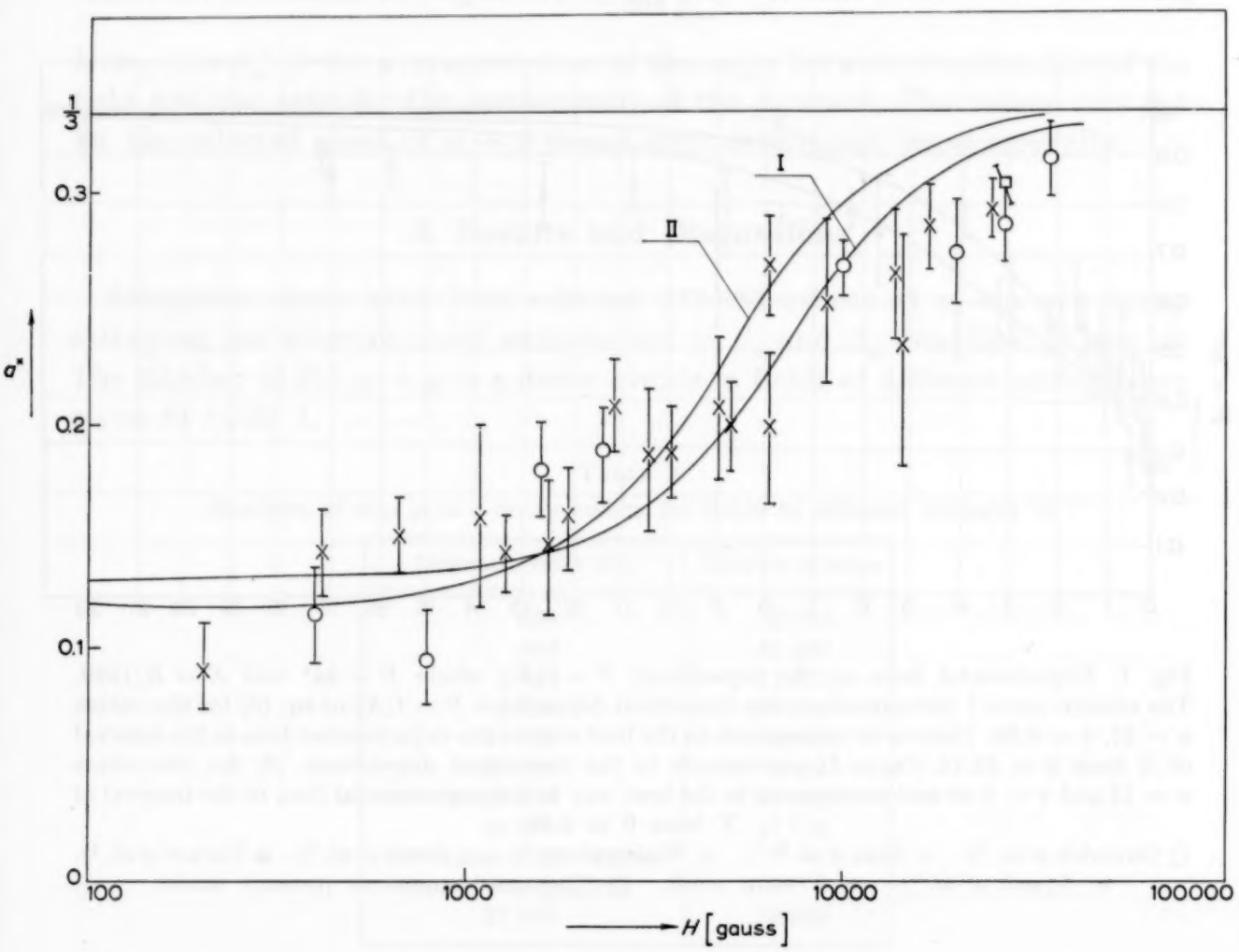

Fig. 2. Experimental and calculated data on the dependence $P = f(X)$. Notations are the same as in fig. 1.
○ Present work. □ "Deluted" emulsions, present work. × Data of other laboratories [1, 3–7].)

TABLE 3

Values of the coefficient $a^* = Pa$ for "diluted" emulsions in the field $H = 27\,000$ G.

$\frac{V_{gel}}{V_{gel}+V_{AgBr}}$	0.51	0.61	0.71	0.76	0.61–0.76
a^*	0.284	0.284	0.323	0.277	0.301
δa^*	0.016	0.016	0.013	0.018	0.009

The δa^* are the standard errors.

The values of the coefficients a^* for μ-mesons in "diluted" emulsions moving along and against the field coincide, just as for non-diluted emulsions:

$$a^*(\uparrow) = 0.297 \pm 0.013, \quad a^*(\downarrow) = 0.305 \pm 0.013.$$

Table 4 illustrates the stability of the values of the coefficients a^* obtained by different scanners. From this table it is clear that the data of different scanners coincide within the statistical errors.

TABLE 4

Values of the coefficient a^* from the data of different scanners

Scanner	"Normal" emulsions $H > 10\,000$ G	"Diluted" emulsions
1	0.254 ± 0.018	0.312 ± 0.022
2	0.282 ± 0.016	0.347 ± 0.020
3	0.294 ± 0.017	0.283 ± 0.023
4	0.284 ± 0.017	0.283 ± 0.021
5		0.338 ± 0.028
6	0.258 ± 0.030	0.278 ± 0.023
7	0.355 ± 0.034	0.246 ± 0.029
Mean value	0.281 ± 0.000	0.301 ± 0.009

Two conclusions can be drawn from the data given in tables 2 and 3:

1) With a sample where μ-mesons are retarded and stopped in longitudinal magnetic fields from 20 000 to 30 000 G, the coefficient a^* does not reach its maximum value $a^* = \frac{1}{3}$. This result is obtained with sufficient statistical reliability.

2) A certain increase in the coefficient a^* is observed as the strength of the field increases from 10 000 G to 35 000 G as well as when the emulsion is "diluted". It should be noted, however, that this conclusion is not so reliable statistically as the first one. The application of the criterion χ^2 gives a probability equal to $W(\chi^2) = 0.3$ that the dependence $a(H)$ observed at $H = 10\,000$ to 35 000 G is a consequence of statistical fluctuations.

The experimental results obtained make it possible, as has been pointed out above, to check the dependence $a^*(H)$ for the emulsion calculated under the assumption of the muonium mechanism of the depolarization of the μ-meson in a substance. The theoretical dependence $a^*(H)$ (see eq. (3)) is a function of two parameters n and τ the choice of which is not practically limited by theoretical considerations.

Figs. (1) and (2) represent the curves $P = f(x)$ corresponding to the theoretical dependence (3) for the values of the parameters n and τ satisfying the

experimental data in the best way possible. The curves were plotted in such a way as to make

$$M = \sum_i \left(\frac{P_{\text{cal},i} - P_{\text{exp},i}}{\delta P_{\text{exp},i}} \right)^2$$

a minimum. The curves I are calculated by using experimental data throughout the interval of variation of X (0 to 22.15). The relevant values n and τ proved to be $n_{\text{I}} = 22$ and $\tau_{\text{I}} = 0.31$; the probability that the dependence $P = f(x)$ thus found corresponds to the experimental data proved to be $W_{\text{I}}(\chi^2) < 0.01$. The curves II correspond to the minimum value of the quantity M as X varies in the interval 0 to 4.09. The values n and τ are $n_{\text{II}} = 12$ and $\tau_{\text{II}} = 0.44$; the probability of the correspondence between the curves II and the experimental results proved to be $W_{\text{II}}(\chi^2) = 0.03$. From the comparison of the curves $P = f(x)$ thus obtained with the experimental values of the quantities P_{exp} it is clear that eq. (3) does not describe the dependence $P_{\text{exp}} = f(x)$ satisfactorily. The fact that the emulsion consists of two components, gelatine and silver bromide, can be roughly allowed for if instead of the dependence $P = f(x)$ described by eq. (3) we assume

$$P = \varepsilon + (1-\varepsilon) \left(1 - \frac{0.5}{1+\tau^{-2}+x^2} \right)^n . \tag{5}$$

Here it is assumed that a certain fraction ε of the μ-mesons stops in the gelatine and does not depolarize at all. Evidently the quantity $\varepsilon < P(x \to \infty)/P(x = 0) \approx 0.3$. The calculation of $P = f(x)$ performed in accordance with the relation (5) for the value $\varepsilon = 0.3$ yields values of P practically coinciding with those obtained when eq. (3) was used. Thus, taking account of the heterogeneity of emulsion cannot improve the agreement between the experimental and calculated dependences $P = f(x)$. The discrepancy between the experimental and calculated dependences $P = f(x)$ is especially conspicuous if one compares P_{exp} and P_{cal} for the values $x > 10$, P_{cal} approximating its maximum value $P = 1$ sufficiently rapidly, while the experimental values P_{exp} remain essentially less than unity. Thus, if one assumes that $P = 1$ ($a = \frac{1}{3}$, V–A interaction) the comparison between the theoretical dependence $P = f(x)$ given by eq. (3) and the experimental data shows that alongside the muonium mechanism of the μ-meson depolarization there is some additional depolarization in the medium, largely responsible for P_{cal} being different from unity for the values $x > 10$.

In conclusion the authors would like to thank V. P. Dzhelepov for the opportunity to irradiate the photoemulsions in the synchrotron of the JINR, D. M. Samoilovich for the development of the emulsions as well as V. M. Kutukova, A. M. Alpers, G. V. Pleshivtsev, S. A. Chueva, B. V. Sokolov and L. V. Surkova for their assistance.

References

1) S. Irear, G. Harris and E. Bierman, Phys. Rev. **107** (1957) 322
2) R. A. Ferrell, Y. C. Lee and M. K. Pal, preprint (1959)
3) Y. C. Sens, R. A. Swanson and V. L. Telegdi, Phys. Rev. **107** (1957) 1465
4) W. H. Barkas, P. C. Giles, H. H. Heckman, F. W. Inman and F. M. Smith, Phys. Rev. **107** (1957) 911
5) A. O. Waissenberg and V. A. Smirnitsky, JETP (in the press)
6) I. I. Gurevich, V. M. Kutukova, A. P. Mishakova, B. A. Nikolsky and L. V. Surkova, JETP **34** (1958) 280
7) G. R. Lynch, I. Orear and Y. Rosendorf, Phys. Rev. Lett. **1** (1958) 12, 471; Phys. Rev. **118** (1960) 284
8) I. I. Gurevich, B. A. Nikolsky and L. V. Surkova, JETP **37** (1959) 318

1.D.2. *Nuclear Physics* **24** (1961) 488—493; © *North-Holland Publishing Co., Amsterdam*
Not to be reproduced by photoprint or microfilm without written permission from the publisher

HINDERED E1 DECAY OF THE 6 keV INDIVIDUAL PARTICLE STATE OF $_{73}Ta^{181}$

U. HAUSER †
Norman Bridge Laboratory of Physics, California Institute of Technology, Pasadena, California ††

Received 16 January 1961

Abstract: The halflife of the 6.25 keV first excited state of Ta^{181} has been determined by a delayed coincidence experiment with a time-to-pulse height conversion method and found to be $t_{\frac{1}{2}} = (6.8 \pm 0.4) \times 10^{-6}$ s. The E1 gamma transition probability of the state is smaller by a factor of 5×10^5 than the single particle estimate in qualitative accord with Nilsson's asymptotic selection rules. The normalized transition probability agrees within a factor of five with four other E1 transitions occurring between levels of neighbouring nuclei which are predicted to be almost identical according to the unified theory.

1. Introduction

Recently Muir and Boehm [1]) reported a 6.25 keV γ-transition in Ta^{181} and concluded that this nucleus has a very low-lying first excited state of this energy.

Strong M-conversion lines were found in the W^{181} decay and very weak indications of conversion lines in the Hf^{181} decay. Further evidence for this line was taken from the appearance of a weak γ-line of this energy in the proportional counter spectrum of the decay of W^{181}. The total conversion coefficient was determined to be $\alpha = 44 \pm 7$, with $M_I/M_{III} = 0.85$, $M_{II}/M_{III} = 1.79$ and $M_{IV,\,V}/M_{III} = 1.76$ which indicate an E1 transition. From the estimated branching ratio of 35 % for the generation of the 6.25 keV radiation in the W^{181} decay and from the fact that in the decay of Hf^{181} there appears, besides the intense 482 keV crossover groundstate transition, a weak 476 keV radiation, the conclusion is drawn that the 6.25 keV transition corresponds to an excited state of Ta^{181} of this energy.

The properties of such a low-lying state are of particular interest. In the following a delayed coincidence experiment is described which proves that the 6.25 keV γ-line follows the K-capture of W^{181} and confirms the existence of the low-lying state. It also determines the lifetime of this level. The decay by a strongly hindered E1 transition is discussed briefly under the aspects of Nilsson's formula [2]) describing the behaviour shell model states in deformed oscillator potentials.

† On leave from 2. Physikalisches Institut der Universität Heidelberg, Heidelberg, Germany.
†† Work performed under the auspices of the U. S. Atomic Energy Commission.

2. Experimental Procedure and Results

The WO_3 source, enriched in W^{180} by a factor of 50, was neutron irradiated in the MTR reactor at Arco, Idaho. It was evaporated on an aluminium foil. Its low energy γ- and X-ray spectrum was measured by an argon filled proportional counter with 10 % methane added at a total pressure of 660 mm Hg. The counter was an aluminium tube of 10 cm diameter. A stainless steel wire of 75 μm diameter served as an anode. The effective length of the counting volume of 15 cm was determined by hypodermic needles serving as guard rings and

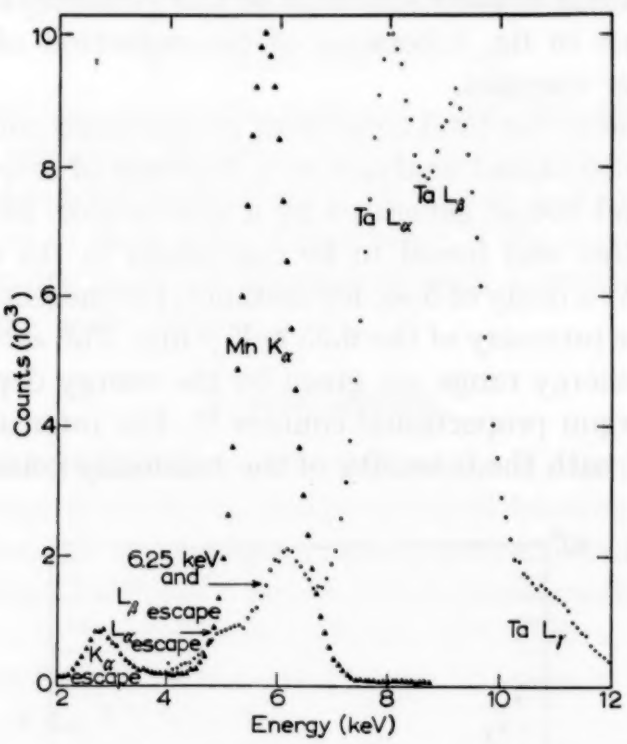

Fig. 1. Proportional counter spectrum of the W^{181} decay (solid circles) with Fe^{55} calibration spectrum (triangles).

fixed in glass insulators. The radiation entered the counter through a beryllium window of 2.5 cm diameter and 0.1 cm thickness. Excellent energy resolution and linearity was obtained after heating the wire in the already filled counter by an electric current to a temperature of about 1000°C for several minutes. The 5.89 keV X-radiation of a Fe^{55} source gave a half-width of the pulse height distribution of 16.7 %. Fig. 1 shows the low energy spectrum of a W^{181} source placed at a distance of 12 cm from the window. In the spectrum the Ta L_α, L_β and L_γ peaks and their escape peaks are clearly resolved. The L_α escape peak coincides with the 6.25 keV γ-ray as already extensively discussed by Muir [1]), but its strong contribution to this line can clearly be seen by comparing its intensity with the neighbouring L_β escape peak.

With the chosen gas pressure, counter dimensions and gas multiplication

factor ($A \approx 1000$), the time lag produced in the coincidence experiment due to the drift velocity of the electrons was a fraction of a μs[3] (ref[3])). The pulse rise time of 0.15 μs was determined only by the upper frequency of the delay-line clipped amplifier used (Hammer N 302). A time constant of 7 μs at the counter wire determined the pulse decay time and the high voltage restoration time.

A coincidence experiment was performed between the Ta K-X-ray, detected by a NaI scintillation counter, and the low energy spectrum, detected by the proportional counter. The source was placed directly on the proportional counter window as well as on the scintillation crystal to get optimum solid angle. The proportional counter spectrum in this geometry is somewhat different from that given in fig. 1 because of the reduction of air absorption in favour of the lower energies.

In a first experiment the total coincident proportional counter spectrum was displayed on a multichannel analyzer as a function of several constant delay times between 0 and 100 μs generated by a univibrator. Besides the 6.25 keV γ-line no other γ-line was found to be coincident in the energy range from 13 keV to 25 keV. At a delay of 5 μs, for instance, the measured background was less than 2 % of the intensity of the 6.25 keV γ-line. The actual intensity limits for γ-lines in this energy range are given by the energy dependent absorption efficiency of the argon proportional counter [3]). The intensity of the 6.25 keV line was compared with the intensity of the randomly coinciding L-lines as a

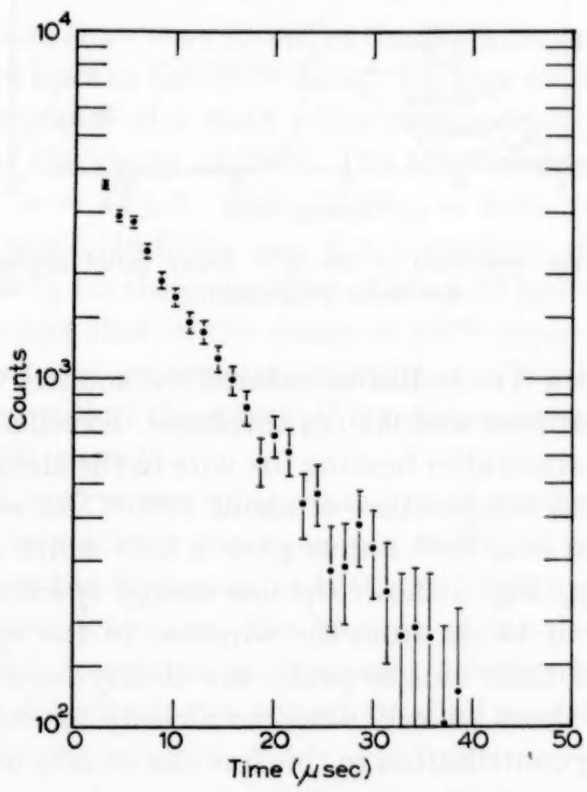

Fig. 2. Coincidence counts of the 6.25 keV γ-ray line versus delay time. The accidental coincidences are subtracted.

function of the delay time. This gave the preliminary result that the lifetime of the state under investigation is about 10^{-5} s.

In a second experiment the lifetime of this state was determined by a time-to-pulse height conversion method. The differential discriminator signal of the Ta K–X-ray channel initiated the sawtooth signal of the time-to-pulse height converter which was fed into the multichannel analyzer. The coincidence gate was opened for 3 μs by the succeeding signal of the differential discriminator measuring the 6.25 keV γ-line. The total time scale used was 72 μs. The time-to-pulse height converter was calibrated with a 1000.0 kHz quartz oscillator.

Fig. 2 shows the result obtained which corresponds to a halflife of

$$t_{\frac{1}{2}} = (6.8 \pm 0.4) \times 10^{-6} \text{ s}.$$

Because of the weak intensity of the 6.25 keV γ-line, the relative high counting rate chosen to get sufficient statistics and the necessarily long time resolution, the contribution of random coincidences due to the L–X-ray lines was appreciable. In the region of short delay times of fig. 2 the random rate was about 60 %, but its intensity could be determined with a statistical error of 0.5 % because of the time scale chosen.

3. Discussion

From the fact that the 6.25 keV γ-line follows the K-capture of W^{181} and that below 110 keV energy (total decay energy minus K-binding energy) no gamma and conversion lines of comparable intensity were found, the conclusion [1]) can be confirmed that Ta^{181} has a very low-lying first excited state. The result of $t_{\frac{1}{2}} = (6.8 \pm 0.4) \times 10^{-6}$s or $\tau = (9.8 \pm 0.6) \times 10^{-6}$ s when combined with the total conversion coefficient of $\alpha = 44 \pm 7$ (ref. [1])) gives a lifetime for photon emission of $\tau_\gamma = (4.4 \pm 0.7) \times 10^{-4}$ s.

From pure lifetime considerations, i.e. the usually used single particle estimate [4]), combined with the empirical trend of the actual multipole transitions [5]), M2 or higher multipole transitions can be ruled out. The state can decay by: 1) a pure E1 transition retarded by a factor of 5×10^5 (the statistical factor in the single particle estimate is neglected), where even a small M2 admixture is improbable because it should be enhanced considerably; 2) a M1 transition, retarded by a factor of 3×10^3; 3) an E2 transition enhanced by a factor of $\approx 10^3$ or a mixture of M1+E2. A pure E2 transition of such an unusual high enhancement can also be excluded because it must be a collective transition of a rotational band different from the well known groundstate rotational band. Therefore the 6.25 keV state should be an intrinsic particle state. Further decision about the multipolarity of the transition cannot be made from the experimental result given above because retardation factors of the order of magnitude mentioned are well known in this region of strongly deformed nuclei for E1 and M1 transitions between intrinsic particle states.

From the conversion coefficient and the subshell ratios Muir and Boehm [1]) concluded that the transition is an anomalous E1 transition very similar in behaviour to E1 transitions in the very heavy element region and fitting well into their conversion systematics [6]). The spin assignment of the 6.25 keV state becomes unique when considering the M2 nature of the 476 keV radiation from the 482 keV $\frac{5}{2}+$ state and the *ft*-values of the K-capture of W^{181}. From this it follows that it is a $\frac{9}{2}-$ state, which indeed is the individual nucleon state predicted as the groundstate or a very low-lying first excited state for Ta^{181} according to Nilsson's level scheme [2]) with the asymptotic quantum number notation [514].

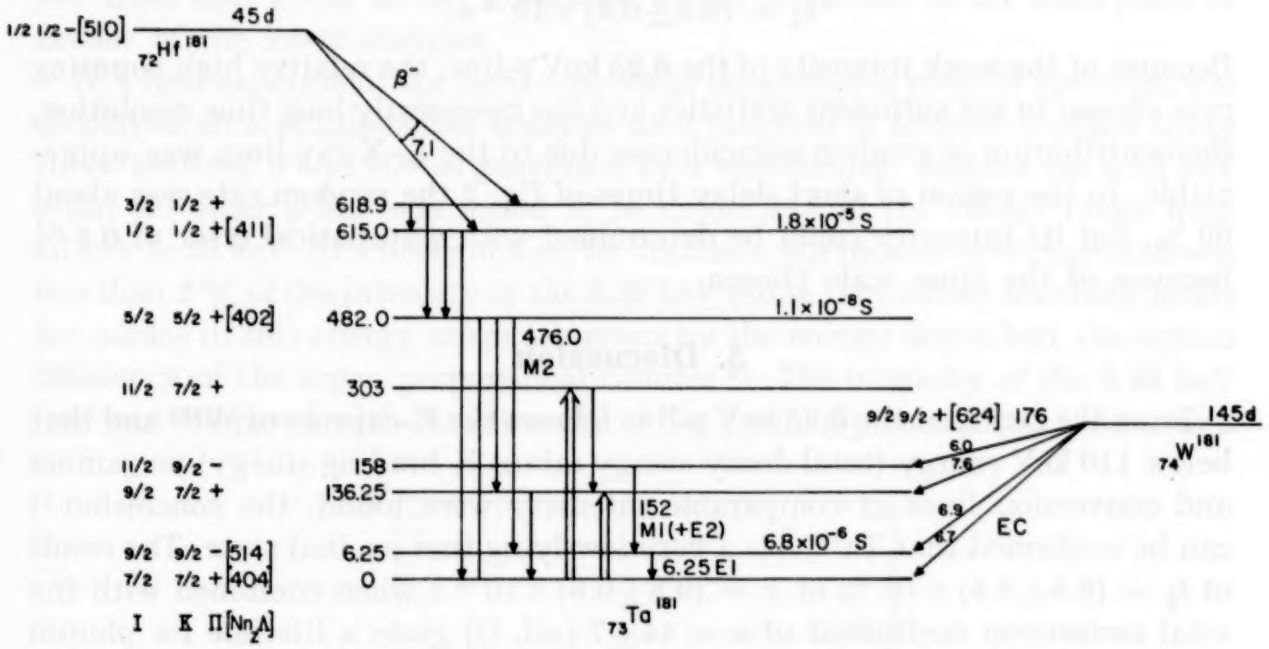

Fig. 3. Level scheme of Ta^{181}. The energies are given in keV. The individual particle states are labelled by Nilsson's quantum numbers.

Muir and Boehm [1]) also determined the nature of the 152 keV transition appearing in the decay of W^{181} to be M1 (+E2) from the conversion electrons. From this they concluded that this is a decay of the first rotational state of 158 keV and spin $\frac{11}{2}-$ of a rotational band belonging to the 6.25 keV intrinsic state. The determined *ft*-values of the electron capture of W^{181} leading to the two different rotational bands of Ta^{181} are also in accord with the Nilsson prediction. Fig. 3 shows the level scheme of Ta^{181}.

It should be noted that the level spacing between the $\frac{9}{2}-$ [514] level and the $\frac{7}{2}+$ [404] groundstate decreases strongly with increasing mass number from $_{71}Lu^{175}$, $_{71}Lu^{177}$, $_{73}Ta^{179}$ to $_{73}Ta^{181}$. The E1 transition probability between these two states was calculated on the basis of Nilsson's wave functions and was found to be relatively insensitive to nuclear deformation changes. Therefore the unified theory predicts for these nuclei almost identical normalized transi-

tion probabilities. It turns out that for these nuclei the five experimentally known normalized transition probabilities are the same within a factor of five, although they are smaller by two orders of magnitude than the predicted value. This is reported in more detail in a separate paper [7]) concerning measurements and analysis of several E1 transition probabilities of neighbouring nuclei.

Asaro *et al.* [6]) defined an empirical L-shell conversion anomaly factor which is the sum of the absolute deviations of the subshell conversion coefficients from the theoretical value normalized on the theoretical total L-shell coefficient. They obtained an almost linear relation when plotting the logarithm of this anomaly factor versus the logarithm of the hindrance factor in the γ-transition probability for several E1 transitions of proton nuclei around $A = 235$. Muir [1]), using their data, got the same result for the anomalous M-conversion of these elements. When inserting the M-shell conversion anomaly factor of the 6.25 keV transition of Ta^{181} into this plot he obtained an estimated hindrance factor of roughly 2×10^5 which agrees surprisingly well with the measured value.

References

1) A. H. Muir and F. Boehm, Bull. Am. Phys. Soc. **4** (1959) 367;
A. H. Muir, Thesis, California Institute of Technology (June 1960) to be published
2) S. G. Nilsson, Mat. Fys. Medd. Dan. Vid. Selsk. **29**, No. 16 (1955);
B. R. Mottelson and S. G. Nilsson, Mat. Fys. Skr. Dan. Vid. Selsk. **1**, No. 8 (1959)
3) W. N. English and G. C. Hanna, Can. J. Phys. **31** (1953) 768;
S. C. Curran, Handbuch der Physik (Springer Verlag, Berlin, 1958) vol. XLV
4) S. A. Moszkowski, in Beta and Gamma-Ray Spectroscopy ed. by K. Siegbahn, (North-Holland Publ. Co., Amsterdam, 1955)
5) M. Goldhaber and A. W. Sunyar, in Beta- and Gamma-Ray Spectroscopy, ed. by K. Siegbahn (North-Holland Publ. Co., Amsterdam, 1955);
D. E. Alburger, Handbuch der Physik (Springer Verlag, Berlin, 1957) vol. XLII
6) Asaro, Stephens, Hollander and Perlman, University of California Radiation Laboratory Report UCRL-8786, (June 1959);
F. Asaro, Bull. Am. Phys. Soc. **4** (1959) 351
7) U. Hauser, K. Runge and G. Knissel, Nuclear Physics, to be published

4.E

Nuclear Physics **24** (1961) 494—499; © *North-Holland Publishing Co., Amsterdam*

Not to be reproduced by photoprint or microfilm without written permission from the publisher

THE DECAY OF Br^{78}

R. RIKMENSPOEL † and D. M. VAN PATTER

Bartol Research Foundation of the Franklin Institute, Swarthmore, Pennsylvania ††

Received 2 January 1961

Abstract: Br^{78} sources have been produced by proton bombardment of isotopically enriched (97 %) thin targets of Se^{18}, in order to investigate the decay scheme of Br^{78}. The Se^{78}(p, n)Br^{78} threshold was measured at 4.40 ± 0.01 MeV, using a slow-fast neutron counter arrangement. Annihilation radiation with a half-life of 6.5 ± 0.1 min was observed for bombardments with $E_p \geqq 4.40$ MeV. Using an anthracene crystal, the end-point of the β^+ spectrum of Br^{78} was measured, and was found to be consistent with the value of 2.54 ± 0.01 MeV calculated from the Se^{78}(p, n) threshold determination. Measurements of the γ-ray spectrum of Br^{78} indicate a γ-ray of 0.613 ± 0.003 MeV, of intensity 0.14 ± 0.015 that of all positons, which is assigned to the known first 2+ state of Se^{78}. Excitation of the known second 2+ state at 1.31 MeV is not observed, occurring with $\leqq 0.4$ % of the decays, with log $ft \geqq 5.9$. The results indicate that the ground state of Br^{78} has spin and parity of 1+.

1. Introduction

Until recently, the adopted level scheme of Br^{78} was based on work of Valley *et al.* [1]) and Buck *et al.* [2, 3]) relating to the (p, n) reaction on natural selenium, and work of Marmier and Preiswerk [4]). This led to a proposed decay scheme which included two low-lying states in Br^{78} at 49 keV (2—) and 157 keV (5—), the latter having a 6.4 min decay. The half-life for the decay of the ground state of Br^{78} was not known, and was said to be $\leqq 6$ min. More recent investigations by Pierson and Coryell [5]) of the Br^{78} decay produced by the $Br^{79}(\gamma, n)$ reaction raised doubts about the validity of this decay scheme.

In connection with investigations of (p, p′γ) spectra from medium-weight even nuclei, γ-radiation with a half-life of 6.5 min was observed from targets containing enriched isotopes of selenium bombarded by protons. It was decided to attempt to clarify the decay scheme of Br^{78}, particularly since the ground-state of Br^{78}(1+) should be readily excited by the Se^{78}(p, n)Br^{78} reaction. By using a proton beam of well defined energy, it should be possible to excite only the ground-state of Br^{78}, and study its decay properties without the complication of competing decays from possible low-lying states. Experiments have been performed

† Now with the Johnson Foundation of the University of Pennsylvania, Philadelphia, Pennsylvania.

†† This research was supported by the United States Air Force through the Air Force Office of Scientific Research of the Air Research and Development Command under contract AF49(638)-512.

1) to establish the energy of the ground state of Br^{78} relative to the ground state of Se^{78},
2) to measure the half-life of the decay of the ground state of Br^{78} and
3) to measure the branching of the decay of Br^{78} to the various known states of Se^{78}.

Following the submission of a preliminary report of these results [6]), it was learned that Pierson and Coryell had extended their investigations, and had reached the same conclusions. Since a full account of their work has now been published [7]), only a brief presentation of the present investigations will be given. In particular, the details of a search for a low-lying isomeric state of Br^{78} will not be given, since a negative result was obtained, in agreement with the work of Pierson and Coryell [7]) who did not find a parent isomer with a half-life of > 10 sec.

2. Source Preparation

Isotopically enriched Se^{78}(96.5 %) was obtained from the Stable Isotopes Division, ORNL, which contained 2.5 % of Se^{80}. Thin targets (of the order of 50 keV thickness) were prepared by vacuum evaporation of the selenium on 0.013 cm gold backings. Br^{78} sources were produced by means of the (p, n) reaction using protons accelerated by the Bartol-ONR Van de Graaff accelerator, with an energy definition of better than 5 keV.

3. The Ground State of Br^{78}

The threshold for the Se^{78}(p, n)Br^{78} reaction was measured at 4.396 ± 0.010 MeV, using the slow-to-fast neutron ratio technique. The experimental data obtained for this threshold are shown in fig. 1. The reproducibility of the data for the counter ratio was ± 2.5 % for $E_p = 4.42$–5.40 MeV. No evidence was found for a (p, n) threshold corresponding to an excited state of Br^{78} with an energy less than 0.20 MeV. The proton energy scale was calibrated with the F^{19}(p, n)Ne^{19} threshold, using the most recent determination of 4.233 ± 0.003 MeV. [8]) This result yields a Q-value for the Se^{78}(p, n)Br^{78} reaction of -4.34 ± 0.01 MeV, which does not agree very well with a recent measurement of -4.37 ± 0.01 MeV obtained by Goodman and Schardt [9]).

The time decay of the annihilation radiation following bombardments of the Se^{78} target at $E_p = 4.42$, 4.52 and 4.62 MeV was measured. The decay curve was composed of two parts: (a) a 6.5 ± 0.1 min activity attributed to Br^{78} and (b) a tail consisting of the 18-min Br^{80} decay and the 4.4-h activity due to Br^{80m}. Extrapolation of the Br^{80} activity to a time immediately following beam bombardment indicated that 1 % of the initial activity was due to Br^{80}.

The β^+ spectrum was measured with a 2.5×1.3 cm anthracene crystal, coupled to a Dumont 6292 photomultiplier. The spectra were displayed on a

100-channel RIDL pulse analyser. The geometry used proved to be not good enough to permit determination of the end-point from a Fermi plot. As an alternative procedure, the $\beta+$ spectra of Ge^{68}, Zn^{63} and Cu^{62}, with end-points of 1.90, 2.34 and 2.93 MeV respectively, were measured in the same geometry as used for Br^{78}. After normalizing the maxima of the various spectra, the energy for the Br^{78} ground-state decay was determined by interpolation, since all the spectra have allowed shapes. The end-point of the Cu^{62} spectrum was taken as 2.93 ± 0.01 MeV, as obtained from a measurement of the $Ni^{62}(p, n)Cu^{62}$ threshold of 4.81 ± 0.01 MeV. In this way, the end-point of the $\beta+$ spectrum of

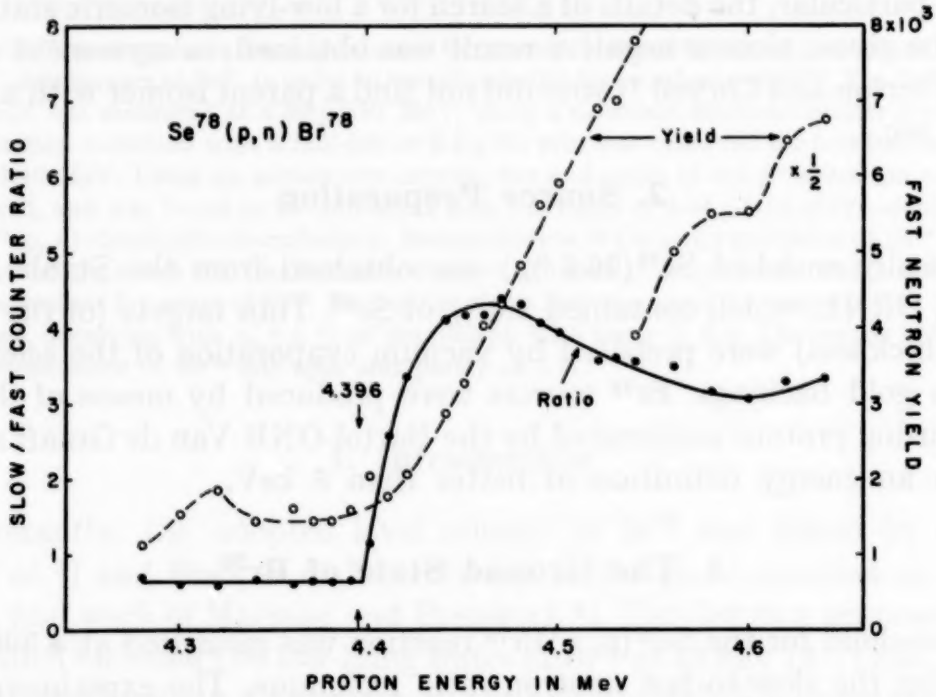

Fig. 1. Measurement of the $Se^{78}(p, n)$ threshold showing (1) slow-to-fast neutron ratio and (2) yield of fast neutrons.

Br^{78} was found to be 2.52 MeV (error $\approx$ 0.05 MeV), which is consistent with the more accurate determination of 2.54 ± 0.01 MeV calculated from the measured value of the $Se^{78}(p, n)$ threshold.

It is concluded that the ground state of Br^{78} is established at an energy of 3.56 ± 0.01 MeV above the ground state of Se^{78}, with a half-life of 6.5 ± 0.1 min. This same conclusion has been reached independently by Pierson and Campbell[7]) and by Goodman and Schardt[9]).

4. The Branching of the $\beta+$ Decay of Br^{78}

The γ-radiation following the decay of Br^{78} was detected by a 5.1×5.1 cm NaI(Tl) crystal coupled to a Dumont 6292 photomultiplier. The spectra were displayed on the 100-channel analyzer. Positons were annihilated in a 1.3 cm aluminium cylinder surrounding the source.

The γ-ray spectrum obtained is shown in fig. 2. In addition to annihilation radiation, a γ-ray of 0.613 ± 0.003 MeV is observed, together with a sum peak at 1.125 MeV. The 0.613-MeV γ-ray is assigned to the known first 2+ level in Se^{78}. The intensity ratio of the 0.613-MeV γ-ray to all positons was found to be 0.14 ± 0.015. No excitation of the known second 2+ level of Se^{78} at 1.31 MeV was observed in this singles spectrum. The intensity ratio to all positons was

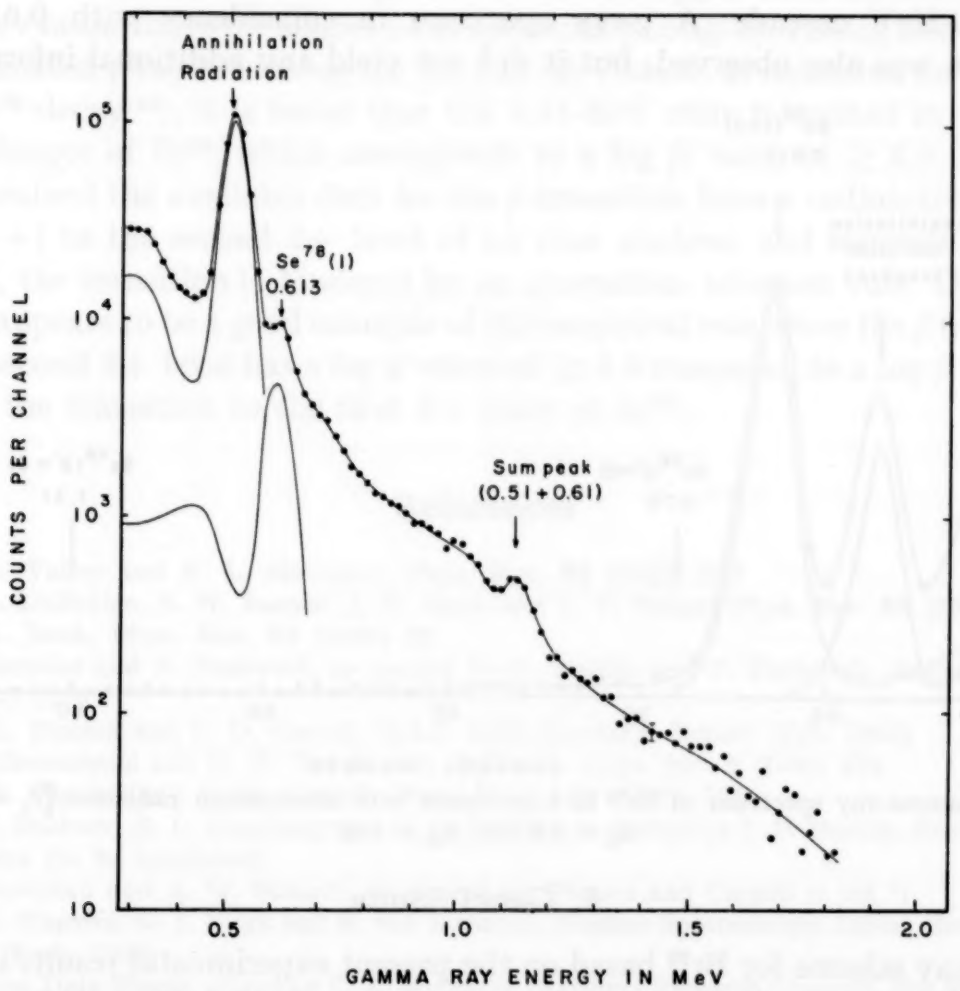

Fig. 2. Gamma-ray spectrum of Br^{78} obtained using a 5.1 cm $\times$ 5.1 cm NaI(Tl) crystal, $d = 5$ cm (source to crystal face).

$\leqq 0.3$ % for the 0.70-MeV cascade radiation (1.31–0.61 MeV transition) and $\leqq 0.2$ % for the 1.31-MeV radiation.

Gamma-gamma coincidence measurements were made using two 5.1×5.1 cm NaI(Tl) crystals, at distances of 3.8 and 5.1 cm from the source to crystal face. The axes of the two crystals were separated by 102°. A 2.5 cm thick lead attenuator was placed between the crystals, to insure that annihilation radiation would not be seen in coincidence with itself. The resolving time of the slow coincidence circuit was measured as 0.2 μsec.

The γ-ray spectrum obtained with a window set at 0.511 MeV is shown in fig. 3. The 0.613 MeV γ-ray is found to be in coincidence with annihilation radiation. The annihilation peak seen in this spectrum can be accounted for by chance coincidences. No other γ-rays coincident with annihilation radiation were observed. The upper limit for 1.31-MeV radiation in coincidence with annihilation radiation is found to be $\approx$ 1.5 % of the intensity of the 0.613-MeV γ-ray in this coincidence spectrum; a similar upper limit of $\approx$ 2.0 % is found for the 0.70-MeV cascade. A γ-ray spectrum in coincidence with 0.613-MeV radiation was also observed, but it did not yield any additional information.

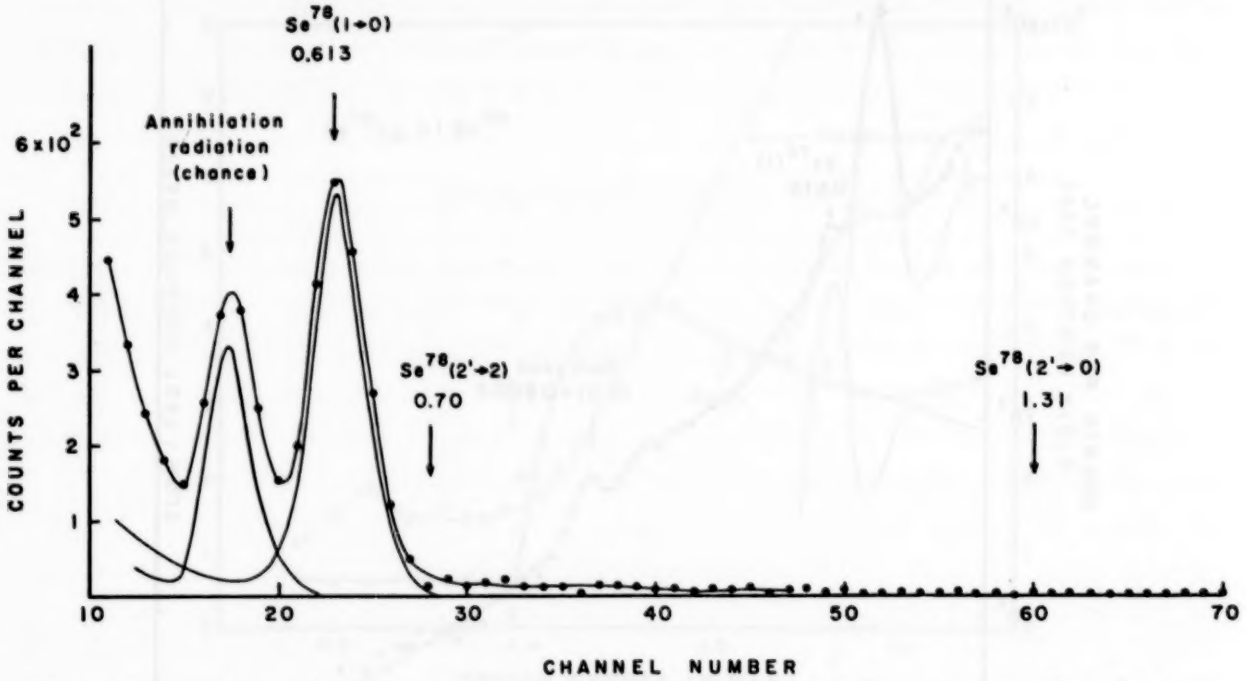

Fig. 3. Gamma-ray spectrum of Br^{78} in coincidence with annihilation radiation, $d_1 = 5.1$ cm, $d_2 = 3.8$ cm, $\theta_{12} = 102°$.

5. Conclusions

A decay scheme for Br^{78} based on the present experimental results is shown in fig. 4. Ratios for electron capture to $\beta+$ decay of 0.07, 0.17 and 0.7 have been

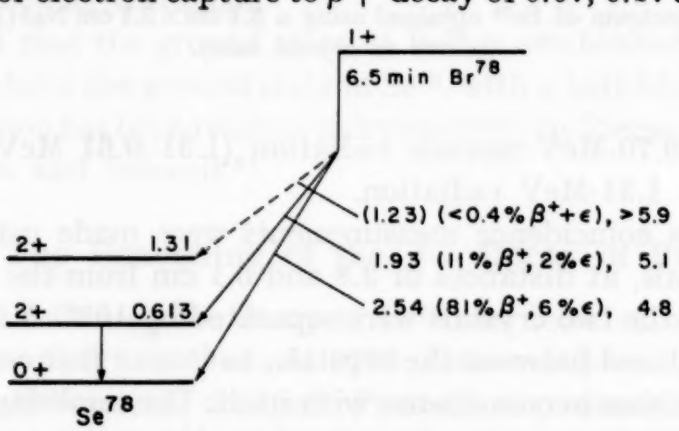

Fig. 4. The decay scheme of Br^{78}, as found from the present experiment.

taken for decays to the ground 0.61 and 1.31-MeV states of Se^{78}, as given in the tables provided by Wapstra *et al.* [10]). Log *ft* values of 4.8 and 5.1 for the branching to the ground state and the first 2+ state of Se^{78} suggest a spin and parity assignment of 1+ for the ground state of Br^{78}. The decay scheme found for Br^{78} is in excellent agreement with that found by Pierson and Coryell [7]).

The most sensitive method for observing excitation of the known second 2+ state of Se^{78} at 1.31-MeV proved to be the upper limit for detection of 1.31-MeV radiation in the singles γ-ray spectrum (see fig. 2). Taking into account the estimated γ-ray branching for the 1.31-MeV state, as indicated for the As^{78} (β^-) Se^{78} decay [11]), it is found that the 1.31-MeV state is excited in $\leqq 0.4$ % of the decays of Br^{78}, which corresponds to a log *ft* value of $\geqq 5.9$. Sakai [12]) has examined the available data for the β-transition from a radioactive parent (spin 1+) to the second 2+ level of an even nucleus, and suggests that, in general, the transition is hindered by an anomalous selection rule. The decay of Br^{78} appears to be a good example of this empirical rule, since the β transition to the second 2+ level has a log *ft* value of $\geqq 5.9$ compared to a log *ft* value of 5.1 for the transition to the first 2+ state of Se^{78}.

References

1) G. E. Valley and R. L. McCreary, Phys. Rev. **56** (1939) 863
2) L. A. DuBridge, S. W. Barnes, J. H. Buck and C. V. Strain, Phys. Rev. **53** (1938) 447
3) J. H. Buck, Phys. Rev. **54** (1938) 25
4) P. Marmier and P. Preiswerk, as quoted by P. Stahlin and P. Preiswerk, Nuovo Cim. **10** (1953) 1219
5) W. R. Pierson and C. D. Coryell, M.I.T. LNS Quarterly Report (Feb. 1958)
6) R. Rikmenspoel and D. M. Van Patter, Bull. Am. Phys. Soc. **5** (1960) 338
7) W. R. Pierson and C. D. Coryell, Phys. Rev. **119** (1960) 755
8) E. H. Beckner, R. L. Bramblett and G. C. Phillips, as quoted by J. B. Marion, Revs. Modern Physics (to be published)
9) A. Goodman and A. W. Schardt, as quoted by Pierson and Coryell in ref. [7])
10) A. H. Wapstra, G. J. Nijgh and R. van Lieshout, Nuclear Spectroscopy Tables (Interscience New York, 1959)
11) Nuclear Data Sheets, edited by C. L. McGinnis (National Research Council), No. 59–5–50
12) M. Sakai, Institute for Nuclear Study, Report No. 19, University of Tokyo (July 1, 1959)

1.E.1

Nuclear Physics **24** (1961) 500—504; © *North-Holland Publishing Co., Amsterdam*

Not to be reproduced by photoprint or microfilm without written permission from the publisher

PROTON CAPTURE IN A^{40}

S. E. ARNELL

Department of Physics, Chalmers University of Technology, Gothenburg

Received 2 January 1961

Abstract: The $A^{40}(p, \gamma)K^{41}$ reaction has been studied in the range of proton energies from 700 keV to 1400 keV using electromagnetic separated isotopes. Fifty-seven excited levels in K^{41} were observed. The target problem was given special attention.

1. Introduction

Electromagnetic separated targets of A^{40} on silver backings were bombarded with protons in the energy range of 0.5 to 1.8 MeV by Broström *et al.* [1]). Four resonances in K^{41} were found in this investigation. The reaction $A^{40}(p, \gamma)K^{41}$ gives information of excited levels above 7.804 MeV (ref. [2])) in K^{41}.

2. Experimental Details

The electrostatic generator of this institute was used as the source of protons. The proton energy scale is based on the value 992.0 ± 0.5 keV [3]) for the strong resonance in the reaction $Al^{27}(p, \gamma)Si^{28}$. The excitation curves were obtained with a heavily shielded 12.7 cm by 10.16 cm long NaI(Tl)-crystal as detector placed at 40° with respect to the proton beam and close to the target.

Targets of A^{40} were prepared by the electromagnetic isotope separator group of this institute. In order to investigate the influence of the backing material as regards the collecting property of the ions a series of separations were performed using copper, silver, platinum, gold, molybdenum, tungsten and tantalum as backing materials and the same ion current and separation time for the different targets. The yield from the prominent resonance in the reaction $A^{40}(p, \gamma)K^{41}$ at $E_p = 1101$ keV was then measured. Of the backing materials mentioned above tantalum, molybdenum and tungsten showed good collecting properties.

In order to find out when a target, using tantalum as backing material, was saturated with argon, a series of targets which had received different amounts of A^{40}-ions were investigated. It was found that a target could store about 4 $\mu g/cm^2$ (ref. [4])) when saturated.

In order to improve the resolution in the resonance yield curve and separate adjacent resonances it was tried to retard the ion beam in the isotope separator

before the ions impinge on the backing material thereby producing targets thinner to the protons. The result is given in fig. 1, which shows the prominent resonance at 1101 keV and an adjacent resonance at 1108 keV at different energies of the argon ions. As the figure illustrates, the improvement of the resolution by diminishing the ion energy is considerable, the observed thickness of the peak at 1101 keV has decreased from 5.7 keV to 2.1 keV when the ion energy is changed from 45 keV to 4.5 keV. This is of great importance when the energy level density is high as is the case at the high excitation of the K^{41}-nucleus being studied in this investigation.

It is of interest that no decrease in the yield of the reaction with saturated targets is found when the ion energy is changed from 45 keV to 4.5 keV, which

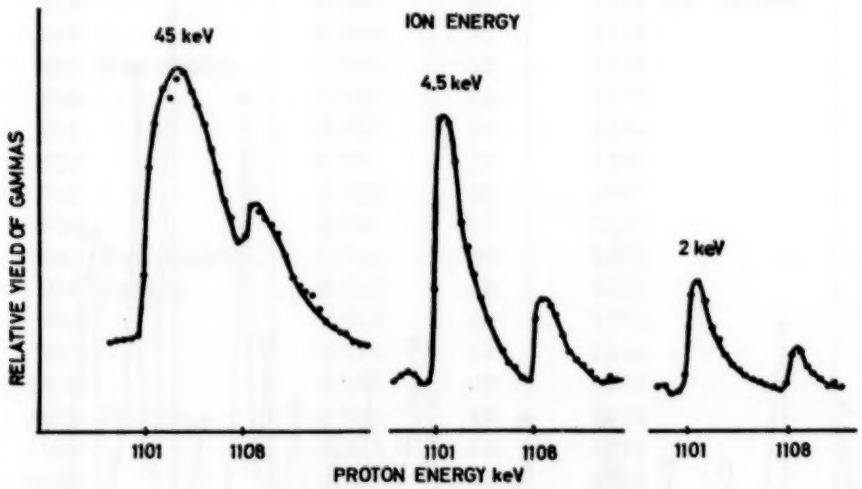

Fig. 1. The improvement in the resolution of the yield curve measurement by retarding the gas ions before they impinge on the backing material.

shows that the maximum density value of the gas ions in the backing material is approximately constant, independent of the accelerating voltage down to low ion energies.

For the target where the argon ions were retarded to 2 keV the decrease in the yield observed may also be due to the fact that the target is thinner to the protons than the proton energy spread. Such an argon target on tantalum could resist one day continuous bombardment with a proton current of about 0.5 μA without showing sign of decrease in the yield indicating diffusion of the ions out of the backing material during bombardment. No cooling of the target was necessary.

3. Result

A series of excitation curves were obtained using backings of tantalum, molybdenum and tungsten. With tantalum as backing material, several targets with different penetration depths of the gas ions were investigated. The result

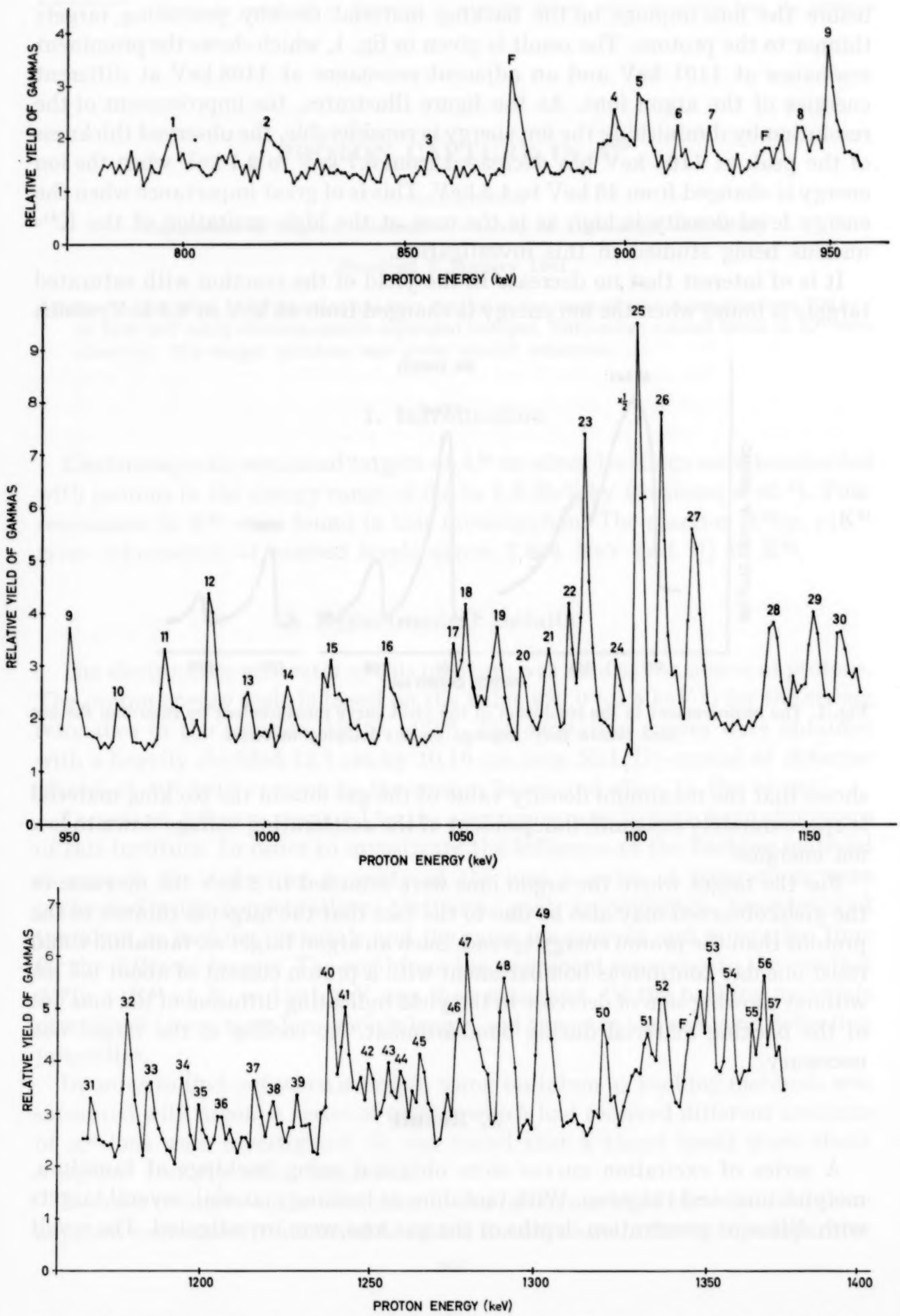

Fig. 2. The excitation function for the yield of gamma rays with energy greater than 1 MeV in the $A^{40}(p, \gamma)K^{41}$ reaction. The peaks marked F are due to the $F^{19}(p, \alpha, \gamma)O^{16}$ reaction.

from an excitation curve with a target where the penetration depth is about 7 $\mu g/cm^2$ (ref. [5])) is given in fig. 2. (The values from the graph of ref. [5]) are multiplied by 2, according to ref. [6])). Table 1 gives the resonance energies.

TABLE 1

Resonance bombarding energies E_p and compound nucleus excitation energies E_x for the $A^{40}(p, \gamma)K^{41}$ reaction

	E_p (keV) (±1)	E_x(MeV) (±0.003)		E_p (keV) (±1)	E_x (MeV) (±0.003)
1	799	8.584	29	1152	8.928
2	819	8.603	30	1162 Ev. double	8.938
3	856	8.639	31	1170	8.946
4	898 Ev. double	8.680	32	1179	8.954
5	904	8.686	33	1186	8.961
6	911	8.693	34	1194	8.969
7	920	8.701	35	1200	8.975
8	942	8.723	36	1207	8.982
9	950	8.731	37	1217	8.991
10	962 Ev. double	8.743	38	1222	8.996
11	973 Double	8.753	39	1229	9.003
12	985	8.765	40	1240	9.014
13	995	8.775	41	1244	9.018
14	1005	8.785	42	1249	9.023
15	1015 Double	8.794	43	1258	9.031
16	1029	8.808	44	1262	9.035
17	1049	8.827	45	1268	9.041
18	1052	8.830	46	1279	9.052
19	1061	8.839	47	1283	9.056
20	1068	8.846	48	1293	9.066
21	1074	8.852	49	1303	9.075
22	1081	8.859	50	1321	9.093
23	1086	8.864	51	1331	9.103
24	1096	8.873	52	1336	9.107
25	1101	8.878	53	1349	9.120
26	1108	8.885	54	1358	9.129
27	1118	8.895	55	1365	9.136
28	1139	8.915	56	1368	9.139
			57	1372	9.143

Very weak resonances have been reported because they are reproducible under such circumstances as mentioned. All resonances found were narrower than 1 keV. The de-excitation of some of the levels will be investigated.

I wish to express my sincere gratitude to Professor N.Ryde for his kind interest in this work, the electromagnetic separator group for performing the separations and Mr. P. Standzenieks for help during the measurements.

References

1) K. J. Broström, T. Huus and I. Koch, Nature **162** (1948) 695
2) E. Lawrence, Tables of Nuclear reaction Q-values, (1959) UCRL 5419
3) I. B. Marion, University of Maryland Physics Department, Technical Report 184 (July 1960)
4) O. Almén and G. Bruece, Nuclear Instruments **12** (1961), to be published
5) K. O. Nielsen, in Electromagnetically Enriched Isotopes and Mass Spectrometry, ed. by M. L. Smith (Butterworths Scientific Publications, London, 1956) p. 77, fig. 5
6) K. O. Nielsen, Thesis, Copenhagen, 1958

2.B:6.B

Nuclear Physics **24** (1961) 505—509; © *North-Holland Publishing Co., Amsterdam*

Not to be reproduced by photoprint or microfilm without written permission from the publisher

AN ABSOLUTE DETECTOR AND PRODUCER OF NUCLEAR ALIGNMENT

B. A. JACOBSOHN † and R. M. RYNDIN ††

CERN, Geneva

Received 16 December 1960

Abstract: For a special type of reaction in which particles of spin one are absorbed or emitted, the consequences of parity and angular momentum conservation are shown to be especially simple and purely geometrical in nature. Such a reaction can serve as an absolute detector of deuteron alignment, as a source of aligned deuterons, or, when followed by a gamma ray, as a source of 100 % linearly polarized photons. Some applications are given.

1. Introduction

A succinct method of examining some consequences of parity invariance for reactions initiated by particles in flight has been discussed by Bohr [1]). In this brief note, we wish to call attention to the consequences of the application of the Bohr symmetry argument to a special type of reaction

$$a(0^+)+b(0^+) \leftrightarrow c(0^+)+d(1^+) \qquad (1)$$

with the indicated spins and parities †††. Certain of these have already been discussed in Bohr's paper. However, since reaction (1) possesses some remarkably simple and unique geometrical properties, we believe that it is useful to present some further consequences here.

As we shall see below, the reaction can, in principle, be used as a source of a known amount of nuclear alignment, an absolute detector of the same, or a source of completely linearly polarized gamma rays ‡. All quantities other than the dependence of the cross section on polar angle are geometrical and are fully determined.

We must confess at the outset that reactions of the above type occur but rarely in nuclear physics. For each case discussed below we mention a few possibilities; the reader will, if interested, doubtless be able to find others for himself. The very simplicity of reaction (1) makes it uninteresting to study it for its own sake, and most applications will require it to be preceded or followed by another nuclear interaction, a requirement which makes its use more diffi-

† Present address: University of Washington, Seattle, Washington, USA.

†† Present address: Joint Institute for Nuclear Research, Dubna, USSR.

††† The parities of any two, or of all four, of the particles can be odd.

‡ The implications of reaction (1) for the case that particle d is a hyperfragment have been discussed in ref. [1]).

cult. A partially compensating feature is, as we shall see, that one can use larger solid angles than one might expect offhand.

There is one application of process (1) which would not require it to be one of a pair of reactions in tandem; namely, as an absolute detector of the degree of alignment achieved by an accelerator of artificially oriented deuterons.

2. Alignment Production

The demonstration of these properties can, with equal brevity, be made using as quantization axis either the direction of flight of particle d [2]) or the direction $\mathbf{n}$ along $\mathbf{k}_0 \times \mathbf{k}_1$; $\mathbf{k}_0$ is the initial, $\mathbf{k}_1$ the final relative momentum, taken positive in the direction of motion of d. To facilitate the comparison with Bohr's discussion, we shall commence with the latter method, but shall then immediately rotate the quantization direction so that it points along $\mathbf{k}_1$.

As the result of applying a reflection in the $\mathbf{k}_0$, $\mathbf{k}_1$ plane, Bohr showed [1]) that the matrix element for any parity-conserving reaction will vanish unless

$$\mathscr{P}_i \mathscr{P}_f = (-1)^{S^f_n - S^i_n}, \tag{2}$$

where $\mathscr{P}_i \mathscr{P}_f$ is the product of all intrinsic parities and $S^{f,i}_n$ represent the sums of all spin components along the $\mathbf{n}$ direction. When applied to reaction (1) proceeding from left to right, eq. (2) implies that the normalized amplitudes which are produced for the three spin projection states are $a^{(n)}_{\pm 1} = 0$, $a_0{}^{(n)} = i$. (We choose the latter phase for convenience.)

Since alignments are conventionally discussed when projected along the direction of flight, we rotate the axes first through $+90°$ about $\mathbf{n} \times \mathbf{k}_1$ (the original x-axis), and then through $+\varphi$ about $\mathbf{k}_1$. The final z-axis is thus along $\mathbf{k}_1$ and the y-axis makes an angle φ with $\mathbf{n}$. It is easy to see that the new amplitudes, which transform like the spherical harmonics Y_{1m} and for which we omit superscripts, are

$$a_{\pm 1} = \frac{1}{\sqrt{2}} e^{\mp i\varphi}, \quad a_0 = 0. \tag{3}$$

To describe the production process we take $\varphi = 0$, and see immediately that reaction (1) produces a fixed amount of d alignment, independently of primary energy and reaction angle,

$$\langle T_{20} \rangle \equiv \frac{1}{\sqrt{2}} \langle 3S_z{}^2 - 2 \rangle = \frac{1}{\sqrt{2}}, \tag{4}$$

$$\langle T_{2\pm 2} \rangle \equiv \tfrac{1}{2}\sqrt{3} \langle S_\pm{}^2 \rangle = \tfrac{1}{2}\sqrt{3}.$$

All other $\langle T_{JM} \rangle$ turn out to be zero. The explicit expressions for these tensor operators are given by Lakin [3]), as are formulae for the effect of these alignments on subsequent reactions.

In searching for candidates for applications of this process to the production of aligned deuterons, one is handicapped in the case of light elements by the ubiquitous isobaric spin selection rule. Reactions such as $C^{12}(\alpha, d)N^{14*}$ to the first 0^+ level are known to proceed with extremely low intensity. A possibility may be $Mg^{24}(\alpha, d)Al^{26*}$. Known and well-separated 0^+ levels in heavy odd-odd nuclei seem to be rare.

3. Polarized Gamma Quanta

If, instead of considering a deuteron, we take $d(1^+)$ to be an excited level which has a gamma emission directly to a 0^+ state, it is easy to show that these photons are emitted with a pure $\sin^2\theta$ angular distribution about the $\mathbf{n}$ direction, and that they are completely linearly polarized, with the magnetic vector lying in the plane containing $\mathbf{k}_\gamma$ and $\mathbf{n}$. A more useful result is found by summing over all directions $\mathbf{k}_1$. We let $\cos\beta = \mathbf{k}_0 \cdot \mathbf{k}_\gamma$. If $\boldsymbol{\varepsilon}_1$ be a unit vector along $\mathbf{k}_\gamma \times \mathbf{k}_0$, then $\boldsymbol{\varepsilon}_2 = \mathbf{k}_\gamma \times \boldsymbol{\varepsilon}_1$, and I_1 and I_2 be the intensities polarized with magnetic fields along $\boldsymbol{\varepsilon}_1$ and $\boldsymbol{\varepsilon}_2$. The result of the averaging is

$$I_1 \approx 1, \quad I_2 \approx \cos^2\beta. \tag{5}$$

In particular, the quanta are completely polarized for $\beta = \frac{1}{2}\pi$. Effects due to the motion of the nucleus d have been ignored.

Well-identified 1^+ states in even-even nuclei for use in the reaction $X(\alpha, \alpha')X^*$ are few, and again one must be on guard against isobaric spin inhibition. There is a probable 1^+, $T = 0$ level in C^{12} at 12.7 MeV which a small fraction of the time emits a gamma to the ground state. A possible level is also provided by Mg^{24}. In Zn^{66} there is a group of states, apparently 1^+, at excitations of 3.8 to 4.9 MeV; unfortunately, those among them which have large branching ratios for the ground state gamma are listed at present as only probable (1^+).

4. Detection of Alignment

To discuss this case, one must invert the roles of initial and final states in the discussion of sect. 2 and note that, whatever might be the state of the incoming d beam, only the amplitude $a_0^{(n)}$ can produce the reaction. After a rotation is made to bring the z-axis along $\mathbf{k}_1$ and appropriate averages taken over the ensemble of incoming d particles, there results the following expression for the differential cross-section:

$$\frac{d\sigma}{d\Omega} = f(E,\theta)\{1 + (2^{-\frac{1}{2}})\langle T_{20}\rangle + (3^{\frac{1}{2}})|\langle T_{22}\rangle| \cos 2(\varphi - \alpha)\}, \langle T_{22}\rangle = |\langle T_{22}\rangle| e^{2i\alpha}. \tag{6}$$

If the d beam comes from a previous parity-conserving two-body reaction and if the y-axis is chosen along the vector $\mathbf{n}$ associated with that reaction, then $\langle T_{22}\rangle$ must be real [3]).

We see from eq. (6) that the *total* cross section, if measured at fixed energy on the one hand with an unpolarized beam and on the other with the beam under study, will yield an absolute measurement of $\langle T_{20} \rangle$ for the latter. Furthermore, $\langle T_{22} \rangle$ can be determined from measurements which integrate over all θ at a fixed φ.

Eq. (6) should be compared with a double elastic scattering at a single θ which, as Lakin [3]) has shown, also gives an absolute measurement of alignment. The latter process involves the squares of the tensor polarizations and cannot distinguish signs. Moreover, the detecting reaction must be observed at fixed polar angle.

The possibilities of using (d, α) elastic scattering as a source, and the T(d, n)He^4 reaction as a detector, of d alignment have recently been discussed [4,5]). Both of those methods depend on the detailed dynamics of the reactions and are not absolute in the sense discussed here. They are useful in limited energy regions near the relevant resonances.

We note in passing that, if a d-producing reaction such as (K, d) elastic scattering should fail by a small amount to conserve parity, the angle α would be linear in the parity nonconserving amplitude.

The remarks that we can make relating to the applications of this detecting reaction follow the same lines as those relevant to the alignment-producing one, modified by the fact that (d, α) reactions are experimentally easier to carry out. Two cases appropriate to the analysis of deuteron alignment have already been observed [6,7]). The reaction Si^{28}(d, α)Al^{26*} to the first excited state of Al^{26} at 0.23 MeV proceeds, for 6 MeV deuterons, with an intensity ≈ 10 % of the ground state transition. O^{16}(d, α)N^{14*} gives a relative yield only slightly smaller.

5. Other Spins and Parities

If the 1^+ level of particle d is replaced in the preceding analysis by 1^-, or by higher spin, the Bohr rule still has relevant predictions to make concerning selection rules. However, it is clear that in all such cases there are at least two independent amplitudes allowed, and it is impossible to express the polarization dependence of the process at all angles as a consequence of geometry alone.

It may be interesting to notice, however, that all such processes must produce 100 % polarization P at each angle, where P is a generalized polarization defined by an extension of the definition given in ref. [3]),

$$P^2 = \frac{1}{2S} \sum_{J>0,\, M} |\langle T_{JM} \rangle|^2. \tag{7}$$

The reason for this is that the final density matrix ρ in the spin space of particle d is that of a pure state since no other spins exist over which one can average. The condition $\rho = \rho^2$ is necessary and sufficient to have $P^2 = 1$ in eq. (7).

The authors wish to thank Prof. L. Madansky for helpful discussion, and to express their gratitude to CERN for its hospitality.

References

1) A. Bohr, Nuclear Physics **10** (1959) 486
2) B. A. Jacobsohn and R. M. Ryndin, Phys. Rev. Letters **6** (1961) 27
3) W. Lakin, Phys. Rev. **98** (1955) 139
4) L. G. Pondrom, Phys. Rev. Letters **2** (1959) 346
5) A. Galonsky, H. B. Willard, and T. A. Welton, Phys. Rev. Letters **2** (1959) 349
6) C. P. Browne, Phys. Rev. **114** (1959) 807
7) C. P. Browne, Phys. Rev. **104** (1956) 1598

1.D.2:
1.E.1

Nuclear Physics **24** (1961) 510—513; © *North-Holland Publishing Co., Amsterdam*
Not to be reproduced by photoprint or microfilm without written permission from the publisher

A DOUBLET AT 3.40 MeV EXCITATION IN Mg^{25}

S. HINDS and R. MIDDLETON
Atomic Weapons Research Establishment, Aldermaston, Berkshire
and
A. E. LITHERLAND †
Clarendon Laboratory, Oxford

Received 6 January 1961

Abstract: The well known 3.40 MeV level in Mg^{25} has been studied by means of the Al^{27}(d, α)Mg^{25} and the Mg^{24}(d, p)Mg^{25} reactions. In both reactions the level was resolved into two components, separated by 9 ± 2 keV, at 3.407 ± 0.007 and 3.398 ± 0.007 MeV. In the (d, p) reaction the level at the lower excitation energy was weakly excited indicating that the upper member is the well known $\frac{3}{2}^-$ state. In the (d, α) reaction the reverse was observed, the lower level being consistently the stronger. The relative intensities of the members of the doublet in the (d, α) reaction suggest that the new level in Mg^{25}, at 3.398 ± 0.007 MeV, has spin $\frac{9}{2}$ and consequently corresponds to the 3.44 MeV ($\frac{9}{2}^+$) level in the mirror nucleus Al^{25}.

1. Introduction

The 3.407 MeV level in Mg^{25} has been extensively studied using the Mg^{24}(d, p)Mg^{25} stripping reaction and has been assigned [1]) a spin and parity of $\frac{3}{2}^-$. However, a comparison of the energy levels of Mg^{25} with those of the mirror nucleus Al^{25} suggests that this level may be a doublet. At 3.44 MeV in Al^{25} there is a level of low proton width which has been assigned [2]) a tentative spin and parity of $\frac{9}{2}^+$. Gove and Litherland [2]) have observed that levels of low proton width in Al^{25} correspond well in excitation energy with some of the known levels of Mg^{25}. Consequently a $\frac{9}{2}^+$ level is expected near 3.44 MeV excitation energy in Mg^{25}.

The existence of this level is also supported by the interpretation of the levels of Mg^{25} and Al^{25} in terms of overlapping rotational bands by Litherland *et al.* [3]). They showed that the first member of the ground state rotational band, having spin and parity $\frac{7}{2}^+$, occurs at almost precisely the same excitation energy (1.61 MeV) in both nuclei. They were also able to identify the second member of the band ($\frac{9}{2}^+$) with the 3.44 MeV state in Al^{25} but were unable to do the same in Mg^{25} since the only state with approximately the same excitation energy was known to have a spin and parity of $\frac{3}{2}^-$. Recently indirect evidence has been obtained by Blair and Hamburger [4]) that the 3.40 MeV level in Mg^{25} may be a doublet. They observed that the 1.61 and 3.40 MeV states were strongly excited

† Seconded from the Atomic Energy of Canada, Chalk River, Ontario, Canada.

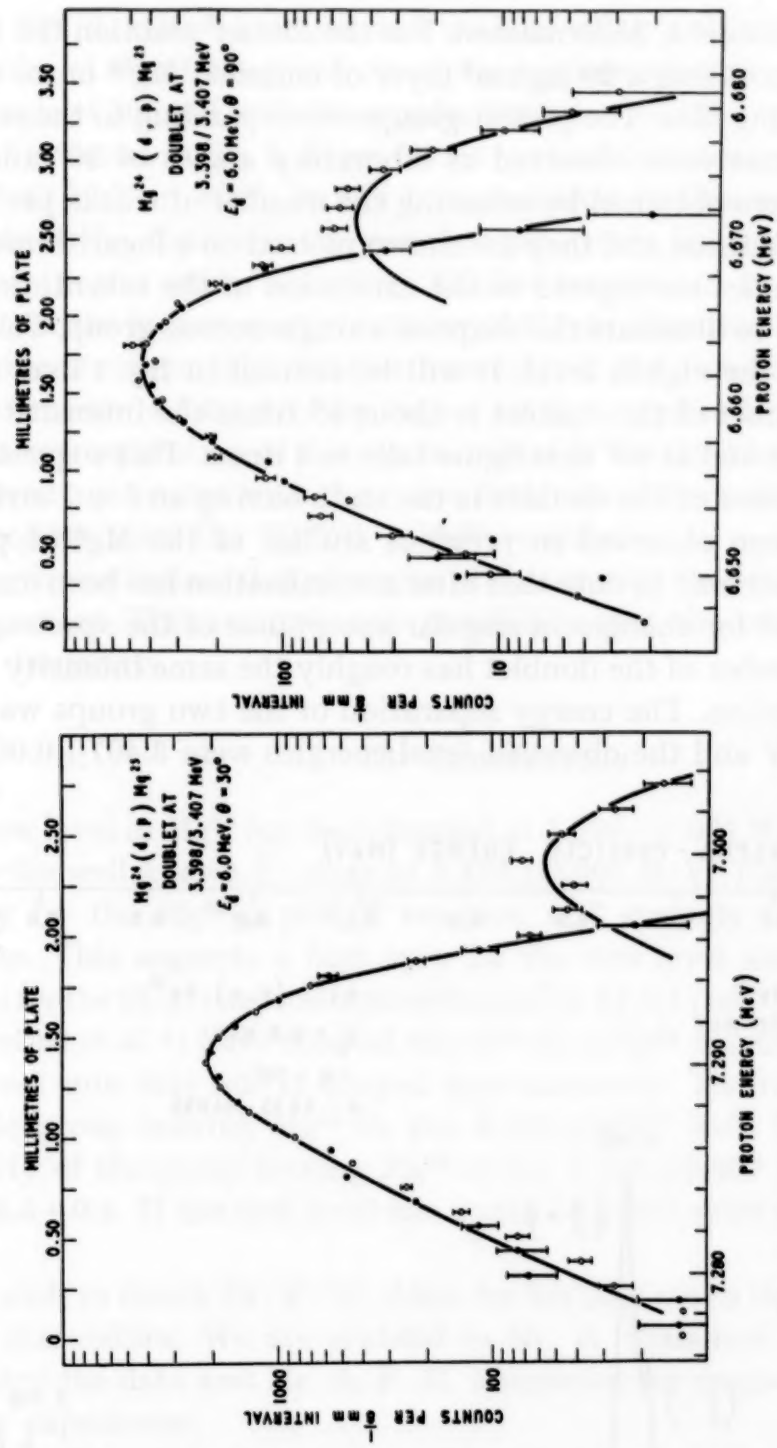

Fig. 1. The proton groups from the reaction Mg^{24}(d, p)Mg^{25} leading to the doublet in Mg^{25} at 3.398 and 3.407 MeV are plotted using open circles. The incident deuteron energy was 6.0 MeV and the angles of the proton emission in the laboratory system were 30° and 90°, repectively. Also shown superimposed upon the doublet, for comparison purposes, is the proton group (solid circles) corresponding to the seventh excited state of Mg^{25}. The solid lines show an analysis of the doublet into two peaks.

by the Mg^{25}(d, d')Mg^{25} reaction. They concluded that as the reaction was expected to excite preferentially the first and second members of the ground state rotational band, the 3.40 MeV level was probably a doublet with one member having a spin and parity of $\frac{3}{2}^-$ and the other $\frac{9}{2}^+$.

2. Results

The Mg^{24}(d, p)Mg^{25} and Al^{27}(d, α)Mg^{25} reactions were studied using the 6 MV Van de Graaff and broad range magnetic spectrograph [5]) at the Atomic Weap-

ons Research Establishment, Aldermaston. For the former reaction the target was prepared by evaporating a 20 μg/cm^2 layer of enriched Mg^{24} on to a thin 9 μg/cm^2 carbon backing film. The proton groups corresponding to the seventh and eight excited states were observed at laboratory angles of 30° and 90°, respectively. These were obtained by counting the number of tracks per $\frac{1}{8}$ mm intervals of nuclear emulsion and they are shown plotted on a logarithmic scale in fig. 1. The solid circles correspond to the excitation of the seventh level of Mg^{25} and are included to illustrate the shape of a single proton group. The open circles correspond to the eighth level. It will be noticed in fig. 1 that at 30° the lower energy member of the doublet is about 40 times the intensity of the higher energy member and at 90° this figure falls to 8 times. This suggests that the lower energy member of the doublet is the state having an $l = 1$ stripping pattern which has been observed in previous studies of the Mg^{24}(d, p)Mg^{25} reaction. It is also of interest to note that after normalisation has been made for exposure duration and for changes in angular acceptance of the spectrograph, the higher energy member of the doublet has roughly the same intensity at the two angles of observation. The energy separation of the two groups was estimated to be 9 ± 2 keV and the observed level energies were 3.407 ± 0.007 and 3.398 ± 0.007 MeV.

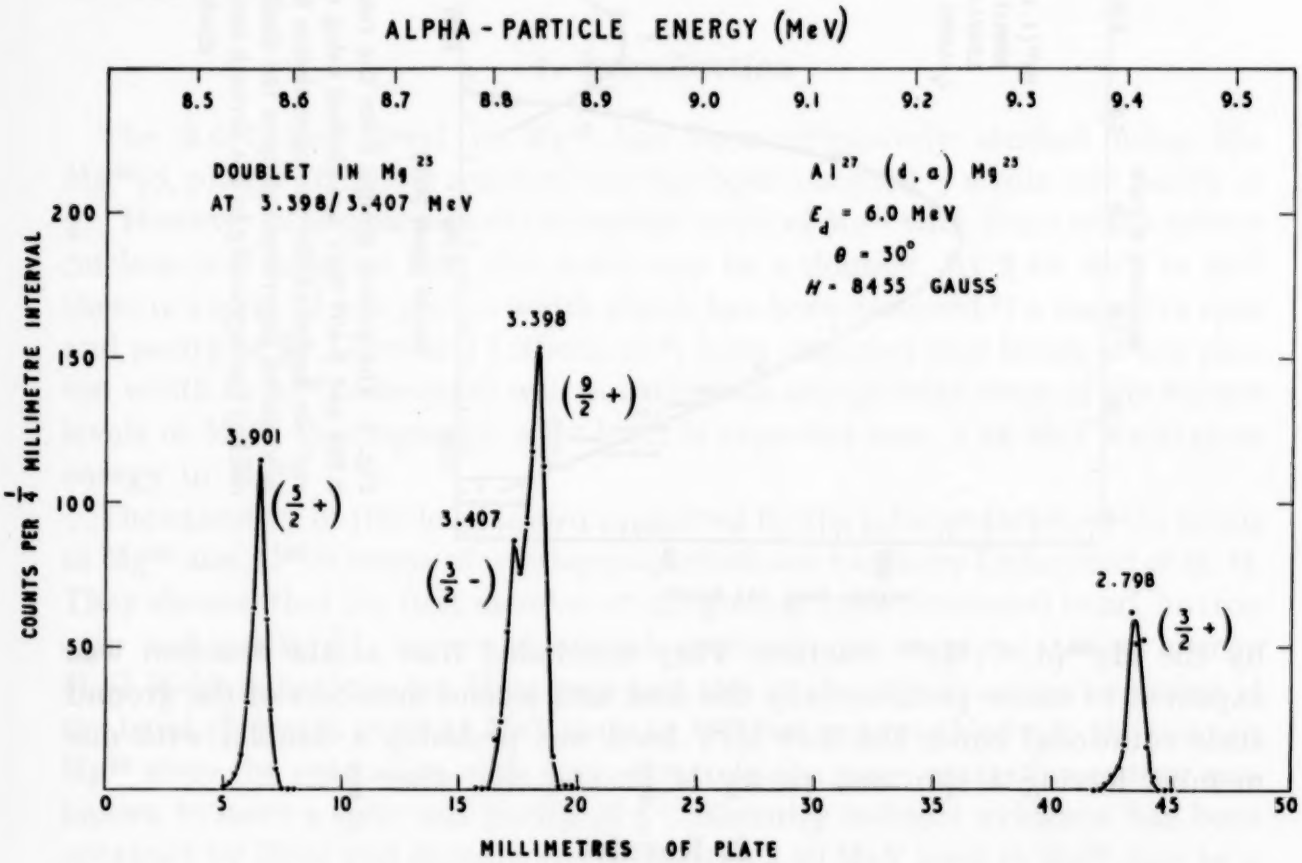

Fig. 2. A portion of the alpha particle spectrum from the Al^{27}(d, α)Mg^{25} reaction. The two alpha particle groups of about 8.83 MeV energy correspond to the members of the doublet discussed in this paper. The alpha particle groups on each side of the doublet are shown for comparison purposes.

The $Al^{27}(d, \alpha)Mg^{25}$ reaction was studied using a thin self-supporting aluminium film of about $10\mu g/cm^2$. An alpha-particle spectrum obtained at a laboratory angle of 30° and with the angular acceptance of the spectrograph restricted to $\pm 1°$ is shown in fig. 2. From this it is clear that there are two excited states near 3.40 MeV in Mg^{25}. It will be noted that in this case the higher energy member of the doublet is the more intense group. Spectra have been measured at other angles using a slightly thicker target and in spite of the inferior resolution the higher energy member of the doublet was consistently observed to be the stronger. The relative intensity of the two members, from several measurements is 2.5 ± 0.4, the higher energy member being the more intense. The energy separation of the two members of the doublet was 9 ± 2 keV which is in good agreement with the value determined from measurements made on the protons from the $Mg^{24}(d, p)Mg^{25}$ reactions.

In both reactions and at all angles of observation the separation of the doublet was constant. This removes any possibility that the new level arises from a target impurity.

3. Conclusions

A new level in Mg^{25} has been located at 3.398 ± 0.007 MeV which is 9 ± 2 keV below the well known $\frac{3}{2}^-$ state at 3.407 ± 0.007 MeV. The new level is excited weakly by the $Mg^{24}(d, p)Mg^{25}$ reaction and strongly by the $Al^{27}(d, \alpha)Mg^{25}$ reaction. This suggests a high spin for the new level and in fact if the cross section for the (d, α) reaction is proportional to $2J+1$ (ref. [6])) a spin of $\frac{9}{2}$ is favoured. Sheline *et al.* [6]) have studied the $Al^{27}(d, \alpha)Mg^{25}$ reaction and for the levels of known spin this rule is obeyed approximately. The intensity of the alpha particle group leaving Mg^{25} in the 3.398 ± 0.007 MeV level divided by the intensity of the group leaving Mg^{25} in the 3.407 ± 0.007 MeV level was found to be 2.5 ± 0.4. If the new level has a spin of $\frac{9}{2}$ this ratio should then be 2.5.

We wish to thank Dr. K. W. Allen for his interest in this work and for some useful discussions. We are grateful to Mr. H. Marchant for his assistance in analysing the data and Mr. A. F. H. Muggleton for preparing the targets used in this experiment.

References

1) P. M. Endt and C. M. Braams, Rev. Mod. Phys. **29** (1957) 683
2) H. E. Gove and A. E. Litherland, Phys. Rev. **107** (1957) 1458
3) A. E. Litherland, H. McManus, E. B. Paul, D. A. Bromley and H. E. Gove, Can. J. Phys. **36** (1958) 378
4) A. G. Blair and E. W. Hamburger, Bull. Amer. Phys. Soc. **5** (1960) 247
5) S. Hinds and R. Middleton, Proc. Phys. Soc. **74** (1959) 196
6) R. K. Sheline, H. L. Nielsen and A. Sperduto, Nuclear Physics **14** (1960) 140

8.B

Nuclear Physics **24** (1961) 514—518; © *North-Holland Publishing Co., Amsterdam*

Not to be reproduced by photoprint or microfilm without written permission from the publisher

APPLICATIONS OF THE SAKATA MODEL FOR ELEMENTARY PARTICLES

ELIZABETH HORMANN

Department of Theoretical Physics, University of Manchester

Received 2 January 1961

Abstract: Simple sub-symmetries of the three-dimensional unitary group are used to describe and classify all interactions, including in particular electromagnetic interactions. It is seen that all known types of interaction, and only these, appear. Application to the leptons succeeds in forbidding the direct electromagnetic μ–e decay. A suggestion is made for the removal of the μ–e mass degeneracy, and the range of applicability of the approach is discussed.

1. Introduction

Many papers have recently been written exploiting a group theory approach [1–5]) to the Sakata model [6]). The purpose of these has been to present a unified scheme for the strongly-interacting particles, and recently of the leptons (the "Nagoya model" [3])) in terms of transformations of the three-vector χ,

$$\chi = \begin{pmatrix} \mathrm{p} \\ \mathrm{n} \\ \Lambda \end{pmatrix}$$

under the three-dimensional unitary group u_3. In the Nagoya model, one then considers p, n and Λ as composites of an isoscalar charged boson B^+ with the leptons, as follows:

$$\mathrm{p} \equiv \langle \mathrm{B}^+ \nu \rangle,$$

$$\mathrm{n} \equiv \langle \mathrm{B}^+ \mathrm{e}^- \rangle,$$

$$\Lambda \equiv \langle \mathrm{B}^+ \mu^- \rangle,$$

so that therefore the leptons too, will transform under u_3.

There are still useful aspects of the Sakata-Nagoya model which should, perhaps, be pointed out explicitly. In particular, as we shall show below, a closer inspection of some of the sub-symmetries of the system within u_3 can succeed in giving a unified classification of all interactions whatsoever, in rigorously forbidding the direct decay $\mu \to \mathrm{e} + \gamma$, and in introducing specific possibilities for the origin of the μ-mass. We shall see that these considerations are, moreover, independent of the Sakata model per se, and apply with equal validity in Thirring's approach to the composite-particle problem [4]).

In the first section we shall discuss the relevant sub-symmetries of u_3. Section 2 is devoted to the classification of the interactions; and in section 3 we discuss the leptons in the light of our considerations.

2. Sub-symmetries of u_3

Like Yamaguchi [1]), we assume that the very strong interactions are invariant under rotations of χ in isospace, and also under the permutation $\mathrm{n} \leftrightarrow \Lambda$. As Wess has noted [5]), the presence of such symmetries implies that these interactions are then necessarily invariant under the three-dimensional unitary unimodular group, of which isospace rotations and the $\mathrm{n} \leftrightarrow \Lambda$ permutation form sub-groups. Schematically, then, we shall say that the very strong interactions must be invariant under isorotations:

$$\chi \equiv \begin{pmatrix} \mathrm{p} \\ \mathrm{n} \\ \Lambda \end{pmatrix} \rightarrow \left(\begin{array}{c|c} u_2 & \\ \hline & 1 \end{array}\right) \begin{pmatrix} \mathrm{p} \\ \mathrm{n} \\ \Lambda \end{pmatrix} \equiv T\chi, \tag{1}$$

where u_2 is some matrix of the two-dimensional unitary unimodular group, and T denotes any rotation in isospace; and under the permutation $\mathrm{n} \leftrightarrow \Lambda$:

$$\begin{pmatrix} \mathrm{p} \\ \mathrm{n} \\ \Lambda \end{pmatrix} \rightarrow \left(\begin{array}{c|cc} 1 & & \\ \hline & 0 & 1 \\ & 1 & 0 \end{array}\right) \begin{pmatrix} \mathrm{p} \\ \mathrm{n} \\ \Lambda \end{pmatrix}.$$

We also know that conservation of the charge-displacement number u is equivalent to invariance under an inversion in isospace (in general, and in the Sakata-Nagoya model in particular),

$$\begin{pmatrix} \mathrm{p} \\ \mathrm{n} \\ \Lambda \end{pmatrix} \rightarrow \left(\begin{array}{cc|c} i & 0 & \\ 0 & i & \\ \hline & & 1 \end{array}\right) \begin{pmatrix} \mathrm{p} \\ \mathrm{n} \\ \Lambda \end{pmatrix} \equiv U\chi. \tag{2}$$

We now note that we must require invariance under another inversion (i.e., one in another sub-space), namely

$$\begin{pmatrix} \mathrm{p} \\ \mathrm{n} \\ \Lambda \end{pmatrix} \rightarrow \left(\begin{array}{c|cc} 1 & & \\ \hline & i & 0 \\ & 0 & i \end{array}\right) \begin{pmatrix} \mathrm{p} \\ \mathrm{n} \\ \Lambda \end{pmatrix} \equiv q\chi. \tag{3}$$

In fact, assuming baryon-number conservation, such a requirement merely gives us conservation of charge.

Now consider the following sub-group of transformations:

$$\begin{pmatrix} \mathrm{p} \\ \mathrm{n} \\ \Lambda \end{pmatrix} \rightarrow \left(\begin{array}{c|c} 1 & \\ \hline & u_2 \end{array}\right) \begin{pmatrix} \mathrm{p} \\ \mathrm{n} \\ \Lambda \end{pmatrix} \equiv Q\chi. \tag{4}$$

We note that Q-invariance and T-invariance together, with their inversions q and U, are necessary and sufficient for invariance under the full u_3. The effect of a general Q-transformation is to mix all states (i.e., all particles) of the same charge which belong to the same irreducible representation of u_3. For example, in the 8-dimensional representation to which, according to the suggestion of e.g. Ikeda, Ogawa and Ohnuki [2]), the ordinary bosons belong, a Q-transformation will mix π^+ and K^+; π^- and K^-, etc.

One now finds that invariance under Q necessarily implies U-invariance and, conversely, that T-invariance implies q-invariance. To show this, we use the fact that any Lagrangian $\mathscr{L}$ (which will be some tensor in the space of u_3) must have an equal number of covariant and contravariant indices if it is to be Lorentz-covariant. Now suppose that $\mathscr{L}$ is a scalar under Q; then there must be contraction over all indices 2 and 3. Thus the number of covariant and contravariant indices 2 are equal, and likewise the indices 3. Thus the same must hold for indices 1 as well, since the total number of covariant and contravariant indices must be equal. The number of covariant indices 1 plus 2 we call N; then under U, we have

$$\mathscr{L} \to (-i)^N (i)^N \mathscr{L} = \mathscr{L},$$

as we set out to show.

3. Classification of the Interactions

We have already assumed that the very strong interactions are invariant under the full u_3. We next suppose that the medium-strong interactions are not invariant under Q (Yamaguchi [1]) suggests that medium-strong interactions are non-invariant under the permutation $n \leftrightarrow \Lambda$; the formulations are equivalent). They are, of course, invariant under T, U and q. Weak interactions, as we know, are not T nor U-invariant. Therefore they cannot be invariant under Q either; but charge conservation demands that they satisfy q-invariance.

TABLE 1
Classification of interactions

Interaction conserves	T	U	Q	q
very strong	yes	yes	yes	yes
medium strong	yes	yes	no	yes
electromagnetic	no	yes	yes	yes
weak	no	no	no	yes
?	no	yes	no	no
?′	no	no	no	no

To consider electromagnetic interactions, we note that if it is assumed that all particles of the same type (e.g. all bosons) have the same interaction with

the electromagnetic field if they have the same charge, as indeed is the case in nature, this implies invariance under Q-transformations.

We assume that the T and Q sub-symmetries are the only physically relevant ones, since by limiting our attention to these alone we obtain an automatic and unique classification of all interactions. The situation is represented in table 1. These are the *only* possibilities. Since interactions ? and ?′ do not conserve charge, one must ignore them for the present.

4. Applications to the Leptons

Consider (ν, e, μ) as a vector transforming under u_3, as e.g. in the Nagoya model [3]). Now invariance under Q will imply as the simplest possibility that the electromagnetic interaction has the form

$$\mathscr{L}_{\mathrm{em}} = (\bar{\nu}\,\bar{\mathrm{e}}\,\bar{\mu}) \left(\begin{array}{c|cc} 0 & & \\ \hline & 1 & 0 \\ & 0 & 1 \end{array}\right) \gamma_\mu A_\mu \begin{pmatrix} \nu \\ \mathrm{e} \\ \mu \end{pmatrix},$$

(omitting constants); the neutrino charge has been assumed zero. But this not only gives the leptons the electromagnetic interaction which we in fact observe, but also rigorously implies the absence of the direct reaction

$$\mu \to \mathrm{e} + \gamma \tag{6}$$

so that we have succeeded in forbidding a contact electromagnetic μ–e decay by the classification given in table 1. (A similar remark has been made by Cabibbo and Gatto [10]), who introduce Q-symmetry ad hoc for the μ and e.)

Alternatively, we could have said that the decay (6) is forbidden by strangeness-conservation. The Nagoya model automatically gives μ a charge-displacement number 0, and e and ν the charge-displacement number 1. The first consequence of this assignment (and therefore, since verified, the first evidence in favour of it) is the forbiddenness of the decay (6). But note that strangeness-conservation is itself a consequence of Q-invariance. The Q-invariance contains the fact that strangeness is conserved in electromagnetic interactions.

We also see that the μ–e mass degeneracy may be removed by allowing the μ to have medium-strong interactions. (This has already been noted by Yamaguchi [1]), but we may now put the suggestion within the mathematical framework of the Nagoya model.) One may, in particular, allow the leptons the interaction

$$\mathscr{L}_{\mathrm{ms}} = (\bar{\nu}\,\bar{\mathrm{e}}\,\bar{\mu}) \left(\begin{array}{c|c} 0 & \\ \hline & 1 \end{array}\right) \begin{pmatrix} \nu \\ \mathrm{e} \\ \mu \end{pmatrix} \pi'^0, \tag{7}$$

(omitting constants) as the only strong interaction in which the leptons take part; π'^0 is the isoscalar boson whose existence is required in the Sakata-Nagoya

model. This suggestion is particularly interesting because it has been made in the past starting from quite different considerations [7]); we could then identify π'^0 with Schwinger's [8]) σ-particle. Note however that π'^0 must be a pseudoscalar in space-time, while the work of some authors [10]) suggests that a σ-particle with the desired properties may be a scalar.

In conclusion, it should be remarked that our considerations are not strictly limited to the Sakata-Nagoya model, but apply with equal validity in the Thirring approach [4]). Thirring regards p, n and Λ as composite particles belonging to the same irreducible representation of u_3 as the other baryons, the basis being three fundamental fields $\psi_\alpha(\alpha = 1--3)$ with the appropriate characteristics. In this case the leptons may be regarded as composites of the ψ's with a charge-boson,

$$\begin{pmatrix} \nu \\ \mathrm{e} \\ \mu \end{pmatrix} = \begin{pmatrix} \langle \mathrm{B}^- \psi_1 \rangle \\ \langle \mathrm{B}^- \psi_2 \rangle \\ \langle \mathrm{B}^- \psi_3 \rangle \end{pmatrix}.$$

The rest of the analysis then follows through automatically.

The author wishes to express her thanks to Dr. P. Roman for his help and encouragement, to Dr. S. F. Edwards for kindly consenting to read and comment on the manuscript and to Dr. F. Mandl for helpful discussions. This work was made possible by a Fulbright Foundation Fellowship.

References

1) Y. Yamaguchi, Prog. Theor. Phys. Supp. **11** (1959) 1, 37
2) Ikeda, Ogawa and Ohnuki, Prog. Theor. Phys. **22** (1959) 715; Prog. Theor. Phys. **23** (1960) 1073
3) Maki, Nakagawa, Ohnuki and Sakata, Prog. Theor. Phys. **23** (1960) 1174
4) W. Thirring, Nuclear Physics **14** (1959) 565
5) J. E. Wess, Nuovo Cim. **15** (1960) 52
6) S. Sakata, Prog. Theor. Phys. **16** (1956) 686
7) I. Saavedra, Nuclear Physics **11** (1959) 569
8) J. Schwinger, Ann. Phys. **2** (1957) 407
9) N. Cabibbo and R. Gatto, Phys. Rev. Lett. **5** (1960) 114
10) W. S. Cowland, Nuclear Physics **8** (1958) 397;
I. R. Gatland, Nuclear Physics **9** (1958/59) 267;
S. N. Gupta, Phys. Rev. **111** (1958) 1436, 1698

1.E.1:
3.A

Nuclear Physics **24** (1961) 519—523; © *North-Holland Publishing Co., Amsterdam*
Not to be reproduced by photoprint or microfilm without written permission from the publisher

HIGH ENERGY GAMMA RAYS IN THE DECAY OF 27h Ho^{166}

P. G. HANSEN, K. WILSKY
Chemistry Department, Research Establishment Risø, Denmark

D. J. HOREN and LUNG-WEN CHIAO
Lawrence Radiation Laboratory, Berkeley, California †

Received 19 January 1961

Abstract: The gamma-ray spectrum of 27h Ho^{166} has been re-investigated by means of a three-crystal pair-spectrometer and coincidence techniques. Two new gamma rays with energies of 1747 ± 5 and 1825 ± 5 keV establish a new level at 1826 keV in Er^{166}. The log *ft* value for the β-decay to this state is $5.2^{+0.3}_{-0.4}$ and suggests an allowed, unhindered transition. Single particle assignments for this level are discussed.

1. Introduction

The investigations of the decay of 27h Ho^{166} reported by previous workers were performed with small NaI(Tl) crystals [1–3]). In some cases (e.g., refs. [1, 4])) the data seemed to indicate the presence of weak gamma rays with energies higher than those reported. It was considered worthwhile to determine whether such gamma rays actually exist in this decay, especially since their presence would probably require an allowed, unhindered β-transition.

2. Experimental

Holmium sources were prepared by neutron irradiation of holmium oxide. The high-energy singles spectrum was measured in a 7.6 cm diam. × 7.6 cm long NaI(Tl) crystal and a three-crystal pair-spectrometer. The latter consisted of a 3.8 diam. × 2.5 cm long NaI(Tl) centre crystal and used two 7.6 cm diam. × 7.6 cm long crystals in the sides. The side crystals were shielded from direct radiation. Their outputs were fed into a conventional fast-slow coincidence circuit ($2\tau = 10^{-7}$s), which gave an output only when each side crystal simultaneously detected a 511-keV gamma ray. The output of the slow coincidence circuit was used to gate a 256-channel analyzer.

To measure the singles spectrum, a holmium source was surrounded by 0.5 cm carbon to reduce bremsstrahlung from the high energy electrons and placed 15.5 cm from the 7.6 cm × 7.6 cm crystal. A 0.076 cm tin and 0.013 cm copper absorber was placed before the crystal to reduce detection of the 80-keV

† Work supported in part by the U. S. Atomic Energy Commission.

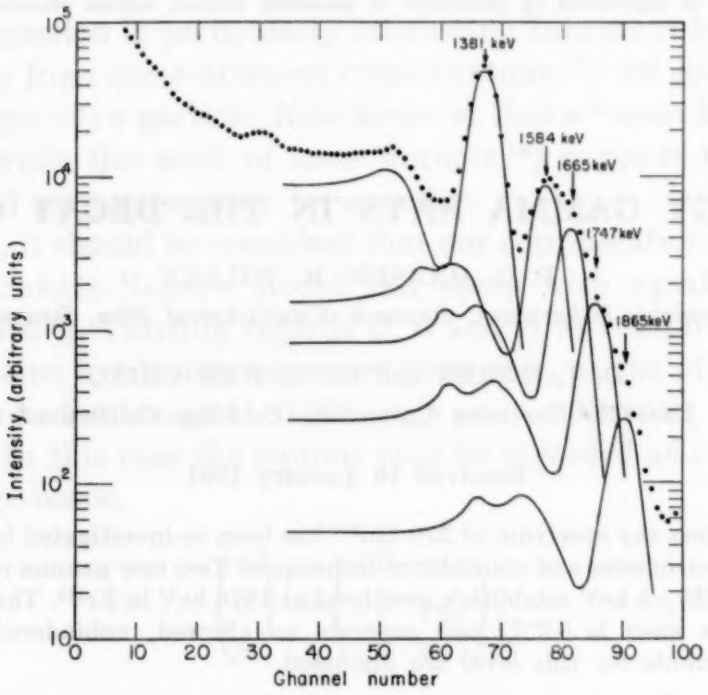

Fig. 1. Singles gamma-ray spectrum 27 h Ho^{166} taken with a 7.6 cm × 7.6 cm NaI(Tl) crystal.

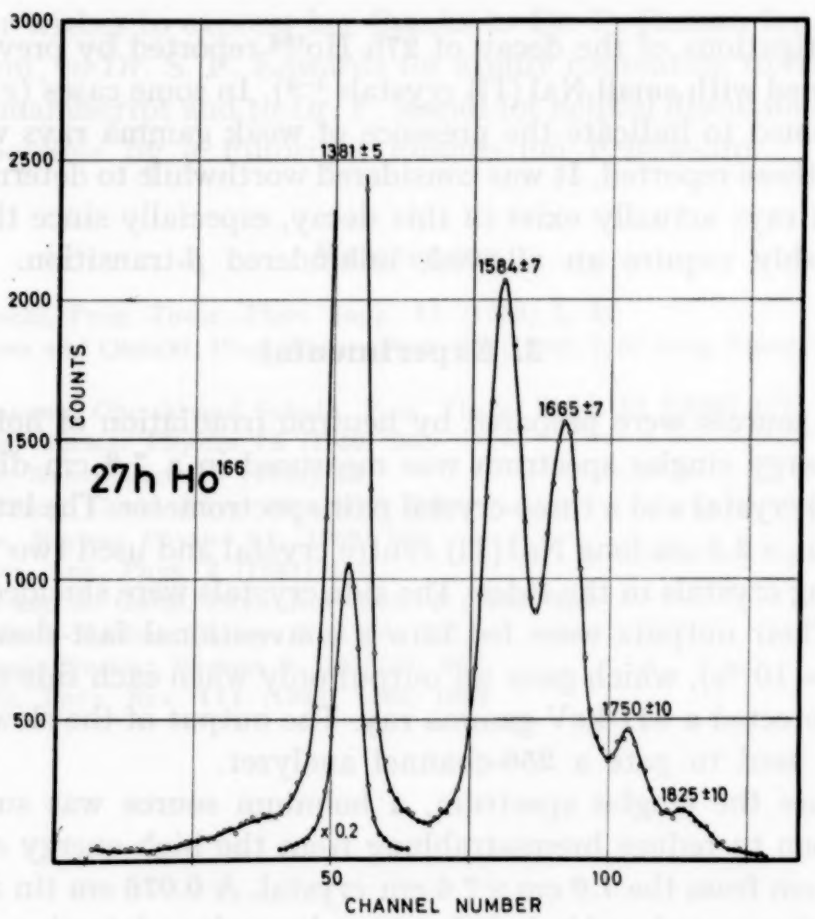

Fig. 2. Gamma rays from the decay of 27 h Ho^{166} measured with a three-crystal pair spectrometer. The source was placed to give a 20 000 c/s counting rate in the central crystal. Data were collected during four successive ten hour intervals. The four spectra and calibrations showed shift during this period of less than 1 %. The calibrations were performed with sources of La^{140} and Co^{60} and in singles with sources of Eu^{152}, Na^{22}, Cs^{137} and Sc^{46}.

gamma ray and K X-rays. Fig. 1 shows the high-energy single spectrum so obtained. Analysis revealed the presence of gamma rays with energies of 1747 and 1825 keV in addition to the previously known gamma rays of 1380, 1582 and 1663 keV.

For the pair spectrometer measurement, one source was prepared by neutron irradiation of holmium oxide and another was obtained from the decay of 82h Dy^{166} which was produced by double neutron capture in Dy^{164}. Both sources gave identical results, verifying that the 1747- and 1825-keV gamma rays were emitted in the decay of 27h Ho^{166}.

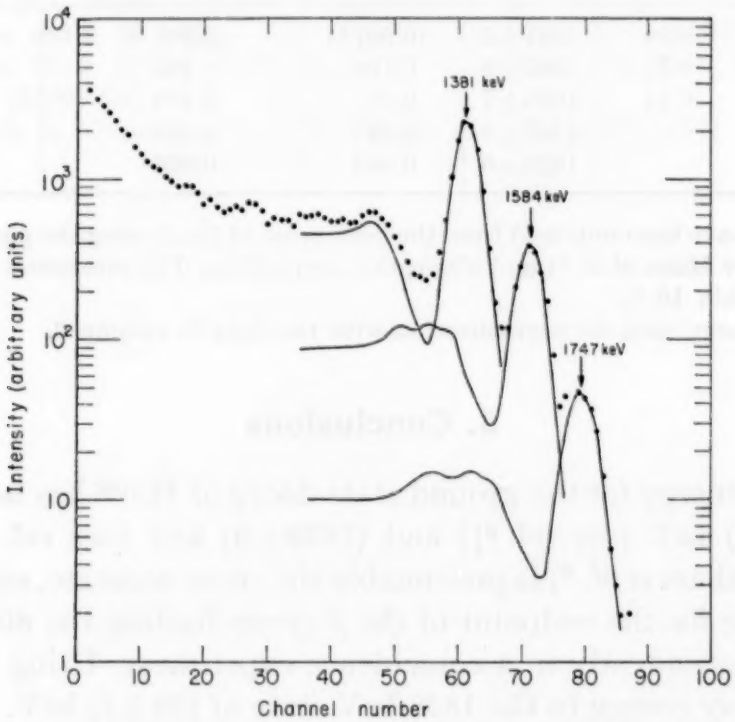

Fig. 3. High energy gamma-ray spectrum in coincidence with 80-keV gamma rays and K X-rays. For this spectrum the low energy gamma rays were detected in a 2.5 cm × 0.64 cm NaI (Tl) crystal and the high energy gamma rays in a 7.6 cm × 7.6 cm crystal. The crystals were mounted in 90° geometry with a graded lead antiscattering shield.

Fig. 2 shows the pair spectrum obtained in a 40 h run. For this data the source was surrounded by polyethylene, 3 mm lead and 0.7 mm cadmium. In calibrating the pair spectrometer, use was made of the accurate gamma-ray energies determined by Marklund *et al.* [3]) as well as external standards.

The two highest energy gamma rays suggest the existence of a 1826-keV level in Er^{166} decaying to the ground state and first excited state. This assumption was confirmed by a gamma gamma coincidence experiment with the 80-keV transition. In addition to the previously observed 1380 and 1582 transition, the 1747-keV gamma-ray was found to be in coincidence with the 80-keV gamma ray (see fig. 3).

In table 1 we summarize the relative intensities of the high energy gamma rays obtained in this investigation.

TABLE 1

Energies and intensities of high-energy gamma rays from 27h Ho^{166}

Marklund *et al.*		This investigation			
E_γ (keV)	Intensity (%)	E_γ (keV)	7.6 cm × 7.6 cm (relative intensity)	Pair spectrometer (relative intensity) [a]	Coinc. with 80 keV and KX (relative intensity)
1379.8±0.4	0.90	1381±5	(0.90) [b]	(0.90) [b]	0.90) [b]
1582.4±0.4	0.21	1584±5	0.198	0.182	0.187
1663.0±0.5	0.11	1665±7	0.101	0.104	
		1747±5	0.037	0.025	0.029
		1825±5	0.007	0.008	

[a] The intensities have been obtained from the peak areas of fig. 2 using the pair production cross sections given by Mann *et al.* [5]) and absorption corrections. The intensities are believed to be accurate to within 10 %.

[b] This value has been used for normalization with the data in column 2.

3. Conclusions

The β-decay energy for the ground state decay of Ho^{166} has been determined to be (1854±5) keV (see ref. [6])) and (1839±5) keV (see ref. [2])). The value obtained by Graham *et al.* [6]) is presumably the most accurate, especially since a consistent value for the endpoint of the β-group feeding the 80-keV state was determined independently in a coincidence experiment. Using this value, one obtains a β-decay energy to the 1826-keV state of (28±7) keV. Assuming that this state de-excites solely by the 1747- and 1825-keV transition, one finds a log *ft* value of $5.2^{+0.3}_{-0.4}$ for this 0.033 % branch.

The most likely classification for this β-group is then as allowed, unhindered. In terms of the unified model this requires [7]) $\Delta K = 0.1$ and no change in the asymptotic quantum number. The odd nucleus Ho^{166} has been assigned zero spin and odd parity [6, 8]). This corresponds to the single particle configuration $p\frac{7}{2}^-$ [523], $n\frac{7}{2}^+$ [633]. From available orbitals in this region [7]) it is seen that the allowed, unhindered β-decay can only proceed to a two neutron state characterised by the quantum numbers $\frac{5}{2}^-$ [523], $\frac{7}{2}^+$ [633] which give the allowed spin and parity of 1^-.

Allowed, unhindered β-transitions between the $p\frac{7}{2}^-$ [523] orbital and the $n\frac{5}{2}^-$ [523] orbital have been observed in a number of odd-mass nuclei in the Tb–Ho region [7]). In addition, three transitions of this type have recently been observed [9]) in the decay of 11.8 min Ho^{162} and 68 min Ho^{162m}. It is, therefore, not surprising that this transition is also observed in the beta decay of Ho^{166}.

The authors are indebted to Mr. O. B. Nielsen of the Institute for Theoretical Physics, Copenhagen for helpful discussions and for communicating his results prior to publication.

References

1) A. W. Sunyar, Phys. Rev. **93** (1954) 1345
2) J. M. Cork, M. K. Brice, R. G. Helmer and R. M. Woods, Jr., Phys. Rev. **110** (1958) 526
3) I. Marklund, B. Van Nooijen and F. Grabowski, Nuclear Physics **15** (1960) 533
4) E. Bodenstedt, H. J. Körner, C. Günther and J. Radeloff, Nuclear Physics **22** (1960) 145
5) L. G. Mann, W. E. Meyerhof and H. I. West, Phys. Rev. **92** (1953) 1481
6) R. L. Graham, J. L. Wolfson and M. A. Clark, Phys. Rev. **98** (1955) 1173A
7) B. R. Mottelson and S. G. Nilsson, Mat. Fys. Skr. Dan. Vid. Selsk. **1**, No. 8 (1959)
8) L. S. Goodman, W. J. Childs, R. Marrus, I. P. K. Lindgren and Y. A. Cabezas, Bull. Am. Phys. Soc. **5** (1960) 344
9) M. Jørgensen, O. B. Nielsen and O. Skilbreid, Nuclear Physics **24** (1961) 443

7.C

Nuclear Physics **24** (1961) 524—526; © *North-Holland Publishing Co., Amsterdam*

Not to be reproduced by photoprint or microfilm without written permission from the publisher

THE ELECTRIC POLARIZABILITY OF THE NEUTRON IN THE STATIC MESON THEORY

AKIRA KANAZAWA †

Department of Physics, Purdue University, Lafayette, Indiana ††

Received 19 December 1960

Abstract: The electric polarizability of the neutron is recalculated in the framework of the static meson theory. The recalculated values of the electric polarizability are $\alpha = 1.1\times10^{-42}$ cm^3 for a Gaussian cut-off with cut-off momentum $k_c = 5.6$ meson mass, and $\alpha = 1.0\times10^{-42}$ cm^3 for an inverse square cut-off with the same cut-off momentum. These values are almost half of those which were obtained by Barashenkov and Barbashov.

In recent years many attempts [1]) have been made to observe or predict the electric polarizability of the neutron, among which is the calculation of Barashenkov and Barbashov [2]) by means of Chew's cut-off theory. However, their calculation is unsatisfactory in several respects. The main objections are that they failed to take into account the contribution from the catastrophic interaction between pions and the external electric field, fig. 1b, and that they have not included all the time-ordered diagrams corresponding to fig. 1a. The polarizability has been recalculated in this paper taking into account the above terms. The fully relativistic calculation of the problem has been carried out by S. Tani and the author and will be published elsewhere [3]).

We start from the following interaction Hamiltonian:

$$
\begin{aligned}
H_I &= H_1+H_2+H_3,\\
H_1 &= \left(\frac{f}{\mu}\right)\int \psi^*(t)\rho(\mathbf{x})\tau_\alpha\boldsymbol{\sigma}\nabla\phi_\alpha(\mathbf{x},t)\psi(t)\mathrm{d}\mathbf{x}-\delta m\psi^*(t)\psi(t),\\
H_2 &= e\int \phi_\alpha T_{\alpha\beta}\dot{\phi}_\beta A_0(\mathbf{x})\mathrm{d}\mathbf{x},\\
H_3 &= -e^2\int(\phi_1^2+\phi_2^2)A_0A_0\mathrm{d}\mathbf{x}.
\end{aligned}
\tag{1}
$$

It should be noted that H_3 is the sum of the catastrophic interaction $\frac{1}{2}e^2(\phi_1^2+\phi_2^2)A_\mu A_\mu$ and the surface dependent interaction $\frac{1}{2}e^2(\phi_1^2+\phi_2^2)(n_\mu A_\mu)^2$. The function $\phi(\mathbf{x},t)$ represents the meson field with mass μ, and $\dot{\phi}$ is its time derivative. We denote by $A_0(\mathbf{x})$ the scalar potential, which describes the exter-

† On leave of absence from the Department of Physics, Hokkaido University, Sapporo, Japan.

†† Work supported by the National Science Foundation.

nal constant electric field and by $\psi(t)$ the nucleon field with mass m, which satisfies

$$(-i\partial_t+m)\psi(t) = 0. \tag{2}$$

The density function $\rho(\mathbf{x})$ represents the extension of the interaction between nucleon and pion, and f is the rationalized pseudovector coupling constant. By $T_{\alpha\beta}$ we denote the elements of the matrix

$$T = \begin{pmatrix} 0 & 1 \\ -1 & 0 \end{pmatrix}.$$

The S-matrix element corresponding to any Feynman diagram can be calculated quite analogously to the case of relativistic field theory [4]), if we simply note that

$$\langle T(\psi(t), \psi^*(t'))\rangle_0 = \frac{i}{(2\pi)}\int \frac{\mathrm{e}^{-ip_0(t-t')}\,\mathrm{d}p_0}{p_0-m+i\varepsilon}. \tag{3}$$

The two lowest order diagrams which contribute to the electric polarizability are given in fig. 1.

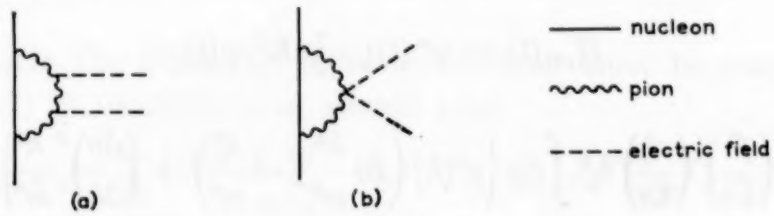

Fig. 1

The corresponding matrix elements are

$$M_a = -2\pi\delta(0)\left(\frac{f}{\mu}\right)^2 e^2\frac{8}{(2\pi)^4} \tag{4a}$$
$$\int \mathrm{d}\mathbf{q}\,\mathrm{d}\mathbf{q}'\mathrm{d}^4k\,\frac{v(k)v(k'')k_0{}^2(\boldsymbol{\sigma}\cdot\mathbf{k}'')(\boldsymbol{\sigma}\cdot\mathbf{k})a(\mathbf{q})a(\mathbf{q}')}{(k_0-i\varepsilon)[k_0{}^2-(\omega''-i\varepsilon)^2][k_0{}^2-(\omega'-i\varepsilon)^2][k_0{}^2-(\omega-i\varepsilon)^2]} - \tfrac{1}{2}M_b,$$

$$M_b = 2\pi\delta(0)\left(\frac{f}{\mu}\right)^2 e^2\frac{2}{(2\pi)^4}\int \mathrm{d}\mathbf{q}\,\mathrm{d}\mathbf{q}'\,\mathrm{d}^4k\,\frac{v(k)v(k'')(\boldsymbol{\sigma}\cdot\mathbf{k}'')(\boldsymbol{\sigma}\cdot\mathbf{k})a(\mathbf{q})a(\mathbf{q}')}{(k_0-i\varepsilon)[k_0{}^2-(\omega''-i\varepsilon)^2][k_0{}^2-(\omega-i\varepsilon)^2]}, \tag{4b}$$

where ω, ω', and ω'' are the meson energies corresponding to the momenta k, $k' = k+q$, and $k'' = k+q+q'$ respectively; $v(k)$ and $a(\mathbf{q})$ are the Fourier transform of $\rho(\mathbf{x})$ and $A_0(\mathbf{x})$; i.e.

$$v(k) = \int \rho(\mathbf{x})\mathrm{e}^{i\mathbf{k}\cdot\mathbf{x}}\,\mathrm{d}\mathbf{x}, \quad a(\mathbf{q}) = \frac{1}{(2\pi)^3}\int A_0(\mathbf{x})\,\mathrm{e}^{-i\mathbf{q}\cdot\mathbf{x}}\,\mathrm{d}\mathbf{x} = -i\mathbf{E}\frac{\partial}{\partial\mathbf{q}}\delta(\mathbf{q}), \tag{5}$$

where E is the constant external electric field.

It should be noted here that the second term in (4a) comes from the δ-function term of the propagator:

$$\langle P(\dot{\phi}(x), \dot{\phi}(y))\rangle_0 = -\tfrac{1}{2}\frac{\partial^2}{\partial t^2}\Delta_F(x-y) - i\delta^4(x-y). \tag{6}$$

It is well known that the contribution from this δ-function term must cancel with that of the surface dependent interaction, which is just one-half of the interaction H_3 in the present case.

If we carry out the integration with respect to k_0 in (4), the first term in M_a vanishes and we have

$$M_a + M_b = \tfrac{1}{2}M_b$$
$$= 2\pi i\delta(0)\left(\frac{f}{\mu}\right)^2 e^2 \frac{1}{(2\pi)^3}\int \mathrm{d}\mathbf{q}\,\mathrm{d}\mathbf{q}'\,\mathrm{d}\mathbf{k}\,\frac{v(\mathbf{k})v(\mathbf{k}'')(\boldsymbol{\sigma}\cdot\mathbf{k}'')(\boldsymbol{\sigma}\cdot\mathbf{k})a(\mathbf{q})a(\mathbf{q}')}{\omega^2\omega''^2} \tag{7}$$

The electric polarizability α can be uniquely obtained if we compare (7) with the effective S-matrix element, i.e.

$$M_{\mathrm{eff}} = -i\int \mathrm{d}t H_{\mathrm{eff}}(t) = -2\pi i\delta(0)(-\tfrac{1}{2}\alpha E^2), \tag{8}$$

where

$$H_{\mathrm{eff}}(t) = \psi^*(t)(-\tfrac{1}{2}\alpha\mathbf{E}^2)\psi(t). \tag{9}$$

The result is

$$\alpha = \left(\frac{f^2}{4\pi}\right)\left(\frac{e^2}{4\pi}\right)\tfrac{16}{3}\int \mathrm{d}k\left\{v^2(k)\left(10\frac{k^4}{\omega^6} - 8\frac{k^6}{\omega^8}\right) + \left(\frac{\mathrm{d}v}{\mathrm{d}k}\right)^2\frac{k^4}{\omega^4}\right\}\left(\frac{1}{\mu^3}\right). \tag{10}$$

Numerical values † for two choices of the cut-off function v are

$$\begin{aligned} &\alpha = 1.1\times 10^{-42}\,\mathrm{cm}^3 \quad \text{for} \quad v = \exp\{-(k/5.6)^2\}, \\ &\alpha = 1.0\times 10^{-42}\,\mathrm{cm}^3 \quad \text{for} \quad v = 1/\{1+(k/5.6)^2\}. \end{aligned} \tag{11}$$

These values are consistent with current experiments [1]).

The author wishes to thank Professor M. Sugawara for the hospitality extended to him at Purdue University.

† Barashenkov *et al.* have obtained the numerical values $\alpha = 1.8$ for the Gaussian cut and $\alpha = 1.6$ for the inverse square cut.

References

1) V. S. Barashenkov and I. P. Stakhanov, Soviet Physics JETP **5** (1957) 144;
Iu. A. Aleksandrov and T. I. Bondarenko, Soviet Physics JETP **4** (1957) 612;
A. S. Baldin, Proc. Padua-Venice Conf. on Fundamental Particles (1957);
A. Langsdorf, R. O. Lane and J. E. Monahan, Phys. Rev. **107** (1957) 1077;
R. M. Thaler, Phys. Rev. **114** (1959) 827;
V. I. Goldansky, O. A. Karpukhin, A. V. Kutsenko and V. V. Pavlovskays, Nuclear Physics **18** (1960) 473;
G. Breit and M. L. Rustgi, Phys. Rev. **114** (1959) 830;
L. L. Foldy, Phys. Rev. Letters **3** (1959) 105
2) V. S. Barashenkov and B. M. Barbashov, Nuclear Physics **9** (1958) 427
3) A. Kanazawa and S. Tani, Progr. Theor. Phys. **25** (1961);
see also T. Ueda and S. Sawamura, Progr. Theor. Phys. **24** (1960) 519
4) M. H. Friedman, Phys. Rev. **97** (1955) 1123

10.E *Nuclear Physics* **24** (1961) 527—528; © *North-Holland Publishing Co., Amsterdam*

ERRATA

D. Robson, Polarizations in (d, p) reactions, Nuclear Physics **22** (1960) 34.

Eq. (3.3) as it appears on p. 40 is incomplete. The actual equation should read

$$\sigma(\theta) = A^*A+\tfrac{2}{3}(B^*B+C^*C)+(\tfrac{1}{2}\cos^2\theta+\tfrac{1}{6})D^*D + \tfrac{4}{3}\,\mathrm{Re}\,[A^*(C+D\cos\theta)]+\tfrac{2}{3}\,\mathrm{Re}\,(C^*D)\cos\theta. \quad (3.3)$$

D. Robson, Spin-orbit effects in the stripping reaction involving polarized particles, Nuclear Physics **22** (1960) 47.

In this article the following three corrections must be made:

(1) Eq. (2.7) is incorrect and should read

$$\rho_{\mu_p M_B, \mu'_p M'_B} = \sum_{IM} \langle T^{IM} \rangle \sum_{\mu_d \mu'_d M_A} (\hat{I}_A)^{-2} I_{\mu_p M_B;\, \mu_d M_A} T^{IM}_{\mu_d \mu'_d} I^{\dagger}_{\mu'_d M_A;\, \mu'_p M'_B}. \quad (2.7)$$

(2) The factor $A(\alpha', lj)$ occurring in eqs. (2.9)–(2.13) and in the equation for $H(\alpha\alpha', ljp)$ following eq. (2.14) should be starred, viz: $A^*(\alpha', lj)$.

(3) The factor $(2I_A+1)/(2I_B+1)$ occurring in eqs. (2.12) and (2.13) should be inverted (i.e. $(2I_B+1)/(2I_A+1)$ as in eq. (2.11)).

N. K. Glendenning and J. Sawicki, Intrinsic quadrupole moments of deformed nuclei and superfluidity in nuclei, Nuclear Physics **18** (1960) 596.

In the caption to table 3 and elsewhere the factor $(1+\frac{1}{2}\delta)$ should be replaced by $(1+\frac{2}{3}\delta)$. This increases the uniform charge model value of Q_0/ZR^2 by about 5 % at $\eta = 6$. The deformations listed in the last column of table 4 should be decreased by about $\frac{1}{6}\delta^2/(1+\delta)$ or 0.01.

P. S. Dubbeldam, C. C. Jonker and H. J. Boersma, Energy and angular dependence of the left-right asymmetry of D–D neutrons scattered by carbon, Nuclear Physics **15** (1960) 452–463.

In table 3, page 461, the values of $\sigma(\vartheta_1)$ for some values of E_D (1200, 1500 and

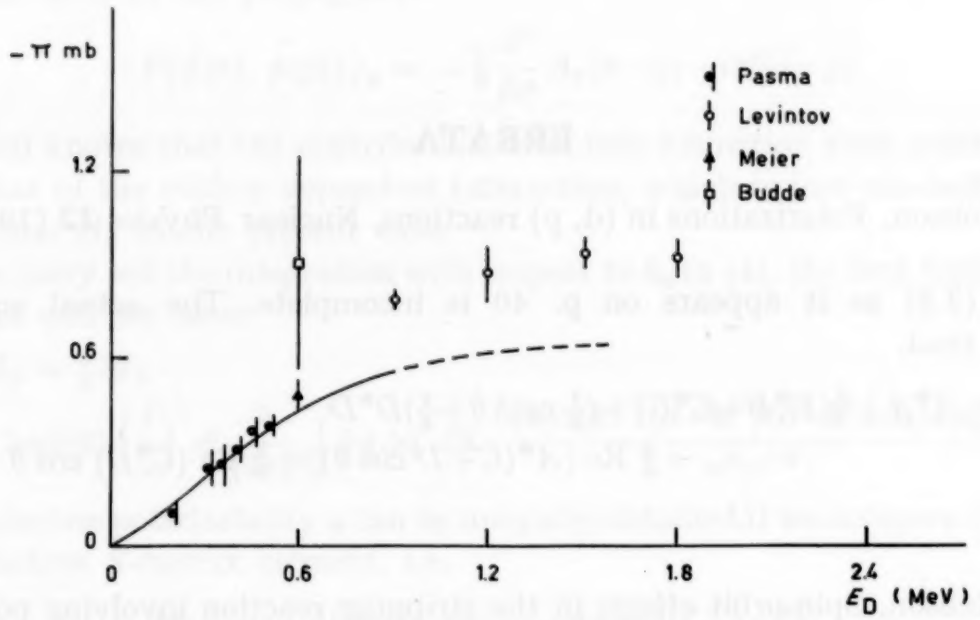

Fig. 5. Values of Π as a function of E_D. The solid curve represents σ_1 *a* sin $2\vartheta_1$ fitted to experimental points.

1800 keV) have been quoted incorrectly from Fowler and Brolley (Rev. Mod. Phys. **28** (1956) 103). In consequence the values of Π at these energies in the table and in fig. 5, page 462, are also wrong.

The pertinent part of table 3 is given here as well as the correct fig. 5.

TABLE 3 (partly)

Ref.	$\vartheta_{1\,\mathrm{lab}}$	E_D (keV)	$-P_1$ (%)	$\sigma(\vartheta_1)$ (mb)	$-\Pi$
Levintov *et al.*	49°	900	13.7 ± 0.4	5.8	0.79 ± 0.02
		1200	13.8 ± 1.4	6.3	0.87 ± 0.09
		1500	15.8 ± 0.9	5.9	0.93 ± 0.05
		1800	16.8 ± 1.0	5.5	0.92 ± 0.06

2.E

Nuclear Physics **24** (1961) 529—534; © *North-Holland Publishing Co., Amsterdam*

Not to be reproduced by photoprint or microfilm without written permission from the publisher

SCATTERING BY Si^{28} OF PROTONS OF ENERGY 10.0—12.3 MeV

A. V. COHEN and J. A. COOKSON

Atomic Weapons Research Establishment, Aldermaston, Berkshire

Received 9 January 1961

Abstract: The excitation curve for inelastic scattering of protons in the energy range 10.0–12.3 MeV shows considerable structure. Angular distributions, both of this reaction and the elastic process, have been determined at two energies, and the elastic results are discussed in terms of the optical model.

1. Introduction

Elastic and inelastic scattering of protons by Si^{28} has previously been studied [1]) as a function of energy using cyclotron-accelerated protons up to 9.45 MeV and by protons of 5 MeV or less accelerated by electrostatic generators [2, 3]), while an angular distribution of 12 MeV cyclotron-accelerated protons exciting the 1.77 MeV state in Si^{28} has also been determined [4]). Resonant structure in a compound nucleus is indicated directly by the excitation curves at lower energies and suggested at the higher energies by a strongly energy-dependent angular distribution for inelastic scattering to the first excited state.

The tandem electrostatic generator of the Atomic Weapons Research Establishment [5]) can produce a 12 MeV proton beam defined in energy to $\approx$ 1 keV. This enables the elastic and inelastic scattering of protons by Si^{28} to be investigated as a function of energy under conditions which might be expected to reveal any fine-structure in the energy dependence. The present report describes such work at proton energies of up to 12.3 MeV.

2. Experimental

A well-collimated 0.5 μA proton beam was directed on to a target consisting of 100 $\mu g/cm^2$ of natural silicon evaporated on a 15 $\mu g/cm^2$ carbon backing. The particle spectrum at a given angle θ to the incident beam direction was examined with a magnetic particle spectrometer [6]) which has a solid angle 0.007 sr and an optimum energy resolution of 1 in 850, so that the various groups of elastically and inelastically scattered particles could be resolved and identified by their corresponding ρ values from which the incident particle energies may also be deduced. The yield of each group was estimated from the area of the associated peak, integrating over momentum, while the proton beam was measured by a Faraday cup placed near the target.

3. Results

The spectrum arising from 10.61 MeV protons incident upon the Si targets was examined, and inelastically scattered protons were observed corresponding to all the known excited states of Si^{28} up to the 7.415 MeV level, though the fifth and sixth states were unresolved. The excitation energies of the levels calculated from several angles are given with estimated errors in table 1 together with the P^{31} (p, α) results of Endt and Paris [7]) and values obtained by Hinds and Middleton [8]) from the $Al^{27}(He^3, \alpha)$ reaction.

TABLE 1

Excitation energies in MeV

Present results	Ref. [7]) ($\pm$8 keV)	Ref. [8]) ($\pm$12 keV)
1.761$\pm$0.009	1.771	
4.602$\pm$0.016	4.617	
4.960$\pm$0.017		4.975
6.242$\pm$0.021		6.276
6.867$\pm$0.023		6.880, 6.889
7.359$\pm$0.025		7.382
7.390$\pm$0.024		7.415

The excitation curve for inelastic scattering at 90° to the first excited state of Si^{28} in the proton energy range 9.95–12.28 MeV was obtained (fig. 1). The

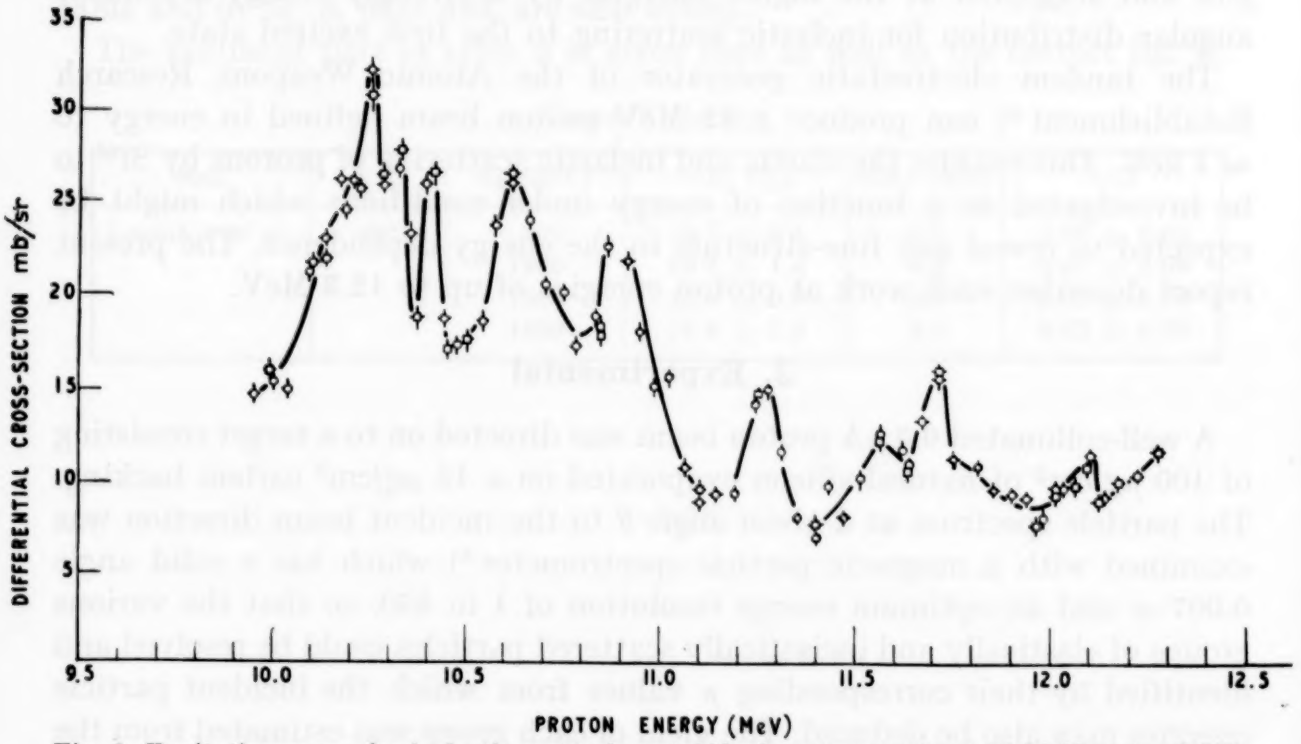

Fig. 1. Excitation curve for inelastic scattering at 90° of protons to the 1.77 MeV state of Si^{28}. Absolute cross sections are subject to an additional $\pm$13 % normalisation error. Squares and circles correspond to separate runs.

energy scale is subject to a ± 20 keV error. The absolute cross-sections, subject to ± 13 % normalisation error, were obtained by reference to the intensity of elastic scattering at forward angles (see below). Structure is evident, and the apparent resonant peak positions with their approximate widths, including some 10 keV instrumental width, are listed in table 2.

TABLE 2
Resonant peak positions

Resonant energy (MeV)	Width (keV)	Excitation of P^{29} (MeV)
10.25	30	12.61
10.32	30	12.68
10.40	40	12.76
10.61	130	12.96
10.88	150	13.25
11.28	120	13.61
11.56	80	13.88
11.73	80	14.05
12.10	50	14.40

However, it is by no means certain either that the structure in the excitation curve is completely resolved, or that the peaks correspond to genuine level positions in the compound nucleus P^{29}. In the reaction Si^{28}(d, p), the excitation curve at a given angle [9]) shows peaks similar to the present results, which are ascribed to interference between a predominantly stripping mechanism and less than 15 % compound nucleus formation. The present peaks may well be due to a similar interference effect with a predominantly direct interaction mechanism. Taken at their face value they represent a level spacing of 200 keV, while similar experiments performed at a P^{29} excitation of 6.5 MeV reveal the same apparent spacing [2, 3]). Studies of other light nuclei suggest that the true level spacing is much closer; thus even at 8.5 MeV excitation, the spacing of levels in Si^{29} formed by the reaction Si^{28}(d, p) is 40 keV (ref. [10])). In the circumstances it was decided not to attempt a detailed study of level distributions and widths, as has been done for the nucleus S^{32} by Clarke *et al.* [11]), in the reaction P^{31}(p, α), where compound nuclear processes predominate.

Angular distributions of elastically scattered protons and protons inelastically scattered to the 1.77 MeV level of Si^{28} were determined in the range $\theta = +10°$ to $\theta = +130°$ at the following two energies:

a) 10.61 MeV, the top of a well-defined peak in the inelastic yield curve;

b) 11.98 MeV, in a trough, and close in energy to a cyclotron measurement [4]).

Figs. 2a and 2b show the elastic scattering at these two energies. The curves show the optical model calculations made by Dr. P. E. Hodgson and Mr. R. N.

Maddison of the Clarendon Laboratory, Oxford, using a Saxon-Woods potential without any spin-orbit term. Absolute values of cross-sections for all the measurements are derived from the predictions this model makes as to the elastic yield at forward angles; in doing this we have allowed for the unresolved groups due to elastic scattering of Si^{29} and Si^{30}. The effect of these isotopes on the shape of figs. 2a and 2b cannot be accurately estimated, but is probably slight. The parameters giving the best fit to these two curves are shown in table 3 together with the parameters used by Glassgold and Kellogg [12]) to describe the elastic scattering of protons at 10 MeV and 17 MeV. The latter

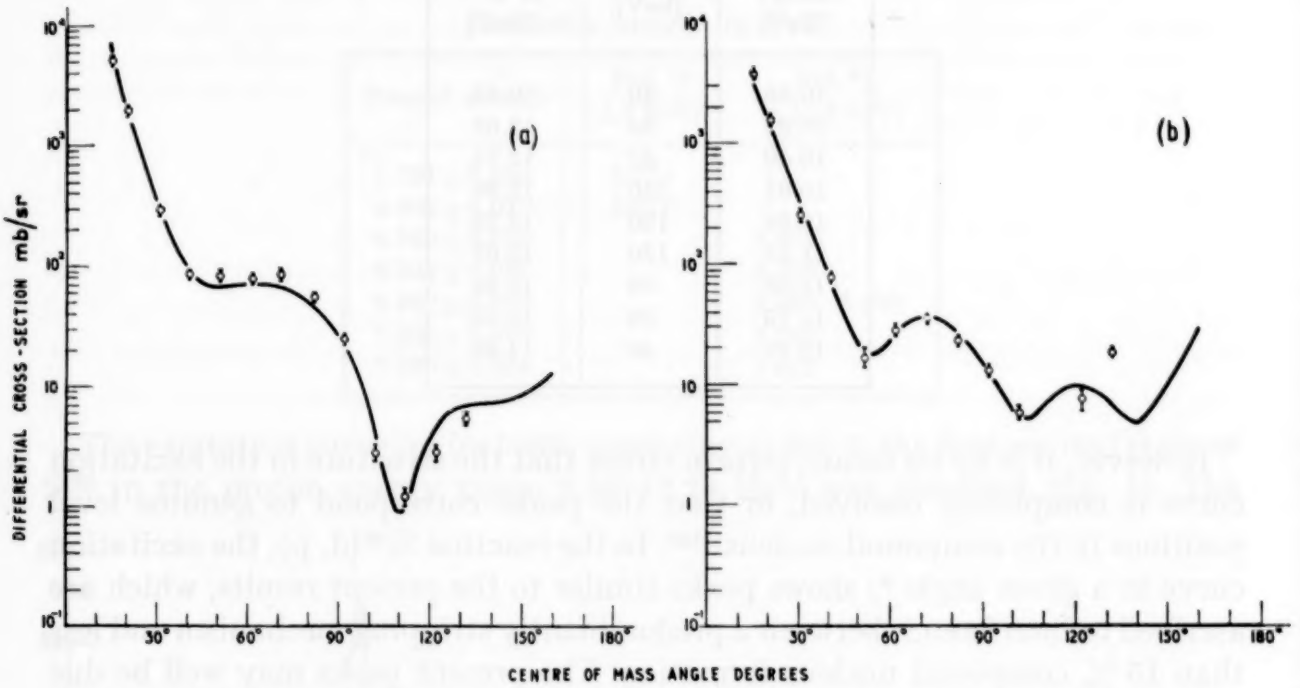

Fig. 2. Angular distributions for elastic scattering of protons by Si. Absolute cross-sections are subject to an additional ±10 % error. (a) Incident proton energy 10.61 MeV. (b) Incident proton energy 11.98 MeV.

parameters are stated to be fairly independent of atomic weight and are calculated on a basis of $r_0 = 1.30\ A^{\frac{1}{3}}$ fm. The present values of r_0 seem rather low but give a better fit than would a higher value.

TABLE 3

Best fit parameters for several energies

	Proton energy (MeV)	$-U$ (MeV)	$-W$ (MeV)	a (fm)	$r_0 A^{-\frac{1}{3}}$ (fm)
Present value	10.61	54	4.5	0.40	1.21
	11.98	57	8.5	0.62	1.11
Ref. [12])	10	53±3	7 ±1	0.68±0.07	1.30
	17	50±2	8 ±1	0.68±0.07	1.30

The optical model cannot be expected to apply where compound nuclear processes are important, so that the values corresponding to 10.61 MeV may well be merely empirical parameters of no direct physical significance. The region near 11.98 MeV appears free of isolated resonances for inelastic scattering to the first excited state. If this is so for the elastic process as well, the parameters corresponding to that energy may properly be compared with those of Glassgold and Kellogg.

Figs. 3a and 3b show the inelastic angular distributions at the two energies. The full curve in fig. 3b is the result of the cyclotron experiment of Conzett [4])

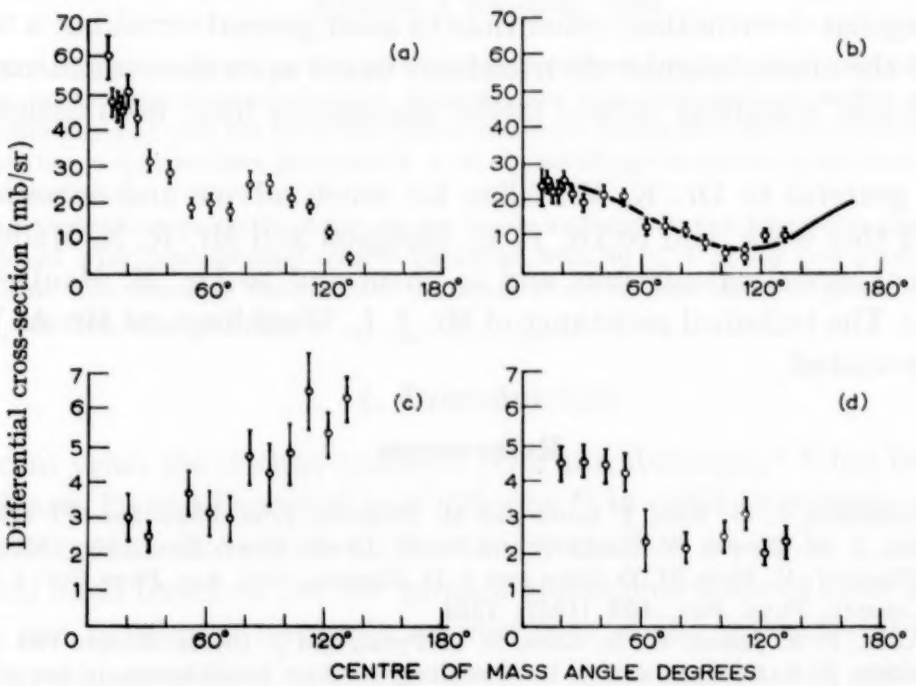

Fig. 3. Angular distributions for inelastic scattering of protons by Si^{28}. Absolute cross-sections are subject to an additional ± 10 % error. (a) 10.61 MeV protons exciting 1.77 MeV level. (b) 11.98 MeV protons exciting 1.77 MeV level; the curve represents the results of Conzett [4]). (c) 10.61 MeV protons exciting 4.62 MeV level. (d) 10.61 MeV protons exciting 4.98 MeV level.

at 12.0 MeV with 0.15 MeV spread in energy. The agreement both in shape and absolute magnitude with the present results despite the very different energy resolutions would be expected in a region free of isolated resonances. Figs. 3c and 3d show the angular distributions at 10.61 MeV of inelastic proton scattering to the second and third excited states of Si^{28} at 4.62 and 4.98 MeV, respectively.

The ground state of Si^{28} is (0^+), and the first excited state is (2^+) (ref. [13])). The seond and third states have spins 4 and 0 respectively (C. Broude and H. E. Gove, private communication). Should inelastic scattering be by a simple undistorted wave direct interaction mechanism [14]) the expected angular distribution for the first excited state is $j_2^2(kR)$. Similar predictions, depending on the assumed parity, may be made for the other levels. The observed angular

distributions are not of this form, and this, together with the strong energy dependence of angular distribution for inelastic scattering to the 1.77 MeV level observed both in the present work and by Greenlees [1]) at lower energies, is additional evidence of the complexity of the mechanism.

4. Conclusions

The excitation curve reveals many overlapping peaks, possibly corresponding to levels in P^{29}. The presence of these is borne out by the energy dependence both of inelastic and elastic processes. It has not proved possible to discuss the inelastic angular distributions other than in most general terms but a tentative analysis of the elastic angular distributions based upon the optical model has been made and empirical optical model parameters have been assigned.

We are grateful to Dr. K. W. Allen for much advice and encouragement throughout this work, and to Dr. P. E. Hodgson and Mr. R. N. Maddison for their optical model calculations and to them and to Dr. N. MacDonald for discussions. The technical assistance of Mr. J. L. Wankling and Mr. A. J. Cole is much appreciated.

References

1) G. W. Greenlees, L. G. Kuo, J. Lowe and M. Petravic, Proc. Phys. Soc. **71** (1958) 347
2) J. Vorona, J. W. Olness, W. Haeberli and H. W. Lewis, Phys. Rev. **116** (1959) 1563
3) H. B. Willard, J. K. Blair, H. D. Cohn and J. D. Kington, Bull. Am. Phys. Soc. **1** (1956) 264
4) H. E. Conzett, Phys. Rev. **105** (1957) 1324
5) K. W. Allen, F. A. Julian, W. D. Allen, A. E. Pyrah and J. Blears, Nature **184** (1959) 303
6) A. V. Cohen, J. A. Cookson and J. L. Wankling, Nuclear Instruments, in the press
7) P. M. Endt and C. H. Paris, Phys. Rev. **106** (1957) 764
8) S. Hinds and R. Middleton, Proc. Phys. Soc. **76** (1960) 545
9) J. A. Kuehner, E. Almqvist and D. A. Bromley, Proc. Int. Conf. on Nuclear Structure, Kingston (1960) (North-Holland Publishing Company, Amsterdam, 1960)
10) C. P. Browne and J. T. Radzyminskii, Nuclear Physics **19** (1960) 164
11) R. L. Clarke, E. Almqvist and E. B. Paul, Nuclear Physics **14** (1960) 472
12) A. E. Glassgold and P. J. Kellogg, Phys. Rev. **109** (1958) 1291
13) J. G. Rutherglen, P. J. Grant, F. C. Flack and W. M. Deuchars, Proc. Phys. Soc. **67** (1954) 101
14) N. Austern, S. T. Butler and H. McManus, Phys. Rev. **92** (1953) 350

1.D.2 *Nuclear Physics* **24** (1961) 535—575; © *North-Holland Publishing Co., Amsterdam*

Not to be reproduced by photoprint or microfilm without written permission from the publisher

EVIDENCE FOR THE EXISTENCE OF ROTATIONAL LEVELS IN ALL EVEN NUCLEI

C. A. MALLMANN †

Argonne National Laboratory, Argonne, Illinois ††

Received 2 December 1960

Abstract: A theory of rotations of even nuclei is developed which is more general than the one based on the hydrodynamical model. It is assumed that the rotational motion can be treated adiabatically and that the three effective moments of inertia and the two effective quadrupole moments are independent parameters. A small centrifugal distortion of the rotor is added as a correction term.

The theoretical predictions for energy levels and gammaray transition probabilities are compared with experimental results for nuclei with $40 \leqq A \leqq 250$ and good agreement is obtained. The trends of the effective moments of inertia and effective quadrupole moments as a function of A are given.

1. Introduction

In recent years the nuclear model of Bohr and Mottelson [1, 2]) has been extended by Marty [3]) and Davydov and Filippov [4]) in order to include rotations of non-axially symmetric nuclei. In this theory the 3+, 4+, 5+, . . . levels of the rotational band based on the 2+ gamma vibrational state of Bohr and Mottelson [1, 2]), are developed naturally as members of the ground state rotational band. Experimental data on energy levels of even nuclei are in agreement with this theory when applied to nuclei far away from closed shells [5, 6, 7]) but in disagreement close to closed shells [7, 8]). Measured gamma-ray transition probabilities agree with the general trends of the predictions as a function of $E(^{2}2+)/E(^{1}2+)$ although some deviations are observed [6, 9 10, 11]) †††.

The fact that the 0+, 2+, 4+, 6+, 8+ rotational levels in strongly deformed even nuclei are members of a system of levels which exist throughout all the even nuclei [12]), the fact that the general trends of the ratios of gamma-ray transition probabilities as a function of $E(^{2}2)/E(^{1}2)$ are predicted correctly by a restricted ‡ [3, 4]) asymmetric rotor theory (the hydrodynamical model), and

† Present address: Departmento de Fisica, Facultad de Ciencias Exactas y Naturales de la Universidad de Buenos Aires, Perú 222, Buenos Aires, Argentina.

†† This paper is based on work performed under the auspices of the U. S. Atomic Energy Commission.

††† The notation $^{1}2$ indicates the first excited spin-two state with positive parity. In the following we shall give the spin of the levels considered and not the parity because we are only considering states with positive parity.

‡ Only two independent moments of inertia and one quadrupole moment.

the fact that the gamma-ray transition probability from the ^{12} state to the ground state follows one law throughout the nuclear chart [13]) ($16 \leqq A \leqq 250$), indicated that a more general asymmetric rotor treatment might lead to still more complete and accurate agreement with experimental results. Davydov, Rabotnov and Chaban [15]) have recently considered such an adiabatic general asymmetric rotor theory with no restrictions on the moments of inertia. They concluded that the agreement with experimental data is not improved and suggested that taking into account the vibration-rotation interaction in the hydrodynamical model [3, 4]) might improve the agreement. This interaction had already been taken into account [7]) as a perturbation of the hydrodynamical model and better agreement obtained for nuclei far away from closed-shells. The present paper introduces the rotation-vibration interaction as a perturbation to the general asymmetric rotor theory (quasi-adiabatic general asymmetric rotor theory) and shows that agreement is obtained with measured energies and gamma-ray transition probabilities in the low lying even parity states in non-closed-shell even nuclei with $40 \leqq A \leqq 250$.

2. Assumptions

We assume that the rotational motion of an even nucleus can be treated quasi-adiabatically. This is equivalent to the assumption that the excited states due to other degrees of freedom of the nucleus have energies which are appreciably higher than the energies due to the rotational motion. Departure of actual nuclei from this behaviour is assumed to be small and hence explainable in terms of perturbation theory. Vibration-rotation interactions are treated in this way.

The wave function φ is then the product of a rotational wave function ψ and an intrinsic wave function ϕ. The intrinsic wave function describes all the other degrees of freedom of the nucleus (vibrations, particle excitations, etc.). We impose the symmetry conditions of Bohr [1, 2, 3]) on the wave function.

The rotational Hamiltonian is given by

$$H^{\mathrm{R}} = \frac{Q_{\mathrm{A}}^{\,2}}{2I_{\mathrm{A}}} + \frac{Q_{\mathrm{B}}^{\,2}}{2I_{\mathrm{B}}} + \frac{Q_{\mathrm{C}}^{\,2}}{2I_{\mathrm{C}}}, \tag{2.1}$$

where A, B and C are the labels for the principal axes of inertia, Q_{A}, Q_{B} and Q_{C} the angular momentum operators, and I_{A}, I_{B} and I_{C} the effective moments of inertia in order of increasing magnitude,

$$I_{\mathrm{A}} \leqq I_{\mathrm{B}} \leqq I_{\mathrm{C}}. \tag{2.2}$$

The three effective moments of inertia are considered to be independent parameters and no attempt is made to calculate them from first principles.

The intrinsic Hamiltonian H_1 is not given explicitly. Each intrinsic state has an energy to which the rotational energies are added. The ground state intrinsic energy is arbitrarily set equal to zero in order to avoid carrying this additive constant throughout the analysis.

For the calculation of gamma-ray transition probabilities in a nucleus of charge Z we use the two effective quadrupole moments

$$k_0 = \sqrt{\frac{5}{16\pi}} \sum_{i=1}^{Z} \int (3z_i^2 - r^2)|\phi|^2 \mathrm{d}t, \tag{2.3}$$

$$k_2 = \sqrt{\frac{15}{32\pi}} \sum_{i=1}^{Z} \int (x_i^2 - y_i^2)|\phi|^2 \mathrm{d}t, \tag{2.4}$$

as parameters and again make no attempt to calculate them from first principles.

3. Energy Levels

We make use of the well known results [14]) on energy levels of asymmetric rotors which are used in molecular spectroscopy. Let us define

$$A = \frac{\hbar}{4\pi I_A}, \quad B = \frac{\hbar}{4\pi I_B}, \quad C = \frac{\hbar}{4\pi I_C}, \tag{3.1}$$

where $\hbar$ is Planck's constant h divided by 2π. Because of eq. (2.2) we have

$$\frac{A}{C} \geqq \frac{B}{C} \geqq 1, \tag{3.2}$$

if we assume that $C > 0$, i.e., $I_C < \infty$. The parameter A/C can then take values between 1 and ∞. For rigid bodies the values of A/C have to satisfy the relation

$$\frac{A}{C} \leqq \frac{1}{1 - \frac{C}{B}}, \tag{3.3}$$

which is a consequence of the following well known relation among the moments of inertia of a rigid body: $I_A + I_B \geqq I_C$. In the hydrodynamical model [3, 4]) the moments of inertia are given by

$$I_\lambda^{\mathrm{H}} = \frac{12MAR_0^2}{8\pi} \beta^2 \sin^2(\gamma - \tfrac{2}{3}\pi\lambda), \quad (\lambda = 1, 2, 3), \tag{3.4}$$

where γ is the parameter which together with β determines the shape of the nucleus. The parameter γ can take values between 0° and 30°. The symbol M represents is the mass of a nucleon, A is the atomic number and R_0 the nuclear radius.

Note that the absolute values of A, B and C are determined by two parameters γ and β and the ratios A/C and B/C are functions of γ only and are given by

$$\frac{A}{C} = \frac{\sin^2(\gamma-\frac{2}{3}\pi)}{\sin^2\gamma} \text{ and } \frac{B}{C} = \frac{\sin^2(\gamma-\frac{2}{3}\pi)}{\sin^2(\gamma-\frac{4}{3}\pi)} \; (I_1 \equiv I_C; I_2 \equiv I_B; I_3 \equiv I_A). \quad (3.5)$$

These ratios do not satisfy the rigid rotor requirement (3.3), except for $\gamma = 0°$. The latter value of γ is used in the model of Bohr and Mottelson [2]). The aforementioned use of only two independent parameters clearly shows that the hydrodynamical model is a restricted case of the general asymmetric rotor we are considering. The moments of inertia considered by Macdonald [6]) are given by

$$I_\lambda{}^M = I_\lambda{}^H\{(I_\lambda{}^H/I_\lambda{}^R)+p\}^{-2}, \quad (\lambda = 1, 2, 3), \quad (3.6)$$

where $I_\lambda{}^R$ are the rigid body moments of inertia and p is a parameter which is independent of β and γ. They also are a special case of those we are considering since he only considered a few different combinations of the parameters p and β. As mentioned in the introduction, Davydov, Rabotnov and Chaban [15]) have also considered the general asymmetric rotor we are considering. The rotational Hamiltonian can be written in the following way:

$$H^R = \frac{hC}{\hbar^2}\left(\frac{A}{C}\,Q_A{}^2 + \frac{B}{C}\,Q_B{}^2 + Q_C{}^2\right). \quad (3.7)$$

The wave function ψ satisfies the following equation:

$$H^R\psi = hC\varepsilon_0\psi, \quad (3.8)$$

where ε_0 is the energy E_0 in units of $hC = \hbar^2/2I_C$, of the (J, τ) spin J level of an asymmetric rotor. It is given by [14])

$$\frac{E_0}{hC} = \varepsilon_0\left(J, \tau, k, \frac{A}{C}\right) = J(J+1)\left\{\beta(k, \tau, J) + \frac{A}{C}\,[1-\beta(k, \tau, J)]\right\}, \quad (3.9)$$

where the subscript 0 indicates that the vibration-rotation interaction effects have not been taken into account, τ labels the $2J+1$ levels of spin J, and the asymmetry parameter k is given by

$$k = \frac{2B-A-C}{A-C}. \quad (3.10)$$

The parameter k can take values between -1 and 1. For rigid rotors, k is -1 for a prolate symmetric top ($B = C$), 1 for an oblate symmetric top ($B = A$) and varies between these two values for asymmetric cases. The function †

† The reader should not confuse the function $\beta(k, \tau, J)$ with the parameter β of Bohr and Mottelson.

β takes values between 0 and 1. Tables for $\beta(k, \tau, J)$ or $E(k, \tau, J)$, which is related to β by

$$\beta(k, \tau, J) = \tfrac{1}{2}\left[1 - \frac{E(k, \tau, J)}{J(J+1)}\right], \tag{3.11}$$

are given in refs. [16–19]).

The symmetry conditions of Bohr [1, 2, 3]) for the nuclear wave functions (see section 6) eliminate some of the $2J+1$ spin J levels of the general asymmetric rotor, i.e., some of the possible τ values, which in the general case take values from $-J$ to J in unit steps, are eliminated. The allowed τ values are given by

$$\tau = K_{-1} - K_1, \tag{3.12}$$

where K_{-1} and K_1, the projection of J on the symmetry axis in the limiting cases of $k = -1$ (rigid prolate top) and $k = 1$ (rigid oblate top) respectively, must both be even numbers. This means that the only rotational wave functions allowed are those which are symmetric for 180° rotations about any of the principal axes of inertia. It is easy to see that the levels so excluded are not found in nuclei. An example of this is the spin-1 state which would lie between the ground state and the first excited spin-2 state. We relabel the allowed τ values in order of increasing τ; this is equivalent to ordering the levels of a given J in order of increasing energies. Eq. (3.9) is now written

$$\varepsilon_0\left({}^nJ, k, \frac{A}{C}\right) = J(J+1)\left\{\beta(k, {}^nJ) + \frac{A}{C}\left[1-\beta(k, {}^nJ)\right]\right\}. \tag{3.13}$$

It has been shown [7, 12]) to be useful to study the energy of the excited states of even nuclei in units of the energy of the ^{12} state. We shall use this method of giving the energy of the excited states of a rotor. Using eq. (3.13) one can show that the ratio $R_0({}^nJ)$ of the energy of the ${}^nJ$ level to the energy of the ^{12} level as a function of $R_0({}^mJ')$, the ratio of the energy of the ${}^mJ'$ level to the energy of the ^{12} level, is given by

$$R_0({}^nJ) = \tfrac{1}{6}J(J+1)\,\frac{\beta(k, {}^mJ') - \beta(k, {}^nJ)}{\beta(k, {}^mJ') - \beta(k, {}^12)} + \frac{J(J+1)}{J'(J'+1)}\,\frac{\beta(k, {}^nJ) - \beta(k, {}^12)}{\beta(k, {}^mJ') - \beta(k, {}^12)}\,R_0({}^mJ'). \tag{3.14}$$

For a given k value this is the equation of a straight line. The segment between the points

$$R_0({}^nJ)_{\frac{A}{C}=\infty} = \tfrac{1}{6}J(J+1)\,\frac{1-\beta(k, {}^nJ)}{1-\beta(k, {}^12)},$$

$$R_0({}^mJ')_{\frac{A}{C}=\infty} = \tfrac{1}{6}J'(J'+1)\,\frac{1-\beta(k, {}^mJ')}{1-\beta(k, {}^12),} \tag{3.15}$$

TABLE 1

Values of $R_0(^nJ)$ for $A/C = \infty$ as a function of k

k	^{2}2	^{1}4	^{2}4	^{1}6	^{1}8
−1.0	∞	3.333	∞	7.000	12.00
−0.9	27.36	3.183	29.90	6.209	9.643
−0.8	14.06	3.029	16.80	5.498	7.947
−0.7	9.652	2.879	12.60	4.929	6.858
−0.6	7.466	2.739	10.62	4.493	6.135
−0.5	6.171	2.613	9.517	4.162	5.627
−0.4	5.323	2.502	8.851	3.907	5.254
−0.3	4.732	2.407	8.430	3.708	4.972
−0.2	4.301	2.325	8.160	3.551	4.752
−0.1	3.978	2.257	7.990	3.425	4.579
0	3.732	2.200	7.887	3.325	4.442
0.1	3.542	2.152	7.832	3.245	4.332
0.2	3.394	2.113	7.813	3.180	4.245
0.3	3.280	2.082	7.818	3.129	4.175
0.4	3.191	2.057	7.811	3.089	4.121
0.5	3.124	2.037	7.874	3.058	4.079
0.6	3.075	2.023	7.911	3.035	4.048
0.7	3.040	2.012	7.947	3.019	4.025
0.8	3.017	2.005	7.976	3.008	4.011
0.9	3.004	2.001	7.994	3.002	4.003
1.0	3.000	2.000	8.000	3.000	4.000

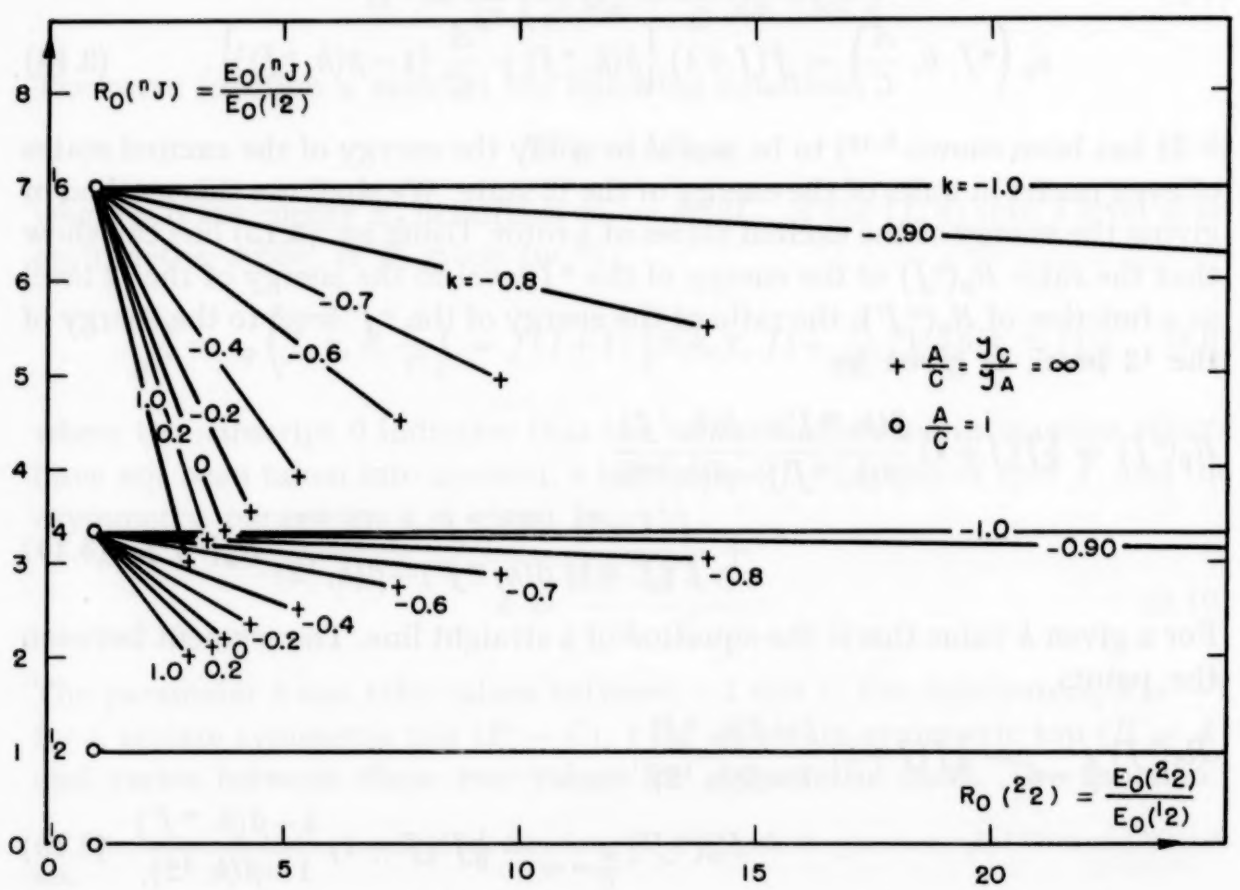

Fig. 1. Plot of $R_0(^12)$, $R_0(^14)$ and $R_0(^16)$ as a function of $R_0(^22)$ for different k values and all possible values of A/C $(1 \leqq A/C \leqq \infty)$.

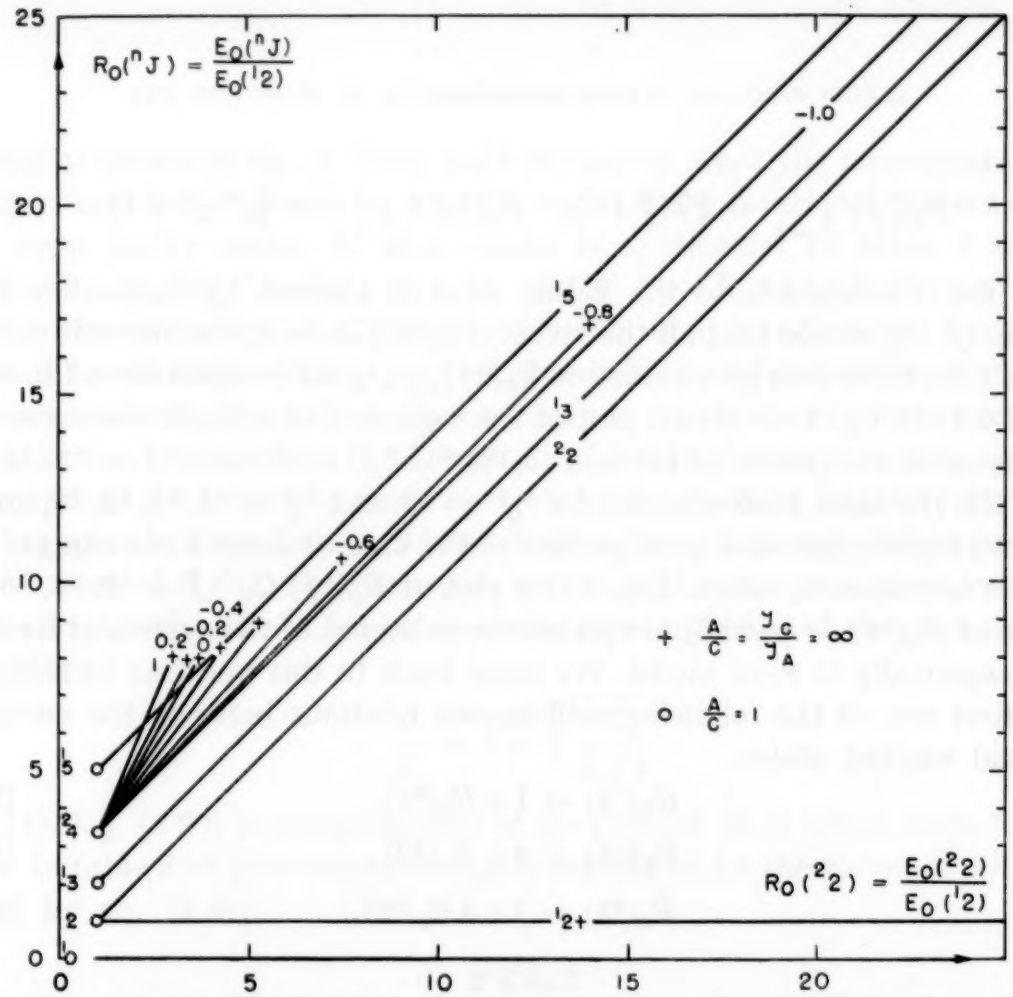

Fig. 2. Plot of $R_0(^12)$, $R_0(^22)$, $R_0(^13)$, $R_0(^24)$ and $R_0(^15)$ as a function of $R_0(^22)$ for different k values and all possible values of $A/C(1 \leqq A/C \leqq \infty)$. Note that the plots of $R_0(^13)$ and $R_0(^15)$ as a function of $R_0(^22)$ are straight lines because of eq. (3.17) and (3.18).

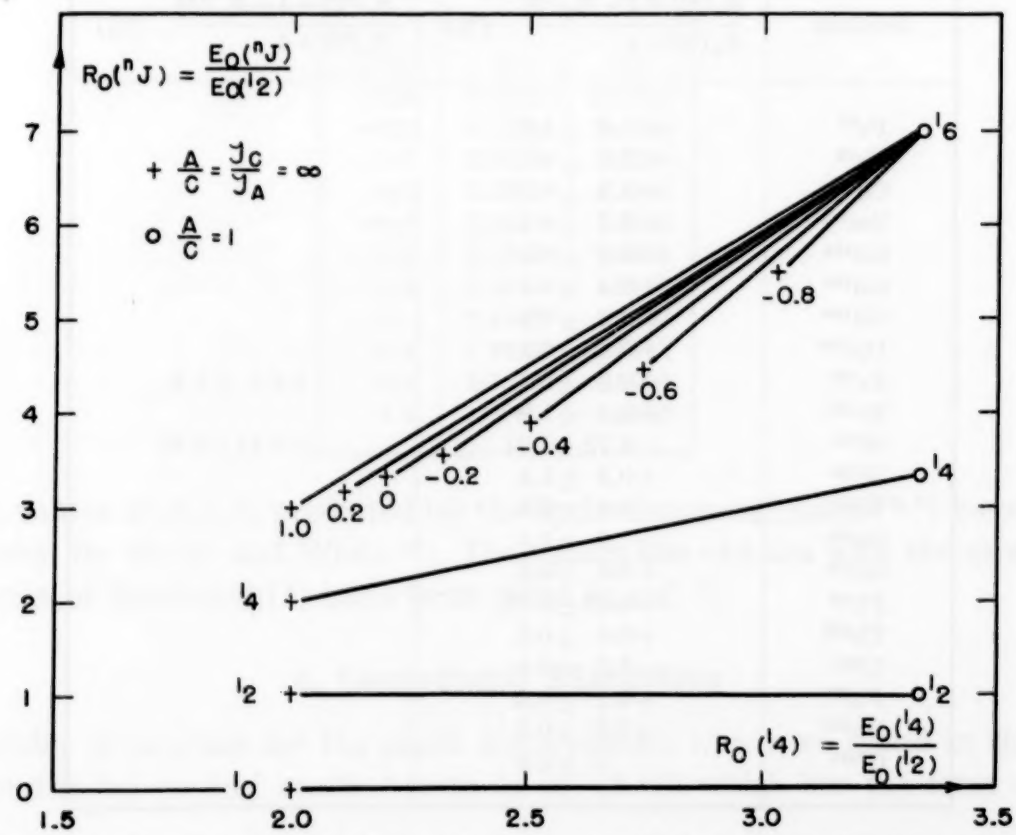

Fig. 3. Plot of $R_0(^12)$, $R_0(^14)$ and $R_0(^16)$ as a function of $R_0(^14)$ for different k values and all possible values of $A/C(1 \leqq A/C \leqq \infty)$.

and

$$R_0({}^nJ)_{\frac{A}{C}=1} = \tfrac{1}{6}J(J+1), \quad R_0({}^mJ')_{\frac{A}{C}=1} = \tfrac{1}{6}J'(J'+1) \tag{3.16}$$

on this line corresponds to the values of A/C allowed by inequality (3.2). From eq. (3.16) we see that all the levels of spin J have the same ratio for A/C equal to 1. In table 1 we give values of $R_0({}^nJ)_{A/C=\infty}$ for k values from 1 to -1 in steps of 0.1. In fig. 1 we give a plot of the segments of straight lines given by (3.14) between the points (3.15) and (3.16) for ${}^mJ' = {}^22$ and ${}^nJ = {}^12$, ^{14}, and ^{16}. Fig. 2 is the same kind of a plot for ${}^mJ' = {}^22$ and ${}^nJ = {}^12$, ^{22}, ^{13}, ^{24}, and ^{15}. These two figures give us a good picture of the kind of spectra one can get with adiabatic asymmetric rotors. Fig. 3 is a plot of $R_0({}^nJ)$ for ${}^nJ = {}^12$, ^{14}, ^{16} as a function of $R_0({}^14)$. It partially explains the existence of the system of levels [12]) found empirically in even nuclei. We come back to this question in section 5.

The first two of the following well-known relations between the energy of rotational excited states:

$$R_0({}^13) = 1+R_0({}^22), \tag{3.17}$$

$$R_0({}^15) = 4+R_0({}^22), \tag{3.18}$$

$$R_0({}^25) = 1+4R_0({}^22), \tag{3.19}$$

TABLE 2

Values of $[R_e({}^22)+1-R_e({}^13)]/[R_e({}^22)+1]$ and $[R_e({}^22)+4-R_e({}^15)]/[R_e({}^22)+4]$ given in percent for nuclei in which the ^{13} level is known (references for the data used are given in section 11)

Nucleus	$\frac{R_e({}^22)+1-R_e({}^13)}{R_e({}^22)+1}$ (%)	$\frac{R_e({}^22)+4-R_e({}^15)}{R_e({}^22)+4}$ (%)
Fe^{56}	$+1.8 \pm 1.6$	
Kr^{82}	$+7.0 \pm 0.1$	
Cd^{110}	-1.5 ± 0.2	
Sm^{152}	-2.2 ± 0.1	
Gd^{154}	-0.8 ± 0.1	
Gd^{156}	-0.4 ± 0.2	
Gd^{158}	$+0.4 \pm 0.3$	
Dy^{160}	$+0.4 \pm 0.3$	
Er^{166}	$+0.8 \pm 0.6$	$+2.5 \pm 1.5$
Er^{168}	$+0.6 \pm 1.0$	
W^{182}	-0.73 ± 0.04	$+0.11 \pm 0.05$
W^{184}	$+0.9 \pm 1.4$	
W^{186}	$+0.3 \pm 0.6$	
Os^{190}	-1.2 ± 2.0	
Os^{192}	$+0.6 \pm 0.2$	
Pt^{192}	$+0.92 \pm 0.07$	
Th^{228}	$+0.6 \pm 0.6$	
U^{232}	-3.0 ± 0.6	
Pu^{238}	$+0.2 \pm 0.3$	
Pu^{240}	$+0.3 \pm 0.2$	
Cf^{250}	0 ± 1.9	

are clearly shown in fig. 2. They hold no matter what the parameters of the rotor are, and hence should be true for nuclei if the rotational picture of low-lying even parity states in even nuclei is applicable. In table 2 we give $[R_e(^22)+1-R_e(^13)]/[R_e(^22)+1]$ and $[R_e(^22)+4-R_e(^15)]/[R_e(^22)+4]$ in % for all nuclei with $40 \leqq A \leqq 250$ for which the spin 3 and/or spin 5 states are known. The subscript e stands for experimental. The references for the data are given in section 11. From the table we conclude that with only three exceptions out of 23 cases the relations (3.17) and (3.18) hold to better than 2 %, and that the deviations get larger the closer one gets to closed shells. Negative deviations seem to appear half way between closed shell nuclei and strongly deformed nuclei.

The values of $R_0(^nJ)$ one can reach with a rigid rotor for a given value of k are on the straight line (3.14) between the points (3.16) and the ones obtained by making

$$\frac{A}{C} = 1 + \sqrt{\frac{2}{k+1}} \tag{3.20}$$

in (3.13). Eq. (3.20) is a consequence of the relation (3.3) which holds for rigid rotors. In table 3 we give values of $R_0(^22)$ calculated for the values of A/C and k related by eq. (3.20).

TABLE 3

Values of the maximum A/C and $R_0(^22)$ values allowed by the rigid rotor model given as a function of k

k	A/C	$R_0(^22)$
−1.0	∞	∞
−0.9	5.4721	3.6204
−0.8	4.1623	2.7428
−0.7	3.5820	2.3559
−0.6	3.2361	2.1280
−0.5	3.0000	1.9752
−0.4	2.8257	1.8652
−0.2	2.5811	1.7188
0	2.4142	1.6287
0.2	2.2910	1.5713
0.5	2.1530	1.5220
1.0	2.0000	1.5000

The values of $R_0(^nJ)$ predicted by the hydrodynamical model [3, 9]) have been computed by Moore and White [20]). The values one obtains with the moments of inertia of Macdonald [6]) have been given in ref. [15]).

4. Centrifugal Distortion

In order to account for the small discrepancies which we found in the last section one has to add another term to eq. (3.13) which has the form of the

centrifugal distortion terms of molecular spectroscopy or the vibration-rotation interaction in the nuclear collective model. We shall assume that the energy of a level in units of hC is given by [7])

$$\varepsilon_b(k, {}^nJ, A/C) = \varepsilon_0(k, {}^nJ, A/C) - b\{\varepsilon_0(k, {}^nJ, A/C)\}^2, \tag{4.1}$$

where b is a constant which will be treated as a parameter. This type of correction term is a first order correction to the pure asymmetric rotor energy level formula. Using eq. (4.1) one can show that $R_b({}^nJ)$ as a function of $R_b({}^mJ')$ is given by

$$R_b({}^nJ) = R_0({}^nJ)\,\frac{R_0({}^nJ)-R_0({}^mJ')}{1-R_0({}^mJ')} + \frac{R_0({}^nJ)}{R_0({}^mJ')}\,\frac{1-R_0({}^nJ)}{1-R_0({}^mJ')}\,R_b({}^mJ'). \tag{4.2}$$

This is the equation of a straight line for particular values of $R_0({}^nJ)$, $R_0({}^mJ')$. The values of b, which give a particular point on this line, may be obtained from the following relation:

$$R_b({}^mJ') = \frac{\varepsilon_0({}^mJ', k, A/C) - b\{\varepsilon_0({}^mJ', k, A/C)\}^2}{\varepsilon_0({}^12, k, A/C) - b\{\varepsilon_0({}^12, k, A/C)\}^2}. \tag{4.3}$$

In comparing experimental results with theoretical predictions one attempts to find for each nucleus a set of parameters $(k, A/C, hC, b)$ which reproduce the observed energy levels. When one knows the energy of the ^{12}, ^{22}, ^{13} and/or ^{15} levels one can determine the value of $R_0({}^22)$ from

$$R_0({}^22) = \frac{R_b({}^13)+R_b({}^22)-1}{R_b({}^13)-R_b({}^22)+1}, \tag{4.4}$$

$$R_0({}^22) = \left\{\frac{7R_b({}^22)+R_b({}^15)-16}{2[R_b({}^15)+4-R_b({}^22)]}\right\} \pm \sqrt{\left\{\frac{7R_b({}^22)+R_b({}^15)-16}{2[R_b({}^15)+4-R_b({}^22)]}\right\}^2 + \frac{12R_b({}^22)}{[R_b({}^15)+4-R_b({}^22)]}}, \tag{4.5}$$

which result from eq. (4.1) making $m = 2$, $J' = 2$; $n = 1$, $J = 3$ and $m = 2$, $J' = 2$; $n = 1$, $J = 5$, respectively, and using eqs. (3.17) and (3.18). If one obtains the same value of $R_0({}^22)$ from eqs. (4.4) and (4.5) by replacing $R_b({}^22)$, $R_b({}^13)$ and $R_b({}^15)$ by the corresponding experimental values $R_e({}^22)$, $R_e({}^13)$ and $R_e({}^15)$, the model is consistent with experiment. Knowing $R_0({}^22)$ we can get other $R_0({}^nJ)$ values from

$$R_0({}^nJ) = \tfrac{1}{2}\left\{\left[\frac{R_0{}^2({}^22)-R_b({}^22)}{R_0({}^22)-R_b({}^22)}\right] - \sqrt{\left[\frac{R_0{}^2({}^22)-R_b({}^22)}{R_0({}^22)-R_b({}^22)}\right]^2 - \frac{4[R_0({}^22)-1]R_0({}^22)}{R_0({}^22)-R_b({}^22)}\,R_b({}^nJ)}\right\}, \tag{4.6}$$

replacing $R_e({}^nJ)$, for $R_b({}^nJ)$ and $R_e({}^22)$ for $R_b({}^22)$. Eq. (4.6) is a consequence of eq. (4.1) with $m = 2$, $J' = 2$. Each pair of values $R_0({}^22)$, $R_b({}^nJ)$ has a value for the k parameter associated with it. One way of determining it is to note that

$$\frac{R_0({}^nJ)-\frac{1}{6}J(J+1)}{R_0({}^22)-1} = \frac{1}{6}J(J+1)\,\frac{\beta(k,\,{}^nJ)-\beta(k,\,{}^12)}{\beta(k,\,{}^22)-\beta(k,\,{}^12)}, \tag{4.7}$$

which is a consequence of eq. (3.14) with $m = 2$, $J' = 2$. The value of the right hand side of the equation can be plotted as a function of k for different ${}^nJ$ values. Knowing the corresponding R_0's one can calculate the left hand side of the equation and determine k. In table 4 we give values of the right hand side

TABLE 4

Values of $J(J+1)[\beta(k,\,{}^nJ)-\beta(k,\,{}^12)]/6[\beta(k,\,{}^22)-\beta(k,\,{}^12)]$ for ${}^nJ = {}^14,\ {}^24,\ {}^16$ and ^{18} as a function of k

k	^{14}	^{24}	^{16}	^{18}
−1.0	0	1.0000	0	0
−0.98	−0.000221	1.0003	−0.00119	−0.00374
−0.96	−0.000892	1.0009	−0.00479	−0.0149
−0.94	−0.00202	1.0029	−0.0108	−0.0333
−0.92	−0.00362		−0.0193	−0.0584
−0.90	−0.00570	1.0081	−0.0300	−0.0894
−0.88	−0.00825		−0.0430	−0.1257
−0.86	−0.01129		−0.0582	−0.1666
−0.84	−0.01480		−0.0753	−0.2113
−0.82	−0.01880		−0.0943	−0.2594
−0.80	−0.02328	1.0313	−0.1150	−0.3102
−0.70	−0.05248	1.0713	−0.2394	−0.5943
−0.60	−0.09186	1.1268	−0.3876	−0.9071
−0.50	−0.1393	1.1958	−0.5488	
−0.40	−0.1922	1.2763	−0.7155	−1.5604
−0.30	−0.2483	1.3660	−0.8823	−1.8835
−0.20	−0.3054	1.4624	−1.0450	
−0.10	−0.3615	1.5634	−1.2002	
0	−0.4150	1.6667	−1.3451	
0.10	−0.4647	1.7699	−1.4773	
0.20	−0.5060	1.8709	−1.5953	
0.30	−0.5490	1.9674	−1.6979	
0.40	−0.5825	2.0570	−1.7846	
0.50	−0.6101	2.1375	−1.8554	
0.60	−0.6318	2.2066	−1.9109	
0.70	−0.6478	2.2620	−1.9519	
0.80	−0.6586	2.3020	−1.9796	
0.90	−0.6651	2.3269	−1.9961	
1.00	−0.6667	2.3333	−2.0000	

of eq. (4.7) for various values of ${}^nJ$. The values of k determined in this way for different levels should be the same if the experiment is in agreement with theory. If we do not know the $R_e({}^13)$ and $R_e({}^15)$ ratios to determine $R_0({}^22)$, then we try

to find a $R_0(^2 2)$ which gives the same k value for all $R_e(^n J)$ values. This can be done graphically or analytically. Having the value of k we can now determine the value of A/C which gives us the values of $\varepsilon_0(k, {}^n J, A/C)$ (eq. (3.13)) which in turn give us the desired R_0's. Knowing A/C and k it is easy to obtain B/C from eq. (3.10). The constant b is now obtained using eq. (4.3) with $m = 2$, $J' = 2$ for example. Having b we can determine all the other R_b's through

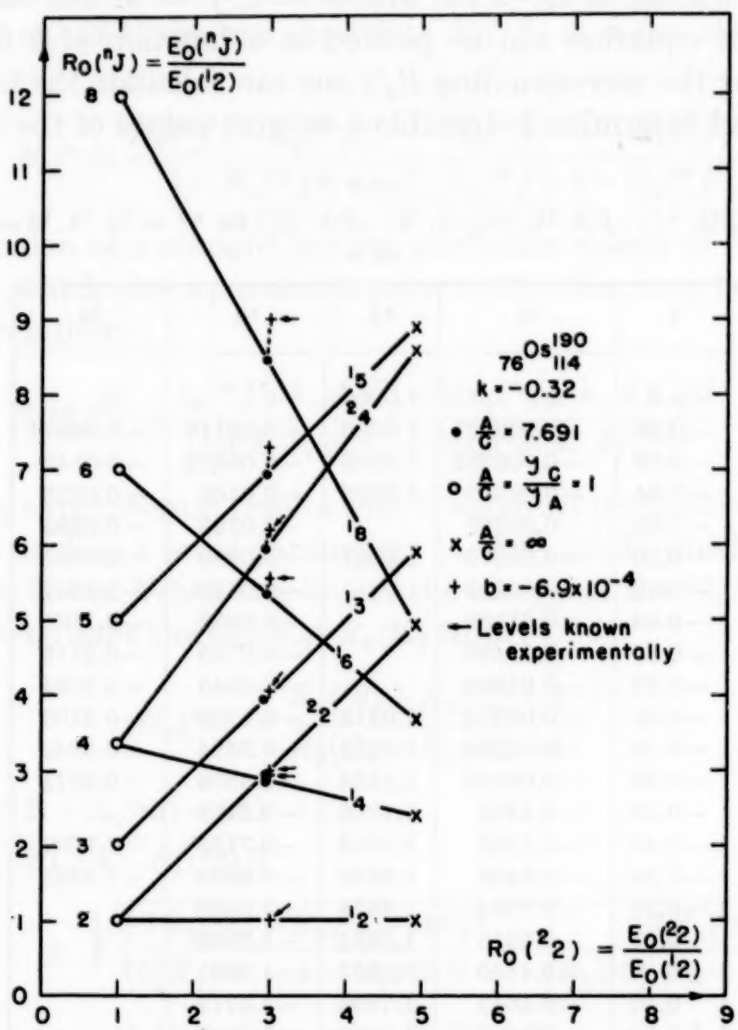

Fig. 4. The full straight lines are a plot of $R_0(^1 2)$, $R_0(^2 2)$, $R_0(^1 3)$, $R_0(^1 4)$, $R_0(^2 4)$, $R_0(^1 5)$, $R_0(^1 6)$ and $R_0(^1 8)$ as a function of $R_0(^2 2)$ for the k value of $Os^{190}(-0.32)$ and all possible values of $A/C (1 \leqq A/C \leqq \infty)$. The dashed lines join the $[R_0(^n J), R_0(^2 2)]$ points with the k and A/C values for $Os^{190}(-0.32, 7.691)$ with the points $[R_b(^n J), R_b(^2 2)]$ for $Os^{190}(b = -6.9 \times 10^{-4})$ which are indicated with a plus sign. The levels known experimentally are indicated with an arrow and no distinction has been made between them and $[R_b(^n J), R_b(^2 2)]$ because they are too close together.

eq. (4.3). The knowledge of the $\varepsilon_b(k, {}^1 2, A/C)$ also allows us to determine hC through the relation

$$hC = \frac{E_e(^1 2)}{\varepsilon_b(k, {}^1 2, A/C)} \tag{4.8}$$

TABLE 5

Comparison of measured energy levels with theoretical predictions. The measured energy of the ^{12} state $[E_e(^12)]$ and the measured values of $R(^nJ)$ for the nuclei indicated in the first column are given in the first row within each nucleus. The second row gives the theoretical values for $R(^nJ)$ calculated with the parameters given in table 6. The third row lists spins and parities (in parentheses) and $R_e(^nJ)$ values for levels which are not identifiable with the predicted members of the ground state rotational band. Experimental errors are indicated in the following way: $986 \pm 3 \equiv 986\ \underline{3}$. References for the data used are given in section 11.

Nucleus	$E_e(^12)$ (keV)	$R(^14)$	$R(^16)$	$R(^18)$	$R(^22)$	$R(^13)$	$R(^24)$	$R(^15)$
$_{22}Ti^{48}_{26}$	986 3	2.333 14 2.339	3.387 17 3.387		2.469 26 2.464	3.008	3.660	
	other levels: (4,3+) 3.286							
$_{26}Fe^{56}_{30}$	845 6	2.467 50 2.463			3.153 35 3.148	4.079 65 4.077		
	other levels: (?)3.479; (2+)3.501; (?)3.691; (?)3.987; (2+)4.009; (?)4.260							
$_{48}Cd^{110}_{62}$	656.3 5	2.348 4 2.343	3.776 6 3.779		2 245 4 2.242	3.293 5 3.021		
	other levels: (?) 3.413							
$_{56}Ba^{134}_{78}$	604.7 2	2.317 1 2.316			1.931 3 1.934		3.259 3 3.286	
	other levels: (≦2)2.596; (≧ 3)2.711; (≧3)2.932							
$_{60}Nd^{144}_{84}$	696.4 4	1.886 2 1.891	2.560 3 2.556		2.240 3 2.240			
	other levels: (1−)3.145; (?)3.291; (?)3.408							
$_{62}Sm^{152}_{90}$	121.80 5	3.009 2 3.011			8.914 10 8.906	10.136 10 10.128		
	other levels: (0+)5.624; (2+)6.658; (1−)7.906							
$_{64}Gd^{154}_{90}$	123.21 4	3.013 2 3.025			8.090 11 8.090	9.162 11 9.161		
	other levels: (0+)5.681; (2, 3)11.36							
$_{64}Gd^{156}_{92}$	88.97 1	3.238 2 3.251	6.565 3 6.569		12.95 3 12.95	14.00 3 14.00		
	other levels: (?)11.8?; (?)12.6?; (4+)16.94; . . .							
$_{64}Gd^{158}_{94}$	79.56 3	3.292 3 3.290	6.774 6 6.768	11.290 20 11.288	14.860 30 14.862	15.800 40 15.802		
	other levels: (?)12.6?; (?)18.67; . . .							
$_{66}Dy^{160}_{94}$	86.7 1	3.271 6 3.271			11.138 18 11.138	12.093 29 12.093	13.333 30 13.313	
	other levels: (1−)13.84; (2−)14.59; . . .							
$_{68}Er^{166}_{98}$	80.57 2	3.294 6 3.291	6.774 30 6.773		9.770 40 9.768	10.686 60 10.678	11.889 50 11.886	13.43 20 13.36
	other levels: (3)15.61; (0+)18.12; (2+)19.13; . . .							
$_{68}Er^{168}_{100}$	79.90 40	3.309 30 3.308	6.872 70 6.861		10.29 10 10 29	11.22 11 11.23	12.47 13 12.47	
	other levels: (3−)13.70; (3−)19.34							

TABLE 5 (continued)

Nucleus	$E_e(^{12})$ (keV)	$R(^{14})$	$R(^{16})$	$R(^{18})$	$R(^{22})$	$R(^{13})$	$R(^{24})$	$R(^{15})$
$_{70}Yb^{170}_{100}$	84.2 2	3.298 8 3.299			14.627 40 14.628	15.542 40 15.543		
	other levels: ?							
$_{72}Hf^{178}_{106}$	93.15 10	3.294 14 3.292	6.792 18 6.779	11.38 12 11.32	15.89 18 16.01			
	other levels: (9, 8−)12.32; (10, 9−)15.89							
$_{74}W^{182}_{108}$	100.09 2	3.291 2 3.290	6.798 4 6.765		12.207 4 12.209	13.302 7 13.305		
	other levels: (1−)12.55; (2−)12.90; (3−)13.74; (4−) 14.88; ...							
$_{74}W^{184}_{110}$	111.13 6	3.275 7 3.275			8.136 1 8.137	9.053 13 9.055		
	other levels: (2−)10.35; (3−)11.07							
$_{74}W^{186}_{112}$	122.48 8	3.319 10 3.314			5.960 20 5.961	6.940 45 6.941	8.491 66 8.252	
	other levels: ?							
$_{76}Os^{186}_{100}$	137.22 2	3.164 3 3.166	6.332 6 6.338		5.598 6 5.598			
	other levels: ?							
$_{76}Os^{190}_{114}$	186.7 1	2.934 3 2.918	5.614 11 5.546	8.904 18 8.995	2.985 3 2.988	4.045 6 4.037	6.220 7 6.193	
	other levels: (4+)5.112; (3−)7.413; ...							
$_{76}Os^{192}_{116}$	205.75 20	2.821 6 2.822			2.377 1 2.377	3.356 7 3.356		
	other levels: ?							
$_{80}Hg^{198}_{118}$	411.76 19	2.43 2 2.43	3.97 3 3.96		2.644 3 2.640			
	other levels: (6+)4.082;							
$_{90}Th^{228}_{138}$	57.48 5	3.241 10 3.246	6.576 23 6.539		16.86 8 16.87	17.80 8 17.81	19.00 8 19.15	
	other levels: (1−)5.698; (3−)6.889; (5−)8.942; (2−)19.54; ...							
$_{90}Th^{232}_{142}$	49.75 25	3.271 60 3.292	6.688 100 6.779	11.15 16 11.32	15.88 30 16.01			
	other levels: (2+)15.54; ...							
$_{92}U^{232}_{140}$	47.20 20	3.311 22 3.298	6.801 50 6.813		18.39 12 18.39	19.34 12 19.34		
	other levels: (1−)11.95; (3−)13.35; (0+)14.68; (2+)15.57; (4+)17.65; ...							
$_{92}U^{234}_{142}$	43.5 7	3.31 2 3.31	6.83 4 6.873		21.20 9 21.20	22.18 9 22.17	23.45 11 23.48	25.00 11 25.07
	other levels: (1−)18.3; (0+)18.6; (4+)21.8; (3+)26.4; ...							
$_{94}Pu^{238}_{144}$	44.07 5	3.292 6 3.314	6.889 14 6.898	11.663 30 11.683	23.349 70 23.351	24.302 80 24.304		
	other levels: (1−)13.73; (0+)21.22; (2+)22.35; ...							
$_{98}Cf^{250}_{152}$	42.20 50	3.327 66 3.328			24.50 40 24.49	25.50 50 25.49		
	other levels: ?							

The constants hB and hA are then easily obtained from the knowledge of hC, A/C and B/C. In fig. 4 we give an example (Os^{190}) of the results of such a calculation. The straight segments (3.14) are given for the k value of Os^{190} (-0.32). The points on these lines which give the correct value of R_0 are indicated; they are joined with a straight segment to the points one gets after the centrifugal distortion correction term has been applied (R_b's). No distinction has been made between the experimental points and those given by the R_b's because they are too close together.

5. Comparison of Energy Levels with Experimental Results

The comparison has been done for nuclei with $40 \leqq A \leqq 250$, the references used are given in section 11. There are 30 nuclei for which enough data are available to make a meaningful comparison. We have always used the energy of the ^{12}, ^{22}, ^{14} and one other level to determine the parameters of the rotor. Fourteen of the 30 nuclei have more than four levels known and hence are a good test for the theory. The other 16 cases only tell us if the data are consistent with theory or not.

The fourteen nuclei are: Cd^{110}, Gd^{156}, Gd^{158}, Dy^{160}, Er^{166}, Er^{168}, Hf^{178}, W^{182}, W^{186}, Os^{190}, Th^{232}, U^{232}, U^{234}, and Pu^{238}. As we can see from table 5 the agreement between theory and experiment is within experimental error with the following exceptions:

Cd^{110}: The ^{13} level is not in agreement with the one predicted by the constants determined by the other four levels. The discrepancy is 10 %. The energy of spin 5 level at 2925 keV is close to the predicted energy for the ^{15} rotational level. It is not considered to be the ^{15} rotational state because it has probably negative parity and because if one assumes it is the rotational state, one predicts a very strong $\approx$ 980 keV gamma-ray ($^15 \rightarrow {}^13$) which is not seen (see section 8).

Os^{190}: The ^{16} and ^{18} levels have an energy which differs by 1 % from the one predicted by the constants determined by the other 5 levels. Note that the ^{24} rotational level is the one at 1161 keV and not the one at 954 keV as has previously been suggested.

The parameters with which the theoretical values given in table 5 were calculated are given in table 6. The parameters of Hf^{178} and Th^{232} have been determined on the assumption that $b = 0$ because the position of the ^{13} level is not known.

The sixteen nuclei for which only four levels of the ground state rotational band are known are: Ti^{48}, Cr^{52}, Fe^{56}, Kr^{82}, Ba^{134}, Nd^{144}, Sm^{152}, Gd^{154}, Yb^{170}, W^{184}, Os^{186}, Os^{192}, Pt^{192}, Hg^{198}, Th^{228}, and Cf^{250}. Their levels are consistent with a set of parameters for the rotor (see tables 4 and 5) with the exception of Kr^{82}, in which, if one assumes that the level ^{13} is the one at 2094 keV, one cannot get a set of parameters for the rotor which would have the level at 1821 keV as the ^{14} level;

Pt^{192}, in which the relation between the energies of the ^{12}, ^{22} and ^{13} levels agrees very well with the rotor model, (see table 3), but the position of the ^{14} level seems to be inconsistent with the rotational picture;

Cr^{52}, which is a closed shell nucleus for which the rotational picture with small perturbations due to the other degrees of freedom of the nucleus does not hold.

TABLE 6

Rotor parameters determined by the measured energy levels. Values of the parameters k, A/C, $\hbar C$, $\hbar B$, $\hbar A$, $\varepsilon_0(^12)$ and $b\varepsilon_0(^12)$ which give the best fit to the measured energy levels (table 5) of the nuclei given in the first column

Nucleus	k	A/C	$\hbar C$ keV	$\hbar B$ keV	$\hbar A$ keV	$\varepsilon_0(^12)$	$b\varepsilon_0(^12)$ %
Ti^{48}	−0.15	9.300	69.88	316.4	649.9	15.22	7.3
Fe^{56}	−0.08	17.17	33.93	286.3	582.5	25.18	1.1
Cd^{110}	0.40	7.490	41.54	230.3	311.1	16.53	4.4
Ba^{134}	0.20	4.855	56.72	187.9	275.4	11.61	8.3
Nd^{144}	1.00	23.00	15.42	354.6	354.6	50.00	9.7
Sm^{152}	−0.69	78.00	2.981	38.56	232.5	40.31	−1.4
Gd^{154}	−0.71	47.59	4.814	37.33	229.1	25.48	−0.46
Gd^{156}	−0.88	39.44	6.931	22.91	273.3	12.81	−0.20
Gd^{158}	−0.94	33.18	8.984	17.66	298.1	8.874	0.20
Dy^{160}	−0.91	25.61	9.357	19.72	239.6	9.284	0.20
Er^{166}	−0.96	17.14	11.62	15.37	199.2	6.964	0.44
Er^{168}	−0.98	16.60	12.39	14.33	205.7	6.467	0.30
Yb^{170}	−0.96	28.45	11.05	17.12	314.5	7.639	0.28
Hf^{178}	−0.93	39.00	9.357	21.76	364.9	9.954	0
W^{182}	−0.89	30.78	9.192	24.25	282.9	10.84	−0.38
W^{184}	−0.93	15.15	14.95	22.35	226.4	7.472	0.49
W^{186}	−0.95	9.404	18.51	22.40	174.1	6.626	0.17
Os^{186}	−0.48	20.69	6.309	38.61	130.5	20.23	−7.4
Os^{190}	−0.32	7.691	15.24	49.92	117.2	12.15	−0.84
Os^{192}	−0.12	5.445	18.65	55.11	101.5	11.08	0.45
Hg^{198}	0	10.55	23.56	136.1	248.6	18.11	3.5
Th^{228}	−0.91	57.67	4.245	15.07	244.8	13.56	0.17
Th^{232}	−0.93	39.00	4.998	11.62	194.9	9.954	0
U^{232}	−0.95	41.82	5.227	10.56	218.6	9.042	0.13
U^{234}	−0.96	46.00	5.011	9.522	230.5	8.686	0.071
Pu^{238}	−0.97	47.63	5.453	9.267	259.7	8.090	0.10
Cf^{250}	−0.98	44.00	5.791	8.282	254.8	7.287	0

In fig. 5 we show the ratios $R_0(^12)$, $R_0(^14)$, $R_0(^16)$, $R_0(^18)$ as a function of the ratio $R_0(^14)$ (full lines) for various values of k. The experimental trends [12]) of the ratios $R_e(^18)$ and $R_e(^16)$ as a function of $R_e(^14)$ are also shown (dashed lines). The dotted lines join the experimental points (theoretical with rotational-vibrational interaction taken into account) with the theoretical points without rotational-vibrational interaction taken into account. As one can see, the empirical curve can be explained for values of $R_e(^14) \geqq 1.8$. Nuclei which have $R_e(^14) \leqq 1.8$ are closed shell nuclei and require a very large perturbation of the

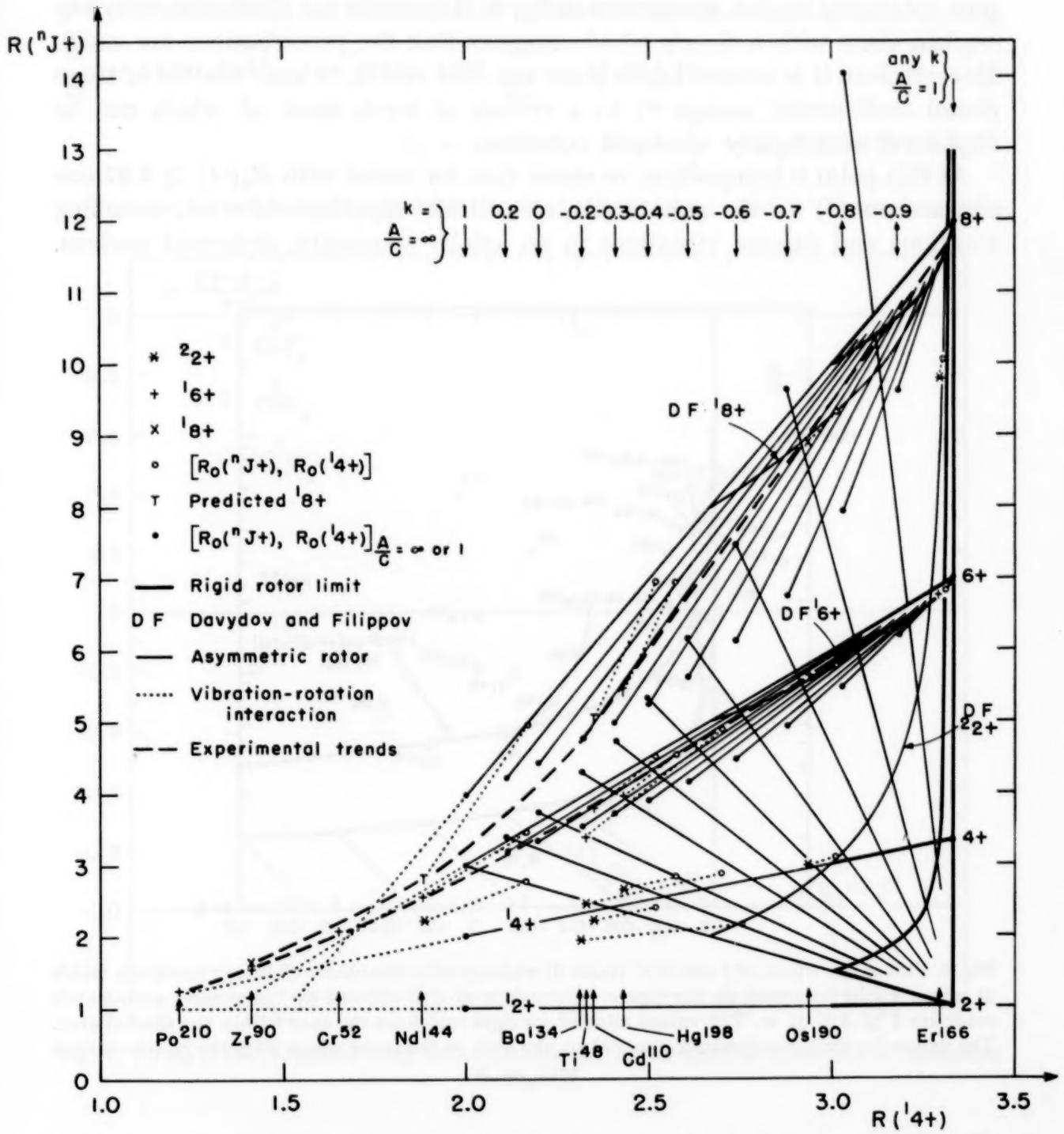

Fig. 5. The figure shows the ratios $R_0(^8)$, $R_0(^6)$, $R_0(^4)$, $R_0(^2)$ and $R_0(^2)$ as a function of the ratio $R_0(^4)$ (full lines) for various values of k. Each straight segment corresponds to a different k value. The heavy full dots at the extreme of the segments are given by $A/C = \infty$ or 1 and k values which are indicated in the upper part of the figure. Davydov and Filippov curves for the ratios and the regions to which rigid rotors are limited (heavy full lines) are also indicated. The experimental trends of $R_e(^8)$ and $R_e(^6)$ as a function of $R_e(^4)$ are also shown (dashed lines). The dotted lines represent $R_b(^nJ)$ as a function of $R_b(^4)$ for particularly interesting values of $R_0(^nJ)$ and $R_0(^4)$. The dotted lines which end at experimental ratios for ^{8}, ^{6}, ^{2} levels start at the R_0 values with which one is able to explain the observed spectrum of the nucleus indicated in the lower part of the figure.

pure rotational motion as one sees in fig. 5. Hence it is not reasonable to try to explain these with a theory which assumes that the perturbations are small. Nevertheless, it is interesting to point out that the $^{1}4$, $^{1}6$ and $^{1}8$ levels of these closed shell nuclei pertain [12]) to a system of levels most of which can be explained with nearly adiabatic rotations.

At this point it is important to stress that for nuclei with $R_e(^{1}4) \geqq 3.27$ one can account [12]) for the same levels, also within experimental error, assuming rotations and gamma vibrations in an axially symmetric deformed nucleus.

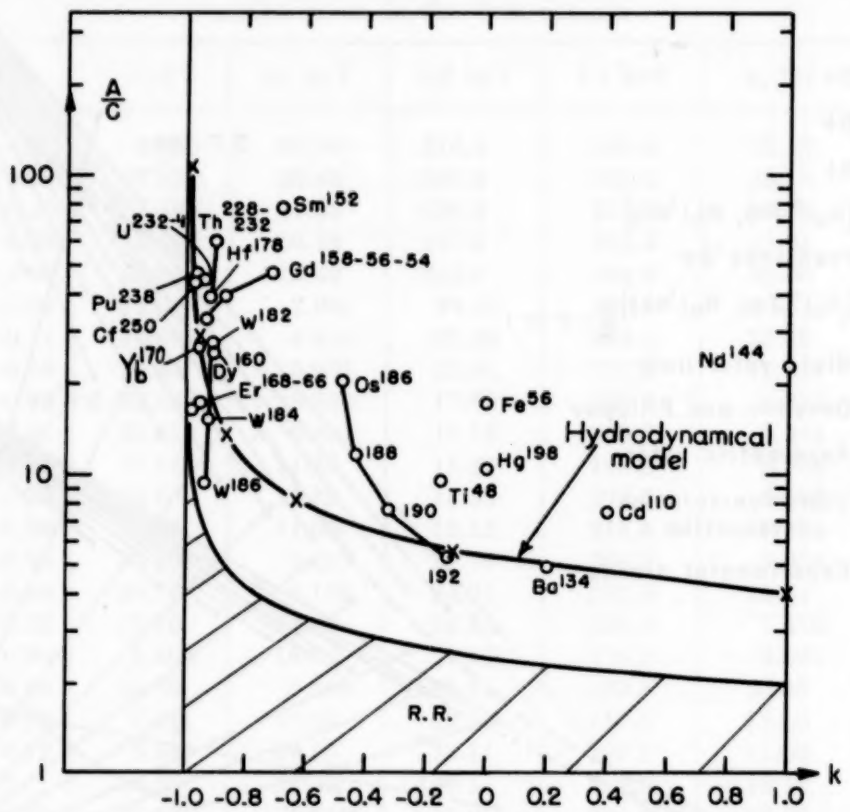

Fig. 6. Plot of the values of k and A/C (table 6) which predict the observed energy spectrum (table 5) of the nuclei indicated on the figure. The values of A/C allowed by the general asymmetric rotor are $1 \leqq A/C \leqq \infty$. The values allowed for rigid rotors are the ones within the shaded area. The values for the hydrodynamical model are the ones on the curve which joins the points marked with an X.

As is well known, the $^{1}2$, $^{1}4$, $^{1}6$, $^{1}8$, levels are then interpreted as a ground state rotational band and the $^{1}3$, $^{2}4$, $^{1}5$, . . . levels are explained as a rotational band based on the $^{2}2$ gamma vibrational state. However, the number of parameters needed is five as compared to four in the present asymmetric rotor picture. The five parameters are: the moment of inertia and vibration-rotation interaction parameter for the ground state rotational band and for the rotational band based on the gamma-vibrational state (4 parameters) plus the gamma vibrational frequency to get the energy of the $^{2}2$ state $\hbar\omega_\gamma + \hbar^2/I = E(^{2}2)$. An exam-

ple of this is Er^{166} for which the five parameters are

$$\frac{\hbar^2}{2I} = 13.50 \text{ keV}, \quad b = 8.35\times10^{-4}, \frac{\hbar^2}{2I_\gamma} = 12.32 \text{ keV},$$

$$b_\gamma = 1\times10^{-4}, \quad \hbar\omega_\gamma + \frac{\hbar^2}{I} = E_e(^22) = 787.4 \text{ keV}.$$

For nuclei with $R_e(^14) \geqq 2.67$ the hydrodynamical model [3, 4]) explains the

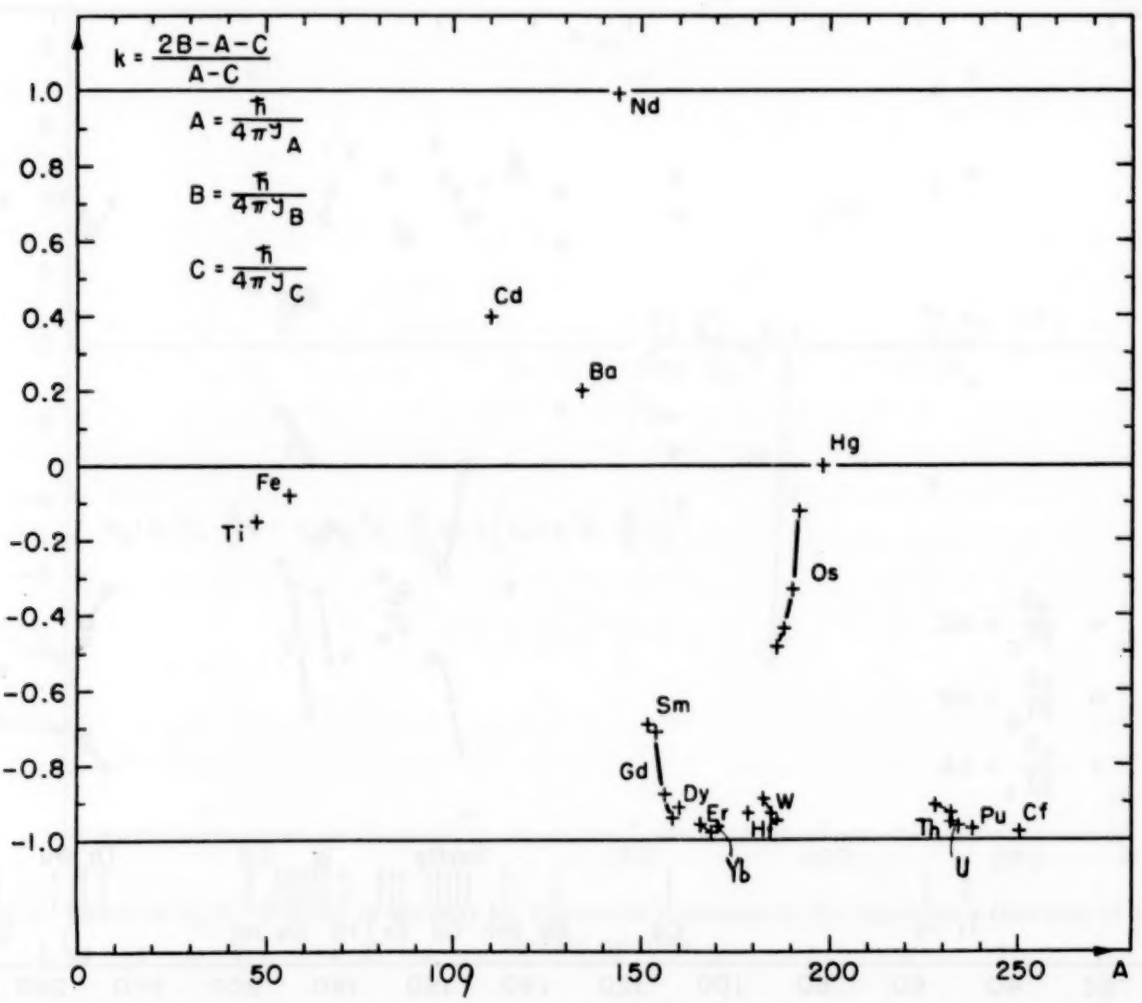

Fig. 7. Values of the parameter k for the nuclei indicated in the figure as a function of the atomic number A.

data on energy levels within experimental errors with a few exceptions [7]). This model has only three parameters (β, γ, b) because of the relation among the three moments of inertia (see eq. (3.4)). The quasi-adiabatic general asymmetry rotor has one parameter more but is capable of explaining the exceptions to the hydrodynamical model and also levels in nuclei out of the region of applicability of the hydrodynamical model $R_e(^14) \leqq 2.67$.

In order to see how the parameters A/C and k obtained for nuclei assuming they are asymmetric rotors compare with those predicted by the rigid rotor

model and by the hydrodynamical model [3,4]) we have given a plot of A/C as a function of k in fig. 6. It is interesting to note that most of the nuclei have effective moments of inertia which do not lie between the rigid rotor limit and the hydrodynamical values. They are closer to the hydrodynamical model than to the rigid rotor.

The behaviour of k, the three effective moments of inertia and the centrifugal

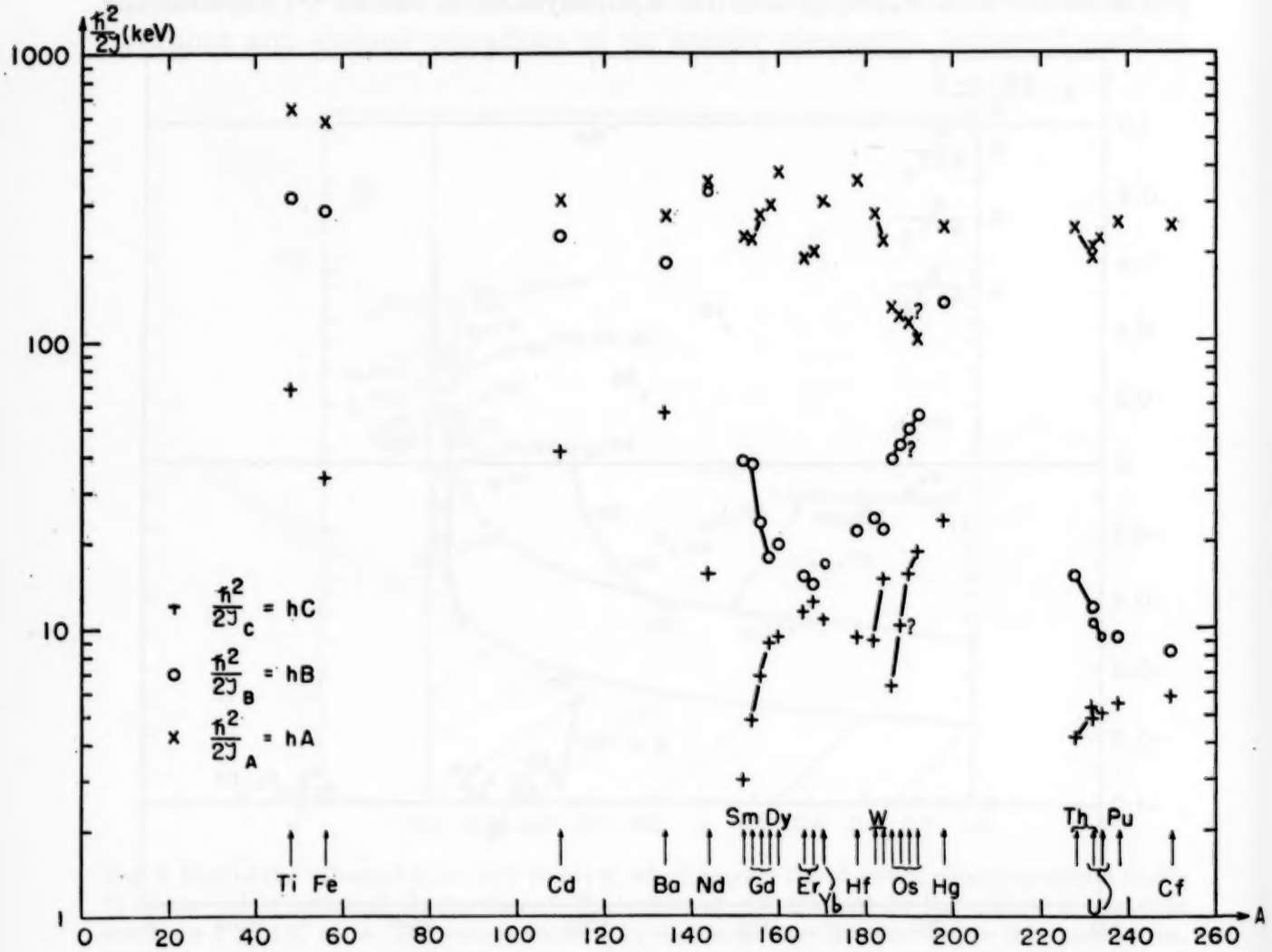

Fig. 8. Value of hC, hB and hA in keV for the nuclei indicated in the lower part of the figure as a function of the atomic number A.

distortion correction to the energy of the first excited state as a function of A are given in figs. 7, 8, and 9. In fig. 8 one clearly sees the regions in which the approximations $hB \equiv hC$ and $hA \approx \infty$ of Bohr and Mottelson are valid. Fig. 9 clearly points out the fact that the perturbations of the rotor are larger close to closed shells.

The existence of levels not belonging to the ground state rotational band (see table 4) clearly points to the existence of other degrees of freedom in the nucleus (vibrations, particle excitations, etc.). The lack of a detailed treatment

of the interaction of these levels with the rotational levels may be the cause for some of the disagreement we found, especially in cases like Os^{190}, Sm^{152}, or nuclei close to closed shells in which non-rotational levels are known to exist between the rotational levels.

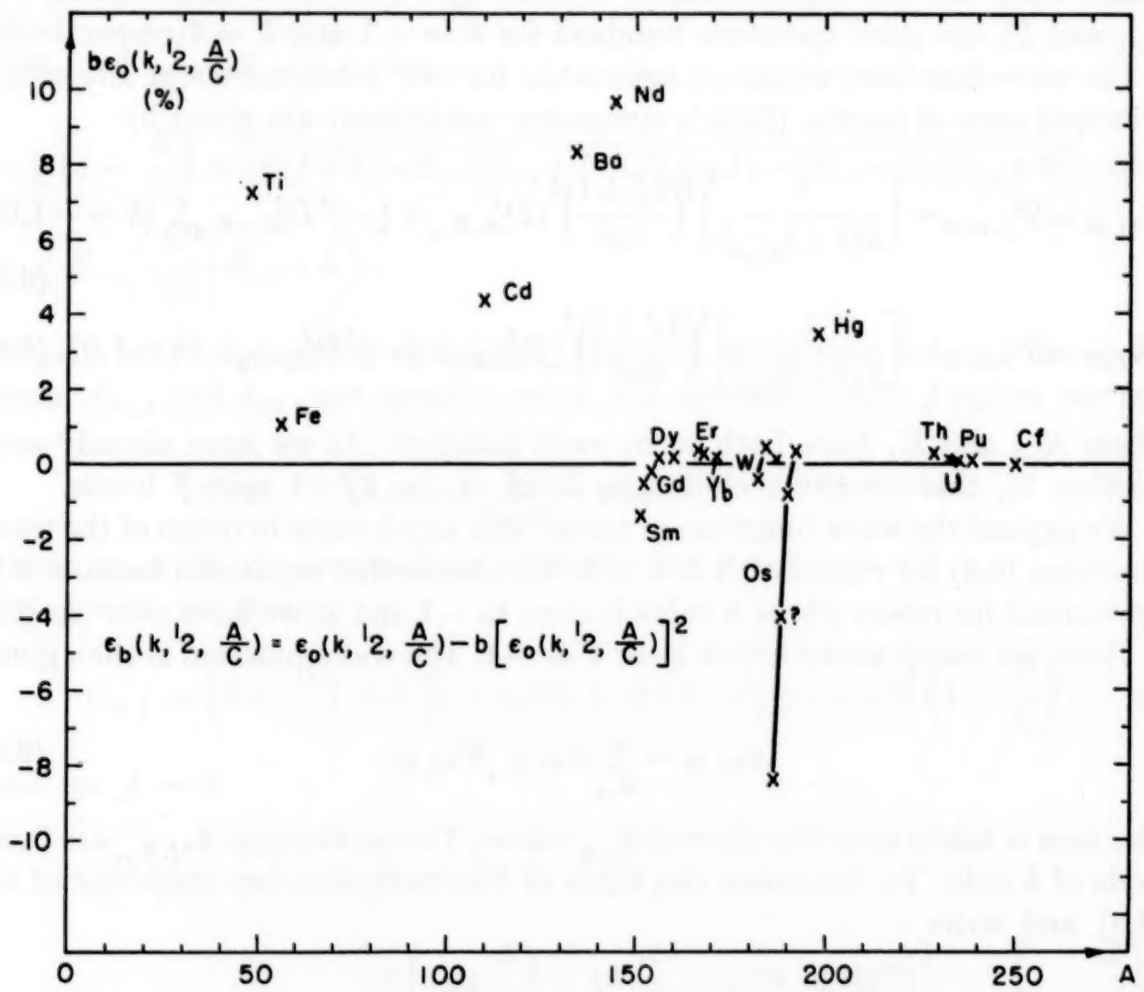

Fig. 9. Value of $b\epsilon_0(k, {}^12, A/C)$ in percent for the nuclei indicated in the figure as a function of the atomic number.

6. Rotational Wave Functions

We should now like to calculate the gamma-ray transition probabilities. In order to do this we have to know the rotational wave functions. As is well known, the wave functions for either a $k = -1$ or a $k = 1$ rotor form a complete set of functions. They are given by

$$\Psi_{J,\tau,M} = \Psi_{J,K_{-1}-K_1,M} = \left(\frac{2J+1}{8\pi^2}\right)^{\frac{1}{2}} D^J_{M,K_{-1}}, \quad (k = -1.0), \tag{6.1}$$

$$\Psi_{J,\tau,M} = \Psi_{J,K_{-1}-K_1,M} = \left(\frac{2J+1}{8\pi^2}\right)^{\frac{1}{2}} D^J_{M,K_1}, \quad (k = 1.0), \tag{6.2}$$

for a state characterized by $\tau = K_{-1} - K_1$, the total angular momentum J, and its projection M on a fixed axis (z axis). K_{-1} and K_1 have been defined in section 3. The D^J_{MK} are functions of the Euler angles specifying the orientation of the principal axes of inertia with respect to a coordinate system fixed in space. They are the representation of rank $2J+1$ of the rotation group [21]). K_{-1} and K_1 are good quantum numbers for $k = -1$ and $k = 1$ respectively.

The wave functions which are symmetric for 180° rotations about any of the principal axes of inertia (Bohr's symmetry conditions) are given by

$$\Psi_{nJ,M} = \Psi_{J,\tau,M} = \left[\frac{1}{2(1+\delta_{K_{-1}0})}\right]^{\frac{1}{2}} \left(\frac{2J+1}{8\pi^2}\right)^{\frac{1}{2}} [D^J_{M,K_{-1}} + (-)^J D^J_{M,-K_{-1}}], \quad (k=-1.0), \tag{6.3}$$

$$\Psi_{nJ,M} = \Psi_{J,\tau,M} = \left[\frac{1}{2(1+\delta_{K_1 0})}\right]^{\frac{1}{2}} \left(\frac{2J+1}{8\pi^2}\right)^{\frac{1}{2}} [D^J_{M,K_1} + (-)^J D^J_{M,-K_1}], \quad (k=1.0), \tag{6.4}$$

where K_{-1} and K_1 have both to be even numbers. As we have already seen (section 3), this condition eliminates some of the $2J+1$ spin J levels.

We expand the wave functions of rotors with any k value in terms of the wave functions (6.3) for rotors with $k = -1$. We choose this expansion because it is convenient for rotors whose k value is close to -1 and as we have seen (section 5) there are many nuclei which have $k \approx -1$. The wave function is then given by

$$\psi_{nJ,M} = \sum_{K_{-1}} A_{nJ,K_{-1}} \Psi_{nJ,M}. \tag{6.5}$$

The sum is taken over the allowed K_{-1} values. The coefficients $A_{nJ,K_{-1}}$ are functions of k only. To determine the value of the coefficients we make use of eq. (3.8) and write

$$\left\langle D^J_{M,K_{-1}} \left| \frac{H^R}{hC} \right| \psi_{nJ,M} \right\rangle - \varepsilon_0 \left({}^nJ, k, \frac{A}{C}\right) \langle D^J_{M,K_{-1}} | 1 | \psi_{nJ,M} \rangle = 0. \tag{6.6}$$

This gives us a homogeneous algebraic equation for each value of K_{-1}. These equations, together with the normalization equation

$$\sum A^2_{nJ,K_{-1}} = 1$$

are enough to determine the coefficients

$$A_{nJ,K_{-1}}.$$

We use the value of ε_0 given by (3.13) and remember that

$$\left\langle \left(\frac{2J+1}{8\pi^2}\right)^{\frac{1}{2}} D^J_{M,K_{-1}} \left| \frac{H^R}{hC} \right| \left(\frac{2J'+1}{8\pi^2}\right)^{\frac{1}{2}} D^{J'}_{M',K'_{-1}} \right\rangle = \delta_{JJ'}\delta_{MM'} \left\langle K_{-1} \left| \frac{H^R}{hC} \right| K'_{-1} \right\rangle, \tag{6.7}$$

in which the only matrix elements which are different from zero are the following ones:

$$\left\langle K_{-1}\left|\frac{H^{\mathrm{R}}}{hC}\right|K_{-1}\right\rangle = \tfrac{1}{2}\left(1+\frac{B}{C}\right)J(J+1)+\left(\frac{A}{C}-\tfrac{1}{2}\frac{B}{C}-\tfrac{1}{2}\right)K_{-1}^2, \quad (6.8)$$

$$\left\langle K_{-1}+2\left|\frac{H^{\mathrm{R}}}{hC}\right|K_{-1}\right\rangle$$

$$= \tfrac{1}{4}\left(1-\frac{B}{C}\right)\sqrt{[J(J+1)-K_{-1}(K_{-1}+1)][J(J+1)-(K_{-1}+1)(K_{-1}+2)]} \quad (6.9)$$

$$= \left\langle K_{-1}\left|\frac{H^{\mathrm{R}}}{hC}\right|K_{-1}+2\right\rangle.$$

There is only one possible value of K_{-1} for spin 0 and spin 3, hence the coefficients $A_{10,0}$ and $A_{13,2}$ are equal to unity. For other even spin J values one gets

$$A_{nJ,K_{-1}} = C_{n,\frac{1}{2}K_{-1}+1}\Big(\sum_{K_{-1}=0}^{J} C^2_{n,\frac{1}{2}K_{-1}+1}\Big)^{-\frac{1}{2}}, \quad (J=\text{even}), \quad (6.10)$$

where we write the expressions explicitly for $J = 2$ and 4.
For $J = 2$, we have

$$C_{n,1} = \left(1+\frac{B}{C}\right)+4\frac{A}{C}-\varepsilon_0({}^n2, k, A/C),\ C_{n,2}=-\sqrt{3}\left(1-\frac{B}{C}\right),$$

and for $J = 4$

$$C_{n,1} = \left[8\left(1+\frac{B}{C}\right)+4\frac{A}{C}-\varepsilon_0({}^n4, k, A/C)\right]$$

$$\left[2\left(1+\frac{B}{C}\right)+16\frac{A}{C}-\varepsilon_0({}^n4, k, A/C)\right]-7\left(1-\frac{B}{C}\right)^2,$$

$$C_{n,2} = -3\sqrt{5}\left(1-\frac{B}{C}\right)\left[2\left(1+\frac{B}{C}\right)+16\frac{A}{C}-\varepsilon_0({}^n4, k, A/C)\right],$$

$$C_{n,3} = 3\sqrt{35}\left(1-\frac{B}{C}\right)^2.$$

The coefficients for odd spin J values are given by

$$A_{nJ,K_{-1}} = C_{n,\frac{1}{2}K_{-1}}\Big(\sum_{K_{-1}=2}^{J-1} C^2_{n,\frac{1}{2}K_{-1}}\Big)^{-\frac{1}{2}}, \quad (J=\text{odd}), \quad (6.11)$$

where we write the expression explicitly for $J = 5$:

$$C_{n,1} = 7\left(1+\frac{B}{C}\right)+16\frac{A}{C}-\varepsilon_0\left({}^n5, k, \frac{A}{C}\right),\quad C_{n,2} = -3\sqrt{3}\left(1-\frac{B}{C}\right).$$

The values of the $A_{\nu_{J,K_{-1}}}$ coefficients have been calculated [22]) as a function of k for the ^{12}, ^{14}, ^{24}, ^{16} levels. Those for the ^{15} and ^{22} states are related to those of the ^{12} state by

$$A_{1_{2,0}} = A_{2_{2,2}} = A_{1_{5,2}}, \tag{6.12}$$

$$A_{1_{2,2}} = -A_{2_{2,0}} = A_{1_{5,4}}. \tag{6.13}$$

7. Selection Rules for Gamma-Ray Transitions

The probability per unit time T for a gamma-ray transition of either electric or magnetic 2^l pole radiation from a state of spin J to one of spin J' is given by

$$T(Ml, J \to J') = \frac{8\pi(l+1)}{l[(2l+1)!!]^2} \frac{1}{\hbar} \left(\frac{E}{\hbar c}\right)^{2l+1} B(Ml, J \to J'), \tag{7.1}$$

where E is the energy difference between the initial and the final state, and $B(Ml, J \to J')$ is the reduced transition probability. The latter is given by

$$B(Ml, J \to J') = \sum_{M',\mu} |\langle JM|M(l,\mu)|J'M'\rangle|^2, \tag{7.2}$$

where $M(l, \mu)$ is the multipole operator which is referred to the space-fixed coordinate system. To refer it to the body-fixed coordinate system we recall that the multipole operator is a Racah tensor and hence that

$$M(l,\mu) = \sum_{\xi} D^l_{\mu\xi} M'(l,\xi), \tag{7.3}$$

where $M'(l, \xi)$ is referred to the body-fixed coordinate system. The reduced transition probabilities are then given by

$$B(Ml, J \to J') = \sum_{M'\mu} |\langle JM| \sum_{\xi} D^l_{\mu\xi} M'(l,\xi)|J'M'\rangle|^2. \tag{7.4}$$

The normal gamma-ray selection rules forbid the E1, E3, ... M2, M4, ... transitions because the states of the rotor all have the same parity. The Ml gamma-ray transitions are forbidden because in (7.4) the rotational matrix elements are zero. This is true for $\xi = \pm 1$ because one cannot connect $D^J_{M,K_{-1}}$ functions which have all even values of K_{-1}. For $\xi = 0$ and $K'_{-1} > 0$ the rotational matrix element is proportional to

$$D^J_{M'+\mu,K'_{-1}} D^1_{\mu,0} D^{J'}_{M',K'_{-1}} + (-)^{J+J'} D^J_{M'+\mu,-K'_{-1}} D^1_{\mu 0} D^{J'}_{M',-K'_{-1}},$$

which in turn is proportional to $1+(-)^{J+J'+J+J'+1}$ which is zero. For $\xi = 0$ and $K'_{-1} = 0$ the rotational matrix element is proportional to

$$[1+(-)^J] D^J_{M'+\mu,0} D^1_{\mu,0} D^{J'}_{M',0} [1+(-)^{J'}],$$

which is zero for $J = J' \pm 1$ because one of the J values is odd, and is proportional to $C(J', 1, J'; 0, 0, 0)$ when $J = J'$ and this Clebsch-Gordan coefficient

is zero. We are left then with the E2, M3, E4, M5, ... allowed gamma-ray transitions of which we are going to consider only the E2 transitions because the other transitions are too slow to compete favourably. Before doing this we should like to see if the experimental results are in agreement with the additional selection rule for M1 transitions. The $^22 \rightarrow {}^12$ transition is the only one for which there are enough empirical data on the E2, M1 admixture to make comparisons meaningful. In table 7 we give all the nuclei for which the % E2

TABLE 7

Percent E2 admixture and energy of the $^22 \rightarrow {}^12$ gamma-ray transition. References for the data used are given in section 11

Nucleus	(% E2)	E_γ(keV)
Fe^{56}	0.4— 2.5	1812
Fe^{58}	84 ± 6	857
Ni^{60}	≧90	827
Zn^{66}	84	732
Ge^{72}	≧95	631
Se^{76}	97 ± 2	660
Kr^{84}	99.9	1008
Zr^{92}	<0.2	896
Ru^{102}	99	630
Pd^{106}	99.5	618
Sn^{116}	92^{+3}_{-12}	818
Te^{122}	92.4± 1.4	693
Te^{124}	50 ±40	723
Te^{126}	97.6± 1.7	753
Xe^{126}	>99	480
Xe^{128}	97.6	540
Ba^{134}	94	562
Ce^{140}	0.1— 1.0	944
Sm^{152}	98.3± 1.1	965
Dy^{160}	96.5± 3.5	879
W^{184}	100	904
Os^{186}	99 ± 1	631
Os^{188}	99.6± 0.4	478
Os^{190}	98	370
Pt^{192}	97.6± 1.0	296
Pt^{194}	99.9	293
Pt^{196}	95.8± 0.5	331
Hg^{198}	60 ± 6	676
Po^{214}	≦50	769

admixture in the $^22 \rightarrow {}^12$ gamma ray has been measured, together with the gamma ray energy. In fig. 9 we have plotted the ratio of the reduced M1 transition probability to the reduced E2 transition probability in cm^{-2} together with the single particle estimate for the same ratio. The latter is given by

$$\left[\frac{B(\mathrm{M1})}{B(\mathrm{E2})}\right]_{\mathrm{s.p.}} \approx 2\times 10^{-25} A^{-4/3}\ \mathrm{cm}^{-2}.$$

It is evident from fig. 10 that most of the transitions have a ratio which is at least 100 times smaller than the single particle estimate. The exceptions are the closed shell nuclei Zr^{92} and Ce^{140} together with Fe^{56}, Te^{124}, Hg^{198}, and Po^{214}.

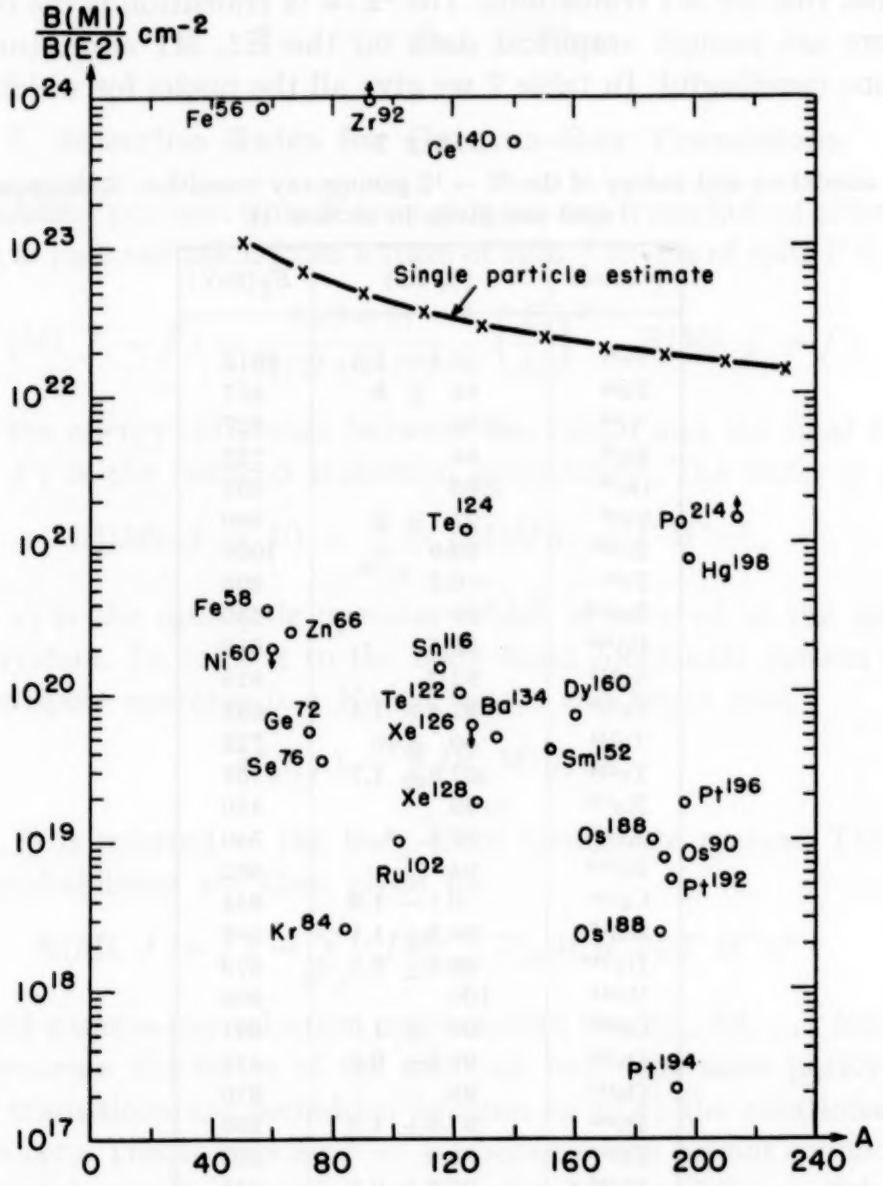

Fig. 10. Ratio of the reduced magnetic dipole (M1) gamma-ray transition probability to the reduced electric quadrupole (E2) gamma-ray transition probability of the $^{2}2 \rightarrow {}^{1}2$ transition in the nuclei indicated in the figure. The full curve is the single particle estimate for that same quantity.

In table 8 we give the reduced M1 transition probabilities in those nuclei in which enough data are available to compute it. One sees that the transitions are slower than the single particle estimate by a factor of at least 100. We may conclude that the empirical data are in agreement with the additional selection rule which forbids M1 transitions.

TABLE 8

Reduced M1 gamma-ray transition probabilities. References for the data used are given in section 11

Nucleus	$\frac{B(\mathrm{M1};\,^2 2 \to {}^1 2)}{e^2}$ (cm^2)
Se^{76}	2.4×10^{-30}
Ru^{102}	6.3×10^{-31}
Te^{122}	3.8×10^{-29}
Sm^{152}	1.2×10^{-30}
Os^{188}	2.6×10^{-31}
Os^{190}	1.7×10^{-30}
Pt^{194}	5.1×10^{-32}
single particle estimate	$\approx 6\times10^{-28}$

8. E2 Gamma-Ray Transition Probabilities

We need to evaluate the reduced transition probabilities given by eq. (7.4) in order to be able to calculate the gamma-ray transition probabilities given by eq. (7.1). We shall not take into account the rotational-vibrational interaction in transition probability calculations. The E2 multipole operator is given by

$$M'(2,\xi) = e\sum_{i=1}^{q} r_i'^2 Y_{2\xi}(\theta'_i, \varphi'_i), \tag{8.1}$$

where q is the number of charges which participate in the motion, e is the elementary charge, and r', θ', φ', is a spherical coordinate system fixed to the rotating body. It is related to the x', y', z', coordinate system by

$$x' = r' \sin\theta' \cos\varphi', \qquad y' = r' \sin\theta' \sin\varphi', \qquad z' = r' \cos\theta'.$$

The x', y', z' axes have been chosen in such a way as to have the following relation to the principal axes of inertia of the rotor

$$z' \to \mathrm{A}, \quad y' \to \mathrm{B}, \quad x' \to \mathrm{C}.$$

The matrix elements are given by

$$\langle JM|M(2,\mu)|J'M'\rangle = e\sum_{\xi}\langle\psi_{nJ,M}|D^2_{\mu\xi}|\psi_{mJ',M'}\rangle\langle\phi|\sum_{i=1}^{q} r_i'^2 Y_{2\xi}|\phi\rangle$$

$$= e[\langle\psi_{nJ,M}|D^2_{\mu 0}|\psi_{mJ',M'}\rangle k_0 + \langle\psi_{nJ,M}|D^2_{\mu 2}+D^2_{\mu -2}|\psi_{mJ',M}\rangle k_2], \tag{8.2}$$

where

$$k_0 = \left\langle \phi \left| \sum_{i=1}^{q} r_i'^2 Y_{20} \right| \phi \right\rangle = \left\langle \phi \left| \sum_{i=1}^{q} \sqrt{\frac{5}{16\pi}}\,(3z_i'^2 - r_i'^2) \right| \phi \right\rangle, \tag{8.3}$$

and

$$k_2 = \left\langle \phi \left| \sum_{i=1}^{q} \tfrac{1}{2} r_i'^2 (Y_{22}+Y_{2-2}) \right| \phi \right\rangle = \left\langle \phi \left| \sum_{i=1}^{q} \sqrt{\frac{15}{32\pi}} (x_i'^2 - y_i'^2) \right| \phi \right\rangle . \quad (8.4)$$

The matrix elements with $\xi = 1$ and -1 in eq. (8.4) are zero because the rotational wave functions have only even values of K_{-1} in the $D^J_{M,K_{-1}}$ functions. The terms of the multipole operator with $\xi = 2$ and -2 can be written in the following way:

$$(D^2_{\mu 2}+D^2_{\mu -2}) \sum_{i=1}^{q} \tfrac{1}{2} r_i'^2 (Y_{22}+Y_{2-2}) + (D^2_{\mu 2}-D^2_{\mu -2}) \sum_{i=1}^{q} \tfrac{1}{2} r_i'^2 (Y_{22}-Y_{2-2}). \quad (8.5)$$

The matrix element due to the term in $D^2_{\mu 2}-D^2_{\mu -2}$ is zero because of the properties of the rotational wave functions and the D^J_{MK} functions. The parameters k_0 and k_2 can be called effective quadrupole moments because they are related to the components of the quadrupole tensor

$$Q_\mu = \left(\frac{16\pi}{5}\right)^{\frac{1}{2}} \sum_{i=1}^{q} \langle \phi | r_i'^2 Y^*_{2\mu} | \phi \rangle \quad (8.6)$$

by the following relations:

$$k_0 = \left(\frac{5}{16\pi}\right)^{\frac{1}{2}} Q_0 , \quad (8.7)$$

$$k_2 = \left(\frac{5}{16\pi}\right)^{\frac{1}{2}} \tfrac{1}{2} (Q_2+Q_{-2}). \quad (8.8)$$

The reduced gamma-ray transition probabilities in units of $e^2 k_0^2$ are given by

$$\frac{B(\mathrm{E2}; {}^nJ \to {}^mJ')}{e^2 k_0^2} = b(\mathrm{E2}; {}^nJ \to {}^mJ')$$

$$= \sum_{\mu M'} |\langle \psi_{nJ,M} | D^2_{\mu 0} | \psi_{mJ'M'} \rangle + \frac{r}{\sqrt{2}} \langle \psi_{nJM} | D^2_{\mu 2} + D^2_{\mu -2} | \psi_{mJ',M'} \rangle|^2, \quad (8.9)$$

where

$$r = \frac{k_2 \sqrt{2}}{k_0} . \quad (8.10)$$

The evaluation of the matrix elements in (8.9) is straightforward. We give the explicit expression for the reduced transition probabilities in units of $e^2 k_0^2$ of gamma-ray transitions connecting states which have been observed experimentally. They are

$$b(\mathrm{E2}; {}^n2 \to {}^1 0) = \tfrac{1}{5} b(\mathrm{E2}; {}^1 0 \to {}^n 2) = \tfrac{1}{5} (A_{n_2,0} + r A_{n_2,2})^2, \quad (8.11)$$

$$b(\mathrm{E2}; {}^n2 \to {}^m2) = b(\mathrm{E2}; {}^m2 \to {}^n2) = \tfrac{2}{7} [2 A_{1_2,0} A_{1_2,2} + r (A^2_{1_2,0} - A^2_{1_2,2})]^2, \quad (8.12)$$

$$b(\mathrm{E2};\,{}^{1}3 \to {}^{n}2) = \tfrac{5}{7}b(\mathrm{E2};\,{}^{n}2 \to {}^{1}3) = \tfrac{5}{14}(A_{n_2,2} - rA_{n_2,0})^2, \tag{8.13}$$

$$b(\mathrm{E2};\,{}^{n}4 \to {}^{m}2) = \tfrac{5}{9}b(\mathrm{E2};\,{}^{m}2 \to {}^{n}4) = \tfrac{1}{126}[(6A_{n_4,0}A_{m_2,0} + \sqrt{15}A_{n_4,2}A_{m_2,2}) + r(A_{m_2,0}A_{n_4,2}\sqrt{15} + A_{m_2,2}A_{n_4,4}\sqrt{35} + A_{m_2,2}A_{n_4,0})]^2, \tag{8.14}$$

$$b(\mathrm{E2};\,{}^{n}4 \to {}^{1}3) = \tfrac{7}{9}b(\mathrm{E2};\,{}^{1}3 \to {}^{n}4) = \tfrac{1}{45}[2\sqrt{3}A_{n_4,2} + r(\sqrt{5}A_{n_4,0} - \sqrt{7}A_{n_4,4})]^2, \tag{8.15}$$

$$b(\mathrm{E2};\,{}^{n}4 \to {}^{m}4) = b(\mathrm{E2};\,{}^{m}4 \to {}^{n}4) = \tfrac{1}{385}[14A_{n_4,4}A_{m_4,4} - 4A_{n_4,2}A_{m_4,2} - 10A_{n_4,0}A_{m_4,0} + r(\{A_{n_4,2}A_{m_4,0} + A_{n_4,0}A_{m_4,2}\}3\sqrt{15} + \{A_{n_4,4}A_{m_4,2} + A_{n_4,2}A_{m_4,4}\}\sqrt{21})]^2, \tag{8.16}$$

$$b(\mathrm{E2};\,{}^{n}5 \to {}^{1}3) = \tfrac{7}{11}b(\mathrm{E2};\,{}^{1}3 \to {}^{n}5) = \tfrac{21}{110}(A_{n_5,2} + rA_{n_5,4})^2, \tag{8.17}$$

$$b(\mathrm{E2};\,{}^{n}5 \to {}^{m}4) = \tfrac{9}{11}b(\mathrm{E2};\,{}^{m}4 \to {}^{n}5) = \tfrac{1}{110}[A_{m_4,2}A_{n_5,2}\sqrt{21} + A_{m_4,4}A_{n_5,4}6 - r(A_{m_4,0}A_{n_5,2}\sqrt{35} + A_{m_4,2}A_{n_5,4}\sqrt{21} - A_{m_4,4}A_{n_5,2})]^2, \tag{8.18}$$

$$b(\mathrm{E2};\,{}^{n}5 \to {}^{m}6) = \tfrac{13}{11}b(\mathrm{E2};\,{}^{m}6 \to {}^{n}5) = \tfrac{1}{770}[A_{m_6,2}A_{n_5,2}8\sqrt{2} + A_{m_6,4}A_{n_5,4}8\sqrt{5} + r(A_{m_6,0}A_{n_5,2}2\sqrt{35} + A_{m_6,2}A_{n_5,4}3\sqrt{2} - A_{m_6,4}A_{n_5,2}6\sqrt{5} - A_{m_6,6}A_{n_5,4}\sqrt{110})]^2, \tag{8.19}$$

$$b(\mathrm{E2};\,{}^{n}6 \to {}^{m}4) = \tfrac{9}{13}b(\mathrm{E2};\,{}^{m}4 \to {}^{n}6) = \tfrac{1}{1430}[A_{m_4,0}A_{n_6,0}15\sqrt{2} + A_{m_4,2}A_{n_6,2}4\sqrt{21} + A_{m_4,4}A_{n_6,4}3\sqrt{10} + r(A_{n_6,2}A_{m_4,0}2\sqrt{35} + A_{n_6,4}A_{m_4,2}\sqrt{210} + A_{m_4,2}A_{n_6,0}\sqrt{30} + A_{m_4,4}A_{n_6,6}3\sqrt{55} + A_{m_4,4}A_{n_6,2})]^2. \tag{8.20}$$

It is interesting to note that the reduced transition probabilities turn out to be proportional to $e^2k_0^2$ and functions of k and r only. The following relations hold:

$$b(\mathrm{E2};\,{}^{1}2 \to {}^{1}0) = \tfrac{14}{25}b(\mathrm{E2};\,{}^{1}3 \to {}^{2}2) = \tfrac{110}{105}b(\mathrm{E2};\,{}^{1}5 \to {}^{1}3), \tag{8.21}$$

$$b(\mathrm{E2};\,{}^{2}2 \to {}^{1}0) = \tfrac{14}{25}b(\mathrm{E2};\,{}^{1}3 \to {}^{1}2) = \tfrac{110}{105}b(\mathrm{E2};\,{}^{2}5 \to {}^{1}3). \tag{8.22}$$

They are a consequence of eqs. (6.12), (6.13), (8.13) and (8.17).

In the hydrodynamical model one has

$$k_0 = \frac{3R^2\beta}{4\pi}\cos\gamma, \tag{8.23}$$

$$k_2 = \frac{3R^2\beta}{4\pi}\frac{\sin\gamma}{\sqrt{2}}. \tag{8.24}$$

For a rigid rotor with charge distribution proportional to its mass distribution

(ρ_e/ρ_m = constant) one obtains

$$k_0 = \frac{\rho_e}{\rho_m}\sqrt{\frac{5}{16\pi}}\,(I_B+I_C-2I_A), \tag{8.25}$$

$$k_2 = \frac{\rho_e}{\rho_m}\sqrt{\frac{15}{32\pi}}\,(I_B-I_C). \tag{8.26}$$

Note that r is always positive in the hydrodynamical model and always negative for a rigid rotor.

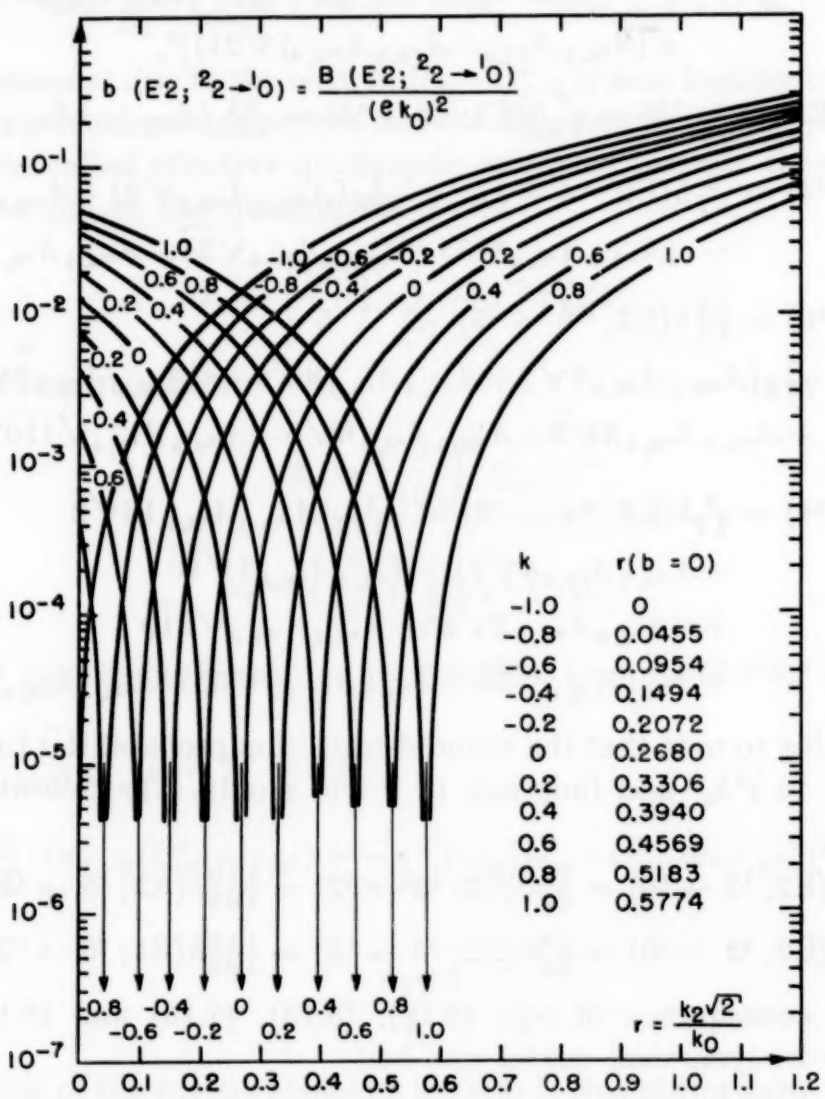

Fig. 11. Plot of the reduced electric quadrupole (E2) transition probabilities in units of $(ek_0)^2$ for the $^22 \rightarrow {}^10$ transition as a function of the ratio of quadrupole moments r for different k values. The inserted table gives the values r for which the E2 reduced transition probability is zero as a function of k. The arrows in the graph indicate the values of r given in the inserted table.

In comparing experimental results with theoretical predictions one needs only one ratio of measured gamma-ray transition probabilities to determine r

assuming that one knows k from the energy level structure. One then predicts all other ratios and is able to compare them with other experimental data. In order to get the effective intrinsic quadrupole moment k_0 one has to know r and one absolute transition probability; k_0 is given by

$$k_0 = \left[\frac{B(\mathrm{E2}; {}^nJ \to {}^mJ')}{e^2 b(\mathrm{E2}; {}^nJ \to {}^mJ')}\right]^{\frac{1}{2}}, \tag{8.27}$$

which is a consequence of eq. (8.9). The effective intrinsic quadrupole moment k_2 is given by

$$k_2 = \frac{r k_0}{\sqrt{2}}. \tag{8.28}$$

Tables of reduced transition probabilities in units of $e^2 k_0^2$ as a function of k and r have been computed [22]). In fig. 11 we give the values of $b(\mathrm{E2}; {}^22 \to {}^10)$ as a function of r for different k values. The table inserted in fig. 11 gives values of (k, r) for which the ${}^22 \to {}^10$ transition is forbidden.

9. Comparison of E2 Gamma-Ray Transition Probabilities with Experiment

The comparison has been made for nuclei with $40 \leqq A \leqq 250$, the references used are given in section 11. Of the 27 nuclei for which we have determined k from the energy level information (section 5) there are 23 for which enough data are known on the gamma-ray transition probabilities to make a meaningful comparison. The nuclei not considered are: Ti^{48}, Gd^{158}, U^{232} and U^{234}. All 23 nuclei have enough data to determine r and then compare at least one predicted ratio of transition probabilities with experimental results. In 17 cases it has been possible to calculate the effective quadrupole moments because of the knowledge of at least one absolute transition probability. In table 9 we give the experimental and theoretical values for the reduced transition probabilities and ratios of gamma-ray transition probabilities (gamma-ray intensities) for the nuclei given in the first column. With the exception of the ${}^22 \to {}^12$ transition of Hg^{198} we have assumed throughout that the gamma-rays are pure E2's. Fe^{56} has not been included because its ${}^22 \to {}^12$ transition is only 2 % E2 and hence violates the selection rules of section 7. The theoretical value is always given below the corresponding experimental value and has been calculated with the k_0 and r values given in table 10.

The agreement of theory with experiment is within experimental errors with the following exceptions:

Ba^{134}, where the ratios $I_\gamma({}^22 \to {}^12)/I_\gamma({}^22 \to {}^10)$ and $I_\gamma({}^24 \to {}^14)/I_\gamma({}^24 \to {}^12)$ disagree by a factor of 3 and 10 respectively;

TABLE

Comparison of experimental E2 gamma-ray transition probabilities with theoretical predictions. The experiment
for the nuclei indicated in column one are given in the first row within each nucleus. The second row gives th
following way 74 6 = 74±6. Referenc

Nucleus	$\frac{B(E2;\,^{12}\rightarrow{}^{10})}{e^2}$ (10^{-50} cm^4)	$\frac{B(E2;\,^{14}\rightarrow{}^{12})}{e^2}$ (10^{-50} cm^4)	$\frac{B(E2;\,^{22}\rightarrow{}^{10})}{e^2}$ (10^{-50} cm^4)	$\frac{I_\gamma(^{22}\rightarrow{}^{12})}{I_\gamma(^{22}\rightarrow{}^{10})}$	$\frac{I_\gamma(^{22}\rightarrow{}^{14})}{I_\gamma(^{22}\rightarrow{}^{10})}$	$\frac{I_\gamma(^{13}\rightarrow{}^{22})}{I_\gamma(^{13}\rightarrow{}^{12})}$	$\frac{I_\gamma(^{13}\rightarrow{}^{14})}{I_\gamma(^{13}\rightarrow{}^{12})}$
Cd^{110}	8.8 10 8.8	12.6	0.50 8 0.52	1.5 5 1.5			
Ba^{134}				4.6 10 1.5			
Nd^{144}		0.75?		47 10 47	0		
Sm^{152}	68.4 38 68.4	113	2.4 4 49	1.1 2 1.1	2.4×10^{-2}	6.2×10^{-5}	(3.6 20)10^{-1} 3.4 $\times10^{-1}$
Gd^{154}	74 6 74	128	92.7	1.0 2 1.0	1.5×10^{-2}	3 $\times10^{-5}$	$\leqq$2.4 $\times10^{-1}$ 1.7 $\times10^{-1}$
Gd^{156}	96.1 38 96.1	135 30 149	94.7	1.1 1 1.1	(5 2)10^{-2} 2.6×10^{-2}	3.6×10^{-6}	(2.2 3)10^{-1} 2.2 $\times10^{-1}$
Dy^{160}	112 10 112	163	9.25	1.3 3 1.3	(4 2)$\times10^{-2}$ 3.6×10^{-2}	5.8×10^{-5}	4 2$\times10^{-1}$ 2.8 $\times10^{-1}$
Er^{166}	115 4 115	250 140 165	3.07	1.1 6 1.1	2.2×10^{-2}	2.8×10^{-4}	(1.9 10)10^{-1} 1.96×10^{-1}
Er^{168}				0.60 15 1.0	1.5×10^{-2}	1.7×10^{-4}	0.35 7 0.15
Yb^{170}	112 3 112	160	4.0	1.45 1.42	4.7×10^{-2}	2.8×10^{-5}	0.33 0.32
Hf^{178}	148 5 148	212	0.34	4.0 8 4.0	0.32 6 0.38		
W^{182}	88 7 88	131	30.2	1.2 1 1.2	2.9×10^{-2}	1.7×10^{-5}	0.17 3 0.23
W^{184}	87.4 90 87.4	126	3.4 10 3.4	0.95 10 1.1	$\approx6.7\times10^{-3}$ 1.7×10^{-2}	1.3×10^{-4}	$\approx$3.3 $\times10^{-1}$ 1.2 $\times10^{-1}$
W^{186}	71 7 71	102	3.5 6 3.5	1.0 2 0.76	3 $\times10^{-3}$	2.5×10^{-3}	$\approx$1.0 1.2 $\times10^{-1}$
Os^{186}	100 100	100 40 160	26	1.3 2 1.3			
Os^{190}	51 5 51	23^{+20}_{-10} 73.8	3.1 10 3.1	0.82 13 0.66	1.7×10^{-7}	(12 3)$\times10^{-2}$ 8.1×10^{-2}	$\leqq$8 $\times10^{-1}$ 4.3 $\times10^{-1}$
Os^{192}	41 4 41	59.4	2.84 6 2.84	0.73 9 0.93		(1.2 3)$\times10^{-1}$ 1.8×10^{-1}	4.5 $\times10^{-1}$
Hg^{198}	26 7 26	36	<2.8 0.7	3.1 3 3.1	1.5×10^{-6}		
Th^{228}	143 11 143	210	20	1.8 3 1.5	7.7×10^{-2} 6.3×10^{-2}	3.8×10^{-6}	3.4 $\times10^{-1}$ 3.8 $\times10^{-1}$
Th^{232}	170 7 170	245	4.36 50 4.36	1.5 2 1.5	6.1×10^{-2}		
Pu^{238}	238 20 238	340	2.09	1.2 2 1.6	(8.4 17)$\times10^{-2}$ 9.4×10^{-2}		(6.6 14)$\times10^{-1}$ 5.3 $\times10^{-1}$
Cf^{250}				1.2 2 1.5	$\lesssim3.9\times10^{-2}$ 3.9×10^{-2}		

a) The ratios quoted are $\frac{I_\gamma(^{24}\rightarrow{}^{12})I_\gamma(^{24}-{}^{13})I_\gamma(^{24}\rightarrow{}^{14})}{I_\gamma(^{24}\rightarrow{}^{22})I_\gamma(^{24}\rightarrow{}^{22})I_\gamma(^{24}\rightarrow{}^{22})}$ and $\frac{I_\gamma(^{24}\rightarrow{}^{16})}{I_\gamma(^{24}\rightarrow{}^{22})}$ in this order. The $I_\gamma(^{24}\rightarrow{}^{12})$ is not known for Os^{19}

values for reduced electric quadrupole (E2) gamma ray transition probabilities and ratios of gamma-ray intensities theoretical values calculated with the values of k, k_0 and r given in table 10. Experimental errors are indicated in the for the data used are given in section 11

$\frac{I_\gamma(^24\to{}^22)}{I_\gamma(^24\to{}^12)}$	$\frac{I_\gamma(^24\to{}^13)}{I_\gamma(^24\to{}^12)}$	$\frac{I_\gamma(^24\to{}^14)}{I_\gamma(^24\to{}^12)}$	$\frac{I_\gamma(^24\to{}^16)}{I_\gamma(^24\to{}^12)}$	$\frac{I_\gamma(^15\to{}^13)}{I_\gamma(^15\to{}^14)}$	$\frac{I_\gamma(^15\to{}^24)}{I_\gamma(^15\to{}^24)}$	$\frac{I_\gamma(^15\to{}^16)}{I_\gamma(^15\to{}^14)}$
3.0 10 2.7	 $\sim 3 \times 10^{-2}$	3.7 15 0.35				
 3.9×10^{-10}	$(1.0\ 5)10^{-1}$ 5.1×10^{-4}	2.6 8 3.0	 7.7×10^{-2}			
$(1.6\ 8)\times10^{-2}$ 1.37×10^{-2}	 1.79×10^{-3}	1.8 9 1.46	 2.9×10^{-2}	 4.1×10^{-2}	 2.4×10^{-3}	$\sim 1.1\times10^{-1}$ 1.9×10^{-1}
 7.8×10^{-3}	 1×10^{-3}	1.3 3 1.3	 1.5×10^{-2}			
$\leqq 0.32$ [a] 0.35 [a]	0.71 15 [a] 0.19 [a]	$\leqq 6 \times 10^{-2}$ [a] 8.4×10^{-1} [a]	 1.9×10^{-5} [a]			

TABLE 10

Values of the parameters k, k_0 and γ which give the best fit to the measured gamma-ray transition probabilities (table 9)

Nucleus	k	k_0 (10^{-25} cm^2)	γ
Cd^{110}	0.40	5.59	0.70
Ba^{134}	0.20		0.57
Nd^{144}	1.00		0.52
Sm^{152}	−0.69	17.3	0.98
Gd^{154}	−0.71	17.7	1.29
Gd^{156}	−0.88	21.3	1.04
Dy^{160}	−0.91	23.5	0.31
Er^{166}	−0.96	23.9	0.17
Er^{168}	−0.98		0.20
Yb^{170}	−0.96	23.6	0.19
Hf^{178}	−0.93	27.2	0.063
W^{182}	−0.89	20.7	0.57
W^{184}	−0.93	20.8	0.21
W^{186}	−0.95	18.8	0.23
Os^{186}	−0.48	20.5	−0.80
Os^{190}	−0.32	15.1	0.44
Os^{192}	−0.12	13.1	0.53
Hg^{198}	0	10.5	0.46
Th^{228}	−0.91	26.5	0.40
Th^{232}	−0.93	29.1	0.18
Pu^{238}	−0.97	34.5	0.10
Cf^{250}	−0.98		0.08

Nd^{144}, where the $B(E2; {}^14 \rightarrow {}^12)$ is only 0.37 times the single particle estimate: from the rotational model one expects it to be of the order of the $B(E2; {}^12 \rightarrow {}^10)$ which according to results of systematics [13]) should be at least 10 times the single particle estimate;

Sm^{152}, where the predicted $B(E2; {}^22 \rightarrow {}^10)$ is 20 times larger than the observed one;

Dy^{160}, where the predicted ratio of gamma-ray intensities $I_\gamma({}^24 \rightarrow {}^22)/I_\gamma({}^24 \rightarrow {}^12)$ is 100 times smaller than the measured one;

Er^{168}, where the order of magnitude of the ratios of gamma-ray transition probabilities predicted by theory agree with experiment, but the values differ by more than the experimental error;

W^{186}, where the predicted ratio of gamma-ray transition probabilities $I_\gamma({}^13 \rightarrow {}^14)/I_\gamma({}^13 \rightarrow {}^12)$ is 10^{-2} times the one estimated indirectly [23]) from the empirical data;

Os^{186}, where the $B(E2; {}^14 \rightarrow {}^12)$ predicted by theory is too high;

Os^{190}, where the predicted $B(E2; {}^14 \rightarrow {}^12)$ is too high and the relative intensities of the gamma-rays depopulating the ^{24} level do not agree with those predicted by theory.

In order to compare the parameters k and r determined empirically with those predicted by the hydrodynamical model [3, 4]) and the rigid rotor theory we have represented them in fig. 12. The hydrodynamical values of r (for $0° \leqq \gamma \leqq 30°$)

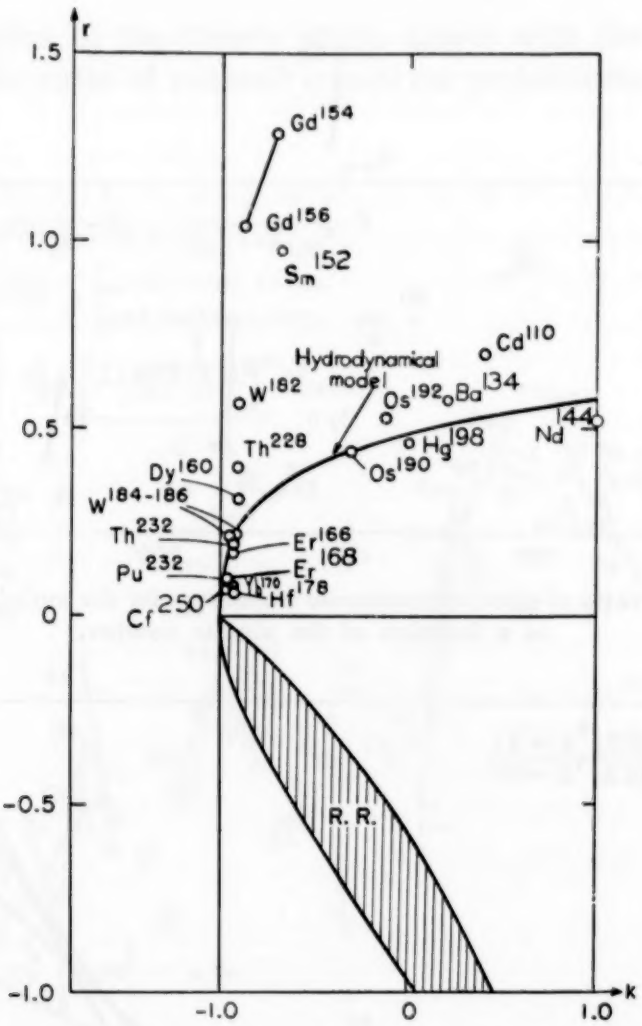

Fig. 12. Plot of the values of k and r (table 10) which predict the observed gamma-ray transition probabilities (table 9) of the nuclei indicated on the figure. The values of r allowed by the general asymmetric rotor theory are $-\infty < r < \infty$. The values allowed for rigid rotors with charge distribution proportional to its mass distribution are the ones within the shaded area. The values for the hydrodynamical model are the ones on the full curve which starts at ($r = 0$, $k = -1$) and ends at ($r = 0.577$, $k = 1$).

are obtained from eqs. (8.23) and (8.24) and the values for k from eqs. (3.10), (3.1) and (3.4). The special case of Bohr and Mottelson ($\gamma = 0°$) has $r = 0$ and $k = -1$. The rigid rotor values of r are obtained with eqs. (8.25) and (8.26) and the ones for k with eq. (3.10) taking into account in both cases the restrictions (3.2) and (3.3). It is interesting to note that the empirical data for r are always positive and in many cases quite close to the hydrodynamical prediction. The rigid rotor has always negative r values and hence is in disagreement with empirical results.

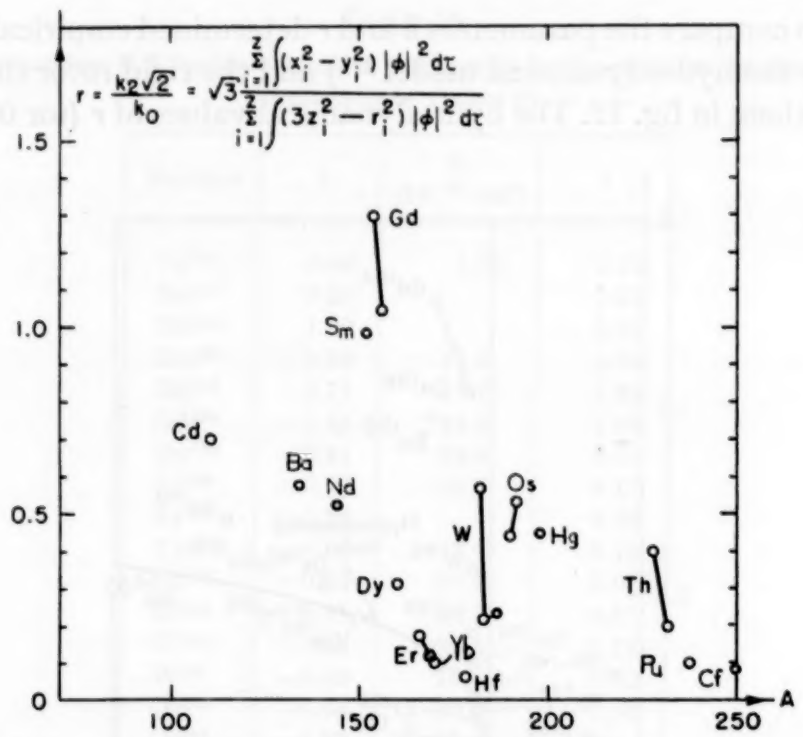

Fig. 13. Values of the ratio of electric quadrupole moments r for the nuclei indicated in the figure as a function of the atomic number.

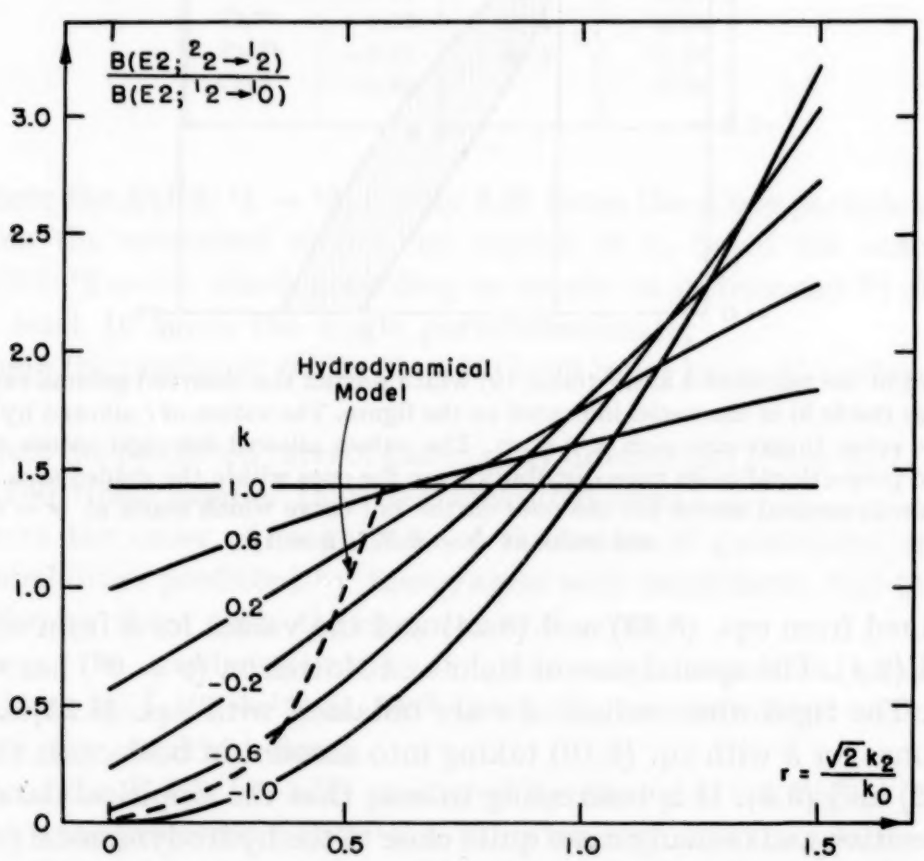

Fig. 14. Plot of the general asymmetric rotor predictions for the ratio of the reduced electric quadrupole (E2) $^2 2 \rightarrow {}^1 2$ gamma-ray transition probability to the reduced E2, $^1 2 \rightarrow {}^1 0$ gamma-ray transition probability as a function of r for different k values. The dashed curve gives the predictions of the hydrodynamical model.

Fig. 13 is a plot of r as a function of the atomic number A. One sees here once more the nuclei for which the assumption $r \approx 0$ (Bohr and Mottelson) is valid. They are the strongly deformed rare earth nuclei and the heavy transuranic elements.

Another prediction of the theory which agrees with the observed data is concerned with the ratio of reduced transition probabilities $B(\mathrm{E2};\ ^{2}2 \rightarrow {}^{1}2)/$

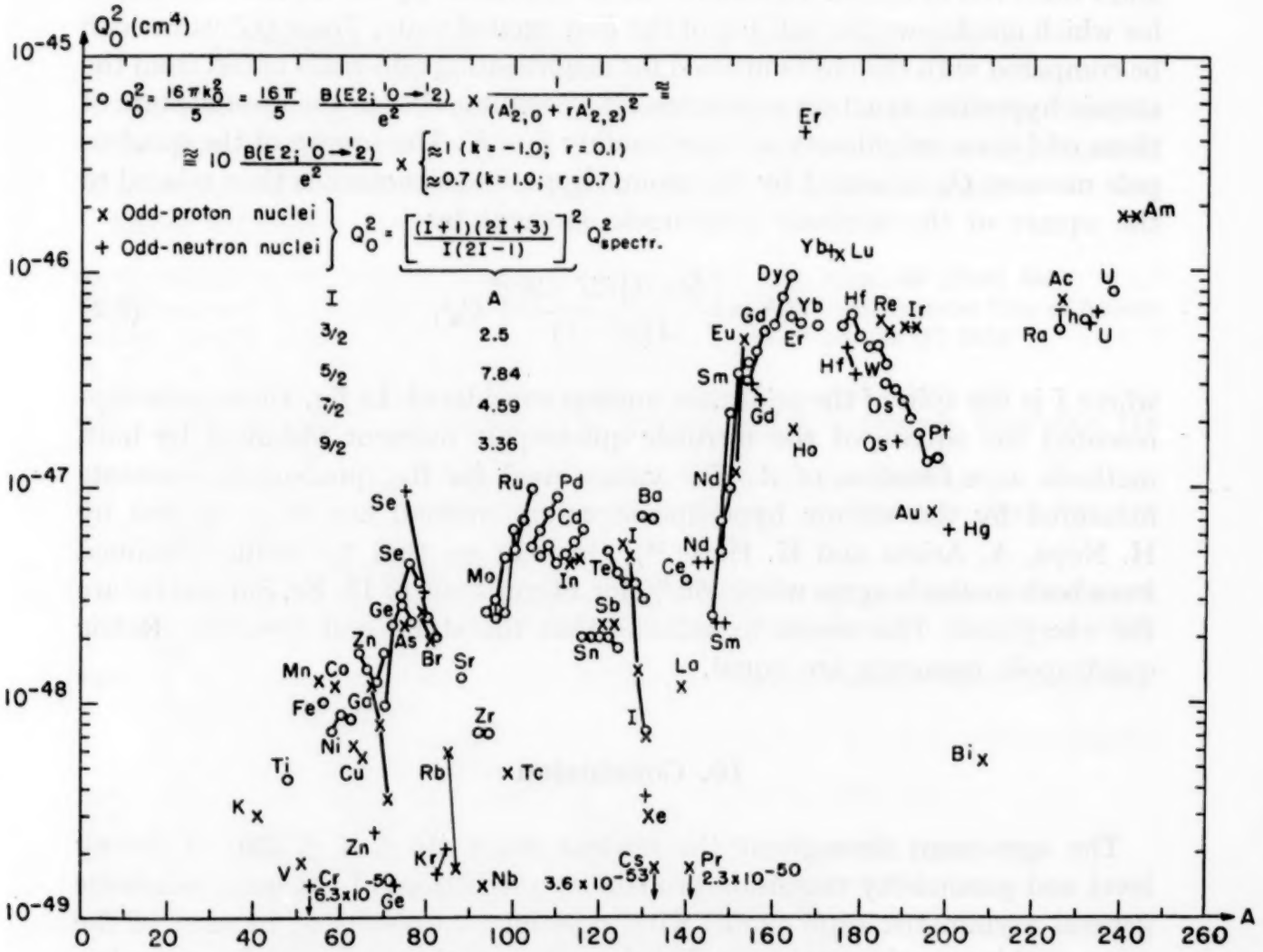

Fig. 15. Plot of the intrinsic electric quadrupole moments Q_0 for the nuclei indicated in the figure as a function of the atomic number. The values obtained from transition probabilities in even nuclei are indicated with circles. The values for odd proton and odd neutron nuclei obtained from atomic hyperfine structure measurements are indicated with an X and a plus sign, respectively.

$B(\mathrm{E2};\ ^{1}2 \rightarrow {}^{1}0)$. Fig. 14 is a plot of this ratio as a function of r for various k values. From Van Patter's [10]) fig. 4, one sees that the experimental ratios vary from 0.07 to 1.5 for nuclei which have corresponding values of (k, r) in the range $(-1, 0) \ldots (> 0, \approx 0.5)$. The present asymmetric rotor theory is able to predict the correct values of the ratios with the values of k and r determined from experimental data as described above.

The square of the effective intrinsic quadrupole moment Q_0 is given by

$$Q_0^2 = \frac{16\pi}{5} \frac{B(\mathrm{E2}; {}^1 0 \to {}^1 2)}{e^2} \frac{1}{5b(\mathrm{E2}; {}^1 2 \to {}^1 0)} \approx 10 \times \frac{B(\mathrm{E2}; {}^1 0 \to {}^1 2)}{e^2}, \quad (9.1)$$

because the value of $5b(\mathrm{E2}; {}^1 2 \to {}^1 0)$ is unity within 30 % for the values of k and r observed in nuclei. This allows us to determine Q_0^2 for all the even nuclei for which one knows the half-life of the first excited state. These Q_0^2 values can be compared with the ones obtained for neighbouring odd-mass nuclei from the atomic hyperfine structure separations if we assume that in the ground state of these odd-mass neighbours we have mainly $I = K$. The square of the quadrupole moment Q_s measured by the atomic hyperfine structure is then related to the square of the intrinsic quadrupole moment by

$$Q_0^2 = \left| \frac{(I+1)(2I+3)}{I(2I-1)} \right|^2 Q_s^2, \quad (9.2)$$

where I is the spin of the odd-mass nucleus considered. In fig. 15 we have represented the square of the intrinsic quadrupole moment obtained by both methods as a function of A. The values used for the quadrupole moments measured by the atomic hyperfine structure method are those quoted by H. Noya, A. Arima and H. Horie [24]). One can see that the values obtained from both methods agree within 50 % for 14 cases out of 17. Er, Sm and Ge are the exceptions. This seems to indicate that the static and dynamic electric quadrupole moments are equal.

10. Conclusion

The agreement throughout the nuclear chart ($40 \leqq A \leqq 250$) of energy level and gamma-ray transition probability predictions of the quasi-adiabatic general asymmetric rotor model with experimental results is, in most of the cases, within experimental error. This fact suggests that the general asymmetric rotor Hamiltonian is an essential part of a more complete Hamiltonian which describes the other degrees of freedom of the nucleus as well as the rotational ones.

The separability of the rotational motion from the other degrees of freedom seems to be quite good already four nucleons away from closed-shells and gets better the farther away one gets from them.. A more detailed study of the other degrees of freedom of the nucleus and their interaction with the rotations should be able to explain, among other things, the levels of non-rotational character and their gamma-ray transition probabilities, the system of levels ${}^1 2$, ${}^1 4$, ${}^1 6$, ${}^1 8$ in even nuclei [12]) for $R({}^1 4) < 2.0$ and the discrepancies with the

rotational model found for nuclei which have very low-lying levels of non-rotational character.

As to the kind of asymmetric rotor involved, the present results seem to indicate once more that the nucleus is not a rigid rotor. The hydrodynamical [34]) model predicts ratios of moments of inertia and ratios of quadrupole moments which are closer to, but not equal to, the empirical ones.

11. References for tables 3, 5, 7, 8, 9 and figs. 4, 5, 10

The references given below are those which did not appear in the Nuclear Data Sheets, National Academy of Sciences, National Research Council, Washington, D. C. up to and including the Set Number 6 of 1959.

Other references used generally are:

D. Strominger, J. M. Hollander and G. T. Seaborg, Revs. Mod. Phys. **30** (1958) 585

W. Scheuer and E. Aisenberg, Proc. Sec. United Nations Intern. Conf. Peaceful Uses of Atomic Energy, Geneva, 1958 (United Nations, Geneva, 1959), paper A/Conf. 15 (P) 2513

D. M. Van Patter, Nuclear Physics **14** (1959/60) 42

I. Marklund, B. Van Nooijen and Z. Grabowski, Nuclear Physics **15** (1960) 533

Ti^{48}: J. W. Knowles, G. Manning, G. A. Bartholomew and P. J. Campion, Phys. Rev. **114** (1959) 1065

Cr^{52}: M. Mazari, W. W. Buechner and A. Sperduto, Phys. Rev. **107** (1957) 1383;
W. C. Porter, D. M. Van Patter, M. A. Rothman and C. E. Mandeville, Phys. Rev. **112** (1958) 468;
J. Konijn, Physica **24** (1958) 377;
J. O. Juliano, C. W. Kocher, T. D. Nainan and A. C. G. Mitchell, Phys. Rev. **113** (1959) 602;
N. Nath, S. S. Malik, M. A. Rothman and D. M. Van Patter, Bull. Am. Phys. Soc. **4** (1959) 258

Fe^{56}: H. E. Gove and C. Broude, Conf. on Reactions between Complex Nuclei, Gatlinburg, Tennessee, May (1960);
B. M. Adams, D. Eccleshall and M. J. L. Yates, Conf. on Reactions between Complex Nuclei, Gatlinburg, Tennessee, May (1960)

Zn^{66}: M. E. Bunker and J. W. Starner, Bull. Am. Phys. Soc. **5** (1960) 253

Zr^{92}: C. F. Coleman, Nuclear Physics **7** (1958) 488;
H. I. West, Jr., L. G. Mann and G. M. Iddings, Phys. Rev. **113** (1959) 881

Pd^{106}: R. L. Robinson, F. K. McGowan and W. G. Smith, preprint (1960)

Cd^{110}: H. W. Taylor and S. A. Scott, Phys. Rev. **114** (1959) 121;
H. W. Taylor and W. R. Frisken, Phys. Rev. **114** (1959) 127;
E. G. Funk (Jr) and M. L. Wiedenbeck, Phys. Rev. **112** (1958) 1247;
E. Boschitz, Z. f. Physik **154** (1959) 90;
U. Cappeler and E. Ganssange, Z. f. Physik **153** (1959) 592;
B. S. Džhelepow and N. N. Zhukovsky, Nuclear Physics **6** (1958) 655

Te^{124}: B. S. Džhelepow and N. N. Zhukovsky, Nuclear Physics **6** (1958) 655

Te^{126}: M. Sakai, H. Ikegami, T. Yamazaki and K. Sugiyama, J. Phys. Soc. Japan **14** (1959) 983;
S. S. Malik, V. R. Potnis and C. E. Mandeville, Nuclear Physics **11** (1959) 691

Xe^{126}: M. Sakai, H. Ikegami, T. Yamazaki and K. Sugiyama, J. Phys. Soc. Japan **14** (1959) 983

Xe^{128}: I. Asplund and T. Wiedling, Arkiv f. Fysik **16** (1960) 219

Ba^{134}: R. K. Girgis and R. van Lieshout, Nuclear Physics **12** (1959) 672

Nd^{144}: S. Ofer, Phys. Rev. **113** (1959) 895;
E. G. Funk, Jr., J. W. Mihelich, C. F. Schwerdtfeger and B. Harmatz, Bull. Am. Phys. Soc. **4** (1959) 247;
P. J. Campion, J. W. Knowles and G. E. Bartholomew, Bull. Am. Phys. Soc. **4** (1959) 247

and private communication (April 1959);
C. A. Mallmann and F. T. Porter, Bull. Am. Phys. Soc. **4** (1959) 324

Sm^{152}: I. Marklund, O. Nathan and O. B. Nielsen, Nuclear Physics **15** (1960) 199;
R. K. Sheline, Rev. Mod. Phys. **32** (1960) 1

Dy^{160}: M. A. Clark, Can. J. Phys. **38** (1960) 262

Er^{166}: K. P. Jacob, J. W. Mihelich, B. Marmatz and T. Handley, Phys. Rev. **117** (1960) 1102

Er^{168}: K. P. Jacob, J. W. Mihelich, B. Marmatz and T. Handley, Phys. Rev. **117** (1960) 1102;
R. G. Wilson and M. L. Pool, Bull. Am. Phys. Soc. **5** (1960) 255

Yb^{170}: B. Marmatz, T. H. Handley and J. W. Mihelich, private communication (June 1960)

W^{182}: C. J. Gallagher, Jr. and J. O. Rasmussen, Phys. Rev. **112** (1958) 1730:
C. J. Gallagher, Jr., J. O. Newton and V. S. Shirley, Phys. Rev. **113** (1959) 1298;
J. J. Murray, F. Boehm, P. Marmier and J. W. M. DuMond **97** (1955) 1007

W^{184}: C. J. Gallagher, D. Strominger and J. P. Unik, Phys. Rev. **110** (1958) 725;
E. Bodensted, E. Matthias, H. J. Körner, E. Gerdau,
F. Frisius and D. Hovestadt, Nuclear Physics **15** (1960) 239;
F. K. McGowan and P. H. Stelson, ORNL-2501 Feb. 15 (1958) p. 14

Os^{190}: W. R. Kane, G. T. Emery, G. Scharff-Goldhaber and M. McKeown, private communication (July 1960)

Hg^{198}: A. H. Wapstra, G. J. Nijgh, N. Salomons-Grobben and L. Th. M. Ornstein, Nuclear Physics **9** (1959) 538

Po^{214}: O. B. Nielsen, private communication to K. Alder, A. Bohr, T. Huus, B. Mottelson, and A. Winther, Rev. Mod. Phys. **28** (1956) 432

Th^{228}: E. Arbman, S. Bjørnholm and O. B. Nielsen, private communication (July 1960);
R. E. Bell, S. Bjørnholm and J. C. Severiens, private communication (July 1960) and Bull. Am Phys. Soc. **5** (1960) 338

Th^{232}: F. E. Durham, D. H. Rester and C. M. Class, Bull. Am. Phys. Soc. **4** (1959) 98; **5** (1960) 110;
F. K. McGowan, Proceedings Paris Conference Nuclear Structure (July 1958);
R. E. Bell, S. Bjørnholm and J. C. Severiens, private communication (July 1960) and Bull. Am. Phys. Soc. **5** (1960) 338;
D. M. Van Patter, Nuclear Physics **14** (1959/60) 42;
F. S. Stephens, Jr., R. M. Diamond and I. Perlman, Phys. Rev. Letters **3** (1959) 435

U^{232}: S. Bjørnholm, A. Knutsen and O. B. Nielsen, private communication (July 1960);
R. E. Bell, S. Bjørnholm and J. C. Severiens, private communication (July 1960) and Bull. Am. Phys. Soc. **5** (1960) 338

U^{234}: S. Bjørnholm and O. B. Nielsen, private communication (July 1960);
R. E. Bell, S. Bjørnholm and J. C. Severiens, Bull. Am. Phys. Soc. **5** (1960) 338 and private communication (July 1960)

Pu^{238}: R. K. Sheline, Rev. Mod. Phys. **32** (1960) 1;
R. E. Bell, S. Bjørnholm and J. C. Severiens, Bull. Am. Phys. Soc. **5** (1960) 338 and private communication (July 1960)

Cf^{250}: S. E. Vandenbosch, H. Diamond, R. K. Sjoblom and P. R. Fields, Phys. Rev. **115** (1959) 115

The author would like to thank J. Weneser for pointing out a mistake in the gamma-ray transition probability formulae and to P. P. Day, M. S. Freedman, E. D. Klema and F. T. Porter for many helpful discussions and suggestions.

References

1) A. Bohr, Mat. Fys. Medd. Dan. Vid. Selsk. **26**, No. 14 (1952)
2) A. Bohr and B. R. Mottelson, Mat. Fys. Medd. Dan. Vid. Selsk. **27**, No. 16 (1953)
3) C. Marty, Nuclear Physics **1** (1956) 58, **3** (1957) 193
4) A. S. Davydov and G. S. Filippov, Nuclear Physics **8** (1958) 237

5) G. R. DeMille, T. M. Kavanagh, R. B. Moore, R. S. Weaver and W. White, Canadian Jour. Phys. **37** (1959) 1036
6) N. Macdonald, Nuclear Physics **14** (1959/60) 70; AWRE NR/P—1/60
7) C. A. Mallmann and A. K. Kerman, Nuclear Physics **16** (1960) 105
8) M. Sakai, INS report 12 (1960) University of Tokyo
9) A. S. Davydov and V. S. Rostovsky, Nuclear Physics **12** (1959) 58
10) D. M. Van Patter, Nuclear Physics **14** (1959/60) 42
11) R. K. Girgis, Thesis, University of Amsterdam (1959)
12) C. A. Mallmann, Phys. Rev. Letters **2** (1959) 507
13) L. Grodzins, Preprint (August 1960)
14) See for example,
G. Herzberg, Infrared and Raman Spectra (D. Van Nostrand Company, New York);
C. H. Townes and A. L. Schawlow, Microwave Spectroscopy (McGraw-Hill Book Company, New York 1955)
15) A. S. Davydov, N. S. Rabotnov and A. A. Chaban, Nuclear Physics **17** (1960) 169
16) E. E. Witmer, University of Pennsylvania Thermodynamics Research Laboratory Technical Report NP-1631 (1950)
17) T. E. Turner, B. L. Hicks and G. Reitwiesner Report 878 (Sept. 1953) Ballistic Research Laboratory, Aberdeen, Md.
18) G. Erlandson, Arkiv f. Fysik **10** (1955) 65
19) C. H. Townes and A. L. Schawlow, Microwave Spectroscopy (McGraw-Hill Book Company, New York 1955), Appendix IV
20) R. B. Moore and W. White, Bull. Am. Phys. Soc. **5** (1960) 378 and private communication
21) See for example, M. E. Rose, Elementary Theory of Angular Momentum (John Wiley and Sons, New York 1957)
22) P. P. Day and C. A. Mallmann, Argonne National Laboratory Report ANL-6184
23) Nuclear Data Sheets, National Academy of Sciences, National Research Council, Washington, D. C.
24) H. Noya, A. Arima and H. Horie, Prog. Theor. Phys. Supplement **8** (1958) 33

1.D.2:
1.D.4

Nuclear Physics **24** (1961) 576—600; © *North-Holland Publishing Co., Amsterdam*
Not to be reproduced by photoprint or microfilm without written permission from the publisher

THE VIBRATIONAL QUADRUPOLE EXCITATION MODEL AND NON-AXIAL ROTATOR MODEL

D. P. GRECHUKHIN

I. V. Kurchatov Atomic Energy Institute, Academy of Sciences, Moscow, USSR

Received 7 September 1960

Abstract: To elucidate the experimental possibilities of checking the non-axial rotator model and the vibrational model for nuclei with nearly equidistant spectra, a detailed comparison was performed of the predictions of these models for the following quantities: 1) the probabilities of E0-, E2-, E4-, and M1-transitions of nuclei; 2) isotopic and isomeric shifts of the levels of atomic electrons; 3) quadrupole moments of nuclei in excited states. Experiments are proposed to check up the non-axial rotator model for nuclei in the region of the transition from the equidistant spectrum to that of the axial symmetrical rotator.

1. Introduction

In the atomic weight intervals $60 \leqq A \leqq 150$ and $190 \leqq A \leqq 214$ the energy spectrum of the levels of even nuclei is closed to equidistant. Originally [1,2]) this spectrum was interpreted in a simple hydrodynamic model of the nucleus as surface quadrupole oscillations of a charge liquid drop. Using this model the basic dependencies of nuclear radiative transitions are explained sufficiently well. Yet the hydrodynamic model yields essentially larger frequencies of the quadrupole oscillations of the nucleus: $\hbar\omega_{\text{hydro}} \approx 2.5$ MeV, than observed in experiment: $\hbar\omega_{\text{exp}} \approx 0.3$ to 1 MeV.

Later, Belyayev [3]) using a somewhat simplified model of shells with allowances for pairing and quadrupole interaction of nucleons, showed the existence of collective quadrupole excitation of the nucleus of the vibrational type. The frequencies of these excitations correspond to those observed, according to the estimate of ref. [3]). We shall designate this model as the VQE model.

A different interpretation was suggested by Davydov and Filippov [4,5]). For describing the states of even nuclei they considered a non-axial rotator model with a fixed form of the nuclear surface. We shall refer to this model as the DF model.

According to the data adduced by Davydov *et al.* [4,5,6,7]) and collected by Van Patter in his survey work [8]) the non-axial rotator model seems at first glance to agree qualitatively with what is observed in experiment.

It is essential, however, to note that in refs. [4–7]) good agreement with the DF model is found in selected nuclei distributed over a broad interval of atomic weights, there being no continuous sequence of the values of the non-axial deformation parameter except for isotopes Os and W.

On the other hand, the following two regions are quite distinct in the graphs of dependencies of the reduced probabilities of the radiative E2-transitions of the nucleus and the relative intensities of the competing E2-transitions as functions of the ratio of the energy of the second and the first excited levels of the nucleus with spin 2^+ represented in ref. [8]):

1) Nuclei with spectra close to those of the axial rotator. The deviations from the curves characterizing the axial rotator can be interpreted for this group of nuclei either as a consequence of the violation of the adiabaticity of the rotation of the nucleus, or, according to the DF model, as a transition to the non-axial rotator.

2) Nuclei with nearly equidistant spectra $E_2(2^+)/E_1(2^+) \leqq 2.5$. The reduced probabilities and relative intensities of the competing transitions for these nuclei do not fit into any smooth curve of dependence on $E_2(2^+)/E_1(2^+)$, but fill in a certain area crossed by the corresponding curve of the dependence on $E_2(2^+)/E_1(2^+)$ in the DF model. Therefore, for the given group of nuclei it is possible to refer only to an approximate qualitative correlation of the DF model and experimental data.

The isotopes Os, W, Gd, Sm, Nd and Pt are in the region of the transition from the axial rotator spectrum to the equidistant spectrum. For this region the DF model is the only model at present. The possibilities of an experimental check-up of the DF model for these nuclei are considered below.

In contrast to the vibrational quadrupole excitation model (VQE model), the non-axial rotator model (the DF model) has not yet, in our view, any convincing theoretical substantiation. Therefore the DF model is considered below as a phenomenological model. The confirmation of refutation of this model should be sought in the comparison with experimental data.

Thus, under discussion are two models qualitatively agreeing with experiment. It is of interest to compare the DF model and the VQE model in detail to gauge the experimental possibilities of checking these models. Considered below with the purpose in view are the results of the calculations in the DF and VQE models of the probabilities of radiative transitions of the nucleus and other physical quantities which can be measured experimentally.

Hydrodynamic approximation is used in the VQE model, for example, for calculating the current of the M1 transitions of the nucleus, since the same approximation is used in the DF model for determining the functional dependce of the moments of inertia of the nucleus on the parameter of the non-axial deformation of the nucleus γ and for calculating the current of the M1-transitions of the nucleus.

In the DF model the values of the moments of inertia $\mathscr{I}_\lambda$ and the dependence $\mathscr{I}_\lambda$ on the parameter of deformation β have not been determined. Accordingly, in the VQE model the inertial parameter of the oscillations of the nucleus B_2

and the dependence of B_2 on β are not considered either. In both DF and VQE models it is assumed that the transition charge density is uniformly spread over the volume of the nucleus.

The values of the principal parameters of the DF model β and γ are taken from experiment; likewise in the VQE model the principal parameter $\bar{\beta}^2 = 5(\hbar\omega/2C_2)$ is determined from the reduced probability of the E2-transition from the first excited level of the nucleus 2^+. Apparently it can be assumed that many results of the simple (formal hydrodynamical) model will hold for other models with vibrational spectrum of excitation provided only that the numerical values of certain parameters are changed.

The vibrational model has been discussed more than once in hydrodynamic approximation (see the references in ref. [2])). Therefore many results given here are well known. Practically all results for the DF model used below were obtained by Davydov *et al.* [4–7]). The basic aim of the present work is to compare the results of these two models and clarify the experimental possibilities of a check-up.

All results for the VQE model are obtained in harmonic approximation. The anharmonic effects are discussed merely qualitatively. In the non-axial rotator model the approximate equidistance of the spectrum $E_2(2^+)/E_1(2^+) \leqq \leqq 2.5$ holds only for the interval of the parameter γ from 25° to 30°. Therefore, those nuclei for which γ falls within this interval are considered in the comparison of the DF and VQE models.

In the DF and VQE models the structure of nuclear excitations is essentially different. Therefore specific notations for the corresponding states and wave functions in each model are used below in the comparison of the DF and VQE models.

2. Spectrum of Levels. Nuclear States

2.1. THE DF MODEL

In the DF model [4, 5]) the nucleus is treated as a three-axis rotator with a rigidity fixed form of surface assigned by the deformation parameters β and γ in the system of the proper axes of the nuclear symmetry:

$$R(\theta, \phi) = R_0\{1+a_0+a_{20}Y_{20}(\theta, \phi)+a_{22}[Y_{22}(\theta, \phi)+Y_{2-2}(\theta, \phi)]\}, \qquad (1)$$

where

$$a_{20} = \beta\cos\gamma \quad \text{and} \quad a_{22} = \beta\sin\gamma/\sqrt{2}.$$

The quantity a_0 can be found from the condition of the conservation of nuclear volume.

To determine the spectrum of rotator levels, the functional dependence of the moments of inertia of the nucleus $\mathscr{I}_\lambda (\lambda = 1, 2, 3)$ on the parameter γ is taken in hydrodynamic approximation [4, 5]) though the absolute quantity $\mathscr{I}_\lambda$

and the dependence $\mathscr{I}_\lambda$ on the parameter β [4,5]) are not determined, but are taken from experiment. Accordingly, for the rotator Hamiltonian $\hat{H}_{\text{rot}}$ we have

$$\hat{H}_{\text{rot}} = \frac{\hbar^2}{2B\beta^2}\frac{1}{2}\sum_\lambda \frac{\hat{M}_\lambda{}^2}{\sin^2(\gamma-\frac{2}{3}\pi\lambda)}, \quad \lambda = 1, 2, 3. \tag{2}$$

The Schroedinger equation for the rotator $\hat{H}_{\text{rot}}\Psi_{IM;\,i} = E_{Ii}\Psi_{IM;\,i}$ is considered in detail in refs. [6,7]). In the notations of the states and functions of the non-axial rotator below we follow these investigations. The wave function of the i-th rotational states with an angular momentum I and magnetic protection M can be represented according to ref. [6]) as

$$\Psi_{IM;\,i}(\theta_j\beta\gamma) = \sum_{K\geq 0} |IK\rangle A_{Ki}(I), \tag{3}$$

where

$$|IK\rangle = \left[\frac{2I+1}{16\pi^2(1+\delta_{K0})}\right]^{\frac{1}{2}} \{\mathscr{D}^I_{MK}(\theta_j)+(-)^I\mathscr{D}^I_{M-K}(\theta_j)\}. \tag{4}$$

θ_j are the Euler angles of the rotator orientation in the laboratory system of coordinates.

For the sake of brevity the rotator states will be denoted by $|IM;\,i\rangle$. A detailed table of the coefficients $A_{Ki}(I)$ is given in ref. [6]) and these values are used below in some calculations. In comparing the DF and VQE models we confine ourselves merely to the lower states of the rotator, i.e. $|00;\,0\rangle$, $|2M;\,1\rangle$, $|2M;\,2\rangle$, $|4M;\,1\rangle$ and $|3M;\,1\rangle$.

2.2. THE VIBRATIONAL MODEL IN HARMONIC APPROXIMATION

In the vibrational model the nucleus in the ground state is regarded as spherical. During the excitation of quadrupole oscillations the sphericity of the nucleus is violated and the surface of the nucleus in the laboratory system of coordinates is described by the deformation parameters α_{2m},

$$R(\vartheta, \varphi) = R_0\{1+\alpha_0+\sum_m \alpha_{2m}Y_{2m}(\vartheta, \varphi)\}, \tag{5}$$

where

$$\alpha_0 = -\left[\frac{1}{4\pi}\sum_m (-)^m\alpha_{2m}\alpha_{2-m}+\frac{1}{3}\sqrt{\frac{5}{4\pi}}\frac{1}{4\pi}C^{20}_{2020}\sum_{m_1m_2m_3}(-)^{m_1}C^{2-m_1}_{2m_2\,2m_3}\alpha_{2m_1}\alpha_{2m_2}\alpha_{2m_3}\right]. \tag{6}$$

The states and spectrum of levels of the nucleus is determined by the Hamiltonian

$$\hat{H}_{\text{vibr}} = \tfrac{1}{2}C_2\sum_m (-)^m\alpha_{2m}\alpha_{2-m}+\tfrac{1}{2}B_2\sum_m (-)^m\dot{\alpha}_{2m}\dot{\alpha}_{2-m}. \tag{7}$$

Here the rigidity parameter C_2 and the inertia parameter B_2 are not calculated but taken from experimental data.

After the quantization of oscillations it is convenient to pass to the creation and annihilation operators of nuclear quadrupole excitation (phonons)

$$\hat{C}_m^+ = \tfrac{1}{2}\left[\left(\frac{2C_2}{\hbar\omega}\right)^{\frac{1}{2}} \alpha_{2m} + i\left(\frac{2}{\hbar\omega B_2}\right)^{\frac{1}{2}} \pi^*_{2m}\right], \tag{8}$$

$$\hat{C}_m = \tfrac{1}{2}\left[\left(\frac{2C_2}{\hbar\omega}\right)^{\frac{1}{2}} \alpha^*_{2m} - i\left(\frac{2}{\hbar\omega B_2}\right)^{\frac{1}{2}} \pi_{2m}\right], \tag{9}$$

where

$$\pi_{2m} = \frac{\partial \hat{H}_{\text{vibr}}}{\partial \dot{\alpha}_{2m}} = B_2 \dot{\alpha}^*_{2m}, \quad \omega = \sqrt{\frac{C_2}{B_2}}. \tag{10}$$

Correspondingly all operators of physical quantities are then written through the operators $\hat{C}_m^+$ and $\hat{C}_m$,

$$\hat{H}_{\text{vibr}} = \tfrac{1}{2}\hbar\omega \sum_m [\hat{C}_m^+ \hat{C}_m + \hat{C}_m \hat{C}_m^+]. \tag{11}$$

The state of the nucleus is determined by the number of phonons v and the angular momentum of the nucleus I. Then the vibrational states are designated $|v; IM\rangle$ in contrast to the rotator states $|IM; i\rangle$. The wave function of the states $|v; IM\rangle$ will be denoted by χ^v_{IM} in contrast to the rotator function Ψ_{IM}. The functions χ^v_{IM} in terms of $\hat{C}_m^+$ can easily be constructed by using the technique

TABLE 1

Function of the ground state χ^0_{00}

$\chi^1_{2M} = C^+_M \chi^0_{00}$
$\chi^2_{IM} = \frac{1}{\sqrt{2}} \sum_{m_1 m_2} C^{IM}_{2m_1 2m_2} C^+_{m_1} C^+_{m_2} \chi^0_{00} \quad (I = 0, 2, 4)$
$\chi^3_{00} = \frac{1}{\sqrt{3}} \sum_{m\lambda} C^{00}_{2\lambda 2m} C^+_m \chi^2_{2\lambda}$
$\chi^3_{6M} = \frac{1}{\sqrt{3}} \sum_{m\lambda} C^{6M}_{4\lambda 2m} C^+_m \chi^2_{4\lambda}$
$\chi^3_{3M} = \frac{1}{\sqrt{3}} \left\{ \sqrt{\frac{5}{7}} \sum_{m\lambda} C^{3M}_{2\lambda 2m} C^+_m \chi^2_{2\lambda} - \sqrt{\frac{2}{7}} \sum_{m\lambda} C^{3M}_{4\lambda 2m} C^+_m \chi^2_{4\lambda} \right\}$
$\chi^3_{4M} = \frac{1}{\sqrt{3}} \left\{ \sqrt{\frac{11}{21}} \sum_{m\lambda} C^{4M}_{2\lambda 2m} C^+_m \chi^2_{2\lambda} + \sqrt{\frac{10}{21}} \sum_{m\lambda} C^{4M}_{4\lambda 2m} C^+_m \chi^2_{4\lambda} \right\}$
$\chi^3_{2M} = \frac{1}{\sqrt{3}} \left\{ \sqrt{\frac{49}{105}} \sum_m C^{2M}_{002m} C^+_m \chi^2_{00} + \sqrt{\frac{20}{105}} \sum_{m\lambda} C^{2M}_{2\lambda 2m} C^+_m \chi^2_{2\lambda} + \sqrt{\frac{36}{105}} \sum_{m\lambda} C^{2M}_{4\lambda 2M} C^+_m \chi^2_{4\lambda} \right\}$

of parentage coefficients. Table 1 lists the states of the functions χ^{ν}_{IM} for the states of interest to us.

2.3. CORRESPONDING STATES IN THE TWO MODELS

From the picture of the DF and VQE spectra we obtain the respective states given in table 2.

TABLE 2
Several corresponding states in the two models

$\|IM; i\rangle$ (DF model)	$\|\nu; IM\rangle$ (VQE model)
$\|00; 0\rangle$	$\|0; 00\rangle$
$\|2M; 1\rangle$	$\|1; 2M\rangle$
$\|2M; 2\rangle$	$\|2; 2M\rangle$
$\|4M; 1\rangle$	$\|2; 4M\rangle$
$\|3M; 1\rangle$	$\|3; 3M\rangle$
$\|4M; 2\rangle$	$\|3; 4M\rangle$
$\|2M; 3\rangle$	$\|3; 2M\rangle$

The excited 0+ level $|2; 00\rangle$ of the vibrational model has no analogue in the DF model. This level in the rotator scheme can be interpreted either as the β-vibrational level or as a level of one-particle origin. The detection of the excited nuclear 0^+ levels and chiefly the investigation of the radiative E2 and conversional E0 transitions from this level is a rather important experiment for checking the DF and VQE models of the nucleus. At present the data on the 0^+ levels of the nuclei are rather scarce and therefore they are not considered here.

3. Reduced Probabilities of E2 and E4 Transitions in DF and VQE Models

All quantities in this section are in the relativistic units $\hbar = m_e = c = 1$, $e^2 = \frac{1}{137}$.

The probability of the EL-radiative transition of the nucleus between the states $Ii \to I'i'$ is determined by the reduced probability of the EL-transition $B(\mathrm{E}L; Ii \to I'i')$; we have

$$W(\mathrm{E}L; Ii \to I'i') = 8\pi e^2 \frac{k^{2L+1}}{[(2L+1)!!]^2} \frac{L+1}{L} B(\mathrm{E}L; Ii \to I'i') \frac{m_e c^2}{\hbar}, \quad (12)$$

where k is the energy of the γ quantum in units of $m_e c^2$ (0.511 MeV). The reduced probability $B(\mathrm{E}L; Ii \to I'i')$ is equal to [2])

$$B(\mathrm{E}L; Ii \to I'i') = \frac{1}{(2I+1)} \sum_{MM'\mu} |\langle I'M'i'|\rho_p r^L Y_{LM}|IMi\rangle|^2. \quad (13)$$

Let us compare the reduced probabilities of the E2 and E4 transitions for the lower respective states of the nucleus in the DF and VQE models.

3.1. THE REDUCED PROBABILITIES IN THE DF MODEL

According to refs. [4, 5]), $B(\mathrm{E2}; Ii \to I'i')$ is in the DF model under the assumption of the uniform distribution of the transition charge density over the volume of the nucleus determined by the operator $\hat{Q}_{2\mu}$,

$$B(\mathrm{E2}; Ii \to I'i') = \frac{5}{16\pi(2I+1)} \sum_{MM'\mu} |\langle I'M'i'|\hat{Q}_{2\mu}|IMi\rangle|^2, \tag{14}$$

where

$$\hat{Q}_{2\mu} = \frac{3}{4\pi} ZR_0^2 \beta 2\sqrt{\tfrac{4}{5}\pi} \left[\cos\gamma \mathscr{D}^2_{\mu 0}(\theta_j) + \frac{\sin\gamma}{\sqrt{2}} \left(\mathscr{D}^2_{\mu 2}(\theta_j) + \mathscr{D}^2_{\mu -2}(\theta_j)\right)\right]. \tag{15}$$

After a simple calculation of the integrals with the functions of the DF model [6, 7]) for the reduced probability we have (see ref. [6]))

$$B(\mathrm{E2}; Ii \to I'i') = \frac{9}{80\pi^2} Z^2 R_0^4 \beta^2 b(\mathrm{E2}; Ii \to I'i'). \tag{16}$$

For estimates in the interval $\gamma \approx 25°$ to $30°$ of interest to us the quantities $b(\mathrm{E2}; Ii \to I'i')$ are obtained in the form of simple functions of $x^2 = [\frac{1}{2}\frac{1}{30}\pi(30-\gamma)]^2$ from the accurate functions given in ref. [6]). For comparing with the VQE model these values $b(\mathrm{E2}; Ii \to I'i')$ are given in table 3.

TABLE 3
Reduced probabilities of E2 transitions of the nucleus

DF model $b(\mathrm{E2}; Ii \to I'i')$	VQE model $c(\mathrm{E2}; \nu I \to \nu' I')$
$b(\mathrm{E2}; 21-00) = 1-x^2$	$c(\mathrm{E2}; 12-00) = 1$
$b(\mathrm{E2}; 22-21) = \frac{10}{7}(1-x^2)/(1+8x^2)$	$c(\mathrm{E2}; 22-12) = 2$
$b(\mathrm{E2}; 22-00) = x^2$	$c(\mathrm{E2}; 22-00) = \frac{4}{7}\bar{\beta}^2/\pi$
$b(\mathrm{E2}; 41-21) = 1.39(1-0.25x^2)$	$c(\mathrm{E2}; 24-12) = 2$
$b(\mathrm{E2}; 41-22) = 0.57x^2$	No transition in harmonic approximation
$b(\mathrm{E2}; 31-21) = \frac{25}{28}x^2$	$c(\mathrm{E2}; 33-12) = \frac{60}{49}\bar{\beta}^2/\pi$
$b(\mathrm{E2}; 31-41) = 1-2.6x^2$	$c(\mathrm{E2}; 33-24) = \frac{6}{7}$
$b(\mathrm{E2}; 31-22) = \frac{25}{28}(1-x^2)$	$c(\mathrm{E2}; 33-22) = \frac{15}{7}$
No analogue	$c(\mathrm{E2}; 20-12) = 2$

3.2. THE REDUCED PROBABILITIES IN THE VQE MODEL

In the vibrational model the operator of the E2-transition is, in terms of operators $\hat{C}_m^+$ and $\hat{C}_m$,

$$(\hat{\mathrm{E}}2)_\mu = \frac{3}{4\pi} Z R_0^2 \left(\frac{\hbar\omega}{2C_2}\right)^{\frac{1}{2}} [\hat{C}_{-\mu}(-)^\mu + \hat{C}_\mu^+]$$

$$+ \frac{3}{4\pi} Z R_0^2 \left(\frac{\hbar\omega}{2C_2}\right) \sqrt{\frac{5}{\pi}} C^{20}_{2020} \sum_{m_1 m_2} (-)^\mu C^{2-\mu}_{2m_1 2m_2} [\hat{C}_{m_1} \hat{C}_{m_2} + (-)^\mu \hat{C}^+_{-m_1} \hat{C}^+_{-m_2}]. \quad (17)$$

Accordingly, we obtain

$$B(\mathrm{E}2; \nu I \to \nu' I') = \frac{9}{80\pi^2} Z^2 R_0^4 \bar{\beta}^2 c(\mathrm{E}2; \nu I \to \nu' I'). \quad (18)$$

The effective deformation of the nucleus $\bar{\beta}^2 = 5(\hbar\omega/2C_2)$ is here introduced for the convenience of comparing with the DF model. The quantities $c(\mathrm{E}2; \nu I \to \nu' I')$ are listed in table 3.

There is no E2-transition $|2; 4M\rangle \to |2; 2M\rangle$ in the vibrational model, in harmonic approximation, due to the degeneration of the levels with $\nu = 2$. This transition can be considered only if the anharmonic terms of the vibrational Hamiltonian are taken into account. On the other hand, in the rotator model there is no analogue to the transition $|2; 00\rangle \to |1; 2M\rangle$ of the VQE model.

Since $c(\mathrm{E}2; 12 \to 00)$ and $b(\mathrm{E}2; 21{-}0)$ are equal to unity (at $\gamma = 30°$) the measurement of the reduced probability of the excitation of the first levels of the nucleus with the spin 2^+ makes it possible to determine the parameters $\bar{\beta}^2$ or β^2 which coincide numerically within the framework of the model assumptions made.

3.3. DISCUSSION OF RESULTS. ANHARMONIC EFFECTS

In the region of nuclei with equidistant spectra β changes (see ref. [7])) in the interval from 0.14 to 0.30 and γ from 25° to 28°. Assuming for the evaluation $\gamma = 27°$ and $\beta = 0.20$ we obtain the following values:

$b(\mathrm{E}2; 22 \to 0) = 0.011$	$c(\mathrm{E}2; 22{-}00) = 0.0073$
$b(\mathrm{E}2; 31 \to 21) = 0.0098$	$c(\mathrm{E}2; 33{-}12) = 0.0156$

Hence it is clear that the reduced probabilities in the DF and VQE models are of the same order of magnitude for retarded transitions.

For some nuclei for which the value of β is known quantitatively table 4 lists the values $[B(\mathrm{E}2; 2' \to 2)/B(\mathrm{E}2; 2'{-}0)]_{\mathrm{exp}}$, and respectively $c(\mathrm{E}2; 2'{-}2)/c(\mathrm{E}2; 2'{-}0)$ and $b(\mathrm{E}2; 2'{-}2)/b(\mathrm{E}2; 2'{-}0)$ according to the harmonic vibrational model and the DF model. The same data for the vibrational model are given in fig. 1 (the second excited level with spin 2+ is cross-hatched).

TABLE 4

Values for the ratios of reduced probabilities in several models. Values $E_2(2+)/E_1(2+)$ and $[B(\mathrm{E2};\ 2'-2)/B(\mathrm{E2};\ 2'-0)]_{\mathrm{exp}}$ are taken from ref. [8]). Values of the β deformation parameter are taken from ref. [7]) in which data of ref. [20]) and ref. [2]) were used

Nucleus	Se^{76}	Se^{78}	Se^{80}	Ru^{100}	Pd^{104}	Pd^{106}	Cd^{110}	Cd^{114}	Te^{122}	Te^{124}	Te^{126}
$\frac{E_2(2+)}{E_1(2+)}$	2.18	2.13	2.20	2.54	2.41	2.20	2.23	2.17	2.23	2.20	2.14
β	0.30	0.27	0.21	0.23	0.21	0.23	0.19	0.20	0.16	0.14	0.16
γ	26.5	27.1	26.5	24.3	24.8	26.5	26.2	26.4	26.2	26.5	27
$\left[\frac{B(2'-2)}{B(2'-0)}\right]_{\mathrm{exp}}$	26.7	30	21	11.6	140	45	30	77	92.4	50	330
$\frac{c(2'-2)}{c(2'-0)}$	122	150	260	210	260	210	310	275	430	560	430
$\frac{b(2'-2)}{b(2'-0)}$	66	87	66	17	19	66	40	50	40	66	85

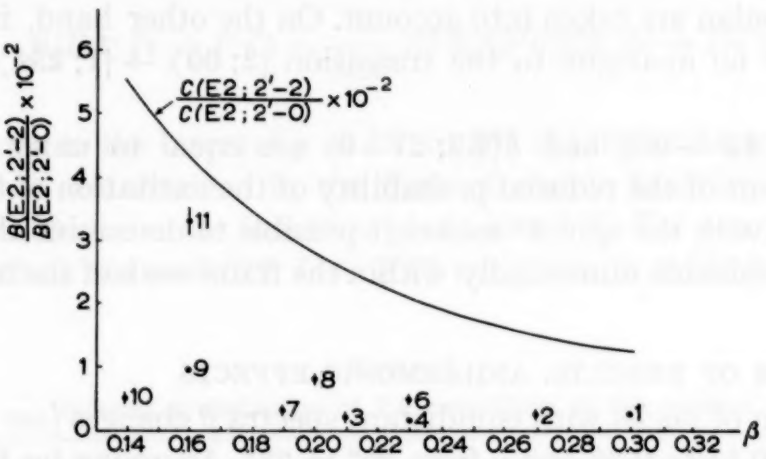

Fig. 1. The quantities $B(\mathrm{E2};\ 2'-2)/B(\mathrm{E2};\ 2'-0)$ and $C(\mathrm{E2};\ 2'-2)/C(\mathrm{E2};\ 2'-0)$ for the vibrational model. The numbers refer to the following nuclei:

1	2	3	4	5	6	7	8	9	10	11
Se^{76}	Se^{78}	Se^{80}	Ru^{100}	Pd^{104}	Pd^{106}	Cd^{110}	Cd^{114}	Te^{122}	Te^{124}	Te^{126}

Cross-hatched points indicate second excited levels with spin 2+.

As is clear from table 4 the numerical agreement of the values $b(\mathrm{E2};\ 2'-2)/b(\mathrm{E2};\ 2'-0)$ with the experimental values is better in the DF model than in the vibrational model. In fig. 2 all experimental points lie substantially below the curve $c(\mathrm{E2};\ 2'-2)/c(\mathrm{E2};\ 2'-0)$ of the vibrational model.

It will be noted, however, that we have been considering the vibrational model in harmonic approximation with an equidistant spectrum, which is not

what we have in reality. If the anharmonic terms in the vibrational Hamiltonian are taken into account, we obtain for the functions of the states $|0; 00\rangle$, $|1; 2M\rangle$ and $|2; 2M\rangle$ the following expressions:

$$X^0_{00} = a_{00}\chi^0_{00} + a_{02}\chi^2_{00} + \sum_{\nu>2} a_{0\nu}\chi^\nu_{00}, \tag{19}$$

$$X^1_{2M} = a_{11}\chi^1_{2M} + a_{12}\chi^2_{2M} + \sum_{\nu>2} a_{1\nu}\chi^\nu_{2M}, \tag{20}$$

$$X^2_{2M} = a_{21}\chi^1_{2M} + a_{22}\chi^2_{2M} + \sum_{\nu>2} a_{2\nu}\chi^\nu_{2M}. \tag{21}$$

Now the E2 transition $X^2_{2M} \to X^0_{00}$ can occur with the annihilation of two phonons and one phonon alike.

If the anharmonic corrections to the functions are small, but $a^2_{21} > 2\bar{\beta}^2/7\pi$, the contribution of the single phonon transition in $X^2_{2M} \to X^0_{00}$ will exceed the contribution of the two-phonon process.

Neglecting all terms with $\nu > 2$ in the wave functions X^0_{00}, X^1_{2M} and X^2_{2M}, and taking into account only single-hhonon E2 transitions, we shall obtain the following rough estimates of the E2 transition probabilities:

$$B(\mathrm{E2}; X_2{}^1 \to X_0{}^0) \approx a^2_{11}\frac{9}{80\pi^2} Z^2 R_0{}^4 \bar{\beta}^2 c(\mathrm{E2}; 12{-}00), \tag{22}$$

$$B(\mathrm{E2}; X_2{}^2 \to X_2{}^1) \approx a^2_{11}a^2_{22}\frac{9}{80\pi^2} Z^2 R_0{}^4 \bar{\beta}^2 c(\mathrm{E2}; 22{-}12), \tag{23}$$

$$B(\mathrm{E2}; X_2{}^2 \to X_0{}^0) \approx a^2_{21}\frac{9}{80\pi^2} Z^2 R_0{}^4 \bar{\beta}^2 c(\mathrm{E2}; 12{-}00), \tag{24}$$

and for the ratio $B(\mathrm{E2}; 2'{-}2)/B(\mathrm{E2}; 2'{-}0)$ in this evaluation we have

$$\frac{B(\mathrm{E2}; 2'{-}2)}{B(\mathrm{E2}; 2'{-}0)} \approx 2\frac{a^2_{11}a^2_{22}}{a^2_{21}} \approx \frac{2}{a^2_{21}}. \tag{25}$$

Thus, for $a^2_{21} \approx \frac{1}{10}$ to $\frac{1}{30}$, which agrees with the estimate $a^2_{21} \approx 0.10$ from the shift of the terms, we obtain just the same degree of agreement as for the DF model. Therefore the ratio $B(\mathrm{E2}; 2'{-}2)/B(\mathrm{E2}; 2'{-}0)$ is not, in our opinion, an essential argument in favour of the rotator model. More important is the ratio $B(\mathrm{E2}; 2'{-}2)/B(\mathrm{E2}; 2{-}0)$ for which, however, there are no sufficiently accurate and complete data.

3.4. E4 TRANSITIONS IN THE DF AND VIBRATIONAL MODEL

For collective E4-transitions the transition operator is of the form

$$(\hat{\mathrm{E}}4_\mu) = \int \rho_\mathrm{p} r^4 Y_{4\mu}\,\mathrm{d}v = \frac{3}{4\pi} Z R_0{}^4 \tfrac{5}{2}\sqrt{\frac{1}{\pi}}\, C^{40}_{2020} \sum_{m_1 m_2} (-)^\mu C^{4-\mu}_{2m_1 2m_2} \alpha_{2m_1}\alpha_{2m_2}. \tag{26}$$

For the rotator transition

$$\alpha_{2m} = \beta\left\{\mathscr{D}^{2*}_{m0}(\theta_j)\cos\gamma + \frac{\sin\gamma}{\sqrt{2}}\left[\mathscr{D}^{2*}_{m2}(\theta_j)+\mathscr{D}^{2*}_{m-2}(\theta_j)\right]\right\} \tag{27}$$

has to be substituted into (26); and for the vibrational model one has to substitute

$$\alpha_{2m} = \frac{\bar{\beta}}{\sqrt{5}}\left[\hat{C}_m + (-)^m \hat{C}^+_{-m}\right]. \tag{28}$$

Accordingly for the reduced probabilities of the E4-transitions in the DF and VQE models we obtain

$$\text{DF:}\quad B(\text{E4};\,41-0) = \frac{9}{16\pi^2} Z^2 R_0^8 \beta^4 \frac{9}{49\pi}, \tag{29}$$

$$\text{VQE:}\quad B(\text{E4};\,24-00) = \frac{9}{16\pi^2} Z^2 R_0^8 \bar{\beta}^4 \frac{9}{35\pi}. \tag{30}$$

Taking into account that β is equal numerically to $\bar{\beta}$ we obtain the ratio of the reduced probabilities of the E4-transition

$$\frac{[B(\text{E4};\,41\text{–}0)]_{\text{DF}}}{[B(\text{E4};\,24\text{–}00)]_{\text{VQE}}} = \frac{5}{7}, \tag{31}$$

Thus the investigation of E4-transitions do not practically permit to differentiate between the rotator model and the vibrational model of the nucleus.

4. Magnetic Dipole Transitions in the DF Model and the VQE Model

The M1 transition probability in the VQE and DF collective models is determined by the reduced probability $B(\text{M1}; Ii \to I'i')$,

$$W(M1; Ii \to I'i') = \frac{8\pi}{9} e^2 k^3 B(\text{M1}; Ii \to I'i') \frac{m_e c^2}{\hbar}, \tag{32}$$

where k is the quantum energy in units of $m_e c^2$ (511 keV), $e^2 = \frac{1}{137}$ and

$$B(\text{M1}; Ii \to I'i') = \frac{1}{(2I+1)} \sum_{MM'\mu} |\langle I'M'i'|\hat{\mathscr{F}}_\mu|IMi\rangle|^2. \tag{33}$$

The operator of the M1-transition $\hat{\mathscr{F}}_\mu = \int \mathbf{Y}^0_{1\mu} r \mathbf{j}_p \, dv$ is calculated in both DF and vibrational model in hydrodynamic approximation. For the proton current $\mathbf{j}_p$ one takes $\mathbf{j}_p = \rho_p \mathbf{v}$ (see ref. [9]), $\mathbf{v}$ being the velocity of the current of the liquid,

$$\mathbf{v} = \tfrac{1}{2} \sum_m \dot{\alpha}_{2m} \nabla(r^2 Y_{2m}). \tag{34}$$

It is assumed that ρ_p is constant over the volume of the nucleus; $\mathbf{Y}^0_{1\mu}$ is the spherical vector of the solenoidal type [22]). After simple calculations for the operator $\hat{\mathscr{I}}_\mu$ we have [9])

$$\hat{\mathscr{I}}_\mu = -i\frac{g_R}{M}\frac{5\sqrt{3}}{7\pi}\sum_\nu C^{1\mu}_{2\mu-\nu 1\nu}\alpha^*_{2\mu-\nu}\hat{I}_\nu \qquad \text{(DF model)}. \tag{35}$$

Here, $\hat{I}_\nu$ is the operator of the spherical ν-th projection of the moment of momentum of the nucleus, g_R is the gyromagnetic factor for collective movement and M is the mass of the nucleon in m_e: $M = 1840$.

The relation (35) holds for the VQE model too, since it is a consequence of the relation

$$\sum_{\mu_1\mu_2}\xi_{\mu_1\mu_2}C^{1M}_{2m2\nu}C^{2\nu}_{2\mu_1 2\mu_2} = -2\sqrt{\tfrac{5}{7}}\sum_{\mu_1\mu_2}C^{1M}_{1n2\mu_1}C^{1n}_{2m2\mu_2}\xi_{\mu_1\mu_2}, \quad \xi_{\mu_1\mu_2} = \xi_{\mu_2\mu_1}. \tag{36}$$

Using the wave functions of the rotator [6]) and the functions of the vibrational states of the nucleus for the reduced probabilities we easily obtain (see ref. [9]) for eq. (37))

$$\begin{aligned} B(\mathrm{M1};\,22-21) &= \left(\frac{g_R\beta}{M}\right)^2\frac{45}{49\pi^2}\frac{\sin^2 3\gamma}{9-8\sin^2 3\gamma} \qquad \text{(DF model)}.\\ B(\mathrm{M1};\,22\to 12) &= \left(\frac{g_R\bar{\beta}}{M}\right)^2\frac{9}{7\pi^2} \qquad\qquad\qquad \text{(VQE model)}. \end{aligned} \tag{37}$$

Taking into account that in the region of equidistant spectrum $\gamma \approx 30°$, we get

$$\frac{\sin^2 3\gamma}{9-8\sin^2 3\gamma} \approx \frac{1-\kappa^2}{1+8\kappa^2} \approx 1, \quad \kappa^2 = [\tfrac{1}{2}\tfrac{1}{30}\pi(30-\gamma)]^2, \tag{38}$$

and we have for the ratio of probabilities

$$\frac{[B(\mathrm{M1};\,2'-2)]_{\mathrm{DF}}}{[B(\mathrm{M1};\,2'-2)]_{\mathrm{VQE}}} = \tfrac{5}{7}\frac{1-\kappa^2}{1+8\kappa^2} \approx \tfrac{5}{7}. \tag{39}$$

In (39) it is assumed that $(g_R)_{\mathrm{DF}} = (g_R)_{\mathrm{VQE}}$.

Let us compare the ratio of probabilities of the competing M1 and E2-transitions in $I_1 \to I_2$ transition of the nucleus. Using the relation (35) between the M1 and E2 transition operators we obtain the same result for the ratio in both the DF model and the VQE model,

$$\begin{aligned} \delta\left(\frac{\mathrm{M1}}{\mathrm{E2}}I_1 \to I_2\right) &= \frac{W(\mathrm{M1};\,I_1-I_2)}{W(\mathrm{E2};\,I_1-I_2)}\\ &= \tfrac{500}{441}\,[I_1+I_2+3][I_2-I_1+2][I_1-I_2+2][I_1+I_2-1]\left(\frac{g_R}{ZkMR_0{}^2}\right)^2. \end{aligned} \tag{40}$$

Hence the ratio

$$\Delta = \delta\left(\frac{\mathrm{M1}}{\mathrm{E2}} I_1 - I_2\right) \Big/ \delta\left(\frac{\mathrm{M1}}{\mathrm{E2}} ; I_3 - I_4\right)$$

is a function of the spins and the transition energies only:

$$\Delta\left(\frac{I_1-I_2}{I_3-I_4}\right) = \left(\frac{k_{3\to4}}{k_{1\to2}}\right)^2 \frac{[I_1+I_2+3][I_2-I_1+2][I_1-I_2+2][I_1+I_2-1]}{[I_3+I_4+3][I_4-I_3+2][I_3-I_4+2][I_3+I_4-1]}. \quad (41)$$

In (40) and (41), we have $M = 1840$. The quantity $k_{i\to i'}$ is in $m_e c^2$ units and R_0 is in $\hbar/m_e c$ units.

The accuracy of determining δ(M1/E2) experimentally is at present nog high and therefore the available data [8, 9, 11]) do not contradict either the DF or the vibrational model.

It will also be noted that the relative phases of the matrix elements of M1 and E2-transitions in the DF and vibrational model coincide. Therefore the determination of the phases of M1 and E2 elements cannot solve the problem of the model.

The same relation holds for static dipole magnetic and quadrupole electric moments of the nucleus in excited states. Therefore the investigation of a change of a correlation function in the cascades of γ quanta, with external magnetic and electric fields switched on simultaneously, is not a critical experiment either.

Though the M1-transitions in the DF and VQE models are retarded, the conversion coefficient for the M1-transition is normal. The corrections for the penetration of the converging electron into the volume of the nucleus for the K and L_I electrons are not large in the present case ($\approx 1\,\%$) and equal in the DF and VQE models. Thus, the investigation of the internal conversion coefficients cannot contribute anything essential to the problem under consideration.

5. Electric Monopole Transitions in Even and Odd-Neutron Nuclei

Alongside E2 and M1 transitions conversional E0 transitions of the nucleus are possible between the states of the nucleus with the same spin I and parities. The general dependences of these transitions are investigated in sufficient detail in refs. [12, 13]). According to refs. [12, 13]) the probability of the E0-transition $Ii \to Ii'$ is determined by the matrix element of the monopole transition

$$\langle Ii'| \sum_{\mathrm{p}}^{Z} r_{\mathrm{p}}^2 |Ii\rangle = R_0^2 \rho(\mathrm{E0}; Ii \to Ii').$$

We shall consider what information on the nuclear structure of the nucleus can be obtained by studying E0-transitions. For this purpose we shall calculate and compare the matrix elements of the E0-transitions in the DF rotator model

and vibrational model. Apart from even nuclei we shall also consider odd-neutron nuclei in the simplest one-particle model nucleon+core, the states of the core being described either in the DF rotator model or the vibrational model. It is assumed that the deformed core remains constant for different states of the nucleus in the DF model.

5.1. THE MODEL FOR EVEN NUCLEI

According to refs. [4, 5]) in the rotator model the wave function of the nucleus is a product of the internal function of a deformed nucleus and the rotational function of a rotational state of the nucleus

$$\Psi_{IM;i}(\beta\gamma\theta_j) = \varphi_{\beta\gamma}(r'_k)\psi_{IM;i}(\theta_j). \tag{42}$$

Since the operator of the E0-transition $\sum_p^Z r_p^2$ is scalar, the matrix element of the E0-transition between rotator states divides into the product

$$\langle \Psi^*_{IM;i'} | \sum_p^Z r_p^2 | \Psi_{IM;i} \rangle = \langle \varphi_{\beta\gamma}(r'_k) | \sum_p^Z (r'_p)^2 | \varphi_{\beta\gamma}(r'_k) \rangle \int \psi^*_{IM;i'} \psi_{IM;i} \, d\Omega. \tag{43}$$

The primes here designate the coordinates of the nucleons in the proper system of the coordinates of the nucleus.

Due to the orthogonality of the rotator wave functions the matrix element of the E0-transition vanishes. Thus the observation of E0-transitions is a critical experiment for the adiabatic DF model. The magnitude of the E0-transition matrix element can serve as a measure of the adiabaticity of the nuclear rotational motion. The corresponding estimates of the E0-transitions matrix elements with allowances for non-adiabaticity are made in ref. [19]). See also ref. [21]) for this subsection.

5.2. THE DF MODEL FOR ODD-NEUTRON NUCLEI

In the case of odd-mass nuclei with a core described according to the DF model, the wave function of the nucleus in the most general form will be represented as an expansion in the rotational states of the core

$$\Phi_{JM;n}(\mathbf{r};\beta\gamma\theta_j) = \sum_{qj;Ii} a^{Jn}_{qjIi} \sum_{\mu m} C^{JM}_{j\mu Im} \Psi_{Im;i}(\beta\gamma\theta_j) f_{qj\mu}(\mathbf{r}). \tag{44}$$

We assume that the deformed core remains constant for all states of the nucleus. In the case of odd-neutron nuclei the contribution of the neutron E0 transition to the matrix element of the E0 transition of the nucleus can be neglected since this contribution is proportional to $Z/A^2 \ll 1$, and for the matrix element of the E0-transition we thus obtain

$$\langle \Phi^*_{JM;n'} | \sum_p^Z r_p^2 | \Phi_{JM;n} \rangle = \langle \varphi_{\beta\gamma} | \sum_p^Z (r'_p)^2 | \varphi_{\beta\gamma} \rangle \sum_{qjIi} a^{Jn}_{qjIi} a^{Jn'*}_{qjIi}. \tag{35}$$

Due to the orthogonality of the functions $\Phi_{JM;n}$ and $\Phi_{JM;n'}$ the matrix element of the E0-transition in this model also vanishes. Accordingly, the observation of E0-transitions in odd-mass nuclei with even core described by the rotator model can yield valuable information on the stability of the surface form of the core with respect to the interaction with an odd neutron in different states.

5.3. THE VIBRATIONAL MODEL FOR EVEN NUCLEI

The E0-transitions of even nuclei in the framework of the vibrational model of the nucleus were considered by the present author [12]). Following below are the results in brief.

The operator of the E0-transition $\sum_p^Z r_p^2$ expressed in terms of $\hat{C}_m^+$ and $\hat{C}_m$ operators is of the form

$$\begin{aligned}(\hat{\mathrm{E}}0) = {} & \frac{3}{4\pi} ZR_0^2 \left(\frac{\hbar\omega}{2C_2}\right) \sum_m (-)^m [\hat{C}_m \hat{C}_{-m} + \hat{C}_m^+ \hat{C}_{-m}^+] \\ & + \frac{3}{4\pi} ZR_0^2 \left(\frac{\hbar\omega}{2C_2}\right)^{\frac{3}{2}} \frac{5}{3} \sqrt{\frac{5}{4\pi}}\, C^{20}_{2020} \\ & \times \{ \sum_{m_1 m_2 m_3} (-)^{m_1} C^{2-m_1}_{2m_2\,2m_3} [(-)^{m_1} \hat{C}^+_{-m_1} \hat{C}_{m_2} \hat{C}_{m_3} \\ & \qquad + (-)^{m_2} \hat{C}_{m_1} \hat{C}^+_{-m_2} \hat{C}_{m_3} + (-)^{m_3} \hat{C}_{m_1} \hat{C}_{m_2} \hat{C}^+_{-m_3}] \\ & + \sum_{m_1 m_2 m_3} (-)^{m_1} C^{2-m_1}_{2m_2\,2m_3} [(-)^{m_3} \hat{C}^+_{-m_1} \hat{C}^+_{-m_2} \hat{C}_{m_3} \\ & \qquad + (-)^{m_2} \hat{C}^+_{-m_1} \hat{C}_{m_2} \hat{C}^+_{-m_3} + (-)^{m_1} \hat{C}_{m_1} \hat{C}^+_{-m_2} \hat{C}^+_{-m_3}] \}. \end{aligned} \tag{46}$$

The first term of the operator is responsible for the E0-transitions with a change of the state of the system by two phonons and the second for the transitions between adjacent states of the nucleus differing by one phonon.

As a result of the calculation of the matrix elements for E0-transitions $\chi^2_{2M} \to \chi^1_{2M}$ and $\chi^2_{00} \to \chi^0_{00}$ we are led to the quantities †

$$\rho(\mathrm{E}0;\, 0'-0) = \langle \chi^{0+}_{00} | \sum_{p=1}^{Z} \left(\frac{r_p}{R_0}\right)^2 | \chi^2_{00} \rangle = \frac{3}{4\pi} Z\bar{\beta}^2 \sqrt{\tfrac{2}{5}}, \tag{47}$$

$$\rho(\mathrm{E}0;\, 2'-2) = \langle \chi^{1+}_{2M} | \sum_{p}^{Z} \left(\frac{r_p}{R_0}\right)^2 | \chi^2_{2M} \rangle = -\frac{3}{4\pi} Z\bar{\beta}^3 \sqrt{\frac{1}{7\pi}}. \tag{48}$$

The estimates of $\rho(\mathrm{E}0;\, 0'-0)$ and $\rho(\mathrm{E}0;\, 2'-2)$ for the nuclei for which $\bar{\beta}^2$ is known are listed in table 5.

It will be noted that for the $2'-2$ transition the estimate (48) for $\rho(\mathrm{E}0;\, 2'-2)$ is a lower limit, since two-phonon E0 transition becomes possible after including anharmonic terms into the Hamiltonian.

† We avail ourselves of this opportunity to correct an error in the value of the matrix element $\langle \chi^{0+}_{00} | \Sigma \bar{\beta}^2 r_p^2 | \chi^2_{00} \rangle$ in ref. [12]): the value given in ref. [12]) should be multiplied by 5.

TABLE 5

Estimates of $\rho(E0; 0'-0)$ and $\rho(E0; 2'-2)$

Nucleus	Se^{76}	Se^{78}	Se^{80}	Ru^{100}	Pd^{104}	Pd^{106}	Cd^{110}	Cd^{114}	Te^{122}	Te^{124}	Te^{126}
$\rho(E0; 0'-0)$	0.465	0.390	0.227	0.352	0.306	0.370	0.262	0.290	0.201	0.153	0.201
$\rho(E0; 2'-2)$	0.0465	0.0332	0.016	0.0275	0.0217	0.0286	0.0168	0.019	0.0108	0.0073	0.0108

5.4. THE VIBRATIONAL MODEL FOR ODD-NEUTRON NUCLEI

In the case of odd-neutron nuclei described by the simplest one-particle model nucleon+core with the vibrational spectrum of the excitations of the core, the function of the nucleus $\Phi_{JM;n}$ will be expanded into a series in the states of the core and a nucleon moving in the spherical core

$$\Phi_{JM;n} = \sum_{qj\nu\lambda} a^{Jn}_{qj\nu\lambda} \sum_{\mu m} C^{JM}_{j\mu\lambda m} \chi^{\nu}_{\lambda m} \psi_{qj\mu}(\mathbf{r}). \tag{49}$$

Neglecting the contribution of the neutron, we obtain for the E0-element

$$\langle \Phi^*_{JM;n'} | \sum_{p}^{Z} \left(\frac{r_p}{R_0}\right)^2 | \Phi_{JM;n} \rangle \tag{50}$$

$$= \frac{3}{4\pi} Z\bar{\beta}^2 \sum_{qj\lambda\nu_1\nu_2} a^{Jn'*}_{qj\nu_2\lambda} a^{Jn}_{qj\nu_1\lambda} \{(2\nu_1+1)\delta_{\nu_1\nu_2} + \tfrac{1}{5} \langle \chi^{\nu_2 +}_{\lambda\mu} | \sum_m (-)^m [\hat{C}_m{}^+ \hat{C}^+_{-m} + \hat{C}_m \hat{C}_{-m}] | \chi^{\nu_1}_{\lambda\mu} \rangle \}.$$

In (50) the contribution of the statical E0-operator

$$(\hat{E}0)_{stat} = \frac{3}{4\pi} Z\bar{\beta}^2 \tfrac{1}{5} \sum_m (C_m C_m{}^+ + C_m{}^+ C_m) \tag{51}$$

is taken into account, which vanishes in the harmonic vibrational model of the even nucleus.

It is very difficult to evaluate the coefficients $a^{Jn}_{qj\nu\lambda}$ with any degree of accuracy at all (see ref. [15])) and therefore it can only be claimed that $\rho(E0; Jn-Jn')$ for the E0-transition of the odd-mass nucleus is of the order of magnitude $\approx (3/4\pi) Z\bar{\beta}^2$. Thus in contrast to the rotator model with an unchanged core, in the vibrational model the matrix elements of the E0-transition do not vanish either in even or odd-mass nuclei.

6. Isotopic and Isomeric Shifts in the Levels of Nuclear Electrons

As a result of the finiteness of the nuclear dimensions the Coulomb field in the nuclear volume essentially differs from the point charge field which leads to the shift ΔE of the shell electron level found for the electrostatic field of a point charge.

The amount of correction to the electron energy term is proportional to the average square of the radius of the proton distribution in the given state of the

nucleus $\langle\sum_p^Z r_p^2\rangle$ and the isotopic shift is determined by the difference $\delta\langle\sum_p^Z r_p^2\rangle$ for the ground states of isotopes,

$$\delta\Delta E = 8\pi Ze^2C_1^2\frac{1}{2I^2(2\sigma)}\frac{a+(1+\sigma)K(a)}{a+(1-\sigma)K(a)}R_u^{2\sigma}\frac{\delta R_u}{R_u}, \tag{52}$$

where $R_u^2 = \frac{5}{3}\langle\sum_p r_p^2\rangle$ (see formula (12) of ref. [16])).

In the case when in odd-mass nuclei there are two close levels with a small difference of energy and a large difference of spins $\delta J \gg 1$ it is possible to measure the relative shift of electron terms arising as a result of the difference in the charge distribution over the nuclear volume in these states of the nucleus. This shift is known as an isomeric level shift.

In a simple one-particle model of the nucleus with a rigid non-deformed core this shift was considered by Weiner [17]). For Hg^{197} the isomeric shift was detected experimentally [18]).

Below we shall consider and compare the isotopic and isomeric shifts of the electron levels in the DF and vibrational models. In the VQE and DF models alike it is assumed that the distribution of proton density over the nucleus is uniform so that the shift of the term is caused by the change of the surface form of the nucleus.

6.1. LEVEL SHIFTS IN THE DF MODEL

For the quantity $\langle\sum_p^Z r_p^2\rangle$ in the rotator model for an arbitrary rotational state of the nucleus we have

$$\langle\sum_p^Z r_p^2\rangle = \langle\varphi_{\beta\gamma}(r'_k)|\sum_p^Z (r'_p)^2|\varphi_{\beta\gamma}(r'_k)\rangle$$
$$= \tfrac{3}{5}ZR_0^2 + \frac{3}{4\pi}ZR_0^2\beta^2 + \frac{9}{40\pi}ZR_0^2\beta^3\cos\gamma[1-4\sin^2\gamma]. \tag{53}$$

In the region of nuclei with equidistant spectra where $\gamma = 30°$ the last term in (53) vanishes and we get

$$\langle\sum_p^Z r_p^2\rangle = \tfrac{3}{5}ZR_0^2 + \frac{3}{4\pi}ZR_0^2\beta^2. \tag{54}$$

Since $\langle\sum_p^Z r_p^2\rangle$ is determined only by the surface form of the core, for the odd-neutron isomers described by an one-particle model with a rigid deformed core the isomeric shift must be equal to zero.

6.2. LEVEL SHIFTS IN THE VIBRATIONAL MODEL

The operator $\sum_p^Z r_p^2$ in the terms $\hat{C}_m^+$ and $\hat{C}_m$ is of the form

$$\sum_p^Z r_p^2 = \tfrac{3}{5}ZR_0^2 + \frac{3}{4\pi}ZR_0^2\left(\frac{\hbar\omega}{2C_2}\right)\sum_m[\hat{C}_m^+\hat{C}_m + \hat{C}_m\hat{C}_m^+]. \tag{55}$$

(In (55) the diagonal term only is taken into consideration). Hence after averaging over the ground state we have

$$\langle 0|\sum_{\mathrm{p}}^{Z} r_{\mathrm{p}}^{2}|0\rangle = \tfrac{3}{5}ZR_0^2 + \frac{3}{4\pi}ZR_0^2\bar{\beta}^2. \tag{56}$$

Thus it is clear from comparing (54) and (56), in the equidistant spectrum region $\langle\sum_{\mathrm{p}}^{Z} r_{\mathrm{p}}^{2}\rangle$ in the rotator model coincides with $\langle 0|\sum_{\mathrm{p}}^{Z} r_{\mathrm{p}}^{2}|0\rangle$ in the harmonic vibrational model. For neutron isomers in the one-particle model with the vibrating core the evaluation $\langle n|\sum_{\mathrm{p}}^{Z} r_{\mathrm{p}}^{2}|n\rangle$ with the functions of the system

$$\Phi_{JM;\,n} = \sum_{\nu\lambda qj} a^{Jn}_{qj\nu\lambda} \sum_{m\mu} C^{JM}_{j\mu\lambda m}\chi^{\nu}_{\lambda m}\psi_{qj\mu}(\mathbf{r}) \tag{57}$$

leads to the quantity

$$\langle\Phi^{*}_{JM;\,n}|\sum_{\mathrm{p}}^{Z} r_{\mathrm{p}}^{2}|\Phi_{JM;\,n}\rangle = \tfrac{3}{5}ZR_0^2 + \frac{3}{4\pi}ZR_0^2\bar{\beta}^2(2\bar{\nu}_n+1), \tag{58}$$

where

$$\bar{\nu}_n = \sum_{\nu}\nu\Big(\sum_{\lambda qj}|a^{Jn}_{qj\nu\lambda}|^2\Big), \tag{59}$$

i.e., $\bar{\nu}_n$ denotes the average number of the virtual phonons in the $\Phi_{JM;\,n}$-state of odd-mass nuclei.

The isomeric shift is determined by the difference

$$\delta\langle n|\sum_{\mathrm{p}}^{Z} r_{\mathrm{p}}^{2}|n\rangle \approx \frac{3}{4\pi}ZR_0^2\bar{\beta}^2\delta\bar{\nu}_n, \quad \delta\bar{\nu}_n = \bar{\nu}_n - \bar{\nu}_{n'}. \tag{60}$$

The average number of phonons $\bar{\nu}$ depends on the strength of the interaction of an odd nucleon with a collective vibrational degree of freedom of the core. The interaction constant is known to be proportional to the angular momentum of a nucleon j. For two states of the nucleus with essentially different j values, $\delta\bar{\nu}$ can be of the order of 1. In this case the isomeric shift can be of the order of the regular volume isotopic shift.

6.3. DISCUSSION

As is clear from eqs. (54), (56), (53) and (58) the results of the rotator model and the vibrational model coincide in the case of the isotopic shift in nuclei with equidistant spectra and essentially differ in the estimate of the isomeric level shift.

There are several isomers in the atomic weight region of interest to us for which it is possible to perform a measurement of the isomeric level shift, namely:

Nucleus	Cd^{113}_{48}	Cd^{115}_{48}	Sn^{121}_{50}	Te^{127}_{52}	Xe^{133}_{54}
$T_{\frac{1}{2}}$	5.11 ij	43 d	400 d	105 d	2.30 d

For the nuclei with $\gamma = 30°$ the DF model predicts an additional isotopic shift depending on the change γ, since in $\langle \sum_p^Z r_p^2 \rangle$ there is the term $(9/40\pi) Z R_0^2 \beta^3 \cos\gamma[1-4\sin^2\gamma]$.

The function $f_0(\gamma) = \cos\gamma[1-4\sin^2\gamma]$ changes rather rapidly from 1 to 0 with the change of γ from 0° to 30 °(see fig. 2). Therefore the change of the isotopic shifts in the isotopes Nd, Sm, Gd, W, Os and Pt where with the change of the number of neutrons there occurs the transition from the equidistant spectrum to the axial symmetrical rotator spectrum (which corresponds to the change γ from 30° to 0°, according to the DF model) can serve as an independent examination of the applicability of the DF model for these nuclei.

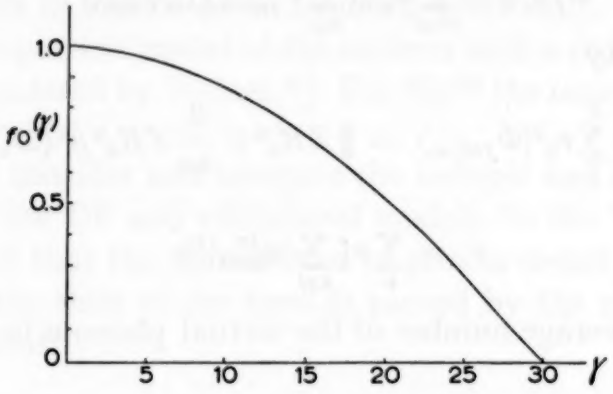

Fig. 2. The function $f_0(\gamma)$.

7. Quadrupole Moments of Odd-Mass Nuclei in Excited States

Let us compare the matrix elements of the static quadrupole moment of the nucleus $\hat{Q}_{2\mu} = \sqrt{4\pi/5}\sum_p^Z r_p^2 Y_{2\mu}(\mathbf{r}_p)$ in the corresponding excited states of the nucleus in the DF model (see ref. [4])) and vibrational model.

7.1. MATRIX ELEMENTS IN THE DF MODEL

The operator $\hat{Q}_{2\mu}$ is of the form

$$\hat{Q}_{2\mu} = \frac{3}{4\pi} Z R_0^2 \beta \sqrt{\frac{4\pi}{5}} \left\{ \cos\gamma\, \mathscr{D}^2_{\mu 0}(\theta_j) + \frac{\sin\gamma}{\sqrt{2}} [\mathscr{D}^2_{\mu 2}(\theta_j) + \mathscr{D}^2_{\mu -2}(\theta_j)] \right\}. \quad (61)$$

Using the wave functions of the states with the spins 2^+, 4^+ and 3^+ we obtain the matrix elements of the quadrupole moment

$$\langle \Psi^*_{2M_1;1} | \hat{Q}_{2\mu} | \Psi_{2M_2;1} \rangle = -\frac{3}{4\pi} Z R_0^2 \beta \sqrt{\frac{4\pi}{5}} f_{12}(\gamma) C^{2M_1}_{2M_2 2\mu}, \quad (62)$$

$$\langle \Psi^*_{2M_1;2} | \hat{Q}_{2\mu} | \Psi_{2M_2;2} \rangle = \frac{3}{4\pi} Z R_0^2 \beta \sqrt{\frac{4\pi}{5}} f_{22}(\gamma) C^{2M_1}_{2M_2 2\mu}. \quad (63)$$

Here, we introduced

$$f_{12}(\gamma) = f_{22}(\gamma) = \frac{3\cos 3\gamma}{\sqrt{1+8\cos^2 3\gamma}}. \tag{64}$$

The function $f_{12}(\gamma)$ is given in fig. 3.

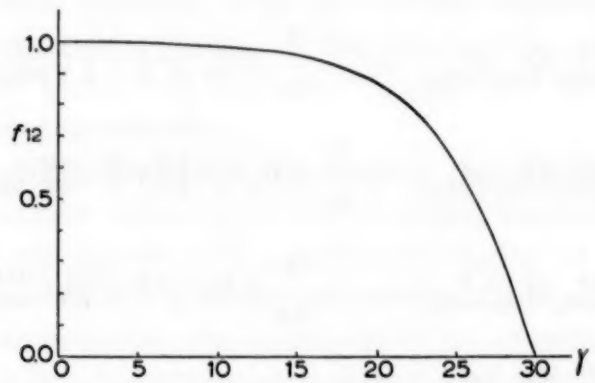

Fig. 3. The function $f_{12}(\gamma)$.

$$\langle \Psi^*_{4M_1;1}|\hat{Q}_{2\mu}|\Psi_{4M_2;1}\rangle = -\frac{3}{4\pi} ZR_0^2\beta\sqrt{\frac{4\pi}{5}} \times 0.51 f_{14}(\gamma) C^{4M_1}_{4M_2\,2\mu}. \tag{65}$$

The function $f_{14}(\gamma)$ is obtained numerically (see fig. 4) with the aid of the rotator functions given in ref. [6]).

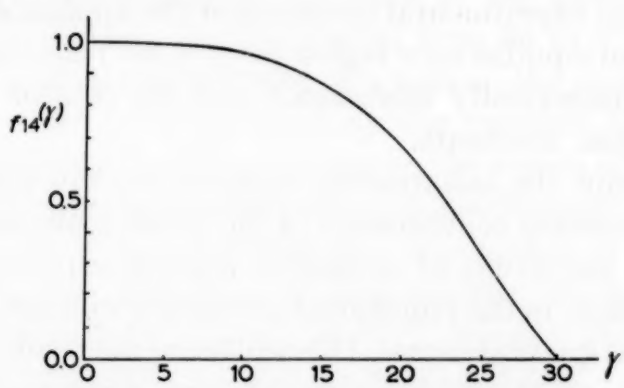

Fig. 4. The function $f_{15}(\gamma)$.

In the case of the state $\Psi_{3M;1}(\theta_j)$ of the rotator, the matrix element of the $\hat{Q}_{2\mu}$-operator is proportional to the Wigner transformation coefficient C^{32}_{3220}; by virtue of an accidental expression ($C^{20}_{3M3-M} \propto [3M^2-3.4]$) the statical quadrupole moment in the 3^+ state of the rotator vanishes

$$\langle \Psi^*_{3M_1;1}|\hat{Q}_{2\mu}|\Psi_{3M_2;2}\rangle \propto C^{32}_{3220} \equiv 0. \tag{66}$$

7.2. MATRIX ELEMENTS IN THE VQE MODEL

In the harmonic approximation the term of the operator $\hat{Q}_{2\mu}$ linear with respect to $(\hbar\omega/2C_2)^{\frac{1}{2}}$ gives no contribution of the static quadrupole moment of

the nucleus. The operator of the quadrupole moment is given by

$$\hat{Q}_{2\mu} = -\frac{3}{4\pi} ZR_0^2 \bar{\beta}^2 \tfrac{2}{5}\sqrt{\tfrac{2}{7}} \sum_{m_1 m_2} (-)^{\mu} C^{2-\mu}_{2m_1 2m_2} [(-)^{m_2} \hat{C}_{m_1} \hat{C}^{+}_{-m_2} + (-)^{m_1} \hat{C}^{+}_{-m_1} \hat{C}_{m_2}], \quad (67)$$

and for the matrix elements $\hat{Q}_{2\mu}$ in the states χ^1_{2M}, χ^2_{2M}, χ^2_{4M} and χ^3_{3M} we find

$$\langle \chi^{1+}_{2M_1} | \hat{Q}_{2\mu} | \chi^1_{2M_2} \rangle = -\frac{3}{4\pi} ZR_0^2 \bar{\beta}^2 \tfrac{4}{5}\sqrt{\tfrac{2}{7}}\, C^{2M_1}_{2M_2 2\mu}, \quad (68)$$

$$\langle \chi^{2+}_{2M_1} | \hat{Q}_{2\mu} | \chi^2_{2M_2} \rangle = \frac{3}{4\pi} ZR_0^2 \bar{\beta}^2 \tfrac{12}{35}\sqrt{\tfrac{2}{7}}\, C^{2M_1}_{2M_2 2\mu}, \quad (69)$$

$$\langle \chi^{2+}_{4M_1} | \hat{Q}_{2\mu} | \chi^2_{4M_2} \rangle = -\frac{3}{4\pi} ZR_0^2 \bar{\beta}^2 \tfrac{8}{7}\sqrt{\tfrac{11}{70}}\, C^{4M_1}_{4M_2 2\mu}, \quad (70)$$

$$\langle \chi^{3+}_{3M_1} | \hat{Q}_{2\mu} | \chi^3_{3M_2} \rangle = 0. \quad (71)$$

The result obtained for the χ^3_{3M} state is rather unexpected; the disappearance of the quadrupole moment in this vibrational state is not so obvious as, for example, for the $\psi_{3M;1}$ state of the rotator. It is noteworthy that the results for the VQE and DF models coincide here.

Though the quadrupole moments of the rotator are proportional to the deformation β, and for the vibrational model proportional to $\approx \bar{\beta}^2$, this fact cannot be used for an experimental check-up of the applicability of the models since in the spectrum equidistance region (at $\gamma \approx 30°$) the functions $f_{tI}(\gamma)$ tend to zero. Thus the numerically vibrational and the rotator model yield close values for quadrupole moments.

Taking into account the anharmonic terms in the vibrational Hamiltonian we obtain a non-vanishing contribution of the quadrupole operator term linear with respect to the amplitude of oscillation and consequently the quadrupole moment of the nucleus in the vibrational model will contain terms linear with respect to $\bar{\beta}$ as well as quadratic ones. This will bring the results of the vibrational model and the data on the rotation model even closer toegether.

8. Possibility of an Experimental Test of the Non-Axial Rotator Model in Angular Correlation of γ-Quantum Cascade

The non-axial rotator model leads to a rather well-pronounced dependence of the quadrupole moments of the nucleus in the excited states of the rotator on the deformation parameter γ in the interval γ from 10 to 30° (see figs. 3 and 4). This dependence is determined by the kinematics of the rotation of the nucleus around three axes of symmetry. Therefore the investigation of the quadrupole moments Q_2 of the excited levels as functions of γ is of interest for an experimental test of the DF model.

The measurement of Q_2 in the excited states is possible through the investigation of angular distribution of γ-quanta emitted after the Coulomb excitation of the nucleus (see ref. [2])) as well as through the measurement of the angular correlation of the γ-quantum cascade as a consequence of the interaction of the quadrupole moment of the nucleus with the field of the medium of the source [10–19]). Below we shall consider only the second method of determining the dependence $Q_2(\gamma)$ since the theory of the attenuation of angular correlation has been elaborated quite well (see ref. [10])) and also because this method is better suited to experimentation.

The application of the method of the angular correlation of the γ-quanta for determining the absolute values $Q_2(\gamma)$ is essentially limited by the fact that the fields of media are not known with a sufficient degree of accuracy and do not even lend themselves easily to rough estimation. This obstacle, however, can be surmounted if we compare the moments $Q_2(\gamma)$ of different isotopes of one element determined by the attenuation of the correlation in the source same medium under identical experimental conditions. In this case unknown parameters of a medium fall out of the final results for the ratio of quadrupole moments of isotopes in the respective excited states.

A similar possibility of checking up the dependence $Q_2(\gamma)$ exists in the case of the even isotopes Nd, Sm, Gd, W, Os and Pt. In this group of isotopes, as was mentioned above, with the change of the number of neutrons there occurs a transition from the equidistant spectrum to the rotator spectrum, which corresponds to the change γ in the interval from 30 to 0°.

If crystals are used as the medium of a source, the correlation attenuation coefficient in this case is determined by the product $(\partial^2 V/\partial Z^2)Q_2\tau$, where $\partial^2 V/\partial Z^2$ is the electric field of the medium in the region of a nucleus and τ the lifetime of the nucleus in the excited state intermediary in the cascade (see the survey of ref. [10])). With this experimental approach it is possible to find the experimental ratio $(Q_2\tau)_\gamma/(Q_2\tau)_{\gamma=0}$ for isotopes with $\gamma \neq 0$ and $\gamma = 0$. Hence to obtain the dependence $Q_2(\gamma)$ it is necessary to measure accurately the lifetime of nuclei in the intermediate excited states of isotopes.

Of special interest is the investigation of the correlation attenuation in the case when a liquid is taken as the medium of the source. In this variant of experiment there is no need to know the lifetimes τ of the nuclei. The coefficients $G_{2\kappa}$ are determined from the observation of the angular correlation of the $\gamma\gamma$ cascade $I_1 \to I_1 \to I_2$,

$$W(\theta) = 1 + \sum_{\kappa} G_{2\kappa} A_{2\kappa} P_{2\kappa}(\cos\theta),$$

since the $A_{2\kappa}$ are known exactly for a given form of the cascade (with definite I, I_1 and I_2, and transition multipolarities).

For liquid sources (under the condition that the lifetime of the nucleus τ in the state I_1 is considerably less than the time of the resolution of the detecting

equipment, while the correlation time τ_c of the liquid is less than τ) the coefficients $G_{2\kappa}$ are, according to refs. [10, 19]), of the form

$$G_{2\kappa} = \frac{1}{1+\lambda_{2\kappa}\tau}, \tag{72}$$

where

$$\lambda_{2\kappa} = \tfrac{3}{80}\left(\frac{eQ_2}{\hbar}\right)^2\left(\frac{\partial^2 V}{\partial Z^2}\right)^2_{\text{aver}}\tau_c\,\frac{2\kappa(2\kappa+1)[4I_1(I_1+1)-2\kappa(2\kappa+1)-1]}{I_1^2(2I_1-1)^2}; \tag{73}$$

$(\partial^2 V/\partial Z^2)^2_{\text{aver}}$ is the average square of the second derivative of the potential of the fluctuating electric field of the source medium.

From (72) we obtain

$$(\lambda_{2\kappa}\tau) = \frac{1-G_{2\kappa}}{G_{2\kappa}}.$$

Let us compare the quantities $(\lambda_{2\kappa}\tau)$ for two isotopes of one element the nuclei of which have $\gamma \neq 0$ and $\gamma = 0$, i.e., let us obtain the ratio $(\lambda_{2\kappa}\tau)_\gamma/(\lambda_{2\kappa}\tau)_0$. It will be emphasized that $G_{2\kappa}$ for isotopes will be measured in the same source medium under identical conditions. According to refs. [4, 5]), we have for the E2 transitions of the rotator (see sect. 3)

$$\frac{1}{\tau} = W(\text{E2}; I_1 \to I_2) = \frac{3}{500\pi}e^2k^5Z^2R_0^4\beta^2 b(\text{E2}; I_1 \to I_2)\,\frac{m_e c^2}{\hbar}. \tag{74}$$

Here k is expressed in $m_e c^2$ units, R_0 in $\hbar/m_e c$ and $e^2 = \frac{1}{137}$.

The values $b(\text{E2}; I_1 \to I_2)$ are given in refs. [4, 5]); following below are the quantities most interesting for the present experiment:

$$b(\text{E2}; 21-0) = \tfrac{1}{2}\left[1+\frac{3-2\sin^2 3\gamma}{\sqrt{9-8\sin^2 3\gamma}}\right], \tag{75}$$

$$b(\text{E2}; 22-0) = \tfrac{1}{2}\left[1-\frac{3-2\sin^2 3\gamma}{\sqrt{9-8\sin^2 3\gamma}}\right], \tag{76}$$

$$b(\text{E2}; 22-21) = \tfrac{10}{7}\,\frac{\sin^2 3\gamma}{9-8\sin^2 3\gamma}. \tag{77}$$

It will be noted here that $b(\text{E2}; 21-0)$ varies from 0.933 to 1 and $b(\text{E2}; 41-21)$ from 1.43 to 1.365, when γ varies from 0 to 30°.

Taking into account that the same medium and the same type of the $\gamma\gamma$-cascade for isotopes with $\gamma \neq 0$ and $\gamma = 0$ are used, we find from (74) for the ratio

$$\frac{(\lambda_{2\kappa}\tau)_\gamma\,k_\gamma^5}{(\lambda_{2\kappa}\tau)_0\,k_0^5} = \frac{k_\gamma^5}{k_0^5}\,\frac{\left(\dfrac{1-G_{2\kappa}}{G_{2\kappa}}\right)_\gamma}{\left(\dfrac{1-G_{2\kappa}}{G_{2\kappa}}\right)_0} = \frac{[b(\text{E2}; I_1-I_2)]_0}{[b(\text{E2}; I_1 \to I_2)]_\gamma}\,f^2_{iI_1}(\gamma). \tag{78}$$

The quantity on the left-hand side of (78) is measured experimentally and that on the right-hand side can be calculated since the value of the parameter γ is determined independently by the ratio of energies $E_2(2+)/E_1(2^+)$ of the first and second levels of the nuclei with spins 2^+.

Of the greatest practical interest are the cascades in which the intermediary levels I_1 are the first excited states of the rotator with spins of 2^+ and 4^+. In these cases (according to refs. [4, 5]) the probabilities $b(\mathrm{E2};\ 21-0)$ and $b(\mathrm{E2};\ 41-21)$ practically do not vary throughout the interval of variation of the parameter γ (see above). For these cases we have

$$f_{iI}^2(\gamma) = \frac{k_\kappa^5}{k_0^5} \frac{\left(\frac{1-G_{2\kappa}}{G_{2\kappa}}\right)_\gamma}{\left(\frac{1-G_{2\kappa}}{G_{2\kappa}}\right)_0}. \tag{79}$$

The functions $f_{12}^2(\gamma)$ and $f_{14}^2(\gamma)$ are given in figs. 5 and 6. Of the greatest interest in the experiment proposed is the region $10° \leqq \gamma \leqq 26°$, where $f_{iI_1}^2$ varies

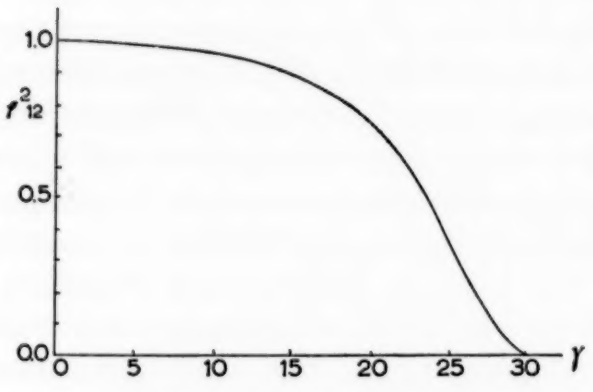

Fig. 5. The function $f_{12}^2(\gamma)$.

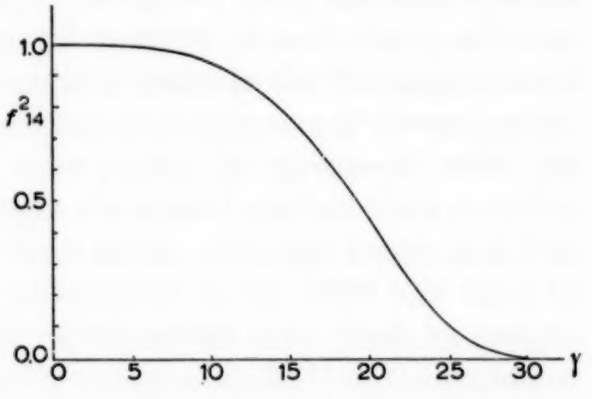

Fig. 6. The function $f_{14}^2(\gamma)$.

rather sharply and the quadrupole moments are not small. In this interval γ the level spectrum is essentially non-equidistant and the comparison of the rotator model and the vibration model are here meaningless, since at present there is no such model for the transitional region from the vibrational spectrum to the axial-symmetrical rotator spectrum. Therefore, the experiment proposed can uniquely establish only the inapplicability of the non-axial rotator model. The most suitable for the experiment are probably Os isotopes for which we have:

Isotope	Os^{186}	Os^{188}	Os^{190}	Os^{192}
γ	18°	19.4°	21.2°	25.2°

References

1) G. Sharf-Goldhaber and J. Wenezer, Phys. Rev. **98** (1955) 212
2) K. Adler, A. Bohr, T. Huus, B. Mottelson and A. Winter, Rev. Mod. Phys. **28** (1956) 432
3) S. T. Beliayev, Mat. Fys. Medd. Dan. Vid. Selsk. **31**, No. 11 (1959)
4) A. S. Davydov and G. F. Filippov, JETP **35** (1958) 440
5) A. S. Davydov and G. F. Filippov, Nuclear Physics **8** (1958) 237
6) A. S. Davydov and V. S. Rostovsky, JETP **36** (1959) 1788
7) A. S. Davydov, Preprint No. 326 of the Joint Institute for Nuclear Research, Dubna, 1959
8) D. M. Van Patter, Nuclear Physics **14** (1959) 42
9) A. S. Davydov and G. F. Filippov, JETP **35** (1958) 703
10) R. M. Steffen, Advances in Physics, a quarterly supplement of the Phil. Mag. **4**, No. 15 (1955) 293
11) S. S. Malik, V. R. Rottvis and C. E. Mandwill, Nuclear Physics **11** (1959) 691
12) D. P. Grechukhin, JETP **32** (1957) 1036
13) E. Church and J. Wenezer, Phys. Rev. **103** (1956) 1035
14) V. S. Rostovsky, JETP **39** (in the press)
15) D. P. Grechukhin, JETP **37** (1959) 1026
16) A. R. Bodmer, Nuclear Physics **9** (1958) 371
17) R. Weiner, Phys. Rev. **114** (1959) 256
18) A. G. Melissonos and S. P. Davis, Phys. Rev. **115** (1959) 130
19) A. Abragam and R. V. Pound, Phys. Rev. **92** (1953) 943
20) P. Stelson and F. McGowen, Phys. Rev. **110** (1958) 489
21) D. P. Grechukhin, JETP **38** (1960) 1891

1.E.1:
3.A

Nuclear Physics **24** (1961) 601—606; © *North-Holland Publishing Co., Amsterdam*
Not to be reproduced by photoprint or microfilm without written permission from the publisher

GAMMA-GAMMA DIRECTIONAL CORRELATION IN Ba^{136} AND Mo^{94}

H. BERNSTEIN and H. H. FORSTER

University of Southern California, Los Angeles

Received 29 December 1960

Abstract: The gamma-gamma directional correlation has been measured for the 1.065 MeV–0.830 MeV gamma cascade in Ba^{136} and for the 0.700 MeV–0.874 MeV cascade in Mo^{94}. The experimental correlation is compatible with either a $4^+(Q)2^+(Q)0^+$ or a $2^+(D+Q)2^+(Q)0^+$ level sequence for the lowest states in either nucleus. A 2^+ assignment for the second excited state leads to a predominantly M1 transition between the second and first excited state, e.g. the quadrupole content in Ba^{136} is 2.7 ± 0.6 %, that of Mo^{94} is 4.4 ± 0.4 %.

1. Introduction

The radioactive decay of Cs^{136}(13d) and of $Nb^{94}(1.8\times10^4 y)$ has been studied by several investigators [1–5]) and the general features of both decay schemes are well known. Ba^{136} and Mo^{94}, the two daughter nuclei in the disintegration of Cs^{136} and Nb^{94}, respectively, have a ground state with spin zero and even parity, and a first excited state with spin 2 and even parity, in agreement with the majority of even-even nuclei. But, as regards the second excited state in either nucleus, no definite spin assignment has been made, although Girgis and Van Lieshout [3]) have pointed out that a 2^+ assignment to the 1900 keV level in Ba^{136} was compatible with the rest of the experimental data. Such an assignment would fit in with the general trend of even-even nuclei [6]) in the region of neutron numbers N such that $24 \leqq N \leqq 88$. For this reason, it seemed advisable to investigate the spin of the second excited state in Ba^{136} and Mo^{94} and the character of the transitions from this state.

2. Experimental Procedure

Thin, uniform sources were placed on a source holder at the centre of a calibrated turntable and were viewed by two identical counters at a distance of 7 cm from the source. Each counter consisted of a 3.8 cm × 3.8 cm thallium activated sodium iodide crystal, coupled optically to a Dumont 6292 photomultiplier. In order to reduce counter to counter scattering, each crystal was shielded by a lead cylinder 2.2 cm thick which was tapered in front to a cone-shaped opening. The solid angle subtended by the crystal at the source was $\frac{1}{4}$ sr. A fast-slow coincidence circuit of the Garwin [7]) type with a resolving time of 14 ns was used for the coincidence measurements. Two single-channel analyzers

were employed to set windows over the photopeaks of the gamma rays, the coincidence of which was to be investigated.

Coincidence data were taken at angles of 90°, 120°, 150° and 180° between the detectors. In addition to the triple coincidences, the number of single counts in each gamma arm was recorded at all settings, in order to keep track of sudden fluctuations and the over-all drift of the instrument. Another precaution was taken to avoid any masking of the effect by a long term drift of the electronic system, e.g. each run was made first in the direction of increasing angles, then in the opposite direction.

A check of the apparatus was made by measuring the angular correlation of the gamma ray cascade in Ni^{60} giving $A_2 = 0.1033 \pm 0.0035$ and $A_4 = 0.0074 \pm \pm 0.0056$ for the angular correlation coefficients, in good agreement with other investigators [8]).

2.1. Ba^{136}

For the investigation of the directional correlation of the 1.065 MeV–0.830 MeV gamma cascade in Ba^{136}, Cs^{136}(13 d) was used. The radioactive source material was obtained by exposing metallic lanthanum to the neutron flux of the Chalk River pile. Cs^{136} was dissolved in concentrated HCl and thin sources were prepared by the insulin mounting technique, using tygon or polyethylene as backing. The decay scheme of Cs^{136} is illustrated in fig. 1 (ref. [3])).

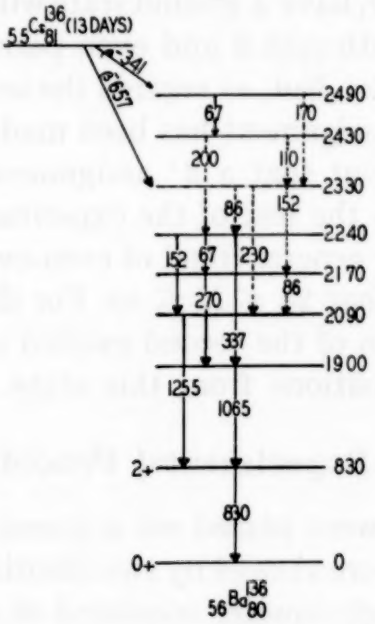

Fig. 1. Decay scheme of Cs^{136}.

The coincidence rate of the gamma rays was determined as described previously, except that additional data were taken at 105° and 135°. A least-squares fit of the data to a correlation function

$$W(\theta) = 1 + A_2 P_2(\cos\theta) + A_4 P_4(\cos\theta)$$

gave, after correction for finite solid angle by a method outlined by Rose [9]) $A_2 = 0.1253 \pm 0.0219$ and $A_4 = 0.0065 \pm 0.0326$. This function is illustrated in fig. 2.

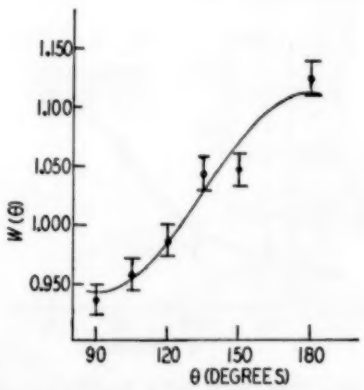

Fig. 2. Directional correlation of the 1065 keV–830 keV cascade in Ba^{136}. The solid curve is the least-squares fit of the data.

2.2. Mo^{94}

$Nb^{94}(1.8 \times 10^4 y)$, obtained by exposing Nb_2O_5 powder to the neutron flux of the Oak Ridge pile, was used for the investigation of the directional correlation of the 700 keV–874 keV gamma cascade in Mo^{94}. Thin sources were prepared by the technique outlined above, after the radioactive powder had been dissolved in concentrated HF at $\approx 100°$C. Fig. 3 is an illustration [4]) of the decay scheme of Nb^{94}. A gamma ray spectrum taken of the source soon after arrival revealed, beside the gamma lines due to Nb^{94}, other lines which were identified tentatively as belonging to Nb^{95} (35 d) and Ta^{182} (112 d), respectively. The coincidence measurements were not started until several months after the sample had been activated in order to allow for the decay of Nb^{95}.

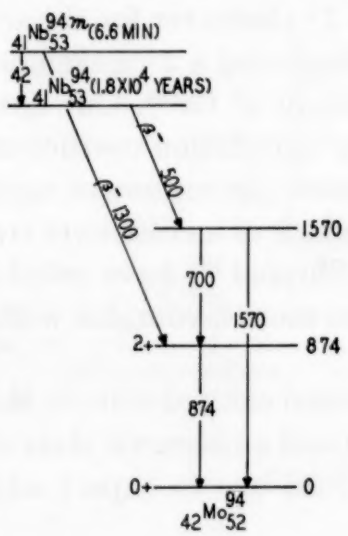

Fig. 3. Decay scheme of Nb^{94}.

The corrected correlation function was found to be

$$W(\theta) = 1 + (0.0865 \pm 0.0080) P_2(\cos\theta) + (0.0243 \pm 0.0125) P_4(\cos\theta).$$

This function is illustrated in fig. 4.

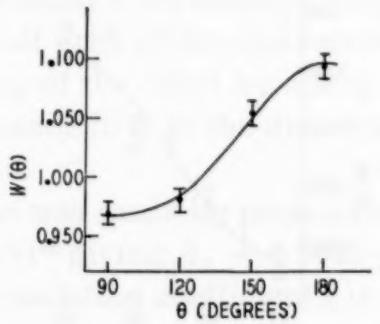

Fig. 4. Directional correlation of the 700 keV–874 keV cascade in Mo^{94}. The solid curve is the least-squares fit of the data.

3. Results and Discussion

The experimental data concerning the angular correlation of the 1.065 MeV–0.830 MeV cascade in Ba^{136} and the 0.700 MeV–0.874 MeV cascade in Mo^{94} do not lead to a unique spin assignment for the second excited state in either nucleus and are compatible both with a $4^+(Q)2^+(Q)0^+$ or a $2^+(M1+E2)2^+(Q)0^+$ sequence. As has been pointed out before, nuclei in this region show predominantly 2^+ character for the second excited state [6]). Girgis and Van Lieshout [3]) have suggested a 2^+ assignment for the 1900 keV level in Ba^{136} on the basis of the decay of La^{136}. Our data tend to suggest the same assignment since the angular correlation coefficients for Ba^{136} are slightly high for a pure E2 upper transition. An argument against a 2^+ assignment to the 1900 keV level would be the lack of a cross-over transition to the ground state. However, as Deliagin and Shipnel [10]) have pointed out, the probability of a cross-over transition becomes more favourable with increasing nuclear deformation.

A 2^+ assignment to the second excited state in Mo^{94} would be compatible with a ground state spin of $4^+(0^+)$ and an isomeric state of $1-(3-)$ in Nb^{94}. However, such an assignment would lead one to expect additional beta transitions between the two nuclei.

If the character of the second excited state is 2^+, then the admixture of M1 to E2 can be found by a method due to Lide and Wiedenbeck [11]), e.g. the angular correlation coefficients A_2 and A_4 can be expressed as

$$A_2 = A_2^{(1)}(\text{mixed}) \cdot A_2^{(2)}(\text{pure}) \text{ and } A_4 = A_4^{(1)}(\text{mixed}) \cdot A_4^{(2)}(\text{pure}).$$

In figs. 5 and 6, $A_2^{(1)}$ and $A_4^{(1)}$ are plotted as a function of the quadrupole content Q for Ba^{136} and Mo^{94}, respectively. For Ba^{136} the experimental data are

compatible with a quadrupole content in the 2^+–2^+ transition of 2.7 ± 0.6 %; for a similar transition in Mo^{94} the quadrupole content would be 4.4 ± 0.4 %.

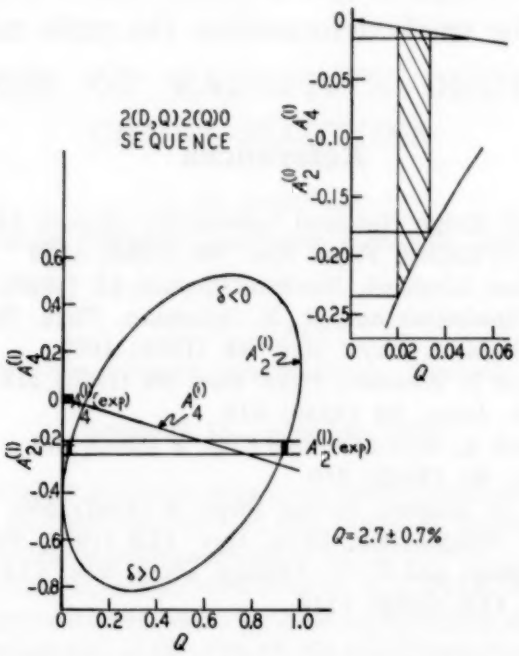

Fig. 5. Partial Legendre coefficients $A_2^{(1)}$ and $A_4^{(1)}$ versus the quadrupole content Q for a 2(D, Q)2 transition. The shaded regions show the values of Q consistent with the experimental values of $A_2^{(1)}$ and $A_4^{(1)}$ obtained for the 1065 keV–830 keV cascade in Ba^{136}.

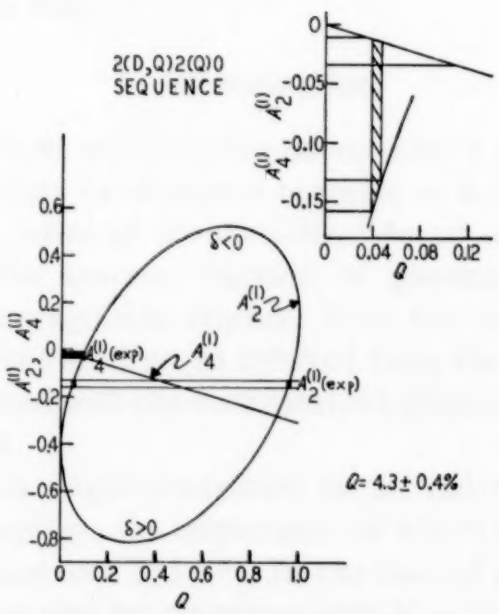

Fig. 6. Partial Legendre coefficients $A_2^{(1)}$ and $A_4^{(1)}$ versus the quadrupole content Q for a 2(D, Q)2 transition. The shaded regions show the values of Q consistent with the experimental values of $A_2^{(1)}$ and $A_4^{(1)}$ obtained for the 700 keV–874 keV cascade in Mo^{94}.

Thus, either transition would be predominantly M1. It may be interesting to note that while for a large number of nuclei the 2^+–2^+ transitions have been

found [6]) to be predominantly E2, cases of enhanced M1 transitions have been recorded [12]). Furthermore, it has been suggested that the ratio of reduced transition probabilities M1/E2 might decrease with increasing deformation of the nucleus and that for small deformation the ratio might be considerably larger than one [13]).

References

1) W. A. Brooksbank, Oak Ridge National Laboratory Report 1474 (1953)
2) J. L. Olsen and G. D. O'Kelley, Phys. Rev. **95** (1954) 1539
3) R. K. Girgis and R. Van Lieshout, Nuclear Physics **12** (1959) 204
4) D. L. Douglas, A. C. Mewherter and R. P. Schuman, Phys. Rev. **92** (1953) 369
5) M. A. Rollier and E. Saeland, Phys. Rev. **94** (1954) 1079
6) G. Scharff-Goldhaber and J. Weneser, Phys. Rev. **98** (1955) 212
7) R. L. Garwin, Rev. Sci. Instr. **24** (1953) 618
8) S. Colombo, A. Rossi and A. Scotti, Nuovo Cim. **2** (1955) 471
9) M. E. Rose, Phys. Rev. **91** (1953) 610
10) N. N. Deliagin and V. S. Shipnel, Soviet Phys. **5** (1957) 309
11) R. W. Lide and M. L. Wiedenbeck, Phys. Rev. **113** (1959) 840
12) H. I. West, Jr., L. G. Mann and G. M. Iddings, Phys. Rev. **113** (1959) 881
13) B. J. Raz, Phys. Rev. **114** (1959) 1116

2.D

Nuclear Physics **24** (1961) 607—613; © *North-Holland Publishing Co., Amsterdam*

Not to be reproduced by photoprint or microfilm without written permission from the publisher

(*N*–*Z*) DEPENDENCE OF RADIATIVE DEUTERON CAPTURE CROSS-SECTIONS

J. H. CARVER

Australian National University, Canberra, Australia

and

G. A. JONES

Atomic Energy Research Establishment, Harwell, England

Received 19 December 1960

Abstract: Induced radioactivity methods have been used to determine the radiative deuteron capture cross-sections for Ni^{58} and Cr^{54} in the range of deuteron energies 3.5–4.5 MeV. When combined with previous measurements [1]) of the Zn^{64}(d, γ) cross-section these results give the (d, γ) cross-sections for nuclei with $N-Z = 2$, 4 and 6. If there is a strong contribution to the cross-sections from direct electric dipole capture they should be proportional to the deuteron penetration factor and to $(N-Z)^2/A^2$. No evidence is found for such a direct contribution. For Ni^{58}($N-Z = 2$) at a deuteron energy of 4.5 MeV, σ(d, γ) = 61±9 μb and σ (d, n) = 85±12 mb. For Cr^{54} ($N-Z = 6$) at a deuteron energy of 4.5 MeV σ (d, γ) = 295±45 μb and σ(d, p) = 75±12 mb. These cross-sections are consistent with an interpretation in terms of the statistical decay of a compound nucleus, the radiative probability being determined from photodisintegration data.

1. Introduction

In a previous paper [1]) we reported the measurement of the cross-section for the Zn^{64}(d, γ)Ga^{66} reaction for deuteron energies of 3.5–4.5 MeV. The results could be interpreted in terms of the statistical decay of a compound nucleus, the cross-section for the inverse reaction of gamma-ray excitation being deduced from photodisintegration studies. Both the radiative capture cross-section and the total cross-section (as inferred from the sum of the (d, n) and (d, p) cross-sections) agreed with the statistical calculations as to their magnitude and energy dependence.

Another process which might contribute to the radiative deuteron capture cross-section is direct capture, the importance of which for (n, γ) reactions has been pointed out by Lane and Lynn [2]). In the case of electric dipole capture the direct cross-section is zero for a nucleus with $N = Z$ if electric polarization of the nucleus and the incident deuteron is neglected. In the more general case in which $N \neq Z$ the effective charge of the deuteron is $(N-Z)e/A$ which may be compared with the effective charge for a proton of Ne/A. For electric dipole radiation the direct (d, γ) cross-section is expected to be proportional to $(N-Z)^2/A^2$ times a deuteron penetration factor.

In order to investigate the possible existence of direct (d, γ) capture in the middle-weight nuclei, we have now measured the cross-section for the Ni^{58}(d, γ) Cu^{60} ($N-Z = 2$) and Cr^{54}(d, γ)Mn^{56}($N-Z = 6$) reactions. Taken together with the previously measured Zn^{64}(d, γ)Ga^{66} ($N-Z = 4$) cross-section these results give the (d, γ) cross-sections for three middle-weight nuclei having $N-Z = 2$, 4 and 6. Allowing for the greater penetration for Cr^{54} a range of $\approx 20:1$ is predicted for the direct electric dipole capture cross-sections.

The method of induced radioactivity was again used. This method leads to a positive identification of the reaction. In contrast to a measurement of the capture gamma-rays the measured cross-sections are independent of the quality of the capture gamma-rays and no complications arise from (d, p, γ) and (d, n, γ) reactions. The radioactive method excludes that contribution to the radiative capture cross-section in which the emission of a primary (low) energy gamma-ray is followed by particle emission (i.e. (d, γ, p) and (d, γ, n) etc. reactions). Since Ni^{59} and Cr^{55} are unstable the (d, γ) products for Ni^{58} and Cr^{54} targets cannot be confused with identical activities produced by the prolific (d, n) reactions in isotopic impurities. Cu^{59} is also unstable so that (d, p) reactions in elemental impurities cannot confuse the Ni^{58}(d, γ) measurement. The same is not true for the Cr^{54}(d, γ) case since Mn^{55} is stable. This complication is discussed later.

2. Experimental Method and Results

The method is essentially the same as that used previously to measure the Zn^{64}(d, γ)Ga^{66} cross-section. Isotopically separated targets of Ni^{58} and Cr^{54} were bombarded with proton beams of $\approx 4\mu$A from the Harwell Van de Graaf at energies of 3.5, 4 and 4.5 MeV. The induced activities were observed with plastic and NaI(Tl) scintillation spectrometers using coincidence techniques to distinguish the relatively weak (d, γ) yields from other induced activities. In addition to the (d, γ) cross-sections we have also measured the Ni^{58}(d, n)Cu^{59} and Cr^{54}(d, p)Cr^{55} cross-sections. These results are useful for making comparisons with the statistical theory.

2.1. THE REACTION Ni^{58}(d, γ)Cu^{60}

The targets used were enriched to 94 % Ni^{58} and were 9.75 mg/cm^2 thick. Typical bombardments were for periods of 20 min. Cu^{60} decays by positon emission with a half-life of 24 min, the gamma-ray spectrum being complex with eight components in the range $E_\gamma = 0.85$–5.0 MeV. The two strongest lines, at 1.332 and 1.76 MeV, are in coincidence and this gamma-ray cascade was observed by measuring the gamma-ray spectrum from a 3.8 cm diam. $\times$ 2.5 cm long NaI(Tl) crystal (counter A) in coincidence with the 1.76 MeV gamma-ray line observed in a 11.4 cm diam. $\times$ 7.6 cm long NaI(Tl) crystal (counter B). The 24 min 1.332 MeV line of Cu^{60} was clearly resolved by this coincidence

arrangement. The only other activity which appeared in the coincidence spectrum was 15 h Na^{24}, presumably produced by the Na^{23}(d, p) reaction in sodium impurities on the target. The 1.38–2.75 MeV coincident gamma-rays of Na^{24} gave rise to a small 15 h component to the 1.3 MeV line in counter A produced maily by events in coincidence with the double escape peak at 1.76 MeV corresponding to absorption of the 2.75 MeV gamma-rays in counter B. The yield of Cu^{60} was obtained from the measured 24 min component of the 1.332 MeV gamma-ray line in the coincidence spectrum. The absolute efficiencies of the apparatus for detecting 2.75 and 1.38 MeV gamma-rays were determined by measuring the coincidence counting rate and the single counting rate in both

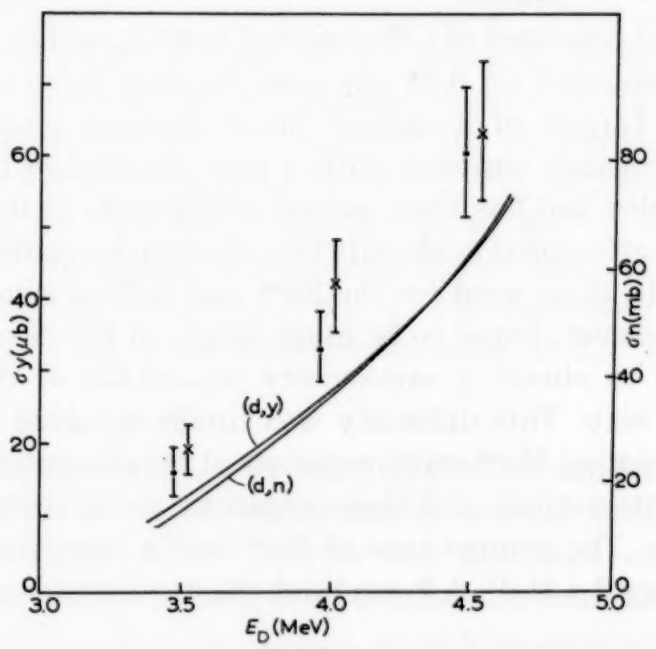

Fig. 1. Cross-sections for the reactions Ni^{58}(d, γ) – denoted by dots – and Ni^{58}(d, n) – denoted by crosses – as a function of deuteron energy. The full curves are given by the statistical theory. (The scale for (d, γ) is to the left and for (d, n) to the right).

arms with a pure Na^{24} source placed in the same geometry as the Ga^{66} sample. The relative efficiencies for the 1.38–2.75 MeV gamma-ray cascade of Na^{24} and the 1.332–1.76 MeV gamma-ray cascade of Cu^{60} were obtained from the compilation of Mott and Sutton [3]). The Cu^{60} decay scheme proposed by Nussbaum *et al.* [4]) was used to evaluate the Ni^{58}(d, γ)Cu^{60} cross-sections from the measured yields. The capture cross-sections, corrected for effective target thickness, are shown in fig. 1 for deuteron energies of 3.5, 4.0 and 4.5 MeV.

2.2. THE REACTION Ni^{58}(d, n)Cu^{59}

The same targets were used as for the (d, γ) measurements. Cu^{59} decays by positon emission with a half-life of 81 sec (Butler and Gossett [5])). Several 1 min bombardments were made and the induced Cu^{59} activity was measured by counting the annihilation radiation in a 3.8 cm diam. × 2.5 cm long NaI(Tl)

crystal placed 60 cm from the source. The (d, n) cross-sections, corrected for effective target thickness, are shown in fig. 1 for deuteron energies of 3.5, 4.0 and 4.5 MeV.

At a deuteron energy of 4.5 MeV the results for Ni^{58} are

$$\sigma(d, \gamma) = 61 \pm 9\ \mu b, \quad \sigma(d, n) = 85 \pm 12\ \mu b,$$
$$\sigma(d, \gamma)/\sigma(d, n) = (0.72 \pm 0.15) \times 10^{-3}.$$

This ratio is nearly constant over the measured range of deuteron energies (3.5–4.5 MeV).

2.3. THE REACTION $Cr^{54}(d, \gamma)Mn^{56}$

The targets used consisted of Cr^{54} enriched to 87 % and in the form of Cr_2O_3. The oxide was deposited on 0.25 mm gold backing using a small amount of plastic bonding. Targets of 8 mg/cm² thickness were prepared in this way. Mn^{56} decays by negaton emission with a half life of 2.58 h. The gamma-ray spectrum is complex and has three strong components at 0.845, 1.81 and 2.13 MeV. Initially we attempted to identify this reaction by gamma-ray coincidence methods similar to those used for the Zn^{64} and Ni^{58} measurements. The Na^{24} impurity was, however, found to be much larger in the chromium case and it was not possible to obtain a satisfactory separation of the Na^{24} and Mn^{56} activities in this way. This difficulty was finally resolved by the use of β–γ coincidence techniques. Mn^{56} emits negatons of maximum-energy, 2.86 MeV in 50 % of the disintegrations and these negatons are in coincidence with 0.845 MeV gamma-rays. The gamma-rays of Na^{24} are in coincidence with negatons of maximum energy 1.4 MeV. A 7 mm thick plastic detector was used to observe

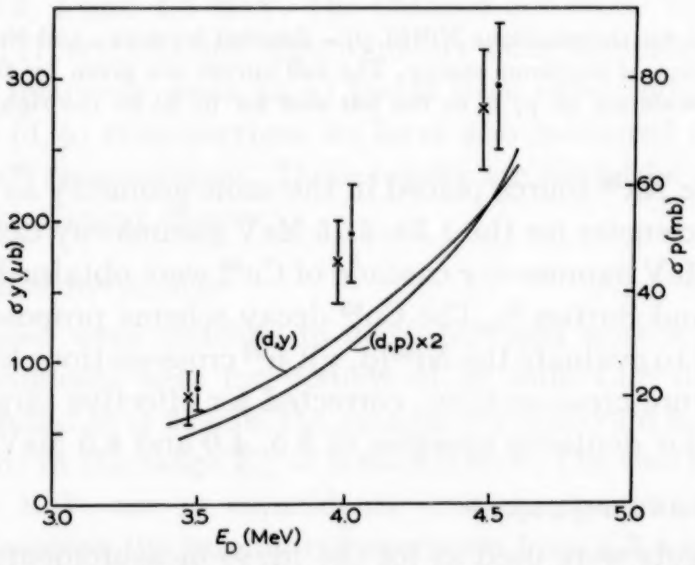

Fig. 2. Cross-sections for the reactions $Cr^{54}(d, \gamma)$ – denoted by dots – and $Cr^{54}(d, p)$ – denoted by crosses – as a function of deuteron energy. The full curves are given by the statistical theory; the theoretical cross-section for (d, p) has been doubled to show the constancy of the ratio of the cross-sections.

the negatons with the bias set so as to exclude the 1.4 MeV β-particles of Na^{24}. The 3.8 cm diam. $\times$ 2.5 cm long NaI(Tl) crystal was used to detect the gamma-rays in coincidence with the Mn^{56} negatons and with this apparatus the β–γ coincidence of 2.58 MeV Mn^{56} was readily observed. The decay scheme given in ref. [6]) was used to evaluate the yields. As remarked in the introduction, a complication arises in the determination of the $Cr^{54}(d, \gamma)Mn^{56}$ cross-section, owing to the fact that Mn^{55} is stable. Thus, any impurity of Mn^{55} in the target material will produce Mn^{56} through the $Mn^{55}(d, p)$ reaction and this will be indistinguishable from that produced in the $Cr^{54}(d, \gamma)$ reaction. In order to estimate the amount of Mn^{55} present in the target material, a sample from the same batch of $Cr_2^{54}O_3$ was irradiated in the reactor "Gleep" for a period of 15 min at a neutron flux of 2×10^8 n/sec. After irradiation the sample was counted as before in the β–γ coincidence arrangement in order to measure the amount of Mn^{56} produced by the $Mn^{55}(n, \gamma)$ reaction. From these results it was estimated that the amount of Mn^{55} impurity in the $Cr_2^{54}O_3$ samples was not greater than 0.1 %. Taking the cross-section for $Mn^{55}(d, p)\ Mn^{56}$ as 100 mb (i.e. larger than $Cr^{54}(d, p)Cr^{55}$ – see below) then this reaction could account for up to 25 % of the yield of Mn^{56} ascribed to $Cr^{54}(d, \gamma)$. The measured $Cr^{54}(d, \gamma)$ cross-sections are shown in fig. 2 for deuteron energies of 3.5, 4.0 and 4.5 MeV.

2.4. THE REACTION $Cr^{54}(d, p)Cr^{55}$

The same targets were used as for the (d, γ) measurements. Cr^{55} decays by negaton emission with a half life of 3.5 min [6]). Several 3 min bombardments were made and the induced Cr^{55} activity was measured with the plastic β-counter. These yields may also include a contribution from 3.8 min V^{52} produced in the $Cr^{54}(d, \alpha)V^{52}$ reaction but the (d, p) yield is expected to predominate. The measured $Cr^{54}(d, p)$ cross-sections are shown in fig. 2.

At a deuteron energy of 4.5 MeV the results for Cr^{54} are

$$\sigma(d, \gamma) = 295 \pm 45\ \mu b, \quad \sigma(d, p) = 75 \pm 12\ mb,$$
$$\sigma(d, \gamma)/\sigma(d, p) = (3.9 \pm 1) \times 10^{-3}.$$

The ratio is nearly constant over the measured range of deuteron energies (3.5–4.5 MeV).

3. Discussion

We shall first compare the measured cross-sections with those calculated from the statistical theory according to which the cross-sections are related to the widths by

$$\sigma(d, x)/\sigma(\text{total}) = \Gamma_x/\Gamma_{(\text{total})}. \qquad (1)$$

It was shown previously [1]) that the total radiation width as measured by induc-

ed radioactivity is given by †

$$\Gamma_\gamma = \frac{4}{\pi}\frac{NZ}{A}\frac{e^2}{\hbar c}\frac{1+0.8x}{MC^2}\frac{\Gamma_g}{\omega_0(E)}\int_0^T \frac{\omega_0(R)\varepsilon^4 \mathrm{d}R}{(\varepsilon^2-E_m^2)^2+(\Gamma_g\varepsilon)^2}.$$

In deriving this expression it was assumed that the cross-section for the inverse process of gamma-ray excitation could be obtained from the ground state photodisintegration data characterised by a giant resonance at an energy E_m with a width Γ_g. We take $E_m = 19$ MeV, $\Gamma_g = 5.5$ MeV and the exchange parameter $x = \frac{1}{2}$. The quantity E is the excitation energy of the capturing state, ε the gamma-ray energy, $R = E-\varepsilon$ the energy of the residual nucleus and ω_0 the level density of states of spin zero. T is the effective "threshold" for secondary particle emission such that for $R > T$ particle emission dominates further gamma-ray emission. The particle widths have been calculated from the data of Blatt and Weisskopf [7]) with a nuclear radius $R = 1.5A^{\frac{1}{3}}\times 10^{-13}$ cm.

Cameron's semi-empirical results for the level densities [8]) have been used to evaluate the various partial widths. The Q-values for the reactions were taken from ref. [6]), the values used being 11.1 MeV for Ni^{58}+d, MeV, 9.7 MeV, for Cu^{59}+n, 4.33 MeV for Ni^{59}+p, 12.9 MeV for Cr^{54}+d, 7.26 MeV for Mn^{55}+n and 9.33 MeV for Cr^{55}+p. Thus T is determined by proton re-emission for Ni^{58} and by neutron re-emission for Cr^{54}. We take $T = 5$ MeV for Ni^{58} and $T = 7.5$ MeV for Cr^{54}. (The results are not very sensitive to changes in T). The total deuteron reaction cross sections have been calculated using the penetrability tables of Sharp, Gove and Paul [9]) assuming a nuclear radius of $(1.5A^{\frac{1}{3}}+1.0)\times 10^{-13}$ cm.

TABLE 1

Results for 4.5 MeV deuterons

Initial nucleus	Reaction	$\sigma_{exp}(\pm 15\ \%)$	$\sigma_{stat\ theor}$	σ_{rel} (direct capture)
Ni^{58}	(d, γ) (d, n) $\frac{(d,\gamma)}{(d,n)}$	61 μb 85 mb 0.7×10^{-3}	48 μb 64 mb 0.75×10^{-3}	61 μb (assuming the measured σ to be totally accounted for by this process)
Zn^{64}	(d, γ) (d, n)+(d, p) $\frac{(d,\gamma)}{(d,n)\times(d,p)}$	80 μb 160 mb 0.5×10^{-3}	86 μb 175 mb 0.49×10^{-3}	192 μb
Cr^{54}	(d, γ) (d, p) $\frac{(d,\gamma)}{(d,p)}$	295 μb 75 mb 3.9×10^{-3}	215 μb 29 mb 7.4×10^{-3}	1280 μb

† There is a misprint in eq. (5) of ref. [1]), the right side of which should be divided by π. Eq. (6) of ref. [1]) is correct.

The calculated cross-sections are compared with the measured values in figs. 1 and 2. It is seen that the agreement with the statistical theory is quite good. A similar conclusion was reached for the $Zn^{64}(d, \gamma)$ and $(d, n)+(d, p)$ measurements.

There is little evidence for a direct electric dipole contribution to the (d, γ) cross-sections. The $(N-Z)^2/A^2$ factor would give a ratio of $\approx 10 : 1$ between the $Cr^{54}(d, \gamma)$ and $Ni^{58}(d, \gamma)$ cross-sections and this ratio is increased to $\approx 20 : 1$ when penetration factors are included. The experimental results for 4.5 MeV deuterons are summarized in table 1 and compared with the statistical calculations and with the relative (d, γ) cross sections predicted by the simple electric dipole direct theory. The last are normalized to the measured $Ni^{58}(d, \gamma)$ cross-section. The results for Zn^{64} are taken from ref. [1]). The measured cross-sections can be accounted for completely by compound-nucleus formation, but the possibility that the direct mechanism may account for up to $\frac{1}{3}$ of the cross-section cannot be ruled out for $N-Z = 6$.

One of us (J. H. Carver) is indebted to Dr. E. Bretscher and to Dr. E. B. Paul for the facilities made available to him while visiting Harwell.

References

1) J. H. Carver and G. A. Jones, Nuclear Physics **11** (1959) 400
2) A. M. Lane and J. E. Lynn, Nuclear Physics **11** (1959) 646
3) W. E. Mott and R. B. Sutton, Enccylopedia of Physics, ed. by S. Flügge (Springer Verlag, Berlin, 1958) Vol. **45**, p. 86
4) R. H. Nussbaum, R. van Lieshout, A. H. Wapstra, N. F. Verster, F. E. L. ten Haaf, G. J. Nijgh and L. T. M. Ornstein, Physica **20** (1954) 555; Phys. Rev. **93** (1954) 255
5) J. W. Butler and C. R. Gossett, Phys. Rev. **109** (1958) 863
6) K. Way, R. W. King, C. L. McGinnis and R. van Lieshout, Nuclear Level Schemes $A = 40$–92, USAEC report No. TID-5399 (1955)
7) J. M. Blatt and V. Weisskopf, Theoretical Nuclear Physics (John Wiley, New York, 1953)
8) A. G. W. Cameron, Can. J. Phys. **36** (1958) 1040
9) W. T. Sharp, H. E. Gove and E. B. Paul, Chalk River Report No. TPI-70 (1953)

2.D

Nuclear Physics **24** (1961) 614—619; © *North-Holland Publishing Co., Amsterdam*

Not to be reproduced by photoprint or microfilm without written permission from the publisher

THE MAGNETIC SPECTROGRAPH DATA ON LEVEL DENSITIES OF LIGHT NUCLEI

N. MACDONALD and A. C. DOUGLAS

Atomic Weapons Research Establishment, Aldermaston

Received 9 January 1961

Abstract: The magnetic spectrograph data on levels in nuclei of mass 18 to 34 are discussed, in relation to nuclear level densities and temperatures. It is pointed out that, contrary to the situation in nuclei with mass about 50, the level densities do not vary in a simple manner with the odd or even character of the nuclei. Some extensions of the magnetic spectrograph work are suggested.

1. Introduction

Quite a considerable amount of information is available on the energies of levels in light and medium mass nuclei, as a result of the magnetic spectrograph analysis of nuclear reactions. The early work of this kind made use mainly of (d, p) and (p, p′) reactions. More recently it has been possible to use other reactions [1]) so that a greater variety of nuclei can be studied.

In the past this information has been obtained as a secondary product of work intended in the first place to provide detailed information about particular levels. However, Ericson [2]) has pointed out that the magnetic spectrograph data are relevant to the study of nuclear level densities and temperatures. This

TABLE 1

Summary of data of Hinds and Middleton [1])

Nucleus	Reaction	Number of states	Maximum energy (MeV)
F^{18}	(He^3, p), (He^3, d)	40	7.5
Ne^{21}	(He^3, p)	67	9.3
Na^{22}	(He^3, α), (d, α)	22	4.8
Mg^{24}	(He^3, d)	39	11.9
Mg^{25}	(d, p), (d, α)	58	8.0
Mg^{26}	(d, p), (t, α), (t, p)	71	10.3
Al^{26}	(He^3, p), (He^3, α)	70	6.9
Mg^{27}	(d, p)	18	5
Mg^{28}	(t, p)	22	7
Si^{28}	(He^3, d)	32	10.4
Si^{29}	(d, p), (He^3, p)	39	8.0
S^{32}	(He^3, d)	24	8.5
Cl^{34}	(He^3, p)	21	4.2

paper discusses the information on these questions which can be obtained from the data of Hinds and Middleton [1]) for nuclei with A between 18 and 34. These data are summarised in table 1 and fig. 1.

Any discussion of level densities based on this kind of experimental data must assume either that almost all levels, in the energy range examined, are detected, or at least that the same proportion of levels escape detection in different nuclei. Now it is quite possible that different reactions pick out different types of level †. For example one would expect (d, p) reactions to pick out single particle levels, and (p, p′) reactions collective levels. For this reason and because the experimental work has not in general been carried out with level densities in mind, we wish †† to draw attention to the value of repeating this kind of work with improved energy resolution, and taking great pains to identify weakly excited levels. Since this adds greatly to the labour involved in establishing the spectra, one has to make a judicious choice of nuclei to examine in more detail. We shall point out some suitable cases.

2. Variation of Level Density with the Type of Nucleus

It is convenient to plot, against excitation energy E, the quantity $\log N(E)$, where N is the number of levels with energy less than or equal to E. Fig. 1 shows in this manner the results of ref. [1]) for nuclei of mass 24 to 32. The curves for Mg^{27}, Mg^{28} and Cl^{34}, which only extend to about $N = 20$, lie slightly above those for Mg^{25}, Mg^{26} and Al^{26} respectively.

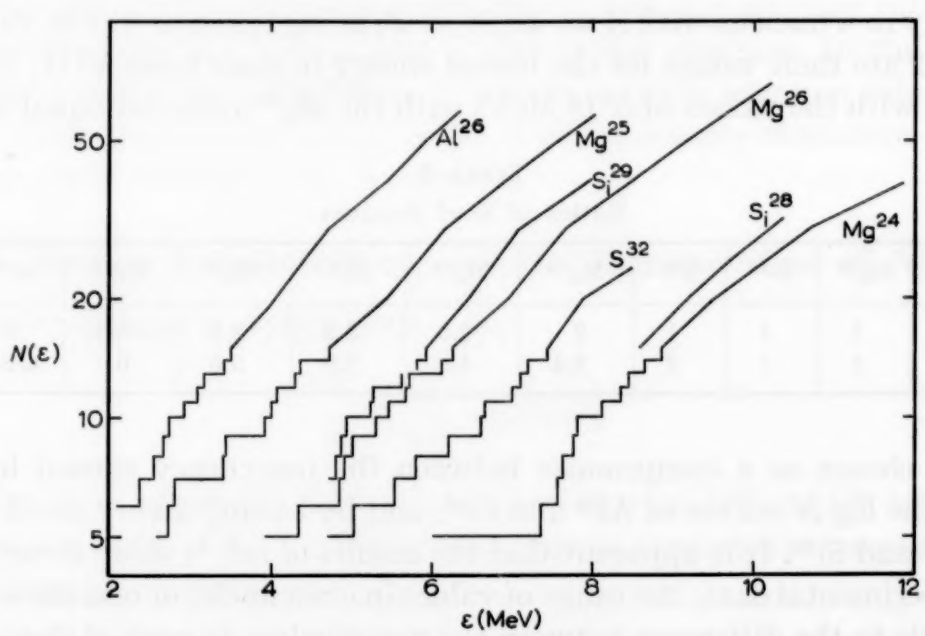

Fig. 1. Number $N(E)$ of levels with energy less than E plotted against E, for various light nuclei.

† It is pertinent to remark that in several cases [1]) more than one reaction has been used to study levels in one nucleus.

†† See also [2]) the remarks of Ericson on the Mn^{56} data.

Ericson [3]) has pointed out that, if one assumes equal pairing energy Δ for a pair of neutrons or a pair of protons, and neglects any pairing interaction between a neutron and a proton, the level densities $\rho(E)$ of odd, odd mass and even nuclei of about the same A should approximately satisfy

$$\rho_{\text{odd}}(E) = \rho_{\text{odd mass}}(E+\tfrac{1}{2}\Delta) = \rho_{\text{even}}(E+\Delta).$$

This has the consequence [2]) that the log $N(E)$ curves lie in the three parallel groups, separated by an energy $\frac{1}{2}\Delta$. This regularity is found [2]) in the magnetic spectrograph data for nuclei with A about 50.

The clear separation of these three groups is not apparent in fig. 1, and a noticeable feature is the difference † between Mg^{24} and Mg^{26}. In this mass region, in which neutrons and protons are filling the same shell, it is presumably not correct to ignore the pairing interaction of a neutron and a proton [5]). Quadruple correlations are also a possibility [6]). One might also expect, whether pairing is considered or not, that level densities should be sensitive to the value of $T_3 = \frac{1}{2}(N-Z)$, the projection of the isobaric spin.

Bardeen and Feenberg [7]) present results for a model which takes into account the dependence of the potential energy on T_3. In their table VIII they give ratios of the level densities in different types of nucleus, namely those with

$$\begin{aligned} A &= 4k, & N-Z &= 0, 2, \ldots, \\ A &= 4k+2, & N-Z &= 0, 2, \ldots, \\ A &= 4k\pm 1, & N-Z &= 1, 3, \ldots, \end{aligned}$$

the density in a nucleus with $A = 4k, N = Z$, being taken as 1. The values ρ in our table 2 are their values for the lowest energy in their table VIII. These are compared with the values of N (8 MeV) with the Mg^{24} value set equal to 1. The

TABLE 2

Ratios of level densities

Nucleus	Mg^{24}	Si^{28}	S^{32}	Mg^{26}	Mg^{28}	Si^{29}	Mg^{25}	Mg^{27}	Al^{26}	Cl^{34}
ρ	1	1	1	2	2.3	3.3	3.3	5.3	8	8
N(8 MeV)	1	1	2	3.4	4.5	3.9	5.5	6	≈ 25	≈ 25

energy is chosen as a compromise between the inaccuracy caused by extrapolating the log N curves of Al^{26} and Cl^{34}, and by having a very small value of N in Mg^{24} and Si^{28}. It is apparent that the results of ref. [7]) share these features of the experimental data; the range of values in even nuclei or odd mass nuclei is comparable to the difference between the mean values in each of these groups, and the smallest level densities occur for even nuclei with $N = Z$.

† The shell structure effect considered by Newton [4]) would give a smaller level density in Mg^{26} than in Mg^{24}.

Any more detailed discussion would require the development of a theory of level densities treating T and T_3 as variables (compare ref. [8])) and suitable for including the effects of residual interactions and deformation. These two factors are known to affect the binding energies of these nuclei in a complicated manner [9]). However, the above discussion indicates that in these nuclei the behaviour of level densities involves more than simply the "odd-even difference" which has been looked for in some heavy ion work [10]). Further magnetic spectrograph work would be most usefully aimed at adding to the information on sets of isobars.

We have excluded from the above discussion the three lightest nuclei studied in the Aldermaston [1]) magnetic spectrograph work, F^{18}, Ne^{21} and Na^{22}. The curves here are not parallel, $N(E)$ being equal for F^{18} and Ne^{21} at about 7.5 MeV. It seems likely that more levels have escaped detection in F^{18} than in Ne^{21}. The nucleus F^{18} is the nearest nucleus, among those examined, to a double closed shell, but the data available for nuclei near $N = 20$, $Z = 20$ suggest that the effect of proximity to a double closed shell is a change in the energy gap, leaving the log N curves parallel †.

No magnetic spectrograph data are available for even nuclei with $N = Z$ in the region $A \approx 50$, since these nuclei are rather deficient in neutrons relative to stable nuclei. However, the compound nucleus calculations of Dostrovsky *et al.* [12]) require an extra energy gap for Fe^{52} and Cr^{48}, to account for the observed behaviour of the reactions $Cr^{50}(\alpha, 2n)Fe^{52}$ and $Ti^{46}(\alpha, 2n)Cr^{48}$. These authors quote a comment by de Shalit that this effect is a result, not of a low density of states in the even nuclei with $N = Z$, but of a selection rule preventing the excitation of $T = 0$ states in the $(\alpha, 2n)$ reaction. In the reactions employed by Hinds and Middleton [1]) there is no such selection rule.

Some evidence for a dependence on $N-Z$ of the density of neutron resonance levels has been presented by Newson [13]).

3. Nuclear Temperatures and the Extrapolation of $N(E)$

Ericson [2]) defines a temperature τ by

$$\frac{1}{\tau} = \frac{\mathrm{d}}{\mathrm{d}E} \log N(E).$$

He points out that for nuclei with $A \approx 55$, and also for Al^{28} and S^{33}, $\log N$ can be approximated quite well by a straight line for an appreciable range of E. This implies that $\tau = T$, where

$$\frac{1}{T} = \frac{\mathrm{d}}{\mathrm{d}E} \log \rho(E)$$

† Data from M.I.T. progress reports for K^{40}, K^{41} and K^{42}, and of C. M. Braams [11]) for Ca isotopes.

defines the temperature commonly used in discussing compound nucleus reactions. Ericson regards this behaviour of N as evidence that T is constant for quite a large range of E. A straight line can be fitted to each of the curves in fig. 1, and to the F^{18} and Ne^{21} curves, for quite a wide range of E. The results for τ are presented in table 3, for nuclei in which 30 or more levels are known.

TABLE 3
Temperatures

Nucleus	States fitted	τ(MeV)
F^{18}	3–21	2.2
Ne^{21}	0–40	1.9
Mg^{24}	9–33	2.5
Mg^{25}	3–40, 4–60	2.1, 2.3
Mg^{26}	8–50	2.2
Al^{26}	0–20, 6–31	1.4, 1.7
Si^{28}	2–35	2.0
Si^{29}	2–32	1.8

One can compare the temperatures τ with the values of T obtained in the analysis of compound nucleus reactions. Storey *et al.* [14]) obtain from their Al^{27}(n, p) data the value $T = 1.75$ MeV, for excitation energy 3 to 11 MeV. From the Al^{27}(p, p′) data of Gugelot [15]) these authors obtain $T = 2.3$ MeV, for excitation energy 8 to 12 MeV. Temperatures obtained from the analysis of heavy ion induced reactions [16]) are also consistent with the τ values of table 3, On the other hand our values are mostly appreciably higher than the temperature $T = 1.45$ MeV, which Facchini *et al.* [17]) give for Mg^{24}, Al^{27}, Si^{28}, P^{31} and S^{32}.

There is evidence [18]) that heavy ion compound nucleus reactions with light targets are best analysed in terms of a temperature increasing as $E^{\frac{1}{2}}$. In some cases, both in the nuclei considered here and in the nuclei for which Ericson [2]) proposes a constant τ, we find, by fitting the log N curves in two (overlapping) energy ranges with straight lines, that the τ values are consistent with this energy dependence. This is illustrated by the pairs of τ values for Mg^{25}, Al^{26} in table 3. It is difficult to distinguish such an increase in τ from the effect of failure to observe all states at high energies. Better energy resolution is required to settle whether the magnetic spectrograph data imply that T is constant in the energy range below neutron binding energy.

Ericson [2]) makes use of the straight line fitted to the log N curve † for Al^{28}, up to about 4.5 MeV, to extrapolate beyond the neutron binding energy ($\approx$ 7.5 MeV). He compares N with $N' = \tau\rho$, where ρ is the value of the level density, obtained by counting the resonance levels observed by Hibdon [20]) in the scattering of neutrons of energy 175 keV to 375 keV on Al^{27}. The two values agree, lending some support to the view that T is constant up to 7.5 MeV in Al^{28}.

† Data of Buechner *et al.* [19]).

More recently Hibdon [21]) has examined many neutron resonance levels in Na^{24}. It would be worth while checking the straight line fit to log N in this case also, so magnetic spectrograph analysis of Na^{23}(d, p) or Mg^{25}(t, α) reactions would be useful. Because of this special interest Na^{24} and Al^{28} would be the most interesting cases in which to perform experiments with improved energy resolution. If one accepts the use of the assumption that τ is constant to extrapolate $N(E)$ to the neutron binding energy in Al^{28}, it implies that one in three of the levels up to this energy were identified in ref. [19]).

The authors wish to thank Dr. S. Hinds and Dr. R. Middleton for providing information on their experiments, and for helpful comments.

References

1) S. Hinds and R. Middleton, Proc. Phys. Soc. **73** (1959) 501; **73** (1959) 721; **74** (1959) 779; **76** (1960) 553; to be published
2) T. Ericson, Nuclear Physics **11** (1959) 481
3) T. Ericson, Nuclear Physics **8** (1958) 265
4) T. D. Newton, Can. J. Phys. **34** (1956) 804
5) V. B. Belyaev, B. N. Zachariev and V. G. Soloviev, JETP **38** (1960) 952
6) V. G. Soloviev, Nuclear Physics **18** (1960) 161
7) J. Bardeen and E. Feenberg, Phys. Rev. **54** (1938) 809
8) C. Bloch, Phys. Rev. **93** (1954) 1094
9) D. M. Brink and A. K. Kerman, Nuclear Physics **12** (1959) 314
10) C. D. Goodman, Proc. Conf. on Reactions between Complex Nuclei (Gatlinburg) 1958, p. 94
11) C. M. Braams, Phys. Rev. **103** (1956) 1310
12) I. Dostrovsky, Z. Fraenkel and G. Friedlander, Phys. Rev. **116** (1959) 683
13) H. W. Newson, contribution Kingston Conf. on Nuclear Structure (1960)
14) R. S. Storey, W. Jack and A. Ward, Proc. Phys. Soc. **75** (1960) 526
15) P. C. Gugelot, Phys. Rev. **93** (1954) 425
16) C. E. Hunting, contribution 2nd Conference on Reactions between Complex Nuclei (Gatlinburg) 1960
17) U. Facchini, I. Iori and E. Menichella, Nuovo Cim. **16** (1960) 1109
18) A. Zucker, Proc. Int. Conf. on Nuclear Structure (Dunod, Paris, 1959), p. 261
19) W. W. Buechner, M. Mazari and A. Sperduto, Phys. Rev. **101** (1956) 188
20) C. T. Hibdon, Phys. Rev. **114** (1959) 179
21) C. T. Hibdon, Phys. Rev. **118** (1960) 514; to be published

7.C: 8.B

Nuclear Physics **24** (1961) 620—629; © *North-Holland Publishing Co., Amsterdam*

Not to be reproduced by photoprint or microfilm without written permission from the publisher

PION-HYPERON RESONANCES IN PION PRODUCTION IN HYPERON-NUCLEON COLLISIONS

S. N. BISWAS and V. GUPTA

Tata Institute of Fundamental Research, Bombay

Received 19 December 1960

Abstract: A brief survey of the one-pion production phenomena in hyperon-nucleon collisions is presented. Equalities and inequalities among the cross-sections for the various pion production reaction based on the hypothesis of charge-independence, are given. The effect of the resonances of the pion-nucleon and pion-hyperon systems in the final state is considered. The modification of these results due to the restricted symmetry hypothesis is also pointed out. Finally, the possibility of ascertaining the relative Σ–Λ parity from the angular distribution is indicated.

1. Introduction

A number of theoretical papers [1]) have suggested the possible existence of resonances for the pion-hyperon system similar to the well-known low energy pion-nucleon (3, 3) resonance. Of the various possibilities [1]) pointed out the most favoured one seems to be a resonance in the isobaric spin $T = 1$ and angular momentum $J = \frac{3}{2}$ state of the pion-hyperon system. The experimental data [2, 3]) on $K^- + p \to Y + \pi$ reactions at 400 MeV/c laboratory momentum for K^- does seem to indicate just such a resonance. The cross-section $\sigma(\Sigma^\pm) \approx 38$ mb for $K^- + p \to \pi^\mp + \Sigma^\pm$ is nearly twice the S-wave limit, thus suggesting a P-wave contribution. The slight forward peaking in $\pi^+\Sigma^-$ and backward for $\pi^-\Sigma^+$ seems to indicate the $P_{\frac{3}{2}}$ state. Further the largeness of $\sigma(\Sigma^\pm)$ compared to $\sigma(\Sigma^0) \approx 6$ mb for $K^- + p \to \Sigma^0 + \pi^0$ suggests that the resonance could be in the $T = 1$ state. Again noticing that the $(\Lambda\pi^0)$ production cross-section $\sigma(\Lambda)$ increases with energy while $\sigma(\Sigma^0)$ stays fairly constant one could conjecture that the large enhancement of the $\sigma(\Lambda)$ might be due to a possible resonance in $T = 1$ state of the $\Lambda\pi$-system also, it being known that $(\Sigma^0\pi^0)$ cannot exist in a $T = 1$ state. Recently [7]) some positive experimental support for a $\Lambda\pi$-resonance in the $T = 1$ state has been reported in the reaction $K^- + p \to \Lambda + \pi + \pi$ at a laboratory momentum of 1150 MeV/c for K^-. The angular momentum state, however, is not yet known.

One would also expect the occurrence of the pion-hyperon resonance in processes involving pion production in hyperon-nucleon collisions. However, in these processes a competing pion-nucleon resonance would be expected to be

present. In this note we have, on the basis of the charge independence hypothesis, analysed the reactions

$$\Sigma^{\pm}+\mathrm{N} \rightarrow \Sigma+\mathrm{N}+\pi, \tag{1a}$$

$$\Sigma^{\pm}+\mathrm{N} \rightarrow \Lambda+\mathrm{N}+\pi, \tag{1b}$$

$$\Lambda+\mathrm{N} \rightarrow \Lambda+\mathrm{N}+\pi, \tag{1c}$$

$$\Lambda+\mathrm{N} \rightarrow \Sigma+\mathrm{N}+\pi. \tag{1d}$$

The consequences of the assumption that only one isobaric state of the pion-hyperon or the pion-nucleon system in the final state is predominant are explored. The question of the angular momentum state associated with the dominant isobaric spin state has been left open. The results of such considerations have been expressed in the form of equalities and inequalities among the various production cross-sections. These relations immediately provide a means to test experimentally the possible existence of the resonances in the final state products. At present, though, the experimental data are rather meagre. Total cross-sections for hyperon-nucleon collisions around 150 MeV have only been measured [3]), but the data are not very reliable. At lower energies, however, some information regarding the Λ-nucleon interaction is available from hypernuclear data. The threshold laboratory hyperon kinetic energy required for the reactions (1a), (1b), (1c) and (1d) are respectively [4]) 325, 146, 314 and 492 in MeV. We have not considered the Σ–N processes giving K-meson and deuteron production (akin to pion and deuteron production in N–N collisions) as these require much higher threshold. We hope, though, that a direct experimental test of our calculation would be possible in the near future. In sect. 2, the effect of the pion-nucleon resonance is considered by combining the pion and the nucleon isobaric spins first and then adding the hyperon isobaric spin to obtain the total isobaric spin for the final state. Similarly in sect. 3, the effect of the pion-hyperon resonance is considered.

Further, a modification of the results of sect. 2 has been obtained (in sect. 4) by introducing the doublet approximation for the hyperons. No attempt has been made to predict these results in terms of nucleon-nucleon data, which is essentially invoking global symmetry. The failure of global symmetry in explaining strange-particle data is well-known [5]). Finally in the last section we present a simple angular momentum analysis of the reactions.

2. Isobaric Spin Analysis

2.1. GENERAL

We consider the processes $\mathrm{Y}+\mathrm{N} \rightarrow \mathrm{Y}+\mathrm{N}+\pi$, where Y stands for the Σ or Λ hyperon, and use the Gell-Mann-Nishijima (abbreviated as G–N) isobaric assignments for the baryons. To obtain the total isobaric spin T of the final

state we combine first the isobaric spins of the pion and the nucleon to give $T' = \frac{1}{2}$ or $\frac{3}{2}$, to which then add the isobaric spin of the final Y to give T. If charge independence holds, one can specify all the independent amplitudes for all the reactions (1) by the subscripts $(2T, 2T')$. We denote the various amplitudes by

$$\Gamma_{11}, \Gamma_{13}, \Gamma_{31}, \Gamma_{33} \text{ for reactions (1a)},$$

$$\gamma_{11}, \gamma_{33} \text{ for reactions (1b)},$$

$$\Omega_{11} \text{ for reactions (1c)},$$

$$\omega_{11}, \omega_{33} \text{ for reactions (1d)}.$$

For the $\Sigma^{\pm}$-hyperon in the initial state there are 22 reactions and for the Λ-hyperon in the initial state there are 14. Of these we need consider one half, as the other 18 reactions are related by charge symmetry ($p \to n$, $\Sigma^+ \to \Sigma^-$, $\Sigma^0 \to \Sigma^0$, $\Lambda \to \Lambda$, $\pi^+ \to \pi^-$, etc.) to the first half and thus have same cross-sections under charge independence. For example the reactions $\Sigma^+ + p \to \Sigma^+ + n + \pi^+$ and $\Sigma^- + n \to \Sigma^- + p + \pi^-$ will have the same cross-section. In table 1 we

TABLE 1

Cross-sections for $\Sigma^{\pm} + p \to Y + N + \pi$ on the assumption of charge independence

Reaction	Cross-section
$\Sigma^+ + p \to \Sigma^+ + p + \pi^0$	$\sigma_1 = \frac{3}{5}\lvert\Gamma_{33}\rvert^2$
$\to \Sigma^+ + n + \pi^+$	$\sigma_2 = \frac{2}{3}\lvert\frac{1}{5}\sqrt{5}\,\Gamma_{33} + \Gamma_{31}\rvert^2$
$\to \Sigma^0 + p + \pi^+$	$\sigma_3 = \frac{1}{3}\lvert\frac{2}{5}\sqrt{5}\,\Gamma_{33} - \Gamma_{31}\rvert^2$
$\to \Lambda + p + \pi^+$	$\sigma_4 = \lvert\gamma_{33}\rvert^2$
$\Sigma^- + p \to \Sigma^- + n + \pi^+$	$\sigma_5 = \frac{2}{27}\lvert 2\Gamma_{11} - \frac{1}{2}\sqrt{2}\,\Gamma_{13} + \Gamma_{31} - \frac{2}{5}\sqrt{5}\,\Gamma_{33}\rvert^2$
$\to \Sigma^+ + n + \pi^-$	$\sigma_6 = \frac{1}{3}\lvert\Gamma_{13} - \frac{2}{5}\sqrt{5}\,\Gamma_{33}\rvert^2$
$\to \Sigma^- + p + \pi^0$	$\sigma_7 = \frac{2}{27}\lvert\sqrt{2}\,\Gamma_{11} + \Gamma_{13} + \frac{1}{2}\sqrt{2}\,\Gamma_{31} + \frac{2}{5}\sqrt{10}\,\Gamma_{33}\rvert^2$
$\to \Sigma^0 + n + \pi^0$	$\sigma_8 = \frac{2}{27}\lvert -\Gamma_{11} + \sqrt{2}\,\Gamma_{13} + \Gamma_{31} + \frac{1}{5}\sqrt{5}\,\Gamma_{33}\rvert^2$
$\to \Sigma^0 + p + \pi^-$	$\sigma_9 = \frac{2}{27}\lvert\sqrt{2}\,\Gamma_{11} + \Gamma_{13} - \sqrt{2}\,\Gamma_{31} + \frac{1}{10}\sqrt{10}\,\Gamma_{33}\rvert^2$
$\to \Lambda + n + \pi^0$	$\sigma_{10} = \frac{2}{9}\lvert\gamma_{11} - \gamma_{33}\rvert^2$
$\to \Lambda + p + \pi^-$	$\sigma_{11} = \frac{1}{9}\lvert 2\gamma_{11} + \gamma_{33}\rvert^2$

thus list the cross-sections for the eleven $\Sigma^{\pm}$–p reactions and in table 2 those for the seven Λ–N reactions. The σ_i's given above are, of course, functions of the incoming energy and outgoing pion energy.

TABLE 2

Cross-sections for $\Lambda+p \to Y+N+\pi$ on the assumption of charge independence

Reaction	Cross-section
$\Lambda+p \to \Lambda+p+\pi^0$	$\sigma_{12} = \frac{1}{3}\lvert\Omega_{11}\rvert^2$
$\to \Lambda+n+\pi^+$	$\sigma_{13} = 2\sigma_{12}$
$\to \Sigma^0+p+\pi^0$	$\sigma_{14} = \frac{1}{9}\lvert\sqrt{2}\omega_{13}-\omega_{11}\rvert^2$
$\to \Sigma^0+n+\pi^+$	$\sigma_{15} = \frac{1}{9}\lvert\omega_{13}+\sqrt{2}\omega_{11}\rvert^2$
$\to \Sigma^-+p+\pi^+$	$\sigma_{16} = \frac{1}{2}\lvert\omega_{13}\rvert^2$
$\to \Sigma^+ +n+\pi^0$	$\sigma_{17} = \sigma_{15}$
$\to \Sigma^+ +p+\pi^-$	$\sigma_{18} = \frac{1}{9}\lvert\omega_{13}-2\omega_{11}\rvert^2$

As an immediate consequence of the results embodied in table 1 we can deduce the following triangular inequalities:

$$\sqrt{\sigma_1}+\sqrt{\sigma_3} \geqq \sqrt{\tfrac{1}{2}\sigma_2}, \quad \sqrt{2\sigma_{10}}+\sqrt{\sigma_{11}} \geqq \sqrt{\sigma_4}, \quad \sqrt{\sigma_9}+\sqrt{\sigma_7} \geqq \sqrt{\tfrac{1}{2}\sigma_2}, \tag{2}$$

and similar relations obtained by permuting the σ's involved in an inequality (e.g. $\sqrt{(\frac{1}{2}\sigma_2)}+\sqrt{\sigma_1} \geqq \sqrt{\sigma_3}$, etc.) In case of Λ–N reactions, apart from the equalities already noted in table 2, we can further deduce the following inequalities:

$$(1+\sqrt{2})\sqrt{2\sigma_{16}} \leqq 3\sqrt{\sigma_{15}}+3\sqrt{2\sigma_{18}}, \quad \sqrt{2\sigma_{16}} \leqq \sqrt{2\sigma_{14}}+\sqrt{\sigma_{15}}. \tag{3}$$

Experimental verification of the inequalities (2) and (3) and the equalities $\sigma_{13} = 2\sigma_{12}$ and $\sigma_{15} = \sigma_{17}$ would constitute a definite proof of the charge independence hypothesis in hyperon-nucleon collisions.

2.2. DOMINANT $T' = \frac{3}{2}$ STATE FOR THE FINAL π–N SYSTEM

The existence of the (3,3) resonance in low energy pion-nucleon scattering suggests that the π–N system in the final state will occur predominantly in the $T' = \frac{3}{2}$ state. Further, this assumption is well justified in case of one-pion production in nucleon-nucleon collisions [6]). On the basis of this idea we can make for Σ–N reactions the following approximation:

$$\Gamma_{11} \approx \Gamma_{31} \approx 0, \quad \gamma_{11} \approx 0. \tag{4}$$

Using (4), we have immediately from table 1,

$$\begin{aligned}
4\sigma_1 &= 18\sigma_2 = 9\sigma_3 = \tfrac{12}{5}\lvert\Gamma_{33}\rvert^2, \\
2\sigma_4 &= 18\sigma_{11} = 9\sigma_{10} = 2\lvert\gamma_{33}\rvert^2, \\
2\sigma_5 &= \sigma_7 = \tfrac{2}{27}\lvert\Gamma_{13}+2\sqrt{\tfrac{2}{5}}\Gamma_{33}\rvert^2, \\
\sigma_8 &= 2\sigma_9 \approx \tfrac{2}{27}\lvert\sqrt{2}\Gamma_{13}+\tfrac{1}{5}\sqrt{5}\Gamma_{33}\rvert^2, \\
\sigma_6 &\approx \tfrac{1}{3}\lvert\Gamma_{13}-\sqrt{\tfrac{2}{5}}\Gamma_{33}\rvert^2,
\end{aligned} \tag{5}$$

and the following triangular inequalities:

$$\sqrt{\sigma_5}+\sqrt{\sigma_8} \geqq \tfrac{1}{3}\sqrt{\sigma_6}, \quad \tfrac{1}{2}\sqrt{\sigma_8}+\sqrt{\sigma_5} \geqq \tfrac{1}{3}\sqrt{\tfrac{1}{2}\sigma_1}. \tag{6}$$

The marked differences between (2) and the relations (5) and (6) should make it easy for experiment to establish the existence of the dominance of the $\frac{3}{2}$ isobaric spin state for the π–N system in the final state.

Assuming this resonance for Λ–N reactions we have similarly from table 2 (putting $\omega_{11} = \Omega_{11} \approx 0$)

$$\sigma_{12} = \sigma_{13} = \sigma_{16} \approx 0, \quad \sigma_{15} = \sigma_{17} = \tfrac{1}{2}\sigma_{18} = 2\sigma_{14}. \tag{7}$$

Again (7) and (3) are easily distinguishable.

Another gross method to test the existence of the $T' = \frac{3}{2}$ π–N resonance and charge independence is to compare with experiment the multiplicity of charged to neutral as well as positive to negative Σ-hyperons in all the reactions. These ratios, on the assumption of the $T' = \frac{3}{2}$ π–N resonance, are summarized below in table 3.

TABLE 3

Multiplicities on the assumption of a resonance for $T = \frac{3}{2}$ state of the pion-nucleon system in the final state

Reactions	Multiplicities	
	$R_c = \dfrac{\text{no. of } \Sigma^+}{\text{no. of } \Sigma^-}$	$R_0 = \dfrac{\text{no. of } (\Sigma^+ + \Sigma^-)}{\text{no. of } \Sigma^0}$
$\Sigma^+ + p \to \Sigma + N + \pi$	∞	$\frac{11}{4}$
$\Sigma^- + p \to \Sigma + N + \pi$	$\infty > \sigma_6/3\sigma_5 > 0$	$(2\sigma_6+3\sigma_7)/6\sigma_9 \geqq 2.8$
$\Lambda + p \to \Sigma + N + \pi$	0	2

In case of Λ–p reactions one can show, generally, from table 2 (that is without the assumption of the π–N resonance) that $\infty > R_c > 0.3$ and $0 < R_0 < 2.3$.

Finally it should be remarked that one could assume a dominant $T' = \frac{1}{2}$ state for the π–N system, that is, make the approximation $\Gamma_{13} \approx \Gamma_{33} \approx 0$, $\gamma_{33} \approx 0$ and $\Omega_{33} \approx 0$. However, such a resonance is not indicated by experiment for low energies and we do not consider it in detail.

3. Dominant Pion-Hyperon Isobaric Spin State

In the process $Y + N \to Y + N + \pi$ one could consider the existence of a pion-hyperon resonance rather than the pion-nucleon one discussed in the previous

section. The experimental indications of a Λ–π resonance in the reaction $K^- + p \to \Lambda + \pi + \pi$ have already been pointed out in the introduction. Theoretical work [1]) seems to favour a resonance in the $T = 1$ state. Moreover, the idea of a resonance in state $T = 1$ (the only isobaric spin state common to the π–Σ and π–Λ systems) is attractive because of its compatibility with the 'restricted symmetry' hypothesis [5]) (also cf. sect. 4). To investigate the effect of such resonances in the reactions given by (1) we first combine the Y and π isobaric spins and then add to it the nucleon isobaric spin to obtain the total isobaric spin for the final state. We can then characterize the charge independent amplitudes by the subscript $(2T, T'')$, where T represents the total initial isobaric spin and T'' is just the isobaric spin of the π–Y system in the final state. We denote the various amplitudes by

$A_{32}, A_{31}, A_{11}, A_{10}$ for reactions (1a),

a_{31} and a_{11} for reactions (1b),

B_{11} for reactions (1c),

b_{10} and b_{11} for reactions (1d).

The various cross-sections σ_i in terms of the amplitudes A's and B's are given in table 4.

TABLE 4

Cross-sections σ_i for the $\Sigma + N \to Y + N + \pi$ reactions given in table 1.

	No resonance	Resonance in $T = 1$ state for Σ–π system
σ_1	$\frac{1}{10}\lvert\sqrt{5}\,A_{31} - A_{32}\rvert^2$	$\frac{1}{2}\lvert A_{31}\rvert^2$
σ_2	$\frac{4}{5}\lvert A_{32}\rvert^2$	0
σ_3	$\frac{1}{10}\lvert\sqrt{5}A_{31} + A_{32}\rvert^2$	σ_1
σ_4	$\lvert a_{31}\rvert^2$	$\lvert a_{31}\rvert^2$
σ_5	$\frac{1}{9}\lvert A_{31} - \frac{1}{5}\sqrt{5}A_{32} - A_{11} + \sqrt{2}A_{10}\rvert^2$	$\frac{1}{9}\lvert A_{31} - A_{11}\rvert^2$
σ_6	$\frac{1}{9}\lvert -A_{31} - \frac{1}{5}\sqrt{5}A_{32} + A_{11} + \sqrt{2}A_{10}\rvert^2$	σ_5
σ_7	$\frac{1}{18}\lvert\frac{3}{5}\sqrt{5}A_{32} + A_{31} + 2A_{11}\rvert^2$	$\frac{1}{18}\lvert A_{31} + 2A_{11}\rvert^2$
σ_8	$\frac{2}{9}\lvert\sqrt{\frac{2}{5}}A_{32} + A_{10}\rvert^2$	0
σ_9	$\frac{1}{18}\lvert\frac{3}{5}\sqrt{5}A_{32} - A_{31} - 2A_{11}\rvert^2$	σ_7
σ_{10}	$\frac{2}{9}\lvert a_{31} - a_{11}\rvert^2$	$\frac{2}{9}\lvert a_{31} - a_{11}\rvert^2$
σ_{11}	$\frac{1}{9}\lvert a_{31} + 2a_{11}\rvert^2$	$\frac{1}{9}\lvert a_{31} + 2a_{11}\rvert^2$

For notation see text.

Notice that the number of amplitudes required for the various reactions is still the same. This is but to be expected because the number of amplitudes should be independent of the manner in which we combine the isobaric spins in the final state. Moreover, the equalities ($\sigma_{13} = 2\sigma_{12}$) and $\sigma_{15} = \sigma_{17}$ and the inequalities (2) and (3) will also hold for the σ_i's given in terms of the amplitudes A, a, B and b. Interesting differences arise when the assumption of a Y–π resonance is made. For the case of resonance for $T'' = 1$, only the two amplides A_{31} and A_{11} remain and furthermore the inequalities

$$\sqrt{2\sigma_{10}}+\sqrt{\sigma_{11}} \geqq \sqrt{\sigma_4}, \tag{7a}$$

$$\sqrt{\sigma_5}+\sqrt{\sigma_7} \geqq \sqrt{2\sigma_1}, \tag{7b}$$

are obtained. The equalities are noted in table 4. These are to be compared with the inequalities (6) for the π–N resonance. Also, comparing the equalities for π–N resonance and π–Y resonance it is clear that they compete and that experiment should be able to distinguish as to which resonance prevails.

For reactions given by (1b) and (1c) only one isobaric state, namely $T'' = 1$, is possible for the π–Λ system. In case of reactions of the type (1d) the assumption of the $T'' = 1$ resonance for Σ–π leads to

$$\sigma_{14} = 0, \quad \sigma_{15} = \sigma_{17} = 2\,\sigma_{16} = 2\sigma_{18} \approx \tfrac{1}{3}|b_{11}|^2.$$

The multiplicities, i.e. the ratios R_c and R_0, given by table 3 are summarized below in table 5 on the assumption of the resonance for $T'' = 1$. The results for the resonances for $T'' = 0$ and 2 can be similarly deduced from table 4.

TABLE 5

Multiplicities on the assumption of a resonance for $T = 1$ state of the π–Σ system in the final state

Reactions	Multiplicities	
	R_c	R_0
$\Sigma^+ + p \to \Sigma + N + \pi$	0	1
$\Sigma^- + p \to \Sigma + N + \pi$	1	$\frac{2\sigma_5+\sigma_7}{3\sigma_7} \geqq 1$
$\Lambda + p \to \Sigma + N + \pi$	3	2

R_c and R_0 are defined in table 3.

The above table for multiplicities with $T'' = 1$ π–Σ resonance is to be compared with table 3 with the $T = \frac{3}{2}$ resonance for the π–N resonance. The differences are marked enough for experiment to distinguish between the two resonances.

4. Restricted Symmetry

It is now generally believed that the global symmetry model of strong interactions ($g_{N\pi} = g_{\Lambda\pi} = g_{\Sigma\pi} = g_{\Xi\pi}$) fails [5]) to explain the observed data on strange particle reactions involving K-mesons. However the 'restricted symmetry' hypothesis ($g_{N\pi} \neq g_{\Lambda\pi} = g_{\Sigma\pi} \neq g_{\Xi\pi}$) seems to be compatible [5]) with experiment. In this section we present the results obtained on the basis of restricted symmetry by forming the two isobaric doublets

$$\Sigma^+, \quad (\Lambda - \Sigma^0)/\sqrt{2} \quad \text{and} \quad (\Lambda + \Sigma^0)/\sqrt{2}, \quad \Sigma^-$$

out of the hyperons. The further symmetry thus induced leads to new relations between the σ_i's in addition to those given by (2). The new equalities for $\Sigma^{\pm} + p \to Y + N + \pi$ reactions are

$$\sigma_6 = 0, \quad \sigma_3 = \sigma_4, \quad \sigma_8 = \sigma_{10}, \quad \sigma_9 = \sigma_{11}, \tag{8}$$

and the new triangular inequalities are

$$\sqrt{\sigma_5} + \sqrt{\sigma_7} \geqq \sqrt{2\sigma_3}, \quad \sqrt{\tfrac{1}{2}\sigma_5} + \sqrt{\sigma_9} \geqq \sqrt{\sigma_1}. \tag{9}$$

If there exists a $T = \frac{3}{2}$ π–N resonance in the final state then a single amplitude Γ_{23} characterizes the reactions and we have, in addition to (8),

$$6\sigma_1 = 12\sigma_2 = \tfrac{8}{3}\sigma_3 = 12\sigma_8 = 24\sigma_9 \approx |\Gamma_{23}|^2, \quad \sigma_1 = \sigma_7, \quad \sigma_2 = \sigma_5. \tag{10}$$

The multiplicities R_c and R_0 are also modified and are tabulated in table 6 for the $T = \frac{3}{2}$ π–N resonance.

TABLE 6

Multiplicities R_c and R_0 on the basis of the 'restricted symmetry' hypothesis

Reaction	$R_c = \dfrac{\text{no. of } \Sigma^+}{\text{no. of } \Sigma^-}$	$R_0 = \dfrac{\text{no. of } \Sigma^+ + \Sigma^-}{\text{no. of } \Sigma^0}$
$\Sigma^+ + p \to \Sigma + N + \pi$	∞	$\frac{2}{3}$
$\Sigma^- + p \to \Sigma + N + \pi$	0	2

The above table and results given by (8) and (10) are to be compared to table 3 and the equalities (5) of sect. 2.

5. Angular Momentum and Parity Analysis and Angular Distributions

It is known that the momentum dependence of the pion-production cross sections in nucleon-nucleon collisions well supports, as far as experimental information goes, the view that pions are emitted in a p-state only. This fact

can be easily understood from the basic Yukawa interaction $N \rightarrow N+\pi$ with the assumption that the nucleon is extremely heavy compared to pions. However, the extension of this conclusion to pions produced in two-nucleon collision is not necessarily correct, for the two nucleons in some of intermediate states may have large relative momentum, in which case the above argument may not be right. But the predominance of p-wave pions may fairly well be correct near the threshold for pion production. We have, however, in the present case considered both s and p wave final pions.

The angular momentum analysis, for the reactions given by (1), proceeds in the same way as for the $N+N \rightarrow N+N+\pi$ reactions (see ref. [6])). However, there is no Pauli principle in the Y–N case to reduce the number of allowed states. The other difference is that the relative parities $P_{\Sigma N}$ and $P_{\Lambda N}$ (in obvious notation) will determine the parity of the initial and final states and should influence the angular distributions. Only from the reactions given by (1b) and (1d) one would expect to infer the Σ–Λ relative parity $P_{\Sigma\Lambda}$. Limiting ourselves to pions produced in s or p states with respect to the baryons we give some of the possible angular distributions for the pions in table 7 below.

TABLE 7

Pion angular distributions

Initial state		Final state	Angular distribution	Total J	Parity
$P_{\Lambda\Sigma} = +$	$P_{\Lambda\Sigma} = -$				
$^1S_0$	$^3P_0$	$(^3S_1, p)$	isotropic	0	+
$^3P_0$	$^1S_0$	$(^1S_0, s)$	isotropic	0	−
$^3S_1$	$^1P_1$ or $^3P_1$	$(^1S_0, p)$ $(^3S_1, p)$	$\cos^2\theta$ $\sin^2\theta$	1	+
$^1P_1$ or $^3P_1$	$^3S_1$	$(^3S_1, s)$	isotropic	1	−

The parities in the table are given on the assumption that the relative parity $P_{\Sigma N} = +$. The angular distributions are those of the pions produced in the reactions (1b) and (1d). For other notations see Fermi [6]).

In table 7 the notation followed is that of Fermi [6]). The parities of the states are given, for the sake of definiteness, on the assumption that $P_{\Sigma N}$ is +, i.e., even. It is clear from table 7 that one can determine $P_{\Lambda\Sigma}$ from the angular distribution if the initial state is either $^3S_1$, $^1P_1$ or $^3P_1$.

Now, if we assume that the π–N system in the final state is produced with angular momentum $J = \frac{3}{2}$ and the hyperon in an s-state relative to it, then, for the final state, allowed values of total angular momentum are $J = 1$ or 2. Thus the assumption of the π–N (3, 3) resonance would permit only the initial

states $^3S_1$, $^1P_1$ or $^3P_1$. If the initial state is a pure S or P state, it is clear from table 7 that a study of the angular distribution would reveal whether $P_{\Lambda\Sigma}$ is odd or even. Our assumption of $P_{\Sigma N} = +$ is not restrictive: corresponding conclusions can be drawn for $P_{\Sigma N} = -$ in a similar way.

6. Conclusion

In the previous sections we have presented equalities and inequalities, between the cross-sections for the reactions $Y+N \to Y+N+\pi$ and also multiplicities of the Σ-hyperons produced. These results are based on the assumption of charge independence and further were given for both the Gell-Mann-Nishijima scheme and the 'Restricted Symmetry' model of the strange particle interactions. Further the effect of a resonance in a definite isobaric spin $T = \frac{3}{2}$ for the π–N and $T = 1$ for the π–Σ system in the final state was investigated. The resonances in the two systems were found to compete. It was remarked earlier that the results for the various cases mentioned above are sufficiently different to be distinguishable by experiment. Thus, an experimental verification of our results, apart from supporting charge independence of hyperon interactions, can also decide whether a π–Σ or a π–N resonance exists and whether restricted symmetry is valid or not. These questions cannot be answered by the available data on hyperon-nucleon collisions. We hope that a comparison with experiment will be possible in the near future.

References

1) D. Amati, A. Stanghellini and B. Vitale, Nuovo Cim. **13** (1959) 1143;
M. Nauenberg, Phys. Rev. Lett. **2** (1959) 351;
A. Komatsuzawa, R. Sugano and Y. Nogami, Prog. Theor. Phys. **21** (1959) 151
2) R. H. Capps, Phys. Rev. **119** (1960) 1753
3) L. W. Alvarez, Report of the High Energy Conference at Kiev (1959), p. 52
4) H. C. Meyer and W. G. Holladay, Nuovo Cim. Suppl. **3** (1960) 387
5) A. Salam, Kiev Conference (1959);
S. S. Saxena and S. N. Biswas, Nuovo Cim. **17** (1960) 748;
M. L. Gupta, Nuovo Cim. **16** (1960) 737
M. Ross and G. Shaw, Phys. Rev. **115** (1959) 1773;
T. Sakuma and S. Furui, Prog. Theor. Phys. **23** (1960) 552;
B. d'Espagnat and J. Prentki, Nuovo Cim. **15** (1960) 130
6) A. M. Rosenfeld, Phys. Rev. **96** (1954) 139
E. Fermi, Nuovo Cim. Suppl. **2** (1955) 17
7) M. Alston, Rochester Conference (1960);

1.D.2:
2D:2.F

Nuclear Physics **24** (1961) 630—641; © *North-Holland Publishing Co., Amsterdam*
Not to be reproduced by photoprint or microfilm without written permission from the publisher

PROTONS AND DEUTERONS FROM Al^{27} BOMBARDED BY 14.8 MeV NEUTRONS

R. N. GLOVER and E. WEIGOLD

Department of Nuclear Physics, Australian National University, Canberra

Received 2 January 1961

Abstract: Angular distributions for direct interaction proton groups corresponding to individual Mg^{27} levels are measured and shown to agree with theoretical predictions. Nuclear temperatures of 1.55 ± 0.15 MeV and 0.49 ± 0.02 MeV are found for the reactions (n, pγ) + (n, pn) and (n, np), respectively. Cross sections for proton emission are: total 273 ± 20 mb; (n, pγ) + + (n, pn) 89 mb compound nucleus, 27 mb direct interaction; (n, np) 157 mb. Spins are assigned to several Mg^{27} levels from analysis of the present experiment and of previous Mg^{26}(d,p) Mg^{27} experiments.

Angular distributions of deuteron groups corresponding to Mg^{26} levels at 0, 1.83 and 3.6 MeV are measured. Reduced widths are extracted and shown to agree with the predictions of the rotational model.

1. Introduction

Proton emission from aluminium bombarded with 14 MeV neutrons has been studied on numerous occasions [1–10]). Level structure has been demonstrated [4, 8, 10]) and correlated with Mg^{27} levels known from the Mg^{26}(d, p)Mg^{27} reaction [11]). Crude angular distributions have been obtained from nuclear emulsion experiments [2, 3]). Experiments with counter telescopes have measured only the energy spectrum at a given forward angle [6, 7, 8, 10]). Using nuclear emulsions Overseth and Peck [5]) attempted to measure angular distributions corresponding to transitions to individual levels of the residual Mg^{27} nucleus. However, examination of their energy and angular distributions suggests that the majority of their analysed tracks were recoil protons.

The emission of deuterons has been reported by Colli *et al.* [12]) but angular distributions were not measured.

The aim of the present experiment is to provide quantitative data on proton and deuteron emission from aluminium by detailed study of energy and angular distributions.

2. Experimental Method

The counter telescope and associated equipment were described earlier [13]). The experiment was carried out and the data analysed essentially as before [14]). The target was an aluminium foil of diameter 2.9 cm and thickness 7.1 mg/cm^2. Four sets of data, each consisting of four runs per angle of observation, were recorded. For each run particles in the energy range 1–15 MeV were detected.

3. The Reactions $Al^{27}(n, p)Mg^{27}$ and $Al^{27}(n, np)Mg^{26}$

3.1. GENERAL

Approximately 30 000 protons emitted from aluminium were recorded. No 15 MeV protons were present in the 0° spectrum, thus proving the absence of water or other hydrogenous contamination. Peaks with relative intensities

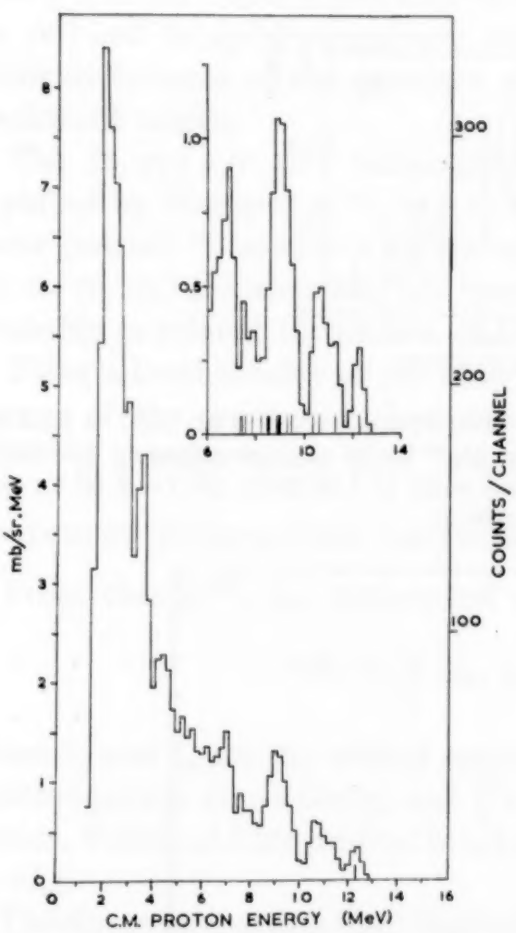

Fig. 1. Corrected proton energy spectrum at 40°. Inset: direct interaction contribution. Lines indicate the positions of known Mg^{27} levels.

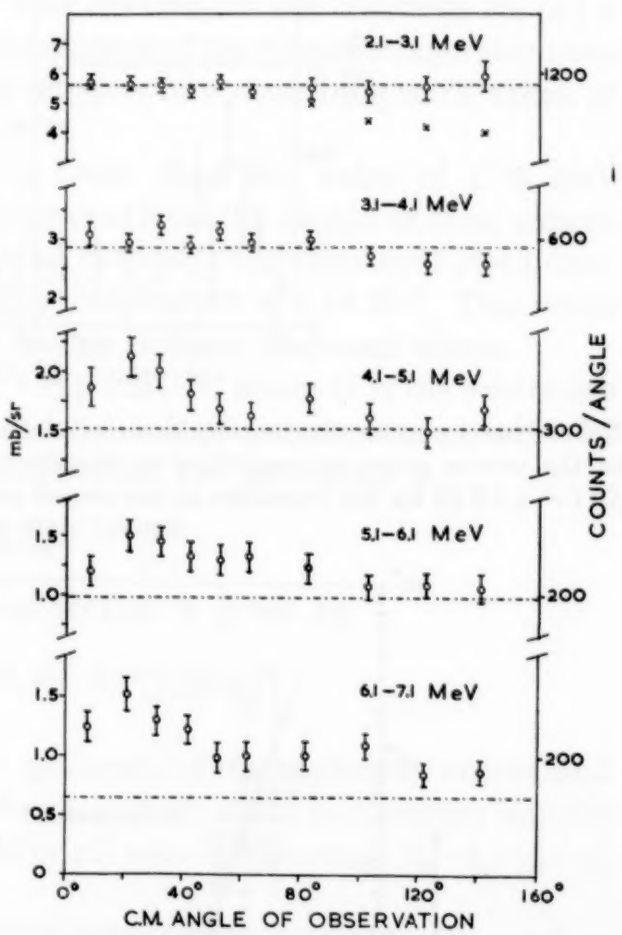

Fig. 2. Proton angular distributions 2.1–7.1 MeV. Broken lines represent the compound nucleus contribution calculated from the ordinates of the points lying on the lines defining the temperatures (fig. 4). In the 2.1–3.1 MeV interval points are shown uncorrected (×) and corrected (○) for loss of low energy protons.

agreeing with previous observations [8, 10]) and at energies corresponding to known Mg^{27} levels [15]) were observed in the proton spectra (fig. 1). Angular distributions are shown in figs. 2 and 3. That for the energy interval 2.1–3.1 MeV (fig. 2) was anisotropic. A similar effect was observed in earlier nuclear emulsion experiments [2–4]). However, the anisotropy is due to low energy protons being absorbed in the target or degraded to an unobservable energy.

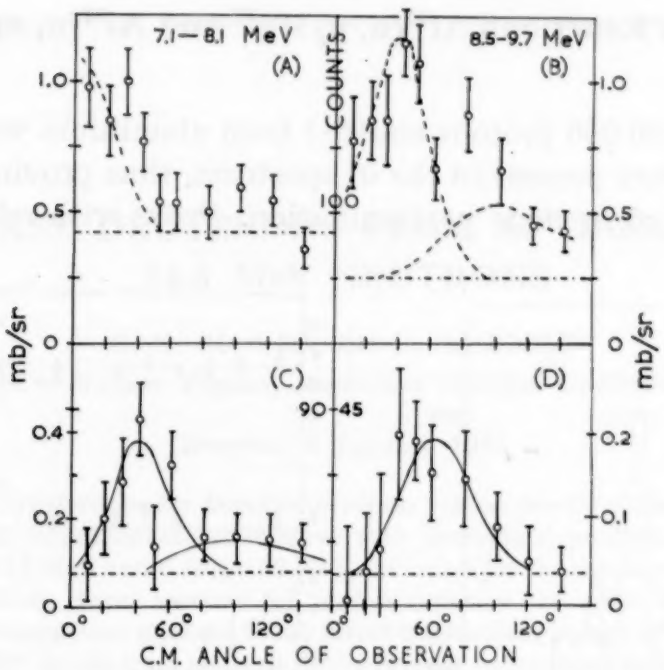

Fig. 3. Proton angular distributions in terms of the level structure. (A) $l = 0$ fit. (B) $l = 1+3$ fit for the proton group corresponding to transitions to Mg^{27} levels at approximately 3.5 MeV. (C) $l = 1+3$ fit for the transition to the second excited state at 1.69 MeV. (D) $l = 2$ fit for the ground state transition.

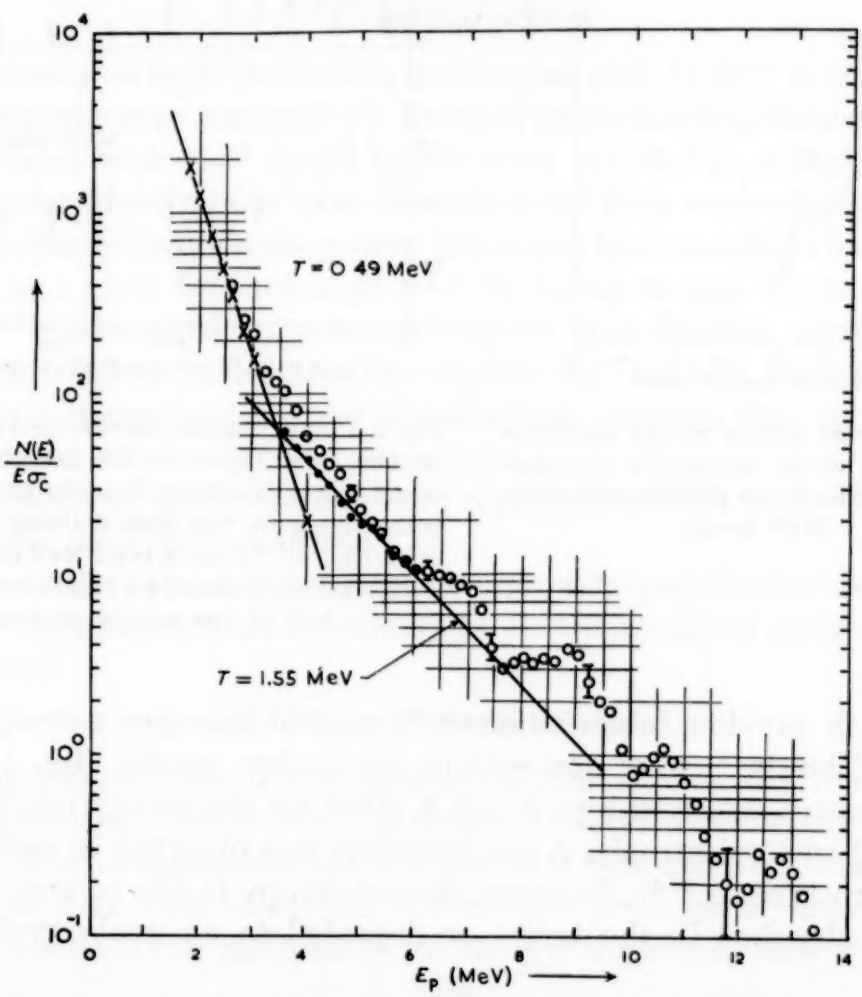

Fig. 4. Conventional statistical theory plot using the cross sections for compound nucleus formation derived by Shapiro [16]). The (n, np) temperature was found from points × in the range 1.8–3.0 MeV obtained at forward angles. The points ○ were given by spectra taken at backward angles. The points ● in the range 4.0–6.4 MeV, which have been corrected for the (n, np) contribution, were used to derive the (n, pγ) + (n, pn) temperature.

Correction for this loss of low energy protons, which is a function of angle because of the dependence of proton energy on angle of observation in the laboratory system, produces isotropy.

3.2. COMPOUND NUCLEUS CONTRIBUTION

From a conventional statistical theory plot (fig. 4) nuclear temperatures of 1.55 ± 0.15 MeV and 0.49 ± 0.02 MeV were derived for the reactions (n, pγ)+(n, pn) and (n, np), respectively. Determination of the former temperature was difficult because of the presence of level structure even in spectra taken at backward angles.

The (n, pγ)+(n, pn) temperature is lower than the value of 1.75 MeV reported by Storey *et al.* [9]), as is to be expected from the design of their experiment (see ref. [14]) section 3.2). Haling *et al.* [3]) found their statistical plot linear, i.e. no (n, np) contribution, and quoted a temperature of 1.16 MeV. This result probably is related to the loss of low energy protons discussed above.

Using a level density of the form $U^{-2}\exp 2(aU)^{\frac{1}{2}}$, where U is the excitation energy of the residual nucleus corrected for a Mg^{27} pairing energy of -2.1 MeV [17]), a value of 5.1 MeV^{-1} was derived for the parameter a.

3.3. DIRECT INTERACTION CONTRIBUTION

From theory [18]) the differential cross section is given by

$$\sigma(\theta) \propto \sum_{l} \langle l_n, l_p, 0, 0|l, 0\rangle^2 [j_l(Qr_0)]^2,$$

where l_n and l_p are the orbital angular momenta of the captured neutron and emitted proton respectively, and Q is the magnitude of the momentum transfer vector. Values of l are limited to all odd or all even in the range $|l_n - l_p| \leqq l \leqq |l_n + l_p|$.

The direct interaction contributions were fitted by this formula using a radius of 4 fm, slightly smaller than the nuclear radius.

Fig. 5 shows the Al^{27} ground state configuration on the Nilsson model [19]). To excite the Mg^{27} ground state rotational band, the incoming neutron enters the $s_{\frac{1}{2}}$ orbit No. 9 and the proton is emitted from the $d_{\frac{5}{2}}$ orbit No. 5. For this band the selection rule given above allows only $l = 2$ transitions. The ground state transition was indeed fitted by an $l = 2$ distribution (fig. 3D). The angular distribution (not shown) for the first excited state, which is a member of the ground state band, also suggested an $l = 2$ transition, but the statistical accuracy was poor because the energy interval considered had to be restricted to avoid a contribution from the neighbouring more intense group.

The angular distribution of the proton group corresponding to the 1.69 MeV level required an $l = 1$ fit. This level must therefore have odd parity. The experimental points beyond 60° could be fitted by an $l = 3$ transition. The

angular distribution was then given by a sum of Bessel functions of the form $(j_1^2+j_3^2)$. The lowest odd parity band may be excited by addition of a neutron to the $f_{\frac{7}{2}}$ orbit No. 14 and removal of a $d_{\frac{5}{2}}$ proton from orbit No. 5. The theory then predicts a distribution of the form $(j_1^2+j_3^2+1.9j_5^2)$ in agreement with experiment.

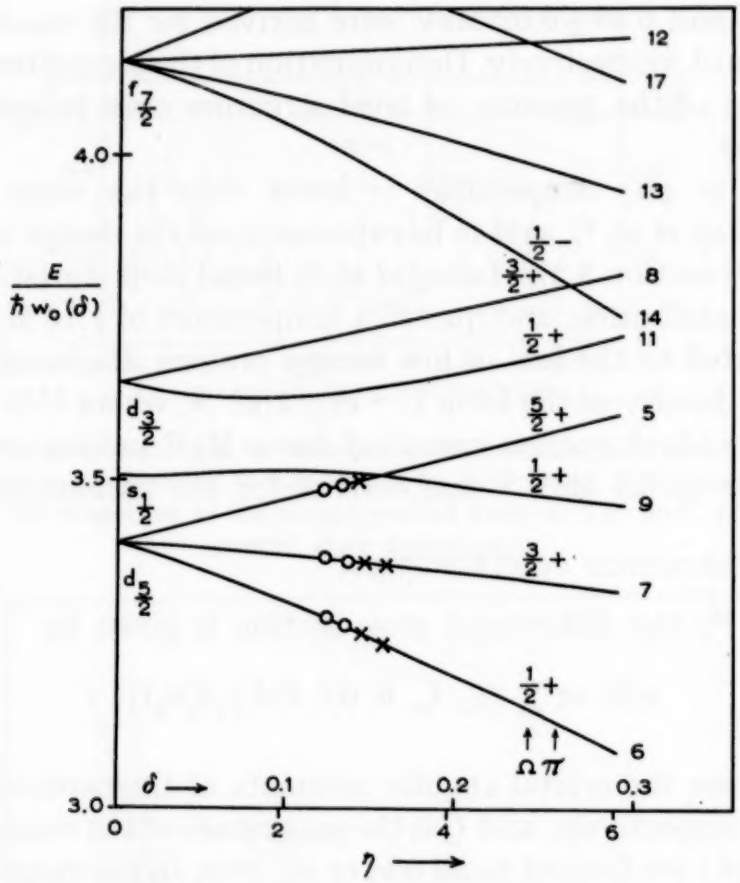

Fig. 5. Nilsson diagram for Al^{27} ground state, deformation parameter $\eta \approx 3$. The neutrons are denoted by circles and protons by crosses.

The angular distribution corresponding to excitation of levels around 3.5 MeV (fig. 3B) can also be fitted by the form $(j_1^2+j_3^2)$, indicating strong excitation of the odd parity level at 3.56 MeV. However, because of the resolution of the scintillation counter, several levels probably contribute and the distribution could be adjusted to contain $l = 2$ or even $l = 0$ contributions.

The remaining angular distributions (figs. 2 and 3A) showed that direct interaction effects were present at proton energies as low as 4 MeV, i.e. excitation energies as high as 8 MeV of the residual Mg^{27} nucleus.

3.4. CROSS SECTIONS

The cross sections, determined as previously described (see ref. [14]) sect. 3.4), were

Total: 273 ± 20 mb,

$(n, p\gamma)+(n, pn)$: { 89 mb compound nucleus, 27 mb direct interaction,

(n, np): 157 mb compound nucleus.

Using activation techniques Hudson and Morgan [20]) obtained a value of (80 ± 8) mb for the (n, p) cross section at 14.8 MeV. The present results therefore suggest an (n, pn) cross section of 36 mb.

4. Spin Assignments to Mg^{27} Levels

Information on the spins of various Mg^{27} levels can be obtained from the present experiment and from analysis, based on the Nilsson model, of Mg^{26}(d, p) Mg^{27} experiments [11, 21]). Relevant formulae are given in sect. 5.1. Fig. 6 shows the spin assignments.

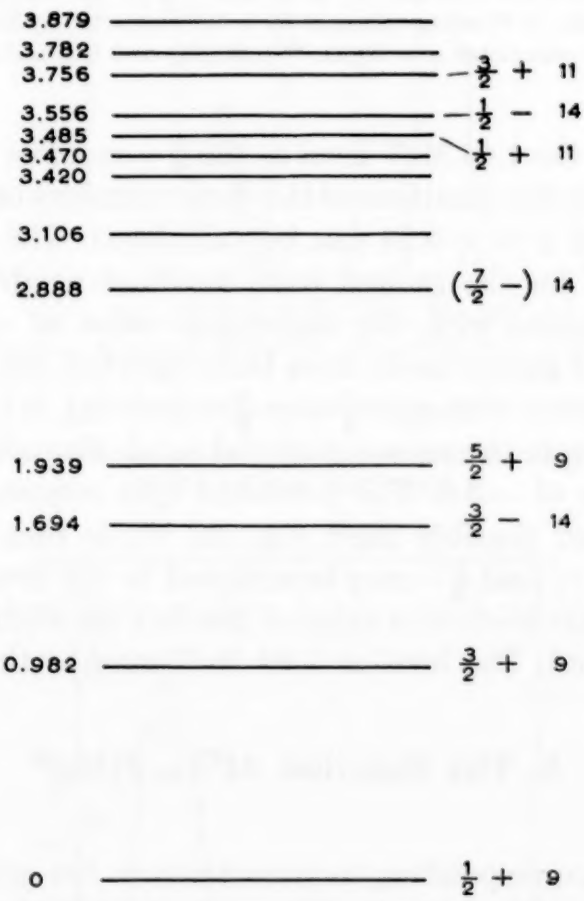

Fig. 6. Tentative spin assignments for Mg^{27} levels reported by [15]). The right hand column denotes the Nilsson orbit involved.

The assumption that the levels at 0.98 and 3.76 MeV are the next members of $K = \frac{1}{2}$ rotational bands based on the ground state (orbit No. 9) and the 3.50 MeV level (orbit No. 11) respectively, leads to a reasonable value of

approximately 250 keV for $\hbar^2/2I$ in both cases, using theoretical values of the decoupling parameter a. Such an identification is strongly suggested by the agreement of the experimental and theoretical reduced widths (table 1) and indicates a spin of $\frac{3}{2}+$ for both levels. The assignment of odd parity to the level

TABLE 1

$Mg^{26}(d, p)Mg^{27}$ analysis

Excitation (MeV)	Spin [a])	Orbit	$(2I+1)\theta^2$ [b])	Reduced widths (θ^2)	
				Experimental	Predicted [c])
0	$\frac{1}{2}+$	9	0.032	0.016	0.016
0.98	$\frac{3}{2}+(\frac{5}{2}+)$	9	0.034	0.009	0.008
3.50	$\frac{1}{2}+$	11	0.028	0.014	0.012
3.76	$\frac{3}{2}+(\frac{5}{2}+)$	11	0.064	0.016	0.012

[a]) The spins in brackets are the alternative values allowed by the stripping reaction.
[b]) Mean of the results of refs. [11, 21]) using values of $(2I+1)\theta^2$ extracted by Macfarlane and French [22]).
[c]) Assuming deformation parameter $\eta = 3$ (ref. [23])), $\theta_0^2(2s) \approx 0.043$ and $\theta_0^2(1d) \approx 0.034$ (ref. [22]), p. 257).

at 1.69 MeV favours the 1.94 MeV level as the $\frac{5}{2}+$ member of the ground state rotational band. From the positions of the three members of this band values of $\hbar^2/2I = 259$ keV and $a = +0.26$ can be calculated. The former agrees well with values of $\hbar^2/2I$ for the ground state bands of neighbouring nuclei, e.g. ref. [24]); the latter agrees with the theoretical value of $+0.4$.

Since only two odd parity levels have been reported, viz. those at 1.69 MeV and 3.56 MeV, the latter with spin $\frac{1}{2}-$ or $\frac{3}{2}-$ (ref. [11])), it is reasonable to suppose that they belong to the same rotational band. For orbit No. 14 the parameter a has a value of -3.6. The predicted spin sequence, which has been observed for Al^{25} and possibly Mg^{25}, e.g. ref. [24]), is then $\frac{3}{2}-$, $\frac{7}{2}-$ and $\frac{1}{2}-$. Therefore spins of $\frac{3}{2}-$ and $\frac{1}{2}-$ may be assigned to the levels at 1.69 and 3.56 MeV respectively. This leads to a value of 240 keV for $\hbar^2/2I$, similar to that for the ground state band. The level at 2.89 MeV may be the $\frac{7}{2}-$ member.

5. The Reaction $Al^{27}(n, d)Mg^{26}$

5.1. GENERAL

Deuteron groups corresponding to transitions to the ground state and first excited state were identified (fig. 7). The peak at 4.8 MeV corresponds to a new level at 3.6 MeV which has recently been reported independently by Blair and Hamburger [25]) and by Hinds and Middleton [15]). The low energy peak may be due to several unresolved levels. Using the tabulations of Lubitz [26]), based on the Butler stripping theory [27]), theoretical angular distributions were fitted to the observed experimental distributions (figs. 8–10). Reduced widths (table 2)

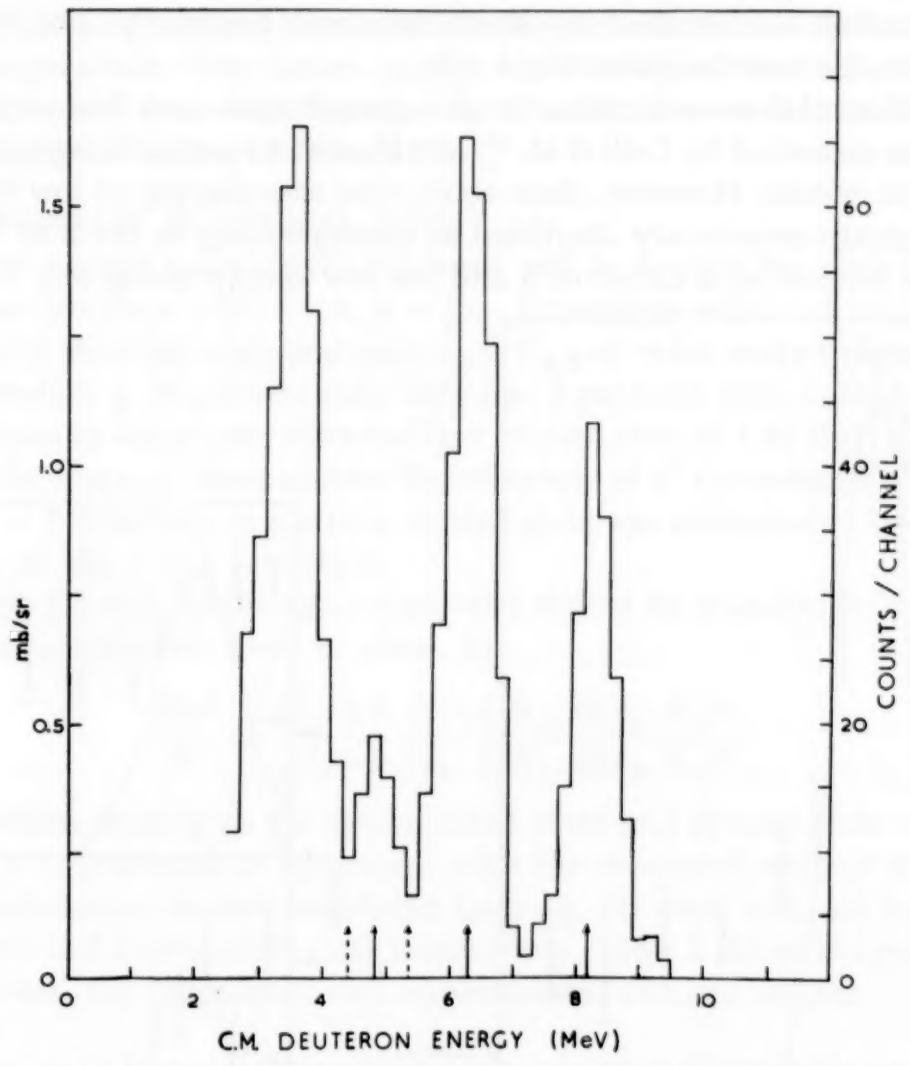

Fig. 7. Corrected deuteron spectrum at 30°. The arrows indicate known Mg^{26} levels at 0, 1.83, 2.97, 3.6 and 3.97 MeV.

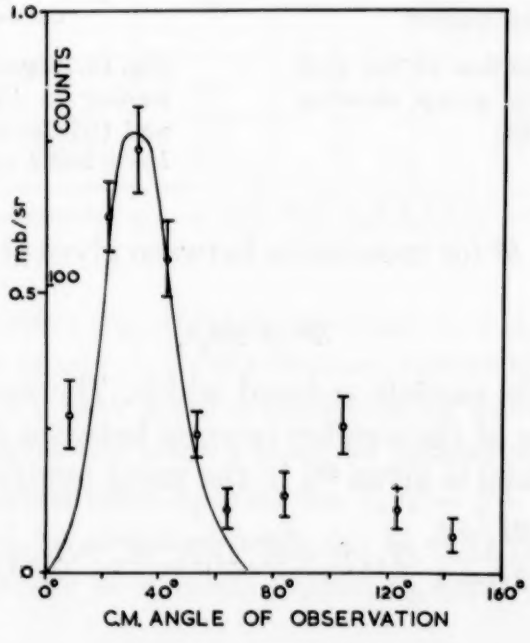

Fig. 8. Angular distribution of the ground state deuteron group showing $l = 2$ fit.

were extracted as described by Macfarlane and French [22]). The total cross section for the reaction was 30 ± 4 mb.

The differential cross sections for the ground state and first excited state transitions measured by Colli *et al.* [12]) at 17°, are in reasonable agreement with the present results. However, their count rate rose sharply at low energies so that the group erroneously identified as corresponding to the 2.97 MeV level was more intense by a factor of 3 and the low energy group was not visible.

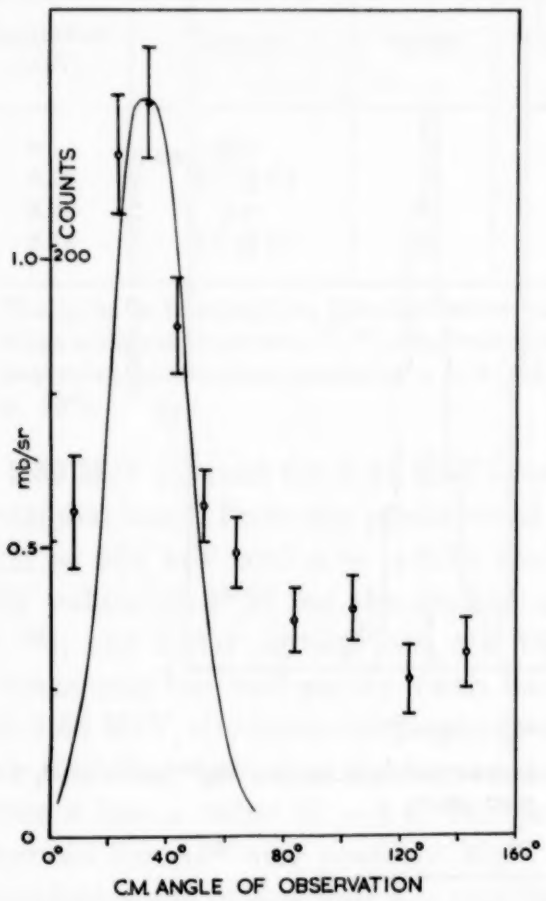

Fig. 9. Angular distribution of the first excited state deuteron group showing $l = 2$ fit.

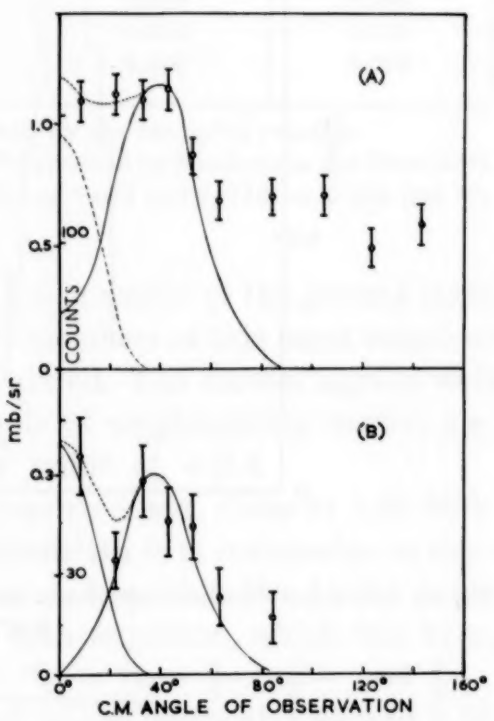

Fig. 10. Angular distributions of deuterons leading to (A) level(s) around 4.9 MeV and (B) the 3.6 MeV level. In both cases $l = 0$ and $l = 2$ fits using radii of 5.1 fm are shown.

The reduced width θ^2 for transitions between given states of two nuclei may be written

$$\theta^2 = S\theta_0^2, \tag{1}$$

where θ_0^2 is the single particle reduced width. The spectroscopic factor S is essentially the square of the overlap integral between the relevant states and for the rotational model is given [28]) in the usual notation by

$$S_{lj} = g^2 \frac{2I_1+1}{2I_2+1} \langle I_1, j, \pm K, \Omega | I_2, K_2 \rangle^2 \langle \varphi_2 | \varphi_1 \rangle^2 C_{jl}^2(\Omega), \tag{2}$$

where the subscripts 1 and 2 refer in the present case to the final and initial nucleus respectively. The factor $\langle\varphi_2|\varphi_1\rangle$, the overlap of the initial and final vibrational states, is as usual assumed to be unity. The coefficients C_{lj} can be derived from the tables of Nilsson [19]).

5.2. GROUND STATE ROTATIONAL BAND

The Mg^{26} ground state rotational band will be excited by pick up of the unpaired proton from orbit No. 5, $\Omega = \frac{5}{2}+$. Transitions with $l = 2$ are predicted for this band since the only non-zero C_{lj} is $C_{2,\frac{5}{2}}$ of value unity independent of the deformation η. Experimentally only $l = 2$ patterns were indeed observed for transitions to the ground state and first excited state at 1.83 MeV (figs. 8 and 9). From the shape of these angular distributions at 0° the reduced width for a possible $l = 0$ transition to the first excited state was estimated to be not more than 1 % of the $l = 2$ transition.

From eqs. (1) and (2) the ratio of reduced widths for transitions to members of the same rotational band is given by

$$\frac{(\theta^1)^2}{\theta^2} = \frac{2I_1{}^1+1}{2I_1+1}\,\frac{\langle I_1{}^1, j, K_1, \Omega|I_2, K_2\rangle^2}{\langle I_1, j, K_1, \Omega|I_2, K_2\rangle^2}. \tag{3}$$

For transitions leading to the first excited state and ground state of Mg^{26} a ratio of 1.8 is predicted in agreement with the measured ratio of 2.1.

The spectroscopic factors calculated from eq. (2) were 0.33 and 0.6 for the ground state and first excited state respectively. Table 2 shows the good agreement between the theoretical and experimental reduced widths.

TABLE 2

Al^{27}(n, d)Mg^{26} analysis

Excitation (MeV)	Spin	l	r_0	Orbit	Reduced widths	
					Experimental	Predicted [a])
0	0+	2	5.1	5	0.011	0.011
1.9	2+	2	5.4	5	0.024	0.021
3.6	(2, 3)+	(0), 2	5.1	7	0.009	0.012

[a]) Assuming deformation parameter $\eta = 3$ (ref. [23])) and $\theta_0{}^2(1d) = 0.034$ (ref. [22])).

5.3. THE 3.6 MeV LEVEL

This angular distribution (fig. 10B) showed an $l = 2$ stripping pattern and a peak at 0°. If the latter is an $l = 0$ contribution, rather than a distorted wave effect, the spin of the 3.6 MeV level is restricted to 2+ or 3+. To produce a dominant $l = 2$ transition the proton must be picked up:

(i) from the highest filled $d_{\frac{5}{2}}$ orbit No. 7, $\Omega = \frac{3}{2}+$ (hence two rotational bands could be obtained with (a) $\Omega = 1$, (b) $\Omega = 4$);

(ii) from admixture of a much higher $d_{\frac{3}{2}}$ orbit No. 8, $\Omega = \frac{3}{2}+$.

For the $\Omega = 1$ band the first observable member would have spin 2+, since the normal ground state of the band, $I = K = \Omega = 1+$, is not allowed by symmetry requirements. The calculated spectroscopic factor of 0.36 yields a reduced width in reasonable agreement with the experimental value (table 2). The alternative spin 3+ yields essentially the same width.

The possibilities (ib) and (ii) may be dismissed. For the $\Omega = 4$ band, to which this level can belong only if the 0° peak is not due to an $l = 0$ transition, the theoretical reduced widths are too small by at least a factor 2. Pick up from orbit No. 8 would require an implausibly large admixture of this orbit in the Al^{27} ground state configuration (80 % if the spin is 2+).

The 3.6 MeV level would therefore seem to be explained on the rotational model by pick up of a core proton from orbit No. 7. The apparent absence of this level in a Mg^{25}(d, p)Mg^{26} experiment [21]) is then understandable. In the present experiment the levels at 2.97 and 3.97 MeV are only weakly excited, if at all. Since the (d, p) experiment excites these levels by addition of a neutron, probably to orbit No. 9, their absence in the (n, d) experiment is not surprising.

5.4. LOW ENERGY DEUTERON GROUP

The angular distribution (fig. 10) again required an $l = 0+2$ fit. However, further analysis is not justified in view of the poor stripping pattern and the number of unresolved Mg^{26} levels in this energy range.

The authors are indebted to Professor E. W. Titterton for his interest and encouragement and to Dr. D. C. Paeslee, Dr. K. Kumar and Mr. D. W. Lang for theoretical discussions. One of us (E. W.) would like to acknowledge the award of a scholarship from the Australian Institute of Nuclear Science and Engineering.

References

1) D. L. Allan, Proc. Phys. Soc. **70** A (1957) 195
2) G. Brown, G. C. Morrison, H. Muirhead and W. T. Morton, Phil. Mag. **2** (1957) 785
3) R. K. Haling, R. A. Peck and H. P. Eubank, Phys. Rev. **106** (1957) 971
4) P. V. March and W. T. Morton, Phil. Mag. **3** (1958) 1256
5) O. E. Overseth and R. A. Peck, Phys. Rev. **115** (1959) 993
6) L. Colli and U. Facchini, Nuovo Cim. **5** (1957) 309
7) L. Colli, M. Pignanelli, A. Rytz and Z. Zurmühle, Nuovo Cim. **9** (1958) 280
8) L. Colli, F. Cvelbar, S. Micheletti and M. Pignanelli, Nuovo Cim. **14** (1959) 1120
9) R. S. Storey, W. Jack and A. Ward, Proc. Phys. Soc. **75** (1960) 526
10) W. Jack and A. Ward, Proc. Phys. Soc. **75** (1960) 833
11) S. Hinds, R. Middleton and G. Parry, Proc. Phys. Soc. **71** (1958) 49
12) L. Colli, F. Cvelbar, S. Micheletti and M. Pignanelli, Nuovo Cim. **14** (1959) 81
13) R. N. Glover, K. H. Purser and E. Weigold, Nuclear Instruments (to be published)
14) R. N. Glover and K. H. Purser, Nuclear Physics **24** (1961) 431
15) S. Hinds and R. Middleton, private communication (1960) (contribution to International Conference on Nuclear Structure, Kingston, Canada)
16) M. M. Shapiro, Phys. Rev. **90** (1953) 171
17) A. G. W. Cameron, Can. J. Phys. **36** (1958) 1040

18) N. Austern, S. T. Butler and H. McManus, Phys. Rev. **92** (1953) 350
19) S. G. Nilsson, Mat. Fys. Medd. Dan. Vid. Selsk. **29**, No. 16 (1955)
20) O. M. Hudson and I. L. Morgan, Bull. Am. Phys. Soc. **4** (1959) 97
21) J. R. Holt and T. N. Marsham, Proc. Phys. Soc. **66** A (1953) 258
22) M. H. Macfarlane and J. B. French, NYO-2846 (1959); Rev. Mod. Phys. **32** (1960) 567
23) G. R. Bishop, Nuclear Physics **14** (1959) 376
24) A. E. Litherland, H. McManus, E. B. Paul, D. A. Bromley and H. E. Gove, Can. J. Phys. **36** (1958) 378
25) A. G. Blair and E. W. Hamburger, Bull. Am. Phys. Soc. **5** (1960) 36
26) C. R. Lubitz, AECU 3990 (1957)
27) S. T. Butler, Nuclear Stripping Reactions (Wiley, New York, 1957)
28) G. R. Satchler, Ann. Phys. **3** (1958) 275

9.B

Nuclear Physics **24** (1961) 642—656; © *North-Holland Publishing Co., Amsterdam*

Not to be reproduced by photoprint or microfilm without written permission from the publisher

MECHANISM OF INTERACTION OF FAST NUCLEONS WITH NUCLEI

V. S. BARASHENKOV, V. M. MALTSEV and E. K. MIKHUL

Joint Institute for Nuclear Research, Dubna, USSR

Received 1 October 1960

Abstract: The paper presents the results of the calculations of intranuclear cascades generated by a 9 GeV proton in photoemulsion nuclei. From comparing these results with the available experimental data it follows that an intranuclear cascade mechanism is operating in nucleon-nucleus collisions at $E = 9$ GeV just as at lower energies. What the nucleon-nucleus interaction mechanism is like at very high energies ($E \gg 10$ GeV) – whether it is a nucleon-tube mechanism or an intranuclear cascade mechanism – is still an open question. The present paper is a direct continuation of ref. [1]).

1. Introduction

Quite a few papers have recently been concerned with the investigation of different aspects of the interaction between 9 GeV protons and nuclei [1–18]). This keen interest is largely due to the two following facts:

1) From the investigation of nucleon-nucleus interactions it is possible to obtain interesting information on the elementary NN-interaction event. For example, it is possible to determine the total cross section of NN-interaction σ_t by experimental data on the length of the fast nucleon mean free path in photoemulsion; the investigation of the energy spectra of particles produced in nucleon-nucleus interactions furnishes information on the spectra of particles produced in NN-collisions and makes it possible to evaluate the average energy lost by the nucleon in one NN-collision event, etc. Some related questions will be considered in the next section.

2) Several authors (see for example refs. [21,22])) expressed the supposition that already at 9 or 10 GeV the "intranuclear cascade mechanism" occurring at lower energies (see ref. [23])) must be replaced by the "tube mechanism" when the primary nucleon interacts with several nucleons of the nucleus at once.

At present there is no unanimous opinion on this question among physicists. Ref. [1]) offers arguments against the tube model and points out that the basic experimental data do not contradict the intranuclear cascade mechanism. Yet no results of the numerical calculations of these cascades were presented †. In ref. [8]) it is also pointed out that the tube mechanism cannot explain all

† Lukin *et al.* noted [10]) that the inferences of ref. [1]) on the mechanism of interaction between 9 GeV protons with a nucleus are in agreement with the results of experiments on cosmic rays with an average energy $E = 100$ GeV (for detail see ref. [29])).

experimental data. The authors of this investigation hold that the interaction of a 9 GeV nucleon with a nucleus has a character intermediary between the tube model and the intranuclear cascade model. Friedlander [11]), on the contrary, holds that the tube mechanism is the basic one at $E = 9$ to 10 GeV.

To discriminate between the two nucleon-nucleus interaction mechanisms under discussion, we performed numerical calculations for the intranuclear cascade and compared the results with experimental data. As will be shown below, the results of the calculations explain the experiments, quite well. Taking account of the objections raised in ref. [1]) against the tube mechanism, we yet think it possible to claim that the intranuclear cascade mechanism occurs in the interaction of 9 GeV protons with photoemulsion nuclei just as at lower energies.

It stands to reason that we mean the interpretation of merely the chief experimental facts, such as averages of particles of different types, their energy and angular distributions. In details, of course, there may be deviations from the intranuclear cascade mechanism or at any rate from that approximate model which we considered †.

2. Cross Sections of Interaction of Fast Particles with Nucleons of Nuclei

To calculate intranuclear cascades it is necessary above all to know the cross sections of interaction of 9 GeV nucleons with the nucleons of the nuclei. To determine these cross sections we shall make use of the experimental value of a mean free path in photoemulsion.

Usually the cases of elastic scattering of fast particles on nuclei are not detected in the track scanning of fast particles in photoemulsion. At high energies elastic scattering is almost entirely diffractional and occurs at very small angles which are the smaller the larger the nuclei. A special technique is necessary to detect a small curvature of tracks in elastic nuclear scattering (cf. ref. [15])). As a rule, elastic scattering on hydrogen †† occurring at comparatively large angles is only detected apart from inelastic interactions.

† D. I. Blokhintsev noted that in the interaction of fast particles with nuclei a whole group of nucleons may leave the nucleus as a result of a fluctuation in the density of nuclear matter [24]). V. I. Veksler drew our attention to the fact that the expulsion of large splinters out of the nucleus can also occur due to a mechanism similar to the propagation of a shock wave in a dense substance. In our approximate calculations we do not take into account these possible nucleon-nucleus interaction mechanisms.

†† Of course, those cases of elastic scattering on hydrogen when the particles scatter at very small angles are not detected either. Estimates showed that at energies $E \lesssim 10$ GeV the contribution of such undetected interactions does not change appreciably the length of the mean free path. At higher energies the bulk of particles elastically scattered on hydrogen gets into the region of small angles and this should be taken into account in calculations (in this case σ_t in eq. (1) should be replaced by σ_{in}; see below).

The mean free path in these cases is equal to

$$L = \frac{1}{\sum_i N_i \sigma_{in}^i + N_H \sigma_t}, \quad (1)$$

where N_H is the number of hydrogen nuclei in 1 cm³ of photoemulsion, N_i the number of nuclei of other elements in 1 cm³ of photoemulsion, σ_t is the total cross section of interaction of the primary particles (pion, nucleon, K-meson, etc.) with hydrogen and σ_{in}^i is the cross section of inelastic interaction of this particle with other nuclei.

At high energies when the wave length of the particles interacting with photoemulsion is much less than the size of the nuclei an optical model can be applied quite well. If the elastic non-diffractional scattering is neglected, which is justified at high energies, the cross sections σ_{in}^i are expressed in this case through the parameters of the nuclei (which can be taken, for example, from experiments on the scattering of fast electrons on nuclei) and through the total cross section of the interaction of a primary particle with the nucleons of a nucleus σ_t.

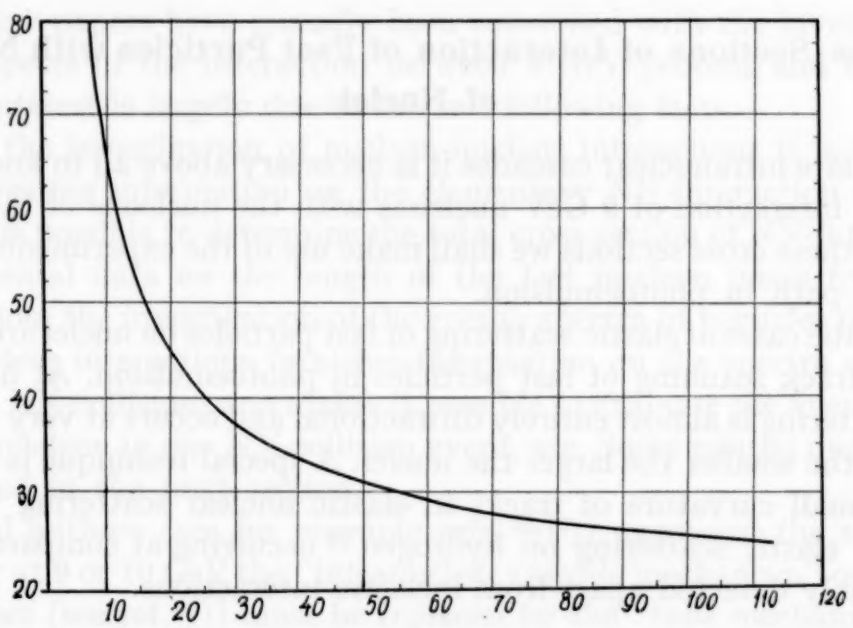

Fig. 1. Dependence of the mean free path of particles in photoemulsion L on the total cross-section of the interaction of these particles with nucleons σ_t.

Values of L in cm are marked off on the axis of the ordinates and values of σ_t in units 10^{-27} cm² on the axis of the abscissa.

Fig. 1 lists the calculated values $L = L(\sigma_t)$. As was shown by calculations, the difference of the paths $L(\sigma_t)$ in Inford G-5 and NIKFI-R photoemulsions is insignificant. The curve in fig. 1 is applicable to both types of emulsion – not only for nucleons but also for particles of other kinds. The applicability of the curve improves with the growth of energy.

In a number of cases the use of the dependence $L = L(\sigma_t)$ is the only method of determining the quantity σ_t (cf. ref. [18])).

The cross sections thus obtained are cross sections, averaged with respect to isobaric spin, of interaction with nucleons bound in nuclei. Yet at high energies $E \gg E_F \approx 30$ MeV the binding energies in nuclei can be neglected and these cross sections prove to be very close to those for the interactions with free nucleons (cf. ref. [18])).

In ref. [9]) the value $L \leqq 35.7 \pm 0.7$ cm was obtained for the mean free path of a 9 GeV proton. The corresponding cross section of the NN-interaction is $\sigma_t \geqq (32 \div 35) \times 10^{-27}$ cm^2 (see fig. 1). If the value $\sigma_{el} = 8.6 \times 10^{-27}$ cm^2 is assumed for the elastic scattering cross section in accordance with ref. [25]), then $\sigma_{in} \geqq (23$ to $26) \times 10^{-27}$ cm^2. We shall select $\sigma_t = 35 \times 10^{-27}$ cm^2 and $\sigma_{in} = 26 \times 10^{-27}$ cm^2.

3. Nuclear Model and Experimental Data Used in Calculation of Intranuclear Cascade

In the calculations we assumed that the nuclear properties can be described by the Fermi-Gas model. It was also assumed that the nucleons are distributed uniformly within a sphere with a radius $R = r_0 A^{\frac{1}{3}}$ (A is the atomic weight of the nucleus) †. The value $r_0 = 1.35 \times 10^{-13}$ cm was used for determining the value of the contant r_0. In ref. [23]) it was shown that the results of the calculation of the intranuclear cascade obtained within the framework of tnis model for energies $E < 2$ GeV are in sufficiently good agreement with experiment. It can well be expected that the applicability of this model will improve with the growth of energy.

It will be noted that at energies $E \gtrsim 1$ GeV the concrete selection of a nuclear model has an essential effect only on the characteristics of low-energy b-particles †† and, to a certain extent, g-particles. Now, the characteristics of fast particles change little when the nuclear parameters vary widely.

To simplify the problem all characteristics of πN- and NN-interactions within the nuclei are regarded as averaged over the isobaric spins of mesons and

† Neglecting the diffuseness of the nuclear boundary is an approximation better suitable for heavy than for light nuclei. It does not introduce essential errors within the limits of the accuracy of the photoemulsion data available at present with which the results of the calculations will be compared. Yet in other cases there may arise appreciable deviations from experiments.

We are indebted to D. I. Blikhintsev, M. G. Meshcheryakov and A. A. Tyapkin who, while discussing the results of the calculations drew our attention to the phenomena in which these deviations are observed. This problem is being studied in detail.

†† Just as it was done in ref. [1]) all particles observed after nucleon-nucleus collisions will be divided into three types: s-, g- and b-particles. This division is justified by the fact that in photoemulsion each of these types has a characteristic type of tracks (for detail see ref. [1])). Table 1 lists the values of the energy of pions and nucleons, necessary for further discussion, for each of these three types.

nucleons. As was shown by estimates, this averaging yields a satisfactory approximation. Besides, all characteristics of inelastic collisions of nucleons and mesons with the nucleons of the nucleus are regarded as averaged with respect to the events in which different numbers of particles are produced. Since we shall regard the characteristics of nucleon-nucleus collisions as also averaged with respect to the events with different numbers of particles produced, this approximation cannot introduce any appreciable distortions into the results of the calculations.

TABLE 1

Pion and nucleon energy values

	Kinetic energy (GeV)	
	Nucleons	π-mesons
s-particles (shower particles)	0.5 ÷9	$0.08 \div T_{\pi max}$; $T_{\pi max} \approx 8$
g- particles (cascade particles)	0.03÷0.5	0.015÷0.08
b-particles (particles with black tracks)	<0.03	<0.15

In the case of NN-collisions the entire region of energies was divided into five intervals; in the case of πN-collisions four energy intervals were considered. The characteristics of elastic and inelastic NN- and πN-collisions, with the exception of the total cross sections σ_t, were regarded as constant for each of these intervals and were taken from experimental investigations [26]), both energy and angular distributions of secondary particles being taken into account The values of the total cross sections $\sigma_t(E)$ determining the path and the point of the collision of a nucleon and a pion in the nucleus were assigned with a considerably smaller pitch ΔE, which practically did not differ from assigning a continuous curve.

Table 2 liststs the energy intervals under consideration.

TABLE 2

Energy intervals ΔE (GeV)

NN	πN
9 ÷4.5	8 ÷3
4.5÷1.5	3 ÷1
1.5÷1	1 ÷0.5
1 ÷0.5	<0.5
<0.5	

The division of the energy interval $E > 1$ GeV into smaller intervals is not feasible owing to the lack of detailed experimental data. However, the contribution of particles with very high energies must be fairly small since the average energy of pions and nucleons after the first (NN)-collision $E_\pi \approx 1$ GeV and $E_N \approx 3.5$ GeV [19, 20]), which is considerably less than the maximum energy $E = 9$ GeV. On the other hand, the division of the lower-energy region into smaller intervals can essentially affect only the results of the calculations for b-particles, since the energy of the primary proton is sufficiently high, and s-particles and a larger part of the g-particles are produced in the collisions of high-energy nucleons and pions with a nucleon of the nucleus. Yet in the most essential region $E \approx 1$ GeV the true characteristics of NN- and πN-collisions do not change considerably as compared with their averages used in the calculations.

The characteristics of the first inelastic NN-collision ($E = 9$ GeV) were calculated by the statistical theory of the multiple particle production with allowances for the peripheral NN-interactions on the strength of experimental investigations [19, 20]) and theoretical papers [17, 27, 28]). The data on the elastic scattering of nucleons are taken from ref. [25]). The cross sections σ_t and σ_{in} are determined in sect. 2.

4. Calculation Method

The calculations of the intranuclear cascades were performed by the Monte-Carlo method for the case of relativistic three-dimensional kinematics with allowances for multiple particle production.

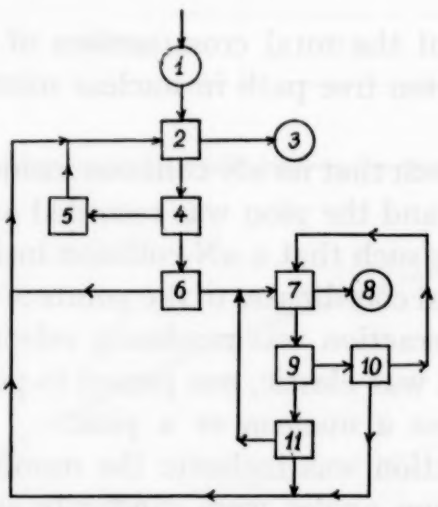

Fig. 2. Scheme of calculation of intra-nuclear cascades. The meaning of individual blocks is clear from the text.

The following calculating procedure was used (see the scheme in fig. 2):

1) The coordinates of the point of the entry of the primary proton into the nucleus were randomly selected.

2) Using the value of the total cross section of the interaction of nucleons σ_t the value of the nucleon free path in nuclear substance $L_N = L_N(\sigma_t)$ was randomly selected.

3) If the value L_N was such that no NN-collision inside the nucleus was possible, the calculation stopped. The number of the protons N_{nl} which have not interacted with the nucleus determines the cross section of the reaction

$$\sigma_r = \pi r_0^2 A^{\frac{2}{3}} \left(1 - \frac{N_{nl}}{N_t}\right), \tag{2}$$

where N_t is the total number of the protons colliding with the nucleus.

4) If the value L_N was such that NN-collision occurs inside the nucleus, the three-dimensional coordinates of the point of collision were determined and the type of NN-interaction was randomly selected as either elastic or inelastic.

5) If NN-interaction was elastic, one passed to point 2). The number of nucleons N_{el} which have experienced one or several elastic collisions inside the nucleus and come out determines the cross section of the quasi-elastic interaction with the nucleus

$$\sigma_{sel} = \pi r_0^2 A^{\frac{2}{3}} \frac{N_{el}}{N_t} \tag{3}$$

(elastic scattering on the bound nucleon in the nucleus).

6) If NN-interaction was inelastic the number of the particles produced, their energy and emission angles were randomly selected †. Then one passed to point 2) or to point 7) depending on whether the particle produced was a nucleon of a pion.

7) Using the values of the total cross section of pion-nucleon interaction $\sigma_t(E)$ the value of the pion free path in nuclear matter $L_\pi = L_\pi(\sigma_t)$ was randomly selected.

8) If the value L_π is such that no πN-collision inside the nucleus was possible the calculation stopped and the pion was recorded as having left the nucleus.

9) If the value L_π was such that a πN-collision inside the nucleus was possible, the three-dimensional coordinates of the points of collision were determined and the type of πN-interaction was randomly selected as elastic or inelastic.

10) If πN-interaction was elastic, one passed to point 2) or 7) depending on whether the particle was a nucleon or a pion.

11) If the πN-interaction was inelastic the number of particles produced, their energy and emission angles were randomly selected. Then one passed

† The angular and energy distribution of the particles produced in the first NN-collision were assigned directly in the laboratory system of coordinates. For the subsequent NN- and πN-collisions the angular and energy distributions were taken from ref. [26]) in which they are given only for the centre-of-mass system. In these cases the random selection was performed in the centre-of-mass system after which each particle was transferred to the laboratory system of coordinates.

either to point 2) or point 7) depending on whether the particle was a nucleon or a pion.

As was mentioned in the previous section, in the calculation use was made of the characteristics of NN- and πN-interactions averaged over the values of isobaric spin. To single out charged particles in the total number of particles formed as a result of inelastic nucleon-nucleus collisions, we assumed that protons account for 50 % of all nucleons and $\frac{2}{3}$ of all pions are charged. At high energies when many particles are produced this approximation is fully justified.

Otherwise our calculations do not differ essentially from similar calculations performed by Metropolis *et al.* [23]).

5. Results of Calculations. Comparison with Experiment

5.1. NUCLEON-NUCLEUS INTERACTION CROSS SECTIONS

Table 3 lists the values of the cross sections σ_r and σ_{sel} for an average light nucleus (N_7^{14}), an average heavy nucleus (Nb_{41}^{94}) and an average nucleus (Ga_{31}^{70}) of the NIKFI-R photoemulsion calculated by eqs. (2) and (3).

TABLE 3

Calculated cross-section values

Type of nucleus	σ_1 (10^{27} cm^2)	σ_{sel} (10^{27} cm^2)	σ_{sel}/σ_d
Light nucleus	243± 5	40± 4	0.30±0.03
Medium nucleus	836±12	87±12	0.41±0.06
Heavy nucleus	1090±15	107±16	0.43±0.06

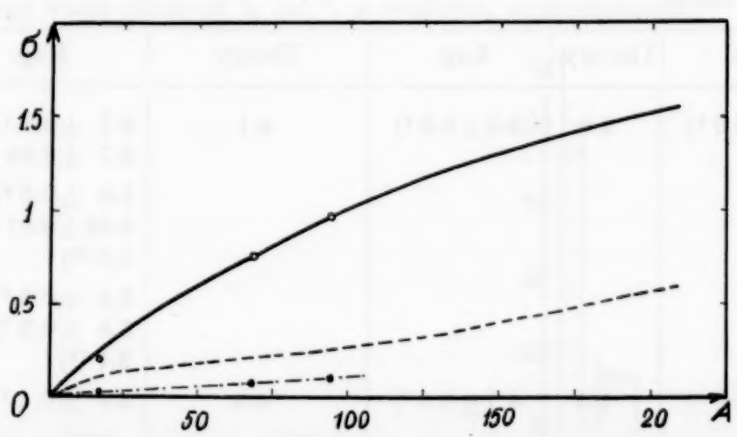

Fig. 3. Cross-sections of interaction of nucleons with nuclei at $E = 9$ GeV. The solid line designates inelastic scattering σ_{in}, the dashed line the diffractional cross-section σ_d, the dot-and-dash line designates an interpolationary line for the values of σ_{sel}, and ○ and ● are the cross-sections σ_{in} and σ_{sel} calculated by the Monte-Carlo method. Cross-sections are given in the units of 10^{-24} cm^2.

The probability of nucleon-nucleus collisions at which the energy transferred by the primary proton to a nucleon of the nucleus completely passes into the kinetic recoil energy of this nucleus must be small at high energies. If these collisions are neglected, the total cross section of inelastic processes

$$\sigma_{\text{in}} = \sigma_{\text{r}} - \sigma_{\text{sel}}.$$

As is clear from fig. 3 the values σ_{in} thus obtained are very close to the curve $\sigma_{\text{in}} = \sigma_{\text{in}}(A)$, calculated directly by an optical model (cf. sect. 2)).

Table 3 also lists the ratios of the cross section σ_{sel} to that of the diffractional scattering on the nucleus σ_{d} calculated by the optical model (cf. fig. 3). Approximately $\frac{1}{3}$ of all cases of elastic scattering of a 9 GeV proton on the nucleus are elastic scattering on a bound nucleon in the nucleus. This agrees with the experimental results obtained in photoemulsion.

5.2. CHARACTERISTICS OF PARTICLES PRODUCED

Tables 4–6 and figs. 4–9 represent the available experimental data for s- and g-particles and the respective calculated quantities. Cases of diffractional scattering on nuclei are not included among nucleon-nucleus collisions, in accordance with the conditions of measurement in refs. [1, 6–10]).

The methodological conditions of measurements and the selection criteria for different types of nucleon-nucleus interactions as well as their analysis are different in all these investigations. Therefore direct comparison of measurements prove to be impossible, as a rule. The tables and figures indicate all results

TABLE 4

Average number of particles produced in one nucleon-nucleus event

Type of particles	Group of light nuclei		Group of heavy nuclei		Per average nucleus of photoemulsion	
	Exp.	The ory	Exp.	Theory	Exp.	Theory
s-particles	3.0 ± 0.2 [1])	2.9	3.5 ± 0.3 [1])	4.1	3.2 ± 0.2 [1]) 3.7 ± 0.05 [8])	3.7
s-protons					1.0 ± 0.5 [9]) 0.68 ± 0.07 [7]) 1.0 [10])	0.9
s-pions					3.3 ± 0.5 [9]) 3.8 ± 0.3 [7]) [a]) 3.1 [10])	2.8
g-particles	1.4 ± 0.1 [1])	1.5	4.1 ± 0.5 [1])	4.0	3.1 ± 0.4 [1])	3.2
g-protons g-pions				$\left.\begin{matrix}\text{prot.} \\ \text{pions}\end{matrix}\right\} \gg 1$	$\frac{\text{prot.}}{\text{pions}} = 4.6$	

[a]) The number of π-mesons given here exceeds the number of all s-particles (see the first line of this table) and evidently is considerably over estimates.

TABLE 5

Average angle (in degrees) which contains half of the particles produced in the collision of a 9 GeV proton with nuclei

Type of particles	Group of light nuclei		Group of heavy nuclei		Per average nucleus of photoemulsion	
	Exp.	Theory	Exp.	Theory	Exp.	Theory
s-particles	22.5±1 [1])	24	27.5±1.5 [1])	29	25.0±1.5 [1])	28
s-protons					≈29 [9]) [a])	22.5
s-pions					36.5±8.8 [9]) [a])	30
g-particles	56.5±3 [1])	48	65±3 [1])	69	65±3 [1])	63

[a]) These values of angles were obtained only for stars with a number of relativistic tracks (of s-particles) $n_s \geqq 3$, a large number of narrow showers with $n_s < 3$ being neglected. This may account for the fact that in ref. [9]) larger values of $\theta_{\frac{1}{2}}$ were obtained than in ref. [1]).

TABLE 6

Average kinetic energy of particles (in GeV) produced in the collision of a 9 GeV proton with nuclei

Type of particles	Group of light nuclei		Group of heavy nuclei		Per average nucleus of photoemulsion	
	Exp.	Theory	Exp.	Theory	Exp.	Theory
s-particles					3.0 ±0.5 [1])	
					3.5 ±0.5 [7]) [a])	2.5
s-pions					0.85 ±0.2 [1])	
					0.60 ±0.18 [6])	0.52
					0.65 ±0.2 [7, 9])	
					0.63 ±0.1 [10])	
g-protons	0.132±0.020 [1])	0.16	0.118±0.012 [1])	0.15	0.120±0.012 [1])	0.15
g-pions					0.040±0.003 [1])	0.048

[a]) This value is very close to the average kinetic energy of the protons produced in NN-collision $\bar{E} = 3.6 \pm 0.5$ GeV. Since the spectrum of protons after nuclear collision should be considerably softer, the energy value obtained in ref. [7]) is evidently overestimated.

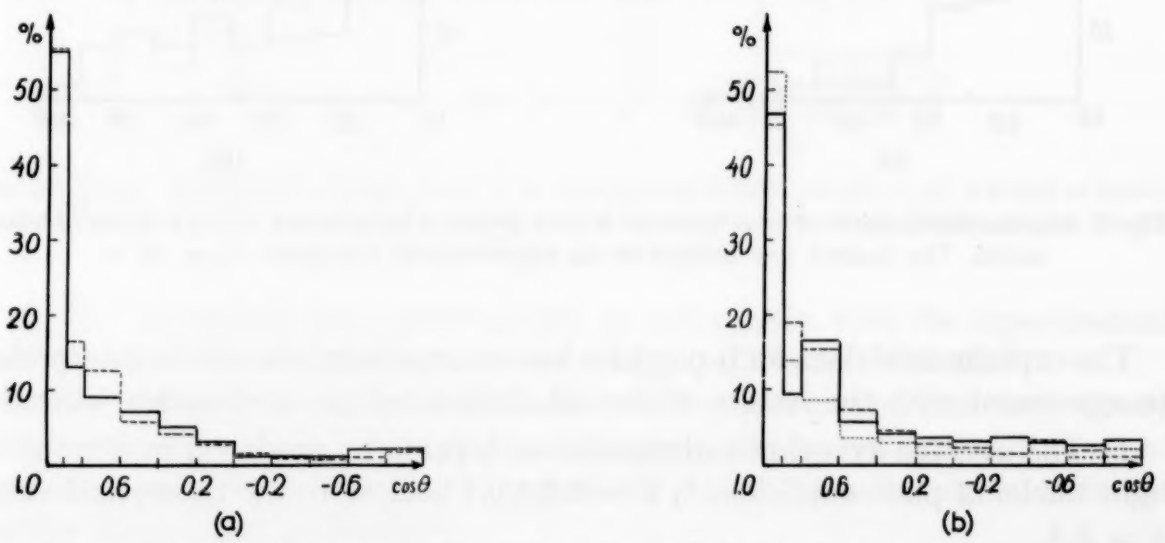

Fig. 4. Angular distributions of s-particles. a) is for a group of light nuclei, b) for a group of heavy nuclei. The dashed line designates experimental histograms from ref. [1]); the dotted line is an experimental histogram from ref. [31]).

of measurements known to us. Experimental values are given as a rule without critical appraisal.

The data cited show that the experimental and theoretical characteristics of s- and g-particles are in good agreement.

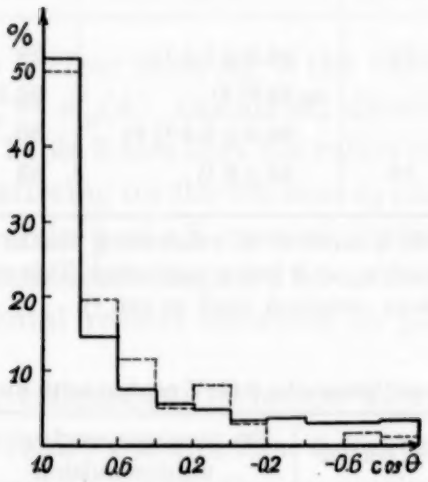

Fig. 5. Angular distribution of s-pions produced in the interaction of 9 GeV proton with the average nucleus of photoemulsion. The dashed line designates an experimental histogram from ref. [9]).

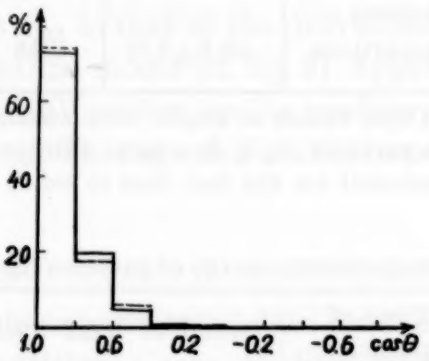

Fig. 6. Angular distribution of s-protons produced in the interaction of 9 GeV proton with the average nucleus of photoemulsion. The dashed line designates an experimental histogram from ref. [9]).

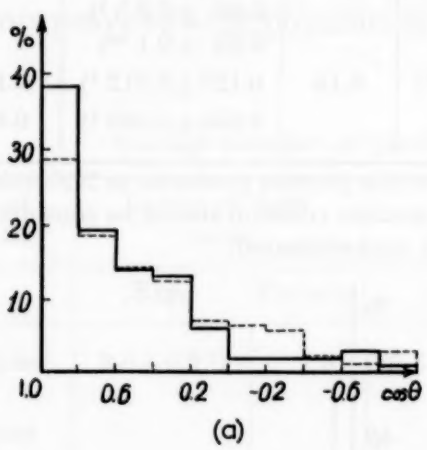

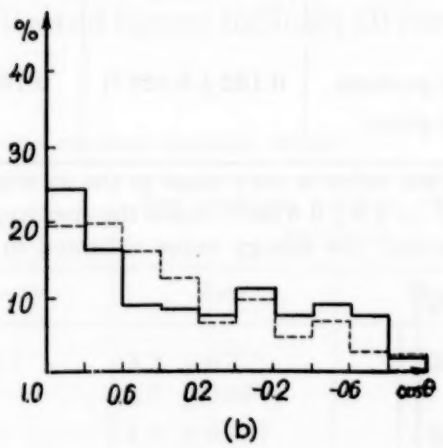

Fig. 7. Angular distribution of g-particles. a) is for a group of light nuclei, b) for a group of heavy nuclei. The dashed line designates an experimental histogram from ref. [1]).

The experimental data for b-particles known at present can also be interpreted in agreement with the results of the calculations of the intranuclear cascade:

1) The average experimental number of b-particles produced in a group of light nuclei of photoemulsions [1]) $\bar{n} = 3.3 \pm 0.1$ is close to the theoretical value $\bar{n} = 3.5$.

2) With allowance for the nucleons "evaporated" from the excited nucleus the experimental and theoretical numbers of particles produced in a group of heavy nuclei also prove to be nearly equal.

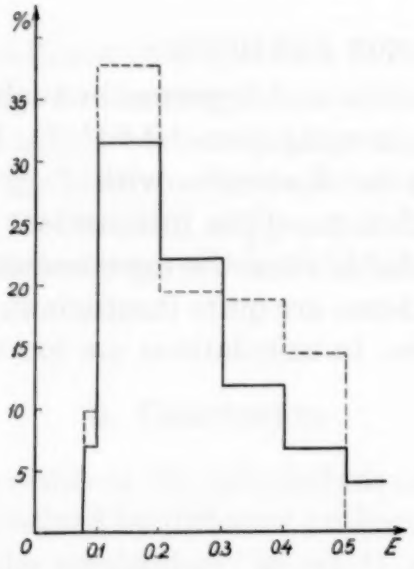

Fig. 8. Energy distribution of pions produced in the interaction of 9 GeV proton with the average nucleus of photoemulsion. The dashed line designates an experimental histogram plotted by the data of ref. [9]). (Methodical conditions in this paper excluded the possibility of observing π-mesons with $E > 0.54$ GeV). Values of the kinetic energy of pions in the laboratory system of coordinates E are given in GeV.

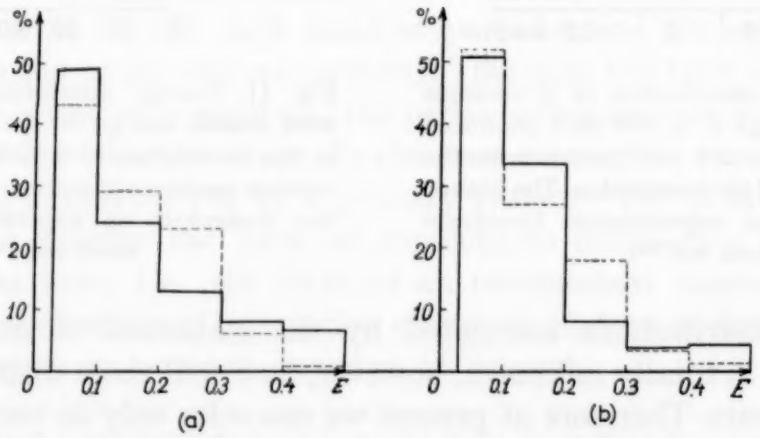

Fig. 9. Energy distribution of g-particles. a) is for a group of light nuclei, b) for a group of heavy nuclei. The dashed line designates an experimental histogram from ref. [1]). Values of the kinetic energy E are given in GeV.

3) The calculated pion spectrum has, in accordance with the experimental data of refs. [1, 9]), a maximum in the energy region $50 \div 100$ MeV.

4) The theoretical angular distributions of b-particles decrease very slowly with increasing angle θ while the average angle which contains half of all b-particles emitted from the nucleus equals 70° to 90°. This also agrees with the results of the measurements [1]).

Yet the results of the theoretical calculations of the characteristics of b-particles depend on the specific assumptions concerning the model of the nucleus and are therefore less definite than the above-mentioned data for s- and g-particles.

5.3. PRODUCTION OF STRANGE PARTICLES

The production of K-mesons and hyperons in nucleon-nucleus collisions was studied in photoemulsion investigations [1, 3, 9, 12, 13]). The most detailed results are obtained in refs. [1, 13]) for K-mesons with $E \leqq 150$ MeV.

The results of the calculations of the intranuclear cascades for strange particles are now rather unreliable since the experimental data on the interaction of these particles with nucleons are quite insufficient. This especially applies to the interaction of hyperons. In calculations use has to be made of the angular

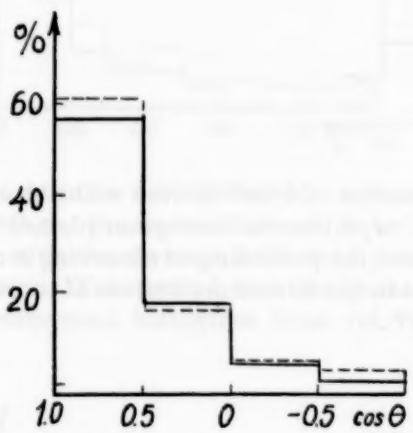

Fig. 10. Angular distribution of K^+-mesons with kinetic energy $E \leqq 150$ MeV produced in the interaction of 9 GeV proton with the average nucleus of photoemulsion. The dashed line designates an experimental histogram from ref. [13]).

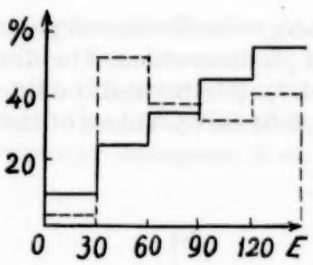

Fig. 11. Energy distribution of K^+-mesons with kinetic energy $E \leqq 150$ MeV produced in the interaction of 9 GeV proton with the average nucleus of photoemulsion. The dashed line designates an experimental histogram from ref. [13]).

and energy distributions calculated by the statistical theory of multiple production. It is totally unknown, however, how well these distributions agree with experiments. Therefore at present we can refer only to very rough qualitative results of the calculations of intranuclear cascades with the participation of strange particles.

Since K-mesons are produced already inside the nucleus and the cross section of their interaction with nucleons is less than the cross-sections of NN- and πN-interactions, K-mesons should on the average undergo a smaller number of interactions in the nucleus than nucleons or pions. Besides, since the probability of K-meson production rapidly decreases with the decrease of energy of colliding particles, the characteristics of K-mesons, should, in rough approximation, be determined largely by the first NN-collision.

Figs. 10 and 11 represent the comparison of experimental distributions with the results of the calculations by the statistical theory of the multiple production of K-mesons in NN-collisions at $E = 9$ GeV. It can be seen that angular distributions are in good agreement but the experimental energy spectrum is "softer".

The evaluation of one collision of a K-meson in a nucleus changes little the theoretical histogram in fig. 10 (for comparison with the experimental data [13])) the theoretical curve is averaged over very large angular intervals) but yields an energy distribution very close to the experimental figure.

The experimental value[13]) $(K^-/K^+) \approx \frac{1}{20} \ll 1$ of the ratio of the numbers of K^-- and K^+-mesons qualitatively agrees with the calculated value, though it is quantitatively $3 \div 5$ times as large †.

6. Conclusion

The comparison of the results of the calculations of the intranuclear cascade with experimental data obtained by different authors, alongside the arguments put forth against the "tube mechanism" in ref. [1]), makes it possible to claim that the intranuclear cascade mechanism occurs at $E = 9$ GeV as well as at lower energies.

The opposite conclusion drawn by Friedlander [11]) is based on the consideration of a narrow group of facts which besides, can be accounted for in terms of the intranuclear cascade mechanism ††.

At energies $E \gg 10$ GeV both incident particles and nucleus are strongly compressed (in the centre-of-mass system). Therefore the time of the interaction with a nucleus is very small and the perturbation wave is unable to spread transversely further than by $\hbar/\mu_\pi c$. In this case interaction occurs only with a tube of nuclear substance cut by a primary particle. Yet in this case as well interaction can assume the form of consecutive interaction with separate nucleons of the tube, i.e., the form of an intranuclear cascade.

Just which mechanism of interaction occurs in nucleon-nucleus collisions at very high energies is an open question at present.

We are grateful to K. D. Tolstov for discussions of different problems involved in nucleon-nucleus interactions at high energies and to M. G. Shafranova for the discussion of experimental data.

† It will be noted that in ref. [13]) an analysis is made of only 80 tracks of K-mesons ($77K^+$ and $3K^-$). Therefore experimental errors are fairly large.

†† A detailed analysis and criticism of the work by Friedlander is given in ref. [30]).

References

1) V. S. Barashenkov *et al.*, Nuclear Physics **14** (1959/60) 522, Atomnaya Energia **7** (1959) 376
2) V. I. Veksler, Proc. 2nd Intern. Conf. on Peaceful Uses of Atomic Energy; Reports by Soviet scientists (Moscow, 1959) V. 1, p. 253
3) Proc. 8th Ann. Intern. High Energy Physics Conf., Geneva (1958), p. 309
4) N. P. Bogachev *et al.*, Atomnaya Energia **4** (1958) 281
5) N. P. Bogachev *et al.*, JETP **37** (1959) 1225
6) G. L. Bayatian *et al.*, JETP **36** (1959) 690
7) G. B. Zhdanov *et al.*, JETP **37** (1959) 611
8) G. B. Zhdanov, V. M. Maksimenko, M. I. Tretyakova and M. N. Shcherbakova, JETP **37** (1959) 620
9) N. P. Bogachev *et al.*, JETP **38** (1960) 432
10) Yu. T. Lukin, Zh. S. Takibaev and E. V. Shalagina, JETP **38** (1960) 1074
11) E. Friedlander, Nuovo Cim. **14** (1959) 796
12) N. I. Kostanashvili and O. A. Shakhulashvili, JETP (to be published)
13) V. A. Beliakov *et al.*, Preprint no. 434 of the Joint Institute for Nuclear Research (1959)
14) V. A. Beliakov *et al.*, Proc. Ann. High Physics Conf., Kiev (1959)
15) V. P. Bannik, V. G. Grishin, V. B. Liubimov and M. I. Podgoretsky, Preprint no. 377 of the Joint Institute for Nuclear Research (1959)
16) V. S. Barashenkov and N. N. Huang, JETP **36** (1959) 1319
17) V. S. Barashenkov, Report at the 2nd All-Union Inter-University Conf. on field theory and elementary particles, Uzhgorod (1960) (to be published in: Forschritte der Fhysik)
18) V. S. Barashenkov, Uspekhi Fiz. Nauk **72** (1960) 53; Preprint no. 509 of the Joint Institute for Nuclear Research (1960)
19) N. P. Bogachev *et al.*, JETP **38** (1960) 1346
20) I. P. Gramenitsky, M. I. Podgoretsky, R. M. Lebedev *et al.* (to be published)
21) E. L. Feinberg, JETP **28** (1955) 241; Uspekhi Fiz. Nauk **58** (1956) 193
22) I. A. Ivanovskaya and D. S. Chernavsky, Nuclear Physics **4** (1957) 29
23) N. Metropolis, R. Bivins, M. Storm, A. Turkevich, J. M. Miller and G. Friedlander, Phys. Rev. **110** (1958) 185; 204
24) D. I. Blokhintsev, JETP **33** (1957) 1295
25) P. K. Markov *et al.*, JETP **38** (1960) 1471
26) M. M. Bloch, E. M. Harth, V. T. Cocconi *et al.*, Phys. Rev. **103** (1956) 1484, 1489;
M. E. Blevins, M. M. Block and I. Leitner, Phys. Rev. **112** (1958) 1287;
R. M. Kalbach, I. I. Lord and C. H. Tsao, Phys. Rev. **113** (1959) 325, 330;
N. P. Bogachev, Thesis of the Joint Institute for Nuclear Research (1960);
S. M. Korenchenko, Thesis of the Joint Institute for Nuclear Research (1960);
and other works (see a list of refs. in refs. [18, 23]))
27) V. S. Barashenkov, V. M. Maltsev and E. K. Mihul, Nuclear Physics **13** (1959) 583
28) V. S. Barashenkov and V. M. Maltsev, Nuclear Physics **17** (1960) 377
29) Yu. T. Lukin and Zh. S. Takibaev, Vestnik of the Kazakh SSR **1** (1959) 78;
T. P. Lazareva and P. A. Usik, Proc. Intern. Conf. on Cosmic Rays **1** (1960) 71 (Moscow, 1959)
30) K. D. Tolstov, a Report at the 2nd All-Union Inter-University Conf. on field theory and elementary particles, Uzhgorod (1960) (to be published);
K. D. Tolstov, Nuclear Physics (to be published)
31) N. P. Bogachev, S. A. Buniatov, Yu. P. Merekhov and V. M. Sidorov, DAN SSSR **121** (1958) 617

2.C

Nuclear Physics **24** (1961) 657—665; © *North-Holland Publishing Co., Amsterdam*

Not to be reproduced by photoprint or microfilm without written permission from the publisher

RESONANCES IN THE $K^{39}(p, \gamma)Ca^{40}$ REACTION FROM 1.0 TO 2.1 MeV

R. A. POPE, D. V. FRECK and W. W. EVANS

Research Laboratory, Associated Electrical Industries, Aldermaston Court, Aldermaston, Berks.

Received 19 December 1960

Abstract: Resonances have been found at $E_p = 1133.0 \pm 1.4$, 1311.7 ± 1.6, 1349.3 ± 1.6, $1579.9 \pm \pm 1.9$, 1769.7 ± 2.1 and 2046.7 ± 2.5 keV, half-widths all being less than 0.5 keV. A number of closely-spaced resonances in the region of $E_p = 1880$ keV have also been observed. The main features of decay at each resonance have been investigated.

1. Introduction

The excited states of self-conjugate doubly-magic Ca^{40} are well known up to 6 MeV from inelastic proton scattering [1]). The first level at 3.35 MeV is a 0^+ pair-emitting state [2, 3]), the second state at 3.73 MeV is a 3^- state [4]), the 3.900-MeV level most probably [5]) has spin 2 and the 4.483-MeV state is probably a 1^- state [6]).

The $K^{39}(p, \gamma)Ca^{40}$ reaction has been investigated from $E_p = 0.5$ to 1.15 MeV by Simao and Sellschop [7]) using 20–30 keV thick metallic potassium targets and beam currents from 50 to 100 μA. Resonances were found at $E_p = 883$, 925, 980 and 1150 keV (all ± 10 keV), the last resonance being about 10 times more intense than any of the others. The angular distribution of the ground state γ-ray from the 1150-keV resonance level indicated an E1 transition. Cascade γ-rays to the 3.73-MeV and 3.348-MeV levels were also observed.

Towle, Berenbaum and Matthews [8, 9]) have also studied this reaction from $E_p = 0.8$ to 1.8 MeV with up to 5μA of protons on 5 keV KI targets. They found resonances at 1120, 1300, 1338 and 1566 keV (all ± 5 keV), decay to the ground state being predominant for all except the resonance at 1338 keV. Cascades through the levels at 3.348, 3.73, 3.90 and possibly 4.483 MeV were seen, and the probability of a cascade through a higher level was inferred for the 1300 keV resonance. Angular distributions suggested 1^+, 1^- or 2^- for the 1120, 1300 and 1566 keV resonance levels.

Since the proton energy ranges for these two groups of experiments overlapped, it seemed clear that the resonance measured as 1150 ± 10 keV by Simao and Sellschop must be the same as that measured as 1120 ± 5 keV by Towle *et al.*, indicating a discrepancy between the two energy scales outside the quoted errors. The present work was undertaken to clear up this discrepancy, to

search for new resonances and to investigate the decay of the resonance levels found.

2. Experimental

Target backings were discs of electro-polished sheet tungsten, chosen for low γ-yield under proton bombardment [10]). Evaporated targets of KI and KBr, thickness both 5 and 20 keV at $E_p = 1$ MeV, were prepared, taking care to transfer them immediately from the evaporation plant to a desiccator for storage until required, since both compounds are extremely deliquescent. If the targets are exposed to a damp atmosphere, or if they are breathed on, the interference colours visible in the thin target film disappear as the material becomes white and opaque. Resonance measurements on targets which have absorbed moisture show that they are considerably thickened, making low-yield resonances more difficult to observe.

Because the targets proved fragile under irradiation, proton currents were kept below 2μA at 1 MeV and even less at the higher energies to avoid evaporation of target material. A strongly-focused beam tended to burn off the target in one spot, so the beam was deliberately slightly de-focused to fill the area of the target (about 1 cm^2). To reduce unwanted counts from stray beam, a tungsten diaphragm was placed immediately before the target. This was cleaned with emery cloth whenever the target was changed.

A liquid air trap served to minimise the deposition of carbon on the target surface. Initially, the target was heated to maintain it at about 200° C, as indicated by a thermocouple in contact with the rear of the target, as additional protection against deposition of impurities from the vacuum system [11]), but the heating was eventually dispensed with because it increased the possibility of burn-off. In fact, since a fresh target was inserted at least once a day, the shift in resonance energy caused by carbon build-up was found to be certainly less than 0.2 keV during the time a target was in the vacuum system.

γ-rays were detected by a 10.2 cm diameter, 10.2 cm long NaI(Tl) crystal optically coupled via a 1.27 cm long perspex light pipe to an E.M.I. 6099A photomultiplier. The scintillation counter was shielded from background γ-rays and x-rays from the machine by a 14.0 cm thick cylindrical lead shield. For γ-ray yield measurements, pulses from the counter passed through a 50 C amplifier to a scaler controlled by a timing unit and a beam current integrator, while for γ-ray spectra the amplifier output was fed to a 100-channel Sunvic pulse-height analyser. The γ-ray energy calibration was effected by detecting known γ-rays from the radioactive sources Na^{22}, Cs^{137}, Co^{60} and Sb^{124}, and extended to higher energies with the 6.14 MeV gamma ray from the $F^{19}(p, \alpha\gamma)O^{16}$ reaction. The energies of the more intense γ-ray peaks could be measured to an accuracy of ± 1.5 % and values given are the mean of several determinations.

Protons were accelerated by a pressurised Van de Graaff generator [12]) and their energy stabilised and measured with an electrostatic analyser [13]) capable of absolute measurement of proton energy to better than one part in a thousand. In the present work, however, it was found more convenient to measure (p, γ) resonance energies relative to a standard resonance in the $F^{19}(p, \alpha\gamma)O^{16}$ reaction previously determined [14]) absolutely as 873.5 ± 0.7 keV. It should be noted, however, that our values for the $F^{19}+p$ resonances are about a part in a thousand higher than the weighted mean values adopted by Marion [15]) from a consideration of the absolute measurements of a number of workers.

The limit of error for each resonance in the present work has been taken as that of our absolute values of the $F^{19}+p$ resonances, 0.80 parts in 10^3, plus 0.4 parts in 10^3, which is the extreme deviation of any relative determination from the mean, giving a total of 1.2 parts in 10^3.

3. Results

The results are summarised in table 1, which includes the resonance energies found by Simao and Sellschop and Towle *et al.*, for comparison. Our γ-ray yield

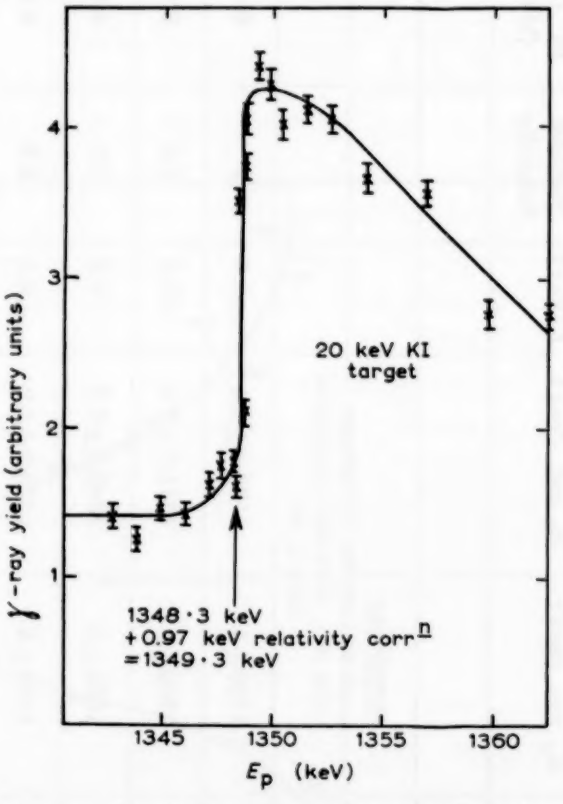

Fig. 1. Thick target yield curve at the 1349.3 keV resonance.

below 1 MeV was too low for any resonances to be observed. This is consistent with the findings of Simao and Sellschop that the resonances below 1 MeV are only 0.1 or less of the intensity of their 1150 keV resonance.

TABLE 1

Summary of results

Simao and Sellschop [7])	Towle *et al.* [8, 9])	Present work				
E_p res. (keV)	E_p res. (keV)	E_p res. (keV)	Γ (keV)	Approx. relative intensity	Corr. level in Ca^{40} (MeV)	Mean features of decay
883±10						
925±10						
980±10						
1150±10	1120±5	1133.0±1.4	<0.5	1	9.44	Ground state and cascade through 3.73
	1300±5	1311.7±1.6	<0.5	1.5	9.61	Ground state and cascade through 3.90
	1338±5	1349.3±1.6	<0.5	2.5	9.65	No ground state. Cascade through 3.73 and 3.90
	1566±5	1579.9±1.9	<0.5	2.2	9.87	Ground state and cascade through 3.35
		1769.7±2.1	<0.5	1.8	10.06	No ground state. Cascade through 3.73 and 3.90
		2046.7±2.5	<0.5	8.0	10.33	Ground state and cascade through 3.35
		resonances in 1880 region	<1.0	3.5 max.	~10.16	No ground state. Cascades through 3.35 and other levels

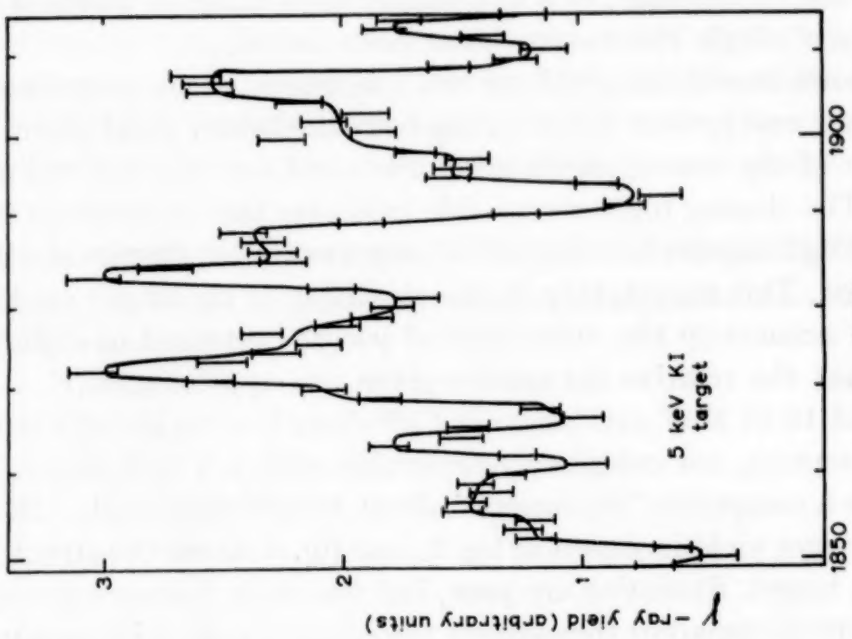

Fig. 3. Thin target yield curve in the resonance region around 1880 keV.

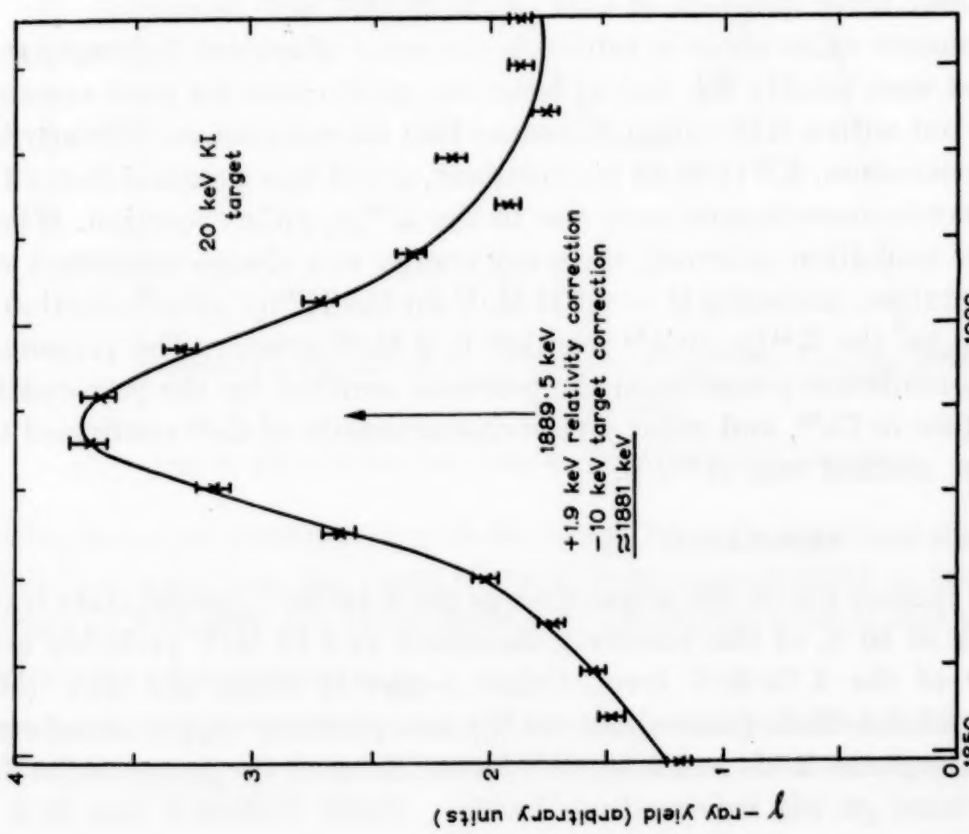

Fig. 2. Thick target yield curve in the resonance region around 1880 keV.

Our first resonance, the only one directly comparable with the results of Simao and Sellschop, is 17 keV lower than their value, while our first four resonances are, on average, 12.5 keV higher than those of Towle *et al.* In addition, two new single resonances have been found.

Fig. 1 shows one of our yield curves. The resonance is very narrow, so that the resonance energy was taken as the half-maximum yield point on the low-energy side of the curve, eliminating the need for any correction for target thickness. The sloping high-energy side indicates the variation in target thickness caused by irregular burning-off of target material, despite the limitation of beam current. This uncertainty in the condition of the target made it difficult to compare accurately the intensities of γ-rays measured in different irradiations, so that the relative intensities given are approximate.

At around 10.16 MeV excitation in Ca^{40} there is a region of narrow, closely-spaced resonances, not completely resolvable with a 5 keV target, which combine to give a composite "resonance" about 35 keV wide with a 20 keV target. The thick target yield is shown in fig. 2, and fig. 3 shows the structure revealed with a thin target. Statistics are poor, but the main features are reproducible. Fine structure is apparent throughout the energy range, with many indications of small peaks too numerous to follow in detail, but only in this region is the intensity sufficient to justify a closer examination.

A single run above 2.1 MeV with a 20 keV target indicated about four unresolved resonances between 2.14 and 2.20 MeV, the thick target intensity rising to about three quarters of that of the 2046.7 keV resonance.

Each resonance value given in table 1 is the mean of several determinations. Targets used were mostly KI, but at least one yield curve for each resonance was carried out with a KBr target to ensure that the resonances were attributable to the potassium. K^{39} is 93.38 % abundant, and it was assumed that all the single resonances investigated were due to the $K^{39}(p, \gamma)Ca^{40}$ reaction. When a ground state transition occurred, the γ-ray energy was always consistent with this interpretation, assuming $Q = 8.331$ MeV for the $K^{39}(p, \gamma)Ca^{40}$ reaction [17]). The Q-value for the $K^{41}(p, \gamma)Ca^{42}$ reaction is 2 MeV greater. The presence of 0.51-MeV annihilation γ-rays from the positons emitted by the pair-emitting 3.35-MeV state in Ca^{40}, and other γ-rays characteristic of Ca^{40} confirmed that the reaction studied was $K^{39}+p$.

3.1. THE 1133.0 KeV RESONANCE

The most intense line in the γ-spectrum is the 9.44-MeV ground state transition. A peak of 40 % of this intensity measured as 3.72 MeV probably arises from decay of the 3.73-MeV level. Other γ-rays of about 5.2 MeV (10 % intensity) and 6.1 MeV (also about 10 %) are probably upper members of cascades through the 3.73- and 3.35-MeV levels. Some of the decay to the 3.73-MeV level must go via intermediate levels.

3.2. THE 1311.7 keV RESONANCE

The 9.61-MeV ground state line is prominent, with a 35 % γ-ray of 3.85 MeV which is probably mainly from the 3.90-MeV level, although there may be a contribution from the 3.73-MeV level also. A γ-ray of 5.77 MeV (5 %) probably results from direct transitions to the levels at 3.90 and 3.73, while one of 6.26 MeV (5 %) must be the transition to the 3.35-MeV state. Once again a large part of the decay through the 3.90 and 3.73-MeV levels must go through higher intermediate levels.

One of the γ-ray spectra taken at this resonance is shown in fig. 4. The peak

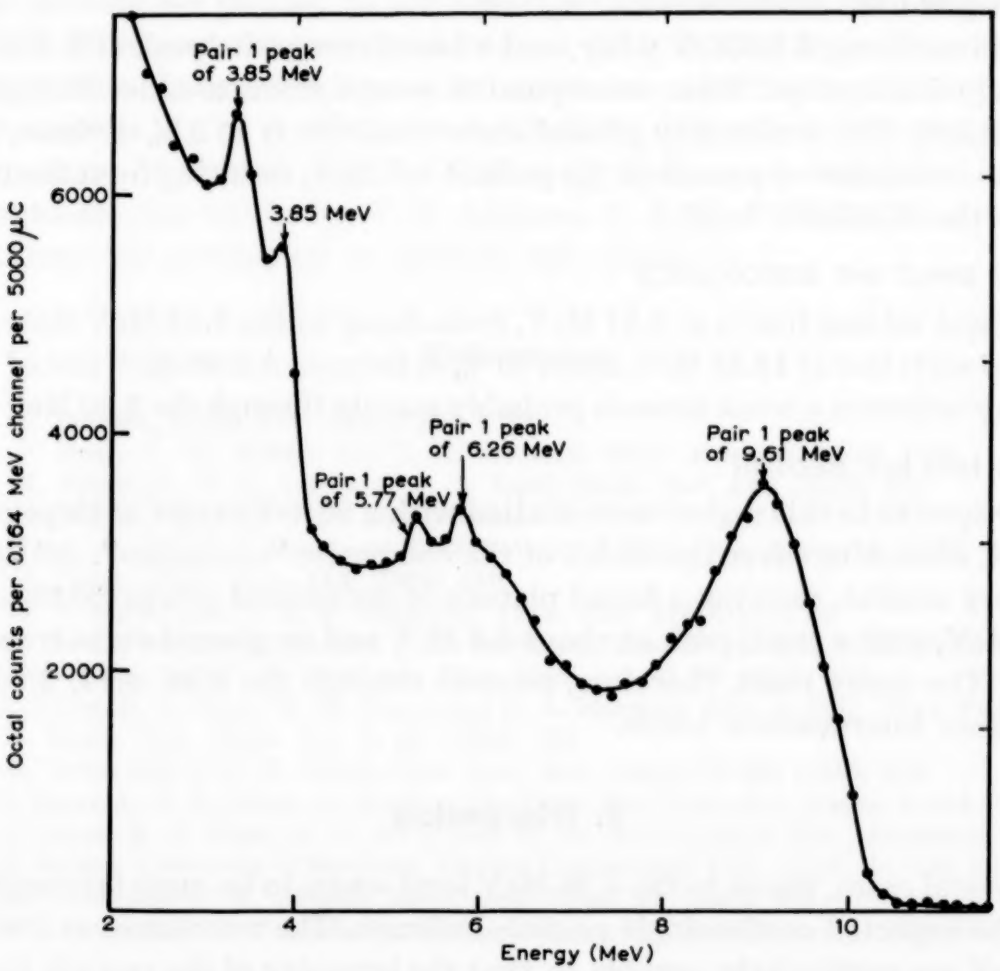

Fig. 4. Gamma ray spectrum at the 1311.7 keV resonance.

resulting from pair production with the escape from the crystal of one 0.51-MeV annihilation quantum (the "pair 1" peak) is most prominent at high energies, although at 3.85 MeV the photoelectric or full-energy peak is still visible.

3.3. THE 1349.3 keV RESONANCE

Two prominent lines of about equal intensity were measured as 3.86 and 5.83 MeV, representing unresolved lower and upper members of cascades through the 3.73 and 3.90-MeV levels.

Any ground state transition was less than 2 % of these. The presence of 0.51-MeV γ-rays from positon annihilation indicated a weak decay through the 3.35-MeV level.

3.4. THE 1579.9 keV RESONANCE

A strong line at 9.87 MeV is the ground state transition, and one of about equal intensity at 6.46 MeV must be the transition to the 3.35-MeV state, which is confirmed by a strong 0.51-MeV line. Decay through the 3.73 and 3.90-MeV levels appears to be weak (5 %).

3.5. THE 1769.7 keV RESONANCE

There is a strong 3.83-MeV γ-ray, and a broad composite peak at 6.2 MeV of about equal intensity. These correspond to γ-rays from cascades through the 3.73 and 3.90-MeV levels. Any ground state transition is < 2 % of these. There is also an indication of a small (5 %) peak at 6.7 MeV, resulting from the transition to the 3.35-MeV level.

3.6. THE 2046.7 keV RESONANCE

The most intense line is at 6.91 MeV, from decay to the 3.35-MeV state, with a ground state line at 10.33 MeV about 70 % as intense. A 3.90-MeV line of 10 % intensity indicates a weak cascade probably mainly through the 3.90 MeV level.

3.7 THE 1880 keV REGION

γ-ray spectra in this region were studied with a 20 keV target at three proton energies, chosen to cover the width of the composite "resonance". All spectra were very similar, showing a broad plateau of unresolved γ-rays extending up to 6.8 MeV, with a small peak at about 3.8 MeV and no ground state transition visible. The decay must, therefore, proceed through the 3.35, 3.73, 3.90-MeV and higher intermediate levels.

4. Discussion

In several cases, decay to the 3.35-MeV level seems to be more favoured than would be expected on the single particle estimate. The resonances at 1580 and 2047 keV are particularly notable in that the intensity of the cascade through the 3.35-MeV level is equal to, or greater than, that of the ground state transition although both states are 0^+. There would appear to be grounds for suggesting that some of the higher excited states might be collective in origin, built upon the first excited 0^+ state which might have a stable deformation contrasting with the spherical ground state. This possibility is more likely for a case like Ca^{40}, where the first excited state is formed from the ground state by the excitation of two particles from the $d_{\frac{3}{2}}$ shell to the $f_{\frac{7}{2}}$ shell [5]). It is also one way of explaining the 1^- level at 4.483 MeV, which Shook [6]) suggests is an octupole vibrational level, although 1^- excitations of purely collective character are

not likely to occur at low energies according to the interpretation of Lane and Pendlebury [17]), who postulate the 3^- state at 3.73 MeV as an octupole vibration. The 4.483-MeV level might be the first octupole vibration of a deformed intrinsic-particle first excited state, whereas the 3^- state at 3.73 MeV results from octupole vibration about the spherical ground state.

The 1880 keV resonance region may correspond to a band of collective levels based on the first excited state, since no ground state gamma rays are observed, but transitions to the 3.35-MeV state are evident.

The authors are pleased to acknowledge the advice and encouragement of Dr. S. E. Hunt and the continued interest of Dr. D. R. Chick. They also wish to thank Mlle. Janine Perchereau for assistance with the experimental work. The comments of Dr. A. M. Lane of A.E.R.E., Harwell, on the possibility of deformations of excited states of Ca^{40} were much appreciated.

Thanks are also due to Dr. T. E. Allibone, C. B. E., F. R. S., Director of the Laboratory for permission to publish this paper.

References

1) C. M. Braams, Phys. Rev. **101** (1956) 1764
2) R. D. Bent, T. W. Bonner and J. H. McCrary, Phys. Rev. **98** (1955) 1325
3) R. M. Kloepper, R. B. Day and D. A. Lind, Phys. Rev. **114** (1959) 240
4) R. H. Helm, Phys. Rev. **104** (1956) 1466
5) Y. Hirao, E. Okado, I. Miura and T. Wakatsuki, J. Phys. Soc. Japan **13** (1958) 233
6) G. B. Shook, Phys. Rev. **114** (1959) 310
7) J. de V. Simao and J. P. F. Sellschop, Phys. Rev. **106** (1957) 98
8) J. H. Towle, R. Berenbaum and J. H. Matthews, Proc. Phys. Soc. A **70** (1957) 84
9) R. Berenbaum and J. H. Matthews, Proc. Phys. Soc. A **70** (1957) 445
10) S. E. Hunt, R. A. Pope, W. W. Evans and D. A. Hancock, Brit. J. Appl. Phys. **9** (1958) 443
11) S. E. Hunt, Proc. Phys. Soc. A **65** (1952) 982
12) D. R. Chick and D. P. R. Petrie, Proc. Inst. Elec. Engrs. B **103** (1956) 132
13) S. E. Hunt, D. P. R. Petrie, K. Firth and A. Trott, Proc. Inst. Elec. Engrs. B **103** (1956) 146
14) S. E. Hunt, R. A. Pope, D. V. Freck and W. W. Evans, Phys. Rev., December (1960)
15) J. B. Marion, University of Maryland, Physics Department, Tech. Rept. No. 184, July (1960)
16) P. M. Endt and C. M. Braams, Revs. Mod. Phys. **29** (1957) 683
17) A. M. Lane and E. D. Pendlebury, Nuclear Physics **15** (1960) 39

4.E

Nuclear Physics **24** (1961) 666—674; © *North-Holland Publishing Co., Amsterdam*

Not to be reproduced by photoprint or microfilm without written permission from the publisher

SYSTEMATIC TRENDS IN HALF-LIVES OF BETA-DECAYING NUCLEIDES

G. ANDERSSON

The Gustaf Werner Institute for Nuclear Chemistry, University of Uppsala, Sweden

Received 26 September 1960

Abstract: Linear relationships between log $T_{\frac{1}{2}}$ and A are shown to exist among neutron deficient Pb and Tl nucleides, if odd and even mass numbers are taken separately and $T_{\frac{1}{2}}$ is the pure beta half-life. The same simple systematics is found to apply to numerous other series of alternate isotopes, neutron rich as well as neutron deficient ones, indicating its usefulness in predicting half-lives. Attempts to establish the conditions for occurrence of these regularities meet with difficulties owing to the lack of experimental data. The probable spin and parity dependence of the systematics may enable it to suggest level assignments in certain cases of isomerism.

1. Introduction

It goes without saying that the search for unknown nucleides is much facilitated if their properties can be predicted. The use of alpha decay systematics in the heavy mass region is perhaps the most well-known example. Isomeric transitions offer other cases where half-life as well as energy show systematic trends.

For beta emitters the situation is rather different. It is true that the disintegration energy available often can be predicted with some accuracy [1]). This is not a readily measurable quantity, however, since beta spectra are continuous and usually complex; furthermore, the endpoint does not necessarily correspond to a ground state transition. The experimental difficulties become especially discouraging in the regions where the search for new beta-decaying nucleides must now take place.

In most cases the half-lives in principle should be more accessible to experimental determination. As to the possibility of making predictions, however, one has to take into account that an observed beta half-life is most often the result of contributions from several branches of different forbiddenness, the relative strengths of which are likely to vary considerably even within series of isotopes of the same type. Thus, although it is well known that half-lives of beta-decaying nucleides tend on the whole to decrease with increasing distance from the stability line, there has been little reason to expect a systematic variation with, for instance, mass number.

It is the purpose of the present communication, however, to point out that such trends do exist in many cases and to give a preliminary discussion of their implications.

2. Half-life Systematics of Pb and Tl Isotopes

To large extent nuclear spectroscopic work at this Institute has been concerned with highly neutron deficient Pb and Tl isotopes. Their half-lives have been accurately determined and mass assigned by following the decay of conversion electron lines from electromagnetically mass separated sources in a high-resolving spectrometer.

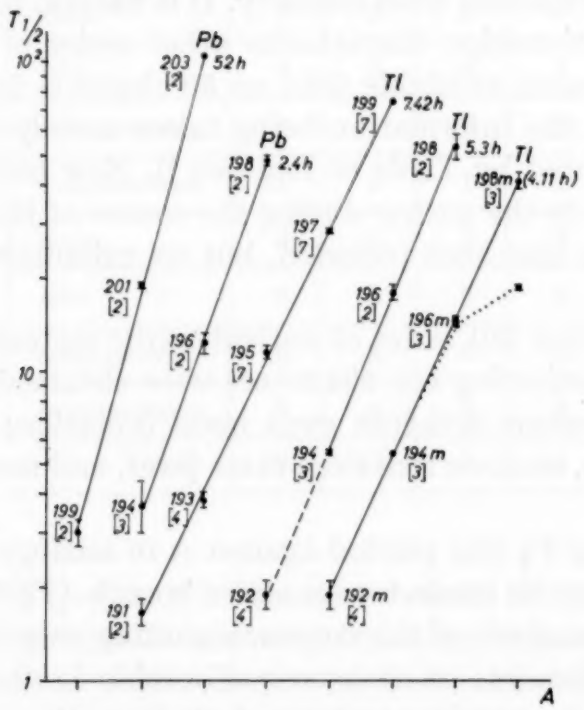

Fig. 1. Semilogarithmic plot of beta half-life against mass number for neutron deficient Pb and Tl nucleides. Tl^{198m} and Tl^{196m} have been corrected for internal branches; the uncorrected half-lives are indicated by dotted lines. Note that different scales have been used for the various lines. Reference numbers are given within brackets.

When the half-lives so obtained, together with some additional ones from the literature [2]), are plotted on a logarithmic scale against A for constant Z, odd mass and even mass isotopes being taken separately, linear relationships appear as shown in fig. 1.

The curve furthest to the right is of particular interest. It represents the beta half-lives of isomeric 7+ states in even-mass Tl isotopes [3, 4]). Tl^{194m} and Tl^{192m} are assumed to be nearly 100 % beta-decaying, whereas in the remaining two cases the observed half-life has been corrected for experimentally determined internal branches. The resulting straight line may be said to demonstrate the

exclusive connection of this systematics with beta decay. A direct use of the uncorrected values would give the dotted curve.

In Tl^{192} an 11.4 min activity has been ascribed to the 7+ state with reasonable certainty, leaving the possibility open of a similar half-life for the ground state [4]). This interpretation is seen to lead to a nice fit with the even-mass ground state line.

3. Additional Experimental Evidence

The lines in fig. 1 represent the most neutron deficient isotopes of each kind known so far, whereas the inclusion of higher mass numbers would cause more or less pronounced deviations from linearity. It is natural to raise the question, whether similar relationships characterize other series of nucleides far from stability. For this reason available data on 50 elements from Pb down to As have been surveyed, the information being taken mainly from Nuclear Data Sheets [2]), complemented by Table of Isotopes [5]). New half-life values, which have become known to the author during the course of the work up to about 1 August 1960, have also been included, but no exhaustive literature search has been made.

In this way altogether 201 series of nucleides (the metastable states of even-mass Tl isotopes constituting the 201*st* one) were obtained, which divide into four main groups: neutron deficient even mass (notation: nde), neutron deficient odd mass (ndo), neutron rich even mass (nre), and neutron rich odd mass nucleides (nro).

For each series, log $T_{\frac{1}{2}}$ was plotted against A in analogy with fig. 1. In one case correction had to be made for an alpha branch (Tb^{149}).

The results of an analysis of the curves, including only isotopes outside the stable ones of each element, are summarized in table 1, where the main groups have been subdivided according to type of nucleus. It was found suitable to classify the information in the following way:

+ if a straight line can be drawn within reported or reasonable error limits of at least three points, starting with the most neutron rich or neutron deficient isotope, respectively;

(+) additional cases where out of three consecutive points a straight line through the two extremes predicts the half-life of the intermediate nucleide within a factor 2 (this criterion was considered useful from the practical point of view of predicting half-lives);

(−) greater deviations from linearity, if the generally recognized trend of decreasing half-life with increasing distance from the stability line is still retained;

− if even the last-mentioned trend is violated.

A striking fact immediately revealed by the survey is the dominance of cases where pertinent data are missing. This is true in particular of the even-proton series, obviously as a result of the numerous stable isotopes of these elements and also partly due to the rather loosely founded principle of discarding data within the stability region. The experimental situation, however, is far from satisfactory even in many of the cases classified. It seems possible that several

TABLE 1

Statistics of series of alternate isotopes in As–Pb as to agreement with beta half-life systematics

Type of nucleus		+	(+)	−	(−)	Data missing
nde	even	1	2	0	0	22
	odd	5	6	4	1	10
ndo	even-proton	4	1	0	2	18
	even-neutron	11	3	1	2	8
nre	even	0	2	0	3	20
	odd	6	6	3	3	7
nro	even-proton	3	3	0	2	17
	even-neutron	3	4	0	3	15
	Total	33	27	8	16	117

For notation, see text.

of the series labelled (−) may be brought over to the positive side by more accurate half-life determinations, changes in mass assignment or the discovery of new members of the series. Improved data and additional information, however, may as well work the opposite way, destroying apparent agreements with a linear relationship. That fortuitous cases may occur is shown by the neutron deficient even-mass Gd isotopes, where the alpha-emitter Gd^{150} would fit rather well into this beta systematics.

Although the individual figures given in table 1 thus are likely to change with time, some general features can be distinguished already at this stage. The expected existence of appreciable deviations from a linear log $T_{\frac{1}{2}}$ versus A plot, for one thing, is well demonstrated, predominantly in odd nuclei (cf. subsection 4.2). On the other hand, the number of positive cases, seemingly statistically distributed between neutron rich and neutron deficient series of isotopes and among nuclei of the various types, is surprisingly large. Already the indicated 70 % chance of making a fair half-life prediction by interpolation should make this simple systematics useful.

A suitable test case was afforded by the earlier unknown Au^{190}, for which a

straight line defined by mass numbers 194, 192 and 188 indicated a 36 min period (fig. 2). The experiments, which are described elsewhere [6]), were arranged with regard to this prediction, and the half-life of Au^{190} was obtained as (38.8± 1.8) min. It may be added that a recently reported new half-life value of Au^{188} [8]) implies a deviation from the earlier beautiful linearity of the 194–192–188 plot, but is better in line with the somewhat longer half-life of Au^{190} found than with that originally predicted.

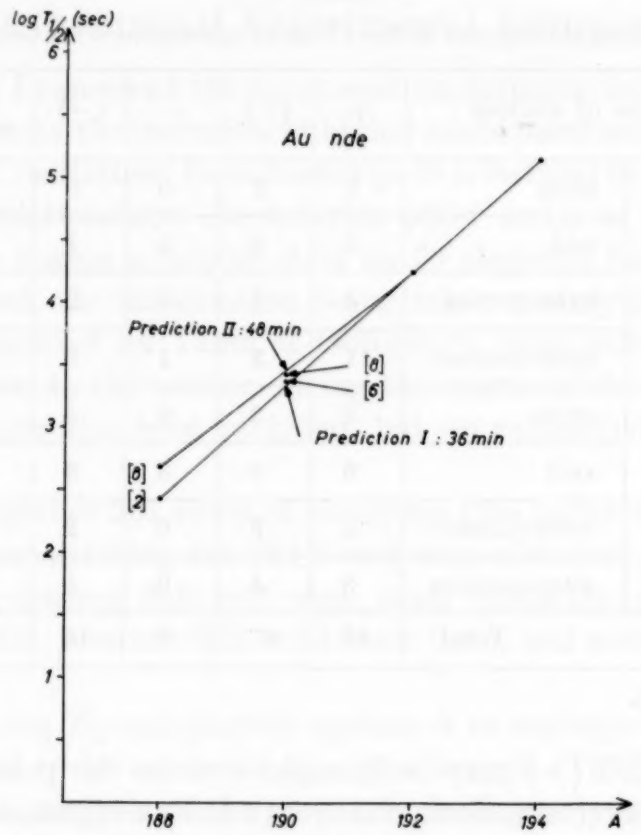

Fig. 2. Half-life systematics of neutron deficient even-mass Au isotopes, used to predict the half-life of Au^{190}. The two lines correspond to different values reported for Au^{188}. Experimental results for Au^{190} in fair agreement with both predictions are indicated. Reference numbers are given within brackets.

To make full use of this systematics, and in particular to be able to extrapolate in the diagrams, the conditions leading to simple regularities in beta-decay half-lives have to be established. Although it does not seem possible to obtain a coherent picture of the situation on the basis of the present incomplete experimental material, it is certainly tempting to speculate on some probable controlling factors as done in the next section.

4. Discussion

4.1. ENERGY DEPENDENCE

Consider first the simplified case that a series of alternate isotopes all decay with a 100 % beta branch to the ground state of the isobar. As long as spin and

parity of both parent and daughter do not change, one expects a constant *ft*-value for the transition. That is, since *f* is roughly proportional to some constant power of the transition energy, a systematic behaviour of the half-life in this case can be explained as a direct reflection of the regularities in the nuclear mass surfaces, as expressed for instance in the Way-Wood systematics[1]).

Branched decay makes the picture more complicated. The fact that the systematic trends are found for the most neutron rich or neutron deficient isotopes of an element would seem to support the assumption that the increase in available disintegration energy with increasing distance from stability is part of the explanation. If the disintegration energy is large enough compared with the spacings of levels populated in the decay, changes in the relative contributions from the various branches may become negligible so that the resulting reduced decay probability can still be considered constant within the series of isotopes concerned.

Some of the experimental data, however, are hard to reconcile with such an interpretation of the regularities. This is true, for instance, of Br^{84}, Eu^{154}, Tm^{167}, Tl^{199} and Pb^{203}, all of which are members of well-behaving series but are known to decay through several branches having large energy differences relative to the total disintegration energy. Another point of interest in this connection is the probability that with increasing disintegration energy, additional levels of favourable spin and parity become available in the daughter nucleus.

If there is a direct correlation between beta half-life and total disintegration energy one should also expect shell effects to show up in the systematics. Indications in this direction are observed, most apparent in the cases of Sn^{132} ($Z = 50$, $N = 82$) and I^{135}($N = 82$). On the other hand, Eu^{145}($N = 82$) fits a straight line.

The fact that so many series of isotopes tend to follow a strictly linear dependence of log $T_{\frac{1}{2}}$ on A should perhaps not be overemphasized, however interesting it may seem. In reality the straight line may be merely a sufficiently good approximation of a more complicated curve within a restricted mass range, especially when the linearity is based on three points only. It deserves to be mentioned, however, that the present systematics includes up to 5 points in several cases and may extend over as much as 5 decades in half-life.

4.2. INFLUENCE OF LEVEL ASSIGNMENT

To return to the simplified case discussed in the beginning of subsection 4.1, constancy of spin and parity was assumed for the states involved as a condition for a systematic behaviour of the half-lives. Consequently, one might expect a discontinuity in the relation between $T_{\frac{1}{2}}$ and A if there is a sufficiently large change of ground state assignment within the series of decaying nucleides. A similar change in the daughter nucleides, however, would be less likely to show

up, because the original ground state may still be available for the decay as a low-lying excited level.

An attempt to confront this hypothesis with experimental data [2]) gives the following results. Out of the altogether eight highly non-systematic cases, seven are series of odd nuclei, which may be significant. Both spin and parity changes among the parent states are reported in four of these cases. Only spin

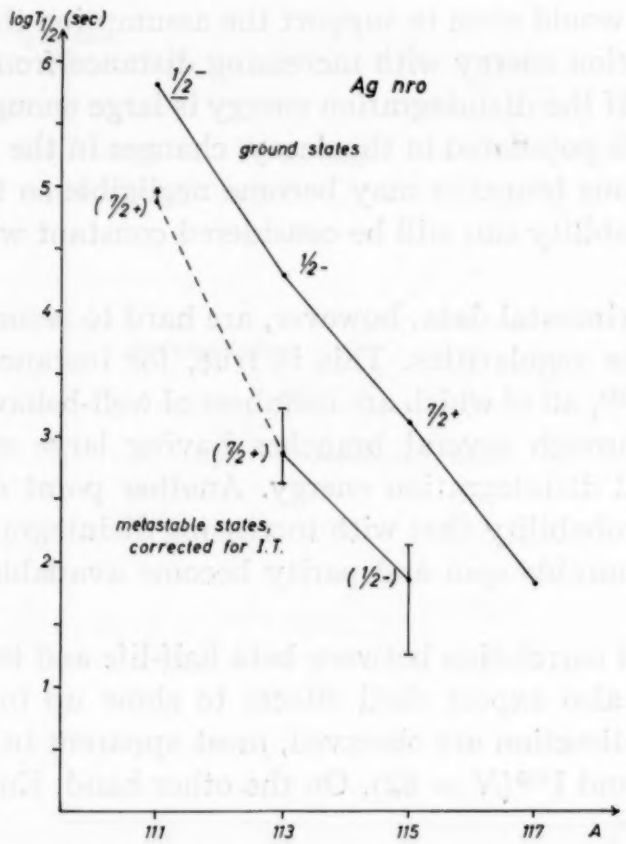

Fig. 3. Beta half-lives assigned to neutron rich odd-mass Ag isotopes with level assignments according to ref. [2]). The systematics would suggest a change of assignments in Ag^{115}.

change is indicated in one case and in the remaining two cases relevant data are missing. The eighth non-systematic series is that formed by the neutron deficient odd-mass Ir isotopes, where spin-parity assignments of the lower-mass members are also unknown. A change of parity of the ground state would seem less probable in this case, but the possibility that for instance the half-life assigned to Ir^{185} is due to a metastable state, with the ground state considerably shorter, can hardly be excluded.

Examination of the 33 series which fit closely to straight lines reveals that level information is insufficient in 19 cases, constant spin-parity assignment of parents probable in 9 cases, and spin change alone occurring in 4 cases. The remaining case is that of neutron rich odd-mass Ag isotopes with a reported spin and parity change. This will be discussed somewhat further.

The Ag isotopes of interest are 111, 113, 115 and 117. While the ground states of the two first-mentioned nuclei are well established as $\frac{1}{2}^-$, a level crossing has been indicated between 113 and 115, making a $\frac{7}{2}^+$ level, known to be metastable in 111 and 113, the ground state of 115. Instead $\frac{1}{2}^-$ is assigned to the isomeric state of this nucleus [2]). The log $T_{\frac{1}{2}}$ versus A plot shown in fig. 3 suggests a change of these assignments. Unfortunately the branching ratios β^-/I.T. for the metastable states are inaccurately known, but it seems reasonable to combine the two sets of experimental points in the way indicated in the figure. This would imply constant parity and small spin changes within each family.

The neutron rich even-mass isotopes of Sb represent another case, in which the half-life systematics suggests which states may be assigned the same parity and similar spin values. (See fig. 4.) It may be remarked that in the 3^- series, as

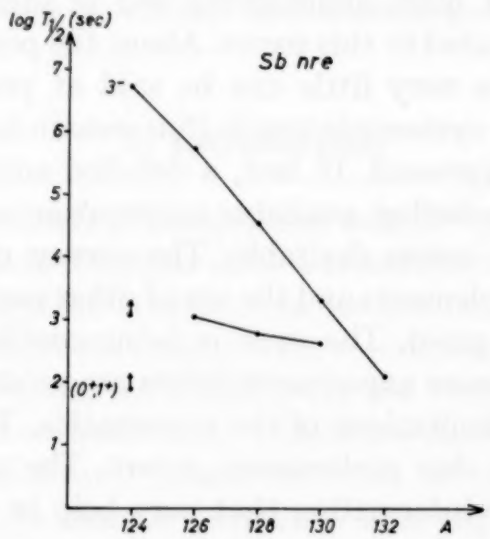

Fig. 4. Systematics of beta half-lives assigned to neutron rich even-mass isotopes of Sb (ref. [2])), indicating which states may be given similar spin-parity assignments.

indicated in the figure, assignment to the ground state is well established for mass 124 and preferred for mass 130, while the members of mass 126 and 128 are both considered metastable [2]). In such questions the present systematics cannot of course contribute to any judgment.

Provided that the constancy of spin and parity of the parent is a determining factor, even nucleides would be expected to be particularly well-behaved. As seen in table 1, the experimental evidence unfortunately is very meagre and does not seem to allow any conclusions to be drawn. It may be mentioned, that one of the (—) cases, Sn nre, can be easily explained as being due to a shell effect (cf. subsection 4.1). In other non-linear series one may trace the influence of the level structure of the daughter nuclei.

A very interesting question is whether a sufficiently high disintegration energy and, hence, the availability of a richer variety of levels in the daughter nucleus would tend to wash out the dependence of the beta half-life on spin and

parity of the decaying state. The coinciding half-life values of 2^- Tl^{194} and 7^+ Tl^{194m} and probably of the corresponding states in Tl^{192} (see fig. 1) seem to indicate this possibility. However, one isolated case is certainly an insufficient basis for a discussion of this problem.

5. Concluding Remarks

The simple half-life systematics first observed among the neutron deficient Pb and Tl isotopes has been found to apply to a considerable number of other series of nucleides in the Z-region surveyed. From a practical point of view this gives some hope that a better understanding of the conditions governing the systematics will make it useful not only in predicting half-lives, but also in judging the validity of mass assignments and in identifying corresponding isomeric states, as indicated in this paper. About the possible physical implications of the regularities very little can be said at present.

Several aspects of the systematic trends thus remain to be studied, before any definite rules can be expressed. In fact, a detailed analysis of every series of nucleides concerned, including available information on beta decay energies and level assignments, seems desirable. The survey of data has also to be extended to additional elements and the use of other parameters in plotting the curves must be investigated. The work is being continued along these lines.

Above all, however, more experimental data are needed in order to establish the potentialities and limitations of the systematics. This is one of the main reasons for publishing this preliminary report. The author would be most grateful to receive any information that may help in extending the investigation.

References

1) K. Way and M. Wood, Phys. Rev. **94** (1954) 119
2) Nuclear Data Sheets, National Academy of Sciences - National Research Council (Washington D.C., 1958, 1959)
3) B. Jung and G. Andersson, Nuclear Physics **15** (1960) 108
4) G. Andersson, I. B. Häller and R. Ringh, J. Inorg. Nucl. Chem. (in press)
5) D. Strominger, J. M. Hollander and G. T. Seaborg, Revs. Mod. Phys. **30** (1958) 585
6) G. Andersson and R. Ringh, Arkiv Fysik **18** (1960) 385
7) B. Jung and J. Svedberg, private communication
8) N. Poffé, G. Albouy, R. Bernas, M. Gusakow, M. Riou and J. Teillac, J. Phys. Radium **21** (1960) 343

1.E.1:
3.A

Nuclear Physics **24** (1961) 675—681; © *North-Holland Publishing Co., Amsterdam*
Not to be reproduced by photoprint or microfilm without written permission from the publisher

γ-RAYS FROM THE 1.14 MeV RESONANCE IN $B^{10}(p, \gamma)C^{11}$

A. N. JAMES

Cavendish Laboratory, Cambridge

Received 6 January 1961

Abstract: γ-rays from the 1.14 MeV resonance in $B^{10}(p, \gamma)C^{11}$ were observed using a 15.2 cm long by 10.2 cm diameter NaI(Tl) scintillation spectrometer. As well as the ground state γ-rays, cascades through the 4.32 and 6.48 MeV states were observed, the 6.48 MeV state decaying partly by a cascade through the 4.32 MeV level. A spin of $\frac{5}{2}-$ is proposed for the 9.74 MeV level in C^{11}.

1. Introduction

The $B^{10}(p, \gamma)C^{11}$ reaction is in competition with $B^{10}(p, \alpha_0)Be^7$ and $B^{10}(p, \alpha_1\gamma)Be^7$. The first two of these reactions show a broad resonance [1]) in their yield at 1.14 MeV, at this energy the cross section for the third is about 10 mb [2–4]). The cross section [2–4]) at the maximum of the resonance for $B^{10}(p, \gamma)C^{11}$ is about 5 μb yielding, therefore, one 9.74 MeV γ-ray for every 2000 of the 431 keV γ-rays which follow the emission of α_1. Chadwick, Alexander and Warren [3]) as well as Hunt, Pope and Evans [4]) observed weak 'intermediate energy' γ-rays which they attributed to cascade radiation. This paper is concerned with a closer examination of these radiations.

A separated B^{10} target nominally 400 $\mu g/cm^2$ thick on a Tantalum backing was bombarded by proton beams from 10 to 20 μA and at energies from 0.75 MeV to 1.30 MeV. The target was found to contain about 4 % B^{11}. A 15.2 cm long by 10.2 cm diameter NaI(Tl) scintillation spectrometer was used to examine the γ-rays. The front face of the crystal was 23 cm from the target, a collimator of 10 cm of lead restricted the sensitive volume of the crystal to the central 5 cm diameter cylinder. A 5 cm lead surround reduced the background counting rate above 2 MeV to 10 counts per min. Extra lead screening was required between the beam defining stops and the crystal in order to reduce the counting rate of 6 MeV γ-rays from the $F^{19}(p, \alpha\gamma)O^{16}$ reaction.

In order to minimize the effect on the counting system of the high counting rate for 431 keV γ-rays (and, after some bombardment, of the 478 keV γ-rays emitted in the 53 day β-decay of Be^7) a lead absorber 1.3 cm thick was interposed between the target and the counter. This transmitted 50 % of the γ-rays > 2 MeV but only 10 % at 0.43 MeV. The pulses from the scintillation counter were clipped to 1μs and amplified. A biased amplifier with a gain of one trans-

mitted only those pulses corresponding to more than 1 MeV, these were then stretched and sorted using a conventional 150-channel kicksorter.

Fig. 1 is a typical pulse-height spectrum obtained with this system in a 30 min run. Such spectra were analysed into separate components by comparison with the single line spectrum shapes found for 2.62 MeV (RdTh), 4.43 MeV ($Be^9(\alpha, n)C^{12*}$, Polonium-Beryllium neutron source and $B^{11}(p, \gamma)C^{12}$), 6.14 MeV ($F^{19}(p, \alpha\gamma)O^{16}$) and 8.06 MeV ($C^{13}(p, \gamma)N^{14}$). Directly after each spectrum had been recorded the energy scale was calibrated with the proton beam still on by observing RdTh and Polonium-Beryllium sources to avoid rate dependent effects.

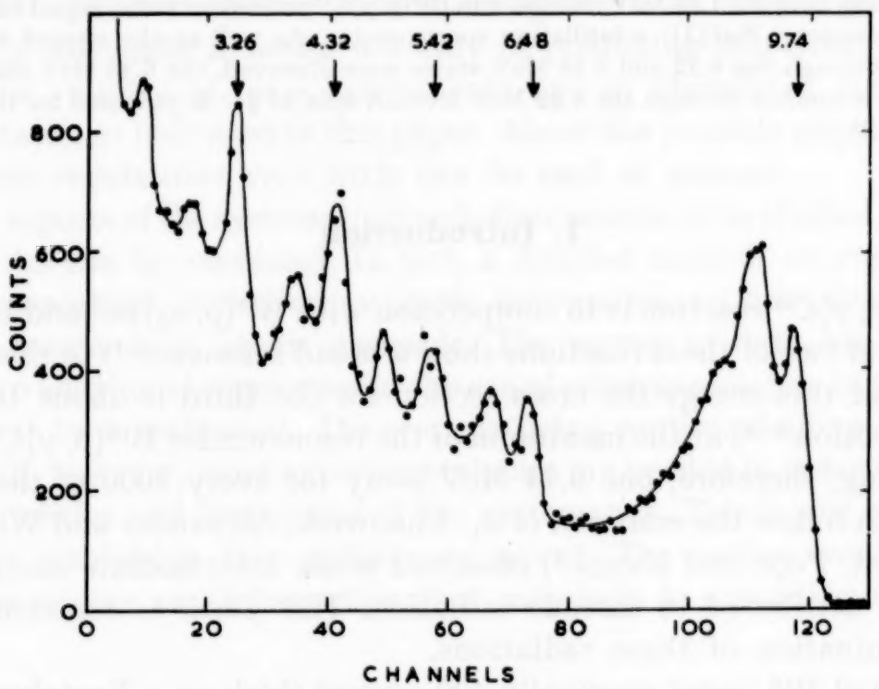

Fig. 1. γ-ray spectrum from $B^{10}(p, \gamma)C^{11}$ observed with a 15.2 cm by 10.2 cm NaI(Tl) crystal at 65° to the proton beam ($E_p = 1.16$ MeV).

The γ-ray spectra from the $B^{10}(p, \gamma)C^{11}$ reaction were observed at 90° for a series of proton energies between 0.75 and 1.30 MeV. The variation of the spectrum with angle was studied at 1.16 MeV, angular distributions for γ-rays at 9.74, 6.48, 5.42, 4.32 and 3.26 MeV being obtained.

2. Results

As the proton energy was varied three γ-rays were observed to change their energy according to $E_\gamma = Q + \frac{10}{11}E_p - E_x$, where $Q = 8.70$ MeV for $B^{10}(p, \gamma)C^{11}$ (ref. [1])). After correcting for target thickness the energy of these γ-rays correspond to direct transitions to the ground state ($E_x = 0$) and excited states at $E_x = 4.32 \pm 0.03$ and $E_x = 6.49 \pm 0.03$ MeV in C^{11}. These energies correspond well with the energies of the second and fifth excited states [5, 6]) of C^{11}. (In the

rest of the paper γ-rays are referred to in terms of their energy at 1.14 MeV proton energy; see table 1).

Other strong γ-rays appearing in the spectrum had energies of 4.36 and 6.50 MeV. The first of these was in part due to cascade radiation of 4.43 MeV from $B^{11}(p, \gamma)C^{12}$. In the intensity measurements this contribution was allowed for by using the $B^{11}(p, \gamma)C^{12}$ peaks at 12.6 MeV and 17.0 MeV observed for the B^{10} target (not shown on fig. 1), to normalize a γ-ray spectrum for $B^{11}(p, \gamma)C^{12}$ measured at 1.14 MeV. The correction was less than 20 % of the intensity of the 4.36 MeV line. A weaker γ-ray of 2.2 MeV was also observed which, on intensity grounds, was assigned to the 6.48 → 4.32 MeV transition.

In all the spectra, the peak at 4.9 MeV was too large to be accounted for by the one-escape peak of the 5.42 MeV γ-ray. Two possible γ-rays which could account for this are the 4.93 and 4.81 MeV components of a cascade through the 4.81 MeV level. It was not possible definitely to verify the presence of either of these γ-rays.

One other weak γ-ray showed in most of the spectra, its energy, 7.7 MeV, seems to indicate a direct transition to the 1.99 MeV first excited state.

No variation of the 90° relative intensities with proton energy was found †. The relative intensities at 1.14 MeV, shown in table 1, are corrected for the measured angular distribution. They were obtained by measuring the area under the peaks, due allowance being made for the variation of efficiency with energy. Both forward and backward angles were observed in the distribution measurements, in all cases the distribution appeared to be very close to $P_0 + a_2 P_2 (\cos \theta)$.

TABLE 1

Relative intensities and angular distributions of the γ-rays of $B^{10}(p, \gamma)C^{11}$

γ-ray energy (MeV)	Assignment	Relative intensity	$\left(\frac{0°}{90°}\right)$ Ratio	a_2
9.74	9.74→0	100±20	1.35±0.10	+0.21±0.06
6.48	6.48→0	20±2	0.67±0.10	−0.25±0.08
5.42	9.74→4.32	18±2	0.77±0.10	−0.17±0.08
4.9	4.81 cascade	10±5		
4.32	4.32→0	28±4	0.82±0.05	−0.13±0.05
3.26	9.74→6.48	30	1.75±0.10	+0.40±0.04
2.2	6.48→4.32	(7)		
7.7	9.74→1.99	(5)		
3.41	9.74→6.34	<15		
2.0	1.99→0	< 7		
Others 2−8		< 4		
Others 8−10		<15		

† This, together with the observation that no forward-backward asymmetry was found in the proton energy range 0.75—1.30 MeV, indicates that the observed γ-ray spectrum can be considered as arising from a single resonance.

3. Coincidence Measurements

In order to verify that the intermediate energy γ-rays are in fact due to cascades from the 9.74 MeV level of C^{11}, coincidence measurements were made. A NaI(Tl) crystal 5.7 cm long by 4.8 cm diameter with a similar counting sys-

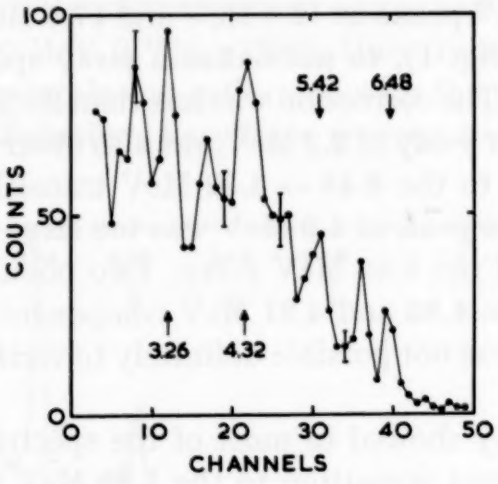

Fig. 2. Large counter spectrum in coincidence with counts between 2 and 7 MeV in the small crystal (large counter at 0°; six hour run).

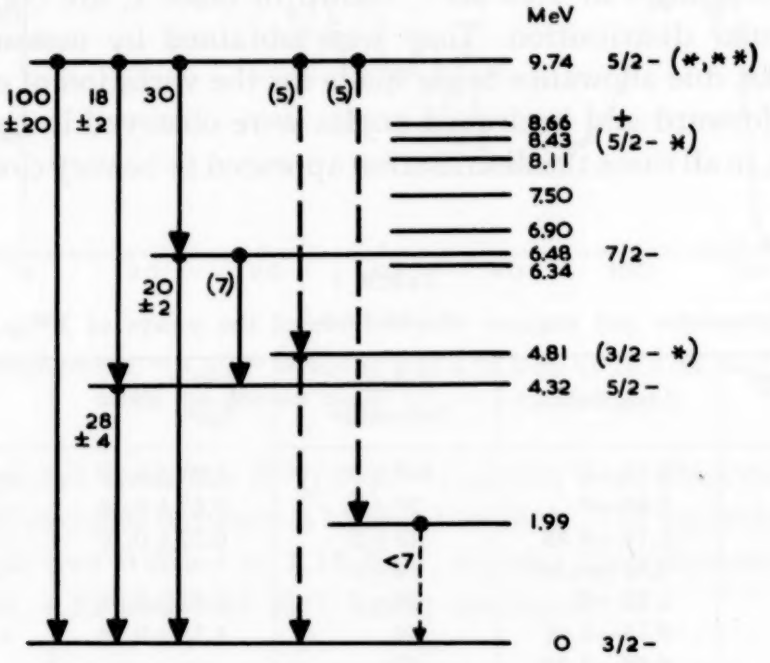

Fig. 3. Decay scheme of the 9.74 MeV C^{11} level.

tem to the larger crystal was placed at 90° to the proton beam. A coincidence system with a resolving time of 1μs was used to select for kicksorting only those pulses from the 15 cm × 10 cm NaI(Tl) which were in coincidence with pulses in a known energy range in the smaller crystal. The larger crystal was placed at either 0° or −90° to the proton beam and in the same plane as the small crystal.

Fig. 2 shows the spectrum observed in coincidence with pulses from 2 — 7

MeV with the large crystal at 0°. The random coincidence rate was negligibly small. The four main γ-rays were identified, 3.26, 4.32, 5.42 and 6.48 MeV, as before the 4.32 MeV γ-ray was mixed with the $B^{11}(p, \gamma)C^{12}$ 4.43 MeV radiation in coincidence with 12.6 MeV radiation. A weak component of 4.9 MeV could not be ruled out. In addition to measurements at 0° and 90° (table 2) with the large energy window (2 — 7 MeV), it was shown that the 6.48 MeV γ-ray was in coincidence only with the 3.26 MeV γ-ray and that the 3.26 MeV γ-ray was in coincidence with both 6.48 and 4.32 MeV γ-rays. One third of the transitions from the 6.48 MeV state cascaded through the 4.32 MeV state. The proposed decay scheme, with the measured intensities, is shown in fig. 3.

TABLE 2

Results of correlation measurements

γ-ray energy (MeV)	Triple correlation (0°/90°) ratio [7])	
	Case I	Case II
6.48		1.0±0.2
5.42		1.0±0.2
4.32	(1.2±0.2)	
3.26	1.8±0.2	

4. Discussion

Using the value $(2J+1)\Gamma_\gamma(9.74) = 10$ eV, deduced by Chadwick, Alexander and Warren [3]), the relative intensities of table 1 give the partial γ-ray widths $(2J+1)\Gamma_\gamma$ for the 5.42 and 3.26 MeV γ-rays. These are given in table 3, which also gives the experimental values of $(2J+1)|M|^2$, the partial width in Weisskopf units, deduced from the assumption of E1, M1 or E2 radiation [8]). The values of $(2J+1)|M|^2$ for M1 radiation all fall well within the ranges found by Wilkinson [8]). However, the widths are also consistent with E1 radiation,

TABLE 3

Experimental partial γ-ray widths

γ-ray energy (MeV)	$(2J+1)\Gamma_\gamma$ (eV)	$(2J+1)\lvert M\rvert^2$ (ref. [8]))			A(M1) ($J = \frac{5}{2}$) [11])
		E1	M1	E2	
9.74	10	0.02	0.5	40	0.7
5.42	1.8	0.02	0.5	130	0.7
3.26	3	0.16	4.3	2700	6.0

particularly that the 3.26 MeV γ-ray. If the radiation is quadrupole then the widths are very large, particularly since the single particle units in which they are expressed are large, a value of $r_0 = 1.5\times10^{-13}$ cm being used [8]). Since all three levels, 6.48, 4.32 and ground state, are formed by $l = 1$ stripping in the B^{10}(d, n)C^{11} reaction [5]) they all have negative parity and the γ-rays of table 3

must all have the same multipolarity †, most probably M1 but certainly dipole. The spins of the ground state and 6.48 MeV state are most probably $\frac{3}{2}-$ and $\frac{7}{2}-$ from (d, n) stripping and comparison with B^{11}. For dipole radiation to both levels the 9.74 MeV state must have $J = \frac{5}{2}$; if in addition the radiation is M1, the parity is negative.

The 9.74, 6.48, 5.42 and 3.26 MeV γ-rays (table 1) have only one definitely known origin in the decay scheme; analysis of their angular distributions is therefore worthwhile. Theoretical angular distributions were calculated from the tables of Ferguson and Rutledge [7]).

Assuming a $\frac{5}{2}+$ state, the maximum possible anisotropy for the E1 transition to the $\frac{7}{2}-$ state at 6.48 MeV by considering mixtures of s and d-wave proton capture is 1.3, well short of the observed value 1.75. For p-wave capture to $\frac{5}{2}-$ the angular distributions for the three primary γ-rays can all be fitted by assuming channel spin $\frac{5}{2}$ with between 90 and 100 % M1 in an M1–E2 mixture. The spin of the 4.32 MeV level was taken as $\frac{5}{2}-$. Admixture of channel spin $\frac{7}{2}$ does not greatly affect the agreement provided that the intensity of E2 is increased. The angular distribution of the 6.48 MeV γ-ray is in agreement with this scheme when the transition is assumed to be $E2(\frac{7}{2}- \rightarrow \frac{3}{2}-)$. The triple correlations of table 2 are not in disagreement with this scheme. However, the ground state α particle distribution found by Cronin [9]) is not entirely in favour of this scheme as it requires a larger proportion of channel spin $\frac{7}{2}$ than $\frac{5}{2}$ in the formation of the 9.74 MeV state.

It is interesting to note that the branching of the 6.48 MeV level to the 4.32 MeV level favours the assignments of fig. 3. If both the 6.48 and 2.16 MeV γ-rays are M1 then the extreme single particle model [8, 10]) predicts

$$\Gamma_\gamma(6.48, \mathrm{M1})/\Gamma_\gamma(2.16, \mathrm{M1}) \approx 30,$$

whereas, if the 6.48 MeV γ-ray is E2,

$$\Gamma_\gamma(6.48, \mathrm{E2})/\Gamma_\gamma(2.16, \mathrm{M1}) \approx \tfrac{1}{10}.$$

Kurath's calculations [11]) of M1 transition strengths at the most probable [12]) value of the intermediate coupling parameter $a/K = 4.5$ predict, with one exception, less variation in the strengths of transitions between low lying odd parity levels [5, 6]) than a factor of 10. The exception is the $\frac{7}{2}- \rightarrow \frac{5}{2}-$ transition, which is vanishingly small. If the ground state is $\frac{3}{2}-$ the 6.48 MeV γ-ray seems too weak relative to the 2.16 MeV γ-ray to be one of the M1 transitions treated by Kurath. The assumption of E2 for the transition can only be accommodated if the 2.16 MeV M1 transition is inhibited and the spin of the 6.48 MeV level is $\frac{7}{2}-$. The branching ratio, which is very similar to that for the B^{11} 6.78 MeV

† The possibility that the 9.7 MeV state is $\frac{7}{2}-$ with the 9.74 MeV γ-ray being E2 and the others of table 3 being M1–E2 mixtures is ruled out by the combination of angular distributions for the two γ-rays in the cascade through the 6.48 MeV state (taken as $\frac{7}{2}-$).

state, therefore favours the assignment of the ground, 4.32 and 6.48 MeV states to the lowest $\frac{3}{2}-$, $\frac{5}{2}-$ and $\frac{7}{2}-$ Kurath levels.

The calculated strengths [11]) of the transitions from highly excited $\frac{5}{2}-$ states of the intermediate coupling shell model show a rapid variation with a/K near $a/K = 4.5$. However, both $\frac{5}{2}-^*$ at $a/K = 4.5$ and $\frac{5}{2}-^{**}$ at $a/K = 6$ agree with the M1 strengths for the 9.74 MeV level shown in last column of table 3 (this column expresses the experimental results in the units of ref. [11]); the $(2J+1)$ factor has been divided out). Both possibilities predict a weaker transition to the $\frac{3}{2}-^*$ level which would agree with the probable cascade through the 4.81 MeV level. It is not possible at present to distinguish which roles the $\frac{5}{2}-$ C^{11} levels at [5]) 8.43 and 9.74 MeV play in the intermediate coupling model.

The 8.66 MeV level [5]) and the 6.34 MeV level [6]) most probably have positive parity. Limits on possible E1 transitions from the 9.74 MeV level to those levels are given by the experimental limits on 3.41 MeV and 8.66 MeV γ-rays (table 1). In both cases the E1 widths must be less than 0.05 Weisskopf units. This is not inconsistent with Wilkinson's analysis [8]).

5. Conclusion

None of the experimental data is inconsistent with the sequence $\frac{3}{2}-$, $\frac{5}{2}-$, $\frac{3}{2}-$, $\frac{7}{2}-$ and $\frac{5}{2}-$ for the spins and parities of the 0, 4.32, 4.81, 6.48 and 9.74 MeV levels of C^{11}.

The isotopic boron targets were supplied by A.E.R.E. Harwell. It is a pleasure to thank Mr. D. D. Stewart for his willing co-operation in running and maintaining the Cavendish Laboratory's 1.4 Cockcroft-Walton generator. The author is indebted to the Department of Scientific and Industrial Research for the support of a Research Fellowship.

References

1) F. Ajzenberg-Selove and T. Lauritsen, Nuclear Physics **11** (1959) 1
2) R. B. Day and T. Huus, Phys. Rev. **95** (1954) 1003
3) G. B. Chadwick, T. K. Alexander and J. B. Warren, Can. J. Phys. **34** (1956) 381
4) S. E. Hunt, R. A. Pope and W. W. Evans, Phys. Rev. **106** (1957) 1012
5) A. N. James, A. T. G. Ferguson and C. P. M. Johnson, Nuclear Physics (to be published)
6) S. Hinds and R. Middleton, Proc. Phys. Soc. (to be published)
7) A. J. Ferguson and A. R. Rutledge, CRP-615 (1957)
8) D. H. Wilkinson, Phil. Mag. **1** (1956) 127
9) J. W. Cronin, Phys. Rev. **101** (1956) 298
10) V. F. Weisskopf, Phys. Rev. **83** (1951) 1073
11) D. Kurath, Phys. Rev. **106** (1957) 975
12) A. J. Ferguson, H. E. Gove, J. A. Kuehner, A. E. Litherland, E. Almqvist and D. A. Bromley, Phys. Rev. Letters **1** (1958) 414

1.D.2 *Nuclear Physics* **24** (1961) 682—694; © *North-Holland Publishing Co., Amsterdam*

Not to be reproduced by photoprint or microfilm without written permission from the publisher

COLLECTIVE EXCITATIONS CORRESPONDING TO QUADRUPOLE NUCLEAR SURFACE VIBRATIONS

A. S. DAVYDOV

Moscow State University, Moscow, USSR

Received 26 October 1960

Abstract: The solutions of the set of equations for the rotation-vibrational spectrum of non-spherical nuclei are investigated, γ vibrations being taken into account in the equations. It is shown that zero spin excited states can refer to β vibrations as well as to γ vibrations.

1. Introduction

Quadrupole vibrations of the surface of a spherical nucleus are usually described [1]) with the help of five variables b_μ ($\mu = 0, \pm 1, \pm 2$), each of which corresponds to a classical oscillator of frequency ω. The elementary excitations in this case are determined by excitation of phonons possessing an energy $\hbar\omega$, angular momentum 2 and angular momentum projection μ. If degeneracy corresponding to states with different values of the angular momentum projection is neglected, two-phonon excitations of an energy $2\hbar\omega$ will be three-fold degenerate ($I = 0, 2, 4$) and three-phonon excitations will be five-fold degenerate ($I = 0, 2, 3, 4, 6$) etc.

For a theoretical investigation of the interaction of the surface vibrations with the motion of separate nucleons and in particular for the investigation of collective motions in non-spherical nuclei it is convenient to describe the nuclear deformations by two parameters β and γ ($0 \leqq \gamma \leqq \frac{1}{3}\pi$) which define at each given instant the shape of the nucleus and by three Eulerian angles θ_i defining the orientation of the nucleus in space instead of employing the five coordinates b_μ. As shown by A. Bohr [1]) in this case the wave function for stationary states corresponding to a definite total angular momentum I can be written down in the form of the product of two functions

$$\Psi_I(\beta, \gamma, \theta_i) = F(\beta)\Phi(\gamma, \theta_i),$$

which satisfy the equations

$$[T_\gamma + \tfrac{1}{4}\sum_{l=1}^{3} A_l \hat{I}_l^2 - \Lambda]\Phi(\gamma, \theta_i) = 0, \tag{1.1}$$

$$\left[-\frac{\hbar^2}{2B}\frac{1}{\beta^4}\frac{\partial}{\partial\beta}\left(\beta^4\frac{\partial}{\partial\beta}\right) + \tfrac{1}{2}C\beta^2 + \frac{\hbar^2\Lambda}{2B\beta^2} - E\right] F(\beta) = 0, \tag{1.2}$$

where $\hat{I}_l$ are the projections of the angular momentum operator on the coordinate axes connected to the nucleus, and where

$$T_\gamma = -\frac{1}{\sin 3\gamma}\frac{\partial}{\partial\gamma}\left(\sin 3\gamma\,\frac{\partial}{\partial\gamma}\right), \tag{1.3}$$

$$A_l = \sin^{-2}(\gamma - \tfrac{2}{3}\pi l), \quad l = 1, 2, 3. \tag{1.4}$$

The function $F\Phi$ is defined in a space of volume element

$$d\tau = \beta^4|\sin 3\gamma|\, d\beta d\gamma d\theta_1 \sin\theta_2 d\theta_2 d\theta_3.$$

In the case of non-magic nuclei the interaction between nucleons of unfilled shells with nucleons of the nuclear core results in violation of spherical symmetry of the nucleus. The interaction between such nucleons and the deformation of the nuclear core can be expressed by the operator

$$H_{\text{int}} = -\beta\sum_p K_p(r_p)\left\{\cos\gamma Y_{20}(\theta_p\varphi_p) + \frac{\sin\gamma}{\sqrt{2}}\left[Y_{2,2}(\theta_p\varphi_p) + Y_{2,-2}(\theta_p\varphi_p)\right]\right\},$$

where the summation refers to all "external" nucleons.

This operator is usually averaged over the states of motion of nucleons possessing a definite angular momentum and angular momentum projection j_3. Thus it is implied that the nucleus is axially symmetric. However, in the general case, for many nuclei the projection of the angular momentum of a given nucleon is not an integral of motion. Consequently, diagonal as well as non-diagonal matrix elements of the operator H_{int} should be taken into account. The problem of determining the potential energy as a function of the parameters β and γ reduces to the solution of a secular equation. The potential energy operator can then be obtained in the form

$$V(\beta\gamma) = \tfrac{1}{2}C\beta^2 + \beta\chi(\cos 3\gamma). \tag{1.6}$$

In the following we shall consider only small vibrations near the equilibrium point, which corresponds to a minimum potential energy (1.6). In other words we put

$$V(\beta, \gamma) = \tfrac{1}{2}C(\beta - \beta_0)^2 + \tfrac{1}{2}C_\gamma\beta_0^2(\gamma - \gamma_0)^2, \tag{1.7}$$

where the quantities C, C_γ, β_0 and γ_0 are regarded as parameters of the theory. It should be noted that stability of the nucleus with respect to variation of the parameter γ is closely connected with the deviation of the nuclear shape from spherical symmetry. For $\beta_0 = 0$ the potential is independent of γ and for $\beta_0 \neq 0$ "stability" always holds. Thus the "γ unstable" potential considered by Wilets and Jean [2]) is not possible for $\beta_0 \neq 0$.

If $\frac{1}{2}C\beta^2$ is replaced by eq. (1.7) in the nuclear Hamiltonian operator, the stationary state wave function should be sought in the form of a product of the

wave functions $\Phi(\gamma, \theta_i)$ and $F(\beta)$ obeying the equations

$$[T_\gamma + \tfrac{1}{4}\sum_{l=1}^{3} A_l \hat{I}_l^2 + W(\gamma) - \Lambda]\Phi(\gamma, \theta_i) = 0, \tag{1.8}$$

$$\left[-\frac{\hbar^2}{2B}\frac{\mathrm{d}^2}{\mathrm{d}\beta^2} + \tfrac{1}{2}C(\beta-\beta_0)^2 + \frac{\hbar^2(\Lambda+2)}{2B\beta^2} - E\right]\beta^2 F(\beta) = 0, \tag{1.9}$$

where

$$W(\gamma) = D(\gamma-\gamma_0)^2, \tag{1.10}$$

$$D = \frac{BC_\gamma}{\hbar^2}\beta_0^4, \quad C_\gamma = \omega_\gamma{}^2 B. \tag{1.11}$$

The quantity ω_γ here can be called the "γ vibration frequency". For $\beta_0 = 0$ eqs. (1.8) and (1.9) are the same as eqs. (1.1) and (1.2).

The purpose of the present paper is an investigation of the set of generalized equations (1.8) and (1.9). For the sake of generality the solution of these equations for spherical nuclei ($\beta_0 = 0$) will be examined in sect. 2. Solutions corresponding to non-spherical non-axial nuclei ($\gamma_0 > 10°$) will be considered in sect. 3. The case of non-spherical axially symmetrical nuclei will be considered in sect. 4. Conditions under which rotational excitations can be separated from γ and β vibrations of the nuclear surface are deduced. It is shown that zero spin excited nuclear states can be divided into β and γ vibrations which differ with respect to their properties. It is shown that in some states (spin 3), it is impossible to separate γ vibrations from rotational excitations in axially symmetric nuclei. In other states this can be done only approximately. Corrections to rotational states of non-axial nuclei due to interaction with β as well as γ vibrations are found.

2. Collective Excitations in Spherical Atomic Nuclei

The equations (1.8) and (1.9) can be solved exactly in the case of spherical nuclei and yield the well known spectrum with uniformly spaced energy levels. Consider first eq. (1.8). Introducing the variable $z = (BC)^{\frac{1}{2}}\hbar^{-1}\beta^2$, $\omega = C^{\frac{1}{2}}B^{-\frac{1}{2}}$ and $f = \beta^2 F(\beta)$ we can transform (1.8) to the form

$$\left[z\frac{\mathrm{d}^2}{\mathrm{d}z^2} + \tfrac{1}{2}\frac{\mathrm{d}}{\mathrm{d}z} - \frac{z}{4} - \frac{\Lambda+2}{4z} + \frac{E}{2\hbar\omega}\right] f(z) = 0. \tag{2.1}$$

Denoting

$$E = 2\hbar\omega(n+s+\tfrac{1}{4}), \tag{2.2}$$

$$\Lambda+2 = 4s(s-\tfrac{1}{2}), \tag{2.3}$$

we obtain for $f(z) = z^s W(z)\exp(-\tfrac{1}{2}z)$ the equation

$$\left\{z\frac{\mathrm{d}^2}{\mathrm{d}z^2} + (2s+\tfrac{1}{2}-z)\frac{\mathrm{d}}{\mathrm{d}z} + n\right\} W(z) = 0,$$

which has solutions satisfying the imposed boundary conditions for positive values of n in the form of a hypergeometric function

$$W(z) = F(-n, 2s+\tfrac{1}{2}, z), \tag{2.4}$$

where, according to (2.3),

$$S = \tfrac{1}{4}(1+\sqrt{9+4\Lambda}). \tag{2.3a}$$

The wave function Φ_I and parameter Λ are defined by eq. (1.1) for each value of the total angular momentum. For states with zero angular momentum, the function Φ_0 depends only on γ and eq. (1.1) changes into

$$(T_\gamma - \Lambda)\Phi_0 = 0,$$

the solutions of which are Legendre polynomials

$$\Phi_0(\gamma) = P_\lambda(\cos 3\gamma) \tag{2.5}$$

for

$$\Lambda = 9\lambda(\lambda+1), \quad \lambda = 0, 1, 2, \ldots. \tag{2.6}$$

Inserting (2.6) into (2.3) and taking into account (2.2), we can verify that states with zero spin can possess an energy

$$E^0_{n\lambda} = \hbar\omega[\tfrac{5}{2}+2n+3\lambda]. \tag{2.7}$$

These states are described by the wave function

$$\Psi_{n\lambda} = F_{sn}(\beta)P_\lambda(\cos 3\gamma),$$

where

$$F_{sn}(\beta) = \frac{N}{\beta^2}\left(\frac{\sqrt{BC}\beta^2}{\hbar}\right)^s \exp\left(-\frac{\sqrt{BC}\beta^2}{2\hbar}\right) F\left(-n, 2s+\tfrac{1}{2}, \sqrt{BC}\,\frac{\beta^2}{\hbar}\right) \tag{2.8}$$

for $s = 1+\frac{3}{2}\lambda$. Here, N is a normalizing factor. The first zero spin (0^+) excited state with an energy $2\hbar\omega$ corresponds to the quantum numbers $n = 1$, $\lambda = 0$. These excitations may be called "pure β vibrations". The next 0^+ excited state with energy $3\hbar\omega$ corresponds to a different type of motion with quantum numbers $n = 0$, $\lambda = 1$. Excitations 0^+ with $n = 0$, $\lambda \neq 0$ will be called "pure γ vibrations".

The solutions of eq. (1.1) for $I \neq 0$ can be written as

$$\Phi_I(\gamma, \theta_i) = \sum_{K \geqq 0} |IK\rangle g^{(I)}_K(\gamma), \tag{2.9}$$

where

$$|IK\rangle = \left[\frac{2I+1}{16\pi^2(2+\delta_{K0})}\right]^{\frac{1}{2}} \{D^I_{MK}(\theta_i)+(-1)^I D^I_{M,-K}(\theta_i)\}.$$

The function $g_K^I(\gamma)$ in (2.9) satisfies the following symmetry conditions:

$$\begin{aligned} &\text{a)}\ g_K^I(\gamma) = 0 \text{ if } K \text{ is an odd number,} \\ &\text{b)}\ g_K^I(\gamma) = (-1)^I g_{-K}^I(\gamma), \\ &\text{c)}\ g_K^I(\gamma) = (-1)^{\frac{1}{2}K} g_K^I(-\gamma). \end{aligned} \tag{2.9a}$$

From symmetry conditions a) and b) it follows that no collective excitations of the quadrupole type can exist with $I = 1$. The following wave functions [3]) correspond to the first two spin 2 excitations:

$$\Psi_{2ni} = F_{sn}(\beta)\Phi_{2i}, \quad i = 1, 2,$$

where

$$\begin{aligned} \Phi_{21} &= |20\rangle \cos\gamma + |22\rangle \sin\gamma, \qquad \text{with } \Lambda = 4,\ s = \tfrac{3}{2}, \\ \Phi_{22} &= |20\rangle \cos 2\gamma - |22\rangle \sin 2\gamma, \quad \text{with } \Lambda = 10,\ s = 2. \end{aligned}$$

The functions $F_{sn}(\beta)$ are defined by (2.8). If (2.2) is taken into account it will be seen that the excitation energies $\Delta E = E - E_0$ of these states are given respectively by the equations

$$\Delta E_{n1}^{(2)} = \hbar\omega(2n+1), \qquad \Delta E_{n2}^{(2)} = 2\hbar\omega(n+1), \qquad n = 0, 1, \ldots.$$

Spin 3 excited states correspond to the wave functions

$$\Psi_{3n\lambda} = |32\rangle P_\lambda^1(\cos 3\gamma) F_{ns}(\beta),$$

where P_λ^1 is an associated Legendre polynomial and

$$S = 1 + \tfrac{3}{2}\lambda.$$

The excitation energy of these states is correspondingly

$$\Delta E_{n\lambda}^{(3)} = \hbar\omega(2n + 3\lambda + 3).$$

3. Collective Excitations of Non-Spherical Non-Axial Nuclei

The solution of (1.9) should be considered in the case of non-spherical atomic nuclei. For small oscillations about the equilibrium position, eq. (1.9) can be written in the form

$$\left\{\frac{\hbar^2}{2B}\frac{\mathrm{d}^2}{\mathrm{d}\beta^2} - W_\Lambda(\beta) + E\right\} f(\beta) = 0, \quad f(0) = 0, \tag{3.1}$$

where

$$W_\Lambda(\beta) = \tfrac{1}{2}C(\beta-\beta_0)^2 + \frac{\hbar^2(\Lambda+2)}{2B\beta^2} \approx W_\Lambda(\beta_\Lambda) + \tfrac{1}{2}C_\Lambda(\beta-\beta_\Lambda)^2, \tag{3.2}$$

$$\beta_\Lambda = \beta_0 + \frac{\hbar^2(\Lambda+2)}{BC\beta_\Lambda{}^3}, \tag{3.3}$$

$$C_\Lambda = C\left[1 + \frac{3\hbar^2(\Lambda+2)}{BC\beta_\Lambda{}^4}\right]. \tag{3.4}$$

After introducing the parameters $\omega = \sqrt{(C/B)}$, $\not{p} = \beta_\Lambda/\beta_0 \geqq 1$ and $\mu^2 = \hbar\omega/C\beta_0^2 = 2\beta_{00}^2/\beta_0^2$, where β_{00}^2 is the mean square amplitude of zero vibrations of the nuclear surface, eqs. (3.3) and (3.4) can be transformed to

$$(\not{p}-1)\not{p}^3 = (\Lambda+2)\mu^4, \tag{3.3a}$$

$$C_\Lambda = C[1+3(\Lambda+2)(\mu/\not{p})^4]. \tag{3.4a}$$

Furthermore

$$W_\Lambda(\beta_\Lambda) = \hbar\omega\left[\frac{(\not{p}-1)^2}{2\mu^2} + \frac{\Lambda+2}{2}\left(\frac{\mu}{\not{p}}\right)^2\right]. \tag{3.5}$$

If we now introduce the new variable

$$\zeta = \frac{\not{p}(\beta-\beta_\Lambda)}{\mu_1\beta_\Lambda}, \quad \mu_1^4 = \mu^4\frac{C}{C_\Lambda}, \tag{3.6}$$

which varies between $-\not{p}/\mu_1 \leqq \zeta < \infty$ and also a new function $f(\beta) = v(\zeta)\exp(-\frac{1}{2}\zeta^2)$, we obtain from eqs. (3.1) a new equation

$$v'' - 2\zeta v' + 2\nu v = 0 \tag{3.6a}$$

for the function $v(\zeta)$ which satisfies the boundary conditions

$$v\left(-\frac{\not{p}}{\mu_1}\right) = 0, \quad \exp(-\tfrac{1}{2}\zeta^2)v(\zeta) \to 0 \quad \text{for } \zeta \to \infty.$$

The quantity ν is related to the energy of the nucleus by the equation

$$\nu = \frac{E-W_\Lambda(\beta_\Lambda)}{\hbar\omega_\Lambda} - \tfrac{1}{2}, \quad \omega_\Lambda = \sqrt{\frac{C_\Lambda}{B}}.$$

The solution of eq. (3.6a) is

$$v(\zeta) = H_\nu(\zeta) \equiv [2\Gamma(-\nu)]^{-1}\sum_{l=0}^{\infty}\frac{(-1)^l}{l!}\Gamma\left(\frac{l-\nu}{2}\right)(2\zeta)^l.$$

The collective nuclear excitation energy corresponding to the parameter Λ is defined by the formula

$$E_{\Lambda\nu} = \hbar\omega\left\{(\nu+\tfrac{1}{2})\sqrt{1+3(\Lambda+2)\left(\frac{\mu}{\not{p}}\right)^4} + \tfrac{1}{2}(\Lambda+2)\left(\frac{\mu}{\not{p}}\right)^2 + \frac{(\not{p}-1)^2}{2\mu^2}\right\}, \tag{3.7}$$

where ν is the root of the transcendental equation

$$H_\nu\left(-\frac{\not{p}}{\mu_1}\right) = 0. \tag{3.8}$$

In the general case collective excitations corresponding to a definite angular momentum I are of a complex nature. However, under conditions when the

"non-adiabaticity parameter" is such that $\mu < \frac{1}{3}$, the quantity $\mu_1 \approx \mu$ and the root of equation (3.8) assumes values close to integers

$$\nu \approx n = 0, 1, 2, \ldots .$$

Moreover, in this case,

$$p = 1+\mu^4(\Lambda+2)+ \ldots$$

and the collective excitation energy can be expressed by the formula

$$E_{\Lambda n} = \hbar\omega(n+\tfrac{1}{2})+ \frac{\hbar^2}{2B\beta_0^2}(\Lambda+2)\left[1+3\mu^2(n+\tfrac{1}{2})-\mathscr{D}\frac{\hbar^2}{B\beta_0^2}(\Lambda+2)\right]^2, \quad (3.9)$$

where

$$\mathscr{D} = \tfrac{1}{2}\mu^4[1+\tfrac{57}{4}(n+1)\mu^2] \approx \tfrac{1}{2}\mu^4.$$

The last two terms in (3.9) take into account the connection between β vibrations and rotation and γ vibrations of the nucleus.

Thus β vibrations can be separated from the total collective excitation of the nucleus only under the condition that $\mu < \frac{1}{3}$, that is, if the zero vibrations are small compared to the parameter β_0.

We shall now consider eq. (1.8) for non-axially symmetric nuclei with $\gamma_0 > 10°$. A new function $\varphi = \sqrt{|\sin 3\gamma|}\,\Phi$ will first be introduced. Function φ obeys the equation

$$\left\{\frac{\partial^2}{\partial\gamma^2}+\tfrac{9}{4}[1+\sin^{-2}(3\gamma)]-\tfrac{1}{4}\sum_{l=1}^{3}A_l(\gamma)\hat{I}_l^2-W(\gamma)+\Lambda\right\}\varphi(\gamma,\theta_i) = 0. \quad (3.10)$$

According to (1.10) in the case of small oscillations about the equilibrium point one has $W(\gamma) = D(\gamma-\gamma_0)^2$. Replacing in (3.10) coefficients A_l and $\sin 3\gamma$ by their values for $\gamma = \gamma_0$ and introducing $\xi = \gamma-\gamma_0$ we get the equation

$$\left\{\frac{\partial^2}{\partial\xi^2}-D\xi^2+\tfrac{9}{4}[1+\sin^{-2}(3\gamma_0)]-\tfrac{1}{4}\sum_{l=1}^{3}A_l(\gamma_0)\hat{I}_l^2+\Lambda\right\}\varphi = 0. \quad (3.10a)$$

It should be noted that function $\varphi(\gamma,\theta_i)f(\beta)$ is defined in the space of volume element $d\tau = d\beta d\gamma d\theta_1 \sin\theta_2 d\theta_2 d\theta_3$. After substituting $\varphi(\xi,\theta_i) = g^I(\xi)\Psi_I(\theta_i)$ we obtain the two equations

$$\left[\tfrac{1}{2}\sum_{l=1}^{3}A_l(\gamma_0)\hat{I}_l^2-\varepsilon(I)\right]\Psi_I(\theta_i) = 0, \quad (3.11)$$

$$\left(\frac{\partial^2}{\partial\xi^2}-D\xi^2+L\right)g^I(\xi) = 0, \quad (3.12)$$

where

$$\varepsilon(I) = 2[\Lambda-L+\tfrac{9}{4}(1+\sin^{-2}(3\gamma_0))]. \quad (3.13)$$

Eq. (3.11) has been solved in the adiabatic theory for non-axial nuclei [3, 4]).

The energy levels $\varepsilon(I)$ and wave functions $\Psi_I(\theta_i)$ were determined in these papers. It was shown, in particular, that two solutions with the energies

$$\varepsilon_\tau(2) = \frac{9[1+(-1)^\tau\sqrt{1-\frac{8}{9}\sin^2(3\gamma_0)}]}{\sin^2(3\gamma_0)}, \quad \tau = 1, 2$$

correspond to spin 2 states.

For $I = 3$ there is one solution

$$\varepsilon(3) = 18\sin^{-2}(3\gamma_0),$$

etc.

The solutions of eq. (3.12) can be expressed in terms of Hermite polynomials H_λ,

$$g^I{}_L(\xi) = \exp(-\tfrac{1}{2}\sqrt{D}\xi^2)H_\lambda(\xi D^{\frac{1}{4}}), \quad \xi = \gamma-\gamma_0, \tag{3.14}$$

for each value of the parameter L equal to

$$L = \sqrt{D}(2\lambda+1), \quad \lambda = 0, 1, \ldots. \tag{3.15}$$

Thus from (3.13) and (3.15) it follows that the parameter Λ which defines the collective excitation energy in expressions (3.7) and (3.9) is equal to

$$\Lambda = \tfrac{1}{2}\varepsilon_\tau(I)+\sqrt{D}(2\lambda+1)-\tfrac{9}{4}[1+\sin^{-2}(3\gamma_0)]. \tag{3.16}$$

Substituting (3.16) into (3.9) and taking into account (1.11) we obtain after subtracting the zero vibration energy ($n = \lambda = 0$, $\varepsilon(0) = 0$) the expression

$$\Delta E_{\tau n\lambda}(I) = n\hbar\omega+\lambda\hbar\omega_\gamma+\frac{\hbar^2\varepsilon_\tau(I)}{4B\beta_0{}^2}-\frac{\hbar^2\mu^2}{2B\beta_0{}^2}\{\mu^2(\tfrac{1}{2}\varepsilon_\tau(I)+2\lambda\sqrt{D})(\tfrac{1}{2}\varepsilon_\tau(I)+2\sqrt{D}(1+\lambda)$$
$$-\tfrac{1}{2}-\tfrac{9}{2}\sin^{-2}(3\gamma_0))-3n[\tfrac{1}{2}\varepsilon_\tau(I)+\sqrt{D}(1+2\lambda)-\tfrac{1}{4}(1+9\sin^{-2}(3\gamma_0))]-\tfrac{3}{4}[\varepsilon_\tau(I)+4\sqrt{D\lambda}]\}. \tag{3.17}$$

In the adiabatic approximation ($\mu = 0$) the collective excitation energy is therefore equal to the sum of the β and γ vibration energies and the rotation energy. It is significant that zero spin γ vibrations are possible. It is noteworthy that if, in accordance with (1.7), the coefficient defining the γ vibration potential energy equals $C_\gamma\beta_0{}^2$, the frequencies of these vibrations will be $\omega_\gamma = (C_\gamma/B)$. Hence even for small values of $C_\gamma\beta_0{}^2$ the γ vibration frequency may be comparatively large. The 0^+ excited states observed experimentally in non-axially symmetric nuclei may therefore contain two types of excitations (β and γ vibrations) which significantly differ in their properties. In excited states with $I \neq 0$ the rotational excitations are related to the γ and β vibrations in a complicated way (especially for non-vanishing values of n and λ) and can be separated from the total excitation only for small values of the non-adiabaticity parameter μ. With an accuracy to a normalization factor the collective excita-

tion wave function can be written down in the form

$$\Psi^I_{\tau n\lambda} = f(\beta)\varphi(\beta\theta_i) = \Psi_{I\tau}(\theta_i)\exp(-\tfrac{1}{2}\zeta^2)H_n(\zeta)\exp(-\tfrac{1}{2}\sqrt{D}\xi^2)H_\lambda(\xi D^{\frac{1}{4}}),$$

where $\xi = \gamma - \gamma_0$ and ζ are defined by eq. (3.6).

Formula (3.17) takes into account coupling of the rotational excitations to γ and α vibrations. It follows from it that the corrections to rotational levels in states with $n = \lambda = 0$ can be represented in the form

$$-a[\varepsilon_\tau(I)]^2 - b\varepsilon_\tau(I),$$

where $\varepsilon_\tau(I)$ is the rotational energy which does not take into account the connection between the rotation and surface vibrations. Due to the presence of zero γ vibrations the significance of the second term in the correction may be larger than in the case of rotational and β vibration excitation coupling (for a fixed value of γ) examined in the paper of Davydov and Chaban [6]). For calculation of the excitation energy of nuclei with $\mu > \frac{1}{3}$ one should employ formula (3.7) in which the values of Λ from (3.16) are inserted. Rotational excitations can be separated from γ vibrations (for $I \neq 0$ and $\lambda \neq 0$) only in nuclei with $\gamma_0 > 10°$. In the case of axially symmetric nuclei ($\gamma_0 = 0$) for some states (e.g., spin 3 states) no such possibility exists whereas in other states it may be realized approximately.

4. Collective Excitations of Non-spherical Axially Symmetric Nuclei

The solutions of eq. (1.8) considered in the preceding section are valid if the inequality $\gamma_0 \gg \xi$ is fulfilled and therefore they cannot be used in the case of small values of γ_0. In the present section we shall consider the solution of eq. (1.8) for the case of axially symmetric nuclei ($\gamma_0 = 0$).

For small vibrations about the equilibrium point $\gamma_0 = 0$ the operator

$$T_\gamma = -\frac{1}{\gamma}\frac{\partial}{\partial\gamma}\left(\gamma\frac{\partial}{\partial\gamma}\right) \tag{4.1}$$

and the equation which determine the collective excitations with spin 0 assume the form

$$\left(\frac{1}{\gamma}\frac{\partial}{\partial\gamma}\left(\gamma\frac{\partial}{\partial\gamma}\right) - D\gamma^2 + \Lambda\right) g_0(\gamma) = 0. \tag{4.2}$$

The solution of this equation can be expressed through the degenerate hypergeometric function

$$g_0(\gamma) = \exp(-\tfrac{1}{2}\sqrt{D}\gamma^2)F(-\lambda, 1, \sqrt{D}\gamma^2)$$

for the values

$$\Lambda_\lambda = (4\lambda+2)\sqrt{D}. \tag{4.3}$$

The zero spin state energies can be obtained by inserting (4.3) into eq. (3.7). For $\mu < \frac{1}{3}$ the simpler formula (3.9) can be employed. By subtracting from the expressions thus obtained their values for $n = \lambda = 0$ which correspond to the ground state energy, the excitation energy of spin 0 excited states can be determined.

For $\mu < \frac{1}{3}$ the ground state energy will be

$$E_{00}(0) = \tfrac{1}{2}\hbar\omega + \frac{\hbar^2(1+\sqrt{D})}{B\beta_0^2}\left\{1+\mu^2[\tfrac{3}{2}-2\mu^2(1+\sqrt{D})]\right\}. \tag{4.4}$$

and hence if (1.11) is taken into account the excitation energy of the nucleus may be written down as

$$\Delta E_{n\lambda}(0) = n\hbar\omega+\hbar\omega_\gamma\{2\lambda-8\mu^4\lambda[(1+\lambda)\sqrt{D}+1] +3\mu^2 n(2\lambda+1)+3\mu^2\lambda\}+3n\mu^2\frac{\hbar^2}{B\beta_0^2}.$$

It should be mentioned here that in axially symmetric nuclei, in the adiabatic approximation ($\mu = 0$) the first excited state corresponding to zero spin γ vibrations has an energy of $2\hbar\omega_\gamma$ just as in the case of spherical nuclei the first zero spin 0 vibration has an energy of $2\hbar\omega$.

In states with $I \neq 0$ the rotation energy operator should be taken into account in equation (1.8). The coefficients A_ι of this operator which depend on γ (1.4) cannot be replaced by their values at $\gamma = \gamma_0 = 0$ since in this case the coefficient A_3 becomes infinite.

Besides the case of $I = 0$, solutions of (1.8) can also be derived for $I = 3$ inasmuch as in these states there is only one term

$$\Phi_3(\gamma, \theta_i) = |32\rangle g_2^{(3)}(\gamma)$$

in the sum in (2.9). Inserting this value into (1.8) and taking into account that

$$\langle 32|\tfrac{1}{4}\sum_\iota A_\iota \hat{I}_\iota^2|32\rangle = 9\sin^{-2}(3\gamma),$$

we get an equation which determines functions for small deviations from the equilibrium position

$$\left[\frac{1}{\gamma}\frac{\partial}{\partial\gamma}\left(\gamma\frac{\partial}{\partial\gamma}\right) - D\gamma^2 - \frac{1}{\gamma^2} + \Lambda - 3\right] g_2^{(3)}(\gamma) = 0.$$

The solution of this equation can also be expressed through a degenerate hypergeometric function with the values

$$\Lambda_\lambda^{(3)} = 3+4(\lambda+1)\sqrt{D}. \tag{4.5}$$

Thus in a spin 3 excited state an additional term in the potential energy determining the γ vibrations arises as a result of the rotational motion. The

minimum potential energy $W(\gamma) = D\gamma^2+1/\gamma^2$ measured in $\hbar^2(2B\beta_0^2)^{-1}$ units corresponds to $\gamma_m = D^{-\frac{1}{4}} = (2\gamma_{00}^2)^{\frac{1}{2}}\beta_0^{-1}$, where $\gamma_{00}^2 = \frac{1}{2}\hbar(C_\gamma B)^{-\frac{1}{2}}$ are the mean square amplitudes of the zero vibrations. Therefore, when an axially symmetric nucleus goes over to an excited state with $I = 3$, the axial symmetry of the nucleus is violated. Thus the rotational energy of an axially symmetric nucleus and γ vibrations are intimately related in a state with a spin 3. In order to obtain the energy of spin 3 states the ground state (0^+) energy should be subtracted from the expressions obtained. For $\mu = 0$ we get

$$\Delta E_{n\lambda}(3) = n\hbar\omega+2\hbar\omega_\gamma(\lambda+\tfrac{1}{2})+\frac{3\hbar^2}{2B\beta_0^2}.$$

The first excited state of this type which corresponds to the quantum numbers $n = \lambda = 0$ may be termed "rotational excitation". The dependence of the wave function of this state on the Eulerian angles and γ is given by the function

$$\Phi_{300}(\gamma, \theta_i) = y e^{-\frac{1}{2}y^2}|32\rangle, \quad \text{if} \quad y^2 = \sqrt{D}\gamma^2.$$

This state may be compared with the first γ vibration of spin 0 ($n = 0$, $\lambda = 1$). The wave function of this state does not depend on the Eulerian angles

$$\Phi_{001}(\gamma, \theta_i) = (1-y^2)e^{-\frac{1}{2}y^2}.$$

The energy difference between these states is determined by the expression

$$E_{01}(0)-E_{00}(3) = \hbar\omega_\gamma-\frac{3\hbar^2}{2B\beta_0^2}, \quad \text{if} \quad \mu = 0.$$

Consider now the excitations corresponding to a spin of 2. Substituting (2.9) in (1.8) with $\gamma_0 = 0$ we arrive at a set of two differential equations

$$[T_\gamma+\tfrac{3}{4}(A_1+A_2)+D\gamma^2-\Lambda]g_0(\gamma)+\frac{\sqrt{3}}{4}(A_1-A_2)g_2(\gamma) = 0, \tag{4.6}$$

$$\tfrac{1}{4}\sqrt{3}(A_1-A_2)g_0(\gamma)+[T_\gamma+\tfrac{1}{4}(A_1+A_2)+A_3+D\gamma^2-\Lambda]g_2(\gamma) = 0.$$

In the case of small vibrations about the equilibrium position $\gamma_0 = 0$, only terms of the zero and first order in γ may be retained in the coefficients A_1+A_2 and A_1-A_2.

The equations (4.6) then simplify to

$$\begin{aligned}\left[-\frac{1}{\gamma}\frac{\partial}{\partial\gamma}\left(\gamma\frac{\partial}{\partial\gamma}\right)+D\gamma^2-\Lambda+2\right]g_0(\gamma)-\tfrac{4}{3}\gamma g_2(\gamma) &= 0,\\ -\tfrac{4}{3}\gamma g_0(\gamma)+\left[-\frac{1}{\gamma}\frac{\partial}{\partial\gamma}\left(\gamma\frac{\partial}{\partial\gamma}\right)+D\gamma^2+\frac{1}{\gamma^2}-\Lambda+1\right]g_2(\gamma) &= 0.\end{aligned} \tag{4.7}$$

The equations (4.7) have two orthogonal solutions $g_{01}(\gamma)$, $g_{21}(\gamma)$ and $g_{02}(\gamma)$,

$g_{22}(\gamma)$. Thus even for small γ vibrations of axially symmetric nuclei, the quantum number K is not an integral of motion. According to symmetry rule c) in (2.9a) the function $g_2(\gamma)$ should vanish for $\gamma = 0$. In order to obtain approximate solutions of (4.7) we put $g_{21}(\gamma) = 0$ and then function g_{01} will be a solution of the equation

$$\left[-\frac{1}{\gamma}\frac{\partial}{\partial\gamma}\left(\gamma\frac{\partial}{\partial\gamma}\right)+D\gamma^2-\Lambda+2\right]g_{01}(\gamma) = 0. \tag{4.8}$$

A second solution of equations (4.7) which is orthogonal to the first is $g_{02}(\gamma)$ and the function $g_{22}(\gamma)$ which satisfies the equation

$$\left[-\frac{1}{\gamma}\frac{\partial}{\partial\gamma}\left(\gamma\frac{\partial}{\partial\gamma}\right)+D\gamma^2+\frac{1}{\gamma^2}-\Lambda+1\right]g_{22}(\gamma) = 0. \tag{4.9}$$

Solving equations (4.8) and (4.9) we get

$$g_{01\lambda}(\gamma) = \exp(-\tfrac{1}{2}\sqrt{D}\gamma^2)F(-\lambda, 1, \sqrt{D}\gamma^2), \quad \Lambda_1 = 2+(4\lambda+2)\sqrt{D},$$
$$g_{22\lambda}(\gamma) = \exp(-\tfrac{1}{2}\sqrt{D}\gamma^2)D^{\frac{1}{4}}\gamma F(-\lambda, 2, \sqrt{D}\gamma^2), \Lambda_2 = 1+4(\lambda+1)\sqrt{D}.$$

These solutions correspond to substituting the values $A_1 = A_2 = \frac{4}{3}$ for the coefficients A_l in (4.6). In this approximation quantum number K is an integral of motion.

In the same approximation the wave functions of collective excitations with spins of $I \geqq 4$ can be represented by the product

$$\Phi_{IK} = |IK\rangle g_K^{(I)}(\gamma), \quad K = 0, 2, \ldots I.$$

Employing the functions in (1.8), taking into account (4.1) and $A_1 = A_2 = \frac{4}{3}$, $A_3 = \frac{1}{3}-\gamma^{-2}$ we find

$$g_K^I(\gamma) = \exp(-\tfrac{1}{2}\sqrt{D}\gamma^2)(\sqrt{D}\gamma^2)^{\frac{1}{4}K}F(-\lambda, \tfrac{1}{2}K+1, \sqrt{D}\gamma^2).$$

In this case

$$\Lambda_{K\Lambda}^I = (4\lambda+K+2)\sqrt{D}+\tfrac{1}{3}[I(I+1)-\tfrac{3}{4}K^2]. \tag{4.10}$$

Inserting (4.10) into (3.7) or (3.9) and subtracting the ground state energy (4.4) we can determine the energy of the corresponding excited states.

In the simplest case when $\mu = 0$ the excitation energy of an axially symmetric nucleus calculated in this way can be expressed by the formula

$$E_{n\lambda}(I) = n\hbar\omega+\hbar\omega_\gamma(2\lambda+\tfrac{1}{2}K)+\frac{\hbar^2[I(I+1)-\frac{3}{4}K^2]}{6B\beta_0^2}. \tag{4.11}$$

The first term in this expression corresponds to β vibrations and the second takes into account γ vibrations and rotation in states with $K \neq 0$; the last term corresponds to the rotational energy. In deriving (4.10) it was assumed that quantum number K is a good quantum number. This assumption may be

justified only in the case of strongly deformed nuclei (large β_0). For $K \neq 0$ part of the rotational energy accounted for by the second term will then be much greater than the part due to the third term.

In conclusion a few additional words should be said about the spin 0 excited states considered above. These excited states may be of two types. They may be β vibrations corresponding to quantum numbers $n \neq 0$, $\lambda = 0$ and γ vibrations corresponding to quantum numbers $n = 0$, $\lambda = 0$. Direct transitions from these excited states to the ground state with $n = \lambda = 0$ may be possible via emission of conversion electrons. In other words these transitions refer to electric monopole transitions E0. As is well known, in the generalized model of the nucleus the E0 transition operator can be expressed by the series

$$\mathfrak{M}(\mathrm{E0}) = A + B\beta^2 + C\beta^3 \cos 3\gamma + \ldots . \tag{4.12}$$

The first, constant term in the operator (4.11) does not contribute to E0 transitions. Transitions of this type between excited spin 0 β-vibrational states and the ground state can be caused by the second (quadratic) term in (4.12); E0 transitions between excited spin 0 γ-vibrational states and the ground state can be due to the third (cubic) term in (4.12) Thus an experimental investigation of the E0 transition probability may permit one to distinguish between these two types of excited states.

References

1) A. Bohr, Mat. Fys. Medd. Dan. Vid. Selsk. **26**, No. 14 (1952)
2) L. Wilets and M. Jean, Phys. Rev. **102** (1956) 788
3) Z. Jankovic, Nuovo Cim. **14** (1959) 1174
4) A. S. Davydov and G. F. Filippov, JETP **35** (1958) 440; Nuclear Physics **8** (1959) 237
5) A. S. Davydov and V. S. Rostovsky, JETP **36** (1959) 1788; Nuclear Physics **12** (1959) 58
6) A. S. Davydov and A. A. Chaban, Nuclear Physics **20** (1960) 499
7) A. S. Davydov, Izv. Akad. Nauk SSSR, Ser. Fiz. **23** (1959) 792

6.C

Nuclear Physics **24** (1961) 695; © *North-Holland Publishing Co., Amsterdam*
Not to be reproduced by photoprint or microfilm without written permission from the publisher

ON THE SYMBOL FOR THE CURIE UNIT

The symbol c for the curie unit at present in use is not satisfactory, inasmuch as it violates the general rule of writing unit symbols derived from proper names with a capital letter. The question of an adequate symbol for curie is under discussion in the SUN Commission and it is understood that the eventual decision will very probably be to recommend the symbol Cur. Without in any way anticipating the Commission's decision, it has been decided, purely as a matter of convenience, from now on to adopt the symbol Cur for the curie unit in *Nuclear Physics*.

10.A

NEWS ITEM

INTERNATIONAL CONFERENCE ON ELEMENTARY PARTICLES

An international conference on elementary particles will take place from 14 to 20 September 1961 at Aix-en-Provence, France, under the sponsorship of the Commissariat à l'Énergie atomique, Ministère des Affaires étrangères and the Service des Relations culturelles, Ministère de l'Éducation nationale.

The French organizing committee consists of MM. Armenteros (École Polytechnique/CERN), Berthelot (CEA/Orsay), Bishop (Orsay), Falk (CEA), Gregory (École Polytechnique), Jean (Orsay), Messiah (CEA), Moch (Collège de France), Souriau (Marseille), Teillac (Orsay). The Secretary General is M. B. Gregory.

For further information apply to Miss E. W. D. Steel, Secretary, The Scientific Conference Secretariat, CERN, Geneva 23, Switzerland.

10.D *Nuclear Physics* **24** (1961) 696—698; © *North-Holland Publishing Co., Amsterdam*

BOOK REVIEWS

M. A. LEONTOVICH (Respondible Editor), J. TURKEVICH and HICKS (Translation Editors), *Plasma Physics and the Problem of Controlled Thermonuclear Reactions*, Vol. II. (Pergamon Press, 20 articles, 457 pages. £ 8)

This is a translation into English of volume II of the four volumes on plasma physics, published for the Geneva Conference 1958. The book is a collection of Russian articles on theoretical and experimental subjects, written mainly in the period 1953—1955.

The articles are original research articles, but since they are 5—7 years old, the book seems not very interesting now for people working with plasma physics. The book covers roughly the period of plasma physics before the importance of the many varieties of instabilities were discovered and, by articles of Shafronov, the discovery of kink and sausage instabilities of pinches. Therefore the book has interest as source material mainly. However, even if one is interested in three of the articles only, it might be less expansive to buy the whole volume, due to the trouble of translating from Russian.

The book is printed by photografic methods from a typewritten text. This seems very reasonable, as it means saving of time of money, even so it seems to the reviewer that the book comes too late and that the price is high. It might have been wiser if the publisher had translated and published volume IV first, as this volume contains the most recent articles.

Torkil Hesselberg Jensen

ROBERT V. MEGHREBLIAN and DAVID K. HOLMES, *Reactor Analysis*, McGraw-Hill Series in Nuclear Engineering (McGraw-Hill, London 1960. v—795 p. £ 7.11s.)

The field of reactor engineering is surprising. Nobody had any idea that this field existed in 1938. Today it is a fairly completely developed engineering dicipline and a text can be written like the present book. "Reactor analysis" deals with "the mathematical study of the nuclear behaviour of reactors based on certain approximate physical models". Thus reactor analysis and reactor physics are considered different topics, the former of special engineering interest, the latter of more fundamental or basic scientific interest. Personally I do not believe that a satisfactory education is obtained by the study of reactor analysis alone in this meaning of the subject, whereas I would be inclined to think that a study of reactor physics would be adequate. However, a book like "Reactor Analysis" is a very useful tool for anybody who wants to undertake practical and detailed reactor calculations. The book contains the material used in the ORSORT course. In addition to this material about twice as much subject matter is dealt with in considerable detail. The reader is assumed to have the general background of first courses in mathematical physics, analytical methods applied to engineering problems, and modern physics. In spite of this the two first chapters are devoted to a short survey of some of the concepts encountered in modern physics. This part of the book is not good. The rest is excellent and a lot of material is presented which has never before been dealt with in text book form.

"Reactor Analysis" deals only with the topics which are encountered in other reactor physics textbooks i.e. the development of reactor theory from transport theory and slowing down, via the bare homogeneous thermal reactor, reflected reactors, heterogeneous reactors, reactor kinetics etc. to perturbation theory.

With its nearly 800 pages and very thorough and systematic treatment the book becomes somewhat of a handbook in reactor calculations, although of course a reactor engineer may find himself involved in many design calculations and engineering problems the solution of which has

to be sought elsewhere. Here I think of subjects like shielding problems, heat transfer, safety, properties of materials, just to mention a few.

To state it very briefly, "Reactor Analysis" is one of the many books which are very useful for a reactor engineer. One may even say it is one of the McGraw-Hill Series in Nuclear Engineering which together with others may eventually make this series a complete set of tools for the study of this large subject.

O. Kofoed-Hansen

L. R. B. ELTON, *Introductory nuclear theory* (Pitman & Sons Ltd., London 1959. xi—286 p. 40 s.)

The boom in nuclear physics, besides producing great new quantities of physicists, physics laboratories, and physics journals, has also called into being an expanding variety of new physics courses that are offered to the students of universities and technical schools. Each institution faces its own special problems and solves them with its private recipe of courses, that may range from the purely cultural courses that attempt to describe the intellectual content of modern physics to highly specialized instruction in elementary particle physics, reactor engineering, or nuclear chemistry, etc. This great proliferation in courses has been paralleled by the production of a flood of text books that assist the students and teachers of these new courses.

The present text book is intended for final honours physics students (corresponding about to the beginning of graduate instruction in American universities); the student is assumed to have a previous acquaintance with quantum mechanics but no previous knowledge of the properties of nuclei. The course is developed with a view to providing exercise in the use of quantum mechanics simultaneously with the elucidation of the features of the atomic nucleus. This mixture is a fairly common and useful one, combining the advantages of giving to the nuclear physics student the essential tools of his trade at as early a stage as is possible, and also motivating the study of quantum mechanics with illustrations from a developing and interesting field of study.

The difficulties in adopting such a course arise largely from the necessity of finding in each case a method of derivation appropriate to the rather elementary quantal experience of the students. Thus, the present course is at its best in the discussion of scattering and reaction processes. The quantal formulation of scattering problems is clearly developed in the text, including the separation of centre of mass and relative coordinates, the definitions of the cross sections, the partial wave expansion etc. These general results are then applied to the two nucleon scattering problem (without polarization effects), the continuum theory, resonances, and the optical model.

The balance between simplicity, and elegance and generality is less successfully sustained in some other parts of the book, especially in the discussion of beta decay and gamma emission. In the discussion of the latter problem the author does not permit himself any of the general and powerful tools of the quantal angular momentum calculus (this is true throughout the whole book) but rather confines himself to a derivation of the transition rates for the two lowest multipoles M1 and E1. Thus, a rather long chapter, which starts with a derivation of time dependent perturbation theory, ends with the single application to the photodisintegration of the deuteron (and the inverse process).

The problem sets at the end of each chapter should be quite useful to the students. The problems are partly mathematical exercises in the techniques developed in the text, and partly examples of the types of problem that occur in the understanding and analysis of empirical nuclear data. A useful adjoint to these latter exercises is the twenty page table of nuclear data included at the end of the book.

Taken all together it would seem that this book should be especially useful to beginning nuclear physics students who have had only a very elementary course in quantum mechanics. The relatively low price should help to bring the book within the financial reach of most students, while the small size (286 pages) brings it within the carrying ability of all.

B. R. Mottelson

H. ENGEL and K. O. THIELHEIM, *Kernenergie-Technik* (Verlag Moderne Industrie, Munich 1960. 300 p. DM 36).

This book is intended as a help for engineers who have previously been working in other fields, but want to read an introductory survey on nuclear energy. For this reason only practical results are given and the mathematical and physical theory of reactors is not described.

The book is divided into four main sections. The first of these gives in about a hundred pages a very brief summary of technical aspects of nuclear reactors such as background material from nuclear physics, reactor physics, control of the chain reaction, shielding, thermal aspects, ore extraction and uranium purification, isotope separation, heavy water production and radiation detection. It is evident from this list and the relatively few pages allotted to these subjects that little detail can be obtained and in some of the cases one would even be inclined to think that too little material can be given in order to obtain even a scanty survey.

Thus, I do not believe that it is of great help to the reader to learn on half a page that scintillation counters do not enter in reactor control (but are useful radiation detectors), to be introduced to the principle underlying their operation, to learn that they function in the same way as visual X-ray screens, that they are used with electron-multipliers and electronics equipment, that several materials are used as scintillators, that scintillation counters have a very short time resolution and are therefore suited especially for coincidence work or time of flight work and that they may be used for energy spectrometry. I do not think that all these words are explained just by being stated and I see that I have spent nearly half an ordinary page by telling about all the words mentioned in this little section, so there cannot be a great deal more in the book. This case is an especially bad example, but there is, in general, too much of the same calibre throughout the book.

About another hundred pages are used on description of special types of reactors and about sixty pages deal with reactor economics, plans for the future in US, UK, USSR, Euratom and West Germany and ship propulsion, including data for "Lenin" and "Savannah" as well as for some ship projects. Finally, a few pages describe fusion and speculations on hopes for the future.

All told, the book contains a lot of information and, in general, it may very likely be of use for its purpose. It also contains an excellent list of references to more detailed descriptions.

O. Kofoed-Hansen

J. B. MARION and J. L. FOWLER (Editors), *Fast Neutron Physics, Part I: Techniques* (Interscience Publishers, New York XIII-961 p. $ 29.00).

This book constitutes volume IV of Interscience monographs and texts in physics and astronomy and the first of two volumes on fast neutron physics. Like many other modern physics texts the individual chapters are written by outstanding specialists. Thus the book may be said to consist of 24 individual scientific review papers under the four main headings: 1. Neutron Sources, 2. Recoil Detection Methods, 3. Detection by Neutron Induced Methods and 4. Special Techniques and Problems.

On nearly 1000 pages a wealth of diversified subject matter is described, as can be seen from two extreme quotations which I shall permit myself to make. Thus on page 400 the reader finds a short paragraph on neutrino detectors: "The giant detector for neutrino observation is a large version of the cadmium loaded scintillator" and where credit for much of the progress in the field of high efficiency liquid scintillation neutron detectors is given to the Los Alamos group who developed these counters for the neutrino experiment. As the other extreme I have chosen the following quotation from another kind of fast neutron "physics" on page 900: "Children exposed to the bomb tend to be smaller in size and to mature later than unexposed children" from the section on fast neutron radiation hazards where among other material one finds an account on human exposures with a subsection on Hiroshima and Nagasaki.

It will be understood from these two quotations that even an apparently specialized field like fast neutron physics deals with so many individual topics that a comprehensive book on the subject is best written as done in the present case, in which authoritative specialists bring their individual contributions and the entire material is collected into a well edited volume. The book is very much to be recommended for anybody who wants to specialize in this subject.

O. Kofoed-Hansen

AUTHOR INDEX

AITKEN, J. H. *see* DIXON

ALI-ZADE, S. A., *see* GUREVICH

ALLAN, D. L., An experimental test of the statistical theory of nuclear reactions 274

ANDERSSON, G., Systematic trends in half-lives of beta-decaying nucleides 666

ANDRÉ, G. O., *see* VAN BEEK

ARIMA, A., Residual interaction and the deformation of nuclei 69

ARNELL, S. E., Proton capture in A^{40} 500

BARASHENKOV, V. S., V. M. MALTSEV and E. K. MIKHUL, Mechanism of interaction of fast nucleons with nuclei 642

BELIAEV, S. T., Concerning the calculation of nuclear moment of inertia 322

BERÉNYI, D., *see* MÁTHE

BERNSTEIN, H. and H. H. FORSTER, Gamma-gamma directional correlation in Ba^{136} and Mo^{94}. 601

BISWAS, S. N. and V. GUPTA, Pion-hyperon resonances in pion production in hyperon-nucleon collisions 620

BOZÓKI, G., E. FENYVES and L. JÁNOSSY, Measurement of the collision mean free path of penetrating shower producing cosmic ray neutrons in lead. 412

BROWN, G. E., J. A. EVANS and D. J. THOULESS, Vibrations of spherical nuclei 1

CARVER, J. H. and G. A. JONES, (N-Z) dependence of radiative deuteron capture cross-sections 607

CERINEO, M., *see* CINDRO

CHIAO, LUNG-WEN, *see* HANSEN

CHRISTY, R. F. and I. DUCK, γ rays from an extranuclear direct capture process. 89

CINDRO, N., M. CERINEO and A. STRZAŁKOWSI, (d, α) reactions on some light nuclei at 13 MeV 107

CIULLI, S. and J. FISCHER, A convergent set of integral equations for singlet proton-proton scattering 465

COHEN, A. V. and J. A. COOKSON, Scattering by Si^{28} of protons of energy 10.0—12.3 MeV. 529

COOKSON, J. A., *see* COHEN

DAGLEY, P., W. HAEBERLI and J. X. SALADIN, The C^{13} (p, n) N^{13} reaction cross section from the threshold to 13 MeV 353

DAVYDOV, A. S., Collective excitations corresponding to quadrupole nuclear surface vibrations 682

DEUTSCH, J. P. et P. LIPNIK, Dépendance angulaire de la corrélation

β—γ (polarisé circulaire) dans Au ^{198}. 138
DEVANATHAN, V., *see* RAMAKRISHNAN
DIXON, W. R. and J. H. AITKEN, Absolute cross section of the K^{39} (n, p) A^{39} reaction for 2.5 MeV neutrons 456
DOUGLAS, A. C., *see* MACDONALD
DUCK, I., *see* CHRISTY
ESTULIN, I. V., A. S. MELIORANSKY and L. F. KALINKIN, Transitions between low-lying excited states of Mn^{56} and Ho^{166} 118
EVANS, J. A., *see* BROWN
EVANS, W. W., *see* POPE
FENYVES, E., *see* BOZÓKI
FISCHER, J., *see* CIULLI
FORSTER, H. H., *see* BERNSTEIN
FRECK, D. V., *see* POPE
GALLAGHER, Jr., C. J. and H. L. NIELSEN, The 5.3 sec isomer of W^{183} . . 422
GERHOLM, T. R., B.-G. PETTERSSON, B. VAN NOOIJEN and Z. GRABOWSKI, Penetration matrix elements and nuclear structure effects in Tl^{203} . . 177
GERHOLM, T. R., *see* GRABOWSKI
GERHOLM, T. R., *see* PETTERSSON
GERHOLM, T. R., *see* PETTERSSON
GERHOLM, T. R., *see* PETTERSSON
GLAGOLEV, V. V., V. PETRŽÍLKA and K. D. TOLSTOV, On isobaric excitation of nucleons in collisions with fast particles 126
GLOVER, R. N. and K. H. PURSER, Protons and deuterons from Ni^{58} bombarded by 15.9 MeV neutrons 431
GLOVER, R. N. and E. WEIGOLD, Protons and deuterons from Al^{27} bombarded by 14.8 MeV neutrons 630
GOEBEL, K., D. HARTING, J. C. KLUYVER, A. KUSUMEGI and H. SCHULTES, The C^{12} (p, pn) C^{11} and Al^{27} (p, 3pn) Na^{24} cross-sections at 591 MeV 28
GOTŌ, T., On the nature of the electromagnetic field 388
GRABOWSKI, Z., B.-G. PETTERSSON, T. R. GERHOLM and J. E. THUN, Penetration matrix elements and nuclear structure effects in Ta^{181} 251
GRABOWSKI, Z., *see* GERHOLM
GRABOWSKI, Z., *see* PETTERSSON
GRATOT, I., *see* OLKOWSKY
GRECHUKHIN, D. P., The vibrational quadrupole excitation model and non-axial rotator model 576
GREENLEES, G. W., J. S. LILLEY, P. C. ROWE and P. E. HODGSON, The elastic scattering of 29 MeV He^3 by Al, V and Cu 334
GROTE, L. C., U. KRECKER, U. KUNDT, K. LANIUS, G. MANSKE and H. W. MEIER, Inelastic π^--nucleon interactions at 7.5 GeV 300
GUPTA, S. N., Relativistic one-pion exchange nuclear potential 160

GUPTA, V., *see* BISWAS
GUREVICH, I. I., B. A. NIKOLSKY and S. A. ALI-ZADE, Asymmetry of the angular distribution of electrons from $\mu \rightarrow$ e—decay 480
HAEBERLI, W., *see* DAGLEY
HANSEN, P. G., K. WILSKY, D. J. HOREN and LUNG-WEN CHIAO, High energy gamma rays in the decay of 27h Ho^{166} 519
HARTING, D., *see* GOEBEL
HAUSER, U., Hindered E1 decay of the 6 keV individual particle state of $_{73}Ta^{181}$ 488
HINDS, S., R. MIDDLETON and A. E. LITHERLAND, A doublet at 3.40 MeV excitation in Mg^{25} 510
HODGSON, P. E., *see* GREENLEES
HOREN, D. J., *see* HANSEN
HORMANN, E., Applications of the Sakata model for elementary particles 514
JACOBSOHN, B. A. and R. M. RYNDIN, An absolute detector and producer of nuclear alignment 505
JAMES, A. N., The C^{13} (d, n) N^{14} reaction 132
JAMES, A. N., γ-rays from the 1.14 MeV resonance in B^{10} (p, γ) C^{11} . . . 675
JÁNOSSY, L., *see* BOZÓKI
JONES, G. A., *see* CARVER
JØRGENSEN, M., O. B. NIELSEN and O. SKILBREID, Levels in Ho^{162} and Dy^{162} 443
KALINKIN, L. F., *see* ESTULIN
KANAZAWA, A., The electric polarizability of the neutron in the static meson theory 524
KARDON, B., D. KISS, I. LOVAS and Z. ZÁMORI, γ—γ angular correlation in the Ti^{48} (n, γ) Ti^{49} reaction 151
KAUFMANN, W. and H. WÄFFLER, A search for parity-forbidden alpha-decay from the 8.88 MeV (2^-) state in O^{16} 62
KISS, D., *see* KARDON
KLUYVER, J. C., *see* GOEBEL
KRECKER, U., *see* GROTE
KROMMINGA, A. J. and I. E. MCCARTHY, Simplified discussion of backward peaking in direct interactions 36
KUNDT, U., *see* GROTE
KUSUMEGI, A., *see* GOEBEL
LANIUS, K., *see* GROTE
LAWSON, R. D. and M. H. MACFARLANE, A rotational model for Fe^{57} . . 18
LE PAPE, M., *see* OLKOWSKY
LILLEY, J. S., *see* GREENLEES
LIPNIK, P., *see* DEUTSCH
LITHERLAND, A. E., *see* HINDS

LOMON, E. L. and N. NAUENBERG, The $^1S_0$ nucleon interaction in the boundary condition model 474
LOMSADZE, Ju. M., Concerning a "strong" coupling method in the quantized field theory 143
LOVAS, I., *see* KARDON
MACDONALD, N., and A. C. DOUGLAS, The magnetic spectrograph data on level densities of light nuclei 614
MACFARLANE, M. H., *see* LAWSON
MALLMANN, C. A., Evidence for the existence of rotational levels in all even nuclei 535
MALTSEV, V. M., *see* BARASHENKOV
MANSKE, G., *see* GROTE
MARIS, TH. A. J., A remark on the isobaric spin space. 346
MÁTHE, Gy., T. SCHARBERT and D. BERÉNYI, Investigations on the decay scheme of I^{131} in the low energy region of gamma-rays 318
MCCARTHY, I. E., *see* KROMMINGA
MEIER, H. W., *see* GROTE
MELIORANSKY, A. S. *see* ESTULIN
MIDDLETON, R., *see* HINDS
MIKHUL, E. K., *see* BARASHENKOV
MONAHAN, J. E., S. RABOY and C. C. TRAIL, Measurement of the energy of the gamma radiation from neutron capture by hydrogen 400
NAUENBERG, N., *see* LOMON
NIELSEN, H. L., *see* GALLAGHER, Jr.
NIELSEN, O. B., *see* JØRGENSEN
NIKOLSKY, B. A., *see* GUREVICH
OLKOWSKY, J., I. GRATOT et M. LE PAPE, Sections efficaces des réactions (p, n) et (p, 2n) sur Nd^{150} 84
OLKOWSKY, J. et J. RAYNAL, Sur la détermination du potentiel imaginaire dans le modèle optique 269
PANDYA, S. P. and S. K. SHAH, Nuclear interactions in the shell model 326
PELLEGRINI, F., (d, α) reactions on C^{12}, O^{16} and Mg^{24}. 372
PETRŽÍLKA, V., *see* GLAGOLEV
PETTERSSON, B.-G., T. R. GERHOLM, Z. GRABOWSKI and B. VAN NOOIJEN, Penetration matrix elements and nuclear structure effects in Tl^{201} . . 196
PETTERSSON, B.-G., J. E. THUN and T. R. GERHOLM, Experimental determination of the conversion coefficient of the 412 keV E2 transition in Hg^{198} 243
PETTERSSON, B.-G., J. E. THUN and T. R. GERHOLM, Magnetic and quadrupole interactions in Hg^{197m} angular correlations 223
PETTERSSON, B.-G., *see* GRABOWSKI
PETTERSSON, B.-G., *see* GERHOLM

POPE, R. A., D. V. FRECK and W. W. EVANS, Resonances in the K^{39} (p, γ) Ca^{40} reaction from 1.0 to 2.1 MeV 657
PURSER, K. H., *see* GLOVER
RABOY, S., *see* MONAHAN
RAMACHANDRAN, G., *see* RAMAKRISHNAN
RAMAKRISHNAN, A., V. DEVANATHAN and G. RAMACHANDRAN, Elastic photoproduction of neutral pions from deuterium 163
RAYNAL, J., *see* OLKOWSKY
RIKMENSPOEL, R. and D. M. VAN PATTER, The decay of Br^{78} 494
ROBSON, D., Polarizations in (d, p) reactions, erratum 528
ROBSON, D., Spin-orbits in the stripping reaction involving particles, erratum 527
ROWE, P. C., *see* GREENLEES
RYNDIN, R. M., *see* JACOBSOHN
SALADIN, J. X., *see* DAGLEY
SCHARBERT, T., *see* MÁTHE
SCHULTES, H., *see* GOEBEL
SETH, K. K., On the spin dependence of neutron strength functions . . 169
SHAH, S. K., *see* PANDYA
SKILBREID, O., *see* JØRGENSEN
STRZAŁKOWSKI, A., *see* CINDRO
TER-MIKAELYAN, M. L., Emission of fast particles in a heterogeneous medium 43
THOULESS, D. J., *see* BROWN
THUN, J. E., *see* GRABOWSKI
THUN, J. E., *see* PETTERSSON
THUN, J. E., *see* PETTERSSON
TOLSTOV, K. D., *see* GLAGOLEV
TRAIL, C. C., *see* MONAHAN
VAN BEEK, A. M. K. and G. O. ANDRÉ, The polarization of protons Be^{9} (d, p) Be^{10} and Li^{6} (d, p) Li^{7} for 1.63 MeV deuterons 102
VAN LOEF, J. J., Activations cross sections for (n, p) reactions in some medium-weight nuclei with D + D neutrons 340
VAN NOOIJEN, B., *see* GERHOLM
VAN NOOIJEN, B., *see* PETTERSSEN
VAN PATTER, D. M., *see* RIKMENSPOEL
WÄFFLER, H., *see* KAUFMANN
WEIGOLD, E., *see* GLOVER
WILSKY, K., *see* HANSEN
YAMAZAKI, K., A new variational method for calculating excited energy levels and its application to the anharmonic oscillator 313
ZÁMORI, Z., *see* KARDON

SUBJECT INDEX

1. Nuclear Structure

1.B *Two- and three-body problems*

Measurement of the energy of the gamma radiation from neutron capture by hydrogen, J. E. Monahan, S. Raboy and C. C. Trail 400

The $^1S_0$ nucleon interaction in the boundary condition model, E. L. Lomon and N. Nauenberg 474

1.D *Nuclear models*

1.D.1 *Shell model*

Nuclear interactions in the shell model, S. P. Pandya and S. K. Shah 326

1.D.2 *Collective model*

A rotational model for Fe^{57}, R. D. Lawson and M. H. Macfarlane . . . 18

Hindered E1 decay of the 6 keV individual particle state of $_{73}Ta^{181}$, U. Hauser 488

A doublet at 3.40 MeV excitation in Mg^{25}, S. Hinds, R. Middleton and A. E. Litherland 510

Evidence for the existence of rotational levels in all even nuclei, C. A. Mallmann 535

The vibrational quadrupole excitation model and non-axial rotator model, D. P. Grechukhin 576

Protons and deuterons from Al^{27} bombarded by 14.8 MeV neutrons, R. N. Glover and E. Weigold 630

Collective excitations corresponding to quadrupole nuclear surface vibrations, A. S. Davydov 682

1.D.4 *Relationship between different models*

Vibrations of spherical nuclei, G. E. Brown, J. A. Evans and D. J. Thouless 1

Residual interaction and the deformation of nuclei, A. Arima 69

The vibrational quadrupole excitation model and non-axial rotator model, D. P. Grechukhin 576

1.E *Properties of nuclei*

1.E.1 *Energy levels*

Transitions between low-lying excited states of Mn^{56} and Ho^{166}, I. V. Estulin, A. S. Melioransky and L. F. Kalinkin 118

γ—γ angular correlation in the Ti^{48} (n, γ) Ti^{49} reaction, B. Kardon, D. Kiss, I. Lovas and Z. Zámori 151

Penetration matrix elements and nuclear structure effects in Tl^{201}, B.-G. Pettersson, T. R. Gerholm, Z. Grabowski and B. Van Nooijen . 196

Investigations on the decay scheme of I^{131} in the low energy region of gamma-rays, Gy. Máthe, T. Scharbert and D. Berényi 318

The 5.3 sec isomer of W^{183}, C. J. Gallagher, Jr., and H. L. Nielsen . . . 422

Levels in Ho^{162} and Dy^{162}, M. Jørgensen, O. B. Nielsen and O. Skilbreid 443

Proton capture in A^{40}, S. E. Arnell 500

A doublet at 3.40 MeV excitation in Mg^{25}, S. Hinds, R. Middleton and A. E. Litherland 510

High energy gamma rays in the decay of 27h Ho^{166}, P. G. Hansen, K. Wilsky, D. J. Horen and Lung-Wen Chiao 519
Gamma-gamma directional correlation in Ba^{136} and Mo^{94}, H. Bernstein and H. H. Forster 601
γ-rays from the 1.14 MeV resonance in B^{10} (p, γ)C^{11}, A. N. James . . . 675

1.E.6 *Nuclear moments of inertia*

Concerning the calculation of nuclear moment of inertia, S. T. Beliaev 322

2. Nuclear Reactions

2.A *General properties*

2.A.1 *Cross-sections, energy relations*

The C^{12} (p, pn) C^{11} and Al^{27} (p, 3 pn) Na^{24} cross-sections at 591 MeV, K. Goebel, D. Harting, J. C. Kluyver, A. Kusumegi and H. Schultes 28
Sections efficaces des réactions (p, n) et (p, 2n) sur Nd^{150}. J. Olkowsky, I. Gratot et M. Le Pape 84
Activation cross sections for (n, p) reactions in some medium-weight nuclei with D + D neutrons, J. J. Van Loef 340
Absolute cross section of the K^{39} (n, p)A^{39} reaction for 2.5 MeV neutrons, W. R. Dixon and J. H. Aitken 456

2.B *Angular distributions, correlations; polarization*

(d, α) reactions on some light nuclei at 13 MeV, N. Cindro, M. Cerineo and A. Strzalkowsi 107
The C^{13} (d, n)N^{14} reaction, A. N. James 132
An absolute detector and producer of nuclear alignment, B. A. Jacobsohn and R. M. Ryndin 505

2.C *Resonance reactions; R-matrix theory*

The C^{13} (p, n) N^{13} reaction cross section from threshold to 13 MeV, P. Dagley, W. Haeberli and J. X. Saladin 353
Resonances in the K^{39} (p, γ) Ca^{40} reaction from 1.0 to 2.1 MeV, R. A. Pope, D. V. Freck and W. W. Evans 657

2.D *Statistical model*

An experimental test of the statistical theory of nuclear reactions, D. A. Allan 274
Protons and deuterons from Ni^{58} bombarded by 14.9 MeV neutrons, R. N. Glover and K. H. Purser 431
($N-Z$) dependence of radiative deuteron capture cross-sections, J. H. Carver and G. A. Jones 607
The magnetic spectrograph data on level densities of light nuclei, N. MacDonald and A. C. Douglas 614
Protons and deuterons from Al^{27} bombarded by 14.8 MeV neutrons, R. N. Glover and E. Weigold 630

2.E *Optical model*

Sections efficaces des réactions (p, n) et (p, 2n) sur Nd^{150}, J. Olkowsky, I. Gratot et M. Le Pape 84
On the spin dependence of neutron strength functions, K. K. Seth 169
Sur la détermination du potentiel imaginaire dans le modèle optique, J. Olkowsky et J. Raynal 269
The elastic scattering of 29 MeV He^3 by Al, V and Cu, G. W. Greenlees, J. S. Lilley, P. C. Rowe and P. E. Hodgson 334
Scattering by Si^{28} of protons of energy 10.0—12.3 MeV, A. V. Cohen and J. A. Cookson 529

2.F *Direct interaction (other than stripping)*

Simplified discussion of backward peaking in direct interactions, A. J. Krominga and I. E. McCarthy 36
γ rays from an extranuclear direct capture process, R. F. Christy and I. Duck 89
The C^{13} (p, n) N^{13} reaction cross section from the threshold to 13 MeV, P. Dagley, W. Haeberli and J. X. Saladin. 353
(d, α) reactions on C^{12}, O^{16} and Mg^{24}, F. Pellegrini 372
Protons and deuterons from Ni^{58} bombarded by 14.9 MeV neutrons, R. N. Glover and K. H. Purser. 431
Protons and deuterons from Al^{27} bombarded by 14.8 MeV neutrons, R. N. Glover and E. Weigold. 630

2.G *Stripping and pick-up*

The polarization of protons Be^{9}(d, p) Be^{10} and Li^{6}(d, p) Li^{7} for 1.63 MeV deuterons, A. M. K. Van Beek and G. O. André 102
(d, α) reactions on some light nuclei at 13 MeV, N. Cindro, M. Cerineo and A. Strzałkowsi 107
The C^{13} (d, n) N^{14} reaction, A. N. James 132

2.J *Fission and spallation*

The C^{12} (p, pn) C^{11} and Al^{27} (p, 3pn) Na^{24} cross-sections at 5.91 MeV, K. Goebel, D. Harting, J. C. Kluyver, A. Kusumegi and H. Schultes 28

2.L *Scattering processes (except two-nucleon system and meson scattering)*

The elastic scattering of 29 MeV He^{3} by Al, V and Cu, G. W. Greenlees, J. S. Lilley, P. C. Rowe and P. E. Hodgson 334
A convergent set on integral equations for singlet proton-proton scattering, S. Ciulli and J. Fischer 465

3. Electromagnetic Radiation

3.A *Gamma radiation*

Transitions between low-lying excited states of Mn^{56} and Ho^{166}, I. V. Estulin, A. S. Melioransky and L. F. Kalinkin 118
γ-γ angular correlation in the Ti^{48} (n, γ) Ti^{49} reaction, B. Kardon, D. Kiss, I. Lovas and Z. Zámori 151
Investigations on the decay scheme of I^{131} in the low energy region of gamma-rays, Gy. Máthe, T. Scharbert and D. Berényi 318
Measurement of the energy of the gamma radiation from neutron capture by hydrogen, J. E. Monahan, S. Raboy and C. C. Trail 400
The 5.3 sec isomer of W^{183}, C. J. Gallagher, Jr., and H. L. Nielsen 422
High energy gamma rays in the decay of 27h Ho^{166}, P. G. Hansen, K. Wilsky, D. J. Horen and Lung-Wen Chiao 519
Gamma-gamma directional correlation in Ba^{136} and Mo^{94}, H. Bernstein and H. H. Forster 601
γ-rays from the 1.14 MeV resonance in B^{10} (p, γ) C^{11}, A. N. James 675

3.B *Internal conversion*

Penetration matrix elements and nuclear structure effects in Tl^{203}, T. R. Gerholm B.-G. Pettersson, B. Van Nooijen and Z. Grabowski 177
Penetration matrix elements and nuclear structure effects in Tl^{201}, B.-G. Pettersson, T. R. Gerholm, Z. Grabowski and B. Van Nooijen. 196
Experimental determination of the conversion coefficient of the 412 keV E2 transition in Hg^{198}, B.-G. Pettersson, J. E. Thun and T. R. Gerholm 243

Penetration matrix elements and nuclear structure effects in Ta^{181}, Z. Grabowski, B.-G. Pettersson, T. R. Gerholm and J. E. Thun 251

3.C *Extranuclear effects*

Magnetic and quadrupole interactions in Hg^{197m} angular correlations, B.-G. Pettersson, J. E. Thun and T. R. Gerholm. 223
Penetration matrix elements and nuclear structure effects in Ta^{181}, Z. Grabowski, B.-G. Pettersson, T. R. Gerholm and J. E. Thun 251

4. Beta Decay; Parity

4.E *Analysis of data*

The decay of Br^{78}, R. Rikmenspoel and D. M. Van Patter 494
Systematic trends in half-lives of beta-decaying nucleides, G. Andersson . . . 666

5. Alpha Decay

A search for parity-forbidden alpha-decay from the 8.88 MeV (2^-) state in O^{16}, W. Kaufmann and H. Wäffler 62

6. Methods and Instruments

6.B *Theoretical*

A new variational method for calculating excited energy levels and its application to the anharmonic oscillator, K. Yamazaki 313
An absolute detector and producer of nuclear alignment, B. A. Jacobsohn and R. M. Ryndin 505

6.C *Constants, standards and units*

On the symbol for the curie unit 695

7. Quantum Field Theory

7.A *General*

Concerning a "strong" coupling method in the quantized field theory, Ju. M. Lomsadze 143
A convergent set of integral equations for singlet proton-protons scattering, S. Ciulli and J. Fischer 465

7.C *π-meson field (scattering and nuclear forces)*

On isobaric excitation of nucleons in collisions with fast particles, V. V. Glagolev, V. Petřzílka and K. D. Tolstov 126
Relativistic one-pion exchange nuclear potential, S. N. Gupta 160
Elastic photoproduction of neutral pions from deuterium, A. V. Ramakrishnan, A. V. Devanathan and G. Ramachandran 163
The electric polarizability of the neutron in the static meson theory, A. Kanazawa 524
Pion-hyperon resonances in pion production in hyperon-nucleon collisions, S. N. Biswas and V. Gupta 620

8. Elementary Particles

8.A *Experimental*

Dépendance angulaire de la corrélation β—γ (polarisé circulaire) dans Au^{198}, J. P. Deutsch et P. Lipnik 138

Inelastic π^--nucleon interactions at 7.5 GeV, L. C. Grote, U. Krecker, U. Kundt, K. Lanius, G. Manske and H. W. Meier 300
Asymmetry of the angular distribution of electrons from $\mu \rightarrow$e-decay, I. I. Gurevich, B. A. Nikolsy and S. A. Ali-Zade 480

8.B *Theory; interactions, transformation properties*

Emission of fast particles in a heterogeneous medium, M. L. Ter-Mikaelyan . . 43
A remark on the isobaric spin space, Th. A. J. Maris 346
Applications of the Sakata model for elementary particles, E. Hormann . . . 514
Pion-hyperon resonances in pion production in hyperon-nucleon collisions, S. N. Biswas and V. Gupta 620

8.C *Fundamental theory of matter*

On the nature of the electromagnetic field, T. Gotō 388

9. Cosmic Radiation

9.B *Passage of particles through matter*

Emission of fast particles in a heterogeneous medium, M. L. Ter-Mikaelyan 43
Measurement of the collision mean free path of penetrating shower producing cosmic ray neutrons in lead, G. Bozóki, E. Fenyves and L. Jánossy 412
Mechanism of interaction of fast nucleons with nuclei, V. S. Barashenkov, V. M. Maltsev and E. K. Mikhul 642

10. News Items

10.A *News items*

International Conference on Elementary Particles 695

10.D *Book reviews*

W. D. Allen, Neutron detection (J. Schiellerup Petersen). 176
M. A. Leontovich (Responsible Editor), J. Turkevich and Hicks (Translation Editors), Plasma Physics and the Problem of Controlled Thermonuclear Reactions, Vol. II (Torkil Hesselberg Jensen) 696
Robert V. Meghreblian and David K. Holmes, Reactor Analysis (O. Kofoed-Hansen) 696
L. R. B. Elton, Introductory nuclear theory (B. R. Mottelson) 697
H. Engel and K. O. Thielheim, Kernenergie. Technik (O. Kofoed-Hansen) . 698
J. B. Marion and J. L. Fowler (Editors), Fast neutron physics, Part I: Techniques (O. Kofoed-Hansen) 698

10.E *Errata*

D. Robson, Spin-orbits in the stripping reaction involving particles 527
D. Robson, Polarizations in (d, p) reactions 527
N. K. Glendenning and J. Sawicki, Intrinsic quadrupole moments of deformed nuclei and superfluidity in nuclei. 527
P. S. Dubbeldam, C. C. Jonker and H. J. Boersma, Energy and angular dependence of the left-right asymmetry of D-D neutrons scattered by carbon 527